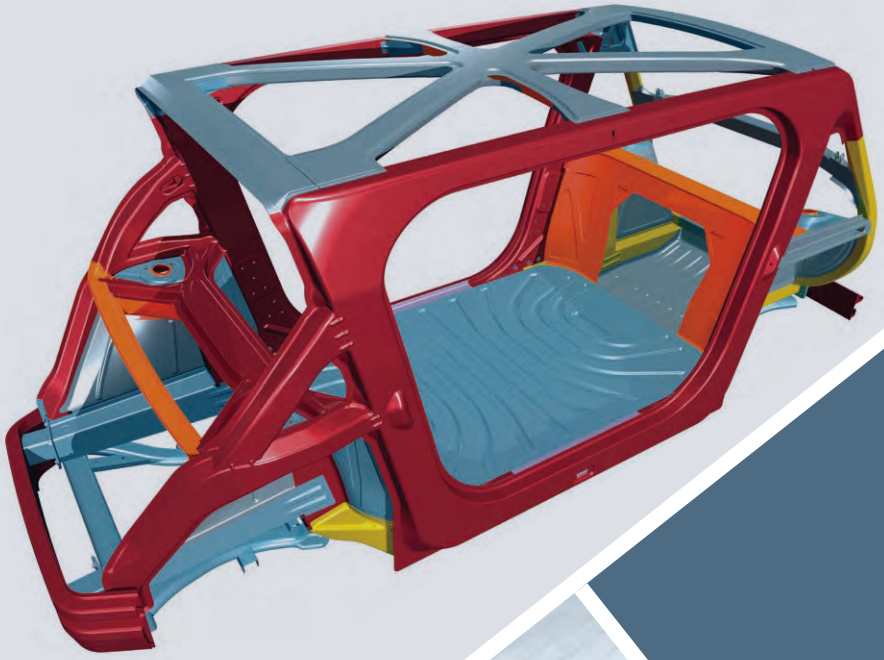

Steel E-Motive
Engineering Report

Development of a new vehicle and body structure for a fully autonomous, Mobility as a Service vehicle, featuring the latest advanced high-strength steel material grades and manufacturing processes

STEEL E-MOTIVE

IN PARTNERSHIP WITH

WorldAutoSteel

RICARDO

1 August 2023

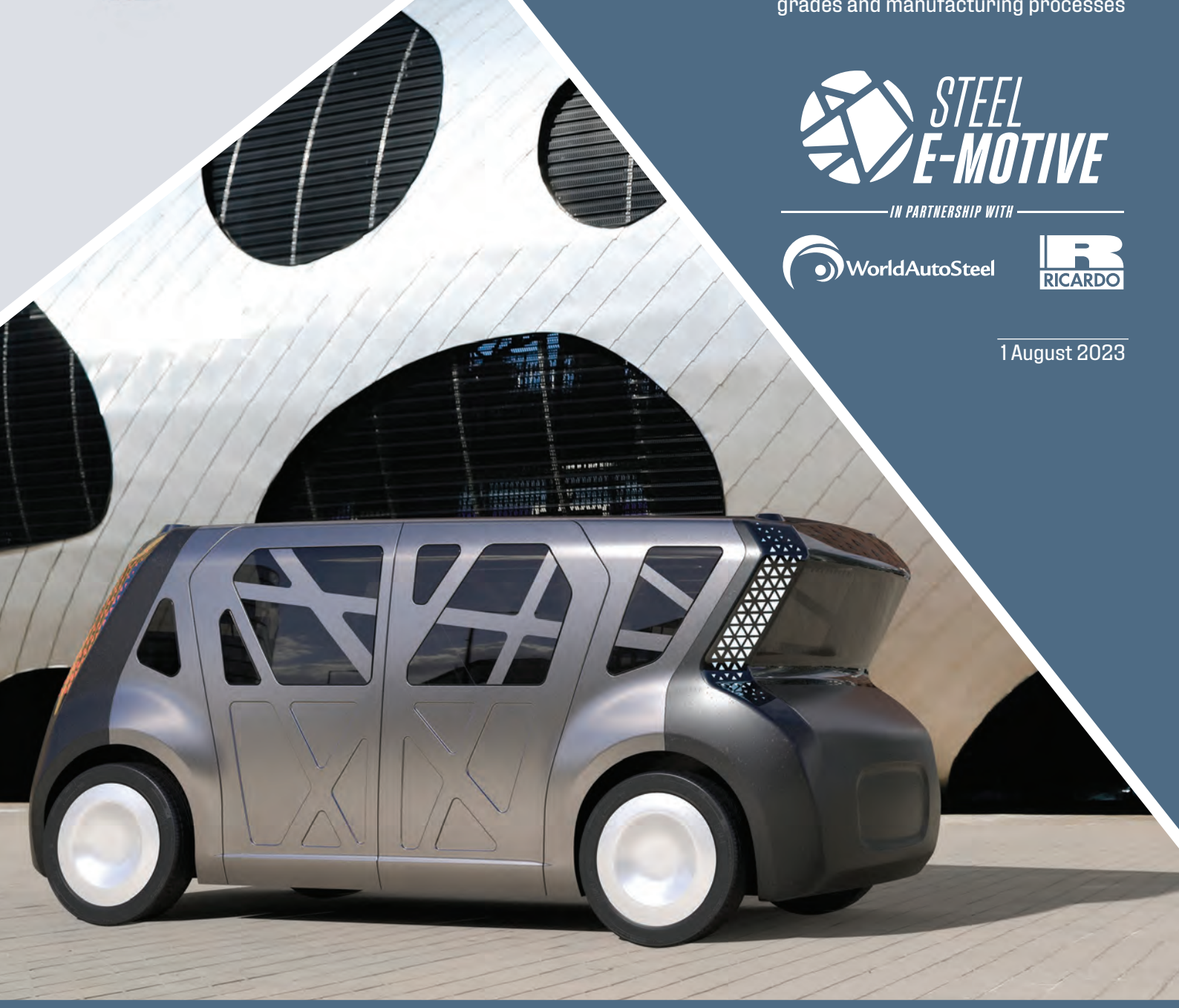

CONTENTS

1.0 Preface

This report documents the results of the Steel E-Motive engineering programme. The Steel E-Motive programme is the most recent addition to WorldAutoSteel's series of initiatives demonstrating steel solutions that help address the affordable, sustainable and safe mobility challenges that are facing automakers, governments and policy makers around the world.

This programme follows the Ultra-Light Steel Auto Body (ULSAB) 1998, the Ultra-light Steel Auto Closures (ULSAC) 2000, Ultra-light Steel Auto Suspension (ULSAS), ULSAB-AVC (Advanced Steel Concepts) 2021 and Future Steel Vehicle (FSV) 2013.

WorldAutoSteel has commissioned Ricardo (https://www.ricardo.com/en), to conduct the engineering development of 2 vehicle design concepts, codenamed SEM1 and SEM2, which are fully autonomous battery electric vehicles for use in Mobility as a Service (MaaS) operations. With its engineering partner ARRK, the vehicle designs were developed from "clean sheet", with the specific focus on the body structure, demonstrating how the latest Advanced High-Strength Steels (AHSS) can be applied to address the requirements and challenges for this next generation of personal transportation vehicle.

1.1 WorldAutoSteel member companies

- ANSTEEL
- ArcelorMittal
- Baowu
- CSC
- Erdemir
- HBIS Group
- Hyundai Steel
- JFE
- JSW
- Kobelco
- Nippon Steel
- Nucor
- POSCO
- Tata Steel
- Ternium
- Usiminas
- U.S. Steel
- Voestalpine

1.2 Steel E-Motive programme engineering service providers

- Ricardo (lead)
- ARRK (support)

1.3 Steel E-Motive lead project team members

Cees Ten Broek, Director, WorldAutoSteel
George Coates, Technical Director, WorldAutoSteel
Kate Hickey, Communications Manager, WorldAutoSteel
Russ Balzer, Technical Manager, WorldAutoSteel
Angela Erhart, Administrator, WorldAutoSteel
Neil McGregor, Chief Engineer, Ricardo
Owain Davies, Chief Engineer, Ricardo
Anne-Lise Gras, Programme Manager, Ricardo
Phil Crowther, Vehicle Integration Head, Ricardo

1.4 Steel E-Motive Core Team members

Ansteel, Lin Li
ArcelorMittal, Jerome Favero
ArcelorMittal, Jimmy Lam
Baosteel, Changwei Lian
Baosteel, Han Fei
China Steel, Cheng-Kai, Chiu Huang
Erdemir, Elvin Özcan
Erdemir, Mehmet Bulut Özyiğit
HBIS Group, Ziliu Xiong
Hyundai, Dong Yul Lee
Hyundai, Brandon Hance
Hyundai, Dae Young Kim
Hyundai, Jongmin Lee
JFE, Keiji Nishimura
JFE, Toshiaki Urabe
JFE, Tsuyoshi Shiozaki
JSW, Kinshuk Roy
Kobe Steel, Yoichi Mukai
Kobe Steel, Daisuke Matsuwaka
Nippon Steel, Akira Usami
Nippon Steel, Shunji Hiwatashi
Nippon Steel, Sato Masahiko
Nucor, Arnie Newsome
Nucor, Dean Kanelos
POSCO, Barney Jaehyun Kim
POSCO, Jiwoong Ha
POSCO, Haea Lee
POSCO, Jongcheol Park
Tata Steel, Peter Jones
Ternium, Juan Pablo Pedraza
U. S. Steel, Vasant Pednekar
USIMINAS, Tulio Melo
USIMINAS, Aldo Barbosa
Voestalpine, Enno Arenholz
Voestalpine, Reinhard Hackl

Project advisors and technical consultants:

Donald E. Malen, Senior Technical Advisor, University of Michigan
Hesham Ezzat, Senior Technical Advisor, American Iron and Steel Institute
Mike Davenport, Auto Steel Partnership
John Catterall, Auto Steel Partnership

1.5 Ricardo project delivery team

Maurizio Tancredi

Vladimir Jirasek

Patrik Pakut

Martin Vlcek

Ben Lowe

Tom Timpson

Terry McKie

Tom Van Dicjk

Nik Hill

Marco Raugei

Louise Wilson

Rebecca Roper

Kathryn Bellamy

Harry Jones

Fabian Fiquet

2.0 Executive Summary

2.1 Introduction & motivation for the Steel E-Motive programme

Privately owned passenger cars have long been the go-to transportation mode for personal, land-based mobility. A number of influencing factors are now contributing to a significant shift in personal transportation modes. Climate change threatens the health, safety and wellbeing of everyone on the planet, with a significant reduction in Greenhouse Gas emissions identified as the primary solution to global warming. The transition from fossil fuelled internal combustion engines to hybrid and electric propulsion systems should help address climate change to some extent, but the impact of this will also be dependant on the ability to decarbonise vehicle manufacture and electricity used to charge vehicle batteries.

Population growth and societal changes such as the growth of mega-cities, continued urbanisation trends, personal expenditure and vehicle ownership & running costs will also change the demands on personal transportation. Despite advances in vehicle safety technologies, car design and the introduction of vehicle safety tests, requirements and legislation, fatalities, and serious injuries as a result of road traffic accidents are still excessive. Future mobility solutions must continue the path of for improved road safety.

The continuous development and implementation of new technologies into passenger cars and clean energy will help to address the challenges and accelerate the shifts in transportation modes. The first generation of Battery Electric Vehicles (BEV) technologies are already well established. The continued growth in BEV sales and shifts to clean energy electricity sources are expected to result in an overall reduction in GHG emissions from passenger cars in the coming years. Subsequent generations of BEVs will feature improvements in battery technology and charging, offering higher capacity at lower costs and production carbon intensity.

Autonomous vehicle technologies continue to develop and become more accessible. Vehicles featuring SAE levels 1 to 3, with semi-autonomous functions such as hands-free driving are starting to become mainstream. A number of fully autonomous vehicles (SAE level 5) are currently in pilot and demonstration phases, with mainstream rollout expected in the 2030 to 2035 period. Fully autonomous vehicles will enable freedoms and potential not experienced with human operated vehicles so far. Passenger convenience can be enhanced from the leisure or work time gained from not operating (driving) the vehicle. Disabled and physically impaired persons could have more readily available access to transportation with fully autonomous vehicles. The connectivity required from autonomous vehicle to vehicle (V2V) and vehicle to infrastructure (V2X) will enable traffic flows to be better controlled and regulated, resulting in improved journey times, and reduced traffic congestion. With proper regulation, autonomous vehicles should result in fewer traffic collisions, with deaths and serious injuries reduced. With excessive speed, appropriate use of safety restraint systems (seatbelts) and drug and alcohol misuse cited as the primary cause of road traffic deaths and injuries, autonomous vehicles should prohibit such violations in operation. Cost of ownership benefits could also be realised with reduced labour costs for vehicle operation and shared mobility (increased vehicle occupancy) lowering journey costs for users.

The Steel E-Motive programme encapsulates the emerging trends in shared mobility and vehicle technologies and has delivered new vehicle concept designs that demonstrate how Advanced High Strength Steels can help to deliver a cost effective, sustainable and safe transportation solution of the future.

2.2 Key Results From The Steel E-Motive Programme

The Steel E-Motive programme has engineered 2 vehicle design concepts, with specific focus on the AHSS body structures. SEM1 is a compact, 4 passenger vehicle intended for city type journeys, such as home to office, home to school, shopping and leisure activities. It has a 75kWh battery electric propulsion system with a front axle, single speed electric motor. SEM2 is a larger derivate of SEM1, seating up to 6 passengers and is intended for longer, higher capacity journeys such as city to city and city to airport type journeys. SEM2 features a larger 96kWh battery and front and rear electric motors. Both vehicles are specifically engineered to have full (SAE level 5) autonomy operating 100% of the time. Both SEM1 and SEM2 have 4-wheel steering, enabling a smaller turning radius which enhances vehicle manoeuvrability in confined spaces such as parking lots and hotel forecourts.

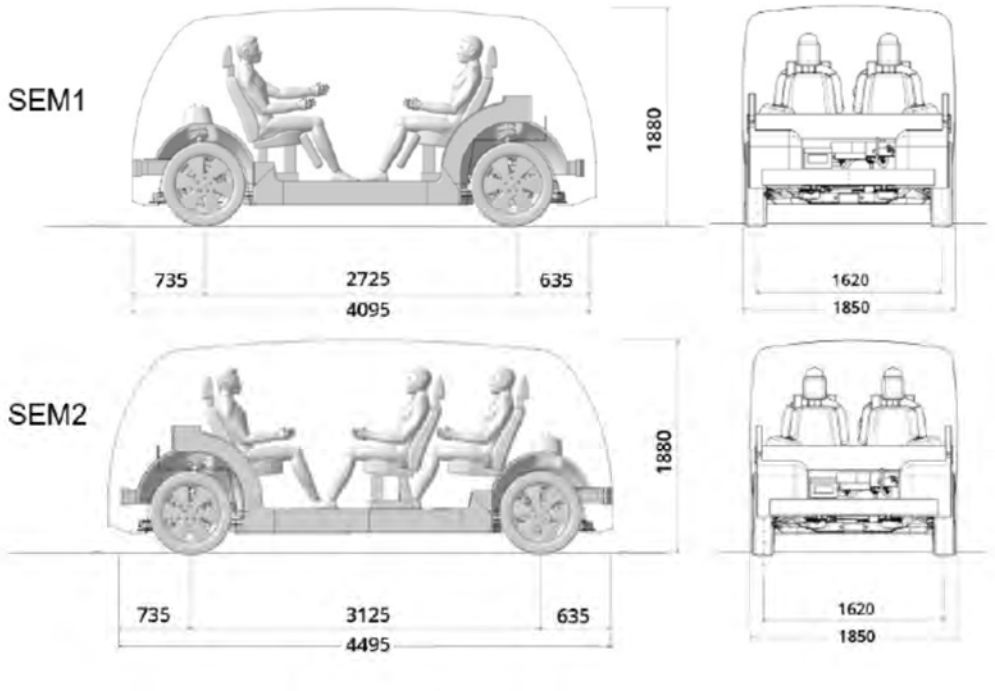

Figure 2.2.1 SEM1 and SEM2 overall vehicle dimensions

The vehicle curb and gross weights of SEM1 and SEM2 are summarised below.

	SEM1	SEM2
Vehicle curb weight (kg)	1512	1873
Vehicle gross weight (kg)	2012	2548

A styling exercise was undertaken to develop a brand identify for the Steel E-Motive vehicles and an exterior styling A surface developed. A complete vehicle 3D packaging and layout study was undertaken, sizing and positioning the occupants and major vehicle systems such as powertrain, chassis, electrical, safety. This coupled with the exterior styling A surface provided a “workable” volume, from which the AHSS body structure could be engineered. Computer Aided Engineering (CAE) optimisation tools were used to help determine the main

loadpaths through the body structure. These were then interpreted and developed into the preliminary body structure concept. The body structure main section profiles and joint designs were then optimised and AHSS grades and fabrication methods selected for the primary concept. CAE structural analyses were then used to guide the design and AHSS grade and gauge assignment.

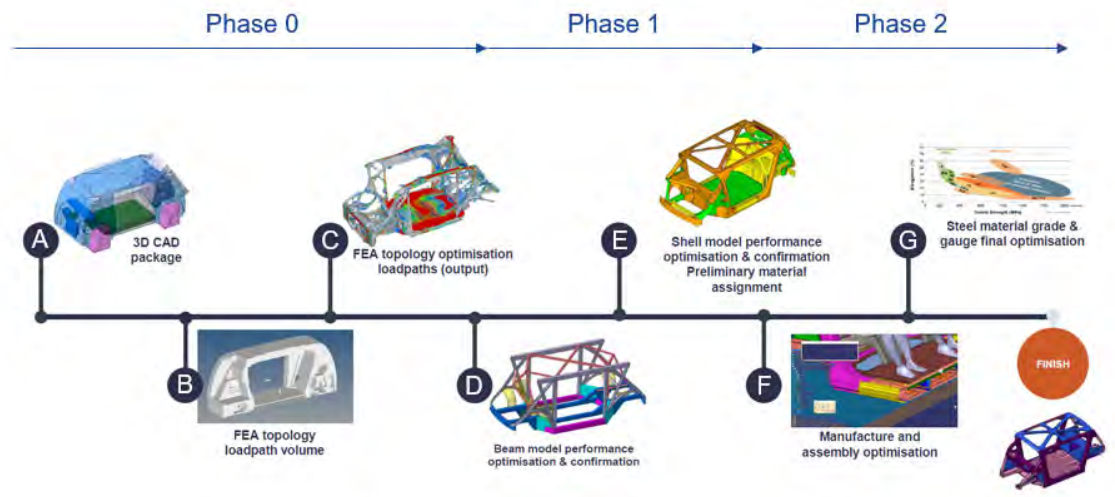

Figure 2.2.3 Approach for the development of Steel E-Motive body structure

Figure 2.2.4 shows the final SEM1 body structure and body in white designs and AHSS grade utilisation.

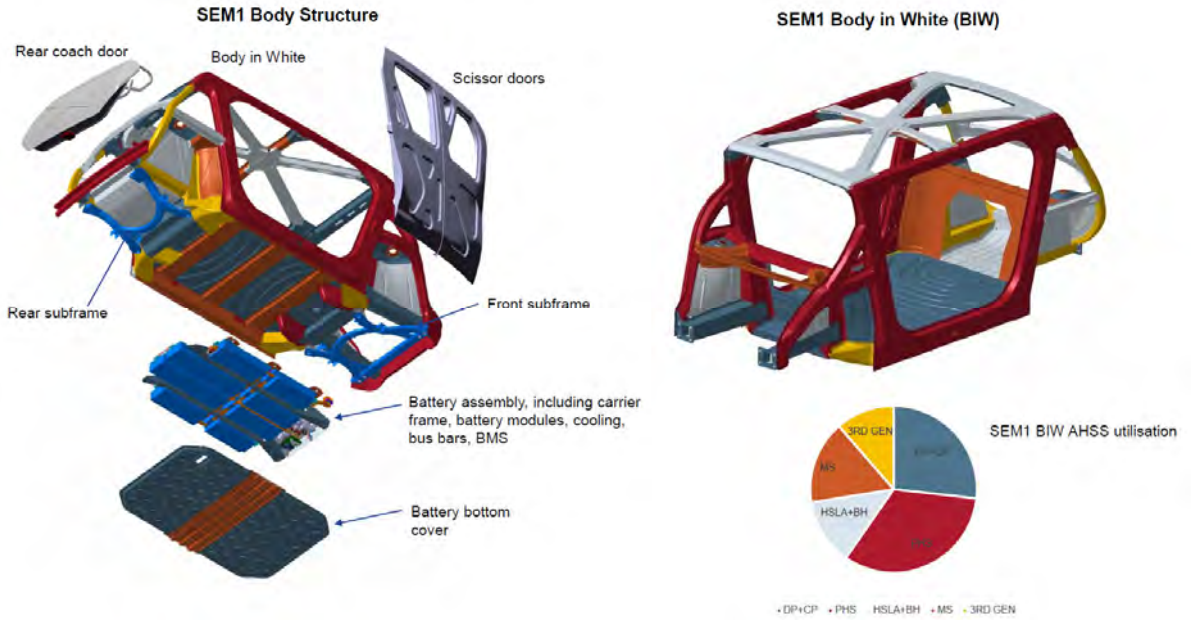

Figure 2.2.4 SEM1 body structure, body in white and AHSS grade utilisation

The SEM1 vehicle and body structure achieved the following performance attributes:

Vehicle performance and range: maximum vehicle speed = 130kph, up to 500km range on a single charge (WLTC cycle), vehicle turning circle radius of 7.4m, achieved by using 4-wheel steering.

Cabin comfort and ergonomics: Comfortable ingress and egress (entry and departure) from the vehicle is ensured by 1) a low step in height 2) wide (>1.0m) door aperture/opening width 3) flat floor interior (enabled by electric powertrain and unique battery frame concept (see below)). 4 occupants are seated in an inward facing configuration

Weight: Vehicle curb weight = 1512kg. This is 27% lighter than a typical current production battery electric vehicle of comparable size to SEM1. This was achieved by removing the driver interface systems (such as steering wheel, pedals, instrument cluster), applying expected weight savings as a result of battery technology improvements, AHSS body in white weight optimisation savings and secondary savings achieved from a complete vehicle weight optimisation study. The final body in white achieved a weight of 282kg. This is calculated to be 25% lighter than an expect/benchmark weight for a vehicle of comparable size and proportions. This was achieved using a combination of AHSS grades and properties, using gauges as low as 0.7mm in thickness, coupled with appropriate design and body construction methods.

Lifecycle greenhouse gas emissions: A complete vehicle lifecycle assessment and optimisation study was performed, concluding that a reduction of up to 86% CO_2 equivalent greenhouse gas emissions could be achieved comparing a current (2022) battery electric vehicle and SEM1 in full operation in Europe in 2035. This reduction was achieved considering a number of factors and measures, including, efforts to decarbonise vehicle production such as “green steel” and reduced carbon batteries, optimising vehicle design, minimising weight and scrap, considering future electricity grid decarbonisation using renewable sources such as wind and solar power, considering the operational efficiency improvements of autonomous vehicles, extending the lifetime of the vehicle and batteries and assuming increased passenger occupancy in order to reduce the number of specific vehicle journeys per passenger-kilometer.

Safety: SEM1 is engineered to the latest high speed crashworthiness tests and requirements. Computer Aided Engineering crash simulations were used to evaluate and optimise the vehicle design:

- USNCAP 56kph frontal rigid barrier (FFB). Maximum deceleration pulse of 33.1g and maximum intrusion of 1.8mm. These are expected to provide good levels of occupant protection.
- IIHS 64kph front offset deformable barrier (ODB). Maximum deceleration pulse of 20.5g and maximum intrusion value of 5.2mm. These are expected to enable SEM1 vehicle to achieve the IIHS “good” rating (highest) for this test.
- IIHS 64kph front small overlap rigid barrier (SORB) test. Maximum deceleration pulse of 19.9g and maximum intrusion value 74mm. These are expected to enable SEM1 vehicle to achieve the IIHS “good” rating (highest) for this test.
- IIHS 60kph side moveable deformable barrier. Minimum intrusion clearance from seat centreline calculated at 296mm versus >180mm target. These are expected to enable SEM1 vehicle to achieve the IIHS “good” rating (highest) for this test.
- USNCAP 32kph side pole (4 locations assessed). IIHS side crash intrusion targets were used to assess occupant protection performance in this loadcase. Performance

indicated that IIHS “good” rating to be achieved. This loadcase is particularly challenging for protection of propulsion battery. Results showed that there is no risk of contact between battery housing structure and modules. This means that there is minimal risk to rupture and damage to the battery which may lead to thermal runaway and fire incidents.

- FMVSS305 EV Rear 80kph 70% overlap moving deformable barrier. Maximum acceleration pulse of 22g and 30mm intrusion. Results suggest minimum risk of injury to occupants.
- IIHS roof crush. Achieved roof strength load to vehicle weight ratio (SWR) of 9.58, exceeding the requirement of >4.00 for attaining IIHS “good” rating.
- Additionally, SEM1 was assessed for the EuroNCAP 50kph 50% overlap moving progressive deformable barrier (MPDB) and NHTSA 90kph oblique deformable barrier front loadcases. In both cases the predicted deceleration pulses and intrusion levels demonstrated good levels of performance.
- For all crashworthiness loadcases, the body structure maintained it’s integrity around the passenger compartment and battery housing.
- One of the most significant engineering challenges in the Steel E-Motive programme was achieving the IIHS “good” rating for the 64kph front SORB test and the low pulse and intrusion levels in the 56kph FFB test. These crash loadcases have conflicting requirements on the body structure. The SORB test requires a very strong front corner structure such that the vehicle can react the barrier crash loads enabling the vehicle to “glance” off the barrier. This results in lower crash pulse and intrusion levels. The front FFB loadcase requires a structure that will crush and collapse progressively in a controlled manor, to fully decelerate the vehicle and minimise pulse and intrusion. The balance was achieved through careful design of the front crash structure and selection and tuning of the AHSS grades and gauges.
- The Steel E-Motive vehicles will also benefit from the advanced safety features and functionality that fully autonomous vehicles bring, such as collision avoidance and autonomous emergency braking. With these system, the likelihood of an accident should be significantly reduced. Should a collision occur, the occupants and battery are sufficiently protected by the AHSS body structure. Whilst the development and engineering of the autonomous vehicle systems was not specifically addressed in the Steel E-Motive programme, the body structure design does account for the positioning, packaging and mounting of the autonomous sensors and processors.

Stiffness and strength: SEM1 body structure achieves static torsional stiffness of 63,285Nm/degree versus a target of 25,000Nm/degree. This means that the risk of issues such as “squeak and rattle” of body and trim parts would be minimised. The static vertical bending stiffness was calculated at 13,438N/mm versus a target of 9,000N/mm.

The body structure was assessed for fatigue and durability using quasi-static loads and non-linear stress FEA. The results showed no areas of concern. The predicted peak stresses in the body structure were well below the infinite life fatigue strengths for the AHSS grades selected.

Noise Vibration & Harshness (NVH): First body structural mode at 32Hz and first battery mode at 35Hz. These attain sufficient decoupling from other vehicle system modes such as powertrain and suspension. The attachment dynamic stiffness (driving point inertance) at key chassis interfaces are at least 5 to 10 times the local bushing stiffness. This ensures that the Steel E-Motive vehicle achieves competitive interior noise and vibration levels

Manufacture and assembly: The SEM1 BIW is divided into 3 main zones – the front mid and rear. Each zone is then subdivided into primary assemblies and sub-assemblies. The definition of the zones, assemblies and sub-assemblies follows a conventional high-volume passenger car with a stamped steel body structure. This means that existing vehicle manufacture and assembly facilities could be used for the mass production of SEM1 (and SEM2). This reduces investment and capital expenditure costs for the vehicle. Production volumes of >250,000 vehicles per year would be possible with such manufacturing methods.

Vehicle Cost and Total Cost of Ownership: Both Steel E-Motive vehicles feature stamped steel body structures, using high volume manufacturing methods which deliver low unit costs. The body structure uses fabrication methods that help to deliver high material utilisation and low scrap rates, reducing the overall quantity of steel required and contributing to lower overall cost. SEM1 and SEM2 are based on a common platform principle. SEM2 features 68% carry over/common parts from SEM1. Vehicle operator running costs and passenger journey costs are expected to be competitive with alternative personal transport modes due to the autonomous driving characteristics and fleet volumes assumed in operation.

2.3 Key Innovations

Using the newest steel grades and fabrication processes, Steel E-Motive's portfolio enables tailoring vehicle properties that achieve significant safety, cost, and comfort advantages with eight key innovations only possible using steel:

1. **Autonomous vehicle AHSS body structure**, specifically engineered to accommodate fully autonomous vehicle operating conditions and requirements. The front occupants are positioned rear facing towards the front of the vehicle and the BIW B pillars are housed within the door structure**.** The passenger side doors have a "scissor" type motion (sliding). The seating position and door configuration enable a more open, spacious feeling interior compared to a conventional passenger car. A wide door aperture provides improved occupant ingress and egress to and from the vehicle. The body in white achieves competitive weight and stiffness performance as a result of structural loadpath optimisation, section size and joint design optimisation and the stiffness and strength properties of AHSS.

2. **AHSS Passenger Protection Zone** provides excellent crashworthiness protection for the rear-facing front passengers in the event of a frontal or side collision.

3. **Short Front Crash Zone** structure meets the most stringent global crash requirements. Dual Phase (DP) Tailor Welded Blanks enable efficient design.

4. **Small Overlap Front Crash Glance Beam,** a specific module of the front crash structure that guides ("glances") the vehicle along the IIHS 64kph small overlap impact barrier. This results in reduced crash intrusion and deceleration pulse values. The glance beam allows the front crash structure to deform in front crash loadcases with greater offsets, such as IIHS moderate overlap and frontal rigid barrier.

5. **(Rocker) Hex beam energy absorbers,** made of roll-formed DP steel, are low cost, compact, and weight efficient devices providing side crash energy absorption, providing protection for the occupants and propulsion battery.

6. **Hydroformed in-door B-Pillars**, featuring a compact cross section profile providing greater glazed area for better passenger visibility. The side doors provide coverage for most of the body structure side area, therefore the conventional body side outer A surface panels have been deleted, providing cost and weight savings.

7. **Integrated Battery Carrier Frame.** The battery is integrated into the body in white lower structure, resulting in the conventional “generation 2” battery housing side and upper/cover parts to be deleted. The battery modules, cooling system and electrical connectors are mounted to an AHSS carrier frame. The frame is then inserted and bolted into the BIW housing cavity. The BIW floor acts as the battery top cover and the BIW rocker provides side crash protection. The installed frame enables a compact package, resulting in low floor height and flat floor which gives improved occupant ergonomics. A 3-sheet bottom cover provides protection from underneath. The integrated carrier frame results in significant cost and weight saving without compromising battery safety, durability. The battery modules are easily accessible, meaning that the individual damaged or expired modules could be easily replaced instead of replacing the complete battery pack.

8. **Semi-glazed lattice roof structure.** A large, glazed area enhances the open & spacious feel to the cab, whilst the structural members provide the stiffness and strength required

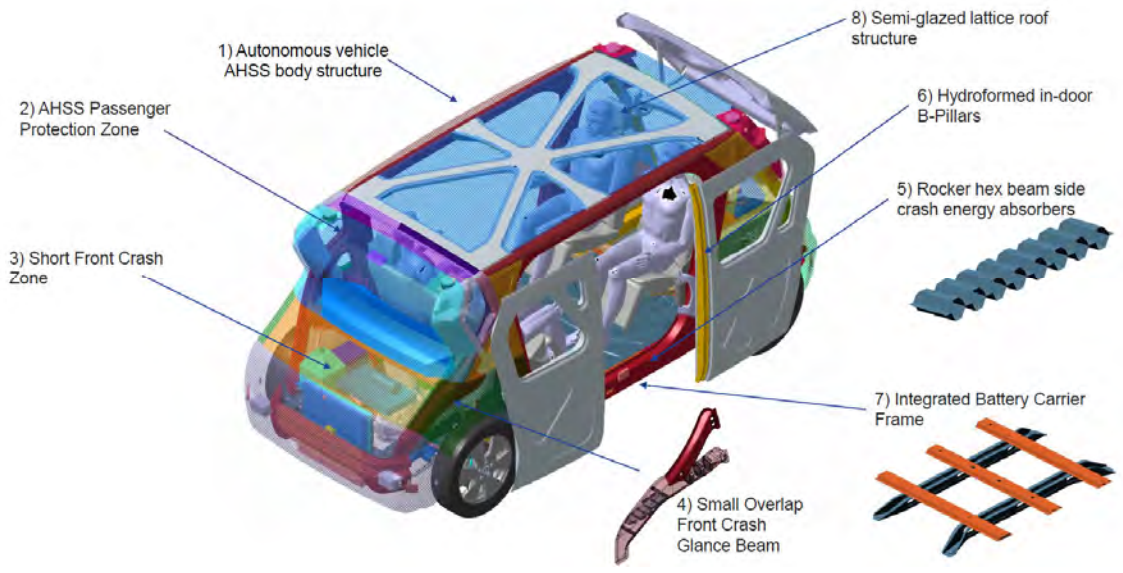

Figure 2.3.1 Steel E-Motive key innovations (shown on SEM1)

2.4 Development of SEM2 variant

The larger SEM2 vehicle variant was engineered during the concept definition Phase 0 where the base layout, package and specifications were determined. Detailed engineering of the body structure was undertaken during Phase 2, concurrently with the development of SEM1. The target was to maximise part commonality between SEM1 and SEM2 such that costs and manufacturing complexity could be minimised. The additional size and space of SEM2 was achieved by increasing the vehicle wheelbase and overall length by 400mm, with the mid zone effectively extended at a point rearwards of the midpoint. This enabled the front

and rear zones to be largely carry over/common with SEM1. The scissor doors are largely carryover as an additional C pillar was incorporated to maintain a common body side door aperture profile. Commonality in the SEM1/SEM2 roof structures was achieved by creating an add-on roof portion at the rear of SEM2. Figure 2.4.1 shows SEM1 and SEM2 at vehicle level and Figure 2.4.2a shows a comparison of the body structures.

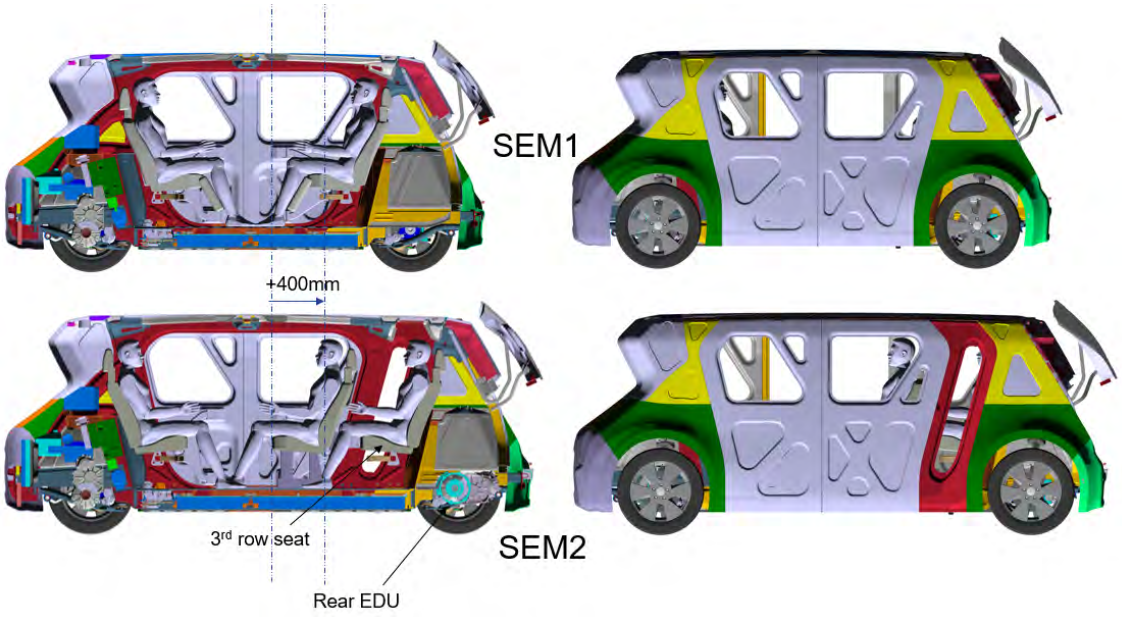

Figure 2.4.1 Comparison of SEM1 and SEM2 vehicles

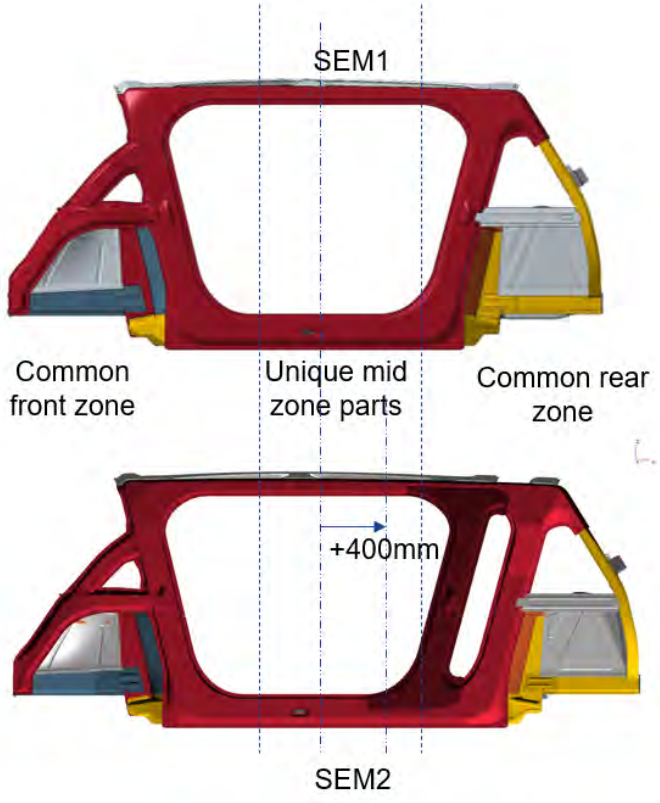

Figure 2.4.2a SEM1 and SEM2 Body in White

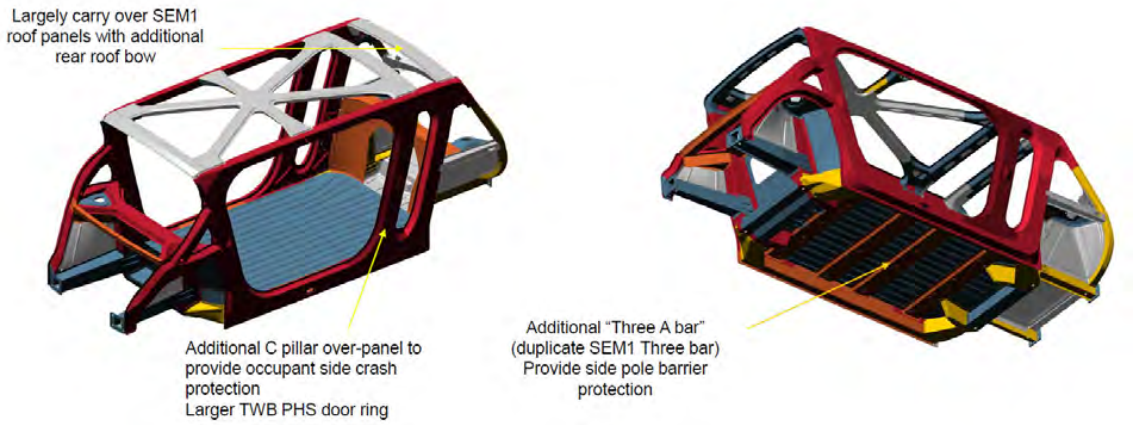

Figure 2.4.2b SEM2 Body in White

By adopting a platform approach, 156 out of a total of the 229 BIW parts (68%) are common between SEM1 and SEM2. 53 unique BIW parts are required for SEM2 and 20 parts are common geometry but will require material grade change. The SEM2 BIW weight achieved 323kg versus a target of 361.9kg.

The battery capacity of SEM2 was increased to 96kWh, ensuring the vehicle performance and range in line with the targets. The same carrier frame concept was used for the SEM2 battery pack. Part commonality was assured using SEM1 design of carrier frame cross members. Unique SEM2 frame longitudinals and battery bottom covers were required due to the increased length and wheelbase.

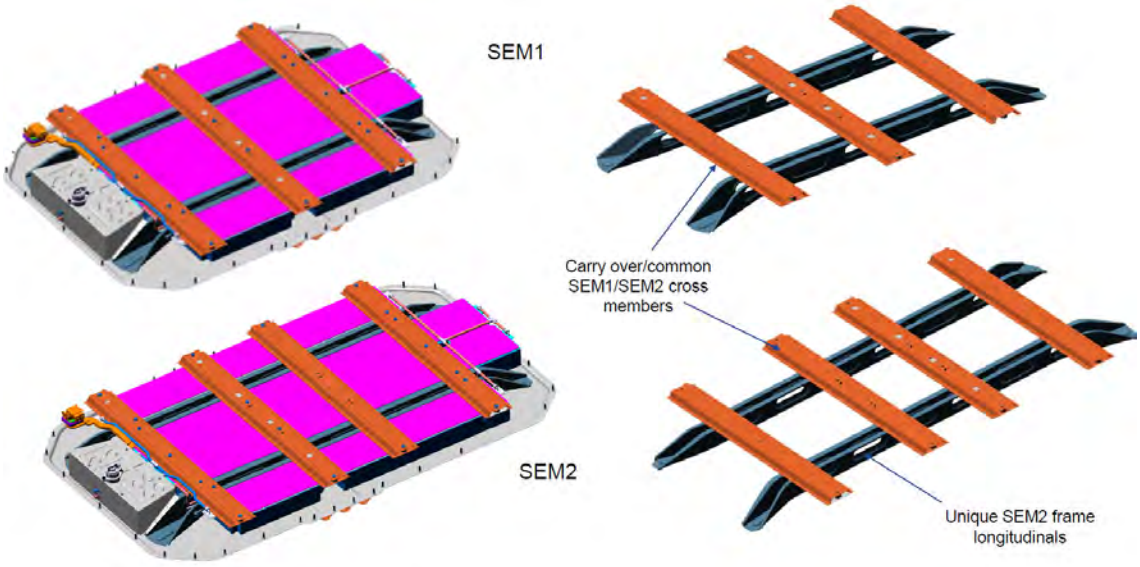

2.5 Additional SEM1 and SEM2 engineering studies conducted by academic institutions

Throughout the Steel E-Motive programme, a number of supporting studies and projects were undertaken by academic institutions. This enabled undergraduate and research students to apply and develop their engineering skills on an advanced vehicle technology programme, whilst the Steel E-Motive programme benefited from the external perspectives and expansion of the Steel E-Motive vehicle concepts beyond their original brief.

1) Development of hydrogen fuel cell powered variant of SEM1. Loughborough University (UK), MEng student final year engineering project. The study successfully demonstrated a SEM1 vehicle concept design with the powertrain converted to an hydrogen fuel cell. Performance simulations were used to validate the vehicle range and support the fuel cell specification. A 3D CAD design study packaged the main powertrain systems and components (shown in Figure 2.5.1)

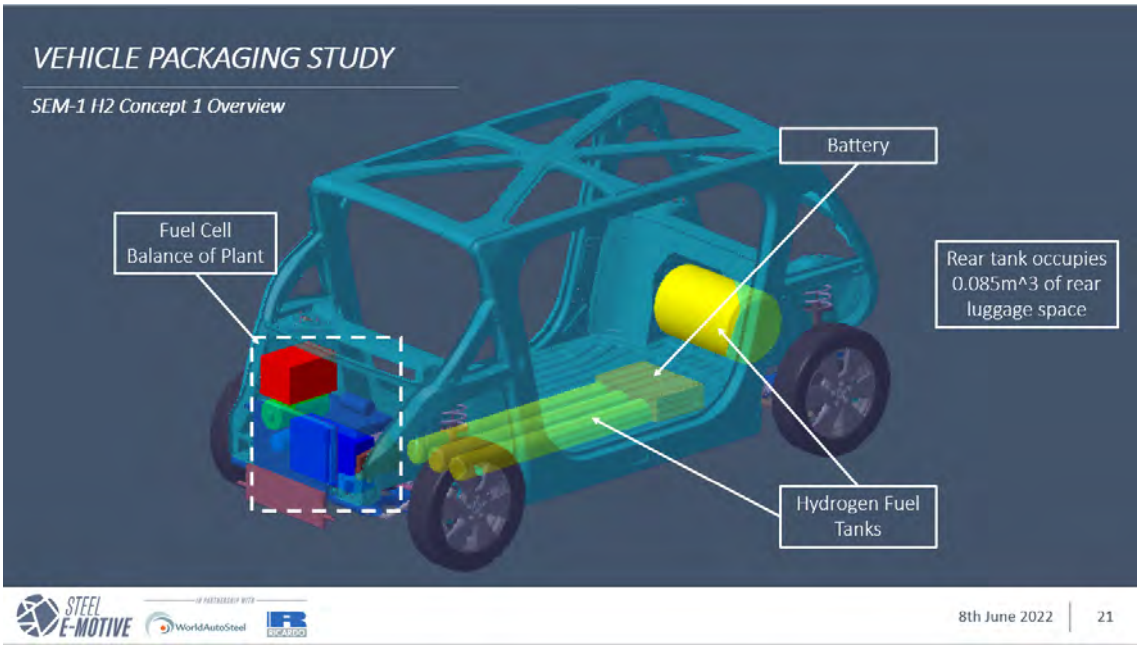

Figure 2.5.1 Loughborough University (UK) MEng final year engineering project to develop fuel cell powertrain variant concept of SEM1

2) Michigan Tech University (MTU) – Senior Capstone Project #1: Steel E-Motive Side Door Functionality, Door Hinge Assessment

   The MTU Senior Capstone Design Team, sponsored by WorldAutoSteel and the Auto/Steel Partnership, were challenged to develop an improved door and hinge for the Steel E-Motive side closure mechanism. MTU's design solution uses a four-bar linkage hinge design to keep the door parallel to the body of the vehicle to avoid damage to either the door or the body. The team used a 4:1 gear ratio for the drive motor to open the door. Finally, one of the pins in the secondary arm linkage is accessible by passengers and removable, allowing users to manually push the door open in the event of an emergency.

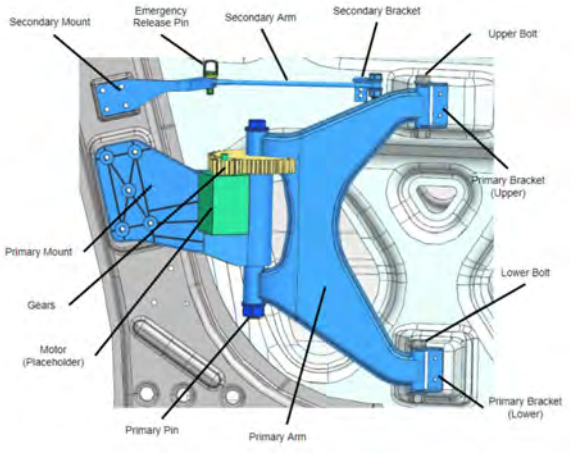

Figure 2.5.2 MTU Capstone project to enhance the design of SEM1 scissor door hinge and drive mechanism

3) The Ohio State University undertook a Senior Capstone Project to confirm the viability of a complex Resistance Spot Weld (RSW) joint comprising of 5 individual sheet layers for SEM1 BIW. This 5-layer stack-up weld project demonstrated technical capability that allow manufacturers to leverage current manufacturing infrastructure, lowering investment costs and improving sustainability.
The welded joint under consideration was the front extended passenger protection zone of the car, specifically the vertical dash brace and upper glance beam reaction area. The various material grades include MS1200, PHS2000, and MS2000 with gauges of 1 to 2 mm and coatings of EG and AS150 (for the PHS grades). The conclusions of the study were as follows:

    1. A five-layer stack-up spot weld can be successfully created with advanced high strength steels using a range in number of pulses, currents, forces, and times, indicating sufficient process robustness.
    2. Simufact Welding successfully models weld nugget development and final weld size, that allows parameter selection avoiding costly trial and error practices.
    3. Using a pulsation current schedule with descending current pulses was just as successful in creating welds as using the same current level pulses. This was perhaps assisted by joint symmetry.

    A single spot weld for a five-layer stack-up has greater time and cost efficiency than welding a two-layer and a three-layer stack-up into a combined five layers

4) Michigan Technological University (MTU) undertook a Senior Capstone Project to develop a solution for expanding the application of SEM2 vehicle from passenger carrying to goods carrying vehicle. A rapid conversion system was engineered, allowing the vehicle to be transformed from passenger transportation by day to goods carrying by night. This would enable the vehicle to achieve a higher operational time, increasing revenue and profit for operators.

Figure 2.5.3 shows the design concept for the rapid interior configuration system. This design showcases two pairs of T-shaped rails placed in the fore-aft direction of the vehicle. These T-Rails are compatible with a slider system that connects to the bottom of each seat leg. The rails allow adjustment of the interior seats and rapid removal by the use of a depot-based pallet jack accessory

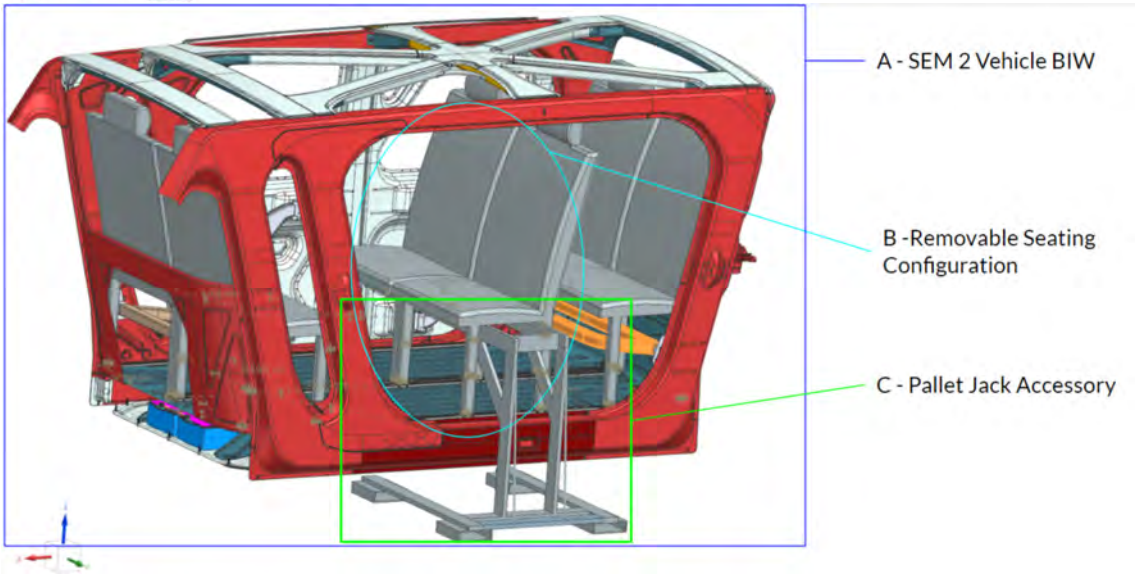

Figure 2.5.3: System level concept – rapid adaptation of SEM2 to autonomous delivery services

3.0 Motivation for Steel E-Motive project: Addressing future transportation challenges

3.1 Introduction

The future of mobility is changing. The mass transportation challenges faced by cities and heavily populated areas can be addressed by automotive technologies and innovations that are forecast to be implementable within the next decade. The fully autonomous vehicle concepts Steel E-Motive, operating in a ride hailing, Mobility as a Service (MaaS) role has the potential to offer a safer, convenient, comfortable, and cost-effective transportation mode. By reducing the net number of vehicles on the road, the impacts of traffic congestion can be alleviated. The Steel E-Motive vehicle concepts are powered by a battery electric powertrain, resulting in zero tailpipe emissions. Vehicle lifetime greenhouse gas (GHG) vehicle emissions can be reduced by considering that electricity supply (for charging the Steel E-Motive batteries) will come from an increasingly renewable (or “green”) source such as wind or solar energy. Vehicle manufacturers and their suppliers, including the steel producers are implementing new production approaches and facilities enabling significant reductions in greenhouse gas emissions. With the combined effects of lower carbon intensive production methods, renewable energy sources, vehicle efficiency built into the design and operation and increasing passenger occupancy rates through ride hailing, it is estimated that lifecycle greenhouse gas emissions could be reduced by up to 86% compared to current day battery electric vehicles operating as personalised taxis. Additionally, the Steel E-Motive MaaS vehicle concept will enable improved mobility access for the underserved population, such as disabled or physically impaired and those living in remote regions with limited or reduced access to public transport.

3.2 Future Transportation Challenges, PESTEL Analysis

The urban transportation challenges of the future are well documented and understood. A PESTEL analysis (Political, Economic, Social, Technology, Environmental and Liability) enables a comprehensive, holistic evaluation of the challenges and is a solid precursor for defining the solutions and the subsequent requirements and specifications of vehicles such as Steel E-Motive. Figure 3.2 shows a PESTEL analysis undertaken for Steel E-Motive.

Political	Economic	Social	Technological	Environmental	Legal
- Global trade policies and tariffs - Global trade policies and tariffs - Global energy security - Global stability, (conflict) - Urbanisation, housing, health and living standards - Population growth - Taxation policies (e.g. environment related) - Reduced road traffic injuries and towards zero fatalities	- Access to credit and credit costs - Impact of high inflation - Economic growth - Cost of living (housing, food, clothing, leisure) - Global and local transportation costs - Raw material costs (iron, steel, precious metal) - Cost of environmental impacts (floods, heatwave)	- Consumer behaviour changes (rent/lease vs outright ownership, on-demand, leisure time utilisation, convenience, lifestyle, flexible working) - Ageing population - Access to healthcare and improving living standards - Serving the underserved (impaired, disabled) - Cost of living and wage growth - Environmental awareness and responsibility	- Digital and communications growth (connectivity, processing, radar, lidar, computation, artificial intelligence, big data, GPS & mapping) - Infrastructure improvements (road, rail, sea) - Vehicle propulsion system technologies (battery electric, hydrogen, charging) - Innovations in materials and manufacturing - Green energy supply and innovations	- Global and local climate change agreements and policies - Local air quality policies and directives - Towards complete life cycle evaluation, policies and regulation - Land, river and sea pollution - Recycling, reuse disposal policies - Scarce resources availability and impacts - Noise pollution	- Liability and insurance (WRT autonomous vehicles) - Product warranty and recall - Data protection and data security - Labour laws and regulation - Intellectual property management

Figure 3.2.1 PESTEL analysis

The PESTEL analysis highlights societal trends, such as changes in consumer habits and behaviour, disposable income challenges, health and living standard changes and an increasing awareness and concern by the general population of environmental challenges and impacts. The environmental impacts of transportation and industrialisation are being addressed by global and regional leaders in the form of legislation and targets on greenhouse gas emissions, pollutants and recycling. This is driving developments in low carbon technologies for all types of transportation (land, sea, air) as well as clean & green energy sources such as wind and solar power. Digital and connectivity technologies continue to expand and develop and are being embraced by the automotive industry, enabling features such as autonomous and active safety to be deployed. The PESTEL analysis provides a good foundation for determining future trends which may impact vehicle development and technology.

3.4 Autonomous Vehicle Technology Roadmap

A roadmap analysis (Figure 3.4.1) of future autonomous and Mobility as a Service vehicles was constructed to confirm the validity and expected implementation timing for Steel E-Motive. The top half of the roadmap describes the *enabling factors* which are expected to develop, mature or be implemented within the next 30 years, which will empower the growth of autonomous and MaaS. The lower half describes the expected *outcomes* as a result of the enablers.

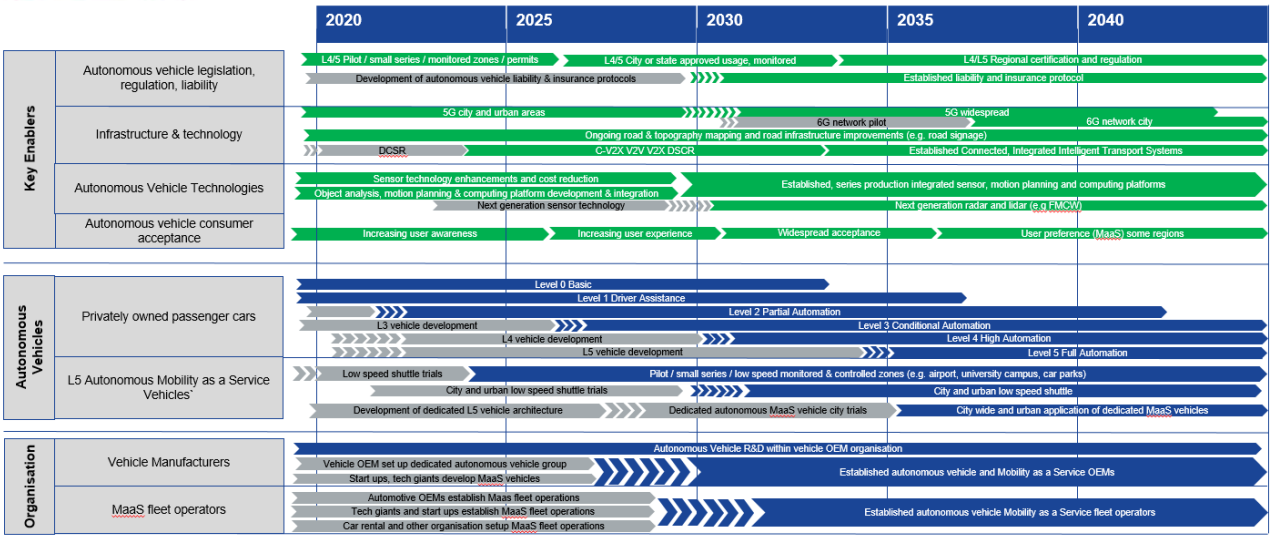

Figure 3.4.1 Autonomous vehicle and Mobility as a Service roadmap (see enlarged version in Appendix 4)

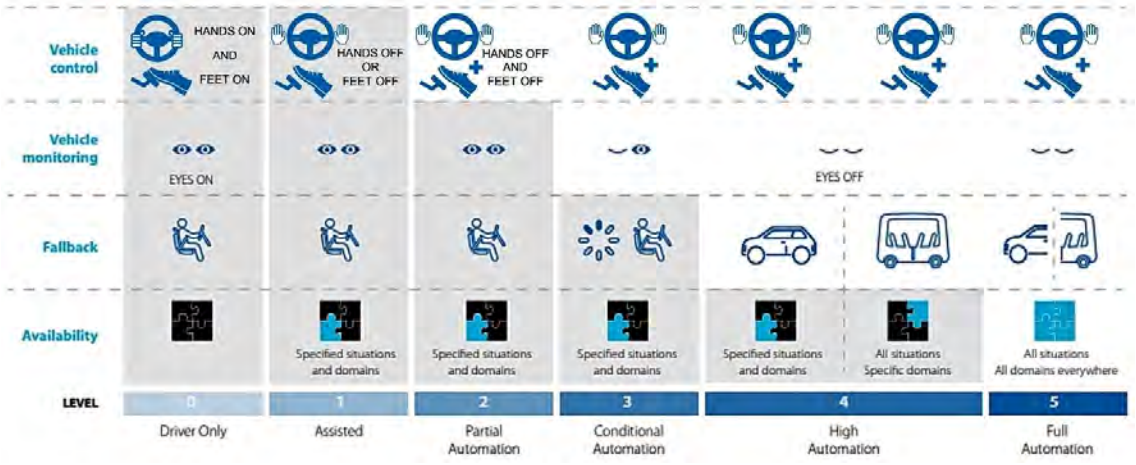

Figure 3.4.2 SAE definitions of autonomous vehicles + explanation

One significant challenge for autonomous vehicles is establishing the liability and insurance responsibilities. In present-day privately-owned vehicles, the operator (driver) is primarily responsible for accidents and damage to vehicles, where the cause can be specifically attributed. Vehicle manufacturers and infrastructure providers can also be liable depending on the nature and cause of accidents. With fully autonomous vehicles, there is no human in-vehicle operator. The users' input to the vehicle or service will be to define a journey start and end point. The calculation of the vehicle route, the control of the vehicles' speed and direction and the decisions it makes will be managed by an on-board computer and will be based on the information it receives from sensors and the pre-programmed algorithms. In the event of an accident or collision involving a fully autonomous vehicle, the liability will then shift from the vehicle operator (driver) to the organisation responsible or liable for governing the actions of the vehicle. This could be the vehicle OEM, the technology supplier or fleet operator. This significant shift in responsibility and liability requires collaboration and agreement between government authorities, vehicle OEMs and lawyers to determine protocols and policies for autonomous vehicles. Additionally, governments and policy makers will be required to develop and implement new legislation, ensuring the safe

operation of autonomous vehicles on public highways. During the timeframe of the Steel E-Motive project, several autonomous vehicle pilot trials were taking place on public highways, where temporary permits or licenses were granted by national or regional authorities. Examples of draft legislation being reviewed at the time of Steel E-Motive project include Article 11 of EU Regulation No. 2019/2144, permitting European Small Series Type Approval (EUSSTA) of fully automated M and N category vehicles, with manufacturers permitted to register up to 1500 vehicles per year. [https://www.interregs.com/articles/spotlight/draft-eu-regulations-on-the-type-approval-of-fully-automated-vehicles-published-000241]. Many of the current autonomous vehicle trials require a capable driver to be present. By 2030, the permits to operate are expected to be expanded to larger city-wide fleet trials without trained drivers. By 2035, it is expected that suitable legislation and liability protocols will be established, enabling the operation of fully autonomous vehicles on existing public highways.

The continued development and growth in motion sensing, computational, infrastructure and communication technologies are a key enablers to fully autonomous vehicles. Radar and lidar sensor technologies are currently mature enough to enable fully autonomous vehicle operation. Future development will focus on performance enhancements, size, cost, and safety improvements. Motion detection, calculation and computation technologies will also undergo continued development, enabling greater capacity, cost reduction and safety. Steel E-Motive vehicles are intended to be operated on existing highways therefore offsetting requirements for purpose built, dedicated road networks for autonomous vehicles (i.e., geofenced). Existing highways may require some developments and enhancements to cater for fully autonomous vehicles. The detection of vehicles, objects and road signs requires a clear and unobstructed view from the vehicle, therefore minor improvements to road traffic junctions, roundabouts, traffic signage and signals may be required. Autonomous vehicles are reliant on constant, uninterrupted communication between other vehicles (“V2V”) and stationary objects such as traffic signals and monitoring stations (“V2X”). Existing V2V and V2X protocols are already established, such as DCSR (Dedicated Short-Range Communications). Wider communications systems such as 4G and 5G networks are also required for autonomous vehicles. These are currently widespread in urban areas and network coverage is increasing. Where 4G and 5G networks are not available then autonomous vehicles may have restricted operation by geofencing. In the future, higher capacity, faster and more reliable networks such as 6G and satellite communications are likely to be introduced, with the higher bandwidth enabling enhanced journey reliability and infotainment. Autonomous vehicles also require detailed topological data of the road networks. In many cases, present day mappings largely meet the requirements for autonomous vehicles.

3.5 Addressing the requirements of Smart Cities

Smart Cities are a response to an increasing world of connectivity, where data and information gathered from sensors to manage assets and is processed and to manage resources and services efficiently. Data can be collected from citizens, devices, buildings, and assets that is processed and analysed to monitor and manage traffic and transportation systems, power plants, utilities, water supply networks, waste, crime detection, information systems, schools, libraries, hospitals, and other community services. Fully autonomous Mobility as a Service vehicles such as the Steel E-Motive concepts will play an important role in Smart Cities of the future.

Combining the autonomy, connectivity and efficiency aspects of future vehicles will assist Smart Cities to improve the transportation of passengers and goods, easing congestion, reducing pollution and improving safety.

4.0 Steel E-Motive Vehicle Targets and Requirements

4.1 Introduction – approach and considerations for the derivation of Steel E-Motive targets and requirements

The requirements for a fully autonomous vehicle are in many instances quite different to a conventional human operated passenger car. The use cases, mode of operation and interaction with the vehicle users is quite different. Additionally, there is little if any reference data available for existing autonomous vehicles such that the Steel E-Motive targets and requirements could be verified. The approach for deriving targets and requirements for Steel E-Motive was therefore based on an evaluation of the vehicle user (occupant) and the vehicle fleet operator or owners' requirements and expectations, coupled with knowledge and experience from conventional passenger cars. Vehicles also have regulatory requirements such as the protection of occupants and the high voltage battery in the event of collisions. Prior to deriving the vehicle targets, the key user and operator expectations for the Steel E-Motive vehicle were collaboratively defined within the project team. These key expectations were then used to derive numerical targets for the vehicle and cascaded to the vehicle systems and subsystems.

Passenger comfort and convenience: Fully autonomous MaaS vehicles represent a modal shift in urban transportation. They will also need to compete with privately owned and human driven vehicles for several years to come. In order to initiate a demand and a shift to MaaS operations, a high degree of passenger comfort and convenience is required. The term "comfort" can be interpreted as alleviation from disturbances and annoyances that vehicle users are subjected to throughout the complete journey. Examples of disturbances and annoyances that users can be subjected to include vibrations and motion sensations as a result of road inputs and vehicle manoeuvres, noises, and harmonics as a result of the vehicle operation, such as road (tyre noise), bump noises, wind noise, electric machine noises, squeaks and rattles and temperature & humidity differences and expectations. The vehicle interior, spaciousness and ergonomics also contributes to passenger comfort. Convenience describes the *ease of use* of the service. The Steel E-Motive project did not specifically consider the ride hailing and connectivity aspects of MaaS operations, but users would expect a rapid and reliable on-demand response, seamlessly interfacing with existing transportation methods such as rail, bus and ferry services. The vehicle would be expected to operate effectively and reliably in a diverse number of locations, from enclosed city and urban areas to more remote locations. Vehicles also need to be designed with a range of users in mind. This includes babies and small children, through to the elderly, disabled and visually impaired. The design should also consider the fact that the autonomous nature of the vehicle, assistance for disabled or persons with special needs would be reduced as there is effectively no vehicle driver.

Safety: Autonomous vehicles feature enhanced active and pre-emptive safety systems that should reduce or minimise the likelihood of a vehicle to vehicle or vehicle to object collision by automatic control of the vehicle speed and direction. The Steel E-Motive vehicle is designed to operate in a mixed traffic mode where autonomous and human operated vehicles operate on the same highway. The likelihood of a low or high-speed collision can therefore not be completely eliminated. For this reason, high speed crash and safety regulations and requirements have been applied for the Steel E-Motive design. This is to ensure that risk of serious injuries and fatalities are minimised in the event of a collision. The Steel E-Motive design also features a battery electric propulsion system, where the high voltage batteries are vulnerable and susceptible to damage in the event of a collision. This can lead to increased risk of fires and injuries if the battery is not sufficiently protected. New

users of autonomous vehicles may also be wary and sceptical of their safety given the removal of human driver. It is therefore important to alleviate such fears or opinions by demonstrating a reassuring level of vehicle safety performance. This can be communicated to users in advance via brand awareness and marketing.

Total cost of ownership: Total cost of ownership is relevant to both the vehicle user and the operator or owner. From the users' perspective, there will be an expectation of journey price competitiveness, with respect to private vehicle ownership and human operated taxis. The MaaS operators will be seeking to maximise operating profits, minimising investment costs, minimising the return-on-investment duration and minimising financial risks associated with the operations.

Environment and sustainability: The contribution of passenger cars and vehicle emissions to the climate change challenges is well understood and actions such as global climate agreements and local emissions and pollution regulations are in place to address the issues. The pace of transition to more sustainable modes of transportation is reliant on governments, regulators and now the vehicle users. There is now a common awareness and acceptance that mobility users' choice of transportation mode can significantly impact climate change. One of the key objectives from the Steel E-Motive project is to demonstrate that the use of the latest steel material grades and manufacturing processes, coupled with efficient design and optimisation a ride sharing vehicle can enable significant greenhouse gas (GHG) emissions.

Once the key attribute requirements for the Steel E-Motive vehicle were defined, a thorough target setting activity was undertaken. The following sections describe the derivation and justification of the numerical targets in more detail.

4.2 Vehicle Requirements and Targets

4.2.1 SEM1 Vehicle performance targets and overall dimensions

Target	Value	Comment
Overall vehicle length (mm)	4100	Overall vehicle dimensions describe a compact vehicle, fitting between European B-C segment sized passenger car
Overall vehicle width (mm)	1850	
Overall vehicle height (mm)	1850	
Wheelbase (mm)	2725	
Track, front and rear (mm)	1620	
Vehicle turning circle (metres)	<7.6	To align with common city taxi regulations such as London Condition of Fitness. Enabling high degree of vehicle manoeuvrability
Autonomy level (SAE)	5	Fully autonomous 100% of time in all conditions and highways. No direct human control interfaces (i.e., steering wheel, pedals, turn indicators)
Vehicle curb weight (kg)	<1640	
Vehicle Gross Vehicle Weight GVM, (kg)	<2140	Based on 4 passengers + 150kg payload No towing requirement No roof carrying requirement (e.g., roofbox)
Vehicle acceleration 0-102km/h (sec)	<9	
Maximum vehicle speed km/h	130	
Towing requirements		(vehicle not required to perform towing operation)
Range on 1 full battery charge(km)	>500	Based on a WLTC drive cycle
Battery charging Time (minutes)	<20	From 10% to 90% State of Charge (See 6.2.2 for battery requirement & specifications) Assume fixed charging location (no inductive charging requirement) Standard charger interface. Vehicle side location for charge socket
Expected vehicle life (km)	>500,000	Based on expectation for taxi vehicle. Subject to revision depending on LCA impact
Sustainability and Life Cycle performance		Steel E-Motive should demonstrate the benefits that steel can offer as a sustainable material. The project should demonstrate the maximum potential for reduction in greenhouse gas emission and outline the sensitivities in the approach and calculation of greenhouse gas emissions
Body manufacturability and vehicle assembly		To use conventional sheet steel fabrication processes for the body structure (for example, but not limited to; hot and cold stamping, roll forming, roll stamping, hydroforming). Body assembly to use Resistance Spot Welding (RSW), laser welding, brazing, structural adhesives, mechanical fasteners Utilise a conventional high volume vehicle assembly processes and approaches The design to be suitable for production in global locations and facilities
Anticipated production volumes (per year)	250,000	
Anticipated Start of Production (SOP) date	2030 to 2035	
Luggage volume capacity (litres)	400	To have separate, lockable luggage compartment. Luggage volume based on available volume in passenger and luggage compartment

Passenger ergonomics		To have a minimum side door aperture opening width >1.0m To be compliant with disabled user requirements (e.g., wheelchair, ramp access) To seat 4 passengers comfortably, assuming 95% ile mannequin To accommodate breadth of potential users (e.g., babies, children, elderly)
Vehicle servicing and repair		Steel E-Motive design to ensure that minor service points (such as coolant, screen wash, brake fluid reservoir) to be readily accessible without the requirement for hand tools. Ensure major servicing of parts such as brake pads & discs, tyres can be completed within industry standard timelines and efforts Major repair parts such as high voltage battery can be undertaken in competitive timelines

4.2.2 Body in White (BIW) targets

Target	Value	Comment
Body in white weight (kg)	<309	Target BIW weight derived from statistical regression analysis of reference vehicles (see Figure 4.4.2.1 below)
BIW cost ($)		The design should demonstrate the lowest cost feasibly possible whilst achieving structural performance targets
Static torsional stiffness (Nm/deg)	>25,0000	Fully trimmed BIW. BIW + battery + subframes, + bumper beams + closures + glazing
Static vertical bending stiffness (N/mm)	>9,000	
1st body modal frequency	>28Hz	
1st battery modal frequency	>35Hz	
Chassis attachment point dynamic stiffness (N/mm)	> 5x dynamic bushing stiffness	
Panel resonances	>50Hz	
BIW Durability		Predicted linear stresses to be within expected fatigue or proof stress limits. Loadcases considered: Fatigue loadcases: • Braking fatigue • Acceleration fatigue • Cornering fatigue LH • Vertical 30degree positive fatigue • Settling at GVW • Maximum rebound • Limit forwards braking • Limit cornering LH Abuse loadcases: • Maximum bump load • Maximum bump and braking load • Pothole braking

A vehicle's body in white (BIW) is one of the largest and heaviest parts of a vehicle, significantly contributing to the vehicle kerb weight. Lower vehicle weight results in reduced powertrain size (battery and motor). Additionally, "weight spiral" effects mean that a lighter vehicle can itself be reduced in weight as components such as suspension parts are required to take lower static and dynamic loads. With a significant contribution to vehicle weight, the BIW also has a significant impact on overall vehicle Greenhouse Gas (GHG) emissions. Reducing the material content in the body results in lower GHG emissions in the vehicle production stage and a lower weight results in lower energy consumption during the vehicle use phase also. Using less material also results in lower overall cost of the product. In order to define a weight target for the BIW, a benchmarking statistical approach was applied. A data sample from comparable vehicles was assembled and the statistical relationship between key vehicle and system dimensions (such as overall length, width and height, weight) was calculated and evaluated. With Steel E-Motive being one of the first full design of battery electric fully autonomous vehicles there are no matching vehicles or datasets to compare against. Instead, vehicles of comparable architectures, such as vans and people carriers were used for the analysis. Figure 4.2.2.1 shows the statistical evaluation of "vehicle box size" versus BIW weight. Vehicle box size is defined as the effective surface area of a hypothetical box placed around the extremities of the vehicle. This parameter was selected as the Steel E-Motive concepts features a "one box" type architecture, with the weight of the "box" effectively influenced by the surface area.

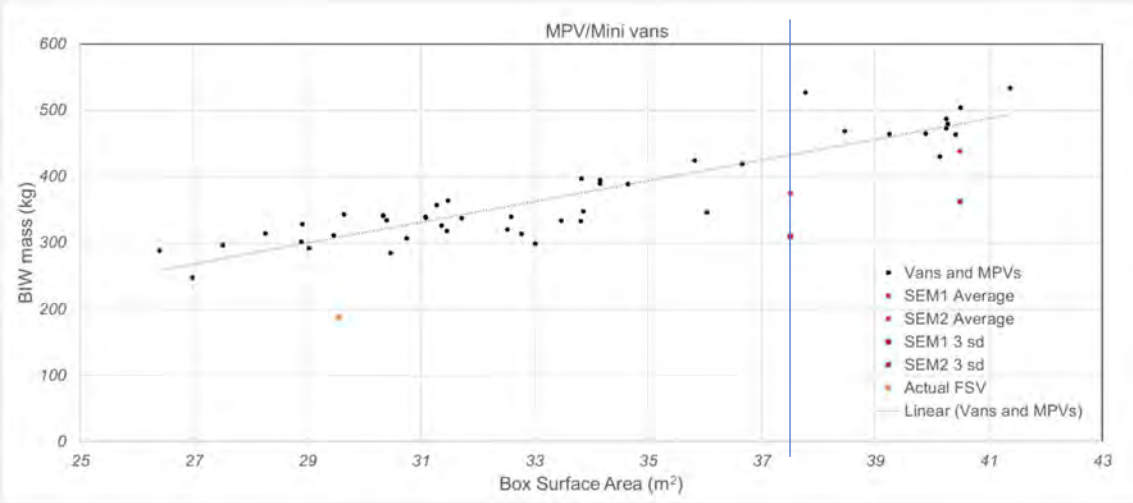

Figure 4.2.2.1 Statistical regression analysis of MPV & Minivan BIW weight versus Box Surface Area. Analysis courtesy of Donald E Malen, University of Michigan. Data source from a2mac1

The statistical analysis shows that there is a consistent relationship between the weight of the BIW in the reference vehicle data sample and the box surface area. The regression r^2 coefficient = 0.83, confirms the level of correlation (where 1.0 represents a direct correlation between the two data parameters). With the relationship between BIW weight and box surface area established, the expected weight of the Steel E-Motive BIW could be estimated given the overall vehicle dimensions (obtained from vehicle dimension targets). With vehicle length = 4095mm, width = 1850mm and height = 1880mm, an overall box surface area for SEM 1 vehicle is calculated at 37.5m. Using the mathematical relationship between BIW

weight and box area, the “expected” BIW weight for SEM1 is calculated as 374kg. This would be the expected weight for a current production vehicle, such as an MPV or minivan with the given dimensions. For the Steel E-Motive project, a certain degree of innovation and technology would expect to yield a more lightweight BIW. In order to account for this, a factor of 3 times the standard deviation of the statistical dataset is applied. This results in the BIW weight target of 309kg. This value is the effective BIW weight target applied for SEM1. The BIW is defined as the steel body structure and excludes the high voltage battery and structure, front and rear subframe, doors, seats, glazing, front, and rear bumper beams.

4.2.3 Vehicle safety and crashworthiness targets

Steel E-Motive SEM1 and SEM2 vehicles are intended for operation in mixed mode traffic (both autonomous and human operated). To ensure absolute protection of the occupants and other road users, the Steel E-Motive concepts were engineered to meet high speed crash test regulations and requirements. A summary of the tests, requirements and targets is shown in Figure 4.2.3.1. The crash tests and requirements were selected to ensure the design is compliant and compatible with vehicle global safety standards. The Steel E-Motive SEM1 crash performance was evaluated and developed using Finite Element Analysis (FEA) simulation. The FEA models were setup to replicate the real-world crash events, and according to standard simulation approach and methodologies. In order to simplify the calculation process, crash test dummies and air bags were omitted from the models and calculations. The crashworthiness evaluations were determined from acceleration pulse and occupant compartment intrusion levels.

Table 4.2.3.1 Summary of Vehicle Crash Test Loadcases and Targets

	Test	Vehicle Speed	Barrier Type	Target	Additional Info
Front	USNCAP full frontal rigid barrier ("FFB")	56kph	Rigid, 100%	Vehicle acceleration pulse <35g Front bulkhead intrusions <40mm No damage to battery	Acceleration to be measured at B pillar location or equivalent. Acceleration pulse processed using sliding mean approach Where possible, pulse and intrusion levels should achieve lowest value. Targets are maximum permitted values
	Insurance Institute Of Highway Safety (IIIHS) front Offset Deformable Barrier (ODB)	64kph	40% overlap, deformable	Vehicle acceleration pulse <35g Occupant compartment intrusion levels below values as described in Table 4.4.3.3. Values to demonstrate "good" rating No damage to battery	
	Insurance Institute Of Highway Safety (IIIHS) Small Offset Rigid Barrier (SORB)	64kph	25% overlap, rigid barrier	Vehicle acceleration pulse <35g Occupant compartment intrusion levels below values as described in Table 4.4.3.4 Values to demonstrate "good" rating No damage to battery	
Side	USNCAP rigid pole	32kph (note, moving barrier/pole)	Rigid pole, 254mm diameter, 15degrees to perpendicular. In line with front occupant head location	Occupant compartment intrusion levels below values described in Figure 4.4.3.5 (IIHS targets). For battery intrusion test locations, >30mm of intrusion clearance between battery	USNCAP requirement describes occupant (dummy) injury levels. IIHS intrusion levels applied for this test (see below). 3 additional test locations evaluated
	IIHS side barrier	60kph	IIHS deformable barrier, 1900kg, design ii	Occupant compartment intrusion levels below values described in Figure 4.4.3.5 Values to demonstrate "good" rating No damage to battery	
Rear	FMVSS305 EV	80kph (moving barrier)	Deformable barrier (FMVSS301). 70% overlap	<35g pulse <40mm occupant compartment intrusion No damage to battery	
Roof crush	FMVSS216a/ IIHS	Quasi-static loading, 127mm fixed displacement	Rigid plenum	Measured force to exceed 4 x Strength To Weight Ration (SWR), based on vehicle gross weight	

Front crash loadcases

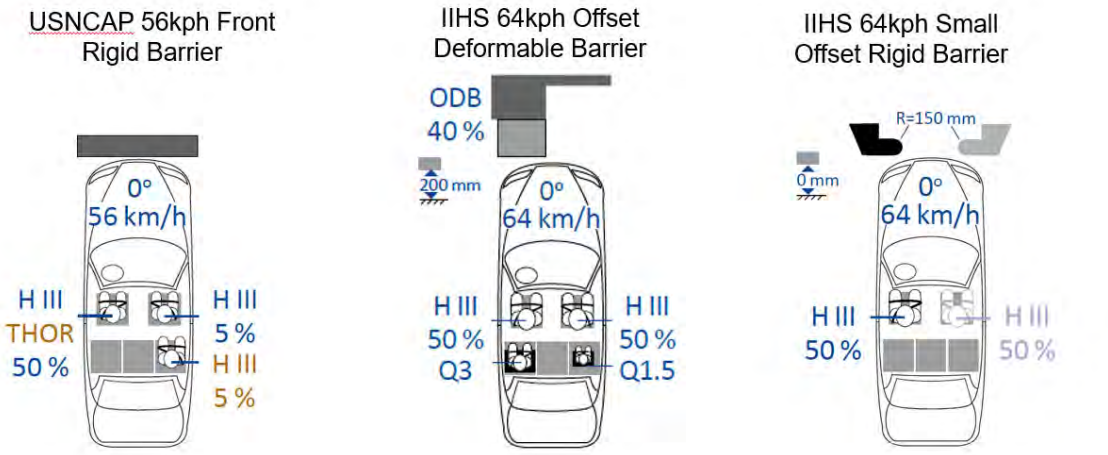

Figure 4.2.3.2 Front Crash Test Configurations

The objective of the USNCAP 56kph rigid barrier test is to ensure the vehicle is able to absorb sufficient crush energy in the event of a frontal impact, such that the occupants' injuries are minimised. The rigid test barrier results in the vehicle's moving kinetic energy is mainly converted to crush energy in the structure. A front crash structure is therefore required to decelerate the vehicle progressively without the occupant compartment being compromised by high intrusion. This challenge is particularly compounded with smaller vehicles, where the available front crush length is lower.

The IIHS 64kph ODB or moderate overlap test aims to simulate a high-speed vehicle to vehicle impact. The deformable crash barrier results in some of the vehicle kinetic energy being absorbed by crush in the barrier. One of the main challenges and objectives of this test is minimising injury as a result of intrusion into the occupant compartment. The high velocity and energy levels involved further make this more challenging.

The IIHS 64kph small overlap rigid barrier test (SORB) replicates a high-speed vehicle impact into a rigid stationary object. The lateral overlap between barrier and front of the vehicle is 25%. The combined effect of the high impact velocity, the rigid barrier, and the small overlap results in a considerable challenge for the management of the crash loads and protection of the occupants. The real-world test is applied to both the driver and passenger sides. With the symmetrical left to right design of Steel E-Motive (and the lack of "driver"), the loadcase was applied to the left side of the vehicle only.

The IIHS test protocols are primarily intended to inform the consumer (general public) on the safety performance of new vehicles and assist purchasing decisions. Vehicles are independently tested, and a rating system applied to advise on the relative safety performance. Vehicles are awarded "good", "acceptable", "marginal" and "poor" depending on the measured intrusion values, occupant (dummy) injuries and level and performance of active safety systems. As dummies and air bags were not considered in Steel E-Motive crash simulations, the ratings were based on structural intrusion levels alone. The acceleration pulses were noted as a reference. Acceleration pulses >35g were deemed unacceptable. The intrusion measurement locations are defined in the IIHS test protocol [https://www.iihs.org/media/ec54a7ea-1a1d-4fb2-8fc3-b2e018db2082/1A5oYw/Ratings/Protocols/current/small_overlap_test_protocol.pdf] and

shown in Figure 4.2.3.4 below. The locations are defined for a conventional human operated vehicle, where risk of injury can occur from protruding objects such as the steering wheel and brake pedal. The fully autonomous Steel E-Motive vehicle features no such direct vehicle control interfaces, and a decision was made during the programme to position the front occupant in a rear facing configuration. To account for this, modifications to the front crash intrusions measurement locations were made on the Steel E-Motive vehicle. The steering wheel, brake pedal, parking brake pedal locations were deleted. To account for the rear facing forward position of the front occupants and the proximity of the head to structure and glazing, two additional measurement locations were added at the upper front hinge pillar. An additional measurement location was added to the upper dash panel to ensure no intrusion occurred to the front seat back. The front intrusion measurement locations for Steel E-Motive as shown in Figure 4.2.3.5

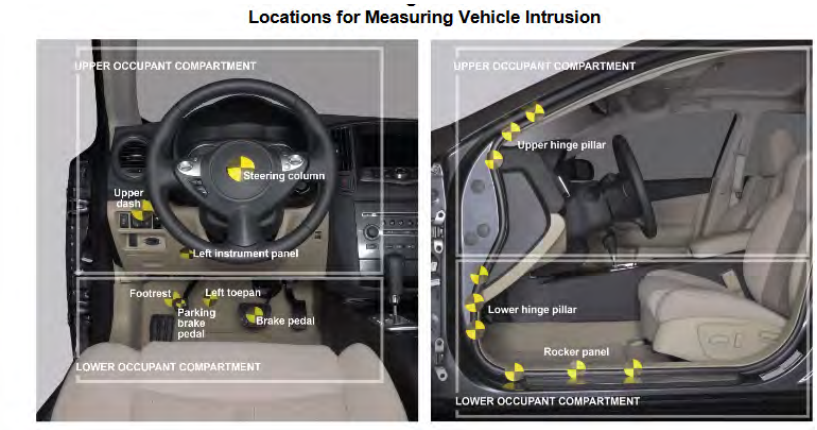

Figure 4.2.3.4 IIHS front crash intrusion measurement locations for conventional vehicle

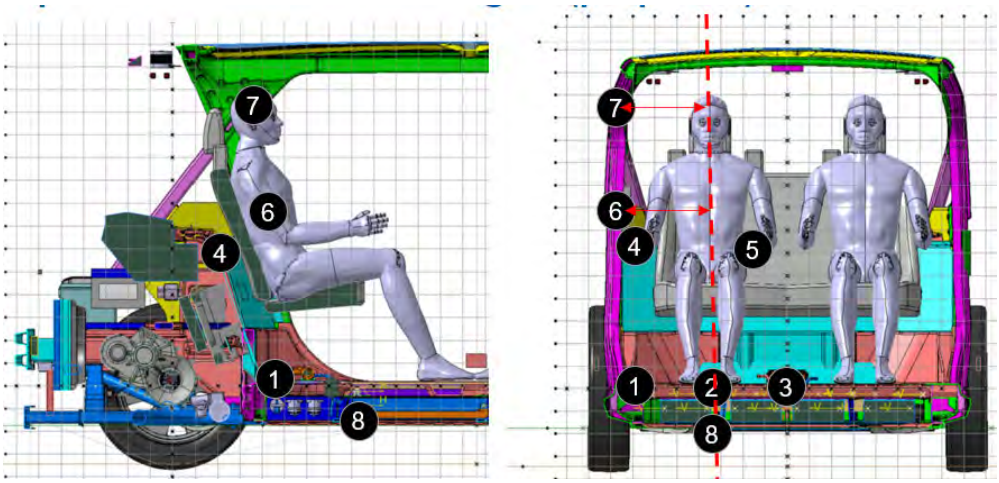

Figure 4.2.3.5 Steel E-Motive front crash intrusion measurement locations

The front crash target intrusion target values were based on IIHS values that achieve a “good” safety rating. The targets values are summarised in Figure 4.2.3.6 below.

Measurement Location	IIHS 64kph 40% offset deformable barrier	IIHS 64kph 25% small overlap rigid barrier
1,2,3	< 150mm	<150mm
4, 5	<50mm	<75mm
6,7	>180mm clearance between intrusion point and seat centreline	
8	No contact between battery module and structure	

Figure 4.2.3.6 IIHS front crash intrusion targets for Steel E-Motive vehicles

Side crashworthiness loadcases

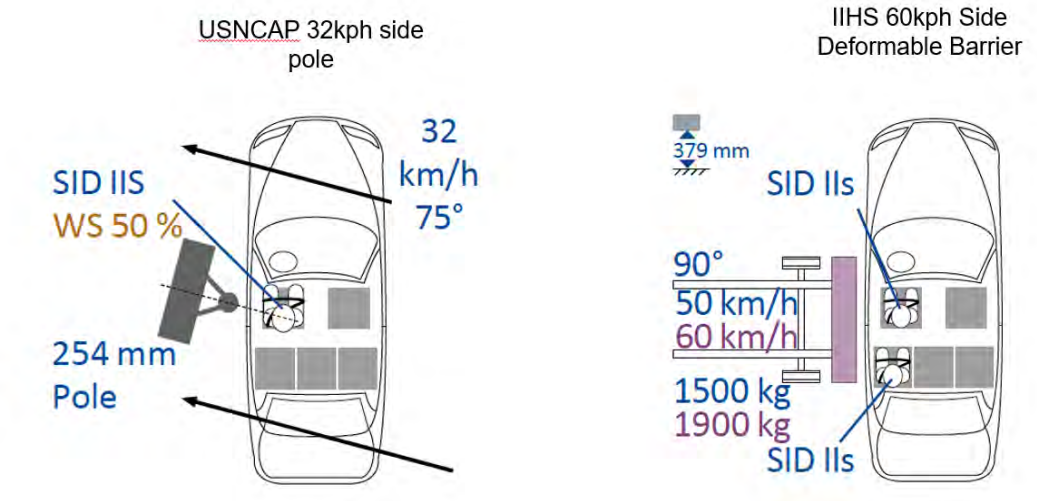

Figure 4.2.3.7 Side crash test configurations

The USNCAP side pole test considers a crash event where the vehicle strikes a static object such as a lamppost or road sign from the side, hence a test pole diameter of 254mm. The vehicle impact velocity is 32kph, at an angle of 75degrees. The pole and impact position is aligned to the driver's head. The primary objective of the test is to ensure the occupants are sufficiently protected from the impact resulting in reduced injury risk. Given the proximity of the high voltage batteries to the extremities of the vehicle, there is also a considerable risk of damage to the cells in this test. Damage to the battery cells can lead to leakage of the electrolytes and a thermal runaway event (fire). An additional intrusion clearance criteria of >30mm was therefore added for this to test in order to ensure the batteries remain undamaged. This means that there should be a minimum distance of 30mm between the outside of the battery module case and the body structure/battery housing. The USNCAP test protocol calls for the pole test in one location (in line with the drivers' head). To ensure a robust design and enhanced level of safety and protection for the occupants the Steel E-Motive project considered and engineered for 3 additional pole test locations as shown in

Figure 4.2.3.8. Position 1) is the required test location, in line with the drivers' head. Position 2) is located at the X coordinate centreline of the vehicle and poses challenges due to distance from supporting vertical structures in the body such as A and C pillars. Test position 3) is aligned with the rear occupants' head, ensuring sufficient protection is offered for rear passengers. Position 4) is located at a midpoint between the vehicle centreline (position 2) and the rear vertical "C" pillar. As per position 2) this location was selected as a potentially vulnerable position for the high voltage battery. Positions 1) and 3) are primarily intended to ensure protection of the occupants and positions 2) and 4) are primarily to ensure protection of the high voltage battery. The targets for the USNCAP side pole (real world) tests are based on measured occupant (or crash test dummy) injury loads and criteria. As the Steel E-Motive FEA simulations did not include dummies or air bags, an alternative approach using the IIHS side barrier targets was employed. The level of occupant protection was determined by the post-crash intrusion clearance to a virtual line in the centre of the occupant seat. The IIHS side barrier test requires >180mm of clearance post-crash in order to achieve a "good" rating. The same target was applied for the USNCAP side pole test.

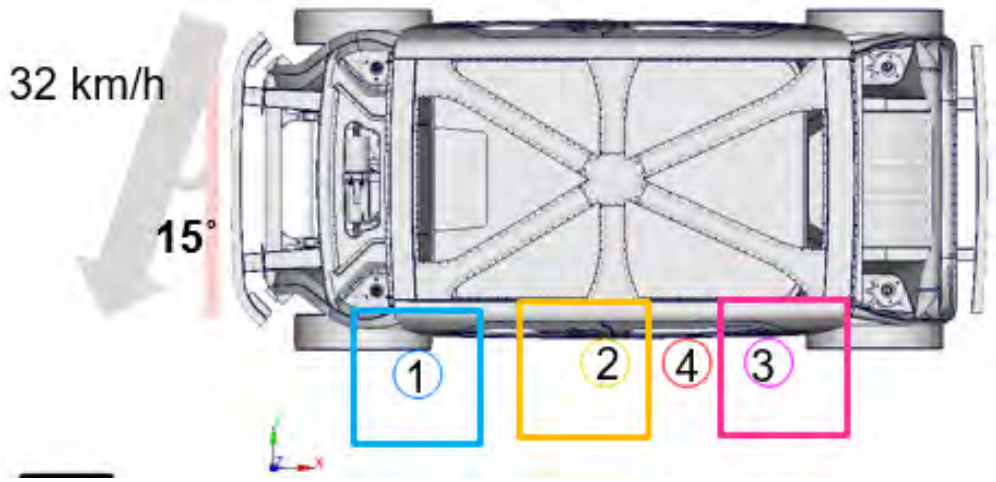

Figure 4.2.3.12 USNCAP side pole test locations

One of the main challenges for any side pole tests is the small contact area of the pole versus the vehicle. This results in very high concentrated loads applied to the body structure during the crash event. Also, there is a much smaller region in the vehicle structure to manage the crash event and loads when compared to front or rear crash tests. With the vehicle occupants and batteries located relatively closer the barrier impact location the crash loads and subsequent intrusions need to be carefully managed, primarily through design of the body and side closure structure and safety restraint systems (e.g., air bags).

The IIHS side barrier test simulates a collision between two vehicles with one vehicle impacting the test vehicle perpendicular to the direction of travel. This scenario is typical of a collision at a traffic T junction. In 2020, the test protocol was updated to consider a more challenging condition, with the impact velocity increased from 50kph to 60kph and the test barrier weight increased from 1500kg to 1900kg. The profile of the barrier was also modified to take into consideration recent changes in vehicle front end design and profile (figure 4.2.3.13)

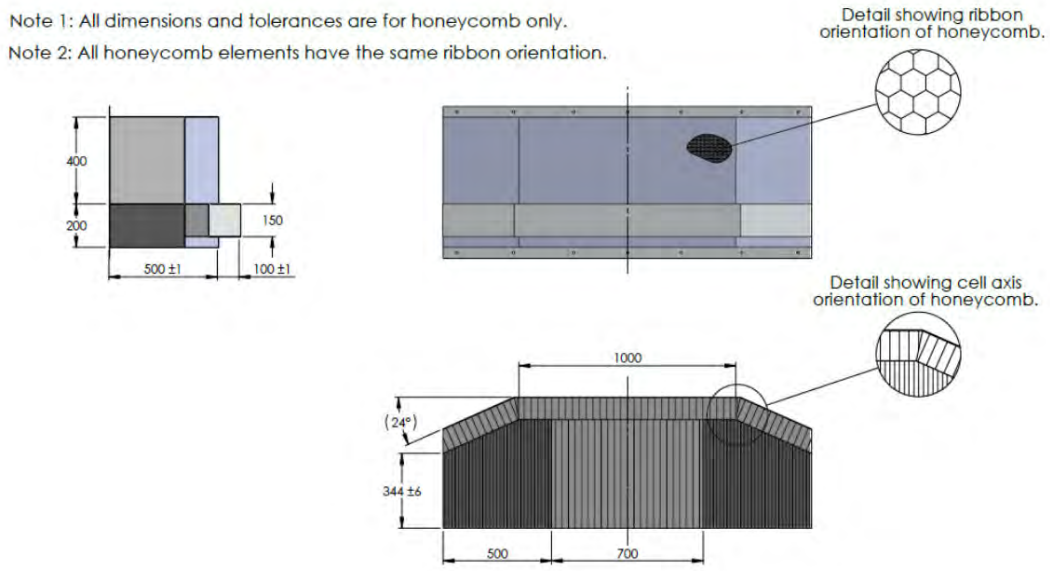

Figure 4.2.3.13 IIHS side barrier (2) dimensions https://www.iihs.org/media/b76a49b5-88db-4535-b08f-c269d59f4934/IanIHw/Ratings/Protocols/current/side_barrier_spec-2.0.pdf

For the Steel E-Motive SEM1 concept, the centre of the test barrier is aligned to a position 156.05cm rearwards of the front wheel centreline as shown in Figure 4.2.3.14

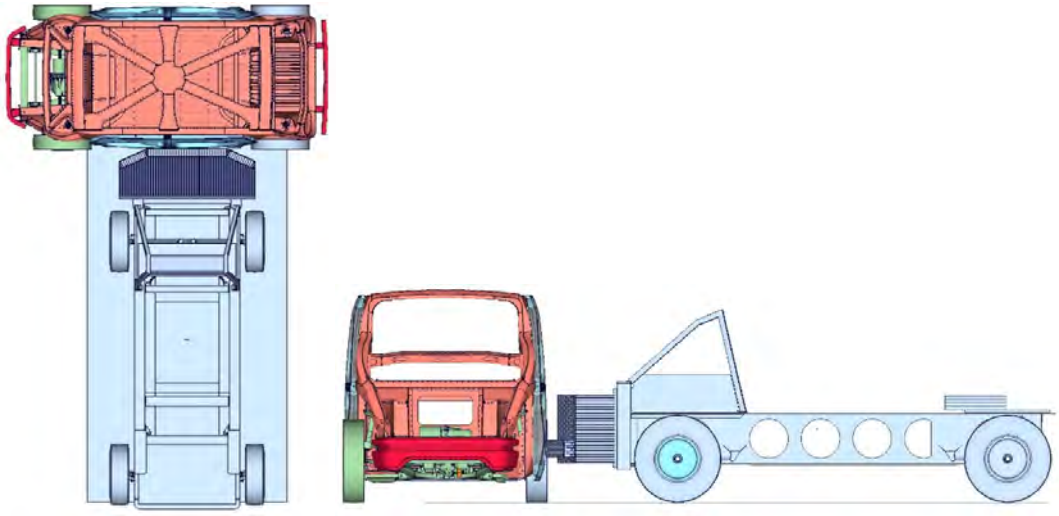

Figure 4.2.3.14 alignment of IIHS side barrier (version 2.0) to Steel E-Motive SEM1 vehicle

One of the main challenges and considerations with the IIHS side barrier test is that the barrier vertical position is above the general floor height. A lower floor height is desired in order to enable better ingress and egress to and from the vehicle, especially for a ride hailing vehicle. This means that the barrier does not initially impact with the outer structure of the body (e.g., the rocker) and there is a limited lateral loadpath across the vehicle. The structure in the vehicle side closures and B-pillar (if any) are the primary contact points and interfaces to the barrier. As per the IIHS front crash protocols, a rating system is applied to the side barrier test based on measured intrusion and dummy injuries. The goal for Steel E-

Motive was to achieve a “good” rating in side crash. The IIHS protocol requires the B pillar intrusion values to be >180mm from the centreline of the seat. [https://www.iihs.org/media/3fe4c863-2726-4823-b924-06b079222929/KktnZQ/Ratings/Protocols/current/side_impact_2.0_ratings_guidelines.pdf]

For the SEM1 vehicle, a decision was taken during the design stage to position the front occupants in a rear facing configuration. The assessment protocol for Steel E-Motive was there modified to ensure that the maximum intrusion at any location is >180mm from the seat centreline. Figure 4.4.3.15 describes the IIHS side crash intrusion target applied for Steel E-Motive. The same target was applied for the USNCAP side pole test.

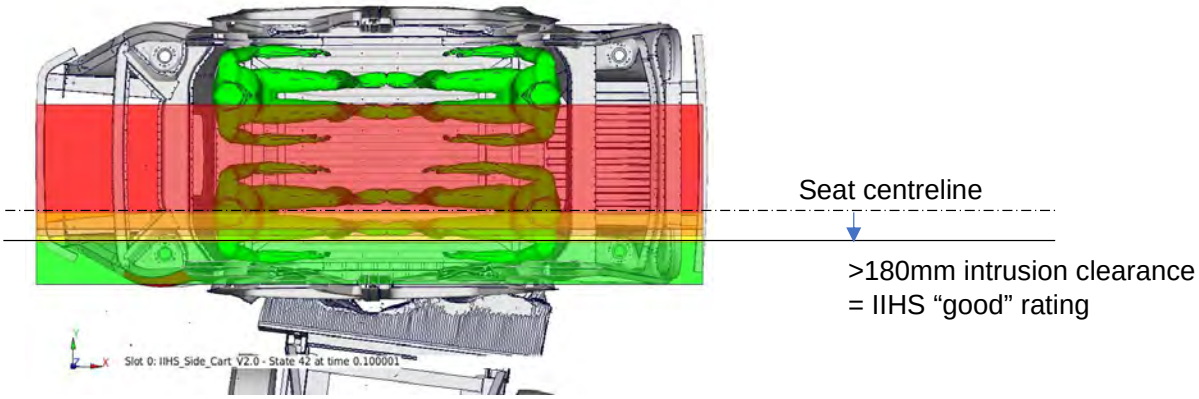

Figure 4.2.3.15 IIHS side crash intrusion targets applied for Steel E-Motive

Rear crashworthiness loadcase

The FMVSS 305 EV (incorporating FMVSS 301) loadcase considers a moving vehicle impacting a stationary vehicle, replicating a collision event in waiting traffic. A deformable barrier with a weight of 1368kg impacts the test vehicle at a speed of 80kph with a 70% overlap. The primary objective of the FMVSS 305 (EV) is to maintain the integrity of the high voltage electrical systems, namely, to prevent damage to the high voltage battery and cables and minimise occupant injury risks. A target of <40mm rear bulkhead intrusion and <35g was applied to ensure a reduced risk of occupant injury. The design approach and philosophy for rear crash load management is similar to the front, where the impact crush energy needs to be carefully managed using crushable body structure elements whilst ensuring the structural intrusions to the occupant compartment and battery are minimised.

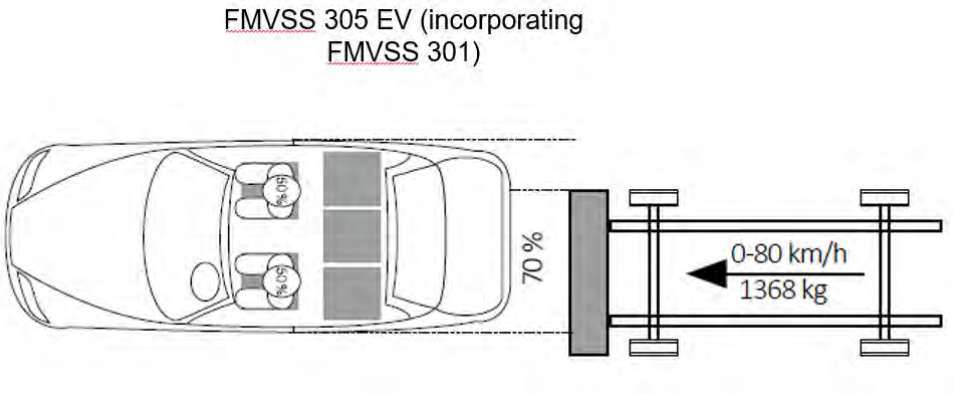

Figure 4.2.3.16 FMVSS 305 EV rear crash test configuration

Roof Crush

The objective of the IIHS roof crush is to ensure the vehicle occupants remain protected in a dynamic vehicle roll over event. The vehicle is maintained in a static upright position with a loading cell position as per the specification shown in Figure 4.4.3.16. A quasi-static load is applied to the vehicle roof structure, up to a point where the load cell displacement reaches 127mm. The peak force in the load cell is measured at this point and the *strength to weight* ratio *(SWR)* is calculated. The SWR is derived from the peak load force at 127mm divided by the vehicle curb weight (in Newtons). The target for Steel E-Motive was to achieve IIHS "good" rating, where the peak force at 127mm displacement is at least 4 times greater than curb weight. Achieving the required roof crush load relies on high strength roof members and suitable loadpath and member strength from the upper to the lower body structure (such as A pillar).

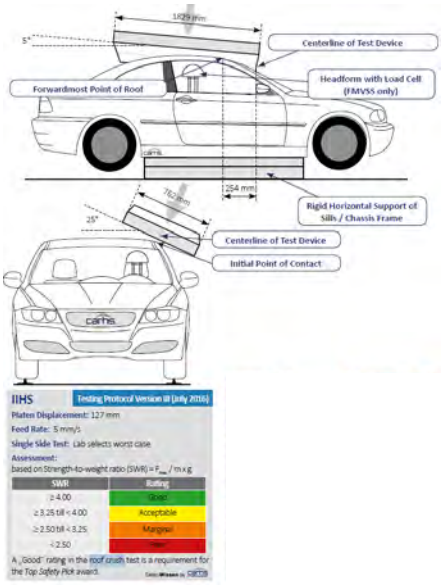

Figure 4.2.3.16 IIHS roof crush test and rating

4.2.4 Vehicle crash reference loadcases

The loadcases and targets outlined in section 4.2.3 were considered as "core" targets, meaning that the Steel E-Motive design was engineered to be meet the performance requirements defined. Additionally, two *reference* crash loadcases were considered to periodically assess the design and quantify the crash performance.

EuroNCAP Moving Progressive Deformable Barrier (MPDB) replicates a car-to-car frontal impact and is designed to improve the crash compatibility between vehicles. The test vehicle impacts at 50kph into a moving deformable barrier, with weight 1400kg, travelling at 50kph, with a frontal impact offset of 50%. The deformable barrier design is engineered to replicate the crush performance of a modern European passenger car. The EuroNCAP assessment of occupant dummy injuries (forces and moments on limbs and joints), intrusion levels and deformation of the impact barrier. For Steel E-Motive, the vehicle acceleration pulse and intrusion values were observed and compared to the front IIHS and USNCAP FFB values. The main challenge for this test is management of the high crush loads as the effective impact velocity is 100kph, whilst ensuring both the test vehicle and barrier collapse progressively, minimising injury risks to the occupants.

Figure 4.2.4.1 EuroNCAP Moving Progressive Deformable Barrier (MPDB) test protocol

At the time of undertaking the Steel E-Motive programme, the NHTSA front 90kph, 35% overlap, 15degrees oblique test was not officially mandated as a requirement or test for production vehicles but was cited as a potential test to be introduced at some point in the future. This loadcase was also considered as a *reference* crash loadcase for the Steel E-Motive programme. A moving deformable barrier of weight 2486kg is impacted into the stationary test vehicle at 90kph, the barrier being at 15degrees to the direction of travel and impacting with a 35% offset to the front. The resultant acceleration pulse and intrusion levels were compared to the core loadcase targets.

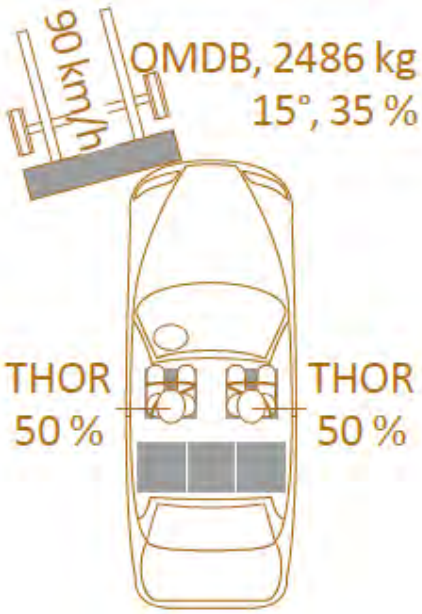

4.2.6 Propulsion Battery Targets

Given the size and weight of high voltage batteries in electric vehicles, the requirements and specifications of the battery can influence the overall vehicle design and architecture.

Figure 4.2.6.1 summarises the requirements and targets for the of the Steel E-Motive high voltage battery

Requirement/Specification/Test	Target	Comment
Battery type and chemistry	-	“agnostic” (see comment below)
Battery capacity (kWh) and voltage	-	To be determined, such that the vehicle can operate effectively within a typical ride hailing/taxi type drive cycle
Overall battery pack weight (kg)		Not specified but should be competitive with market trends and enables fulfilment of vehicle targets (e.g., range, curb weight)
China requirement GB 38031-2020, incorporating 100kN crush load		Battery pack integrity to be maintained. No rupture or electrolyte leakage. Strength of the pack to be determined by the design and strength properties of the material
ISO 12405-2 PSD Random Vibration Fatigue		Battery pack integrity to be maintained. No rupture or electrolyte leakage. Strength of the pack to be determined by the design and strength properties of the material
Debris and jacking intrusion prevention		Battery design to withstand high velocity road debris impact from underneath the vehicle Battery design to withstand a jacking load from underneath the vehicle. Detailed in 4.4.6.2
1st battery modal frequency	>35Hz	System level target (and FEA modelling approach) to ensure full vehicle modal target is achieved

4.2.5.1 Battery chemistry and cell type

The battery cell and chemistry technologies in electric vehicles will continue to evolve considerably in the coming years. Car makers are faced with many options of battery technologies and approaches for integrating them into the vehicle. The intended Start of Production (SOP) date for Steel E-Motive concepts is in the 2030 to 2035 timeframe. By that time, it is anticipated that the battery technology will have evolved even further. Given that the primary focus of the Steel E-Motive project was the design of the body structure, a decision was taken to engineer the vehicle for an “agnostic” battery chemistry type and cell, meaning that the vehicle and body design should enable the freedom for a variety of battery cell types (e.g., pouch, prismatic, cylindrical) and cell technologies (e.g., lithium ion, solid state) to be considered in future designs. To assist the engineering of the body structure, some subsequent assumptions were made on battery type and technologies, such that the module package sizes, and weight could be determined and considered in the overall vehicle design. These specifications are outlined in Section 6.

4.2.5.2 Battery strength and durability requirements

Damage or rupture to high voltage batteries can result in significant hazards to the vehicle occupants and other road users. If the battery cell integrity is compromised, the electrolytes can leak and mix, resulting in very temperatures, thermal runaway (an uncontrollable thermal temperature risk as a result of exothermic chain reaction of secondary cell). Subsequent combustion and fires can release toxic and noxious fumes and must be extinguished using specific methods. In addition to the vehicle safety requirements several battery system

standards and requirements are mandated to ensure the battery is not damaged or ruptured as a result of everyday use or occasional accidental abuse or misuse events.

China standard GB 38031-2020 and GB/T 31467.3-2015 incorporates several requirements for battery electric vehicle batteries including a 100kN crush load applied to the pack. A quasi-static load of magnitude 100kN is applied to the battery pack extremities in the primary vehicle crash loading directions (X and Y), with a cylindrical impactor of diameter 150mmmm. The load application positions are not prescribed, hence the worst-case locations are typically accounted for, as shown in Figure 4.2.5.2.1 below

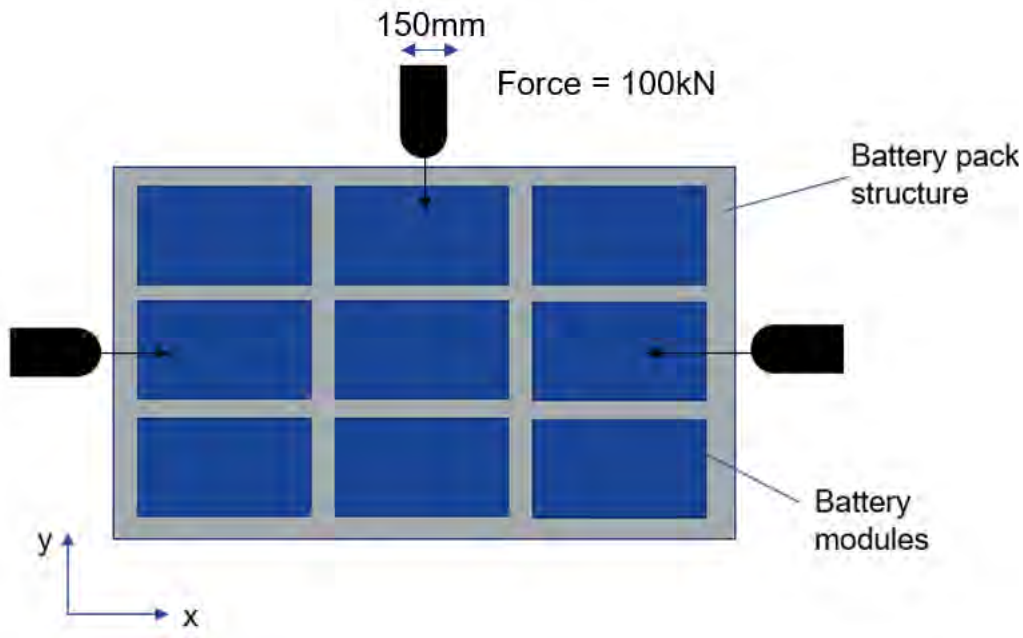

Figure 4.2.5.2.1 Standard GB 38031-2020 incorporating 100kN quasi-static crush load

The standard requires the battery pack to maintain its overall integrity, with no evidence of electrolyte leakage, damage, or rupture to the cells. The battery overall resistance and voltage must remain within prescribed limits. The test can be performed at pack level (for example on a sealed and contained battery pack assembly) or as installed in the vehicle.

To account for potential misuse of the vehicle or battery, the Steel E-Motive design considers a 25G shock test loadcase is applied. Separate loadcases are applied in the X, Y and Z directions according to the profile shown in Figure 4.2.5.2.2. The battery structure integrity must be maintained with no permanent damage to the pack or modules. The material plastic strain limits were used to determine permanent damage to the pack and modules.

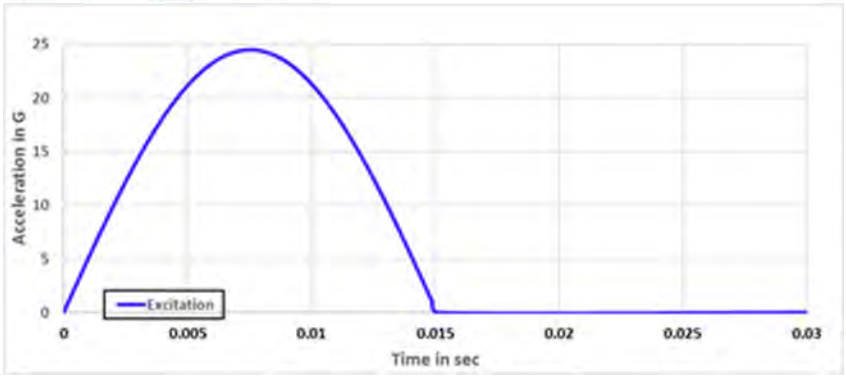

Figure 4.2.5.2.3 25g battery shock test load profile

Battery packs in electric vehicles are typically located in the lower portion of the vehicle, primarily due to package requirements and to achieve a lower overall centre of gravity. This location puts the battery in a vulnerable location. There are risks from road debris and large objects impacting the underside of the vehicle whilst the vehicle is moving, which could rupture the battery modules. The batteries are also located close to designated jacking or lift zones, where the vehicle is raised for service or repair. In some cases, users or technicians can place the vehicle jacking or lifting devices in the incorrect location, such as the battery cover. With these parts of the structure not specifically designed to withstand the lifting load of the vehicle, excessive deformation of the battery cover may lead to contact and high loads acting on the modules, resulting in damage to the cells and subsequent issues with thermal runaway and fires. A similar scenario may occur if the vehicle parked or stopped accidently or by malfunction in the vicinity of an automatic/remotely operated traffic bollard. To account for these misuse situations, 6 battery cover or undertray loading points were identified as potential points of greatest weakness and vulnerability. A load equivalent to half of the vehicle gross weight was applied at each location (independent tests) over a cylindrical impactor of 50mm diameter. The requirements of the test are that no physical contact should occur between the cover and the battery modules. Figure 4.4.6.4 shows the locations for the applied loads and Figure 4.2.5.2.4 shows the loading profile or time history

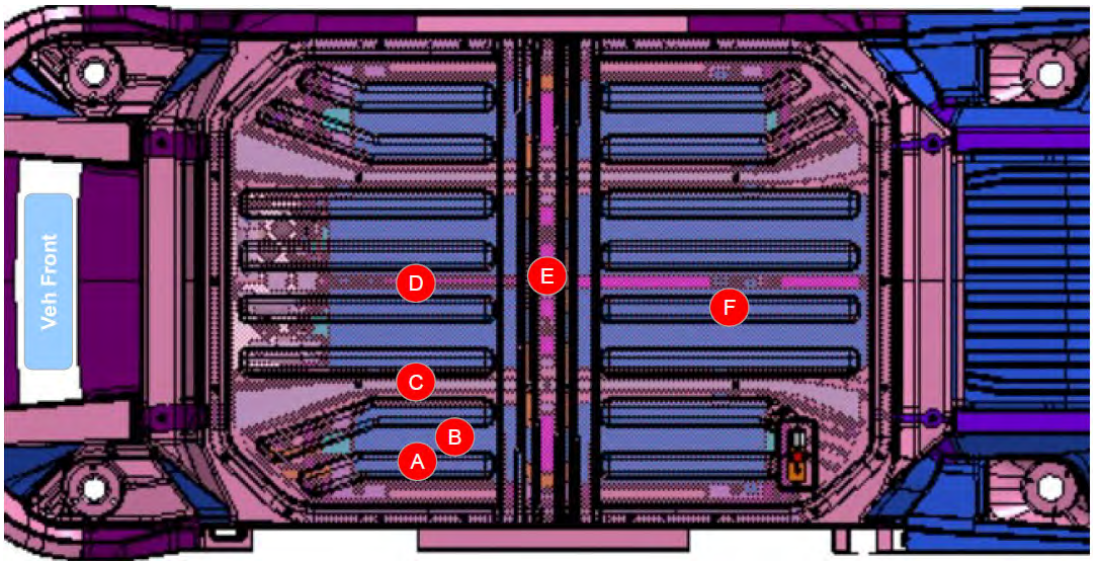

Figure 4.2.5.2.4 Vehicle lifting and jacking misuse loadcase. Locations for misuse vehicle jacking, lifting or debris impact

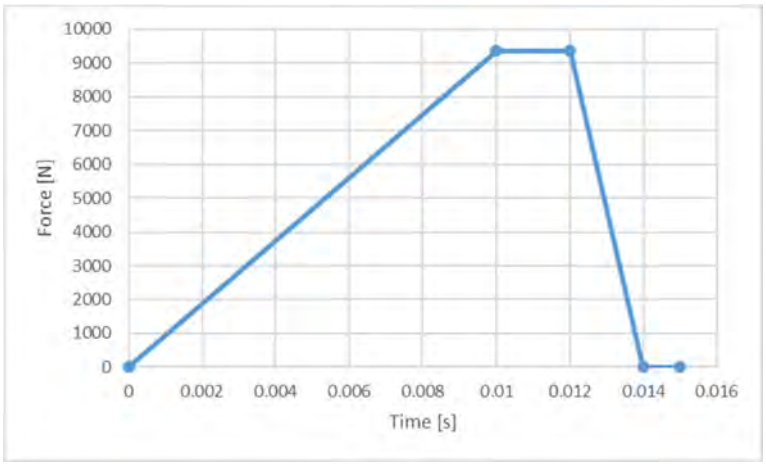

Figure 4.2.5.2.5 Vehicle lifting and jacking misuse loadcase. Force-time profile

During the life of the vehicle, the battery is also subjection to vibration loading as a result of road induced loads and vehicle manoeuvring. The repetitive cycling loading can cause fatigue failure of the battery structure and its components. To ensure fatigue failures don't occur, an ISO 12405-2 Power Spectral Density (PSD) fatigue loading requirement was applied. Figure 4.2.5.2.6 shows the FEA model approach and PSD loading profile. Acceptance of the performance was based on the predicted stresses in the battery and structure being within the material grade fatigue limits.

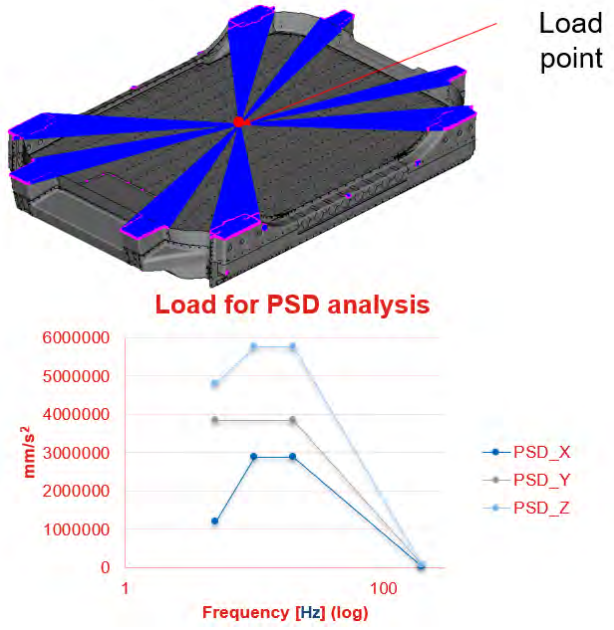

Figure 4.2.5.2.6 Battery PSD fatigue analysis approach and loading

5.0 Steel Grades, Joining Methods and Fabrication Technologies

This section describes the different steel grades and fabrication processes considered in the design and development of Steel E-Motive.

5.1 Steel Grades and Selection Criteria

Automotive steels are commonly classified by a metallurgical designation and strength level. Common designations include low-strength steels (interstitial-free and mild steels); conventional High-Strength Steels (HSS) (carbon-manganese, bake hardenable, high-strength interstitial-free, and high-strength, low-alloy steels); and Advanced High-Strength Steels (AHSS) (dual phase, transformation-induced plasticity, ferritic-bainite, complex phase, martensitic, twinning-induced plasticity, press-hardened and 3rd Generation steels).

The different grades have distinctly different microstructures and deformation characteristics. The results are different performance levels for part formability, crash, and energy management. The Global Formability Diagram compares strength and total elongation (a steel property related to formability) for different types of steel and is shown in Figure 1.

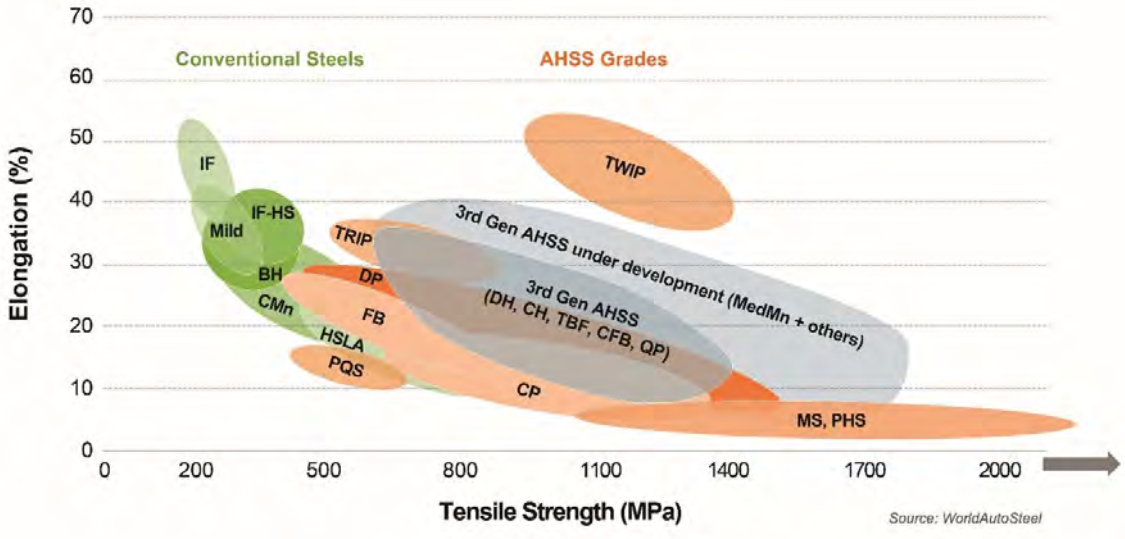

Figure 5.1: *Steel Global Formability Diagram*

The Steel E-Motive Materials Portfolio is a compilation of steel grades considered in the vehicle's design. All are commercially available from our member companies, today or in the near future. These members contributed over 65 grades of AHSS, ranging from the very common dual phase steels to the more complex press-hardened and 3rd Gen steels. The intensive innovation within the auto industry fueled the development of this broad range of materials, where minimum tensile strengths among portfolio grades range from 450 MPa to 2000 MPa. In comparison, and to emphasize the achievement in the automotive steel industry's product development, FutureSteelVehicle, (WorldAutoSteel's previous vehicle concept program) showcased 27 AHSS grades in 2010, with a maximum tensile strength of 1500 MPa. The complete AHSS Materials Portfolio is presented in Table 5.1.

Newer steel grades prosper from improved ductility as well, where steels with strength levels

of 1200 MPa can now achieve 20% elongation, enabling cold forming solutions for more challenging geometries.

The combination of new design technologies, emerging steel grades and advanced steel fabrication processes enabled optimal vehicle lightweighting and safety performance, with significant reductions in Greenhouse Gas (GHG) emissions over the entire vehicle life cycle.

Legend at Bottom					Thickness (mm)	Thickness (mm)	YS (MPa)	YS (MPa)	UTS (MPa)	UTS (MPa)	Tot EL (%)	HR Gage (mm)	CR Gage (mm)		GI or GA Gage (mm)		EG Gage (mm)		Aluminized Gage (mm)
Steel Grade - Written in common format- TENTATIVE	min TS	Type: TENTATIVE	Comment	Direction	Min t	Max t	Min	Max	Min	Max	min	U	U	E	U	E	U	E	U
CR140Y/270T	270	Mild Steel		RD	0.35	4.60	140		270		42	1.6 - 2.0	0.6 - 2.5	0.6 - 1.5	0.6 - 2.5	0.6 - 1.5	0.6 - 2.5	0.6 - 1.5	
CR210Y/340T-BH	340	BH		RD	0.40	3.40	210		340		38	N.A.	0.6 - 3.0	0.6 - 1.5	0.6 - 2.5	0.6 - 1.5	0.6 - 2.5	0.6 - 1.5	
CR260Y/370T-BH	370	BH		RD	0.40	2.80	260		370		34	N.A.	0.6 - 3.0	0.6 - 1.5	0.6 - 2.5	0.6 - 1.5	0.6 - 2.5	0.6 - 1.5	
CR280Y/400T-BH	400	BH		RD	0.50	2.80	280		400		32	N.A.	0.6 - 3.0	0.6 - 1.5	0.6 - 2.5	0.6 - 1.5	0.6 - 2.5	0.6 - 1.5	
CR260Y/410T-IF	410	IF		RD	0.40	2.30	260		410		41	N.A.	0.6 - 2.5	0.6 - 1.5	0.6 - 2.5	0.6 - 1.5	0.6 - 2.5	0.6 - 1.5	
CR300Y/420T-IF	420	IF		RD	0.50	2.30	300		420		33	N.A.	0.6 - 2.5	0.6 - 1.5	0.6 - 2.5	0.6 - 1.5	0.6 - 2.5	0.6 - 1.5	
CR350Y/450T-LA	450	HSLA		RD	0.50	5.00	350		450		25	N.A.	0.6 - 2.5	N.A.	0.6 - 2.5	N.A.	0.6 - 2.5	N.A.	
CR420Y/500T-LA	500	HSLA		RD	0.75	5.00	420		500		24	N.A.	0.6 - 2.5	N.A.	0.6 - 2.5	N.A.	0.6 - 2.5	N.A.	
CR490Y/600T-LA	600	HSLA		RD	0.75	5.00	490		600		22	N.A.	0.6 - 2.5	N.A.	0.6 - 2.5	N.A.	0.6 - 2.5	N.A.	
CR550Y/620T-LA	620	HSLA		RD	0.75	5.00	550		620		21	N.A.	0.6 - 2.5	N.A.	0.6 - 2.5	N.A.	0.6 - 2.5	N.A.	
CR700Y/780T-LA	780	HSLA		RD	0.75	5.00	700		780		17	N.A.	0.6 - 2.5	N.A.	0.6 - 2.5	N.A.	0.6 - 2.5	N.A.	
HR350Y/450T-LA	450	HSLA		RD	1.65	8.50	350		450		25	>1.65	N.A.	N.A.	1.8-5.0	N.A.	N.A.	N.A.	
HR420Y/500T-LA	500	HSLA		RD	1.50	8.50	420		500		24	>1.5	N.A.	N.A.	1.8-5.0	N.A.	N.A.	N.A.	
HR490Y/600T-LA	600	HSLA		RD	1.60	8.50	490		600		22	>1.6	N.A.	N.A.	1.8-5.0	N.A.	N.A.	N.A.	
HR550Y/620T-LA	620	HSLA		RD	1.60	8.50	550		650		21	>1.6	N.A.	N.A.	1.8-5.0	N.A.	N.A.	N.A.	
HR700Y/780T-LA	780	HSLA		RD	2.00	5.00	700		780		17	>2.0	N.A.	N.A.	2.0-5.0	N.A.	N.A.	N.A.	
CR260Y450T-DP	450	DP		RD	0.5	2.2	260	340	450	560	27	N.A.	0.6-2.3	N.A.	0.6-2.3	N.A.	0.6-2.0	N.A.	N.A.
CR290Y490T-DP	490	DP		RD	0.6	2.3	290	390	490	600	25	N.A.	0.6-1.8	N.A.	0.6-2.3	N.A.	0.6-1.8	N.A.	N.A.
CR300Y590T-DP	590	DP		RD	0.7	2.1	300	470	590	700	16	N.A.	0.7-2.1	N.A.	0.7-2.1	N.A.	0.7-2.1	N.A.	N.A.
CR340Y590T-DP	590	DP		RD	0.6	2.3	340	440	590	700	21	N.A.	0.6-2.3	N.A.	0.6-2.3	N.A.	0.6-2.3	N.A.	N.A.
CR420Y590T-DP	590	DP		RD	0.7	2	420	500	590	700	17	N.A.	N.A.	N.A.	0.7-2.0	N.A.	N.A.	N.A.	N.A.
CR420Y780T-DP	780	DP		RD	0.7	2.3	420	550	780	900	15	N.A.	0.7-2.3	N.A.	0.8-2.0	N.A.	0.7-2.0	N.A.	N.A.
CR500Y780T-DP	780	DP		RD	0.7	2.1	500	650	780	900	13	N.A.	0.7-2.1	N.A.	0.7-2.1	N.A.	0.7-1.6	N.A.	N.A.
CR550Y980T-DP	980	DP		RD	0.8	2.1	550	730	980	1130	9	N.A.	0.8-1.2	N.A.	0.8-2.1	N.A.	N.A.	N.A.	N.A.
CR590Y980T-DP	980	DP		RD	0.8	2.1	590	740	980	1130	11	N.A.	0.8-2.0	N.A.	0.8-2.0	N.A.	0.8-2.1	N.A.	N.A.
CR700Y980T-DP	980	DP		RD	0.8	2.1	700	920	980	1130	9	N.A.	0.8-2.3	N.A.	0.8-2.2	N.A.	0.8-1.8	N.A.	N.A.
CR740Y1180T-DP	1180	DP		RD	1	1.8	740	980	1180		7	N.A.	N.A.	N.A.	1.0-1.8	N.A.	N.A.	N.A.	N.A.
CR800Y1180T-DP	1180	DP		RD	1	2.3	800	1200	1180	1300	7	N.A.	1.0-2.3	N.A.	1.0-2.3	N.A.	1.0-1.4	N.A.	N.A.
CR860Y1180T-DP	1180	DP		RD	1	2	860	1100	1180	1300	7	N.A.	1.0-2.0	N.A.	1.0-2.0	N.A.	N.A.	N.A.	N.A.
CR1200Y1470T-DP	1470	DP		RD	1	1.8	1200		1470			N.A.	1.0-1.8	N.A.	N.A.	N.A.	1.0-1.8	N.A.	N.A.
HR330Y580T-DP	590	DP		RD	2	5.5	330	450	580	680	20	2.0-5.5	N.A.	N.A.	N.A.	N.A.	N.A.	N.A.	N.A.
CR330Y590T-DH	590	DH		RD	0.8	2.4	330	440	590	700	26	N.A.	0.8-1.6	N.A.	0.8-2.4	N.A.	0.8-1.6	N.A.	N.A.
CR440Y780T-DH	780	DH		RD	0.8	2	440	550	780	900	19	N.A.	0.8-1.6	N.A.	0.8-2.0	N.A.	0.8-1.6	N.A.	N.A.
CR690Y900T-DH	900	DH					690		900		30	N.A.	maybe	N.A.	maybe	N.A.	maybe	N.A.	N.A.
CR560Y980T-DH	980	DH		RD	1	2	560	740	980	1180	14				1.0-2.0				
CR700Y980T-DH	980	DH		RD	1.0	2.3	700	850	980	1180	14	N.A.	1.0-1.6	N.A.	1.0-2.0	N.A.	1.0-1.6	N.A.	N.A.
CR850Y1180T-DH	1180	DH		RD	1.00	1.80	850	1050	1180	1350	10	N.A.	1.0-1.8	N.A.	N.A.	N.A.	1.0-1.6	N.A.	N.A.
CR360Y590T-CP	590	CP		RD	0.8	2.0	360	500	590	700	17	N.A.	0.8-2.0	N.A.	0.8-2.0	N.A.	0.8-2.0	N.A.	N.A.
CR570Y780T-CP	780	CP		RD	0.8	2.0	570	720	780	920	11	N.A.	0.5-2.1	N.A.	0.8-2.0	N.A.	0.8-1.7	N.A.	N.A.
CR680Y780T-CP	780	CP		RD	0.8	2.0	680	830	780	980	10	N.A.	0.8-2.0	N.A.	0.8-3.0	N.A.	0.8-1.7	N.A.	N.A.
CR700Y980T-CP	980	CP		RD	1.0	2.0	700	900	980	1200	8	N.A.	N.A.	N.A.	1.0-2.0	N.A.	N.A.	N.A.	N.A.
CR780Y980T-CP	980	CP		RD	0.5	2.1	780	950	980	1140	7	N.A.	0.5-2.1	N.A.	0.9-2.1	N.A.	0.5-2.1	N.A.	N.A.
CR900Y1180T-CP	1180	CP		RD	1	1.6	900	1100	1180	1350	5	N.A.	1.0-2.0	N.A.	1.0-2.0	N.A.	1.0-1.6	N.A.	N.A.
HR660Y760T-CP	760	CP		RD	2.0	5.0	660	830	760	960	10	2.0-5.0	N.A.	N.A.	2.0-5.0	N.A.	N.A.	N.A.	N.A.
HR720Y950T-CP	950	CP		RD	1.7	4.5	720	920	950		9	1.7-4.5	N.A.	N.A.	N.A.	N.A.	N.A.	N.A.	N.A.
CR780Y980T-CH	980	CH		RD	1.0	1.7	780	950	980	1140	10	N.A.	1.0-1.7	N.A.	N.A.	N.A.	1.0-1.7	N.A.	N.A.
CR900Y1180T-CH	1180	CH		RD	1.0	1.9	900	1150	1180	1350	8	N.A.	1.0-1.9	N.A.	N.A.	N.A.	1.0-1.9	N.A.	N.A.
CR1000Y1370T-CH	1370	CH		RD	1.0	1.6	1000	1250	1370	1550	5	N.A.	1.0-1.6	N.A.	N.A.	N.A.	1.0-1.6	N.A.	N.A.
HR300Y450T-FB	450	FB		RD	1.8	4.5	300	440	450	550	25	1.8-4.5	N.A.	N.A.	2.0-5.0	N.A.	N.A.	N.A.	N.A.
HR440Y580T-FB	580	FB		RD	2	6	440	600	580	700	16	2.0-6.0	N.A.	N.A.	2.0-5.0	N.A.	N.A.	N.A.	N.A.
HR600Y780T-FB	780	FB		RD	1.8	6	600	800	780	900	14	1.8-6.0	N.A.	N.A.	N.A.	N.A.	N.A.	N.A.	N.A.
CR700Y1180T-medMn	1180	medMn										unknown	unknown	unknown	unknown	unknown	unknown	unknown	unknown
CR340Y590T-RA	590	RA		TD	0.6	2.3	350	480	590		27	N.A.	0.6-2.3	N.A.	N.A.	0.45-2.0	0.6-2.3	N.A.	N.A.
CR400Y600T-RA	600	RA		RD	0.8	2	380	520	590		26	N.A.	0.8-2.0	N.A.	0.8-2.0	N.A.	0.8-2.0	N.A.	N.A.
CR400Y690T-RA	690	RA		RD	0.7	2	400	520	690	800	25	N.A.	0.7-2.0	N.A.	0.7-2.0	N.A.	0.7-2.0	N.A.	N.A.
CR400Y780T-RA	780	RA		RD	0.8	2	400	570	780		22	N.A.	0.8-2.0	N.A.	0.8-2.0	N.A.	0.8-2.0	N.A.	N.A.
CR600Y980T-RA	980	RA		RD	1	2	600	850	980	1130	20	N.A.	1.0-2.0	N.A.	1.0-2.0	N.A.	N.A.	N.A.	1.0-2.0
CR820Y1180T-RA	1180	RA		RD	1	2	820	1100	1180	1330	12	N.A.	1.0-2.0	N.A.	1.0-2.0	N.A.	N.A.	N.A.	1.0-2.0
CR1000Y1500T-RA	1500	RA		RD	1	2	1000		1500			unknown	unknown	unknown	unknown	unknown	unknown	unknown	unknown
CR480Y950T-TW	950	TW		RD	1	2	480	600	950		45	N.A.	1.0-2.0	N.A.	N.A.	N.A.	N.A.	N.A.	N.A.
CR860Y1100T-MS	1100	MS		RD	1	1.6	860	1120	1100	1320	3	N.A.	1.0-1.6	N.A.	N.A.	N.A.	1.0-1.6	N.A.	N.A.
CR950Y1180T-MS	1180	MS		RD	1	2.1	950	1200	1180	1400	3	N.A.	1.0-2.1	N.A.	N.A.	N.A.	1.0-1.8	N.A.	N.A.
CR1030Y1300T-MS	1300	MS		RD	1	2.1	1030	1330	1300	1550	3	N.A.	1.0-2.1	N.A.	N.A.	N.A.	1.2-1.6	N.A.	N.A.
CR1150Y1400T-MS	1400	MS		RD	1	2.1	1150	1400	1400	1600	3	N.A.	1.0-2.1	N.A.	N.A.	N.A.	1.0-1.8	N.A.	N.A.
CR1000Y1470T-MS	1470	MS		TD	0.8	2	1000		1470		5	N.A.	0.8-2.0	N.A.	N.A.	N.A.	N.A.	N.A.	N.A.
CR1200Y1470T-MS	1470	MS		RD	1	2.1	1200	1520	1470	1750	3	N.A.	1.0-2.1	N.A.	N.A.	N.A.	1.0-2.0	N.A.	N.A.
CR1350Y1700T-MS	1700	MS		RD	1	2.1	1350	1700	1700	2000	3	N.A.	1.0-2.1	N.A.	N.A.	N.A.	1.0-2.0	N.A.	N.A.
CR1550Y2000T-MS	2000	MS		RD			1550		2000			unknown	unknown	unknown	unknown	unknown	unknown	unknown	unknown
HR900Y1180T-MS	1180	MS		RD	2	3	900	1150	1180	1400	5	2.0-3.0	N.A.	N.A.	N.A.	N.A.	N.A.	N.A.	N.A.
PHS-CR500T-LA	500	PQS	after	TD	1	2	340	450	410		15	N.A.	N.A.	N.A.	0.5-2.5	N.A.	N.A.	N.A.	1.0-2.0
PHS-CR600T-LA	600	PQS	after	TD	1	2	370	550	550		11	N.A.	1.0-2.0	N.A.	N.A.	N.A.	N.A.	N.A.	1.0-2.0
PHS-CR1500T-MB	480	PHS	before	RD	0.7	3	300	480	480	800	12	N.A.	0.7-3.0	N.A.	0.7-2.5	N.A.	N.A.	N.A.	1.0-3.0
PHS-CR1900T-MB	500	PHS	before	TD	1	2.1	300	520	450	650	16	N.A.	1.0-2.1	N.A.	1.0-2.0	N.A.	N.A.	N.A.	N.A.
PHS-CR1500T-MB	1500	PHS	after	TD	0.7	3	950	1250	1300	1700	5	N.A.	0.7-3.0	N.A.	0.7-2.5	N.A.	N.A.	N.A.	0.7-3.0
PHS-CR1800T-MB	1800	PHS	after	RD	0.7	2						N.A.	0.6-2.0	N.A.	N.A.	N.A.	N.A.	N.A.	N.A.
PHS-CR1900T-MB	1900	PHS	after	TD	1	3					5	N.A.	1.0-3.0	N.A.	1.0-2.0	N.A.	N.A.	N.A.	1.0-3.0
PHS-HR1500T-MB	500	PHS	before	TD	2	8	300		500	750	12	2.0-8.0	N.A.	N.A.	N.A.	N.A.	N.A.	N.A.	N.A.
PHS-HR1900T-MB	520	PHS	before	TD	2	4	300		520	850	10	2.0-4.0	N.A.	N.A.	N.A.	N.A.	N.A.	N.A.	N.A.
PHS-HR1500T-MB	1500	PHS	after	TD	2	6						2.0-6.0	N.A.	N.A.	N.A.	N.A.	N.A.	N.A.	N.A.
PHS-HR1900T-MB	1900	PHS	after	TD	2	4						2.0-4.0	N.A.	N.A.	N.A.	N.A.	N.A.	N.A.	N.A.
PHS-CR1000T-MB	1000	PHS-HD	after	RD	1	2	800	950	950		5	N.A.	1.0-2.0	N.A.	N.A.	N.A.	N.A.	N.A.	1.0-2.0
PHS-CR1200LA-MB	1200	PHS-HD	after	TD	0.75	3						N.A.	N.A.	N.A.	N.A.	N.A.	N.A.	N.A.	0.75-3.0

Table 5.1: *Steel E-Motive Materials Portfolio*

5.1.1 Steel Selection Criterion

The following information list is important when determining the suitability (and availability) of a steel type and grade for component design and functionality requirements:

- Hot-rolled, cold-rolled, and coating availability.
- Thickness and width capabilities.
- Mechanical properties and ranges.
- Joining and assembly requirements.
- Manufacturing process specifications.

AHSS grade development has been driven by the need to balance better performance in ever-more challenging crash regulations, while reducing weight to achieve emissions targets. Third Generation (3rd Gen) AHSS address the automotive industry's need for steels with both higher strength and enhanced formability, allowing more complex geometries to be produced with cold forming, and for some applications, providing an alternative option to press hardening. Even newer versions of the Dual phase (DP), Complex Phase (CP) and Transformation Induced Plasticity (TRIP) steels have been updated to provide additional formability within the same strength range, compared to conventional High Strength Low Alloy (HSLA) steels.

Detailed information about AHSS grades is available at the WorldAutoSteel AHSS Application Guidelines website, at www.ahssinsights.org.

To complement the product portfolio, WorldAutoSteel contributed several advanced fabrication technologies that helped achieve manufacturing feasibility, while also reducing the material production emissions due to higher material utilization or conversion yields. This is a key objective in the project, evidenced by reduced thickness and high-yield fabrication processes selected for many of the vehicle components.

5.1.2 AHSS Grade Development Sequence

The Second Generation (2nd Gen) AHSS grades have essentially a fully austenitic microstructure and rely on a twinning deformation mechanism for strength and ductility. Austenitic stainless steels have similar characteristics, so they are sometimes grouped in this category as well. Second Gen AHSS grades are typically higher-cost grades due to the complex mill processing to produce them as well as being highly alloyed, the latter of which leads to welding challenges.

Third Gen AHSS grades were developed in collaboration with global contributions from research institutes, universities, steel producers and auto makers. Individual automakers may have proprietary definitions of 3rd Gen AHSS grades containing minimum levels of strength and ductility, or specific balances of microstructural components, but no globally accepted standards exist. Starting around 2010, several international consortia formed with the hopes of achieving the next-level properties associated with 3rd Gen steels in a production environment.

Third Gen steels have improved ductility in cold forming operations compared to other steels at the same strength level. As such, they may offer a cold forming alternative to press hardening steels in some applications. Also, while 3rd Gen steels are intended for cold forming, some are appropriate for the hot stamping process.

Like all steel products, 3rd Gen properties are a function of the chemistry and mill processing conditions. There is no one unique way to reach the properties associated with 3rd Gen steels. Steelmakers use their available production equipment with different characteristics, constraints, and control capabilities. Even when attempting to meet the same OEM

specification, steelmakers will take different routes to achieve those requirements. This may lead to each approved supplier having properties which fall into different portions of the allowable range. Manufacturers should use caution when switching between suppliers, since dies and processes tuned for one set of properties may not behave the same when switching to another set, even when both meet the OEM specification.

There are three general types of 3rd Gen steels currently available or in development. All rely on the TRIP effect. Applying the quenching and partitioning (QP) process to the other grades below may create additional high-performance grades.

TRIP-Assisted Bainitic Ferrite (TBF) and Carbide-Free Bainite (CFB)

- TRIP-Assisted Bainitic Ferrite (TBF) and Carbide-Free Bainite (CFB) are descriptions of essentially the same grade. Some organizations group Dual Phase – High Ductility (DP-HD, or DH) in with these. Their production approach leads to an ultra-fine bainitic ferrite grain size, resulting in higher strength. The austenite in the microstructure allows for a transformation induced plasticity effect leading to enhanced ductility.

Quenched and Partitioned Grades, Q&P or simply QP

- Quenching and Partitioning (QP) describes the processing route resulting in a structure containing martensite as well as significant amounts of retained austenite. The quenching temperature helps define the relative percentages of martensite and austenite while the partitioning temperature promotes an increased percentage of austenite stabile room temperature after cooling.

Medium Manganese Steels, Medium-Mn, or Med-Mn

- Medium Manganese steels have a Mn content of approximately 3% to 12%, along with silicon, aluminium, and microalloying additions. This alloying approach allows for austenite to be stable at room temperature, leading to the TRIP effect for enhanced ductility during stamping. These grades are not yet widely commercialized.

5.2 Definition of Steel Types Found in the Steel E-Motive Materials Portfolio

Since the terminology used to classify steel products varies considerably throughout the world, the Steel E-Motive materials portfolio uses a combination of methods to define the steels. Each steel grade is identified by metallurgical type, yield strength and sequenced by minimum ultimate tensile strength (in MPa). To illustrate, DP 500/800 means a Dual Phase steel type with 500 MPa minimum yield strength (YS) and 800 MPa minimum ultimate tensile strength (TS).

5.2.1 Mild (conventional) Steels

Mild steels are the conventional steels historically used in automotive applications and are characterized by low strength and good formability. Drawing Quality (DQ) and Aluminum Killed (AKDQ) steels are examples and often serve as a reference base because of their widespread application and production volume.

5.2.2 Interstitial-Free (IF) Steels (Low strength and high strength)

IF steels have ultra-low carbon levels which reduce their yield strengths, while achieving high work hardening rates. This results in steels with excellent formability as compared to mild

steels. The higher strength grades of IF steel are widely used for structural applications requiring complex geometries and closure applications with more features compared to an aluminum product.

5.2.3 Bake Hardenable (BH) Steels

Bake Hardenable (BH) steels grades are conventional High Strength Steels that exhibit a bake hardening effect. BH steels exhibit an increase in yield strength after room-temperature stamping followed by processing through a thermal cycle comparable to the time-temperature profile used in paint curing (or baking) – approximately 170 °C for 20 minutes. Bake hardenability is characterized by determining the Bake Hardening Index.

BH steel grades have yield strength at shipment from the steel mills of 180 MPa to 300 MPa (approximately 25 ksi to 45 ksi). The grades at the lower strength levels are capable of being produced with a Class A surface finish and are used in applications where dent resistance is desired in thin sheet steel. Applications for the higher strength BH steels include structural parts where Class A surface is not required. The higher strength after forming and baking is the reason automakers might use these in body structure applications, potentially contributing to vehicle lightweighting efforts.

These grades work harden approximately 30 MPa when 2% strain is introduced, either from stamping or during a tensile test, which is similar to dent resistant IF-HS. In contrast to IF-HS, the paint-bake cycle after forming results in an additional yield strength increase. The minimum strength increase from baking is specified by some automakers as 20 MPa to 35 MPa, measured after applying a defined level of strain.

Higher yield strength directly improves the dent performance. Even though BH grades and their non bake hardening counterpart IF-HS grades may have similar yield strength and thickness after forming, BH steels will show superior dent resistance due to the increase in yield strength from the paint baking operation.

Ferrite is the main microstructural phase of BH steels. The strengthening from the paint bake cycle is due to the controlled amount of carbon remaining in solid solution (on the order of 25 ppm) when the steel leaves the production mill. At the baking temperatures after the part is formed, the dissolved carbon migrates to pin any free dislocations created from stamping. This increases the yield strength of the formed part for increased dent resistance. Formability does not suffer since the strength increase occurs after stamping.

5.2.4 High-Strength Low-Alloy (HSLA) Steels

High-strength low-alloy (HSLA) steels were developed as an alternative to alloyed steel, where higher strength was achieved with a much lower alloy content. Lower carbon content and lower alloying content leads to increased ductility, toughness, and weldability compared with grades achieving their strength from only solid solution strengthening such as C-Mn steels. Lower alloying and elimination of post-forming heat treatment makes HSLA steels an economical approach for many applications.

HSLA steels have a microstructure that is mostly precipitation-strengthened ferrite, with the amount of other constituents like pearlite and bainite being a function of the targeted strength level. This steelmaking approach allows the production of sheet steels with yield strength levels now approaching 800 MPa. HSLA steels increase strength primarily by micro-alloying elements contributing to fine carbide precipitation, substitutional and interstitial strengthening, and grain-size refinement. Carbide precipitation and grain-size refinement is achieved with only 0.05% to 0.10% of titanium, vanadium, and niobium, added alone or in combination with each other.

HSLA steels are found in many body-in-white and underbody structural applications where strength is needed for increased in-service loads.

5.2.5 Dual Phase (DP) Steels

DP steels consist of multiple microstructural phases (one a soft phase “Ferrite”, the other a hard phase “Martensite”). The soft ferrite phase is generally continuous, giving these steels excellent ductility. When these steels deform, strain is concentrated in the lower-strength ferrite phase surrounding the islands of martensite, creating the unique high initial work-hardening rate (n-value) exhibited by these steels. Here, the forming process actually increases the strength level of the part, compared to the initial strength level of the steel.

Higher strength DP steels are typically achieved by increasing the martensite volume fraction. Depending on the composition and process route, steels requiring enhanced capability to resist cracking on a stretched edge (as typically measured by hole expansion capacity) can have a microstructure containing significant quantities of bainite.

The work hardening rate plus excellent elongation creates DP steels with much higher ultimate tensile strengths than conventional steels of similar yield strength. For example, DP steels exhibit higher initial work hardening rate, higher ultimate tensile strength, and lower YS/TS ratio than an HSLA with comparable yield strength.

5.2.6 Transformation-Induced Plasticity (TRIP) Steels

Another multi-phase steel with complex metallurgy and production processing, TRIP steels use higher quantities of carbon and other alloying elements than DP steels to achieve uncommon micro-structural phases at or below ambient temperature. TRIP steels contain metastable Austenite, that transforms to the hard phase Martensite during plastic strain of metal forming or crash. During deformation, the TRIP steel microstructure results in higher work hardening rates at higher strain levels, beyond that of DP steels, providing a slight advantage over DP in the most severe stretch forming applications. TRIP steels therefore can be engineered or tailored to provide excellent formability for the manufacturing of complex part shapes and exhibit high work hardening during crash deformation for excellent crash energy absorption. The additional alloying requirements of TRIP steels degrade their resistance spot-welding behavior.

5.2.7 Ferritic-Bainitic (FB) Steels (including Stretch Flangeable - SF)

FB steels have a very fine dual-phase microstructure, achieved from additional alloying and steel processing requirements. These steels are sometimes utilized to meet specific customer application requirements defining Stretch Flangeable (SF) or High Hole Expansion (HHE) capabilities for improved edge stretch capability. They are very formable and are available as hot-rolled products.

The primary advantage of FB steels over HSLA and DP steels is the improved stretchability of sheared edges as measured by the hole expansion test (λ). Compared to HSLA steels with the same level of strength, FB steels also have a higher strain hardening exponent (η) and increased total elongation. Because of their good weldability, FB steels are good candidates for tailored blank applications. These steels also are characterized by both good crash performances and good fatigue properties.

5.2.8 Complex Phase (CP) Steels

CP steels typify the transition to advanced metallurgical complexity to achieve very high ultimate tensile strengths while maintaining reasonably good ductility. The microstructure of CP steels typically contain small amounts of martensite, retained austenite and pearlite within a ferrite/bainite matrix. A thermal cycle that retards recrystallization and promotes the formation of carbo-nitrides precipitation results in extreme grain refinement. DP and TRIP steels do not rely on precipitation hardening for strengthening, and thus the ferrite in these steels is relatively soft and ductile. In CP steels, carbo-nitride precipitation increases the ferrite strength. For this reason, CP steels show significantly higher yield strengths than DP steels at equal tensile strengths of 800 MPa and greater.

Minimizing retained austenite helps improve local formability, since forming steels with retained austenite induces the TRIP effect producing hard martensite. CP steels are characterized by high energy absorption and high residual deformation capacity, excellent features for crash structures including frame rails, pillar reinforcements, fender and bumper beams.

5.2.9 Martensitic (MS) Steel

Martensitic steels are characterized by a microstructure that is mostly all martensite, but possibly also containing small amounts of ferrite and/or bainite. Steels with a fully martensitic microstructure are associated with the highest tensile strength – grades with a tensile strength of 2000 MPa are commercially available, and higher strength levels are under development. Within the group of multiphase steels, MS steels show the highest tensile strength levels.

To create MS steels, the austenite that exists during hot-rolling or annealing is transformed almost entirely to martensite during quenching on the run-out table or in the cooling section of the continuous annealing line. Adding carbon to MS steels increases hardenability and strengthens the martensite. Manganese, silicon, chromium, molybdenum, boron, vanadium, and nickel are also used in various combinations to increase hardenability. This martensite structure can also be developed with post-forming heat treatment. MS steels are often subjected to post-quench tempering (re-heating) to improve ductility, so that extremely high strength levels can be achieved along with adequate ductility for certain forming processes like Roll Forming.

5.2.10 Twinning-Induced Plasticity (TWIP) Steel

TWIP steels have a high manganese content (17-24%) that causes the steel to be fully austenitic at room temperatures. A large amount of deformation is driven by the formation of de- formation twins. This deformation mode leads to the naming of this steel class. The twinning causes a high value of the instantaneous hardening rate (n value) as the microstructure becomes finer and finer. The resultant twin boundaries act like grain boundaries and strengthen the steel. TWIP steels combine extremely high strength with extremely high stretchability. The n value in- creases to a value of 0.4 at an approximate engineering strain of 30% and then remains constant until both uniform and total elongation reach 50%. The tensile strength is higher than 1000 MPa.

5.2.11 Press-Hardened (Hot Formed) Steel (PHS)

Press hardening steels are typically carbon-manganese-boron alloyed steels. They are also commonly known as Press Hardening Steels (PHS) or hot-stamped steels and are characterized by boron levels between 0.002% and 0.005%. They have been in use since the 1990s in to solve the need for very high strength intrusion resistant crash members,

although Hot Stamping as we know it today was developed in 1970s in Sweden. The most used steel since then has been 22MnB5 with slight modifications. The name 22MnB5 means approximately 0.22 wt-% C, approximately (5/4) = 1.25% wt-% Mn, and B alloying, which is why they are often referred to as Boron steels.

For 22MnB5 to reach its high strength after quenching, it must be austenitized first, which means heated above the austenite transformation temperature. During heating, ferrite begins to transform to austenite, and then the Austenite transforms to martensite or other microstructures as the steel is cooled. The microstructures produced from this transformation depends on the cooling rate; achieving the "fully hardened" condition in PHS grades requires an almost fully martensitic microstructure, which means a rapid "quench" or "critical cooling rate". Rapid cooling results also results in parts that retain critical dimensional characteristics, while achieving extremely high strength levels. For energy absorbing applications, there are also tailored parts with "soft zones", where areas on a component will be intentionally developed with other microstructures to ensure higher energy absorption. This is another example of steel's ultimate tunability, a feature that cannot be replicated with other materials.

There are two types of press-hardening or hot forming applications, that will be described in more detail in the Steel E-Motive Manufacturing Processes Section:

- Direct Hot-Forming: the part is formed at very high temperatures (above 850^{o}C), followed by quenching (rapid cooling) to ambient temperature.
- Indirect Hot-Forming: pre-forms the part at room temperature to a high percentage of the final part shape followed by additional high temperature forming and quenching. The press hardened steels for this process must begin with better cold forming properties than is necessary in direct hot forming

5.3 Steel E-Motive Manufacturing Processes

Steel E-Motive targets Mobility as a Service (MaaS) providers, whose primary interest is achieving a profitable business model premised on lowest Total Cost of Ownership (TCO). One of the enablers of low TCO is the ability to utilize the existing automotive manufacturing infrastructure to minimize investment costs and utilize already paid-for assets. The ability to utilize these assets also eliminates the need to produce new equipment that can be energy-intensive and hence unfriendly to the environment. Steel E-Motive can be a catalyst towards achieving Net Zero emissions in 2050, and hence manufacturing process selection is critical to that ambition.

In the automotive industry, conventional stamping processes are commonly used to produce parts in the vehicle body structure. But these processes are also characterized by significant levels of engineered scrap, which translate into greater steel production and emissions associated with these parts. Therefore, there is urgency to form parts via fabrication processes that utilize material production more efficiently. Alternatives to stamping include press hardening, roll forming, roll stamping, hydroforming, and others. Various grades of sheet steel material for these processes are available in the form of coils, and each coil can represent a single material sheet (thickness and grade), laser welded coils, or tailor rolled coils.

Below are brief descriptions of each the various material production processes that were considered for various Steel E-Motive components.

5.3.1 Laser Welded Blanks

A laser welded blank is two or more sheets of steel butt seam-welded together into a single blank which is then stamped into a part. As a result of laser welding technology, a single blank can contain different steel grades, different steel thicknesses, or both. Laser welded blank technology allows for the placement of various steel grades and thicknesses within a specific part, placing steel's attributes where they are most needed and removing weight that does not contribute to part performance. For large parts such as a door ring, individual blanks are joined together prior to stamping. The smaller blanks typically achieve the geometry of the final part much more efficiently, compared to blanking the entire door ring from one blank, and then trimming the center of the ring, creating excessive engineered scrap.

Figure 5.2 shows a laser welded door ring with multiple grades and thicknesses. This technology allowed for a reduction in panel thickness in non-critical areas, thus contributing to an overall weight reduction of the part. The lower strength product in the bottom section of the B-Pillar helps dissipate the crash energy in the event of a side impact, playing a key role in crash energy management.

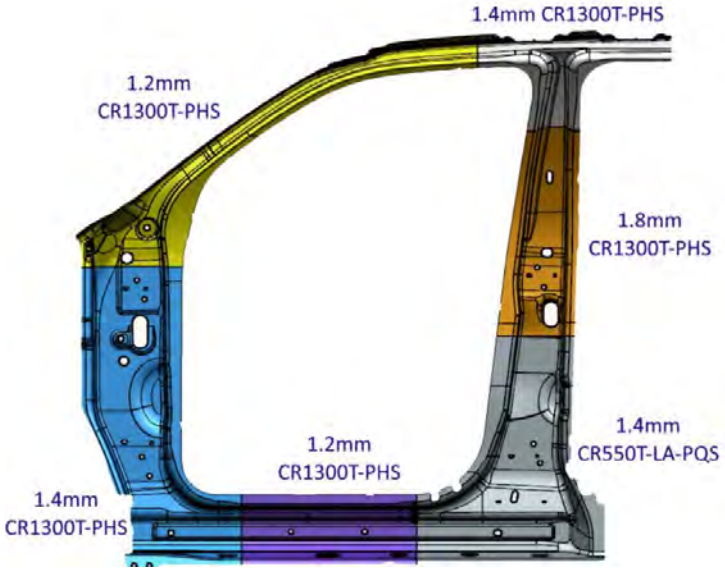

Figure 5.2: *Example of a laser weld blank used for a body side door ring.*

5.3.2 Laser Welded Coil

Laser welded coil is a process of producing a continuous coil of steel from individual separate coils of varying thickness and grades. The basic process takes separate coils prepares the edges, and laser welds these together and re-coils the strip ready for other blanking or to be used as a continuous feed in a transfer press line. See Figure 5.3.

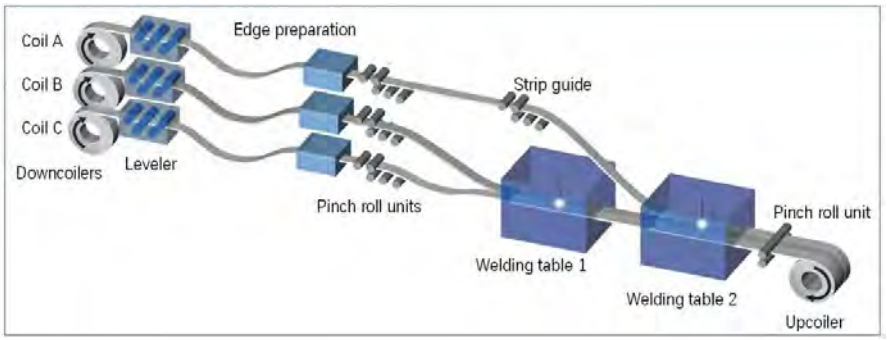

Figure 5.3: *Laser welded coils production process.*

5.3.3 Tailor Rolled Coil

This is a manufacturing process of flexible cold strip rolling by varying the gap between two rolls which allows for different strip thicknesses in the direction of rolling (Figure 5.4). The accurate measuring and controlling technology ensures that strip thickness tolerances are achieved.

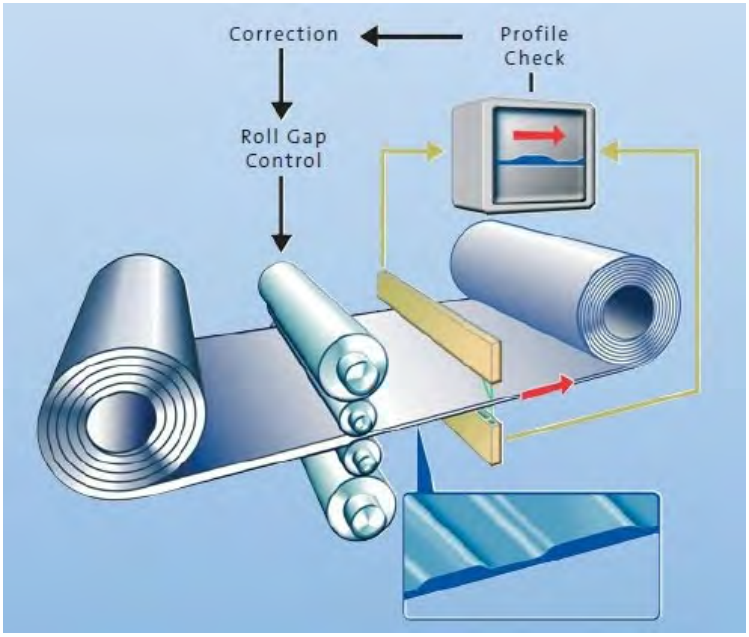

Figure 5.4**:** *The principle of producing a Tailor Rolled Coil.*

A tailor rolled coil can be either used for blanking operations (for stamping or tubular blanks) or can be directly fed into a roll forming line.

5.3.4 Conventional Electric-Resistance-Welded (ERW) Tube

ERW tubes are produced specifically for hydroforming. The process can utilize either a standard single thickness and grade coil, a laser welded coil or a tailor rolled coil, as shown in Figure 5.5.

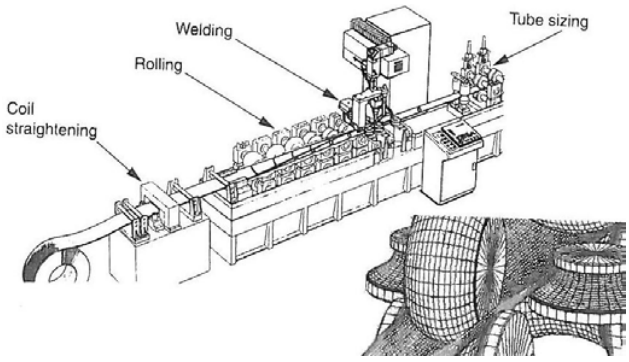

Figure 5.5: *Typical roll form layout for making ERW tubes*

5.3.5 Tubular Blanks (Laser-Welded)

Laser welded tubes used in the hydroforming process are made from individual blanks. This blank is then formed into a tube of constant diameter or a tapered tube. Manufacturing precision welded tubes typically involves continuous roll forming followed by a longitudinal weld created by laser welding.

The bending behaviour of tube depends on both the tubular material and the bending technique. The weld seam is also an area of non-uniformity in the tubular cross section, and therefore influences the forming behaviour of welded tubes. The recommended procedure is to locate the weld area in a neutral position during the bending operation.

Tubular components can be a cost-effective way to reduce vehicle weight and improve safety. Closed sections are more rigid, resulting in improved structural stiffness. Automotive applications include seat structures, cross members, side impact beams, bumpers, engine subframes, suspension arms, and twist beams. All AHSS grades can be roll formed and welded into tubes with large D/t ratios (tube diameter / wall thickness); tubes having 100:1 D/t with a 1mm wall thickness are available for Dual Phase and TRIP grades (example shown in Figure 5.6).

Due to the cold working generated during tube forming, the formability of the tube is reduced compared to the as-received sheet. The work hardening during tube forming increases the yield strength and the tensile strength, thereby allowing the tube to be a structural member. Successful bending requires aligning the targeted radii with the available elongation of the selected steel grade. Subsequent operations like flaring, flattening, expansion, reduction, die forming, bending and hydroforming must consider the tube properties rather than the properties of the incoming flat sheet.

AHSS tubes provide excellent engineering properties suitable for structures, offering competitive advantage through high-energy absorption, high strength, low weight, and cost-efficient manufacturing.

Figure 5.6: *DP 590 formed into a tube w/45 degree bend, then laser welded.*

5.3.6 Roll Forming

Roll forming is a continuous forming process which converts a flat steel strip into an engineered shape using consecutive sets of mated rolls. Each roll makes only an incremental change in the form, but the sum of these small steps can be a fairly complex profile. Two common methods are closed roll forming and open roll forming, which describe the way the metal engages each die section. The typical process consists of a steel uncoiler, a hydraulic hole and notch punch, the roll forming machine with several roll stands, a straightener, an automatic cutting station and the final product unload station.

In the forming process, a coil or long individual strips are fed through a roll forming line which converts the flat sheet to a contoured cross-sectional profile. The unique aspect of this approach is the use of consecutive forming stations, each of which nudges the metal towards the desired shape (Figure 5.7). Based on the targeted profile, a computer calculates the optimal placing and shape of the rollers for maximum efficiency and designs the track. The more advanced the desired shape, the more rollers the material goes through. The roll forming line can bend metal, form metal into tubes, create metal maze-like structures, and punch the metal with holes during the process.

For comparison, in conventional stamping the entire part is formed all at the same time, in one press stroke. The part shape – and especially how complex it can be, is limited when the strains from forming exceed what the metal is capable of achieving before splitting. Conversely, in roll formed parts, only a small amount of forming strain is put into the part during each station and even here, only a small section is bent at any given time. Because of this, more complex shapes can be achieved with an appropriately designed roll forming process.

The rollers are precision-contoured metal dies that shape the incoming sheet metal. In most cases, they are also the powered drive rolls that pull the strip through the roll forming unit. These rollers can be as simple as the cylindrical rollers used to roll luggage through airport scanners, or they can take on more intricate shapes. After the final forming station, the strip is sheared to the ordered product length. Typically, no additional work is needed before shipment, since the final form has been achieved.

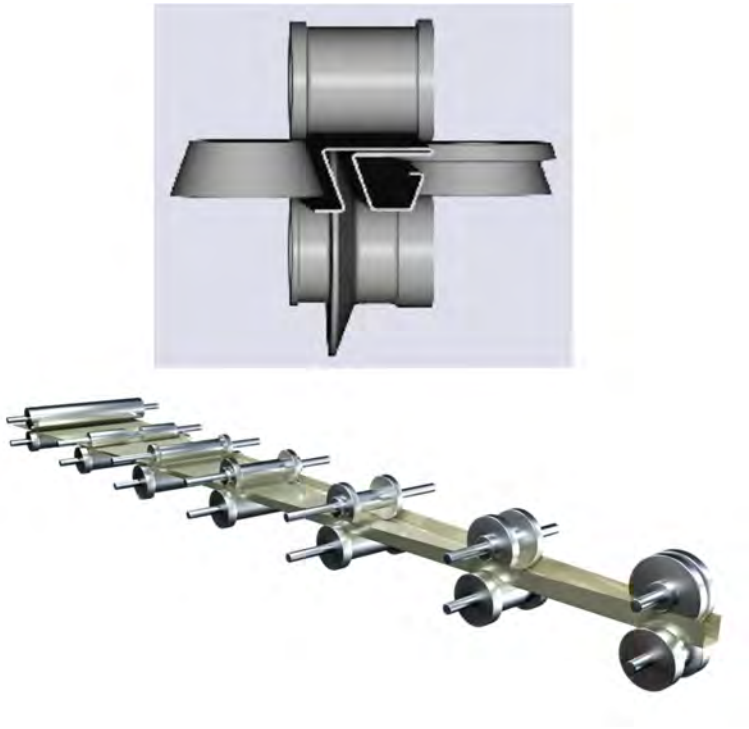

Figure 5.7: *Roll forming rolls and line layout, showing incremental changes in part shape.*

Advantages of the Roll Forming Process

There are a variety of advantages to roll forming. Because of the "assembly line" efficiency of roll forming, long lengths of metal can be produced and cut in large quantities, which reduces cost. Secondary processes such as punching or even welding can be integrated into a single production line. The profiles that can be produced using roll formed sheet steel utilize the material very efficiently, meaning less waste and lower overall steel production emissions, since engineering scrap (waste) is commonly less than 10%.

The roll forming process makes creating lighter-weight steel parts easier compared to other shaping processes, since the wall thickness can be targeted based on the structural needs of the component. Parts can be rolled even if a finish or paint has been applied. While hot forming can produce similarly complex profiles, roll forming is a room temperature process. As such, it avoids the distortion risk associated with hot forming, while being more energy efficient at the same time.

5.3.7 Roll Stamping

Traditional roll forming creates products with essentially uniform cross sections. A newer technique called Roll Stamping enhances the ability to create shapes and features which are not in the rolling axis.

Using a patented process**,** forming rolls with the part shape along the circumferential direction create the desired form, as shown below in Figure 5.8.

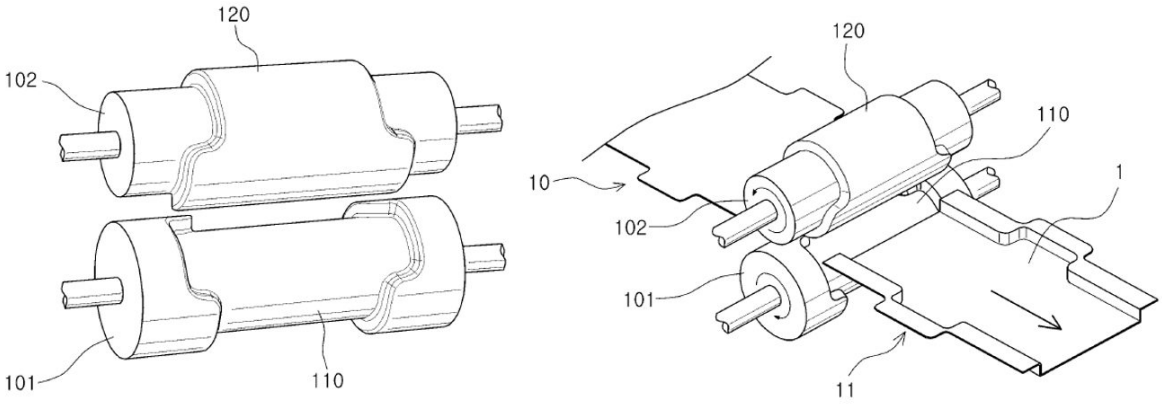

Figure 5.8: *Roll Stamping creates additional shapes and features beyond capabilities of traditional roll forming.*

This approach can be applied to a conventional roll forming line. In the example of an automotive door impact beam, the W-shaped profile in the central section and the flat section which attaches to the door inner panel are formed at the same time, without the need for brackets or internal spot welds (Figure 5.9). Sharp corner curvatures are possible due to the incremental bending deformation inherent in the process.

Figure 5.9**:** *A roll stamped door part formed on a conventional roll forming line eliminates the need for welding brackets at the edges.*

5.3.8 Stress Reverse Forming™

When HSS sheet is press formed, the “springback” phenomenon, in which the sheet tends to return to its original shape after press forming, must be compensated for to maintain accurate part shape. The amount of springback increases with increasing strength levels, and the corresponding tool shape must be designed more precisely to ensure the accurate part shape, which leads to increased time and cost to develop the appropriate tool shape. Corresponding to the need for a cold press forming method that minimizes spring back, the “Stress Reverse Forming™” was developed by a WorldAutoSteel member company. Generally, a small stress is induced into the steel at the bottom dead point (bottom of the press-stroke) during press forming, which leads to the smaller amount of springback and stabilizing part shape. Stress Reverse Forming™ reduces this induced stress by utilizing the Bauschinger effect of steel, which lowers deformation stress after the deformation direction is reversed (Refer to schematic in Figure 5.10.).

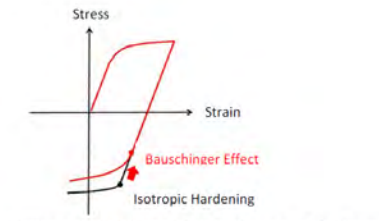

Bauschinger effect (stress–strain relationship) in steel sheet

Figure 5.10**:** *Center roof reinforcement adopted with use of 1470MPa grade cold-rolled UHSS by "Stress Reverse Forming.*

5.3.9 Hydroforming (Tube)

Tube hydroforming creates complex shapes by using internal pressure to expand a tube against a die cavity. Frame rails, engine cradles, roof rails and bows, instrument panel beams, cross members, pillars, and seat frames are among the parts created using hydroforming. Benefits of this approach can include part consolidation, weight reduction, improved stiffness and strength, tighter dimensional tolerances, fewer secondary operations, and reduced cost compared with conventional stamping and welding approaches.

These benefits are highlighted in a truck front end structure shown in Figure 5.11, where hydroforming allowed for consolidation of 31 parts into 18 and resulted in a 31% weight reduction.

Automotive body structures have incorporated hydroformed parts for several years, with recent vehicles using AHSS grades to improve crash energy management and impact performance. Figure 5.11 shows the Nissan Titan hydroformed roof rail:

Figure 5.11: *2016 Nissan Titan XD: Door-To-Roof Support.*

The hydroforming process for tubes usually involves expanding the tube diameter from 3% to 30% depending on the design, materials selected and pressures available for forming.

Tube production commonly utilizes one of three basic methods of hydroforming tubes, categorized by the internal pressure used for the expansion.

In high-pressure tube hydroforming, the tube is placed in the die and the die is closed. Pressurizing the tube now causes the metal to stretch as the circumference increases to conform to the inner circumference of the die – often with tight radii in corners and product features. Higher strength steels may be unable to expand sufficiently to fill the die geometry or create small radii without failure. Furthermore, high pressure could be necessary to obtain the correct geometry with minimum springback or fewer wrinkles compared to low-pressure hydroforming.

Low-pressure tube hydroforming begins with a tube whose circumference is slightly less than the final circumference of the finished geometry. Tube pressurization occurs after placing the tube in an open die, prior to closing. As the die closes, the circumference of the tube changes shape to conform to the closing die. The internal pressure is sufficient to prevent the tube from buckling during the shape change. A small circumference increase combined with a uniform wall thickness means that high strength and lower-formability metals can achieve tighter radii without failure. This low-pressure process is suitable for tubes made from AHSS. This approach results in a change of the shape of the tube cross-section, rather than tube expansion.

5.3.10 Stamping (cold)

In the stamping process, sheet metal is transformed into complex parts using highly specialized computer-aided drafting and manufacturing programs. Sheet metal stamping produces high quality parts quickly and efficiently and is ideal for most large volume production (+ 100,000 parts or vehicles) because conventional presses can produce large stampings at rates up to 15 parts per minute.

The metal is fed into a press, either in blank or coil form, where the stamping tool, also known as a die, creates the desired shape. The die is pressed into or through the metal with tremendous force, and this force is based on the size and strength of the metal being formed (the force used is measured in tons). With a series of operations, the metal can be altered from a relatively simple shape into a complex geometry. Stretch forming is ideal for shallow parts, in that the blank or coil is held tight by binder pressure or beads, and then stretched into the part shape; the stretching adds strength to the final part and typically allowing the smallest of blank sizes. This translates to lower metal waste and production emissions, ever-increasingly important.

Drawing is a more complicated operation and is how vessels or deep depressions are formed. Tension is used to carefully draw the material into a cavity to change its shape. Though the material might stretch while it's drawn, technicians try to avoid stretching as much as possible to keep the material intact. Vehicle oil pans are an example of an automotive part made with drawing.

As the name implies, cold stamping doesn't use heat; instead, the forming and subsequent operations are performed at ambient temperature. Even though no heat is used, final parts come out of the press warm or hot because of the friction that's created between the metal and the die from the force of the press.

When producing parts using a conventional cold stamping process there are various die set-ups that can be considered depending on the final part geometry. Types of dies used are progressive, transfer, compound, and combination. For the Steel E-Motive stamping processes, only a transfer die configuration was considered (Figure 5.12). This process is used for high volume production where several dies are mounted of a common base plate. Material

is fed into the press in blank or coil form and is generally transferred from die to die automatically with robots or carrier arms. When using a single material thickness and grade, a steel coil will be delivered to the stamping plant and blanking operation completed prior to feeding the blank into the transfer press. This can be completed either as part of the transfer press or off-line in a separate operation. When using either a laser welded or tailor rolled blank the blanking operation will normally be completed by the steel service provider and the blank delivered to the stamping plant. The transfer line presses would normally complete the following stamping operations: blank, form, trim, pierce and flange. To keep tooling cost to a minimum the number of stamping dies in a transfer press are kept to the minimum necessary to produce the part. Traditionally the maximum number of stations in a transfer press is six, but through part and die design improvements most OEM's have limited the number of stations to four.

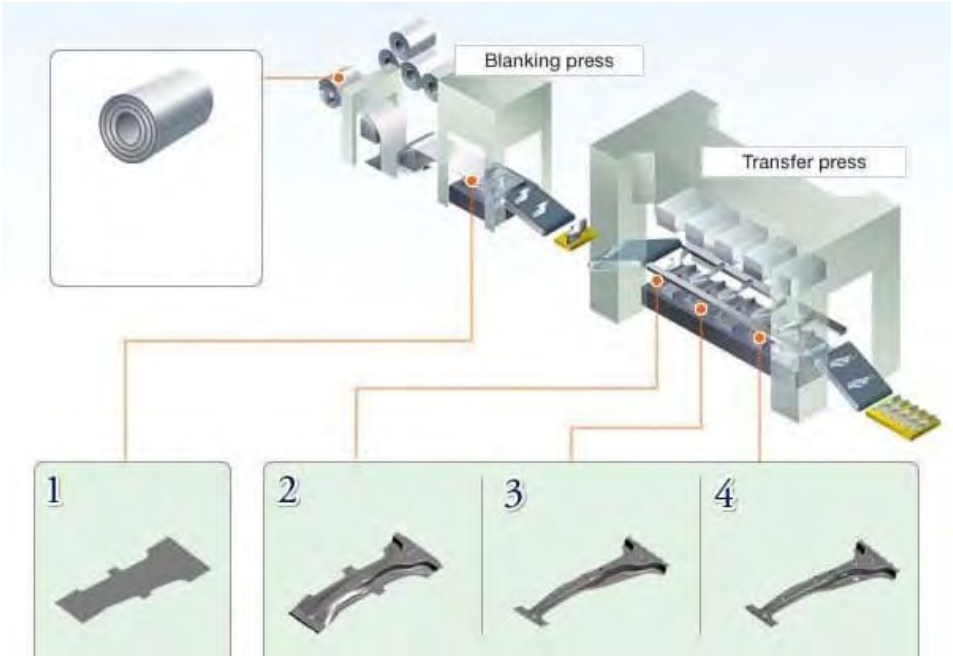

Figure 5.12**:** *Schematic of a typical transfer press layout*

5.3.11 Press Hardening

Press hardening (hot stamping) uses a base material, 22MnB5, ferritic-pearlitic structure, with a tensile strength of approximately of 500 - 650MPA. After the hot stamping, the part develops a martensitic structure and increased strength up to 300% of its original value.

The Direct hot stamping process, shown in Figure 5.13, uses blanks heated in a continuous feed furnace to temperatures between 900 and 950 C°. During this heating process an austenitic structure is formed.

Figure 5.13**:** *Typical direct hot stamping line*

Blanks are then transferred to a stamping die to form the correct geometry. The die is built with cooling lines, to allow rapid cooling of the die and part. This quenching takes place after the forming process has been completed and allows a transformation from the austenitic structure to a martensitic microstructure with a tensile strength of up to 1500 MPa (Figure 5.14).

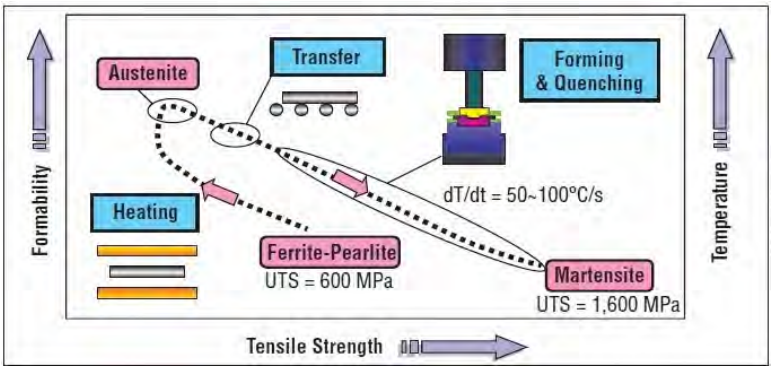

Figure 5.14**:** *Part transformations during the hot stamping process.*

The preparation of the blank for hot stamping is similar to that for a cold stamped part, this applies to both direct and in-direct hot stamping. The difference in the stamping operation comes when the decision is made if the part is to be produced using a direct or indirect stamping process. The indirect process differs from the direct process in that the part can be formed up to 100% of its required geometer prior the transfer of the part to a continuously feed furnace (Figure 5.15). This can be achieved in a similar process as used for cold stamping using a transfer press process. The part is placed in a continuous feed furnace then transferred to the hot stamping die. At this stage there is minimal geometry changes to the part in the die. This process gives minimal post forming trimming operations.

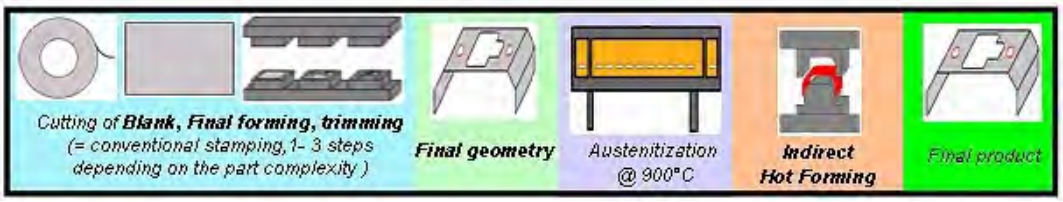

Figure 5.15**:** *In-direct hot stamping process*

This is in contrast to a direct process where no pre-forming of the part is done prior to the hot stamping operation. As minimal stamping operations other than forming can be completed in the direct hot stamping die there is a greater use of post stamping laser trimming operations. In both processes, oxidation of the part due to exposure to the ambient atmosphere may occur a de- scaling operation may be necessary. Due to the extreme hardness of the scale and movement of the blank in the die during the stamping operation, high die wear may result. To address the scale formation in hot stamping operations, steel products are provided that include an Aluminized, Galvanealed, or other barrier coating that prevents oxidation of the surface and formation to address die wear issues and post-process scale removal.

5.4 Various Joining Methods Considered for AHSS and Steel E-Motive

Steel E-Motive concepts can be assembled in an existing automotive manufacturing plant with conventional joining equipment. Aside from the Laser Welding Blank process described in Fabrication Processes, the vehicle components are joined with various processes including resistance spot welding, laser welding, and adhesive bonding. These are briefly described here.

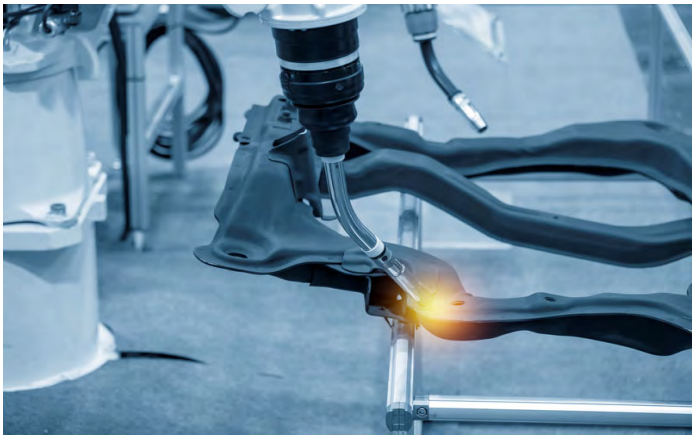

2T and 3T stackups of very high-strength press hardened steels are joined successfully with resistance spot welding in current model production. 2T to 3T stackups have also been joined with little difficulty. The Ohio State University in Columbus, Ohio is presently evaluating the potential for a 5T stackup. Simulated stackups have been achieved with the correct model parameters.

5.4.1 Resistance Spot Welding

Advance High-Strength Steels (AHSS) have been successfully resistance welded in automotive assembly lines for several years. Higher clamping forces are required due to the extreme high strengths of these materials, so these tools must be updated especially in Tier 1 and older assembly shops. Typical weld parameters apply to these materials, but must be more closely controlled, as process variation may impact joint strength and functional performance.

The high strength and hardness associated with AHSS can affect spot weld failure modes during the typical peel testing and chisel testing performed for weld quality evaluation; these “test” failures may occur even though the weld strengths are acceptable for the intended application, so experience is required to interpret these results correctly. With AHSS, full button pulls are less likely due to the high Carbon Equivalent that are likely to produce hard weld nuggets. This fact is compounded by the higher yield strengths of the material that will tend to produce greater stresses concentrating at the edge of the nugget during a peel or chisel tests. Therefore, the conventional modes of testing such as peel and chisel testing may be more likely to initiate interfacial or partial interfacial failure modes.

With AHSS, even full interfacial failures may exhibit high strength, although it may sometimes be challenging to differentiate between an interfacial failure and a “stuck” weld condition (which refers to an unfused bond of unacceptable strength). To improve nugget failure modes with AHSS, the hard martensite must be softened. A simple and effective approach to accomplishing this is to add a temper cycle at the end of the weld, something that can easily be added at the end of the spot-welding cycle.

A sufficient amount of quench time must be included prior to tempering to allow the complete transformation to martensite, and the amount of tempering time and current will dictate how much softening occurs. Of course, the quench time adds cycle time to each weld, so production requirements mandate that this time be kept as short as possible. Depending on how hardenable the steel being welded is, other approaches that slow cooling rates may be helpful. These approaches include current pulsing, current sloping, longer weld times, and short hold times.

The unique physical characteristics of Advanced High Strength Steels (AHSS) present some challenges to welding and bonding processes. AHSS differ from mild steels by chemical composition and microstructure. For high-volume production, it's important to note that these microstructural differences will require different welding parameters for successful joining. Assuming you chose the appropriate welding parameters that allow for a large process window, manufacturing variability will strongly affect the RSW weld quality and performance, and thus additional attention to process control is required.

Material fit-up

One of the great advantages of the RSW process is the action of clamping the material together via the electrode force applied during the process. This fit-up issue, as shown in Figure 5.16, can be very significant especially in welding an AHSS product. In this case the effective required force specified during the process setup is significantly reduced and can

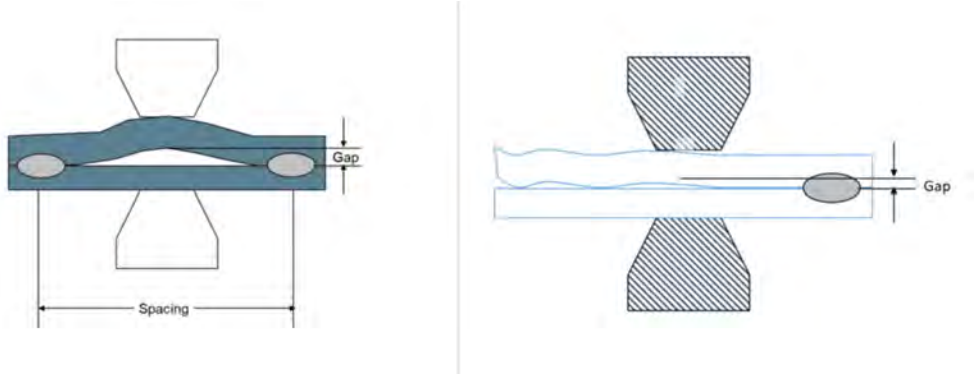

result in an unacceptable weld, over-heating, and severe metal expulsion.

Figure 5.16: *Examples of Pre-Welding Condition/Processing Fit-Up Issues.*

For welding AHSS, higher forces are generally required as a large part of the force is being used to force the parts together in addition to the force required for welding. Also, welding parameters may be set for pre-heating with lower current pulses or current up-slope to soften the material for easier clamping to close the joint gap.

Electrodes Misalignment

In many production applications, electrode misalignment is a common problem during machine set up, and this must be carefully avoided to achieve appropriate nugget shape and strength.

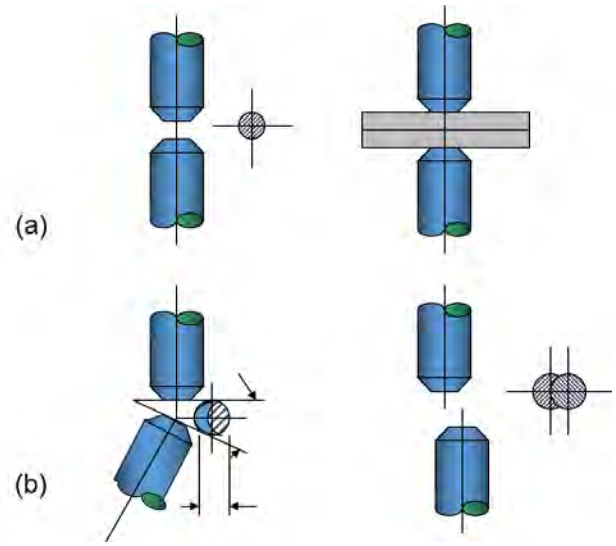

Figure 5.17: *Alignment vs. Misalignment of Electrodes, AHSS and Electrode Geometry*

In these cases, the intended contact between the electrodes is not achieved and thus the current density and the force density (pressure) required for producing an acceptable weld cannot be achieved. With such conditions, overheating, expulsion, sub-size welds and extensive electrode wear will result. Electrode cooling rates are another example of a process variable that must be carefully controlled for AHSS applications; in general, higher cooling rates are necessary to extend electrode life and ensure high joint strength.

Squeeze Time
The squeeze time is the time required for the force to reach the level needed for the specific application. Welding current should be applied only after reaching this force. RSW controllers enable the easy control of squeeze time, just as with the weld time, for example. In many production operations, a squeeze time is used that is too low due to lack of understanding of its function. If squeeze time is too low, high variability in weld quality in addition to severe expulsion will be the result.

The squeeze time required for an application depends on the machine type and characteristics (not an actual welding parameter such as weld time or welding current for example). Some of the more modern force gauges have the capability to produce the curve shown in the Figure so adequate squeeze time will be used. If you do not know what the required squeeze time for your machine/application is, it is recommended to use a longer time.

5.4.2 Laser Welding

Laser welding is growing in more vehicle applications due to inherent weld strength, adaptability to complex weld geometries, and lower part distortion. Automotive applications use a variety of welding joint designs for laser welding in both lap joint and seam butt joint configurations as shown in Figure 5.18. For example, laser butt-welding is used for welding tubes in roll-forming production lines as an alternative method for high frequency induction welding. Seam welds on butt joints need less power from the machine than lap joints due to the smaller weld fusion area, producing less distortion and a smaller heat affected zone (HAZ). Butt joint configurations are more cost efficient, however, the fit up for seam welds can be more difficult to obtain than those of lap joints.

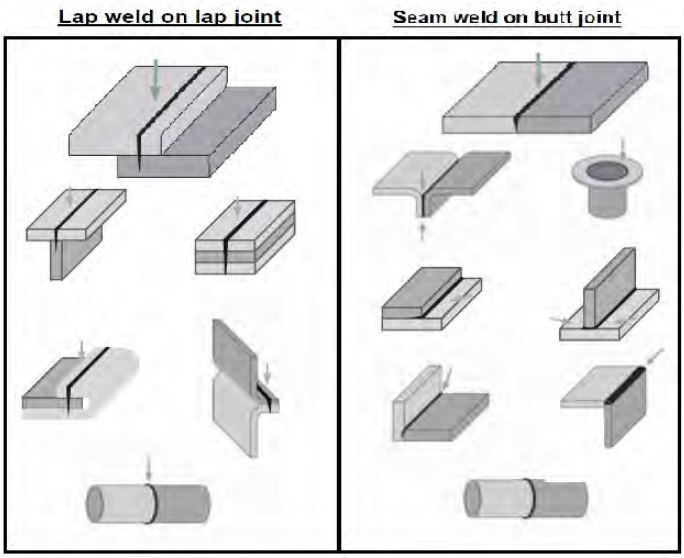

Figure 5.18: *Common seam and joint types for laser welding of automotive applications.*

When seam welding butt joint configurations, a general guideline for fit-up requirements include a gap of 3-10% the thickness of the thinnest sheet being welded, and an offset of 5-12% thickness of the thinnest sheet. Conversely, lap joints can require a gap of 5-10% the thickness of the top sheet being welded.

Laser welding is often used for AHSS lap (overlap) joints, but of course use different parameters compared to seam butt joint configurations. This type of weld is either a conventional weld with approximately 50% penetration in the bottom sheet or an edge weld. Welding is performed in the same way as for mild steels, but the clamping forces needed for a good joint fit-up are higher with AHSS than for mild steels. Lap joints tend to provide a larger process window, which can compensate for some of the manufacturing difficulties with AHSS, including springback and part distortion. To achieve good laser-welded overlap joints for Zn-coated AHSS, a small intermittent gap (0.1-0.2 mm) between the sheets is recommended, which is identical to Zn-coated mild steels. In this way, the Zn does not get trapped in the melt, avoiding pores and other imperfections. An excessive gap can create an undesirable underfill on the topside of the weld.

Studies have shown laser welding Zn-coated steels can be done without using a gap between the overlapped sheets. This is accomplished using dual laser beams. While the first beam is used to heat and evaporate the Zn coating, the second beam performs the welding. The dual laser beam configuration combines two laser-focusing heads using custom-designed fixtures.

AHSS grades can be laser butt-welded and are used in production of tailored products (tailor-welded blanks and tubes). The requirements for edge preparation of AHSS are similar to mild steels – in both cases, a good quality edge and a good fit-up are critical to achieve good quality welds.

If a tailor-welded product is intended for use in a forming operation, a general stretchability test such as the Erichsen Olsen cup test can be used for assessment of the formability of the laser weld. AHSS with tensile strengths up to 800 MPa show good Erichsen test values (Figure 5.19).

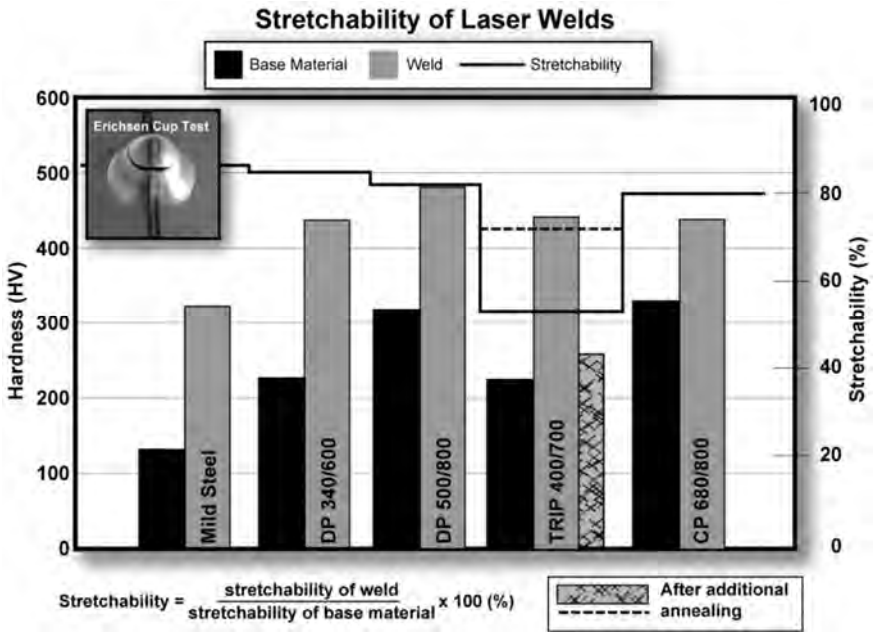

Figure 5.19**:** *Hardness and stretchability of laser butt welds with two AHSS sheets of the same thickness (Erichsen test values describe the stretchability.)*

The hardness of the laser welds for AHSS is higher than for mild steels. However, good stretchability ratios in the Erichsen test can still be achieved when the difference in hardness between weld metal and base metal is only slightly higher for AHSS compared to mild steels. If the hardness of the weld is too high, a post-annealing treatment (using HF-equipment or a second laser scan) may be used to reduce the hardness and improve the stretchability of the weld.

5.4.3 Adhesive Joining

Adhesive bonding is a joining process for metals and non-metals that uses and adhesive or glue, typically in the form of a liquid or a paste. It offers the major advantage of being able to join a wide array of materials but is limited by joint strength and applicable service conditions. Many of the fundamentals are similar to brazing and soldering, in particular the need for wetting and capillary action, and overlapping joint designs that rely on joint area for strength. Adhesives are categorized as thermosetting or thermoplastic. Thermosetting adhesives require a chemical reaction to cure and cannot be remelted once cured. They are the most common adhesives for structural applications and are recommended for AHSS.

Adhesives may be applied a variety of ways, including caulking and spray guns, dipping, rollers, and brushes. Curing may be accelerated by heating or some other energy source. Joining of AHSS with adhesive bonding is a good method to improve stiffness and fatigue strength in comparison to other joining methods (spot welding, mechanical joining, arc welding, and laser welding). If higher joint strengths are needed, the overlapped area may be enlarged. Due to the larger bonding area with adhesive bonding, the local stresses can be reduced and therefore the fatigue strength is increased. These improvements in stiffness and fatigue strength are important factors to consider at the design stage, especially in those cases when AHSS is used to decrease the weight of a component.

In general, the use of AHSS with high-strength structural adhesives will result in higher bond strength than for mild steel if the same sheet thickness is applied. Reduction of sheet thickness will decrease the strength because more peel load will occur.

5.4.4 Non-destructive Evaluation (NDE)

Several non-destructive testing processes have been evaluated for their ability to detect good weld nugget formation, incomplete nugget formation and cracking from LME or hydrogen embrittlement. Laboratory results have been quite repeatable, with UTS phased array showing the most promise. However, trials to conduct similar high-quality evaluations in series production have shown mixed results. Attaching sensors to robot heads interferes little with production, however the in-plant vibration, temperature fluctuations and dirt result in poor reproducibility. When welded components are removed and tested off-line (but still in the production plan), the results are improved and more stable; again phased array shows great promise in this application.

Steel industry partners have modelled LME susceptibility and held production application trials of various NDE methods with the hope of achieving a preferred methodology for automotive OEM's and Tier suppliers. As the technology and application understanding mature, we'll communicate recommendations via the website https://ahssinsights.org/

6.0 Technical Approach

6.1 Overall engineering approach, timing, and organisation

The Steel E-Motive engineering programme was completed within 24 calendar months. The programme was divided into 3 engineering phases with interim review gateways throughout. (Figure 6.1.1). Phase 0 was a 3-month pre-concept study, confirming and validating the vehicle targets, performing vehicle layout and package studies to define the available space for the body structure, develop a preliminary exterior styling them and collate the engineering tools and data inputs which would be used throughout the programme. A 3D FEA topology optimisation was undertaken to determine the key loadpaths for the body structure. A desktop benchmarking study was also conducted to identify autonomous MaaS vehicles currently in development and their basic performance and characteristics. Phase 1 focussed on exploring the vehicle and body concepts based on the outputs from Phase 0. Development was done at complete body level as well as subsystems and modules such as the rocker and longitudinal crush rails. A limited number of steel grades was purposefully considered within Phase 1 to simplify the concept development process. On completion of Phase 1, the body concept designs, and performance were evaluated, validated, and down selected as a primary concept for development in Phase 2. Phase 2 focussed on optimising, refining, and validating the vehicle and body design and performance. The complete steel grade portfolio and fabrication process as detailed in Section 5.0 was applied and considered in Phase 2. The first 12 months of the project were largely undertaken with local and global Covid-19 pandemic restrictions in place. The engineering teams worked remotely (mainly home based), relying on web meetings and email communication. Face-to-face meetings between the WorldAutoSteel members did not occur until Month 14 of the project. In order to keep consortia members regularly informed and updated on technical progress, Engineering Working Groups were established, covering Design, CAE, Target Setting and Life Cycle Assessment. Periodic Working Group meetings were held throughout the Steel E-Motive engineering phases, approximately on a 3 monthly basis. The Working Groups provided an opportunity to brief the consortium members on technical progress as well as enabling members to provide their feedback, thoughts, and suggestions to the engineering teams.

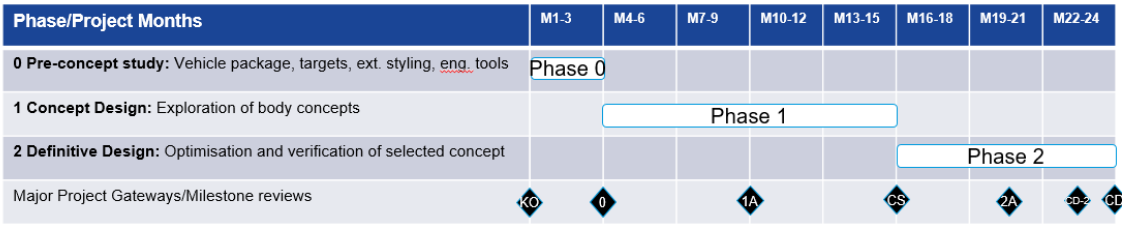

Gateway	Description
KO	**Project Kick off.** Confirmation of project timing, approach, roles, responsibilities, meeting cadence. Data exchange
0	**Phase 0 exit gateway**. Confirmation of targets, package layout, exterior styling theme, engineering approach and tools for Phase 1
1A	**Interim Phase 1 gateway**. Review of vehicle and body performance versus target. Confirmation of programme timing
CS	**Concept Selection**. Selection of vehicle and body for Phase 2. Confirmation that performance targets can be achieved
2A	**Interim Phase 2 gateway.** Review of vehicle and body performance versus target. Confirmation of programme timing
CD-2	**Concept Definition readiness.** Confirm key performance targets are/can be achieved. Confirm design maturity and manufacturability
CD	**Concept Definition.** Final engineering gateway. Confirmation that all performance targets achieved. Concept design is sufficiently mature

Figure 6.1.1 Steel E-Motive engineering programme timing, phases, and gateways

Figure 6.1.2 shows the Steel E-Motive design and engineering maturation steps, from “clean sheet” to completed vehicle and body structure. Firstly, a 3D CAD package study (step A) determined the overall layout of the vehicle, the positioning of the occupants and the main vehicle systems such as battery, chassis, electrical, interior and closures. This defined a “workable” design volume or space for the body structure. This volume was converted to an FEA model (step B). A series of static loadcases (forces) were defined that approximated the loads that the vehicle and body may experience and should therefore be designed for. These include static twist (torsion) and bending, wheel input (e.g., bump,) crashworthiness loads representing front, side, rear, and roof crush. A 3D CAE topology optimisation was performed, where the optimiser software determines the contribution and sensitivity of each element of the design volume based on the applied loads. With the element contribution and sensitivities combined, the main structural loadpaths through the body were defined (step C). The engineering team then interpreted the recommended body structure loadpaths and converted them to a beam model representation (step D). A 3D Finite Element (FE) model of the beam representation was constructed, and simulations performed to verify the structural performance. Finite Element simulations for static stiffness, NVH (modal) and crashworthiness (front, side, rear, and roof crush) confirmed the structural performance, and the model was iterated, varying the main section profiles and joint stiffnesses until a satisfactory level of performance was achieved. The beam model was then converted to shell model, where the design started to resemble a conventional stamped steel body structure (step E). At this stage, design details such as the flanges, panel breaks, manufacturability and assembly were not considered in detail. The objective was to demonstrate that the design concept could achieve the structural performance and weight targets. In parallel with this activity, concepts for body subsystems such as the rocker, battery, longitudinal crush rails were developed using 3D CAD and FEA tools. The subsystem concepts were incorporated into the complete body structure models throughout the development. Once a satisfactory level of structural performance was achieved (end Phase 1), the engineering activities were then focussed on maturing and refining the vehicle and body design to consider the manufacture and assembly and expanding the steel grades and fabrication processes considered to the complete portfolio. A collaborative, 3-day face-to-face workshop event was held to review the body concept design and subsystems to consider the specific steel grades and fabrication processes that would be suitable and enable optimum performance of the structure whist satisfying the manufacture requirements. (step G). The material recommendations from the workshop were then incorporated into the Steel E-Motive concept design and further FEA simulations were performed, focused on more refined steel grade and gauge adjustments to optimise the design until all the performance targets were achieved.

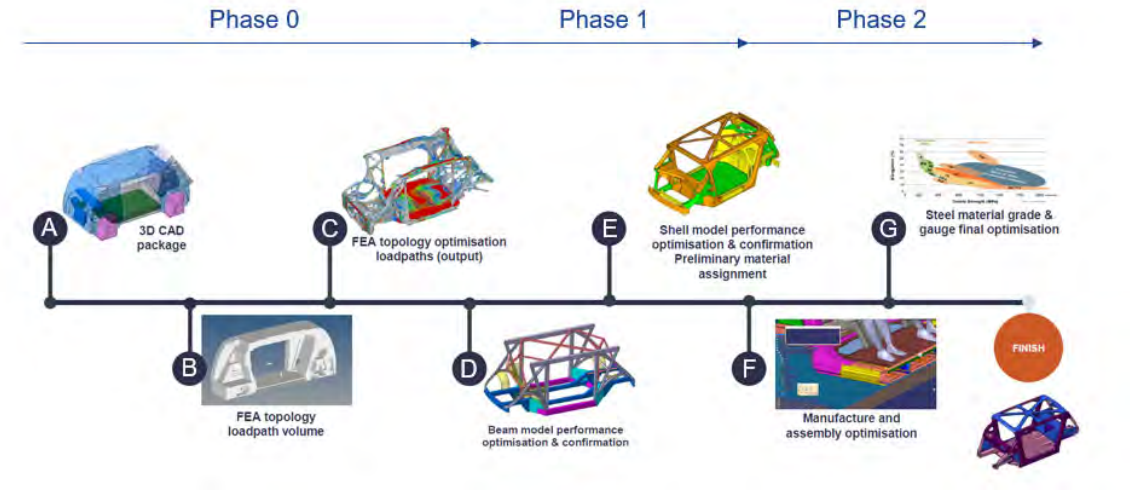

Figure 6.1.2 Engineering approach and maturity of vehicle and body structure concept

6.2 Technical Approach, Phase 0

The objectives of Phase 0 were to establish the basis (or "foundations") for the subsequent body structure design activities in Phases 1 and 2. Design, analysis and engineering activities were undertaken to determine the size, position, and specification of the main vehicle systems such that the body structure could be developed. To assist some of the decision making and the selection of key vehicle system a "MoSCoW" prioritization approach was applied. For each system or topic under consideration, an evaluation was made as to whether the feature or approach was a "must have", "should have", "could have" or "will not have"

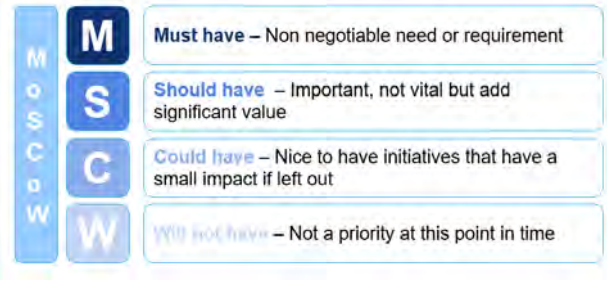

Figure 6.2.1 MoSCoW prioritisation approach.

6.2.1 Powertrain sizing and specification study

The powertrain of battery electric vehicles is typically much larger (by weight and volume) than a typical internal combustion engine. A sizing activity was undertaken to determine the specifications (and therefore size) of the high voltage battery and electric drive unit (EDU). 1D vehicle simulations were performed to determine the EDU and battery specifications that would enable the overall vehicle performance targets (such as range, acceleration, and maximum speed) to be achieved. The e-machine and battery targets were compared to benchmark and reference data and the following powertrain specifications were established.

Requirement	Specification	Comment
Electric drive unit power (kW)	115 (peak)	(230kW continuous)
Electric drive unit driveline	Single speed, fixed ratio, front axle position	
Propulsion battery energy	75kWh	

Propulsion battery energy density (volume)	622 Wh/l for battery module 280 Wh/l for battery pack	Based on market expectation for 2030-2035
Propulsion battery energy density (mass)	377Wh/kg for battery module 266Wh/kg for battery pack	
Propulsion battery voltage	800V	
Number of battery modules		
Battery pack weight target	<360kg	

Figure 6.2.1.1 SEM1 powertrain specification

Electric Drive Units can feature either a fixed single speed gearbox speed or multi-speed. A MoSCoW evaluation suggested single speed EDU for SEM1 would be best suited due to the additional cost, complexity and NVH concerns of muti-speed units.

Figure 6.2.1.2 MoSCoW analysis for SEM1 EDU

The EDU can be positioned to provide traction to the front or rear or both axle of a vehicle. A decision was made to position the single speed EDU to the front axle of SEM1. The primary drivers for this decision being improved package – a rear axle EDU requires more package space with the potential to reduce the available boot volume by 34%. Also, a front axle EDU enables a greater amount of braking energy recovery compared to rear EDU. The vehicle dynamics of a forward braking event result in a dynamic weight shift from the rear to the front axle. This results in a higher braking load and moment on the front axle. With a battery electric vehicle enabling energy recovering to the battery through regenerative braking, a front axle EDU enables a greater proportion of the braking energy to be recovered.

Battery sizing and package considerations

An agnostic approach was taken for the Steel E-Motive battery specification, with no specific cell type of chemistry considered for the battery design. This was intentional, given the rapid pace of battery technology development and the intended, hypothetical production date of 2030-2035 timeframe. The battery was engineered such that different types of battery cells and chemistries could be used within the battery design concept. However, to enable the package, design and structural analysis of the battery, the sizes and specifications as shown in Figure 6.2.1.3 were assumed.

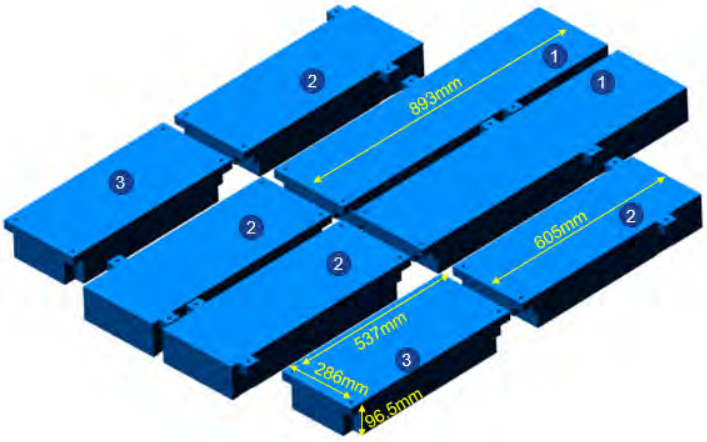

SEM nominal battery capacity: 75kWh
Total module volume: 111.3litres
Module specific power: 674Wh/litre
Module specific weight: 1.78kg/litre
Total module weight = 111.3 x 1.78 = 198.8kg

Figure 6.2.1.3 SEM1 battery module sizing and specifications

6.2.2 Chassis system selection and sizing

The chassis system of a vehicle plays an important role of connecting the wheels and tyres to the body structure and incorporates the steering, suspension, wheels, tyres, brakes subsystems. The chassis design influences several key vehicle attributes, namely, ride comfort, handling and steering feel, noise, vibration & harshness, manoeuvrability, cost, and weight. The chassis also has a secondary contribution to the crashworthiness of a vehicle. Three front suspension types were considered for the Steel E-Motive concept. A multi-link system provides improved wheel control, ride and NVH performance at the expense of higher weight and cost. A Chapman Strut suspension is a relatively simple concept, with low weight and cost with some compromise to wheel compliance and ride. A MoSCoW analysis confirmed that McPherson strut offers the best compromise between cost, ride, NVH and mechanical package. McPherson strut was selected for the front suspension.

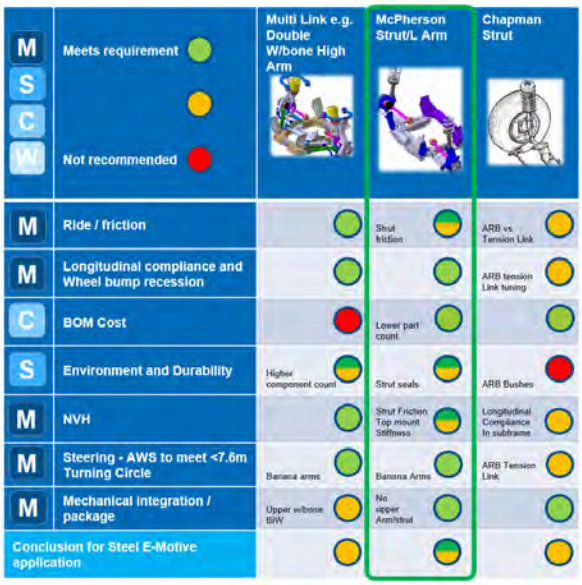

Figure 6.2.2.1 MoSCoW evaluation of front suspension types, confirming selection of MacPherson strut

The wheel and tyre size for SEM1 was specified at 19inches, with an option for 20". This is a larger size than would typically be considered for a vehicle size of SEM1. The reasons for increasing the wheel size were:

- "tall and narrow" profile provides enhanced efficiency, rolling resistance and reduction in frontal area, improving aerodynamics
- balance the overall vehicle style and dimensional proportions, LxWxH

The tyre size was selected as 175/60/R19

Following the selection of suspension type and wheel size, the wheel package envelopes were calculated using 3D CAD. The wheel package envelopes are the volumes that wheels and tyres occupy because of the suspension travel and steering turn envelopes. The volumes must be protected and not encroached by other parts of the vehicle to allow the wheels and tyres to operate unobstructed.

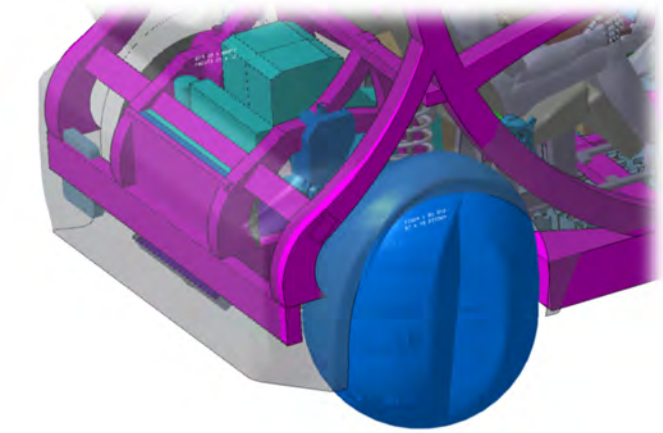

Figure 6.2.2.2 Front wheel and tyre envelopes

Specification	Value	Comment
Front suspension type	McPherson Strut	See MoSCoW analysis
Wheel Bump Stroke (mm)	80	
Wheel Rebound Stroke (mm)	100	
Wheel Rate (inc parasitic/ex tyre - N/mm)	28	
Anti-rollbar type	Passive	
Anti-rollbar dia (mm)	35	
Wheel hub bolt pattern	5 stud	
Wheel Bearing type	Gen 3	
Damper type	Passive, twin tube	
Subframe (fixed/Isolated and fixings)	4 point rigidly mounted	Assume rigidly mounted to contribute to body structure stiffness and strength
Braking System	CAT A	Disc and calliper
Front tyre size	175/60 R19	
Steering System	Rack and Pinion	EPAS Level 5, no steering wheel or column

Figure 6.2.2.2 Front suspension specifications

As per the front suspension, the rear suspension options were evaluated using MoSCoW analysis. One importance consideration for the rear suspension was the requirement for <7.6m turning circle. Given the SEM1 vehicle dimensions, calculations showed that steering of the rear axle was required to meet the vehicle turning circle requirements. The alternative rear suspension options of multi-link, Chapman strut and semi-trailing link have challenges in achieving wheel lock angles. The McPherson strut type was selected for the rear suspension primarily for this reason.

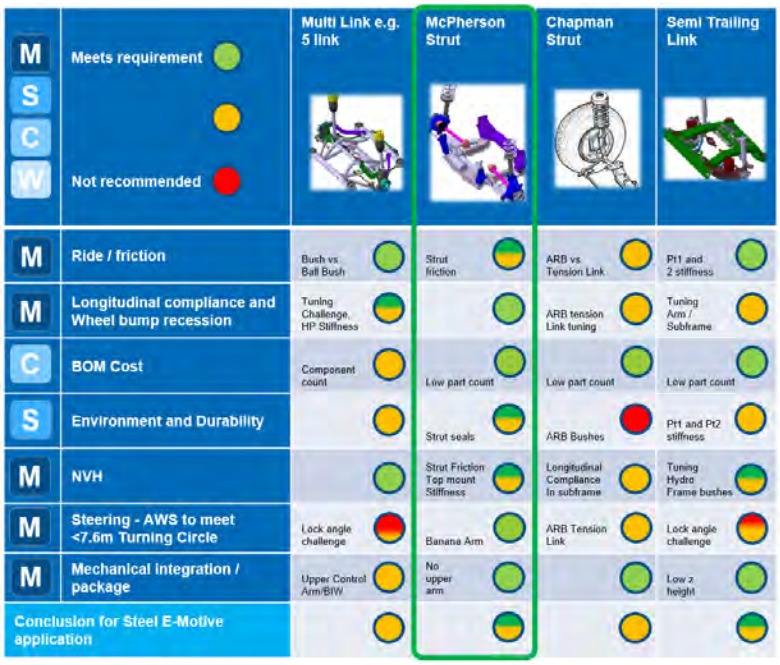

Figure 6.2.2.3 Rear suspension MoSCoW analysis, confirming selection of McPherson strut

Confirmation of achieving the 7.6m turning circle was confirmed by the vehicle steering and suspension geometrical analysis as shown in Figure 6.2.2.4

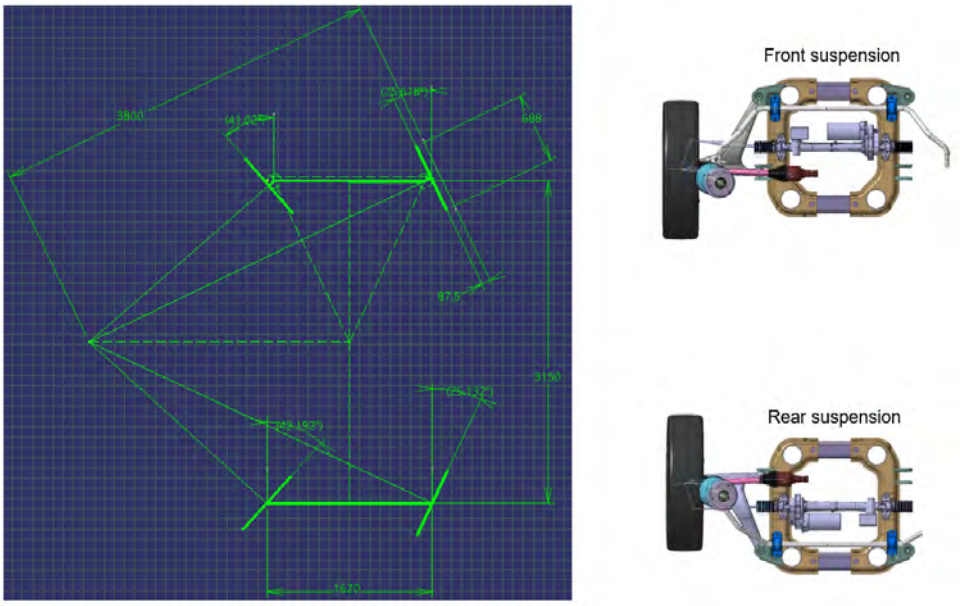

Figure 6.2.2.4 Steering geometry analysis confirming requirement for rear wheel steering (note, this calculation performed for the worst case, long wheelbase variant SEM2)

Figure 6.2.2.5 summarises the overall rear suspension specification for SEM1

Specification	Value	Notes
Geometry	McPherson Strut	See MoScOw analysis
Wheel Bump Stroke (mm)	80	
Wheel Rebound Stroke (mm)	100	
Wheel Rate (inc parasitic/ex tyre - N/mm)	29	
Anti-rollbar type	Passive	
Anti-rollbar dia (mm)	28	
Wheel hub bolt pattern	5 stud	
Wheel Bearing type	Gen 3	
Damper type	Passive, twin tube	
Subframe (fixed/Isolated and fixings)	Rigidly mounted, 4 point	To contribute to body stiffness, NVH and crash performance
Braking System	CAT A	
Steering System	Rack and Pinion	EPAS Level 5, required for <7.6m turning circle requirement

Figure 6.2.2.2 Rear suspension specifications

6.2.3 Vehicle package study

With the SEM1 powertrain and chassis specifications confirmed, 3D CAD package studies defined the overall layout and space claim for the major vehicle systems and occupants. Figure 6.2.3.1 shows the overall approach for the Phase 0 vehicle package and integration studies.

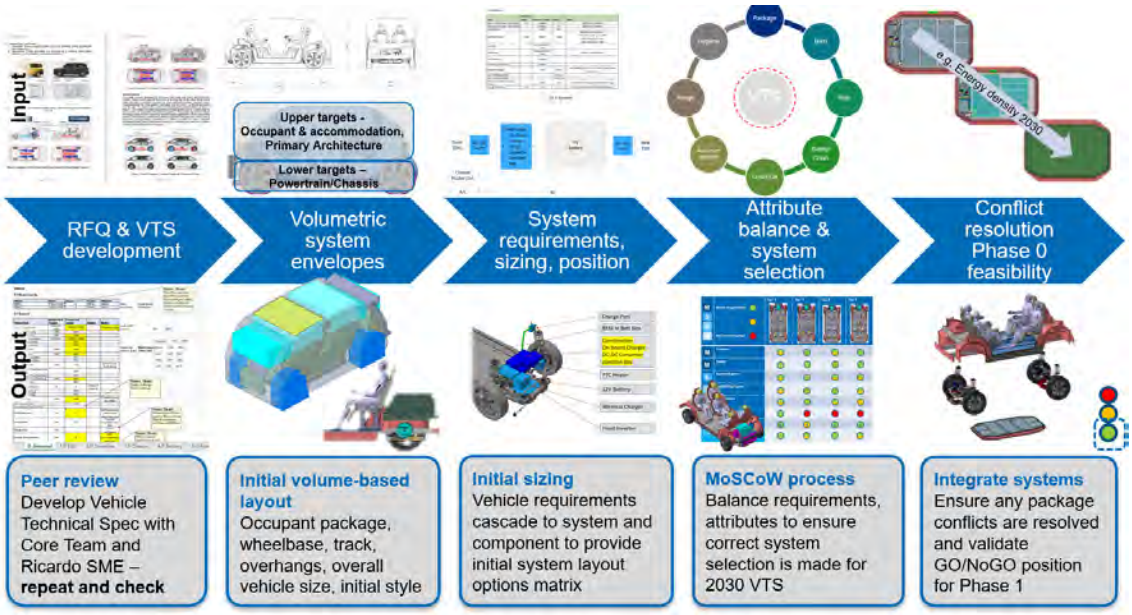

Figure 6.2.3.1 Phase 0 vehicle package and integration studies

Figure 6.2.3.2 shows the overall vehicle size and proportions for the SEM1 vehicle. Note that the front overhang length (735mm) and overall vehicle length (4095mm) were increased from the initial specifications of 635mm and 3095mm respectively in engineering Phase 1. This was to address issues with available crush length and frontal crash performance.

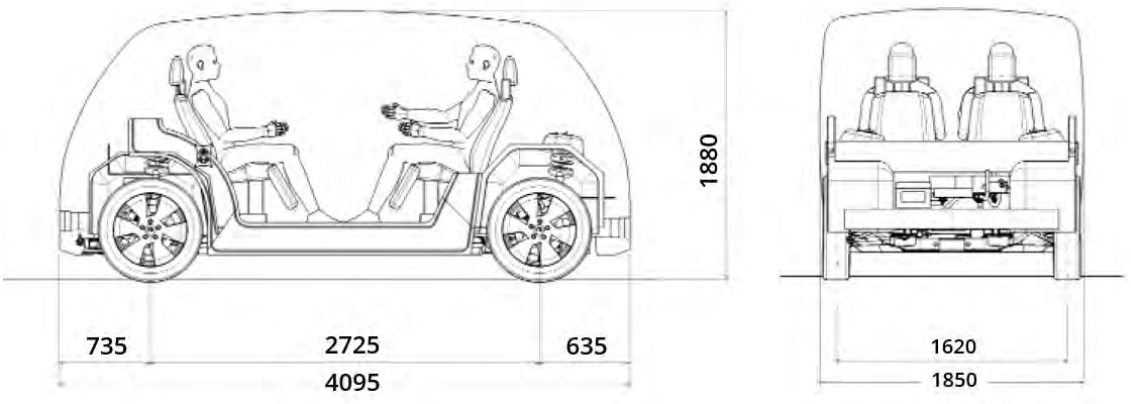

Figure 6.2.3.2 SEM1 overall vehicle dimensions (final design)

Fully autonomous vehicles enable significant freedoms in the positioning of the occupants. With no direct driver interfaces and no requirements for vision and visibility, the occupants can be positioned in unconventional positions and orientations, enabling improved ergonomics, comfort, and interface with devices (e.g., digital screens) and other users.

Occupants are still however subject to requirements of safety and comfort, therefore fixed or allocated seating locations should be defined, such that safety restraint systems can be positioned and engineered for. A study was therefore undertaken to explore the potential occupant seating locations for the Steel E-Motive concepts. The main considerations for the selection of occupant seating locations were comfort, safety, ingress/egress (getting in and out of the vehicle), socialising space, compatibility with SAE level 4 (as a potential future option or consideration), available space for working ability to accommodate the required number of passengers comfortably (4 passengers in SEM1, up to 6 passengers in SEM2). Additional, considerations such package and overall space utilisation, accounting for disabled users, enabling a flat floor and ability to meet the luggage space requirements were also accounted for. A MoSCoW priority analysis was used to assess several different seating options as shown in Figure 6.2.3.3

Figure 6.2.3.3 SEM1 Occupant seating position MoSCoW analysis

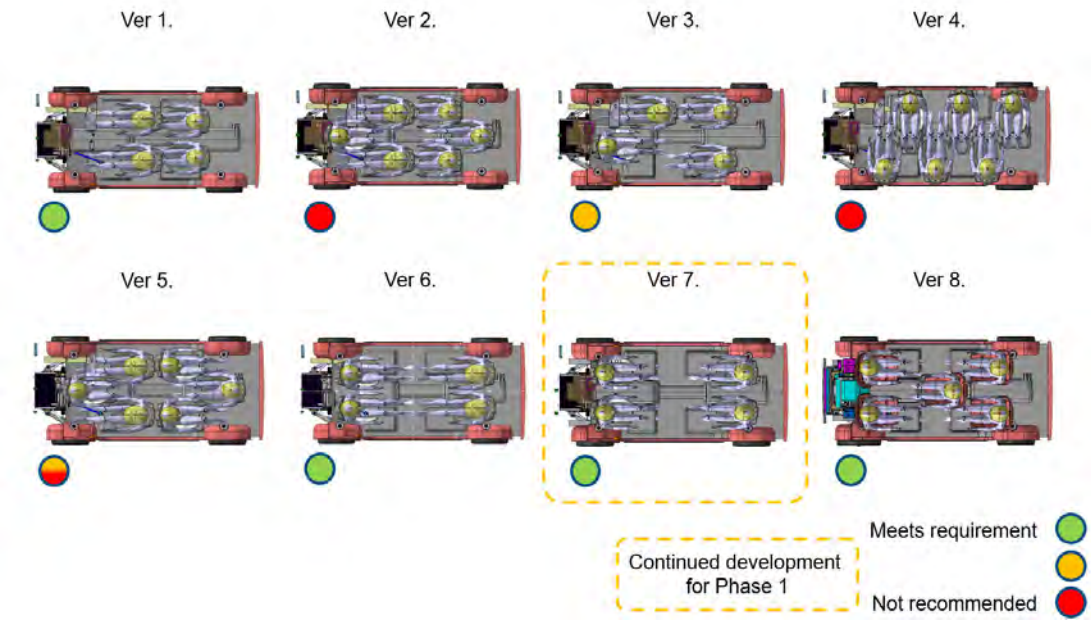

Figure 6.2.3.4 SEM1 occupant position overall evaluation and recommendation

An evaluation of previous research studies and technical papers on the subject of occupant seating positions in autonomous vehicles was conducted. A study by Sofia Jorlöv, Katarina Bohman, Annika Larsson titled “Seating Positions and Activities in Highly Automated Cars – A Qualitative Study of Future Automated Driving Scenarios”, identified preferred seating configurations and activities in fully autonomous vehicles. A sample of occupants were placed in 5 different static seating configurations and polled to determine their preference and feedback. (http://www.ircobi.org/wordpress/downloads/irc17/pdf-files/11.pdf) The study concluded that for longer journeys, a “living room” (inward facing) configuration was preferred. This concurs with the recommendation from the MoSCoW evaluation (version 7). This inward facing configuration was therefore selected as the primary direction for seating in SEM1. The rear facing front occupants would require careful design and engineering of the vehicle structure to account for crash protection, as outlined in subsequent sections of this report.

Further 3D CAD studies were undertaken to determine the optimum positioning of the occupants in the inward (” living room”) seating configuration. Industry guidelines for passenger vehicle seating positions were reviewed and applied (H-Point: The Fundamentals of Car Design & Packaging, Stewart Macey and Geoff Wardle). Dimensions such as seat back angle, head and arm clearance, H point height, heal point height were applied for the occupant positions.

Figure 6.2.3.5 shows the occupant positions in the SEM1 vehicle at the conclusion of Phase 0. The seating positions would be subject to some further adjustment in Phase 1 and 2 of the project to enhance the safety and protection of occupants in frontal impacts.

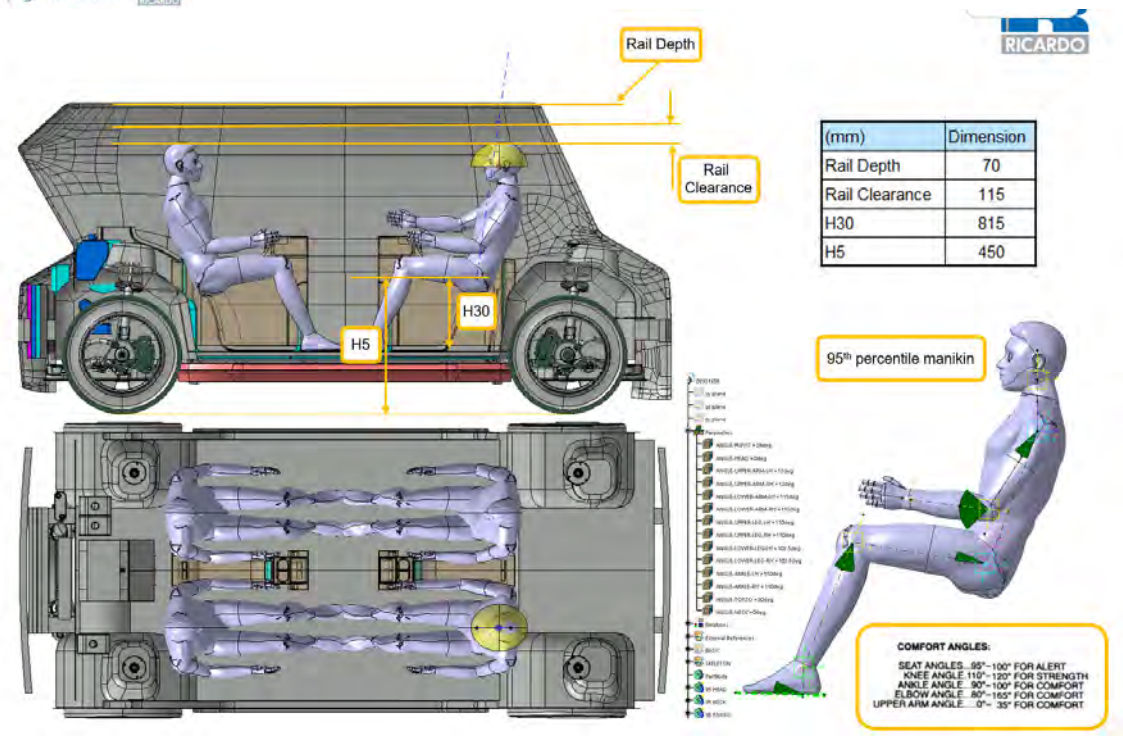

(mm)	Dimension
Rail Depth	70
Rail Clearance	115
H30	815
H5	450

The occupant experience and comfort in a vehicle is also heavily influence by the type and design of the seat. Whilst the specific detail design of the seats was not considered within the Steel E-Motive project, an overall concept for the seat construction was required. The options considered were bench seats, pillar or pilot seats and reversible/swing seats. Given the ride hailing and short to medium journey expectations of SEM1, a bench seat configuration was selected as the primary consideration. This would offer a simpler and lower cost solution than a single pillar seat. It was expected that lack or limited adjustability in a bench seat would be acceptable to vehicle users over shorter durations. The seating configuration for SEM2 is discussed in Section 11. Figure 6.2.3.6 shows the seating configuration for SEM1.

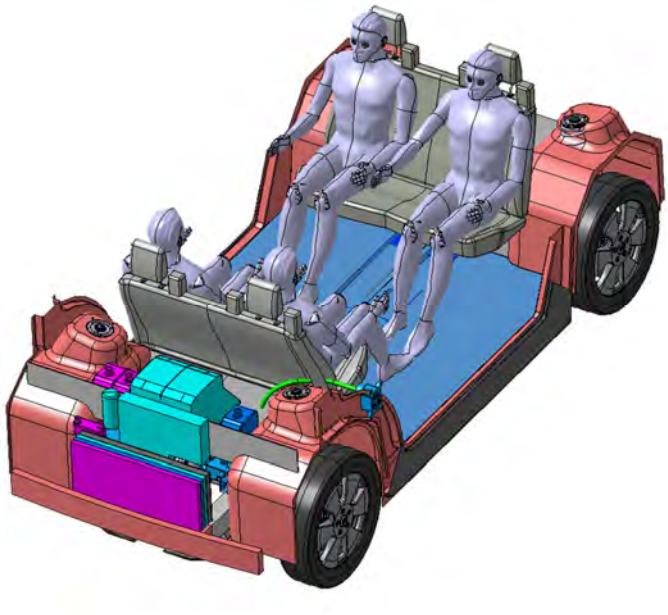

Figure 6.2.3.6 SEM1 bench seating configuration

Consideration for disabled users: Fully autonomous vehicles offer the potential to provide an enhanced quality of life for persons with disabilities. With lower predicted journey costs compared to current private taxi transport and a potentially wider fleet and network of vehicles, MaaS operations should enable disabled users' greater mobility across urban and extra-urban regions. The vehicle design requires adjustment and consideration for disabled users – this was considered in Phase 0. Firstly, standards and requirement for the carriage of disabled passengers were consulted, including The Transport For London (TFL) "Construction and licensing of motor taxis, for use in London – Condition of Fitness" (https://content.tfl.gov.uk/taxi-conditions-of-fitness-update-2019.pdf). A standard for wheelchair dimensions was obtained and incorporated into the 3D CAD study (Figure 6.2.3.7)

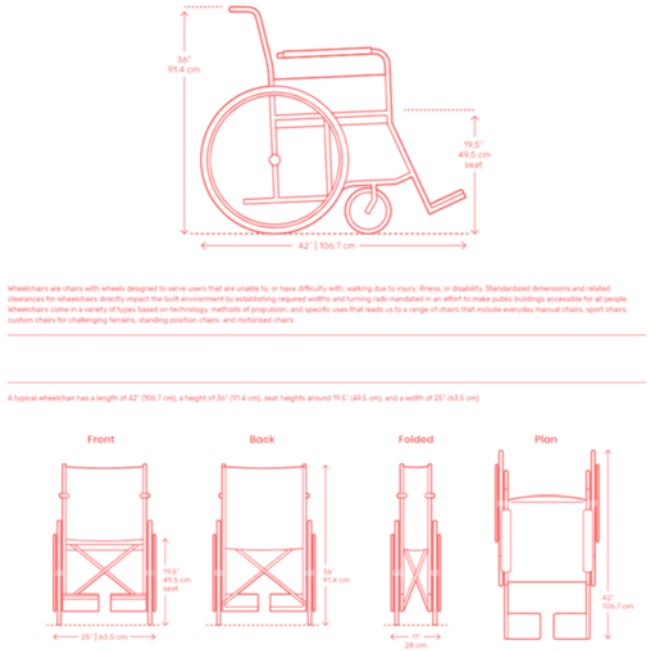

Figure 6.2.3.7 Wheelchair dimensions considered in Steel E-Motive package study

(Source https://www.dimensions.com/element/wheelchairs)

Using this and other references, the following disabled access requirements were defined for Steel E-Motive vehicles:

- Minimum door aperture width when open > 0.75m
- Minimum door angle when opened (swing door) 90 degrees
- Facilitate ramp access from kerb side to vehicle. Vehicle may be fitted with air springs and operate a kerbside “crouch” or “kneel” function in order reduce kerb to vehicle floor height. Target is for maximum ramp angle < 4.0 degrees
- Vehicle interior to have “flat floor”. Wheelchair should be able to manoeuvre freely in the vehicle by manual operation
- Designated fixing points to secure wheelchair during transit
- Provision for grab handles, door opening operation

Luggage capacity, stowage and security is an important requirement for taxi vehicles. The luggage capacity target for SEM1 is 450 litres. Design package studies were undertaken to determine the space claim requirements to achieve the 450litre target.

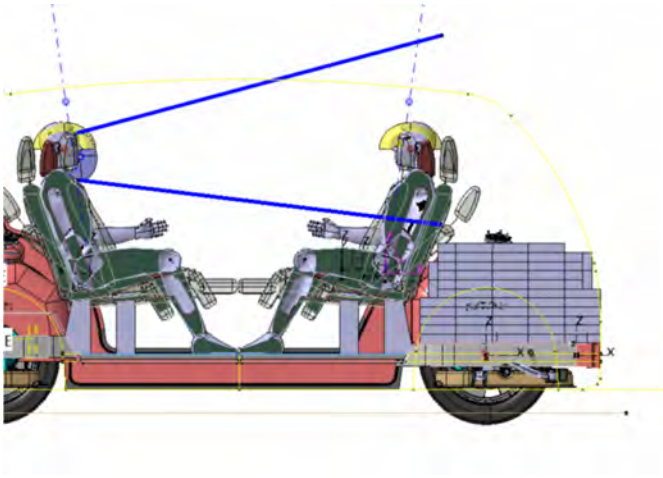

Figure 6.2.3.8 Package space claim study to confirm 450litre luggage capacity

In addition to the propulsion battery and motor, electric vehicles require several additional high voltage components and systems to facilitate the charging and operation. The sizing of these components was based on benchmarking and library data for similar vehicles. The space package positioning for the high voltage components is shown in Figure 6.2.3.9

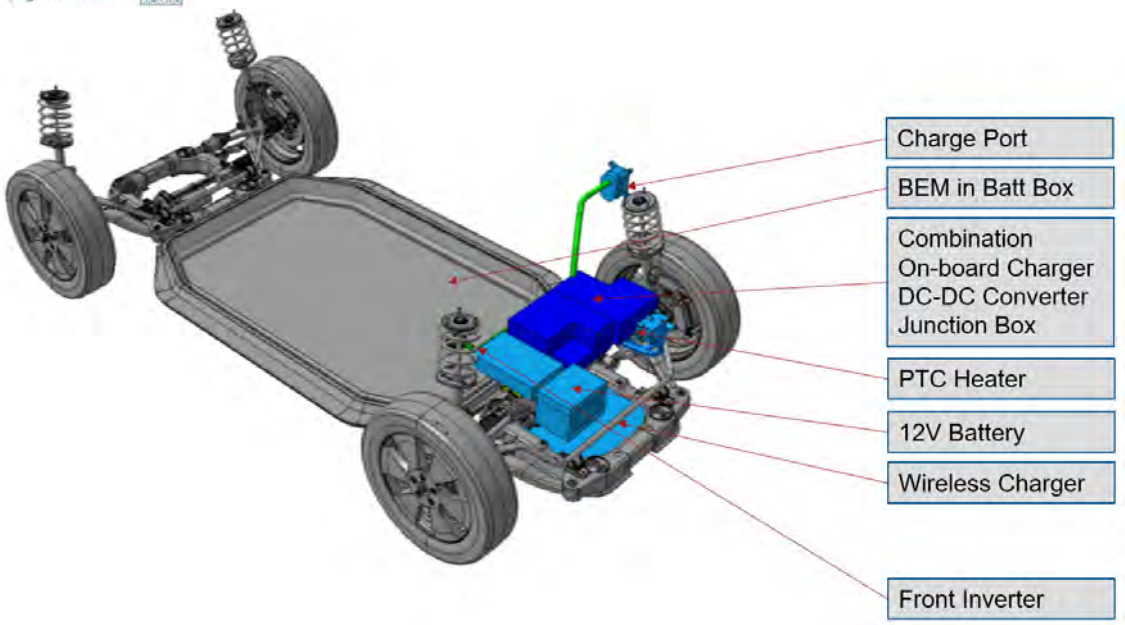

Figure 6.2.3.9 High Voltage system sizing package layout

The vehicle cooling, heating, ventilation, and air conditioning (HVAC) system ensures an appropriate operating temperature for the battery and EDU and conditions the passenger compartment climate to the desired temperature and humidity. The demands on HVAC system for an urban ride hailing vehicle are anticipated to be higher than a conventional passenger car, due the increased frequency of door opening (journey pick-ups and drop offs), the requirement for a large door opening aperture (greater heat loss to/from the vehicle) and the desire to have a spacious feeling interior, which may result in a higher glazed surface area hence greater solar loading into the vehicle.

A schematic layout of the Steel E-Motive thermal system (SEM2 vehicle) is shown in Figure 6.2.3.10. The EDU(s) have a dedicated low temperature cooler circuit, incorporating header tank and heat exchanger(s). The battery pack has a separate cooling circuit with a front mounted chiller pack. The HVAC system comprises of a heat pump, air conditioning compressor, accumulator, and front mounted condenser. HVAC system also requires blower, air vents, ducts, and mixer/valve unit for controlling temperature and humidity via a recirculation valve. The sizing and scaling of the vehicle thermal system and components was based on benchmark and reference data for similar sized vehicles to Steel E-Motive, with adjustments made for the specific ride hailing expectations as described above.

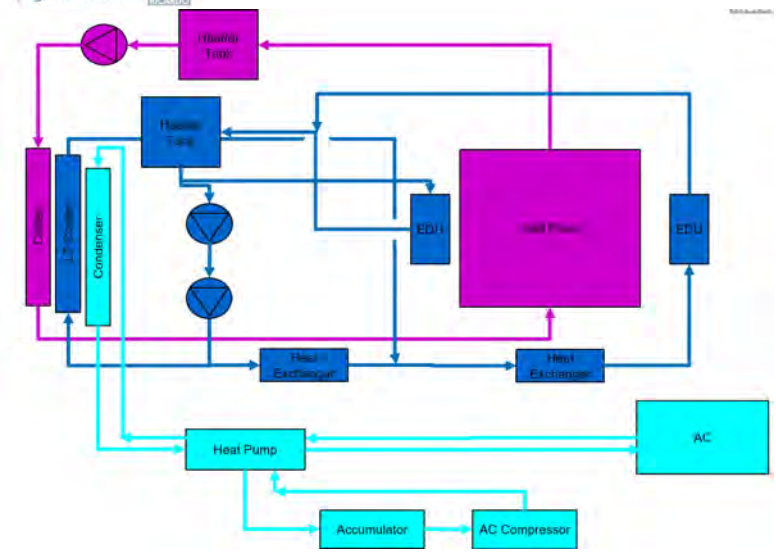

Figure 6.2.3.10 Vehicle thermal system schematic (for SEM2 vehicle featuring a rear EDU)

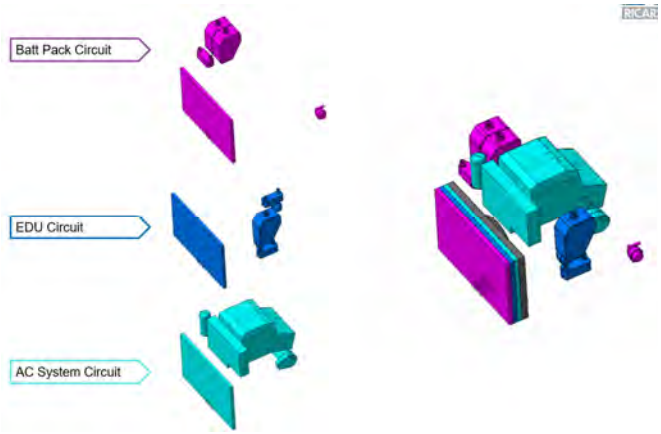

Figure 6.2.3.11 Package volumes for the main thermal system components

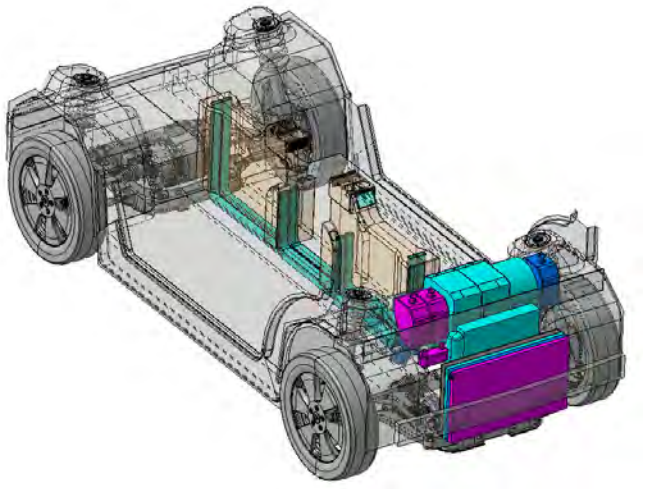

Figure 6.2.3.12 Vehicle thermal systems as packaged (SEM2 vehicle shown)

Autonomous vehicles require systems and components in order to sense the nearby objects and vehicles, recognise and develop a virtual image of the object then make computations to determine the response of the vehicle. The packaging and integration of these systems is not insignificant and required consideration in the development of the Steel E-Motive body structure. The autonomous sensors and controller sizes were positioned as per Figure

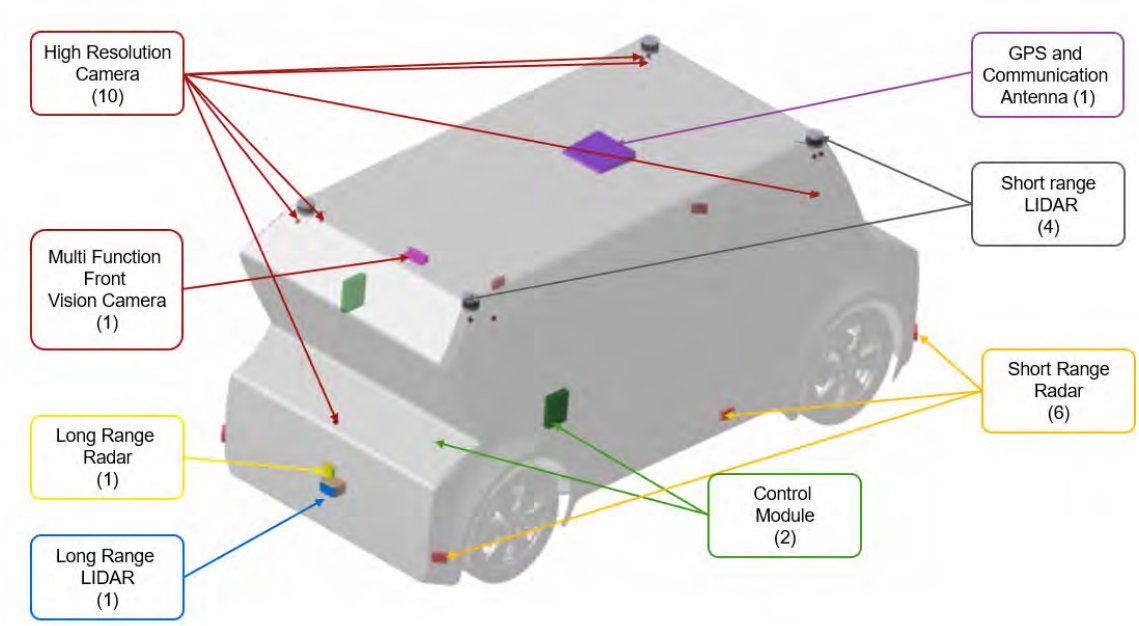

Figure 6.2.3.13 Positioning of level 5 autonomous vehicle sensors

The full level of vehicle autonomy in the Steel E-Motive concepts enabled deletion of the following conventional driver interface components; steering wheel, steering column and adjuster, accelerator pedal and cable, brake pedals, parking brake pedal or parking switch, gear shift controller, turn indicators, rear view & wing mirrors. The main driver information panel would be replaced by a much simpler tablet/screen-based interface. The main interfaces to the occupants are envisaged to be via mobile telephone app, with the vehicle based digital interface primarily for providing journey information, a backup in case of mobile phone/app failure and for fleet operator vehicle service and diagnostics.

The glazing and door openings of a vehicle have a significant impact on the body, it's structural performance and aesthetics. Despite the glazing and doors undergoing detailed design consideration in Phase 1 and 2, a preliminary Phase 0 study was undertaken to define some initial requirements, specifications and sizing of the glazed zones and closures. Firstly, the passenger ergonomics and requirements were considered. Ensuring that users of the Steel E-Motive vehicles can easily enter and exit the vehicle is an important factor in establishing a comfortable and convenient journey experience. With the seating positions already defined where the front occupants are located in a rear facing configuration, the possibility to diverge from a conventional front and rear swing door configuration is made possible. Door concepts including sliding doors, rear hinged swing doors ("suicide doors"), gullwing (roof mounted hinge) and combinations of these were considered and evaluated in a MoSCoW evaluation, as shown in Figure 6.2.3.14. The key requirements and considerations for the vehicle doors were defined as; ease of ingress & egress for the passengers, impact and contribution to overall body stiffness, encroachment/additional vehicle height and width with the doors opened, the package space (cost and weight) for the

mechanism such as sliding rails, contribution, and impact to safety & crashworthiness, potential or restrictions on glazed areas and overall vehicle style impact.

		Tesla Model X P90D 2016	Icona Nucleus Concept	MG Vision-I	2019 Lincoln Continental	Saturn Ion	Kia Sedona SX 3.3 2015
M S C W	Meets requirement / Not recommended	 Gullwing rear door	 Gullwing single door	 Opposed sliding doors	 Rear "suicide" door	 Rear gullwing no B pillar	 Front swing, rear sliding
M	Ingress/Egress						
M	Body Stiffness/NVH						
S	Opened door space (garage/underground)						
S	Mechanism Package						
M	Safety						
C	Glazing						
C	Style (option H compatibility)						
Conclusion for Steel E-Motive application							

Figure 6.2.3.14 Preliminary MoSCoW evaluation of door concepts

The MoSCoW analysis concluded that a side sliding door configuration would provide the best solution for Steel E-Motive. With this preliminary selection of door concept, 3D CAD studies were performed to evaluate the ingress/egress performance and ensure the occupant seating position were compatible. Figures 6.2.3.15 shows the ergonomic evaluation for a 95th percentile male entering/exiting the Steel E-Motive concept. The study shows that with a door aperture of 0.75m, occupants can comfortably enter and leave the vehicle. The door aperture was subsequently be increased to enable improved access and accommodate disabled users' requirements.

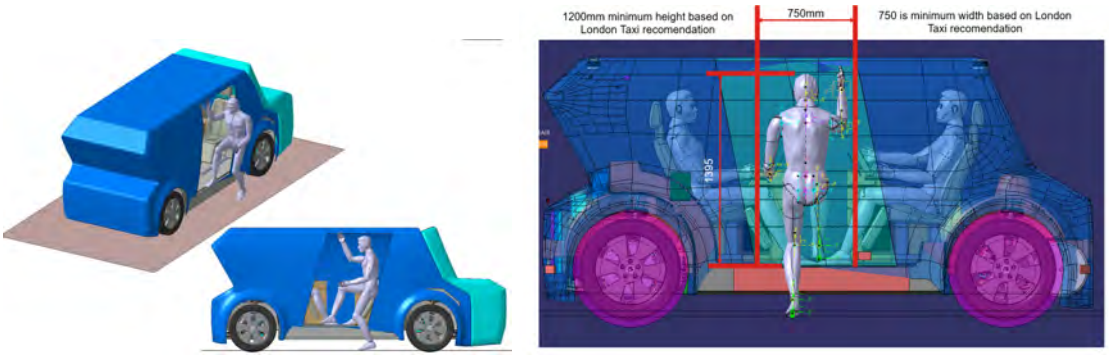

Figure 6.2.3.15 Vehicle ingress/egress study using 95th percentile mannequin

Figure 6.2.3.16 shows the conclusion of a 3D CAD package study of the occupant seating position and sliding door concept. Sliding doors typically have larger section requirements in the y direction, due to the rail and track mechanisms. This can encroach on the occupants seating area and position, especially in a compact sized vehicle such as Steel E-Motive. The

study showed that with a 150mm sliding door overall width (worst case), sufficient clearance to the seated occupant could be maintained.

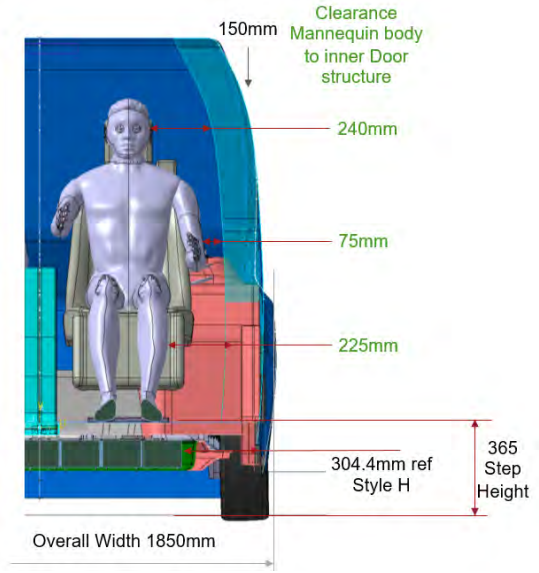

Figure 6.2.3.16 Sliding door to seated occupant package study

The approach and considerations for the detailed development of the side closure concept is described in Section 6.3 and 6.4. The final solution is presented in Section 7.0.

With autonomous vehicles not subjected to direct driver vision and obscuration legislation, the requirements for the glazed surfaces are quite different. Vehicle designers are therefore presented with significant freedoms in the design and location of glazing in autonomous vehicles. Elements of the body structure and other vehicle components can be positioned in locations that would previously be prohibited by the direct driver vision regulations, such as the front windscreen. However, the requirements of the occupants or passengers in autonomous vehicles must also be considered. The ability to have a clear view of the outside from the seated position enhances the occupant's situational awareness in a journey and can help alleviate motion sickness issues. A 3D CAD study identified the potential glazed surfaces in the Steel E-Motive vehicle package (Figure 6.2.3.17). The would be subject to review and alteration during the detail stages in Phase 1 and 2.

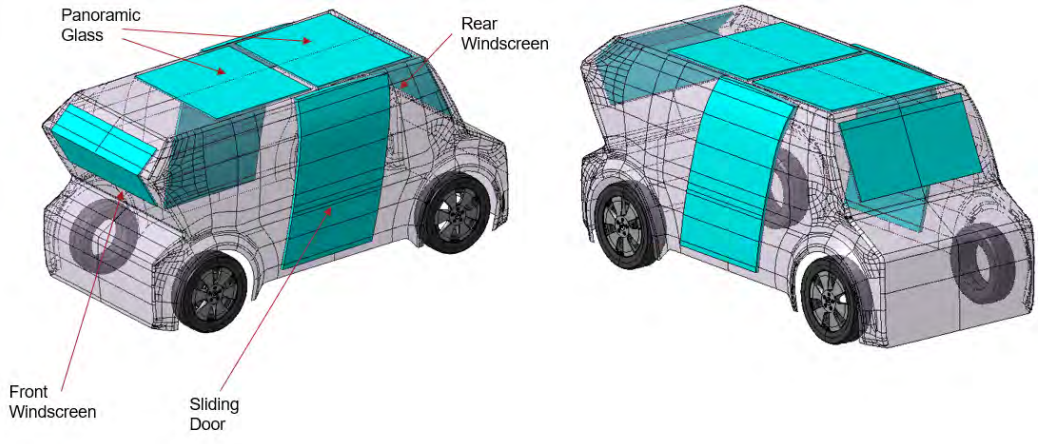

Figure 6.2.3.17 Preliminary glazed surfaces study

Autonomous vehicles are expected to meet the same exterior lighting requirements and regulations which conventional human operated vehicles are subjected to. Exterior lighting is an important aspect of vehicle safety and collision avoidance. Users of autonomous vehicle may also expect the road to be illuminated to provide a sense of security and safety during their journeys. With modern day safety standards, the lighting requirements for passenger cars are significant and require consideration in the vehicle and body design. Front and rear lighting that would meet current legislative requirements was provisioned for in bother the 3D CAD package model and the preliminary vehicle styling as shown in Figure 6.2.3.18.

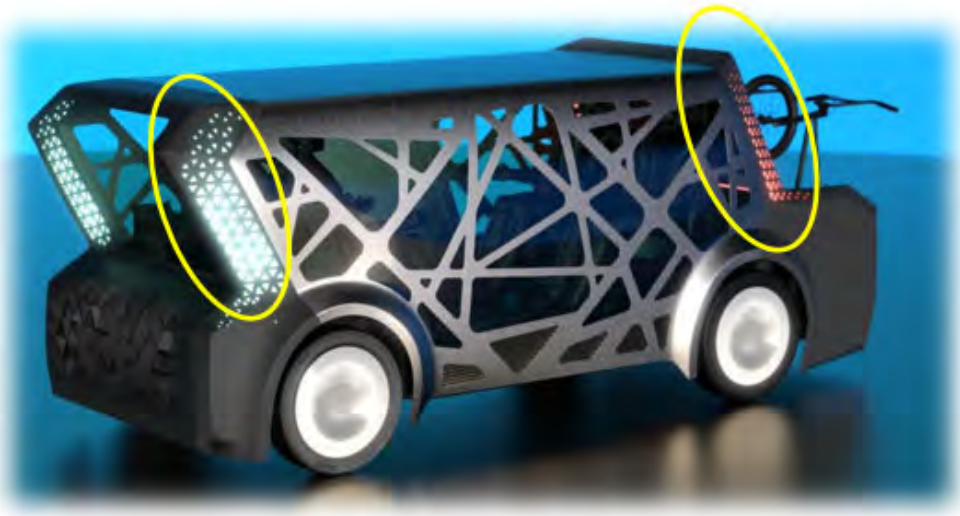

Figure 6.2.3.18 Provision for front and rear exterior lighting in preliminary styling rendering

Combining all the vehicle system requirements, specifications, occupant position considerations and space claims, an overall package model for the Steel E-Motive concept was realised (Figure 6.2.3.19). This essentially defined the volume and position of the major vehicle systems and enabled the development of the body structure in the subsequent phases of the project

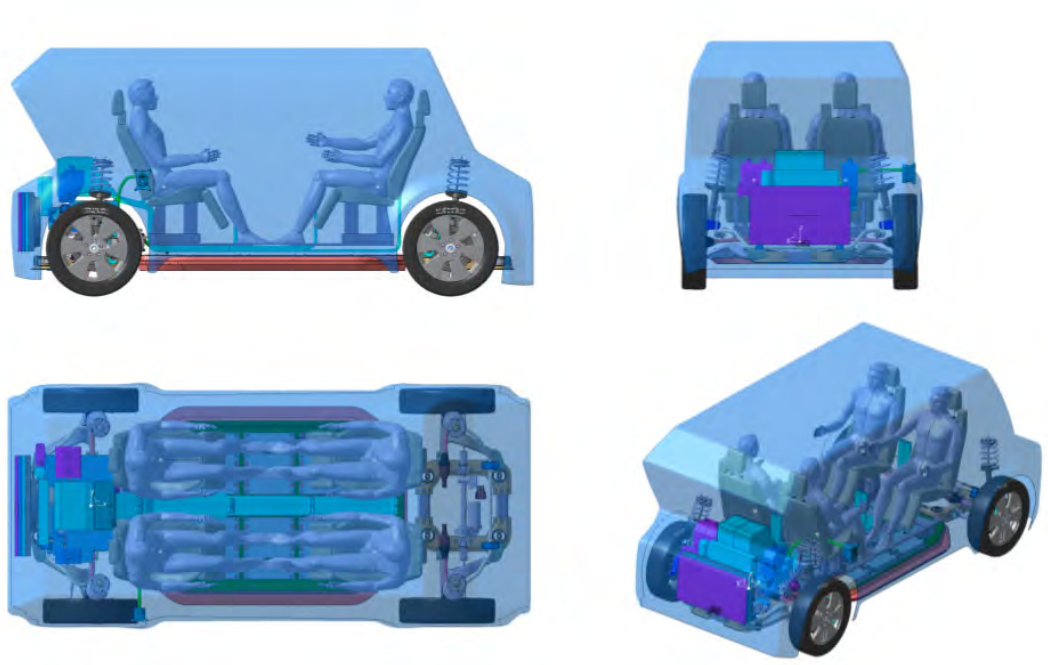

Figure 6.2.3.19 SEM1 Overall vehicle package, Phase 0 (note, the provisional exterior styling theme is applied. See section 6.2.5)

6.2.4 Topology Loadpath Optimisation Simulation

To provide a starting point for the development of the body structure in Phase 1, a 3D topology loadpath optimisation analysis was performed in Phase 0. The objective of the analysis was to define the major structural loadpaths in the body given a set of loads that represent the typical conditions that the vehicle may experience during its lifetime, including crashworthiness loads. The optimisation also supports the development of a weight efficient structure, guiding the design to use structure in appropriate places. The first step of the optimisation is to create a Finite Element model of the available body structure. This was derived from the overall 3D CAD vehicle package study as described in Section 6.2.3 and shown in Figure 6.2.4.1. The interior occupant volume was removed from the overall design volume.

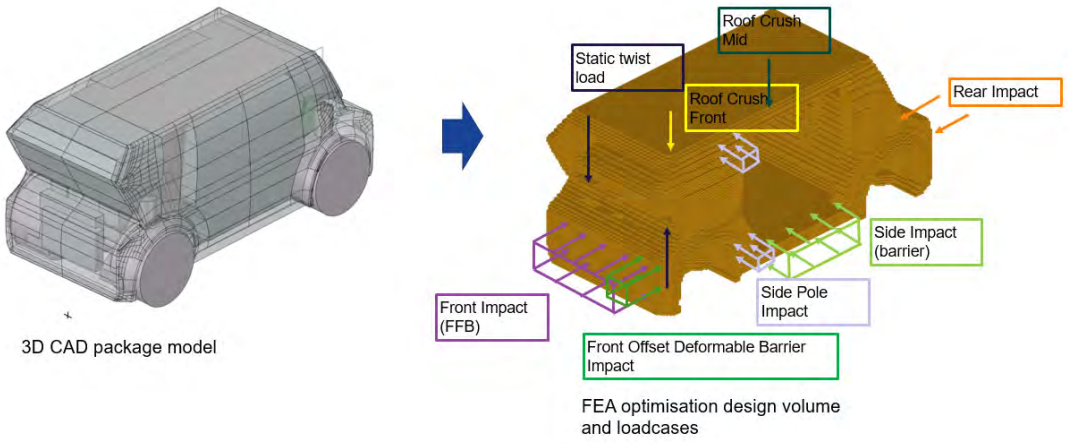

3D CAD package model

FEA optimisation design volume and loadcases

Figure 6.2.4.1 Creation of 3D FEA design volume for topology loadpath optimisation

A set of representative loads (forces) were applied to the FEA mesh volume. The loads applied considered; front crash (FFB), front crash (SORB), side crash (barrier), roof crush (front and mid load), torsion/twisting and vertical bend. The FE optimisation analysis is linear static and the loadpaths in the design volume are calculated based on the element sensitivity. The magnitude of the input loads were therefore normalised to 1.0N, applied as individual loadcase and combined. This enabled the structural loadpaths for specific loadcases to be identified as well as their contribution to the combined loadpaths.

The optimisation software Optistruct was used for the calculation. The software outputs 3D shape data for the loadpaths identified within the design volume. The loadpaths for the combined loadcases is shown in Figure 6.2.4.2

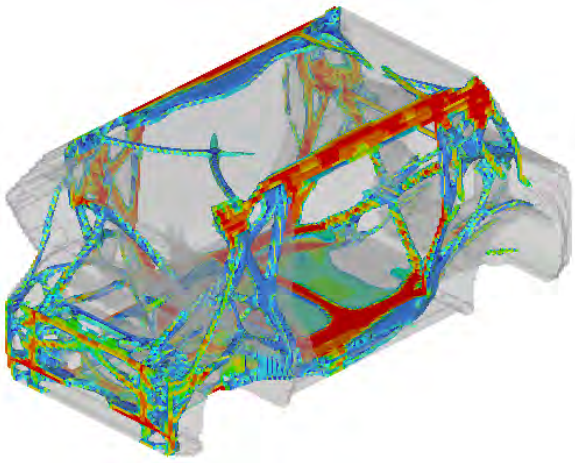

Figure 6.2.4.3 Topology loadpath optimisation considering all (combined) loadcases

The loadpaths considering only the stiffness loadcases (torsion/twist) and vertical bending only loadcases are shown in Figure 6.2.4.4. Should the body structure require improvement or enhancement in static stiffness performance in the subsequent stages of these loadpaths could be referred to and the design enhanced by placing more structure (or section size) in the regions identified.

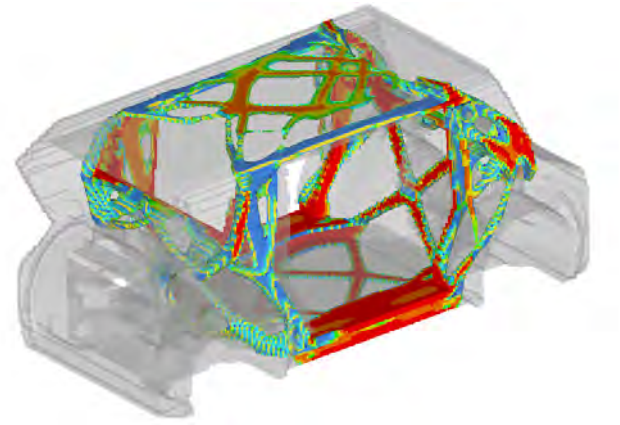

Figure 6.2.4.4 Topology loadpath optimisation considering static torsion and bending loadcases only.

Similarly, the loadpaths for the crash loadcases only could be identified and used to influence the design at later stages as per Figure 6.2.4.5

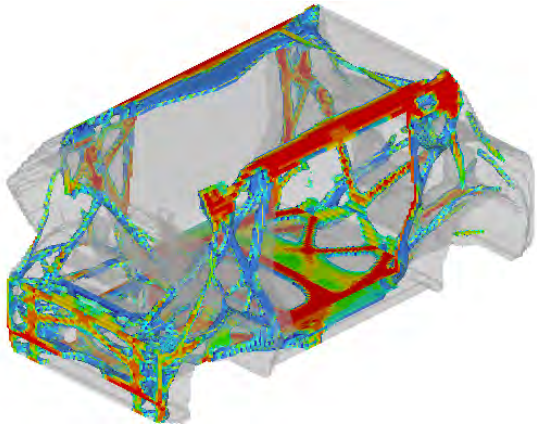

Figure 6.2.4.5 Topology loadpath optimisation considering crash loadcases only

The vehicle closures can contribute to the overall stiffness and strength of a body structure. The door structures cover a significant surface area of side of the vehicle resulting in significant interface with the side crash and pole barriers. Structural reinforcements inside the door offer significant strength and load management in side crash. The side doors create a significant shear panel contributing to the static torsion, bending and NVH modal stiffness of the overall body structure. The topology analyses as described above included no representation of the side closure structures, representing a “worst case”, no contribution scenario. Additional analyses were performed to understand the potential loadpaths and contributions assuming some structural contribution from the side closures. The FEA design volume was modified to include a representation of side closures. Two scenarios were considered: 1) side closure on one side of the vehicle only, the other side being enclosed by the BIW 2) side closures on both sides of the vehicle. The side closure volume was connected to the parent body structure completely around the perimeter, the objective being to try to determine the optimum location for door locks and latches to the body. Figure 6.2.4.6 shows the FEA design volumes for the baseline, no side closures (results as above), single closure on the left side of the vehicle and side closures on both sides of the vehicle

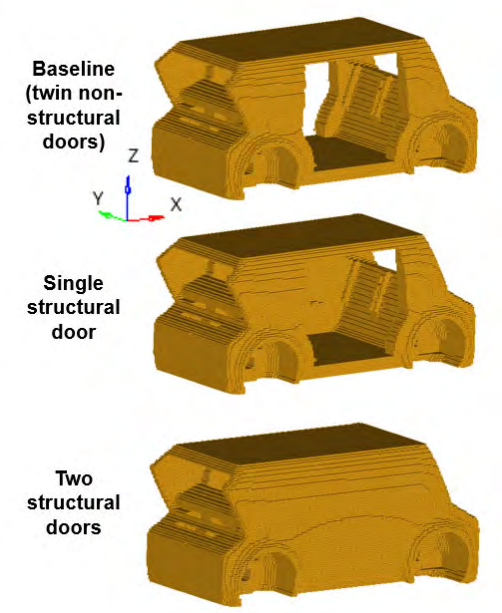

Figure 6.2.4.6 FEA design volumes with different configurations of side closures

The FEA design volumes were subject to the same loadcases and design constraints. The comparative loadpath results from the topology optimisation analyses are shown in Figure 6.2.4.7. The results show that with the single, left side door structure included, an additional vertical loadpath is recommended. With doors considered on both sides of the vehicle, the optimisation recommends vertical and diagonal loadpaths through the doors. The loadpaths in both doors also introduce additional loadpaths into the roof zone, with double diagonal braces intersecting and connecting with the door loadpaths.

The topology loadpath optimisations are intended to be for guidance purpose only and not to prescriptively define the exact layout and loadpaths for the BIW. Engineering interpretation of the 3D loadpaths was assisted using Virtual Reality (VR) tools. The 3D topology loadpath results were translated into VR format. Engineers were then able to review the loadpaths from a full-scale, real-world view collaboratively. The VR tools enabled the engineers to overlay preliminary structural members onto the recommended loadpaths to develop the primary BIW and door structures. The development of the body structure concept was undertaken within Phase 1 of the project and is described in Section 6.3. An example of the 3D topology results as reviewed in the VR application is shown in Figure 6.2.4.8.

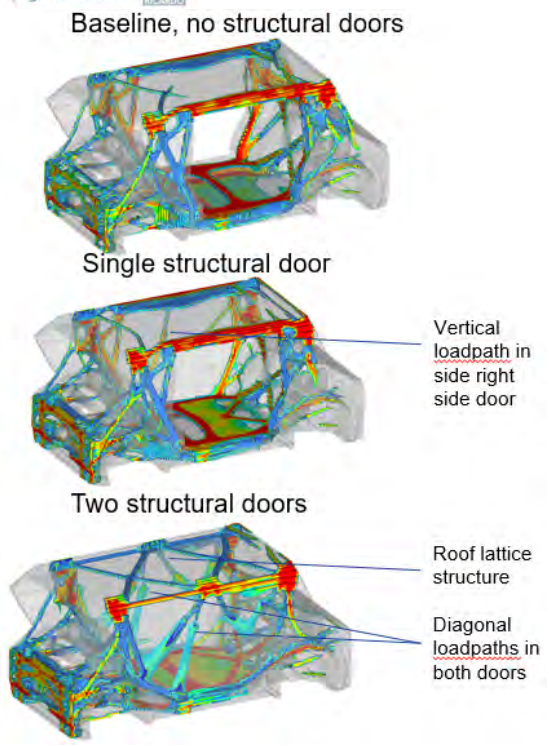

Figure 6.2.4.7 topology loadpath optimisation results with different configurations for the side closures (doors)

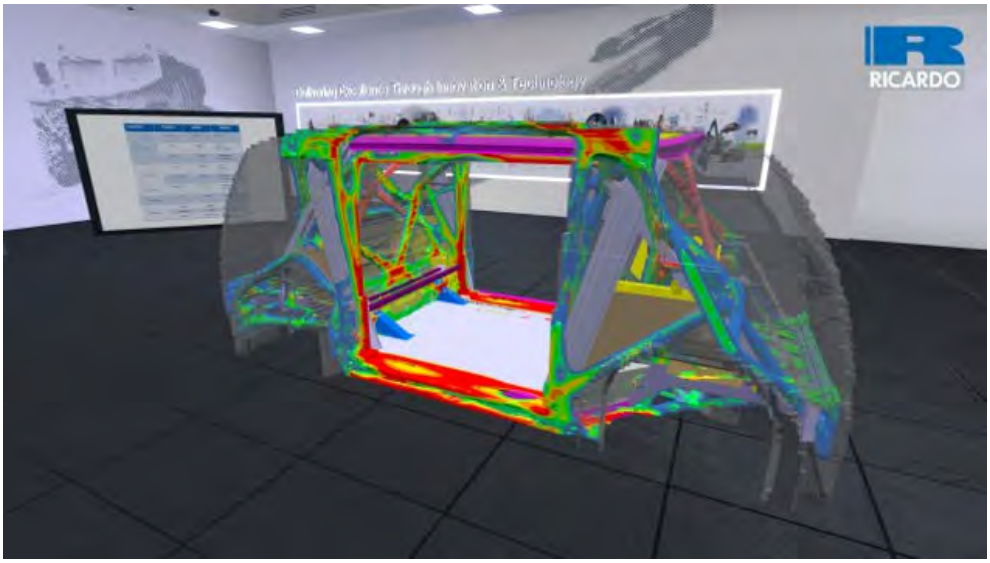

Figure 6.2.4.8 Example of topology loadpath optimisation results using Virtual Reality software

6.2.5 Competitor Vehicle Benchmarking

Competitor vehicle benchmarking is usually undertaken at the start of a new vehicle programme to ensure market competitiveness and appropriate positioning of the vehicle being developed. Benchmark vehicles usually undergo testing and evaluation to establish the key features, specifications, performance attributes and design approach to verify the targets and expectations of the new vehicle. With fully autonomous, MaaS vehicles not expected to enter widespread operation until 2030 at least, the available data for benchmark vehicles was extremely limited. Autonomous MaaS vehicles that were under development were at concept development or prototype stage, hence no physical/hardware testing was possible. Evaluations were therefore limited to “desktop” (literature) based. The desktop benchmarking study aimed to determine the overall vehicle dimensions, seating configurations, door configuration and size, powertrain and autonomous vehicle features of similar vehicle concepts to Steel E-Motive. Figure 6.2.4.1 summarises the high-level features and data that was publicly available at the time of the study.





Feature	Canoo	Nevs Sango	Cruise/Origin	Zoox	Steel E-Motive
Level 5 Autonomy	(level 4)	✓	✓	✓	✓
High speed, (safety cell for >30kph)	✓	?	✓	X	✓
High volume, production feasible	✓	?	?	X	✓
Modular, configurable	✓	✓	✓	?	✓
Manoeuvrable (rear wheel steer)	X	?	?	✓	✓
Innovative features	• Module to frame battery • Configurable interior	• Configurable interior	• NHTSA and FMVSS crash compliant • 1 million mile lifetime • Mainly steel body structure • 2023-25 launch	• Split battery pack	• Side doors >1m aperture • Competitive floor height

Figure 6.2.4.1 High level specifications and features of comparable vehicles to Steel E-Motive. (Data sources: https://www.canoo.com/ https://www.nevs.com/en/pons/ https://getcruise.com/ https://zoox.com/vehicle/) Information believed to be correct at the time of writing.

A comparison of the benchmark vehicle exterior silhouette and dimensions is shown in figure 6.2.4.2. The specific dimensions were estimated and scaled from technical journals and articles and are therefore approximate and subject to errors. The study does show a similarity in the overall vehicle sizes and proportions. Two exterior silhouettes and profiles are shown as these were under consideration at the time of the benchmarking study.

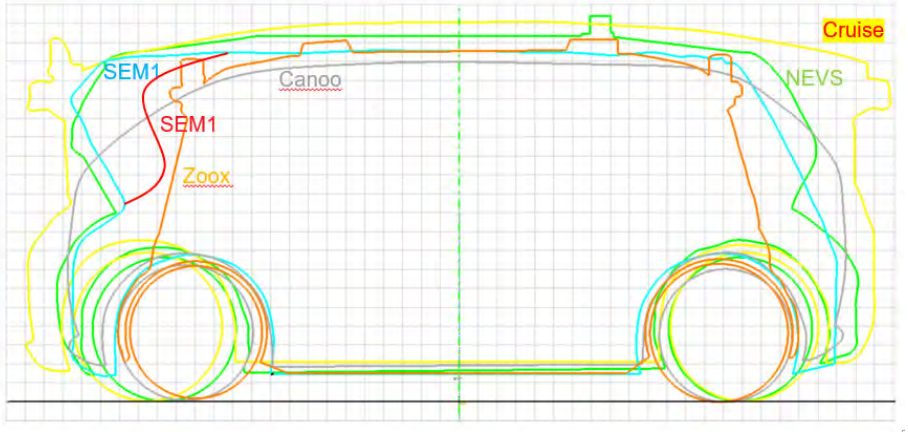

Figure 6.2.4.2 Benchmark vehicle overall size and proportion comparison (note, based on estimated/scaled data from technical journals and articles)

Similarly, the door aperture dimensions were estimated and compared to SEM1. The SEM1 design concluded with an overall door aperture width of 1.07m.

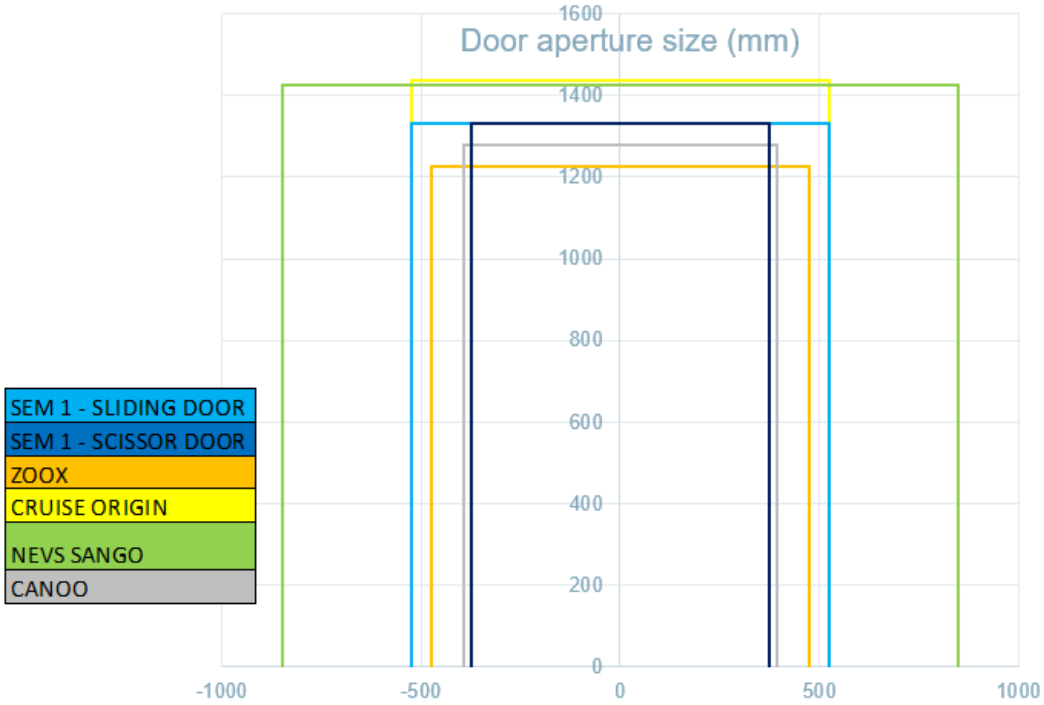

Figure 6.2.4.3 Benchmark vehicle door aperture profiles (note, based on estimated/scaled data from technical journals and articles)

The benchmark evaluation concluded that the GM Cruise vehicle was most aligned to the Steel E-Motive concept, operating at high speed (>40kph), level 5 autonomy, has high volume production intent and is dedicated vehicle design considering the freedoms enabled by full vehicle autonomy. Canoo, NEVS and Zoox were identified as offering lower levels of autonomy or intended to operate at lower maximum speeds than Steel E-Motive and may be intended for low speed off-highway shuttle type transportation. These may have been early

prototype/demonstration vehicles with maximum speed limited for safety. In this case, it is possible that these vehicles may not be compliant with high-speed crash standards and legislation (as in the case of Steel E-Motive). The vehicle structures of these vehicles may differ considerable to vehicles that are compliant with high-speed crash requirements. The vehicles may also be early development vehicles where high speed crash requirements may be considered later in the vehicle development cycle. The vehicles offering level 5 autonomy (NEVS, Cruise, Zoox) all feature interiors with inward (“living room”) seating configuration with double side opening doors on the left and right sides of the vehicle, as shown in Figure 6.2.4.4. Bench type seats feature on the Zoox and Cruise concepts and configurable pilot seats feature in the NEVS concept.

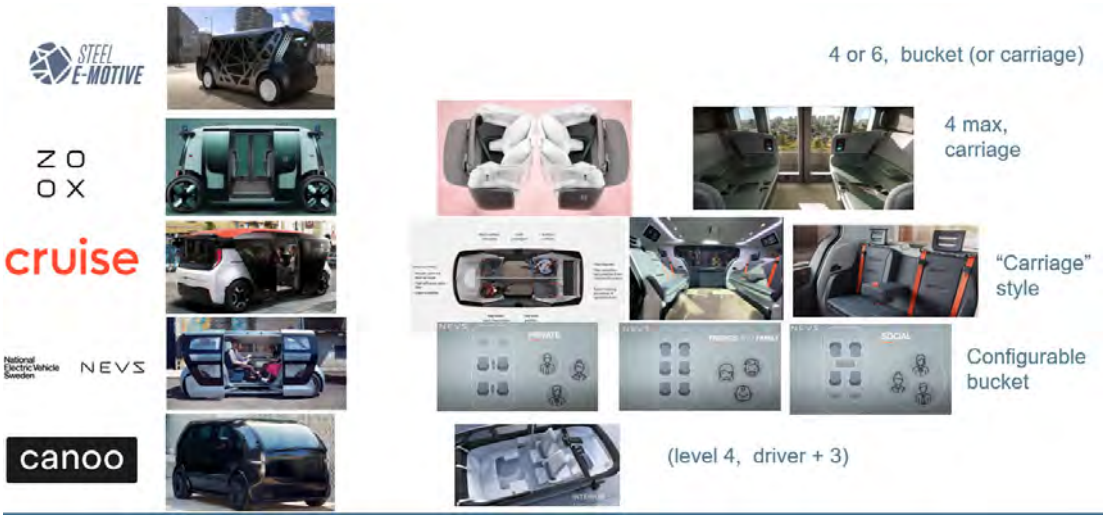

Zoox interior

Cruise interior

NEVS interior

Figure 6.2.4.4 Interior and seating styles of the Zoox, Cruise and NEVS concept vehicles (image source Zoox, Cruise, NEVS)

The desktop benchmarking concluded that Steel E-Motive high-level specifications were aligned to the reference vehicles that were undergoing development at the time. Given the

limited information available, the Steel E-Motive concept would expect to be competitive in the marketplace if it were to enter production in the intended timeframe.

6.2.5 Exterior Styling Study

The primary focus and objectives of the Steel E-Motive project were to develop a fully autonomous vehicle and body concept, demonstrating the suitability of the latest steel grades and manufacturing processes for future vehicles. The styling and exterior aesthetic appearance of the vehicle is also important as it demonstrates and represents the brand (for steel), conveys messages about what the vehicle (and project represents) and the exterior styling and shape also has the potential to influence and impact the definition of the body structure. An exterior styling activity was therefore undertaken within Phase 0 of the project. The styling activity was divided into three stages 1) generation of exterior style themes and concepts 2) review and selection of one exterior styling theme 3) creation of 3D digital (CAD) data of the selected theme and creation of rendering images showing the vehicle style. The exterior styling activity was undertaken by Ricardo's inhouse vehicle design team.

6.2.5.1 Exterior style theme

To provide guidance to the exterior vehicle design group, a "creative design" poll survey was undertaken. The objective of this was to capture the thoughts and ideas of the Steel E-Motive project team of what messages the Steel E-Motive design would expect to represent. A multiple-choice questionnaire presented questions regarding the association of everyday objects, creatures and brands and emotions to the Steel E-Motive project and style. The collective conclusions from the survey would then inform and guide the styling team to create a design that represents and defines the Steel E-Motive concept. A sample of the creative design poll questions and responses are shown in Figure 6.2.5.1.1. The overall poll survey results are shown in Figure 6.2.5.1.2

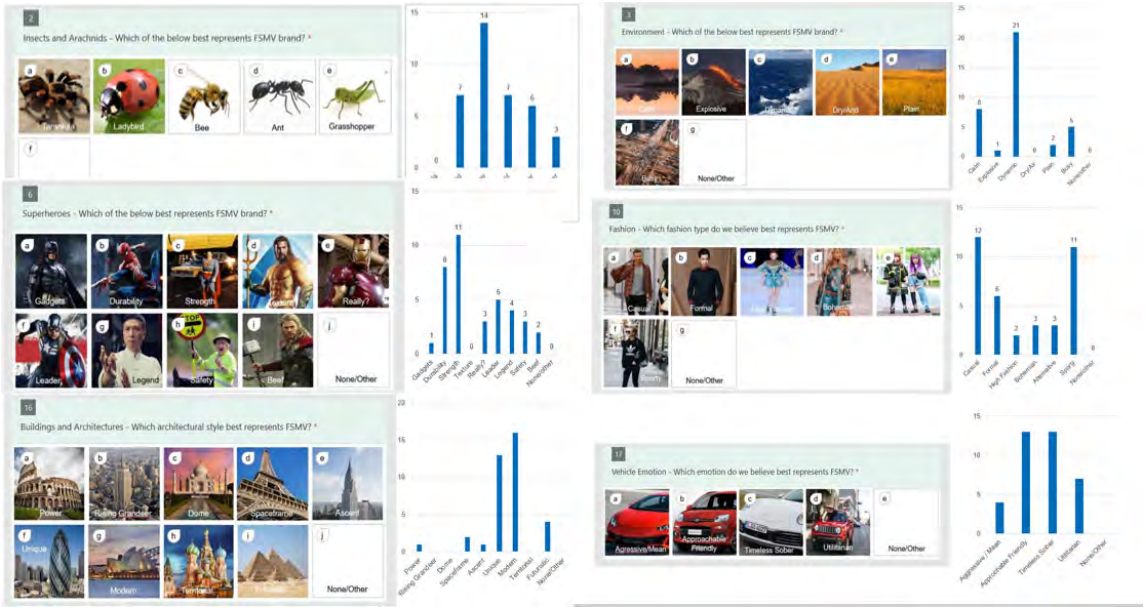

Figure 6.2.5.1.1 Extracts from creative design poll questions and response (see Appendix 4 for larger image)

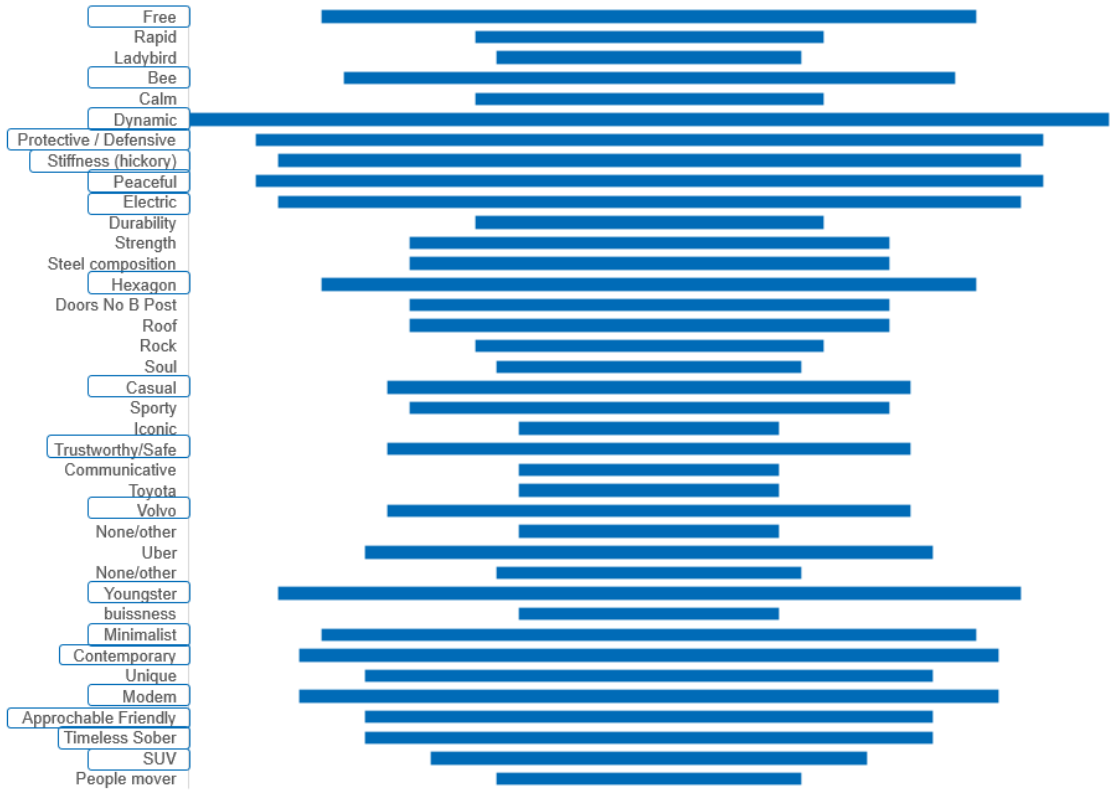

Figure 6.2.5.1.2 Creative design poll overall results, with key “design emotions” highlighted

The results from the creative design poll were reviewed and interpreted by the design team and a vehicle design “styling vision” was created. This was a brief or snapshot of the styling theme and vision and intended to as a reference point and guide for the designers as they created the concept themes.

Figure 6.2.5.1.3 Steel E-Motive styling vision

Several vehicle styling concepts were then generated using freehand sketches, examples of which are shown in Figure 6.2.5.1.4 and 3D design software. Figure 6.2.5.5 shows all the digital renderings of concept themes generated.

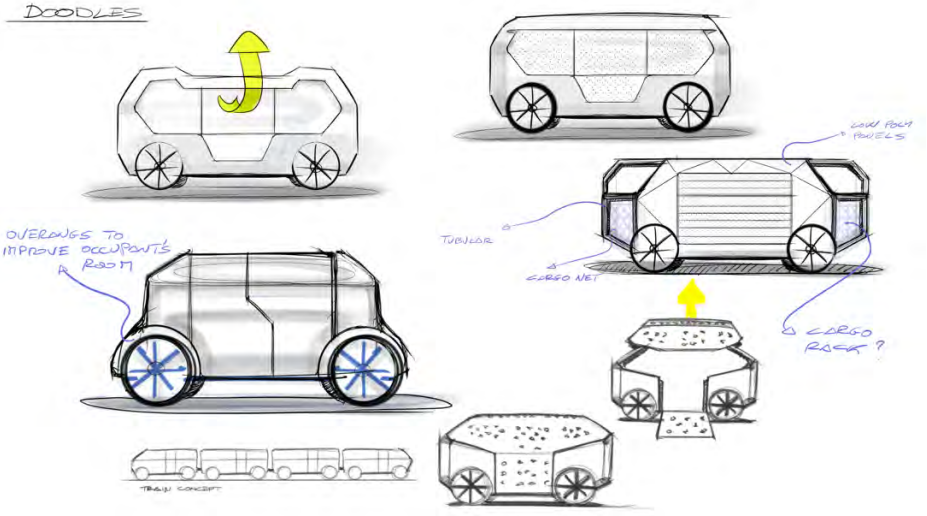

Figure 6.2.5.1.4 Styling concept creation using freehand sketch

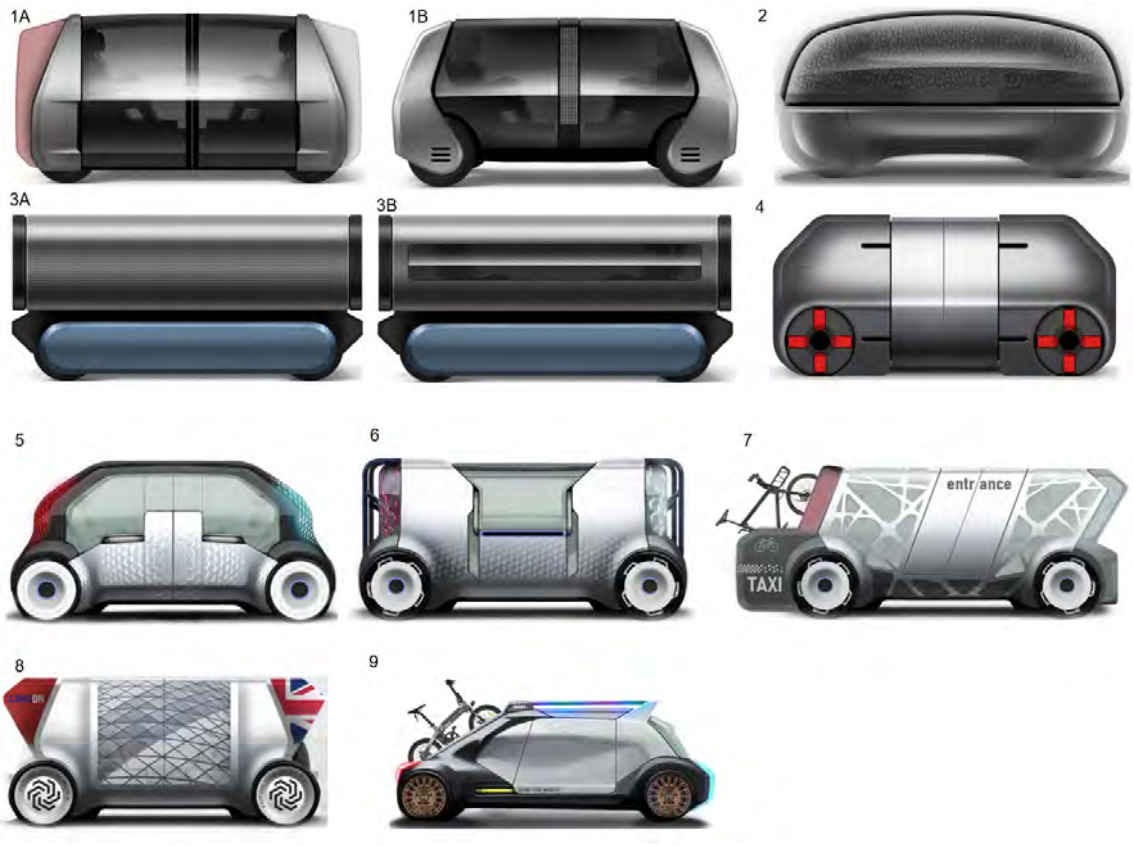

Figure 6.2.5.1.5 Digital renderings of the Steel E-Motive exterior style concept designs

The concept themes were down-selected to 3 concepts using a polling and voting approach within the Steel E-Motive project team. The 3 concepts then underwent an engineering appraisal, to identify issues or benefits that each concept may pose or offer. Figure 6.2.5.1.6 shows the results from the engineering appraisal of the concepts and the results of the concept selection pole. The conclusion from the engineering evaluation was that Concept 7 offered advantages with crashworthiness performance, mechanical package, weight, and cost. Additionally, the exoskeleton concept was viewed as demonstrating a uniqueness and “wow factor”. Concept 7 was therefore selected as the primary concept theme for the Steel E-Motive project. Figures 6.2.5.1.7 and 8 shows the final Phase 0 digital renderings for the selected. The styling theme provided a basis for the engineering teams to work with for the subsequent body engineering activities. The exterior “A” surface provides a boundary where the body design should work to where feasible and possible.

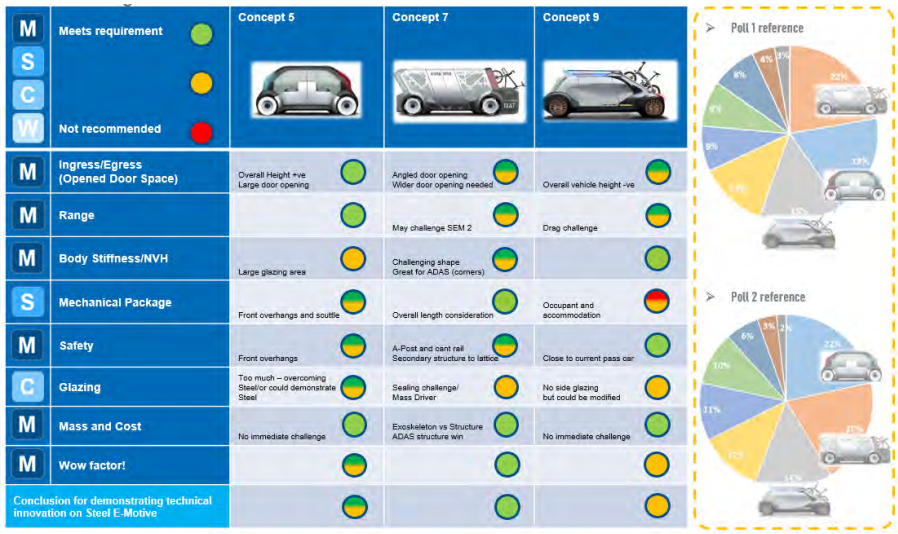

Figure 6.2.5.1.6 Engineering appraisal of 3 selected concepts (see Appendix 4 for larger image)

Figure 6.2.5.1.7 and 8 Digital renderings of Steel E-Motive selected

6.2.7 Vehicle curb weight verification and system weight budget allocation

The curb weight target value for the SEM1 vehicle was defined at 1640kg. An exercise was undertaken to verify this value and allocate the vehicle system weight “budgets” that result in the curb weight value. This would also provide input for Phase 1 activities such as full vehicle crash simulation, where the vehicle weight and weight distribution are required as inputs to the model. The system weight budgets were defined from benchmark data, primarily using a2mac1. (https://www.a2mac1.com/ a2mac1 is a subscription-based service, where current production vehicles undergo teardown to determine system and component weights and dimensions). For some systems, a weight regression analysis was performed, where the weight-dimension trends were calculated for a sample of vehicles and the expected SEM1 weight estimated based on the weight-dimension regression formula and the SEM1 specific dimensions. The data sample used consisted of battery electric vehicles of similar size and specification to SEM1. Figure 6.2.7.1 shows the SEM1 system weight evaluation and estimation. Based on the evaluation, the curb weight of SEM1 was estimated to be 1512kg versus the target value of 1640kg, a difference of 128kg. This overall weight saving would enable benefits to be realised in the vehicle design stage, such as lower crash loads, lower propulsion energy requirements lower durability loads. This may result in secondary or “weight spiral” effects, where the body, chassis and powertrain systems can be downsized because of the inherent weight savings. For the purpose of calculation and simulations in the subsequent development of the SEM1 vehicle, the curb weight was assumed to be 1512kg

System	Budget SEM 1	Description
Body non-structure	169	exterior trim panels, interior trim, seating, interior and exterior lighting, dash/controls interface
Body Structure	309	body in white only, target value based on regression analysis
Front sub-frame	18	
Battery case (structure)	70	
Rear sub-frame	18	
Front suspension	115	springs, damper, knuckle, control arm, anti-roll bar, bushes, brake discs and caliper
Rear suspension	115	springs, damper, knuckle, control arm, anti-roll bar, bushes, brake discs and caliper
Braking	10	booster and master cylinder, ABS and brake lines
Steering	12	EPAS, steering rack and track rods
Tires and wheels	86	
Motor Trans Front	80	
Motor Trans Rear		
Battery system less case	250	fluids, busbars, cooling plate, modules and PDU
Propusion controls	60	charging port, DC:DC inverter,
Electrical-non propulsion	36	wiring harness, 12v battery, fuse box, radar, lidar, cameras, autonomous control unit, switches and sensors
Cooling and heating	30	front cooling pack, header tanks, thermostat valves, cooling hoses, HVAC blower, ducting and vents, air conditioning compressor, heat pump
Closures	100	side doors, tailgate, locks, actuators, hinges, glazing,
Bumpers	34	bumper beams, crush cans, low speed energy absorbers, exterior panels
Estimated Curb Mass	**1512**	kg

Figure 6.2.7.1 SEM1 curb weight verification and system weight budget allocation

6.3 Technical Approach, Phase 1

6.3.1 Introduction and approach

The primary objectives of Phase 1 of the Steel E-Motive project were to develop body structure concepts based on the preliminary sizing and scoping activities undertaken in Phase 0. The conclusion of Phase 1 would see one body structure selected as the primary route and focus for development and verification in Phase 2. With the high voltage propulsion battery being of significant size, weight and structural contribution to the overall body and vehicle performance, the exploration and development of battery concepts was undertaken in parallel with the development of the body structure. Concepts for some of the body subsystems, such as the front and rear crash structures and the rocker were also undertaken in parallel. An interim project Gateway was held midway through Phase 1, where the key design and performance metrics were assessed against the project targets. The body architecture, battery concepts and subsystems were combined and integrated into a single design and evaluated at the Concept Selection <CS> gateway at the end of Phase 1. To simplify the Phase 1 design and analysis activities, the engineering development in Phase 1 purposefully considered a limited, sample of steel material grades. Manufacturing and assembly feasibility was primarily experience and engineering judgement based – detailed evaluation and development was undertaken in Phase 2. Figure 6.3.1.1 shows the timing and interaction of the Phase 1 engineering activities and Figure 6.3.1.2 shows the approach for the development of the body structure.

Work Package / Project Month	3	4	6	8	7	8	9	10	11	12	13	14	15	17
Engineering Phase	0	Phase 1												2
Body architecture concept development		Loadpath, beam structure, key section profiles						Development of stamped unibody structure concept						
Battery concepts development		Development alternative battery structure concepts						Development alternative battery structure concepts						
Body subsystem concept		Front, rear crash structure, rockers, modules												
Closures concept development		Side closure & tailgate concept exploration						Side closure & tailgate concept exploration						
Major Project Gateways/Milestone reviews	◆ 0							◆ TA						◆ CS

Figure 6.3.1.1 Phase 1 engineering activities

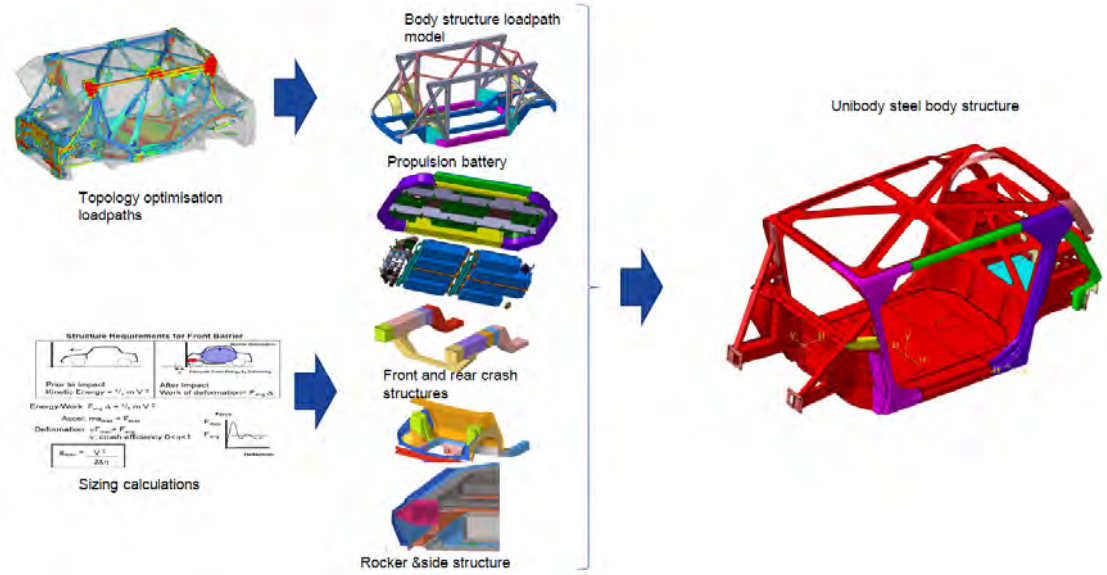

Figure 6.3.1.2 Approach for the development of Phase 1 body structure concept

The first stages of Phase 1 focussed on developing the overall architecture of the body, the layout and sizing of the key structural elements and ensuring the structural performance targets were achievable. In parallel, different concepts for the propulsion battery were developed. This was initially done “standalone” (without considering the native body structure). Once the body architecture was established mid-way through Phase 1, the development of the propulsion battery considered a fully integrated approach with the body structure. Preliminary calculations and concept studies were performed for the front and rear crash structure and subsystems such as the rocker. Similarly, this development was initially done at subsystem level, before the concepts were integrated into the body architecture level mid-way through Phase 1. The Concept Selection <CS> gateway confirmed that the SEM1 targets were achievable given the timing and resources available for the remained of the programme. Some concessions were enabled on the performance targets at this stage, as 100% compliance for all targets would not be expected at this stage of the programme.

6.3.2 Concept Development of Body Architecture

The structural loadpath optimisation undertaken in Phase 0 provided the basis for the development of the overall vehicle and body architecture. At this stage, several different body structure construction types and approaches were considered for the Steel E-Motive concept. A “body on frame” architecture consist of a rolling chassis, with the suspension,

steering and powertrain systems mounted to a ladder frame. A separate, unibody body structure is then mounted to the rolling chassis, usually via isolating rubber mounts. This architecture is suited for vehicles with high payload and towing requirements such as pickup trucks. This high load capacity comes at the penalty of poor overall weight efficiency. A more common architecture for small vehicles and passenger cars is a unibody construction. The load carrying aspects of the chassis are integrated into the body structure. The body structure essentially acts as a “bracket” for all the major systems to attach to. Unibody constructions are more weight and cost efficient than body on frame but lack the load carrying and towing capacity of body on frame design. The growth and development of battery electric vehicles has led to the evolution of “skateboard” concepts. The skateboard chassis contains a base structure or platform, the propulsion battery, power electronics. The suspension, steering and braking systems are also mounted from the platform. An upper body containing the passenger compartment and interior is then mounted to the skateboard. A true skateboard architecture is less weight efficient that a unibody due to the horizontal split between the skateboard and upper body which creates inefficiencies in the loadpaths. The reality is that many battery electric vehicles feature a unibody construction with elements of skateboard features, such as a protective crash structure around the battery, flat floor, and integration of the power electronic systems. Given the targets and requirements for the Steel E-Motive vehicle, the decision was made to use a stamped steel unibody construction. This would enable a weight efficient structure, that could incorporate a flat floor, offer high levels of comfort and crash protection for the occupants and battery and would be suitable for production volumes of greater than 250,000 per year, using existing and conventional manufacturing approaches.

Development of the Steel E-Motive body structure concept started with the loadpath results from the Phase 0 topology optimisation study. The suggested loadpaths were reviewed and interpreted by the design team using 3D CAD and Virtual Reality tools. Figure 6.3.2.1 shows an example of the interpretation of the topology loadpath results resulting in the preliminary beam concept body structure model.

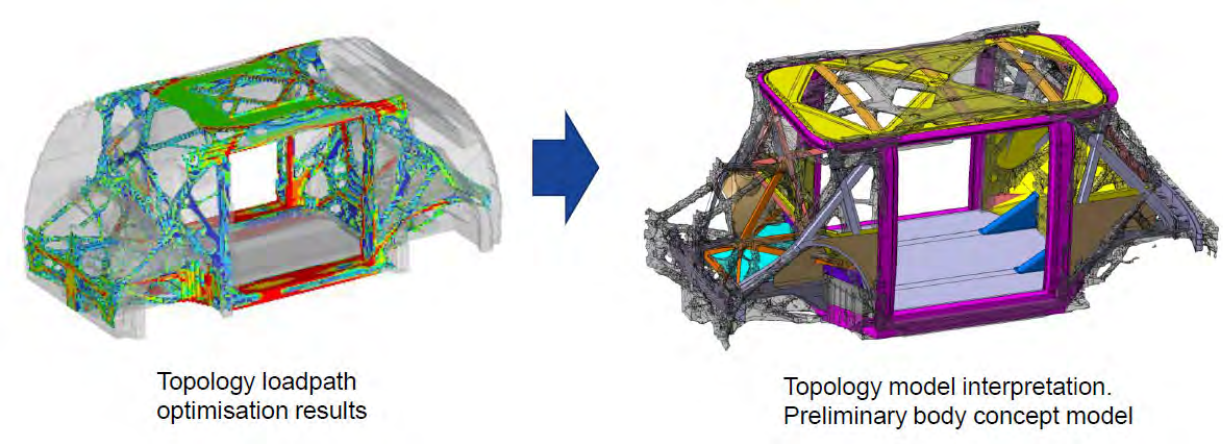

Figure 6.3.2.1 Interpretation of topology loadpath optimisation results into preliminary body structure concept model

The beam concept model featured first approximations for the main section profiles and properties. A Finite Element model of the beam structure body model was created. Front and

rear crash structures were integrated from the body subsystem studies as described in 6.3.3, which were run in parallel to the complete body structure development. Structural analyses were undertaken to evaluate the complete vehicle crashworthiness, static stiffness and NVH modal performance. Analysis iterations were performed, adjusting the beam section profiles and dimensions until satisfactory levels of performance were achieved.

6.3.3 Development of body subsystem and module concepts

Preliminary sizing and development of some of the body subsystems was undertaken at the start of Phase 1 and in parallel to the body architecture study described in 6.3.2. In order to manage crash loads in a frontal impact, a front crash structure is required. The function of the front crash structure is to manage the front impact event by decelerating the vehicle from the impact speed to standstill in a controlled and progressive way, such that the resulting loads on the occupants are not excessive. High levels of vehicle deceleration (or “pulse”) can cause injuries to the head, neck, and internal organs. The crash structure also needs to work with the safety restraint system such as seat belts and airbags can protect the occupants from high pulse levels. Occupant injuries can also occur as a result of the body structure deforming significantly and impacting the occupant. This can cause injuries to more exposed body parts such as legs, feet, arms, and feet. High levels of structural deformation into the occupant compartment are referred to as “intrusion levels”. To achieve satisfactory levels of deceleration pulse and intrusion, a crash structure consisting of collapsible members are engineered to fail and crush in a controlled and predictable manor on impact. Typically, these are longitudinal box sections extending forward from the bulkhead to the front bumper and impact zone. The crush characteristics of regular metallic box sections can be estimated by simple formula. Calculation tools such as MS Excel were used to determine the required crush length for Steel E-Motive. With a pulse target of 35g for the 56kph frontal rigid barrier and an assumed vehicle crash test weight of 1620kg (curb weight +100kg of test equipment), an available crush length of 720mm was required, as shown in Figure 6.3.3.1. These calculations, along with the results from the topology optimisation enabled the creation of front crash structure concept models, as shown in Figure 6.3.3.3. With the guidance of the loadpath optimisation results, a conventional approach of managing the main (primary) crash loads through a longitudinal crush rail, a secondary loadpath through the front subframe and a third or tertiary loadpath through the shotgun was employed. With the unique positioning of the occupants and very short front overhang, the shotgun was oriented more vertically than a conventional passenger car.

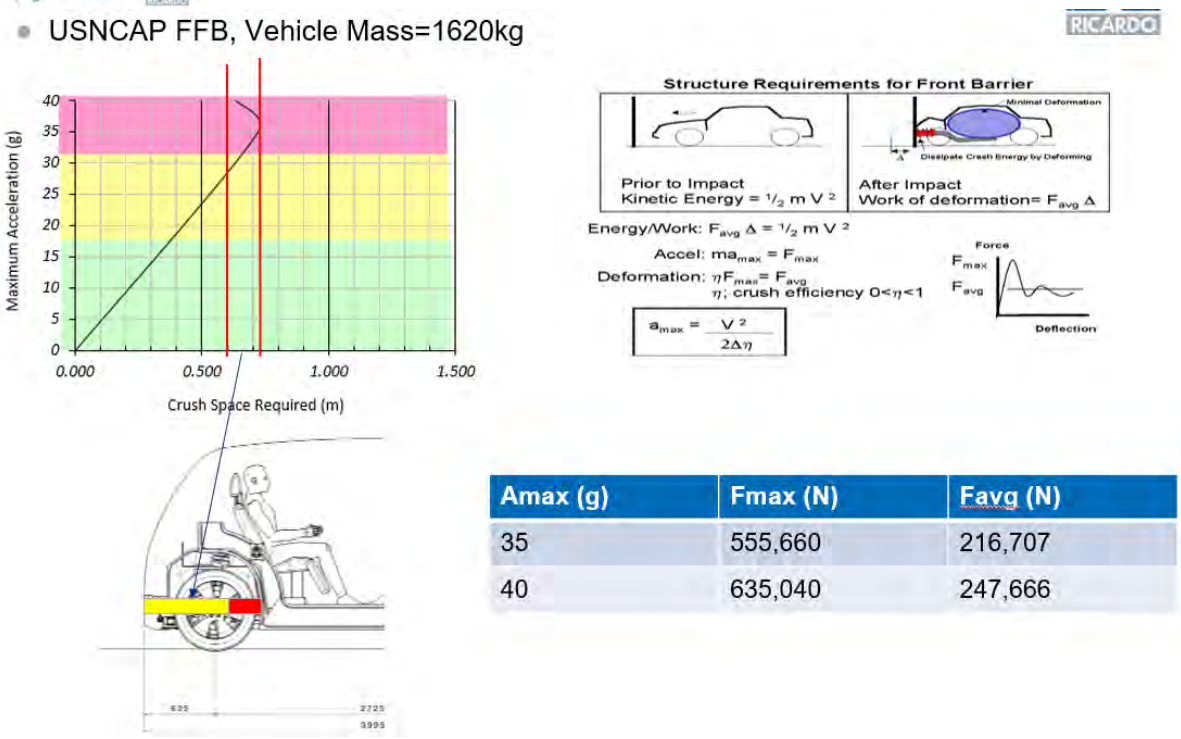

Amax (g)	Fmax (N)	Favg (N)
35	555,660	216,707
40	635,040	247,666

Figure 6.3.3.1 Estimation of required front crush length using formula and MS Excel (calculation tool provided courtesy of Donald E. Malen, Fundamentals of Automobile Body Structure Design, SAE International, 2020, Reference Section 6.2)

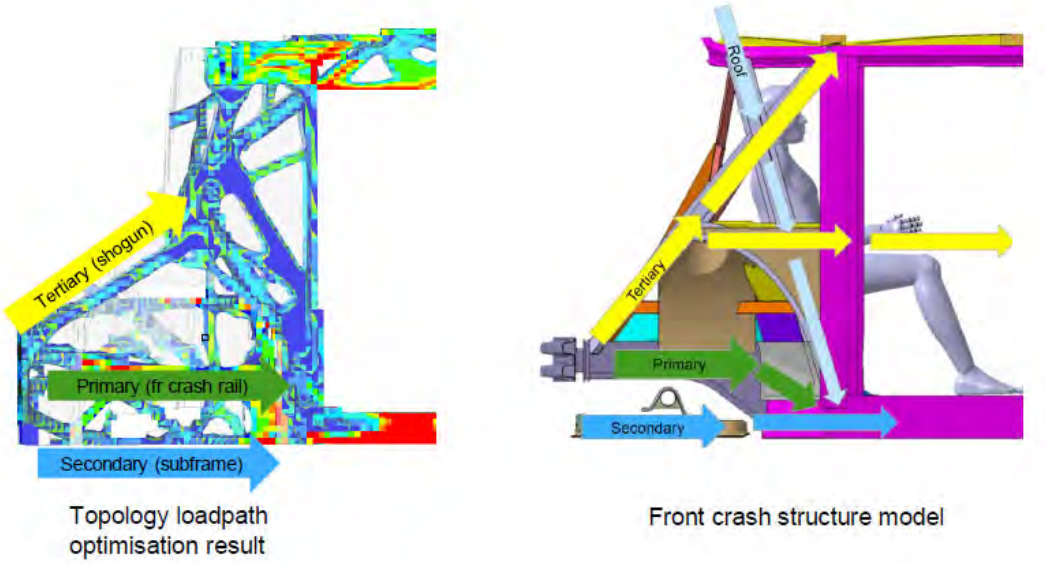

Figure 6.3.3.2 Development of front crash structure concept design using topology loadpath optimisation results. Also shown are the main crash loadpaths

FEA based design studies were performed to understand the sensitivity of the front crash structure design and the contribution of the front subframe and crash rail configuration. A summary of the study is shown in Figure 6.3.3.3. The study concluded that the best crash performance was achieved with an extended (longer) front subframe coupled with tailor

welded crush rail, with steel grades tuned to provide progressive crush and minimise intrusion (Concept 1). The study also showed the sensitivity of the positioning and motion of the EDU in front crash event. The EDU is comparably stiffer and stronger than the front crash structure. The EDU should be engineered to moved downward, towards the ground in a front impact. This should prevent the EDU being pushed rearwards in the front bulkhead which may result in high crash intrusion. The EDU should effectively be moved out of the way to allow the crash structure to work effectively. Based on the front crash studies and results, Concept 1 (shown in Figure 6.3.3.4) was selected as the primary design and incorporated into the complete body structure as described in Section 6.3.2. This concept would undergo further design and material grade refinement throughout the rest of the engineering phases of the project.

			Concept 1	Concept 3a	Concept 3b	Concept 3c
Front Longitudinal Crush Rail Design			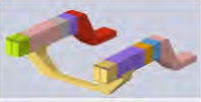			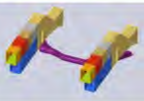
Chassis/subframe design						(no subframe)
Metric		CAE Target (interim)				
FFB	Acceleration	<48G	43	51	56	54
FFB	Intrusion	- [mm]	363	398	375	400
FFB	Max longitudinal force	<350kN	265	261	334	256
ODB	Acceleration	<40G	39	36	X	37
ODB	Intrusion	- [mm]	893	820	X	777
ODB	Max longitudinal force	<350kN	293	253	X	268
Mass - longitudinal		- [kg]	13.6	10.2	13.6	12
Mass - subframe		- [kg]	15.6	14	7.2	X
Overall performance status						

Figure 6.3.3.3 Front crash structure FEA concept design studies evaluating longitudinal crush rail and front subframe configurations (see Appendix 4 for larger image)

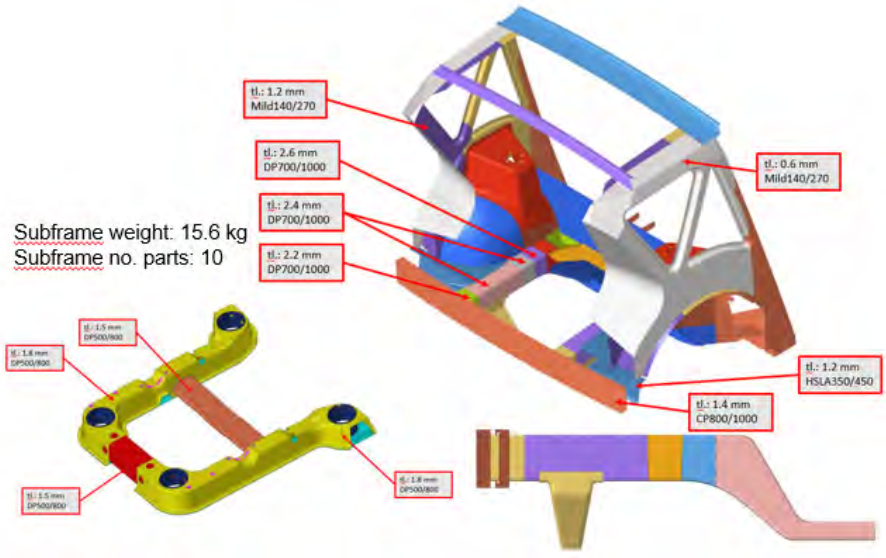

Figure 6.3.3.4 Front crash zone preliminary concept (#1)

Similar concept level studies were performed for the rear crash structure. Here, the objective is to manage the crash loads from a deformable crash barrier only and ensure there is no damage to the propulsion battery. There are also targets for the crash intrusion levels to the occupant compartment. Figure 6.3.3.5 summarises the results from rear crash structure FEA design studies. Concept 1a was selected as the primary rear crash structure concept despite other concepts showing lower battery contact forces. Concept 1a was deemed to have better fabrication and assembly characteristics than the other concepts.

		Concept 1a	Concept 1b	Concept 2	Concept 3a	Concept 3b
Body structure design			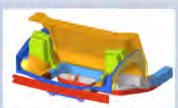	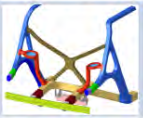	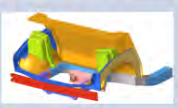	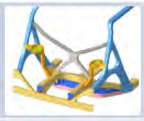
Rear subframe design		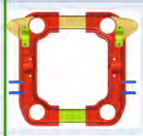	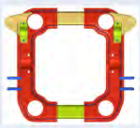	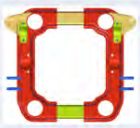	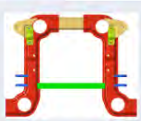	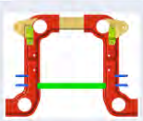
Metric	**CAE Target (subsystem/ interim)**					
Accelerations	<20G	30G	42G	30G	41G	49G
Battery Forces	<70kN	88kN	103kN	79kN	85kN	147kN
Door Intrusion	<40mm	127mm	69mm	48mm	79mm	15mm
Longitudinal Efficiency	-	37%	36%	51%	36%	44%
Body Mass	-	148kg	161kg	132kg	148kg	129kg
Subframe Mass		18.4kg	18.4kg	18.4kg	21.1kg	21.1kg
Overall performance status						

Figure 6.3.3.5 Rear crash structure FEA concept design studies (see Appendix 4 for larger image)

Subsystem development of the rocker and side crash structure was also undertaken. The side crash structure was developed for two crash loadcases: the USNCAP 32kph side pole and the IIHS 60kph side barrier. The side pole test impacts the body structure over a relatively small contact area, primarily loading the rocker, with secondary contribution from the side closures and cantrail in the roof. The IIHS side barrier test primarily loads the side closure's structure. The height of the barrier results in the rocker section missing the impact zone. In both tests, the objective is to ensure the occupants remain protected from intrusion of the body structure and the propulsion batteries remain undamaged. The main challenge with side crash is the relatively small space to manage the crash event compared to front and rear zones.

For the rocker, a strategy was adopted, where the outer part of the rocker featured a crush zone, the objective being to absorb the maximum amount of impact energy and the inner section engineered to be a protection zone, where the intrusion to the propulsion battery and occupant compartment would be minimised. (Figure 6.3.3.6). This is a similar concept as applied to the front and rear crush zones but confined to a much smaller area.

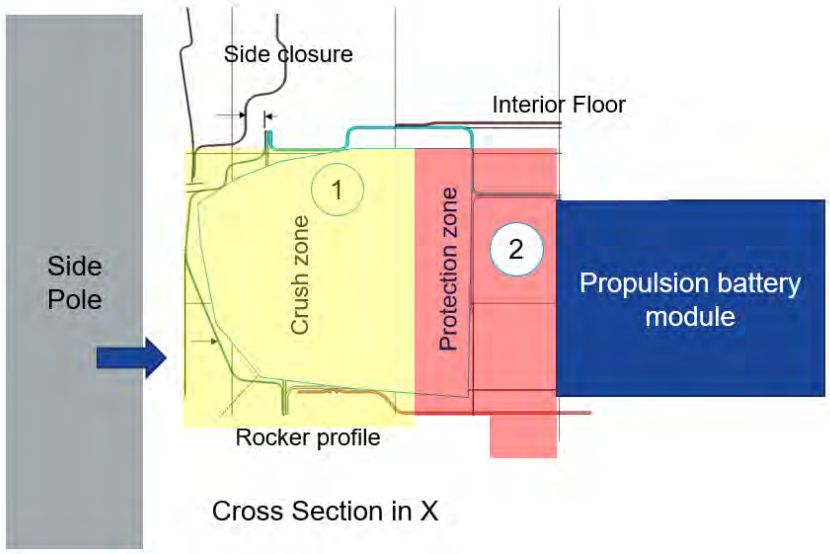

Figure 6.3.3.6 Cross section through rocker and floor showing strategy for outer crushable zone and inner protection zone.

Preliminary FEA studies were performed using a rocker and floor structure subsystem model (Figure 6.3.3.7), to evaluate several different rocker concept designs, adopting the strategy of crush and protection zones.

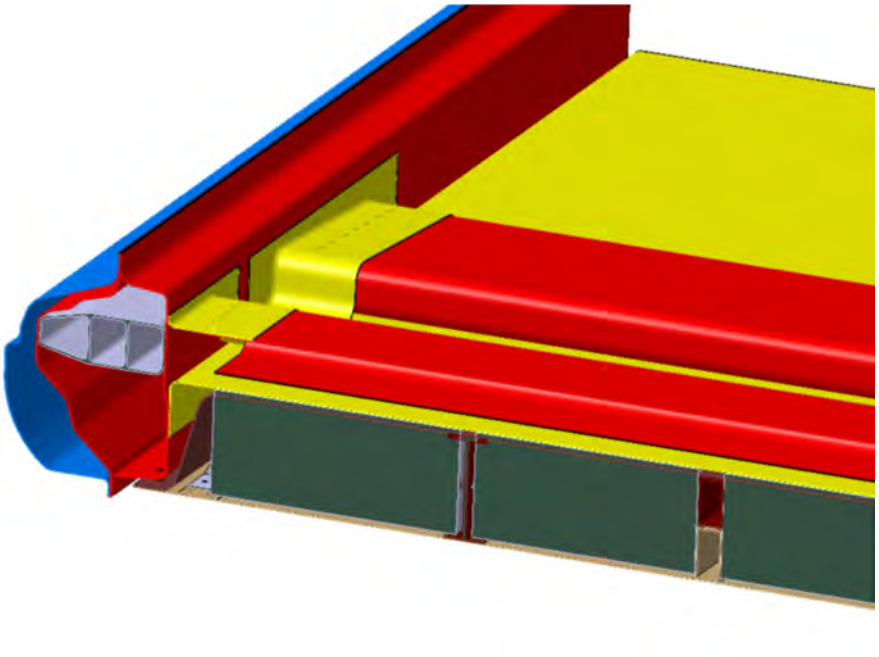

Figure 6.3.3.7 Rocker and floor FEA subsystem model

		(Benchmark study)	Concept 2	Concept 5	Concept 7.3.2
Mid-Zone Design (cross section profile)		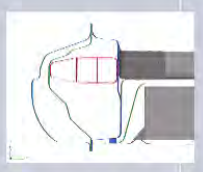	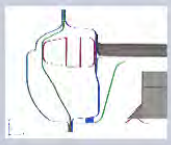		
Design concept		Extruded aluminium crush element, AHSS protection	Fabricated Advanced High Strength Steel crush element	**Coverless battery pack.** Body floor & crossmembers provide top cover.	**Sliding door concept** Re-profiled reinforcement sections, with stabilisers. Swages added to crossmembers. Sill inner increased thickness.
Metric	**CAE Target (subsystem model)**				
Rebound	-	35ms	43ms	33ms	29ms
Pole Force	-	625kN	560kN	552kN	544kN
Floor crush	<25mm	15mm	80mm	11mm	40mm
Rocker energy	>80%	82%	53%	95%	77%
Rocker Mass	<18kg/m	19.8kg/m	14.9kg/m	-	21.9kg/m

Figure 6.3.3.8 Preliminary rocker concept FEA studies, including aluminium extrusion benchmark (See Appendix 4 for larger image)

Firstly, a benchmark evaluation was performed considering an extruded aluminium crushable element. This determined some reference results that subsequent steel designs could be compared to. The subsystem FEA was not able to fully represent a complete side crash event, therefore metrics such as floor crush intrusion, rocker energy and weight per length were used as subsystem evaluation targets. The study concluded that a fabricated steel crushable element was able to match or outperform the aluminium extrusion.

The side closures were undergoing concept design at the same time as the rocker study. One concept under consideration was a sliding side door design, featuring body side rails and tracks along the length of the cantrail and rocker to guide the door during opening and closing. For the door to operate effectively, the lower track of the sliding door concept encroached significantly into the rocker structure. This design was assessed using the FEA subsystem model to understand the potential impact on side crashworthiness performance. The study concluded that the impingement of the closure rails into the rocker compromised the structural performance significantly and the crashworthiness of the rocker could not be recovered to the required levels. This result supported part of the decision not to proceed with sliding doors with body side tracks and rails.

Following the preliminary side crash FEA analyses, further rocker concepts were developed. Design brainstorming meetings were held, and several new concept ideas were generated and subsequently engineered and assessed in the FEA model. Figure 6.3.3.9 shows the concepts generated and the conclusions from the FEA evaluation.

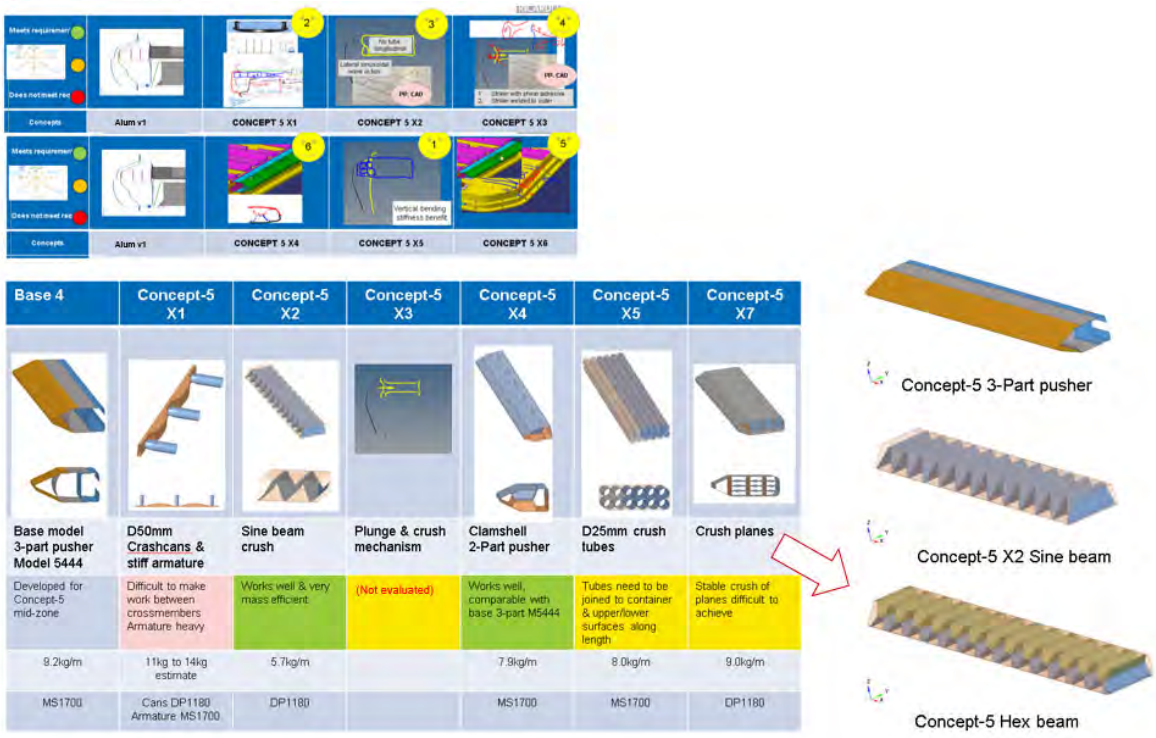

Base 4	Concept-5 X1	Concept-5 X2	Concept-5 X3	Concept-5 X4	Concept-5 X5	Concept-5 X7
Base model 3-part pusher Model 5444	D50mm Crashcans & stiff armature	Sine beam crush	Plunge & crush mechanism	Clamshell 2-Part pusher	D25mm crush tubes	Crush planes
Developed for Concept-5 mid-zone	Difficult to make work between crossmembers Armature heavy	Works well & very mass efficient	(Not evaluated)	Works well, comparable with base 3-part M5444	Tubes need to be joined to container & upper/lower surfaces along length	Stable crush of planes difficult to achieve
9.2kg/m	11kg to 14kg estimate	5.7kg/m		7.9kg/m	8.0kg/m	9.0kg/m
MS1700	Cans DP1180 Armature MS1700	DP1180		MS1700	MS1700	DP1180

Figure 6.3.3.9 Development and assessment of rocker crush element designs (See Appendix 4 for larger image)

The study showed that concept “5x2” gave good crush performance and weight efficiency. The part could either be stamped or roll formed and having a significant number of edge corners in the contact and crush direction resulted in large amounts of material work hardening and energy absorption. The “sine beam” concept evolved into a 2 part “hex” beam, offering greater energy absorption. A Dual Phase steel grade was selected for the hex beam due to its high elongation and energy absorbing qualities. This concept (Figure 6.3.3.10) was selected and incorporated into the complete body structure model for further development.

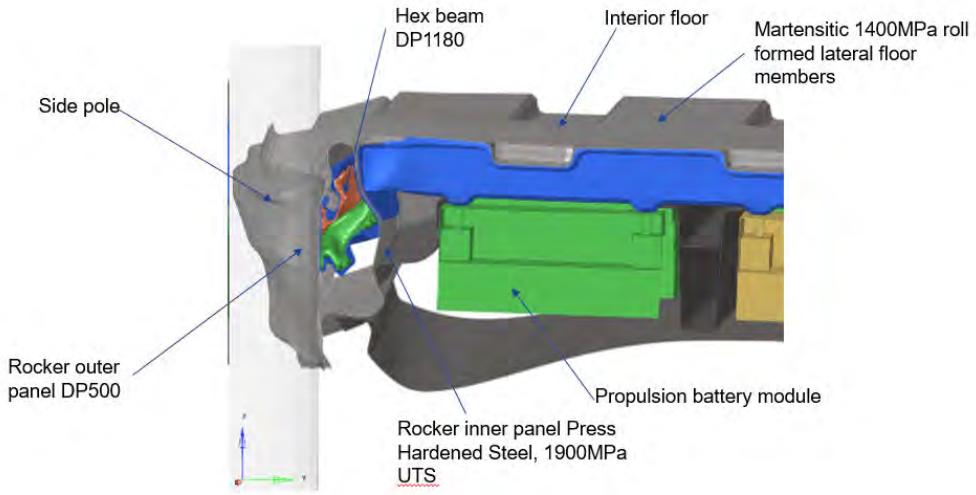

Figure 6.3.3.10 Rocker and floor concept, side pole subsystem FEA model showing the concept design selected for inclusion into the complete body model

6.3.4 Development of Propulsion Battery Concepts

The propulsion battery and supporting structure occupies a significant volume and has a significant contribution to the overall body and vehicle structural performance. Its weight is significant, (up to 1/4 of the vehicle curb weight) and also has the potential to contribute significantly to life cycle greenhouse gas emissions. Being a safety critical component, the battery must be able to withstand low and high-speed crash events as well as the fatigue and abuse loading from regular operation. A concept design study for the battery structure aimed to develop a lightweight design, featuring a low-cost design, achieving low life cycle greenhouse gas emissions, and meeting the structural performance targets. A total of six unique battery concepts were developed and explored.

The first battery concept to be developed was based around a “conventional” sealed pack unit. These are often referred to as “Generation 2” battery pack designs. The battery modules, cooling plates, bus bars and power distribution unit (PDU) are mounted to a stamped steel base plate, which also serves as the bottom protection cover on the underside of vehicle. A steel top cover encapsulates the modules and seals to the base plate, resulting in a fully enclosed battery unit. The pack is mounted to the body structure through fixings on the rockers. Figure 6.3.4.1 shows this concept applied to Steel E-Motive (“Concept 7”). The advantages of this design are improved (or robust) sealing solution, the pack can be manufactured and shipped off-site from the final vehicle assembly and the fully enclosed pack may better stiffness and strength performance. Concept #7 can also be easily integrated to the body and vehicle during assembly. The disadvantages of this design are higher weight and cost, as the top cover function is effectively duplicated by the floor of the BIW, low frequency modal resonance due to the battery modules mounted to a skin plate and potential damage to the modules from debris due to their proximity to the underside of the vehicle.

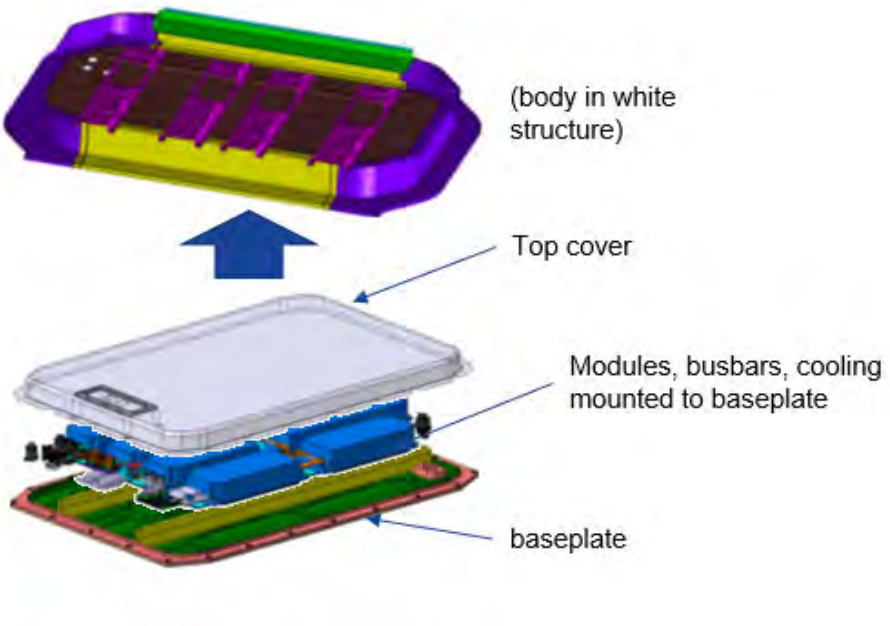

Figure 6.3.4.1 Battery Concept #7, “conventional” sealed battery pack

Battery concept #5 (Figure 6.3.4.2) was an evolution of concept #7, where a weight and cost saving were achieved by deletion of the top cover. The BIW floor design and sealing between the baseplate and rocker underwent design improvements to ensure the pack maintained the required sealing performance.

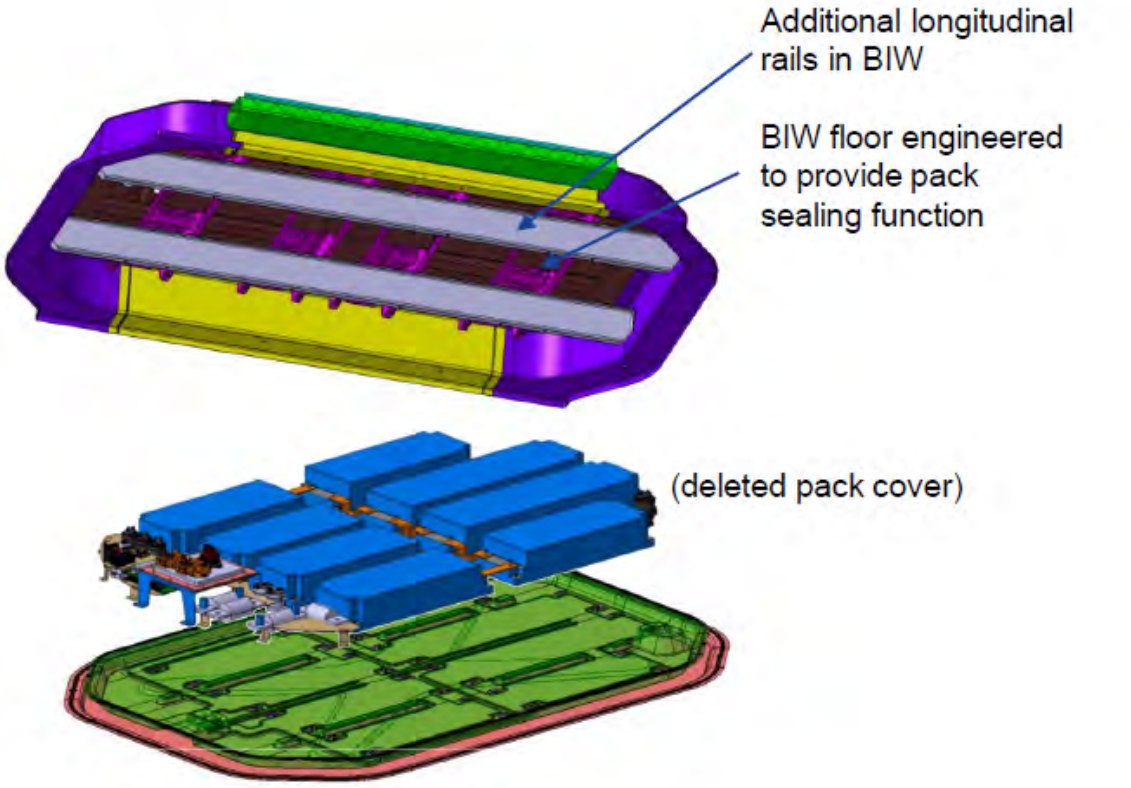

Figure 6.3.4.2 Concept #5, “coverless” pack concept

Battery concept #8 (Figure 6.3.4.3) featured a more radical design with the battery modules mounted (bolted) directly to the body in white, instead of bolting to the battery baseplate. The BIW maintained the sealing function to the floor with the top cover deleted. By attaching the battery modules to the BIW (longitudinal) directly provides improved support and stiffness than mounting to the baseplate. The module locations are also slightly higher than concepts 5 and 7, resulting in a greater clearance between the bottom of the module and the protective baseplate cover. The results in a lower risk of damage as a result of debris impact or incorrect vehicle jacking or lifting from underneath the vehicle. The consequence of this approach is that assembly of the modules to the body is more complex and potentially longer due to increased number of fixings and assembly processes.

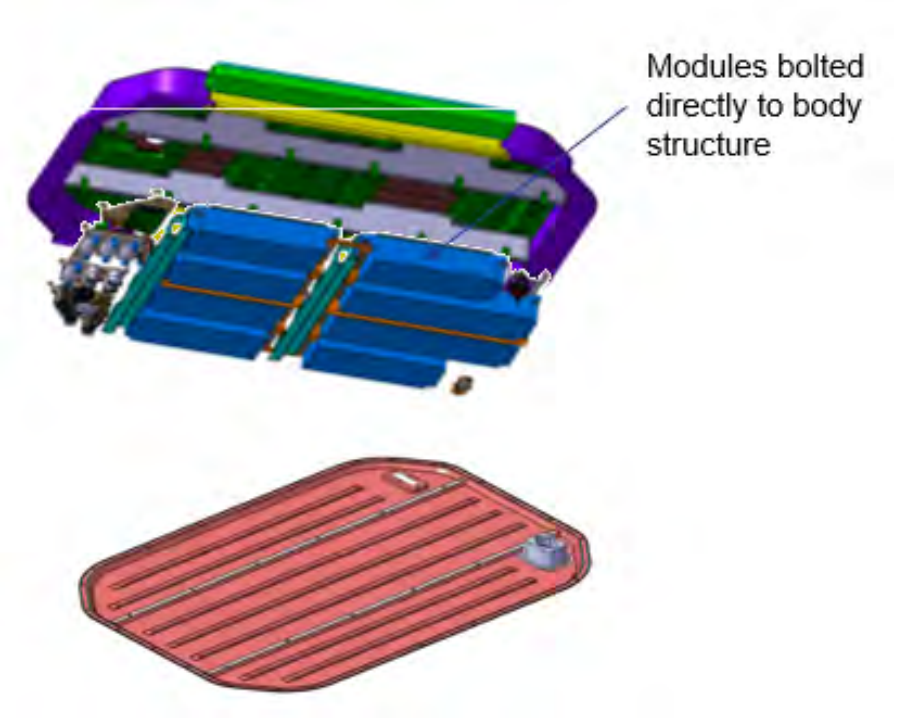

Figure 6.3.4.3 Concept #8, modules to body

The assembly risks and concerns were investigated by undertaking comparative evaluation of the manufacturing steps of concepts 5,7 and 8. The pack sub-assembly, pack and vehicle assembly processes were mapped as shown in Figure 6.3.4.4.

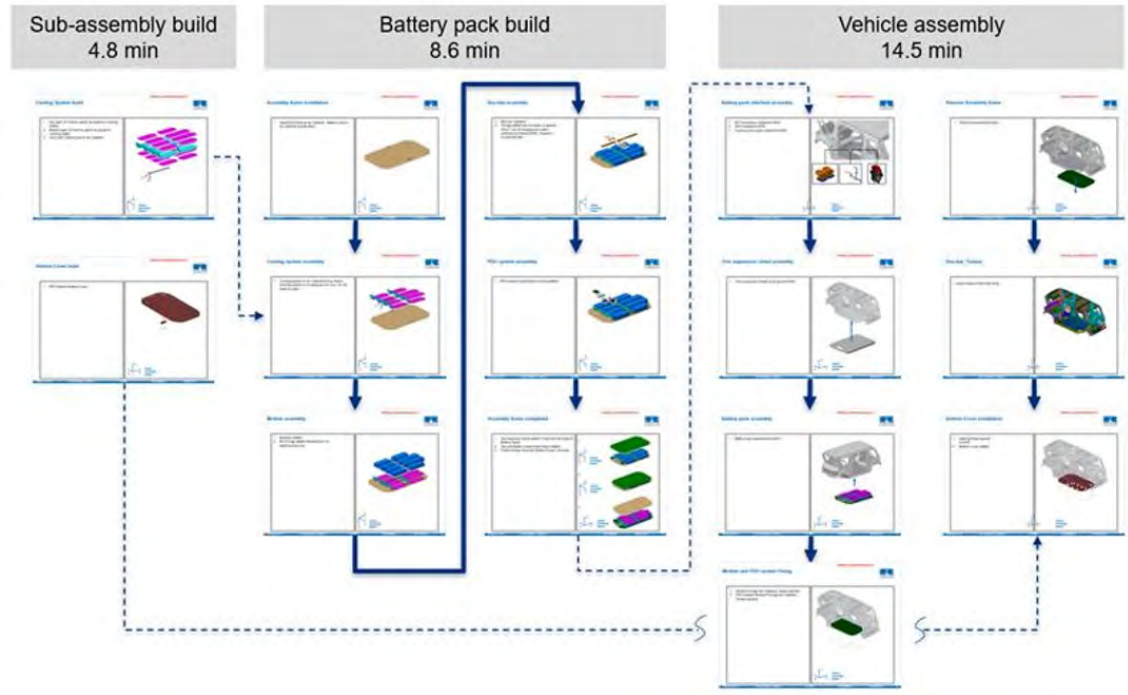

Figure 6.3.4.4 Battery concept #8 assembly process (battery into vehicle only) (See Appendix 4 for larger image)

The manufacturing evaluation concluded that the battery and vehicle assembly “TAKT” time was increased by 15% when compared to concept 7 (Figure 6.3.4.5). Installation of concept 8 battery modules directly to the body structure was identified as particularly challenging. This would require an additional, bespoke vehicle assembly station, where the vehicle would be inverted (upside down), enabling the battery modules to be inserted from above. Concept 8 would also require an additional assembly jig or platen for the modules to be pre-assembled and aligned to prior to the marriage to the body structure.

Concept variant	Assembly time (est seconds – considers series assy)			
	Total time	Battery Sub-assy Build	Battery Pack Build	Vehicle Build
7	1450 (100%)	460	730	260
5	1100 (-24%)	0	570	530
8	1665 (+15%)	290	515	860

Figure 6.3.4.5 Comparison of battery and vehicle assembly times for concepts 7, 5 and 8

Battery concept #9 investigated the potential for extreme levels of integration between the body structure and battery pack, with the pack structure containing the floor element of the BIW (Figure 6.3.4.6)

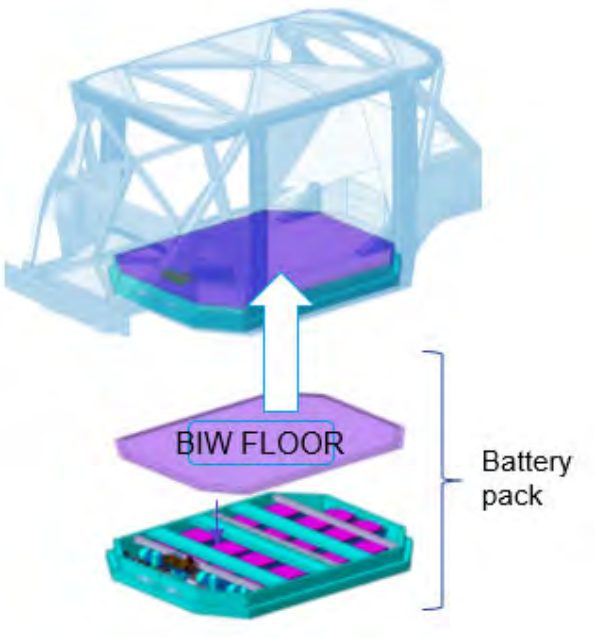

Figure 6.3.4.6 Concept #9, battery pack containing BIW floor structure

The BIW is engineered to feature a void where the conventional floor structure would reside. The battery pack top cover is engineered to be the floor structure of the BIW and assumes it's role when the battery and BIW are married on the vehicle assembly line. The battery top cover is a single panel but dual purpose, enabling weight and cost savings. With this concept, the main challenges are the sealing between the occupant compartment and the battery and ensuring overall structural performance of the body system with the separated floor structure. The design and analysis studies showed that these challenges could be largely overcome.

Battery concept #11 features a structural carrier frame from which the battery modules, power distribution unit, busbars and cooling plates are mounted. The carrier frame provides a stiffer structure to mount the battery components from compared to the other concepts (e.g., mounting from the base plate). Several different concepts of structural frame were considered and explored. The final frame concept featured two Dual Phase grade longitudinal members, primarily providing vertical stiffness with roll formed Martensitic lateral cross members provide load reaction in side crash. The frame features no top cover – the BIW floor provides the upper sealing function. The frame is mounted to the BIW via fixings into BIW floor cross members. After the battery pack is assembled to the BIW, a structural undertray panel is fixed to the base of the BIW, completing the sealing of the battery compartment and providing impact and jacking load resistance from underneath. Figures 6.3.4.6 show the overall Concept #11 layout and the Phase 1 design of the battery pack and structural carrier frame.

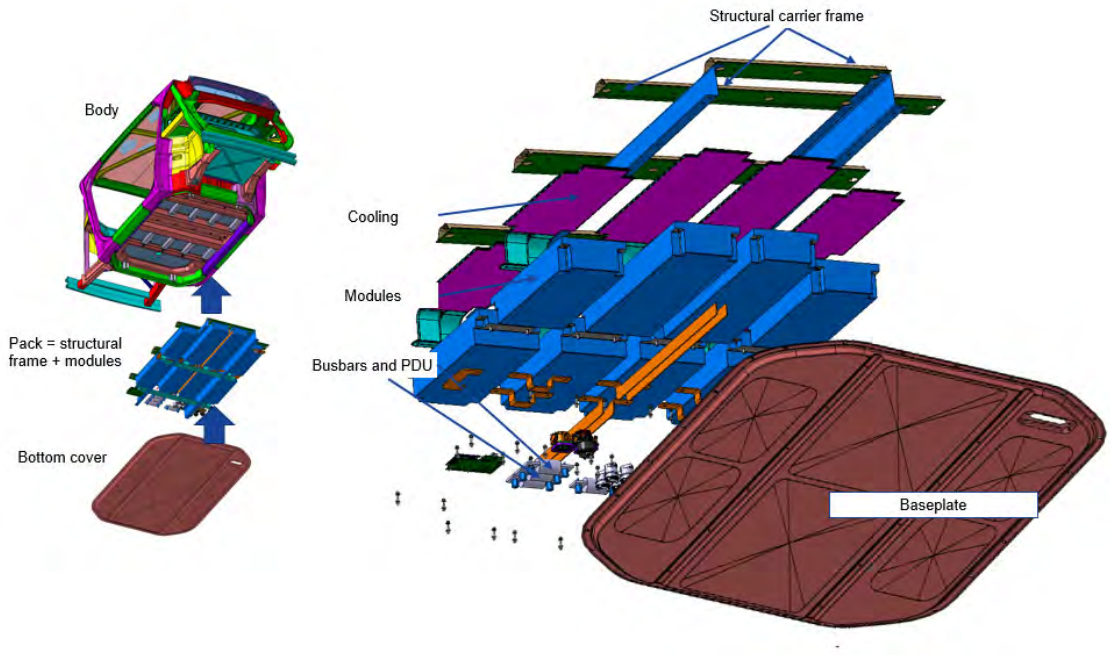

Figure 6.3.4.7 Battery concept #11 (See Appendix 4 for larger image)

Selection of battery concept:

A concept selection matrix was devised to evaluate and identify the battery concept which provided the best overall performance given the requirement of the Steel E-Motive project. A scoring system was used to rate each concept comparatively. A combination of CAD design data, FEA calculations and subjective opinion was used. The main requirements and considerations for the battery concept selection were defined as:

- Battery and BIW sealing. For many of the concepts this was a considerable challenge, requiring more complex design of seals. All designs would meet the requirements for sealing. Higher scores were awarded to concepts with a lower risk and lower complexity of sealing design
- Available internal battery volume: A larger battery internal volume enables a larger battery to be housed and may also offer benefits such as improved cooling. A larger internal battery volume was awarded a higher score. The absolute available volumes were calculated from CAD, therefore the results were aligned to objective metrics
- Thermal runaway suppression: Whilst all packs were expected to meet safety requirements, some back designs would provide better suppression of a thermal runaway incident than other designs. A higher score was awarded to designs with better thermal runaway suppression. This evaluation was purely subjective
- Battery pack weight: This is the overall weight of the battery pack, including supporting structure, frames, busbars, cooling, PDU and cover plate. Values were calculated in CAD. More lightweight concepts were scored higher
- Battery pack and BIW midzone weight. As some concept featured overlap and integration with the packs and BIW, the combine weight was assessed (similar to above)
- Manufacture build time (battery and pack): Higher scoring concepts had relatively simple assembly processes. Lower scoring concepts were estimated to have longer TAKT times and additional build steps, jigs, and fixtures
- Complexity (number of parts): concepts requiring more parts would typically be higher cost and have higher life cycle impact. More simple concepts with lower parts were scored higher
- Debris impact performance: Concepts where the modules are mounted to the baseplate/undertray may potentially have a higher damage risk from road debris and accidental jacking than concepts where the modules are mounted further away from the groundline or have improved protection. Concepts with good protection were scored higher
- Modal performance (pack only). There is an NVH requirement for the first installed battery mode to be >35Hz. In most cases, the battery concepts were able to demonstrate that this target was achieved. Concepts were scored higher where the target was comfortably met, or limited design changes or countermeasures were required
- Body torsion: relates to static torsional stiffness performance. With the battery pack contributing significantly to overall body stiffness, concepts were scored higher where a higher combined torsional stiffness was achieved (evaluated using FEA)
- Service and rework: concepts with easier, shorter, and less complex steps to access the battery in the case of servicing or repair were scored higher
- Cost: whilst no specific costs were calculated at this stage, a subjective approach was taken to evaluate each pack cost comparatively. Packs expected to be lower costs scored higher
- Recycling (End of life): the propulsion battery has a significant contribution to the overall greenhouse gas emissions of a vehicle. Concepts were assessed subjectively as to the recycling efforts and potential
- Demonstration of steel: an additional evaluation where concepts demonstrating unique steel grades, fabrication processes or exceptional performance in steel were scored higher

Each concept was rated 1 to 5 for each of the above assessments. The scoring was undertaken amongst the engineering and design teams. The results of the concept are shown below (Figure 6.3.4.8) and graphically in a radar plot (Figure 6.3.4.9)

Attribute / Battery Concept	Concept 7	Concept 5	Concept 8	Concept 9	Concept 11
Battery (and BIW) sealing	4	2	4	3	4
Available internal batt pack volume	2	3	5	4	5
Thermal runaway suppresion (risk)	5	3	2	4	2
Battery Pack Mass	2	4	5	1	5
Batt Pack and BIW Midzone Mass	2	4	5	1	5
Manufacture Build Time (battery pack and vehicle)	3	5	1	2	5
Complexity (number of parts)	5	2	4	1	6
Debris Impact Performance (	4	4	5	5	5
Modal Performance (Pack only)	3	3	5	4	4
Body Torsion	3	3	5	4	4
Service and Rework	4	5	3.5	3	3.5
Cost	4	4	4	2	5
Recycling (EOL)	4	4	4	2	5
Demonstration of steel	2	3	4	3	4
Total	47	49	56.5	39	62.5

Figure 6.3.4.8 Battery concept evaluation matrix

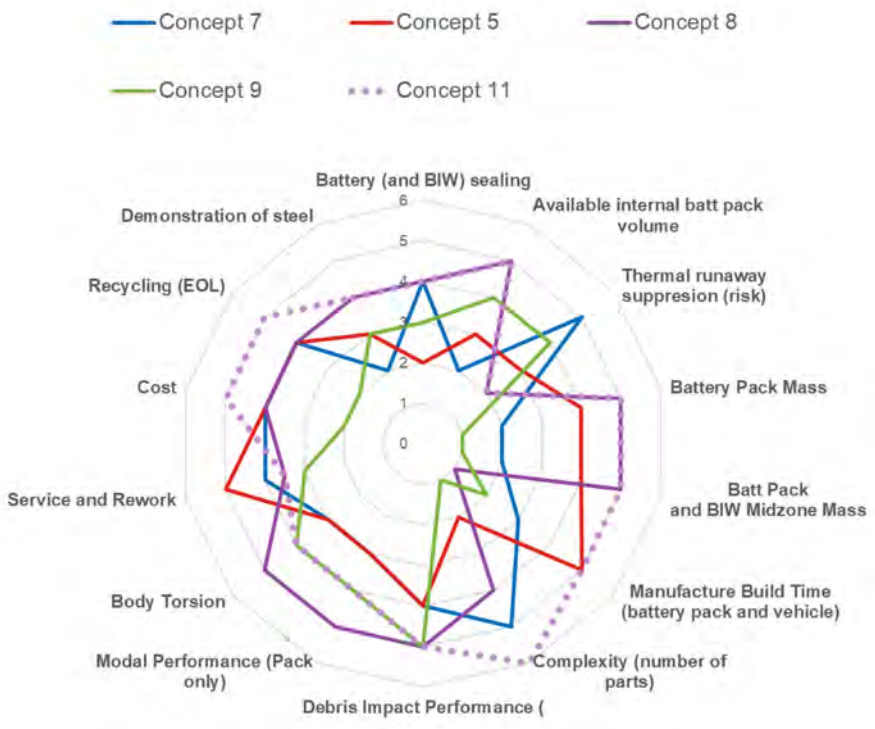

Figure 6.3.4.9 Battery concept evaluation radar plot

The evaluation concluded that concept #11 provided the best overall performance. Assembling the battery modules and components to the carrier frame overcomes the assembly challenges of concepts 8 and 9, whilst the structural carrier frame provides good stiffness and support to the modules, which also have increased clearance to the baseplate meaning better impact resistance. At the time of the study, the engineering teams were not aware of similar concepts in production or in development, hence, concept #11 offered a unique solution and was expected to be able to meet all targets. Preliminary FE analysis of concept #11 confirmed the structural performance. Concept #11 was selected as the primary design direction at the end of Phase 1. Phase 2 focussed on further refinement and validation of concept #11.

6.3.5 Development of closures concepts

The preliminary studies in Phase 0 identified that a “sliding” side door design would be best suited for the Steel E-Motive vehicles. This would improve the accessibility to vehicle users, both able bodied and disabled. The term “sliding” refers to the motion of the doors relative to the vehicle (i.e., along the length of the vehicle instead of hinged and swinging outwards). Achieving a “sliding” side door trajectory could be achieved by different mechanisms. Two such door mechanisms were evaluated in Phase 1; a sliding “track and rail” approach and a “scissor” door approach.

6.3.5.1 Track and rail sliding door

Sliding track and rail side doors are common on larger, present day passenger cars, multi-purpose vehicles (MPV) and light commercial vehicles. An example of a sliding door using track and rails is shown in Figure 6.3.5.1.1

Figure 6.3.5.1.1 Track and rail sliding door, Ford B-Max passenger car (images from a2mac1)

The door is supported and connected to the body at 3 locations; an upper rial, centre rail (which is partially visible on the exterior) and a lower rail. The 3 rails are mounted and integrated into the body structure. The door attaches to the 3 rails via guides and brackets – the upper and lower guides feature a roller wheel which locates inside the door side rails.

The shape and profile of the rail determines the path of the door on opening and closing. The path of the door on initial opening needs to be outwards (laterally) to provide clearance for the door to then slide rearwards. The door rails therefore feature a curved then straight profile as shown in Figure 6.3.5.1.2

Figure 6.3.5.1.2 Ford B-Max sliding door track profile (plan view, image from a2mac1)

The sliding door tracks are integrated into the body structure. The curved profile results in a significant impingement into the body structure as shown in Figure 6.3.5.1.3. This requirement may lead to a degradation to overall structural performance and may compromise side crash performance where the strength of the rocker and cantrail are important. The package for the lower rail is likely to encroach into the battery pack, reducing effective volume and compromising structural integrity.

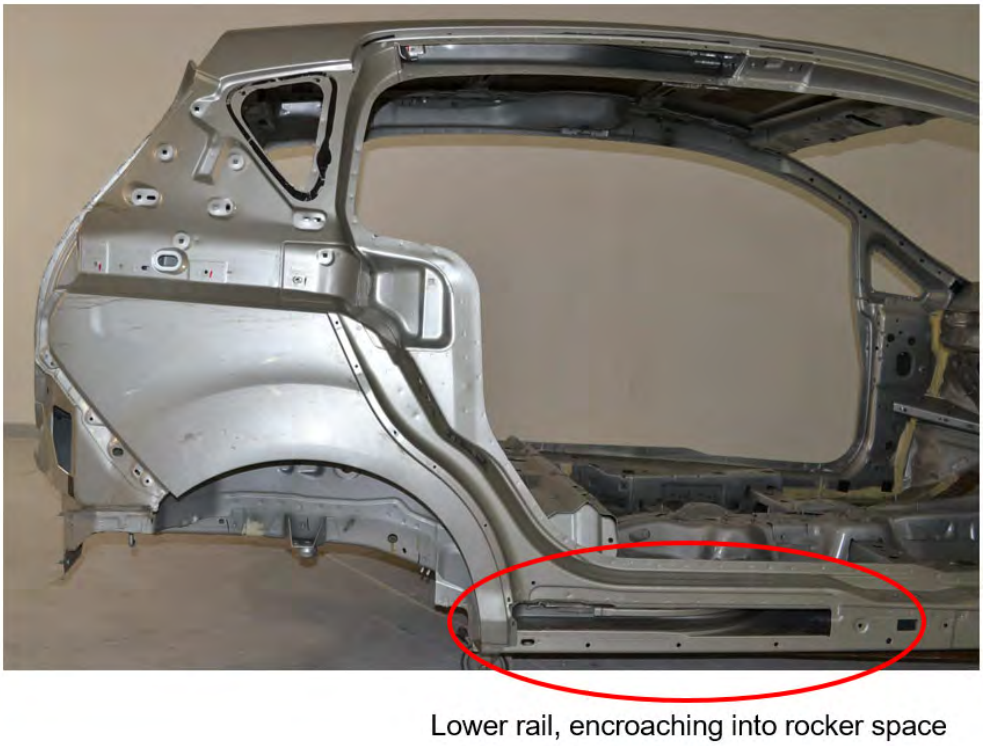

Figure 6.3.5.1.3 Ford B-Max BIW, showing lower sliding door rail position encroaching on rocker and floor (image from a2mac1)

A concept design study was undertaken to develop a track and rail sliding door concept for the SEM1 vehicle. Given the size of the door aperture and the overall length of the vehicle, it was not possible to package a split (2 doors) arrangement due to insufficient space for the

mid track front. A single door sliding to the rear of the vehicle was therefore configured as shown in Figure 6.3.5.1.3.

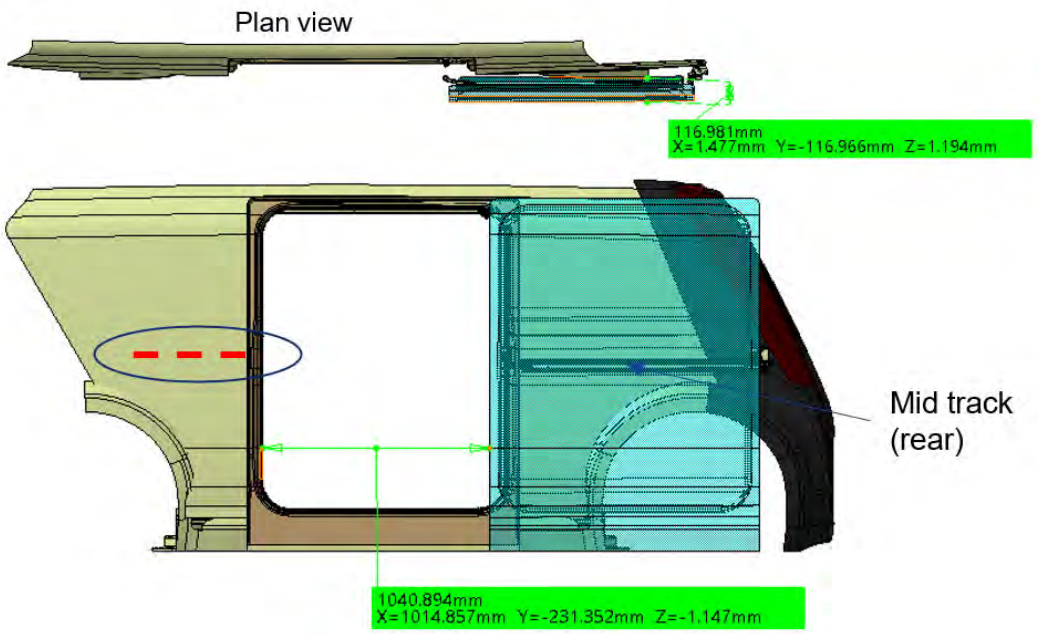

Figure 6.3.5.1.3 SEM1 track and rail sliding door concept study.

The design of the upper and lower door tracks investigated the impact on the rocker and battery compartment. A significant encroachment of the rocker and its crash structure was required to accommodate the lower track. The battery compartment package was also impacted as shown in Figure 6.3.5.1.4.

Design studies attempted to develop countermeasures, however FEA analyses predicted a significant degradation in the side pole crash performance with the sliding door track arrangement.

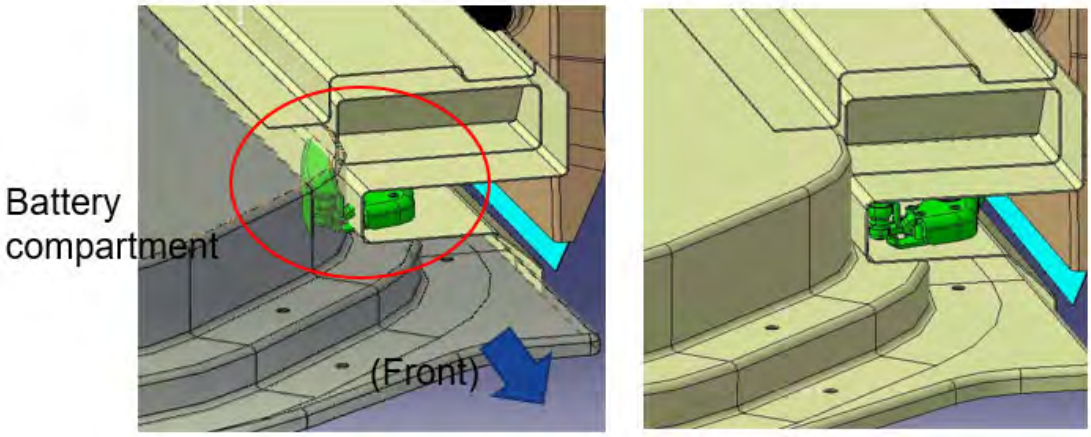

Figure 6.3.5.1.4, battery compartment package clash with sliding door lower track

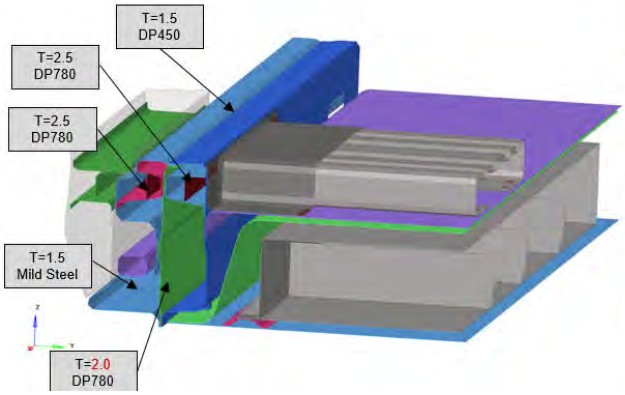

Metric	CAE Target	Status
Rebound	-	29ms
Pole Force	-	718kN
Floor crush	< 25mm	40mm
Sill energy	> 80%	46kJ
Ratio		77%
Sill mass per length	< 18kg/m	21.9kg/m

Figure 6.3.5.1.5 Section in X showing left side rocker, sliding door incorporating lower track. Degradation in structural performance due to packaging of lower track in the rocker

6.3.5.2 Scissor hinge sliding door

"Outward swing door mechanism" (referred to as scissor door mechanism in the Steel E-Motive project) are commonly found on bus and coach vehicles, an example shown below in Figure 6.3.5.2.1

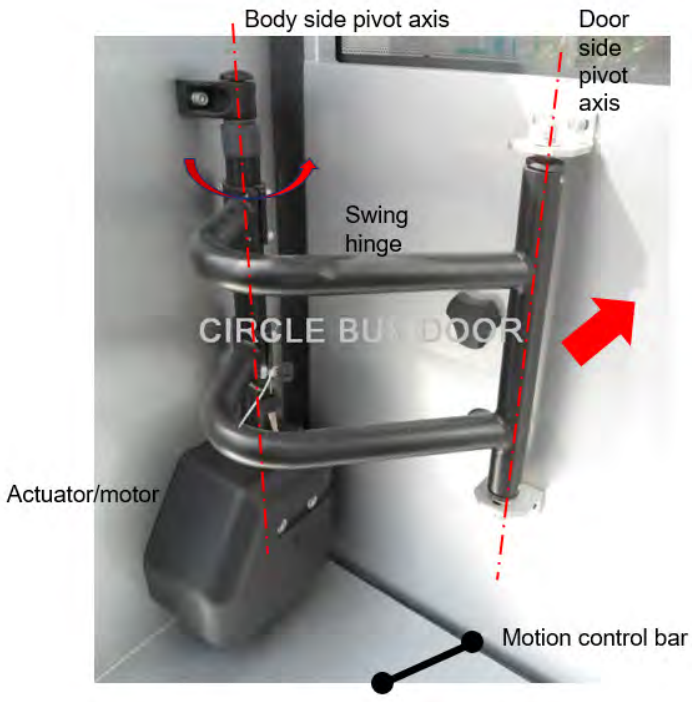

Figure 6.3.5.2.1. Example of scissor (outward swing door mechanism). Image source http://www.circlebusdoor.com/products/eom100-electric-outswing-bus-door-mechanism-for-bus-and-vehicle/

The actuator provides an input torque to the body side pivot bar, rotating the bar through approximately 120degrees. The resultant moment pushes (swings) the door initially outwards away from the door aperture then longitudinally along the length of the vehicle to

provide the opening. A motion control bar constrains the rotational motion of the door around the door pivot axis and guides the door as it opens. The challenges with the scissor door mechanism are the higher distance in lateral offset (or kerbside encroachment) when the door is opened compared to track and rail. The hinge and actuator can be significant in size and encroach on occupant space and the moving parts are a potential injury risk. The hinge on the door side is mounted to the centre of the door structure so some structure is required to support the door side hinge brackets. Preliminary concepts were developed for Steel E-Motive as shown in Figure 6.3.5.2.2.

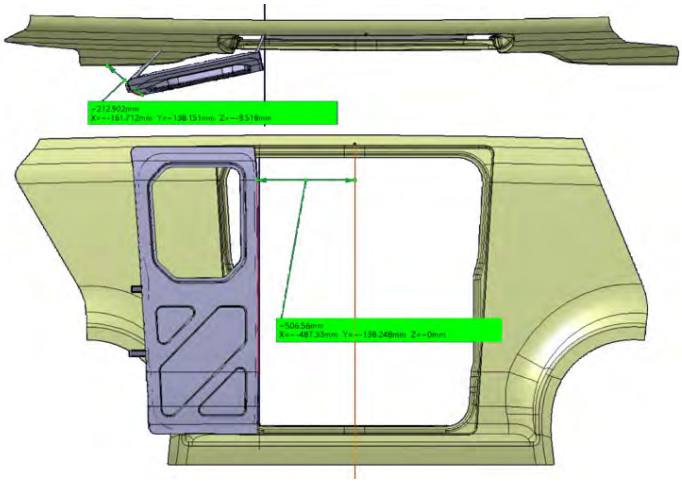

Figure 6.3.5.2.2 Scissor door, preliminary Steel E-Motive concept

The study showed that the hinge and door could be design and packaged effectively and the curb encroachment distance in the open position calculated at 250mm (versus 117mm on the track and rail concept).

During Phase 1, the body structure concept was modified to incorporate inclined A and C pillars which were moved forwards (A) and rearwards (C) in order to improve the loadpath distribution.

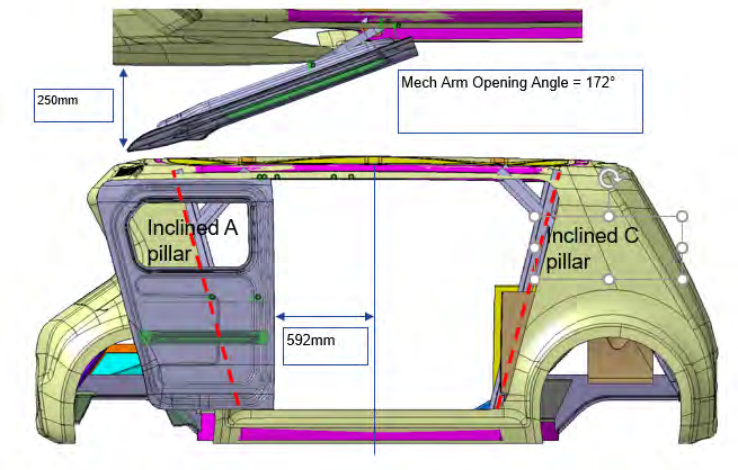

Figure 6.3.5.2.3 Door aperture width increase a door design change

The door aperture increased from 1012mm to 1184mm. The curb side encroachment increased from 138mm to 250mm. The track and rail and scissor door concept then underwent evaluation and concept selection as described below in Section 6.3.5.3

6.3.5.3 Evaluation and selection of sliding door concept

The MoSCoW prioritisation process was used to assist the selection of one sliding door concept to progress and develop in Phase 2. The key criteria identified for the side closures were:

- Mechanical package. The space and encroachment challenges imposed by the door structure, hinge, actuators, and tracks
- Kerbside ingress. This maximum lateral distance that the door opens by, encroaching on to the kerbside
- Opening aperture. The minimum effective distance between the doors when fully open
- Weight. Weight of complete door system, including body side components
- Cost. (note, no specific cost evaluation was done at this stage)
- Glazing. The potential to feature a reasonable sized glazed area on the doors
- Side crash. The challenge or additional risk imposed on side crashworthiness performance by the door design
- Front crash. The challenge or additional risk imposed on front crashworthiness performance by the door design

The MoSCoW evaluation is shown in Figure 6.3.5.3.1. This concluded that the scissor door mechanism posed the least integration challenges compared to the track and rail concept. The higher curb side encroachment in the scissor door design was deemed to be acceptable. The scissor door concept was selected as the primary concept for further development and refinement in Phase 2.

		Scissor	Sliding (track and rail)
M S C W	Meets requirement Not recommended		
M	Mechanical Package	Mech arm and motor can be well packaged. Fixed upper pivot arm easy to package	3 sliding rails provide a lot of packaging challenges taking up a lot of space
S	Kerbside Ingress (Minimal)	Currently ~212mm at open kerbside ingress but can be tuned – 312mm during sweep	
M	Opening Aperture >1000	~1184mm (with detail will be approx. 1050/1100mm)	827mm – overlap of aperture with Dorito door shape
M	Mass (Estimate)	TBC, was 26.4kg/side on Incremental	Was 31.7kg on Incremental, likely to be heavier
M	Cost ($0.00)	Not assessed	
C	Glazing		
M	Side Crash	Door structure can be utilised to help side crash (virtual b-pillar)	Door structure available but slider detrimental to rocker
S	Front Crash	Waistrail tertiary path possible (not assessed)	Waistrail tertiary path possible (not assessed)
Conclusion for SEM1 application			

6.3.5.3 Rear tailgate concept development

The rear closure or tailgate enables access to the rear luggage compartment and forms the rear exterior surface of the vehicle. The tailgate aperture should be sufficient to enable everyday items such as luggage and shopping to be safely stowed. No specific rear closure concept designs were generated in Phase 0. Six concepts were generated within Phase 1 as shown below in Figure 6.3.5.3.1

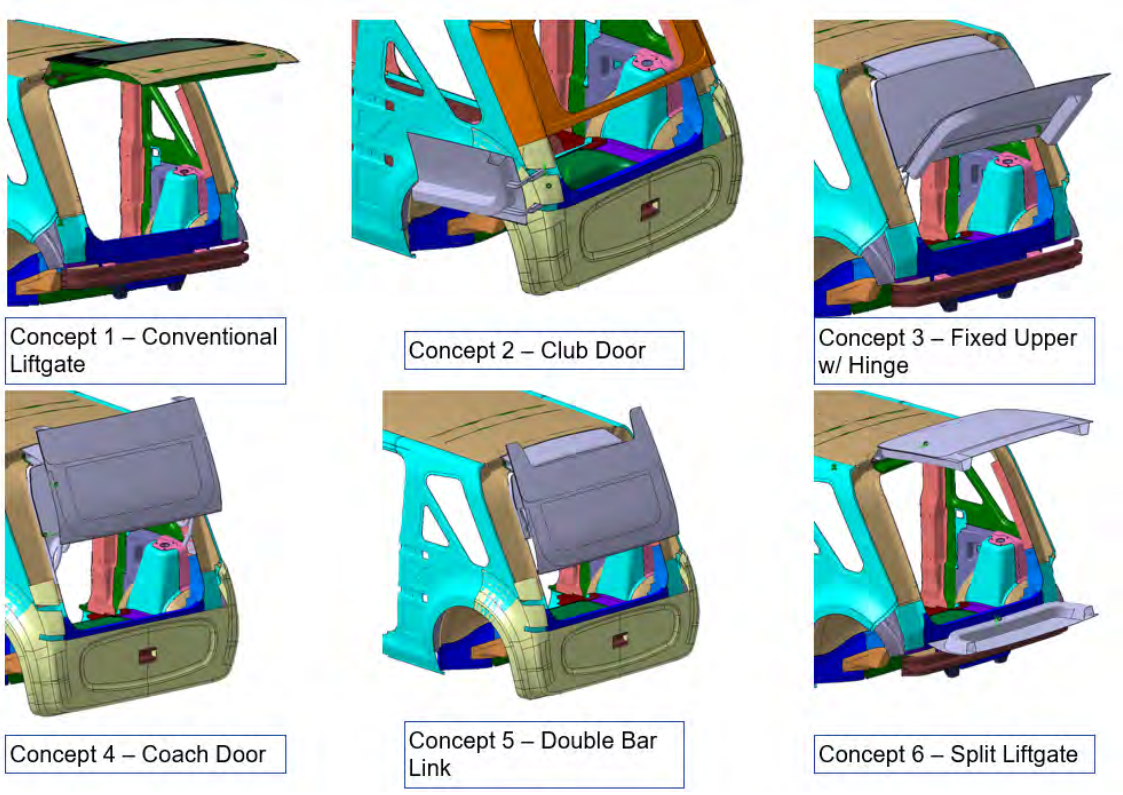

Figure 6.3.5.3.1 Rear tailgate concept designs for SEM1

Concept 1 was based on a conventional liftgate as seen on estate and SUV style passenger cars. The door is mounted to the body via hinges (usually two) mounted to the rear header rail of the body. Gas struts provide assisted opening and powered mechanism are common also. Club door (concept 2) features single or twin doors, hinged on the rear D pillar. Whilst unique in style, the rearward swing motion encroaches on the rear of the vehicle and could be challenging for taxi like operations. Operation of these doors is challenging if the hinges are not oriented vertically. Concept 3 is similar to Concept 1 liftgate, but the upper portion of the closure is fixed (glazing) with just the lower half of the door able to open. Concept 4 coach door is based on a design commonly found on the underside stowage compartments of large coach vehicles. Hinges are mounted on the rear D pillars and a parallelogram hinge mechanism results in a vertical and upward motion of the door with reduced rear encroachment. Concept 5 features a D pillar mounted twin link bar mechanism, similar to concept 4, resulting in a more vertical door motion but with reduced door aperture. Concept 6 is a split rear tailgate, seen on some Sport Utility Vehicles. It provides a large aperture but the drop of the rear liftgate can give challenges when loading and unloading. Given the number of concept design, a descriptive concept selection matrix was devised and populated as shown in Figure 6.3.5.3.2.

BASELINE SELECTED

Attribute	Concept 1 – Conventional Liftgate	Concept 2 – Club Door	Concept 3.1 – Half Liftgate with Exposed Hinge	Concept 3.3 – Half Liftgate with Fiat 500 Hinge	Concept 4.1 – Coach Door	Concept 4.5 – Coach Door Revision	Concept 5 – Double Link Hinge	Concept 6 – Split Liftgate
Tailgate Opening (mm)	1431	449	449	610	688	690	462	1431
Interior Intrusion	N/A	N/A	N/A	N/A	235mm (x) from back of closest passenger	Crank of looped arms currently sits 352mm (x) from back of closest passenger	N/A	N/A
Mechanical Package	Simple hinge design with powered strut mounted to BIW	Connecting arm must be exposed to allow for secondary hinge axis to be outside the vehicle Requires A-Surface to move	Hinges must be exposed to allow for correct sweep that doesn't clash with glazing	Full hinge assembly with base/door plates packages well into BIW	Large connecting arms difficult to package Hinge axis can be changed to allow for more efficient package and eliminate some current clashes	Needs consideration for driving mechanism (Stabilus Powerise or motor) Connecting arms package more efficiently than previous concept 4.1 due to reduced crank throw	Concept needs to be further developed to efficiently package hinge design without BIW clashes	Concept needs to be further developed to efficiently package hinge design without BIW clashes
Kerbside Ingress (mm)	N/A	635	N/A	N/A	N/A	N/A	N/A	N/A
Vehicle Height Impact (m)	1.99 (+0.11)	N/A	N/A	N/A	2.03 (+0.15)	2.03 (+0.15)	1.98 (+0.10)	2.02 (+0.14)
Rear Overhang (mm)	646	695	363	447	185	197	113	296
Overhang at Open Position (mm) (measured from bumper A-Surface)	653	-114	/	258*	/	-66	-40	296
Fixed Glazing	N	Y	Y	Y	Y	Y	Y	N
Rear Box Section Potential (global stiffness contribution)	N	Y	Y	Y	Y	Y	Y	N
Door Panel Mass Estimate (kg)	19.62	7.47	/	10.6	/	11.8	10.6	19.2
Cost Estimate	WIP							

Figure 6.3.5.3.2 Rear closures concept selection matrix (See Appendix 4 for larger image)

The study concluded that Concept 4 coach door provided the best solution for Steel E-Motive vehicles. The hinge mechanism enables reasonable opening aperture and has lower rear encroachment. This helps when operating in confined areas, for example, when the vehicles are queued in a taxi rank or at an airport. Concept 4 coach door was selected for further development and refinement in Phase 2.

6.3.6 Front crashworthiness challenges and strategy

6.3.6.1 Introduction and background to front crashworthiness challenge

One of the most significant challenges encountered during the engineering development of the Steel E-Motive concepts was the achieving front crashworthiness performance. The front crash loadcases and targets are described in Section 4.2.3. One particular challenge was achieving a solution that balanced the conflicting requirements of the USNCAP 56kph full width rigid barrier (FFB) and the IIHS 64kph small overlap rigid barrier (SORB). The FFB test requires a crush zone engineered to decelerate the vehicle progressively and controllably, with minimum deceleration pulse. Crush intrusion into the occupant compartment should also be minimised and be within the targets. Conversely, the SORB test requires a significant amount of strength in the front crash structure. With the 25% front barrier overlap and higher impact velocity, the front crash structure needs to “work” much harder to manage the energy and prevent intrusion. A higher strength structure is required to manage the crash loads in the SORB test, but this is too stiff and strong for the FFB test. This results in high deceleration pulse in FFB as a smaller crush length is used. Essentially the front crash structure needs to be engineered for two quite different requirements. Due to the higher impact speed and small overlap, the SORB test encompasses more of the vehicle than the FFB test. The front suspension, wheels and tyres, rocker and front door structures are all impacted by the crash event and the design of these components and system contribute to crashworthiness performance in SORB. Because of this, a more comprehensive FEA model

was required. Therefore, a complete understanding of the SORB performance and challenges was not possible until mid-way through engineering Phase 1, where the design of the components and systems were sufficiently mature for a representative FEA could be constructed. The front crashworthiness challenge was further compounded by the overall size and compactness of Steel E-Motive – with a short frontend and overhang distance, there is less “metal” to absorb the crush energy. The package space in the front motor compartment is generally more compact, resulting in systems such as the EDU contributing or disrupting the crash structure behaviour.

6.3.6.2 Desktop benchmarking of front crash strategies

The USNCAP 64kph FFB test is well established and the strategies and solutions for achieving performance are well understood. It was established early in Phase 0 and 1 that SEM1 could be engineered to meet the crashworthiness targets for this test by engineering of front longitudinal crush members and rigidly mounted front subframe. The IIHS SORB test was introduced in 2012 and as this is a US specific consumer focussed assessment, IIHS evaluations are typically carried on larger sized vehicles where the sales volumes of smaller compact vehicles (e.g., European A, B, C sized vehicles) are lower compared to D, E segment, SUVs, and pickup trucks. The IIHS publish results from crash tests on their website (https://www.iihs.org/), with more detailed test data made available through their “techdata” portal, requiring a specific account and login. The smallest sized vehicles evaluated by IIHS at the time of the Steel E-Motive project were the BMW i3 and Volvo XC40 recharge (both with hybrid electric powertrain). Both vehicles achieved the highest “good” rating for the SORB and the moderate overlap deformable barrier test. Figure 6.3.6.2.1 shows a still image from the Volvo XC40 test. The video for the test can be viewed at https://www.iihs.org/ratings/vehicle/volvo/xc40-recharge-4-door-suv/2022

Figure 6.3.6.2.1 Volvo XC40 Recharge (2021MY) IIHS 64kph frontal small overlap test

The animation shows that the as the vehicle strikes the barrier, it is deflected laterally, such that by the time the barrier reaches the hinge pillar (as in the still image), the vehicle has moved laterally such that there is reduced contact and impact with the barrier. The vehicle continues with a reasonable onward velocity. The vehicle is said to “glance” off the SORB barrier, resulting in less vehicle kinetic (moving) energy being converted to crush energy, therefore resulting in lower vehicle deceleration levels, lower crush forces in the front structure and lower intrusion levels. Further evaluation of the numerical test data showed

very low cabin intrusion levels and low dummy injury forces. Overall, the XC40 demonstrated a clear (“glance off”) strategy for management of the SORB test. Other observations showed that the front wheel completely detached shortly after impact. It is possible that the front suspension was engineered to fail in this way, such that wheel does not provide a loadpath into the rocker and inhibits the “glance off” motion.

A similar evaluation of the Mazda CX-30 was performed. Again, this vehicle achieved “good” performance for both IIHS front crash tests. Figure 6.3.6.2.2 shows an image from the crash test and the full animations can be seen via the link https://www.iihs.org/ratings/vehicle/Mazda/cx-30-4-door-suv/2020 .

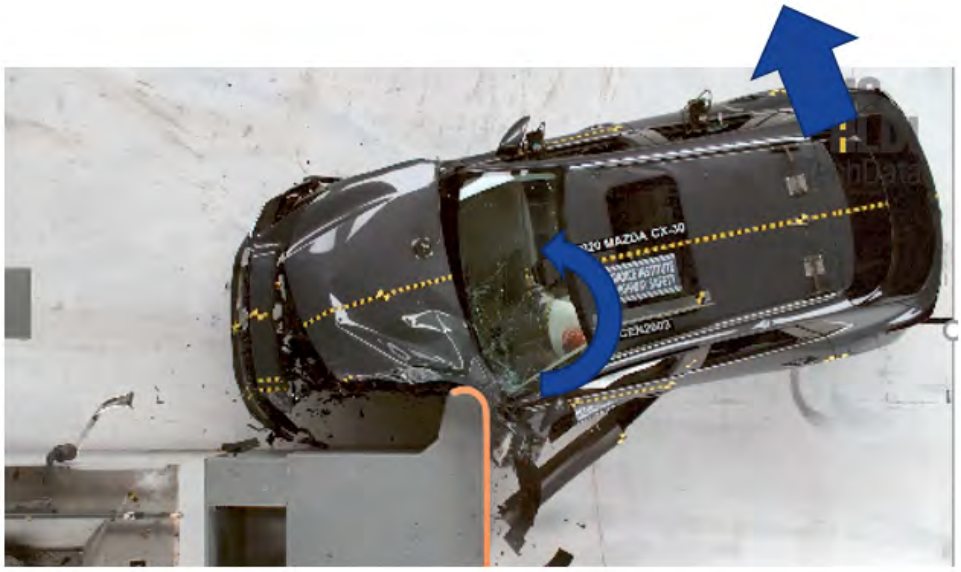

Figure 6.3.6.2.2 Mazda CX-30 2020MY, IIHS small overlap test

Here, the forward motion of the vehicle is seen to stop, with some of the kinetic energy converted to a rotational (yaw) movement. Instead of “glancing” off the barrier, the vehicle is observed to crush then “snag” at the hinge pillar. Further analysis of the test data showed the Mazda CX-30 had slightly higher measured vehicle pulse, cabin intrusions and crash test dummy forces**.** It can be concluded that achieving a “glance off” in SORB may tend to achieve improved crashworthiness performance than a vehicle with a “snag” (note, both vehicles achieve IIHS “good” and “Top Safety Pick” ratings from IIHS. The Safety Restraint System including seat belts and air bags may also contribute to the different performance of the vehicles).

The findings from this benchmarking study were applied and considered for the Steel E-Motive concept compared to a conventional passenger car (“B”) as shown in Figure 6.3.6.3.1.

6.3.6.3 Development of front crashworthiness strategy for Steel E-Motive

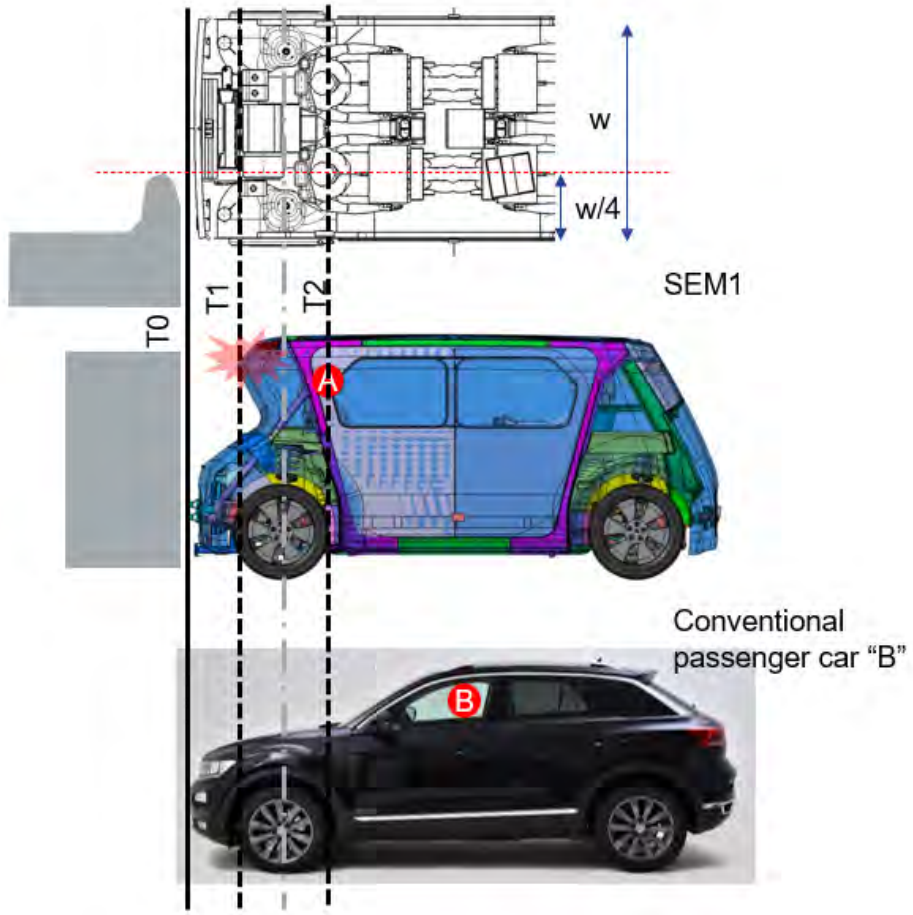

Figure 6.3.6.2.2 Comparison of IIHS SORB crash event for SEM1 compared to a conventional passenger car

The relative positions of the occupant (heads) are shown as positions A and B. For the passenger car B, the SORB crash event is largely completed by the time the vehicle reaches T2. With the front occupant of SEM1 being closer to the crash event, a more comprehensive approach to the management of the loads and protection of the occupant would be required. A strategic decision was made to target a “glance off” crash mode for SEM1 in the SORB test. The justification for this being that a “glance off” results in reduced crush energy for the crash structure to manage, therefore protection of the occupant in a more vulnerable location would be less of a challenge than adopting the “snag” approach.

The strategy for management of the SORB crash event is shown in Figure 6.3.6.2.4.

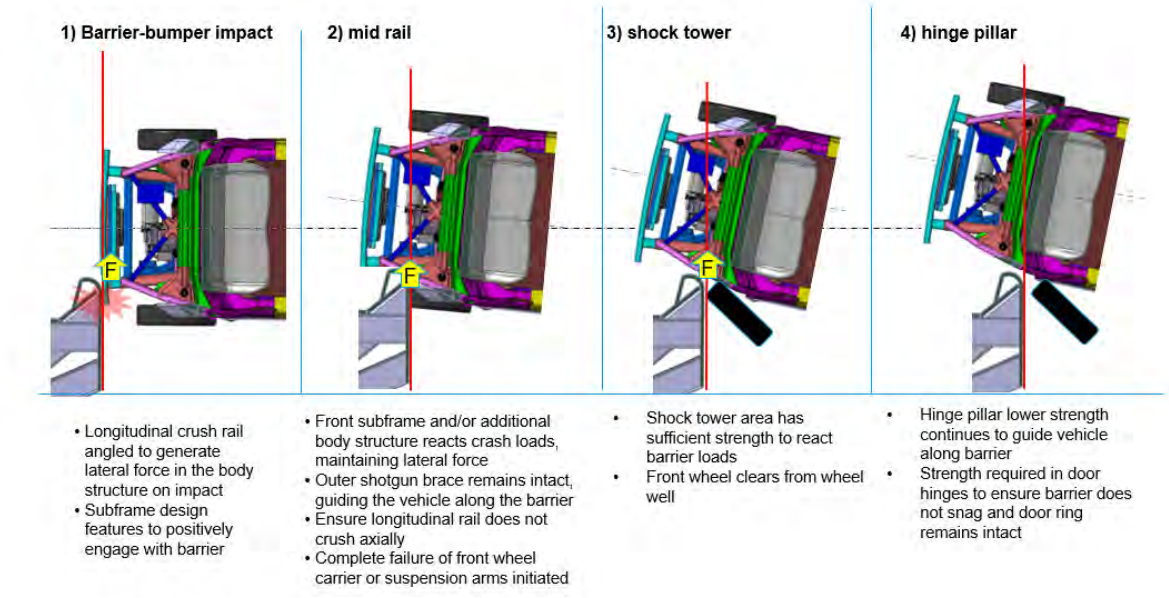

Figure 6.3.6.2.4 SEM1 IIHS 64kph SORB front crash strategy (See Appendix 4 for larger image)

On initial impact, the body structure needs to react with the SORB barrier such that a lateral load is generated. Positioning the longitudinal crash rails with a positive plan view angle towards the barrier should develop a lateral force component. The longitudinal rail should maintain overall shape (i.e., not crush axially). The front subframe could also feature extensions forward, positively engaging with the SORB barrier. The front bumper beam could be engineered such that it bends on impact, enabling a lateral force component to be generated. An additional brace between the front crash rails and/or front subframe would also strengthen the front end and ensure higher lateral load reaction. As the barrier reaches the middle of the motor compartment, there is less structure to react the barrier loads. (This is the collapsible crush zone for management of the FFB energy). A high strength structure is therefore required on the outside of the motor compartment to maintain the interface with the barrier, ensuring the vehicle “slides” or “glances”. The SORB barrier needs to be aligned appropriately (outside) before reaching the shock tower. If the barrier is inboard of the shock tower then a “snag” may occur. The shock tower structure has the potential to provide a good level of lateral load reaction to the barrier loads and provide high lateral acceleration and displacement. With this zone being very high strength and appropriately designed, the barrier should remain outside of the shock tower, continuing the glance motion of the vehicle. As the barrier reaches the hinge pillar, and rocker, high strength structure is required such that the cabin structural integrity is maintained, and intrusion levels are minimised. The side door structure and hinges require sufficient strength such that the SORB barrier does not become lodged into the door front edge.

Considering the above strategy for the SORB test and the crush requirements for the FFB test, the following design approach was proposed for the SEM1 front structure.

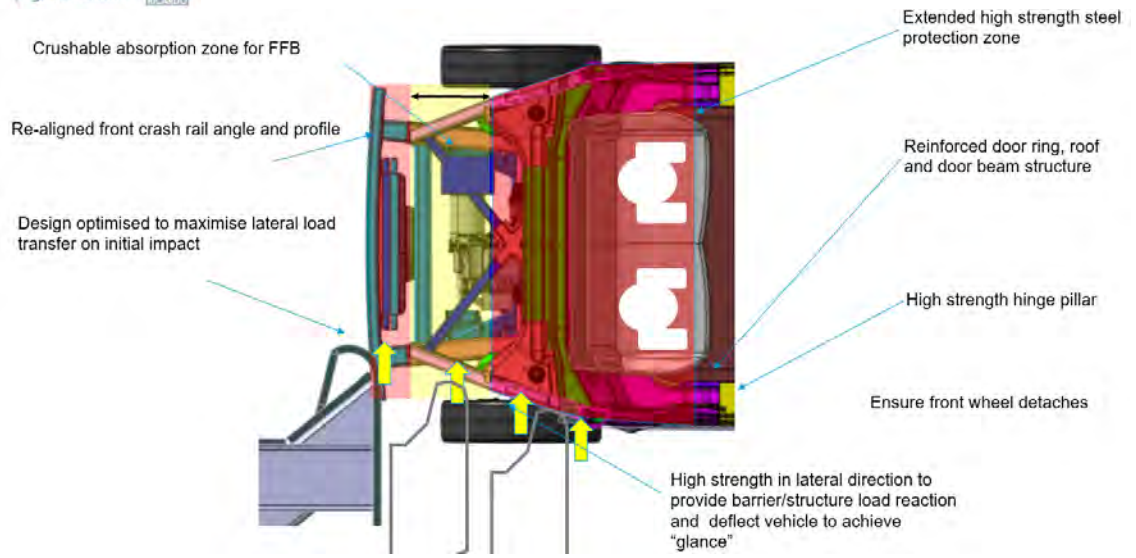

Figure 6.3.6.2.5 Front crash structure design approach for achieving USNCAP FFB and IIHS SORB with “glance off” strategy

The front crash structure is divided into 3 zones. The front zone is engineered to allow longitudinal crush for low speed and FFB impact requirements but must have very high lateral strength for the SORB test. The front zone should be engineered such that very high lateral reaction forces are generated on initial impact. The middle zone (yellow) is protected for FFB. The mid-zone structure must have the freedom to crush axially, absorbing the vehicle kinetic energy with highest efficiency possible, resulting in progressive deceleration. The motor compartment package should ensure that no “stack up” of large components such as the EDU occur in this zone. To maintain the glance motion in the SORB test, an outer lateral structure maintains engagement with the barrier, guiding the vehicle along the desired trajectory. The beam must maintain structural integrity whilst not interfering with the crush requirements in FFB. The rear zone (red) is an extended high-strength passenger safety cell. The zone should begin in front of the shock tower and extending rearwards as required (for side crash also). The objective of the protection zone is to minimise intrusion to the cabin and battery compartment. The front wheel should be engineered to detach during the front crash event and exit the wheel compartment.

6.3.6.4 Development of SEM1 front crash structure, resolving FFB and SORB conflict

Given the strategy and design approach defined above, a simulation led development activity was undertaken to develop the SEM1 vehicle front crash structure. The full vehicle crash FEA model was updated to represent the latest design. Many crash FEA iterations were performed, evaluating the key parameters shown in Figure 6.3.6.4.1 below

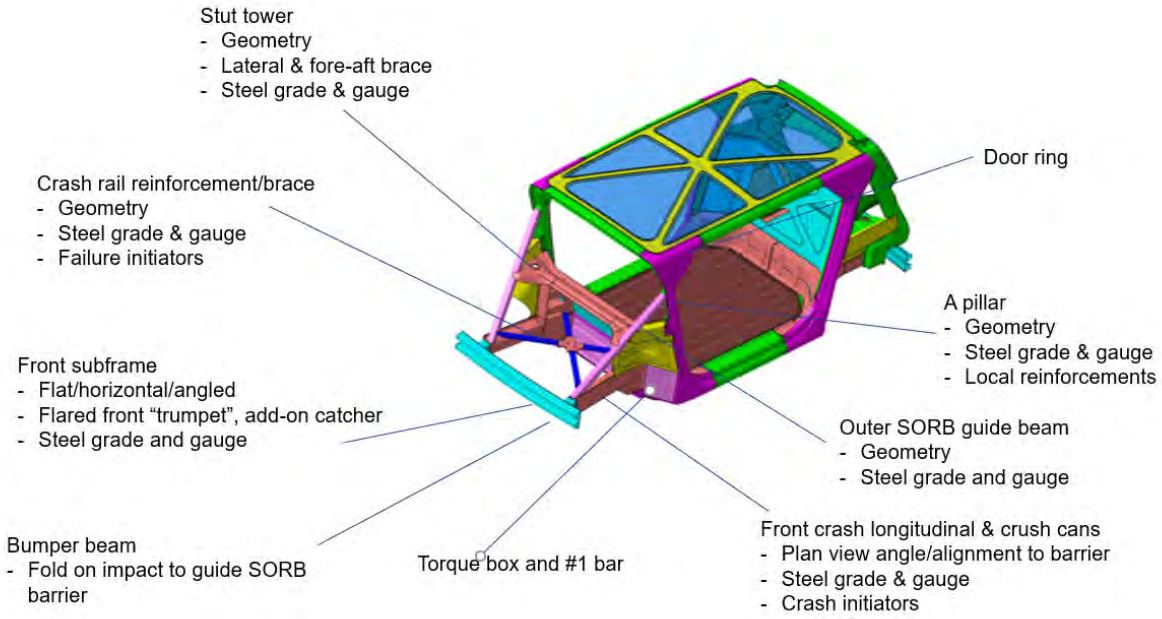

Figure 6.3.6.4.1 summary of design iterations considered in the front crashworthiness development

Figure 6.3.6.4.2 shows the final Phase 1 design of SEM1 BIW

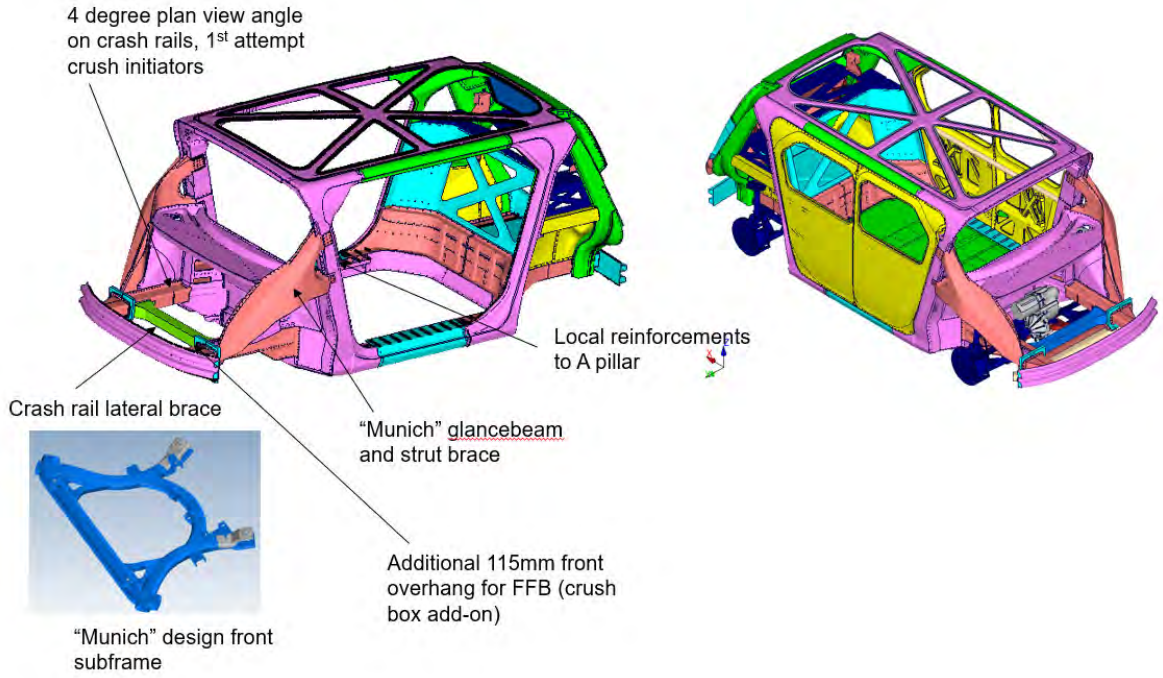

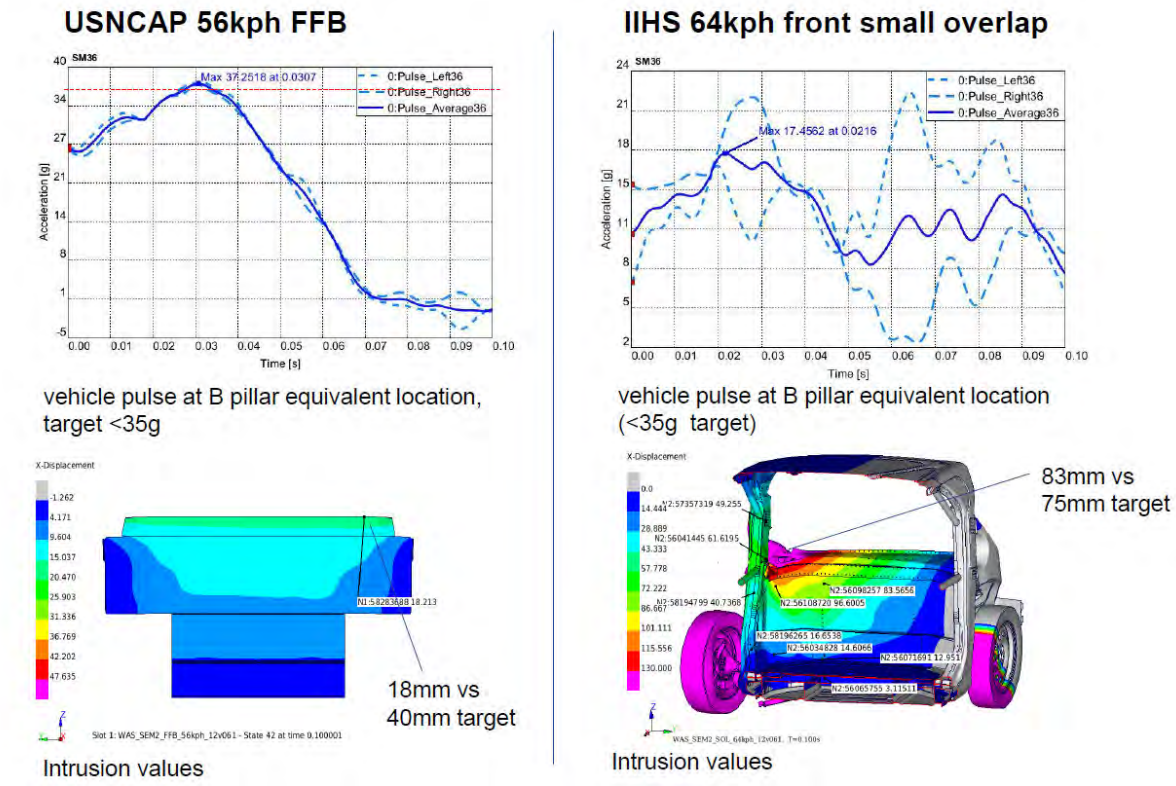

Figure 6.3.6.4.3 front crash FEA results of Phase 1 final design concept

The results show that because of the front crash strategy and design philosophy, the crashworthiness of the Phase 1 SEM1 design was within 10% of the overall performance targets. This was evaluated in the Phase 1 <CS> gateway and accepted as positive indication that the design could achieve 100% target with further engineering development.

6.3.6.5 Considerations for the protection of rear facing front occupants in frontal collision

Positioning the front occupants in a rear facing configuration benefits the spacious and openness feeling of the vehicle interior and takes advantage of the freedoms enabled by fully autonomous driving. The front occupants are however located in a more challenging location with respect to protection from frontal collisions. Compared to a conventional passenger car, the occupant head and torso is located closer to the impact zone, where intrusions of the front structure may impact the occupants causing injuries. The occupant legs and feet are further from the front impact zone and may be subject to a lower injury risk. In a frontal impact, forward facing occupants are decelerated by the safety restrain system, namely the seat belts and air bags. The forces exerted on the occupants from seat belts and air bags can lead to serious injuries to the torso legs and arms. For rear facing occupants in a frontal collision, primary deceleration of the occupant is provided by contact forces between the torso and legs. With a greater contact area than seat belts, the deceleration forces are more distributed over the torso hence injuries may be lower for a rear facing occupant. The risk of neck injury or whiplash is significant in this configuration due to the potential for differential motion and deceleration of the occupant torso and head.

The frontal collision for a rear facing front occupant is equivalent to a forward-facing passenger experiencing a rear impact. The protection of forward-facing occupants in a rear collision is well understood, with regulations, tests and guidelines in place for the seat and headrest design. However, the impact speeds and deceleration levels for a frontal collision are typically higher than a rear collision. The seating structure and headrest design for a rear facing front occupant configuration must therefore be engineered to consider the higher impact loads from frontal impact. The headrest requires particular attention to minimise the risk of whiplash. Advantage could be taken of the autonomous functionality of Steel E-Motive by inhibiting movement of the vehicle if occupants are not seated appropriately. Also, the variability in the sizes of occupants should be accounted for in MaaS (taxi) vehicles. Automatically adjusting headrests could be employed to minimise whiplash injury risks. The specific engineering of the seating structure and restraints systems was not considered within the Steel E-Motive programme, however, consideration for the space and packaging for the front seat structure was provisioned for. The frontal impact crashworthiness targets were also adjusted to account for the rear facing front occupant. The consideration and approach for the rear facing front occupants is summarised in Figure 6.3.6.5.1

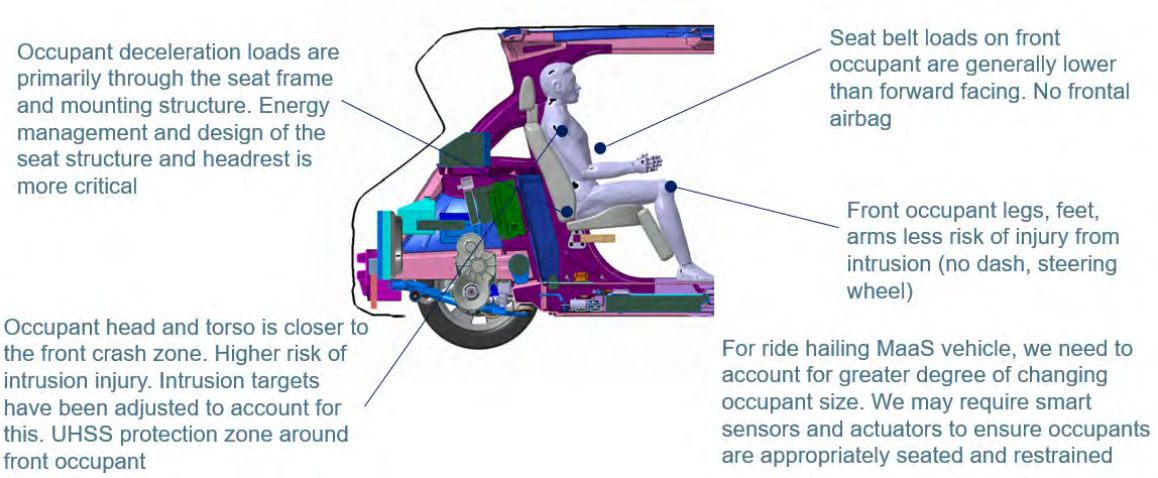

Figure 6.3.6.5.1 Considerations and approach for protection of the rear facing front occupants in a frontal collision (See Appendix 4 for larger image)

6.4 Technical Approach, Phase 2

6.4.1 Phase 2 objectives and approach

The objectives of Phase 2 of the Steel E-Motive programme were to optimise and refine the Phase 1 vehicle and body structure design such that all the performance targets and requirements were achieved. This included ensuring the designs are suitable for manufacturing (e.g., stamping, roll forming, press hardening), body assembly process (including joining methods such as spotwelding, laser welding) and complete vehicle assembly. The complete steel grade portfolio was utilised and applied in the design as well as all the fabrication processes as detailed in Section 5.0.

The combined approach of applying 3D CAD and FEA tools to drive the design continued, with more refined levels of modelling and optimisation applied.

Technical review gateways were held throughout Phase 2 to track the progress and progression towards 100% target achievement. An interim gateway was held midway

through Phase 2 (2A), then 2 “countdown” gateways (CD-2, CD-1) were held in the lead up to the final technical gateway CD (“concept definition”).

At this stage of the project, the covid-19 pandemic restrictions had been lifted in many regions and the project benefitted significantly from several collaborative, face-to-face technical workshop events.

6.4.2 Technical Design Workshop

The first activity undertaken in Phase 2 was an in person, 1-week technical design review workshop. The objectives of the workshop were to:

- Critique the Phase 1 SEM1 body design
- Review the performance results
- Brainstorm design improvement suggestions
- Consider the application of steel grades and fabrication processes from the complete portfolio
- Consider the panel fabrication, body assembly and vehicle assembly requirements and consider these in the design brainstorming
- Develop a CAD “design brief”, giving clear instructions to the 3D CAD teams to initiate the development of the Phase 2 concept

The workshop was attended by the programme technical lead team. The workshop was structured into “deep dive” technical reviews by body zone (i.e., front zone, mid zone, rear zone). Ideas were developed and captured mainly through 2D sketches, whiteboard notes and then documented in MS Excel. Figures 6.4.2.1 show some examples of the output from the workshop.

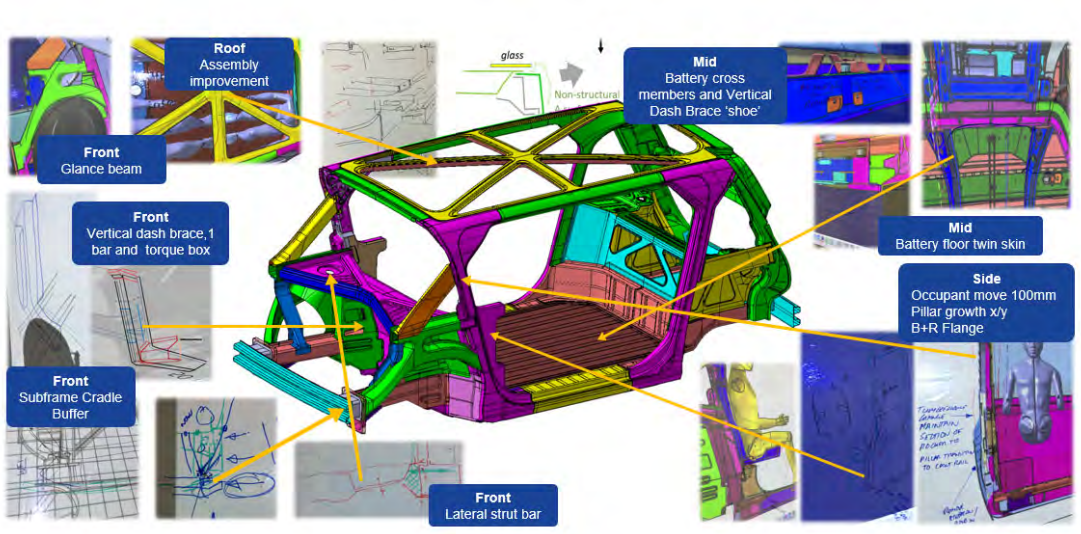

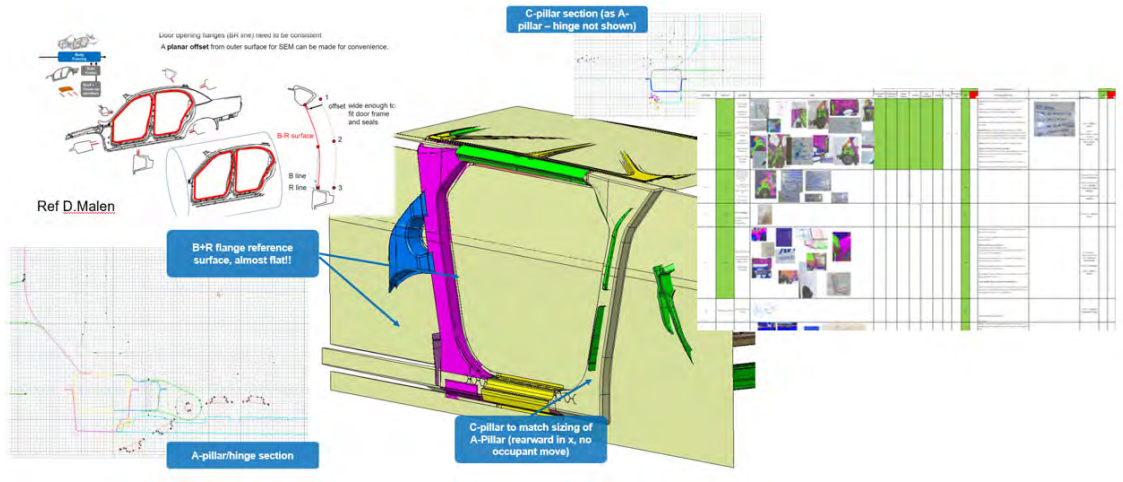

Figure 6.4.2.1 Example outputs for the technical design workshop

Following the design workshop, the 3D CAD and FEA models were created, and structural performance of the body evaluated. The results demonstrated a continued progression towards target achievement. Further design iterations were performed, primarily focussed on optimising the front crash structure and integration of the closures and battery design, which were maturing in parallel with the body concept.

6.4.3 Materials application technical workshop

The WorldAutoSteel consortium features a rich pool of knowledge and experience in the automotive application of Advanced High-Strength Steels, steel manufacturing, steel fabrication, joining and vehicle production & assembly. To canvass this knowledge and enable a democratic approach and selection of steel technologies to the Steel E-Motive concept, a three-day, face-to-face collaborative workshop was held in Los Angeles, mid-way through Phase 2. The objectives of the workshop were:

- Review the project-based steel grade portfolio (Section 5.0) and agree on global grade availability and specification
- Review the Steel E-Motive concept design and identify suitable and optimum steel grades for given subassemblies
- Identify moderate design changes that would enable potential performance improvements
- Explore opportunities to push the boundaries of current steel technologies and their application

Figure 6.4.3.1 shows the overall approach applied during the workshop.

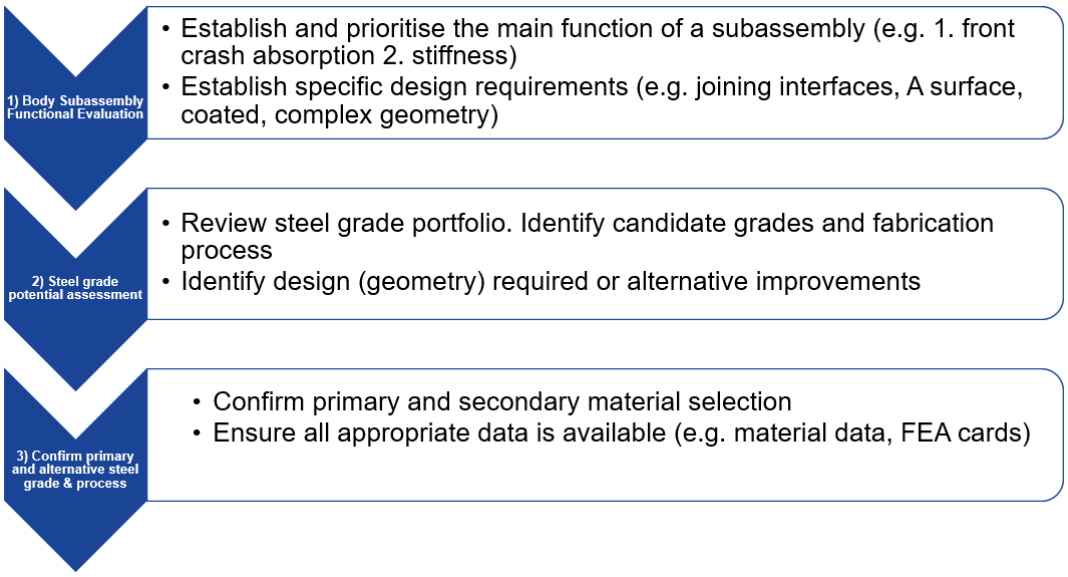

Figure 6.4.3.1 Approach for materials application technical workshop

The approach for the material grade selection was “function led” – meaning that the selection of steel grades and fabrication processes were driven primarily by the body components function and requirements (i.e., “what does the part need to do”). Other requirements such as complex geometries, joining and interfaces to other subassemblies, visible/A surface and corrosion resistant parts were identified and documented for each body subassembly (this was done in advance of the workshop). During the workshop, each subassembly was reviewed, and the functional requirements agreed. Opinions on the potential steel grades was then canvassed, with the pros and cons of each recommendation discussed. The overall vehicle design goals of comfort, safety, sustainability, and cost were considered throughout the discussion and selection. A final selected of “primary” steel grade and “alternative” (second choice) steel grade was then made and documented. In some cases, further discussion and debate was required where unconventional approaches were suggested, such as the application of very thin gauges (<0.7mm) and suitability of 3rd generation grades. The evaluations and recommendations for each subassembly were documented, as per the example shown in Figures 6.4.3.2 to 6.4.3.3

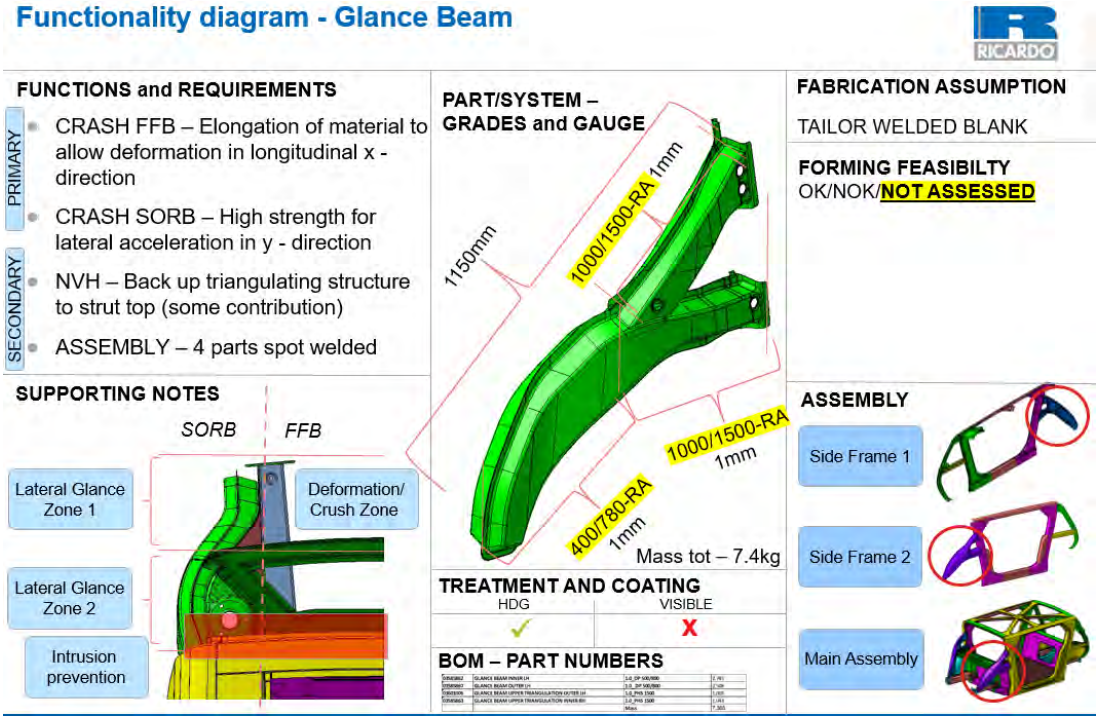

Figure 6.4.3.2 Material technologies workshop – example of subassembly functional evaluation

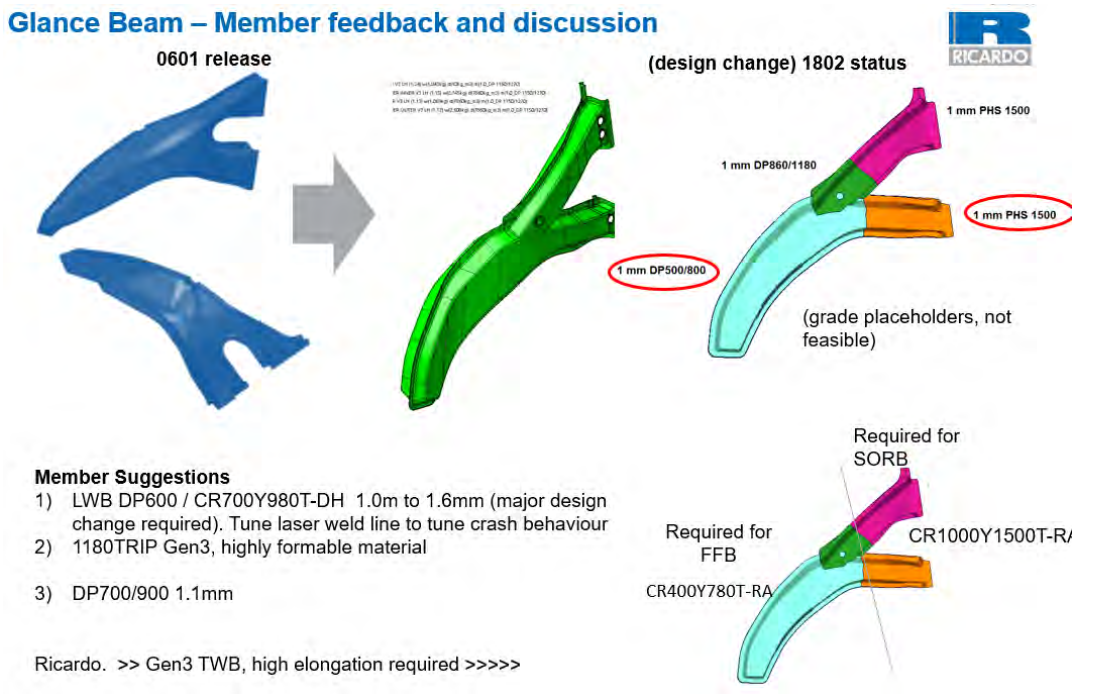

Figure 6.4.3.3 Materials technologies workshop – example of consortium members' feedback

Glance Beam – Final recommendation

Core design

Welding RA1500 to PHS? MS grade to the interface on the A Post for weldability?

HSLA risk of cracking in critical zone

Put the HSLA through the hot form process

Part	Fab'n process	Material Grade	Gauge (mm)	Coating/ Visible
Front		TWB PHS500		
Rear		TWB PHS1500		
Front		HSLA780		
Rear		PHS 1500		

Alternative solutions

Ford Focus Benchmark – DP800

Tailor tempering to soften areas for folding up

1470-MS – challenge for lower part

1300-MS

Part	Fab'n process	Material Grade	Gauge (mm)	Coating/ Visible
	Hydroform	DP1000		
Front		HSLA780		
Rear		PHS 1500		
Front		TWB PHS500		
Rear		TWB PHS1500		
	Air Forming	MS Grade		
	Split Lower in 2	MS1300 or MS1470		

Figure 6.4.3.3 Materials technologies workshop – confirmation of primary and alternative steel grade selection

The workshop successfully delivered a revised specification of steel grades and fabrication processes, that were subsequently used by the engineering teams to assess in CAD and FEA simulations. Further iterations and grade changes were assessed and implement throughout the remainder of Phase 2.

6.5 Engineering Tools

The following engineering tools and software were used throughout the Steel E-Motive engineering programme

Activity / calculation	Software tool and version
3D CAD design	Catia V5
PLM data management	Windchill
FEA model creation	ANSA 21.1.3
FEA linear statics (stiffness, NVH)	Nastran 2019.1
FEA Non-linear (strength, durability)	LS-Dyna R11_1_0_x64
FEA non-linear (crash simulation)	LS-Dyna R11_1_0_x64
FEA structural topology optimisation	Optistruct 2019.2
Lifecycle Analysis	MS Excel tool, originally created by University of California Santa Barbara
Body costing evaluation	MS Excel tool, originally created by Massachusetts Institute of Technology
Project management	Jira

7.0 SEM1 final design

7.1 Vehicle design and key features

The Steel E-Motive vehicle design encompasses many innovative design features and approaches that deliver an autonomous Mobility as a Service vehicle of the future. These are summarised below and detailed in the subsequent sections of the report.

- The Steel E-Motive vehicle design embraces the features and potential of level 5 (full) autonomous driving. The direct driver controls such as steering wheel, pedals, turn indicators are completely removed enabling cabin space and weight saving. The design accommodates space for mounting of the autonomous driving sensors (such as radar and lidar). The front occupants are oriented in a rear facing configuration. To assist entry and egress from the vehicle, the body structure B pillar is removed from the body in white and placed into the side doors. The doors open in a sliding “scissor” action, enabling a wide opening (aperture). For the occupant, this means getting in and out of the vehicle much easier. The rear tailgate features a parallelogram life mechanism (or “coach door”). This minimises the outswing distance, enabling the vehicle to operate in a confined spaces
- The complete vehicle design has been engineered around the propulsion battery (see section 7.4). This results in a space optimised solution, where the battery occupies minimum space, resulting in more space and a flat floor in the cabin
- All four wheels are steered, resulting in a minimum steering circle radius of 7.4m. The vehicle can therefore achieve 180 degree “U turns” in tighter spaces, resulting in more convenient passenger access and journeys. Four-wheel steering also allows Steel E-Motive to “crab steer” when manoeuvring to curb side collections and drop offs
- The design and performance of the body structure delivers high levels of passenger comfort, convenience and safety. This achieved through a combination of innovate design approaches and features in the structure combined with the properties of Advanced High-Strength Steels
- Modular architecture, enabling smaller urban (SEM1) and extra-urban (SEM2) variants. Potential for commercial vehicle application such as light delivery van. Vehicle and body designed for high volume production using conventional, existing manufacturing facilities (see section 7.5)
- Efficient design and use of the latest Advanced High-Strength Steel grades and fabrication processes in the body structure results in a lightweight, cost-effective solution (see section 7.1.4 and 7.2.1)
- A combination of vehicle design features and operation in ride hailing MaaS demonstrates the potential to significantly reduce life cycle greenhouse gas emissions (LCA approach and results are detailed in Section 10)
- Features Steel E-Motive exterior lattice styling, reinforcing the emotion of the steel structure design and visionary vehicle of the future (See Section 10.0)

SAE Level 5 autonomous driving:
- Fully autonomous, SAE level 5
- Deletion of direct driver controls (steering wheel, pedals, dashboard)
- Package accommodation of autonomous vehicle sensors
- Suitable for deployment on existing highway networks, operating alongside Level 1 to 4 vehicles

Spacious, comfortable cabin interior
- Inward facing seating configuration
- Scissor doors with wide door aperture providing improved entry and egress for passengers
- Glazing surfaces maximised, enabling light and airy cabin space environment
- Steel E-Motive frame mounted integrated battery solution results in a flat floor interior and low step in height
- Vehicle systems packaged and positioned to provide maximum interior space

Advanced High Strength Steel Body Structure:
- Achieves high speed vehicle crashworthiness standards. Predicted to achieve IIHS "good" rating
- High stiffness and strength body structure. Good levels of comfort and NVH
- Lightweight steel design
- Significant reduction in lifecycle greenhouse gas emissions comparing 2035 operation to 2020 conventional battery electric vehicle

Optimised propulsion system
- 75kWh battery electric powerunit. Front electric drive unit. Potential for 12 hour operation on a single charge
- Potential for conversion to hydrogen fuel cell powertrain
- All wheel steer, enabling 7.4m turning circle

Figure 7.1.1 Engineering 3D CAD image of SEM1 vehicle. Key design features and achievements (See Appendix 4 for larger image)

7.1.1 SEM1 Vehicle external and internal dimensions

Figure 7.1.1.1 shows the external dimensions of the SEM1 vehicle including a comparison to a typical European C segment passenger car. The overall length of SEM1 is slightly smaller than a C segment vehicle and overall height higher, which is necessary due to the occupant location and more upright position.

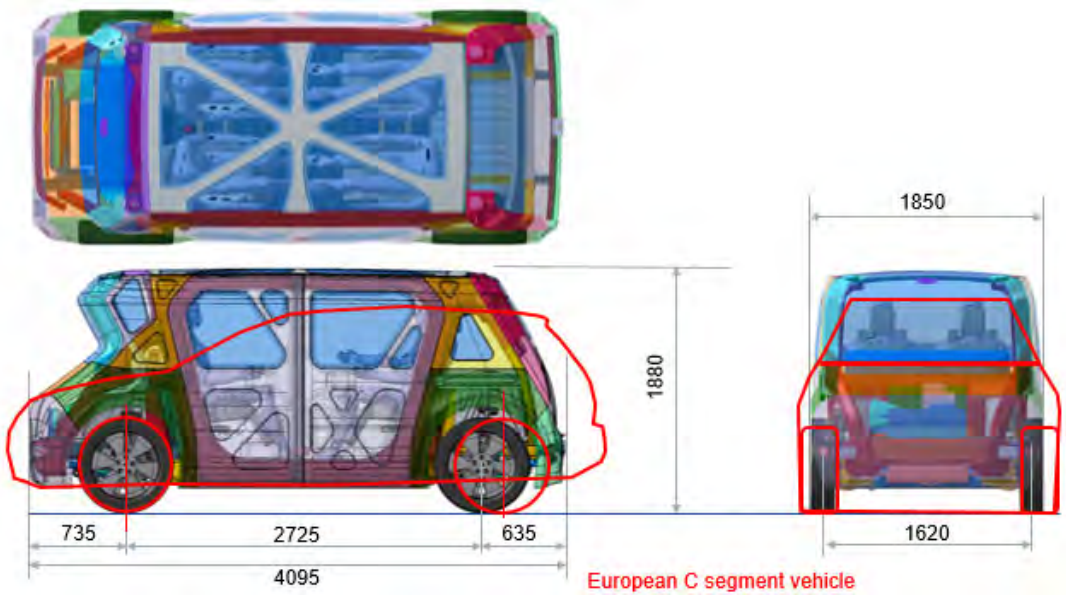

Figure 7.1.1.1 SEM1 vehicle external dimensions

The Steel E-Motive concept features a relatively spacious interior given the overall vehicle dimensions. The occupant positioning and level 5 autonomous features enable this. Overall interior dimensions are show in Figure 7.1.1.2.

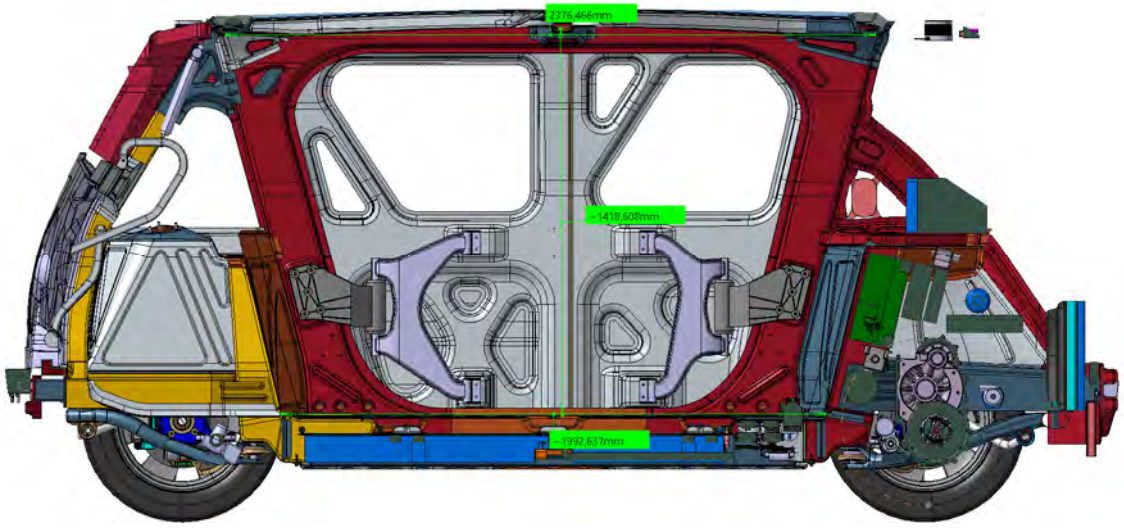

Figure 7.1.1.2 Overall SEM1 interior dimensions

7.1.2 Vehicle design considerations for SAE Level 5 autonomy

The Steel E-Motive concept designs have been engineered to enable SAE Level 5 autonomous operation. This means the vehicle drives itself on a conventional highway, with the human operator or passenger requesting a journey start and end location. The vehicle will manage the route optimisation, interface with the fleet operator network, connect with road traffic infrastructure (such as traffic signals), interface with other vehicles. The onboard vehicle sensors (radars and lidars) with determine the proximity of nearby objects such as other vehicles, stationary objects, pedestrians and will determine its location using satellite Global Positioning Systems (GPS) and 4G telecommunications. The sensory data is processed by an on-board processor and the motion trajectories and vehicle response are calculated. The roadmap in Section 3.3 outlines the development and evolution of the autonomous vehicle technology, concluding that widescale deployment should be feasible in the 2030 to 2035 timeframe. The autonomous vehicle sensors have been positioned and packaged in the Steel E-Motive design. Whilst detailed design of the sensor mounting was not been undertaken, the sensors are positioned in locations with significant supporting structure, such as the top of the A pillar and on roof bow structures. This should ensure requirements such as attachment stiffness and vibration isolation are attainable.

Level 5 autonomy means that the vehicle is controlled autonomously 100% of the time during it’s operation. The user or operator will not directly control the vehicle at any time. This therefore means that the conventional controls such as steering wheel, column, accelerate and brake pedals, gear shift and turn indicator controls can be eliminated from the vehicle. Additionally, the dashboard and driver information panels can be deleted and replaced with on-board information screens. Overall a net weight saving of 135kg is estimated based on deletion of driver controls and addition of autonomous sensors and controls (see figure 7.1.5.3). The vehicle changes associated with Level 5 autonomy also

enable improvements to cabin space and interior. There is no requirement for occupants to view the road or traffic conditions, therefore vision and obscuration requirements do not apply. In the Steel E-Motive concept, the front occupants are therefore positioned in a rear facing orientation and the seating position moved to the front of the vehicle where a conventional vehicle dashboard. This creates an inward “sitting room” configuration, with improved legroom and personal space, enhancing the user’s journey experience.

Figure 7.1.2.1 SEM1 engineering 3D CAD model, section cutaway in X, looking to the front of the vehicle showing front occupant (95th percentile mannequins) in rear facing, front seat configuration. Occupants are positioned where conventional vehicle controls would be located. (doors in open position).

7.1.3 Vehicle design considerations enabling passenger comfort and ergonomics

To enable easier access (ingress and egress) to the vehicle, Steel E-Motive concept features sliding or “scissor” action doors with A and C pillar mounted hinges. Deletion of the body in white B pillar (with the structure located in the doors) enables a wide (1.01m) aperture with the doors in the fully open position. This provides users with very convenient access to the vehicle during pick up and drop offs. The scissor motion of the doors also minimises the distance that the doors swing outwards when opened (referred to as “kerbside encroachment”). This enables the vehicle to manoeuvre closer to the kerbside during passenger pick-ups and drop offs, providing added convenience for users. A completely flat interior floor is enabled in the Steel E-Motive design due to the engineering packaging of the propulsion battery and supporting structure. This facilities easier and unobstructed movement within the vehicle. The floor and step-in heights are also competitive for the size of vehicle and offer convenient access for the user.

	Measurement	Value (mm)
1	Ground clearance	170
2	Interior floor height	365
3	Step in height	392
4	Kerbside lateral encroachment	230.5

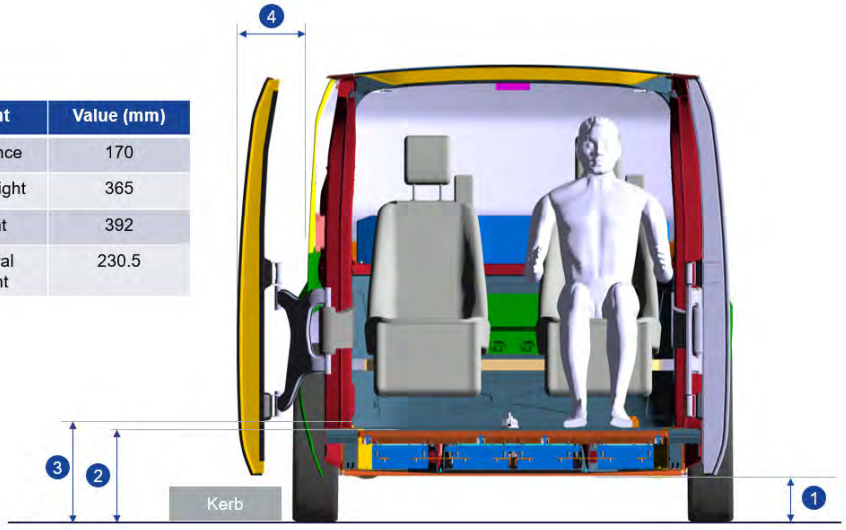

Figure 7.1.3.1 SEM1 ground clearance, floor, step in height and kerbside lateral encroachment

Figure 7.1.3.2 SEM1 occupant ingress and egress study (95th percentile male) using Virtual Reality tools

Figure 7.1.3.3 rear compartment access evaluation using Virtual Reality tools

Figure 7.1.3.4 SEM1 interior space evaluation using Virtual Reality tools

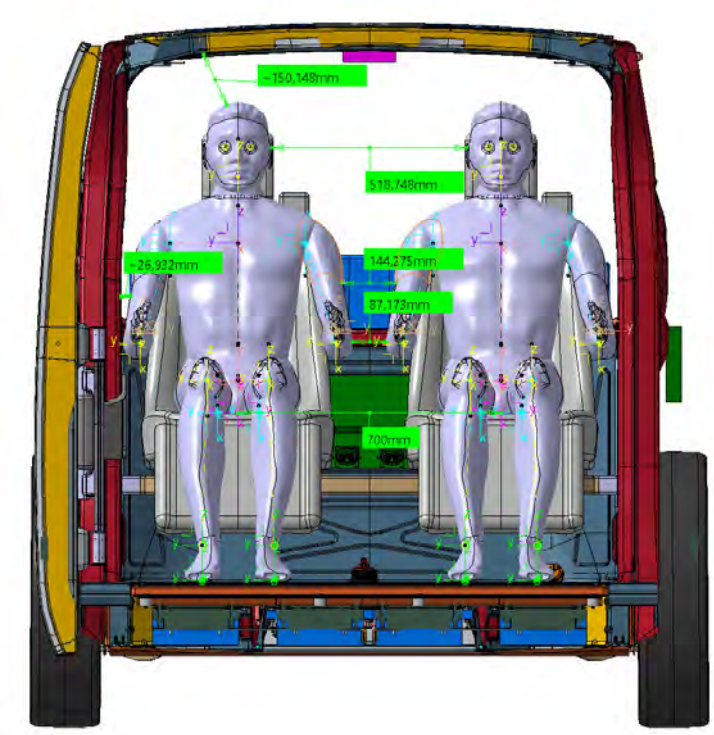

Figure 7.1.3.5 SEM1 occupant seating position and clearance using 95th percentile mannequin

Despite the compact vehicle size, the seating positions in SEM1 provide reasonable levels of clearance from occupant to vehicle and occupant to occupant as show in Figure 7.1.3.5

The 400 litres luggage capacity target was achieved by occupying the combined spaces of the upper and lower boot (388 litres) and additional space made available underneath the bench seats.

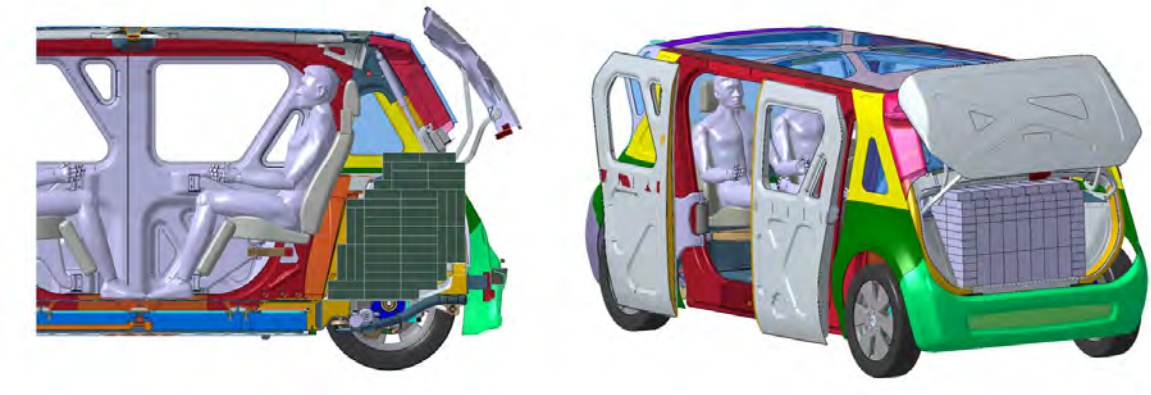

Figure 7.1.3.6 SEM1 luggage capacity estimation. 388litres

Motion sickness can be a common occurrence and aggravation when humans are subjected to journeys by land vehicles where and external vision and focal points are less accessible. This is therefore a risk in autonomous vehicles where the users' vision is likely to be focussed on tasks inside the vehicle. The glazed area of the Steel E-Motive concept has therefore been enhanced in order maximise the natural light potential and minimise the risk and severity of vehicle motion sickness. Despite there being no legal requirements for driver vision or obscuration, a "conventional" front windscreen provides good forward vision and natural lighting. The roof features a lattice structure with large glazed in-fills. The side closures feature fixed glazing incorporated into the lattice styling and the rear tailgate features a fully glazed upper panel. Overall, the Steel E-Motive enables a light and airy interior space despite the compact vehicle size.

7.1.4 Vehicle design considerations for disabled and impaired users

One of the significant benefits and motivational factors for fully autonomous vehicles is the ability to serve the underserved. Users who don't have the ability or capability to drive a conventional vehicle will now be able to enjoy the travel freedoms beyond taxi or public transport services. This includes disabled, elderly and physically impaired users and able-bodied passengers who are recovering from injury or long-term treatment. With journeys being monitored and securely operated, unaccompanied children may also be able to use autonomous vehicle services with some limitations. With the added freedoms that autonomous vehicles enable, the vehicle itself must be fit for purpose for disabled users. Mobility as a Service fleet operators would specifically cater for disabled users by engineering unique vehicle variants that specifically accommodate disabled users. The modifications would include the permanent removal of one or two of the fixed passenger seats and wheelchair tie-down fixings added to the floor and pillar structures. The reduced kerbside encroachment, step in height and flat floor (as described in 7.1.3) ensure that disabled users can conveniently access the vehicle with the assistance of an on-board ramp (not specifically engineered). Virtual Reality (VR) 3D visualisation tools were used to assist confirm the suitability of the Steel E-Motive concept for wheelchair users. Specific vehicles would require minor vehicle adaptations, including the removal of portion of the seat (or engineering of a device to temporarily remove a portion of the bench seat), inclusion of a pull-out wheelchair ramp from the floor structure and addition of wheelchair location points and fixings. Mobility as a Service operators would be expected to adapt a number of vehicles for disabled user needs within their fleets.

Figure 7.1.4.1 SEM1 wheelchair user vehicle access evaluation using Virtual Reality tools

7.1.5 Vehicle weight

A low vehicle weight enables efficiency savings at both the design and operational level. Low weight vehicles generally utilise less material in their construction, resulting in lower greenhouse gas emissions as a result of the manufacture and assembly. Low vehicle weight also results in lower propulsion force and energy needs, enabling a smaller battery for an equivalent range and smaller traction motor. Steel E-Motive SEM1 achieves an estimated unladed weight of 1512kg. The value is derived based on calculations from 3D CAD for the systems specifically engineered (designed) in the Steel E-Motive programme and estimations for other systems based on statistical benchmark data from services such as a2mac1 (https://www.a2mac1.com/).

Figure 7.1.5.1 shows the SEM1 vehicle curb weight breakdown

Subsystem	SEM 1 Status CD	Source/estimation
Body non-structure	177.2	Estimated from a2mac1 statistical analysis. Includes seating, trim panels, glazing, front end clip, exterior panels
Body Structure	282.0	<CD> design value from 3D CAD
Front sub-frame	16.5	<CD> design value from 3D CAD
Battery case (structure)	59.0	<CD> design value from 3D CAD
Rear sub-frame	10.2	<CD> design value from 3D CAD
Front suspension	114.0	<CD> design value from 3D CAD
Rear suspension	114.0	<CD> design value from 3D CAD
Braking	59.7	Estimated from a2mac1 statistical analysis
Steering	26.0	Estimated from a2mac1 statistical analysis (steering rack and tie rods only, no wheel column, EPAS etc)

Tires and wheels	84.0	Estimated from a2mac1 statistical analysis
Motor Trans Front	63.0	Estimated from a2mac1 statistical analysis and Fiat 500e
Battery system less case	245.6	<CD> Ref BOM including 5kg of fluids, busbars, cooling plate, modules and PDU
Propulsion controls	60.0	Estimated from a2mac1 statistical analysis
Electrical-non propulsion	35.7	Estimated from a2mac1 statistical analysis
Cooling and heating	30.0	Estimated from a2mac1 statistical analysis
Closures	109.3	<CD> design value from 3D CAD
Bumpers	26.0	Estimated from a2mac1 statistical analysis
Vehicle curb weight	**1512.2**	**kg**

Weight performance of the body in white and battery structure are discussed in section 7.2.1.

The relative competitiveness of vehicle curb weight can be expressed using comparison of vehicle dimensions and weight performance. Figure 7.1.5.2 shows a comparison of a sample of battery electric vehicles, comparing curb weight to the occupied volume area (vehicle length x vehicle width x vehicle height). The reference vehicle sample includes vehicles with steel, aluminium and mixed/multi-material body structures. A statistical regression analysis enables a “line of fit” to be calculated for the data sample, drawing a relationship between the vehicle curb weight and vehicle occupied volume.

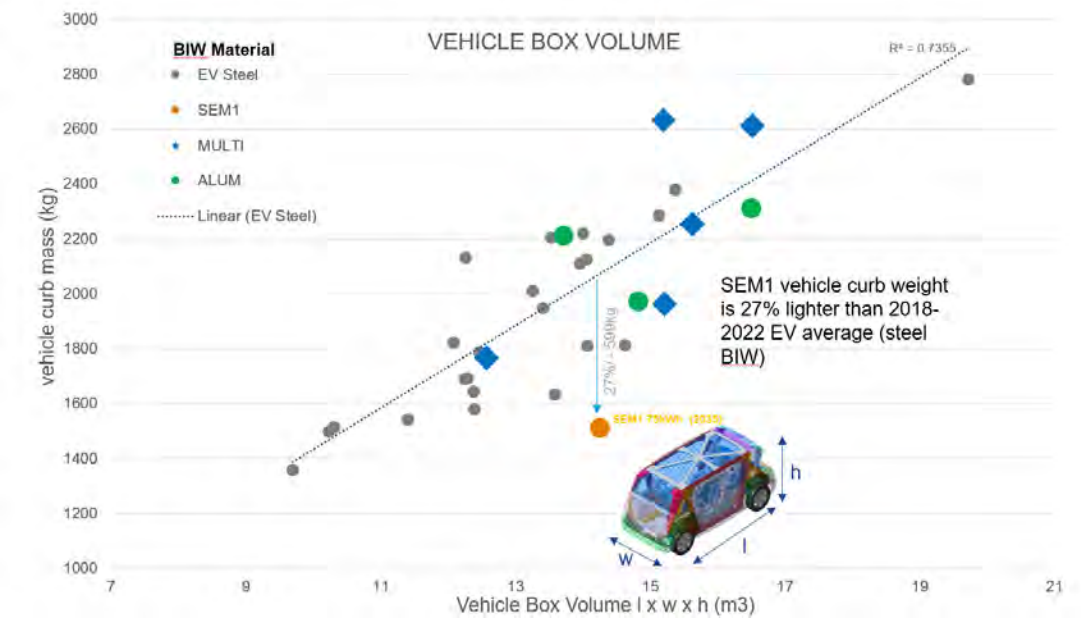

Figure 7.1.5.2 Vehicle curb weight versus box volume comparison. Reference vehicle data source www.a2mac1.com (See Appendix 4 for larger image)

The comparison shows that the Steel E-Motive SEM1 concept has good weight efficiency performance, achieving a curb weight that is 27% lower than the statistical estimation for the vehicle data sample. The study also shows that Steel E-Motive design is competitive compared to vehicles with aluminium and multi-material body structures. One consideration for this calculation is that battery electric vehicle weights are heavily impacted by the

propulsion battery capacity. Many of the sample vehicles with >15m box volume have significantly large batteries (>90kWh), which result in a considerably higher curb weight. However, most of the vehicles within the size of SEM1 do have comparable sizes and specifications of propulsion batteries. Another important consideration in vehicle curb weight calculation is the consideration of autonomy level. Most vehicles in the data sample are level 1 to 2, with conventional driver controls. Steel E-Motive features level 5 autonomy, with the direct driver controls deleted and replaced with an array of motion sensors. Figure 7.1.5.3 shows a projected “weight walk”, comparing the SEM1 vehicle curb weight to a conventional SAE level 1 to 3 vehicle (2022 Model Year). The difference in curb weight can be attributed to; lower weight propulsion battery as a result of expected future battery technology enhancements and efficient Steel E-Motive battery structure design, deletion of the direct driver interfaces, controls and main dashboard, additional weight for autonomous vehicle sensors, estimated weight reduction of other vehicle systems such as suspension, wheels and tyres and weight reduction efforts of the body in white structure (detailed in section 7.2.1).

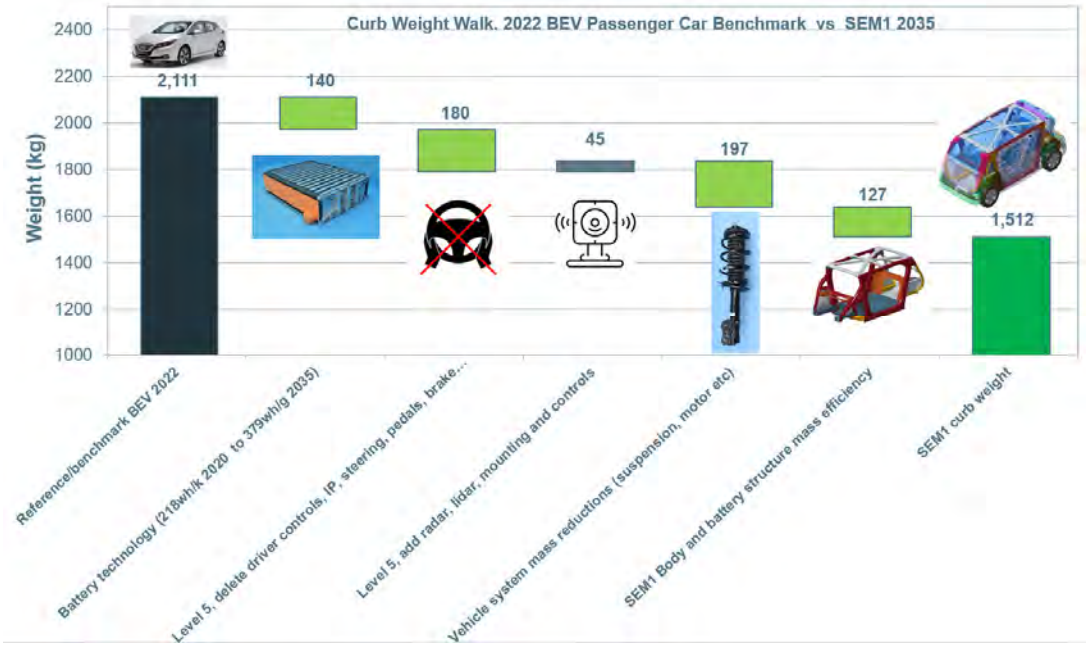

Figure 7.1.5.3 vehicle curb weight walk, comparing 2022 BEV (SAE level 1 to 2) to SEM1

7.2 Steel E-Motive body architecture design and material selection

This section describes the approach and philosophy of the Steel E-Motive body structure design concept with respect to the requirements and the performance achieved. The considerations and justification of the selected material grades and fabrication process are also detailed as well as the geometry and shape considerations. The design decisions were mainly driven and influenced by the requirements and performance targets as defined in Section 4. Section 8 provides comprehensive performance results of SEM1.

7.2.1 Steel E-Motive Body in White (BIW) design, steel grades and fabrication processes

The Steel E-Motive Body in White (BIW) is a monocoque construction consisting of Advanced High Strength Steel (AHSS) sheets, primarily stamped or roll formed parts and assembled using resistance spotwelding (RSW) and laser welding methods. The AHSS steel grades were determined and selected based on the specific requirements of the parts or subassemblies (such as crash, stiffness, formability). Section 7.3 describes the design, AHSS grade selection and fabrication process considerations and selection in detail with respect to each of the specific performance requirements. Figures 7.2.1.1, 7.2.1.2 and 7.2.1.3 show the Steel E-Motive SEM1 BIW design and the application of steel grade family for “core” design. (An “alternative” grade assignment study was performed to further demonstrate and promote the breadth of steel grades available. This is reported in Section 7.5). The Steel E-Motive (core design) BIW uses 34% Press Hardened Steel (PHS), 11% Martensitic, 17% Dual Phase and Complex Phase, 22% 3rd generation (including Retained Austenite, high formability Dual Phase and Complex Phase) and 15% High Strength Low Alloy / Bake Hardenable steels by weight. The Bill of Materials for SEM1 BIW is provided in Appendix 1.1. This details the specific material grade, gauge thickness, weight and fabrication process for each part in the BIW.

Figure 7.2.1.1 Steel E-Motive SEM1 BIW design and distribution of AHSS (See Appendix 4 for larger image)

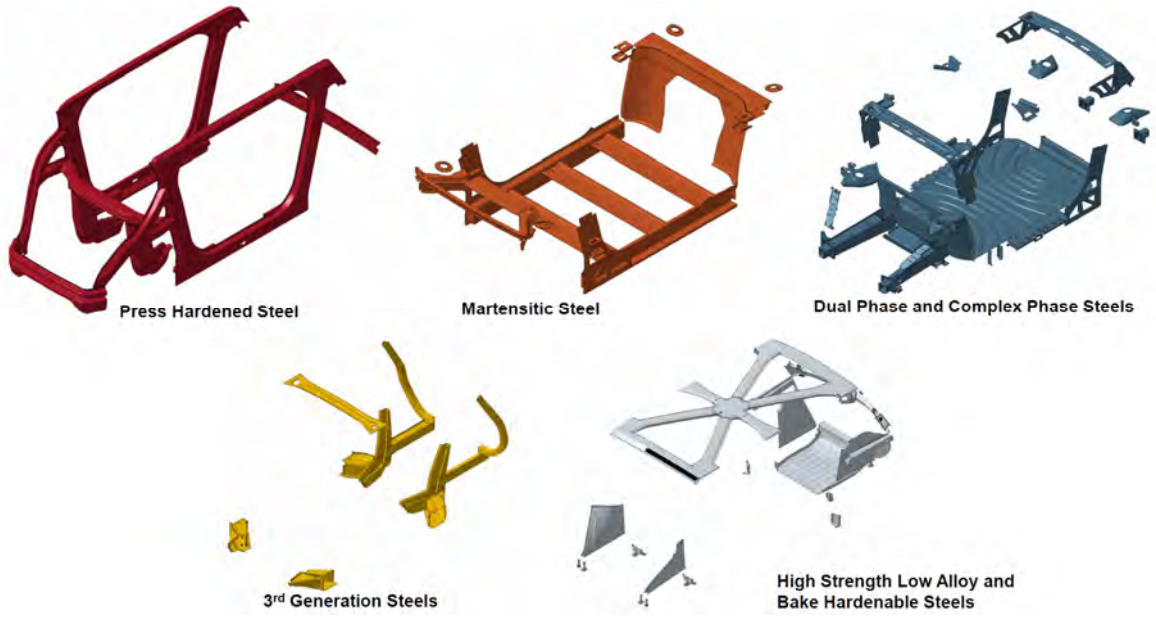

Figure 7.2.1.2 Steel E-Motive BIW AHSS grade allocation (See Appendix 4 for larger image)

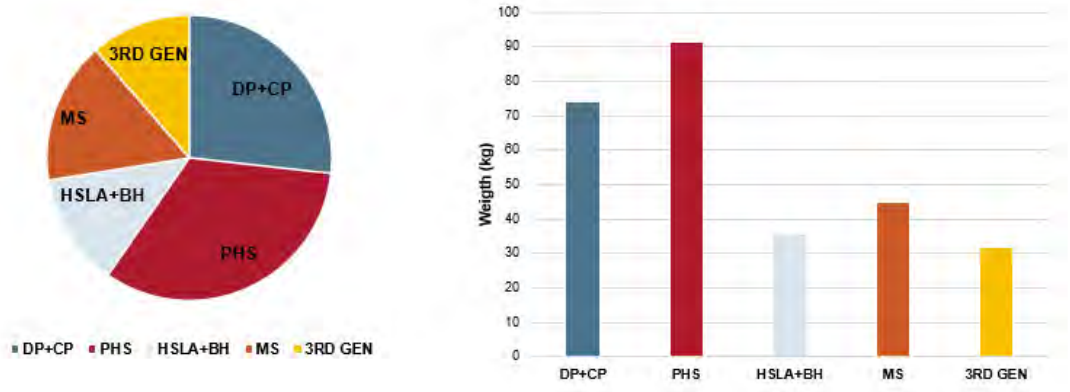

Figure 7.2.1.3 Steel E-Motive BIW AHSS grade distribution (See Appendix 4 for larger image)

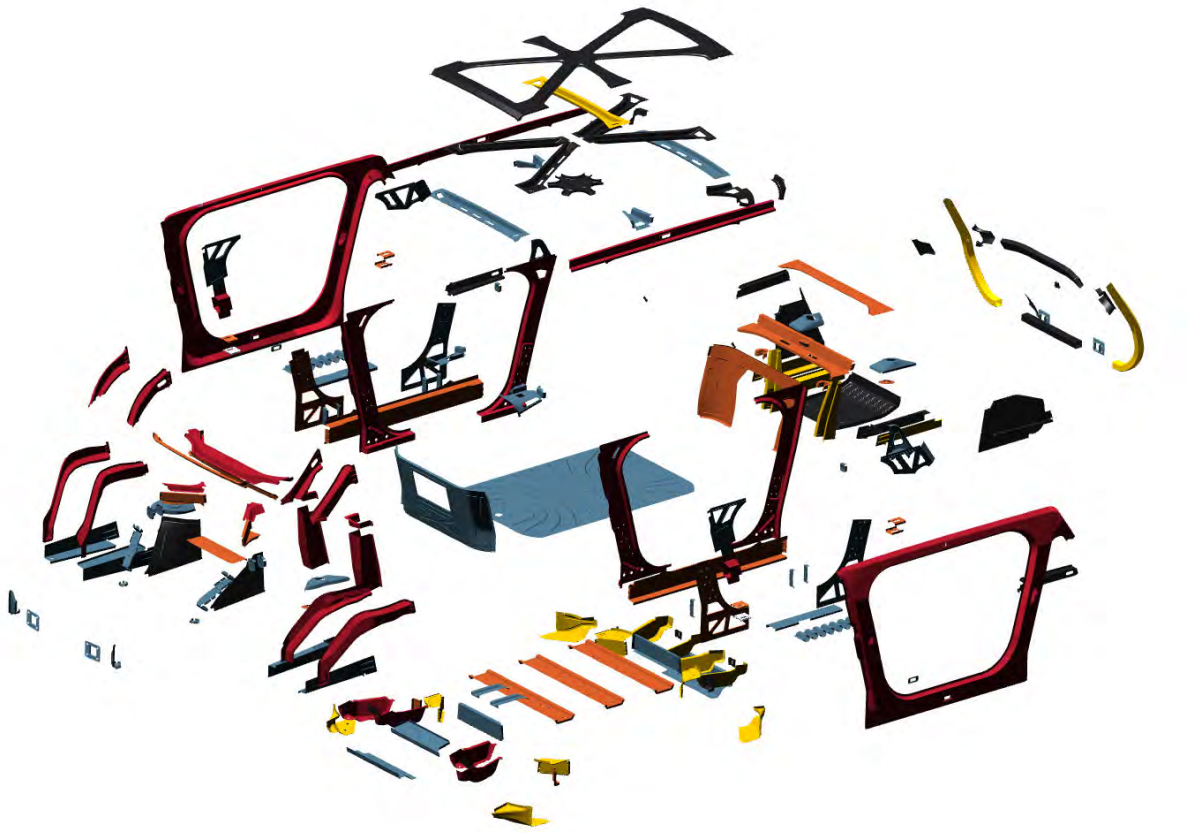

Figure 7.2.1.4 Steel E-Motive SEM1 BIW AHSS grades (exploded view) (See Appendix 4 for larger image)

The Steel E-Motive body structure draws on the various fabrication processes available for sheet steel body structures. Cold forming is widely used as it provides high speed and efficiency for high volume production, facilitates lower cost and high quality. Advanced High-Strength steels feature high elongation properties making cold forming a readily applicable solution for many parts. Roll forming and roll stamping is applied to panels with continuous section profiles. Roll stamping provides an additional freedom for sections with some out of plane curvature or features. (See Section 5). Where very high strength and cold forming methods cannot be applied to parts with complex geometry then Press Hardened Steels (PHS) have been applied. The performance demands of the Steel E-Motive resulted in the requirement for a significant quantity of >1000MPa UTS grades, especially for the management of front and side crash loadcases. Where possible, 3rd generation and martensitic grades were applied. For parts with geometry that fall outside of the forming limits of these grades then Press Hardened Steels were applied. Figure 7.2.1.5 shows the BIW fabrication process usage by weight.

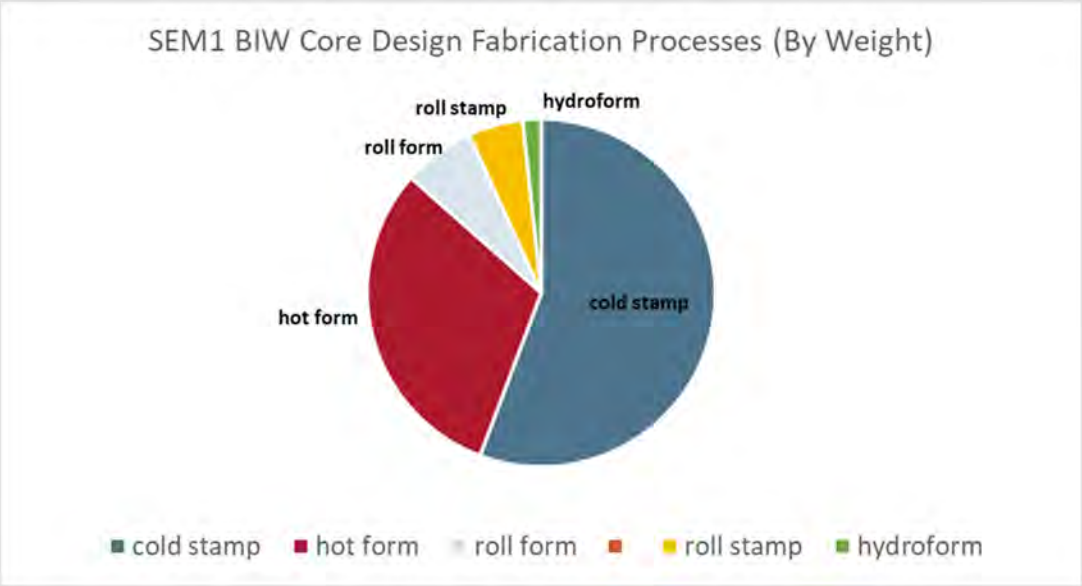

Figure 7.2.1.5 SEM1 BIW fabrication process application by weight

7.2.2 Steel E-Motive body structure design approach and features for weight, stiffness and NVH performance

The Steel E-Motive concept achieves very good body structure weight, static stiffness and NVH performance, as summarised in Figure 7.2.2.1 below.

Loadcase/requirement	Target value	SEM1 performance
Body in white weight	<309.3kg	282kg
Static torsional stiffness	>25,000 Nm/deg	63,285 Nm/deg
Static vertical bending stiffness	>9,000 N/mm	13,438 N/mm
Trimmed BIW first mode	>28Hz	32Hz
Trimmed BIW first battery mode	>35Hz	35Hz
Trimmed BIW local dynamic attachment stiffness	>5 x equivalent dynamic bushing stiffness	5 x dynamic bushing stiffness achieved

Figure 7.2.2.1 SEM1 body weight and stiffness performance versus targets

The main design factors that enable the weight, stiffness and NVH performance are summarised below:

- Optimum structural loadpaths throughout the body. Placing structure where it is needed
- Using the right material in the right place by applying the appropriate Advanced High Strength Steels grades. The Steel E-Motive project portfolio contained steel grades with Ultimate Tensile Strengths up to 2000MPa and gauge thicknesses from 0.4mm to 5.0mm. Technologies such as Tailor Welded Blanks (TWB) and Tailor Rolled Blanks (TRB) enable refinement of steel grade and gauge within in a single part. This enabled a good balance of weight, strength and stiffness to be achieved in the body structure design
- Development of the body structure as a complete system, considering the contribution of the propulsion battery structure and cover, the chassis subframes, closures and bumper beams. The integrated battery solution in the Steel E-Motive concept provides a significant contribution to overall body stiffness performance

- Optimum size and shape of structural members in the body structure. Fabricated steel structures enable cross sections with high polar moment of areas and weight efficiency.
- Local geometry and design features. Orientation and design of the fabricated panel joint flanges. Use of panel swaging and beading to improve local stiffness
- Appropriate selection of joining methods and locations
- Inherent Youngs Modulus value (207GPa) of steel, irrespective of specific steel grade

BIW weight:

The weight target for the SEM1 body in white (BIW) was derived using a similar principle to the vehicle curb weight comparison as described in Section 7.1.5. A dataset of Multi-Purpose Vehicles (MPV) and mini-vans was assembled and statistical regression calculations performed to identify suitable weight versus dimensional relationships as the basis for the target. MPVs and mini-vans were selected as they feature more of an overall "one-box" exterior shape (similar to SEM1), compared to conventional passenger cars featuring two or three box shapes. The BIW occupied box surface area was found to present a strong relationship to the BIW weight and was therefore selected as the primary function to derive the weight target. Figure 7.2.2.2 shows the BIW weight regression evaluation and derivation of weight target. The "Benchmark/average" BIW weight for a vehicle of SEM1 dimensions was calculated using a logarithmic function of the statistical regression relationship and a value of 374.1kg was derived. The BIW weight target was then calculated based on a factor of 3 times the Standard Deviation value of the benchmark average weight. Based on the SEM1 BIW dimensions, the statistical dataset for MPV/mini-vans and the Standard Deviation factor, a target weight value of 309.3kg was derived.

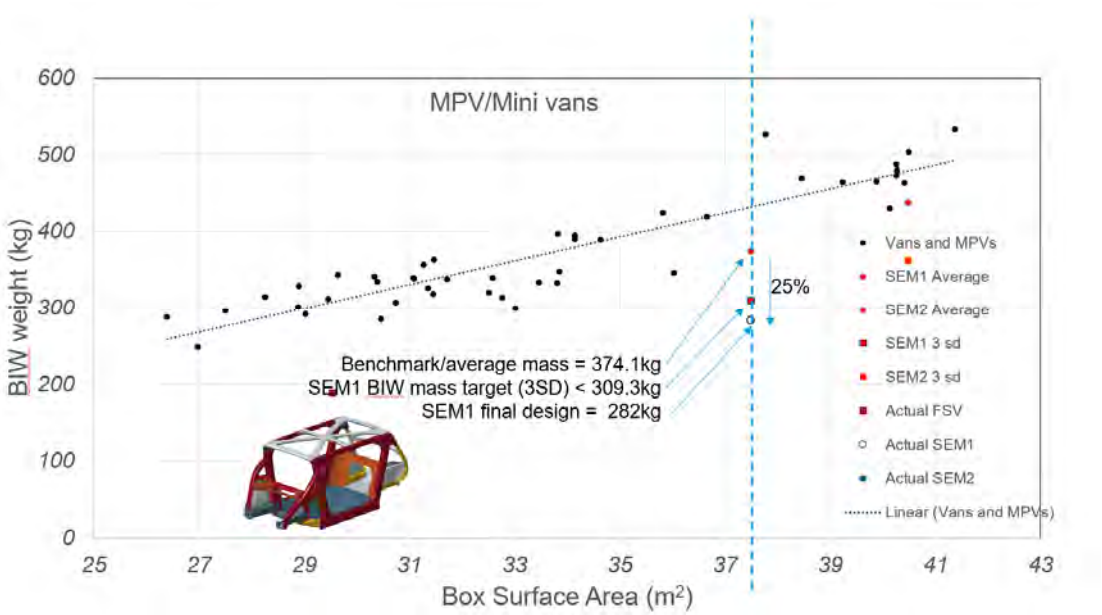

Figure 7.2.2.2 Body In White weight regression analysis (See Appendix 4 for larger image)

The final design weight of the SEM1 body in white is 282kg, representing a 25% improvement on the benchmark/reference vehicle weight and 8% lower than the weight target. The statistical dataset chosen for the BIW weight target setting exercise consisted of MPVs and mini-vans with Internal Combustion Engine powertrain. This was due to the body structure designs being more consistent in shape, therefore providing a good statistical

relationship between weight and dimensions. Battery electric vehicle body structures currently have a larger variability in shape and construction due to the different approaches taken for integrating the propulsion battery. The statistical relationship between BIW weight and dimensions for battery electric vehicles is not as strong as the MPV and mini-van dataset. Nevertheless, a comparison of the SEM1 BIW weight performance and current production (2018 to 2022 model year) battery electric vehicles was performed. Figure 7.2.2.3 shows a similar BIW weight evaluation using the occupied box volume as the dimension parameter. The greater level of data "scatter" demonstrates more inconsistency in the relationship between weight and occupied box volume and therefore unsuitability for weight target derivation (note low the r^2 values which describe the consistency of the dataset relationship of weight and dimensions). This evaluation does however demonstrate good weight efficiency performance of the Steel E-Motive BIW concept. For the data sample evaluated, it can be concluded that the Steel E-Motive AHSS structure has comparable weight performance to aluminium and multi-material body structures. The SEM1 BIW weight is also in line and on a similar trend to the Future Steel Vehicle BIW concept, further demonstrating that steel solutions can be engineered to be as weight efficient as aluminium and multi-material structures. It should be noted that the Steel E-Motive BIW weights quoted do not include considerations for paint and NVH trim pads, which are accounted for in the a2mac1 data, therefore the actual weight performance of SEM1 BIW versus the benchmark a2mac1 data would be slightly reduced.

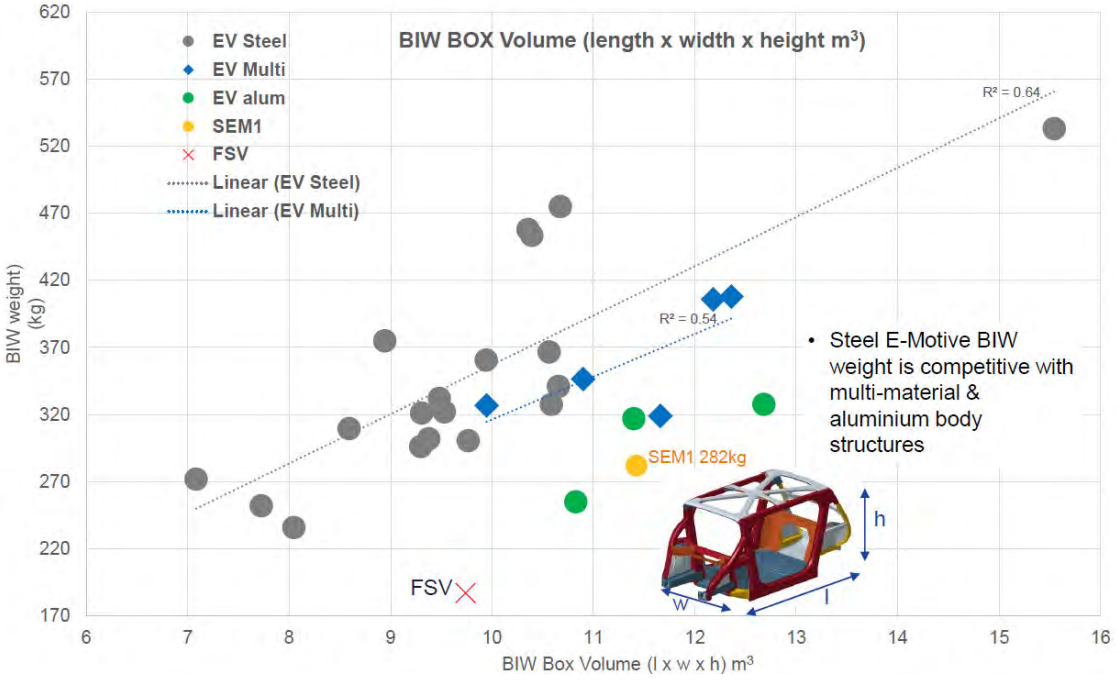

Figure 7.2.2.3 Body In White weight versus occupied box volume comparison. 2018 to 2022 battery electric passenger cars. (data source www.a2mac1.com)

Body Structure Stiffness:

Section 6.2.4 outlines the approach taken for the topology structural loadpath optimisation, a methodology that assists designers to place material in the most appropriate and efficient locations within the available volume of body structure. Section 6.3.2 demonstrates how the outputs from the topology loadpath optimisation were interpreted into the design of the SEM1 body structure. The placement of the key structural members in the Steel E-Motive body structure was guided by the early concept structural topology optimisation. Figure

7.2.2.4 shows the SEM1 body design with the key structural loadpaths highlighted. For a static torsional loadcase with equal and opposite forces applied at the front strut top mount a *front torsion loop* consisting of left and right vertical dash braces, a lateral strut brace and lower #1 bar creates a ring structure to react the twist loads.

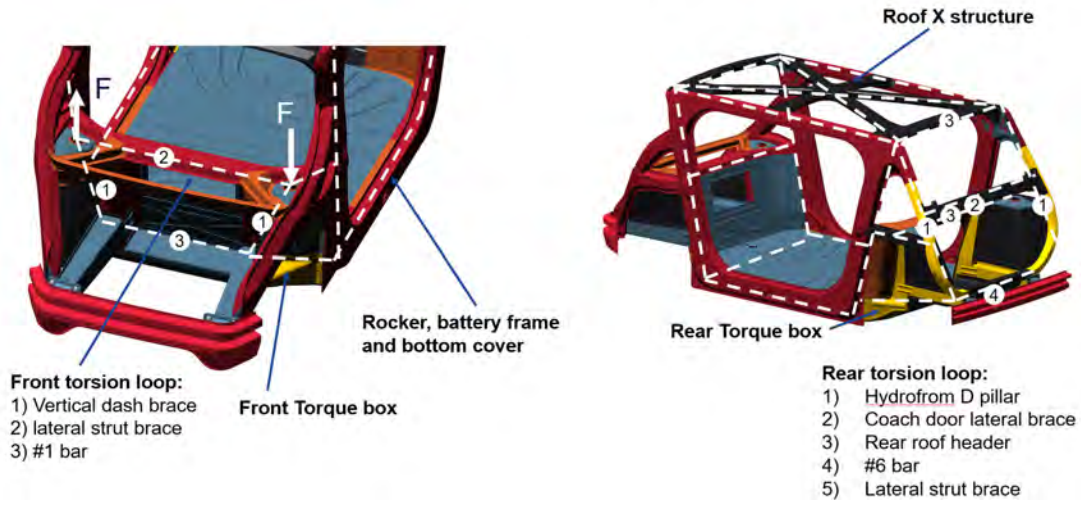

Figure 7.2.2.4 SEM1 body structure key loadpaths (See Appendix 4 for larger image)

The front strut tops themselves are located in close proximity to key structural members such as lateral strut brace and the front crash SORB structure as shown in Figure 7.2.2.5. This provides enhanced local stiffness and integration to the body structure loadpaths.

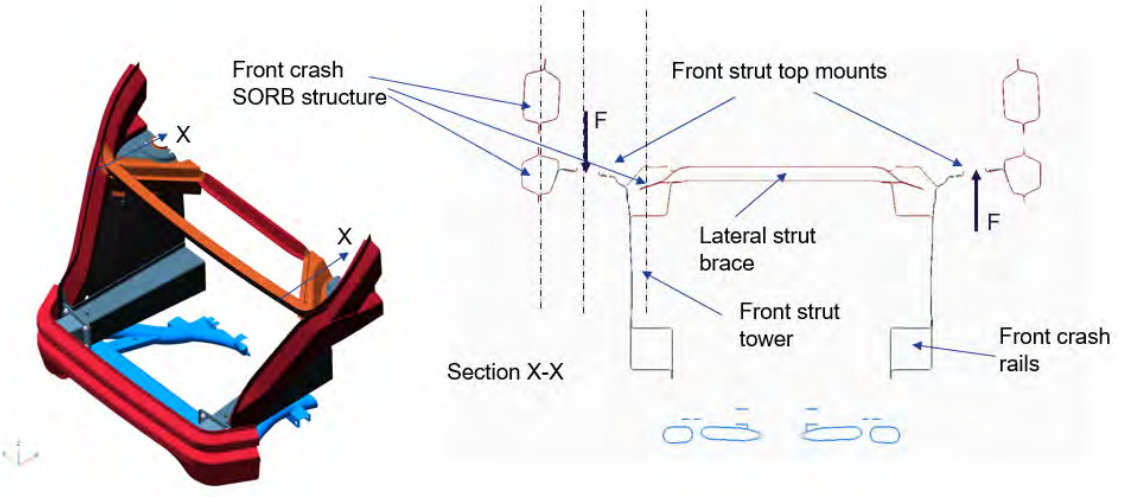

Figure 7.2.2.5 BIW section in X-X through front strut top mounts (See Appendix 4 for larger image)

With the Steel E-Motive concept featuring an open cockpit and B pillarless structure, the loadpaths through the upper and lower sections of the body structure required additional attention and focus in order to ensure the stiffness targets were achieved. Additionally, the propulsion battery is integrated to the body structure via a carrier frame. The BIW features a cavity opening to house the battery. A continuous underbody chassis-type structure ensures the crash and road loads are managed throughout the length of the vehicle as shown in Figure 7.2.2.6

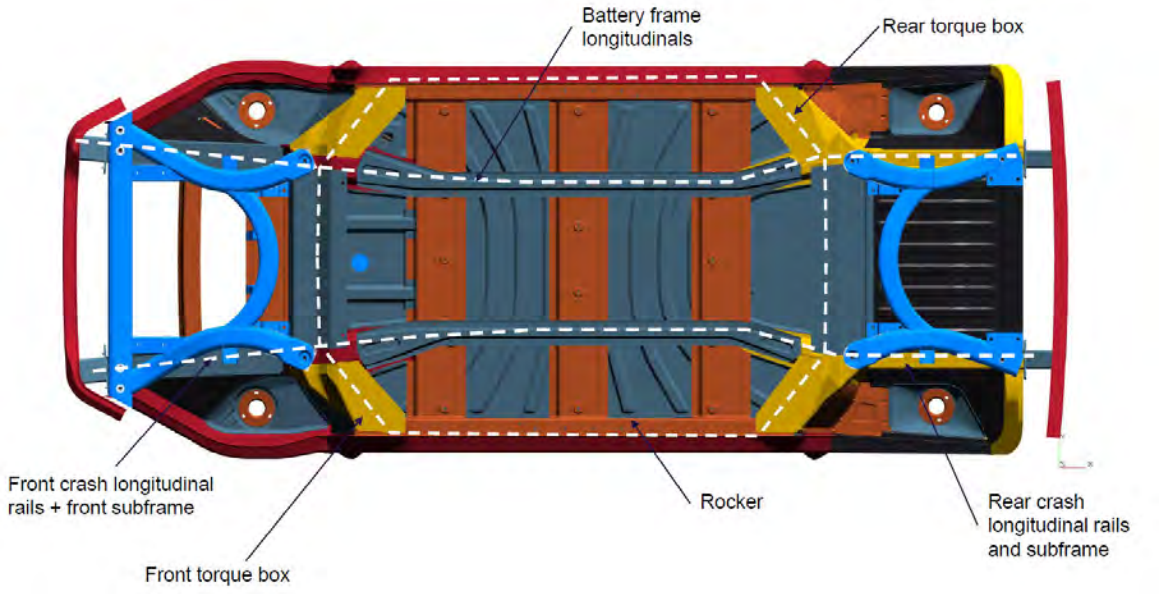

Figure 7.2.2.6 Underbody structural loadpaths and features (note, battery cover plate removed from image for clarity)

The rigidly mounted front subframe and front crash rail longitudinals combine to provide the main element of the forward front structure. The front subframe features forward and rearward lateral braces providing local chassis attachment stiffness as well as assisting front crash loadpaths. The #1 bar and front torque box structures combine to distribute loads from the front subframe and longitudinals outwards to the rocker sections. Additionally, the bolt-in battery carrier frame features longitudinals which align to the front and rear longitudinals. This provides a continuous loadpath (or “spine”) along the length of the vehicle and provides particular contribution to the static and dynamic (NVH) vertical bending stiffness as well as support to the battery modules. The central loadpath is completed by the battery cover plate (Figure 7.2.2.7), which is attached to the BIW via 34 x M8 fixings and to the battery carrier frame by 8 weldnuts. This provides a significant enhancement to body stiffness as well as supporting the sealing function to the battery from outside. The battery carrier frame also contributes to the overall body stiffness. The frame is connected to the body via 22 fixings from the frame cross members to equivalent positioned cross members in the body in white floor as shown in Figure The battery modules are attached to the carrier frame through 4 fixings per module (total 32 fixings).

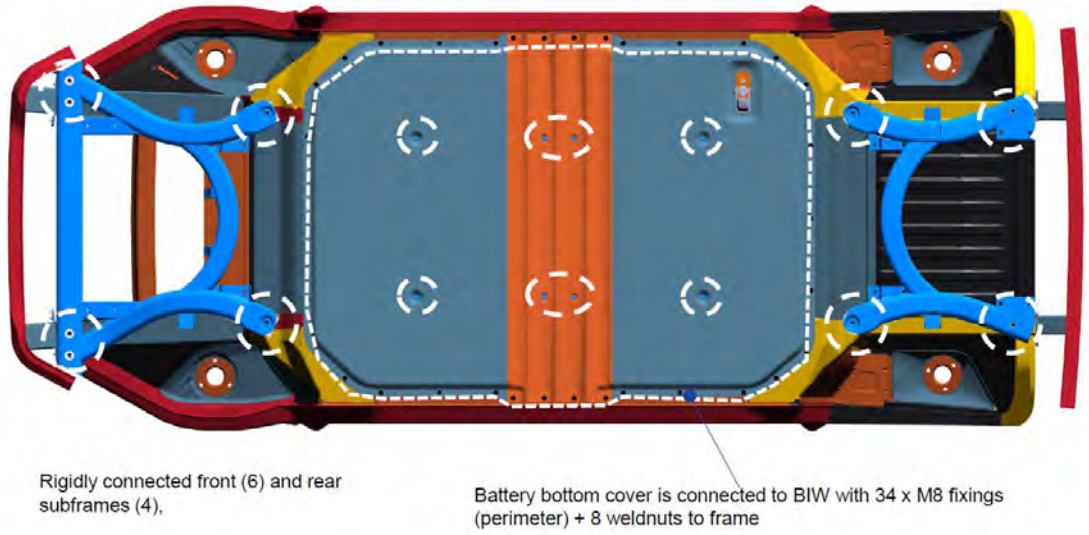

Figure 7.2.2.7 Subframe and battery cover fixings

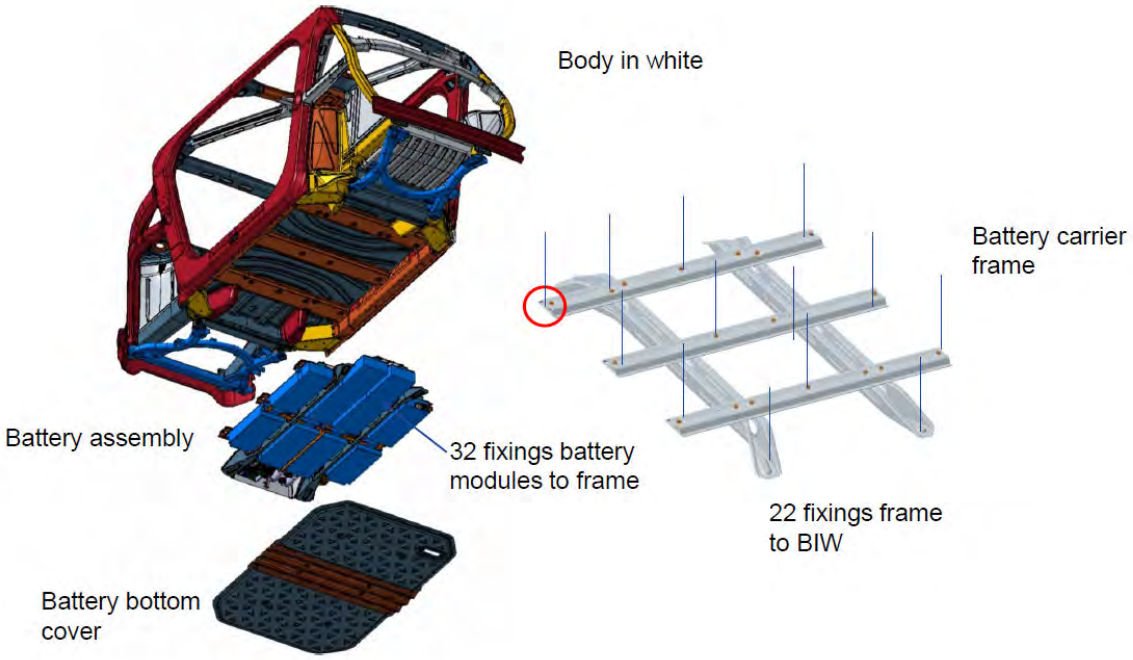

Figure 7.2.2.8 Battery carrier frame fixings to body in white (See Appendix 4 for larger image)

The roof structure features a unique “X brace” configuration, connecting the front and rear corners of the body structure through a central node (Figure 7.2.2.4). The roof structure provides stiffness and crash loadpaths as well as enabling large glazed areas. The rear body structure features single part hydroformed D-pillars which offer a lightweight and stiff solution and forms part of the rear torsion loop.

Stamped and fabricated structures achieve high stiffness and low weight due the ability to produce cross section profiles with high second and polar moment of inertias. When coupled with the inherent high Young’s Modulus of steel, a monocoque body in white structure can

be lightweight and achieve high stiffness. The section profiles and dimensions in the Steel E-Motive body structure concept were guided by CAE optimisation tools, results and requirements from all loadcases including crash, stiffness, strength and weight and design guidelines and principles. Appendix 2.2 shows the cross-section properties for the main parts of the body in white and Figure 7.2.2.9 shows the cross-section profile for the rocker section. The size and configuration of the profile was primarily driven by global body stiffness and side crash requirements.

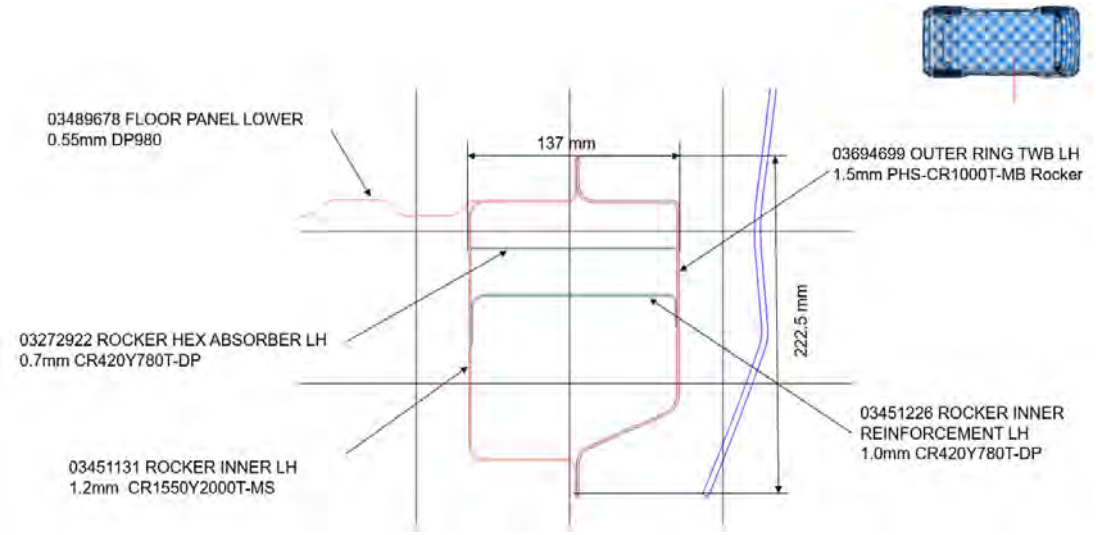

Figure 7.2.2.9 Rocker cross section profile (full BIW section profiles are shown in Appendix 2.2)

Another benefit of fabricated sheet structures is the ability to efficiently locally reinforce sections where specifically needed. The Steel E-Motive body concept features a number of local reinforcements as shown in Figures 7.2.2.10 and 7.2.2.11. The corner gusset reinforcements in the body side structure provide a loadpath through the bending axis of the cross section (Z-Z in Figure 7.2.2.10). This provides improved stiffness and strength through the section.

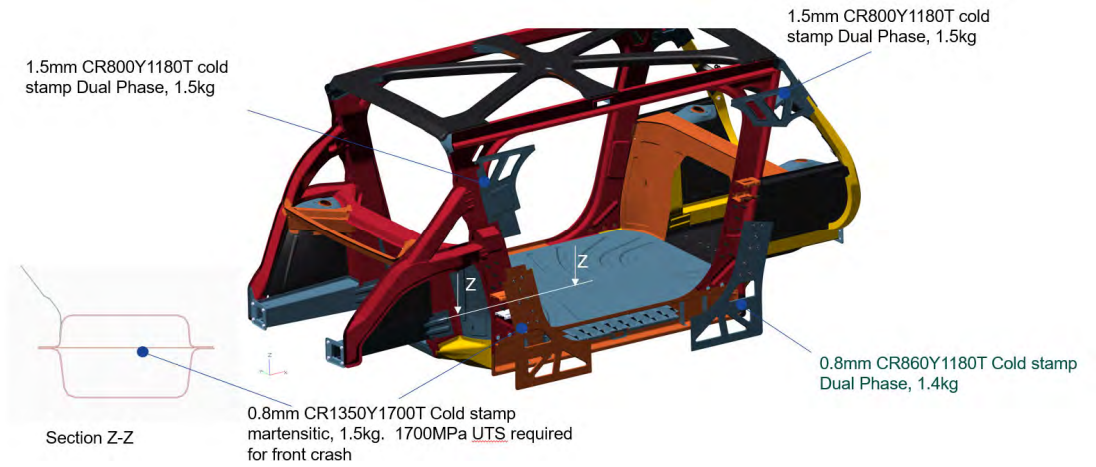

Figure 7.2.2.10 Localised gusset reinforcements adding efficient stiffness and strength improvements (See Appendix 4 for larger image)

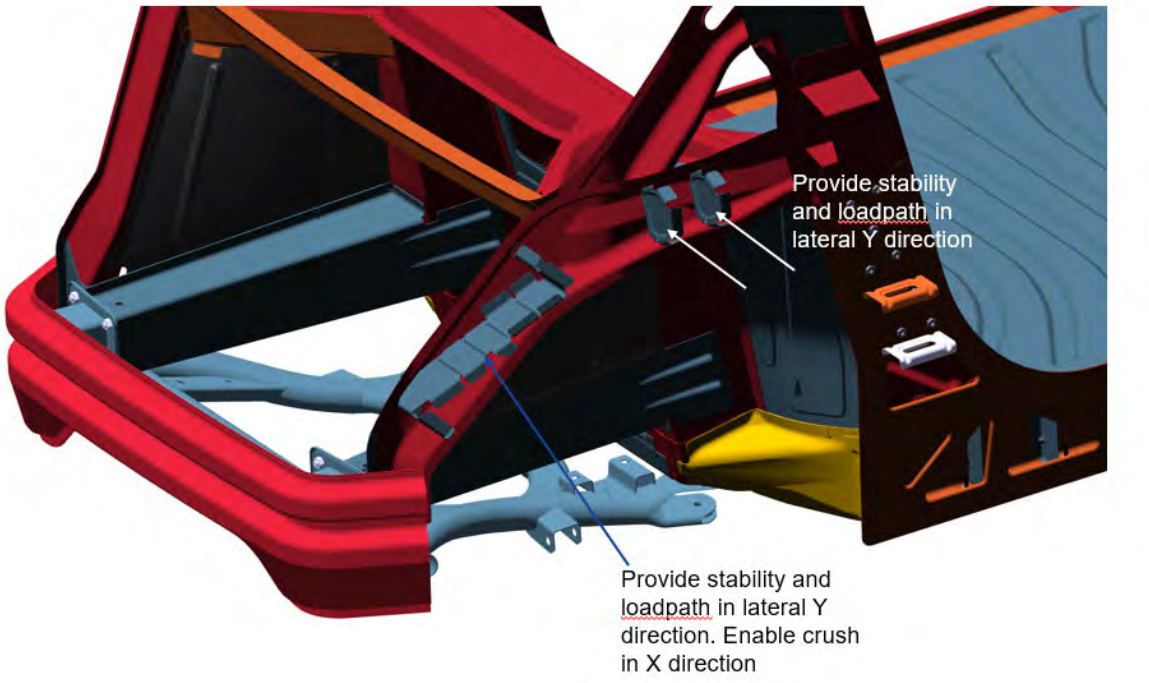

Figure 7.2.2.11 Glance beam reinforcements providing local section support

Gauge thickness for weight, stiffness and strength

The Steel E-Motive body structure utilises the broad range of gauge thicknesses available for sheet steel coils. Thinner gauges such as 0.7mm are applied to large panels which are weight sensitive. For parts such as damper strut tops, where stiffness and strength is required then gauges of 2.4mm can be applied. The selection of each specific panel gauge thickness was based on a number of factors: stiffness, weight, crash strength, durability, formability, availability. CAE gauge optimisations methods as described in section 6.4.5 were used to guide engineers in the selection of panel gauges. Figure 7.2.2.12 and 7.2.2.13 shows the distribution of panel gauge thickness for the Steel E-Motive body in white design.

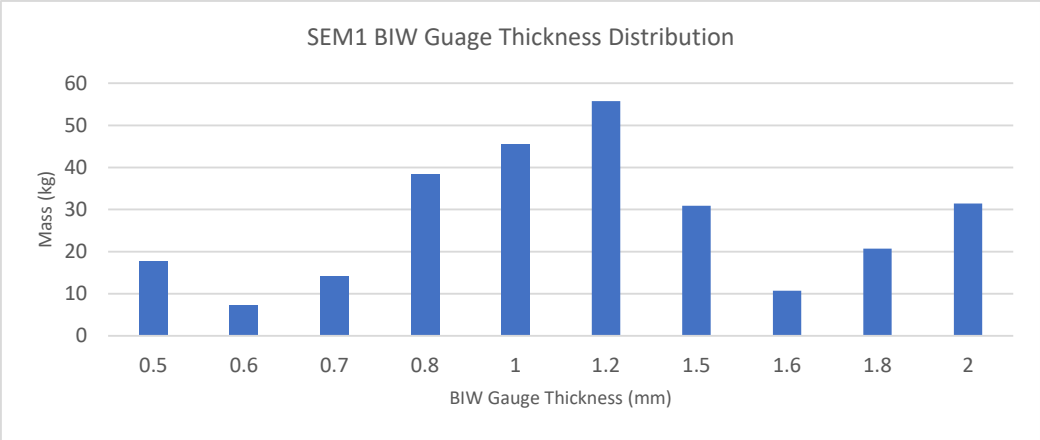

Figure 7.2.2.12 Gauge thickness distribution in SEM1 BIW

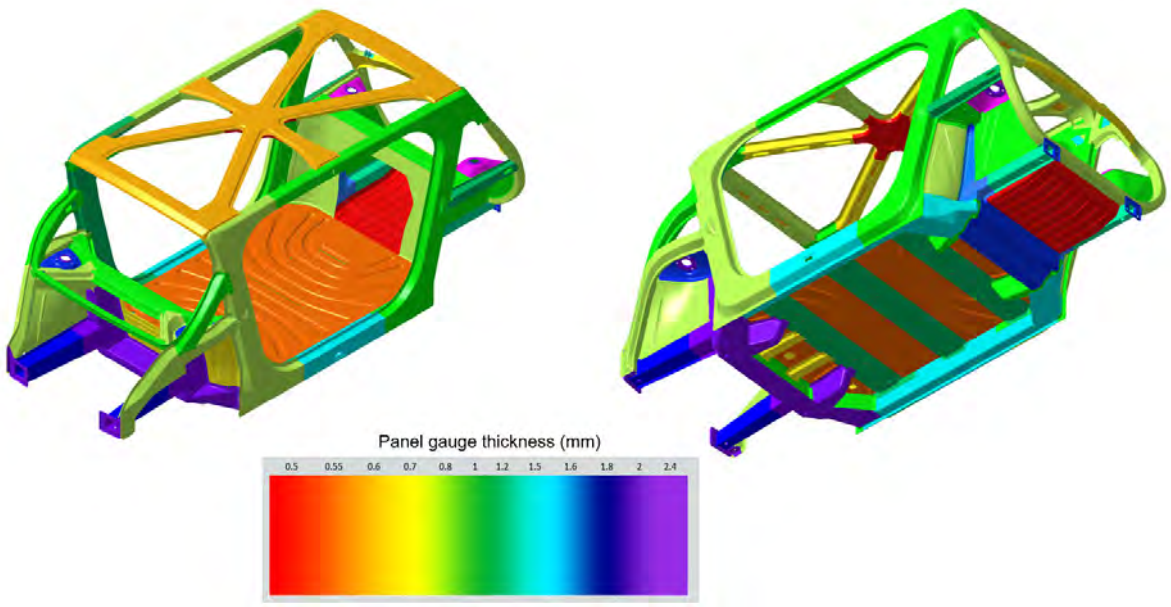

Figure 7.2.2.13 Gauge thickness assignment in SEM1 BIW

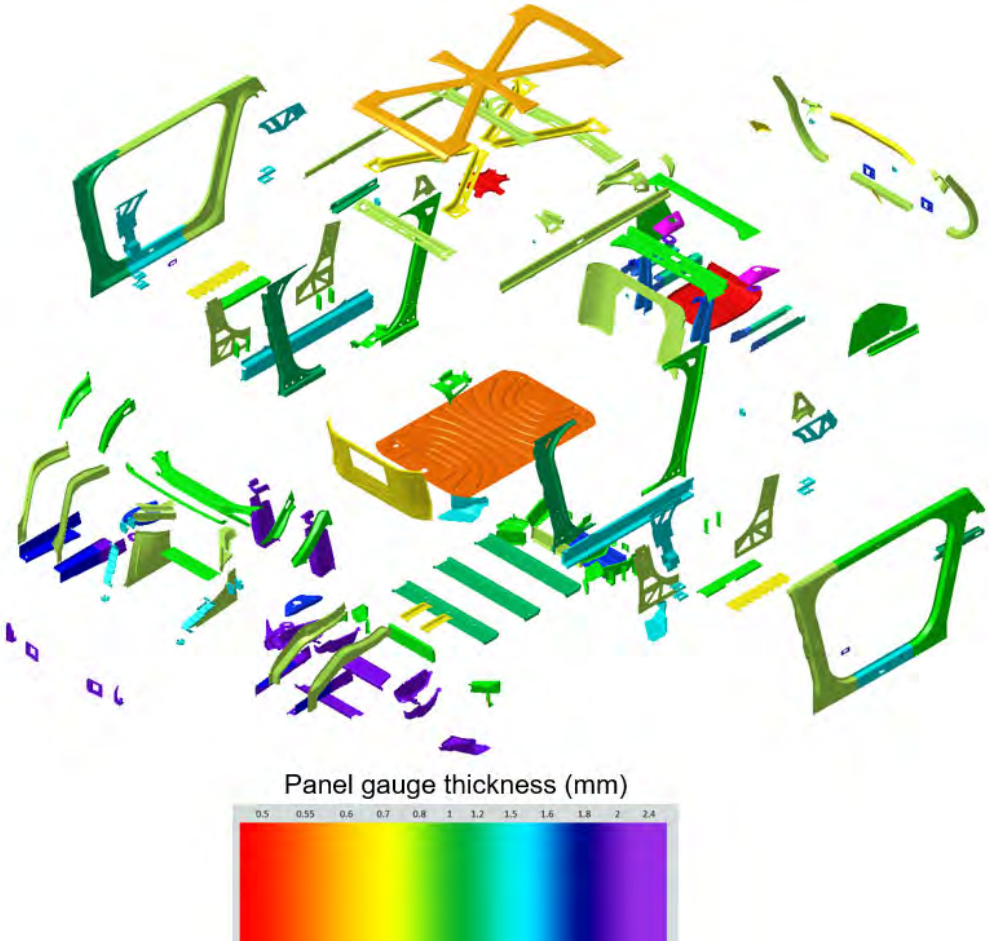

Figure 7.2.2.14 Gauge thickness assignment in SEM1 BIW (exploded view) (See Appendix 4 for larger image)

BIW Joining Methods

The joining methods used in a fabricated body structure have a significant influence on overall stiffness, strength at both body and complete vehicle level. The fabricated steel structure of Steel E-Motive concept uses resistance spotweld (RSW) (more information provided in Section 5) methods as the primary method of joining, with seam/mig welding, seam laser welding and structural adhesive applied in specific locations where required. RSW was selected as the primary joining method as it provides a robust and low-cost solution for stamped steel body structures. RSW enables the joining of up to 5 individual sheets (subject to specific considerations for the design of joint, welding parameters and the potentials for some strength degradation). The Steel E-Motive SEM1 body structure features 3,219 spotwelds though 3 sheet thicknesses (3T), 777 through 3T and 38 4T. The rear D pillars consist of single part hydroformed tube sections which cannot be spotwelded using conventional 2 sided welding guns. To overcome this, single sided spotwelding process is applied. The spotweld positions and pitch (distance between the welds) was optimised based on the requirements from specific loadcases such as crash, stiffness and durability. MIG and laser welding was applied where a constant seam weld was required in the body structure, such as the perimeter of the body floor panel (to provide sealing to the underbody battery compartment)

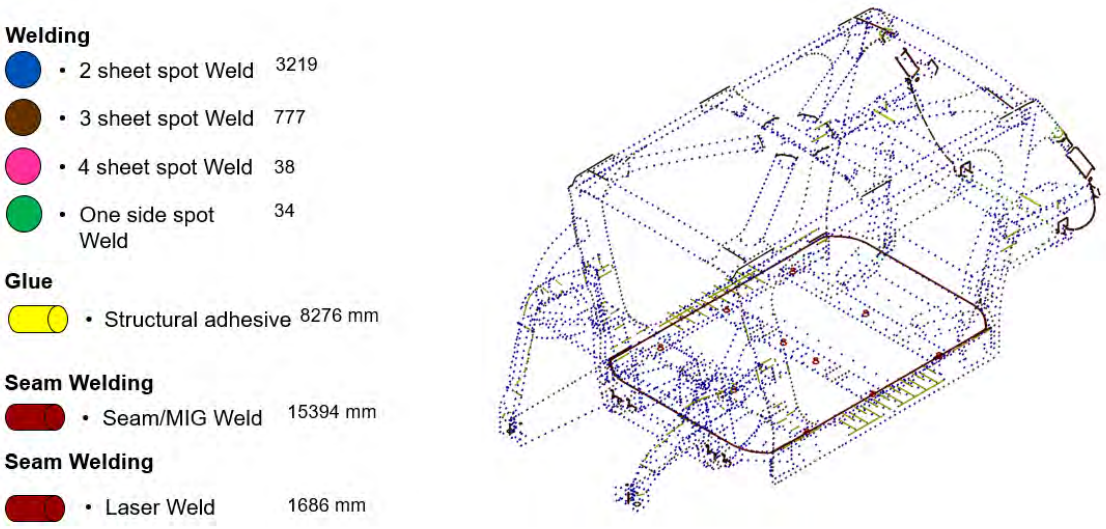

Figure 7.2.2.14 Body in White joining methods (See Appendix 4 for larger image)

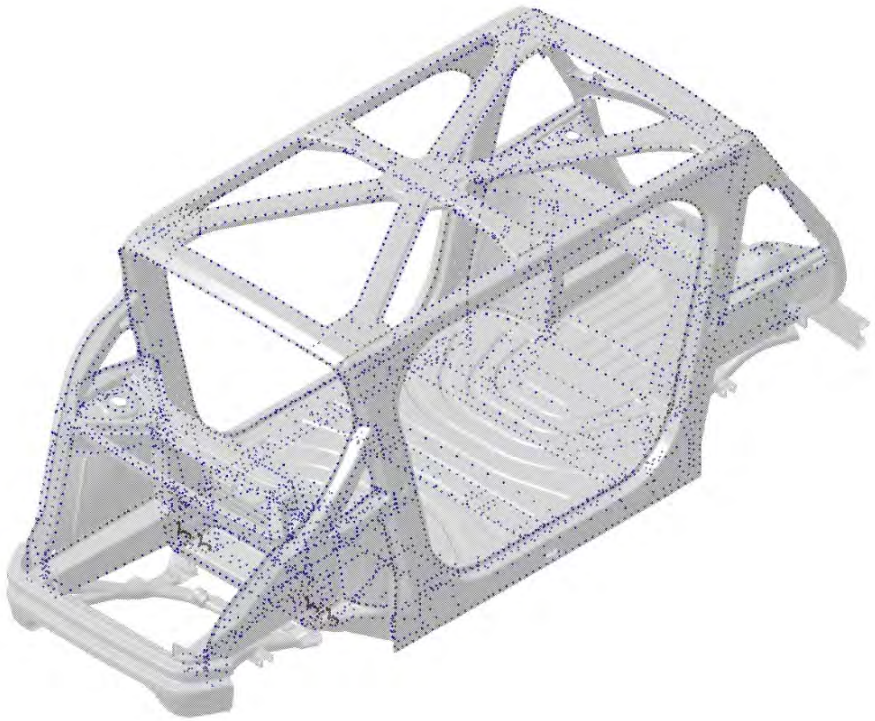

Figure 7.2.2.15 SEM1 Body in White spotweld locations

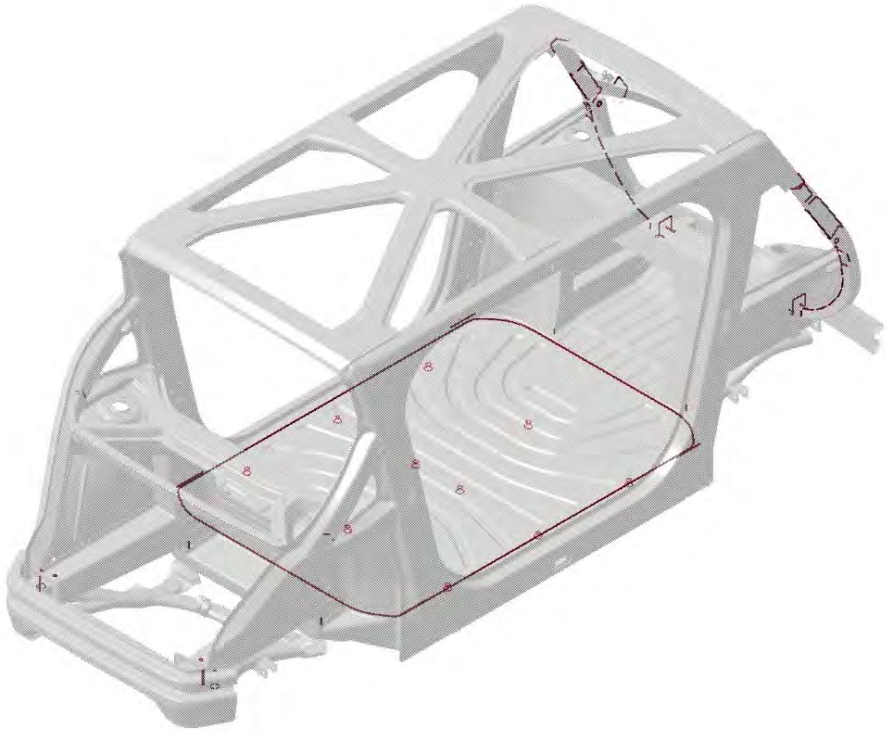

Figure 7.2.2.16 SEM1 Body in White laser weld locations

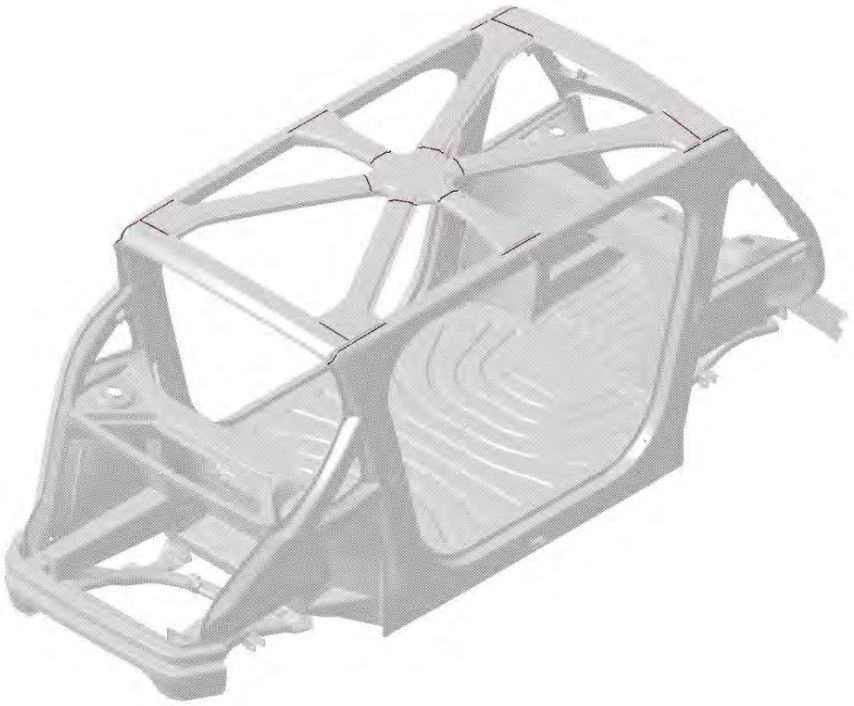

Figure 7.2.2.17 SEM1 Seam weld locations

Further localised stiffening features can be achieved with stamped steel body structures by the introduction of panel swaging. These are depressions or features which are oriented such that bending or in-plane stiffness is increased. These features are employed on large body panels such as front and rear bulkheads, floor panel and battery bottom cover and provide enable increased panel modal frequencies and static stiffness.

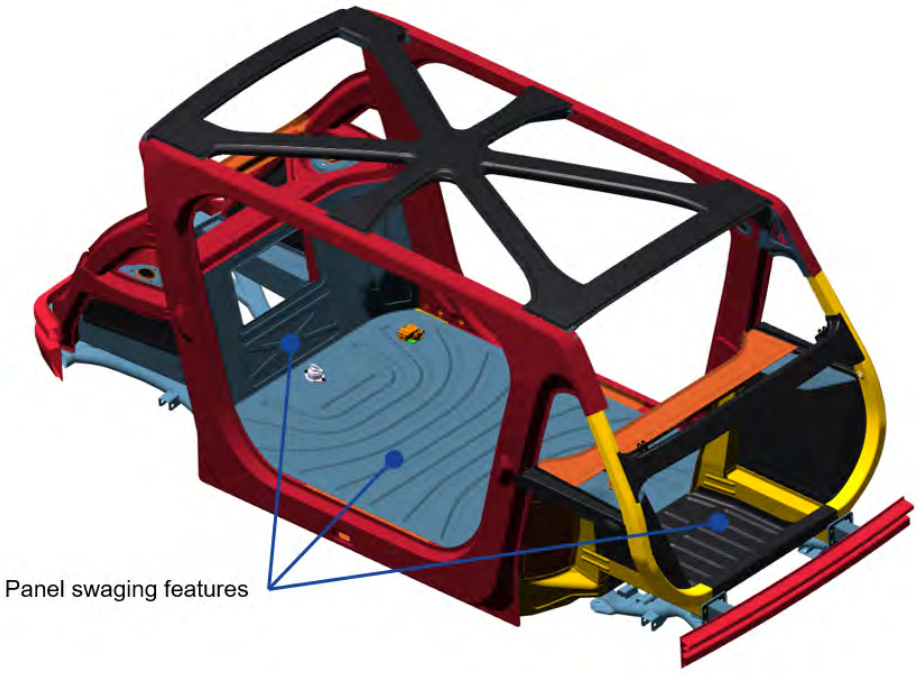

Figure 7.2.2.18 panel swaging features

Attaining a suitable body structure static torsional stiffness performance ensures that the body twist under static and dynamic (i.e. asymmetrical road loads) is well managed and the risk of quality issues such as squeak, rattle, fit and finish are minimised. Appropriate static torsional stiffness also ensures the vehicle chassis is able to perform as required, although specific attributes such as dynamics and handling will be less critical for a fully autonomous vehicle.

The Steel E-Motive body design features described in section 7.2.1 combine to deliver a lightweight and high stiffness structure. The static torsional stiffness of the body structure (including BIW, battery frame, bottom cover, subframes, front windscreen clip and bumper beams was calculated as 63,285 Nm/deg versus a target of 25,000Nm/deg. The BIW alone achieves a torsional stiffness of 34,236Nm/deg. Figure 7.2.2.19 shows the predicted strain energy distribution and displaced shape of the body structure for the static torsional stiffness loadcase. The lower plot shows the rotational twist angle of the body structure along the X axis. It can be observed that the gradient of the line is fairly constant, demonstrating that the torsional stiffness of the body structure is consistent. Significant gradient changes in the plot would highlight localised regions of lower stiffness and it is evident that no such areas are present in the Steel E-Motive structure. This demonstrates a consistent, robust body structure design.

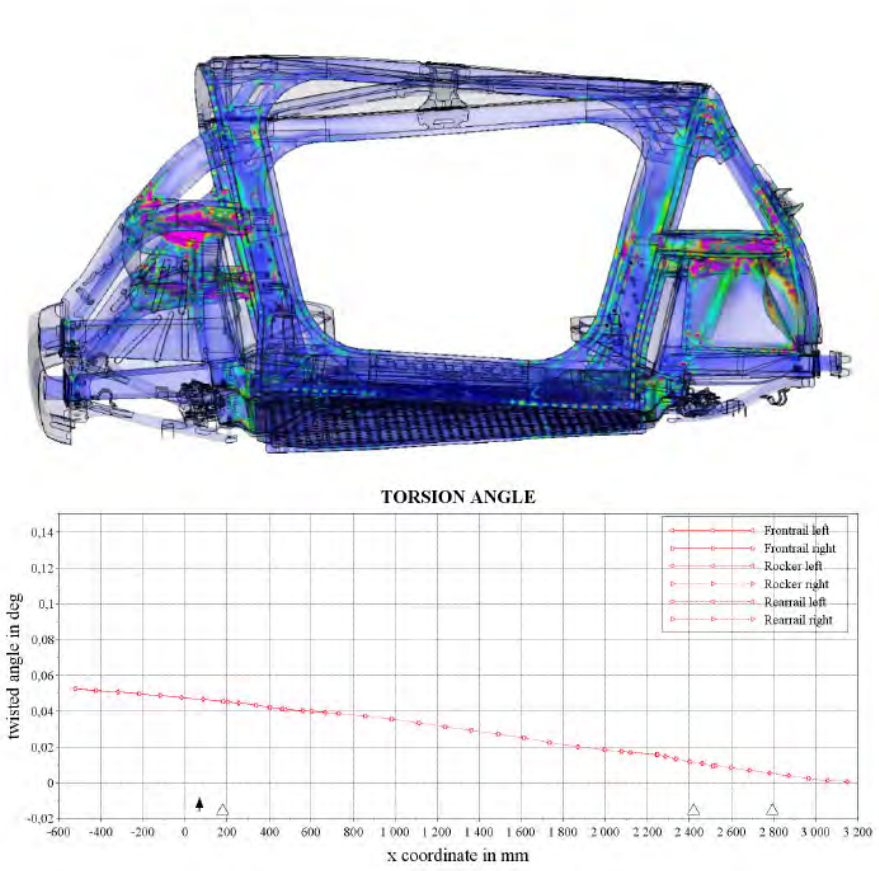

Figure 7.2.2.19 static torsional stiffness displaced shape, strain energy and rotation angle vs length results

The relative contribution of the body structure sub-assemblies to the static torsional stiffness performance were investigated in order to provide further insight into the Steel E-Motive concept. Figure 7.2.1.20 shows the torsional stiffness “walk” from BIW to dressed body. The study shows that the battery frame and cover provide the largest contribution to overall torsional stiffness. The rigidly connected front and rear subframes show a low contribution to torsional stiffness but this is likely caused by the battery frame and cover not being present in that specific loadcases. The combined effect of battery frame, battery cover and rigidly connected subframe is expected to be significant.

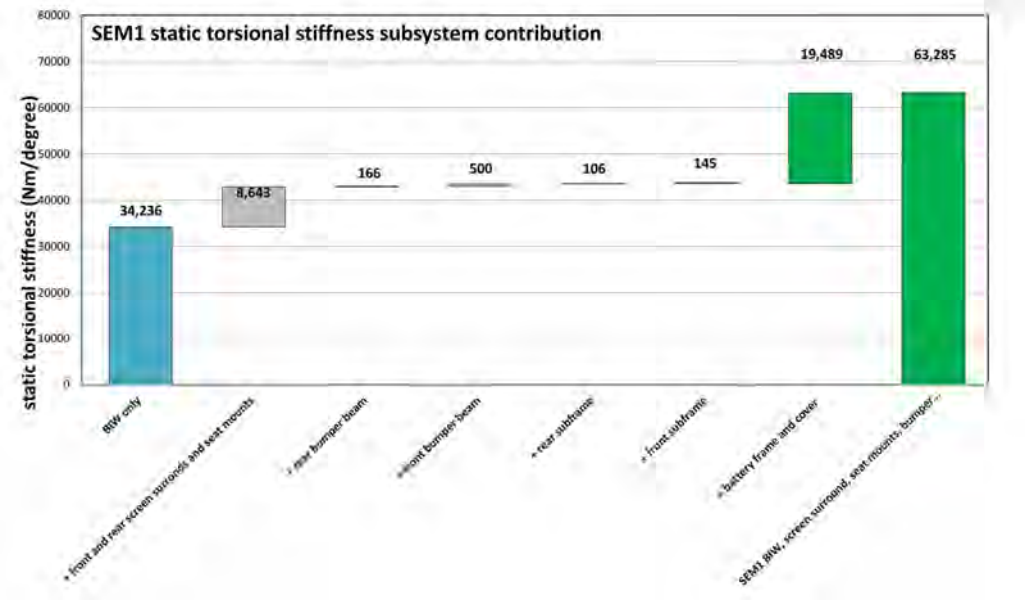

Figure 7.2.1.20 static torsional stiffness contribution

Lightweight design coefficient

Lightweight design coefficient is an industry standard metric to measure the weight efficiency of a body structure. It takes into consideration the static torsional stiffness, weight of the body structure and accounts of the dimensional size. Lightweight design coefficient is calculated using the equation below:

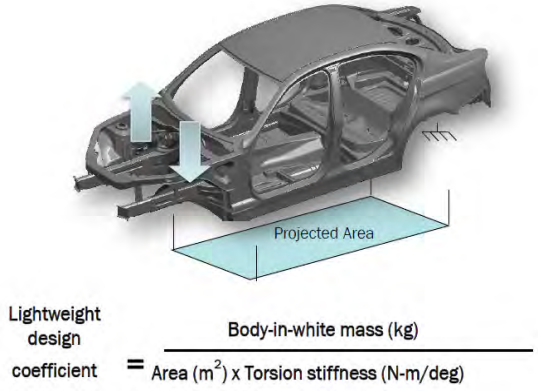

Figure 7.2.2.21 Lightweight design coefficient calculation

A low value of lightweight design coefficient demonstrates a “lightweight” design, where a low body structure weight, combined with high stiffness achieves a low value. Figure

7.2.2.22 shows the calculated lightweight design coefficient for Steel E-Motive compared to a number of current production passenger car body structures. Although the body structure design of Steel E-Motive is different to a conventional passenger car body structure, a comparison of the lightweight design coefficient provides a useful insight into performance of the structure. The comparison shows that the Steel E-Motive BIW achieves a very low value of lightweight design coefficient value of 1.87. The vehicles in the comparison are ICE 2010 to 2018 model year. Despite the difference in age and vehicle type, this still demonstrates that the Steel E-Motive concept is lightweight and high stiffness design.

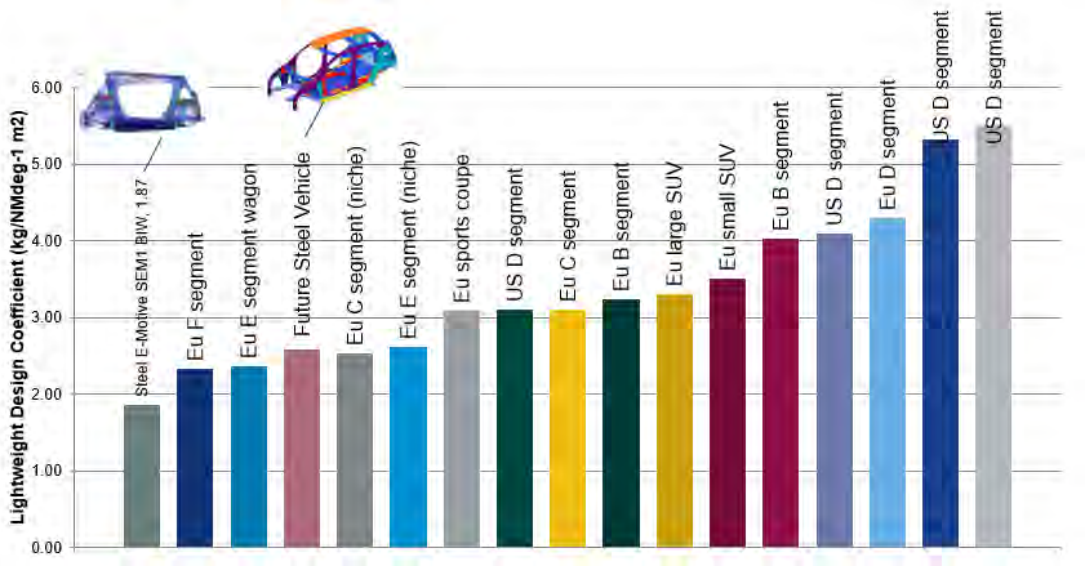

Figure 7.2.2.22 Comparison of lightweight design coefficient

Static vertical bending stiffness

As per the static torsional stiffness loadcases, vertical bending stiffness ensures the body achieves appropriate levels of quality as a result of vertical loads applied within the vehicle (such as passengers and luggage). The Steel E-Motive body structure comfortably achieves the vertical stiffness target and also demonstrate uniform stiffness throughout, as shown in Figure 7.2.2.23

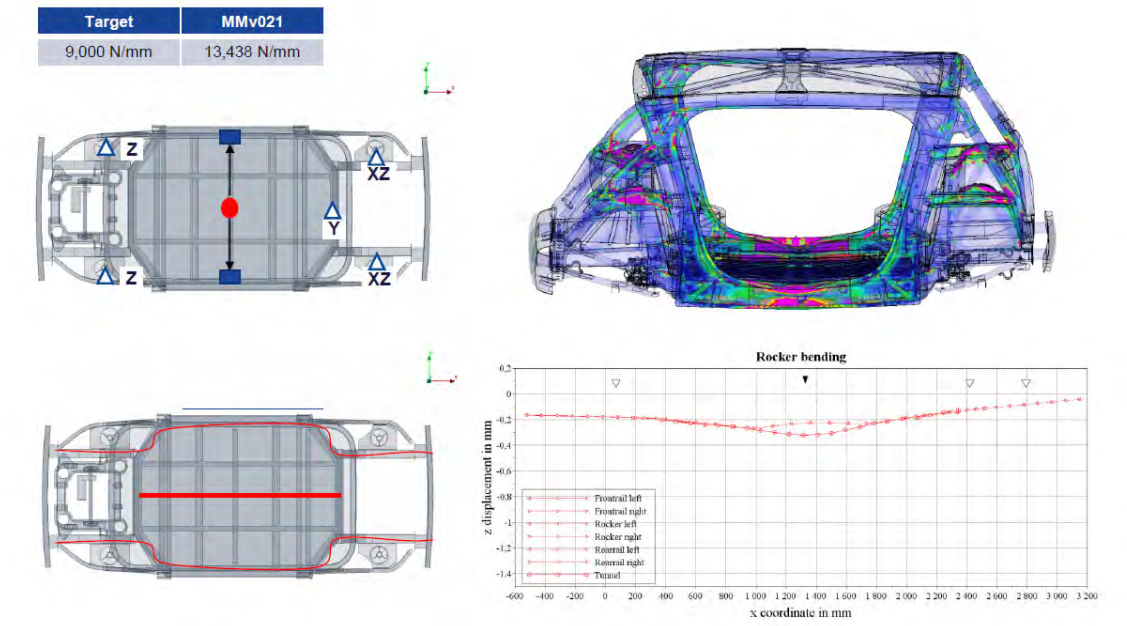

Figure 7.2.2.23 Steel E-Motive body structure static vertical stiffness performance

NVH performance

Noise, Vibration and Harshness (NVH) is an important attribute for achieving good passenger comfort performance. Unwanted and unacceptable levels of noise as a result of road/tyre, wind/aerodynamic and powertrain/motor noise can be a source of annoyance to passengers. Similarly, high levels of vibration in a vehicle can lead to passenger discomfort. Harshness defines the characteristics and interaction of noise and vibration. The Steel E-Motive vehicle has been engineered to achieve competitive levels NVH performance with specific focus on the body structure attributes. Low frequency vibration of the vehicle and body structure (i.e. <50Hz) needs to be addressed in passenger cars due to the mechanics of human response and sensitivity. Many of the vibration excitation sources and system modal frequencies such as the primary vehicle rigid body modes (bounce, pitch, yaw), wheel hop modes, powertrain rigid body modes and body structure modes occur in a similar frequency band, and where coupling of excitation and modes occur can lead to resonances and high vibration amplitudes. To mitigate the risk of modal coupling, a *modal mapping* approach was taken to ensure that the primary excitation and response modes were sufficiently decoupled and acceptable levels of vibration and passenger comfort were achieved. Figure 7.2.2.24 shows the modal map table for the SEM1 vehicle. The x axis defines the modal frequencies and the vertical columns describe the primary excitation sources and the major subsystem modal frequencies. Targets for the body structure modal frequencies were based on achieving sufficient separation from excitation and other system modes. The target for the first body structure mode was set at greater than 28Hz. Additionally, the relatively high weight of the battery may cause a floor heaving mode and induce high vibration amplitudes in the body structure if coupled with other modes. An additional target for the first battery structure mode was defined as greater than 35Hz in order to attenuate the risk of high vibration response. With a unique exterior shape and vehicle interior enabled by the autonomous nature of Steel E-Motive concept, the internal air cavity resonance mode may shift significantly resulting in low frequencies booming noise. This risk was mitigated by FEA calculations to predict the modal frequencies of the interior

air cavity. A target of greater than 40Hz was defined and the first air cavity mode predicted to be 67Hz.

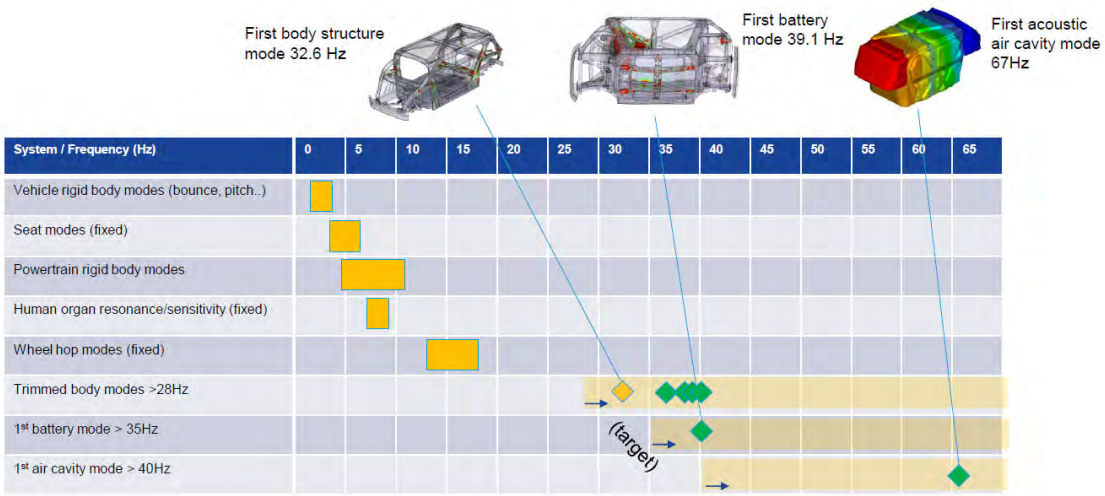

Figure 7.2.2.24 SEM1 Vehicle NVH modal map (See Appendix 4 for larger image)

Figure 7.2.2.25 shows the predicted first body structure mode and strain energy at 32.6Hz

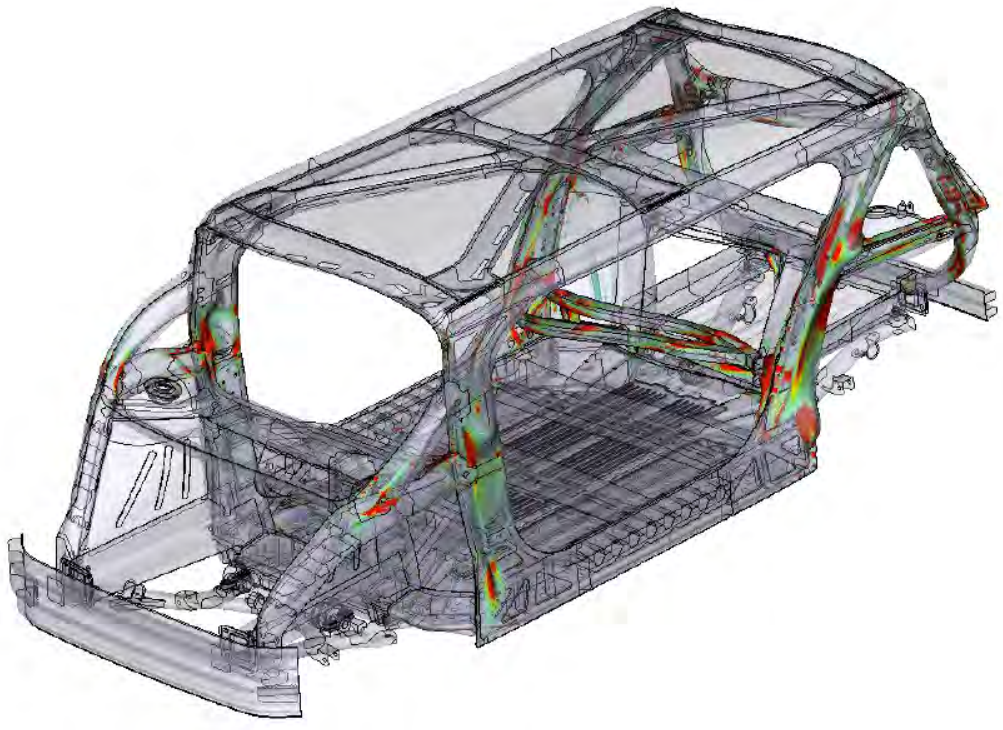

Figure 7.2.2.25 First body structure mode 32.6Hz (versus >28Hz target)

Typically for an automotive passenger car, the first mode shape of the body structure is a twisting or torsion type mode. With Steel E-Motive being a unique shape and construction, a lateral “lozenging” mode shape is observed. The mode shape and strain energy distribution demonstrates a very stiff lower body structure, achieved by the integrated battery structure, subframes, bottom cover, rocker section and floor design. The highest strain energy and compliance is observed in the A and C pillars. The frequency of the first body mode was increased to above the 28Hz target by the introduction of small internal reinforcements (bulkheads) to the A and C pillars as well as structural adhesive applied on the weld flanges.

The first battery mode shape is shown in Figure 7.2.2.26. The mode shape also includes a component of the front roof vertical mode. The displaced shape and strain energy distribution highlights that the battery carrier frame and lateral frame longitudinals and floor cross members contribute to the modeshape and frequency. Specific design and engineering focus was applied to these parts to ensure the first modal frequency of the installed battery structure was above the 35Hz target. Figure 7.2.2.X shows the final design of the battery frame longitudinals and cross members.

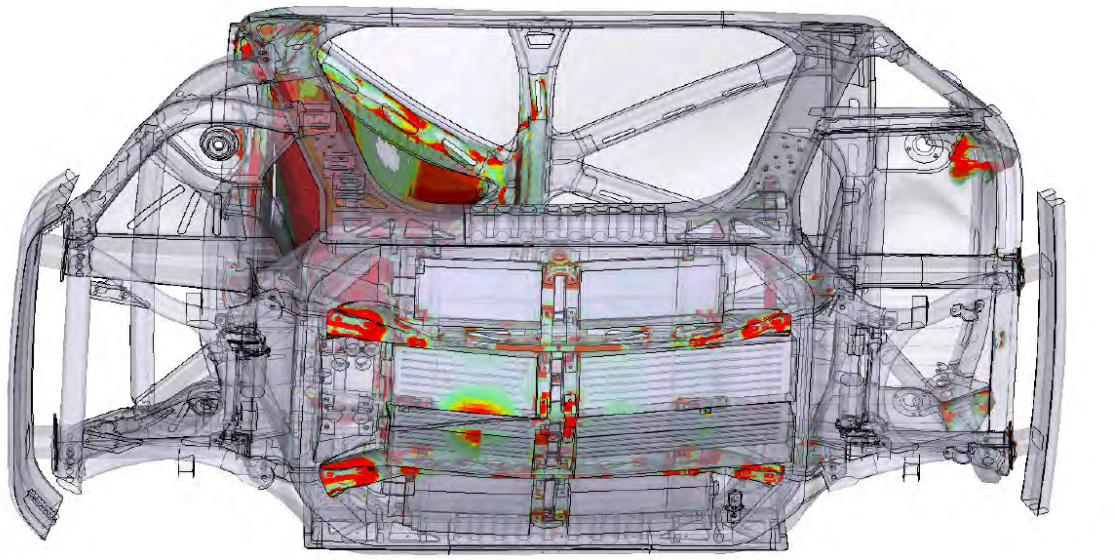

Figure 7.2.2.26 Battery structure first mode (39.1Hz versus >35Hz target)

Figure 7.2.2.27 shows the final design of the battery frame longitudinals and cross members. The longitudinals are a single piece cold stamping using DP450, which with a typical elongation of 25% enable the deep draw section (the width of the longitudinals is driven by the space allocation of the battery modules (not shown)). The single piece cold stamping removes any joins or welds in the parts, improving overall stiffness. Laser cut-outs are added to the longitudinals in specific locations to provide some weight reduction, whilst not compromising stiffness in the critical direction. The lateral cross members consist of top hat cross section profiles and roll stamped (upper) and roll formed (lower) parts. The battery frame cross members are bolted to the body structure floor cross members through fixings as shown in Figure 7.2.1.6. The combined design approach and integration approach delivers a first battery mode that meets the >35Hz target requirement.

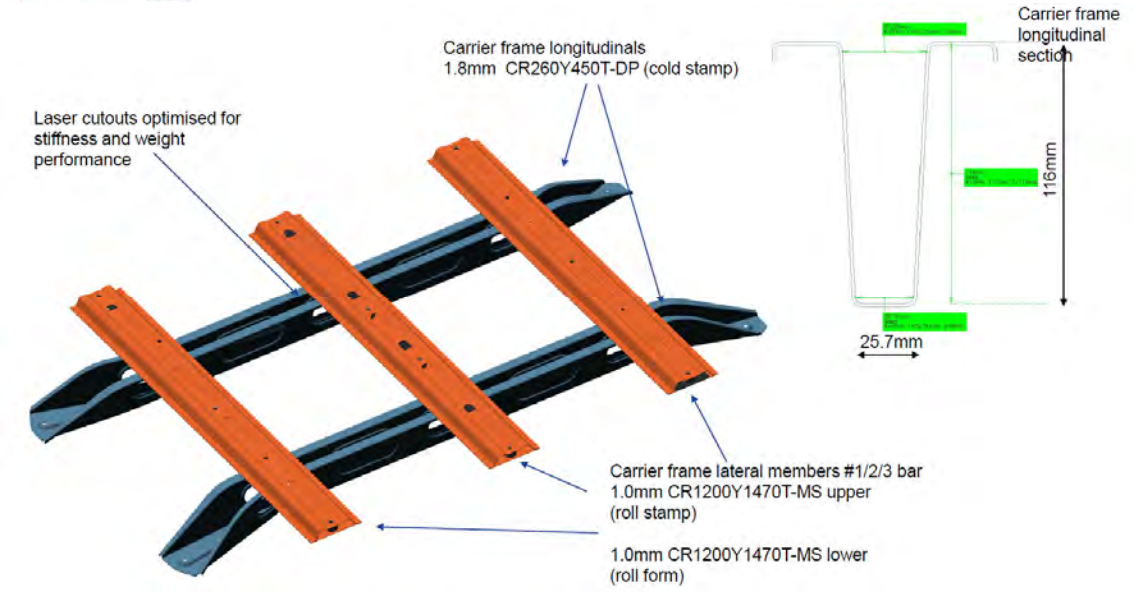

Figure 7.2.2.27 battery carrier frame structural members

Driving Point Inertance/Local Dynamics Stiffness

In addition to the modal mapping approach, the higher frequency structural response (50Hz to 250Hz) of the body structure was assessed and developed for Local Dynamic Stiffness (LDS). LDS is a measure of a key body attachment point dynamic stiffness to a unit dynamic excitation. It is a key factor in the design of body isolation systems and NVH performance for the chassis, body and powertrain systems. For an isolation system to function properly, the body structural dynamic stiffness should be at least 5 times the bushing dynamic stiffness with optimum performance achieved with 10 times stiffness. Suspension bushings are typically rubber or polymeric compounds with their stiffnesses tuned in specific directions for static and dynamic compliance requirements such as vehicle handling and powertrain primary modes. The target for the body side LDS performance is therefore dependant on the bushing isolation stiffness. As the primary focus of the Steel E-Motive programme was the development of the body structure, the design of the chassis system was not considered in detail, therefore the static and dynamic bushing stiffnesses were estimated based on data from vehicles with comparable suspension types and vehicle sizes. The driving dynamics requirements and considerations are assumed to be less significant for a fully autonomous vehicle where there is no direct handling feedback to the occupants. Attributes such as ride comfort and road disturbance impact are however important for achieving good passenger comfort. The evaluation considered the chassis bushes for the *critical loading directions* – these being the primary directions of road loads. For the front suspension, these are the front damper strut top mounts and the lower arm rear bushing and for the rear suspension, the rear damper strut top and the lower arm front bushing. Figure 7.2.2.28 shows the locations of the LDS measurement points, the assumed static bushing stiffness, the predicted local dynamic stiffness (LDS) values from the trimmed BIW model and the calculated ratio of LDS to bushing static stiffness. The results demonstrate the target ratio of 5 times factor of dynamic structural stiffness to dynamic bushing stiffness was achieved and a with a minimum factor of 8 achieved for all locations. This demonstrates that the body structure has sufficient dynamic stiffness performance for the chassis isolation system to operate correctly.

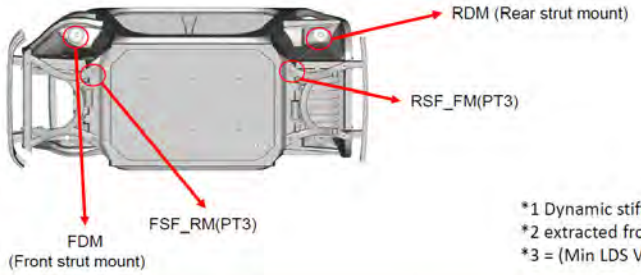

*1 Dynamic stiffness Target =5x(1.6xStatic mount stiffness)
*2 extracted from dynamic stiffness FEA
*3 = (Min LDS Value / Static mount stiffness)

Positon	Direction	Static mount stiffness [N/mm]	Dynamic stiffness Target [N/mm] (*1)	Min LDS value [N/mm] (*2)	Min LDS Frequency [Hz]	LDS/Static stiffness coefficient (*3)
FSF_RM(PT3) (front lower arm rear suspension bush)	X	690	>5,520	41,980	57	61
	Y	1000	>8,000	8,812	65	9
	Z	300	>2,400	11,010	53	37
RSF_FM(PT3) (rear lower arm front suspension bush)	X	690	>5,520	42,140	58	61
	Y	1000	>8,000	16,350	164	16
	Z	300	>2,400	6,571	57	22
FDM (front strut mount)	Local Z	600	>4,800	5,027	53	8
RDM (rear strut mount)	Local Z	600	>4,800	4,870	63	8

Figure 7.2.2.28 shows the predicted frequency dependant local dynamic stiffness curves for front strut mount in Z. Results for the all the attachment points are documented in Appendix 1 of this report.

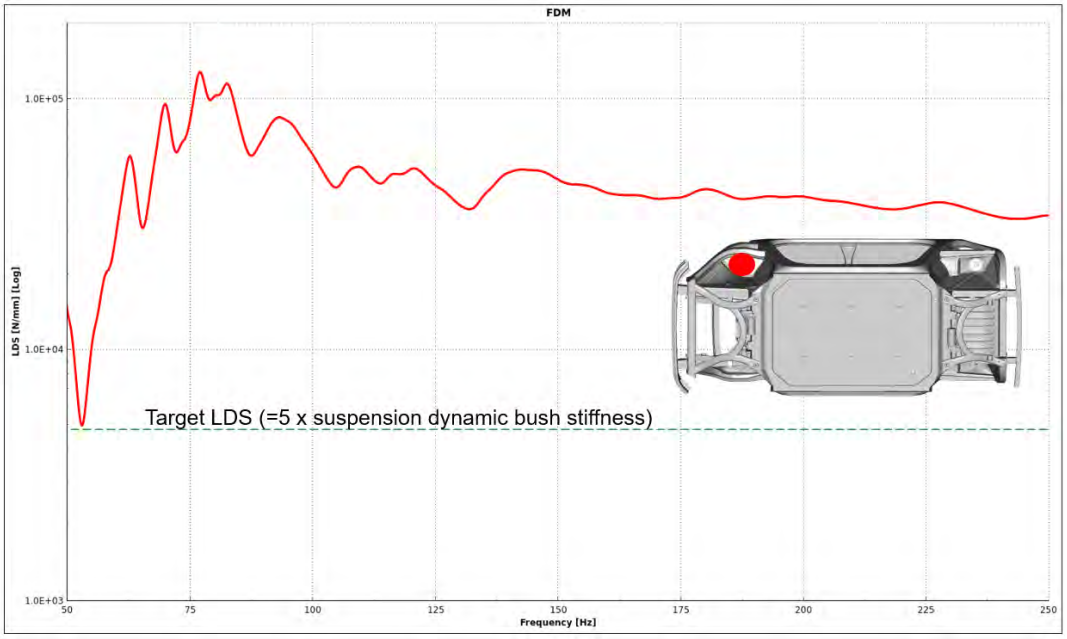

Figure 7.2.2.28 Local Dynamic Stiffness (LDS) of front damper strut top (trimmed BIW FE analysis)

7.2.3 Steel E-Motive body structure design approach and features for front crash performance

The front zone of the Steel E-Motive body structure was designed to serve the following functions:

- Safety: Management of high-speed front crash loads and provide protection to occupants and high voltage battery
- Management of road induced loads and loads and vibrations from the powertrain
- Contribute to local and global body stiffness (as described in Section 7.2.2)
- Provide mounting and support for subsystems such as electric drive unit, cooling pack, HV electronics, HVAC, exterior panels, and glazing
- Management of low-speed collisions (low speed collision and pedestrian protection is generally managed by the bumper plastic trim and was therefore not specifically considered within this project. For a 2035 model year launch it is anticipated that significant enhancements would be made in active and reactive safety systems for low speed and pedestrian protection)

The majority of the front zone design decisions and AHSS grade selections were based on the requirements for front crash performance. This section is therefore dedicated to describing the strategy and design approach for achieving front crash performance. Figure 7.2.3.1 shows the major components or subassemblies of the front crash structure.

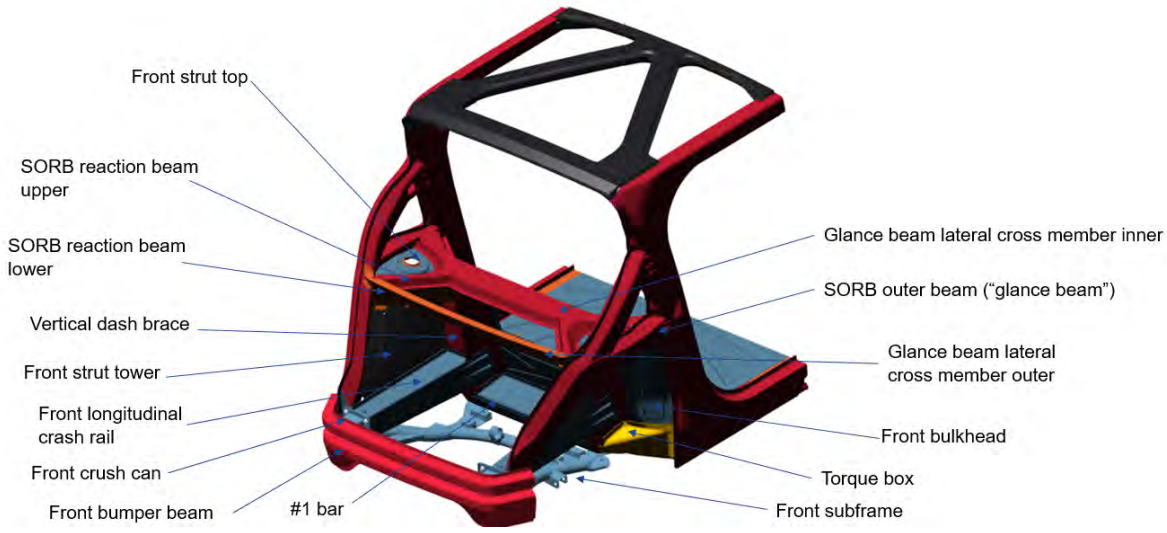

Figure 7.2.3.1 Primary subassemblies in SEM1 front crash structure (See Appendix 4 for larger image)

Table 4.2.3.1 describes the front crash loadcases and targets considered for the Steel E-Motive design. The main challenges and constraints when considering the development of the Steel E-Motive front crash structure are listed below:

- Compact vehicle size, short front overhang, short crush distance, challenging to manage crash loads. Challenging to balance FFB and SORB crash requirements

- The front occupants were positioned in a rear facing forward position, taking advantage of the fully autonomous functionality of the vehicle. This places them closer to the front crash impact zone, resulting in a greater challenge for their protection
- Electric Drive Unit (EDU) package in front compartment. The EDU is very stiff compared the surrounding body structure. In a front crash event, the EDU may “lock out”, resulting in high crash pulse (deceleration loads) and intrusion into the front bulkhead

Section 6.3.6 describes the strategy and approach taken for the Phase 1 development of the front crash structure. The development in Phase 2 focussed on refining and optimising the front crash structure and fine tuning of the AHSS grades and gauges to ensure that the crash targets were achieved, as well as other performance targets such as stiffness and weight. The strategy for the management of the front crash loads was carried over from Phase 1. For the USNCAP 56kph FFB and IIHS 64kph ODB tests the crash loads were managed primarily through the front longitudinal crash rails, providing a “crush zone” for the kinetic energy to be contained and converted to crush energy and the vertical dash braces, #1 bar and front bulkhead providing crush load reaction and preventing intrusion to the cabin. Figure 7.2.3.2 and 7.3.3.3 shows the front zone crush deformation behaviour throughout the stages of the USNCAP 56kph FFB loadcase. The deformation mode is comparable for the IIHS 64kph ODB test, with a single rail being the crushable element.

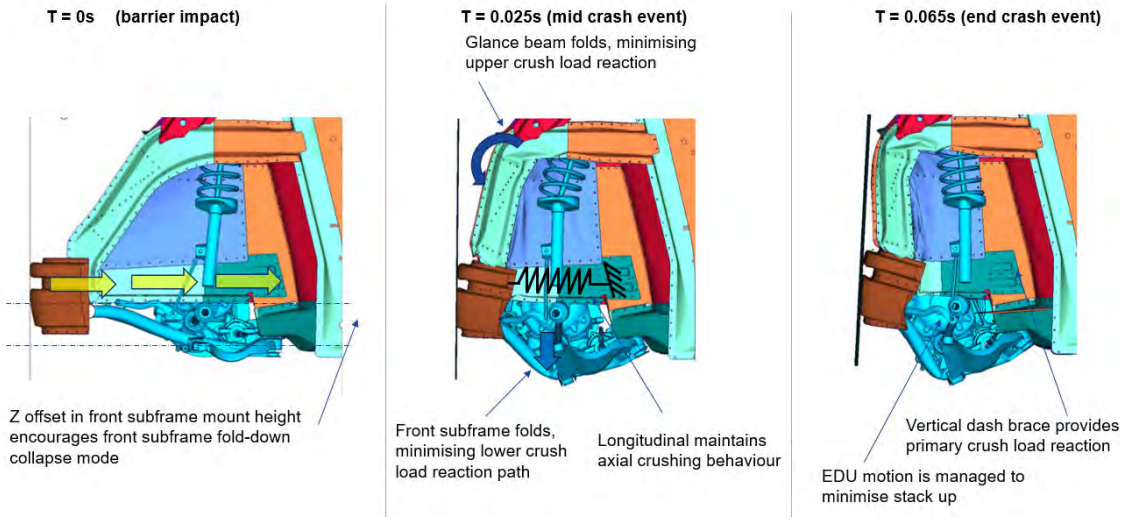

Figure 7.2.3.2 USNCAP 56kph FFB crash test. Vehicle CAE simulation showing the front crush zone deformation behaviour (some parts removed for clarity) (See Appendix 4 for larger image)

The front longitudinal crush rails are engineered to be the primary absorbing elements in the FFB and ODB tests. The rails are cold formed tailor welded blank Dual Phase grade.

The geometry and AHSS grade selection of the front subframe helps to promote a folding collapse mode which minimises longitudinal crush load reaction. The subframe collapse mode is mirrored by the glance outer beam, which also folds around a hinge point in the Z plane in line with the strut tops.

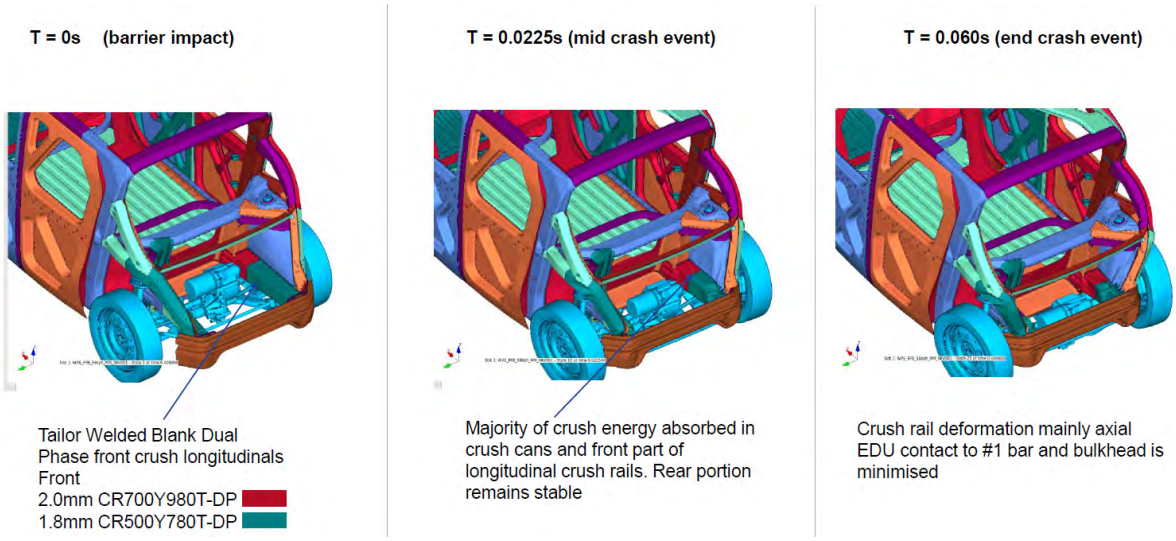

Figure 7.2.3.2b USNCAP 56kph FFB crash test. Vehicle CAE simulation showing the front crush zone deformation behaviour (some parts removed for clarity) (See Appendix 4 for larger image)

Figure 7.2.3.3 shows the vehicle deceleration profile for the USNCAP 56kph FFB loadcase. The peak (instantaneous) predicted pulse is 33.1g and average deceleration rate is 29.9g

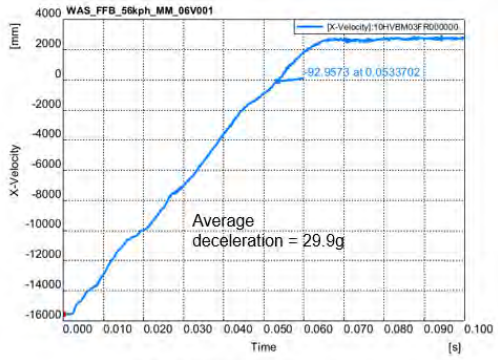

Vehicle velocity versus time

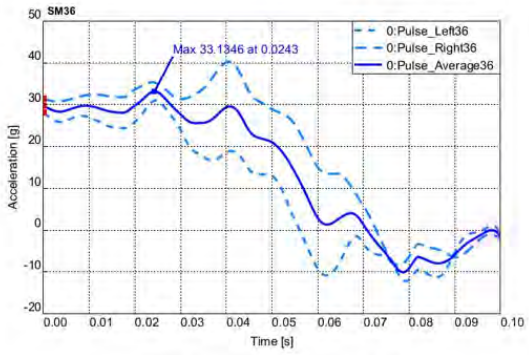

Vehicle acceleration versus time

Figure 7.2.3.3 USNCAP 56kph FFB, predicted vehicle pulse (measured at BIW floor equivalent B pillar position)

Figure 7.2.3.4 shows the predicted intrusion values at the front bulkhead, the maximum value being 2.4mm.

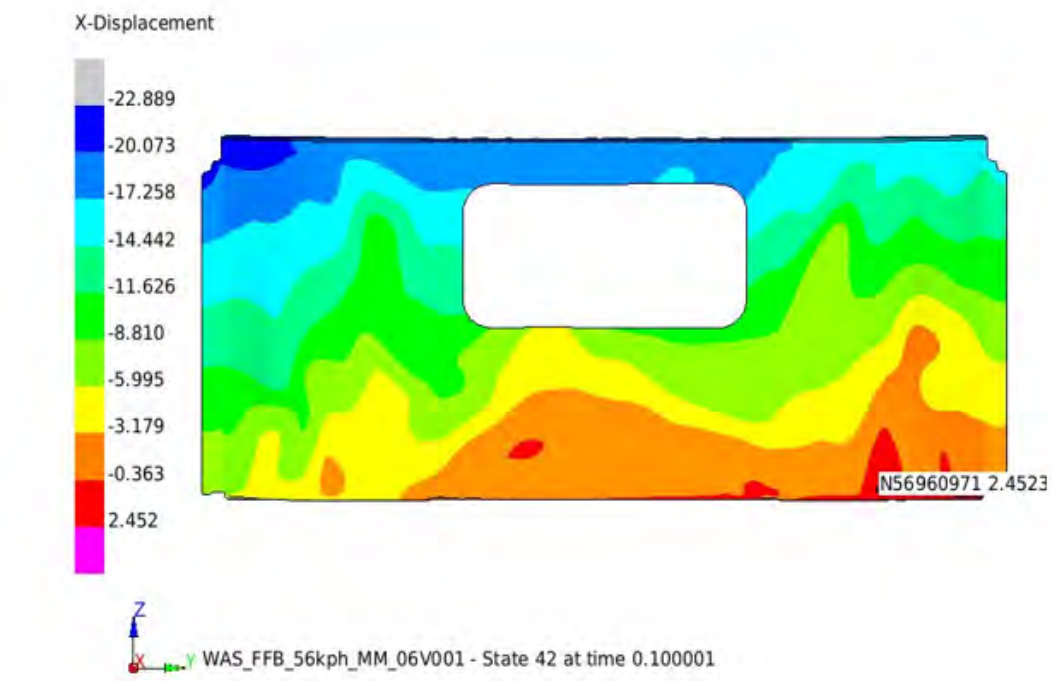

The peak pulse (33.1g) and maximum intrusion (2.4mm) are well within the target values of 35g and 40mm. This suggests that a “good” level of crash protection is provided to the occupants.

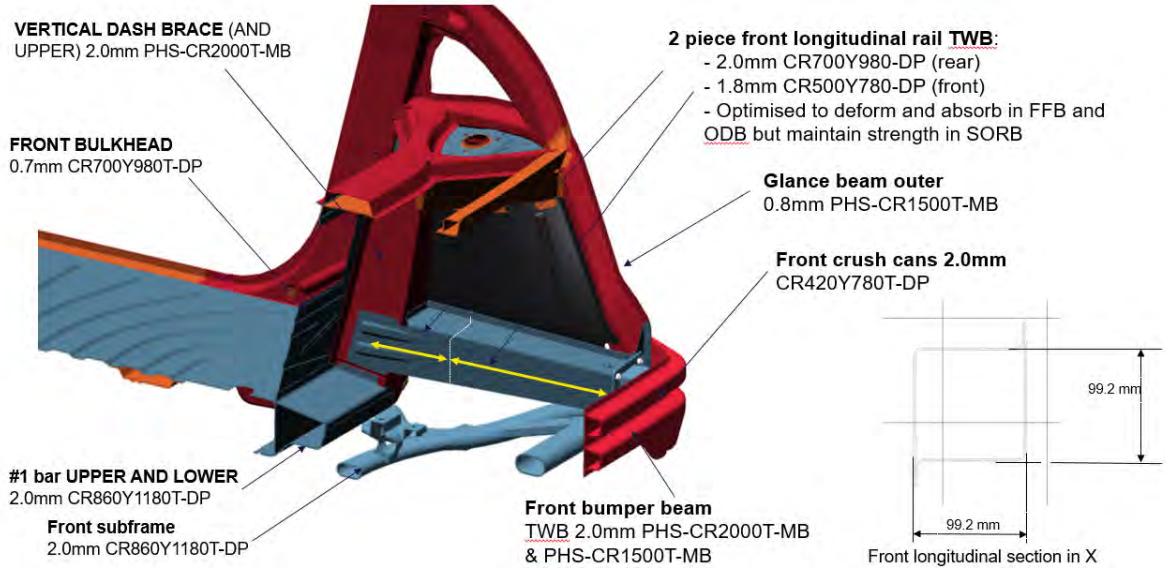

Figure 7.2.3.5 Front crash FFB and ODB key components and AHSS grades & gauges (See Appendix 4 for larger image)

The key elements of the USNCAP FFB and IIHS ODB front crash structure are shown in Figure 7.2.3.5. The front crash performance can be attributed to the combination of design

and AHSS grade selection. The front crush longitudinal rails are comprised of 2 cold stamped “L” profile sections, spot welded along the length. Each section is a Tailor Welded Blank (TWB) with the forward section being 1.8mm CR500Y780-DP and the rear section 2.0mm CR700Y980-DP. The forward section enables the axial crush and the higher strength and stiffer rear section maintains the rail integrity at the interface to the vertical dash brace. The TWB provides an efficient method of achieving different mechanical properties within a single stamped component. The 2 L sections form a closed box section, approximately 99mm square. The front subframe and glance beam outer are engineered to fold in the FFB and ODB crash loadcases as shown in Figure 7.2.3.2. The front subframe is 2.0mm CR860Y1180T-DP throughout and the glance beam outer is 0.8mm PHS-CR1500T-MB. The glance beam outer’s primary function is management of loads in IIHS SORB loadcase and is discussed in detail later. The front subframe gauge and grade provides the stiffness and strength required for chassis loads (durability) whilst enabling appropriate collapse in FFB and ODB. The front subframe construction also contributes to the IIHS SORB crash performance (discussed later). The front longitudinal rails join to the vertical dash brace which forms part of the occupant protection zone as shown in Figure 7.2.3.6. The function of the vertical dash brace is to provide load reaction to the longitudinal crush rails and minimise intrusion into the cabin. A high UTS is required for these parts and given the geometry/shape requirements 2.0mm PHS2000 grade was selected. The lower vertical dash brace provides some crash and body stiffness load transfer to the battery carrier frame longitudinals and is also 2.0mm PHS2000 grade. The lower vertical dash brace parts also house the mounting brackets for the front subframe rear mounting point. The two #1 bar lateral members consist of an upper and lower cold stamped CR860Y1180T-DP and provide intrusion protection to the propulsion battery and also contribute to global body stiffness. The torque box provides some crash load reaction and also body stiffness contribution. These are cold stamped in a 3rd generation AHSS, a high-formability dual phase (DH) grade enables a 1180MPa UTS and up to 10% total elongation allows the subassembly to be made from two parts per side. The front bulkhead provides the final element of the crash intrusion prevention structure and being a large panel with high weight sensitivity and high strength requirement is made from 0.7mm CR700T980T-DP grade.

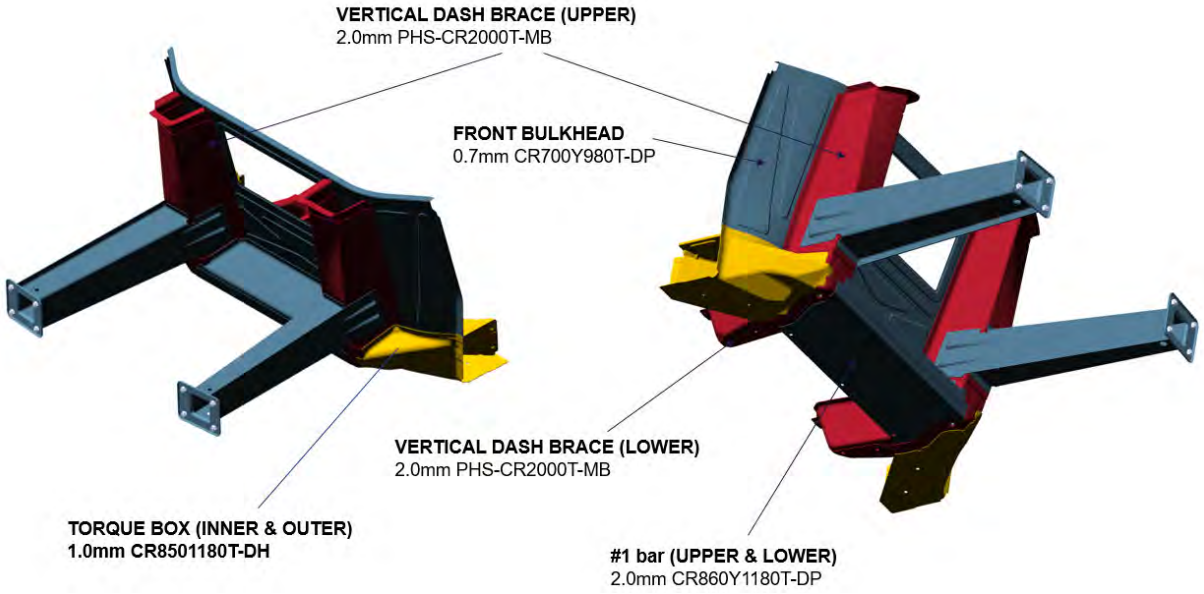

Figure 7.2.3.6 Front crash structure, components and AHSS grades contributing to intrusion prevention

To summarise, the Steel E-Motive front crash performance for the USNCAP 56kph FFB and IIHS 64kph ODB tests can be attributed to the following body structure design features:

- Box section profile longitudinal crush members. AHSS TWB with 1.8mm DP780 and 2.0mm DP980 enabling the progressive and controlled crush behaviour
- Front subframe and glance beam outer structures engineered to fold in FFB test. This enables the longitudinal to crush in a primary axial direction, maximising the crush efficiency and enabling a steady deceleration rate during the crash event. Whilst these components fold in the FFB and ODB loadcases and enable the crush longitudinal to work effectively, the components behave differently in the IIHS SORB loadcase where high lateral load reaction is required to achieve glance off
- Crash load reaction and intrusion members. The PHS2000 vertical dash brace, DP1180 #1 bar, DP980 front bulkhead and DH1180 torque box combine to manage the crash loads and minimise intrusion levels to the cabin

The Steel E-Motive vehicle is also engineered for the IIHS 64kph Small Overlap Rigid Barrier (SORB). This is a challenging test due to the high vehicle impact speed, rigid barrier type and the initial frontal impact overlap of 25%. The approach and strategy for managing the test was devised in the earlier phases of the project and applied to the final concept in Phase 2 (Section 6.3.6). The “glance off” strategy was adopted in order to reduce the conversion of moving vehicle kinetic to crush energy and minimise the resultant deceleration pulse and intrusion levels. Figure 7.2.3.7 to Figure 7.2.3.9 show the key stages of the SORB crash event and the design approach for how the glance off was achieved. The crash event can be broken down into the 3 stages: Stage 1 initial impact with the SORB barrier, Stage 2 mid impact, Stage 3 final stage. As discussed in Section 6.3.6, the strategy for achieving glance off in the Steel E-Motive concept was to initiate and maintain sufficient vehicle lateral acceleration during the SORB crash event such that the vehicle lateral displacement was sufficient for the vehicle to be deflected from the barrier. The high lateral acceleration was achieved by developing an AHSS front crash structure that provides sufficient lateral force reaction with the SORB barrier. This requirement for lateral force reaction ability (or strength) conflicts with the USNCAP FFB and IIHS ODB requirements for absorption or crush longitudinally. The careful design and AHSS grade assignment of the front crash structure enabled both requirements to be met.

IIHS 64kph SORB crash event Stage 1

View from underneath (body structure shown for clarity)
Prior to barrier impact

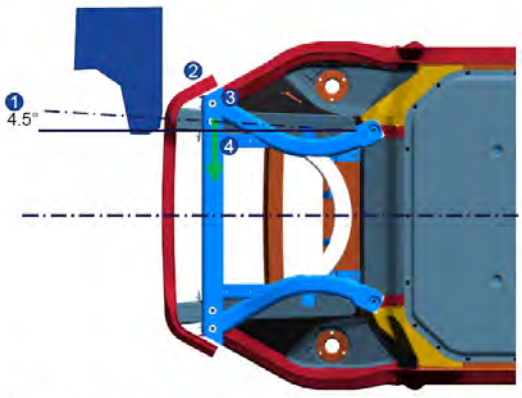

Crash simulation

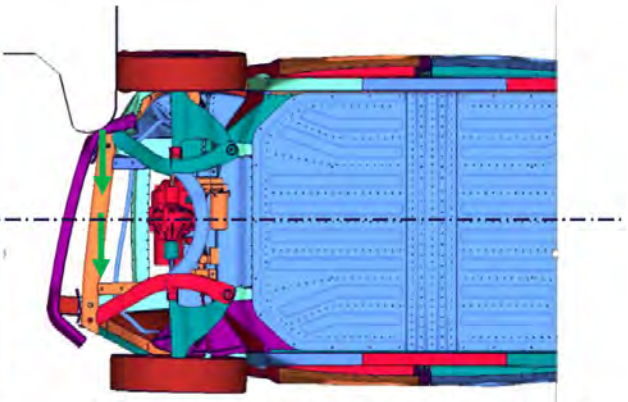

1. Longitudinal crash rail plan view angle 4.5 degrees to align with SORB barrier
2. Front bumper beam outer face is angled to enable swift engagement with front subframe after impact
3. Front subframe rigidly bolted to longitudinal and SORB outer beam
4. Front subframe lateral member provides lateral loadpath

Shortly after barrier impact, features 1,2,3 & 4 combine to provide high strength and load reaction in the lateral direction. This initiates lateral acceleration of the vehicle (i.e. glance off)

Figure 7.2.3.7 IIHS 64kph SORB crash loadcase, impact Stage 1. Design features and crash simulation results.

The initial impact stage (1) of the IIHS SORB crash event is critical for initiating lateral acceleration and deflection from the barrier. The Steel E-Motive front crash structure employs a number of features to achieve this. Firstly, the longitudinal crash rail has a plan view angle of 4.5 degrees. A number of crash simulation iterations were performed to determine the optimum angle of the rail. Angling the rail greater than 4.5 degrees resulted in significant initial crush and collapse of the rail, resulting in the front body structure not being able to withstand the barrier loads through the later stages of the crash event. With an angle of less the 4.5 degrees, the vehicle was observed to “skid” along the longitudinal rail. The front bumper beam profile was angled (in plan view) to align with the shape of the SORB barrier. During initial impact, the front bumper beam deforms slightly and contacts the front subframe, whilst still maintaining contact with the SORB barrier. With the subframe rigidly bolted to the BIW, this provides a direct lateral loadpath from the SORB to the front subframe and body structure. A lateral cross member is positioned at the front of the front subframe to provide a loadpath from the impact side of the vehicle to the non-impact side (left to right in the case of the example shown). Despite the high magnitudes of forces generated, the design features and AHSS properties provide sufficient strength and structural integrity react the SORB barrier loads and initial lateral acceleration of the vehicle.

As the SORB crash event progresses, it is important to maintain the structural integrity of the front crash structure, particularly in the lateral direction. The features shown in Figure 7.2.3.8 show how this was achieved in the Steel E-Motive concept.

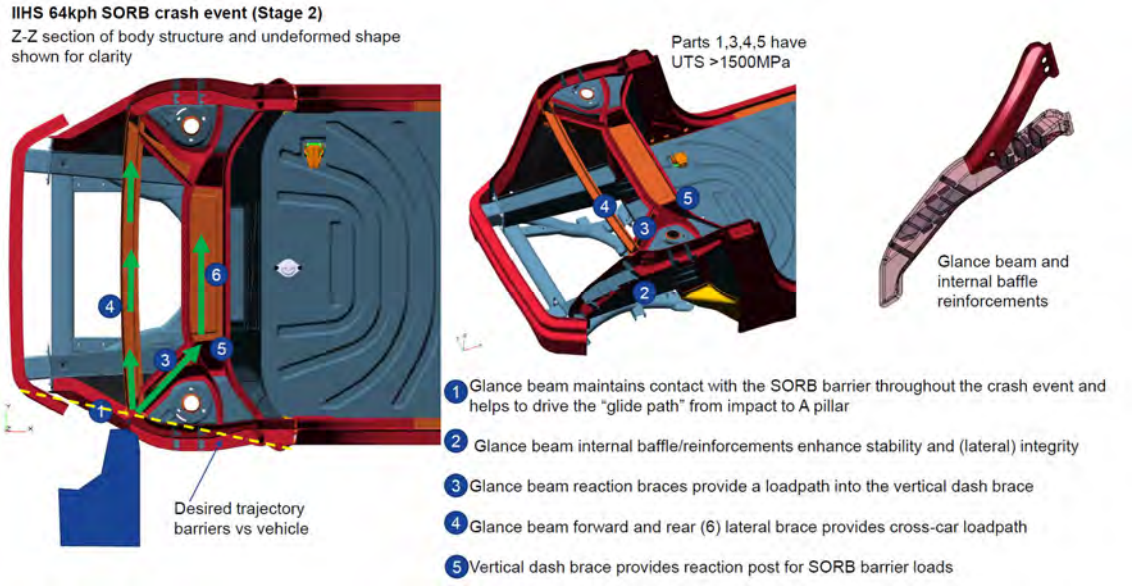

Figure 7.2.3.8 IIHS 64kph SORB front crash. Stage 2 of the crash event, showing the key elements of the body structure that enable and maintain the glance off

The glance beam is a fundamental component in the SORB crash event. It’s geometry approximates the desired trajectory of the barrier to vehicle contact point, starting at the outer face of the longitudinal crush rails and ending by A pillar. The specific plan view profile was optimised to ensure the vehicle glides along the barrier throughout the crash event. Despite the very high loads experienced by the direct contact to the SORB barrier the PHS1500MPa UTS AHSS grade ensures the glance beam largely remains intact and is able to distribute the crash loads to the glance reaction and lateral beams. The DP780 MPa

internal baffles have been optimised to provide additional support and reinforcement to the glance beam section in the lateral direction whilst allowing the beam to fold and collapse in the USNCAP 56kph FFB and IIHS 64kph ODB tests. The glance beam reaction and forward lateral beams (parts 3 and 4 shown in Figure 7.2.3.8) provide loadpaths cross-car and into the vertical dash brace (5). The front damper strut cross members (5) provide an additional cross-car loadpath.

Figure 7.2.3.9 shows the crash simulation results at Stage 2 of the crash event (37ms). The results show that the front crash rail structural integrity is generally maintained. Whilst the glance beam undergoes significant collapse and deformation, it maintains its ability to provide a loadpath to the glance lateral and reaction beams. These structures and loadpaths combine to ensure that the vehicle continues lateral acceleration and deflection from the SORB barrier. An important feature of the SORB glance strategy is to purposefully engineer the front wheel on the struck side to detach during the event. If the front wheel remains within the wheel well, it can provide a loadpath from the SORB barrier to the rocker and this can induce a pivot or hinging effect and limit the lateral deflection of the vehicle from the barrier. Crash simulations confirmed this behaviour.

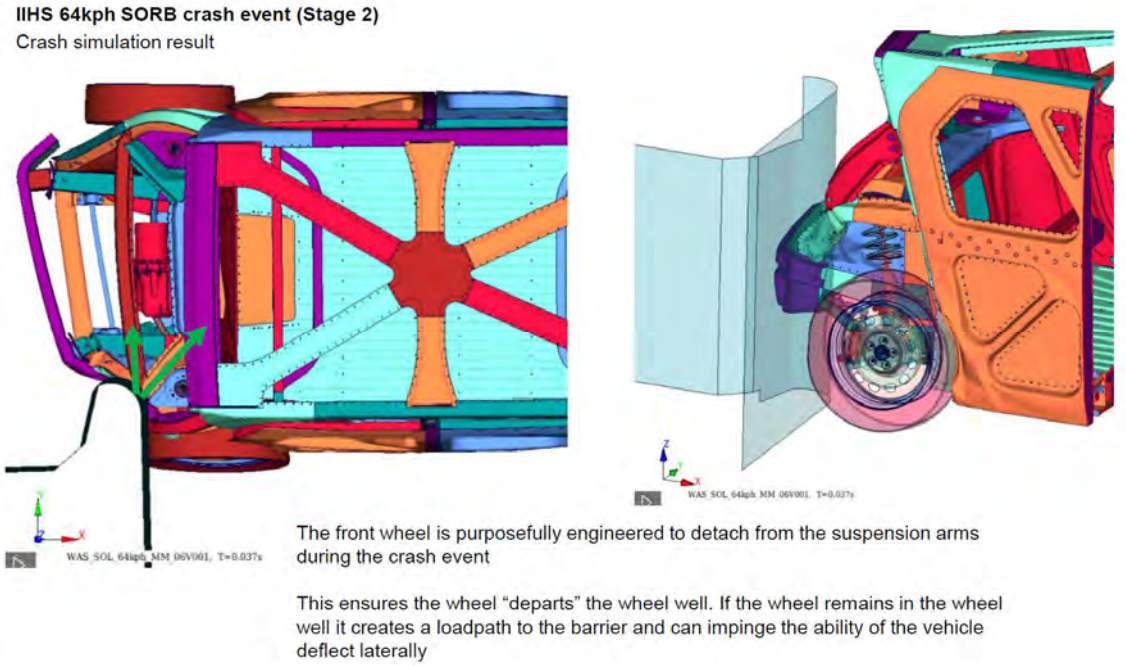

Figure 7.2.3.9 IIHS 64kph SORB crash simulation at 37ms (Stage 2)

Stage 3, the final step in the SORB crash event relies on structure around the front damper strut mounts and A pillar to provide loadpaths. It is important to maintain the lateral glance movement of the vehicle in this stage of the crash event as the vehicle can easily "snag" on the A pillar. Figure 7.2.3.10 shows the key parts of the body structure that contribute the SORB crash event in Stage 3.

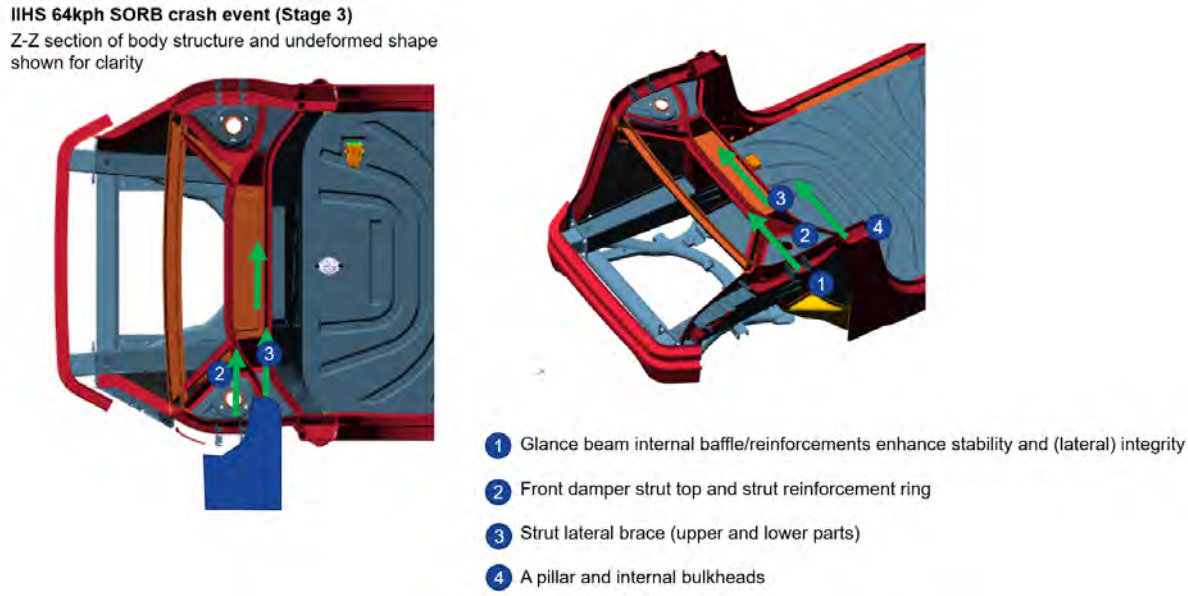

Figure 7.2.3.10 IIHS 64kph SORB front crash. Stage 3 of the crash event, showing the key elements of the body structure that enable and maintain the glance off

To maintain a lateral loadpath in the structure, further bulkhead reinforcements are placed inside the glance beam (1), in line with the front strut top mounts. The front strut top mounts (2) feature a DP1180 main panel (1.8mm) and a MS1470 strut reinforcement ring (2.0mm). This arrangement also provides good stiffness and durability performance. An integrated strut top lateral brace (3) consisting of upper (1.0mm PHS2000) and lower closing plate (1.0mm MS1470) completes the lateral loadpath. The A pillar provides the final component in the SORB event. By applying PHS2000 AHSS in 1.2mm for the inner and outer parts and using internal bulkheads or reinforcements in specific locations helps to maintain the integrity of the structure and the glance motion of the vehicle relative to the SORB barrier. The A pillar outer forms part of the door ring outer panel which is a Tailor Welded Blank and is critical for side crash protection (discussed later).

Figure 7.2.3.11 shows the crash simulation results for Stage 3 of the SORB crash event. The results show that the SORB barrier is close to the outer side of the vehicle, indicating that the vehicle is well on course to achieve a full glance off. Whilst the glance beam has undergone significant deformation, it maintains sufficient integrity to provide a loadpath to the strut mounts and lateral strut brace. The front wheel has completely detached from the chassis and is outboard of the wheel well. Despite some contact with the door outer skin, the wheel does not impact the vehicle glance behaviour.

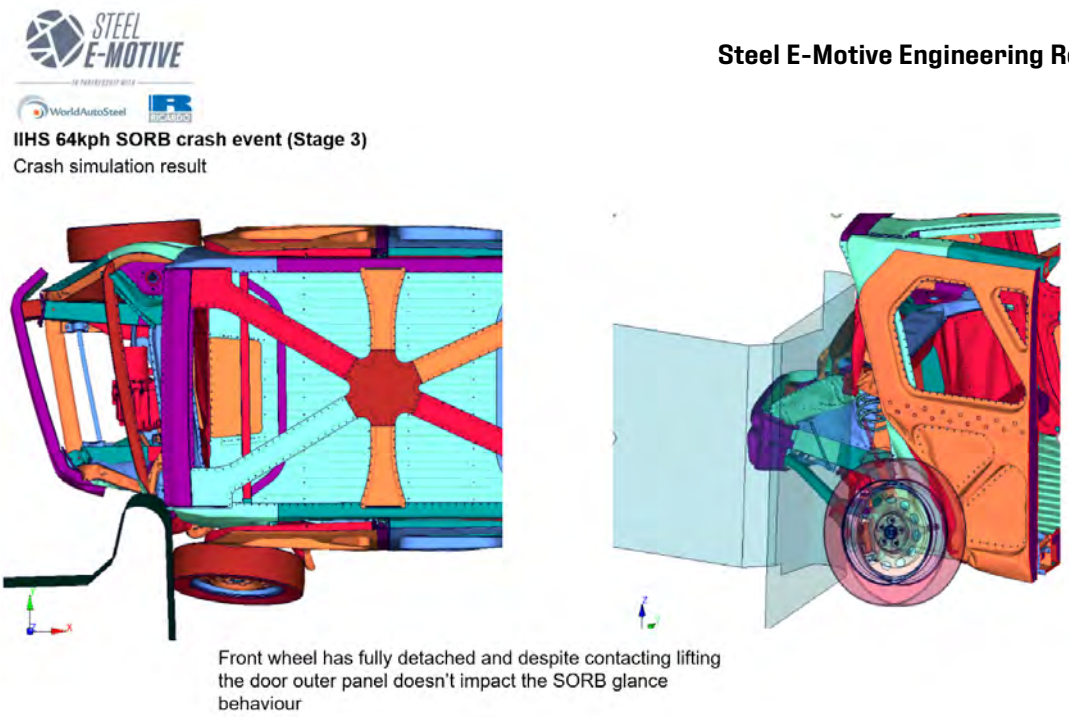

Figure 7.2.3.11 IIHS 64kph SORB crash simulation at 37ms (Stage 3)

The very high strength AHSS grades in this region do not impact the USNCAP 56kph FFB and IIHS 64kph ODB crash performance as they are outside (or rearwards) of the body structure crush zone. They also form part of the intrusion prevention zone or safety cell, providing protection for the vehicle occupants and battery.

The design approach and AHSS grade selection combine to produce impressive crashworthiness performance for the IIHS SORB loadcase, enabled by a vehicle full glance off from the barrier. Figure 7.2.3.12 shows the total lateral displacement of the vehicle over the duration of the SORB impact and the approximate alignment of the crash event Stages 1,2 and 3.

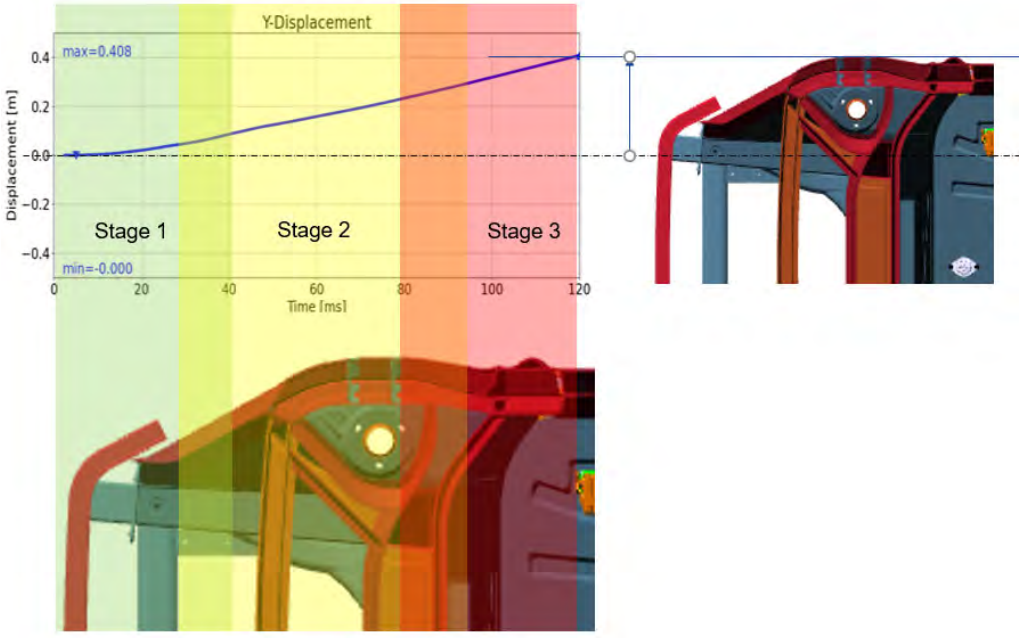

Figure 7.2.3.12 Vehicle lateral displacement vs time during SORB impact and the approximate alignment of the crash event Stages 1,2 and 3.

Figure 7.2.3.12 shows the predicted intrusion levels and deceleration pulse from the crash simulation. The maximum intrusion levels fall within the IIHS “good” rating scale. A maximum vehicle crash pulse of 19.9g was predicted versus the 35g target.

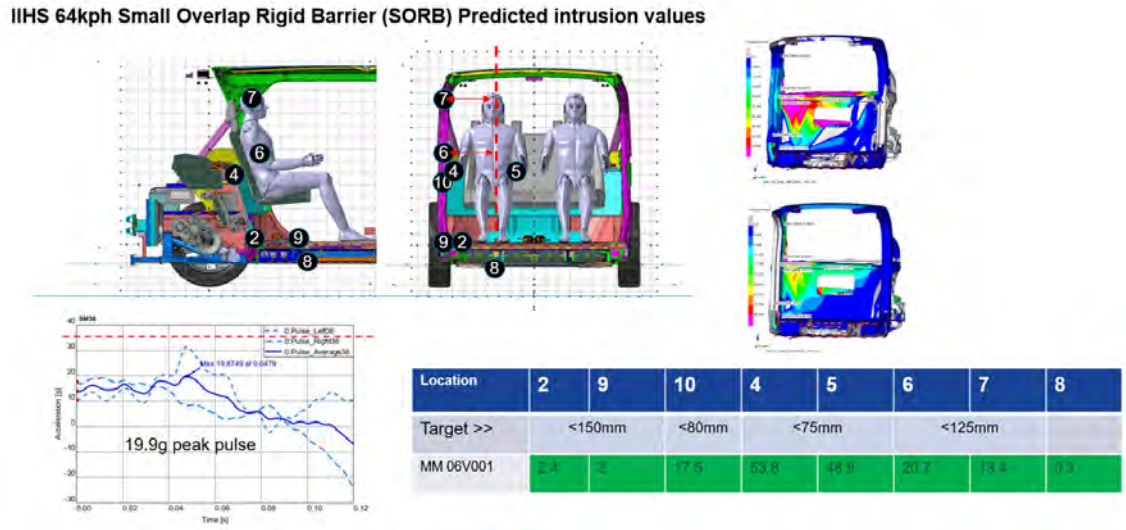

Figure 7.2.3.12 IIHS 64kph SORB vehicle crash simulation results. Predicted vehicle pulse and intrusion values.

The predicted intrusion levels are below the threshold for attaining the IIHS “good” rating. (note, this is the highest safety rating for the SORB test that can be achieved). The IIHS provide access to measured crash test result data for vehicles that have undergone testing within their facilities. Some of this data was extracted, processed and compared with the Steel E-Motive crash simulations results in order to further quantify and validate the performance. Figure 7.2.3.13 shows a graph comparing measured upper dash intrusion values (Y axis, cm) and vehicle pulse (X axis, g) for a sample of 8 current production vehicles, 4 vehicles having Internal Combustion Engines (ICE) and 4 Battery Electric Vehicles (BEVs). All vehicles are D segment sized sedan or Sport Utility Vehicles. During the SORB crash test, the vehicles were observed to either “glance” (or deflect/bounce) from the barrier or “snag”. (“Snag” meaning that the vehicle is fully decelerated by the impact, usually by the time the impact reaches the A pillar. Any remaining vehicle kinetic energy is then converted to vehicle rotation or yaw motion around a point at the A pillar). The results show that that 4 vehicles that have an observed “snag” crash behaviour tend to have higher upper dash intrusion and higher vehicle pulse levels than the “glance” behaviour vehicles. A lower crash deceleration pulse usually results in lower forces acting on the vehicle occupants and lower intrusion levels generally result in lower risk or magnitude of vehicle to occupant contact forces (the Safety Restraint System (seat belt and air bags) also have a significant influence on the forces witnessed by occupants and the subsequent injury levels). Lower intrusion and pulse values are observed in the “glance” vehicles as they maintain a greater forward velocity after the impact with the barrier, hence the deceleration rate is lower, resulting in lower forces and energy levels observed during the impact with the barrier. It should be noted that all 8 vehicles in the data sample achieve the IIHS “good” rating for the SORB test. The predicted results from the SEM1 vehicle crash simulation are plotted on the same graph and show that the vehicle deceleration pulse is comparable to those of the “glance” vehicles. The predicted SEM1 upper dash intrusion values are slightly higher than

the sample vehicles. This may be because SEM1 is a smaller vehicle than the comparative vehicles, having a lower crush length and dash panel closer to the frontal crush zone.

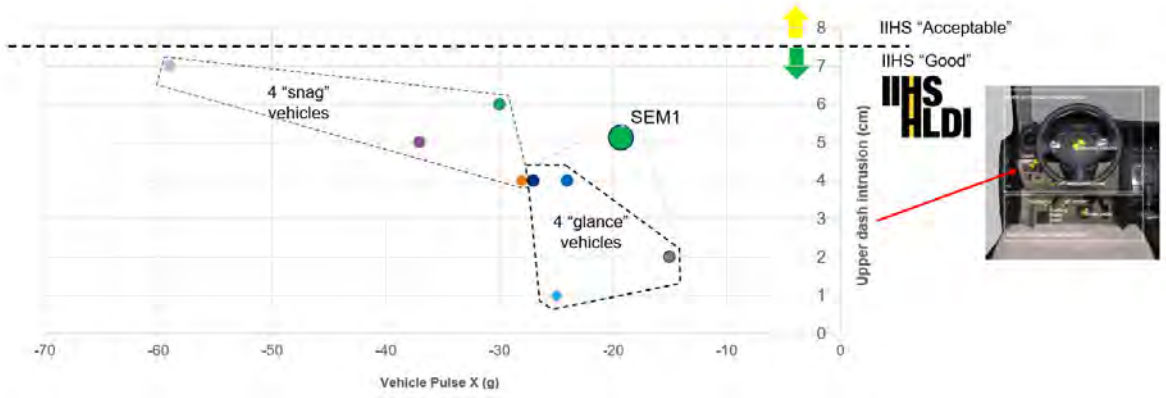

Figure 7.2.3.13 IIHS 64kph SORB crash test. Comparison of measured upper dash intrusion vs vehicle X pulse for sample of 8 vehicles. Data courtesy of https://www.iihs.org/

Figure 7.2.3.14 shows measured data for the same sample of vehicles, comparing vehicle frontal crash dummy Head Injury Criteria (HIC15), (X) and Vehicle deceleration pulse (Y axis, g). HIC15 is a measure of the likelihood and severity of head injury arising from an impact. The assessment is based on the magnitude and duration of acceleration experience by occupant (or crash test dummy) head in an impact. A lower HIC15 value suggests a lower risk and severity of head injury. A HIC15 value lower than 560 is required for vehicles to obtain the IIHS "good" safety rating. The Steel E-Motive programme did not consider crash dummy models in the vehicle simulations therefore no HIC data was calculated. Figure 7.2.3.14 shows a reasonable correlation between measured HIC15 values and vehicle deceleration pulse, with lower HIC15 values correlating to lower vehicle pulse levels. The 4 "glance" vehicles showed generally lower pulse and HIC15 levels than the 4 "snag" vehicles. Again, this can be attributed to the glance behaviour resulting in reduced vehicle velocity change during the impact event. With the Steel E-Motive vehicle achieving a predicted peak pulse of 19.9g, it could be expected that the resultant HIC15 values would be of a similar magnitude as the "glance" vehicles. This would be subject to the design and implementation of a suitable Safety Restraint System. Additionally, the different orientation of the front occupants in SEM1 should be considered when attempting occupant injury and safety assessments in SEM1. The front occupants are rearward facing, therefore the forces acting on the occupants will be different in location and magnitude to a conventional forward facing seating configuration. In a rear facing seat, the main deceleration loads acting on the occupants in a frontal crash event will be via the seat back. This has the potential to reduce loads on the occupant thorax, legs and arms but there is an increased risk of neck injury or whiplash if the head is not properly supported with a suitably designed headrest. For a taxi vehicle, with frequent changes in occupant size, seating technologies such as adaptive headrests may be required in order to ensure occupants are safely positioned in the vehicle and the risks of injuries due to collisions are minimised.

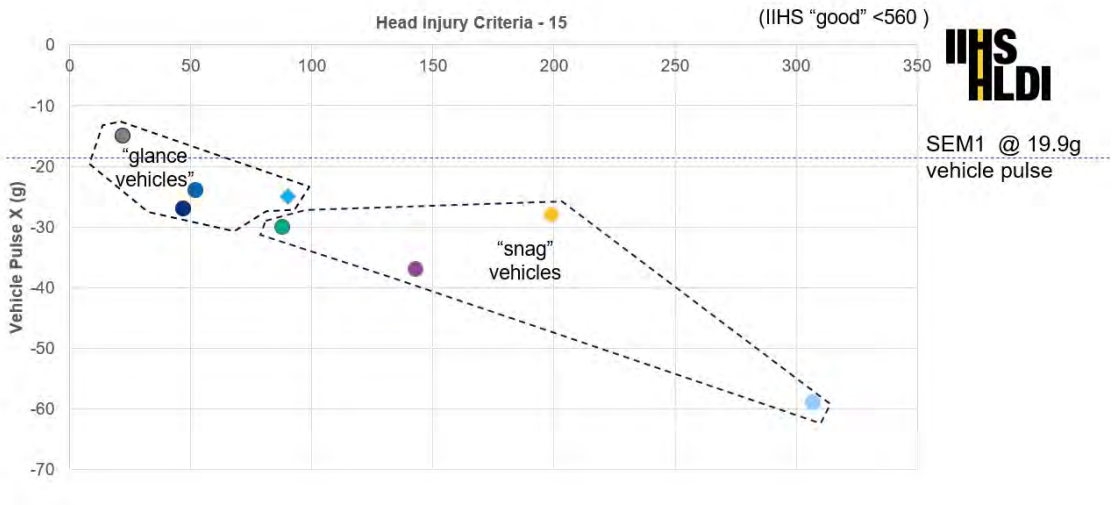

Figure 7.2.3.14 IIHS 64kph SORB crash test. Comparison of measured vehicle X pulse versus Head Injury Criteria for sample of 8 vehicles. Data courtesy of https://www.iihs.org/

The crashworthiness performance of a vehicle should consider the protection of occupants during the impact event itself and the post-event extraction and recovery of the occupants. Removal of the occupants firstly requires the side closures to be opened by the emergency services. Although not specifically engineered for in the Steel E-Motive project, any door locking mechanism and latches would be released or disengaged by the safety restraint system (e.g. air bags). Additional features would enable manual release and opening of the door by internal and externally mounted emergency access handles. Specific guidelines, regulations and tests are typically applied to ensure the forces required to open doors post-impact are not excessive and manageable by emergency services. Examples of this are a 750N maximum door load opening requirement assessed by EuroNCAP. Given the limitations of CAE tools applied for the Steel E-Motive concept, it was not possible to calculate the door opening load for SEM1, however, the efforts to open the door post-impact are generally driven by the level of crash deformation of the door aperture and door structure itself. A significant deformation of the door aperture can result in significant interference (or "jamming") between the door and body structure, which impinges the ability to open the door and extract the occupants. The door and door frame deformation as a result of the crash test loadcases was assessed in the CAE models during the Steel E-Motive project. The final design showed impressive performance as shown in Figure 7.2.3.14. The predicted door frame deformation for the most severe frontal crash loadcase (IIHS 64kph SORB) shows very minimal deformation, suggesting that the door could be opened post-impact within the expected requirements (exact physical tests would be required to validate this). The door frame construction and AHSS usage is discussed in Section 7.2.4.

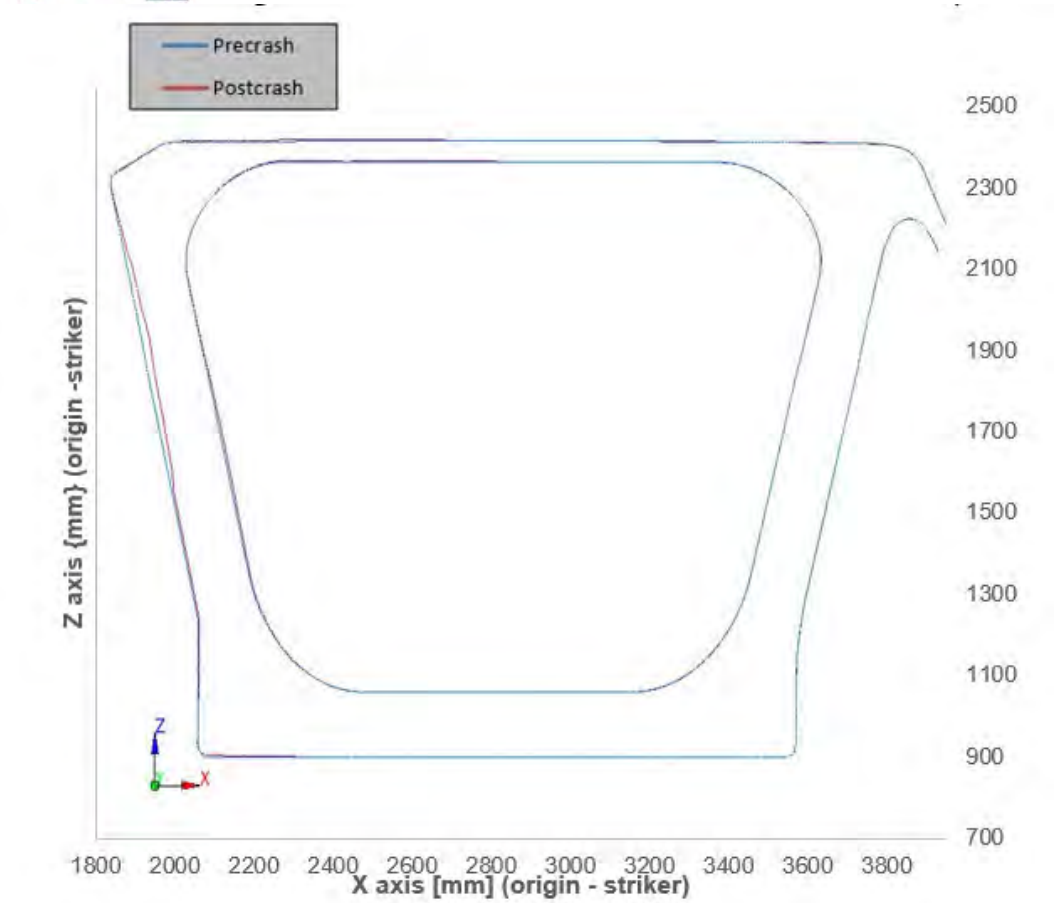

Figure 7.2.3.14 BIW door frame deformation as a result of IIHS 64kph Small Offset Rigid Barrier

Figures 7.2.3.15 to 7.2.3.20 provide a pictorial breakdown of the Advanced High Strength Steel grades and fabrication processes applied in the Steel E-Motive front crash structure.

Front Bumper Beam	
Geometry/design	Bumper beam outer faces angled and oriented to align with IIHS SORB barrier impact location. In early stage of SORB crash event the bumper beam deforms to contact with front subframe providing lateral force loadpath to initiate glance off motion
Part 1: front bumper panel	2.0mm PHS-CR2000T-MB / Hot form
Part 2: rear bumper panel	2.0mm PHS-CR1500T-MB/ Hot form
Part 3: front crush cans	2.0 mm CR420Y780T-DP / Cold Stamp
Part 4: interface panel	1.2mm CR780Y980T-CP / Cold Stamp

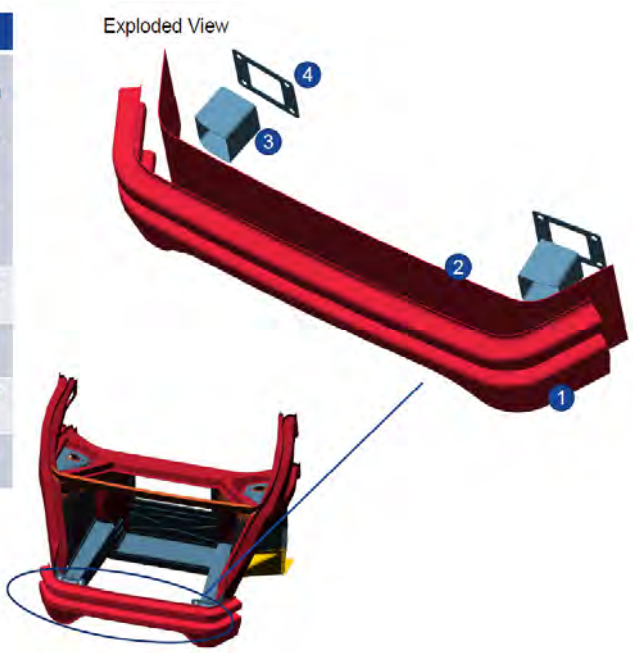

Figure 7.2.3.14 Front bumper beam AHSS grades (See Appendix 4 for larger image)

Front crush zone	
Geometry/design	Longitudinal crush rails 1 and 2 provide primary crush absorption for FFB, ODB and MPDB tests. Tailor Welded blank parts enable uniform axial crush performance and vehicle deceleration. Vertical dash brace parts 4,5, 6 and 7 provide crush load reaction and limits intrusion. One bar parts 8,9 & 10 limit lower intrusion and protect battery
Part 1: LONGITUDINAL MID RAIL INNER FRONT RH	TWB 1.8/2.0_CR500Y780T-DP/CR700Y980T-DP / Cold stamp
Part 2: LONGITUDINAL MID RAIL OUTER FRONT RH	TWB 1.8/2.0_CR500Y780T-DP/CR700Y980T-DP / Cold stamp
Part 3: BUMPER BEAM INTERFACE PLATE FRONT RH	2.0mm CR860Y1180T-DP / Cold stamp
Part 4: VERTICAL DASH BRACE FRONT LH	2.0mm PHS-CR2000T-MB / Hot form
Part 5: VERTICAL DASH BRACE UPPER FRONT	2.0mm PHS-CR2000T-MB / Hot form
Part 6 & 7: VERTICAL DASH BRACE LOWER INNER & OUTER	2.0mm PHS-CR2000T-MB / Hot form
Part 8 & 9: ONE BAR UPPER AND LOWER	1.0mm CR860Y1180T-DP / Cold stamp
Part 10: ONE BAR INNER	2.0mm CR8501180T-DH / Cold stamp
Part 11: STRUT TOWER FRONT RH	0.8mm CR350Y/450T-LA / Cold stamp
Part 12: STRUT TOP FRONT RH	1.8mm CR860Y1180T-DP / Cold stamp
Part 13: STRUT RING FRONT	2.0mm CR1200Y1470-MS / Cold stamp

Figure 7.2.3.15 Front crush zone AHSS grades (See Appendix 4 for larger image)

Glance Beam	
Geometry/design	Plan view profile optimised to guide vehicle along desired SORB barrier trajectory. Design and grades optimised to enable fold in FFB and no rupture in SORB
Part 1: GLANCE BEAM OUTER LH	0.8mm PHS-CR1500T-MB / Hot form
Part 2: GLANCE BEAM INNER LH	0.8mm PHS-CR1500T-MB / Hot form
Part 3: GLANCE BEAM UPPER TRIANGULATION OUTER LH	2.0 mm CR420Y780T-DP / Cold Stamp
Part 4:GLANCE BEAM UPPER TRIANGULATION INNER LH	1.2mm CR780Y980T-CP / Cold Stamp
Part 5: GLANCE BEAM BULKHEADS	1.5mm CR420Y780T-DP CR780Y980T-CP / Cold Stamp
Part 6:GLANCE BEAM BULKHEADS	1.5mm CR420Y780T-DP CR780Y980T-CP / Cold Stamp
Part 7: GLANCE BEAM CAP (and subframe bolt)	2.0mm CR420Y780T-DP / Cold stamp

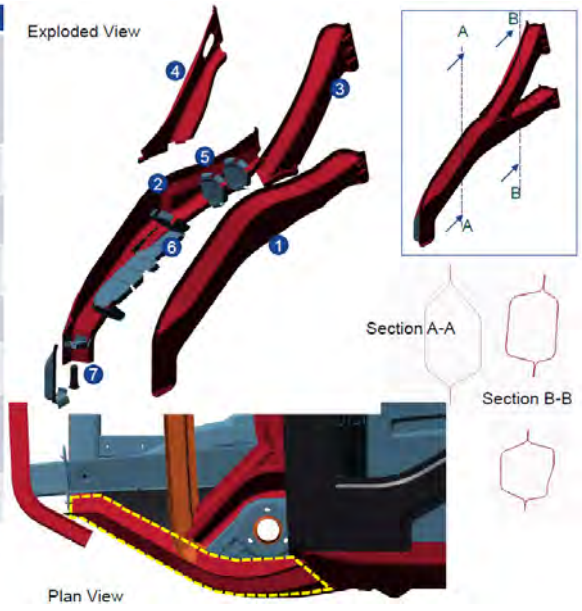

Figure 7.2.3.16 Glance beam AHSS grades (See Appendix 4 for larger image)

SORB Glance Reaction Beams and Damper Strut Top	
Geometry/design	Grades and geometry enable SORB lateral loadpath for glance behaviour
Part 1:GLANCE BEAM UPPER REACTION LH	0.8mm PHS-CR1500T-MB / Hot form
Part 2:GLANCE BEAM LOWER REACTION LH	0.8mm CR1200Y1470T-MS / Cold stamp
Part 3: GLANCE BEAM LATERAL CROSS MEMBER OUTER	1.0mm CR1200Y1470T-MS / Cold stamp
Part 4: GLANCE BEAM LATERAL CROSS MEMBER INNER	1.0mm CR1200Y1470T-MS / Cold stamp
Part 5: STRUT CROSS MEMBER FRONT	1.0mm PHS-CR2000T-MB / Hot form
Part 6: STRUT CROSS MEMBER CLOSING PLATE	1.0mm CR1550Y2000T-MS / Cold stamp
Part 7: STRUT TOP FRONT	1.8mm CR860Y1180T-DP / Cold stamp
Part 8: STRUT RING FRONT	2.0 mm CR1200Y1470-MS / Cold stamp
Part 9: VERTICAL DASH BRACE UPPER FRONT	2.0mm PHS-CR2000T-MB / Hot form
Part 10: VERTICAL DASH BRACE FRONT LH	2.0mm PHS-CR2000T-MB / Hot form
Part 11: STRUT TOWER FRONT LH	0.8mm CR350Y/450T-LA / Cold stamp

Figure 7.2.3.17 SORB glance reaction beam and damper strut top AHSS grades (See Appendix 4 for larger image)

Front Subframe	
Geometry/design	Rigidly connected to BIW at points A (front longitudinal crush rails) B (glance beam), C (Vertical dash brace lower). Provides global body stiffness contribution and crash loadpaths. Front lateral beam (1) provides SORB lateral loadpath Z offset (D) promotes subframe folding collapse mechanism in front FFB, ODB and MPDB loadcases 2.0mm gauge selected as standard for corrosion resistance for chassis parts
Part 1:FRONT SUBFRAME LATERAL BEAM (FRONT)	2.0mm CR860Y1180T-DP / Cold rolled tube
Part 2:FRONT SUBFRAME LONGITUDINAL LH	2.0mm CR860Y1180T-DP / Cold rolled tube
Part 3: FRONT SUBFRAME LATERAL BEAM (REAR)	2.0mm CR860Y1180T-DP / Cold rolled tube
Part 4: MISC. BRACKETS	2.0mm CR860Y1180T-DP / Cold stamp

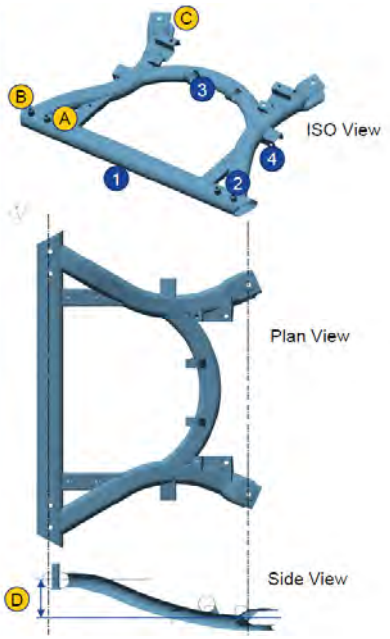

Figure 7.2.3.18 Front subframe AHSS grades (See Appendix 4 for larger image)

Front Crash Protection / Intrusion Zone	
Geometry/design	
Part 1:VERTICAL DASH BRACE FRONT LH	2.0mm PHS-CR2000T-MB / Hot form
Part 2:VERTICAL DASH BRACE UPPER FRONT LH	2.0mm PHS-CR2000T-MB / Hot form
Part 3: VERTICAL DASH BRACE LOWER INNER & OUTER	2.0mm PHS-CR2000T-MB / Hot form
Part 4: ONE BAR UPPER AND LOWER	1.0mm CR860Y1180T-DP / Cold stamp
Part 5: ONE BAR INNER	2.0mm CR8501180T-DH / Cold stamp
Part 6: FRONT BULKHEAD	2.0mm CR860Y1180T-DP / Cold stamp
Part 7: TORQUE BOX OUTER AND INNER	2.0mm CR400Y780T-RA (outer), 1.0mm INNER / Cold stamp
Part 8: STRUT CROSS MEMBER FRONT	1.0mm PHS-CR2000T-MB / Hot form
Part 9: STRUT CROSS MEMBER CLOSING PLATE	1.0mm CR1550Y2000T-MS / Cold stamp
Part 10: A PILLAR OUTER	1.2mm PHS-CR2000T-MB / Hot form (part of TWB OUTER RING)
Part 11: A PILLAR INNER	1.2mm PHS-CR2000T-MB / Hot form

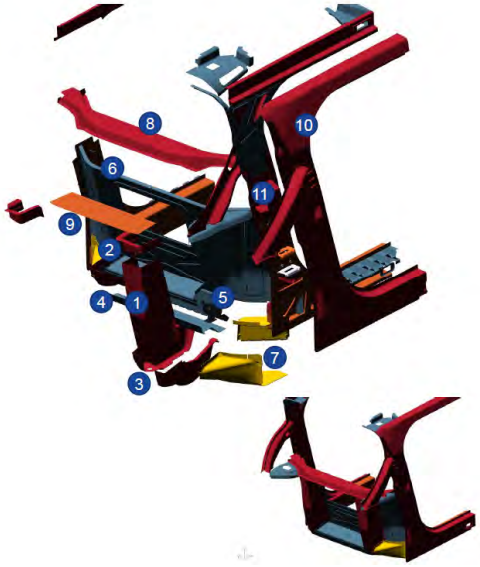

Figure 7.2.3.19 Front crash protection / intrusion prevention zone AHSS grades (See Appendix 4 for larger image)

7.2.4 Steel E-Motive body structure design approach and features for side crash and mid zone performance

The mid zone of the Steel E-Motive body structure consists of the BIW, propulsion battery and carrier frame and scissor doors. The subassemblies combine to deliver structural performance for crash, stiffness and strength requirements. The propulsion battery is described in detail in Section 7.3 and the scissor doors in Section 7.4. This section describe the sub-assemblies combine to deliver side crash performance. Figure 7.2.4.1 shows the key parts of the mid zone structure.

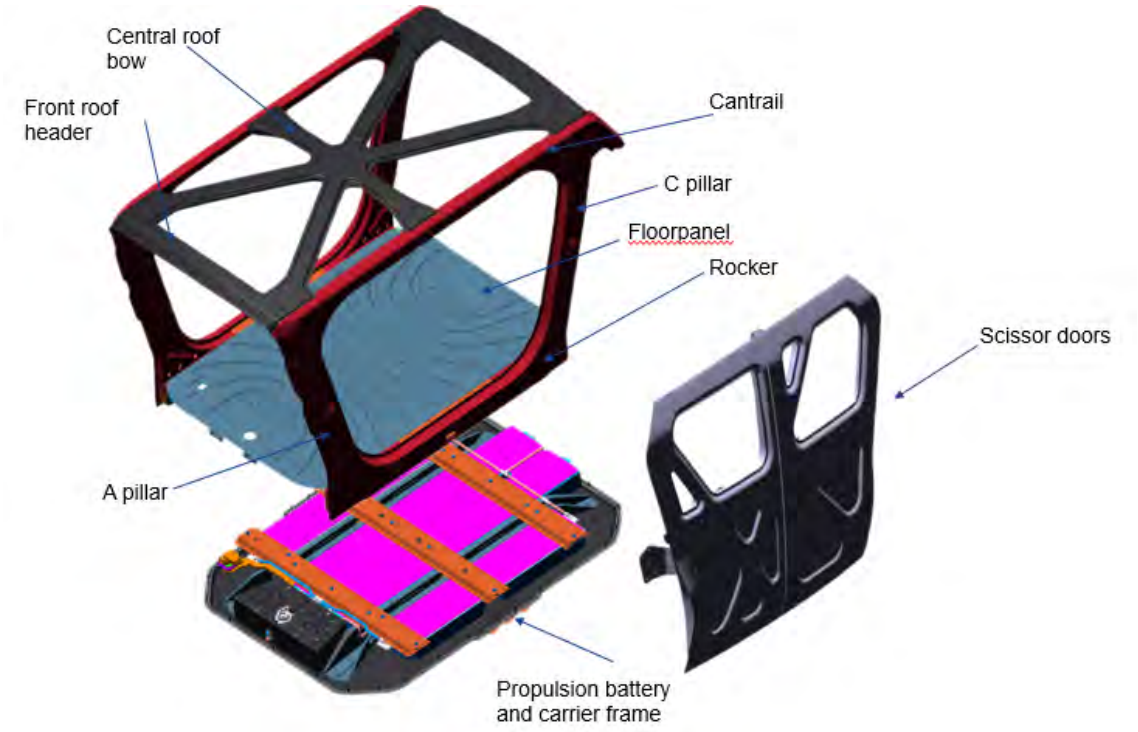

Figure 7.2.4.1 SEM1 body structure mid zone subassemblies and components

The main requirements of the body structure mid zone can be summarised as:

- Provide a comfortable & safe environment for the vehicle occupants
- Provide protection to the occupants and battery in the event of a side impact, roof crush and underbody debris impact
- Provide loadpaths for the front and rear crash zones
- Provide housing and location for the propulsion battery
- Provide aperture and mounting for the scissor doors and interior parts such as seating, trim, glazing and lighting
- Provide required sealing and protection from external elements such rain, solar

The main challenges, constraints, and considerations for the Steel E-Motive mid zone structure were:

- Removal of the B pillar from the body in white structure. This reduces overall BIW strength and stiffness which needs to be compensated elsewhere
- Positioning of the front occupants in a rear facing configuration
- Occupant protection in side crash. Crush load is concentrated over a small area in the side pole test

- Protection of the occupant battery in side crash. Proximity of the propulsion battery to the rocker results in limited crush space to manage the loads and energy
- Achieving a flat floor and floor height, given the requirement to package battery systems
- Comparatively narrow width of the vehicle. Occupants and battery are placed closer to the side crash impact zones compared to larger segment vehicles

Section 4.2 describes the side crash loadcases and targets and Section 6.3.3 describes the preliminary conceptual studies for the Steel E-Motive side crash structure. Figure 7.2.5.2 shows the alignment of the two side crash barrier loadcases to the final SEM1 design and the strategy for the side crash load management and intrusion prevention.

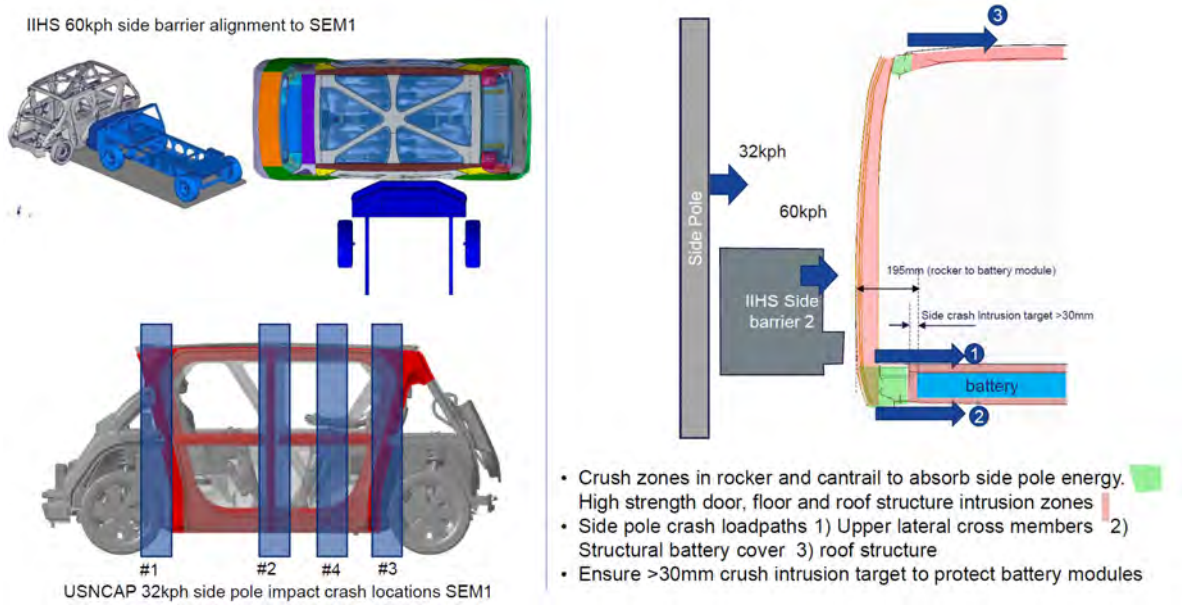

Figure 7.2.5.2 SEM1 side crash barrier alignment and strategy for loadpath and intrusion management (See Appendix 4 for larger image)

For the IIHS 60kph side barrier loadcase, the profile of the barrier largely misses the rocker meaning that the side door structure should be engineered to withstand the majority of the barrier impact loads. Typically, side barrier loads are managed by a vertical B pillar within the BIW structure. In the Steel E-Motive concept, the BIW B pillar is removed to create an open space within the cabin when the doors are open. To compensate for this, the side doors have been engineered with an AHSS B pillar structure effectively within the door structure itself. Crush zones are provisioned for within the rocker structure and cantrail, providing some side crush energy management. The AHSS side closures are full height, with the structure effectively wrapping over the cantrail at the top and rocker at the bottom. With the high strength door structure, a large component the IIHS side barrier crash loads are effectively transferred to the crushable rocker and cantrail parts by the wrap-around door.

The propulsion battery of a battery electric vehicle is particularly vulnerable in a side impact event. The proximity of the battery modules to the side crash event may result in the damage or rupture to the modules, leading to a thermal runaway event and potential vehicle fire. The risk is generally more severe than for the front and rear crash loadcases. The design packaging activity in Phase 0 optimised the battery layout to position the modules, ensuring a maximum distance from the rocker outer surface to the outer face of the modules, thus

enabling the largest side crush distance possible to manage the side crash loads. The body structure was then optimised to use the available crush space to manage the side crash loads. The battery modules were protected by a crushable AHSS member in the rocker section and very high strength steel grades placed between the rocker and battery modules. Very high strength lateral cross members in the floor and battery frame provide loadpaths across the body structure and a battery lower cover plate provides a lower lateral loadpath. The specific design features and AHSS grades applied are discussed later in this section.

IIHS 60kph side barrier performance.

The structural performance targets for the side crash loadcases are detailed in Section 4.0. For the IIHS side barrier test, the requirement is to maintain a >180mm clearance from the maximum point of crush intrusion to the centreline of the occupant seat. Figure 7.2.5.3 shows the predicted side crash intrusion performance from the CAE simulation.

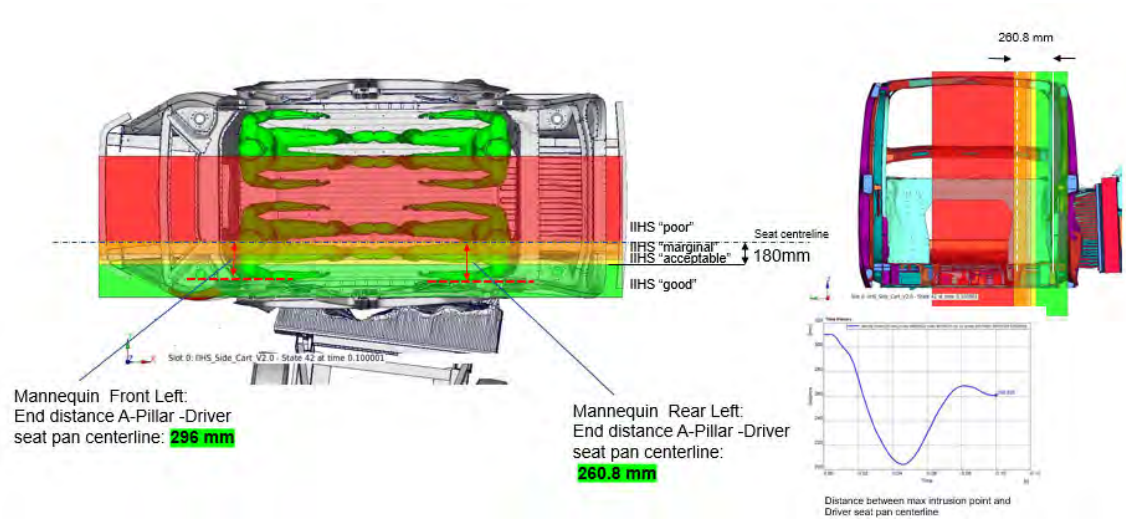

Figure 7.2.5.4 Crash CAE simulation of IIHS 60kph side barrier. Predicted intrusion values are in the IIHS “good” zone. (See Appendix 4 for larger image)

The intrusion clearance attained for the front occupant was calculated at 296mm and 261mm for the rear occupant. This is greater than the 180mm of clearance required in order to achieve the IIHS “good” rating for intrusion performance. Additional measurements such as dummy injury and forces are required in order to achieve and overall “good” rating but these were not considered within the Steel E-Motive programme. The IIHS side barrier CAE results were compared with real world crash test measurements provided by IIHS. Figure 7.2.5.5 shows predicted intrusion values through a horizontal section below the waist rail compared to measured values for a current production C/D segment battery electric vehicle (achieved IIHS “good” rating for side crash). The comparison shows that the predicted crash intrusion values of Steel E-Motive are much less than the measured passenger car. This demonstrates a very good level of occupant protection offered by the Steel E-Motive AHSS body concept for the IIHS side barrier loadcase.

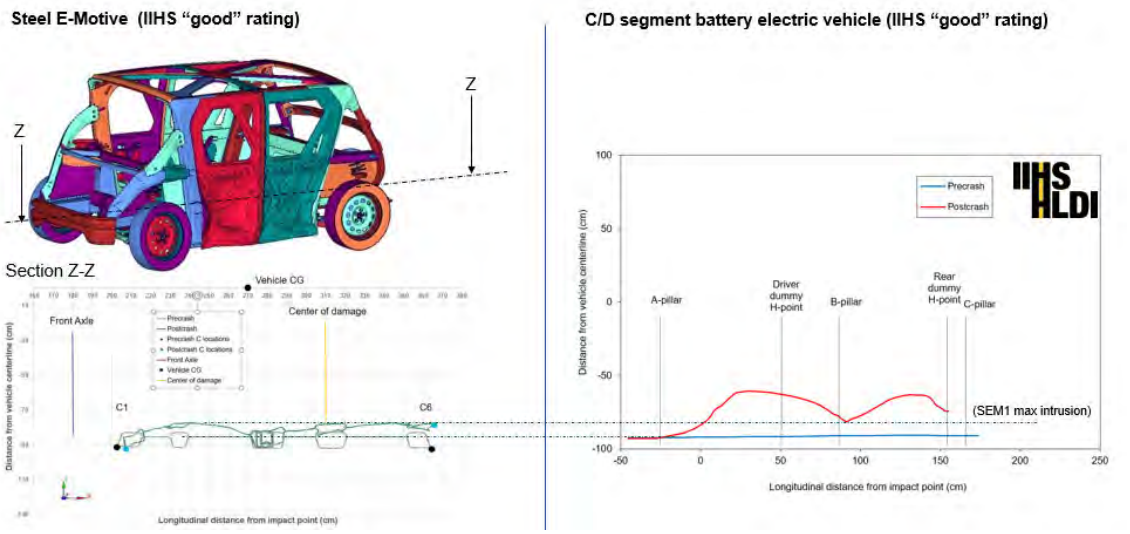

Figure 7.2.5.5 Comparison of predicted (Steel E-Motive) and measured (C/D segment BEV, 2022 model year) intrusion from IIHS 60kph side barrier test

For the USNCAP 32kph side pole test the real-world assessments are based on test dummy injuries alone. As no dummies or SRS was applied for the development of the Steel E-Motive concept, the occupant protection was assessed using the IIHS side barrier intrusion protocol (>180mm intrusion clearance, as described above). Protection of the battery was assessed by the >30mm static intrusion clearance to the outer face of the battery module. Figure 7.2.5.6 shows the predicted intrusion levels for the USNCAP side pole loadcase. For the 4 loadcases/impact positions considered, the predicted intrusion clearance was above the target value of 180mm, demonstrating a good level of occupant protection.

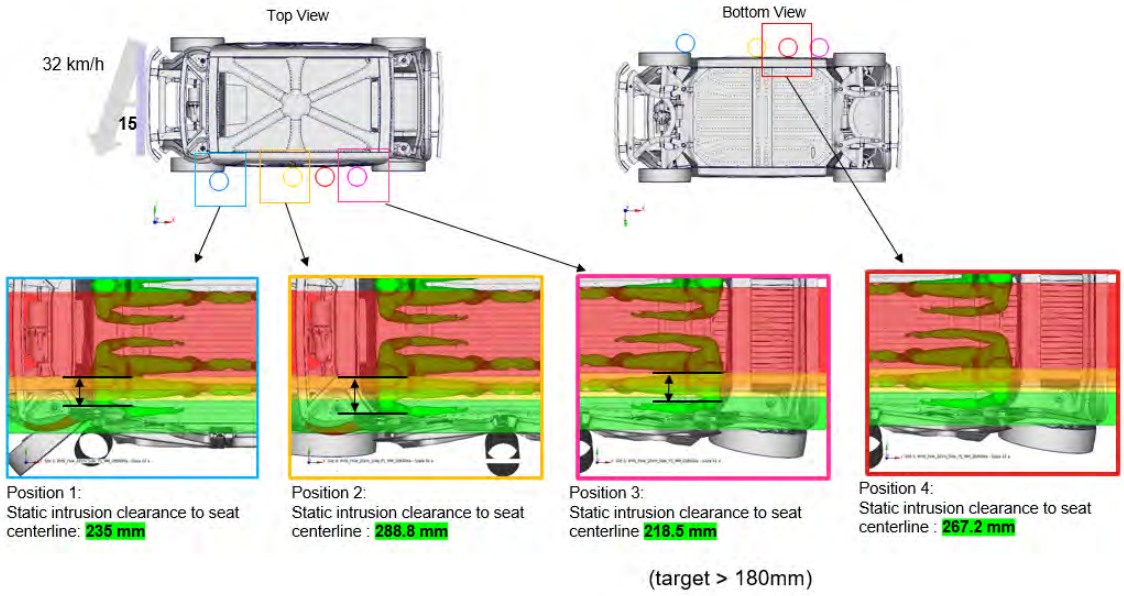

Figure 7.2.5.6 USNCAP 32kph side pole, predicted intrusion values for 4 test locations (See Appendix 4 for larger image)

Figure 7.2.5.7 shows the predicted intrusion values relative to the battery modules for the USNCAP 32kph side pole loadcases. The results show that for the 4 impact locations, the predicted static intrusion values are below the 30mm target and no contact occurs between the body structure and battery modules. This demonstrates that the Steel E-Motive body structure demonstrates a good level of crashworthiness protection of the propulsion batteries in the side pole test.

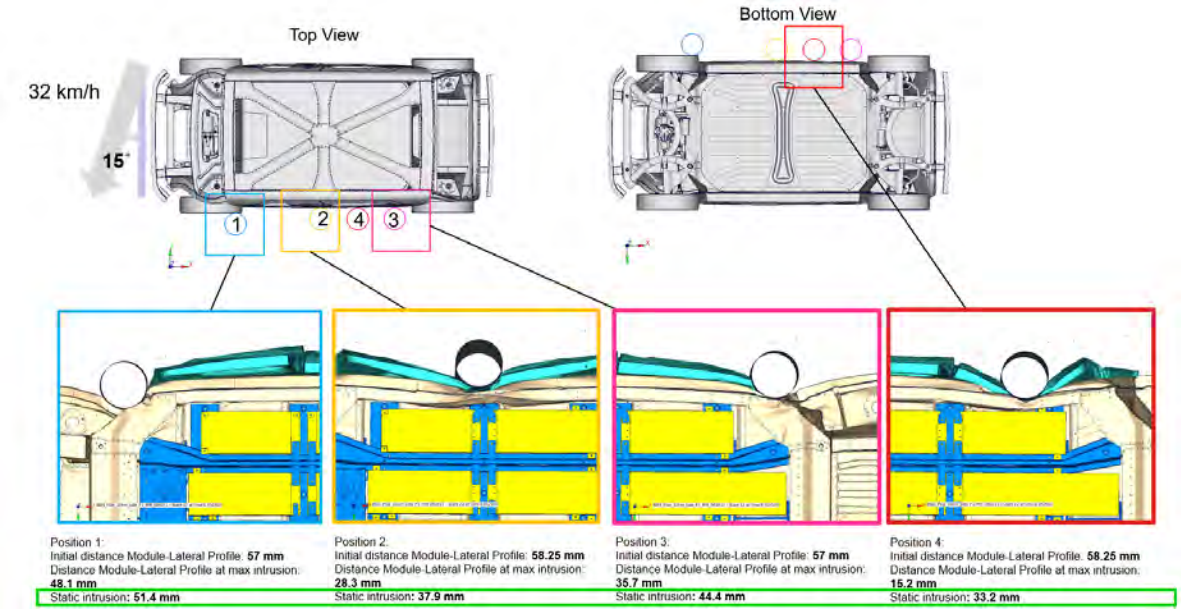

Figure 7.2.5.7 predicted intrusion values for the USNCAP 32kph side pole test (4 locations) (See Appendix 4 for larger image)

AHSS grades and design for protection of front and rear occupants in IIHS side barrier test:

Protection of the occupants and battery for the IIHS side barrier test is provided by the combination and integration of the side door and body structure. The side doors contain 2 B pillar vertical braces, the cross sections of which overlap but do not contact in a no-crash condition. The front door houses a vertical brace on it's rear face and the rear door houses a vertical brace on it's front face. An acute section profile is enabled by hydroforming and high strength achieved by using a CR400Y690T-RA (or "TRIP 690") in 1.2mm. The height of the door vertical braces extend to overlap the cantrail at the top and rocker at the bottom. In a side collision event, the front and rear door vertical braces deform and become interlocked together, providing enhanced overall strength. The vertical braces then come into contact with the rocker and cantrail providing loadpaths into the body in white. The front and rear door vertical braces are joined to horizontal door struts – "U" sectioned roll stamped beams in 1.5mm CR1200Y1470T-MS grade. Despite the vertical positioning of the horizontal door struts being slightly higher than the side barrier impact location, the interaction with the door vertical beams provides a loadpath for the crash loads outwards to the A and C pillars. From the A pillars, the front and rear lateral strut braces provide loadpaths across the vehicle, as shown in Figures 7.2.5.8a, b and c.

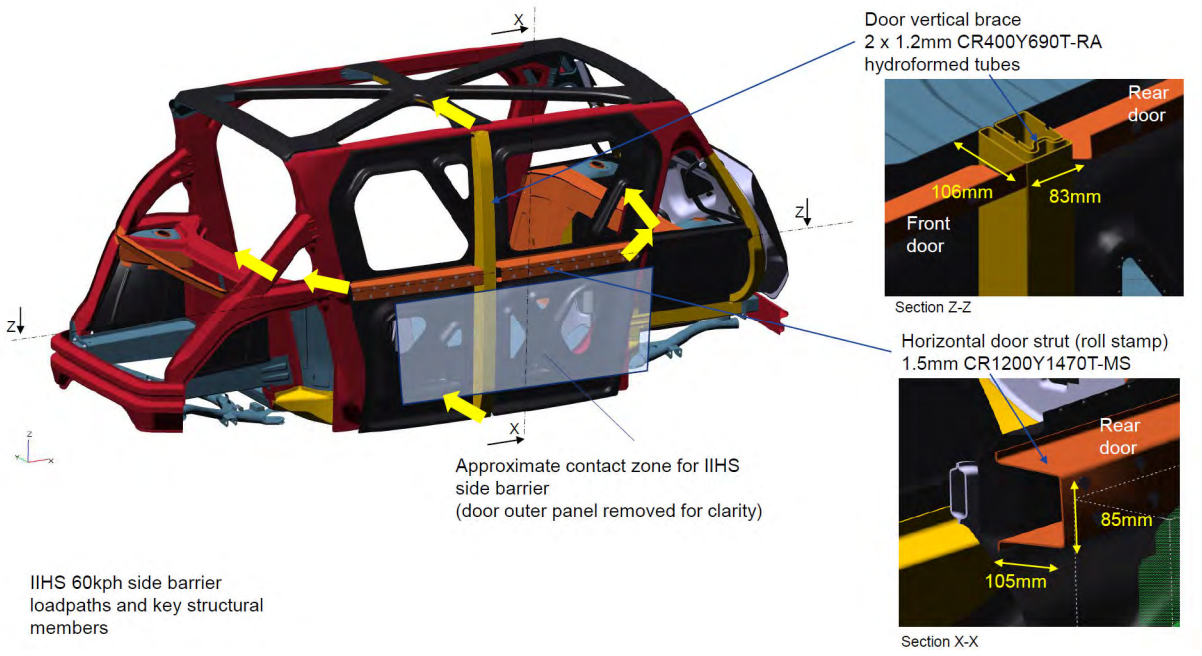

Figure 7.2.5.8a Door structural members and loadpaths into body structure for the IIHS side barrier loadcase (body structure shown for clarity) (See Appendix 4 for larger image)

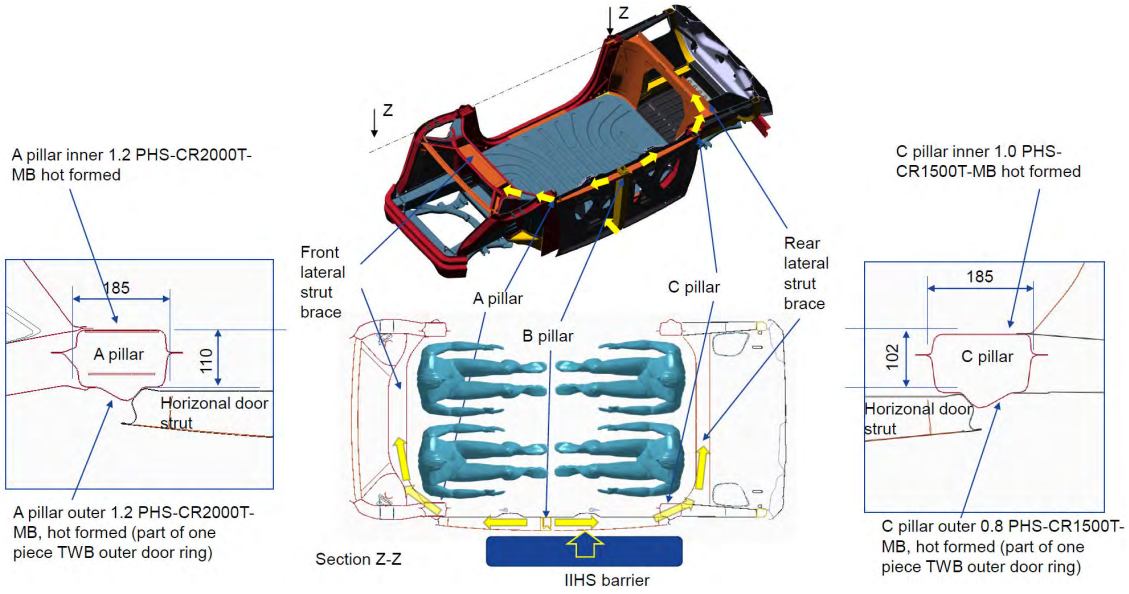

Figure 7.2.5.8b Door structural members and loadpaths into body structure for the IIHS side barrier loadcase (body structure shown for clarity) (See Appendix 4 for larger image)

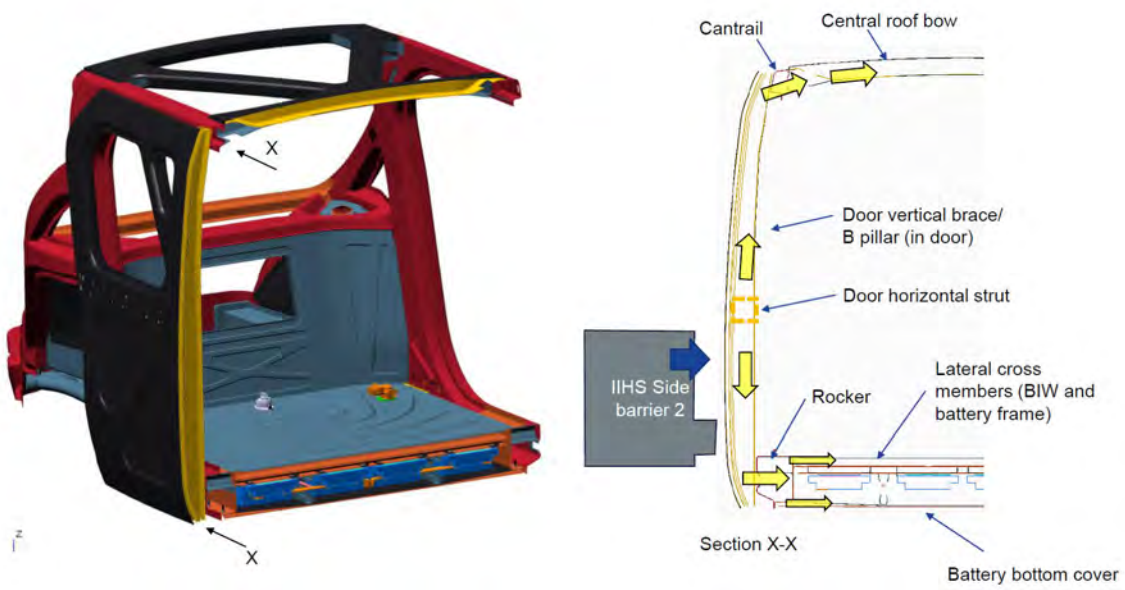

Figure 7.2.5.8c Door structural members and loadpaths into body structure for the IIHS side barrier loadcase (body structure shown for clarity)

The A and C pillars locations are predominantly outboard and in line with the front (A pillar) and rear (C pillar) occupant seating locations. The A and C pillar cross sections and AHSS grades provide very high strength and side crash load reaction, resulting in low crash intrusion values around the occupants.

Figure 7.2.5.8.c shows how the side crash loadpaths are also managed in the vertical plane via the rocker and roof structure. The interlocking vertical door braces (B pillar) combine to provide high bending strength, with minimum plastic deformation, results in a significant transfer of side crash load into the BIW roof and rocker. The construction and contribution of the roof and rocker to side crash is discussed later in this section.

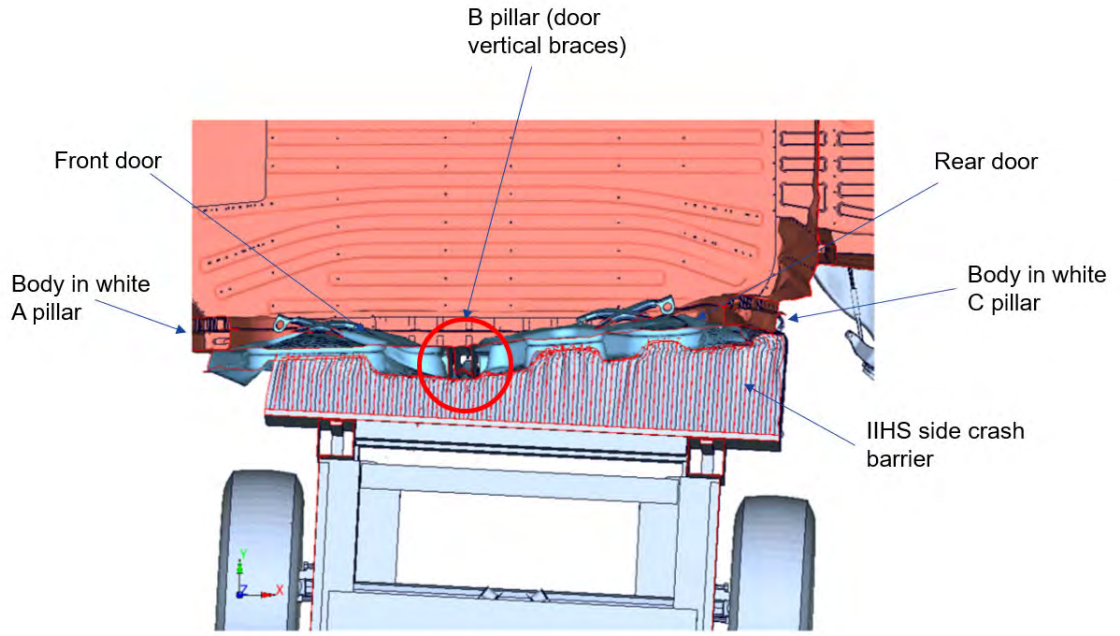

Figure 7.2.5.9 IIHS side barrier crash simulation (end of crash event), section in Z-Z plane showing B pillar/door vertical braces remaining largely undeformed

AHSS grades and design for protection of front and rear occupants side pole crash loadcases.

The management of the side pole crash loads and protection of occupants and battery place greater demands on the body in white structure than the closures, primarily as the impact load is more concentrated over a smaller area contact area and the doors become relatively sacrificial in the during the initial stages of the crash events. Figure 7.2.5.10 shows the impact location for position 1 crash loadcase which is in line with the front occupant head position.

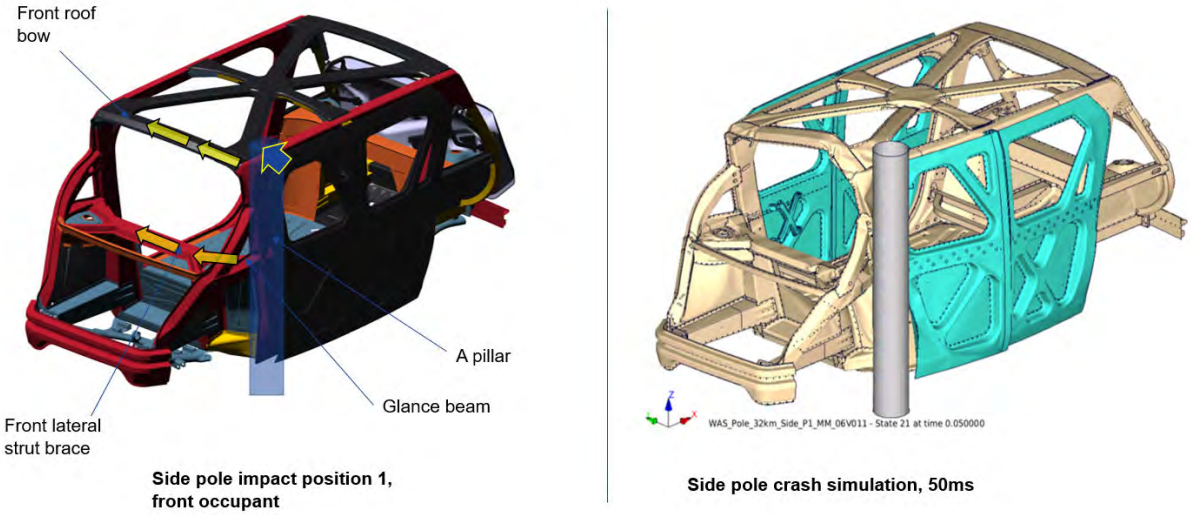

Figure 7.2.5.11 USCAP 32kph side pole crash loadcase, position 1. Loadpaths and crash simulation result (See Appendix 4 for larger image)

The pole impacts the body structure directly on the upper section of the A pillar. The A pillar section and AHSS grades (as described above for the side barrier loadcase) provide primary load reaction. The front lateral strut brace, glance beam and front roof bow header provide lateral loadpaths across the vehicle in a similar way to the IIHS side barrier loadcase (Figure 7.2.5.8b). This results in intrusion levels that are well within the IIHS target intrusion levels that enable “good” rating.

Protection of the rear occupant in the side pole loadcase (position 3) is provide by a similar strategy to the front occupant (position 1). The pole impacts primarily the lower portion of the C pillar, the construction and AHSS grades of which are similar to the A pillar. Cross-car load reaction is provided by the rear torque box and five bar, the rear lateral strut brace and rear roof bow.

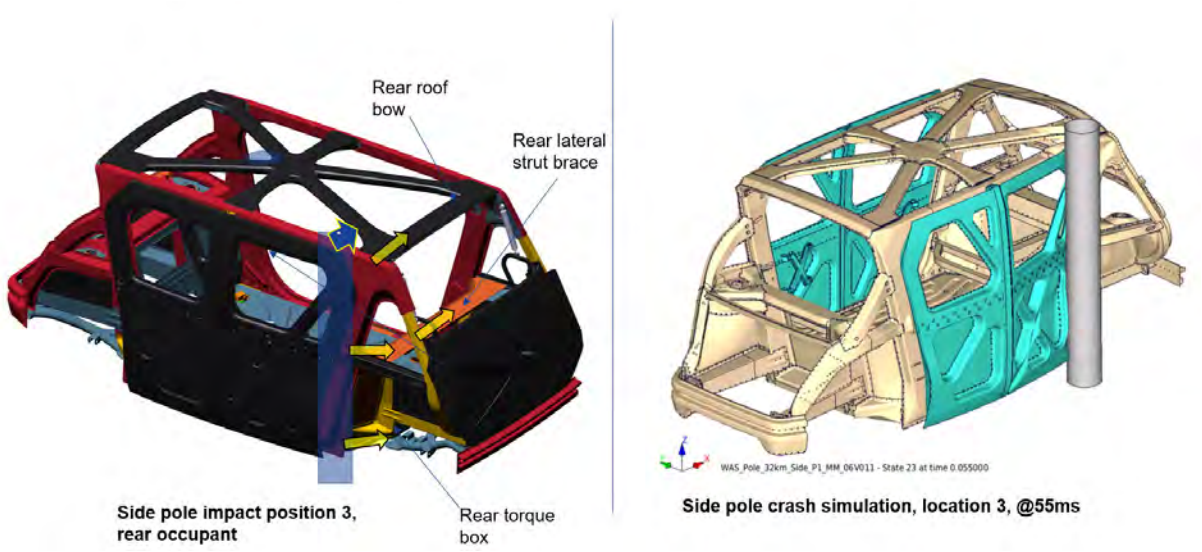

Figure 7.2.5.12 USCAP 32kph side pole crash loadcase, position 3. Loadpaths and crash simulation result (See Appendix 4 for larger image)

Side pole impact locations 2 and 4 are primarily intended to evaluate the body structural integrity for the protection of the batteries. Location 2 is directly in line with the front and rear door split (B pillar) and location 4 is at a midpoint along the length of the rear door. Both positions were selected as potential locations of weakness in the body structure. The strategy for managing the crash loads for positions 2 and 4 is shown in Figure 7.2.5.2. During the initial stages of the pole impact in position 2, the B pillar deforms considerably (due to the small contact area and concentrated load), providing some crush energy absorption, before the pole and door impacts with rocker and floor and roof assembly.

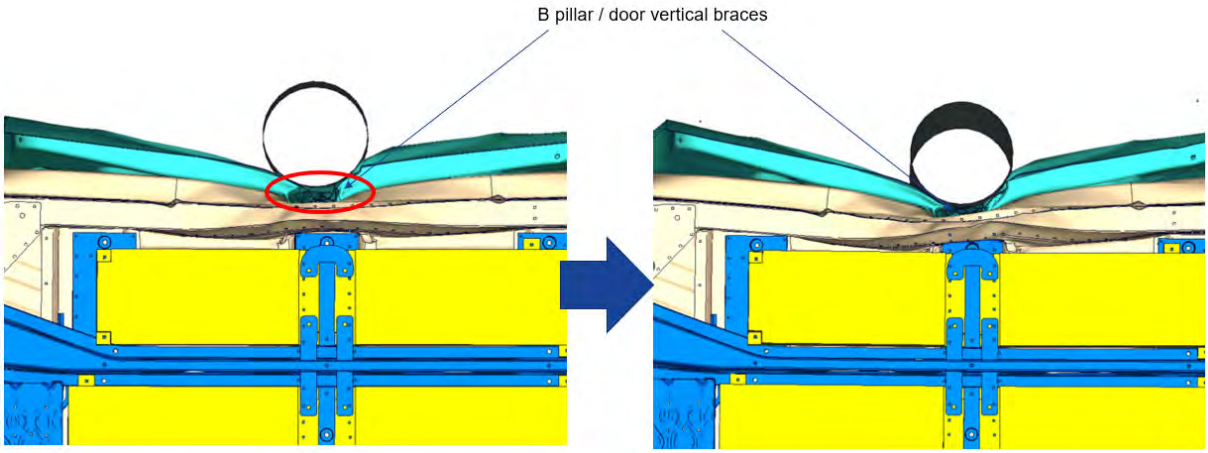

Figure 7.2.5.13 USNCAP 32kph side pole position 2. View from underneath with battery cover removed

Figure 7.2.5.14 shows the main parts of the door, rocker, floor and battery assembly that contribute to the side pole crash performance for positions 2 and 4. (The battery internals e.g. modules, cooling have been removed for clarity). The door, rocker outer panel (outer door ring TWB) and the rocker hex absorber parts act as energy absorbing or crushable elements of the side pole crash strategy (as shown in Figure 7.2.5.2). The rocker hex absorber has been engineered to provide high crush energy absorption with low weight. The part consists of 2 roll formed sheets in DP780, 0.7mm in thickness and spotwelded together. The edges of the 2 sheets produce a “hex” profile, and the large concentration of edges orientated perpendicular to the impact direction result in significant plastic deformation of the part, resulting in a high level crush energy absorption. The rocker hex absorber is supported in the rocker section by a support shelf (not shown) in 1.0mm CR420Y780T-DP.

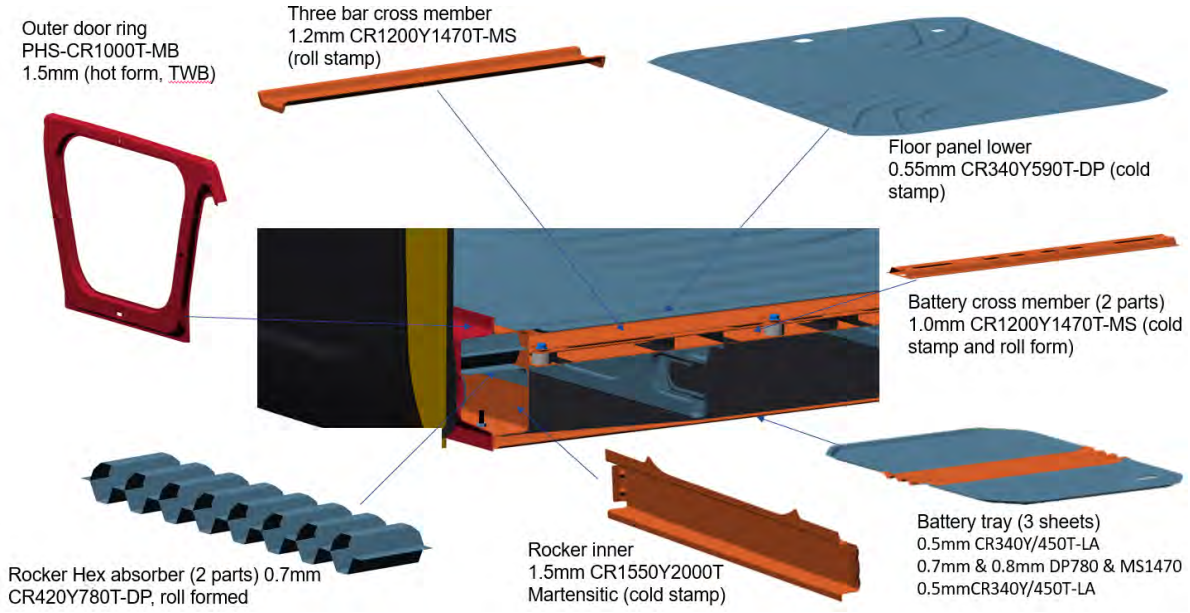

Figure 7.2.5.14 body structure cross section in X at door split point, side pole position 2. (battery modules, cooling plates, interconnects removed for clarity) (See Appendix 4 for larger image)

The second part of the side pole battery protection strategy is the intrusion prevention in the proximity of the battery modules. Here, the higher strength grade steels combine to minimise the penetration of the deformed body structure around the battery modules. Following the crushing of the rocker hex absorber the rocker inner panel in 1.5mm MS2000 grade forms the first part of the battery protection stage. Inboard of the rocker inner panel, the side pole crush loads are dispersed via upper and lower cross vehicle loadpaths as shown in Figure 7.2.5.15.

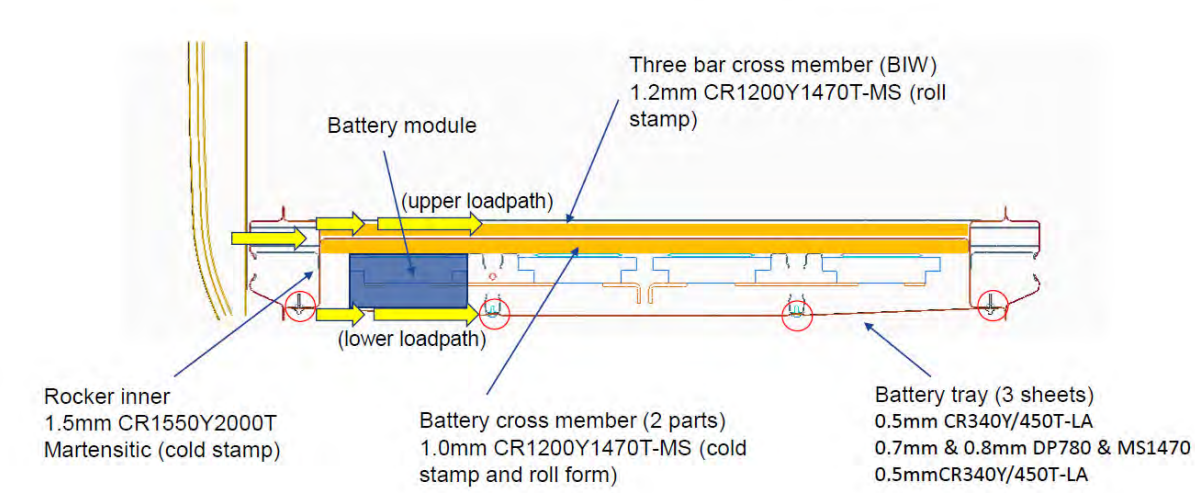

Figure 7.2.5.15 body structure cross section in X showing side pole crash intrusion prevention measures and upper & lower loadpaths (See Appendix 4 for larger image)

The 3 lateral cross members in the BIW floor (“three bar, four bar, five bar”) combined with the 3 battery carrier frame cross members provide high strength upper lateral loadpaths for the rocker crash loads as shown in Figure 7.2.5.16. For side crash pole position 2, the “three bar” cross members are in line with the crush loads. For crash pole position 4, the impact location spans the “three bar” and “four bar” cross member, however both cross members combine to provide overall lateral strength and loadpaths.

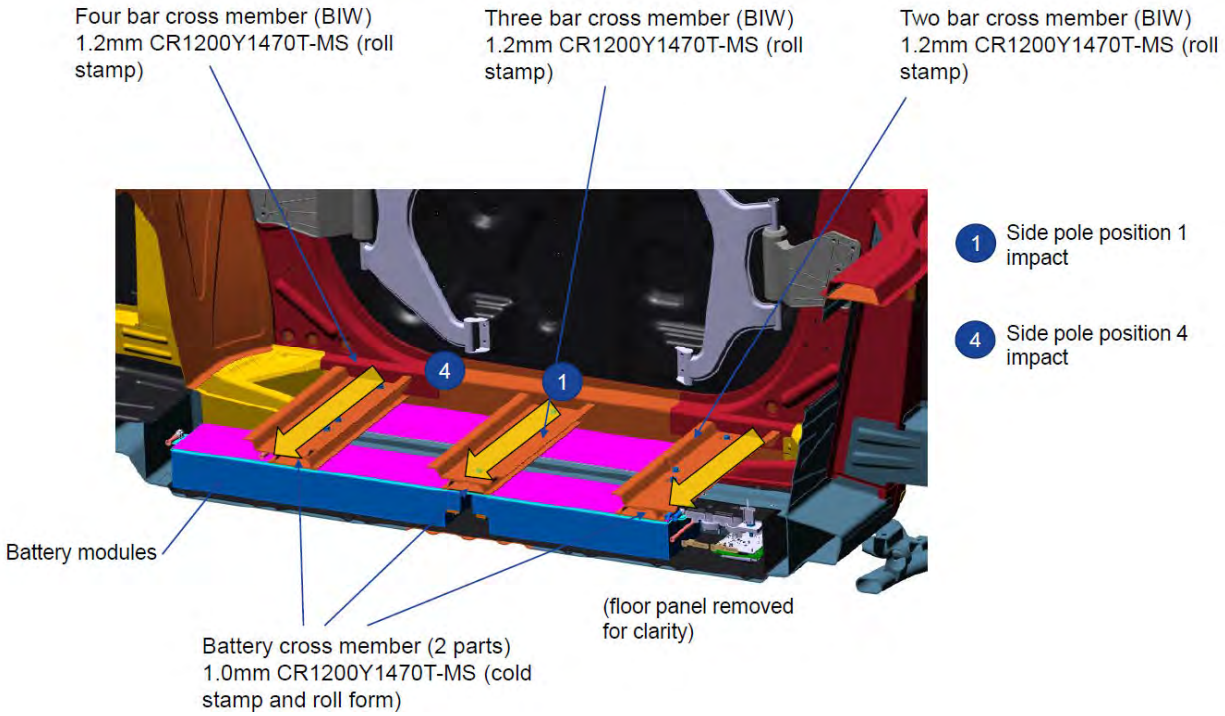

Figure 7.2.5.16 Body structure (floor panel removed) showing body cross members (two, three and four bar) and battery cross members (upper loadpaths) (See Appendix 4 for larger image)

A lower cross vehicle loadpath is provided via the battery tray which is fastened to the rocker via M8 bolts around the perimeter. The battery covers' primary function is to protect the battery from debris impacts and provide sealing externally and internally (discussed in more detail in Section 7.3). The battery tray consists of 3 sandwich sheets which combine to provide the required stiffness and strength performance. The bottom sheet is a TWB part with a MS1470 centre section which provides additional strength to manage the side pole (position 2) impact loads. The lower loadpath provides stability to the rocker section in side pole impact, minimise rotation of the rocker section around the X axis and ensures that the rocker hex absorber functions properly.

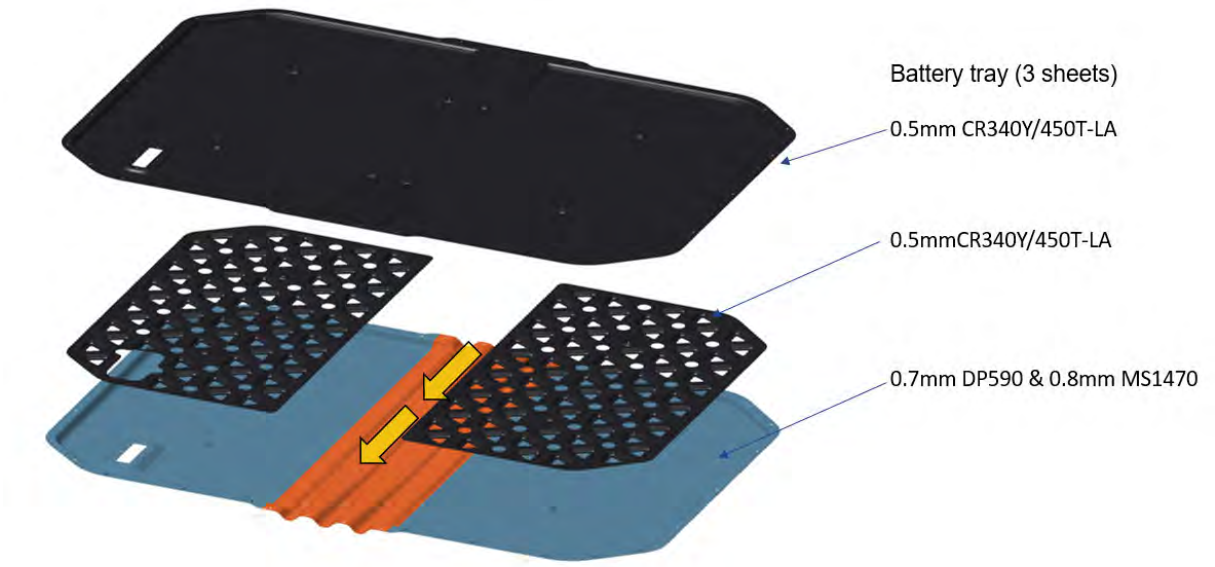

Figure 7.2.5.17 battery tray (exploded view) showing 3 sheet construction and tailor welded lower sheet with MS1470 part to assist side pole crash performance (lower loadpath). The strategy and combination of crush zones and loadpath management around the battery modules results in a maximum intrusion value of 37.9mm for position 2 and 33.2mm for position 4. This means that the body structure does not contact the battery modules for the side pole loadcases, resulting in a significantly lower risk of damage or rupture in a side crash event.

Upper body structure contribution to side crash.

Whilst the lower body structure, namely the scissor doors, rocker, floor and battery structure provide the primary side crash load management, the upper body structure does provide some overall contribution, namely maintaining overall stability of the structure and providing some cross-vehicle loadpaths. Figure 7.2.5.2 shows that the upper body structure is engineered to feature crush and intrusion zones as per the lower structure. With the strength demands on the upper structure being lower in comparison to the lower, AHSS grades of a lower strength were applied. Figure 7.2.5.18 shows the upper structure and forward roof zone that contributes to side pole impact location 1 performance. The A pillar upper (Outer Ring TWB) and cantrail section deform considerably on impact providing some crush energy absorption. The front roof bow section provides the primary upper lateral loadpath to the pole. Whilst the front roof bow does undergo some collapse, the overall strength is sufficient to ensure the intrusion values are well within the targets (Figure 7.2.5.6). For the side pole impact locations 2 and 4, the middle roof bow and roof diagonal members provides upper lateral loadpaths. An 1180MPa 3rd generation Retained Austenite AHSS grade was selected for the mid roof bow inner panel (Figure 7.2.5.18) providing higher strength than DP or CP grades and having formability qualities enabling stamping. Some panels feature lightening holes or cut-outs in the roof structure providing some weight saving benefit.

Roof structure (front)	
Part 1:OUTER RING TWB LH	TWB (A PILLAR PHS-CR2000T-MB 1.2mm, C PILLAR PHS-CR1500T-MB 0.8mm, Cantrail/roof outer PHS-CR1000T-MB 1.5mm, Rocker PHS-CR1000T-MB 1.5mm
Part 2:A POST INNER REINFORCEMENT UPPER	1.5mm CR800Y1180T-DP / Cold stamp
Part 3: ROOF SIDE RAIL INNER LH	0.8mm PHS-CR1500T-MB / Hot form
Part 4: FRONT HEADER INNER	0.8mm CR780Y980T-CP / Roll stamp
Part 5: FRONT HEADER OUTER A-SURFACE	0.6mm CR260Y/370T-BH / Cold stamp
Part 6:DIAGONAL INNER PANEL FRONT	0.7mm CR550Y/620T-LA/ Cold stamp
Part 7: FRONT INNER ROOF HEADER GUSSET MOUNT	1.0mm CR700Y980T-DP / Cold stamp
Part 8: FRONT OUTER ROOF HEADER GUSSET MOUNT	1.0mm CR700Y980T-DP / Cold stamp

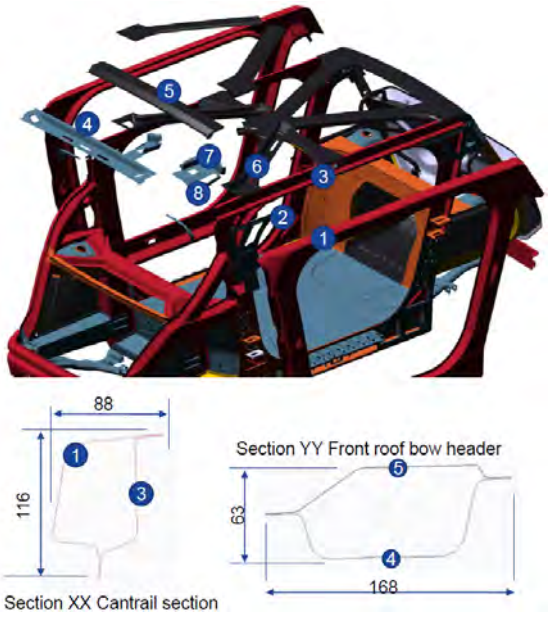

Figure 7.2.5.18 SEM1 mid zone upper structure AHSS grades (See Appendix 4 for larger image)

Roof structure (middle)	
Geometry/design	
Part 1:MID ROOF BOW OUTER A-SURFACE	0.6mm CR260Y/370T-BH / Cold stamp
Part 2:MID ROOF BOW INNER	0.8mm CR820Y1180T-RA / Roll stamp
Part 3:MID INTERSECTION OUTER A-SURFACE PANEL	0.6mm CR260Y/370T-BH / Cold stamp
Part 4: MID INTERSECTION INNER PANEL	0.5_CR260Y/370T-BH / Cold stamp
Parts 5, 7 8 & 9 : DIAGONAL OUTER A SURFACE	0.6mm CR260Y/370T-BH / Cold stamp
Parts 10, 11, 12, 13 :DIAGONAL INNER PANEL	0.7mm CR550Y/620T-LA/ Cold stamp

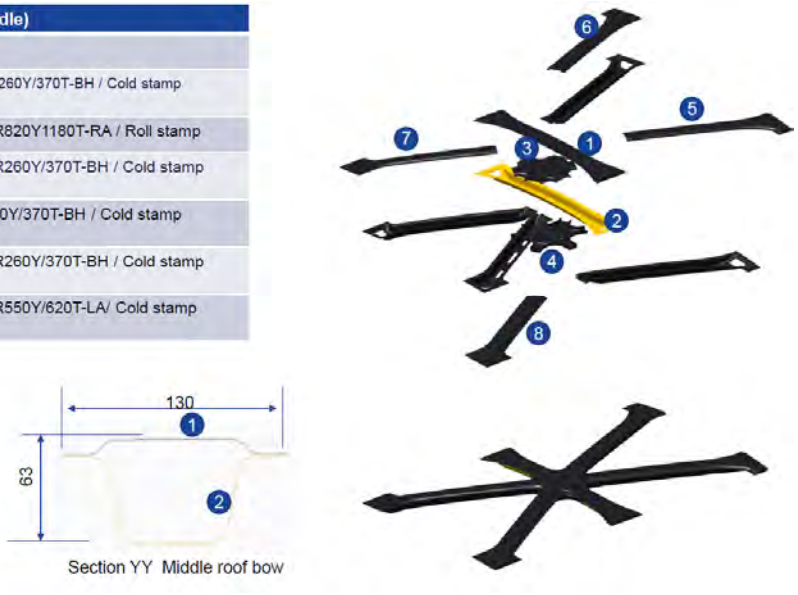

Figure 7.2.5.19 SEM1 mid zone roof structure and AHHS grades (See Appendix 4 for larger image)

The Outer Ring (door ring) is a fundamental part of the body structure mid-zone and contributes significantly to overall body stiffness and strength, front crash, side crash, rear crash and roof crush performance. The part is a large tailor welded blank consisting of 4 unique press hardened steel grades and gauges and provides stiffness and strength benefits compared to individual stamped and spotwelded assembly. The grades and gauges were selected (tailored) based on the specific localised requirements. This part is unique in that the side assembly does not feature a conventional “body side outer” A surface. The PHS TWB outer door ring is essentially the external visible surface. However, given that the scissor doors provide significant coverage of the vehicle side exterior, it was deemed that an

additional body side outer panel was not required (the primary function of a body side outer panel is to provide the A surface and is typically a lower grade, high formability steel such as Bake Hardenable or HSLA). Deleting the body side outer panel enabled a cost saving and approximate overall 27kg weight reduction. With the scissor doors in the open position, the PHS outer door ring will be exposed/visible however, with advances in press hardening fabrication methods it was deemed that a suitable quality of B surface could be attained with additional garnish cover parts/patches added to the exposed surface as required. The front and rear quarters (fenders) of the exterior A surface use a 0.6mm BH370 grade (these parts were not specifically engineered within Steel E-Motive concept design).

Figure 7.2.5.20 SEM1 outer ring and approach for A surfaces (See Appendix 4 for larger image)

The TWB outer door ring features some complex geometric features and underwent forming simulation to develop and demonstrate the feasibility. The forming simulation results for this part (and other body panels) are reported in Appendix 2.

7.2.5 Steel E-Motive body structure design approach and features for roof crush performance

The SEM1 roof crush performance was assessed according to IIHS Roof Strength Protocol Version 1, with the target to achieve “good” rating, which requires a Strength To Weight Ration (SWR) > 4.0. This means that the body structure must be able to withstand a static load of at least four times the curb weight of the vehicle and the displacement of the load platen greater than 127mm. Figure 7.2.5.1 shows the roof crush test specification and the results from the CAE simulation. The results show that a Strength to Weight ratio of 9.58 was achieved, therefore the IIHS “good” rating attained comfortably. The performance can be attributed to the roof structure design and AHSS grade selection. The A pillar is located and oriented approximately in line with the roof load platen device providing a very good primary loadpath, with the section and 2000MPa grade AHSS providing the necessary strength to achieve the load capacity required.

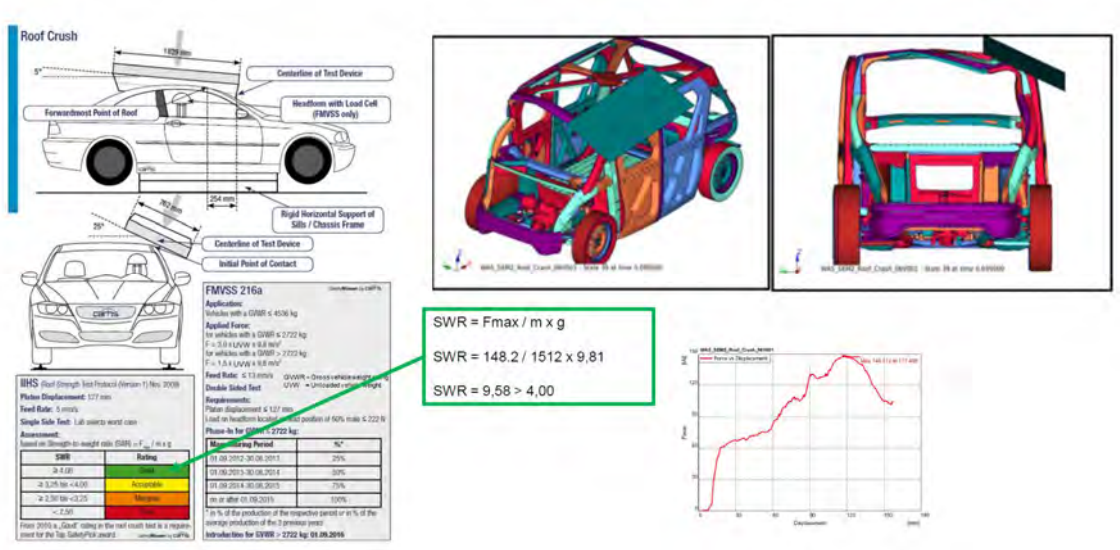

Figure 7.2.5.1 IIHS Roof Crush Strength Evaluation 1 and SEM1 CAE calculation (See Appendix 4 for larger image)

7.2.6 Steel E-Motive body structure design approach and features for rear crash performance

The rear zone of the Steel E-Motive body structure was engineered to deliver the following primary functions and requirements:

- Manage rear collision impact loads
- Provide location/storage of trunk/luggage
- Provide support and manage loads to rear chassis and coach door
- Support to roof and battery structure
- Contribution to global and local (attachment) body stiffness

The specific design challenges and constraints encountered during the development of the Steel E-motive rear structure include:

- Achieving an efficient package space, such that luggage carrying capacity can be achieved
- Compact vehicle size means more challenging to manage rear crash loads. Packaging of rear wheel steer system and impact on body structure
- Integration of hydroformed tube D pillars

The contribution of the rear structure to global and local body stiffness is discussed in Section 7.2.2 of this report and the rear packaging considerations in Section 7.1.3. This section discusses the development of the body structure rear zone development for crashworthiness performance. Figure 7.2.6.1 shows the main subassemblies of the body structure rear zone. The rear zone crash structure was developed and optimised for the FMVSS305 EV, which incorporates FMVSS301 rear impact, an 80kph moving deformable barrier impacting the rear of the vehicle with a 70% overlap. Figure 7.2.6.2 shows the barrier alignment to the body structure and the crash load and energy management strategy. A similar strategy is adopted in the rear structure to the front. The rear longitudinal rails provide the primary crash energy absorption with the subframe engineered to fold allowing the rails to deform uniformly and axially. The rear longitudinal rails are located more inboard toward

the centreline due to the requirement for wheel and tyre package clearance driven by the rear wheel steering lock angle. Vertical dash braces and horizontal beams (five and six bar), rear bulkhead and torque box form the intrusion zones, protecting battery and occupants.

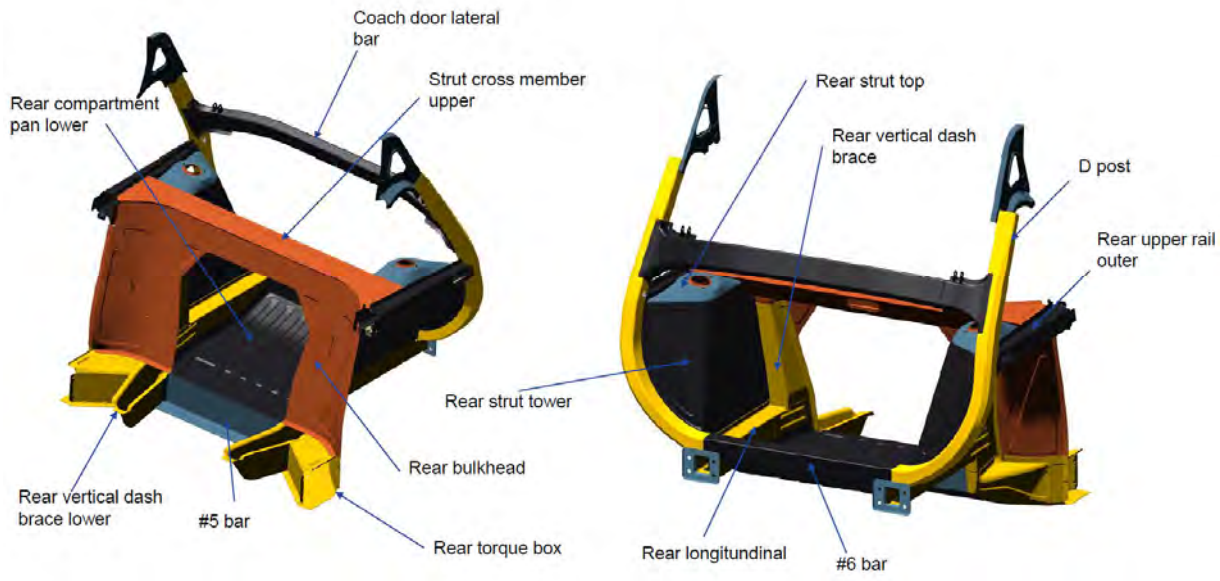

Figure 7.2.6.1 Rear zone subassemblies (See Appendix 4 for larger image)

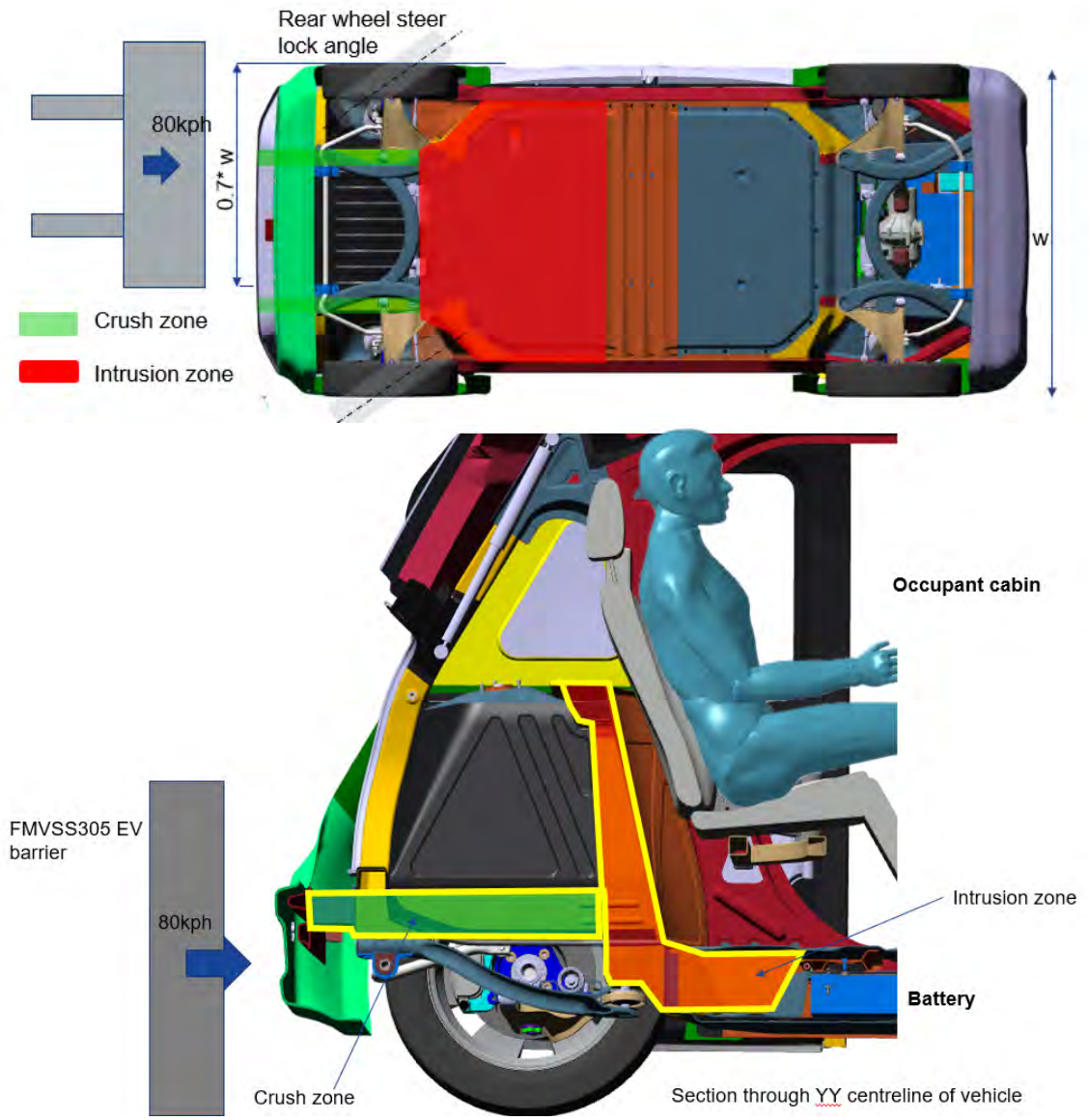

Figure 7.2.6.2 Steel E-Motive rear crash strategy

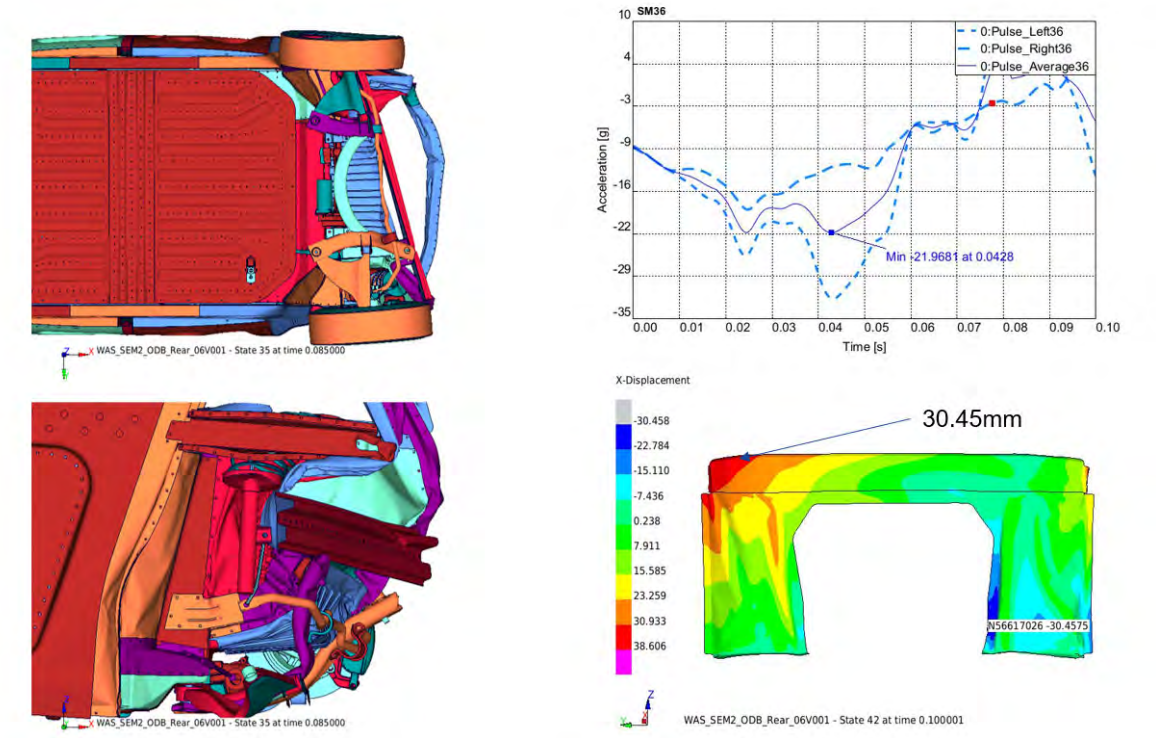

Figure 7.2.6.3 SEM1 FMVSS305 EV rear crash simulation results

The results from the full vehicle crash simulation are shown in Figure 7.2.6.3. A maximum predicted deceleration pulse of 21.9g, cabin intrusion of 30.45mm demonstrates comfortable compliance with the targets (<35g and <40mm intrusion). No contact between the battery modules and body structure was observed, demonstrating compliance with FMVSS305 EV (limiting electrolyte leakage).

Figure 7.2.6.4 shows the design and AHSS grades of the rear crush zone. The PHS rear bumper beam ensures that the barrier loads are distributed across the rear body structure on impact. The rear crush cans and longitudinal rails form the main part of the crush zone, with the grades tuned and optimised using crash CAE tools to achieve the target pulse and intrusion values. A Retained Austenite AHSS grade was selected for the rear lonigitudinals as the work hardening properties provide a greater crush energy absorption than a typical Dual Phase grade, which was required due to the relatively short crush length available.

Rear body structure (crush zone)	
Geometry/design	Crush cans (2) and longitudinal rails (3) tuned to crush axially under FMVSS305 EV loadcase. Longitundinals are 2 grade TWB. Rear subframe is rigidly bolted to BIW and engineered to fold in rear crash
Part 1: REAR BUMPER BEAM	2.0mm PHS-CR2000T-MB / hot formed
Part 2: REAR CRUSH CAN	1.5mm CR350Y600T DP / cold formed
Parts 3: REAR LONGITUDINAL RAILS (2 PARTS)	TWB: (A) 1.6mm CR820Y1180T-RA (B) 1.4mm CR600Y980T-RA / cold formed
Part 4: REAR SUBFRAME	2.0mm CR860Y1180T-DP / hydroformed tubes
Part 5: REAR COMPARTMENT PAN LOWER	0.5mm CR350Y/450T-LA / cold formed

Figure 7.2.6.4 SEM1 Body structure rear zone (See Appendix 4 for larger image)

Rear body structure (intrusion zone)	
Geometry/design	Vertical dash braces provides primary crash load reaction in rear crash. Five bar provides intrusion protection for battery. Rear strut cross member and rear bulkhead provide crush load reaction and intrusion strength
Part 1: REAR VERTICAL DASH BRACE	1.6mm CR820Y1180T-RA / cold formed
Parts 2 & 3: FIVE BAR (INNER & OUTER)	0.8mm CR900Y1180T-CP & 1.8mm CR420Y780T-DP / cold formed
Parts 4 & 5: REAR STRUT CROSS MEMBER (UPPER AND LOWER)	1.0mm CR1200Y1470T-MS
Part 6: REAR BULKHEAD	TWB (A) 1.0mm CR1200Y1470T-MS & (B) 0.8mm CR1000Y1470T-MS

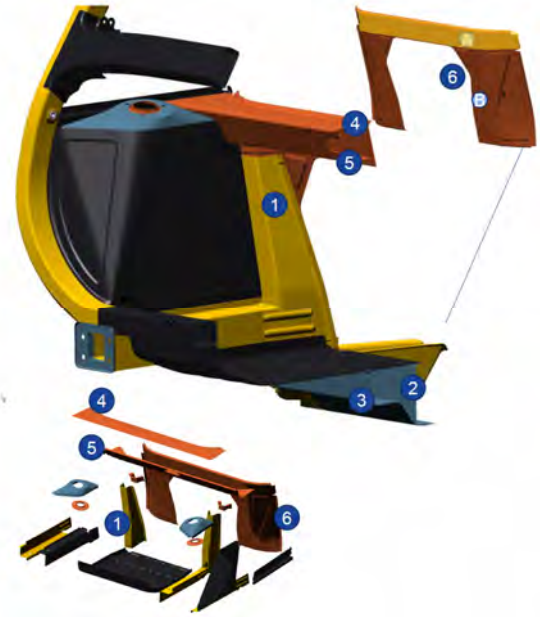

Figure 7.2.6.5 SEM1 Body structure rear zone (See Appendix 4 for larger image)

Protection of occupants and battery in the event of a rear collision is provided primarily by the parts shown in Figure 7.2.6.5. The rear body structure is developed for a single crash loadcase, the requirements from the structural are generally lower than the front crash zone, therefore lower strength steel grades have been applied. The rear vertical dash brace provides significant crush load reaction to the longitudinal rails and braces between the rear strut cross member above and the torque box and five bar in the z plane of the battery. The rear bulkhead consists of a 2 part tailor welded blank in 0.8mm and 1.0mm locally at the top to provide additional strength where required. The rear torque box, five bar and lower vertical dash brace combine to provide crash protection for the battery in rear crash and also

contribute to global body stiffness and strength. Cold stamped Retained Austenite steel grades were selected for the torque box parts, based on the requirements for high strength (~1200MPa UTS) and formability/shape requirements.

Rear body structure (torque box, five bar, lower vertical dash brace)	
Geometry/design	Rear torque box and five bar assembly forms the lower part of the rear crash intrusion zone. The assembly also provides contribution to global body stiffness
Parts 1 & 2: REAR VERTICAL DASH BRACE LOWER (INNER & OUTER)	1.0mm CR820Y1180T-RA / cold formed
Parts 3 & 4: TORQUE BOX REAR (INNER & OUTER)	1.5mm CR400Y780T-RA / cold formed
Part 5: FIVE BAR OUTER	0.8mm CR900Y1180T-CP / cold formed
Part 6: FIVE BAR INNER	0.8mm CR900Y1180T-CP / cold formed

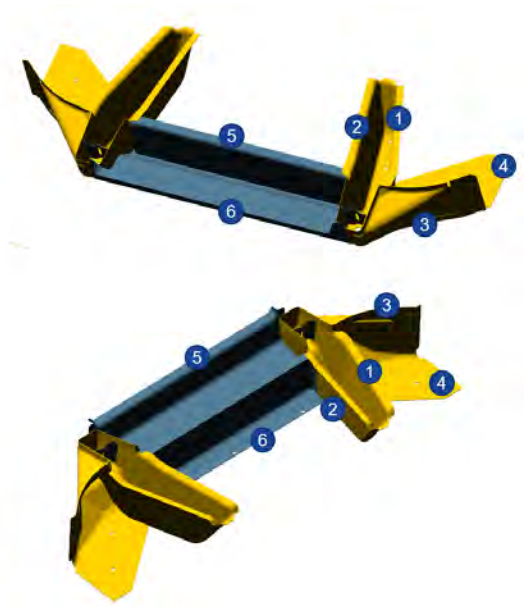

Figure 7.2.6.6 Rear torque box and five bar assembly (See Appendix 4 for larger image)

7.3 Steel E-Motive battery concept

7.3.1 Overview

The Steel E-Motive vehicle features battery electric powertrain with the propulsion battery mounted within the BIW via a carrier frame. Section 6.3 describes the exploration and selection of the battery concept. The SEM1 vehicle features a 75kWh battery capacity, formed from 8 battery modules. The specification of the battery modules are purposefully agnostic, meaning that different battery cell types (pouch, prismatic, cylindrical) could be accommodated within the modules. The final design and AHSS grade selections of the battery are discussed in this section. Figure 7.3.1.1 shows the SEM1 vehicle battery system assembly. The Steel E-Motive concept differs from many current production vehicle batteries by being an “open” (unsealed) unit prior to assembly into the vehicle. The battery modules, cooling plates, interconnects and busbars are assembled onto the structural carrier frame, off-line from the vehicle assembly facility. Typically, this assembly would be a fully sealed/encapsulated unit at this stage –the Steel E-Motive concept is an “un-sealed” battery at this stage. If the battery assembly were to undergo transportation of significant distance (i.e. from an external supplier facility to vehicle final assembly facility) then an additional transportation stillage or carrier device would be required to seal the battery during transit. This would be required to overcome safety requirements such as 1m drop tests. The battery would be removed from the stillage/carrier at the vehicle final assembly and the stillage returned back to the battery supplier facility to be reused. The battery is assembled into the vehicle at the vehicle final assembly facility and located and fasted to the body structure with bolted connections between the carrier frame cross members and body in white floor cross members. A protective battery tray (bottom cover) is then assembled to the underside of the vehicle, sealing the battery within the body structure.

The Steel E-Motive battery concept provides the following advantages and benefits in comparison to current production batteries with sealed pack units:

- Cost and weight saving benefit. The Steel E-Motive battery concept uses the BIW floor as the effective top cover of the battery. The battery pack does therefore not feature a bespoke top cover, enabling cost and weight savings
- The battery carrier frame provides strength and stiffness contribution to the body structure. Typically, the battery is housed a large void in the BIW which can introduce structural weakness or stiffness deficiency. The carrier frame and bottom cover on the Steel E-Motive concept bridges the void, ensuring structural continuity throughout the body structure
- Servicing and repair of the battery will be lower cost. The battery modules and system can be accessed by removing the bottom cover. A damaged or defective battery module would be identified (by the on-board Battery Management System), removed and replaced without having to remove the complete battery pack from the vehicle. This is important for a MaaS vehicle where vehicle usage time is important for Total Cost of Ownership

The AHSS battery carrier frame and tray are discussed in detail in the following sections.

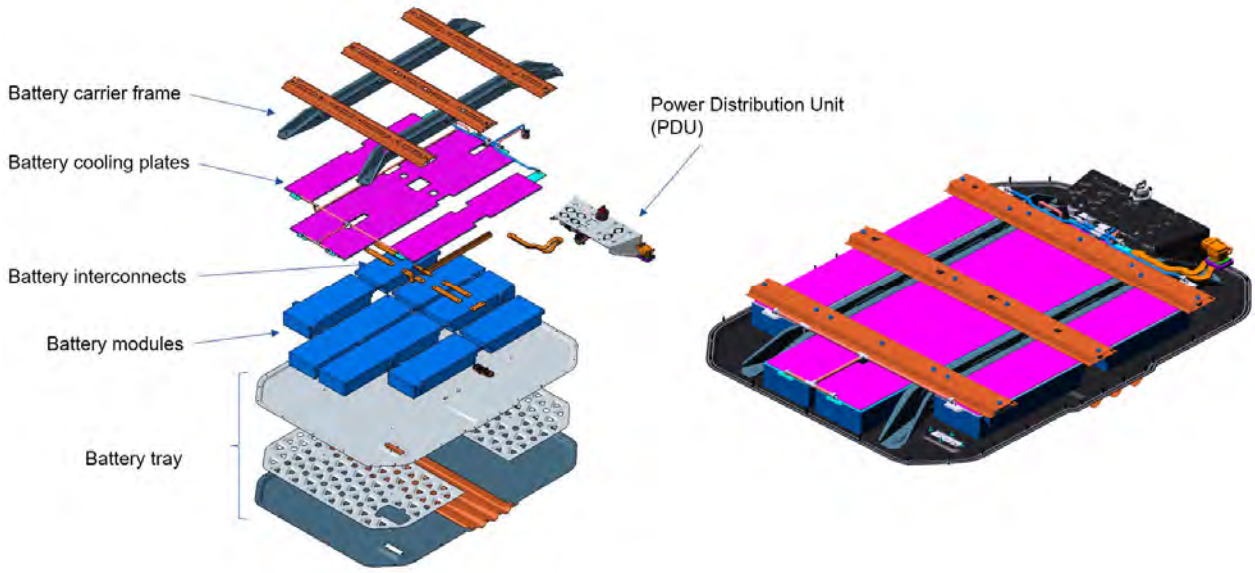

Figure 7.3.1.1 Steel E-Motive battery assembly

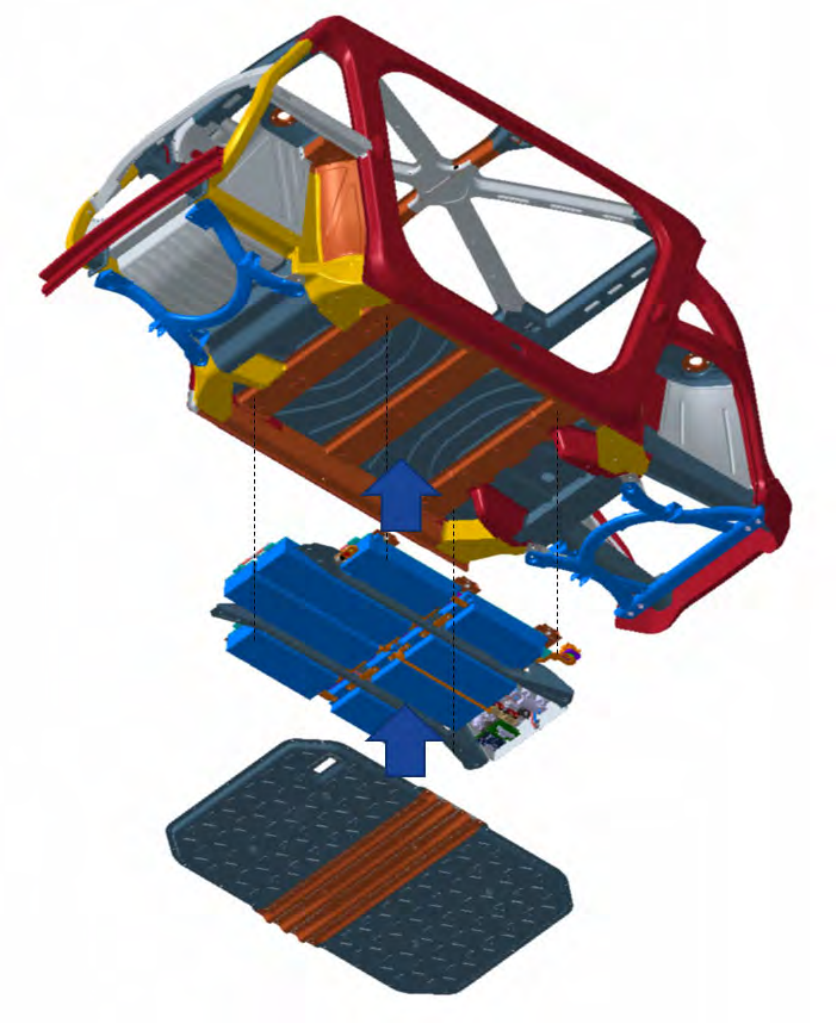

Figure 7.3.1.2 Steel E-Motive battery assembly into body structure

7.3.2 Battery carrier frame

The primary function and requirements of the battery carrier frame are summarised below:

- Support and locate (carry) the battery modules and other battery systems such as cooling, busbars, Power Distribution Unit
- Enable the battery to be assembled “off-line” (i.e. away from the vehicle final assembly
- Provide stiffness and strength contribution to the global body structure (Section 7.2.2)
- Provide sufficient strength and stiffness such that installed NVH modes of the battery are above the 35Hz target
- Provide location and fixing points for connection to the body structure
- Provide a loadpath from the battery tray to the body structure in the event of underbody debris strike or accidental car jacking (lifting)

Figure 7.3.2.1 shows the SEM1 battery frame and AHSS grades applied for the final SEM1 design.

Battery carrier frame	
Part 1 : CARRIER FRAME LONGITUDINAL (LEFT & RIGHT)	1.8mm CR260Y450T-DP / cold formed
Part 2: UPPER CROSS MEMBER #3	1.0mm CR1200Y1470T-MS / roll stamp
Parts 3 & 4: UPPER CROSS MEMBER #2 & 3	1.0mm CR1200Y1470T-MS / roll form
Parts 5,6 & 7: LOWER CROSS MEMBERS #3, #2, #1	1.0mm CR1200Y1470T-MS / roll form

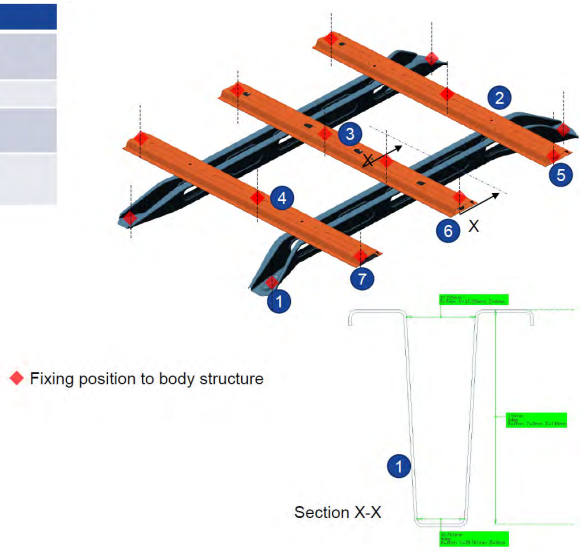

Figure 7.3.2.1 SEM1 battery carrier frame design and AHSS grades (See Appendix 4 for larger image)

The frame longitudinals feature a narrow width profile, enabling a larger packing volume for the battery modules and a deep section, required for higher bending stiffness and enveloping the height of the modules. The front and rear end sections of the longitudinals are flared out to align and marry to the front and rear BIW crash longitudinals and lower parts of the vertical dash braces. This ensures continuity of crash and stiffness loadpaths throughout the body structure. Options for 3 piece longitudinals were considered, with the mid section being a roll formed part and cold stampings at the ends. A single stamped solution was achieved by applying a DP450 AHSS grade, which has good elongation and formability characteristics for the complex geometry and a yield and UTS strength for crash and durability. The single stamped longitudinals would also have slightly improved stiffness compared to a 3 part solution due to the welding required across the 3 part interfaces. The 3 battery frame cross members provide support to the battery modules. The cross members are connect to the longitudinals via bolted joints. The battery modules are suspended from the cross members via fixing bolts. The battery frame cross members align to the BIW floor cross members as shown in Figure 7.2.5.16, and provide a cross vehicle loadpath for side crash loads (Figure 7.2.5.15) . The battery and body in white lateral cross members are MS1470 AHSS grade, and are fabricated using cold stamped, roll formed or roll stamped methods depending on specific geometry of the part. The battery frame (including all the battery parts) is bolted to the body in white via 22 M8 bolted fixings at locations as shown in Figure 7.3.2.1. The frame to BIW fixings and locations ensure that the battery is very well integrated to the parent body structure. This can be demonstrated by the first installed modal frequency of the battery and floor being greater than the 35Hz target (actual value 39.1Hz).

7.3.3 Battery tray and BIW floor sealing

The battery bottom cover (or “battery tray”) was engineered to provide the following functions:

- Protect the battery from impact loads from underneath the vehicle, such as road debris, accidental jacking of the vehicle via the undertray

- Provide a sealing function, protecting the battery from external contaminants such as water and prevent leakage from the battery to outside of the vehicle (e.g. electrolyte, cooling fluid)
- Provide stiffness and strength contribution to body structure
- Provide an aerodynamic cover to the vehicle underside

Figure 7.3.3.1 shows the battery tray construction and AHSS grades

Battery tray (bottom cover)	
Geometry/design	3 sheet steel sandwich cover combines to provide high stiffness and strength. Triangular stamping in 2 provides section depth for stiffness and strength Use of 0.5mm and 0.7mm gauge helps achieve total weight 33.2kg Joining methods: spotweld, laser weld, adhesive
Part 1: BATTERY TRAY UPPER	0.5mm CR340Y/450T-LA / cold formed
Part 2 : BATTERY TRAY TRIANGLECOMB FRONT & REAR	0.5mm CR340Y/450T-LA / cold formed
Part 3: BATTERY TRAY LOWER	TWB (A) 0.7mm CR420Y780T-DP (B) 1.0mm CR1200Y1470T-MS / cold formed

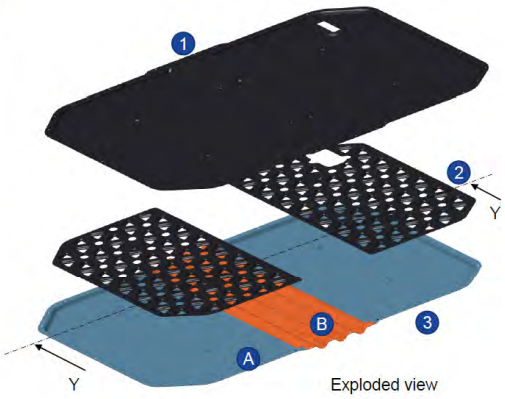

Figure 7.3.3.1 Battery tray design and AHSS grades (See Appendix 4 for larger image)

The battery tray is engineered to provide underbody debris impact protection according to the loadcases defined in Section 4.2.5.2. The performance was developed and assessed using CAE analysis, the results of the final design are shown in Figure 7.3.3.2

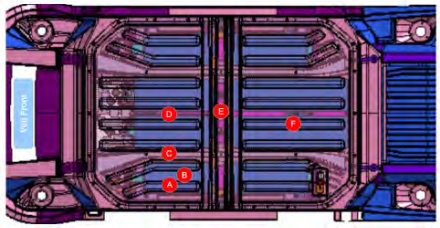

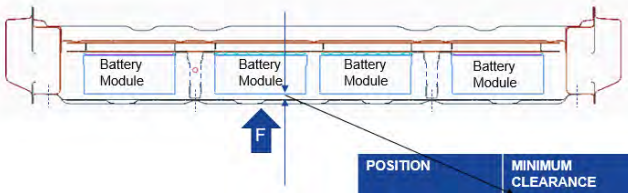

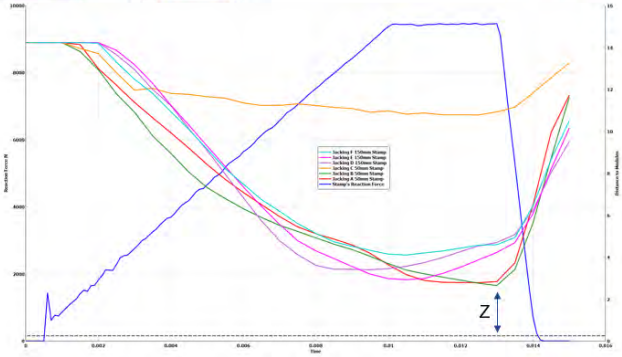

POSITION	MINIMUM CLEARANCE (Z) [mm]
A 50mm Stamp	2.78
B 50mm Stamp	2.64
C 50mm Stamp	10.79
D 150mm Stamp	3.40
E 150mm Stamp	2.92
F 150mm Stamp	4.10

Figure 7.3.3.2 CAE results of battery tray debris and jacking loadcases (See Appendix 4 for larger image)

For all the locations and impactor sizes considered, a minimum clearance distance greater than 2.64mm was calculated, suggesting that the no contact would occur between the battery tray and the battery module in the event of underbody debris impact or accidental jacking. The performance can be attributed to the design concept of the Steel E-Motive battery and the AHSS grades. For impactor location A and B, the strength and stiffness of the AHSS battery tray are sufficient to withstand the impactor loads, with the deflection of tray minimised. The rocker (1) and battery longitudinals provide loadpaths to the body structure. For impactor location C, the battery frame longitudinal provides a direct loadpath to react the load. The worst case impactor locations are D and E, around the centre of the battery and furthest away from the battery frame longitudinals. The AHSS battery tray still manages to prevent contact between the tray and battery modules. This enhanced protection is enabled by the battery architecture and the modules being suspended from the BIW floor, providing a static air-gap clearance between the battery tray and battery modules.

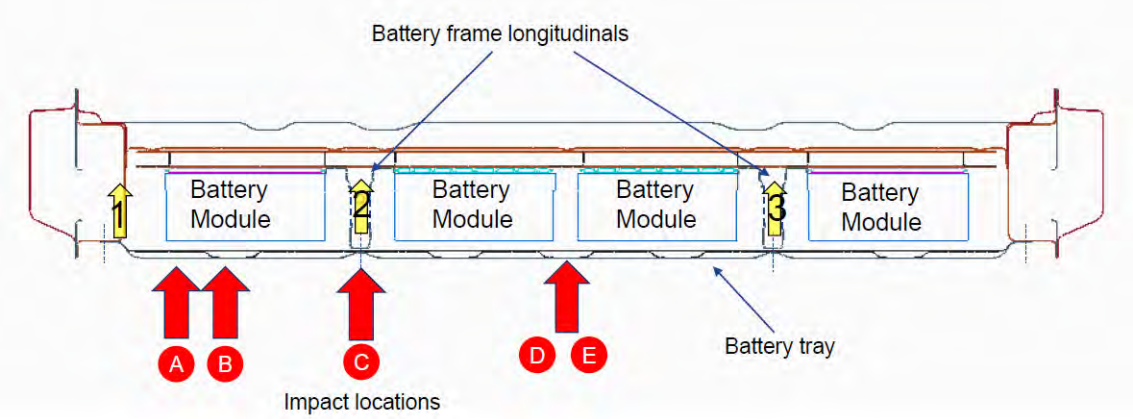

Figure 7.3.3.3 Section in X showing battery, impact locations and loadpaths

The Steel E-motive battery has also been developed for fatigue/durability (Power Spectral Density) performance, drop test and static load crush tests. The results from the CAE analysis demonstrate compliance with the requirements and standards as shown in Figures 7.3.3.4 to 7.3.3.5.

Battery Durability FEA. Predicted PSD Analysis Root Mean Square Von-Mises stress

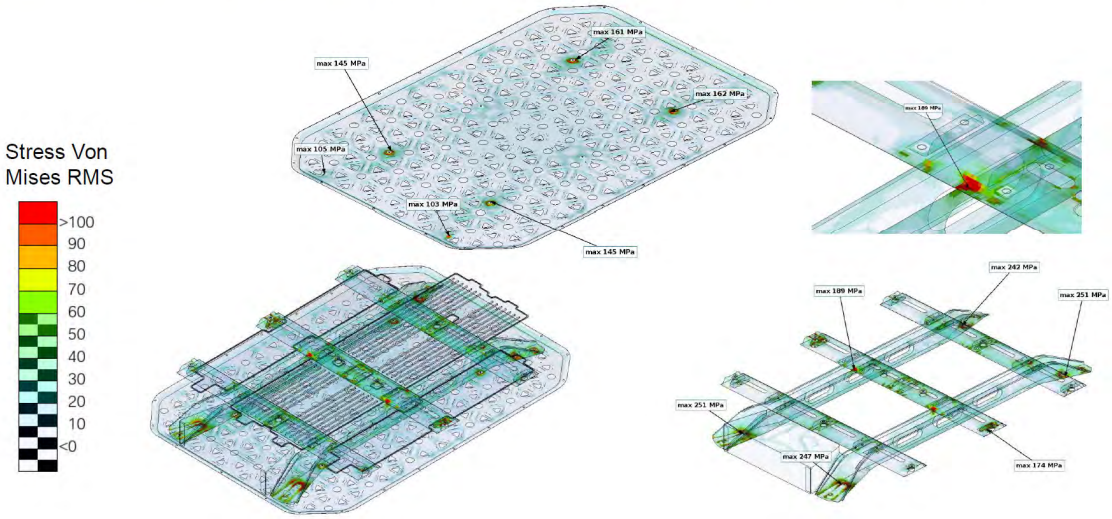

Figure 7.3.3.4 Battery durability FEA. Predicted Von-Mises stresses (Root Mean Square)

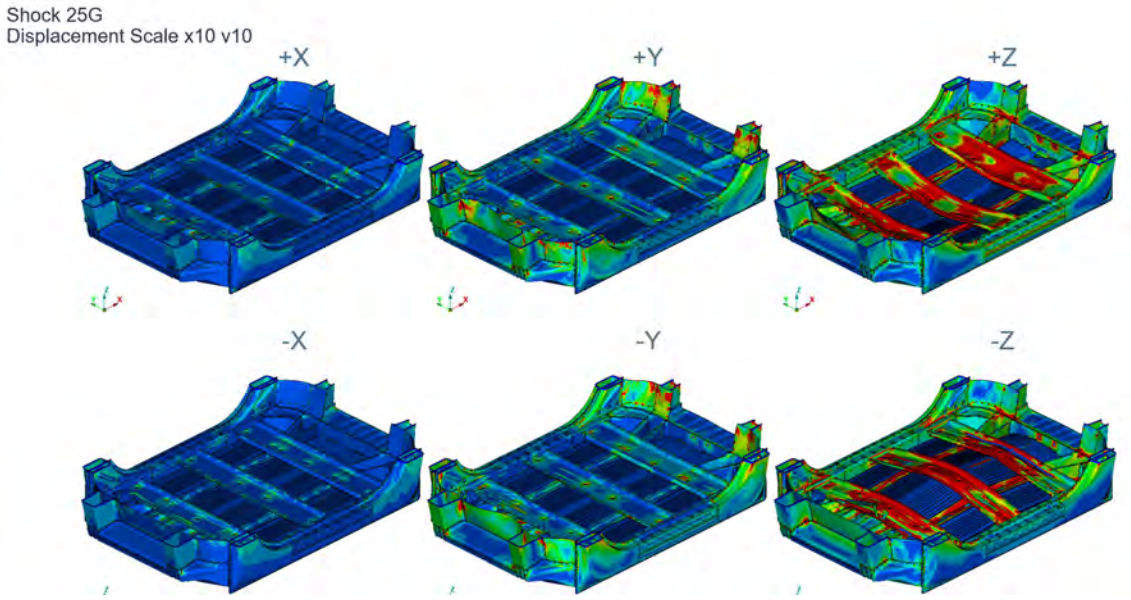

Figure 7.3.3.5 Drop test, 25g shock loading FEA results

Battery sealing:

High voltage batteries pose many safety risks therefore adequate sealing should be provisioned for to prevent the release of any gases from the battery to the passenger compartment, prevent ingress of contaminants from the passenger compartment to the battery compartment (such as fluid/liquid spillages) and prevent ingress of contaminants from outside of the vehicle to the battery compartment (such as water). The Steel E-Motive battery is engineered according to the sealing standards IP6k9k and IP67, requiring ingress protection from dust and water to a depth of 1m for a duration of 30 minutes. Figure 7.3.3.6 shows the sealing configuration for the battery tray.

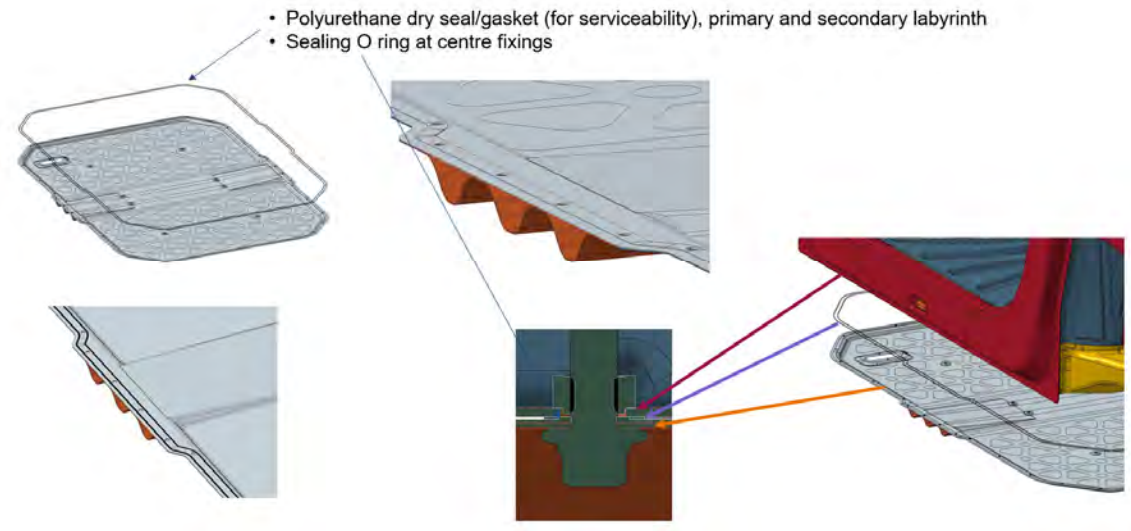

Figure 7.3.3.6 Steel E-Motive battery tray sealing configuration (See Appendix 4 for larger image)

A 2 part (outer and inner) labyrinth dry seal was selected, enabling the cover to be easily removed for battery and module servicing and repair. The battery tray is fastened to the body in white with 36 M8 bolts around the tray perimeter. This ensures appropriate sealing pressure for the labyrinth seal. Additionally the, battery tray is fastened to the battery frame (longitudinals) with 8 M8 bolts. All bolts feature O rings to provide sealing. A key feature of the Steel E-Motive battery is the deletion of the top cover from the pack – this function is provided by the floor of the BIW. This therefore requires BIW to floor to have appropriate sealing treatment. Laser seam welding is applied and for the perimeter weld of the floor panel (Figure 7.2.2.16), providing the appropriate sealing between occupant compartment and the battery. In addition to mechanical/physical seal, the battery compartment would undergo a vehicle production line validation pressure test to ensure the battery compartment sealing was to the required standard. Additionally, battery condition monitoring systems (e.g. temperature) would be installed to alert the occupants and fleet operators to any anomalies with the battery system. In the event of a battery malfunction, the fully autonomous nature of the vehicle would enable the vehicle to manoeuvre and stop in a safe location, open the doors, instruct the occupants to vacate the vehicle and notify the emergency services.

7.4 Steel E-Motive Closures

7.4.1 Side (Scissor) Doors

7.4.1.1 Overview & side door requirements

Section 6.3.5.3 describes the side door concept exploration, evaluation and selection of scissor type doors for the Steel E-Motive design. This section describes the final concept design. The following requirements were considered during the development of the scissor concepts:

- provide closing/encapsulation of body structure whilst in closed position. Enable safe, unobstructed access to the vehicle in the open position

- provide protection and sealing from external elements (e.g. moisture, noise)

- enable visibility/provision glazing

- contribution to vehicle crashworthiness, with respect to protection of occupants and battery

    - side barrier and side pole loadcases have direct impact

    - front and rear crash loadcase contribution

- provide contribution to overall body stiffness, with low cost and weight

- have sufficient durability and strength to withstand fatigue and abuse loads

- meet the aesthetic safety and operational requirements for a fully autonomous vehicle (e.g. condition monitoring, automated controls activation)

- integrated within the overall vehicle styling theme

7.4.1.2 SEM Scissor door design

Figures 7.4.1.2.1 shows the SEM1 scissor doors in the open and closed position and Figure 7.4.1.2.2 shows the hinging and actuator mechanism.

Figure 7.4.1.2.1 SEM1 scissor doors – open and closed positions

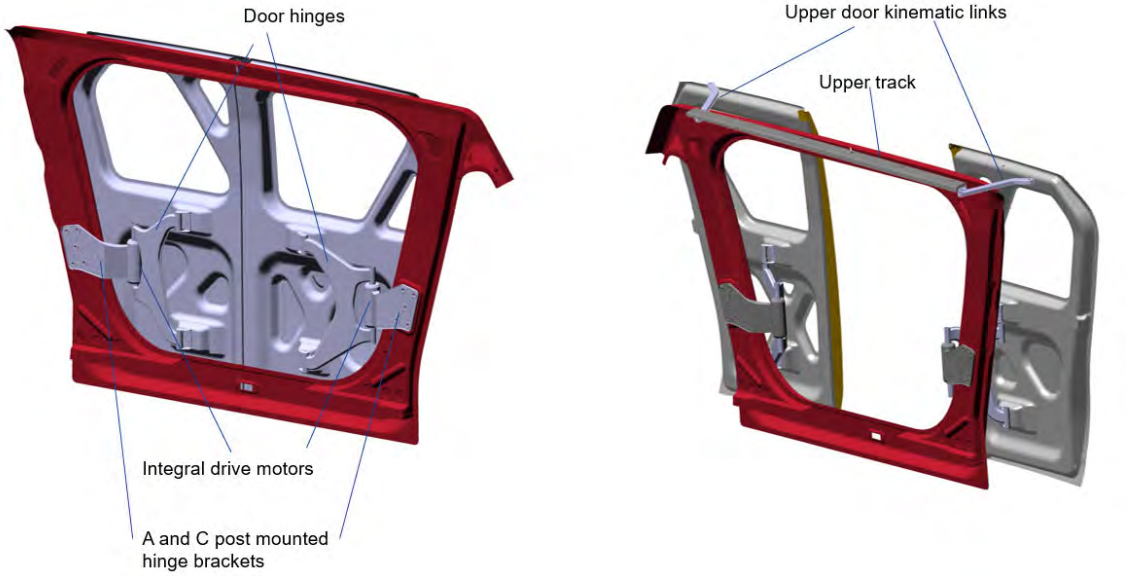

Figure 7.4.1.2.2 SEM1 scissor doors – actuators and hinges

The SEM1 scissor doors have fully automated operation. The electronics and control systems for the doors were not specifically considered within the scope of this project. An electronically controlled integral drive motor provides the primary door opening method. The motors are mounted from A and C pillar hinge brackets. The motor torque is applied to the doors via hinges. A combination of the hinge design and upper kinematic track and links determines the opening motion of the scissor doors as shown in Figure 7.4.1.2.3

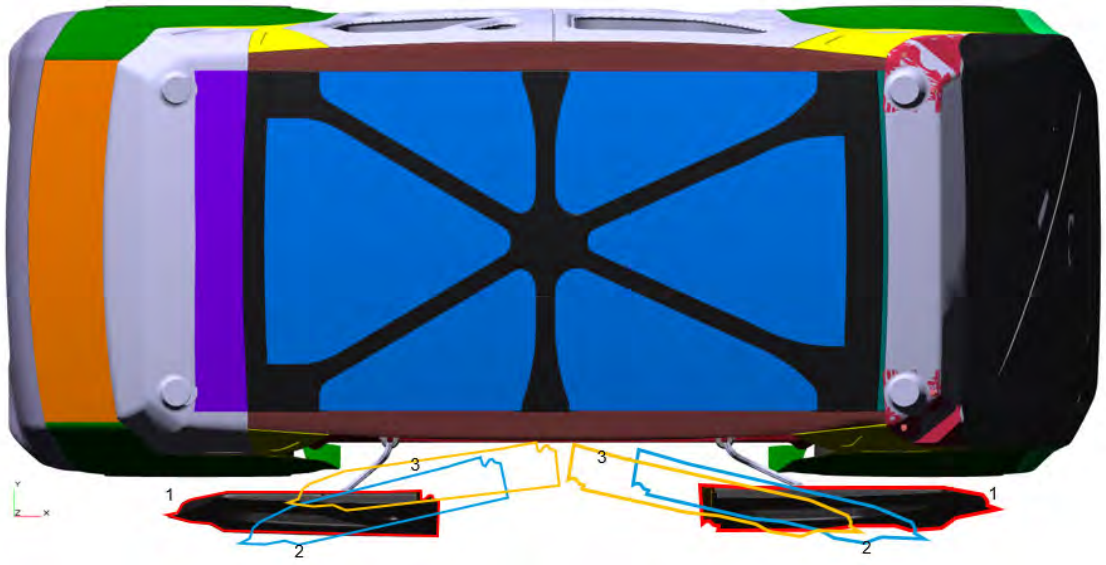

Figure 7.4.1.2.3 SEM1 scissor door closing steps

The scissor door structures feature hydroformed B pillars in RA690 grade and horizontal door beams in roll stamped MS1470. These combine to provide side crashworthiness performance as described in Section 7.2.4. A decision was made during the concept phase to specify fixed glazing in the scissor doors. This was primarily driven by operational safety requirements, however fixed glazing offers cost and weight savings also. Appropriate and automated Heating, Ventilation and Air Conditioning (HVAC) systems would be able to maintain appropriate levels of thermal comfort within the passenger cabin. Figure 7.4.1.2.4 shows the AHSS grades used in the SEM1 scissor door structure.

Scissor Door Structure	
Geometry/design	B pillars (1 & 2) and horizontal door struts (3 & 4) provide main crash loadpaths for IIHS side barrier. B pillars overlap the cantrail (top) and rocker sections (bottom) to provide crash loadpath into BIW structure. Mild steel door inner panels and bake hardenable outer panels. Lattice features provide some
Parts 1 & 2: B PILLAR (FRONT AND REAR)	1.2mm CR400Y690T-RA / Hydroformed
Parts 3 & 4: HORIZONTAL DOOR STRUTS (FRONT AND REAR)	1.5mm CR1200Y1470T-MS / roll stamp
Parts 5 & 6: DOOR INNER PANEL (FRONT AND REAR)	1.2mm Mild140/270 / cold stamp
Parts 7 & 8: DOOR OUTER PANEL(not shown) (FRONT AND REAR)	0.7mm CR280Y/400T-BH / cold stamp

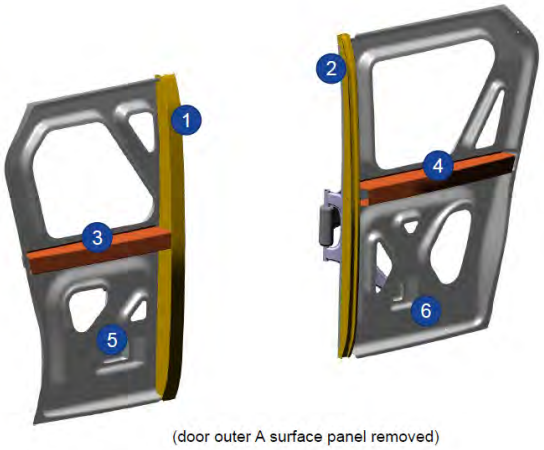

(door outer A surface panel removed)

Figure 7.4.1.2.4 AHSS grades in SEM1 scissor doors (See Appendix 4 for larger image)

7.4.2 Rear tailgate (coach) door

The Steel E-Motive rear door concept was selected during the preliminary concept Phase 0. The “coach door” features a parallel swing arm and powered lift device, resulting in a reduced outward swing distance, providing improved operation in compact spaces.

The tailgate structure features a cold stamped mild steel inner panel and bake hardenable outer A surface panel. The outer A surface features the exterior styling lattice structure features.

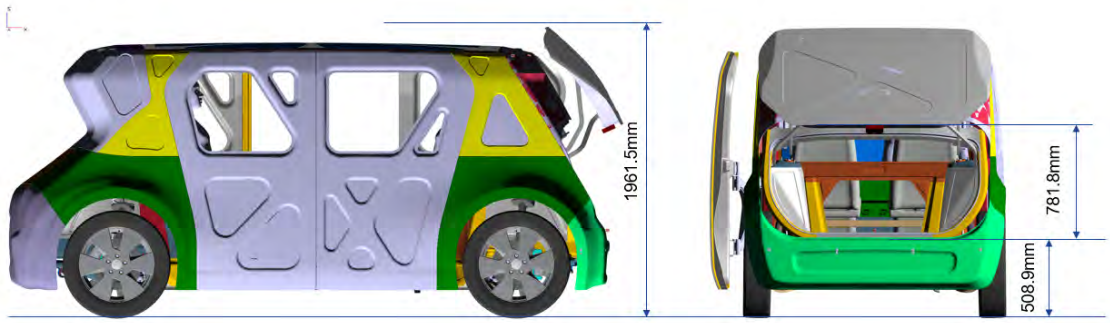

Figure 7.4.2.1 Rear coach door tailgate key dimensions

Rear Tailgate (coach) Door Structure	
Geometry/design	
Part 1 A SURFACE OUTER	0.7mm CR280Y/400T-BH / cold stamp
Parts 2: HORIZONTAL DOOR STRUTS (FRONT AND REAR)	1.2mm MILD STEEL 140/170 cold stamp

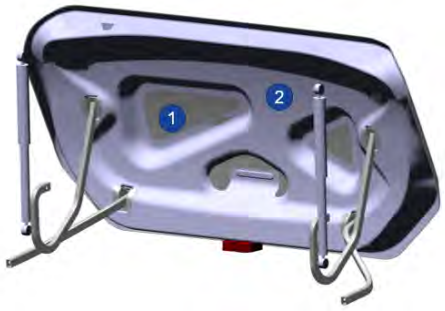

Figure 7.4.2.2 Rear coach door tailgate AHSS grades (See Appendix 4 for larger image)

7.5 Steel E-Motive body in white manufacture and assembly process

The stamping feasibility for the most challenging parts (shape and grade) of the body structure were developed and assessed with the assistance of Autoform stamping simulation software. This was a parallel activity during the design of the body structure. An example of the output from the Autoform stamping simulation is shown in Figure 7.5.1, and the results for the panels evaluated are shown in Appendix 2.1.

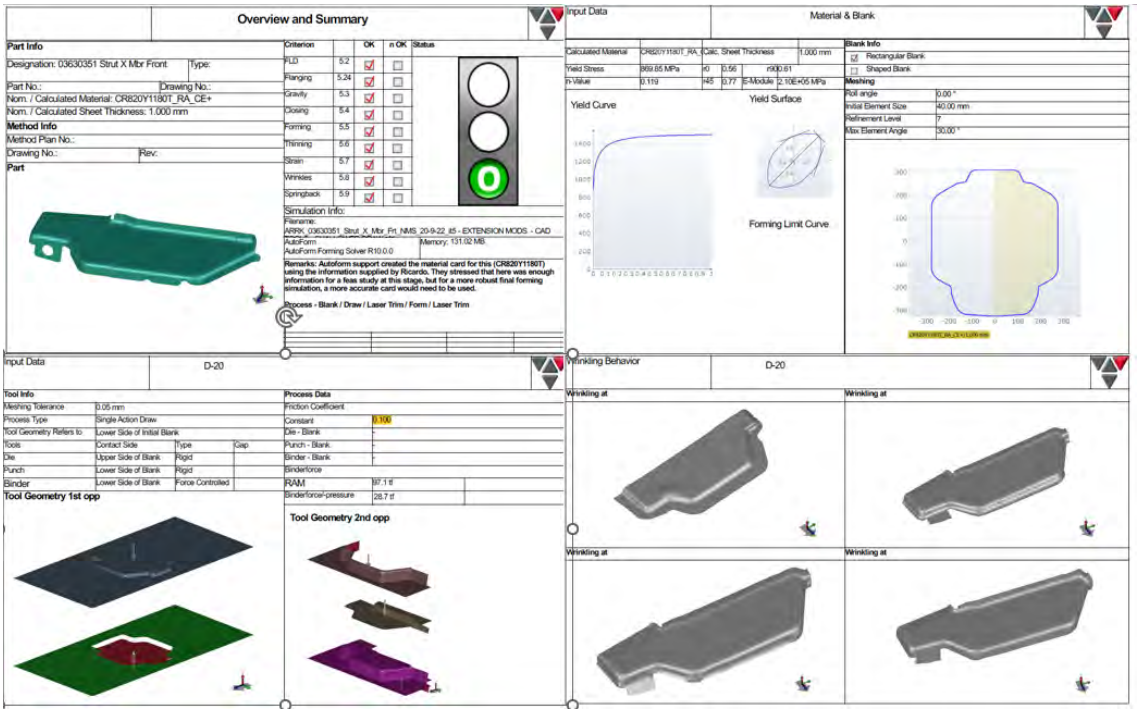

Figure 7.5.1 Example from Autoform stamping simulation output

The Steel E-Motive vehicles have been engineered for high volume production, with an expected capacity of 250,000 vehicles per year, at any global manufacture facility. To achieve the high-volume capacity, conventional body and vehicle assembly processes and procedures have been employed. The body structure is divided into assemblies and sub-assemblies that facilitate the efficient assembly of the body structure. The complete sub-assemblies and body structure assembly process is described in Appendix 2.2. A summary of the main BIW sub assemblies is shown in Figure 7.5.2.

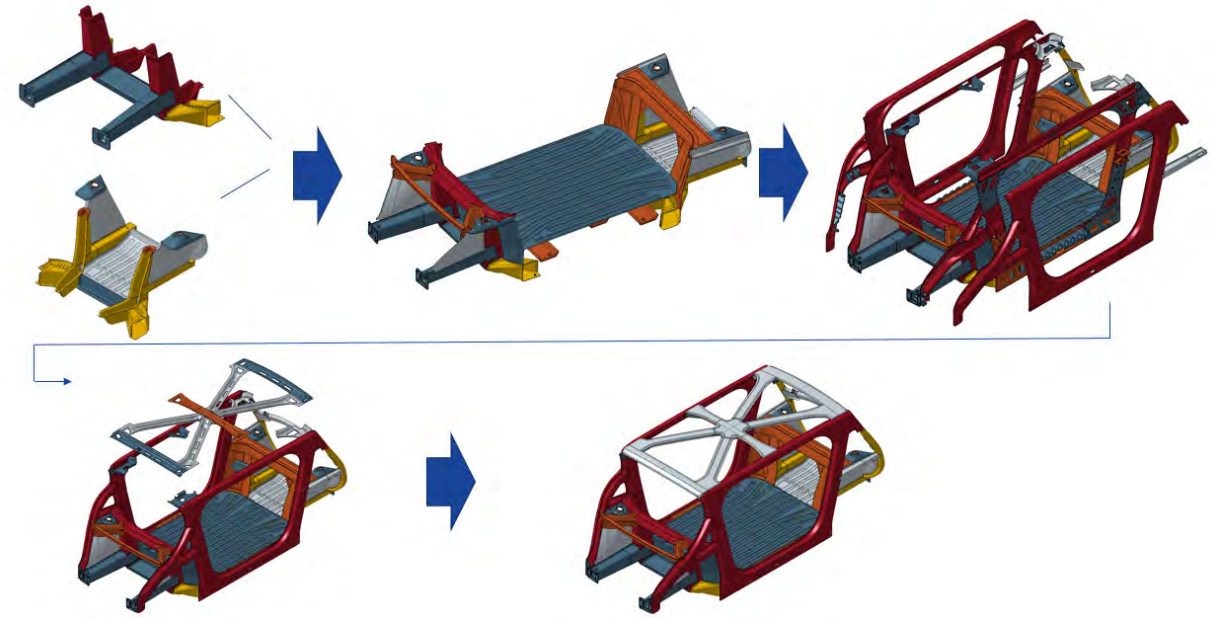

Figure 7.5.2 BIW sub-assemblies (See Appendix 3 for complete body assembly and sub-assembly definition)

7.6 SEM1 body structure cost evaluation

7.6.1 Introduction and approach for cost evaluation

A full costing evaluation of the SEM1 body structure, including BIW, closure, bumper beams and battery frame was undertaken using a modified Excel tool, originally created by The Massachusetts Institute of Technology (MIT). The tool was updated with the material prices at the time of the project. The Covid-19 pandemic saw some significant fluctuations in material prices. The final material prices applied were from November 2022 period, when the disturbance from the pandemic had largely abated. Material costs are defined in the model with a base material price, such as hot or cold steel, then additional price premiums for the specific steel grade (e.g. BH, HSLA, DP, CP, RA, DH, PHS, MS), coatings and finish (hot dip galvanic, AlSi, A surface), tailor welded & tailor coil premium and tube stock premiums. A material scrap price enables cost recovery for return scrap. Nominal vehicle parameters such as powertrain type, overall dimensions, production volumes and platform sharing are defined, along with manufacturing inputs such as energy costs, worker salaries, building and maintenance costs. The body structure is largely defined from the Bill Of Materials, containing material grade, gauge and weight. The part blank sizes are defined, enabling an estimation of part material usage and scrap. The part manufacturing processes are defined, such as blanking, trimming, stamping and rework, roll forming, hydroforming. Different stamping machines can be selected depending on the part size and complexity. The costing tool calculates body structure total cost, and breakdowns for material cost, manufacturing costs and paint costs. The tool also makes an interpolation on total vehicle cost.

7.6.2 SEM1 cost estimates

Figure 7.6.2.1 shows the costing tool calculations for SEM1 body structure and vehicle

	Body structure parts cost ($) *1	Paint costs ($)	Assembly costs ($)	Total body structure cost ($)	Total Vehicle MSRP ($) *2
BIW	1203	130	146	1818	40,406
Battery frame	154				
closures	186				
Total	**1543**				

*1 includes: Equipment, Tooling, Building, Maintenance, Energy, Labour, Overhead, Process, Materials (excludes: assembly & paint costs)

*2 includes approximates for battery, powertrain, electrical, interior, chassis. Does not include costs for autonomous vehicle systems (such as radar & lidar)

Figure 7.6.2.1 SEM1 body structure and vehicle cost estimates

Figure 7.6.2.2 shows the contributions to the body in white parts costs

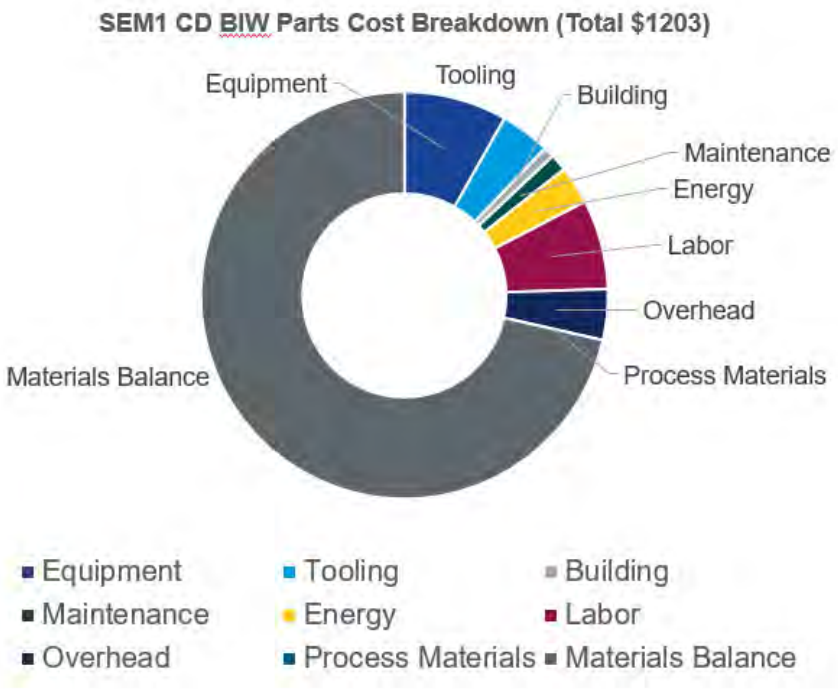

Figure 7.6.2.2 SEM1 Body in White parts cost contribution

Figure 7.6.2.3 shows a pareto of the highest 45 part costs in the SEM1 BIW

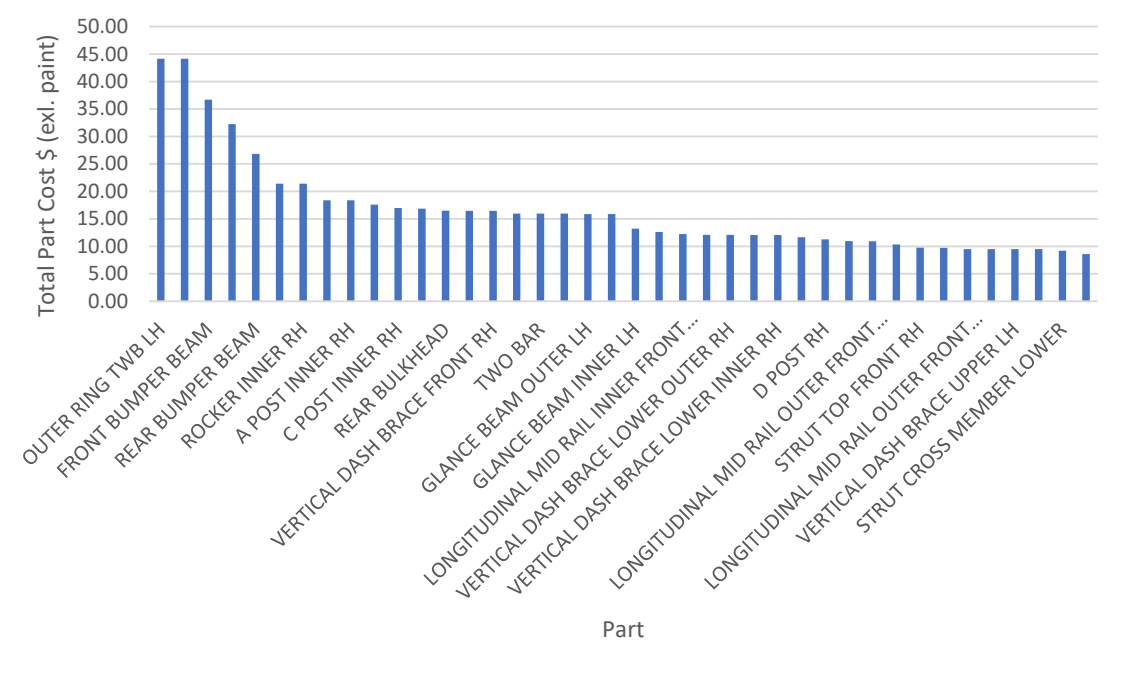

The following cost saving measures were introduced to the body structure design throughout the development of SEM1

- Use of conventional high volume steel stamping, fabrication and assembly methods
- Deletion of the BIW body side outer panel. The side closures cover much of the body side outer surface, hence it was therefore deemed that a low grade (BH/HSLA) body panel with specific purpose to be the A surface would be redundant and not required. The quality of the visible PHS panel when the doors are in the open position as deemed to be acceptable. Lightweight cover/garnish trim panels could be added to areas where the surface quality was deemed unacceptable. In addition to the cost saving, an estimated weight reduction of 26kg is achieved by deletion of the body side outer panels
- SEM1 and SEM2 battery housing features innovative “coverless” housing. The BIW floor assumes the role of the battery top cover
- BIW weight saving. SEM1 is estimated to be 25% lower in weight than a vehicle of similar dimensions. The weight saving would also equate to a reasonable cost saving.
- Use of AHSS grade qualities to achieve greater part integration, resulting in a lower number of part and lower tooling costs. An example of this is the front torque box, where the high formability and high strength characteristics of Retained Austenite AHSS enabled an existing 3 part assembly to be converted to a lower cost 2 part assembly.

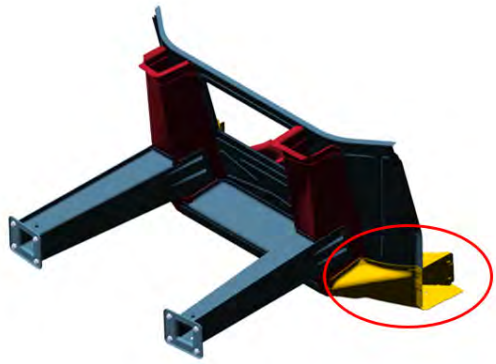

2 part FRONT TORQUE BOX (INNER & OUTER)
1.0mm CR8501180T-DH

7.7 Body in white alternative AHSS grades and fabrication processes study

The AHSS selected for the final concept design of SEM1 were based on the engineering and performance requirements, such as strength, durability, formability, cost and weight. Given the breadth of AHSS available, it is widely acknowledged that there could be multiple alternative grade and fabrication solutions for a given part. To demonstrate this, an "alternative AHSS grades" study was performed. Each part in the BIW was review and assessed with respect to it's performance requirements and potential for alternative AHSS grade and fabrication process. Alternative grades and processes were assigned on a subjective basis (additional CAE analyses would be required to confirm the feasibility of the alternative grades). The complete Bill of Materials for the alternative AHSS grades study is in Appendix 1B. A narrative on the selection and justification of alternative AHSS grade and process is provided in the BoM. Figure 7.7.1 shows the comparison AHSS grade distribution of the SEM1 BIW baseline (or "core") design compared to the alternative grades. Appendix 1.5 shows the BIW Bill of Materials for the alternative grade configuration.

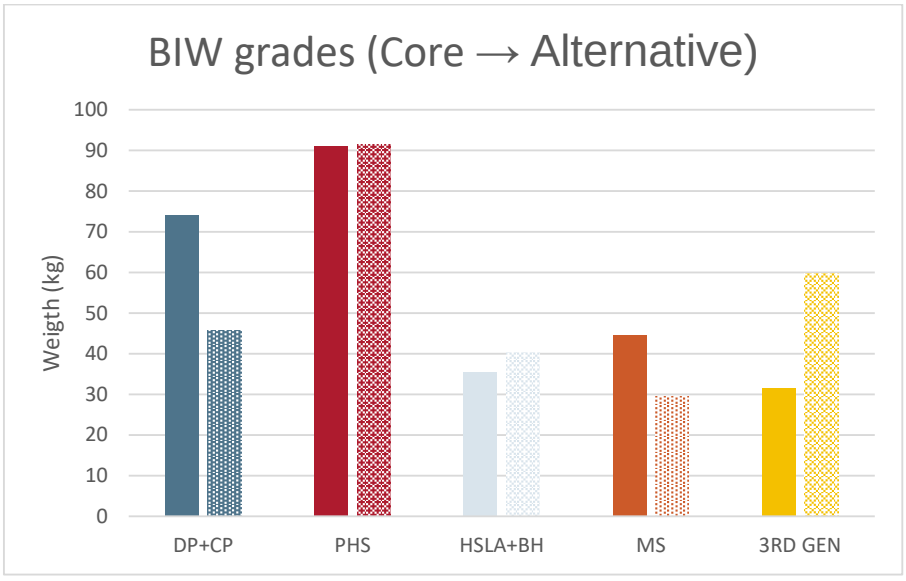

Figure 7.7.1 Comparison of AHSS grade use in SEM1 "core design" BIW and alternative grades

8.0 SEM1 performance

8.1 Introduction & overview

This section describes the specification and performance of the final SEM1 design. For reference and completeness, the results are presented in table and graphical formats.

8.1.1 Vehicle dimensions, exterior & interior

(refer to Section 7.13 and Section 11.0 SEM2 and comparison to SEM1 vehicle dimensions)

8.2 Front crashworthiness

	Vehicle Crashworthiness			
	Loadcase	Target Value	Result Value	Comments
Front (core loadcases)	US - NCAP 56 km/h FFB	<35 G Deceleration	33.1	- progressive, controlled collapse of crush rail - front subframe collapse encourages EDU ride down, reducing impact to front bulkhead
		< 40 mm bulkhead intrusion	2.5	- see Figure 8.2.2
	IIHS 64 km/h 40% ODB	<35 G Deceleration	20.5	Targets described in Figure 4.2.3.
		Footwell intrusion (1,2,3) < 150mm	1) 2.4 2) 4.1 3) 1.4	Intrusion values are within IIHS "good" rating
		Bulkhead Intrusion (4,5) < 50mm	4) 3.4 5) 5.2	- see Figure 8.2.3
		A pillar Y intrusion (6,7) >180mm clearance to seat centreline	6) >180mm 7) >180mm	
		No contact body structure to battery	(no contact observed)	
	IIHS 64 km/h 25% SORB	<35 G Deceleration	19.9	- IIHS "good" rating achieved. Vehicle exhibits "glance off" motion with 420mm lateral deflection - intrusion levels close to target but within 75mm IIHS "good" target
		Footwell intrusion (1,2,3) < 150mm	1) 2.0 2) 2.4 3) 4.2	- very stable A pillar and door ring - see Figure 8.2.4
		Bulkhead Intrusion (4,5) < 75mm	4) 53.8 5) 48.9	
		A pillar Y intrusion (6,7) >180mm clearance to seat centreline	6) >180 7) >180	
		No contact body structure to battery	(no contact observed)	
Front (reference loadcase)	OEM Centre Rigid Pole 64km/h, 253mm Pole	<40 G Deceleration	39	<40g pulse for all loadcases < 70mm dash intrusions
		< 80 mm bulkhead intrusion	1.6	Passenger cell integrity remains good
	NHTSA 90kph 35% 15 degree oblique	<40g	31.9	- see Figure 8.2.5 to 8.2.7
		<80mm intrusion	70	
	NCAP - MPDB	<40 G Deceleration	33.3	
		< 80 mm bulkhead intrusion	1.3	

Figure 8.2.1 SEM1 front crashworthiness results (from full vehicle simulation)

USNCAP 56kph 0 degree frontal rigid barrier (FFB)	
Model level	V06v001
Peak pulse (g)	33.1 g (@ B pillar) sliding mean
Peak intrusion (mm)	2.5 mm

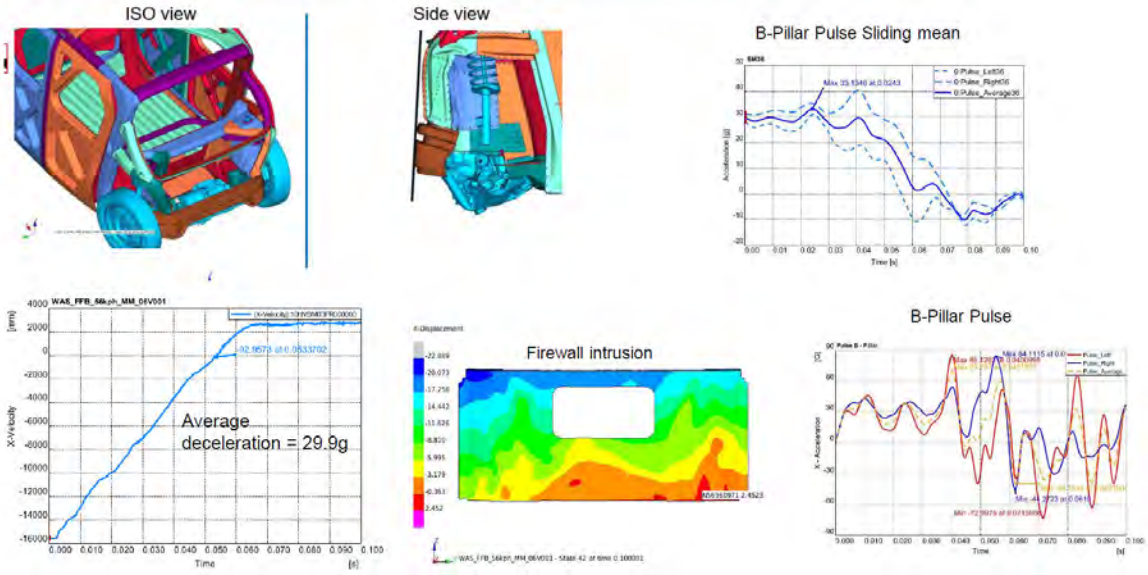

Figure 8.2.2 SEM1 USNCAP 50kph front FFB crash simulation results

IIHS 64kph 40% Moderate Overlap (Offset Deformable Barrier "ODB")	
Model level	V06v001
Peak pulse (g)	20.5 g (@ B pillar) sliding mean
Peak intrusion (mm)	17.6 mm

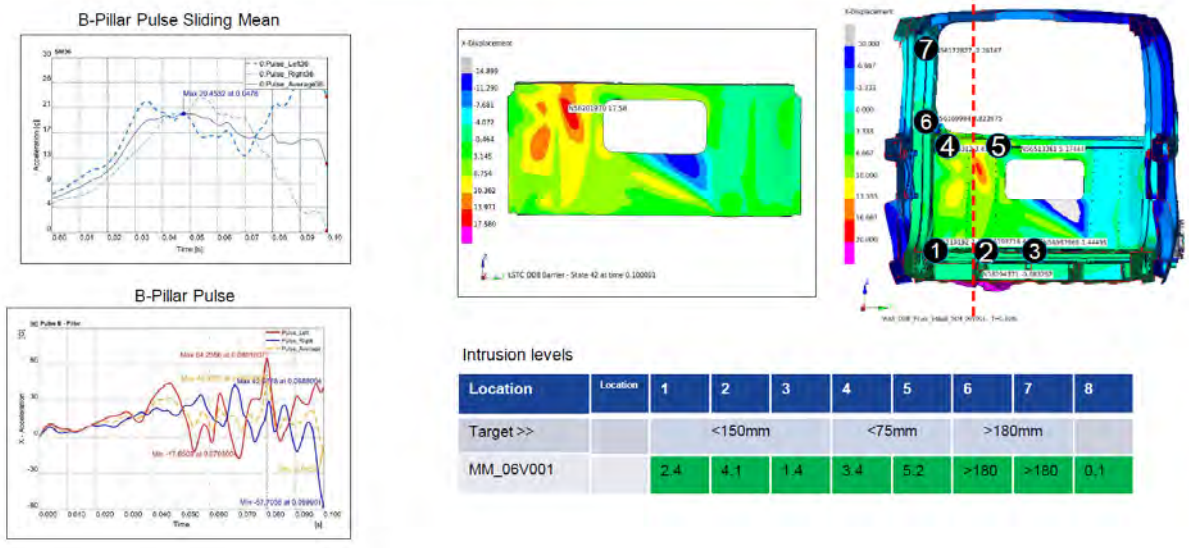

Intrusion levels

Location	Location	1	2	3	4	5	6	7	8
Target >>		<150mm			<75mm		>180mm		
MM_06V001		2.4	4.1	1.4	3.4	5.2	>180	>180	0.1

Figure 8.2.3 SEM1 IIHS 64kph ODB crash simulation results

IIHS 64kph 25% Small Overlap (Small Offset Rigid Barrier "SORB")	
Model level	V06v001
Peak pulse (g)	19.9 g (@ B pillar) sliding mean
Peak intrusion (mm)	74.6 mm

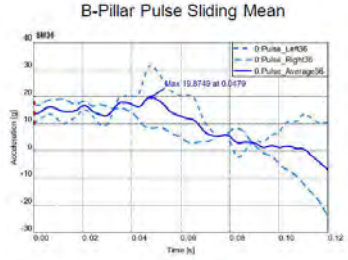

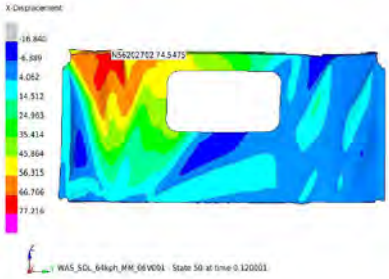

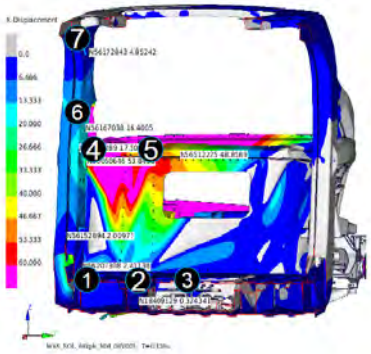

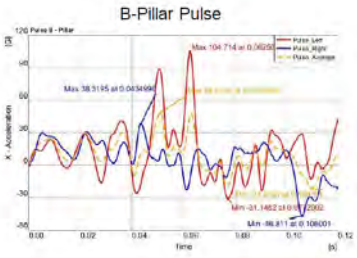

Location	1	2	3	4	5	6	7	8
Target >>	<150mm			<75mm		>180mm		
MM 06V001	2.4	2.0	4.2	53.8	48.9	>180	>180	0.3

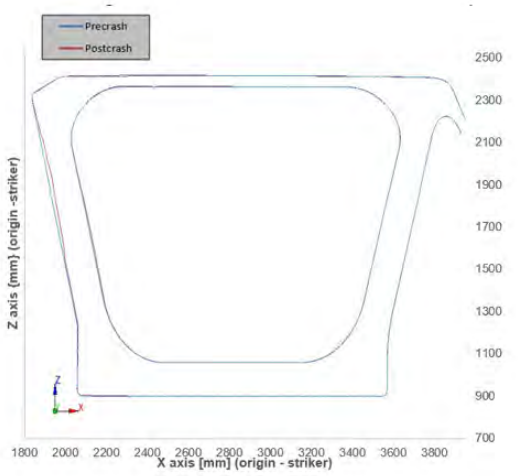

Figure 8.2.4 SEM1 IIHS 64kph front SORB crash simulation results

Reference Loadcase: Front 64kph Rigid Pole	
Model level	V06v001
Peak pulse (g)	39.0 g (@ B pillar) sliding mean
Peak intrusion (mm)	1.6 mm

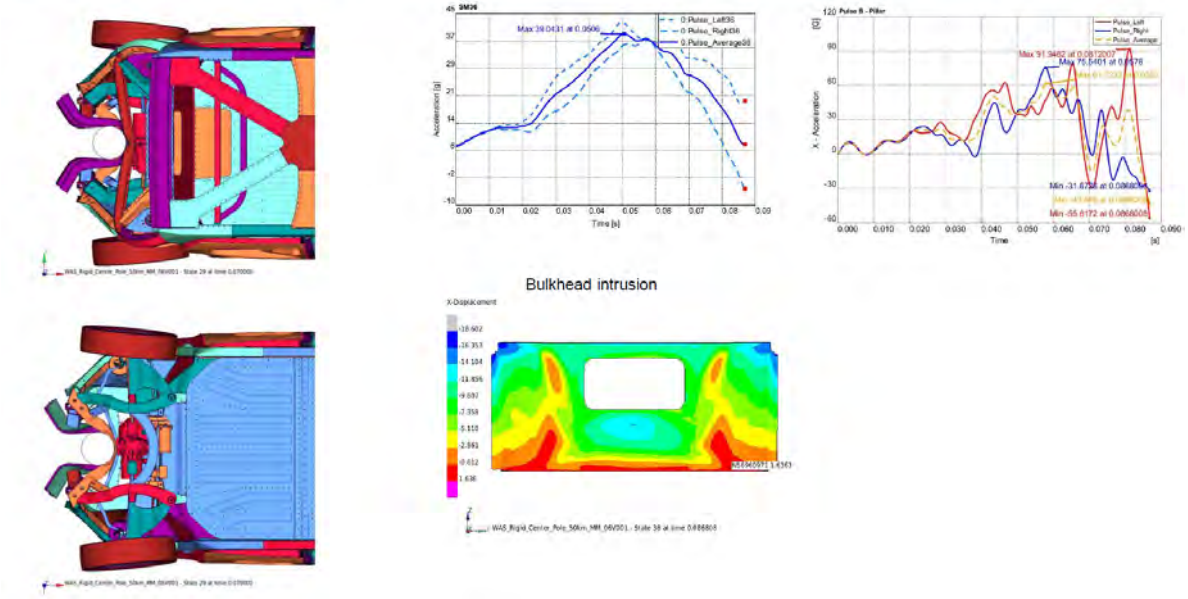

Figure 8.2.5 SEM1 Front 64kph 254mm rigid pole crash simulation results

Reference Loadcase: NHTSA front 90kph Oblique Moving Deformable Barrier (OMDB)	
Model level	V06v001
Peak pulse (g)	32.0 g (@ B pillar) sliding mean
Peak intrusion (mm)	70.1 mm

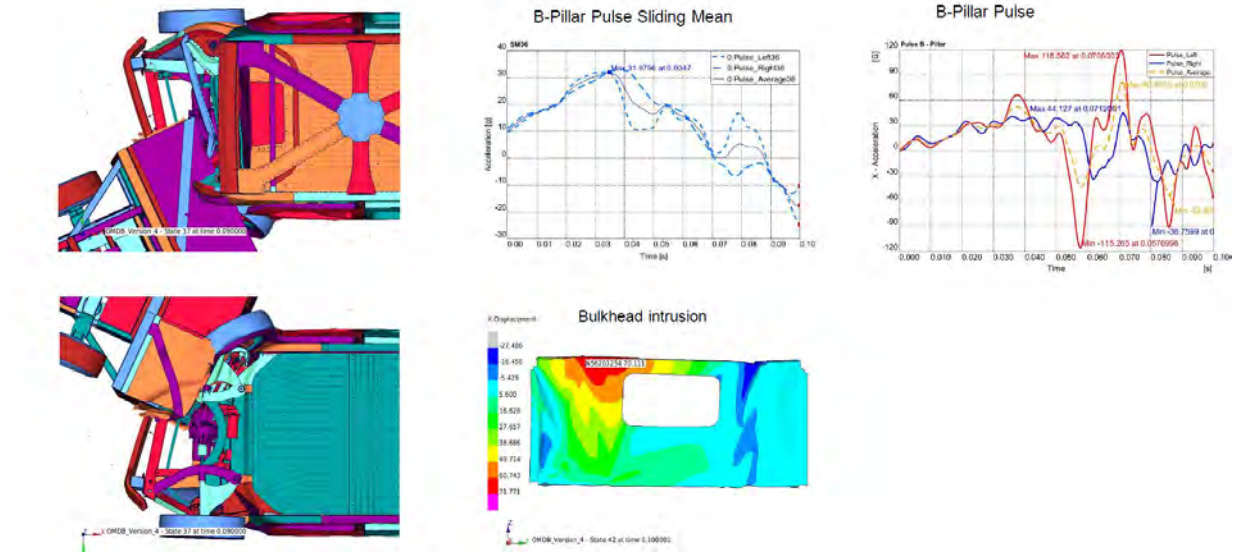

Figure 8.2.6 SEM1 NHTSA 90kph front OMDB crash simulation results

Reference loadcases. Euro NCAP MPDB, 50km/h	
Model level	V06v001
Peak pulse (g)	33.3 g (@ B pillar) sliding mean
Peak intrusion (mm)	1.4 mm

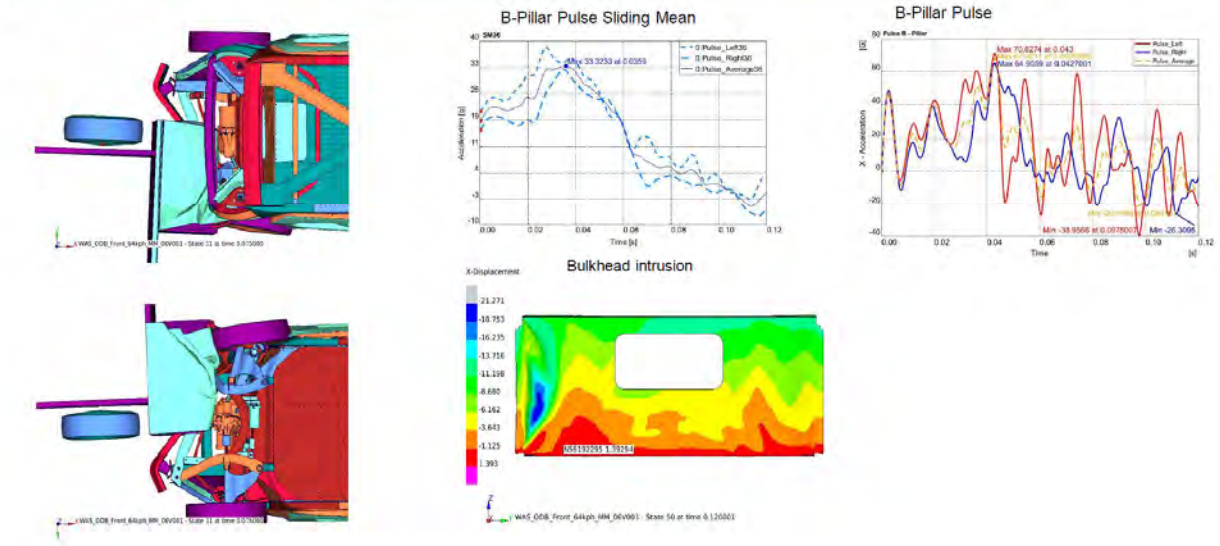

Figure 8.2.7 SEM1 EuroNCAP 50kph Front Moving Progressive Deformable Barrier (MPDB)

8.3 Side crashworthiness

	Vehicle Crashworthiness			
	Loadcase	Target Value	Result Value	Comments
Side	SIDE IIHS 60 km/h MDB	"good" = >180mm intrusion clearance to driver seat c/l	296	Occpant intrusion clearance is compfortably achieved (note IIHS 2 barrier). = IIHS "good" rating >30mm intrusion clearance to battery
	SIDE US-NCAP 32km/h Rigid pole D254mm	(IIHS side barrier intrusion targets >180mm clearance)	236	- Occupant intrusion levels are acceptable (by applying IIHS intrusion guidelines to USNCAP pole) - > 30mm clearance to HVC battery achieved
		> 30 mm clearence inner rocker to battery module	33	

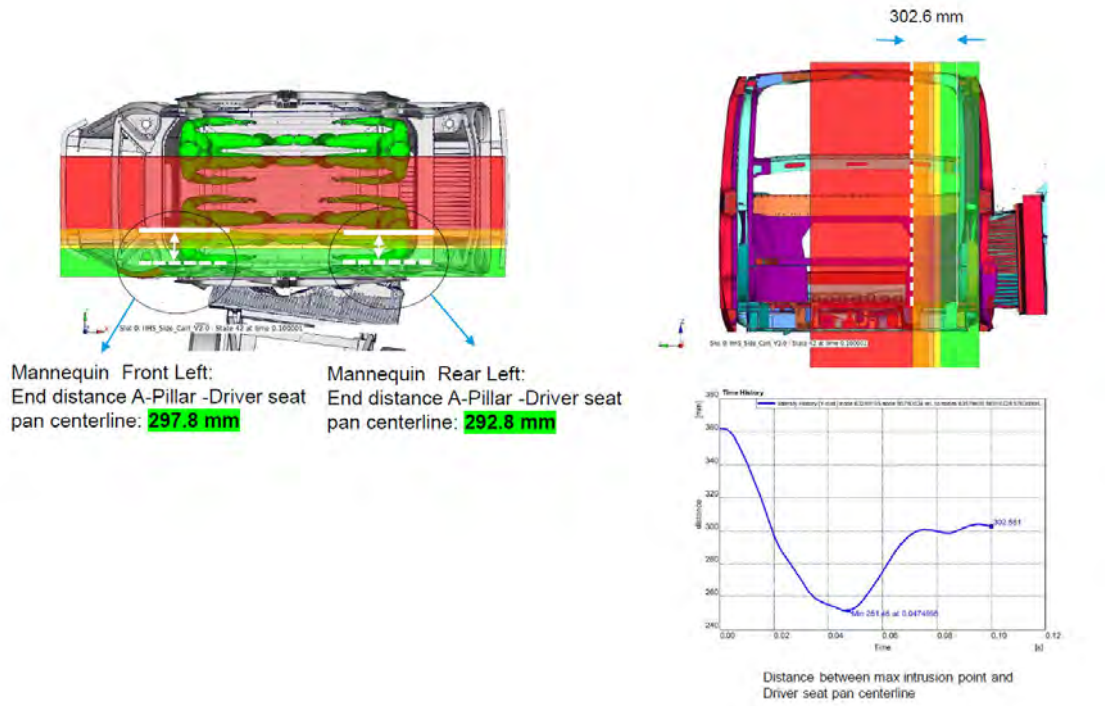

Figure 8.3.2 IIHS 60KPH side barrier (II) crash simulation results (See Appendix 4 for larger image)

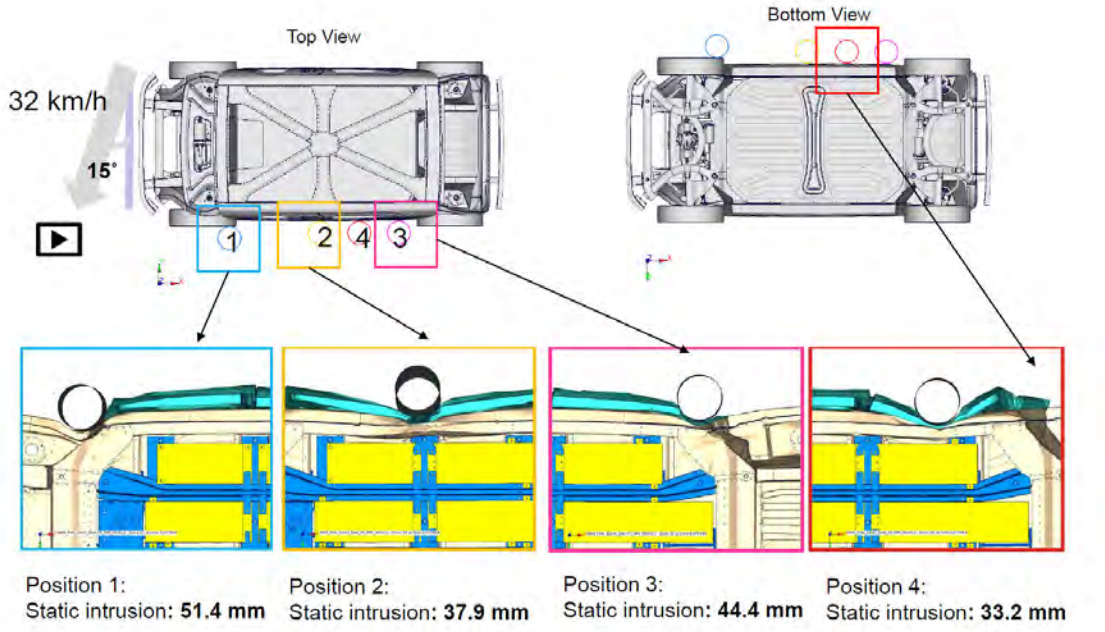

Figure 8.3.3 USNCAP 32kph side pole crash simulation results, battery protection (See Appendix 4 for larger image)

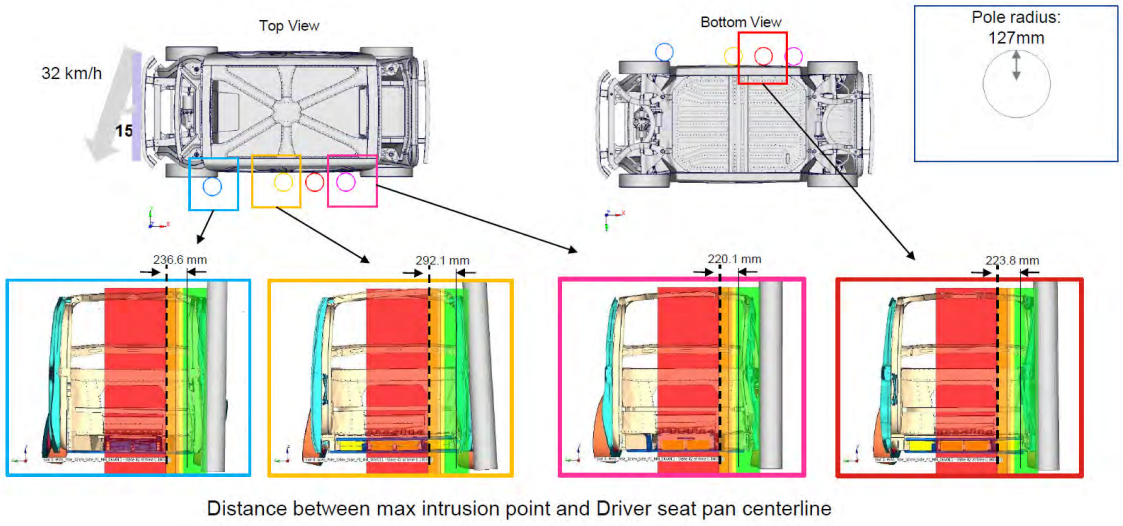

Figure 8.3.4 USNCAP 32kph side pole crash simulation results, occupant protection (See Appendix 4 for larger image)

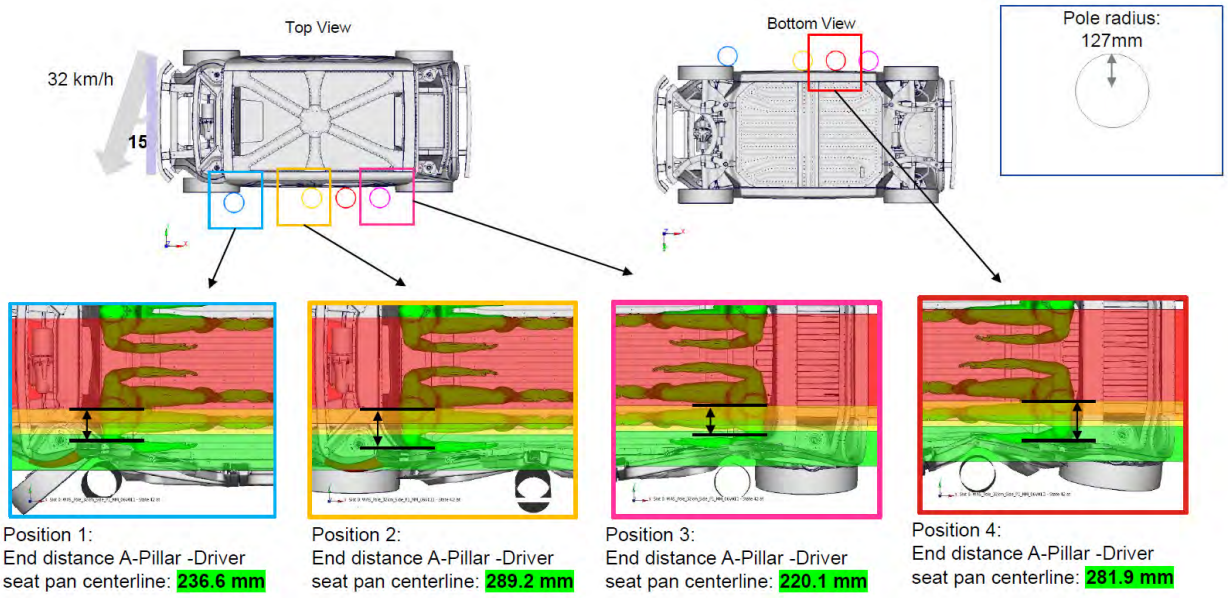

Figure 8.3.5 USNCAP 32kph side pole crash simulation results, occupant protection (See Appendix 4 for larger image)

8.4 Rear crashworthiness, FMVSS305 EV

Rear FMVSS305 EV, 80kph 70% Deformable barrier	
Model level	V06v001
Peak pulse (g)	21.9 g (@ B pillar) sliding mean
Peak intrusion (mm)	30.5 mm

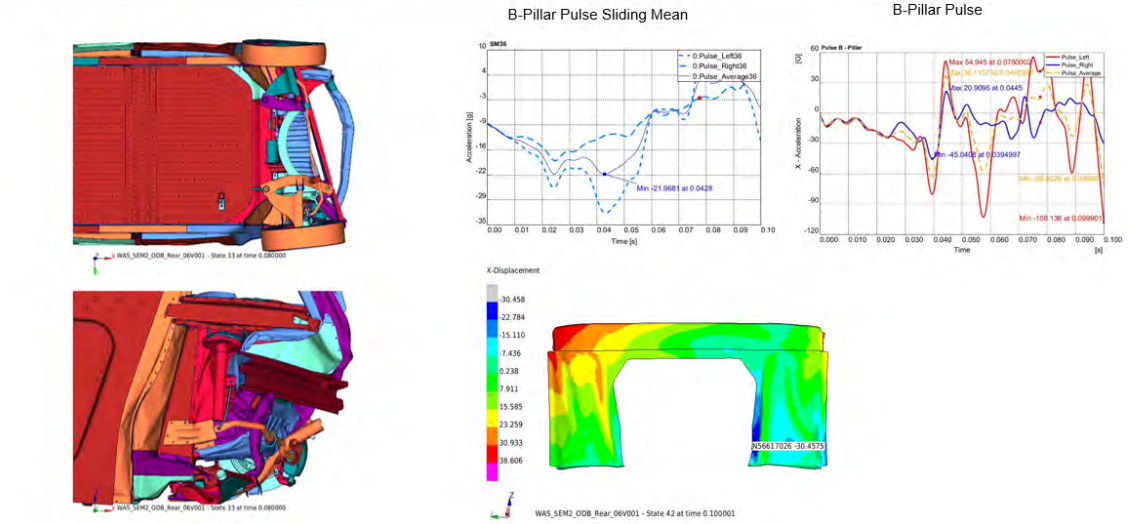

Figure 8.4.1 Rear crash simulation results, FMVSS305 EV

8.5 Roof crush

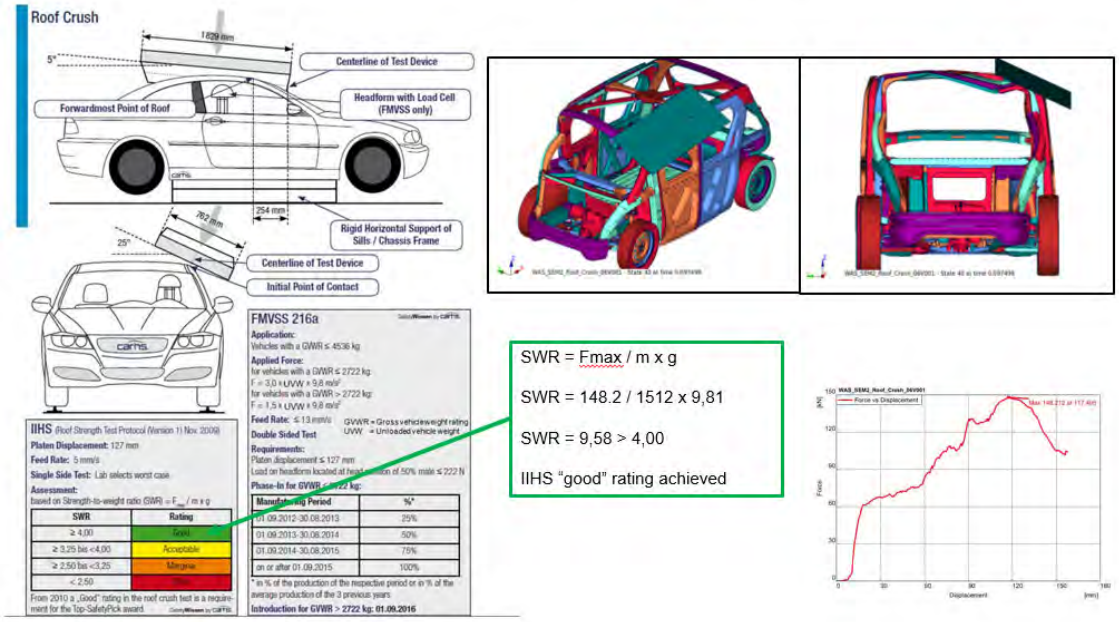

Figure 8.5.1 Roof crush strength simulation results

8.6 Vehicle and subsystem weight

Subsystem	SEM 1 weigth (kg)	*Comment*
Body non-structure	*177.2*	Estimated from a2mac1 statistical analysis. Includes seating, trim panels, glazing, front end clip, exterior panels
Body In White	*282.0*	<CD> design from CAD
Front sub-frame	*16.5*	<CD> design from CAD
Battery case (structure)	*59.0*	<CD> design from CAD
Rear sub-frame	*10.2*	<CD> design from CAD
Front suspension	*114.0*	Design New Architecture
Rear suspension	*114.0*	Design New Architecture
Braking	*59.7*	Estimated from a2mac1 statistical analysis
Steering	*26.0*	column, EPAS etc)
Tires and wheels	*84.0*	Estimated from a2mac1 statistical analysis
Motor Trans Front	*63.0*	Estimated from a2mac1 statistical analysisk and Fiat 500e
Motor Trans Rear (N/A SEM1)		Estimated from a2mac1 statistical analysis and technology roadmap
Battery system less case	*245.6*	Ref BOM including 5kg of fluids, busbars, cooling plate, modules and PDU
Propusion controls	*60.0*	Estimated from a2mac1 statistical analysis
Electrical-non propulsion	*35.7*	Estimated from a2mac1 statistical analysis
Cooling and heating	*30.0*	Estimated from a2mac1 statistical analysis (+BYD HAN EV, Xpeng P7 vehicles)
Closures	*109.3*	<CD> design from CAD
Bumpers	*26.0*	Estimated from benchmark regression (Xpeng P7 vehicles)
Vehicle Curb Weight	**1512**	
Maximum payload	500	based on 4 occupants and luggage
Gross Vehicle Weight GVW	**2012**	

8.7 Body in White Stiffness and NVH

BIW Stiffness & NVH			
Item	**Target Value**	**Result**	**Comments**
BIW Weight (kg)	<309	282	
Static Torsional Stiffness (kNm/deg) (kNm/deg)	>25	63.285	63,285Nm/deg is trimmed BIW (including battery, subframes, bumper beam). 43,000Nm/deg BIW only
Static Vertical Bending (kN/mm)	>9	13.438	trimmed BIW
1st Mode (trimmed) Hz	>28	32	32Hz = first lateral body mode
Installed battery 1st mode (Hz)	>35	35	trimmed BIW
Dynamic attachment point stiffness (inertance / point mobility)	>5-10x bush stiffness	OK	target achieved

8.7 BIW durability

Results from static FEA assessment.

	Loadcase	Max stress (MPa)	Location	Comment
Fatigue	Braking fatigue	127	F1	Predicted stresses are within material fatigue limits
		140	R1	
	Acceleration fatigue	111	F1	
		170	R1	
	Cornering fatigue LH	180	F2	
		194	R1	
	Settling at GVW-proof	106	F1	
		147	R1	
	Max rebound	134	F1	
		215	R1	
	Limit forward braking	236	F3	
		122	R1	
Abuse	Limit cornering LH	248	F2	
		163	R1	
	Vertical 30deg positive fatigue	364	F1	
		507	R1	
	Max bump and braking	341	F1	
		440	R1	
	Pothole braking	474	F3	
		597	R1	

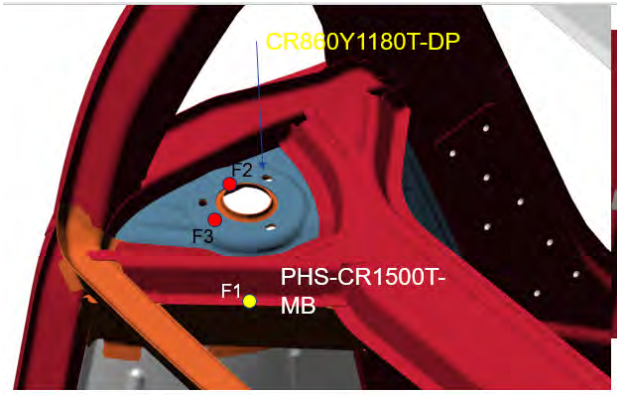

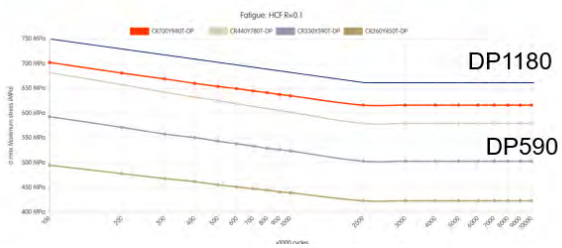

8.10 Body system cost evaluation

	Body structure parts cost ($) *1	Paint costs ($)	Assembly costs ($)	Total body structure cost ($)	Total Vehicle MSRP ($) *2
BIW	1203	130	146	1818	40,406
Battery frame	154				
closures	186				
Total	**1543**				

*1 includes: Equipment, Tooling, Building, Maintenance, Energy, Labour, Overhead, Process, Materials (excludes: assembly & paint costs)

*2 includes approximates for battery, powertrain, electrical, interior, chassis. Does not include costs for autonomous vehicle systems (such as radar & lidar)

8.11 Battery structural performance

HV Battery			
Item	**Target Value**	**Results Status**	**Comments**
Battery Pack Power SEM1 (kWh)	>75	75	
Pack Energy Density Wh/l Wh/kg	2022 - 165-270Wh/l 11-224Wh/kg	 622Wh/l (mod) 377Wh/kg (mod) 280Wh/l (pack) 266Wh/kg (pack)	Wh/l - >600Wh/l for Module Wh/kg - >300Wh/kg for Module
ECE R100 Vibration/Fatigue	Endurance Stress of Material selection	Pass	
ISO 12405-2 PSD Random Vibration	Endurance Stress of Material selection	Pass	
GB/T 31485 and 31467 Crush	Pass/Fail	Pass	
Intrusion - Jacking	J - 50% GVW (50mm coin)	Pass	
1st battery Modal (Hz)	>35	35	
Battery Pack Mass (kg)	<360	304	
Battery Enclosure Mass (kg)	<70	59	

9.0 Sustainability and Lifecycle Analysis

9.1 Introduction

The contribution of transportation modes to greenhouses gas (GHG) emissions, and hence global warming, is well documented and understood. Vehicle OEMs, fleet operators and transport users all have responsibilities to limit individual and collective environmental impacts to the planet, and contribute to meeting national and global climate change mitigation objectives. Mobility as a Service transport solutions such as Steel E-Motive have the potential to contribute to the net reduction in GHG emissions and help achieve these global targets and also specific policy objectives.

Life Cycle Assessment (LCA) is a methodology that considers a product's entire life cycle, with cradle-to-grave assessments typically utilising a boundary to include impacts from raw material extraction and production (manufacturing phase), through its useful life (use phase), and to the end-of-life disposal or recycling of the product (end-of-life phase). It also takes into account the full life cycle of energy sources used across all lifecycle phases. This LCA approach was applied throughout the development of the Steel E-Motive concept.

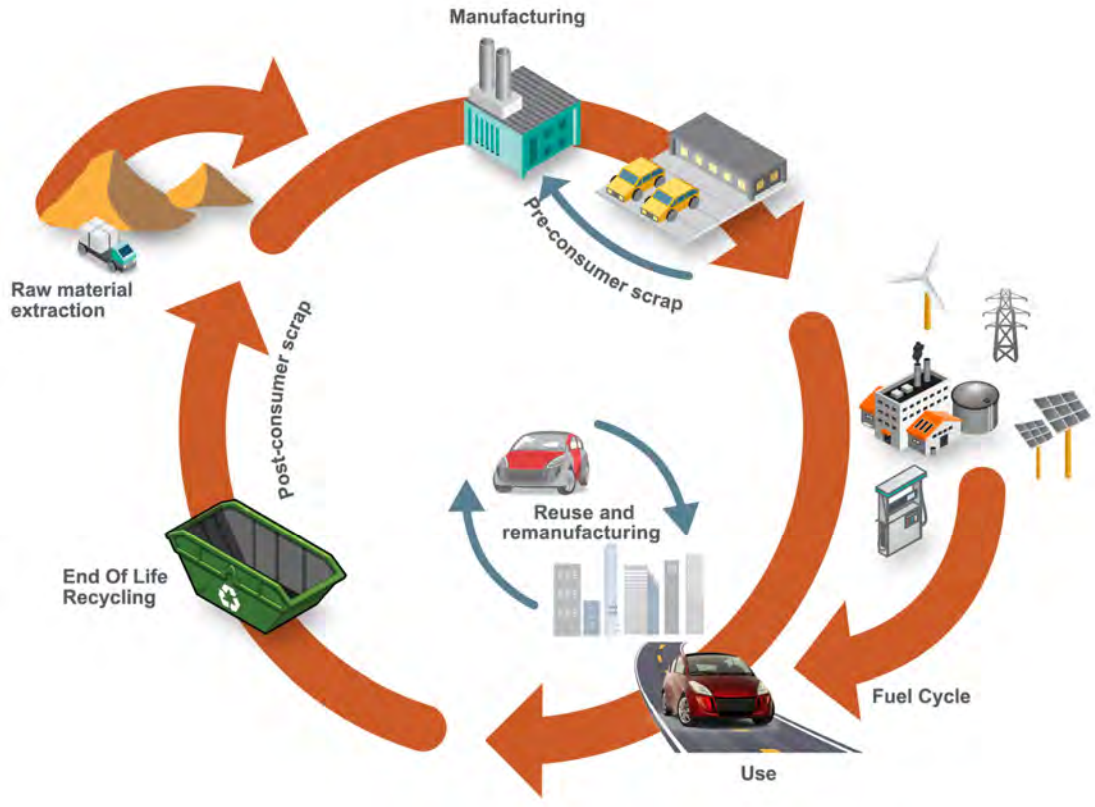

Figure 9.1.1 Life Cycle Assessment, considering the entire life of the vehicle, from raw material extraction to end of life

LCA can cover a range of environmental impacts; in this study the focus was on GHG emissions (through the GWP-100 indicator) and total energy consumption (through the Cumulative/Primary Energy Demand and Fossil Energy Consumption indicators).

The GHG emissions and total energy contributions from the vehicle manufacture and assembly, vehicle use and end of life/recycling phases were calculated using a Microsoft Excel

LCA tool created for WorldAutoSteel by Dr. Roland Geyer at the University of California Santa Barbara (UCSB). As the specific LCA calculation processes, guidelines and legislation is currently being defined and the MaaS vehicle have the potential to operate in different modes and regions, a calculation sensitivity approach was applied which demonstrated the influence of different vehicle operational boundary conditions, manufacture and design considerations on the total vehicle GHG values. The LCA results for the Steel E-Motive vehicle and sensitivities were compared to a present day “reference” battery electric vehicle (BEV).

9.2 Lifecycle Analysis Technical Approach and UCSB tool enhancements & adjustments for Steel E-Motive

The primary inputs to the UCSB LCA tool are: general vehicle specification, such as powertrain type (BEV), vehicle size/category (B-C segment), vehicle drive cycle type (WLTP) and total life (mileage). A breakdown of the approximate vehicle material composition is also required. The UCSB LCA tool has embedded datasets and formulae which are combined with the specific vehicle inputs to calculate GHG (kg CO_2 equivalent) and total primary energy consumption (Mega Joules). The embedded datasets include material CO_2 emissions (per kg), vehicle drive cycle energy consumption, fossil fuel embedded emissions, electricity grid supply CO_2 and calculations for the end of vehicle life contributions, using different approaches and methodologies.

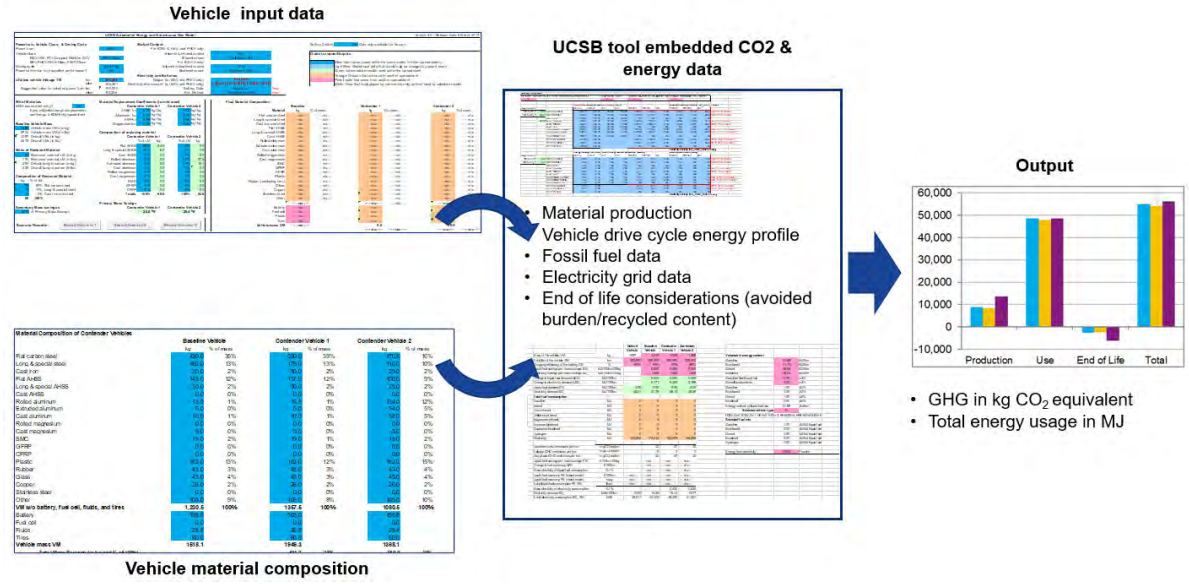

Figure 9.2.1 UCSB Life Cycle Analysis tool data flow (See Appendix 4 for larger image)

Vehicle life cycle performance can vary considerably depending on where the vehicle is manufactured and operated. To account for this, life cycle performance of the Steel E-Motive concept was calculated for Europe, US, China, Japan and India regions.

With the Steel E-Motive concept assuming a hypothetical manufacturing date of 2030, a number of specific enhancements and additional datasets were added to the UCSB model, summarised below (specific details of the enhancements are reported later)

- **Steel and Aluminium primary production:** “Baseline” (non-decarbonised) values contained within the UCSB dataset were validated and checked. Steel and aluminium makers are making significant progress in the decarbonisation of primary materials. By

2035, a significant proportion of the material in a vehicle construction is expected to be manufactured using decarbonised production methods. The UCSB tool was updated with decarbonised (or "green") steels and aluminium. These were calculated using GaBi simulation tools and validated with WorldAutoSteel members.

- **Propulsion battery production emissions data**: Whilst the Steel E-Motive concept features a purposefully "agnostic" battery technology and chemistry, the LCA model dataset was updated to include future forecasts and projections of battery decarbonisation potential. Data from Ricardo's collaborative research programmes on battery decarbonisation were included.
- **Electricity grid supply mix and associated GHG emission values:** With the Steel E-Motive vehicle being battery electric propulsion, the energy source for the vehicle during its use phase is provided by 100% electricity grid supply. With increasing amounts of renewable energy (such as wind and solar power) being deployed in grid networks, the potential for vehicle GHG emissions during the use phase could be reduced significantly. The electricity grid mix estimates in the UCSB model were updated with forecasts up to 2040 using data from the International Energy Agency (IEA World Energy Outlook, 2021) (IEA, 2021).
- **Vehicle life cycle performance:** This is usually calculated and reported in total kg CO_2-eq (greenhouse gases expressed in units of carbon dioxide equivalents), and MJ (total primary energy, expressed in units of oil equivalents). Mobility as a Service (MaaS) and ride hailing vehicles target increased utilisation and occupancy rates enabling journey cost savings for the user and reducing traffic congestion. This is also results in net vehicle life cycle emission reductions, as fewer vehicles are required to transport the same or a greater number of people. MaaS vehicles may also have a longer lifetime (total kilometers) than private or taxi vehicles, resulting in lower overall life cycle emissions, as this may result in a lower number of vehicles produced, with lower production greenhouse gas emissions. To account for this, the metric/measurement applied for the Steel E-Motive LCA calculations was changed to kg CO_2-eq per passenger-kilometer. The GHG emissions and total primary energy calculated for the total life cycle of the Steel E-Motive were divided by the average number of occupants assumed during the vehicle service life, multiplied by the total expected lifetime kilometers of the vehicle. This was deemed to be a more representative metric for MaaS vehicles and to demonstrate the importance and potential of ride sharing in addressing transportation contributions to GHG emissions.

For the LCA calculations and sensitivity studies, a number of different vehicle input parameters were evaluated. These are summarised and described in the table below.

LCA parameter	Value
description	Text description of the LCA model (e.g. "reference", "Steel E-Motive baseline"
Su-title Level 1	Further model description (e.g. "drivecycle smoothing" study
power train	(is Battery Electric for all vehicles in the LCA study)
% ethanol	(=0% for all (BEV) vehicles in the LCA study)
Vehicle class	(= "FSV A class" for all vehicles in the LCA study. This is standard option in UCSB tool
Driving cycle	Standard test drive cycle used for use phase calculation (e.g. WLTP)
Driving cycle smoothing reduction	% reduction in drive cycle energy, based on autonomous vehicle speed and throttle control potential
Lifetime km	Total expected life of vehicle (kilometers)
Battery lifetime (km)	Total expected life of propulsion battery (kilometers)
pyrometall. LIB recycling share	Propulsion battery recycling approach
Grid mix (both SDS and STEPS for future scenarios)	Electricity grid supply timeline (data from IEA)
Region	Vehicle operation (grid supply) location (Europe, US, Japan, China, India)
EoL method	LCA End of life methodology (avoided burden, recycled content)
"green" steel share	% steel of reduced carbon production steel used (100% = all steel used in vehicle is manufactured using decarbonised process)
"green" Al share	% of reduced carbon production aluminium used (100% = all aluminium used in vehicle is manufactured using decarbonised process)
Vehicle occupancy (ride sharing)	Number of vehicle occupants in LCA calculations

Figure 9.2.2 LCA model input parameters (See Appendix 4 for larger image)

- **Lithium-ion battery end-of-life recycling:** at the end of the vehicle's service life, its lithium-ion battery pack may be recycled in two main ways, either by feeding it to a high-temperature furnace (pyrometallurgical recycling), or by subjecting it to a series of wet chemical separation processes (hydometallurgical recycling). The former process is currently prevalent because it can use the same facilities that are already used for primary metal ore smelting; however, it is very energy demanding, and it does not allow the recovery of lithium or any of the of the lightweight battery components (e.g., the graphite anode). In contrast, the latter process is significantly less energy-intensive, and allows a high recovery rate for all battery materials; however, it is not yet commercially used on a large scale because the hitherto limited quantities of EoL EV batteries have not yet led to sufficiently lucrative economies of scale. In light of the above, a 50%/50% mix of pyrometallurgical/hydrometallurgical recycling was conservatively assumed for the EoL treatment of the batteries in the reference "present day" (~2020) battery electric vehicle (BEV), whereas 100% hydrometallurgical recycling was assumed in all other scenarios for Steel E-Motive vehicles based on a hypothetical 2030 manufacture and start-of-operation date.
- **Electricity grid supply mix scenarios:** LCA calculations for all scenarios ("baseline" current vehicle and all sensitivity variations of future Steel E-motive vehicle) were repeated twice to accommodate two alternative future electricity grid mix evolution scenarios, respectively corresponding to the International Energy Agency (IEA) World Energy Outlook (WEO) "Sustainable Development Scenario" (SDS), and "Stated Policies Scenario" (STEPS). More detail on this aspect of the calculations is provided below in **Section 9.3.2.3**.
- **End of life allocation method:** In LCA, a number of alternative EoL allocation methods are possible, whereby different shares of the impacts arising from material recycling are assigned respectively to the product generating the EoL waste materials, vs. the product that subsequently uses the recycled materials as inputs in its production process. In this study, two such methods were considered, respectively referred to as

"cut-off" (or "100:0") and "avoided burden" (or "0:100"). More detail on this aspect of the calculations is provided below in **Section 9.3.2.7**.

9.3.2 Reference taxi vehicle definition ("baseline" vehicle)

An important consideration in LCA calculations is to establish an appropriate "reference point" (or vehicle) from which subsequent calculations and sensitivities can be made. For Steel E-Motive, the reference starting point was assumed to be a "present day" (~2020) battery electric vehicle (BEV), operating in taxi mode, with driver plus one occupant. The vehicle and battery lifetime was assumed to be 300,000km, and the construction using 100% conventional (i.e. 0% "green") steel and aluminium. The vehicle end of life methodology used the Avoided Burden approach (whereby the recycled metals are assumed to displace equivalent quantities of their virgin counterparts, and are assigned corresponding emission and energy demand credits). 50% pyrometallurgical recycling was assumed for the battery packs. The reference taxi vehicle curb weight was estimated using the statistical reference data study (Figure 7.1.5.2), and assuming the same overall dimensions to Steel E-Motive SEM1, equates to an estimated curb weight of 1,949kg. The material utilisation was based on data from a similar vehicle specification and is shown in Figure 9.3.2.1. The vehicle occupancy rate was assumed to be 1.4, based on a combination/average of "empty" and passenger carrying journeys.

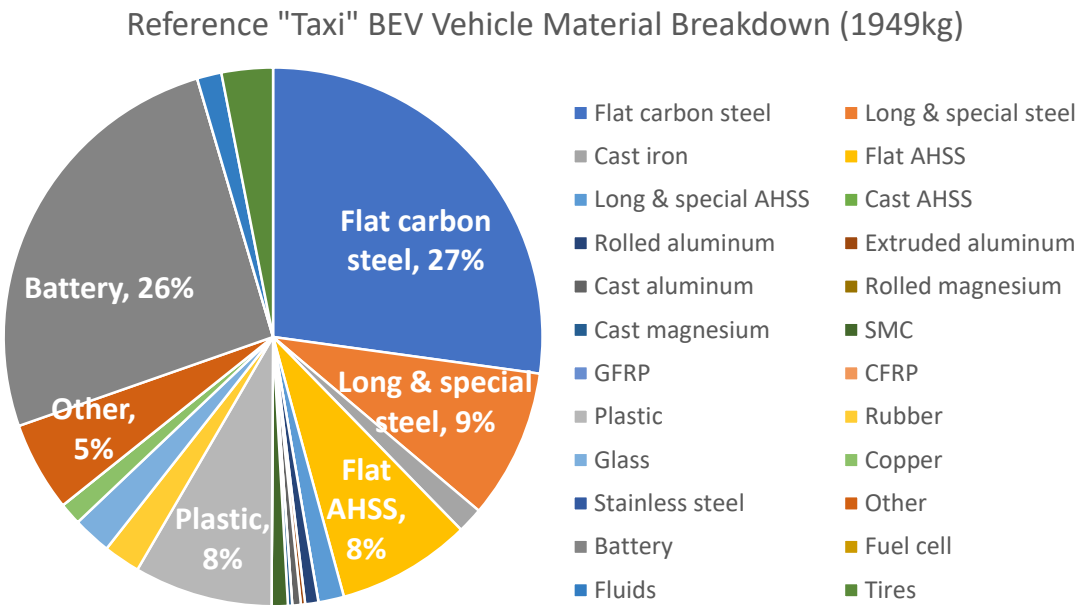

Figure 9.3.2.1 Reference taxi vehicle material breakdown

9.3.1 Steel E-Motive "default" vehicle definition

The Steel E-Motive vehicle life cycle calculations were based on a hypothetical 2030 manufacture and 2030 to 2035 start-of-operation date. The electricity grid supply mix was therefore updated to include the average of the IEA scenario estimations for 2030 and 2040. The nominal SEM1 vehicle curb weight of 1,512kg was applied in the LCA model and the vehicle Bill of Materials updated as per the breakdown shown in Figure 9.3.1.1 below. For comparative purposes, 0% of "green" steel and "green" aluminium were considered, as well as a vehicle occupancy rate of 1.4, standard WLTP drive cycle with zero autonomous drive cycle smoothing, and equal 300,000km battery and vehicle lifetimes. The Avoided Burden allocation method was used for the end-of-life calculation as the default.

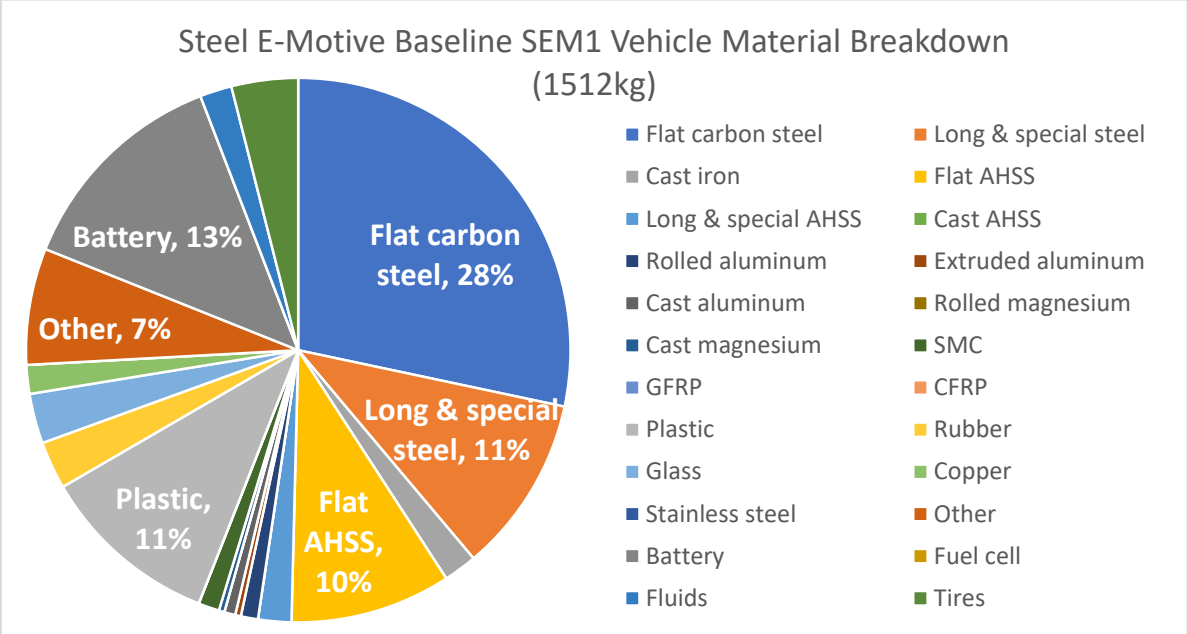

Figure 9.3.1.1 Steel E-Motive SEM1 vehicle material breakdown

9.3.2 Steel E-Motive LCA sensitivity studies

9.3.2.1 Reduced carbon steel and aluminium production

The production of steel firstly involves the conversion of iron ore to pig iron - conventional methods use a Blast Furnace (BF). In the first stage of this process, the iron ore (containing iron oxides) is mixed with coke (derived from coal), which acts as the reducing agent, and other elements such as limestone and then forced air (oxygen) are passed through the mixture, resulting in the chemical reduction of the iron oxides in the ore to impure metallic “pig” iron. A secondary Basic Oxygen Furnace (BOF) process is then used to drive down the carbon content and impurities in pig iron, by forcing oxygen through it at very high (supersonic) velocities for a duration of 25 to 45 minutes, the result being low-carbon steel. The molten low-carbon steel is then poured (or tapped) from the BOF furnace for subsequent processing into steel products, such as slabs, blumes and billets using continuous casting process. This conventional steel making process is referred to BF-BOF. Though BOF steelmaking is a very energy-efficient process (separating the iron from the oxygen at less that two times the theoretical minimum), the use of coke as a reducing agent and the subsequent generation of CO and CO2 offers opportunities for carbon reduction.

The Electric Arc Furnace (EAF) process is an alternative to the BOF and used primarily for converting scrap steel (as opposed to virgin iron ore) to molten steel. A very high electrical current is passed through graphite electrodes, exposing the charged material (scrap steel) to an electric arc, producing molten steel. The steel is then refined and passed to continuous casting process. EAF can be lower cost and significantly less carbon intensive than BOF where the source electricity is generated from renewable sources and the advantage of lower cost off-peak electricity rates can be applied. Approximately 70% of global steel production uses BF-BOF process and 30% EAF.

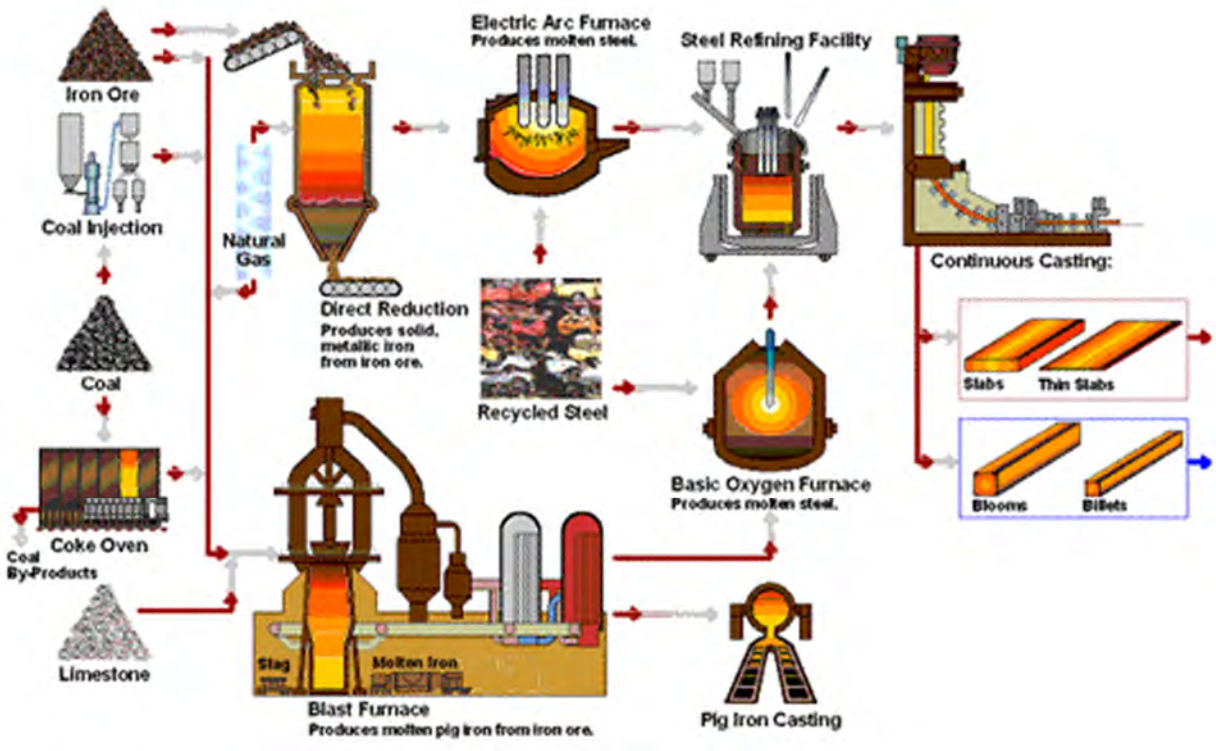

Figure 9.3.2.1.1 Steel production methods (courtesy of AISI https://www.steel.org/steel-technology/steel-production/)

https://worldsteel.org/about-steel/about-steel/steelmaking/

Steel producers are then developing and implementing new iron & steel production methods to significantly reduce GHG emissions – these are commonly referred to as “green” steels.

An alternative to the Blast Furnace method for iron production from virgin iron ore is the Direct Reduced Iron (DRI) process. Instead of using coal-based coke to chemically reduce the iron ore to metallic iron, hydrogen is used as the reducing agent, at a temperature below the iron melting point, resulting in a “direct” conversion from iron ore to iron. The energy consumption and GHG emissions of DRI are therefore lower than conventional Blast Furnace method. The DRI method produces hot-iron briquettes or sponge iron which can then be converted to steel using BOF and EAF methods. Also, importantly, using hydrogen in the DRI method provides further potential to decarbonise the steel production process. Hydrogen produced via water electrolysis powered by renewable electricity (“green” hydrogen) in a DRI process combined with EAF steel production, once again using renewable electricity, provides the best overall potential for decarbonised steel production. At the time of the Steel E-Motive project, a small number of DRI pilot production facilities were in operation, with many larger scale plants planned or under construction. Assuming a hypothetical production timeframe of 2030-2035 for the Steel E-Motive concept, it may be expected that “green” steel will be more widely available, and the latter was therefore considered within the vehicle LCA studies. (Note: “green” steel has the same chemical and mechanical properties as BF-BOF steels and can therefore be assumed as a direct substitution within automotive body structures).

In order to evaluate the potential reduction in GHG emissions with green steel production, an LCA sub-model using GaBi software was constructed, modelling the comparison between the conventional BF-BOF production route, and the low-carbon green-H_2-DRI-EAF route. The

process flows for the BF-BOF and DRI-EAF routes are shown in Figure 9.3.2.1.2 and the GaBi modelling approach for the latter is shown in Figure 9.3.2.1.3.

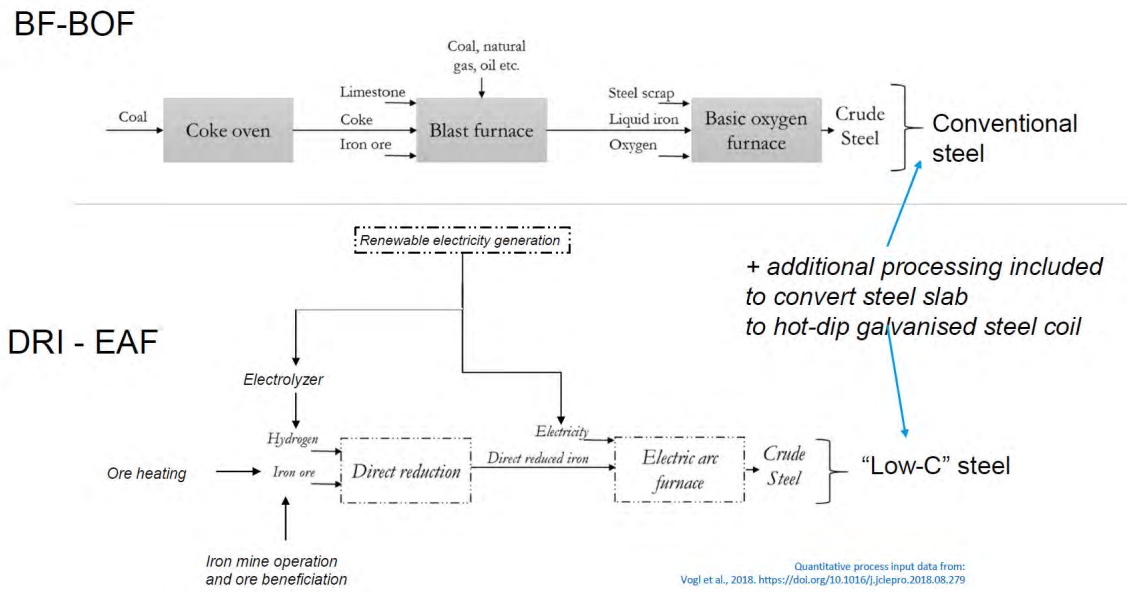

Figure 9.3.2.1.2 Life Cycle Analysis modelling considerations for BF-BOF and DRI-EAF steel production methods (See Appendix 4 for larger image)

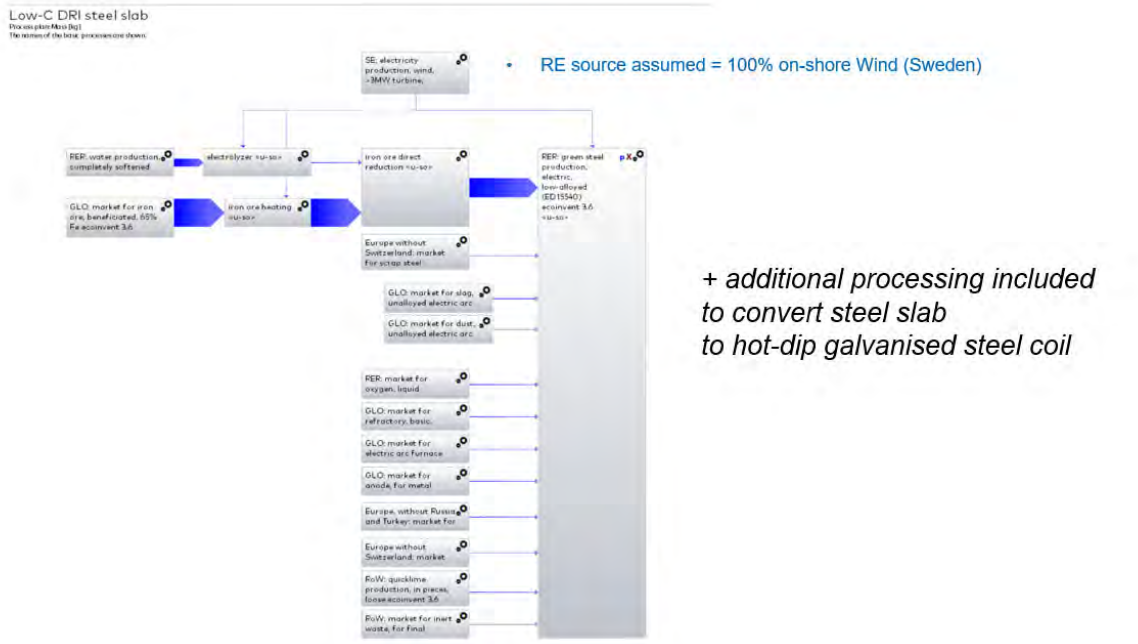

Figure 9.3.2.1.3 GaBi modelling of DRI-EAF steel production (See Appendix 4 for larger image)

The results from the GaBi LCA modelling showed the potential to reduce the GHG emissions for hot drip galvanised steel production from 3 $kgCO_2eq/kg$ (BF-BOF steel) to 0.6 $kgCO_2eq/kg$ (DRI-EAF), i.e., a factor-of-5 reduction. Also, the demand for fossil fuel primary energy resources for green steel production was predicted to be reduced by a factor of 3.8.

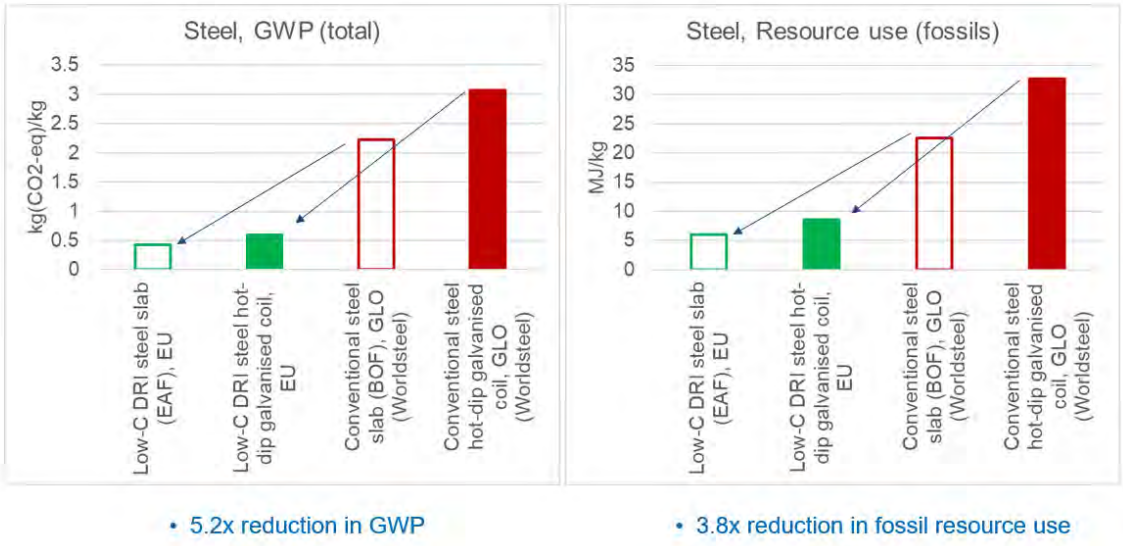

Figure 9.3.2.1.4 Predicted GHG emissions and fossil fuel primary energy demand effects of "green" steel production. (BF-BOF data provided by WorldSteel association). (See Appendix 4 for larger image)

The results from these calculations were embedded within the UCSB LCA Excel tool and applied in subsequent vehicle sensitivity studies.

9.3.2.2 Propulsion battery GHG contribution

Present-day propulsion batteries in electric vehicles can contribute up to 30% of the total vehicle production greenhouse gas emissions. Vehicle manufacturers and suppliers are therefore developing battery technologies resulting in significant reductions in GHG emissions. Given the hypothetical production dates, estimates on the potential reductions were estimated for the 2030 to 2035 timeframe. Results and data from a Ricardo led study for the European Commission was applied to the UCSB LCA tool (Ricardo et al., 2020). (https://op.europa.eu/o/opportal-service/download-handler?identifier=1f494180-bc0e-11ea-811c-01aa75ed71a1&format=pdf&language=en&productionSystem=cellar&part=)

Parameter	Modelled setting/value	Modelling intermediate and final outputs
Chemistry	NMC solid-state	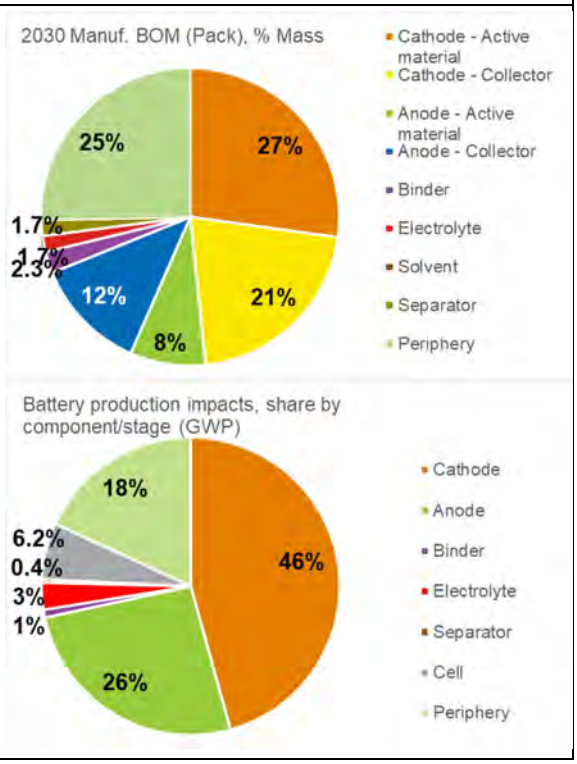
Energy density	500 Wh/kg (cell) 375 Wh/kg (pack)	
Capacity	75 kWh	
Manufacturing year/location	2030, EU (plus sensitivities for CN, US, JP)	
Manufacturing energy source	100% Renewable electricity, EU (plus sensitivities for CN, US, JP grid mix in 2030)	
Calculated 2030 output manufacturing impact (pack)	25.2 $kgCO_2e/kWh$ (pack)	

Figure 9.3.2.2.1 Considerations and data applied for modelling propulsion battery decarbonisation in Steel E-Motive (Ricardo modelling for a 2030 battery pack)

Figure 9.3.2.2.2 shows the predicted impacts of the introduction of new battery technologies and battery manufacturing decarbonisation for a European facility. Using Ricardo data and methodology, the production GHG contribution for a 2020 battery pack was calculated to be significantly higher than the baseline assumption in the UCSB model (the default calculation parameters in the UCSB were understood to be pessimistic). An estimated 72% reduction in GHG emissions for the battery production was estimated, comparing 2020 to 2030 technologies, primarily due to improved energy density (resulting in fewer materials) and 100% use of renewable electricity in manufacturing. This value excludes considerations for end-of-life methodologies and recycling.

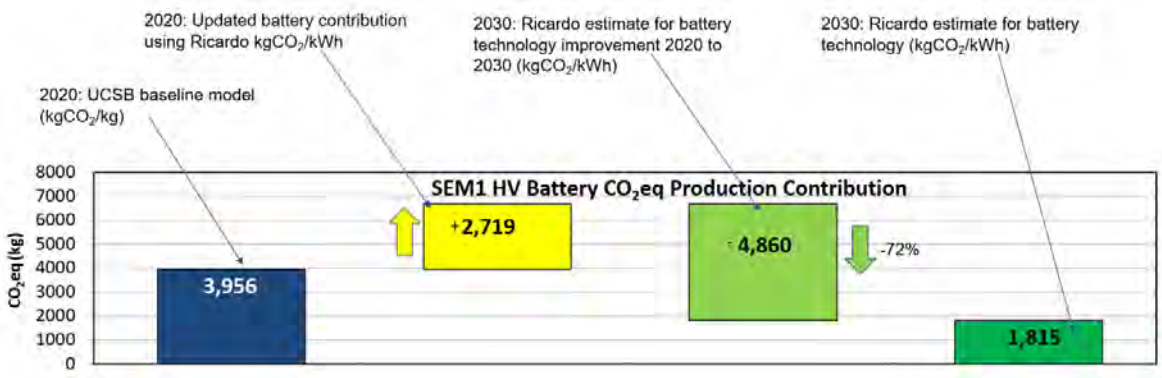

Figure 9.3.2.2.2 SEM1 battery production GHG contribution (Europe), 75kwH battery

9.3.2.3 Electricity grid carbon intensity

The “fuel” for Battery Electric Vehicles comes from mains grid supplied electricity, which is generated from many sources such as coal, gas, nuclear and renewables (wind, solar, hydro-electric). The differing electricity sources and projected future trends were considered in the Steel E-Motive LCA calculations. International Energy Agency (IEA) World Energy Outlook (WEO) https://iea.blob.core.windows.net/assets/4ed140c1-c3f3-4fd9-acae-789a4e14a23c/WorldEnergyOutlook2021.pdf (IEA, 2021) scenarios were used. Specifically, the IEA provide predictions for electricity grid supply carbon intensity for a “Sustainable Development Scenario” (SDS), where global climate targets would be achieved, and also for a “Stated Policies Scenario” (STEPS), a more conservative scenario assuming not all government targets would be achieved. Forecast data for Europe, US, China, India and Japan for SDS and STEPS were extracted and included in the UCSB model and Steel E-Motive LCA calculations. The IEA provide data and estimates for 2020, 2030, 2040 and 2050. Hybrid grid mix scenarios for “2020 to 2030” and “2030 to 2040” were derived from the data (Figure 9.3.2.2.3) and applied to the UCSB tool and Steel E-Motive calculations.

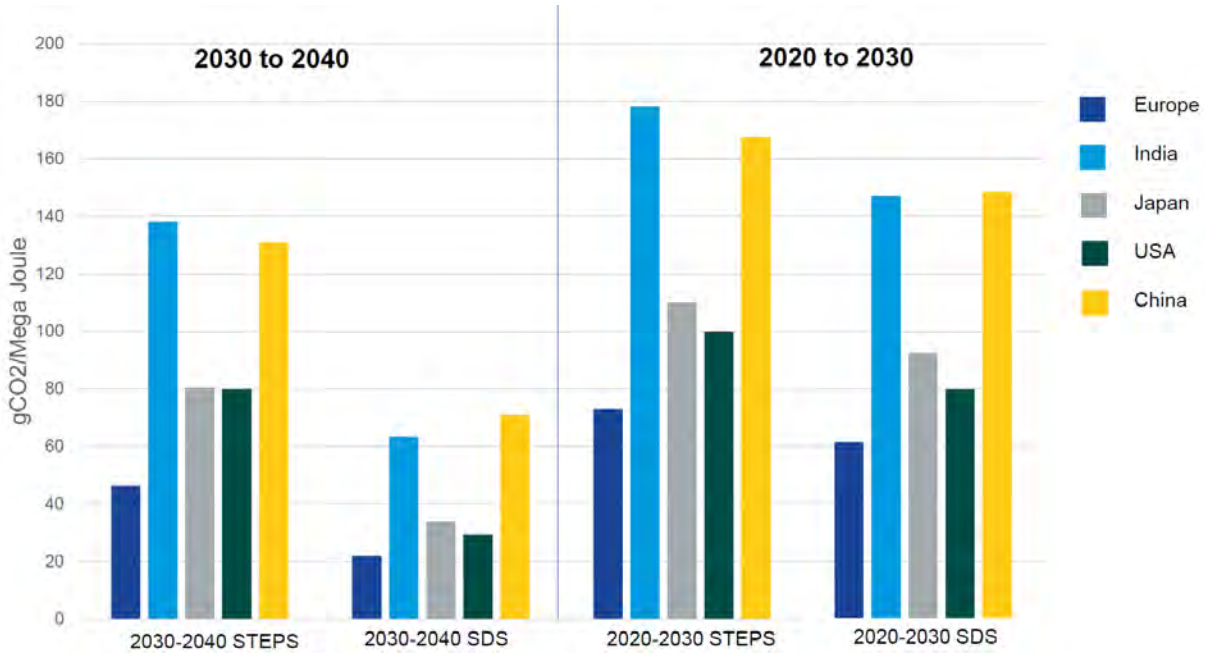

Figure 9.3.2.2.3 Electricity grid carbon intensity data used applied for Steel E-Motive LCA (data source taken from IEA WEO 2021)

9.3.2.4 Autonomous MaaS Vehicle real world driving cycle, and drive cycle smoothing

Autonomous vehicles and MaaS vehicles will operate differently to conventional human-operated vehicles. A ride hailing vehicle with increased passenger occupancy will have a different drive cycle compared to a conventional private or taxi passenger. Also, the ability for autonomous vehicles to communicate with other vehicles (“V2V”) and road infrastructure such as traffic signals (“V2X”) may unlock additional efficiencies through advanced control in response to the data received. For example, with the vehicle communicating with traffic signals, an autonomous vehicle will know when the signal is about to change to red/stop, and can therefore adjust its speed accordingly. On approach to the signal, the autonomous vehicle has the possibility to reduce its speed ahead of a red signal changing to green, therefore

maintaining more of its kinetic energy and reducing overall vehicle energy consumption. This enables “drive cycle smoothing”. A value of 15% reduction in overall vehicle energy consumption was therefore assumed to model autonomous control cycle smoothing.

A combined traffic and vehicle simulation modelling approach was taken for assessing the Steel E-Motive vehicles over a MaaS drive cycle. Firstly, a one-dimensional (1D) vehicle energy simulation model (Figure 9.3.2.5.2) was constructed to simulate the SEM1 and SEM2 vehicle energy consumption over specific duty or drive cycles. Ricardo’s in-house software code IGNITE was used with the modelling input parameters as per table 9.3.2.5.1.

	Value	Unit	Source
Vehicle			
Vehicle type	SEM1 BEV	-	0_General
Drive	FWD		0_General
Kerb mass	1640	kg	0_General
GVW total	2140	kg	0_General
Aero Cd	0.35	-	0_General
Aero Frontal Area	3.0	m2	CAD estimate
overall height	1880	mm	0_General
overall width	1850	mm	0_General
Vmax	130	km/h	0_General
Accel time for 0-102km/h	9	s	0_General
Braking system	CAT A	-	8.0 Chassis
Tyre, front & rear	175/60 R19	-	8.0 Chassis
Battery			
Battery capacity	75	kWh	4.0 Battery
Battery voltage	800	V	4.0 Battery
Module capacity	agnostic	Ah	4.0 Battery
Module voltage	44-50	V	4.0 Battery
Number of module	8	-	4.0 Battery
EDU			
Number of speed	1	-	6.0 EDU
Motor continuous power	115	kW	6.0 EDU
Motor peak power	230	kW	6.0 EDU

Table 9.3.2.5.1 IGNITE vehicle simulation model input parameters

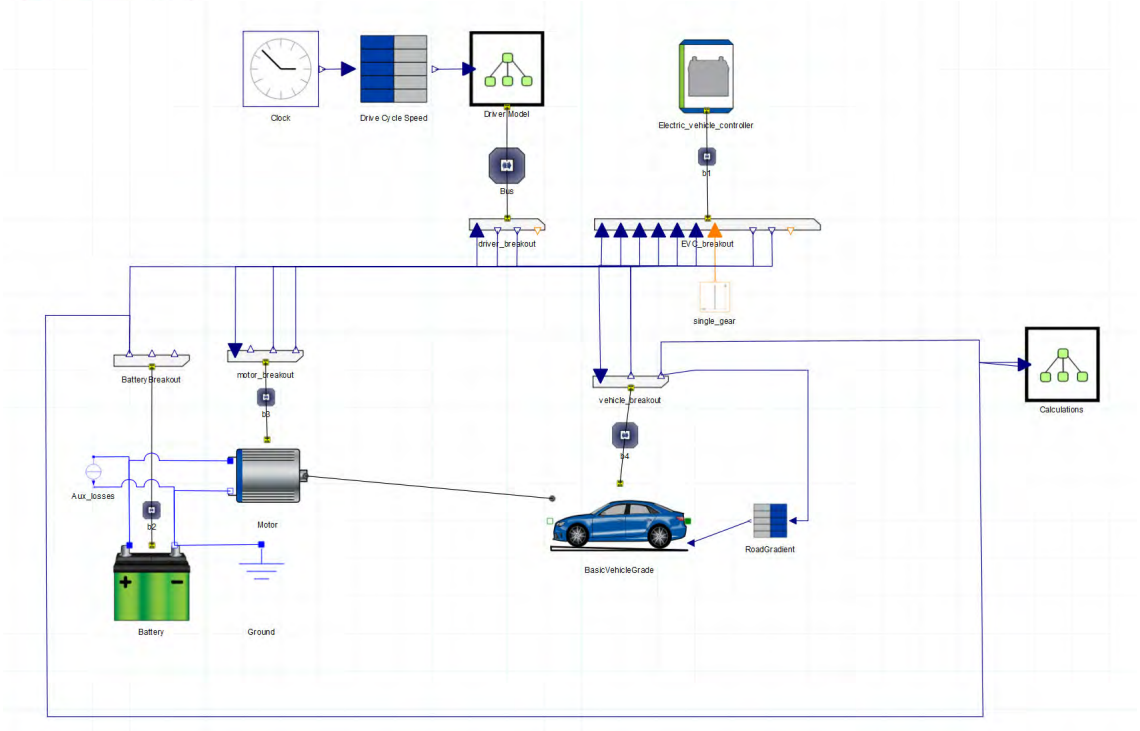

Figure 9.3.2.5.2 1D IGNITE vehicle energy simulation model schematic (See Appendix 4 for larger image)

Vehicle energy consumption is usually calculated for standard, defined drive cycle profiles such a Worldwide Harmonised Light Vehicle Test Procedure (WLTP) and Federal Test Procedure 76 (FTP-75). The drive cycle for the Steel E-Motive SEM1 vehicle is expected to be more aggressive than the defined drive cycles, due to the more frequent instances of stop-start events (i.e., passenger collection and drop-offs) and operation within city centres. Real world drive cycles applicable for SEM1 were therefore defined such that more realistic vehicle energy consumption values could be calculated and used as input into the LCA studies. Additionally, the vehicle energy usage calculations were used to confirm the 75kWh battery specification. Daily usage profiles were devised, combining the real world SEM1 specific drive cycles, resulting in expected battery State of Charge (SoC) estimations, which were used to confirm the available vehicle operation (or “up time”) throughout a daily cycle. The real world SEM1 drive cycles were calculated using the traffic modelling software tool SUMO (https://www.eclipse.org/sumo/). The tool enables modelling of road networks, with vehicle traffic models injected, enabling individual vehicle drive profiles to be extracted and used as an input to the IGNITE energy simulation model. The predicted vehicle energy usage for the calculated real world drive cycles was then used to estimate the daily battery SoC status, and as an input to the UCSB simulation tool. The process flow is shown in Figure 9.3.2.5.3

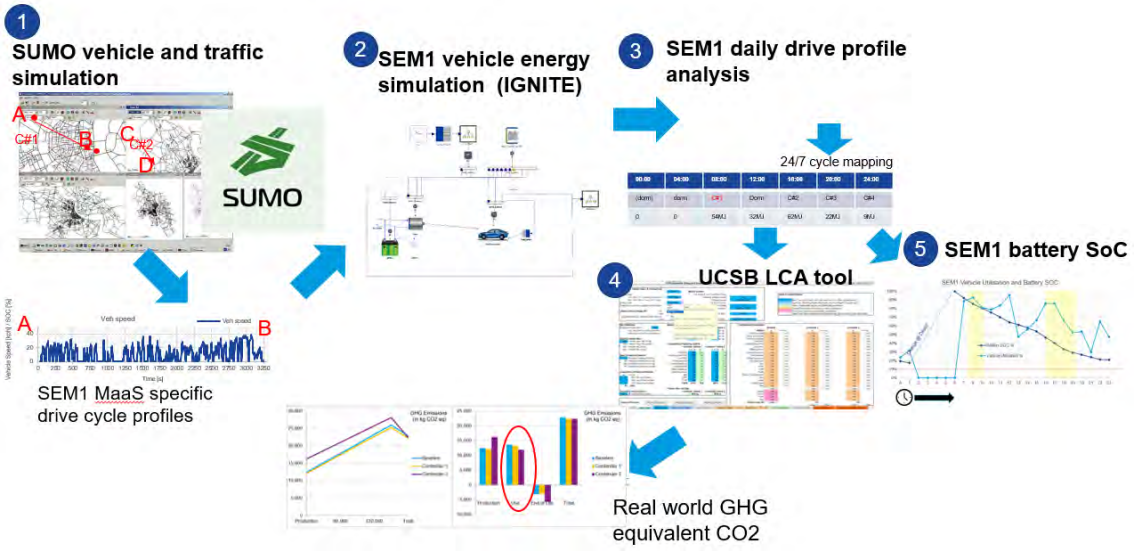

Figure 9.3.2.5.3 Traffic & drive cycle generation, vehicle energy simulation, Life Cycle Analysis process flow applied in Steel E-Motive (See Appendix 4 for larger image)

The SUMO traffic flow and drive cycle generation activity used the Brighton and Hove area of the UK as the basis for the real-world drive cycle routes. Brighton and Hove is a medium sized seaside city, situated on the South Coast of the UK. It contains a mixture of rural, suburban and urban city environments. The topology features some moderate hills and gradients inland. The city has good rail and public transport networks, and the city centre and arterial routes suffer from traffic congestion at peak times. Five unique journeys profiles or “missions” were defined for the Brighton and Hove area. These were selected based on anticipated journeys that SEM1 would likely operate. A hypothetical fleet depot location was assumed on the outskirts of the city, from which the main vehicle charging and servicing operations would be undertaken. The SUMO tool has the functionality to model different traffic congestion levels, therefore scenarios for “low” (off peak) and “high” (peak) were calculated. Figure 9.3.2.5.4 shows a map of the mission routes and Table 9.3.2.5.5 shows the output from the SUMO traffic simulation modelling.

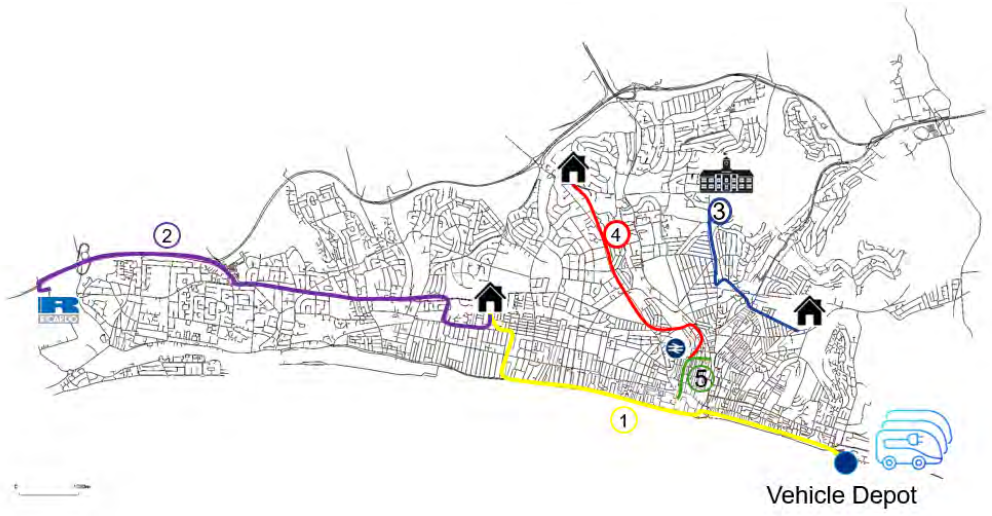

Figure 9.3.2.5.4 Map of SEM1 SUMO model mission routes (See Appendix 4 for larger image)

Mission number	Description	Journey distance (km)	Journey type	Journey time (minutes) (low traffic/off peak)	Average vehicle speed (km/h) (low traffic/off peak)	Journey time (minutes) (high traffic/peak)	Average vehicle speed (km/h) (high traffic/peak)
1	Depot to home collection	8.37	Suburban to suburban	11.9	41.7	13	37.6
2	Home to office	9.11	Suburban to rural	10.0	53.8	10.0	53.8
3	Home to school	3.22	Suburban to suburban	6.2	30.4	6.2	30.4
4	Home to city centre train station	4.08	Suburban to city	7.1	33.9	7.1	33.9
5	City centre journey	1.67	City centre	3.6	27.1	9.2	11.5

Table 9.3.2.5.5 SUMO traffic modelling output for SEM1 missions (See Appendix 4 for larger image)

The outputs from the SUMO traffic simulation were verified using Google maps journey time predictions and from personal experience of the missions/journeys. For each mission, unique vehicle drive cycles were produced in the form of vehicle speed versus time profiles, examples of which are shown in Figure 9.3.2.5.6.

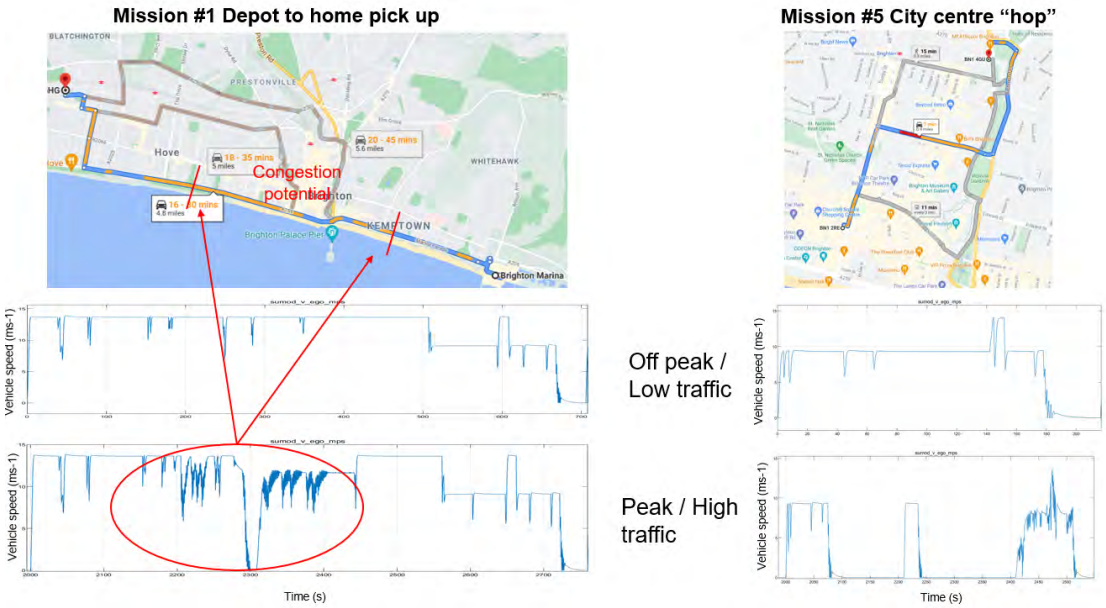

Figure 9.3.2.5.6 SUMO traffic modelling drive cycle profiles for low and high traffic scenarios (See Appendix 4 for larger image)

The mission drive cycle profiles were then used as inputs to the vehicle energy simulation model. This enabled the vehicle energy consumption over the drive cycle, as well as the battery SoC state to be calculated. To account for varying vehicle occupancy, the vehicle energy consumption was calculated for *low weight* and *high weight* scenarios. The calculated SEM1 vehicle energy consumption values for the 5 mission profile, in low & high traffic and low and high weight scenarios is shown in Figure 9.3.2.5.7.

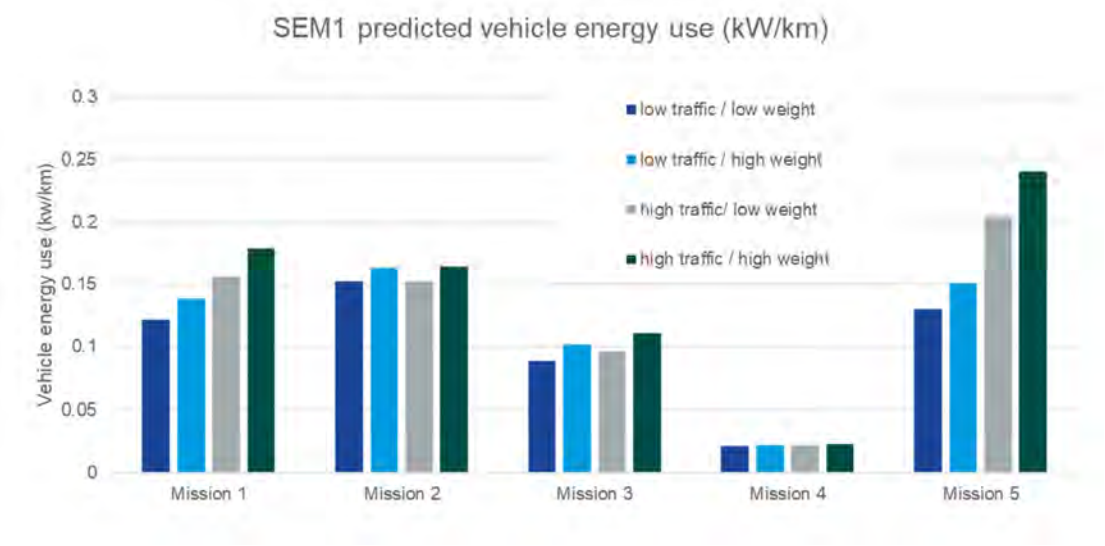

Figure 9.3.2.5.7 SEM1 predicted vehicle energy consumption for Brighton and Hove city mission profiles (values without autonomous vehicle cycle smoothing)

It should be noted that the Mission 4 has a (home) starting point at a higher altitude and destination than sea level in the city centre, therefore the downhill gradient results in overall low levels of vehicle energy consumption. The predicted vehicle energy consumption values were then used for the use phase calculations in the complete vehicle LCA calculations (discussed later). The SEM1 battery capacity and SoC through a typical daily operation were evaluated by combining the mission profiles 1 to 5 over a 24-hour period. The daily profile was assembled subjectively, based on expected journeys for a Monday to Friday period. A more thorough approach would require real-world vehicle tracking and measurement of present-day vehicles such as taxis. Figure 9.3.2.5.7 shows how the mission profiles were combined over a 24-hour duration. Between the hours of 02:00 and 06:00, the vehicle is expected to be based at the fleet operator's depot, undergoing checking, maintenance and battery charging. The vehicle would ramp up service from 06:00, with a high demand for home to office, home to school and home to train station journeys until 10:00. Demand would then expect dwindle, with a switch to more recreational journeys such as home to shopping centres. Drive cycles 2,3 and 4 are expected to be appropriate for these journeys. Demand would expect to decrease considerably after lunchtime before increasing for the evening rush hour between 15:00 (school closing) and 18:00 (office closing). Journey types would switch to recreational during the evening, with home to city and inner city journeys. Demand would then be reduced from 23:00 to 02:00 hours when the vehicle would return to the fleet depot. Combinations of low/high traffic and low/high vehicle weight cycles and vehicle energy consumption were selected depending on the expected traffic conditions and vehicle occupancy during the 24-hour profile. The vehicle energy simulation model calculated the required propulsion energy demand from the battery. It did not consider the vehicle ancillary or "hotel" energy requirements which need to be included for battery SoC estimations. A standard 2.5kW ancillary load was added to the propulsion energy requirement. This was considered worst case, accounting for the autonomous vehicle system electrical loads and heating, ventilation and air conditioning (HVAC) which were assumed to be higher than a conventional passenger car due to the higher frequency of door operation and the wider door opening area, resulting in a higher thermal loading on the vehicle interior.

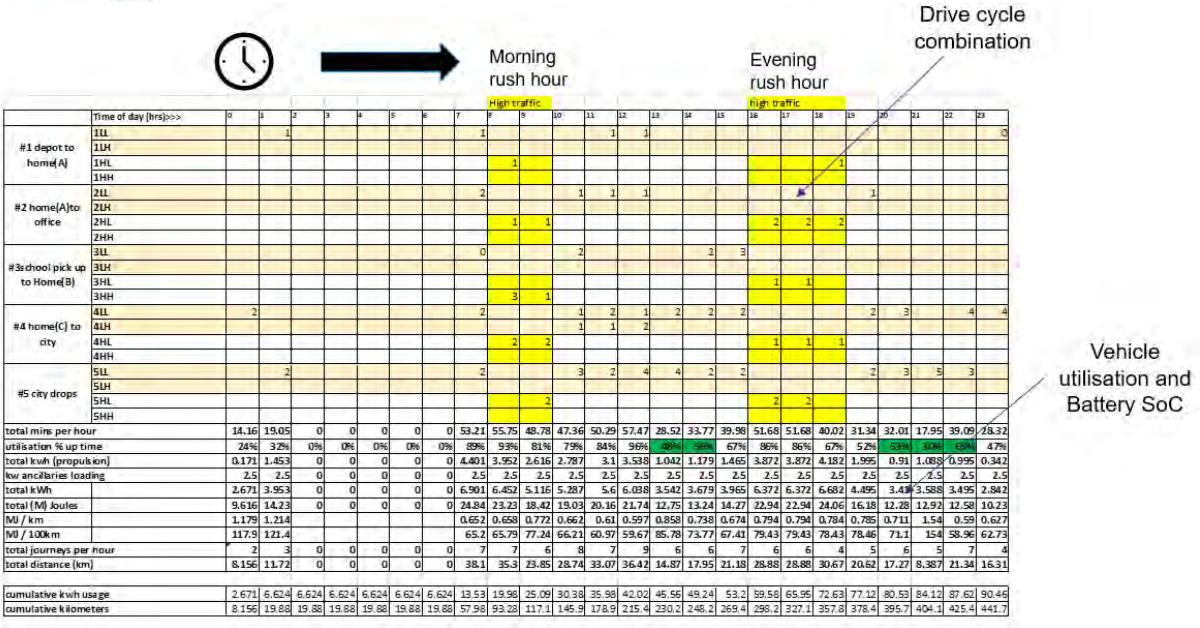

	Time of day (hrs)>>>	0	1	2	3	4	5	6	7	8	9	10	11	12	13	14	15	16	17	18	19	20	21	22	23
										High traffic								High traffic							
#1 depot to home(A)	1LL		1						1				1	1											0
	1LH																								
	1HL									1										1					
	1HH																								
#2 home(A)to office	2LL								2			1	1	1							1				
	2LH																								
	2HL									1	1							2	2	2					
	2HH																								
#3school pick up to Home(B)	3LL								0			2				2	3								
	3LH																								
	3HL																	1	1						
	3HH									3	1														
#4 home(C) to city	4LL	2							2			1	2	1	2	2	2				2	3		4	4
	4LH											1	1	2											
	4HL									2	2							1	1	1					
	4HH																								
#5 city drops	5LL		2						2			3	2	4	4	2	2				2	3	5	3	
	5LH																								
	5HL										2							2	2						
	5HH																								
total mins per hour		14.16	19.05	0	0	0	0	0	53.21	55.75	48.78	47.36	50.29	57.47	28.52	33.77	39.98	51.68	51.68	40.02	31.34	32.01	17.95	39.09	28.32
utilisation % up time		24%	32%	0%	0%	0%	0%	0%	89%	93%	81%	79%	84%	96%	48%	56%	67%	86%	86%	67%	52%	53%	30%	65%	47%
total kwh (propulsion)		0.171	1.453	0	0	0	0	0	4.401	3.952	2.616	2.787	3.1	3.538	1.042	1.179	1.465	3.872	3.872	4.182	1.995	0.91	1.088	0.995	0.342
kw ancillaries loading		2.5	2.5	0	0	0	0	0	2.5	2.5	2.5	2.5	2.5	2.5	2.5	2.5	2.5	2.5	2.5	2.5	2.5	2.5	2.5	2.5	2.5
total kWh		2.671	3.953	0	0	0	0	0	6.901	6.452	5.116	5.287	5.6	6.038	3.542	3.679	3.965	6.372	6.372	6.682	4.495	3.41	3.588	3.495	2.842
total (M) Joules		9.616	14.23	0	0	0	0	0	24.84	23.23	18.42	19.03	20.16	21.74	12.75	13.24	14.27	22.94	22.94	24.06	16.18	12.28	12.92	12.58	10.23
MJ / km		1.179	1.214						0.652	0.658	0.772	0.662	0.61	0.597	0.858	0.738	0.674	0.794	0.794	0.784	0.785	0.711	1.54	0.59	0.627
MJ / 100km		117.9	121.4						65.2	65.79	77.24	66.21	60.97	59.67	85.78	73.77	67.41	79.43	79.43	78.43	78.46	71.1	154	58.96	62.73
total journeys per hour		2	3	0	0	0	0	0	7	7	6	8	7	9	6	6	7	6	6	4	5	6	5	7	4
total distance (km)		8.156	11.72	0	0	0	0	0	38.1	35.3	23.85	28.74	33.07	36.42	14.87	17.95	21.18	28.88	28.88	30.67	20.62	17.27	8.387	21.34	16.31

cumulative kwh usage	2.671	6.624	6.624	6.624	6.624	6.624	6.624	13.53	19.98	25.09	30.38	35.98	42.02	45.56	49.24	53.2	59.58	65.95	72.63	77.12	80.53	84.12	87.62	90.46
cumulative kilometers	8.156	19.88	19.88	19.88	19.88	19.88	19.88	57.98	93.28	117.1	145.9	178.9	215.4	230.2	248.2	269.4	298.2	327.1	357.8	378.4	395.7	404.1	425.4	441.7

Figure 9.3.2.5.8 24 hour SEM1 vehicle mission profile, combining mission segments #1 to #5, at low/high traffic and low/high weight (See Appendix 4 for larger image)

The output from the 24-hour mission profile study was overall vehicle utilisation (%) and calculated battery SoC state (%) (Figure 9.3.2.5.9). Assuming the battery is at 98% SoC at the start of the day (assuming a full 100% SoC is not achievable in real life), it was predicted that the vehicle could operate on a full charge until 19:00hrs. Given the expected low journey demand period during the afternoon, the vehicle would be able to recharge at the main depot, and with a high capacity charger, a full charge could be re-established in time to support the high demand evening rush hour. With the vehicle assuming a high vehicle occupancy, driverless operation, it could be expected that the high degree of soiling of the interior may occur during the daily operation. Fleet operators may therefore be inclined to bring vehicles in for cleaning, inspection throughout the day. The mid-day charging operation would enable the vehicle to undergo simultaneous valeting and inspection.

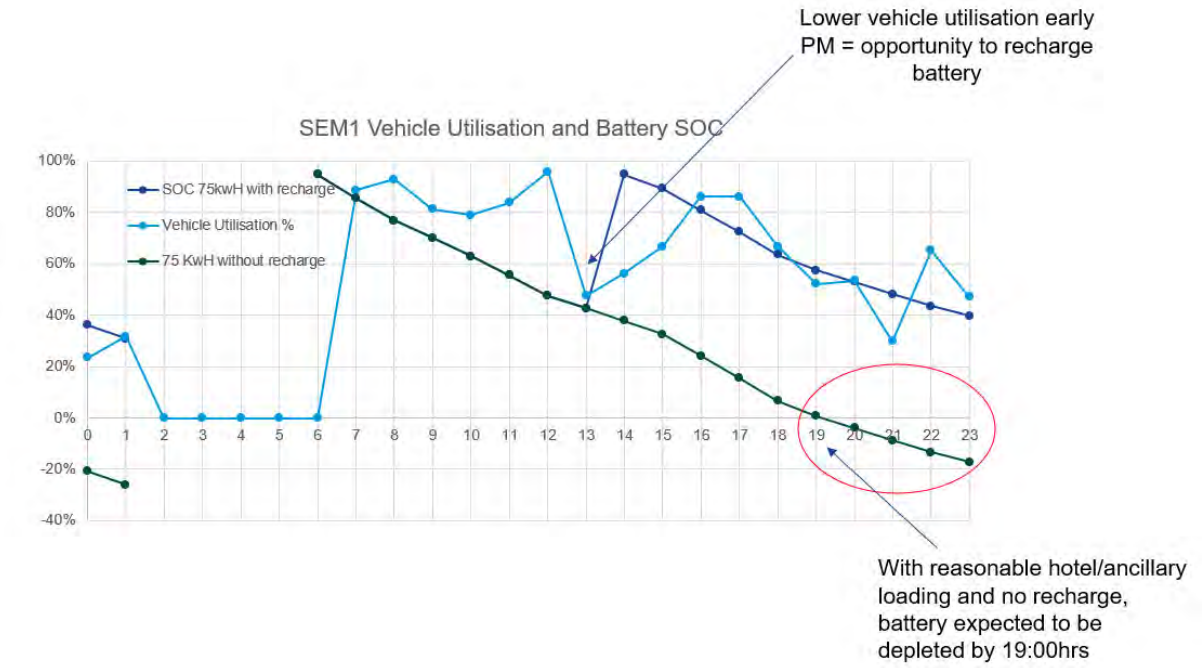

Figure 9.3.2.5.9 Predicted SEM1 vehicle utilisation (%) and battery state (SoC) over 24 hour duty cycle (autonomous vehicle drive cycle smoothing not applied)

This study concluded that the SEM1 vehicle and battery specification is able to support the expected journey requirements and demands of a typical city.

9.3.2.6 Vehicle and battery life extension. Increased vehicle occupancy

Passenger cars and vehicles are typically engineered for a given lifetime duration, in order to satisfy warranty and consumer expectations. Extending the life of a vehicle means that a lower cumulative number of new vehicles are required to maintain a given fleet size. A lower number of vehicles in turn leads to lower cumulative GHG emissions for the fleet as a whole. This is accounted for in the Steel E-Motive calculations as the GHG contribution is expressed as $kgCO_2$-eq/(passenger·kilometer). Therefore extending the required life of a vehicle reduces the $kgCO_2$-eq/(passenger·kilometer) value. A default consideration of 300,000km vehicle lifetime was considered, extended up to 600,000km as a stretch potential for the 2035 market. Similarly, extending the propulsion battery life will have a net beneficial impact on life cycle emissions. The Steel E-Motive battery design is engineered such that the individual battery modules are easily accessible and replaceable. This would enable failed battery modules to be easily replaced where typically the complete may be replaced currently. This was modelled in the LCA calculations by assuming a default battery life of 300,000km and an extended battery life of 600,000km.

9.3.2.7 End of life methodology sensitivity

In LCA, the “cut-off” EoL allocation method (also referred to as “100:0”) requires that the environmental impact associated to the recycling of the waste materials generated at EoL be excluded from the system boundary of the product under assessment, and that at the same time no impact credit be assigned for the virgin materials that such EoL recycling allows to displace. At the opposite end of the scale in terms of EoL impact allocation, the “avoided burden” method (also referred to as “0:100”) requires that 100% of the impact associated to the recycling of the waste materials generated at EoL be assigned to the product under

assessment, in addition to the full impact credit for the corresponding virgin materials that are assumed to be displaced; however, to avoid double counting, in this method no material input to manufacturing may be assumed to be of secondary (i.e., recycled) origin.

In this study, this latter “avoided burden” method was adopted as the default option, while a separate sensitivity analysis was carried out to investigate the effect of the alternative use of the “cut-off” method.

9.4 Life cycle analysis results

Figure 9.4.1 summarises the 11 lifecycle analysis studies and boundary conditions. 2 reference/baseline conditions and 9 Steel E-Motive sensitivity studies were evaluated. These included alternative assumptions on LCA end-of-life modelling methodology, lifetime vehicle activity (and battery lifetime), alternative operational energy consumption sensitivities, sensitivities on the use of ‘green’ steel and on vehicle occupancy rates.

Scenario n.	1	2	3	4	5	6	7	8	9	10	11
description	*BASELINE: 2018-2030 grid mix, private/taxi, EU*	*Future grid mix, private/taxi, EU*	*Future grid mix, private/taxi, EU, recycled content EoL*	*Future grid mix, 100% low-C steel, private/taxi, EU*	*Future grid mix, extended life, 2 batt, private/taxi, EU*	*Future grid mix, extended life, 1 batt, private/taxi, EU*	*Future grid mix, private/taxi, "real world" cycle, EU*	*Future grid mix, autonomous, private/taxi, "real world" cycle, EU*	*Future grid mix, ride sharing low, EU*	*Future grid mix, ride sharing high, EU*	*Future grid mix, extended life, 100% low-C steel, autonomous, ride sharing high, EU*
Title Level 1	*Baseline vehicle*								*Increased*		
Title Level 2	*2018*	*Steel e-Motive; Default*	*Recycled*	*Low-C steel*	*Extended life, 2*	*Extended life, 1*	*"Real-World"*	*"Real-World"*	*Ride sharing low*	*Ride sharing*	*Extended life,*
Title Level 3	*Baseline*										
power train	**BEV**	**BEV**	**BEV**	**BEV**	**BEV**	**BEV**	**BEV**	**BEV**	**BEV**	**BEV**	**BEV**
% ethanol	0%	0%	0%	0%	0%	0%	0%	0%	0%	0%	0%
Vehicle class	FSV A-class	FSV A-class	FSV A-class	FSV A-class	FSV A-class	FSV A-class	FSV A-class	FSV A-class	FSV A-class	FSV A-class	FSV A-class
Driving cycle	WLTP	WLTP	WLTP	WLTP	WLTP	WLTP	real-world cycle	real-world cycle	WLTP	WLTP	WLTP
Driving cycle smoothing reduction	0%	0%	0%	0%	0%	0%	0%	-15%	0%	0%	0%
Lifetime km	300,000	300,000	300,000	300,000	600,000	600,000	300,000	300,000	300,000	300,000	600,000
Battery lifetime (km)	300,000	300,000	300,000	300,000	300,000	600,000	300,000	300,000	300,000	300,000	600,000
pyrometall. LIB recycling share	50%	0%	0%	0%	0%	0%	0%	0%	0%	0%	0%
Grid mix (both SDS and STEPS for future scenarios)	2018	2030-2040	2030-2040	2030-2040	2030-2040	2030-2040	2030-2040	2030-2040	2030-2040	2030-2040	2030-2040
Region	**Europe**	**Europe**	**Europe**	**Europe**	**Europe**	**Europe**	**Europe**	**Europe**	**Europe**	**Europe**	**Europe**
EoL method	Av.Burden	Av.Burden	Recycled content	Av.Burden	Av.Burden	Av.Burden	Av.Burden	Av.Burden	Av.Burden	Av.Burden	Av.Burden
"green" steel share	0%	0%	0%	100%	0%	0%	0%	0%	0%	0%	100%
"green" Al share	0%	0%	0%	0%	0%	0%	0%	0%	0%	0%	0%
Vehicle occupancy (ride sharing)	1.4	1.4	1.4	1.4	1.4	1.4	1.4	1.4	2	3	3

Figure 9.4.1 Lifecyle analysis studies and model boundary conditions (See Appendix 4 for larger image)

Figure 9.4.2 shows the absolute calculated life-cycle GHG emissions, in units of $kgCO_2$-eq/(passenger·kilometer), for the 11 scenarios studied, with the individual contributions of vehicle manufacturing, vehicle use and end of life phase presented. The difference between use phase emissions under, respectively, SDS and STEPS electricity grid mix scenarios are also presented. For the baseline Steel E-Motive scenario (2), the breakdown and contributions to the vehicle manufacture GHG are shown in the accompanying pie chart.

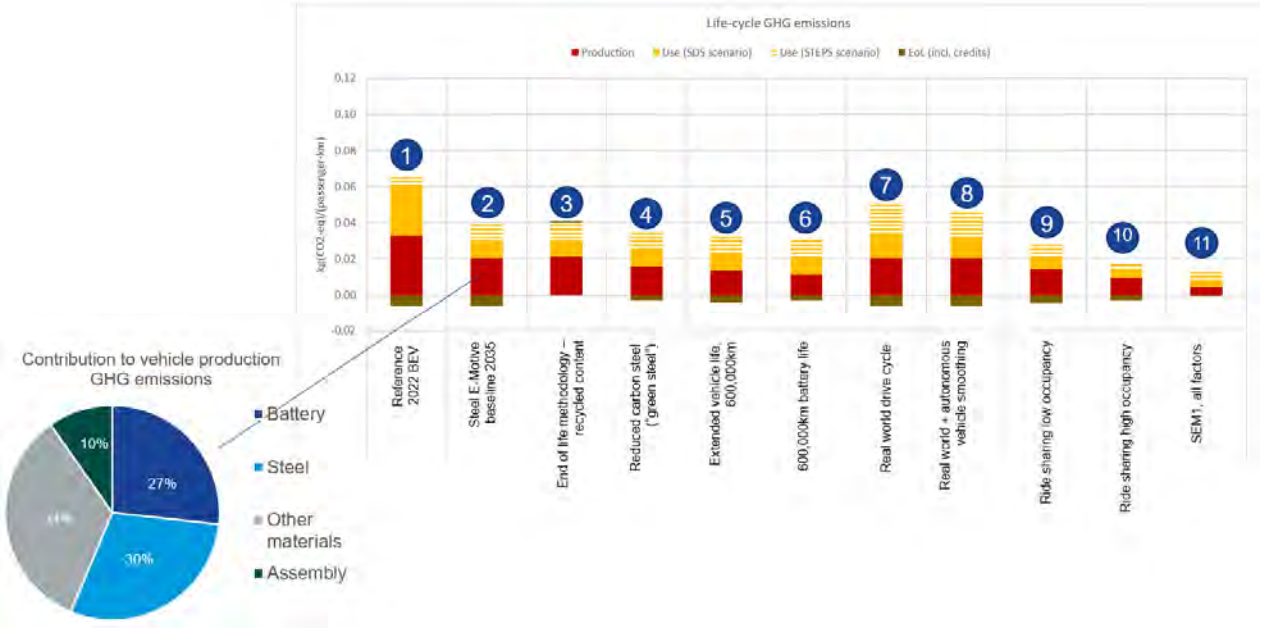

Figure 9.4.2 lifecycle analysis GHG CO_2 calculations (CO_2 equivalent per passenger-kilometers) (See Appendix 4 for larger image)

Figure 9.4.3 shows the total lifecycle GHG emissions for the 11 scenarios, expressed as a percentage of the reference 2022 BEV. Figure 9.4.4 provides a narrative on the comparative results for Europe region.

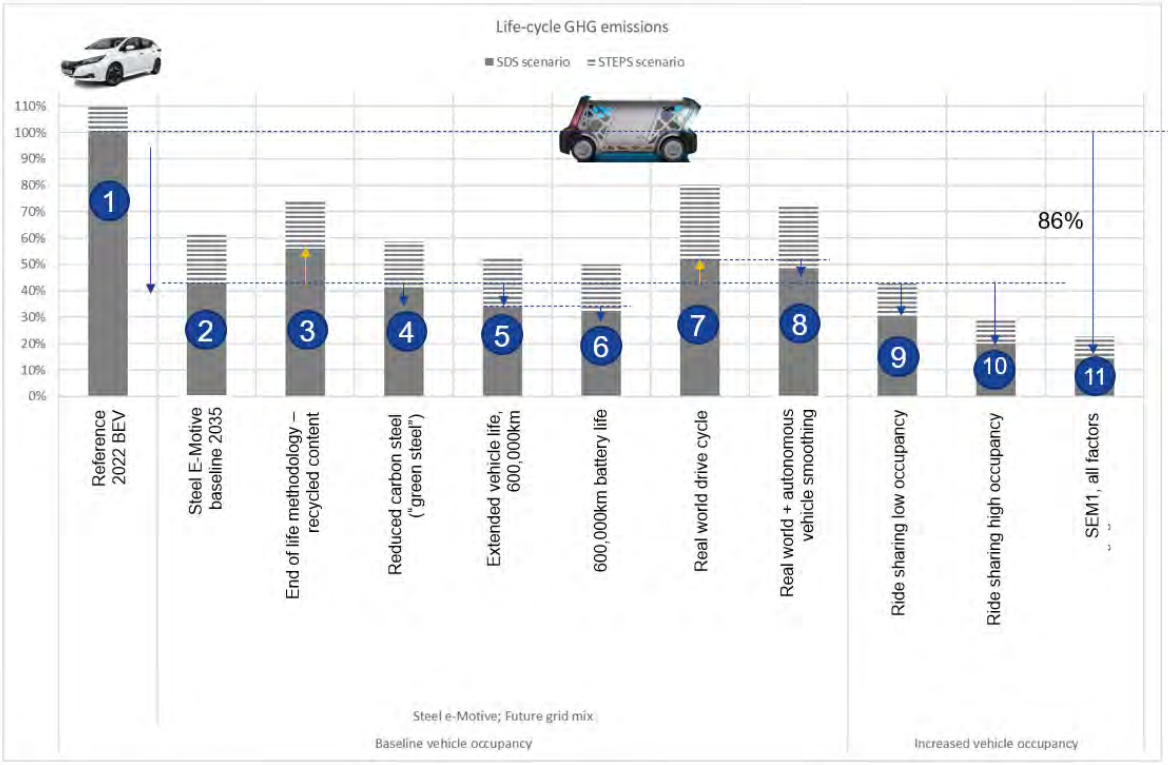

Figure 9.4.3 lifecycle analysis GHG CO_2 calculations, expressed as % of reference 2022 BEV (See Appendix 4 for larger image)

Model/result number	Description	Key Result
1	Reference BEV, 2022	Used as datum/reference for SEM
2	Baseline Steel E-Motive. 25% vehicle weight reduction versus (1), 2030-2040 electricity grid mix	57% life cycle GHG reduction compared to (1)
3	Steel E-Motive. As (2) with End of Life methodology changed from *avoided burden* method to *recycled content*	Recycled content EOL methodology results in a 13% increase in lifecycle GHG
4	Steel E-Motive. As (2) with all AHSS in the vehicle substituted with decarbonised steel production	22% reduction in vehicle production GHG emissions. 3% decrease in GHG over vehicle lifecycle. Note, the effect is diluted due to the GHG contribution in the use phase
5	Steel E-Motive. As (2), with vehicle lifetime kilometers increased from 300,000km (2) to 600,000km (5)	20% reduction in vehicle lifecycle GHG
6	Steel E-Motive. As (5), with battery lifetime increased from 300,000km to 600,000km	A further 7% reduction in lifecycle GHG emissions compared to (5)
7	Steel E-Motive. As (2) with real-world driving cycle. (all other models assume a standard WLTP drive cycle)	Real world drive cycle results in overall 21% increase in lifecycle GHG emissions
8	Steel E-Motive. As (7) with effect of autonomous vehicle drive cycle smoothing	7% reduction in lifecycle GHG emissions compared to (7)
9	Stee E-Motive. As (2) with vehicle occupancy passenger increased from 1.4 to 2.0	30% reduction in lifecycle GHG emissions compared to (2)
10	Stee E-Motive. As (2) with vehicle occupancy passenger increased from 1.4 to 3.0	53% reduction in lifecycle GHG emissions compared to (2)
11	Steel E-Motive. As (2), with combined effects of (4), (5), (6), (10)	86% reduction in lifecycle GHG emissions compared to reference 2022 BEV vehicle (1))

Figure 9.4.4 LCA results narrative (See Appendix 4 for larger image)

The LCA calculations were also separately performed for Europe, United States, China and Japan regions, where the corresponding region-specific electricity grid carbon intensities were applied (Figure 9.3.2.2.3). Results for the regional variances and the overall potential reduction in GHG values are shown in Figure 9.4.5.

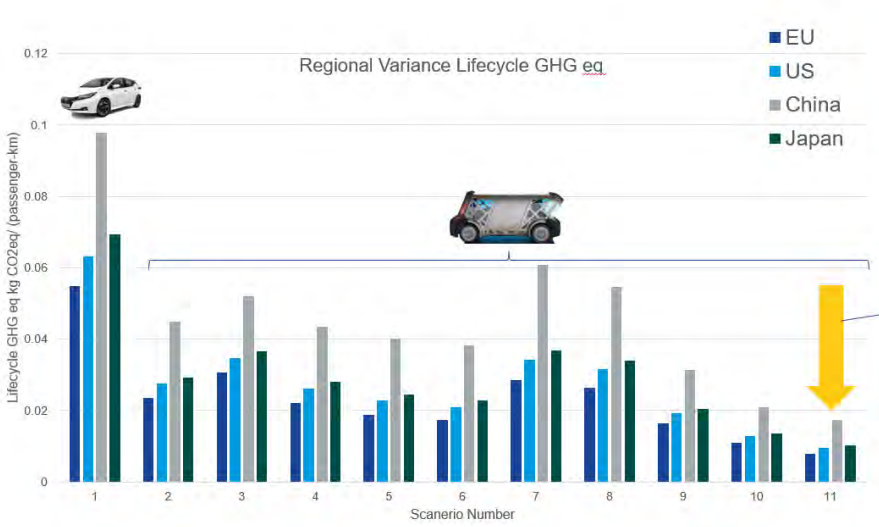

Country	Max GHG Potential from 2022 Reference
EU	86%
US	85%
China	82%
Japan	85%

Figure 9.4.5 Lifecycle calculations for Eu, US, China and Japan regions (See Appendix 4 for larger image)

9.5 Life cycle analysis results discussion and conclusions

Fully autonomous Mobility as a Service vehicles such as the Steel E-Motive concept have the potential to address the ongoing and future requirements for decarbonisation of passenger transportation. The Steel E-Motive concept demonstrates the potential to reduce lifecycle greenhouse gas emissions by up to 86%, when compared to a present day battery electric vehicle operating as a taxi. This potential can be realised by adopting the following measures:

- Reducing vehicle production and manufacturing embedded emissions, by utilising 100% reduced carbon (“green”) steel, improving battery technology and increasing the use of renewable electricity in battery manufacturing, and increasing/improving battery recycling.
- Ensuring the vehicle weight of autonomous vehicles is managed, and the potential weight reduction benefits are realised and implemented. The Steel E-Motive body structure and battery housing demonstrates good weight efficiency.
- Increasing the overall lifespan of the vehicle and battery. The fatigue and durability properties of AHSS can enable enhanced vehicle lifetime. The Steel E-Motive battery design enables easy replacement of specific modules (i.e., those which may fail or be damaged), which should enable an overall extended battery life.
- Autonomous vehicle control providing smoothing of the drive cycle. The vehicle acceleration and deceleration rates can be optimised to match the driving conditions and road topography. This reduces energy consumption and subsequent GHG emissions.
- Increasing passenger occupancy rates to at least 3 per vehicle via MaaS.

The projected net GHG emissions for the Steel E-Motive vehicle operating with the flexibilities described above already represent a very significant reduction vs. the current baseline. Achieving net zero emissions would require additional measures such as manufacturing offsetting manufacturing impacts (e.g. through compensatory credits from atmospheric carbon capture and storage) and transitioning to 100% renewable electricity grid.

10.0 Exterior Vehicle Styling

The SEM1 exterior vehicle styling was adjusted to take into account any necessary adjustments that were made during the engineering development of the body structure. The selected styling theme was maintained. Figure 10.0.1 to 10.0.10 show the final exterior vehicle styling images for SEM1, with in-situ renderings included to demonstrate real life application.

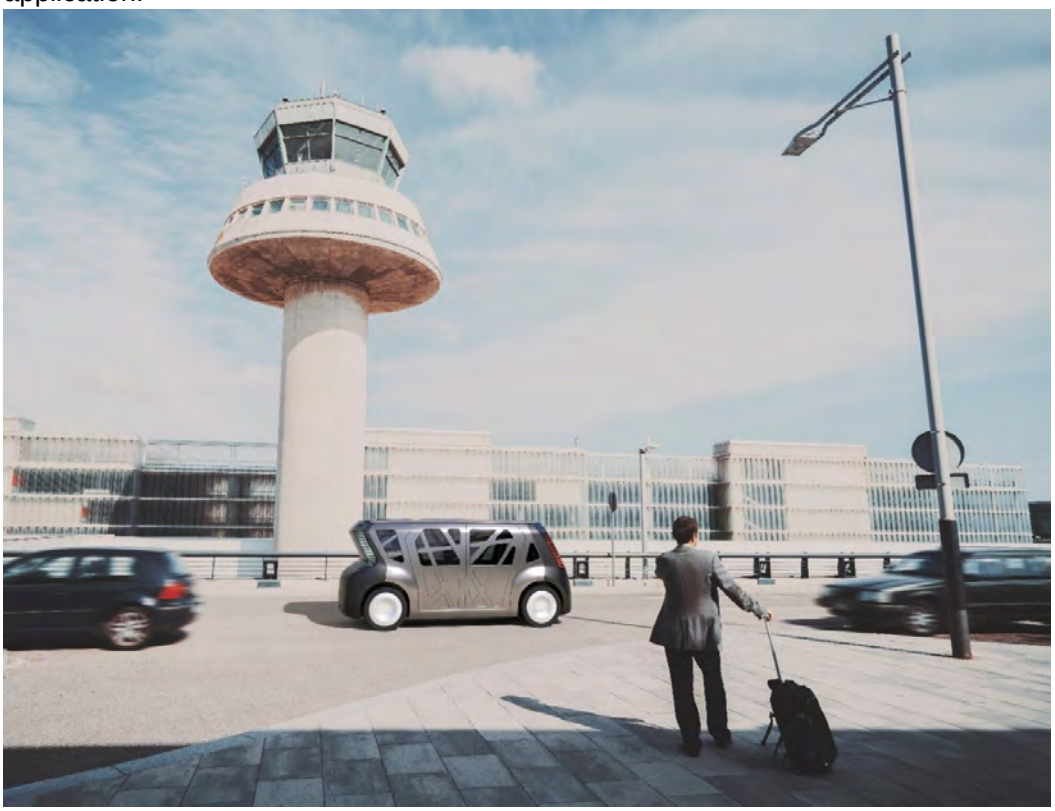

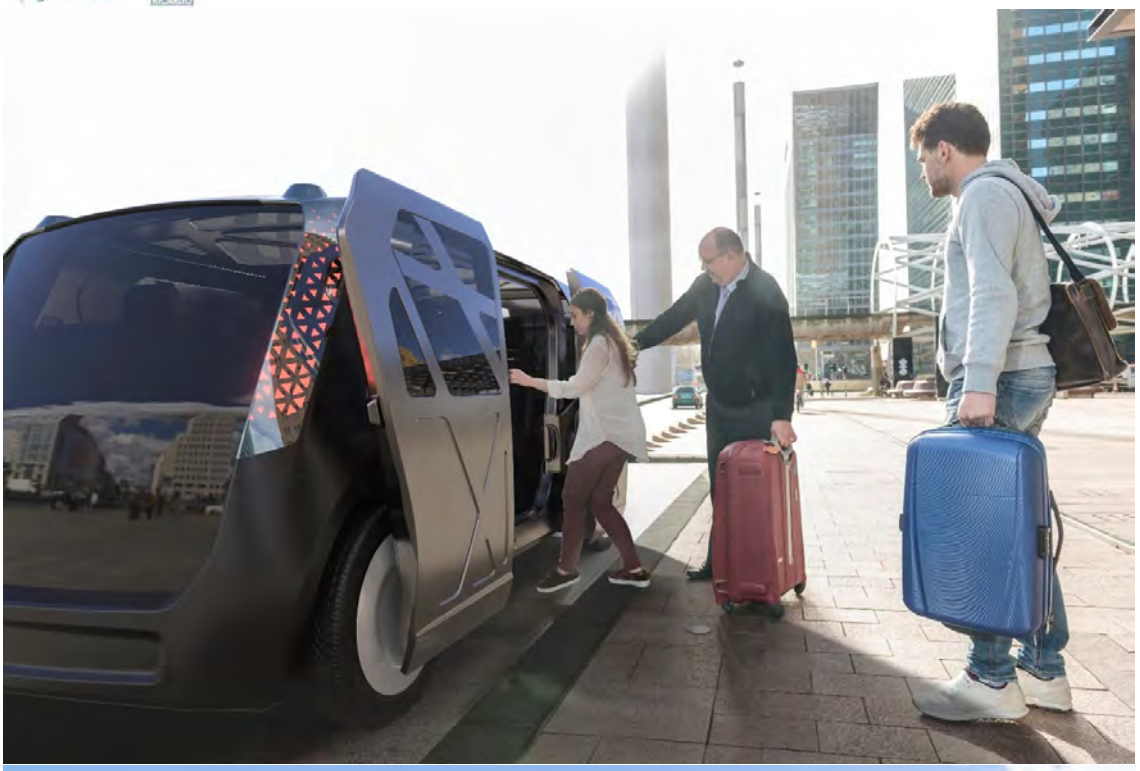

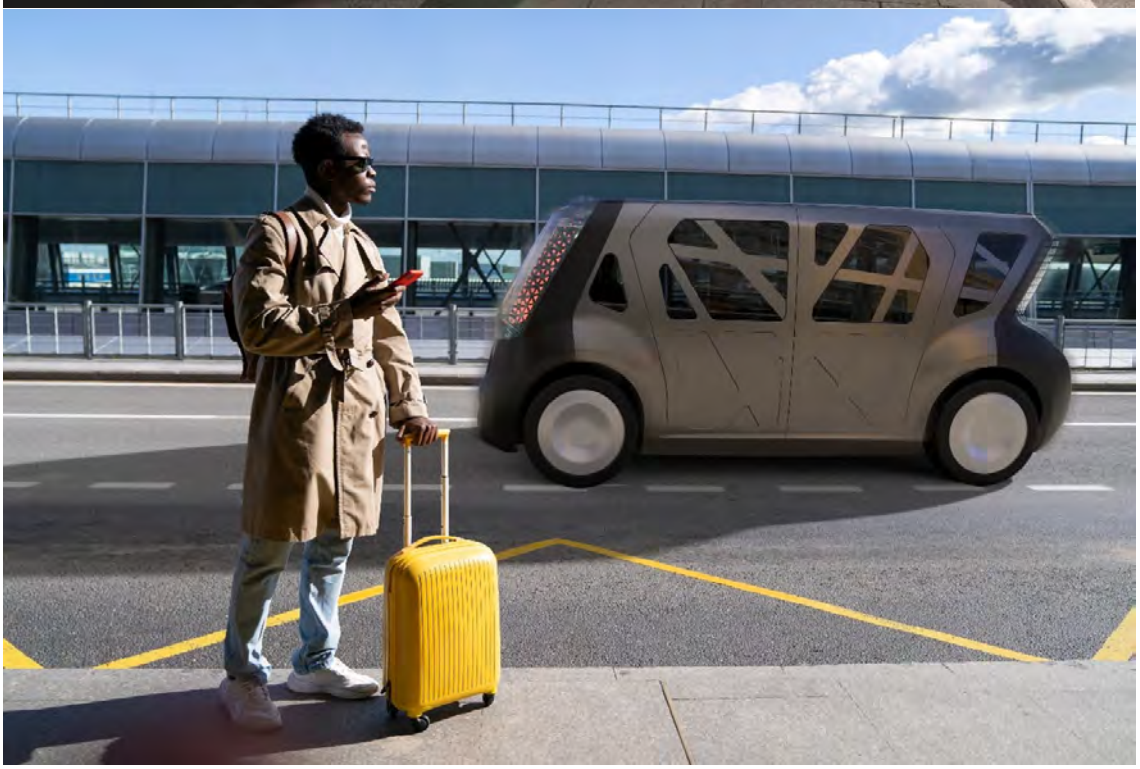

11.0 Design and development of SEM2, extra-urban 6 passenger variant

11.1 Introduction & Objectives

The Steel E-Motive concept is engineered to enable multiple vehicle variants to be developed from a common basis (or platform). The main detailed engineering activities focussed on the smaller 4 passenger SEM1, as documented in this report. To demonstrate the platform and scalability principals, a larger 6 passenger variant SEM2 was engineered, using a combination of 3D CAD design and “desktop” engineering approach.

11.2 SEM2 Targets

Target	SEM1	SEM2	Comment
Overall vehicle length (mm)	4100	4495	
Overall vehicle width (mm)	1850	1850	
Overall vehicle height (mm)	1850	1850	
Wheelbase (mm)	2725	3125	(SEM2 +400mm wheelbase stretch)
Track, front and rear (mm)	1620		
Vehicle turning circle (metres)	<7.6	<9.5	
Autonomy level (SAE)	5		
Vehicle curb weight (kg)	<1640	<1800	
Vehicle Gross Vehicle Weight GVM, (kg)	<2140	<2600	Based on 6 passengers + 150kg payload No towing requirement No roof carrying requirement (e.g. roofbox)
Vehicle acceleration 0-102km/h (sec)	<9		SEM2 has front and rear EDU to provide additional traction effort
Maximum vehicle speed km/h	130		
Towing requirements			(vehicle not required to perform towing operation)
Range on 1 full battery charge(km)	>500	>500	Battery size increased to 96kwH
Battery charging Time (minutes)	<20		
Target vehicle life (km)	>500,000		
Sustainability and Life Cycle performance	Demonstrate ability to make a significant contribution to net zero lifetime vehicle greenhouse gas emissions		
Body manufacturability and vehicle assembly	Maximise commonality between parts		To use conventional sheet steel fabrication processes for the body structure (for example, but not limited to; hot and cold stamping, roll forming, roll stamping, hydroforming). Body assembly to use Resistance Spot Welding (RSW), laser welding, brazing, structural adhesives, mechanical fasteners Utilise a conventional high volume vehicle assembly processes and approaches

			The design to be suitable for production in global locations and facilities
Anticipated production volumes (per year)	250,000	100,000	Lower volume for SEM2
Anticipated Start of Production (SOP) date	2030 to 2035		
Luggage volume capacity (litres)	400		
Passenger ergonomics	Comfortably seat 4 passengers	Comfortably seat 6 passengers	To have a minimum side door aperture opening width >1.0m To be compliant with disabled user requirements (e.g., wheelchair, ramp access) To seat 4 passengers comfortably, assuming 95% ile mannequin To accommodate breadth of potential users (e.g., babies, children, elderly)
Vehicle servicing and repair			Steel E-Motive design to ensure that minor service points (such as coolant, screen wash, brake fluid reservoir) to be readily accessible without the requirement for hand tools. Ensure major servicing of parts such as brake pads & discs, tyres can be completed within industry standard timelines and efforts Major repair parts such as high voltage battery can be undertaken in competitive timelines

With the exception of weight, the SEM2 BIW performance targets were targeted to be the same as SEM1. The same weight-dimension regression analysis principals (Figure 4.2.2.1) as applied for SEM1 BIW weight were applied for SEM2. Using the same approach, a target value of 362kg was defined for SEM2 BIW.

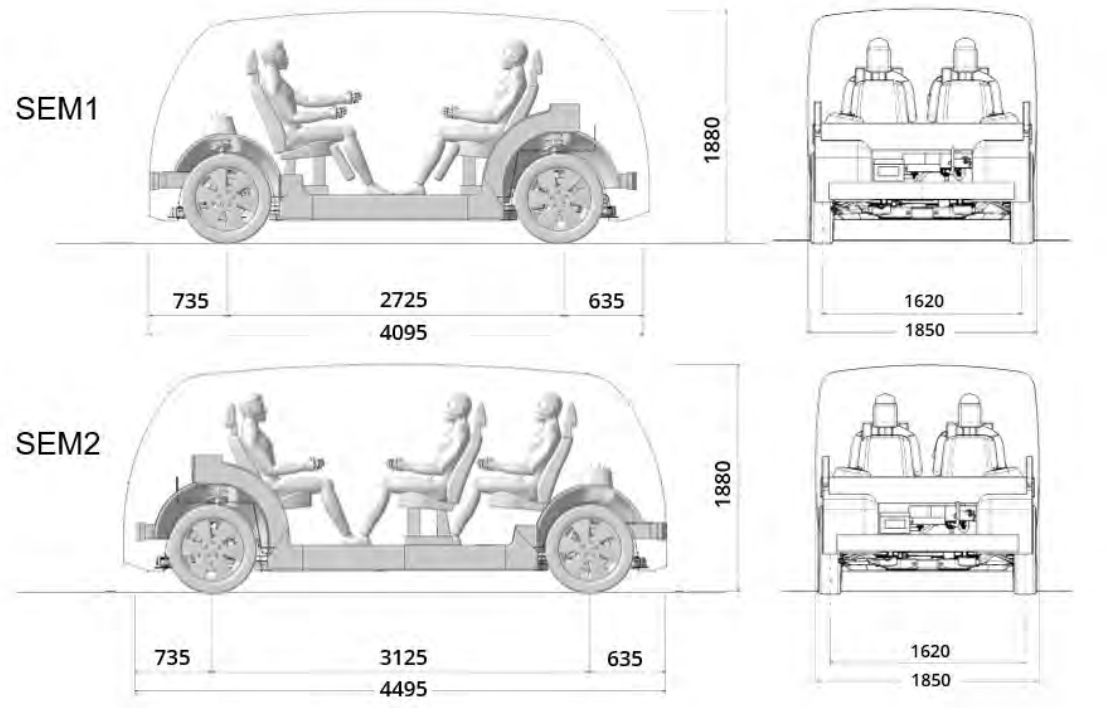

11.3 Technical Approach

Consideration for the development of the SEM2 variant was provided during the preliminary concept development and vehicle package study in Phase 0. To account for the higher kerb and gross weights, an additional rear EDU was specified, in order to provide additional tractive effort and power when required. The front EDU was changed from single speed (SEM1) to 2 speed (SEM2). The greater size of SEM2 was achieved by increasing the wheelbase by 400mm rearwards of the door split line. This would enable the front and rear body structure zones to be largely common and carry-over from SEM1, with SEM2 specific parts for the mid zone. The 6 occupants are accommodated with an additional 3rd row of seating, with the middle row of seats converted to sliding and folding to enable passenger ingress/egress access. The SEM1 3D CAD data was used as the basis for the detailed development of the SEM2 variant. A subject and desktop attribute appraisal approach was then taken to determine further modifications to SEM2 that may be required.

11.4 SEM2 vehicle concept

11.4.1 SEM2 Vehicle layout, weight analysis & occupant positioning

Figure 11.4.1.1 shows the comparison of SEM1 and SEM2 vehicle design, proportions, and interior configuration. The scissor doors are largely carry-over from SEM1, with the exception of the rear door outer surface profile which is adjusted to match the effect of stretched wheelbase. The wide door opening aperture and low step in height is maintained in SEM2, providing good access for the occupants.

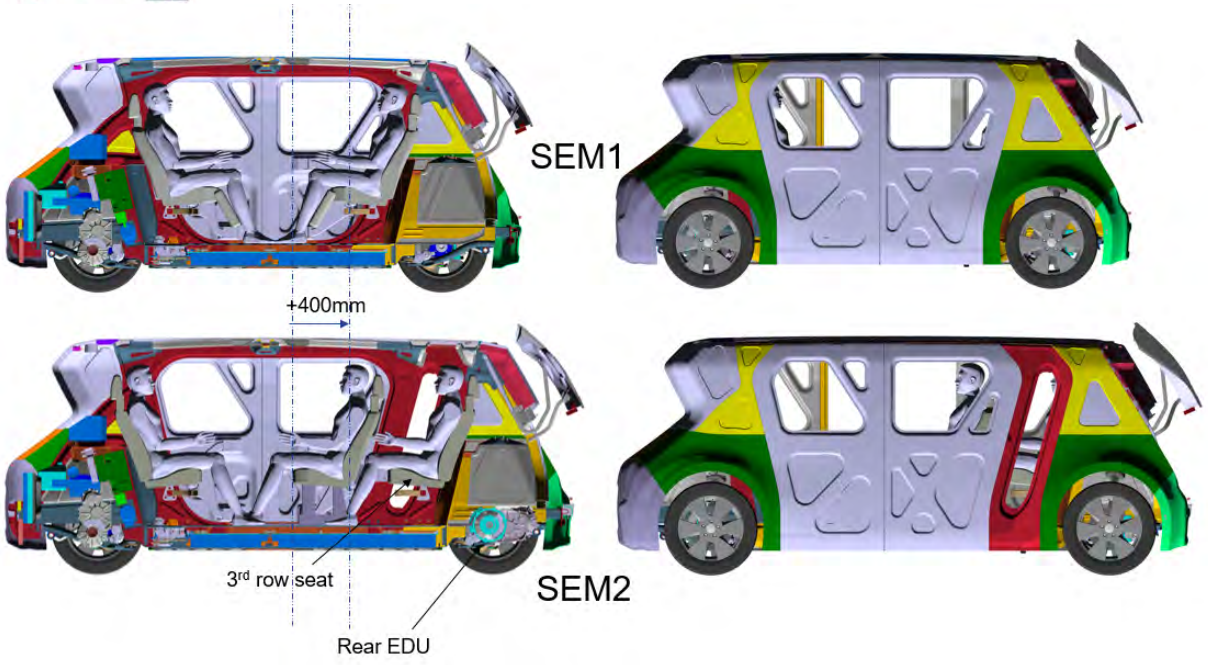

Figure 11.4.1.1 Comparison of SEM1 and SEM2 vehicles and interior configuration

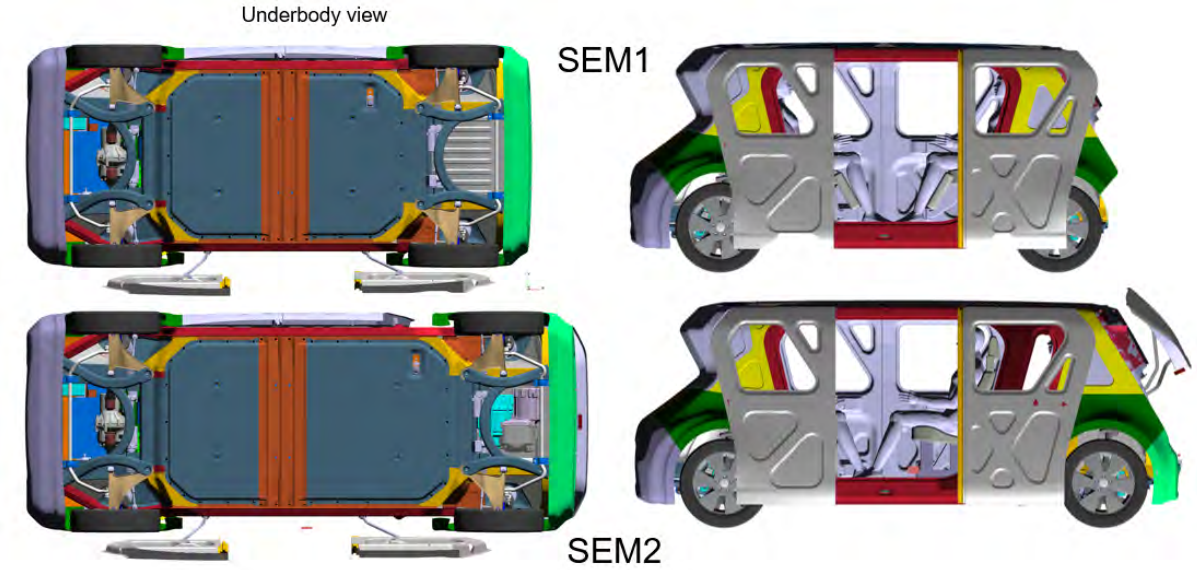

Figure 11.4.1.2 Comparison of SEM1 and SEM2 complete vehicle

The vehicle curb and gross weights were estimated based on the carry over SEM1 systems (green text in Figure 11.4.1.3) and new/modified parts and systems for SEM2 (red text in Figure 11.4.1.3). SEM2 is estimated to have a curb weight value 24% higher than SEM1. The SEM2 Gross Vehicle Weight (GVW) was estimated to be 2548kg.

Subsystem	SEM 1	SEM 2	SEM2 comment
Body non-structure	*177.2*	*293.2*	*additional seat row, glazing, trim size*
Body In White	*282.0*	*323*	*from 3D CAD and adjusted BoM*
Front sub-frame	*16.5*	*16.5*	*carry over SEM1*
Battery case (structure)	*59.0*	*70*	*from 3D CAD model*
Rear sub-frame	*10.2*	*10.2*	*carry over SEM1*
Front suspension	*114.0*	*131.1*	*SEM2 chassis parts for higher GVW*
Rear suspension	*114.0*	*131.1*	*SEM2 chassis parts for higher GVW*
Braking	*59.7*	*65.7*	*10% large disc and caliper for SEM2*
Steering	*26.0*	*26*	*carry over SEM1*
Tires and wheels	*84.0*	*96.6*	*SEM2 chassis parts for higher GVW*
Motor Trans Front	*63.0*	*72.45*	*SEM2 chassis parts for higher GVW*
Motor Trans Rear (N/A SEM1)		*80*	*SEM2 rear EDU only*
Battery system less case	*245.6*	*295.6*	*SEM2 96kwH battery*
Propusion controls	*60.0*	*60*	*carry over SEM1*
Electrical-non propulsion	*35.7*	*36*	*minor adjustment for SEM2*
Cooling and heating	*30.0*	*30*	
Closures	*109.3*	*109.3*	*adjustment to rear door outer skin geometry. No mass impact*
Bumpers	*26.0*	*26*	*carry over SEM1*
Curb mass	**1512.2**	**1872.7**	**kg**
Curb mass delta		**24%**	SEM2 has 24% higher curb mass than SEM1
Maximum payload	500	675	
Gross Vehicle Weight GVW	2012.2	2547.7	
GVW delta		27%	SEM2 has 27% higher GVW than SEM1

Figure 11.4.1.3 Comparison of SEM1 and SEM2 subsystem weight, vehicle curb and gross weight

As per the SEM1 development, Virtual Reality tools were used to assess and confirm the occupant positioning and ingress/egress performance. The middle row seats are configured as sliding and folding enabling access for the third row.

Figure 11.4.1.4 SEM2 Virtual Reality assessment of occupant position, ingress and egress

11.4.2 SEM2 Body structure

The SEM2 BIW is designed to use maximum carry-over/commonality with SEM1. The higher vehicle curb and gross weights result in higher crush and energy levels for frontal and rear crash loadcases, therefore some adjustments were required to in order to ensure the crashworthiness performance was in line with SEM1 and targets. Figures 11.4.2.1 and 11.4.2.1 show where changes to the AHSS grade or gauge thickness was made for specific SEM2 parts. These changes were estimated on an engineering judgement basis. Full vehicle crash simulation as performed for SEM1 would be required to validate these recommendations. In some cases, existing SEM1 tooling could be used for some of the unique SEM2 front and rear zone parts. Full forming feasibility calculations would be required to validate this. The SEM2 BIW weight is 323kg versus a target of 361.9kg.

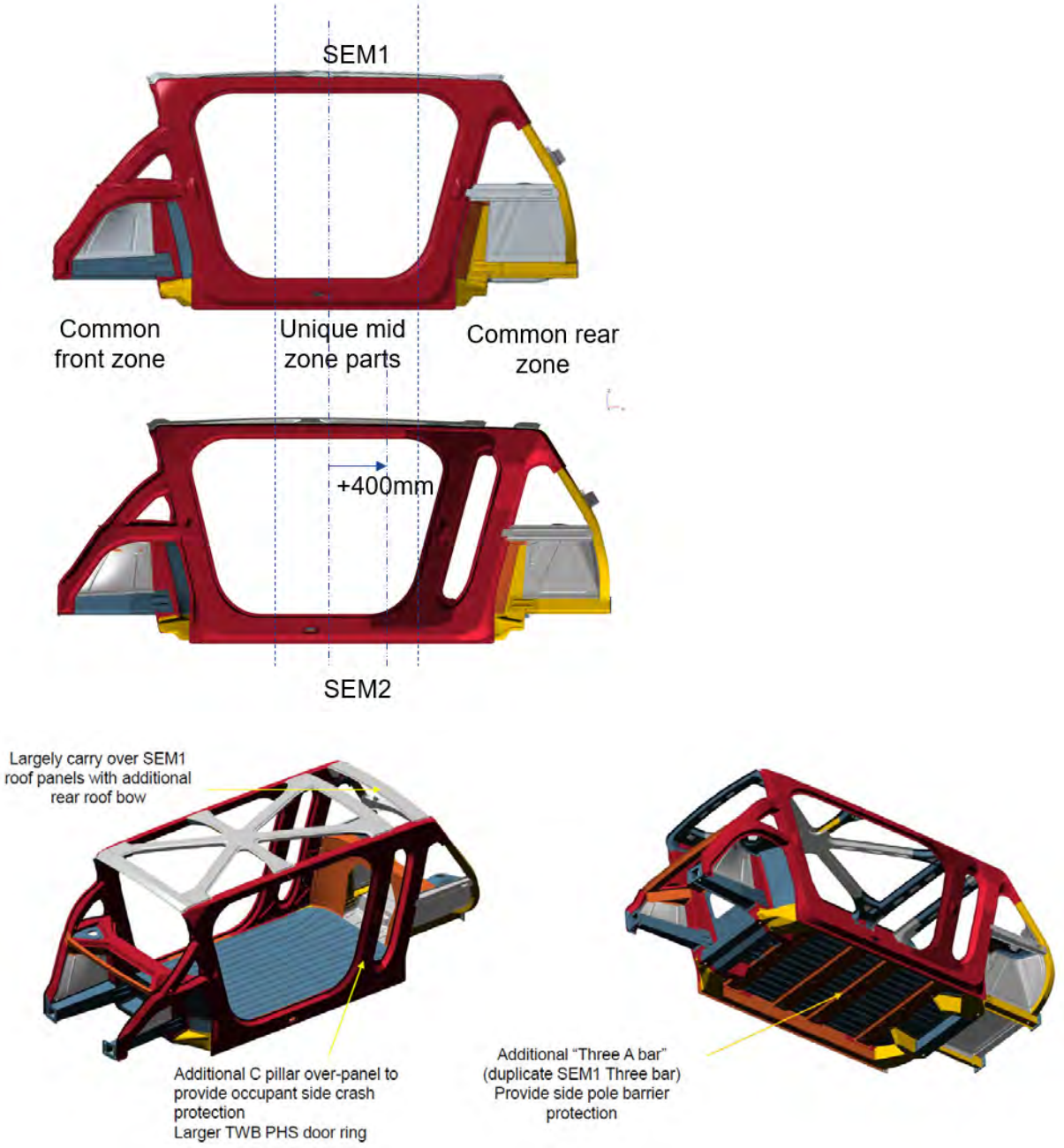

Figure 11.4.2.1 SEM2 BIW design approach and commonality with SEM2

Part Number	Part Name	AHSS Grade	Gauge (mm)	C = Carry over SEM1 G = grade/gauge change N = New geom	Part Mass (kg)	SEM2 change
03643418_2	GLANCE BEAM LOWER REACTION RH	CR1200Y1470T-MS	1.2	G	0.72	change from 0.8mm to 1.2mm
03640761_2	GLANCE BEAM UPPER REACTION RH	PHS-CR1500T-MB	1.0	G	0.52	change from 0.8mm to 1.2mm
03553269_2	LONGITUDINAL MID RAIL OUTER FRONT RH	CR500Y780T-DP/CR700Y980T-DP	2.0	G	3.51	change from 1.8mm/2.0mm TWB to to 2.0mm throughout
03506010_2	LONGITUDINAL MID RAIL OUTER FRONT LH	CR500Y780T-DP/CR700Y980T-DP	2.0	G	3.51	change from 1.8mm/2.0mm TWB to to 2.0mm throughout
03585863_2	GLANCE BEAM UPPER TRIANGULATION INNER LH	PHS-CR1500T-MB	1.2	G	1.12	change from 0.8mm to 1.2mm
03642244_2	GLANCE BEAM LOWER REACTION LH	CR1200Y1470T-MS	1.2	G	0.72	change from 0.8mm to 1.2mm
03553270_2	LONGITUDINAL MID RAIL INNER FRONT RH	CR500Y780T-DP/CR700Y980T-DP	2.0	G	3.79	change from 1.8mm/2.0mm TWB to to 2.0mm throughout
03618587_2	GLANCE BEAM OUTER RH	PHS-CR1500T-MB	1.2	G	2.63	change from 0.8mm to 1.2mm
03618591_2	GLANCE BEAM UPPER TRIANGULATION OUTER RH	PHS-CR1500T-MB	1.2	G	1.27	change from 0.8mm to 1.2mm
03640760_2	GLANCE BEAM UPPER REACTION LH	CR1200Y1470T-MS	1.2	C	0.42	change from 0.8mm to 1.2mm
03618590_2	GLANCE BEAM UPPER TRIANGULATION INNER RH	PHS-CR1500T-MB	1.2	G	1.12	change from 0.8mm to 1.2mm
03643540_2	GLANCE BEAM LATERAL CROSS MEMBER OUTER	CR1200Y1470T-MS	1.2	G	1.52	change from 0.8mm to 1.2mm
03601008_2	GLANCE BEAM UPPER TRIANGULATION OUTER LH	PHS-CR1500T-MB	1.2	G	1.27	change from 0.8mm to 1.2mm
03506011_2	LONGITUDINAL MID RAIL INNER FRONT LH	CR500Y780T-DP/CR700Y980T-DP	2.0	G	3.51	change from 1.8mm/2.0mm TWB to to 2.0mm throughout
03640758_2	STRUT CROSS MEMBER FRONT	PHS-CR2000T-MB	1.2	G	3.31	change from 1.0mm to 1.2mm
03618589_2	GLANCE BEAM INNER RH	PHS-CR1500T-MB	1.2	G	2.56	change from 0.8mm to 1.2mm
03585867_2	GLANCE BEAM OUTER LH	PHS-CR1500T-MB	1.2	G	2.63	change from 0.8mm to 1.2mm

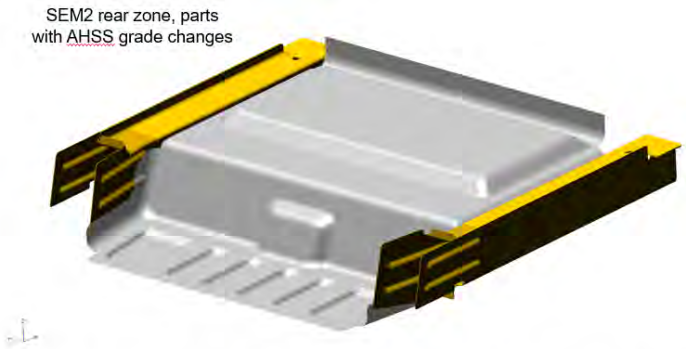

Part Number	Part Name	AHSS Grade	Gauge (mm)	C = Carry over SEM1 G = grade/gauge change N = New geom	Part Mass (kg)	SEM2 change
03596995_2	REAR COMPARTMENT PAN LOWER	CR_HSLA350/450	0.5	N	2.89	New geometry for rear EDU package
03477701_2	LONGITUDINAL REAR RAIL INNER RH	CR820Y1180T-RA_1.4_CR600Y980	1.8	G	1.90	change from 1.4mm/1.6mm TWB to 1.6mm
03476382_2	LONGITUDINAL REAR RAIL INNER LH	CR820Y1180T-RA_1.4_CR600Y980	1.6	G	1.90	change from 1.4mm/1.6mm TWB to 1.6mm
03477703_2	LONGITUDINAL REAR RAIL OUTER RH	CR820Y1180T-RA_1.4_CR600Y980	1.6	G	1.81	change from 1.4mm/1.6mm TWB to 1.6mm
03476381_2	LONGITUDINAL REAR RAIL OUTER LH	CR820Y1180T-RA_1.4_CR600Y980	1.6	G	1.81	change from 1.4mm/1.6mm TWB to 1.6mm

Figure 11.4.2.2 Unique SEM2 BIW parts: front and rear zones (See Appendix 4 for larger image)

The SEM2 mid zone features more unique parts and less commonality with SEM1 due to the geometric changes as a result of the +400mm length increase. Nevertheless, a significant number of common parts were enabled in the mid zone by incorporating a largely carry-over roof structure, A pillar inners and floor cross members (two, three, four bars) as shown in Figure 11.4.2.3.

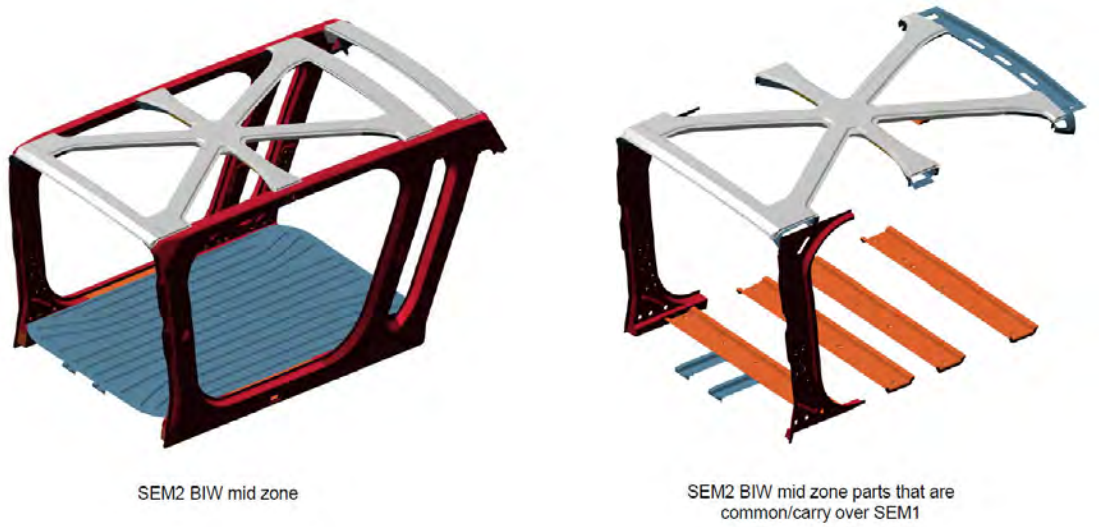

Figure 11.4.2.3 Unique SEM2 BIW parts: mid zones, common/carry over from SEM1

The overall BIW part commonality between SEM1 and SEM2 is shown in Figure 11.4.2.4. From a total of 229 SEM2 BIW parts, 68% are carry-over/unmodified from SEM1, 9% are carry-over from SEM1 but with a material grade or gauge thickness change (subject to forming feasibility) and 23% are unique parts with unique tooling. This platform commonality approach ensures SEM2 (and also SEM1) achieves an overall competitive BIW and vehicle cost.

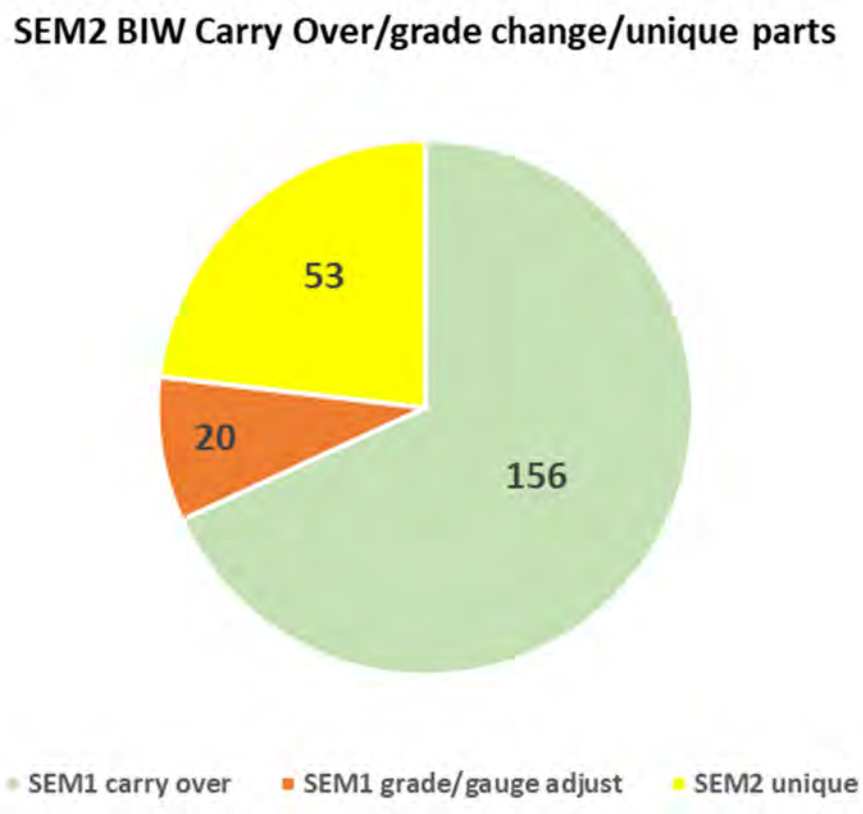

Figure 11.4.2.4 SEM2 BIW part commonality with SEM1

11.4.3 SEM2 Propulsion battery

The SEM2 propulsion battery energy is increased to 96kWH configured with 8 modules. The modules are mounted to 4 structural roll formed and roll stamped Martensitic grade cross members, which are common in design and AHSS grade with SEM1. The SEM2 battery longitudinals are unique to SEM2 and cold formed in DP1180. The SEM2 battery bottom cover applies the same concept and AHSS grades as SEM1 design (Figure 7.2.5.17).

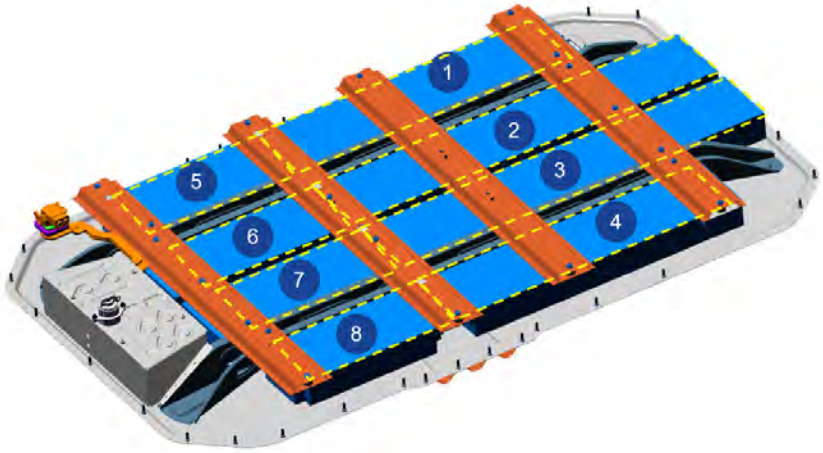

Figure 11.4.3.1 SEM2 96kwH battery and module configuration

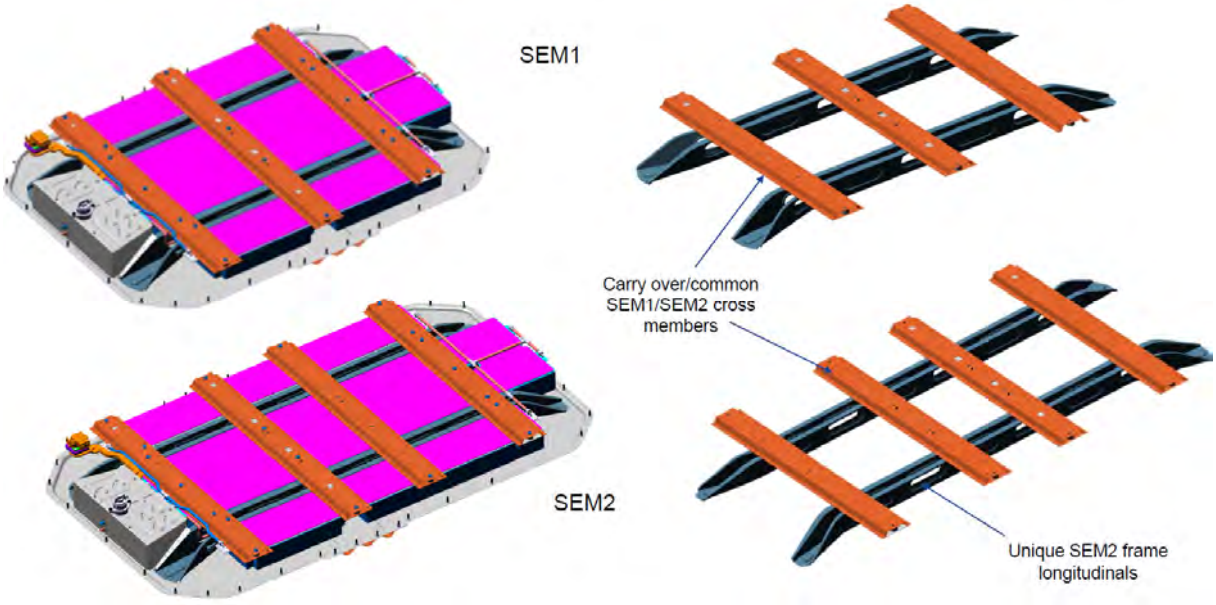

Figure 11.4.3.1 Comparison of SEM1 and SEM2 batteries and carrier frames

11.5 SEM2 subjective performance evaluation

A subjective performance evaluation was performed to help guide the SEM2 design and advise any AHSS grade and gauge changes.

Attribute/Requirement	Impact of SEM1 to SEM2	Design mitigation and countermeasures
Front crash	SEM2 higher 24% curb mass, therefore front crash will have higher energy levels to manage	Increase strength of front longitudinals to enable greater energy absorption. Increase gauge thickness of PHS2000 SORB parts
Side crash	IIHS side barrier. Larger side aperture. Heavier vehicle. SEM1 has very good side barrier crash performance Pole: Alignment to occupant won't change so no issue expected. Pole to HV battery potentially an issue with stretched door aperture	Additional C pillar to protect 3rd row occupants
Rear crash & roof crush	Higher GVW. SEM1 performance is comfortable so no significant issue expected	None
Body stiffness and NVH	Stretched, longer body structure therefore modal frequencies expected to reduce, potentially below target. Higher battery mass will further reduce the batter first mode	Additional structural adhesive applied to recover NVH modal frequencies
Durability	Higher curb mass = higher durability loads. SEM1 has some margin on durability performance so no change is expected	None
BIW Mass	SEM2 BIW mass increase will be: additional/stretch mid-zone section. Impact of secondary countermeasures. There could be a –ve mass spiral effect with more mass being required due to higher curb mass. E.g. body needs to be heavier due to heavier battery	None
Cost	New mid-zone panels (tooling) and increased grade and gauges in front zone	Cost increases expected to be in line with other vehicle platform approach
Life Cycle Assessment	Higher vehicle mass, more steel. Less aggressive real world duty cycle (less city stop-start) Need to ensure high occupancy rate >2	None
Manufacture & assembly	Don't expect significant manufacture issues beyond usual vehicle variant lines	
HV battery, jacking, China crush, PSD	Higher mass, higher jacking load. Larger battery cover area. More challenging to meet targets	None

Figure 11.5.1 Subjective performance evaluation for SEM2 (See Appendix 4 for larger image)

CAE calculations are required in order to validate the subjective evaluations.

12.0 Additional SEM1 and SEM2 engineering studies conducted by academic institutions

This section describes supporting/complementary engineering studies undertaken by global academic institutions using Steel E-Motive concept and data as a basis. These studies serve to further demonstrate the validity of the Steel E-Motive concept and provide students the opportunity to develop and demonstrate their engineering learning on a futuristic vehicle.

12.1 Concept development of hydrogen fuel cell SEM1 variant

This study was undertaken by a final year UK undergraduate study as part of a Masters of Engineering Degree in Automotive Engineering at Loughborough University. The student supported the Steel E-Motive project design activities at Ricardo during a “gap year”.

Objectives of the study:

- Optimise a Fuel Cell Hybrid configuration for Steel E-Motive to maximise performance while keeping system cost and weight to a minimum.

- Explore the feasibility of a Fuel Cell Hybrid configuration to be used in Steel E-Motive when compared to original BEV variant

Technical Approach:

1. Produce a vehicle simulation and fuel cell system model, using MATLAB and Simulink, to output PEMFC performance characteristics based on adjustable vehicle parameters
2. Using data obtained from objective 1.1, create analysis of generated FCHV system performance in context of MaaS application
3. Using optimised system parameters, explore packaging feasibility of a fuel cell system in SEM-1 while changing as little architecture as possible
4. Using data obtained from objective 1.1 as well as data obtained from 2030 roadmaps and other literature sources, construct an analysis of the generated FCHV system and its feasibility of being used as a fleet vehicle for MaaS applications

The following slides are taken from the final engineering report for the study, demonstrating fuel cell simulation modelling & optimisation and 3D CAD package study.

Model Construction

Model Overview

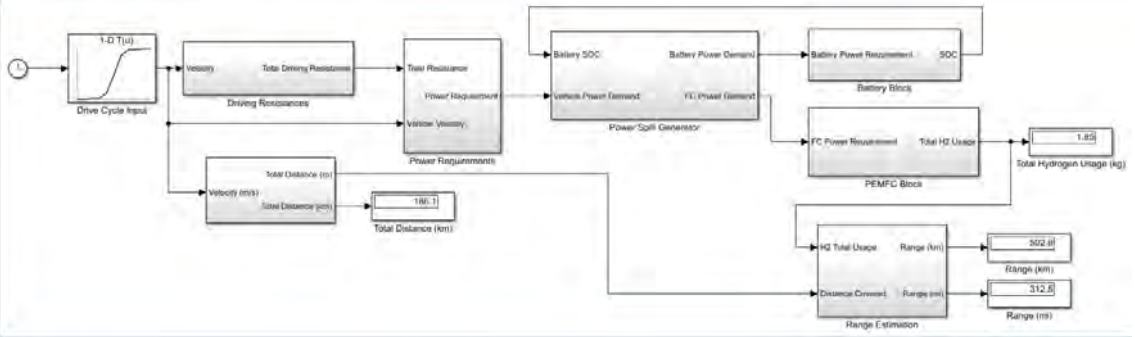

Model Construction

Model Inputs

- System inputs ran through preliminary MALTAB script before running simulation
  - *Vehicle Parameters*
  - *Drive Cycle*
  - *Battery Parameters*
  - *PEMFC Parameters*
- Drive Cycle Input
  - *Primary: WLTP Class 3b*
  - *Secondary: New York City Cycle*

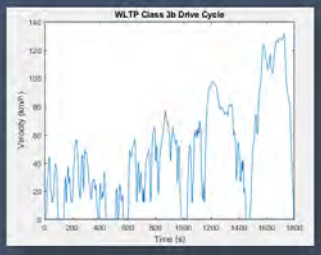

Elapsed Time: 1800 Seconds
Distance Covered: 23.26 km

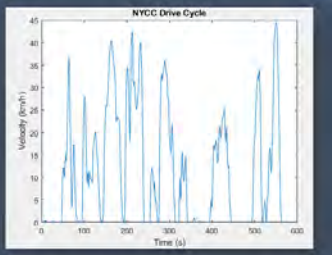

Elapsed Time: 599 Seconds
Distance Covered: 1.89 km

Model Construction

PEMFC Block

- Battery Block Principles:
  - *Input: Fuel Cell Power Requirement*
  - *Output: H2 Usage*
- Assumes cell behaviour is uniform across pack
- Accounts for parasitic losses and auxiliary component load
- Polarization Curve scaled to meet 2030 FCHJU targets
  - *Cell Power Density = 2 W/cm2*

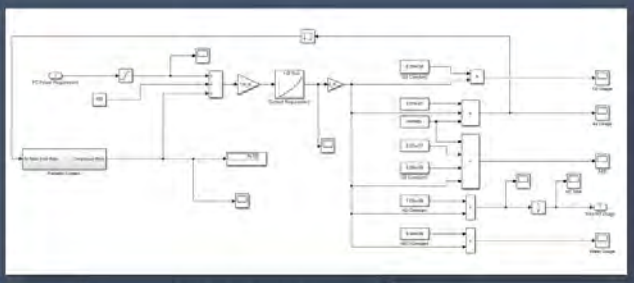

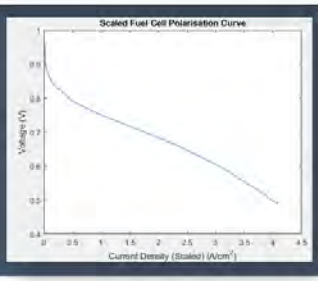

MODEL CONSTRUCTION

Hybrid Power Split

- Battery:Fuel Cell Power Split Dictated by battery state of charge (SOC)
  - *Linear relationship between 65-100% SOC*
  - *Non-Linear <65%*
- Aim of hybrid system is to maintain SOC between 50-65% during operation
- When battery SOC is below threshold, fuel cell power output is increased to recharge battery

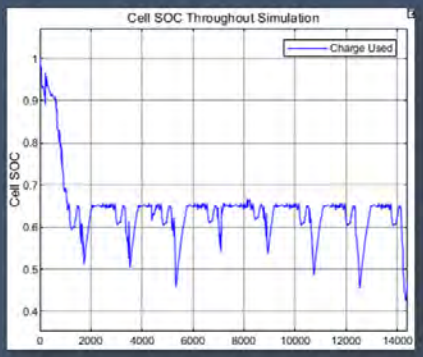

System Optimisation & Results

Parameter Selection

- 4 parameters chosen to optimise for system and use case
- Measured parameters shown below
- Fuel Cell cost and Battery cost and mass figures obtained from APC roadmap
  - *Fuel Cell Cost = 54 $/kW*
  - *Battery Cost = 77 $/kWh*
  - *Battery Gravimetric Density = 240 Wh/kg*
- Fuel Cell mass derived from benchmarking Toyota Mirai and Hyundai Nexo stack system
  - *Fuel Cell Gravimetric Density = 1.53 kW/kg*
- Performance coefficient created to quantify system performance → $S = \frac{Ra^2}{(m_{FC}+m_B)\cdot(C_{FC}+C_B)}$

Parameter	Value 1	Value 2	Value 3	Unit
Number of Fuel Cells	300	400	500	/
Battery Capacity	1	2	3	kWh
Power Split Lower Bound	0.2	0.25	0.3	/
Power Split Upper Bound	0.5	0.6	0.7	/

Parameter	Abbreviation	Unit
Range	Ra	km
Fuel Cell System Cost	C_{FC}	$
Fuel Cell System Mass	m_{FC}	kg
Battery Pack Cost	C_B	$
Battery Pack Mass	m_B	kg
Performance Coefficient	S	/

System Optimisation & Results

Optimisation Results

Parameter	Value	Unit
Number of Fuel Cells	300	/
Fuel Cell Stack Power	120	kW
Battery Pack Capacity	1	kWh
Power Split Lower Bound	0.3	/
Power Split Upper Bound	0.6	/
Range	504	km
Powertrain Mass	82.6	kg
Powertrain Cost	6557	$
Performance Coefficient	0.469	/

First Optimisation Run

Parameter	Optimal Value	Unit
Number of Fuel Cells	260	/
Fuel Cell Power	104	kW
Battery Pack Capacity	1.6	kWh
Power Split Lower Bound	0.3	/
Power Split Upper Bound	0.6	/
Range	502.8	km
Powertrain Mass	74.64	kg
Powertrain Cost	5739.2	$
Performance Coefficient	0.59	/

Second Optimisation Run

Parameter	Value 1	Value 2	Value 3	Value 4	Value 5	Value 6	Unit
Number of Fuel Cells	260	270	280	290	300	310	/
Battery Capacity	1	1.2	1.4	1.6	/	/	kWh

System Optimisation & Results

Final Results

- Maximum range target: 402km
  - *UITP Taxi Benchmark Study*
- H2 consumption target: 1kg/100km
  - *FCHJU 2030 SoA Target*

Parameter	Optimal Value	Unit
Number of Fuel Cells	260	/
Fuel Cell Power	104	kW
Battery Pack Capacity	1.6	kWh
Power Split Lower Bound	0.3	/
Power Split Upper Bound	0.6	/
Range	502.8	km
Powertrain Mass	74.64	kg
Powertrain Cost	5739.2	$
Performance Coefficient	0.59	/

Drive Cycle	Parameter	Value	Unit
WLTP 3b	Range	502.8	km
	H2 Consumption	0.994	kg/100km
NYCC	Range	823	kg
	H2 Consumption	0.607	kg/100km

8th June 2022 | 17

VEHICLE PACKAGING STUDY

H2 Packaging Benchmark – Toyota Mirai 2

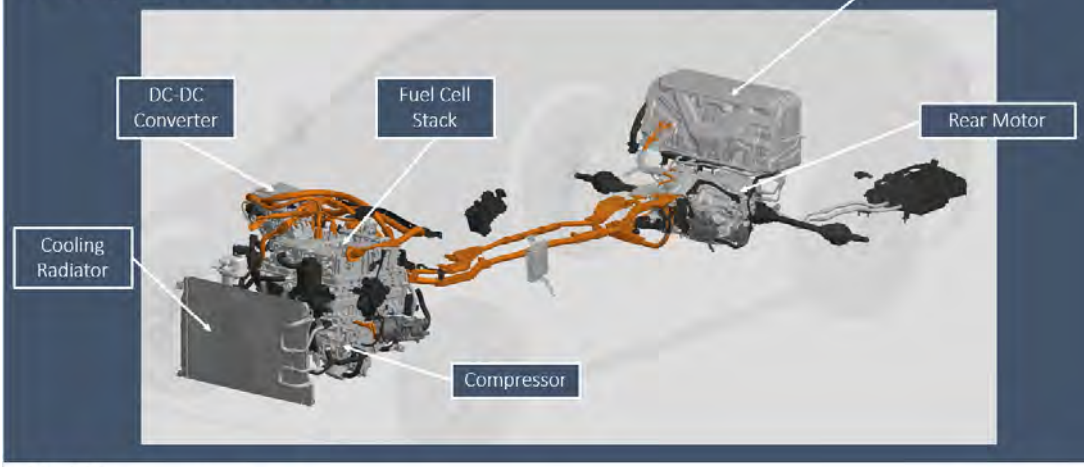

8th June 2022 | 19

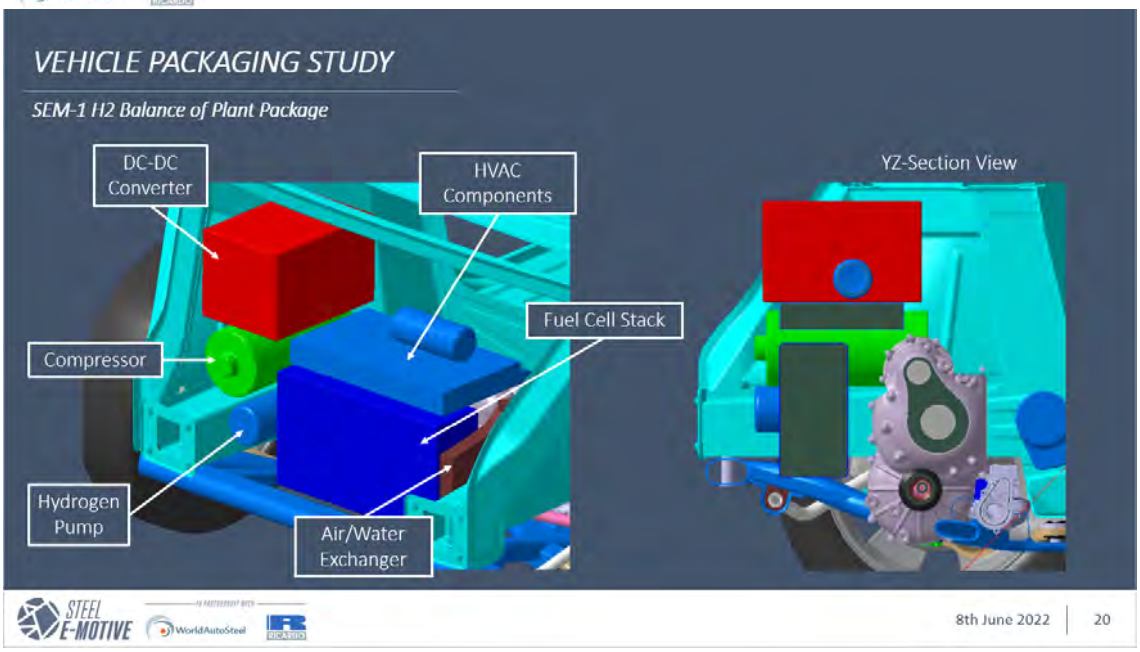
VEHICLE PACKAGING STUDY
SEM-1 H2 Balance of Plant Package
DC-DC Converter
HVAC Components
Fuel Cell Stack
Compressor
Hydrogen Pump
Air/Water Exchanger
YZ-Section View
8th June 2022
20

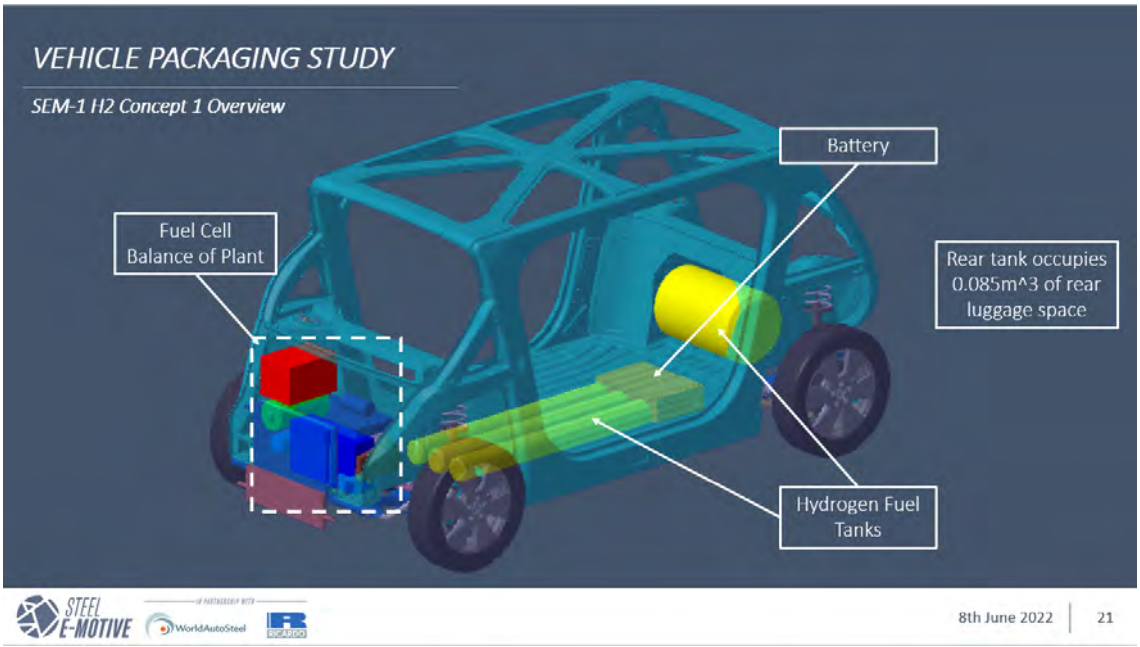
VEHICLE PACKAGING STUDY
SEM-1 H2 Concept 1 Overview
Battery
Fuel Cell Balance of Plant
Rear tank occupies 0.085m^3 of rear luggage space
Hydrogen Fuel Tanks
8th June 2022
21

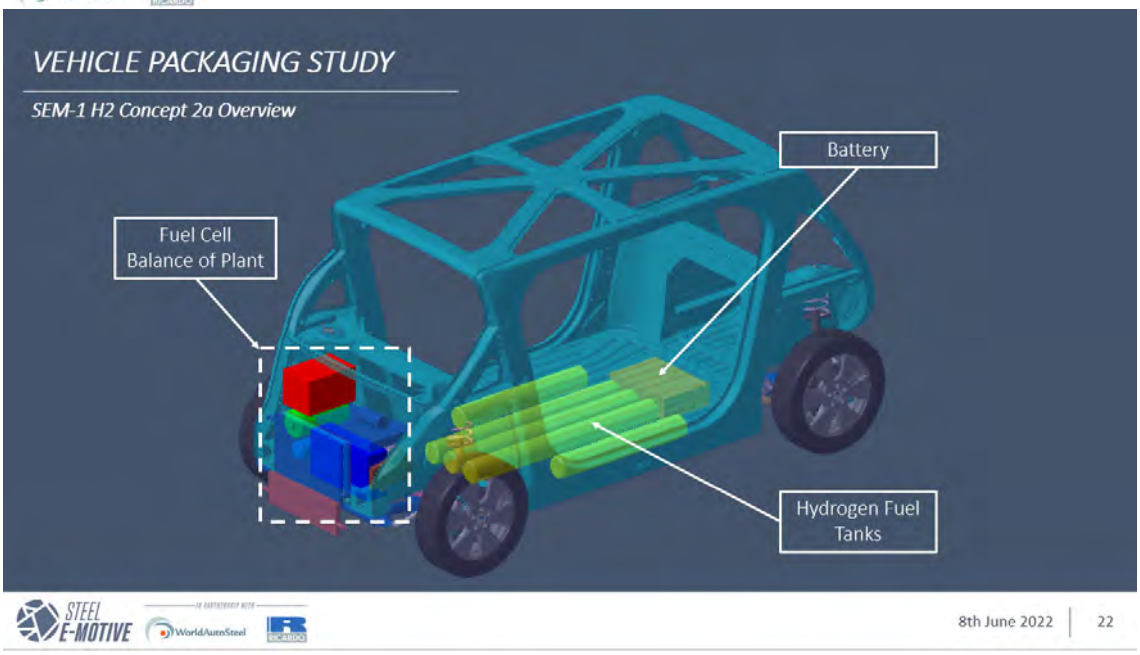
VEHICLE PACKAGING STUDY
SEM-1 H2 Concept 2a Overview
Battery
Fuel Cell
Balance of Plant
Hydrogen Fuel
Tanks
8th June 2022
22

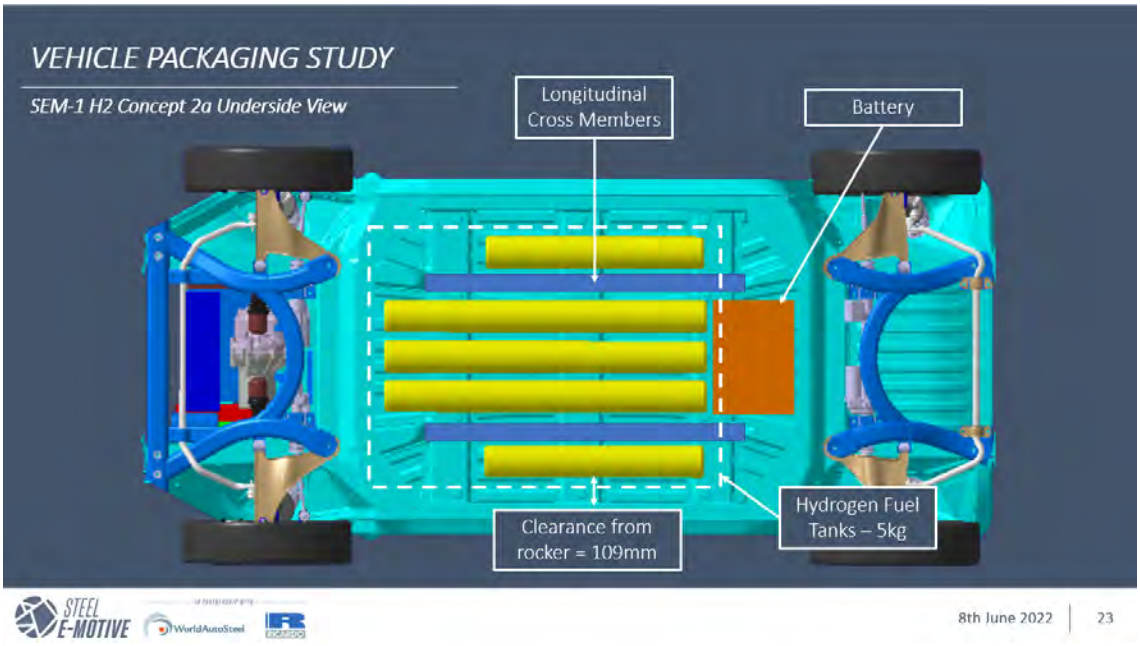
VEHICLE PACKAGING STUDY
SEM-1 H2 Concept 2a Underside View
Longitudinal
Cross Members
Battery
Hydrogen Fuel
Tanks – 5kg
Clearance from
rocker = 109mm
8th June 2022
23

VEHICLE PACKAGING STUDY

SEM-1 H2 Concept 2b Underside View

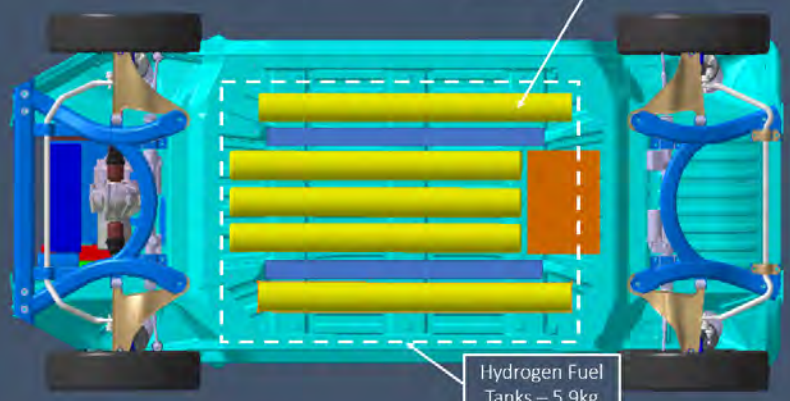

Future Work

Model Enhancements

SIMULATION MODEL

- Create automated hybrid system optimisation process
- Create secondary power split control strategy
- Implement full battery recharge strategy

CAD PACKAGE

- Further work to understand complete mechanical package in detail
  - *i.e. tank packaging, cable and pipe routing*

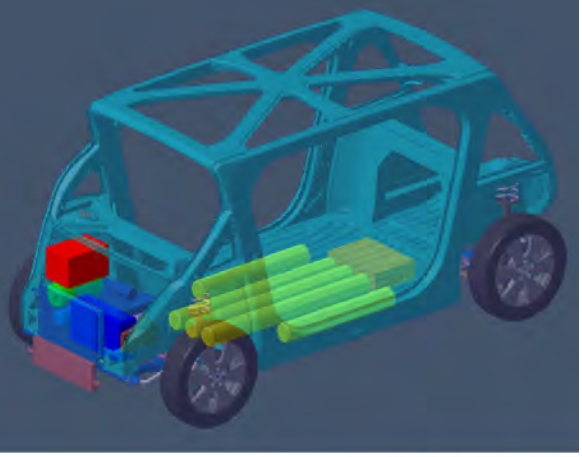

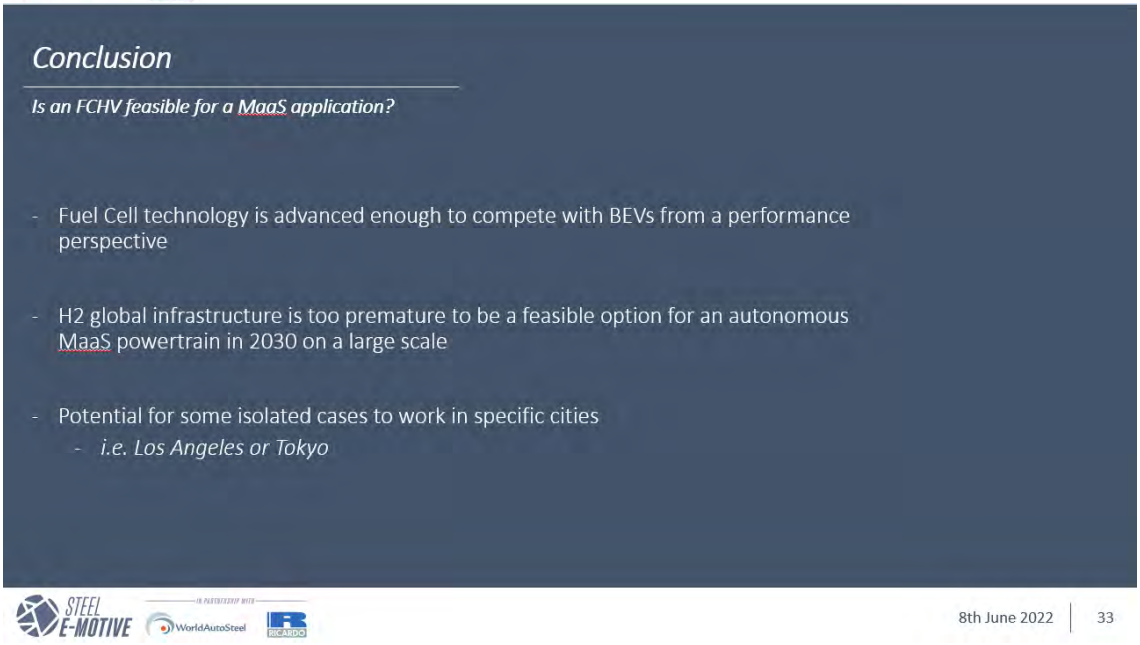

12.2 Michigan Technological University – Senior Capstone Project #1: Steel E-Motive Side Door Functionality, Door Hinge Assessment

MTU Senior Capstone Team: Gavin Sheffer, Leander Daavettila, Rob Oestreich, Steven Turnbull, Andrew Mitteer, and Jesse Ebenhoeh

Status
2 Semester program, complete

Introduction / Background
The MTU Senior Capstone Design Team, sponsored by WorldAutoSteel and the Auto/Steel Partnership, was challenged to design a new door hinge for the Steel E-Motive side closure mechanism. The current hinge design was provided as a reference, but a few operational issues were identified for this team's assessment and engineering study.

- The previous hinge design interferes with the all-wheel steering, meaning in emergency situations, passengers could get trapped in the vehicle. For SEM1, it was also observed that when the wheels are turned, they would block the doors from opening fully, constraining passenger exit (Figure 1 below).
- An emergency release mechanism was needed to allow users to escape in the event a crash or electrical failure prevented the doors from opening.
- Power requirements and electric motor sizing for the hinge mechanism needed to be defined.

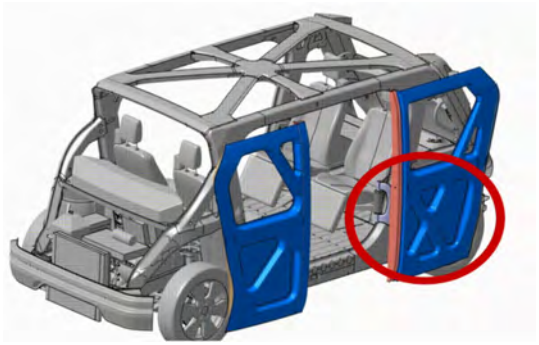

Figure 1: Side door opening constrained by present hinge mechanism and wheel position.

Project Details, Results

MTU's design solution uses a four-bar linkage hinge design to keep the door parallel to the body of the vehicle to avoid damage to either the door or the body. The team used a 4:1 gear ratio for the drive motor to open the door. Finally, one of the pins in the secondary arm linkage is accessible by passengers and removable, allowing users to manually push the door open in the event of an emergency (see Figure 2).

Their solution includes pressing a button to open and close the door. The stepper motor receives the input from the button and rotates the gears; the gears then rotate the primary arm which drives the door. The primary arm is mounted to the door in two locations with bolts. The secondary arm is added to the mechanism to create a four-bar linkage, which helps maintain door orientation during operation. An emergency release was designed and added to the secondary arm to release the four-bar linkage. This allows the door to swivel around a turned wheel in the event of an emergency.

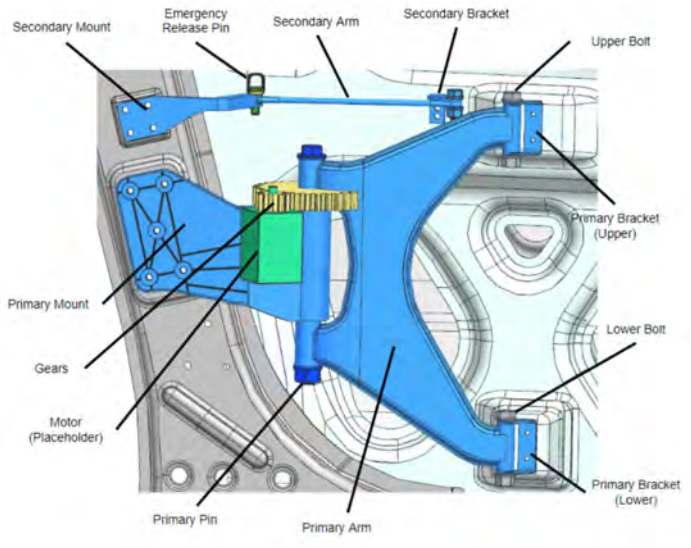

Figure 2: 3D model of the final design less the gear cover for clarity.

The emergency release was designed for safety and manufactur-ability. The emergency release pin was simplified to utilize off-the-shelf pins. A relay is suggested to cut power to the motor and allow the door to be manually pushed open. A gear cover was added for safety to protect the occupants from getting pinched by the gears. To maintain and service the design, each part of the assembly was designed to be attached with threaded fasteners. A gear drive was created so we could use a more cost-efficient motor. The gear ratio decreased the amount of torque required. The material was chosen based on strength and sustainability.

Conclusions

The CAD geometry and the quarter-scale prototype were able to meet all the engineering requirements and objectives. The CAD model defines the mass and emergency release mechanism, and the kinematics are verified by the quarter-scale prototype. The FEA simulation verified *set and sag* under normal and abusive loading conditions. In identifying specifications required for the full model, the projected production cost for one mechanism is $471. This includes stamped and cast components, off-the-shelf components such as the stepper motor and fasteners, and the cost of assembly. The team compared using AHSS for the components as opposed to an aluminum alloy. Steel components are stronger, half the price of aluminum, and produce 1/3 of the carbon emissions compared to the same amount of aluminum.

The prototype was 3D printed from PLA plastic at quarter scale. This serves as a model to be shown by Auto/Steel Partnership for future presentations. It was also used to verify the kinematics of the door motion.

12.3 The Ohio State University - Senior Capstone Project #3: Welding Capabilities of a Five Sheet Stack-up of High-Strength Steels Using Resistance Spot Welding

OSU Senior Welding Engineering Capstone Team: Rachel Blankenship, Koushin Jacquet, Hunter Flading

Status
2 Semester program – complete

Introduction/Background
WorldAutoSteel sponsored The Ohio State University's Senior Capstone Projects to confirm viability of a complex RSW joint comprising of 5 individual sheet layers for Mobility as a Service (MaaS) vehicles. Our hope is that this 5 layer stack-up weld project will demonstrate technical feasibility that allows manufacturers to leverage current manufacturing infrastructure, lowering investment costs and improving sustainability.

AHSS are widely used in the automotive industry for resistance spot welding (RSW); however, they come with many challenges. These include susceptibility to hydrogen cracking, martensite formation during rapid cooling, and porosity. The same weld parameters that are successfully used for mild steel assembly applications must be adapted with higher levels of quality control to achieve required weld integrity and production reliability – but these weld conditions and QC practices are now well-understood and implemented in industry.

The Steel E-Motive vehicles are composed of welds made using spot welding, laser welding, and structural adhesive. Steel grades being used in the vehicle include press hardened steels (PHS), martensitic steels (MS), 3rd generation steels and dual phase steels (DP).
The welded joint under consideration is in the front extended passenger protection zone of the car, specifically the vertical dash brace and upper glance beam reaction area. The various material grades include MS1200, PHS2000, and MS2000 with gauges of 1 to 2 mm and coatings of EG and AS150 (for the PHS grades). Current practice for these types of joints is to create a singular spot weld with the bottom 3 sheets, which would include the strut cross member closing plate, the glance beam lower reaction LH, and the vertical dash brace upper front LH. This 3-sheet stack (Group 2) would then be welded to a 2-sheet stack (Group 1) composed of the top two layers of the 5 stack, the strut cross member front and the glance beam upper reaction LH. The cross section of this joint as well as its position within the vehicle can be seen in Figure 1 below.

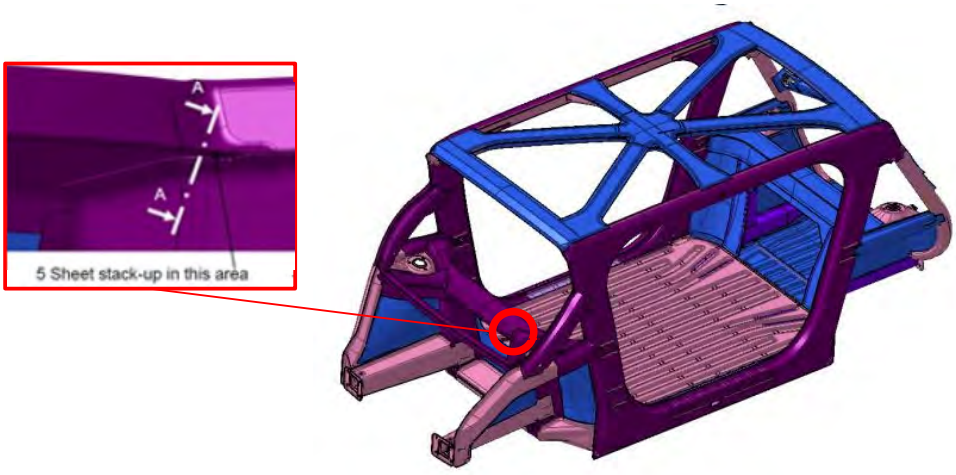

Figure 1: SEM1 body structure and front extended passenger protection zone, showing joint location

Project Details, Results
This team's plan was to create a single 5-t stack-up RSW joint total stack thickness = 6 mm (see Table 1). Project Objectives:

1) Determine optimal RSW parameters for a 5-T stack-up.

2) Determine whether 5-stack resistance spot weld is possible, or if a 2 plus 3 stack resistance spot weld is needed.

Group Number	Stack-up Position	Part Number	Name	Grade	Gauge (mm)	Coating
1	Top	03640760	Glance Beam Upper Reaction LH	MS 1200/1470	1.0 spec; 1.2 actual	EG
1	2	03640758	Strut Crossmember Front	PHS2000	1.0 spec, 1.2 actual	AS150
2	3	03671385	Vertical Dash Brace Upper Front LH	PHS2000	2.0	AS150
2	4	03642244	Glance Beam Lower Reaction LH	PHS2000	1.0 spec, 1.2 actual	AS150
2	Bottom	03642357	Strut Cross Member Closing Plate	MS2000	1.0	EG

Table 1: Individual components, steel grades in 5-t Stack-up.

Steps

Task 1 - Our team first conducted a literature search, where previous experiments and projects were studied to acquire a background on the 5T stack-up. These included procedures and results of 3T and 4T stack-ups performed previously by other scholars (in our research found no current examples of successful spot welding of 5 sheets simultaneously).

Next, we referenced previous work by WorldAutoSteel and used lessons learned to guide parameter selection decisions for our welding trials.

Task 2 - We acquired materials from WorldAutoSteel members, who sent 2 types of materials with varying thicknesses for this project. The joint in question included MS1200, PHS2000, and MS2000 of varying coatings and thicknesses. Members were able to supply PHS2000 was provided with an AS150 coating and 2 sheet thicknesses = 1.2 mm and 2.0 mm, and MS (Martensitic) 1500 steel, with EG coating and 1.2 mm thickness.

Expert conclusion is that the thickness variation was less important than the symmetry of the joint, and the metallurgical chemistries which were quite similar for grades belonging to the same product family.

Task 3 - The parameters for the welding process were determined using Simufact Welding 2021, a welding simulation software. The literature found in Task 1 was used as a basis for welding parameter selection and lab trials.

Task 4 - Welding Trials and Inspection. Using the Obara MFDC resistance spot welder and parameters determined in Task 3, various welds were conducted and evaluated via destructive testing, to determine optimal parameterization to meet target weld criteria. Samples were mounted and prepared for microscopic visual analysis.

For experimental purposes, RSW welding trials were performed with five flat coupons representing the stack-up materials, thicknesses and coatings. The benefits of welding all 5 coupons at once versus welding 2 separate stacks and then joining those together include lower power, cost, increased efficiency and decreased welding time. Additional benefits include less electrode wear between welds and less time cleaning electrodes due to a singular weld. The penetration also gradually increases with each pulse to the weld.

Task 5 - Data Analysis. Macroscopic pictures were taken of the samples and evaluated to compare weld nugget size, porosity, deformation, cracking, and indentation.

Conclusions

4. A five-layer stack-up spot weld can be successfully created with advanced high strength steels using a range in number of pulses, currents, forces, and times, indicating sufficient process robustness.
5. Simufact Welding successfully models weld nugget development and final weld size, that narrows parameter selection avoiding costly trial and error practices.
6. Using a pulsation current schedule with descending current pulses was just as successful in creating welds as using the same current level pulses. This was perhaps assisted by joint symmetry.
7. A single spot weld for a five-layer stack-up has greater time and cost efficiency than welding a two-layer and a three-layer stack-up into a combined five layers.

12.4 Michigan Tech University – Senior Capstone Project #2: Adaptation of SEM2 from People Mover to Commercial Delivery Vehicle

MTU Senior Capstone Team: Kyle Davis, Nick Palatka, Evan Larson, Logan Pietila, Blake Pietila, Tej Bergin

Status
2 Semester program, 1 semester complete

Introduction / Background
This Senior Capstone Design Team was sponsored by World Auto Steel and Ricardo Engineering (UK engineering and consultancy firm), to develop a solution for expanding the servicability within a 24-hour period for Steel E-Motive 2 (SEM2), their extra-urban autonomous electric vehicle concept. The SEM2 vehicle is a stretched 6-passenger commuter targeting longer journeys, with expanded occupancy or additional luggage capacity. In non-commuting hours, the Mobility Fleet Operator would like to continue revenue generation by quickly adapting the vehicle for commercial delivery services. Currently, occupant packaging contrasts with the storage requirements of a package delivery vehicle, thus the SEM2 vehicle's can only be utilized to either transport people or goods. Our project objective is to develop interior seating that enables quick removal and adaptation to an optimal delivery van.

Project Details, Results
From the requirements outlined by WorldAutoSteel, the team focused further research on interior vehicle and seat design. Modern delivery methods, delivery vehicle layout, passenger vehicle seat safety requirements, and seat folding or locking mechanisms were sub-categories of research that hold value within the scope of the project. The main takeaways from our research include different pin and slot mechanisms that are incorporated into a preliminary design for a quick release system. We also benchmarked a vertical folding seat based on International Harvester designs and we have modified these for application to the SEM2 vehicle's specific needs.

The quick release system will benefit MSP technicians responsible for performing the conversion of multiple SEM2 vehicles in its fleet at their depot during off-commuting hours. In under 30 minutes, the fleet operators (MSP) must be able to convert the vehicle from a vehicle stressing passenger comfort to an autonomous delivery van and vice versa, using common tools and techniques while meeting all necessary safety standards and regulations. The fleet operators that provide the robo-taxi service are not expected to see any major disruption in ride services, however they may observe improved utilization and profitability if they use the vehicles for package delivery.

Our current engineering requirements include:
- maximum total payload of 675 kg (6 passengers and 6 seats)
- individual seat weight of 30kg (6 seats)
- total volumetric storage space requirement of 1 cubic meter
- total seating width equal to or less than 1220 mm
- changeover time less than 30 minutes and
- minimal number of changeover movements (fewer than 50 for the complete conversion from passenger to cargo transportation)

Concept Solutions
A graphical rendering of our selected system-level concept is provided in Figure 1. This design showcases two pairs of T-shaped rails placed in the fore-aft direction of the vehicle. These T-Rails are compatible with a slider system that connects to the bottom of each seat leg. A sliced view of the rails and slider system are seen in Figure 2. On each slider, in the port-starboard direction, a circular slot approximately 20 mm in diameter (dependent on pin material and size) is cut-out to allow for the insertion of a spring-loaded steel pin. This pin engages both the slider as well as an equivalent slot cut into the rail, to allow the seat to be locked into a specified position along the rail (Figure 3). The rails run the full length of the vehicle's interior, and allow for 3

seating modules to be placed and locked into a position. Insertion and removal of the slider on the rails will be possible through narrow sections on the rails where the slider can be vertically lifted or placed on the rail system.
In order to “drop the seats" onto the rails without manual lifting, the team has designed an accompanying “pallet jack accessory” that will be able to hold, transport, and lower the seating modules onto the rail system through the use of an industry standard pallet jack with a lifting range of 6 inches. The pallet jack accessory can be seen in Figure 1, item C.

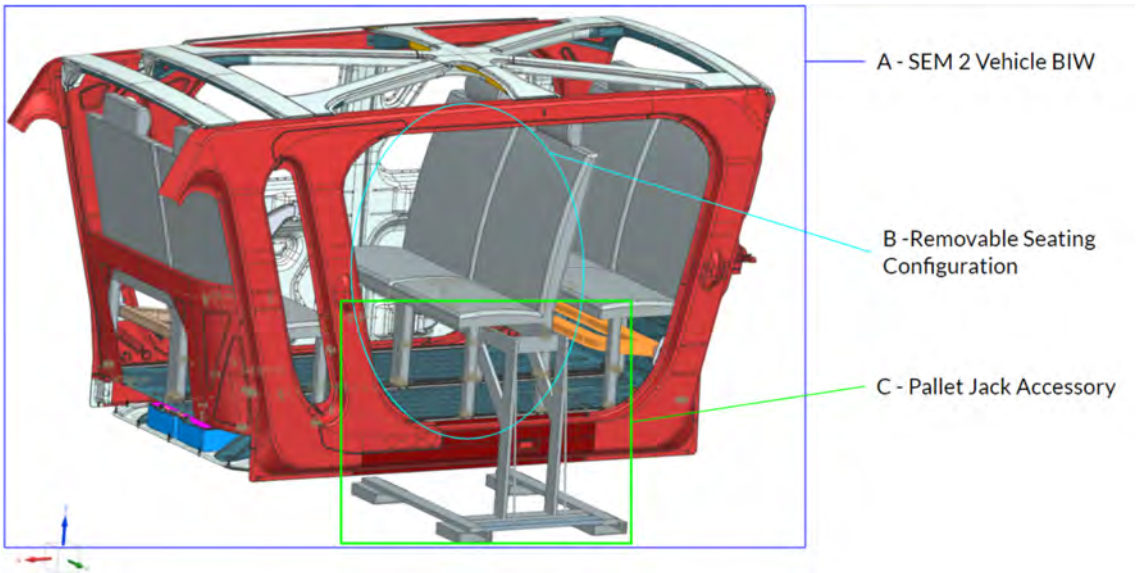

Figure 1: System level concept – rapid adaptation of SEM2 to autonomous delivery services

The slider mechanism, seen in Figure 2, will house a ball roller bearing that allows for the translational motion along the rail to slide the seats into position.

The roller bearing bolts into the slider mechanism allowing for easy replacement. The T-Rails are then bolted to the structural members of the vehicle, where engineers from WorldAutoSteel have confidence the design can withstand any and all static and dynamic loading scenarios. The rails will feature a narrow section near the center allowing for the removal of the seating module. This narrow section is tapered to allow the slider to be “homed” and slid into its final, fixed position.

Figure 2: T-rail system for fast removal of seats.

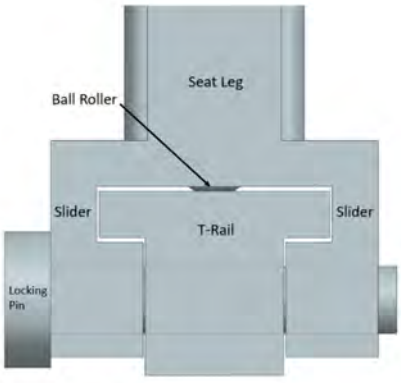

The arms of the pallet jack system reach out to allow a set of seats to be placed on the rail at one time. The pallet jack will drive through the open slots on the ground, lift the seats to the vehicle, align itself using markings on the vehicle and drop the seats into the rails where they can then be manually moved to their correct position. The system is designed to remove and insert these seats as fast as possible, while exerting minimum effort that might stress the MSP technician. With ease of use and safety being the critical elements of every project, we've removed manual lifting from the equation, as well as ensured a factor of safety of 2 is kept for all required crash loads under our current design.

Many integral components are COTS parts and can be bought in bulk to use for mass production as well as reserved parts, helping maintain low cost of ownership for the MSP. The components that are not COTS items, such as the rails and sliders, can be manufactured using high volume, low cost fabrication techniques such as stamping. Assembly of the system will be just as easy,

as all components are connected together using industry standard fastening and welding techniques.

Conclusions

Validation – to confirm the ease of changeover and our objectives, a simulation was conducted to estimate the time and difficulty of changing from delivery service to people transporter. In a warehouse setting, a location was established as the “vehicle maintenance spot”. We developed a “seat module storage area” approximately 30 meters aways. In this simulation, the following steps were conducted:

1. A pallet jack was pre-staged near the vehicle, signaling the beginning of the conversion and timer.
2. A technician walked 30 m to the seating storage area and picked up the seats via accessory.
3. They carried seats back over to the vehicle and aligned the pallet jack with the vehicle door.
8. Lowered seats onto the rail system and removed the pallet jack accessory from the
1. vehicle.
9. Slid the seats into the correct position and inserted the locking pin into its slot.

This simulation was repeated two more times to replicate the insertion of all six seats. To remove the seats, the steps would be reversed. After five runs of this simulation, ensuring adequate time to perform each simulated step, the average time to complete the simulation was 5
minutes 17 seconds with a total of 24 required movements.

These values were well within the 30 minute and 50 movement objectives. For further validation, we’ll repeat these simulations in the opposite direction, ie removing the seats to transform to the delivery van. Finally, in Phase 2 of this project we’ll continue to evaluate seat frame / track componentry to ensure robustness and durability in the proposed solutions.

Appendices

Appendix 1.1 SEM1 Body in White Bill of Materials

CAD PART NUMBER	PART NAME	Gauge thickness (mm)	Material Grade (code)	Advanced High Strength Steel Category	Part mass (kg)	Fabrication Process
03272922	ROCKER HEX ABSORBER LH	0.7	CR420Y780T-DP	Dual Phase	0.70	Roll form
3438889	A POST INNER LH	1.2	PHS-CR2000T-MB	Press Hardened Steel	5.06	Hot form
03440399	C POST INNER LH	1.0	PHS-CR1500T-MB	Press Hardened Steel	4.02	Hot form
3451131	ROCKER INNER LH	1.5	CR1550Y2000T-MS	Martesitic	7.40	Cold stamp
3451226	ROCKER INNER REINFORCEMENT LH	1.0	CR420Y780T-DP	Dual Phase	1.06	Cold stamp
3451542	ROOF SIDE RAIL INNER LH	0.8	PHS-CR1500T-MB	Press Hardened Steel	2.15	Hot form
3470012	MID ROOF BOW MOUNT LH	0.8	CR700Y980T-DP	Dual Phase	0.41	Cold stamp
03503803	A POST INNER REINFORCEMENT LH	0.8	CR1350Y1700T-MS	Martesitic	1.46	Cold stamp
3510150	C POST INNER REINFORCEMENT LH	0.8	CR860Y1180T-DP	Dual Phase	1.36	Cold stamp
03553241	A POST INNER RH	1.2	PHS-CR2000T-MB	Press Hardened Steel	5.06	Hot form
3553252	FRONT INNER ROOF HEADER GUSSET MOUNT RH	1.0	CR700Y980T-DP	Dual Phase	1.26	Cold stamp
03553334	C POST INNER RH	1.0	PHS-CR1500T-MB	Press Hardened Steel	4.02	Hot form
03553361	ROCKER INNER RH	1.5	CR1550Y2000T-MS	Martesitic	7.40	Cold stamp
03553374	ROCKER INNER REINFORCEMENT RH	1.0	CR420Y780T-DP	Dual Phase	1.06	Cold stamp
03553378	ROCKER HEX ABSORBER RH	0.7	CR420Y780T-DP	Dual Phase	0.70	Roll form
03553379	ROOF SIDE RAIL INNER RH	0.8	PHS-CR1500T-MB	Press Hardened Steel	2.15	Hot form
3553390	REAR INNER ROOF HEADER GUSSET MOUNT RH	0.8	HSLA490/600	High Strength Low Alloy	1.26	Cold stamp
03553397	A POST INNER REINFORCEMENT RH	0.8	CR1350Y1700T-MS	Martesitic	1.46	Cold stamp
03553400	C POST INNER REINFORCEMENT RH	0.8	CR860Y1180T-DP	Dual Phase	1.36	Cold stamp
03559985	MID ROOF BOW MOUNT RH	0.8	CR700Y980T-DP	Dual Phase	0.41	Cold stamp
3572146	INNER ROCKER BULKHEAD LH	1.0	CR420Y780T-DP	Dual Phase	0.11	Cold stamp
03573480	INNER ROCKER BULKHEAD RH	1.0	CR420Y780T-DP	Dual Phase	0.11	Cold stamp
03598246	REAR OUTER ROOF HEADER GUSSET MOUNT LH	0.8	CR490Y/600T-LA	High Strength Low Alloy	0.14	Cold stamp
03599223	REAR INNER ROOF HEADER GUSSET MOUNT LH	0.8	CR490Y/600T-LA	High Strength Low Alloy	0.67	Cold stamp
03470750	FRONT INNER ROOF HEADER GUSSET MOUNT LH	1.0	CR700Y980T-DP	Dual Phase	0.63	Cold stamp
03620666	REAR OUTER ROOF HEADER GUSSET MOUNT RH	0.8	CR550Y/620T-LA	High Strength Low Alloy	0.14	Cold stamp
3629368	ROCKER FRONT CAP INNER LH	1.0	CR1200Y1470T-MS	Martesitic	0.14	Cold stamp
03636509	FRONT OUTER ROOF HEADER GUSSET MOUNT LH	1.0	CR700Y980T-DP	Dual Phase	0.22	Cold stamp
03636520	FRONT OUTER ROOF HEADER GUSSET MOUNT RH	1.0	CR700Y980T-DP	Dual Phase	0.22	Cold stamp
03636521	ROCKER REAR CAP INNER LH	1.0	CR550Y/620T-LA	High Strength Low Alloy	0.14	Cold stamp
03636524	ROCKER REAR CAP INNER RH	1.0	CR550Y/620T-LA	High Strength Low Alloy	0.14	Cold stamp
03647858	ROCKER FRONT CAP INNER RH	1.0	CR1200Y1470T-MS	Martesitic	0.14	Cold stamp
03694699	OUTER RING TWB LH	TWB 1.2, 1.0	TWB_PHS-CR2000T-MB, 1.2, PHS-CR1000T-MB Upp	Press Hardened Steel	16.69	Hot form
03703692	SLEEVE FRONT LH	SOLID	NA_EN8	Mild Steel	0.35	(solid part)
03703694	SLEEVE FRONT RH	SOLID	NA_EN8	Mild Steel	0.35	(solid part)
3703801	A POST INNER REINFORCEMENT UPPER LH	1.5	CR800Y1180T-DP	Dual Phase	1.46	Cold stamp
03703802	A POST INNER REINFORCEMENT UPPER RH	1.5	CR800Y1180T-DP	Dual Phase	1.46	Cold stamp
03707049	A POST INNER REINFORCEMENT UPPER REAR LH	1.5	CR800Y1180T-DP	Dual Phase	1.13	Cold stamp
03707053	A POST INNER REINFORCEMENT UPPER REAR RH	1.5	CR800Y1180T-DP	Dual Phase	1.13	Cold stamp
03707551	SLEEVE REAR LH	SOLID	NA_EN8	Mild Steel	0.33	(solid part)
03707552	SLEEVE REAR RH	SOLID	NA_EN8	Mild Steel	0.33	(solid part)
03709256	OUTER RING TWB RH	TWB 1.2, 1.0	TWB_PHS-CR2000T-MB, 1.2, PHS-CR1000T-MB Upp	Press Hardened Steel	16.69	Hot form
03721342	BULKHEAD_C_PILLAR_MIDDLE_LH	1.5	CR1550Y2000T-MS	Martesitic	0.19	Cold stamp
03722991	BULKHEAD_C_PILLAR_LOWER_LH	1.5	CR1550Y2000T-MS	Martesitic	0.19	Cold stamp
03725754	BULKHEAD_C_PILLAR_MIDDLE_RH	1.5	CR1550Y2000T-MS	Martesitic	0.19	Cold stamp
03725762	BULKHEAD_C_PILLAR_LOWER_LH	1.5	DP 800/1180	Dual Phase	0.19	Cold stamp
03730371	BULKHEAD_A_POST_REINFORCEMENT_UPPER_LH	1.5	CR1550Y2000T-MS	Martesitic	0.24	Cold stamp
03730603	BULKHEAD_A_POST_REINFORCEMENT_LOWER_L	1.5	CR1550Y2000T-MS	Martesitic	0.24	Cold stamp
03730608	BULKHEAD_A_POST_REINFORCEMENT_UPPER_RI	1.5	CR1550Y2000T-MS	Martesitic	0.24	Cold stamp
03730609	BULKHEAD_A_POST_REINFORCEMENT_LOWER_R	1.5	CR1550Y2000T-MS	Martesitic	0.24	Cold stamp
3747655	OUTER RING REINF. PLATE LH	2.0	CR340Y590T-DP	Dual Phase	0.08	Cold stamp
03748482	INNER ROCKER BULKHEAD LH	1.0	CR420Y780T-DP	Dual Phase	0.11	Cold stamp
03749650	INNER ROCKER BULKHEAD RH	1.0	CR420Y780T-DP	Dual Phase	0.11	Cold stamp
03750014	OUTER RING REINF. PLATE RH	2.0	CR340Y590T-DP	Dual Phase	0.08	Cold stamp
3820779	REINFORCEMENT LATCH RIGHT LH	1.5	PHS-CR1000T-MB	Press Hardened Steel	0.56	Hot form
3824181	REINFORCEMENT LATCH LEFT LH	1.5	PHS-CR1000T-MB	Press Hardened Steel	0.55	Hot form
03842798	REINFORCEMENT LATCH LEFT RH	1.5	PHS-CR1000T-MB	Press Hardened Steel	0.55	Hot form
03842803	REINFORCEMENT LATCH RIGHT RH	1.5	PHS-CR1000T-MB	Press Hardened Steel	0.56	Hot form
3451626	FRONT HEADER OUTER A-SURFACE	0.6	CR260Y/370T-BH	Bake Hardenable	1.15	Cold stamp
03451793	FRONT HEADER INNER	0.8	CR780Y980T-CP	Complex Phase	1.67	Roll stamp
03461692	MID ROOF BOW OUTER A-SURFACE	0.6	CR260Y/370T-BH	Bake Hardenable	1.05	Cold stamp
03462738	MID ROOF BOW INNER	0.8	CR820Y1180T-RA	Retained Austenite	1.77	Roll stamp
03475937	DIAGONAL OUTER A-SURFACE PANEL FRONT LH	0.6	CR260Y/370T-BH	Bake Hardenable	0.78	Cold stamp
03476375	REAR HEADER OUTER A-SURFACE	0.6	CR260Y/370T-BH	Bake Hardenable	1.21	Cold stamp
03476383	DIAGONAL OUTER A-SURFACE PANEL REAR LH	0.6	CR260Y/370T-BH	Bake Hardenable	0.81	Cold stamp
03476397	REAR HEADER INNER	0.8	CR780Y980T-CP	Complex Phase	1.69	Roll stamp
03484374	DIAGONAL INNER PANEL REAR LH	0.7	CR550Y/620T-LA	High Strength Low Alloy	1.35	Cold stamp
03496795	MID INTERSECTION OUTER A-SURFACE PANEL	0.6	CR260Y/370T-BH	Bake Hardenable	0.63	Cold stamp
03512374	MID INTERSECTION INNER PANEL	0.5	CR260Y/370T-BH	Bake Hardenable	0.62	Cold stamp
03483873	DIAGONAL INNER PANEL FRONT LH	0.7	CR550Y/620T-LA	High Strength Low Alloy	1.29	Cold stamp
03512803	DIAGONAL OUTER A-SURFACE PANEL FRONT RH	0.6	CR260Y/370T-BH	Bake Hardenable	0.78	Cold stamp
03512805	DIAGONAL INNER PANEL FRONT RH	0.7	CR550Y/620T-LA	High Strength Low Alloy	1.29	Cold stamp
03512806	DIAGONAL OUTER A-SURFACE PANEL REAR RH	0.6	CR260Y/370T-BH	Bake Hardenable	0.81	Cold stamp
03512808	DIAGONAL INNER PANEL REAR RH	0.7	CR550Y/620T-LA	High Strength Low Alloy	1.35	Cold stamp
03476381	LONGITUDINAL REAR RAIL OUTER LH	TWB	TWB_1.6_CR820Y1180T-RA_1.4_CR600Y980T-RA	Retained Austenite	1.51	Cold stamp
03476382	LONGITUDINAL REAR RAIL INNER LH	TWB	TWB_1.6_CR820Y1180T-RA_1.4_CR600Y980T-RA	Retained Austenite	1.56	Cold stamp
03477701	LONGITUDINAL REAR RAIL INNER RH	TWB	TWB_1.6_CR820Y1180T-RA_1.4_CR600Y980T-RA	Retained Austenite	1.56	Cold stamp
03477703	LONGITUDINAL REAR RAIL OUTER RH	TWB	TWB_1.6_CR820Y1180T-RA_1.4_CR600Y980T-RA	Retained Austenite	1.51	Cold stamp
03484382	D POST LH	0.8	CR400Y690T-RA	Retained Austenite	2.05	Hydroform
3486016	STRUT TOWER REAR LH	1.0	CR350Y/450T-LA	High Strength Low Alloy	2.13	Cold stamp
3486032	STRUT TOP REAR LH	2.4	CR340Y590T-DP	Dual Phase	1.64	Cold stamp
3491092	D POST INNER UPPER LH	0.8	CR340Y590T-DP	Dual Phase	0.42	Cold stamp
3553188	STRUT CROSS MEMBER LOWER REAR	1.0	CR1200Y1470T-MS	Martesitic	2.75	Cold stamp
03553189	STRUT CROSS MEMBER REAR UPPER	1.0	CR1200Y1470T-MS	Martesitic	1.94	Cold stamp
03553338	STRUT TOWER REAR RH	1.0	CR350Y/450T-LA	High Strength Low Alloy	2.13	Cold stamp
03553340	STRUT TOP REAR RH	2.4	CR340Y590T-DP	Dual Phase	1.64	Cold stamp
03553521	TORQUE BOX INNER UPPER REAR LH	1.0	CR400Y780T-RA	Retained Austenite	0.78	Cold stamp
03553522	TORQUE BOX INNER UPPER REAR RH	1.0	CR400Y780T-RA	Retained Austenite	0.78	Cold stamp
3555308	FIVE BAR INNER	0.8	CR900Y1180T-CP	Complex Phase	0.96	Cold stamp
03557786	D POST RH	0.8	CR400Y690T-RA	Retained Austenite	2.05	Hydroform
03557884	D POST INNER UPPER RH	0.8	CR340Y590T-DP	Dual Phase	0.42	Cold stamp
3558422	UPPER RAIL INNER REAR RH	0.8	CR350Y/450T-LA	High Strength Low Alloy	0.84	Cold stamp
03558955	UPPER RAIL OUTER REAR RH	1.2	CR350Y/450T-LA	High Strength Low Alloy	1.25	Cold stamp

CAD PART NUMBER	PART NAME	Gauge thickness (mm)	Material Grade (code)	Advanced High Strength Steel Category	Part mass (kg)	Fabrication Process
03560014	REAR SUBFRAME BUSHMOUNT FRT RH	EN8	EN8	Mild Steel	0.36	(solid part)
03560015	REAR SUBFRAME BUSHMOUNT RR LH	EN8	EN8	Mild Steel	0.36	(solid part)
03560016	REAR SUBFRAME BUSHMOUNT RR RH	EN8	EN8	Mild Steel	0.36	(solid part)
3559093	BUMPER BEAM INTERFACE PLATE REAR LH	1.8	CR860Y1180T-DP	Dual Phase	0.31	Cold stamp
03570677	BUMPER BEAM INTERFACE PLATE REAR RH	1.8	CR860Y1180T-DP	Dual Phase	0.32	Cold stamp
03572151	FIVE BAR OUTER	1.8	CR420Y780T-DP	Dual Phase	3.93	Cold stamp
3593060	VERTICAL DASH BRACE UPPER REAR LH	1.6	CR820Y1180T-RA	Retained Austenite	2.32	Cold stamp
03593521	VERTICAL DASH BRACE UPPER REAR RH	1.6	CR820Y1180T-RA	Retained Austenite	2.32	Cold stamp
03596982	REAR BULKHEAD	TWB 1.0, 0.8	TWB_1.0_CR1200Y1470T-MS, 0.8_CR1000Y1470T-MS	Martesitic	4.57	Cold stamp
03596995	REAR COMPARTMENT PAN LOWER	0.5	CR350Y/450T-LA	High Strength Low Alloy	2.61	Cold stamp
3630350	VERTICAL DASH BRACE LOWER OUTER REAR LH	1.0	CR820Y1180T-RA	Retained Austenite	0.89	Cold stamp
03630351	VERTICAL DASH BRACE LOWER INNER REAR LH	1.0	CR820Y1180T-RA	Retained Austenite	0.73	Cold stamp
03633267	BULKHEAD SUBFRAME BUSH LH	1.0	CR350Y/450T-LA	High Strength Low Alloy	0.06	Cold stamp
03633268	BULKHEAD SUBFRAME BUSH RH	1.0	CR350Y/450T-LA	High Strength Low Alloy	0.06	Cold stamp
03634578	VERTICAL DASH BRACE LOWER OUTER REAR RH	1.0	CR820Y1180T-RA	Retained Austenite	0.89	Cold stamp
03634581	VERTICAL DASH BRACE LOWER INNER REAR RH	1.0	CR820Y1180T-RA	Retained Austenite	0.73	Cold stamp
3716555	VERTICAL DASH BRACE UPPER REAR LH	1.8	CR1200Y1470T-MS	Martesitic	0.22	Cold stamp
03716556	VERTICAL DASH BRACE UPPER REAR RH	1.8	CR1200Y1470T-MS	Martesitic	0.22	Cold stamp
3736010	BRAKET COACH DOOR UPPER LH	1.5	CR350Y/450T-LA	High Strength Low Alloy	0.72	Cold stamp
03736011	BRAKET COACH DOOR UPPER RH	1.5	CR350Y/450T-LA	High Strength Low Alloy	0.05	Cold stamp
3736543	BRAKET STABILUS LH	1.5	CR350Y/450T-LA	High Strength Low Alloy	0.03	Cold stamp
03736547	BRAKET STABILUS RH	1.5	CR350Y/450T-LA	High Strength Low Alloy	0.03	Cold stamp
3750809	TORQUE BOX REAR LH	1.5	CR400Y780T-RA	Retained Austenite	1.65	Cold stamp
03753560	COACH DOOR LATERAL BAR	0.7	CR350Y/450T-LA	High Strength Low Alloy	1.82	Cold stamp
03753727	COACH DOOR LATERAL BAR REINFORCEMENT INN	0.7	CR350Y/450T-LA	High Strength Low Alloy	0.20	Cold stamp
03753729	COACH DOOR LATERAL BAR REINFORCEMENT INN	0.7	CR350Y/450T-LA	High Strength Low Alloy	0.20	Cold stamp
03753730	COACH DOOR LATERAL BAR REINFORCEMENT OU	0.8	CR350Y/450T-LA	High Strength Low Alloy	0.31	Cold stamp
03753731	COACH DOOR LATERAL BAR REINFORCEMENT OU	0.8	CR350Y/450T-LA	High Strength Low Alloy	0.31	Cold stamp
03753743	TORQUE BOX REAR RH	1.5	CR400Y780T-RA	Retained Austenite	1.65	Cold stamp
03753904	SIX BAR	0.8	CR350Y/450T-LA	High Strength Low Alloy	1.33	Cold stamp
3755567	UPPER RAIL INNER REAR LH 2	1.0	CR350Y/450T-LA	High Strength Low Alloy	0.84	Cold stamp
03755570	UPPER RAIL OUTER REAR LH 2	1.2	CR350Y/450T-LA	High Strength Low Alloy	1.25	Cold stamp
03765101	UPPER RAIL BULKHEAD REAR LH	1.5	CR420Y780T-DP	Dual Phase	0.11	Cold stamp
03765106	UPPER RAIL BULKHEAD REAR RH	1.5	CR420Y780T-DP	Dual Phase	0.11	Cold stamp
3776067	STRUT RING REAR LH	2.0	CR1200Y1470-MS	Martesitic	0.23	Cold stamp
03776068	STRUT RING REAR RH	2.0	CR1200Y1470-MS	Martesitic	0.23	Cold stamp
03489683	TWO BAR	1.2	CR1200Y1470T-MS	Martesitic	3.25	Roll stamp
3489678	FLOOR PANEL LOWER	0.5	CR340Y590T-DP	Dual Phase	14.56	Cold stamp
3489675	THREE BAR	1.2	CR1200Y1470T-MS	Martesitic	3.26	Roll stamp
3489676	FOUR BAR	1.2	CR1200Y1470T-MS	Martesitic	3.25	Roll stamp
3753899	PDU SUPPORT LONGID RIGHT	0.7	CR340Y590T-DP	Dual Phase	0.27	Cold stamp
03753903	PDU SUPPORT LONGID LEFT	0.7	CR340Y590T-DP	Dual Phase	0.27	Cold stamp
3438410	ONE BAR INNER	1.0	CR8501180T-DH	High Formability Dual Pha	1.27	Cold stamp
03439464	FRONT SUBFRAME BUSHMOUNT RR RH	SOLID	N/A_EN8	Mild Steel	0.36	(solid part)
03439413	FRONT SUBFRAME BUSHMOUNT RR LH	SOLID	N/A_EN8	Mild Steel	0.36	(solid part)
03448749	VERTICAL DASH BRACE LOWER OUTER FRONT LH	2.0	PHS-CR1500T-MB	Press Hardened Steel	2.05	Hot form
03448755	VERTICAL DASH BRACE LOWER OUTER FRONT RH	2.0	PHS-CR1500T-MB	Press Hardened Steel	2.05	Hot form
03448854	TORQUE BOX FRONT RH	2.0	CR400Y780T-RA	Retained Austenite	2.15	Cold stamp
03469873	TORQUE BOX FRONT LH	2.0	CR400Y780T-RA	Retained Austenite	1.94	Cold stamp
03475858	FRONT SUBFRAME BUSHMOUNT FRT LH	SOLID	N/A_EN8	Mild Steel	0.45	(solid part)
03475860	FRONT SUBFRAME BUSHMOUNT FRT RH	SOLID	N/A_EN8	Mild Steel	0.45	(solid part)
03506010	LONGITUDINAL MID RAIL OUTER FRONT LH	TWB 2.0, 1.8	1.8/2.0_CR500Y780T-DP/CR700Y980T-DP	Dual Phase	3.16	Cold stamp
03506011	LONGITUDINAL MID RAIL INNER FRONT LH	TWB 2.0, 1.8	1.8/2.0_CR500Y780T-DP/CR700Y980T-DP	Dual Phase	3.13	Cold stamp
03553245	BUMPER BEAM INTERFACE PLATE FRONT LH	2.0	CR860Y1180T-DP	Dual Phase	0.58	Cold stamp
03553253	BUMPER BEAM INTERFACE PLATE FRONT RH	2.0	CR860Y1180T-DP	Dual Phase	0.58	Cold stamp
03553269	LONGITUDINAL MID RAIL OUTER FRONT RH	TWB 2.0, 1.8	1.8/2.0_CR500Y780T-DP/CR700Y980T-DP	Dual Phase	3.16	Cold stamp
03553270	LONGITUDINAL MID RAIL INNER FRONT RH	TWB 2.0, 1.8	1.8/2.0_CR500Y780T-DP/CR700Y980T-DP	Dual Phase	3.13	Cold stamp
03585862	GLANCE BEAM INNER LH	0.8	PHS-CR1500T-MB	Press Hardened Steel	1.72	Hot form
03585863	GLANCE BEAM UPPER TRIANGULATION INNER LH	1.0	PHS-CR1500T-MB	Press Hardened Steel	0.92	Hot form
03585867	GLANCE BEAM OUTER LH	0.8	PHS-CR1500T-MB	Press Hardened Steel	1.75	Hot form
03601006	GLANCE BEAM UPPER TRIANGULATION OUTER LH	1.0	PHS-CR1500T-MB	Press Hardened Steel	1.04	Hot form
03601008	FRONT BULKHEAD	0.7	CR700Y980T-DP	Dual Phase	4.83	Cold stamp
3603910	STRUT TOP FRONT LH	1.8	CR860Y1180T-DP	Dual Phase	1.59	Cold stamp
3614349	GLANCE BEAM LATERAL CROSS MEMBER INNER	1.0	CR1200Y1470T-MS	Martesitic	1.45	Cold stamp
03618387	GLANCE BEAM OUTER RH	0.8	PHS-CR1500T-MB	Press Hardened Steel	2.19	Hot form
03618389	GLANCE BEAM INNER RH	0.8	PHS-CR1500T-MB	Press Hardened Steel	1.72	Hot form
03618390	GLANCE BEAM UPPER TRIANGULATION INNER RH	1.0	PHS-CR1500T-MB	Press Hardened Steel	0.92	Hot form
03618391	GLANCE BEAM UPPER TRIANGULATION OUTER RH	1.0	PHS-CR1500T-MB	Press Hardened Steel	1.08	Hot form
03618394	STRUT TOP FRONT RH	1.8	CR860Y1180T-DP	Dual Phase	1.59	Cold stamp
03630344	VERTICAL DASH BRACE LOWER INNER LH	2.0	PHS-CR1500T-MB	Press Hardened Steel	1.82	Hot form
03630345	VERTICAL DASH BRACE LOWER INNER RH	2.0	PHS-CR1500T-MB	Press Hardened Steel	1.82	Hot form
03633392	BULKHEAD - SUBFRAME BUSH LH	2.0	CR350Y/450T-LA	High Strength Low Alloy	0.39	Cold stamp
03633394	BULKHEAD - SUBFRAME BUSH RH	2.0	CR350Y/450T-LA	High Strength Low Alloy	0.39	Cold stamp
03640758	STRUT CROSS MEMBER FRONT	1.0	PHS-CR2000T-MB	Press Hardened Steel	2.73	Hot form
03640760	GLANCE BEAM UPPER REACTION LH	0.8	PHS-CR1500T-MB	Press Hardened Steel	0.52	Hot form
03640761	GLANCE BEAM UPPER REACTION RH	0.8	PHS-CR1500T-MB	Press Hardened Steel	0.52	Hot form
03642244	GLANCE BEAM LOWER REACTION LH	0.8	CR1200Y1470T-MS	Martesitic	0.47	Cold stamp
03642357	STRUT CROSS MEMBER CLOSING PLATE	1.0	CR1550Y2000T-MS	Martesitic	1.09	Cold stamp
3643340	GLANCE BEAM LATERAL CROSS MEMBER OUTER	1.0	CR1200Y1470T-MS	Martesitic	1.27	Cold stamp
03643407	STRUT TOWER FRONT LH	0.8	CR350Y/450T-LA	High Strength Low Alloy	1.46	Cold stamp
03643408	STRUT TOWER FRONT RH	0.8	CR350Y/450T-LA	High Strength Low Alloy	1.46	Cold stamp
03643418	GLANCE BEAM LOWER REACTION RH	0.8	CR1200Y1470T-MS	Martesitic	0.47	Cold stamp
3670456	ONE BAR OUTER LOWER	2.0	CR860Y1180T-DP	Dual Phase	3.31	Roll form
3670457	ONE BAR OUTER UPPER	2.0	CR860Y1180T-DP	Dual Phase	2.51	Cold stamp
03671385	VERTICAL DASH BRACE UPPER FRONT LH	2.0	PHS-CR2000T-MB	Press Hardened Steel	0.62	Hot form
03671386	VERTICAL DASH BRACE UPPER FRONT RH	2.0	PHS-CR2000T-MB	Press Hardened Steel	0.62	Hot form
03671429	VERTICAL DASH BRACE FRONT LH	2.0	PHS-CR2000T-MB	Press Hardened Steel	4.51	Hot form
03686769	VERTICAL DASH BRACE FRONT RH	2.0	PHS-CR2000T-MB	Press Hardened Steel	4.51	Hot form
03691527	TORQUE BOX INNER FRONT LH	1.0	CR8501180T-DH	High Formability Dual Pha	0.72	Cold stamp
03706556	TORQUE BOX INNER FRONT RH	1.0	CR8501180T-DH	High Formability Dual Pha	0.72	Cold stamp
03724993	GLANCE BEAM CAP LH	2.0	CR420Y780T-DP	Dual Phase	0.38	Cold stamp
03724994	GLANCE BEAM CAP RH	2.0	CR420Y780T-DP	Dual Phase	0.38	Cold stamp
03725636	GLANCE BEAM BULKHEAD 2 LH	1.5	CR420Y780T-DP	Dual Phase	0.81	Cold stamp
03727963	FRONT SUBFRAME BUSHMOUNT FRT OTR LH	SOLID	N/A_EN8	Mild Steel	0.29	(solid part)
03727964	FRONT SUBFRAME BUSHMOUNT FRT OTR RH	SOLID	N/A_EN8	Mild Steel	0.29	(solid part)
3729099	GLANCE BEAM BULKHEAD 4 LH	1.5	CR420Y780T-DP	Dual Phase	0.09	Cold stamp
03730823	GLANCE BEAM BULKHEAD 2 RH	1.5	CR420Y780T-DP	Dual Phase	0.45	Cold stamp
3730837	GLANCE BEAM BULKHEAD 4 RH	1.5	CR420Y780T-DP	Dual Phase	0.09	Cold stamp
3764468	GLANCE BEAM BULKHEAD 5 LH	1.5	CR420Y780T-DP	Dual Phase	0.18	Cold stamp
03764469	GLANCE BEAM BULKHEAD 6 LH	1.5	CR420Y780T-DP	Dual Phase	0.18	Cold stamp
03764609	GLANCE BEAM BULKHEAD 5 RH	1.5	CR420Y780T-DP	Dual Phase	0.18	Cold stamp
03764610	GLANCE BEAM BULKHEAD 6 RH	1.5	CR420Y780T-DP	Dual Phase	0.18	Cold stamp
3776065	STRUT RING FRONT LH	2.0	CR1200Y1470-MS	Martesitic	0.23	Cold stamp
03776066	STRUT RING FRONT RH	2.0	CR1200Y1470-MS	Martesitic	0.23	Cold stamp

Appendix 1.2 SEM1 Battery Bill of Materials

CAD PART NUMBER	PART NAME	CAD/PLM gauge & grade code	Gauge thickness (mm)	Material Grade (code)	Advanced High Strength Steel Category	Part mass (kg)	Subassembly mass (kg)	Forming
	BATTERY STRUCTURE	(blank)					54.90	
3647932	BATTERY TRAY UPPER	0.5_CR340Y/450T-LA	0.5	CR340Y/450T-LA	High Strength Low Allo	9.96		Cold stamp
3647933	BATTERY TRAY LOWER	0.7/0.8_CR420Y780T-DP/CR	TWB 0.7, 0.8	DP780 & MS1470	Dual Phase and Marter	14.66		Cold stamp
3747661	WAS_PDU BRACKET_MUNICH	CR550Y/650T-LA	1	CR550Y/650T-LA	High Strength Low Allo	2.29		Cold stamp
3775874	BATTERY TRAY TRIANGLECOMB FRON	0.5_CR340Y/450T-LA	0.5	CR340Y/450T-LA	High Strength Low Allo	3.17		Cold stamp
03786286	BATTERY TRAY TRIANGLECOMB REAR	0.5_CR340Y/450T-LA	0.5	CR340Y/450T-LA	High Strength Low Allo	3.07		Cold stamp
3496839	Structural Plate Crossmember_001_M	CR1200Y1470T-MS_1	1	CR1200Y1470T-MS	Martensitic	1.61		Roll stamp
03496835	Structural Plate Crossmember_004_M	CR1200Y1470T-MS_1	1	CR1200Y1470T-MS	Martensitic	1.61		Roll form
03496838	Structural Plate Crossmember_002_M	CR1200Y1470T-MS_1	1	CR1200Y1470T-MS	Martensitic	1.61		Roll form
3496832	Structural Plate_004_MUNICH	CR1200Y1470T-MS_1	1	CR1200Y1470T-MS	Martensitic	1.45		Roll form
03496836	Structural Plate_002_MUNICH	CR1200Y1470T-MS_1	1	CR1200Y1470T-MS	Martensitic	1.45		Roll form
03496837	Structural Plate_001_MUNICH	CR1200Y1470T-MS_1	1	CR1200Y1470T-MS	Martensitic	1.45		Roll form
3702273	BATTERY FRAME LONGITUDINAL LEFT	CR860Y1180T-DP_1.5	1.5	CR860Y1180T-DP	Dual Phase	5.99		Cold stamp
03702274	BATTERY FRAME LONGITUDINAL RIGH	CR860Y1180T-DP_1.5	1.5	CR860Y1180T-DP	Dual Phase	5.99		Cold stamp
3720375	SUPPORT BRACKET_11	CR550Y/650T-LA_0.7	0.7	CR550Y/650T-LA	High Strength Low Allo	0.03		Cold stamp
03720376	SUPPORT BRACKET_12	CR550Y/650T-LA_0.7	0.7	CR550Y/650T-LA	High Strength Low Allo	0.03		Cold stamp
03720377	SUPPORT BRACKET_13	CR550Y/650T-LA_0.7	0.7	CR550Y/650T-LA	High Strength Low Allo	0.03		Cold stamp
03720378	SUPPORT BRACKET_21	CR550Y/650T-LA_0.7	0.7	CR550Y/650T-LA	High Strength Low Allo	0.03		Cold stamp
03720379	SUPPORT BRACKET_22	CR550Y/650T-LA_0.7	0.7	CR550Y/650T-LA	High Strength Low Allo	0.03		Cold stamp
03720380	SUPPORT BRACKET_23	CR550Y/650T-LA_0.7	0.7	CR550Y/650T-LA	High Strength Low Allo	0.03		Cold stamp
03720381	SUPPORT BRACKET_24	CR550Y/650T-LA_0.7	0.7	CR550Y/650T-LA	High Strength Low Allo	0.03		Cold stamp
03720382	SUPPORT BRACKET_31	CR550Y/650T-LA_0.7	0.7	CR550Y/650T-LA	High Strength Low Allo	0.03		Cold stamp
03720383	SUPPORT BRACKET_32	CR550Y/650T-LA_0.7	0.7	CR550Y/650T-LA	High Strength Low Allo	0.03		Cold stamp
03720384	SUPPORT BRACKET_33	CR550Y/650T-LA_0.7	0.7	CR550Y/650T-LA	High Strength Low Allo	0.03		Cold stamp
03723001	SUPPORT BRACKET_25	CR550Y/650T-LA_0.7	0.7	CR550Y/650T-LA	High Strength Low Allo	0.03		Cold stamp
03723002	SUPPORT BRACKET_26	CR550Y/650T-LA_0.7	0.7	CR550Y/650T-LA	High Strength Low Allo	0.03		Cold stamp
03723005	SUPPORT BRACKET_27	CR550Y/650T-LA_0.7	0.7	CR550Y/650T-LA	High Strength Low Allo	0.03		Cold stamp
03723007	SUPPORT BRACKET_28	CR550Y/650T-LA_0.7	0.7	CR550Y/650T-LA	High Strength Low Allo	0.03		Cold stamp
03723008	SUPPORT BRACKET_14	CR550Y/650T-LA_0.7	0.7	CR550Y/650T-LA	High Strength Low Allo	0.03		Cold stamp
03723010	SUPPORT BRACKET_15	CR550Y/650T-LA_0.7	0.7	CR550Y/650T-LA	High Strength Low Allo	0.03		Cold stamp
03723011	SUPPORT BRACKET_16	CR550Y/650T-LA_0.7	0.7	CR550Y/650T-LA	High Strength Low Allo	0.03		Cold stamp
03723014	SUPPORT BRACKET_17	CR550Y/650T-LA_0.7	0.7	CR550Y/650T-LA	High Strength Low Allo	0.03		Cold stamp
03723017	SUPPORT BRACKET_37	CR550Y/650T-LA_0.7	0.7	CR550Y/650T-LA	High Strength Low Allo	0.03		Cold stamp
03723018	SUPPORT BRACKET_36	CR550Y/650T-LA_0.7	0.7	CR550Y/650T-LA	High Strength Low Allo	0.03		Cold stamp
03723019	SUPPORT BRACKET_35	CR550Y/650T-LA_0.7	0.7	CR550Y/650T-LA	High Strength Low Allo	0.03		Cold stamp
03723021	SUPPORT BRACKET_34	CR550Y/650T-LA_0.7	0.7	CR550Y/650T-LA	High Strength Low Allo	0.03		Cold stamp

Appendix 1.3 SEM1 scissor doors Bill of Materials

CAD PART NUMBER	PART NAME	Gauge thickness (mm)	Material Grade (code)	Advanced High Strength Steel Category	Part mass (kg)	Subassembly mass (kg)	Forming
03747733	SCISSOR DOOR ASY					84.05	
03645751	REAR DOOR MOTOR				9.35		
03645752	FRONT DOOR MOTOR				9.35		
03750018	REAR DOORS_VAR 02						
03750084	OUTER DOOR RR	0.7	CR280Y/400T-BH	Bake Hardenable	7.20		Cold stamp
3750089	B-PILLAR RR	1.2	CR400Y690T-RA	Rentained Austenite	4.07		hydroform
03750085	INNER DOOR RR	1.2	Mild 140/270	Mild Steel	14.14		Cold stamp
03750087	DOOR STRUT	1.5	CR1200Y1470T-MS	Martensitic	3.01		roll stamp
03786561	REAR DOOR BRKTS BOTTOM				0.32		
03786558	REAR DOOR BRKTS TOP				0.32		
3786580	BRKT SUPPORT CUP REAR	1.2	Mild 140/270	Mild Steel	0.34		Cold stamp
03843042	DOOR SPLIT RR	1.2	Mild 140/270	Mild Steel	0.33		Cold stamp
03750017	FRONT DOORS_VAR 02						
3613567	DOOR STRUT 04	1.2	CR400Y690T-RA	Rentained Austenite	5.57		Cold stamp
03750471	INNER DOOR FR	1.2	Mild 140/270	Mild Steel	12.36		Cold stamp
03750465	OUTER DOOR FR	0.7	CR280Y/400T-BH	Bake Hardenable	6.97		Cold stamp
03750473	DOOR STRUT	1.5	CR1200Y1470T-MS	Martensitic	2.67		roll stamp
03786548	FRONT DOOR BRKTS BOTTOM				0.32		
03786545	FRONT DOOR BRKTS TOP				0.32		
03786579	BRKT SUPPORT CUP FRONT	1.2	Mild 140/270	Mild Steel	0.43		Cold stamp
03843038	DOOR SPLIT FR	1.2	Mild 140/270	Mild Steel	0.46		Cold stamp
03776787	SCISSOR DOOR GLUE				0.00		
03776789	SCISSOR DOOR WELDS				0.68		
03786540	FRONT DOOR BOTTOM ARM 2				2.68		
03786537	REAR DOOR BOTTOM ARM 2				3.13		

Appendix 1.4 Coach door Bill of Materials

CAD PART NUMBER	PART NAME	Gauge thickness (mm)	Material Grade (code)	Advanced High Strength Steel Category	Part mass (kg)	Subassembly mass (kg)	Forming
03777904	COACH DOOR MUNICH - TAILGATE					22.17	
03777906	COACH DOOR MUNICH - A-SURFACE SHEET		BH450	Bake Hardenable	7.36		Cold stamp
03777910	COACH DOOR MUNICH -INNER SHEET	1.2	MILD STEEL 140/170	Mild Steel	14.18		Cold stamp
03777912	COACH DOOR MUNICH - LOCK MECHANISM				0.22		
03777916	COACH DOOR MUNICH - LEFT LOWER ARMS BRACKET	1	HSLA350/450	High Strength Low Alloy	0.13		Cold stamp
03777919	COACH DOOR MUNICH - RIGHT LOWER ARMS BRACKE	1.5	HSLA350/450	High Strength Low Alloy	0.13		Cold stamp
03777920	COACH DOOR MUNICH - LEFT UPPER ARMS BRACKET	1.5	HSLA350/450	High Strength Low Alloy	0.08		Cold stamp
03777921	COACH DOOR MUNICH - RIGHT UPPER ARMS BRACKET	1	HSLA350/450	High Strength Low Alloy	0.08		Cold stamp

Appendix 1.5 SEM1 BIW Alternative grades Bill of Materials

		Core Design							Alternative Design		
CAD PART NUMBER	PART NAME	Gauge thickness (mm)	Material Grade (code)	Advanced High Strength Steel Category	Part mass (kg)	Forming	Secondary Grade Consideration	Secondary Fabrication	Revised Gauge Thickness (mm)	Estimate Part Mass (kg)	Comment
03556695	WAS. BIW ASY. MUNICH									274.08	
03438409	SIDE ASSEMBLY										
03272922	ROCKER HEX ABSORBER LH	0.7	CR420Y780T-DP	Dual Phase	0.70	Roll form	CR420Y780T-DP	Cold stamp	0.7	0.70	0.7mm selected for mass. Lowest gauge available for DP & DH at that strength. Process could change to cold stamp
3438889	A POST INNER LH	1.2	PHS-CR2000T-MB	Press Hardened Steel	5.06	Hot form	PHS-CR2000T-MB	TRB Hot form	1.15	4.85	2000MPa UTS required. MS2000 considered but infeasible forming. TRB may enable some weight saving on large part
03440399	C POST INNER LH	1.0	PHS-CR1500T-MB	Press Hardened Steel	4.02	Hot form	CR1000Y1500T-RA	Cold stamp	1	4.02	1 supplier for this grade. Potential for PHS1500 substitution in future. Subject to cold forming feasibility
3451131	ROCKER INNER LH	1.5	CR1550Y2000T-MS	Martesitic	7.40	Cold stamp	CR1550Y2000T-MS	Cold stamp	1.4	6.90	Potential for weight saving by placing thickness where required
3451226	ROCKER INNER REINFORCEMENT LH	1.0	CR420Y780T-DP	Dual Phase	1.06	Cold stamp	CR500Y980T-DP	Cold stamp	0.8	0.85	grade increase may enable downgauge to 0.8mm. 2kg weight saving
3451542	ROOF SIDE RAIL INNER LH	0.8	PHS-CR1500T-MB	Press Hardened Steel	2.15	Hot form	CR1000Y1500T-RA	Cold stamp	0.8	2.15	1 supplier for this grade. Potential for PHS1500 substitution in future. Subject to cold forming feasibility
3470012	MID ROOF BOW MOUNT LH	0.8	CR780Y980T-DP	Dual Phase	0.41	Cold stamp	CR700Y980T-DP	Cold stamp	0.8	0.41	Strength critical for side crash. No alternatives for 980MPa UTS and 0.8mm
03503803	A POST INNER REINFORCEMENT LH	0.8	CR1350Y1700T-MS	Martesitic	1.46	Cold stamp	PHS-CR1800T-MB	Hot form	0.7	1.27	>1700MPa strength required. MS selected for lower cost. PHS-CR1800T-MB is available in 0.7mm so some mass saving may be achieved
3510150	C POST INNER REINFORCEMENT LH	0.8	CR860Y1180T-DP	Dual Phase	1.36	Cold stamp	CR860Y1180T-DP	Cold stamp	0.8	1.36	>1180MPa strength required. PHS, MS & RA could provide the strength would may not be cost competitive against DP
03553241	A POST INNER RH	1.2	PHS-CR2000T-MB	Press Hardened Steel	5.06	Hot form	PHS-CR2000T-MB	TRB Hot form	1.15	4.85	2000MPa UTS required. MS2000 considered but infeasible forming. TRB may enable some weight saving on large part
3553252	FRONT INNER ROOF HEADER GUSSET MOUNT RH	1.0	CR700Y980T-DP	Dual Phase	1.26	Cold stamp	CR700Y980T-DP	Cold stamp	1.0	1.26	>980MPa strength required. CP, PHS, RA don't offer cost advantage
03553334	C POST INNER RH	1.0	PHS-CR1500T-MB	Press Hardened Steel	4.02	Hot form	CR1000Y1500T-RA	Cold stamp	1	4.02	1 supplier for this grade. Potential for PHS1500 substitution in future. Subject to cold forming feasibility
03553361	ROCKER INNER RH	1.5	CR1550Y2000T-MS	Martesitic	7.40	Cold stamp	CR1550Y2000T-MS	TRB Hot form	1.4	6.90	Potential for weight saving by placing thickness where required
03553374	ROCKER INNER REINFORCEMENT RH	1.0	CR420Y780T-DP	Dual Phase	1.06	Cold stamp	CR500Y980T-DP	Cold stamp	0.8	0.85	grade increase may enable downgauge to 0.8mm. 2kg weight saving
03553378	ROCKER HEX ABSORBER RH	0.7	CR420Y780T-DP	Dual Phase	0.70	Roll form	CR420Y780T-DP	Cold stamp	0.7	0.70	0.7mm selected for mass. Lowest gauge available for DP & DH at that strength
03553379	ROOF SIDE RAIL INNER RH	0.8	PHS-CR1500T-MB	Press Hardened Steel	2.15	Hot form	CR1000Y1500T-RA	Cold stamp	0.8	2.15	1 supplier for this grade. Potential for PHS1500 substitution in future. Subject to cold forming feasibility
3553390	REAR INNER ROOF HEADER GUSSET MOUNT RH	0.8	HSLA490Y600	High Strength Low Alloy	1.26	Cold stamp	HSLA490Y600	Cold stamp	0.8	1.26	HSLA expected to give best option for 600MPa UTS and 0.8mm gauge
03553397	A POST INNER REINFORCEMENT RH	0.8	CR1350Y1700T-MS	Martesitic	1.46	Cold stamp	PHS-CR1800T-MB	Hot form	0.7	1.27	>1700MPa strength required. MS selected for lower cost. PHS-CR1800T-MB is available in 0.7mm so some mass saving may be achieved
03553400	C POST INNER REINFORCEMENT RH	0.8	CR860Y1180T-DP	Dual Phase	1.36	Cold stamp	CR860Y1180T-DP	Cold stamp	0.8	1.36	>1180MPa strength required. PHS, MS & RA could provide the strength would may not be cost competitive against DP
03559985	MID ROOF BOW MOUNT RH	0.8	CR700Y980T-DP	Dual Phase	0.41	Cold stamp	CR700Y980T-DP	Cold stamp	0.8	0.41	Strength critical for side crash. No alternatives for 980MPa UTS and 0.8mm
3572146	INNER ROCKER BULKHEAD LH	1.0	CR420Y780T-DP	Dual Phase	0.11	Cold stamp	CR700Y780T-LA	Cold stamp	1.0	0.11	Same UTS as DP grade. Some cost reduction potential. Higher Yield value of HSLA may be an issue with side crash
03573480	INNER ROCKER BULKHEAD RH	1.0	CR420Y780T-DP	Dual Phase	0.11	Cold stamp	CR700Y780T-LA	Cold stamp	1.0	0.11	Same UTS as DP grade. Some cost reduction potential. Higher Yield value of HSLA may be an issue with side crash
03598246	REAR OUTER ROOF HEADER GUSSET MOUNT LH	0.8	CR490Y/600T-LA	High Strength Low Alloy	0.14	Cold stamp	CR490Y/600T-LA	Cold stamp	0.8	0.14	
03598223	REAR INNER ROOF HEADER GUSSET MOUNT LH	0.8	CR490Y/600T-LA	High Strength Low Alloy	0.67	Cold stamp	CR490Y/600T-LA	Cold stamp	0.8	0.67	
03470750	FRONT INNER ROOF HEADER GUSSET MOUNT LH	1.0	CR700Y980T-DP	Dual Phase	0.63	Cold stamp	CR700Y980T-DP	Cold stamp	1.0	0.63	>980MPa strength required. CP, PHS, RA don't offer cost advantage
03626666	REAR OUTER ROOF HEADER GUSSET MOUNT RH	0.8	CR550Y/620T-LA	High Strength Low Alloy	0.14	Cold stamp	CR550Y/620T-LA	Cold stamp	0.8	0.14	
3629368	ROCKER FRONT CAP INNER LH	1.0	CR1200Y1470T-MS	Martesitic	0.14	Cold stamp	CR1000Y1500T-RA	Cold stamp	1.0	0.14	1 supplier for this grade. Potential for PHS1500 substitution in future. Subject to cold forming feasibility
03636509	FRONT OUTER ROOF HEADER GUSSET MOUNT LH	1.0	CR700Y980T-DP	Dual Phase	0.22	Cold stamp	CR700Y980T-DP	Cold stamp	1.0	0.22	>980MPa strength required. CP, PHS, RA don't offer cost advantage
03636520	FRONT OUTER ROOF HEADER GUSSET MOUNT RH	1.0	CR700Y980T-DP	Dual Phase	0.22	Cold stamp	CR700Y980T-DP	Cold stamp	1.0	0.22	>980MPa strength required. CP, PHS, RA don't offer cost advantage
03636521	ROCKER REAR CAP INNER LH	1.0	CR550Y/620T-LA	High Strength Low Alloy	0.14	Cold stamp	CR700Y780T-LA	Cold stamp	0.9	0.13	potential for minor weight saving: increase gauge to 780MPa UTS, decrease gauge to 0.9mm
03636524	ROCKER REAR CAP INNER RH	1.0	CR550Y/620T-LA	High Strength Low Alloy	0.14	Cold stamp	CR700Y780T-LA	Cold stamp	0.9	0.13	potential for minor weight saving: increase gauge to 780MPa UTS, decrease gauge to 0.9mm
03647858	ROCKER FRONT CAP INNER RH	1.0	CR1200Y1470T-MS	Martesitic	0.14	Cold stamp	CR1000Y1500T-RA	Cold stamp	1.0	0.14	1 supplier for this grade. Potential for PHS1500 substitution in future. Subject to cold forming feasibility
03694699	OUTER RING TWB LH	TWB 1.2, 1.0	TWB_PHS-CR2000T-MB, 1.2, P	Press Hardened Steel	16.69	Hot form	TWB_PHS-CR2000T-MB, 1.2, P	TWB hot form	TWB 1.2, 1.0	16.69	2000MPa required for A pillar outer panel. TWB is good solution for this panel
03703692	SLEEVE FRONT LH	SOLID	NA. ENB	Mild Steel	0.35	(solid part)	NA. ENB			0.35	
03703694	SLEEVE FRONT RH	SOLID	NA. ENB	Mild Steel	0.35	(solid part)	NA. ENB			0.35	
3703801	A POST INNER REINFORCEMENT UPPER LH	1.5	CR800Y1180T-DP	Dual Phase	1.46	Cold stamp	CR1200Y1470T-MS	Cold stamp	1.3	1.26	Potential for weight saving, change 1.5mm DP1180 to 1.3mm MS1470
03703802	A POST INNER REINFORCEMENT UPPER RH	1.5	CR800Y1180T-DP	Dual Phase	1.46	Cold stamp	CR1200Y1470T-MS	Cold stamp	1.3	1.26	Potential for weight saving, change 1.5mm DP1180 to 1.3mm MS1470
03707049	A POST INNER REINFORCEMENT UPPER REAR LH	1.5	CR800Y1180T-DP	Dual Phase	1.13	Cold stamp	CR1200Y1470T-MS	Cold stamp	1.3	0.98	Potential for weight saving, change 1.5mm DP1180 to 1.3mm MS1470
03707053	A POST INNER REINFORCEMENT UPPER REAR RH	1.5	CR800Y1180T-DP	Dual Phase	1.13	Cold stamp	CR1200Y1470T-MS	Cold stamp	1.3	0.98	Potential for weight saving, change 1.5mm DP1180 to 1.3mm MS1470
03707051	SLEEVE REAR LH	SOLID	NA. ENB	Mild Steel	0.33	(solid part)	NA. ENB			0.33	
03707052	SLEEVE REAR RH	SOLID	NA. ENB	Mild Steel	0.33	(solid part)	NA. ENB			0.33	
03709256	OUTER RING TWB RH	TWB 1.2, 1.0	TWB_PHS-CR2000T-MB, 1.2, P	Press Hardened Steel	16.69	Hot form	TWB_PHS-CR2000T-MB, 1.2, P	TWB hot form	TWB 1.2, 1.0	16.69	2000MPa required for A pillar outer panel. TWB is good solution for this panel
03721342	BULKHEAD_C_PILLAR_MIDDLE_LH	1.5	CR1550Y2000T-MS	Martesitic	0.19	Cold stamp	CR1550Y2000T-MS	Cold stamp	1.5	0.19	2000MPa UTS required. MS provides lower cost solution
03722991	BULKHEAD_C_PILLAR_LOWER_LH	1.5	CR1550Y2000T-MS	Martesitic	0.19	Cold stamp	CR1550Y2000T-MS	Cold stamp	1.5	0.19	2000MPa UTS required. MS provides lower cost solution
03727254	BULKHEAD_C_PILLAR_MIDDLE_RH	1.5	CR1550Y2000T-MS	Martesitic	0.19	Cold stamp	CR1550Y2000T-MS	Cold stamp	1.5	0.19	2000MPa UTS required. MS provides lower cost solution
03725762	BULKHEAD_C_PILLAR_LOWER_LH	1.5	DP 800/1180	Dual Phase	0.19	Cold stamp	DP 800/1180	Cold stamp	1.5	0.19	2000MPa UTS required. MS provides lower cost solution
03730371	BULKHEAD_A_POST_REINFORCEMENT_UPPER_LH	1.5	CR1550Y2000T-MS	Martesitic	0.24	Cold stamp	CR1550Y2000T-MS	Cold stamp	1.5	0.24	2000MPa UTS required. MS provides lower cost solution
03730603	BULKHEAD_A_POST_REINFORCEMENT_LOWER_LH	1.5	CR1550Y2000T-MS	Martesitic	0.24	Cold stamp	CR1550Y2000T-MS	Cold stamp	1.5	0.24	2000MPa UTS required. MS provides lower cost solution
03730608	BULKHEAD_A_POST_REINFORCEMENT_UPPER_RH	1.5	CR1550Y2000T-MS	Martesitic	0.24	Cold stamp	CR1550Y2000T-MS	Cold stamp	1.5	0.24	2000MPa UTS required. MS provides lower cost solution
03730609	BULKHEAD_A_POST_REINFORCEMENT_LOWER_RH	1.5	CR1550Y2000T-MS	Martesitic	0.24	Cold stamp	CR1550Y2000T-MS	Cold stamp	1.5	0.24	2000MPa UTS required. MS provides lower cost solution
3747655	OUTER RING REINF. PLATE LH	2.0	CR340Y590T-DP	Dual Phase	0.08	Cold stamp	CR700Y780T-LA	Cold stamp	1.8	0.07	higher grade in HSLA may provide some cost and weight improvement
03748482	INNER ROCKER BULKHEAD LH	1.0	CR420Y780T-DP	Dual Phase	0.11	Cold stamp	CR700Y780T-LA	Cold stamp	1.0	0.11	Same UTS as DP grade. Some cost reduction potential. Higher Yield value of HSLA may be an issue with side crash
03748650	INNER ROCKER BULKHEAD RH	1.0	CR420Y780T-DP	Dual Phase	0.11	Cold stamp	CR700Y780T-LA	Cold stamp	1.0	0.11	Same UTS as DP grade. Some cost reduction potential. Higher Yield value of HSLA may be an issue with side crash
03750014	OUTER RING REINF. PLATE RH	2.0	CR340Y590T-DP	Dual Phase	0.08	Cold stamp	CR700Y780T-LA	Cold stamp	2.0	0.08	higher grade in HSLA may provide some cost and weight improvement
3820779	REINFORCEMENT LATCH RIGHT LH	1.5	PHS-CR1000T-MB	Press Hardened Steel	0.56	Hot form	CR1200Y1470T-MS	cold stamp	1.2	0.44	potential for cost and weight saving, changing to MS1470 1.2mm. Cold stamping feasibility to be checked
3824181	REINFORCEMENT LATCH LEFT LH	1.5	PHS-CR1000T-MB	Press Hardened Steel	0.55	Hot form	CR1200Y1470T-MS	cold stamp	1.2	0.44	potential for cost and weight saving, changing to MS1470 1.2mm. Cold stamping feasibility to be checked
03842798	REINFORCEMENT LATCH LEFT RH	1.5	PHS-CR1000T-MB	Press Hardened Steel	0.55	Hot form	CR1200Y1470T-MS	cold stamp	1.2	0.44	potential for cost and weight saving, changing to MS1470 1.2mm. Cold stamping feasibility to be checked
03842803	REINFORCEMENT LATCH RIGHT RH	1.5	PHS-CR1000T-MB	Press Hardened Steel	0.56	Hot form	CR1200Y1470T-MS	cold stamp	1.2	0.44	potential for cost and weight saving, changing to MS1470 1.2mm. Cold stamping feasibility to be checked
03439435	ROOF ASSEMBLY	(b)	(blank)								
3451626	FRONT HEADER OUTER A-SURFACE	0.6	CR260Y370T-BH	Bake Hardenable	1.15	Cold stamp	CR210Y340T-BH	cold stamp	0.6	1.15	Minor cost saving with lower grade. Unlikley structural performance would be compromised
03451793	FRONT HEADER INNER	0.8	CR780Y980T-CP	Complex Phase	1.67	Roll stamp	CR780Y980T-CP	cold stamp	0.8	1.67	980MPa grade delivers roof crush. No lower cost alternatives. No potential to reduce gauge
03466192	MID ROOF BOW OUTER A-SURFACE	0.6	CR260Y370T-BH	Bake Hardenable	1.05	Cold stamp	CR210Y340T-BH	cold stamp	0.6	1.05	Minor cost saving with lower grade. Unlikley structural performance would be compromised
03462738	MID ROOF BOW INNER	0.8	CR820Y1180T-RA	Retained Austenite	1.77	Roll stamp	N/A		0.8	1.77	1180MPa required for side crash strength. Part geometry has forming challenges (wrinkling hence RA higher elognation)
03470597	DIAGONAL OUTER A-SURFACE PANEL FRONT LH	0.6	CR260Y370T-BH	Bake Hardenable	0.78	Cold stamp	CR210Y340T-BH	cold stamp	0.6	0.78	Minor cost saving with lower grade. Unlikley structural performance would be compromised
03476375	REAR HEADER OUTER A-SURFACE	0.6	CR260Y370T-BH	Bake Hardenable	1.21	Cold stamp	CR210Y340T-BH	cold stamp	0.6	1.21	Minor cost saving with lower grade. Unlikley structural performance would be compromised
03476383	DIAGONAL OUTER A-SURFACE PANEL REAR LH	0.6	CR260Y370T-BH	Bake Hardenable	0.81	Cold stamp	CR210Y340T-BH	cold stamp	0.6	0.81	Minor cost saving with lower grade. Unlikley structural performance would be compromised
03476397	REAR HEADER INNER	0.8	CR780Y980T-CP	Complex Phase	1.69	Roll stamp	CR780Y980T-CP	cold stamp	0.8	1.69	980MPa grade delivers roof crush. No lower cost alternatives. No potential to reduce gauge
03484374	DIAGONAL INNER PANEL REAR LH	0.7	CR550Y/620T-LA	High Strength Low Alloy	1.35	Cold stamp	CR550Y/620T-LA	cold stamp	0.7	1.35	0.7mm gives good weight, 620MPa UTS good strength, HSLA lower cost
03496795	MID INTERSECTION OUTER A-SURFACE PANEL	0.6	CR260Y370T-BH	Bake Hardenable	0.63	Cold stamp	CR210Y340T-BH	cold stamp	0.6	0.63	Minor cost saving with lower grade. Unlikley structural performance would be compromised
03512374	MID INTERSECTION INNER PANEL	0.5	CR260Y370T-BH	Bake Hardenable	0.62	Cold stamp	CR210Y340T-BH	cold stamp	0.5	0.62	Minor cost saving with lower grade. Unlikley structural performance would be compromised
03483873	DIAGONAL INNER PANEL FRONT LH	0.7	CR550Y/620T-LA	High Strength Low Alloy	1.29	Cold stamp	CR550Y/620T-LA	cold stamp	0.7	1.29	0.7mm gives good weight, 620MPa UTS good strength, HSLA lower cost
03512803	DIAGONAL OUTER A-SURFACE PANEL FRONT RH	0.6	CR260Y370T-BH	Bake Hardenable	0.78	Cold stamp	CR210Y340T-BH	cold stamp	0.6	0.78	Minor cost saving with lower grade. Unlikley structural performance would be compromised
03512805	DIAGONAL INNER PANEL FRONT RH	0.7	CR550Y/620T-LA	High Strength Low Alloy	1.29	Cold stamp	CR550Y/620T-LA	cold stamp	0.7	1.29	0.7mm gives good weight, 620MPa UTS good strength, HSLA lower cost
03512806	DIAGONAL OUTER A-SURFACE PANEL REAR RH	0.6	CR260Y370T-BH	Bake Hardenable	0.81	Cold stamp	CR210Y340T-BH	cold stamp	0.6	0.81	Minor cost saving with lower grade. Unlikley structural performance would be compromised
03512808	DIAGONAL INNER PANEL REAR RH	0.7	CR550Y/620T-LA	High Strength Low Alloy	1.35	Cold stamp	CR550Y/620T-LA	cold stamp	0.7	1.35	0.7mm gives good weight, 620MPa UTS good strength, HSLA lower cost
03464903	REAR ASSEMBLY MUNICH	(b)	(blank)								
03476381	LONGITUDINAL REAR RAIL OUTER LH	TWB	TWB 1.6, CR820Y1180T-RA 1.4	Retained Austenite	1.51	Cold stamp	TWB 1.6, CR850Y1180T-DH 1.4	TWB cold stamp	TWB	1.51	DH may give improved crash performance. Also potential for tailor rolled blanks, common grade with thickness profile tuned to give crush profile
03476382	LONGITUDINAL REAR RAIL INNER LH	TWB	TWB 1.6, CR820Y1180T-RA 1.4	Retained Austenite	1.56	Cold stamp	TWB 1.6, CR850Y1180T-DH 1.4	TWB cold stamp	TWB	1.56	
03477701	LONGITUDINAL REAR RAIL INNER RH	TWB	TWB 1.6, CR820Y1180T-RA 1.4	Retained Austenite	1.56	Cold stamp	TWB 1.6, CR850Y1180T-DH 1.4	TWB cold stamp	TWB	1.56	
03477703	LONGITUDINAL REAR RAIL OUTER RH	TWB	TWB 1.6, CR820Y1180T-RA 1.4	Retained Austenite	1.51	Cold stamp	TWB 1.6, CR850Y1180T-DH 1.4	TWB cold stamp	TWB	1.51	
03484382	D POST LH	0.8	CR400Y690T-RA	Retained Austenite	2.05	Hydroform	CR700Y980T-DP	cold stamp	1.2	3.07	690MPa UTS contributes to roof crush and side crash performance. Hydroform could be replaced with multiple conventional cold stamp parts
3486016	STRUT TOWER REAR LH	1.0	CR350Y/450T-LA	High Strength Low Alloy	2.13	Cold stamp	CR350Y/450T-LA	cold stamp	0.8	1.71	1.0mm required for stiffness contribution. 350MPa Yield provides contribution to rear crash structure. HSLA low cost
3486032	STRUT TOP REAR LH	2.4	CR340Y590T-DP	Dual Phase	1.64	Cold stamp	CR500Y/620T-LA	cold stamp	2.4	1.64	High thickness required for stiffness and durability. HSLA may give slight cost advantage (has same elongation as DP590)
3491092	D POST INNER UPPER LH	0.8	CR340Y590T-DP	Dual Phase	0.42	Cold stamp	CR550Y/620T-LA	cold stamp	0.8	0.42	HSLA may enable slight cost saving
3553188	STRUT CROSS MEMBER LOWER REAR	1.0	CR1200Y1470T-MS	Martesitic	2.75	Cold stamp	CR1000Y1500T-RA	TRB cold stamp	0.95	2.61	1 supplier for this grade. Potential for MS1470 substitution in future. Subject to cold forming feasibility. High strength required as it contributes to rear crash intrusion. Tailor Rolled Blank may enable weight saving potential
03553189	STRUT CROSS MEMBER REAR UPPER	1.0	CR1200Y1470T-MS	Martesitic	1.94	Cold stamp	CR1000Y1500T-RA	TRB cold stamp	0.95	1.84	
03553338	STRUT TOWER REAR RH	1.0	CR350Y/450T-LA	High Strength Low Alloy	2.13	Cold stamp	CR350Y/450T-LA	cold stamp	1.0	2.13	1.0mm required for stiffness contribution. 350MPa Yield provides contribution to rear crash structure. HSLA low cost
03553340	STRUT TOP REAR RH	2.4	CR340Y590T-DP	Dual Phase	1.64	Cold stamp	CR550Y/620T-LA	cold stamp	2.4	1.64	High thickness required for stiffness and durability. HSLA may give slight cost advantage (has same elongation as DP590)
03553521	TORQUE BOX INNER UPPER REAR LH	1.0	CR400Y780T-RA	Retained Austenite	0.78	Cold stamp	PHS-CR1000T-MB	hot form	1.0	0.78	High strength and complex geometry part. PHS is suitable alternative
03553522	TORQUE BOX INNER UPPER REAR RH	1.0	CR400Y780T-RA	Retained Austenite	0.78	Cold stamp	PHS-CR1000T-MB	hot form	1.0	0.78	High strength and complex geometry part. PHS is suitable alternative
3555308	FIVE BAR INNER	0.8	CR900Y1180T-CP	Complex Phase	0.96	Cold stamp	TRB CR900Y1180T-CP	TRB cold stamp	0.75	0.90	Tailor Rolled Blank may enable some weight and performance improvement but challenging to get <0.8mm base thickness
03557786	D POST RH	0.8	CR400Y690T-RA	Retained Austenite	2.05	Hydroform	CR700Y980T-DP	cold stamp	1.2	3.07	690MPa UTS contributes to roof crush and side crash performance. Hydroform could be replaced with multiple conventional cold stamp parts
03557884	D POST INNER UPPER RH	0.8	CR340Y590T-DP	Dual Phase	0.42	Cold stamp	CR550Y/620T-LA	cold stamp	0.8	0.42	HSLA may enable slight cost saving
3558422	UPPER RAIL INNER REAR RH	0.8	CR350Y/450T-LA	High Strength Low Alloy	0.84	Cold stamp	CR350Y/450T-LA	cold stamp	0.8	0.84	
03558955	UPPER RAIL OUTER REAR RH	1.2	CR350Y/450T-LA	High Strength Low Alloy	1.25	Cold stamp	CR350Y/460T-LA	cold stamp	1.1	1.15	Tailor Rolled Blank may enable some weight and performance improvement
03560013	REAR SUBFRAME BUSHMOUNT FRT LH	ENB	ENB	Mild Steel	0.36	(solid part)	ENB			0.36	
03560014	REAR SUBFRAME BUSHMOUNT FRT RH	ENB	ENB	Mild Steel	0.36	(solid part)	ENB			0.36	
03560015	REAR SUBFRAME BUSHMOUNT RR LH	ENB	ENB	Mild Steel	0.36	(solid part)	ENB			0.36	
03560016	REAR SUBFRAME BUSHMOUNT RR RH	ENB	ENB	Mild Steel	0.36	(solid part)	ENB			0.36	
3559093	BUMPER BEAM INTERFACE PLATE REAR LH	1.8	CR800Y1180T-DP	Dual Phase	0.31	Cold stamp	PHS-CR1500T-MB	hot form	1.5	0.26	Higher grade may enable gauge reduction from 1.8mm to 1.5mm
03570677	BUMPER BEAM INTERFACE PLATE REAR RH	1.8	CR800Y1180T-DP	Dual Phase	0.32	Cold stamp	PHS-CR1500T-MB	hot form	1.5	0.26	Higher grade may enable gauge reduction from 1.8mm to 1.5mm
03572151	FIVE BAR OUTER	1.8	CR420Y780T-DP	Dual Phase	3.93	Cold stamp	CR420Y780T-DP	TRB cold stamp	1.6	3.49	Tailor Rolled Blank may enable some weight and performance improvement
3593060	VERTICAL DASH BRACE UPPER REAR LH	1.6	CR820Y1180T-RA	Retained Austenite	2.32	Cold stamp	PHS-CR1500T-MB	hot form	1.4	2.03	With higher yield and UTS some weight saving may be possible with 1.4mm gauge
03593521	VERTICAL DASH BRACE UPPER REAR RH	1.6	CR820Y1180T-RA	Retained Austenite	2.32	Cold stamp	PHS-CR1500T-MB	hot form	1.4	2.03	With higher yield and UTS some weight saving may be possible with 1.4mm gauge
03596982	REAR BULKHEAD	TWB 1.0, 0.8	TWB_1.0 CR1200Y1470T-MS,	Martesitic	4.57	Cold stamp	CR1000Y1470T-MS	TRB cold stamp	TWB 1.0, 0.8	4.57	TRB may enable more tailored thickness, resulting in potential weight saving and performance improvement
03596995	REAR COMPARTMENT PAN LOWER	0.5	CR350Y/450T-LA	High Strength Low Alloy	2.61	Cold stamp	CR350Y/450T-LA	cold stamp	0.5	2.61	
3630350	VERTICAL DASH BRACE LOWER OUTER REAR LH	1.0	CR820Y1180T-RA	Retained Austenite	0.89	Cold stamp	PHS-CR1500T-MB	hot form	0.8	0.72	With higher yield and UTS some weight saving may be possible with 0.8mm gauge
03630351	VERTICAL DASH BRACE LOWER INNER REAR LH	1.0	CR820Y1180T-RA	Retained Austenite	0.73	Cold stamp	PHS-CR1500T-MB	hot form	0.8	0.59	With higher yield and UTS some weight saving may be possible with 0.8mm gauge
03633267	BULKHEAD SUBFRAME BUSH LH	1.0	CR350Y/450T-LA	High Strength Low Alloy	0.06	Cold stamp	CR350Y/450T-LA	cold stamp	1.0	0.06	
03633268	BULKHEAD SUBFRAME BUSH RH	1.0	CR350Y/450T-LA	High Strength Low Alloy	0.06	Cold stamp	CR350Y/450T-LA	cold stamp	1.0	0.06	
03634578	VERTICAL DASH BRACE LOWER OUTER REAR RH	1.0	CR820Y1180T-RA	Retained Austenite	0.89	Cold stamp	PHS-CR1500T-MB	hot form	0.8	0.72	With higher yield and UTS some weight saving may be possible with 0.8mm gauge
03634581	VERTICAL DASH BRACE LOWER INNER REAR RH	1.0	CR820Y1180T-RA	Retained Austenite	0.73	Cold stamp	PHS-CR1500T-MB	hot form	0.8	0.59	With higher yield and UTS some weight saving may be possible with 0.8mm gauge
3716555	VERTICAL DASH BRACE UPPER REAR LH	1.8	CR1200Y1470T-MS	Martesitic	0.22	Cold stamp	PHS-CR1900T-MB	hot form	1.7	0.20	Higher grade PHS may enable some weight saving. Assume 1.7mm
03716556	VERTICAL DASH BRACE UPPER REAR RH	1.8	CR1200Y1470T-MS	Martesitic	0.22	Cold stamp	PHS-CR1900T-MB	hot form	1.7	0.20	Higher grade PHS may enable some weight saving. Assume 1.7mm
3736010	BRAKET COACH DOOR UPPER LH	1.5	CR350Y/450T-LA	High Strength Low Alloy	0.72	Cold stamp	CR350Y/450T-LA	cold stamp	1.5	0.72	
03736011	BRAKET COACH DOOR UPPER RH	1.5	CR350Y/450T-LA	High Strength Low Alloy	0.05	Cold stamp	CR350Y/450T-LA	cold stamp	1.5	0.05	
3736543	BRAKET STABILUS LH	1.5	CR350Y/450T-LA	High Strength Low Alloy	0.03	Cold stamp	CR350Y/450T-LA	cold stamp	1.5	0.03	

Appendix 1.6 SEM2 Body in White Bill of Materials

Part Number	Part Name	AHSS Grade	Gauge (mm)	C = Carry over SEM1 G = grade/gauge change N = New geom	Part Mass (kg)	SEM2 change
03596995_2	REAR COMPARTMENT PAN LOWER	CR_HSLA350/450	0.5	N	2.89	New geometry for rear EDU package
03477701_2	LONGITUDINAL REAR RAIL INNER RH	CR820Y1180T-RA_1.4_CR600Y980	1.8	G	1.90	change from 1.4mm/1.6mm TWB to 1.6mm
03476382_2	LONGITUDINAL REAR RAIL INNER LH	CR820Y1180T-RA_1.4_CR600Y980	1.6	G	1.90	change from 1.4mm/1.6mm TWB to 1.6mm
03477703_2	LONGITUDINAL REAR RAIL OUTER RH	CR820Y1180T-RA_1.4_CR600Y980	1.6	G	1.81	change from 1.4mm/1.6mm TWB to 1.6mm
03476381_2	LONGITUDINAL REAR RAIL OUTER LH	CR820Y1180T-RA_1.4_CR600Y980	1.6	G	1.81	change from 1.4mm/1.6mm TWB to 1.6mm
03439435_2	ROOF ASSEMBLY	(blank)	(bl			
04033954	REAR BACK HEADER OUTER A-SURFACE	CR260Y/370T-BH	0.6	N	1.21	
04034062	REAR BACK HEADER INNER	CR780Y980T-CP	0.8	N	1.74	
03512808_2	DIAGONAL INNER PANEL REAR RH	CR_HSLA550/620	0.7	C	1.35	
03512806_2	DIAGONAL OUTER A-SURFACE PANEL REAR RH	CR260Y/370T-BH	0.6	C	0.81	
03512803_2	DIAGONAL OUTER A-SURFACE PANEL FRONT RH	CR260Y/370T-BH	0.6	C	0.78	
03475917_2	DIAGONAL OUTER A-SURFACE PANEL FRONT LH	CR260Y/370T-BH	0.6	C	0.78	
03512374_2	MID INTERSECTION INNER PANEL	CR260Y/370T-BH	0.5	C	0.62	
03512805_2	DIAGONAL INNER PANEL FRONT RH	CR_HSLA550/620	0.7	C	1.29	
03462738_2	MID ROOF BOW INNER	CR820Y1180T-RA	0.8	C	1.77	
03476397_2	REAR HEADER INNER	CR780Y980T-CP	0.8	N	1.69	
03476383_2	DIAGONAL OUTER A-SURFACE PANEL REAR LH	CR260Y/370T-BH	0.6	C	0.81	
03461692_2	MID ROOF BOW OUTER A-SURFACE	CR260Y/370T-BH	0.6	C	1.05	
03496795_2	MID INTERSECTION OUTER A-SURFACE PANEL	0.6_CR260Y/370T-BH	0.6	C	0.64	
03451793_2	FRONT HEADER INNER	CR780Y980T-CP	0.8	C	1.67	
03484374_2	DIAGONAL INNER PANEL REAR LH	CR_HSLA550/620	0.7	C	1.35	
03451626_2	FRONT HEADER OUTER A-SURFACE	CR260Y/370T-BH	0.6	C	1.15	
03476375_2	REAR HEADER OUTER A- SURFACE	CR260Y/370T-BH	0.6	N	1.20	
03483873_2	DIAGONAL INNER PANEL FRONT LH	CR_HSLA550/620	0.7	C	1.29	
03489673_2	FLOOR ASSEMBLY	(blank)	(bl			
03489683_2	TWO BAR	CR1200Y1470T-MS	1.5	C	4.05	
03753899_2	PDU SUPPORT LONGID RIGHT	CR340Y590T-DP	0.7	C	0.27	
03489678_2	FLOOR PANEL LOWER	DP980	0.5	N	17.97	
03753903_2	PDU SUPPORT LONGID LEFT	CR340Y590T-DP	0.7	C	0.27	
03489675_2	THREE BAR	CR1200Y1470T-MS	1.5	C	4.06	
03489676_2	FOUR BAR	CR1200Y1470T-MS	1.5	C	4.05	
03974152_2	THREE A BAR	CR1200Y1470T-MS	1.5	N	4.06	
03438409_2	SIDE ASSEMBLY	(blank)				
03725762_2	BULKHEAD_C_PILLAR_LOWER_LH	1.5_DP 800/1180	1.5	C	0.19	
03766055_2	A POST BULKHEAD COVER RH	PHS-CR2000T-MB	1.5	N	0.18	
03451131_2	ROCKER INNER LH	CR1550Y2000T-MS	1.2	N	7.23	
03553378_2	ROCKER HEX ABSORBER RH	CR420Y780T-DP	0.7	N	0.98	
03636524_2	ROCKER REAR CAP INNER RH	CR_HSLA550/620	1.0	N	0.14	
03707552_2	SLEEVE REAR RH	NA_EN8		N	0.33	
03730603_2	BULKHEAD_A_POST_REINFORCEMENT_LOWER_LH	CR1550Y2000T-MS	1.5	C	0.24	
03725754_2	BULKHEAD_C_PILLAR_MIDDLE_RH	CR1550Y2000T-MS	1.5	C	0.19	
03440399_2	C POST INNER LH	PHS-CR1500T-MB	1.2	N	4.83	
03553252_2	FRONT INNER ROOF HEADER GUSSET MOUNT RH	CR700Y980T-DP	1.0	C	0.62	
03620666_2	REAR OUTER ROOF HEADER GUSSET MOUNT RH	CR_HSLA550/620	0.8	N	0.14	
03636509_2	FRONT OUTER ROOF HEADER GUSSET MOUNT LH	CR700Y980T-DP	1.0	C	0.22	
03758190_2	A POST BULKHEAD COVER LH	PHS-CR2000T-MB	1.5	N	0.18	
03598246_2	REAR OUTER ROOF HEADER GUSSET MOUNT LH	CR_HSLA490/600	0.8	N	0.14	
03438889_2	A POST INNER LH	PHS-CR2000T-MB	1.2	C	5.06	
03721342_2	BULKHEAD_C_PILLAR_MIDDLE_LH	CR1550Y2000T-MS	1.5	C	0.19	
03503803_2	A POST INNER REINFORCEMENT LH	CR1350Y1700T-MS	1.0	C	1.79	
04034061	REAR BACK INNER ROOF HEADER GUSSET MOUNT R	CR_HSLA490/600	0.8	N	0.30	
04033949	REAR BACK INNER ROOF HEADER GUSSET MOUNT L	CR_HSLA490/600	0.8	N	0.95	
03975789	SEM2 EXTENSION PILLAR OUTER LH	TWB_PHS-CR2000T-MB Apillar 1.	TWB	N	3.90	
04034069	REAR OUTER BACK ROOF HEADER GUSSET MOUNT R	CR_HSLA550/620	0.8	N	0.13	
04034066	REAR OUTER BACK ROOF HEADER GUSSET MOUNT L	CR_HSLA490/600	0.8	N	0.13	
03998634	SEM2 EXTENSION PILLAR REINFORCEMENT LH	CR860Y1180T-DP	0.8	N	0.92	
03998485	SEM2 EXTENSION PILLAR INNER LH	PHS-CR1500T-MB	1.2	N	4.79	
04028496	SEM2 EXTENSION PILLAR OUTER RH	TWB_PHS-CR2000T-MB Apillar 1.	TWB	N	3.90	
04028609	SEM2 EXTENSION PILLAR INNER RH	PHS-CR1500T-MB	1.2	N	4.78	
04028555	SEM2 EXTENSION PILLAR REINFORCEMENT RH	CR860Y1180T-DP	0.8	N	0.92	
03553374_2	ROCKER INNER REINFORCEMENT RH	CR420Y780T-DP	1.0	N	1.63	
03573480_2	INNER ROCKER BULKHEAD RH	CR420Y780T-DP	1.0	C	0.11	
03707053_2	A POST INNER REINFORCEMENT UPPER REAR RH	1.5_CR800Y1180T-DP	1.5	N	1.13	
03703694_2	SLEEVE FRONT RH	NA_EN8		C	0.35	
03730371_2	BULKHEAD_A_POST_REINFORCEMENT_UPPER_LH	CR1550Y2000T-MS	1.5	C	0.24	
03766045_2	REINFORCEMENT LATCH LOWER RH	PHS-CR1000T-MB	1.5	N	0.62	
03707551_2	SLEEVE REAR LH	NA_EN8		N	0.33	
03730608_2	BULKHEAD_A_POST_REINFORCEMENT_UPPER_RH	CR1550Y2000T-MS	1.5	C	0.24	
03647858_2	ROCKER FRONT CAP INNER RH	CR1200Y1470T-MS	1.0	N	0.14	
03559985_2	MID ROOF BOW MOUNT RH	CR700Y980T-DP	0.8	C	0.41	
03510150_2	C POST INNER REINFORCEMENT LH	CR860Y1180T-DP	0.8	N	1.36	
03470750_2	FRONT INNER ROOF HEADER GUSSET MOUNT LH	CR700Y980T-DP	1.0	C	0.62	
03572146_2	INNER ROCKER BULKHEAD LH	CR420Y780T-DP	1.0	N	0.11	
03751415_2	REINFORCEMENT DOOR LATCH LH	PHS-CR1500T-MB	1.5	N	0.25	
03636521_2	ROCKER REAR CAP INNER LH	CR_HSLA550/620	1.0	N	0.14	
03451542_2	ROOF SIDE RAIL INNER LH	PHS-CR1500T-MB	0.8	N	2.46	
03707049_2	A POST INNER REINFORCEMENT UPPER REAR LH	CR800Y1180T-DP	1.5	N	1.13	
03636520_2	FRONT OUTER ROOF HEADER GUSSET MOUNT RH	CR700Y980T-DP	1.0	C	0.22	
03694699_2	OUTER RING TWB LH	TWB_PHS-CR2000T-MB Apillar 1.	TWB	N	18.62	
03703802_2	A POST INNER REINFORCEMENT UPPER RH	CR800Y1180T-DP	1.5	N	1.22	
03272922_2	ROCKER HEX ABSORBER LH	CR420Y780T-DP	0.7	N	0.98	
03599223_2	REAR INNER ROOF HEADER GUSSET MOUNT LH	CR_HSLA490/600	0.8	C	0.65	
03553361_2	ROCKER INNER RH	CR1550Y2000T-MS	1.2	N	7.23	
03470012_2	MID ROOF BOW MOUNT LH	CR700Y980T-DP	0.8	C	0.41	
03553241_2	A POST INNER RH	PHS-CR2000T-MB	1.2	C	5.06	
03730609_2	BULKHEAD_A_POST_REINFORCEMENT_LOWER_RH	CR1550Y2000T-MS	1.5	C	0.24	
03766044_2	REINFORCEMENT DOOR LATCH RH	PHS-CR1500T-MB	1.5	N	0.25	
03753845_2	REINFORCEMENT LATCH LOWER LH	PHS-CR1000T-MB	1.5	N	0.62	
03553397_2	A POST INNER REINFORCEMENT RH	CR1350Y1700T-MS	1.0	C	1.79	
03748482_2	INNER ROCKER BULKHEAD 02 LH	CR420Y780T-DP	1.0	C	0.11	
03709256_2	OUTER RING TWB RH	TWB_PHS-CR2000T-MB Apillar 1.	TWB	N	18.64	
03553390_2	REAR INNER ROOF HEADER GUSSET MOUNT RH	CR_HSLA490/600	0.8	C	0.65	
03703692_2	SLEEVE FRONT LH	NA_EN8		N	0.35	
03629368_2	ROCKER FRONT CAP INNER LH	CR1200Y1470T-MS	1.0	N	0.14	
03750014_2	OUTER RING REINF. PLATE RH	CR340Y590T-DP	2.0	N	0.08	
03703801_2	A POST INNER REINFORCEMENT UPPER LH	CR800Y1180T-DP	1.5	N	1.22	
03553379_2	ROOF SIDE RAIL INNER RH	PHS-CR1500T-MB	0.8	N	2.46	
03722991_2	BULKHEAD_C_PILLAR_LOWER_LH	CR1550Y2000T-MS	1.5	N	0.19	
03553400_2	C POST INNER REINFORCEMENT RH	CR860Y1180T-DP	0.8	N	1.36	
03451226_2	ROCKER INNER REINFORCEMENT LH	CR420Y780T-DP	1.0	N	1.63	
03747655_2	OUTER RING REINF. PLATE LH	CR340Y590T-DP	2.0	C	0.08	
03749650_2	INNER ROCKER BULKHEAD 02 RH	CR420Y780T-DP	1.0	C	0.11	
03553334_2	C POST INNER RH	PHS-CR1500T-MB	1.2	N	4.83	
03808141	DS-WAS-1430_SCISSOR DOOR ASY_SEM2	(blank)				
03645751	REAR DOOR MOTOR	(blank)		C	9.35	
03645752	FRONT DOOR MOTOR	(blank)		C	9.35	
04033463	REAR DOORS_SEM2	(blank)				
04033467	DOOR SPLIT RR_SEM2	S101-Mild 140/270	1.2	N	0.33	
04033464	DOOR STRUT_SEM2	CR1200Y1470T-MS	1.5	N	3.68	
04033465	BRKT SUPPORT CUP REAR_SEM2	S101-Mild 140/270	1.2	N	0.34	
04033468	B-PILLAR RR_SEM2	CR400Y690T-RA	1.2	N	4.07	
04033470	INNER DOOR RR_SEM2	S101-Mild 140/270	1.2	N	14.86	
04033466	REAR DOOR BRKTS BOTTOM_SEM2	(blank)		N	0.32	
04033469	OUTER DOOR RR_SEM2	CR280Y/400T-BH	0.7	N	7.19	
04033471	REAR DOOR BRKTS TOP_SEM2	(blank)		N	0.32	
03750017	FRONT DOORS_VAR 02	(blank)				
03843038	DOOR SPLIT FR	S101-Mild 140/270	1.2	C	0.46	
03786548	FRONT DOOR BRKTS BOTTOM	(blank)		C	0.32	
03786579	BRKT SUPPORT CUP FRONT	S101-Mild 140/270	1.2	C	0.43	
03786545	FRONT DOOR BRKTS TOP	(blank)		C	0.32	
03750473	DOOR STRUT	CR1200Y1470T-MS	1.5	C	2.94	
03750465	OUTER DOOR FR	CR280Y/400T-BH	0.7	C	2.94	
03750471	INNER DOOR FR	S101-Mild 140/270	1.2	C	12.36	
03613567	DOOR STRUT 04	CR400Y690T-RA	1.2	C	5.57	
03786540	FRONT DOOR BOTTOM ARM 2	(blank)		C	2.68	
03776787	SCISSOR DOOR GLUE	(blank)		C	0.00	
03776789	SCISSOR DOOR WELDS	(blank)		C	0.69	
03786537	REAR DOOR BOTTOM ARM 2	(blank)		C	3.13	
			68%	156	SEM1 carry over	
			9%	20	SEM1 grade/gauge adjust	
			23%	53	SEM2 unique	
				229	TOTAL	

Appendix 2.1 Panel formability simulation results

A pillar Inner

OEM: ARRK
Vehicle Program: Steel E-Motiv
Project Name: Phase 2

Sheet metal forming simulation

Name:Nick Sephton
Department: Engineering
Date: 16-06-2022 Page1 of 8

Overview and Summary

Part Info

Designation: 03438889-Body.1	Type:Heating
Part No.:	Drawing No.:
Nom. / Calculated Material: 22MnB5	
Nom. / Calculated Sheet Thickness: 1.000 mm	

Method Info

Method Plan No.:	
Drawing No.:	Rev:

Part

Criterion		OK	n OK
FLD	5.2	☑	☐
Wrinkles	5.24	☑	☐
Gravity	5.3	☑	☐
Closing	5.4	☑	☐
Forming	5.5	☑	☐
Thinning	5.6	☑	☐
Martensite	5.7	☑	☐
Temperature	5.8	☑	☐
Hardness		☑	☐

Status: 0

Simulation Info:
Filename:03438889_A_Pillar_Inner_LH_NMS_16-6-22_it9 - NEW CAD.afd

AutoForm AutoForm Forming Solver Thermo R10.0.0	Memory: 685.30 MB

d

Process - Blank Die / Heating / Draw / Quenching / Laser Trim

OEM: ARRK
Vehicle Program: Steel E-Motiv
Project Name: Phase 2

Sheet metal forming simulation

Name:Nick Sephton
Department: Engineering
Date: 16-06-2022 Page2 of 8

Input Data

Material & Blank

Calculated Material	22MnB5	Calc. Sheet Thickness			1.000 mm
Yield Stress		r0	1.00	r90	1.00
n-Value		r45	1.00	E-Module	

Yield Curve

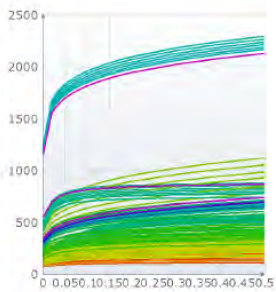

Yield Surface

MU - Part to Blank
56.34 %

RAM tonnage - 110.3 tf

Blank Info

☐ Rectangular Blank
☑ Shaped Blank

Meshing

Roll angle	0.00 °
Initial Element Size	20.00 mm
Refinement Level	6
Max Element Angle	30.00 °

Blank Size - 1821.64 mm X 1021.57 mm

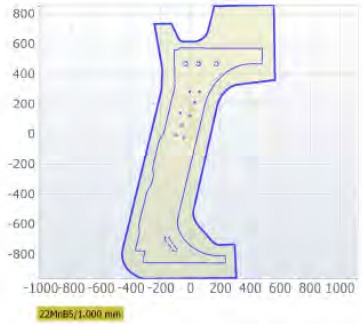

Wrinkling Behavior	D-20	

Wrinkling at -49.68 mm

Wrinkling at -23.90 mm

Wrinkling at -8.94 mm

Wrinkling at 0.00 mm

Formability	K-40	

Advanced Formability

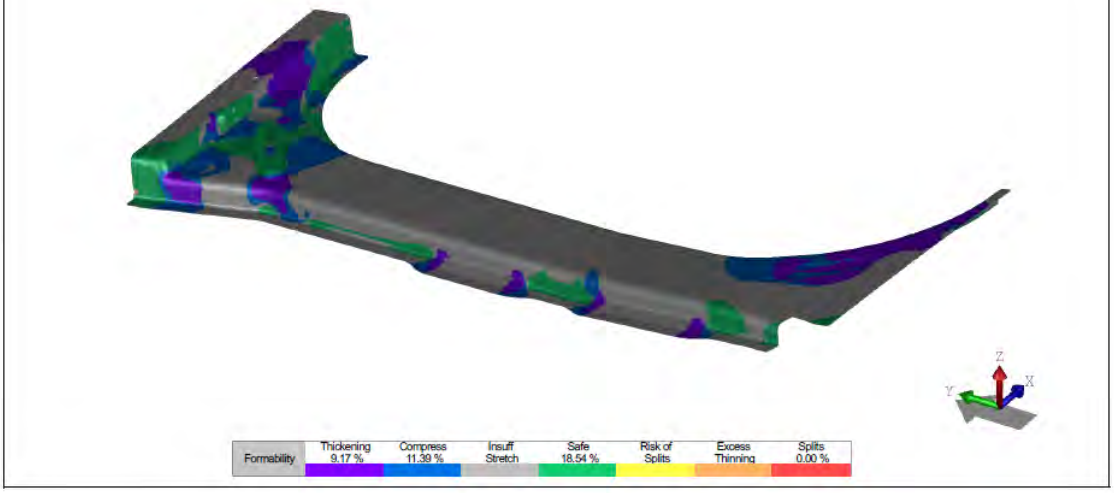

Thinning	K-40

Thinning

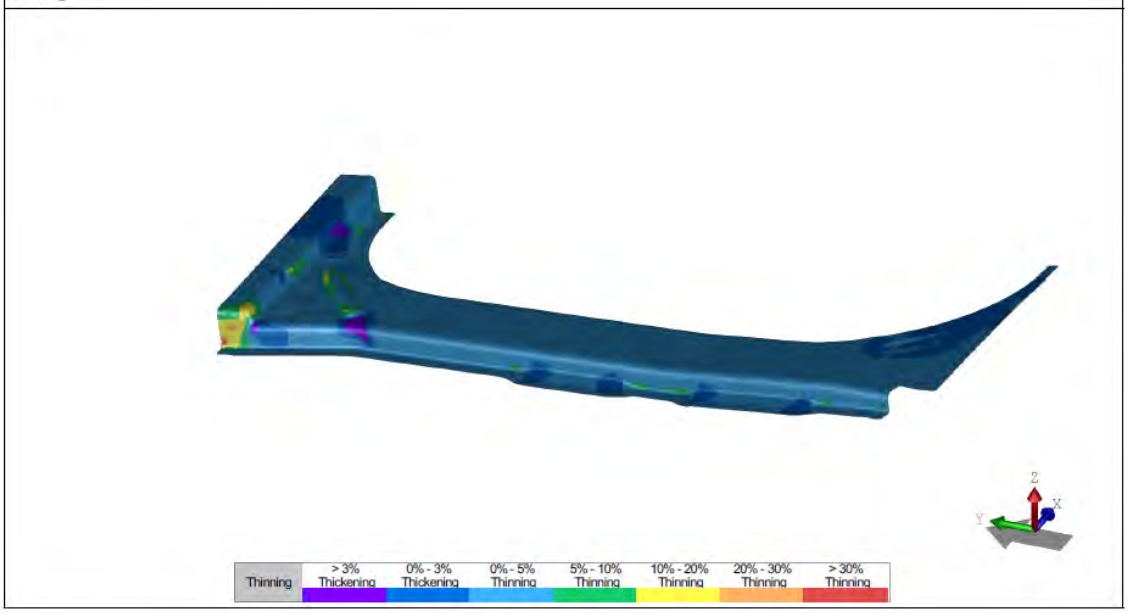

C pillar Inner

Overview and Summary

Part Info

Designation: 03440399-03328225 - C-PILLAR INNER LH	Type:Heating
Part No.:	Drawing No.:
Nom. / Calculated Material: 22MnB5	
Nom. / Calculated Sheet Thickness: 1.000 mm	

Method Info

Method Plan No.:	
Drawing No.:	Rev:

Part

Criterion		OK	n OK
FLD	5.2	☐	☐
Wrinkles	5.24	☑	☐
Gravity	5.3	☑	☐
Closing	5.4	☑	☐
Forming	5.5	☑	☐
Thinning	5.6	☑	☐
Martensite	5.7	☑	☐
Temperature	5.8	☑	☐
Hardness		☑	☐

Status

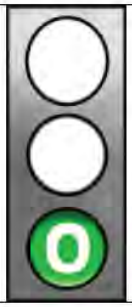

Simulation Info:

Filename:
ARRK_03440399_C_Pillar_Inner_LH_NMS_31-8-22_it4 - EXTENSION MODS 3 -

AutoForm
AutoForm Forming Solver Thermo R10.0.0

Memory: 1450.10 MB

in

Process - Blank Die / Heating / Draw / Quenching / Laser Trim

Input Data	Material & Blank

Calculated Material	22MnB5	Calc. Sheet Thickness			1.000 mm	
Yield Stress		r0	1.00	r90	1.00	
n-Value		r45	1.00	E-Module		

Yield Curve

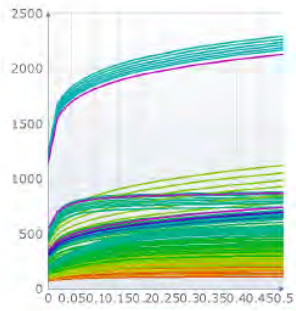

Yield Surface

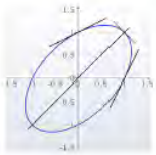

MU - Part to Blank

52.17 %

RAM tonnage - 146.0 tf

Blank Info	
☐ Rectangular Blank	
☑ Shaped Blank	
Meshing	
Roll angle	0.00 °
Initial Element Size	20.00 mm
Refinement Level	5
Max Element Angle	22.50 °

Blank Size - 1778.49 mm X 1025.66 mm

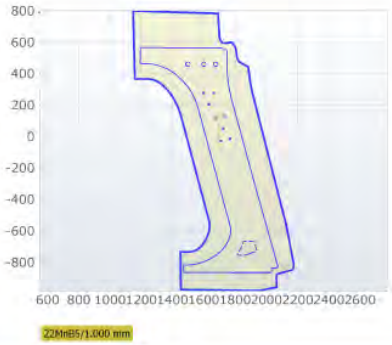

Wrinkling Behavior	D-20

Wrinkling at -54.97 mm

Wrinkling at -27.67 mm

Wrinkling at -10.10 mm

Wrinkling at -1.00 mm

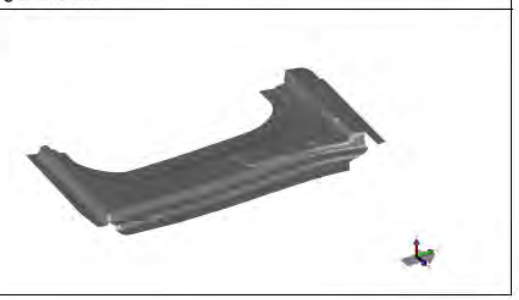

Formability	K-40	

Advanced Formability

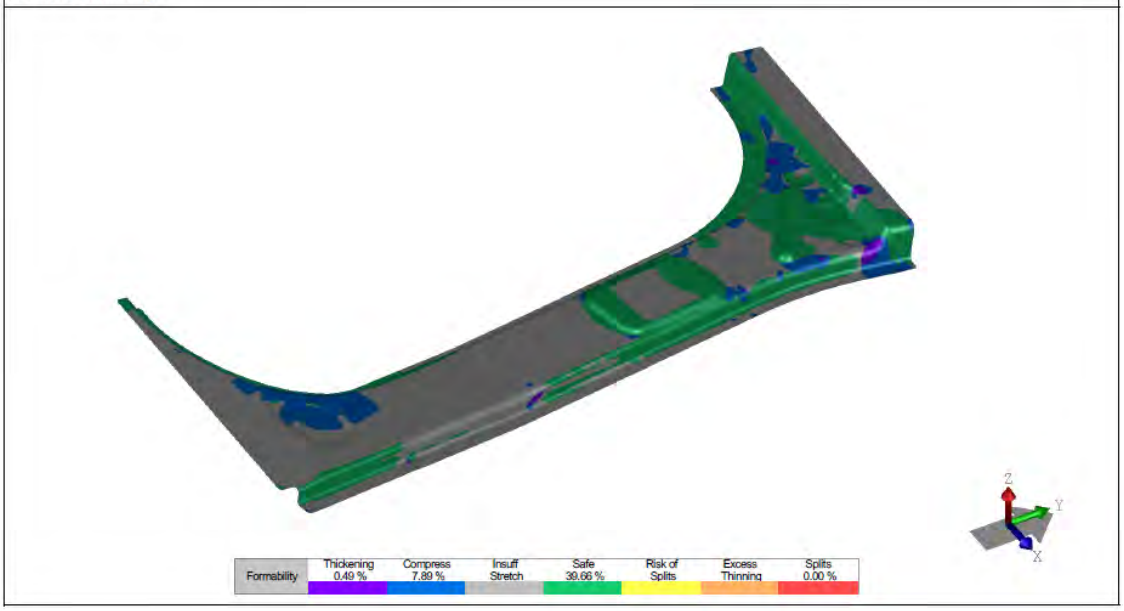

Thinning	K-40	

Thinning

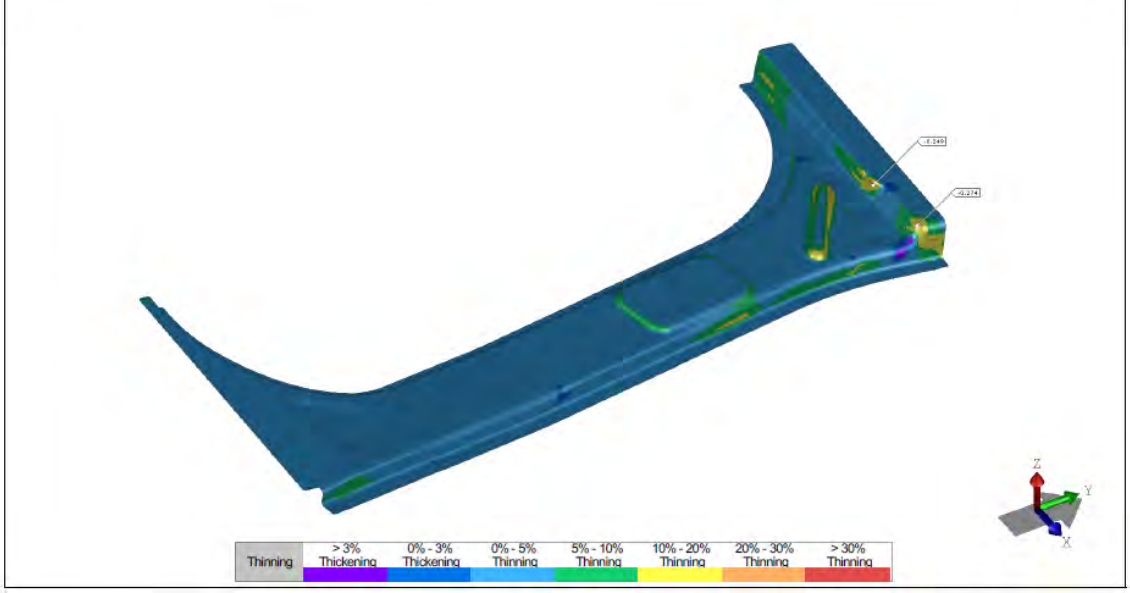

Wrinkling	K-40	

Thickness

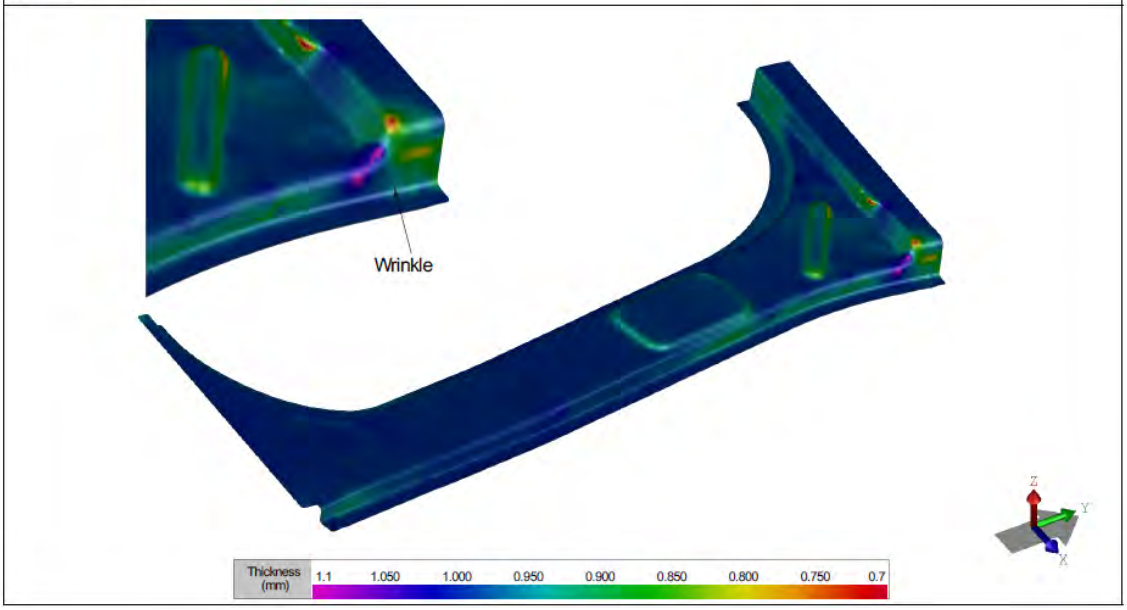

Temperature	K-40	

Temperature

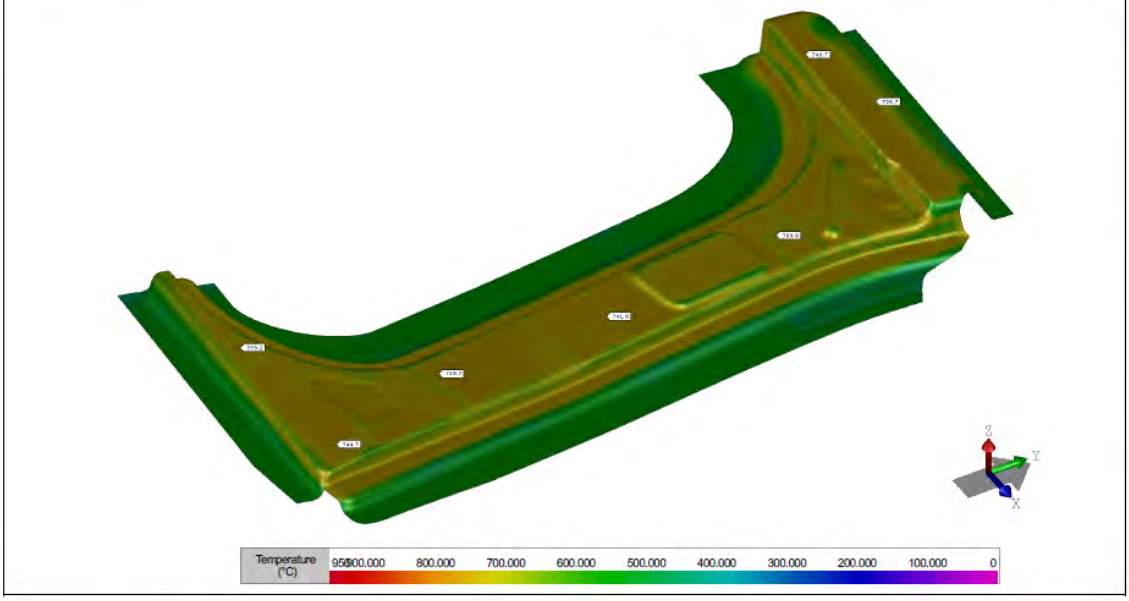

Vertical Dash Brace Lower

Overview and Summary

Part Info

Designation: 03448749 VERTICAL DASH BRACE OUTER	Type: Single Action Draw
Part No.:	Drawing No.:
Nom. / Calculated Material: Usibor1500_150mm_700C	
Nom. / Calculated Sheet Thickness: 2.000 mm	

Method Info

Method Plan No.:	
Drawing No.:	Rev:

Part

Criterion		OK	n OK	Status
FLD	5.2	☑	☐	
Flanging	5.24	☐	☐	
Gravity	5.3	☑	☐	
Closing	5.4	☑	☐	
Forming	5.5	☑	☐	
Thinning	5.6	☑	☐	
Martensite	5.7	☑	☐	
Temperature	5.8	☑	☐	
Hardness		☑	☐	

Simulation Info:

Filename: ARRK_03448749_Vertical_Dash_Brace_LH_NMS_26-8-22_it13 - EXTENSION MODS 2

AutoForm | Memory: 654.15 MB

AutoForm Forming Solver Thermo R10.0.0

Process - Blank Die / Heating / Draw / Quenching / Laser Trim

Input Data — Material & Blank

Calculated Material	Usibor1500_150mm	Calc. Sheet Thickness			2.000 mm
Yield Stress		r0	1.00	r90	1.00
n-Value		r45	1.00	E-Module	

Yield Curve

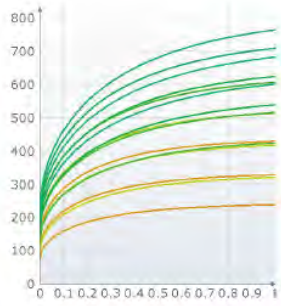

Yield Surface

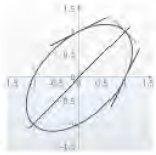

MU - Part to Blank

45.67 %

RAM Tonnage - 160.1 tf

Blank Info

- ☐ Rectangular Blank
- ☑ Shaped Blank

Meshing

Roll angle	0.00 °
Initial Element Size	20.00 mm
Refinement Level	5
Max Element Angle	22.50 °

Blank Size - 774.31 mm X 475.17 mm

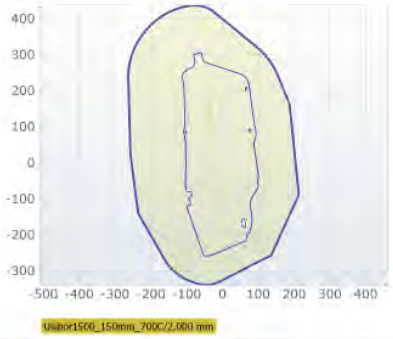

Formability	T-40	

Advanced Formability

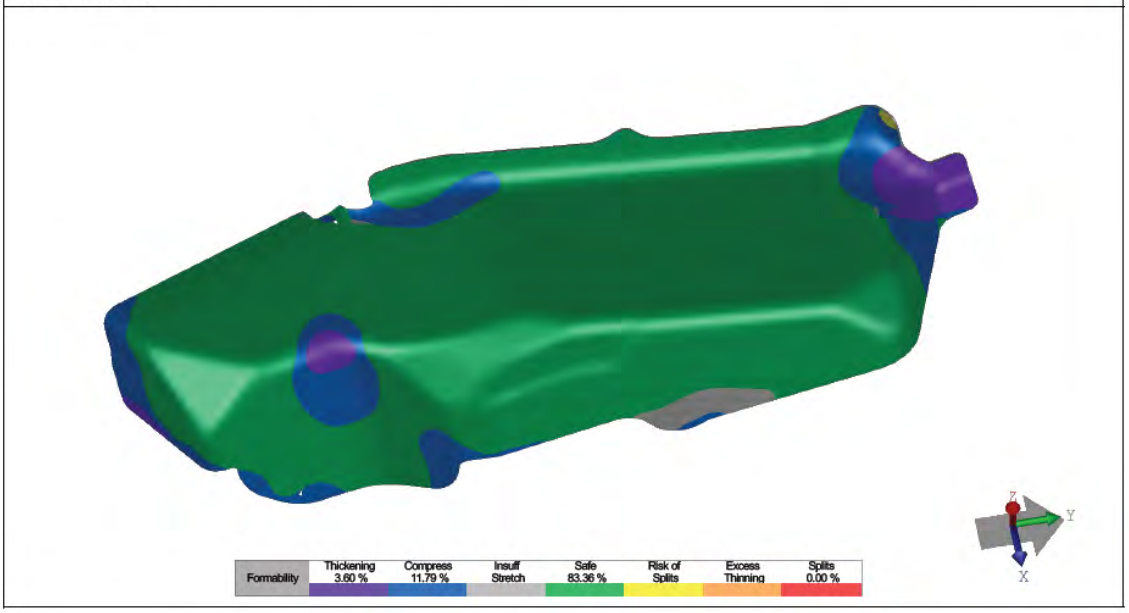

Thinning	T-40	

Thinning

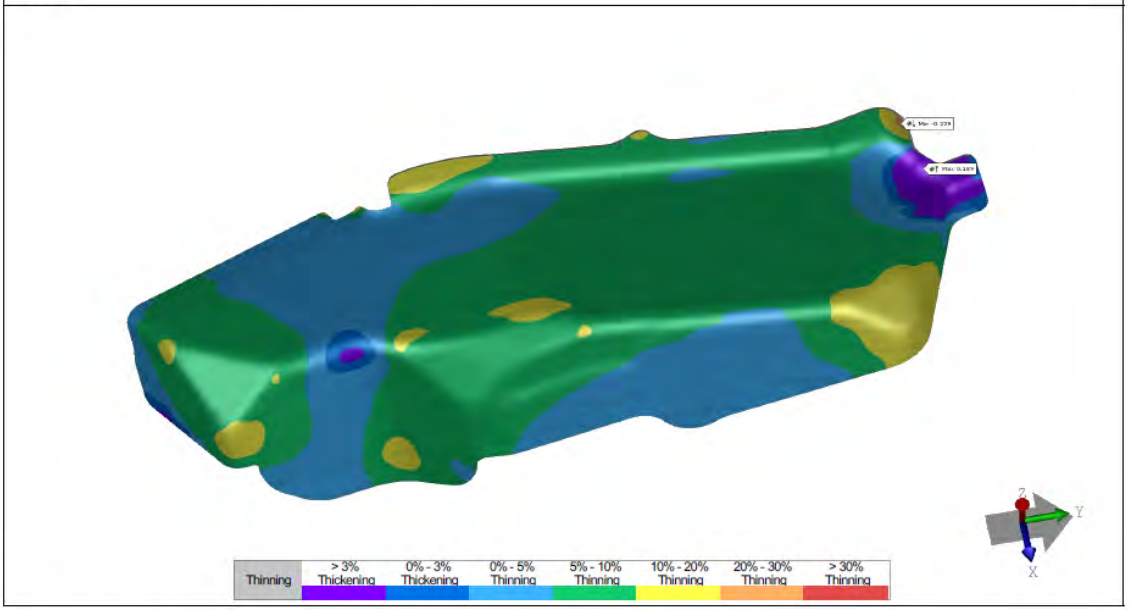

Temperature	D-20	

Temperature

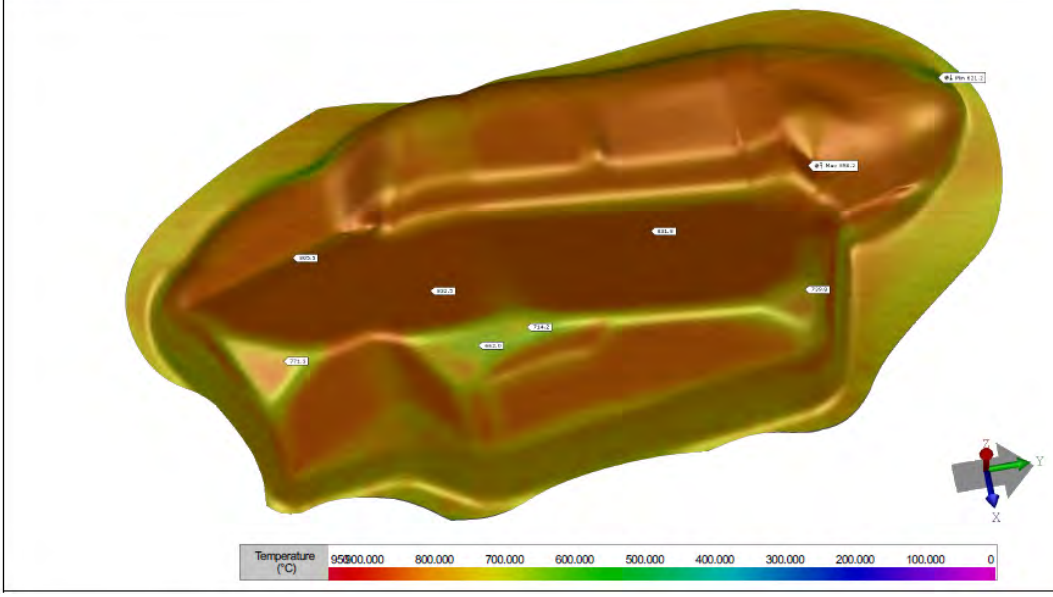

Wrinkling Behavior	T-40	

Wrinkling at -78.0mm

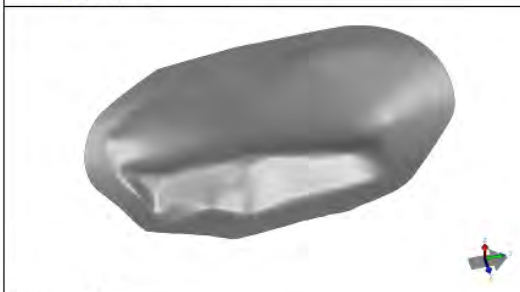

Wrinkling at -38.0mm

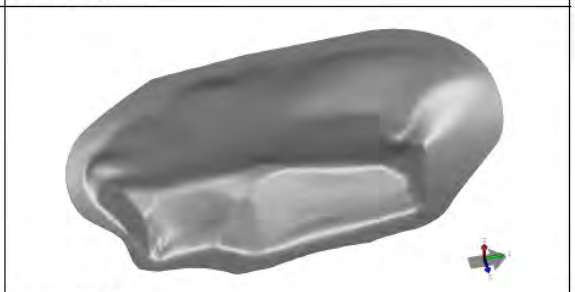

Wrinkling at -9mm

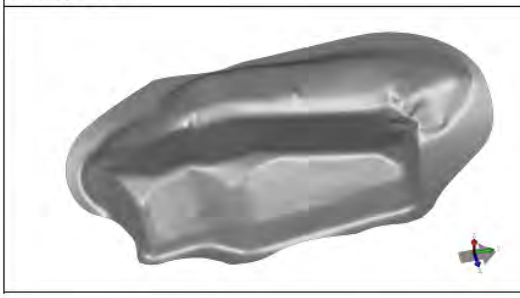

Wrinkling at -1.5mm

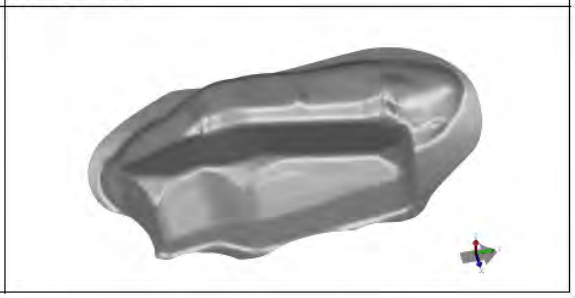

Rocker Inner

Overview and Summary

Part Info

Designation: 03451131 ROCKER INNER LH MW	Type:Heating
Part No.:	Drawing No.:
Nom. / Calculated Material: 22MnB5	
Nom. / Calculated Sheet Thickness: 1.500 mm	

Method Info

Method Plan No.:	
Drawing No.:	Rev:

Part

Criterion		OK	n OK	Status
FLD	5.2	☑	☐	
Flanging	5.24	☐	☐	
Gravity	5.3	☑	☐	
Closing	5.4	☑	☐	
Forming	5.5	☑	☐	
Thinning	5.6	☑	☐	
Martensite	5.7	☑	☐	
Temperature	5.8	☑	☐	
Hardness		☑	☐	

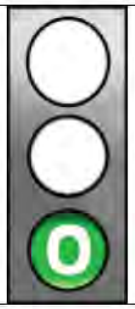

Simulation Info:

Filename:ARRK_03451131-Rocker_Inner_NMS_24-2-22_it1.afd

AutoForm AutoForm Forming Solver Thermo R10.0.0	Memory: 629.87 MB

Input Data — Material & Blank

Calculated Material	22MnB5	Calc. Sheet Thickness			1.500 mm
Yield Stress		r0	1.00	r90	1.00
n-Value		r45	1.00	E-Module	

Yield Curve

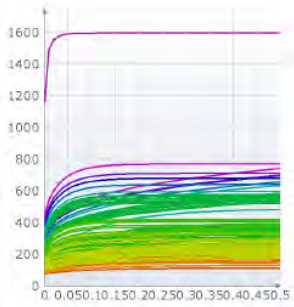

Yield Surface

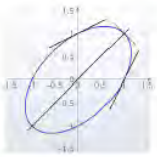

MU - Part to Blank

84.18 %

Blank Info

☑ Rectangular Blank

☐ Shaped Blank

Meshing

Roll angle	0.00 °
Initial Element Size	40.00 mm
Refinement Level	7
Max Element Angle	30.00 °

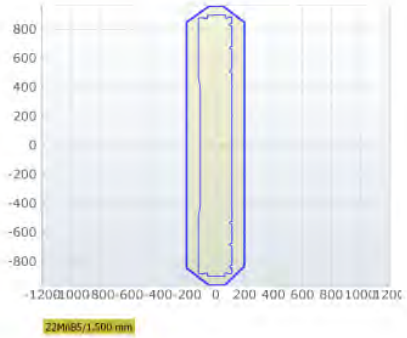

Input Data	D-20	D-20

Tool Info				Process Data		
Meshing Tolerance	0.05 mm			Friction Coefficient		
Process Type	Single Action Draw			Constant	0.450	
Tool Geometry Refers to	Lower Side of Initial Blank			Die - Blank	-	
Tools	Contact Side	Type	Gap	Punch - Blank	-	
Die	Upper Side of Blank	Rigid		Binder - Blank	-	
Punch	Lower Side of Blank	Rigid		Binderforce		
Binder	Lower Side of Blank	Gap Controlled	0.50 mm	RAM	153.0 tf	
				Binderforce/-pressure	105.5 tf	

Tool Geometry 1st opp

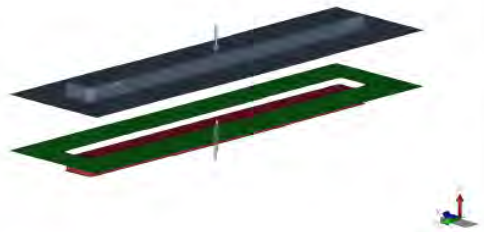

Formability	T-30

Advanced Formability

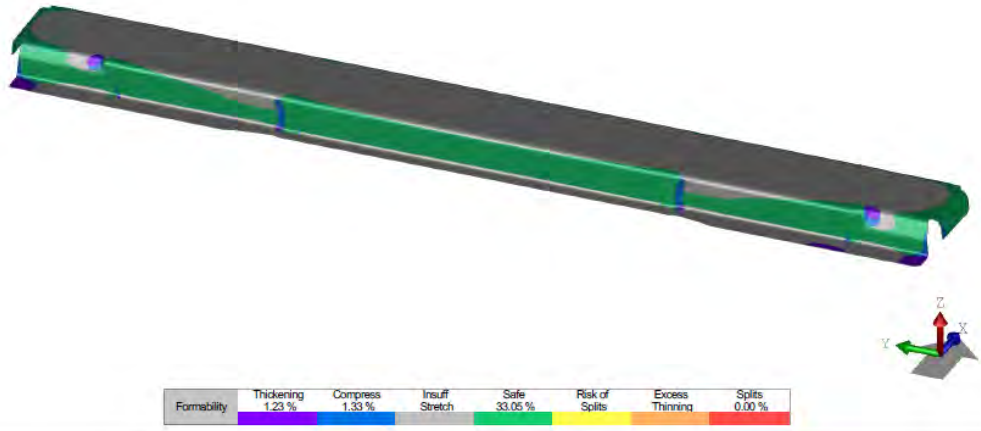

Formability	T-30

FLD

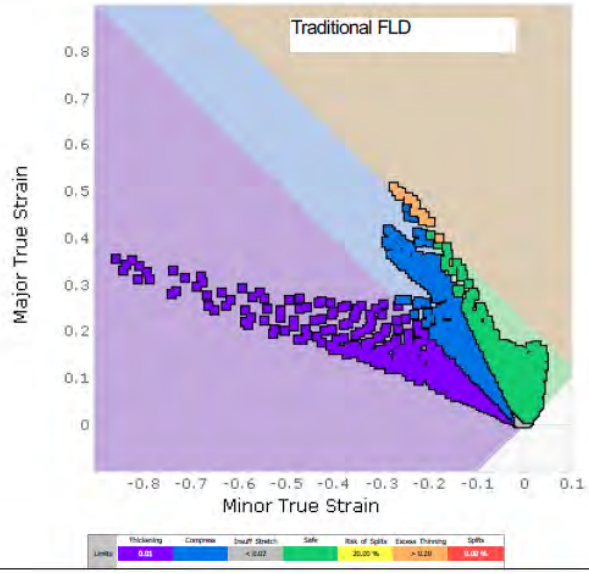

Thinning	T-30

Thinning

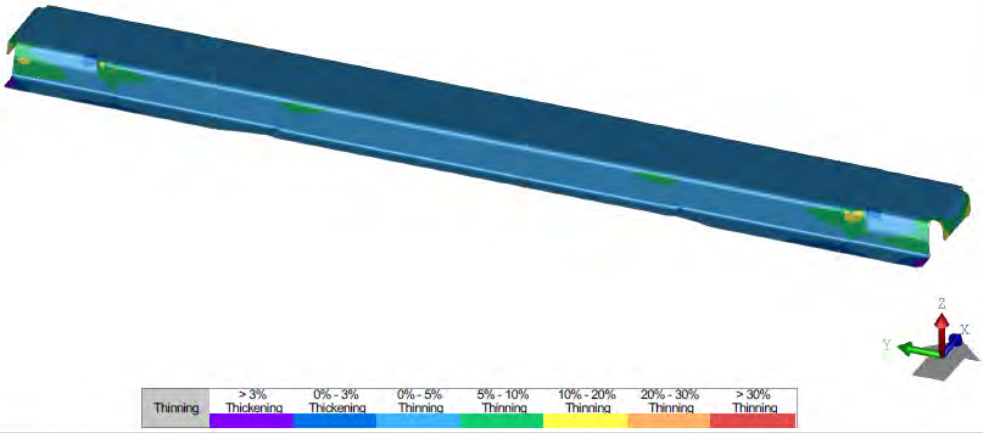

Wrinkling Behavior	H-10

Wrinkling at -51.47 mm	Wrinkling at -24.71 mm
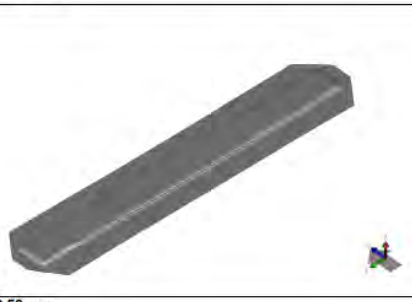	
Wrinkling at -9.50 mm	**Wrinkling at 0.00 mm**
	

Roof side rail inner

Overview and Summary

Part Info

Designation: 03451542-Body.1 | Type: Single Action Draw

Part No.: | Drawing No.:

Nom. / Calculated Material: Usibor1500_150mm_700C

Nom. / Calculated Sheet Thickness: 0.800 mm

Method Info

Method Plan No.:

Drawing No.: | Rev:

Part

Criterion		OK	n OK	Status
FLD	5.2	☐	☐	
Flanging	5.24	☐	☐	
Gravity	5.3	☑	☐	
Closing	5.4	☑	☐	
Forming	5.5	☑	☐	
Thinning	5.6	☑	☐	
Martensite	5.7	☑	☐	
Temperature	5.8	☑	☐	
Hardness		☑	☐	

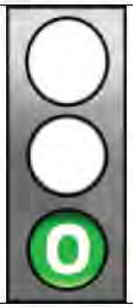

Simulation Info:

Filename:ARRK_03451542_Roof_Side_Rail_Inner_LH_NMS_7-6-22_it1.afd

AutoForm
AutoForm Forming Solver Thermo R10.0.0 | Memory: 1169.46 MB

Remarks: No issues

Process - Blank Die / Heating / Draw / Quenching / Laser Trim

Input Data	Material & Blank

Calculated Material	Usibor1500_150mm	Calc. Sheet Thickness				0.800 mm	
Yield Stress		r0	1.00	r90	1.00		
n-Value		r45	1.00	E-Module			

Yield Curve

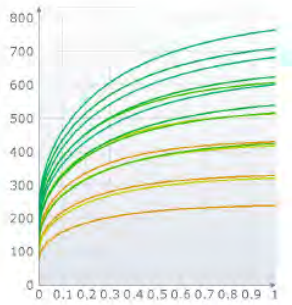

Yield Surface

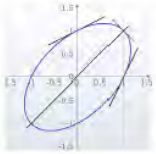

MU - Part to Blank

33.06 %

RAM Tonnage - 400.0 tf

Blank Info	
☑ Rectangular Blank	
☐ Shaped Blank	
Meshing	
Roll angle	0.00 °
Initial Element Size	40.00 mm
Refinement Level	5
Max Element Angle	22.50 °

Blank Size - 2410.00 X 430.00 mm

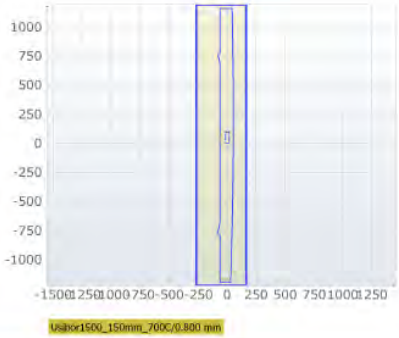

Formability	T-40

Advanced Formability

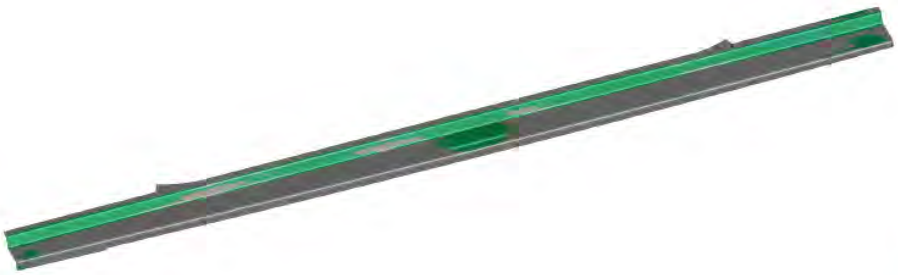

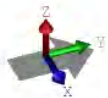

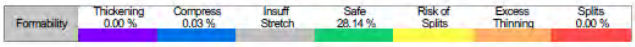

Thinning	T-40	

Thinning

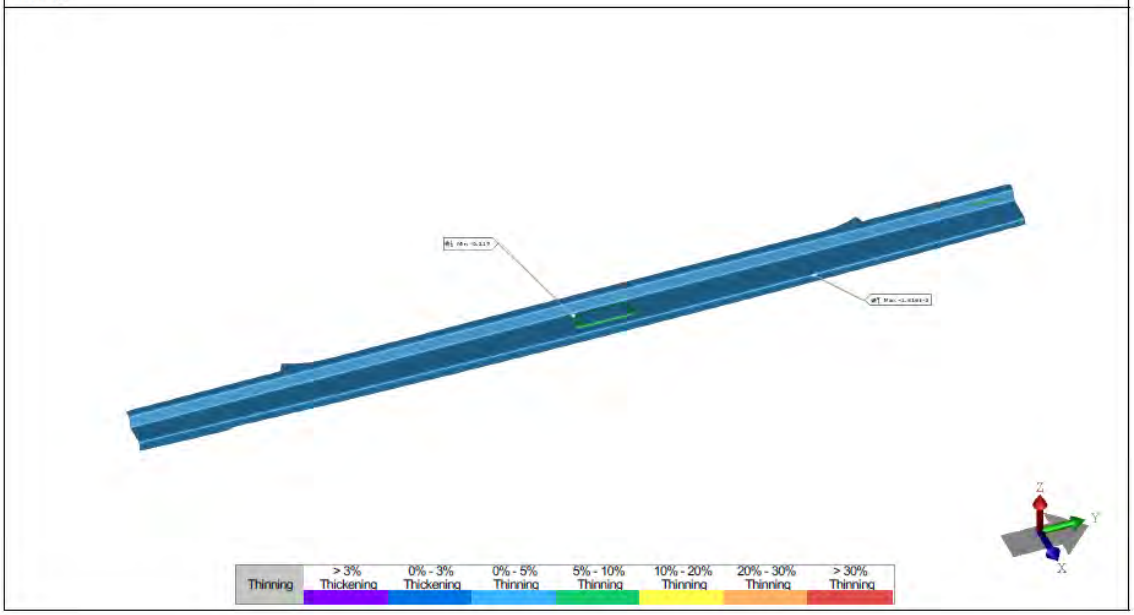

Wrinkling Behavior	T-40	

Wrinkling at

Wrinkling at

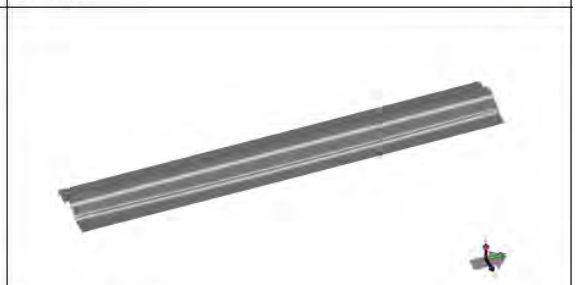

Wrinkling at

Wrinkling at

Front Header

Overview and Summary

Part Info

Designation: 03451793-FRONT HEADER | Type: Single Action Draw

Part No.: | Drawing No.:

Nom. / Calculated Material: SSAB_CR780Y980T_CP

Nom. / Calculated Sheet Thickness: 0.800 mm

Method Info

Method Plan No.:

Drawing No.: | Rev:

Part

Criterion		OK	n OK	Status
FLD	5.2	☑	☐	
Flanging	5.24	☐	☐	
Gravity	5.3	☑	☐	
Closing	5.4	☑	☐	
Forming	5.5	☑	☐	
Thinning	5.6	☑	☐	
Strain	5.7	☑	☐	
Wrinkles	5.8	☑	☐	
Springback	5.9	☑	☐	

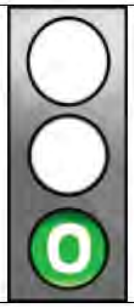

Simulation Info:

Filename: ARRK_03451793_Front_Header_NMS_1-9-22_it6 - EXTENSION MODS 2 - EXTENDED

AutoForm | Memory: 1666.34 MB

AutoForm Forming Solver R10.0.0

Process - Blank Die / Draw / Trim, CAM Pierce & Pierce / Trim, CAM Pierce and Pierce

Input Data — Material & Blank

Calculated Material	SSAB_CR780Y980T	Calc. Sheet Thickness			0.800 mm
Yield Stress	848.99 MPa	r0	0.88	r90	0.91
n-Value	0.094	r45	1.02	E-Module	2.00E+05 MPa

Yield Curve

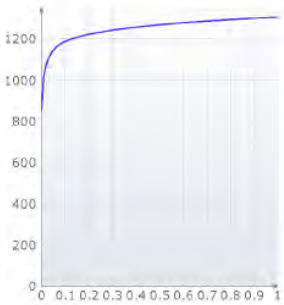

Yield Surface

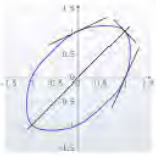

Forming Limit Curve

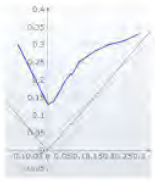

MU - Part to Blank

42.65 %

Blank Info

☐ Rectangular Blank

☑ Shaped Blank

Meshing

Roll angle	0.00 °
Initial Element Size	20.00 mm
Refinement Level	6
Max Element Angle	22.50 °

Blank Size - 1553.95 mm X 444.44 mm

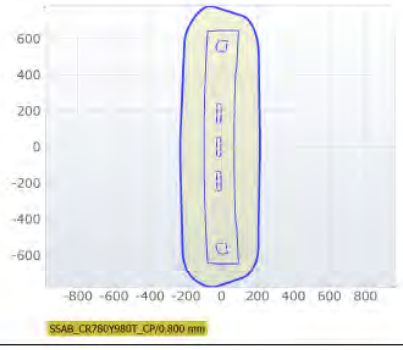

Input Data	D-20	D-20

Tool Info				Process Data		
Meshing Tolerance	0.05 mm			Friction Coefficient		
Process Type	Single Action Draw			Constant	0.100	
Tool Geometry Refers to	Lower Side of Initial Blank			Die - Blank	-	
Tools	Contact Side	Type	Gap	Punch - Blank	-	
Die	Upper Side of Blank	Rigid		Binder - Blank	-	
Punch	Lower Side of Blank	Rigid		Binderforce		
Binder	Lower Side of Blank	Force Controlled		RAM	539.5 tf	
				Binderforce/-pressure	180.0 tf	

Tool Geometry 1st opp

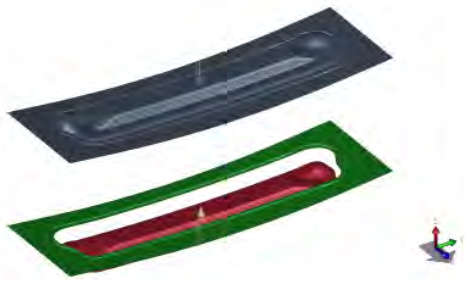

Formability	T-30

Advanced Formability

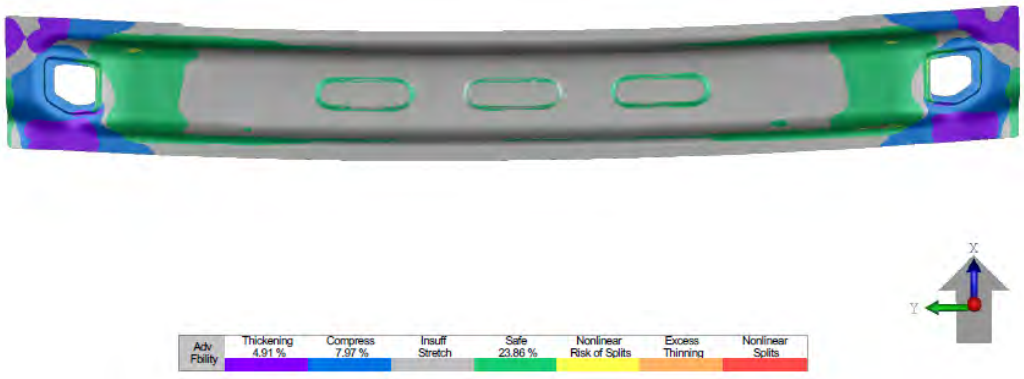

Thinning	T-30	

Thinning

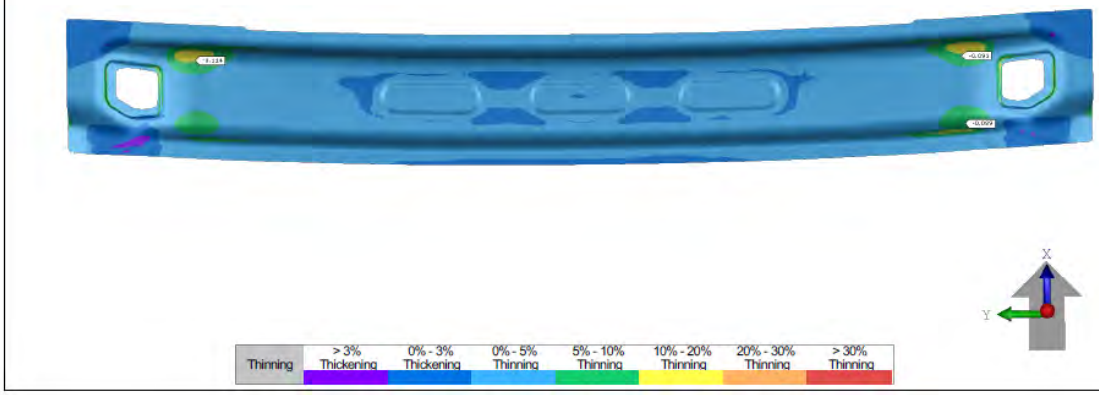

Wrinkles	T-30	

Wrinkles

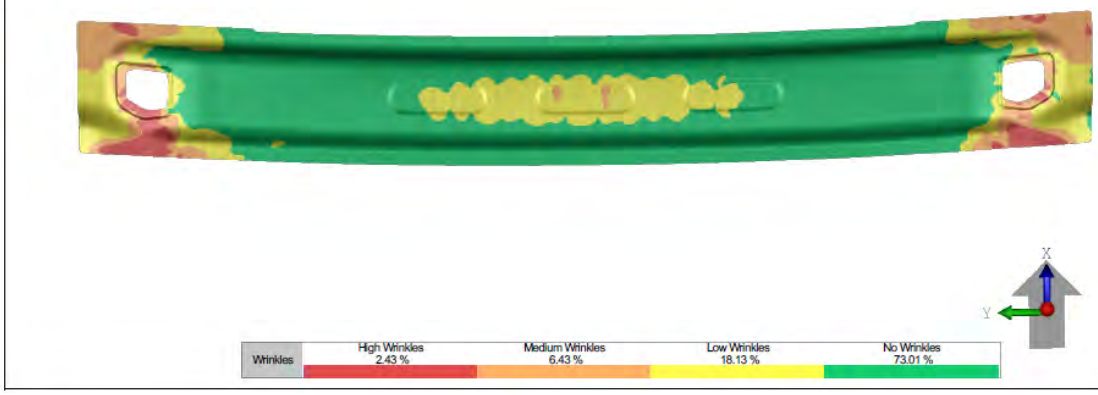

Wrinkling Behavior	D-20	

Wrinkling at -37.86 mm	Wrinkling at -16.37 mm
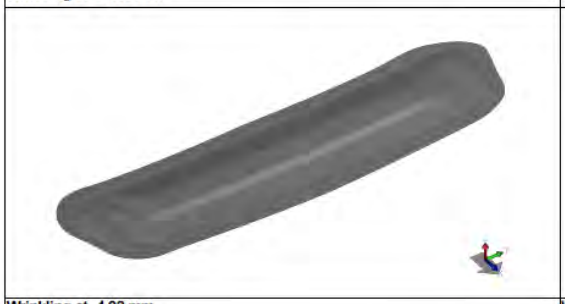	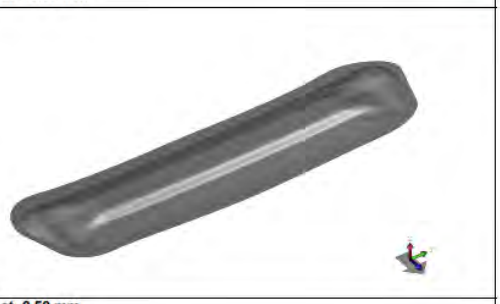
Wrinkling at -4.92 mm	**Wrinkling at -0.50 mm**
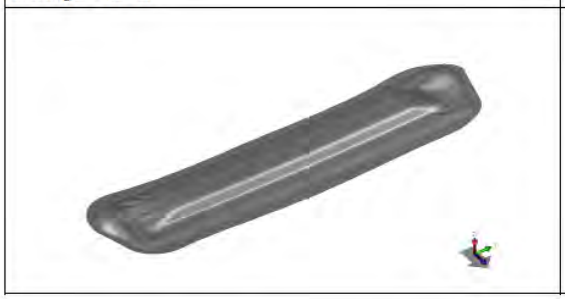	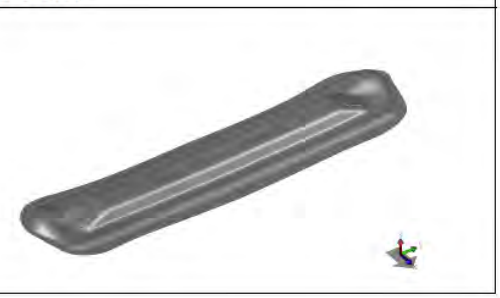

Springback	M-40	

Springback

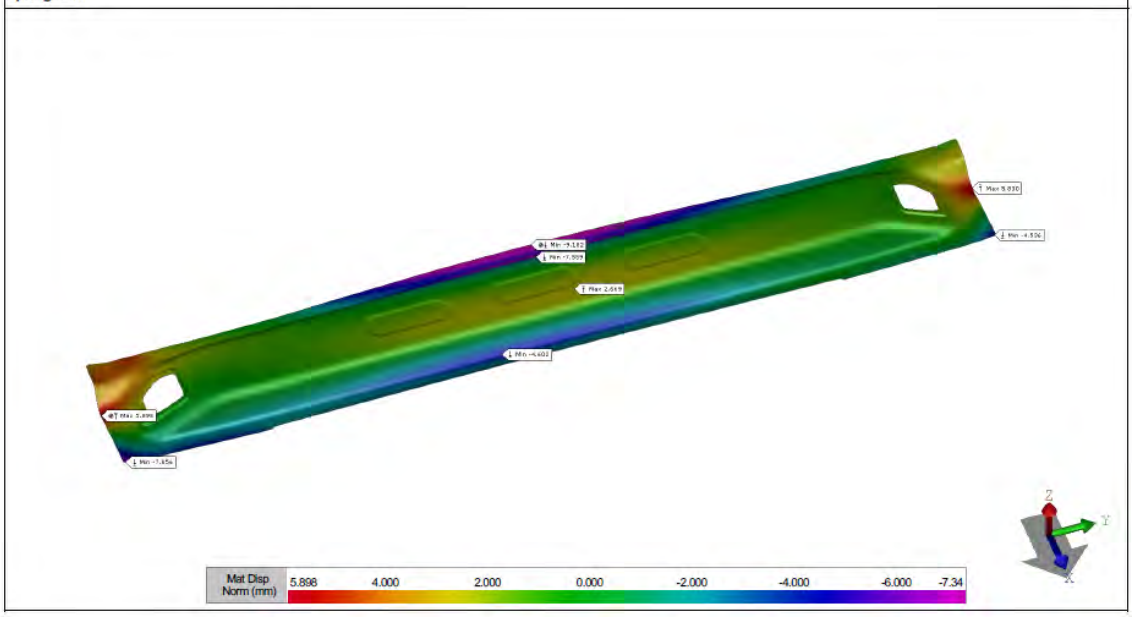

Inner roof frame middle

Overview and Summary

Part Info

Designation: 03462738 INNER ROOF FRAME MIDDLE	Type: Single Action Draw
Part No.:	Drawing No.:
Nom. / Calculated Material: CR820Y1180T_RA_CE+	
Nom. / Calculated Sheet Thickness: 0.800 mm	

Method Info

Method Plan No.:	
Drawing No.:	Rev:

Part

Criterion		OK	n OK	Status
FLD	5.2	☑	☐	
Flanging	5.24	☐	☐	
Gravity	5.3	☑	☐	
Closing	5.4	☑	☐	
Forming	5.5	☑	☐	
Thinning	5.6	☑	☐	
Strain	5.7	☑	☐	
Wrinkles	5.8	☑	☐	
Springback	5.9	☑	☐	

Simulation Info:

Filename: ARRK_03462738_Inr_Roof_Frame_Middle_NMS_8-9-22_it2 - EXTENSION MODS 1 -

AutoForm AutoForm Forming Solver R10.0.0	Memory: 1157.50 MB

Process - Blank / Draw / Laser Trim

Input Data — Material & Blank

Calculated Material	CR820Y1180T_RA_(	Calc. Sheet Thickness			0.800 mm
Yield Stress	869.85 MPa	r0	0.56	r90	0.61
n-Value	0.119	r45	0.77	E-Module	2.10E+05 MPa

Yield Curve

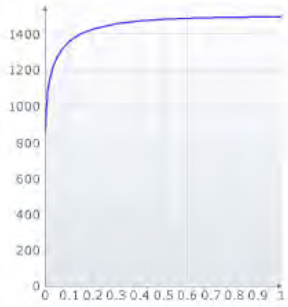

Yield Surface

Forming Limit Curve

MU - Part to Blank

45.39 %

Blank Info

☐ Rectangular Blank

☑ Shaped Blank

Meshing

Roll angle	0.00 °
Initial Element Size	20.00 mm
Refinement Level	6
Max Element Angle	22.50 °

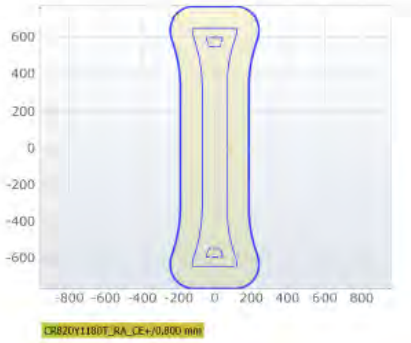

Input Data	D-20	D-20

Tool Info			
Meshing Tolerance	0.05 mm		
Process Type	Single Action Draw		
Tool Geometry Refers to	Lower Side of Initial Blank		
Tools	Contact Side	Type	Gap
Die	Upper Side of Blank	Rigid	
Punch	Lower Side of Blank	Rigid	
Binder	Lower Side of Blank	Force Controlled	

Process Data		
Friction Coefficient		
Constant	0.100	
Die - Blank	-	
Punch - Blank	-	
Binder - Blank	-	
Binderforce		
RAM	488.2 tf	
Binderforce/-pressure	184.4 tf	

Tool Geometry 1st opp

Formability	M-40

Advanced Formability

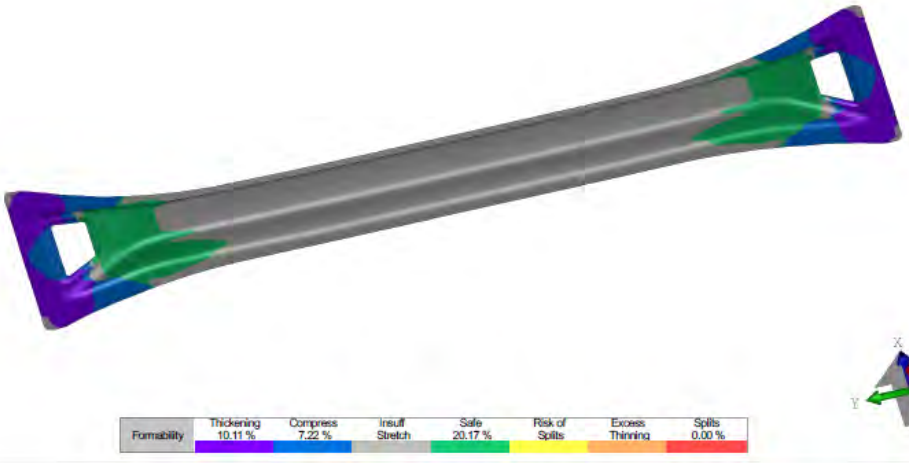

Thinning	M-40	

Thinning

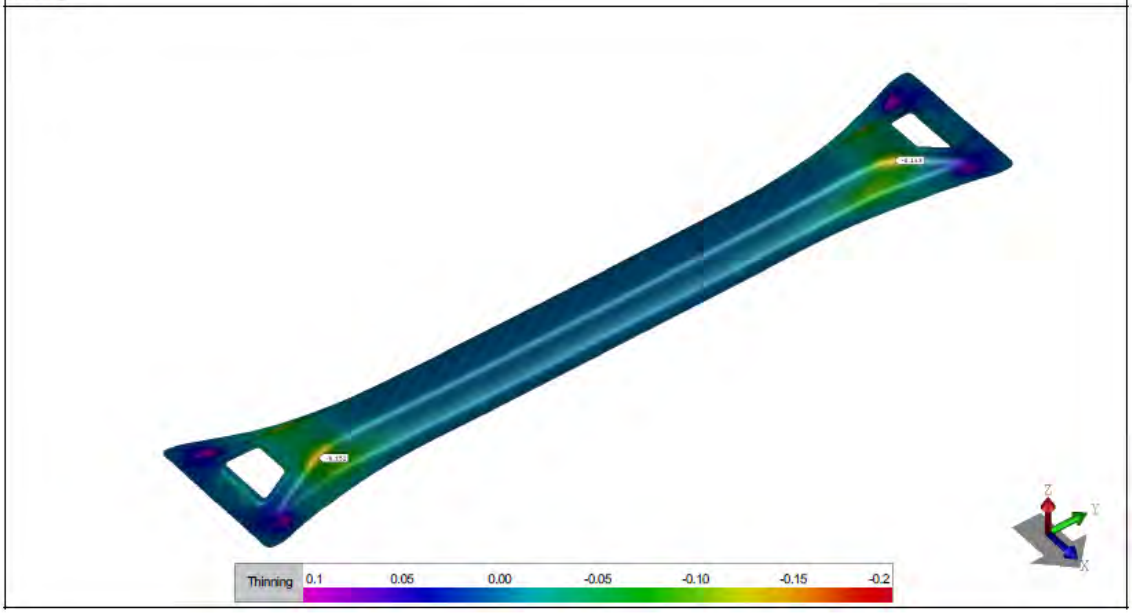

Wrinkles	M-40	

Wrinkles

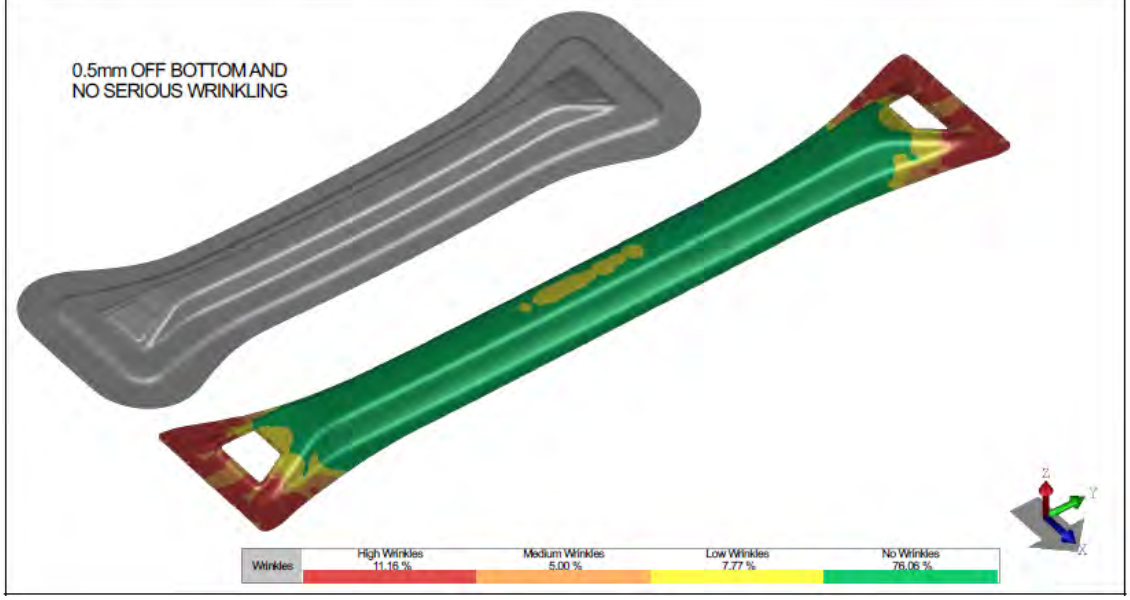

Wrinkling Behavior	D-20	

Wrinkling at -42.55 mm	Wrinkling at -26.32 mm
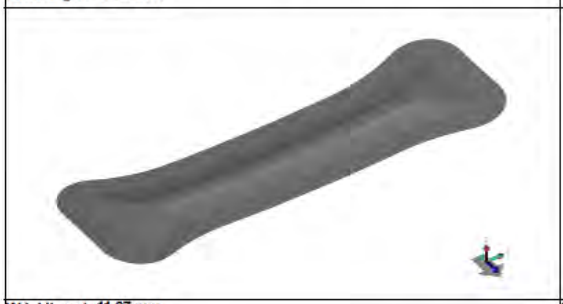	
Wrinkling at -11.07 mm	**Wrinkling at -1.50 mm**
	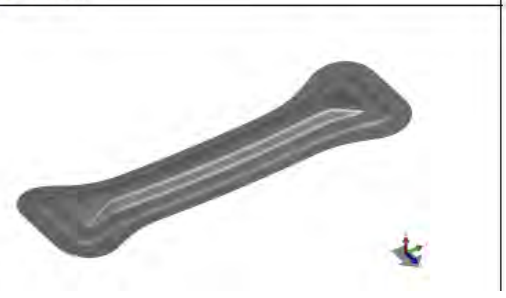

Springback	M-40	

Springback

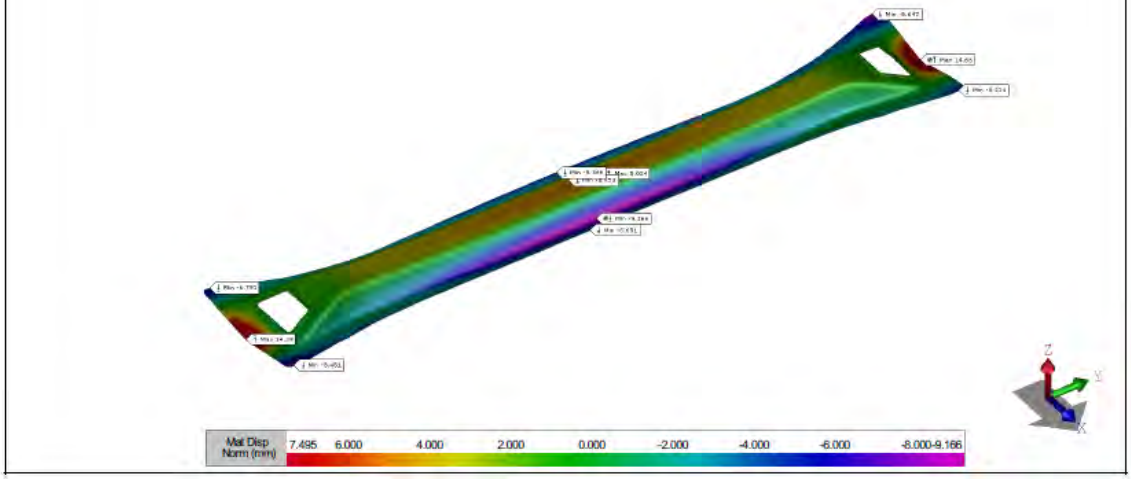

Front Torque Box

Overview and Summary

Part Info

Designation: 03469873 Torque Box Front | Type: Single Action Draw

Part No.: | Drawing No.:

Nom. / Calculated Material: RA780 - CE

Nom. / Calculated Sheet Thickness: 1.800 mm

Method Info

Method Plan No.:

Drawing No.: | Rev:

Part

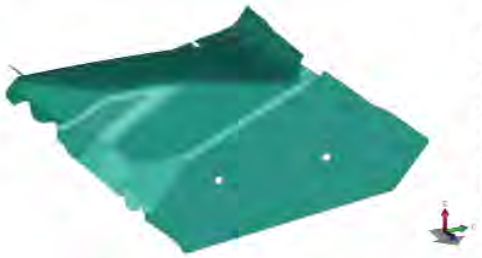

Criterion		OK	n OK	Status
FLD	5.2	☑	☐	
Flanging	5.24	☑	☐	
Gravity	5.3	☑	☐	
Closing	5.4	☑	☐	
Forming	5.5	☑	☐	
Thinning	5.6	☑	☐	
Strain	5.7	☑	☐	
Wrinkles	5.8	☑	☐	
Springback	5.9	☑	☐	

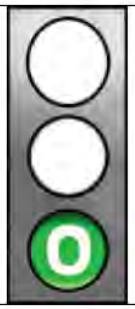

Simulation Info:

Filename:
ARRK_03469873_Front_Torque_Box_NMS_22-9-22_it1 - EXTENSION MODS 1 - CAD

AutoForm
AutoForm Forming Solver R10.0.0

Memory: 138.98 MB

Input Data — Material & Blank

Calculated Material	RA780 - CE	Calc. Sheet Thickness			1.800 mm
Yield Stress	509.85 MPa	r0	1.00	r90	1.00
n-Value	0.186	r45	1.00	E-Module	2.10E+05 MPa

Yield Curve

Yield Surface

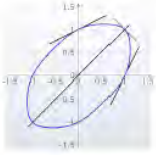

Forming Limit Curve

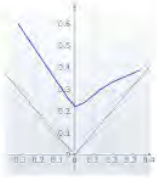

Blank Info

☐ Rectangular Blank

☑ Shaped Blank

Meshing

Roll angle	0.00 °
Initial Element Size	40.00 mm
Refinement Level	7
Max Element Angle	30.00 °

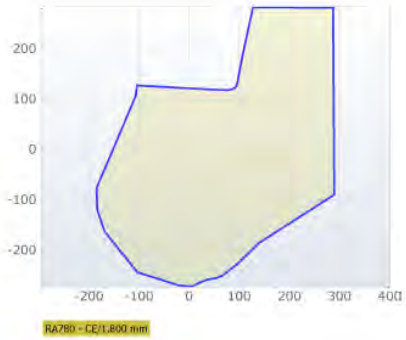

Input Data	D-20	D-20

Tool Info			
Meshing Tolerance	0.05 mm		
Process Type	Single Action Draw		
Tool Geometry Refers to	Upper Side of Initial Blank		
Tools	Contact Side	Type	Gap
Upr Steel	Upper Side of Blank	Rigid	
Upr Pad	Upper Side of Blank	Force Controlled	
Punch	Lower Side of Blank	Rigid	

Process Data		
Friction Coefficient		
Constant	0.100	
Die - Blank	-	
Punch - Blank	-	
Binder - Blank	-	
Binderforce		
RAM	223.1 tf	
Binderforce/-pressure	101.0 tf	

Tool Geometry 1st opp

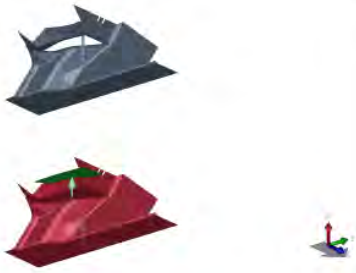

Tool Geometry 1st opp

Formability	T-50

Advanced Formability

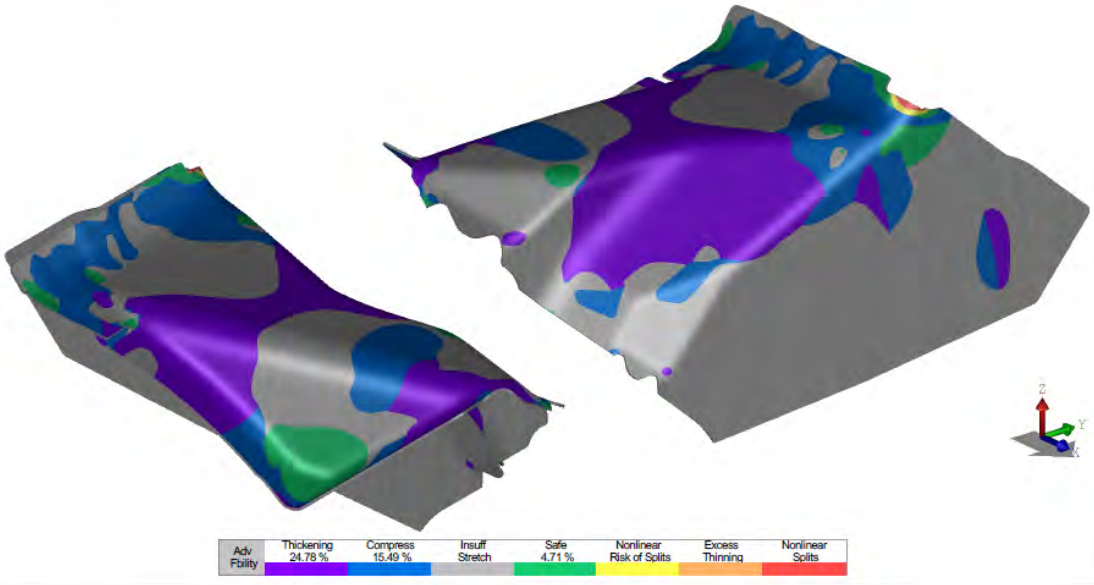

Thinning	T-30	

Thinning

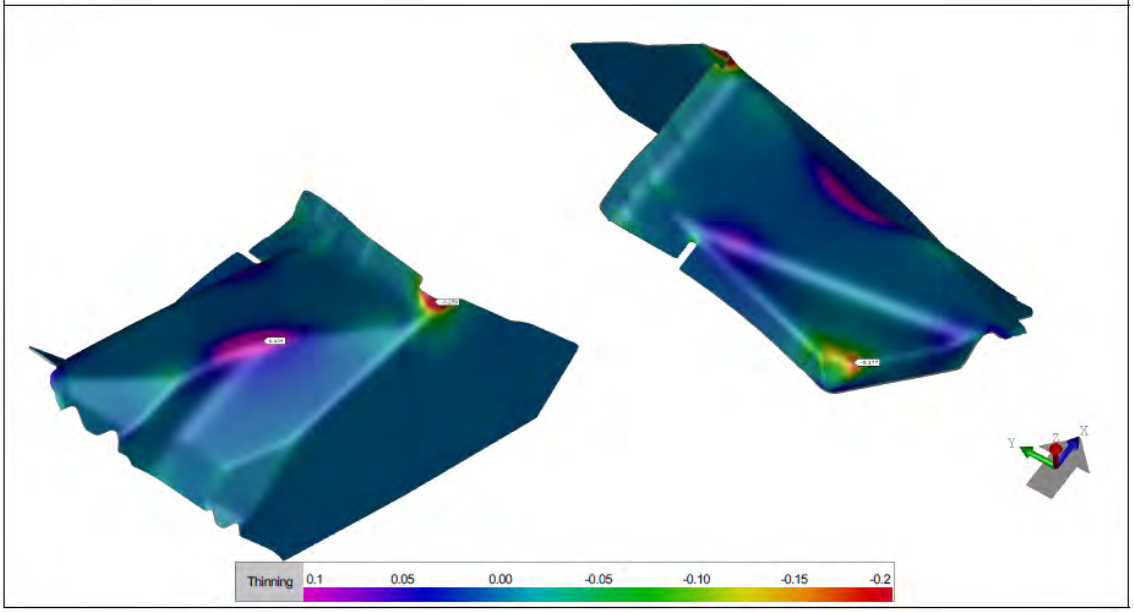

Wrinkles	T-30	

Wrinkles

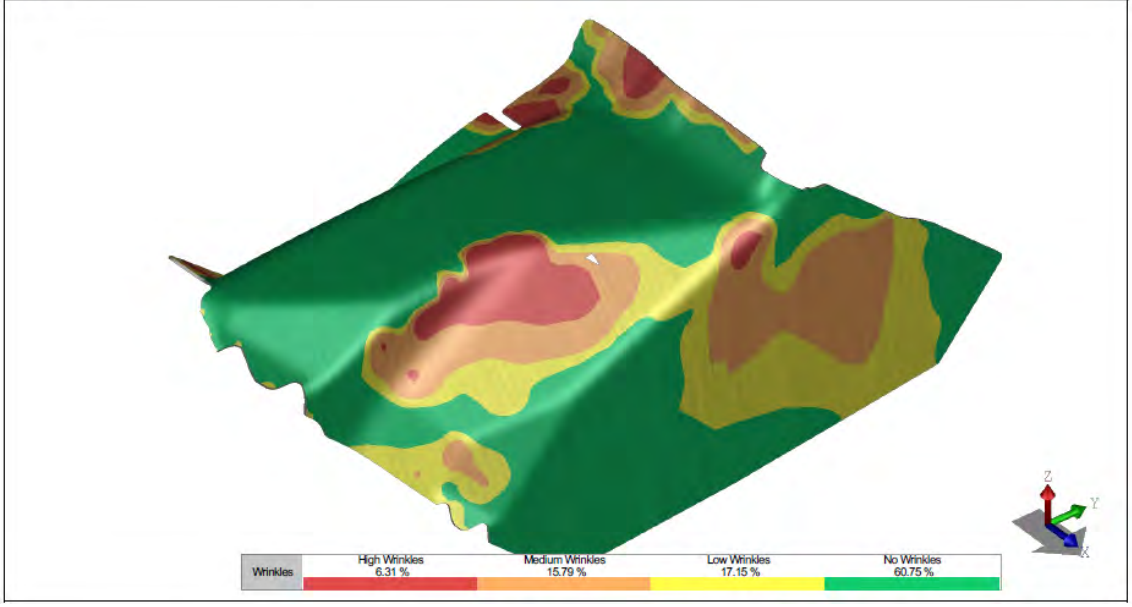

Max Failure	T-30	

Max Failure (Advanced)

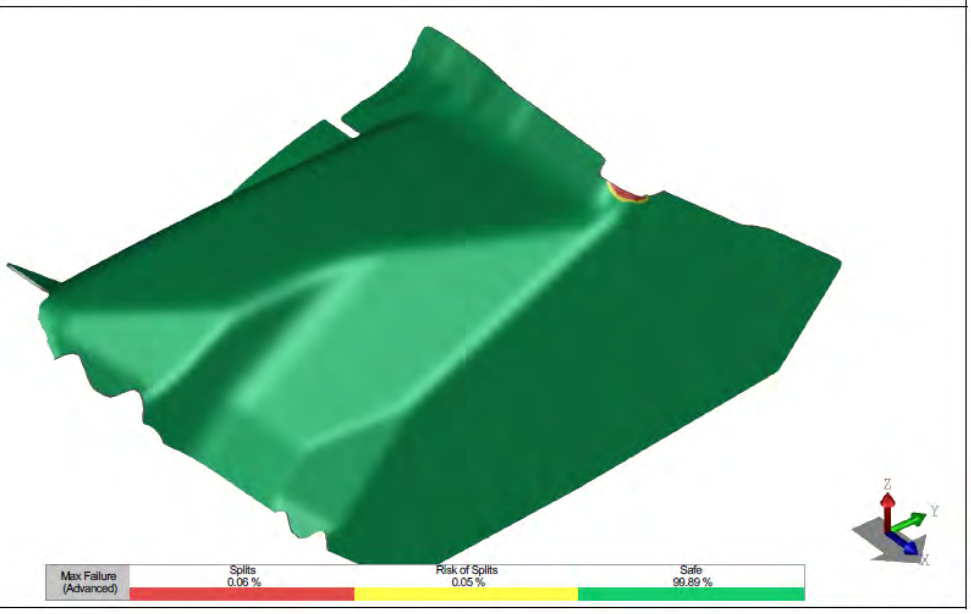

Wrinkling Behavior	D-20	

Wrinkling at -128.02 mm

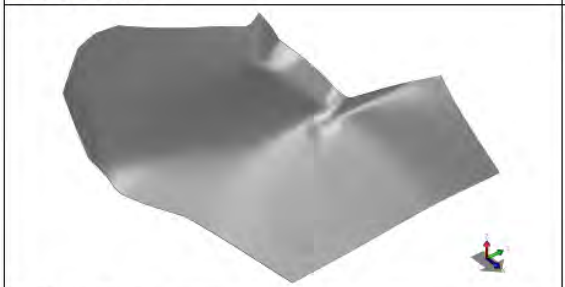

Wrinkling at -35.91 mm

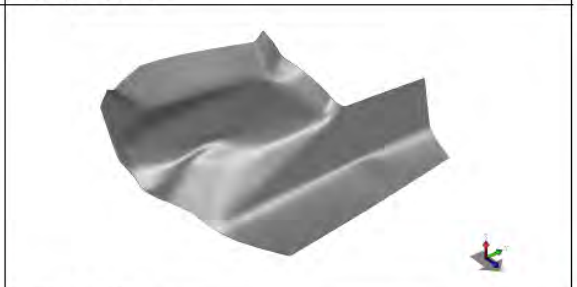

Wrinkling at -353.14 mm

Wrinkling at -31.44 mm

Mid roof bow mount LH

Overview and Summary

Part Info

Designation: 03470012 ROOF CROSSMEMBER REINF	Type:
Part No.:	Drawing No.:
Nom. / Calculated Material: Dual_Phase_980_HY	
Nom. / Calculated Sheet Thickness: 0.800 mm	

Method Info

Method Plan No.:	
Drawing No.:	Rev:

Part

Criterion		OK	n OK	Status
FLD	5.2	☑	☐	
Flanging	5.24	☑	☐	
Gravity	5.3	☑	☐	
Closing	5.4	☑	☐	
Forming	5.5	☑	☐	
Thinning	5.6	☑	☐	
Strain	5.7	☑	☐	
Wrinkles	5.8	☑	☐	
Springback	5.9	☑	☐	

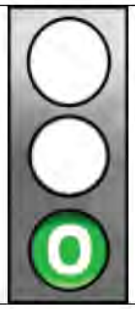

Simulation Info:

Filename:
ARRK_03470012_Mid_Roof_Bow_Mount_LH_NMS_12-8-22_it3 - EXTENSION MODS 1

AutoForm AutoForm Forming Solver R10.0.0	Memory: 140.97 MB

Process - Blank Die / Form / CAM Flange / Pierce

Input Data — Material & Blank

Calculated Material	Dual_Phase_980_HY	Calc. Sheet Thickness			0.800 mm
Yield Stress	745.58 MPa	r0	0.93	r90	1.04
n-Value	0.128	r45	0.95	E-Module	2.10E+05 MPa

Yield Curve

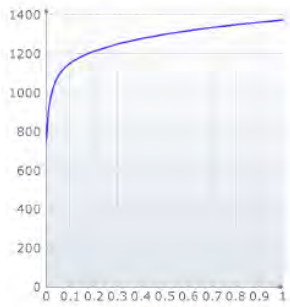

Yield Surface

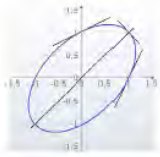

Forming Limit Curve

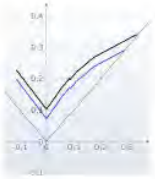

MU - Part to Blank

81.31 %

Blank Info

☐ Rectangular Blank

☑ Shaped Blank

Meshing

Roll angle	90.00 °
Initial Element Size	40.00 mm
Refinement Level	6
Max Element Angle	22.50 °

Blank size - 285.41 mm X 363.38 mm

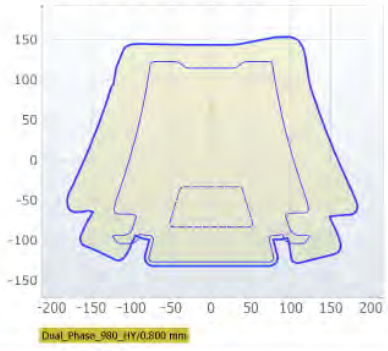

Formability	T-30	

Advanced Formability

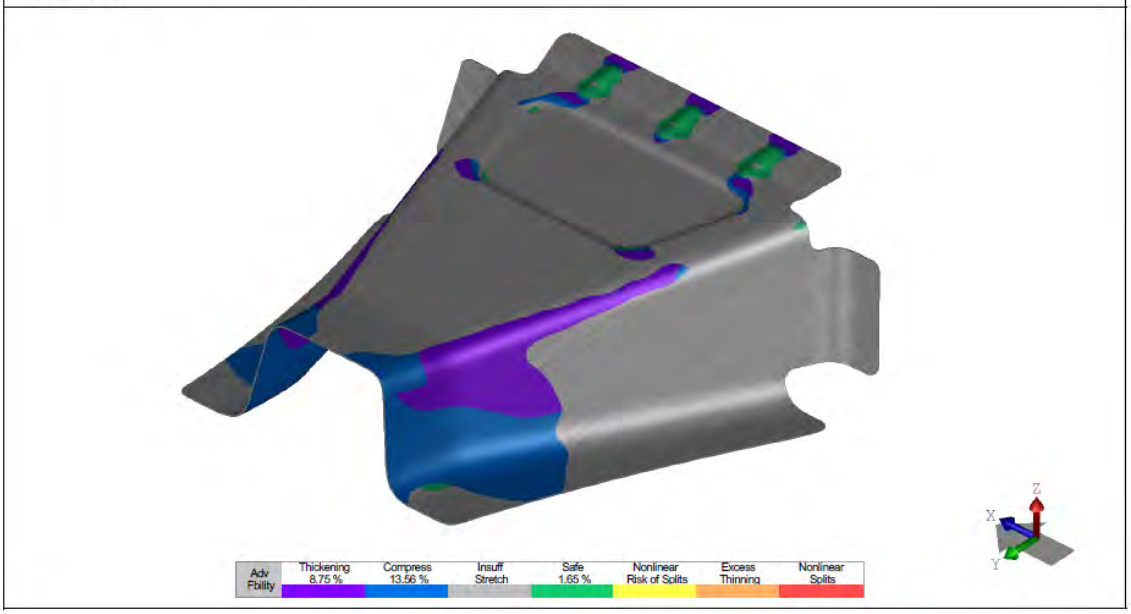

Thinning	T-30	

Thinning

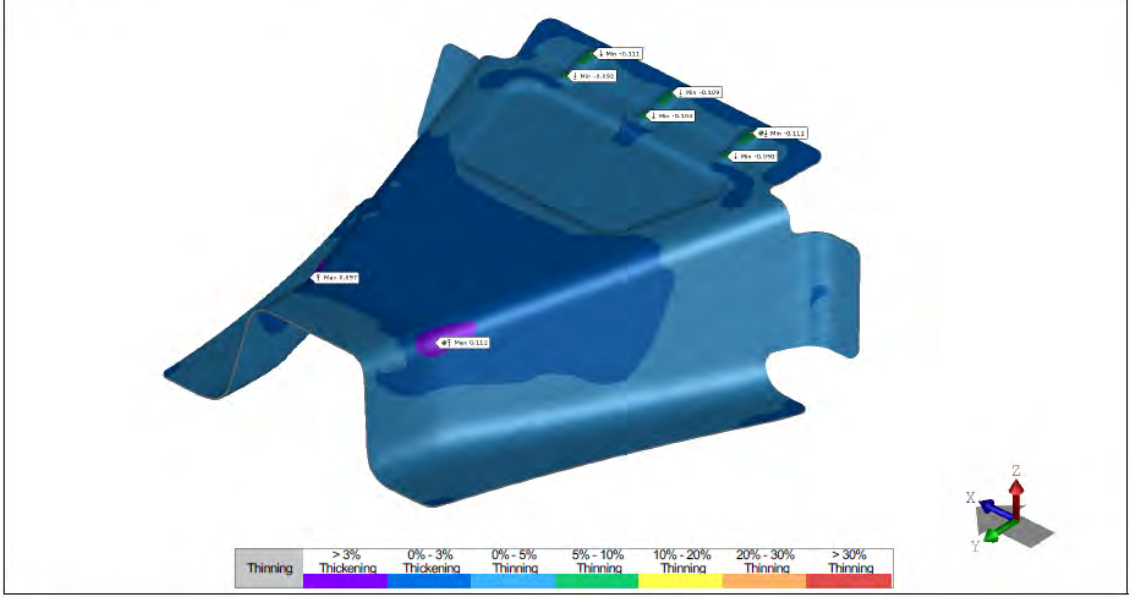

Wrinkles	T-30	

Wrinkles

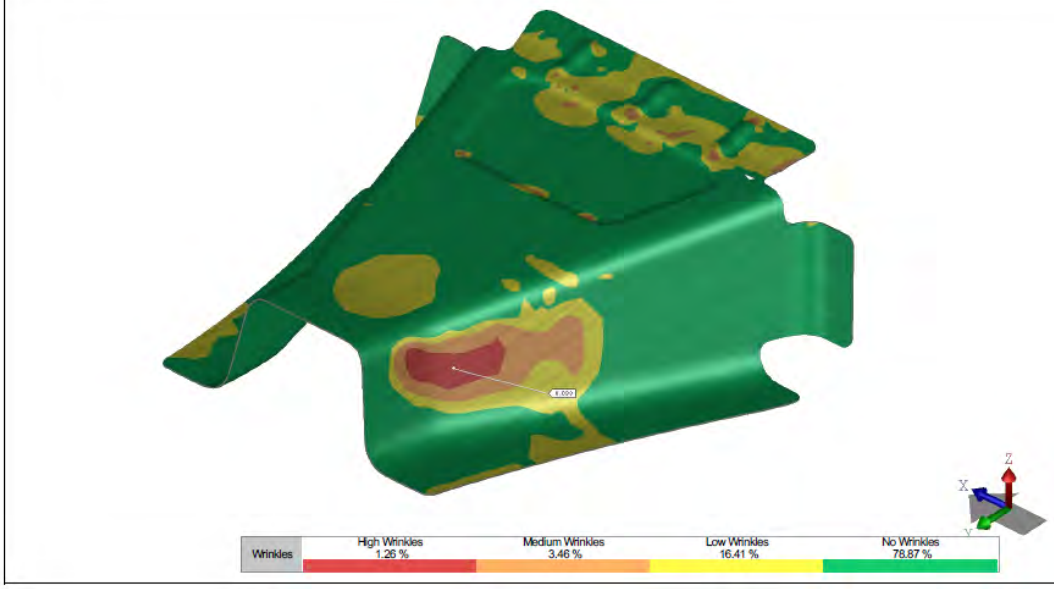

Max Failure	T-30	

Max Failure (Advanced)

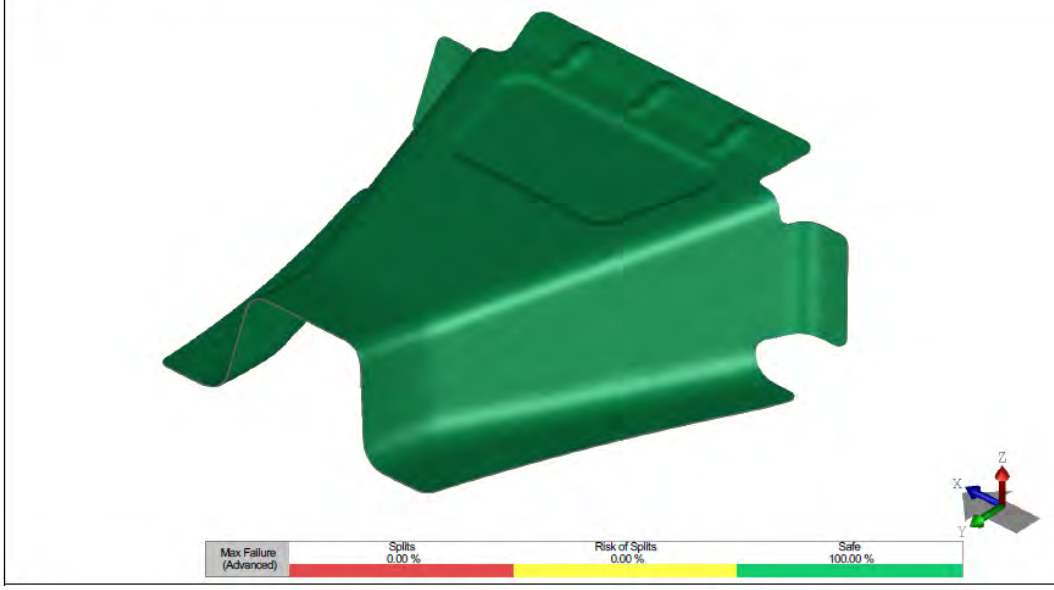

Springback	M-40	
Springback		

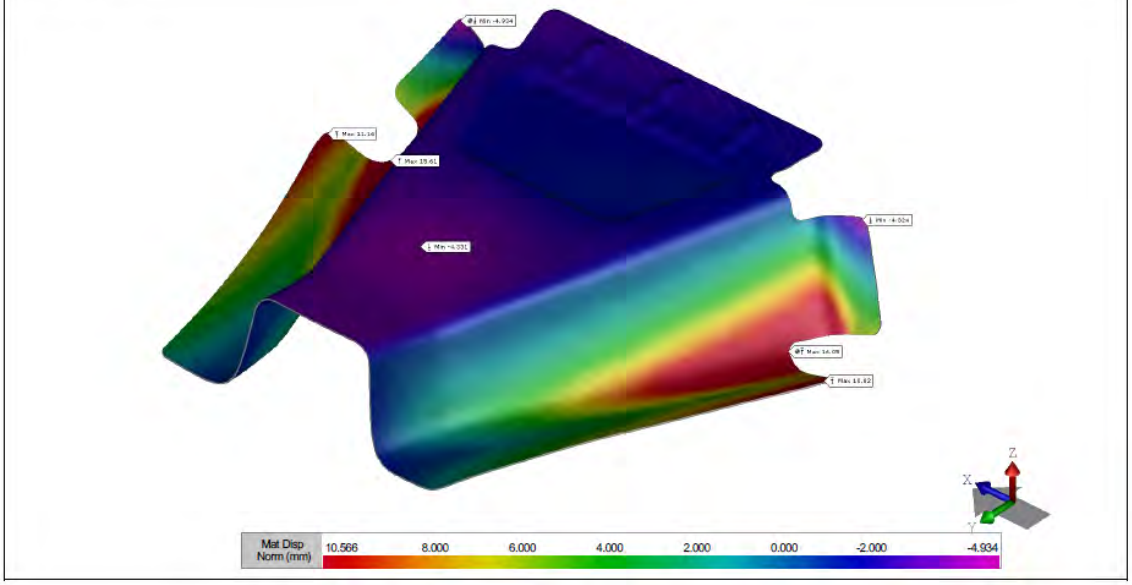

Front Header Roof Innerr Gusset Mount LH

Overview and Summary

Part Info

Designation: 03470750-A-PILLAR TOP CORNER LH	Type:
Part No.:	Drawing No.:
Nom. / Calculated Material: CR700Y980T-DH-GI_DP1000-HD-Z	
Nom. / Calculated Sheet Thickness: 1.000 mm	

Method Info

Method Plan No.:	
Drawing No.:	Rev:

Part

Criterion		OK	n OK	Status
FLD	5.2	☑	☐	
Flanging	5.24	☑	☐	
Gravity	5.3	☑	☐	
Closing	5.4	☑	☐	
Forming	5.5	☑	☐	
Thinning	5.6	☐	☑	
Strain	5.7	☑	☐	
Wrinkles	5.8	☑	☐	
Springback	5.9	☑	☐	

Simulation Info:

Filename:
ARRK_03470750_Frt_Header_Rf_Inr_Gusset_Mount_LH_NMS_15-9-22_it6 -

AutoForm — Memory: 576.48 MB
AutoForm Forming Solver R10.0.0

Process - Blank Die / Draw / Form / Form / Laser trim

Input Data	Material & Blank

Calculated Material	CR700Y980T-DH-GI_DP1000-HD-Z	Calc. Sheet Thickness				1.000 mm
Yield Stress	776.93 MPa	r0	0.86	r90	0.98	
n-Value	0.142	r45	1.26	E-Module	2.10E+05 MPa	

Yield Curve

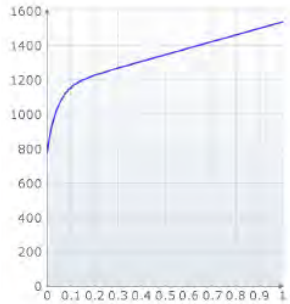

Yield Surface

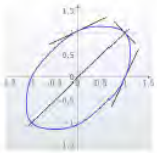

Forming Limit Curve

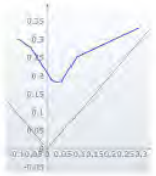

MU - Part to Blank

36.65 %

Blank Info

☐ Rectangular Blank

☑ Shaped Blank

Meshing

Roll angle	0.00 °
Initial Element Size	40.00 mm
Refinement Level	6
Max Element Angle	22.50 °

Blank size - 616.95 mm X 798.55 mm

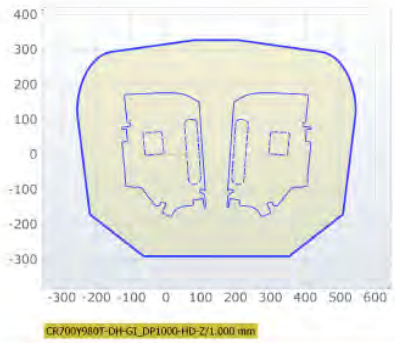

Input Data	D-20

Tool Info

Meshing Tolerance	0.05 mm		
Process Type	Single Action Draw		
Tool Geometry Refers to	Lower Side of Initial Blank		
Tools	Contact Side	Type	Gap
Die	Upper Side of Blank	Rigid	
Punch	Lower Side of Blank	Rigid	
Binder	Lower Side of Blank	Force Controlled	

Process Data

Friction Coefficient		
Constant	0.150	
Die - Blank	-	
Punch - Blank	-	
Binder - Blank	-	
Binderforce		
RAM	295.0 tf	
Binderforce/-pressure	19.7 tf	

Tool Geometry 1st opp

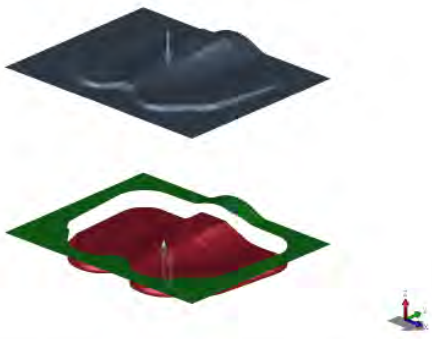

Tool Geometry 2nd opp

Tool Geometry 3rd opp

Formability	T-70	

Advanced Formability

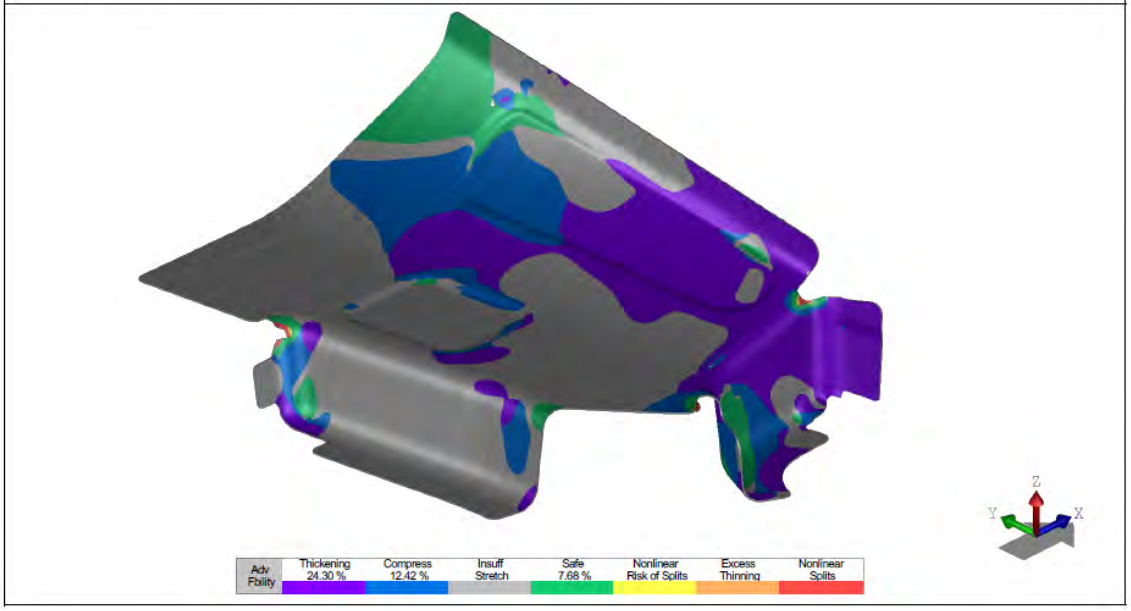

Thinning	T-70	

Thinning

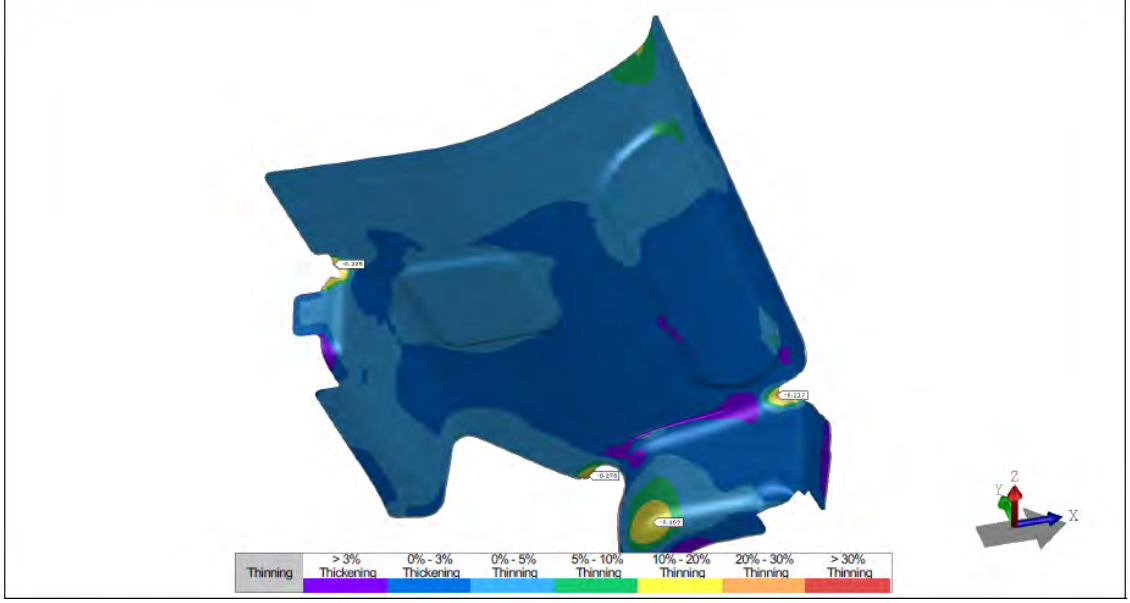

Wrinkles	T-70	

Wrinkles

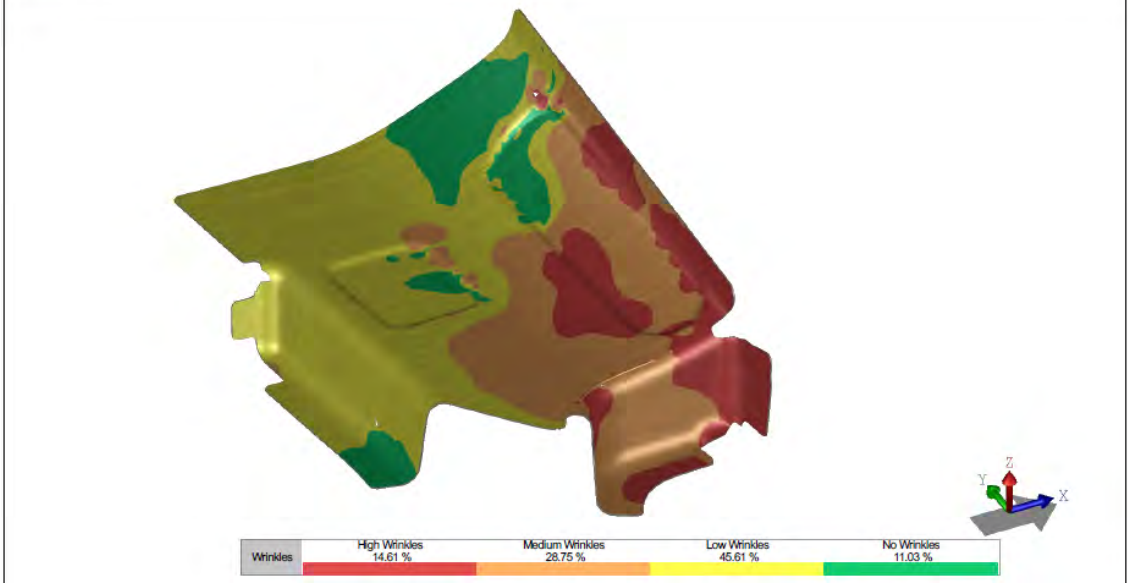

Max Failure	T-70	

Max Failure (Advanced)

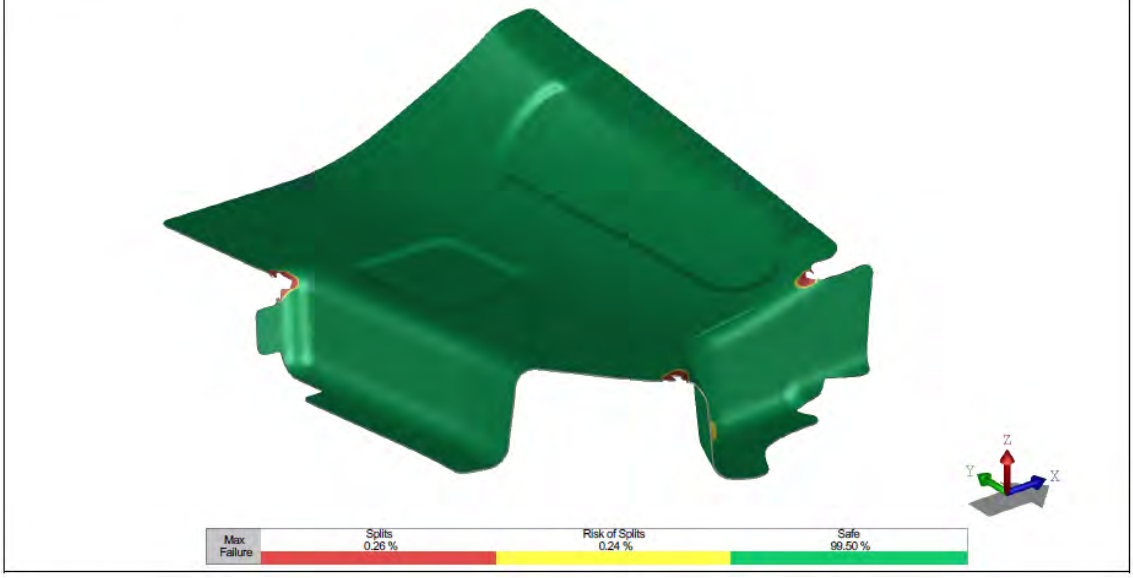

Wrinkling Behavior	D-20	

Wrinkling at -26.65 mm

Wrinkling at -1.00 mm

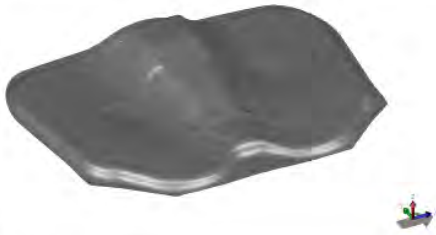

Wrinkling at -35.42 mm

Wrinkling at -0.50 mm

Springback	M-80	

Springback

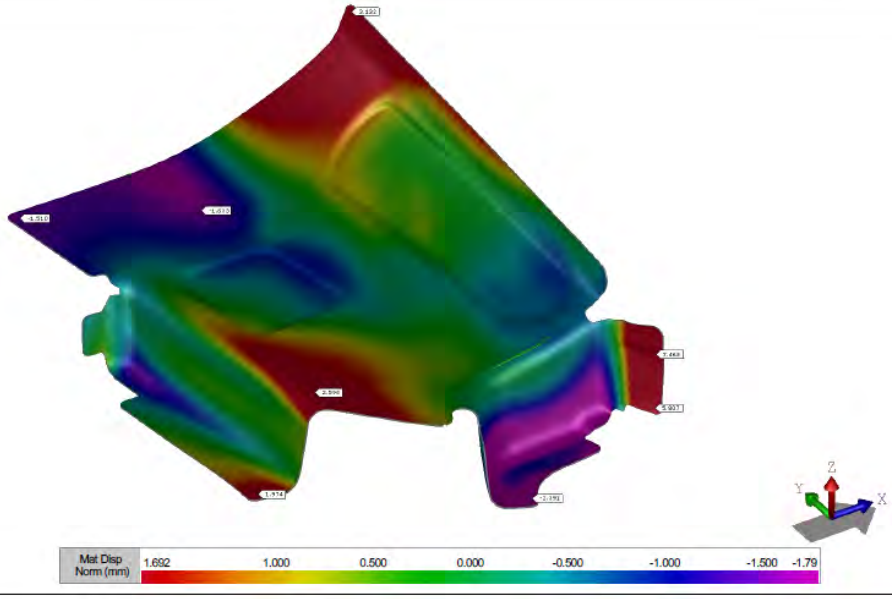

Roof Frame Inner Rear Lower

Overview and Summary

Part Info

Designation: 03484374 - ROOF FRAME ANGLE RR LE	Type: Single Action Draw
Part No.:	Drawing No.:
Nom. / Calculated Material: HD550LAD+Z_2.0-2.5	
Nom. / Calculated Sheet Thickness: 0.700 mm	

Method Info

Method Plan No.:	
Drawing No.:	Rev:

Part

Criterion		OK	n OK
FLD	5.2	☑	☐
Flanging	5.24	☐	☐
Gravity	5.3	☑	☐
Closing	5.4	☑	☐
Forming	5.5	☑	☐
Thinning	5.6	☑	☐
Strain	5.7	☑	☐
Wrinkles	5.8	☑	☐
Springback	5.9	☑	☐

Status

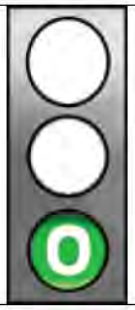

Simulation Info:

Filename: ARRK_03484374_Roof_Frame_Angle_Rr_Lwr_MW_NMS_7-9-22_it5 - EXTENSION

AutoForm AutoForm Forming Solver R10.0.0	Memory: 790.16 MB

Remarks: Part mods elimated splits. All OK for prototype.

Process - Blank Die / Draw / Trim, CAM Pierce & Pierce / Trim, CAM Pierce & Pierce

Input Data — Material & Blank

Calculated Material	HD550LAD+Z_2.0-2	Calc. Sheet Thickness			0.700 mm
Yield Stress	588.00 MPa	r0	0.61	r90	0.78
n-Value	0.117	r45	1.19	E-Module	2.10E+05 MPa

Yield Curve

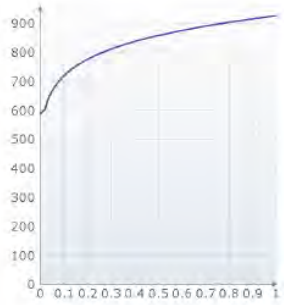

Yield Surface

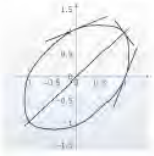

Forming Limit Curve

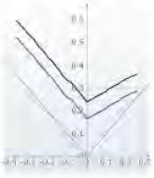

MU - Part to Blank

45.82 %

Blank Info

☐ Rectangular Blank

☑ Shaped Blank

Meshing

Roll angle	0.00 °
Initial Element Size	20.00 mm
Refinement Level	6
Max Element Angle	22.50 °

Blank Size - 1433.46 mm X 528.25 mm

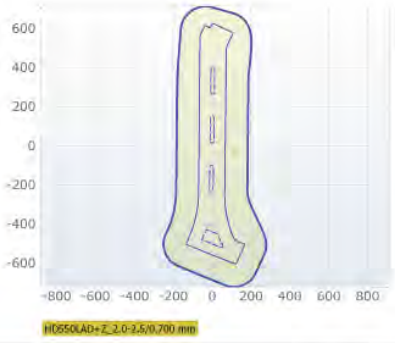

Input Data	D-20	D-20

Tool Info			
Meshing Tolerance	0.05 mm		
Process Type	Single Action Draw		
Tool Geometry Refers to	Lower Side of Initial Blank		
Tools	Contact Side	Type	Gap
Die	Upper Side of Blank	Rigid	
Punch	Lower Side of Blank	Rigid	
Binder	Lower Side of Blank	Force Controlled	

Process Data		
Friction Coefficient		
Constant	0.100	
Die - Blank	-	
Punch - Blank	-	
Binder - Blank	-	
Binderforce		
RAM	257.8 tf	
Binderforce/-pressure	106.3 tf	

Tool Geometry 1st opp

Formability	T-30

Advanced Formability

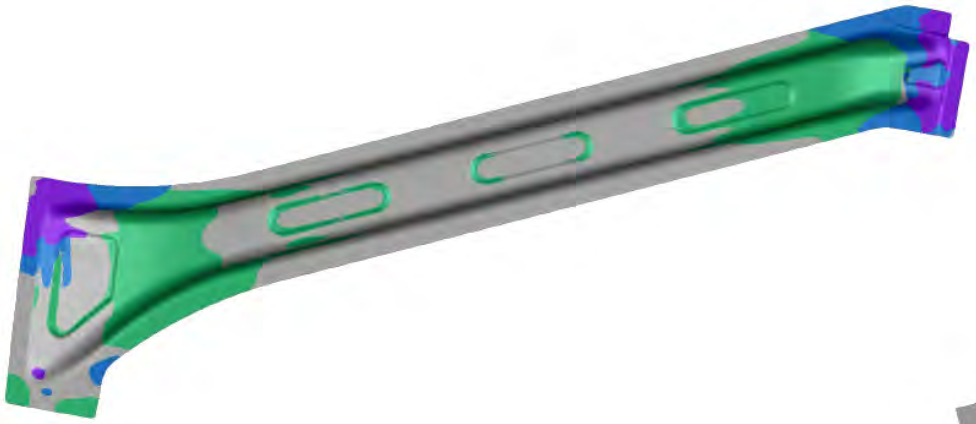

Thinning	T-30	

Thinning

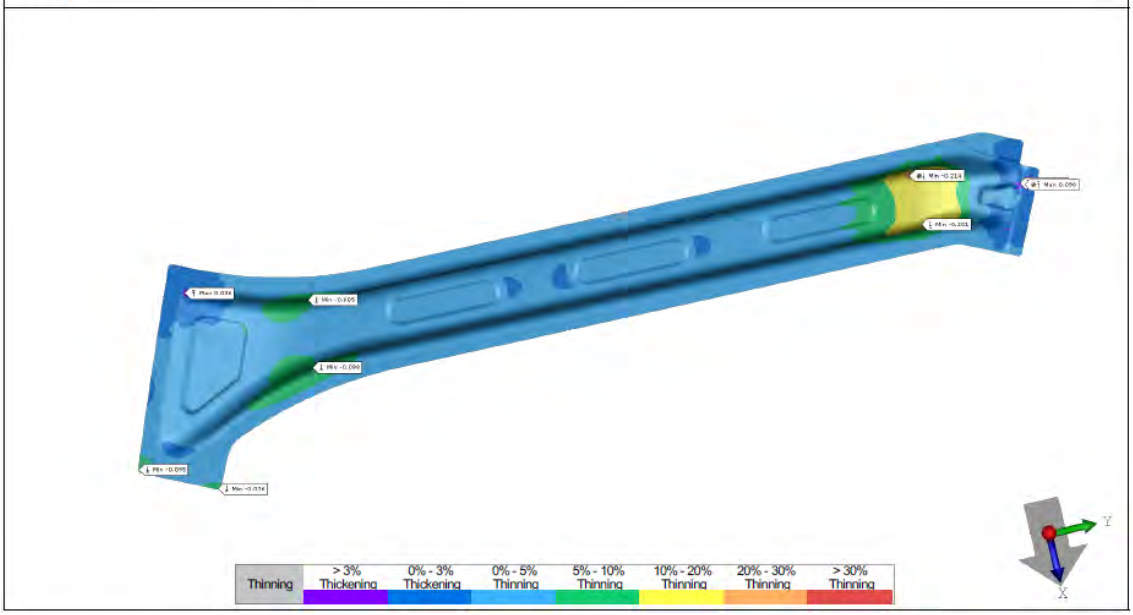

Wrinkles	T-30	

Wrinkles

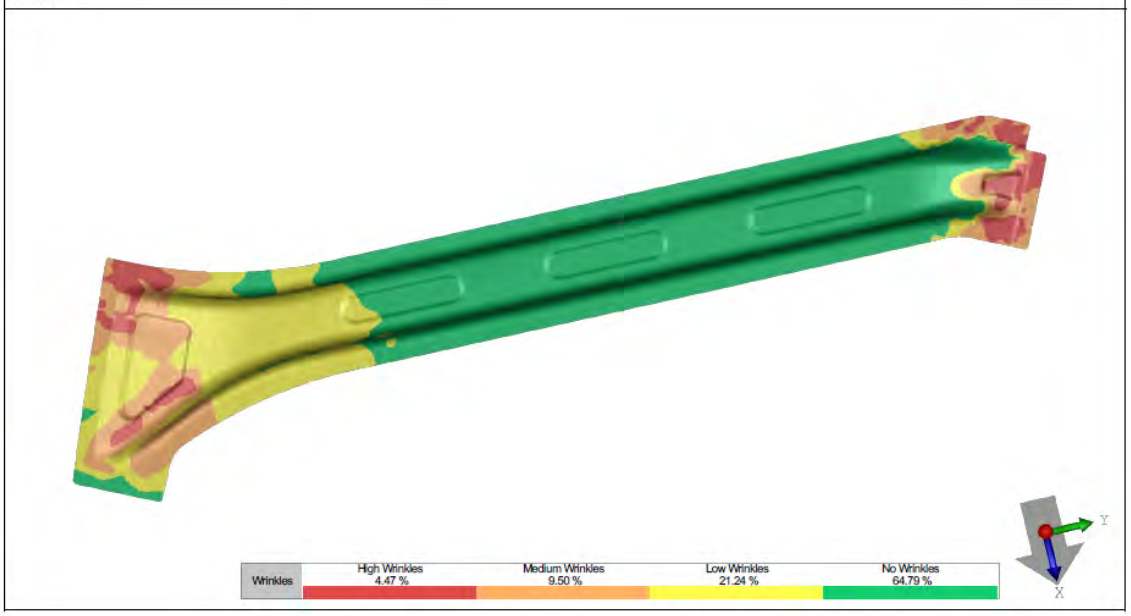

Max Failure	T-30	

Max Failure

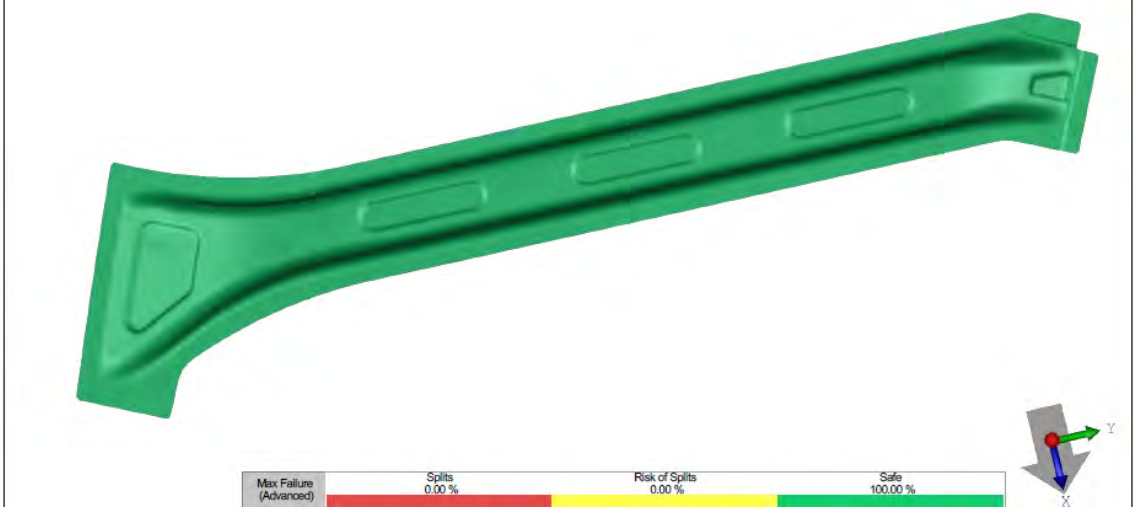

Wrinkling Behavior	D-20	

Wrinkling at -39.51 mm

Wrinkling at -19.39 mm

Wrinkling at -6.06 mm

Wrinkling at -1.50 mm

Springback	M-40

Springback

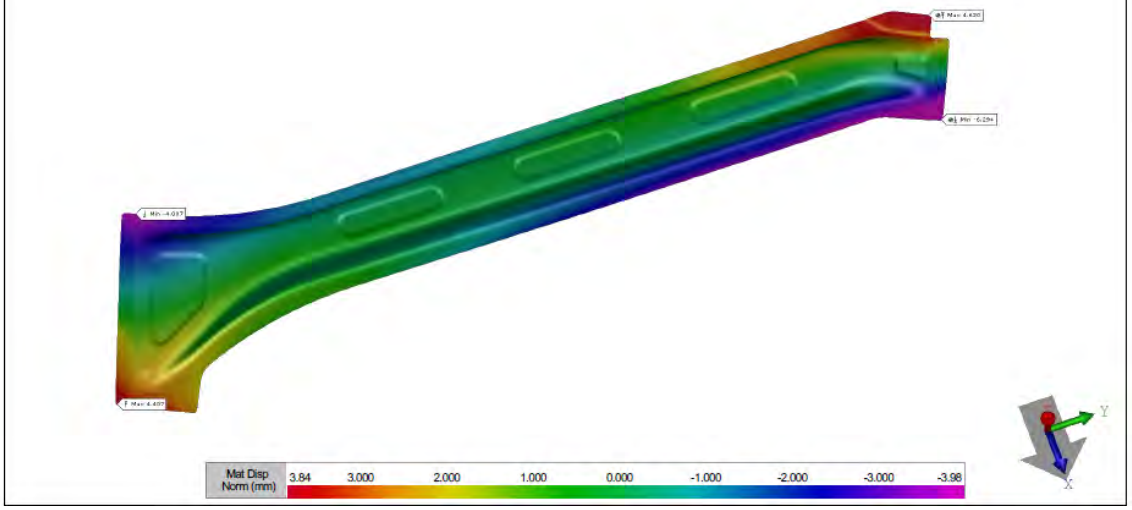

D post upper inner reinforcement

Overview and Summary

Part Info

Designation: 03491092-Body.1	Type:
Part No.:	Drawing No.:
Nom. / Calculated Material: SG-HC340-590DPD+Z-1.0	
Nom. / Calculated Sheet Thickness: 0.800 mm	

Method Info

Method Plan No.:	
Drawing No.:	Rev:

Part

Criterion		OK	n OK	Status
FLD	5.2	☑	☐	
Flanging	5.24	☑	☐	
Gravity	5.3	☑	☐	
Closing	5.4	☑	☐	
Forming	5.5	☑	☐	
Thinning	5.6	☑	☐	
Strain	5.7	☑	☐	
Wrinkles	5.8	☑	☐	
Springback	5.9	☑	☐	

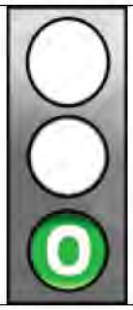

Simulation Info:

Filename:
ARRK_03491092_D_Post_Inr_Upr_LH_NMS_15-8-22_it4 - EXTENSION MODS 3 - INC

AutoForm AutoForm Forming Solver R10.0.0	Memory: 636.70 MB

Remarks: Wrinkling issues on flanges are solved by adding a slip pad on the flanging operation.

Proces - Blank Die / Draw / CAM Trim & Trim & Pierce / Trim / Flange

Input Data	Material & Blank

Calculated Material	SG-HC340-590DPD+Z-1	Calc. Sheet Thickness			0.800 mm
Yield Stress	380.00 MPa	r0	0.85	r90	1.05
n-Value	0.165	r45	0.95	E-Module	2.10E+05 MPa

Yield Curve

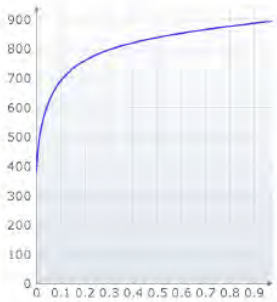

Yield Surface

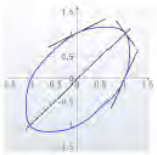

Forming Limit Curve

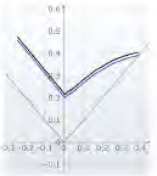

MU - Part to Blank

41.39 %

Blank Info

- ☐ Rectangular Blank
- ☑ Shaped Blank

Meshing

Roll angle	0.00 °
Initial Element Size	40.00 mm
Refinement Level	6
Max Element Angle	22.50 °

Blank Size - 860.64 mm X 484.93 mm

Input Data	D-20

Tool Info

Meshing Tolerance	0.05 mm		
Process Type	Single Action Draw		
Tool Geometry Refers to	Lower Side of Initial Blank		
Tools	Contact Side	Type	Gap
Die	Upper Side of Blank	Rigid	
Punch	Lower Side of Blank	Rigid	
Binder	Lower Side of Blank	Force Controlled	

Process Data

Friction Coefficient		
Constant	0.100	
Die - Blank	-	
Punch - Blank	-	
Binder - Blank	-	
Binderforce		
RAM	184.5 tf	
Binderforce/-pressure	66.6 tf	

Tool Geometry 1st opp

Formability	F-40	

Advanced Formability

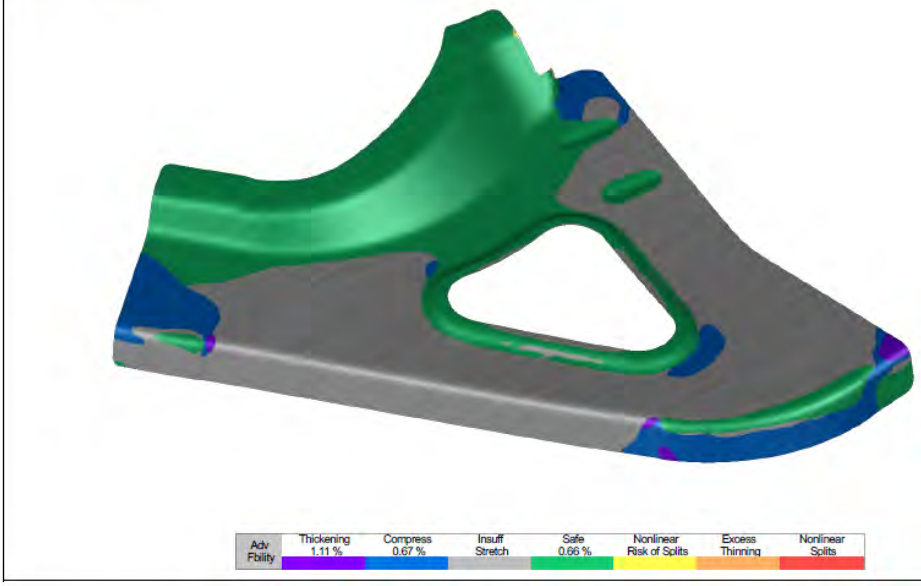

Wrinkles	F-40	

Wrinkles

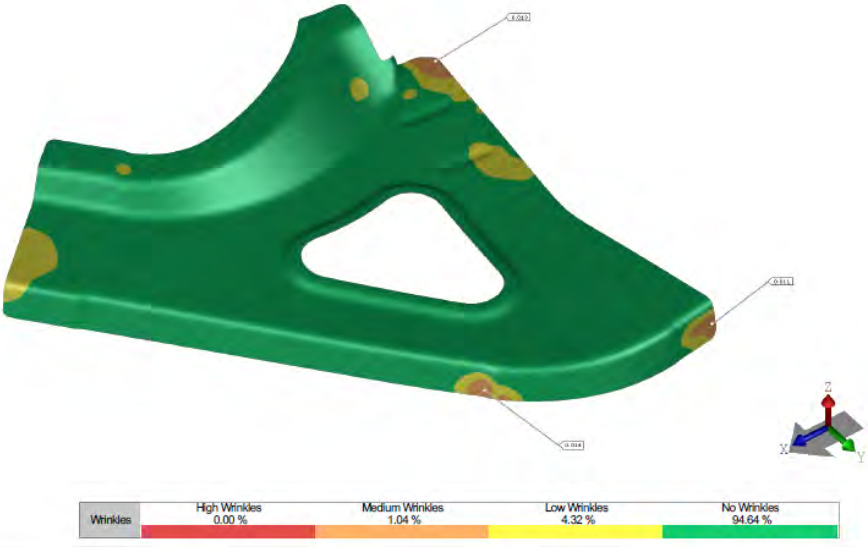

Max Failure	F-40	

Max Failure (Advanced)

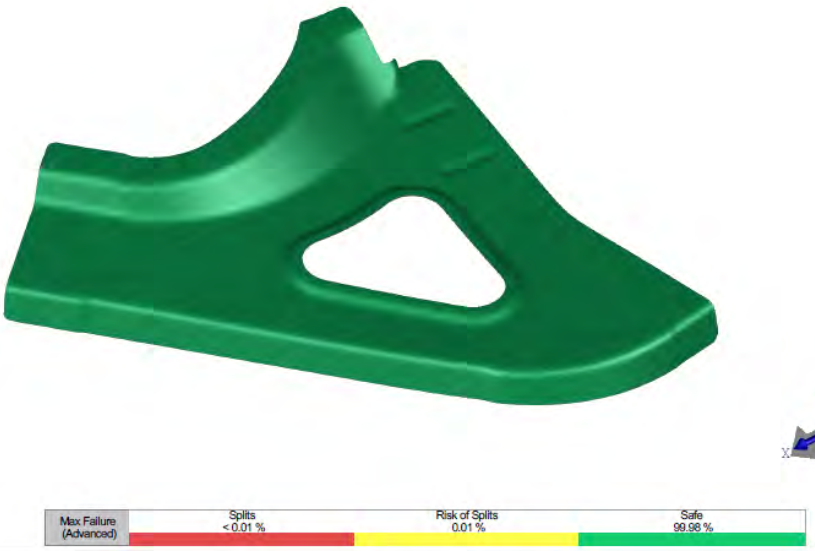

Wrinkling Behavior	D-20	

Wrinkling at -11.48 mm

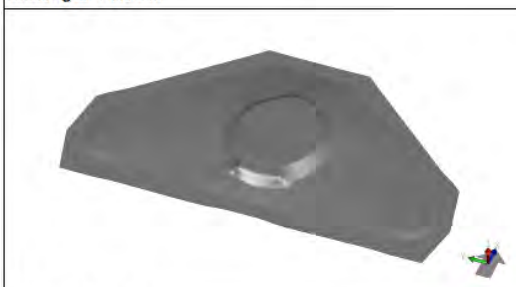

Wrinkling at -3.31 mm

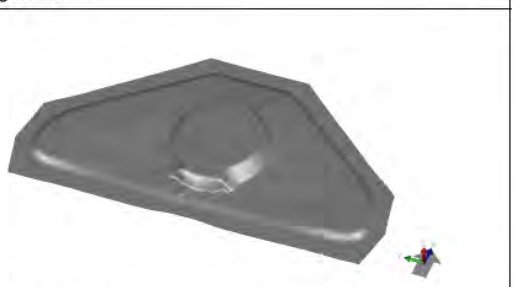

Wrinkling at -0.50 mm

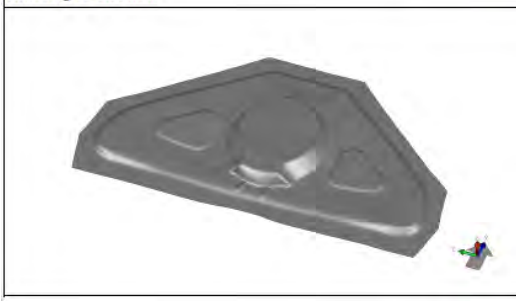

Wrinkling at -8.38 mm

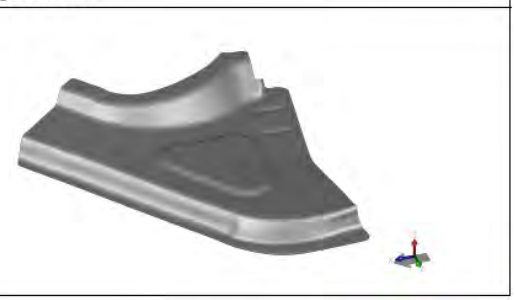

Springback	T-50

Springback

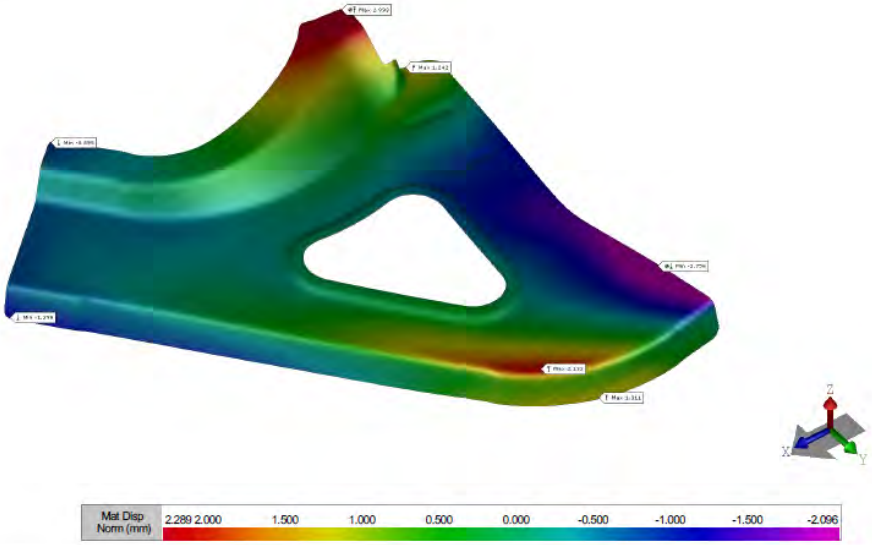

Front rail angled outer

Overview and Summary

Part Info

Designation: 03506010 FRONT RAIL ANGLED OUTER LH	Type:
Part No.:	Drawing No.:
Nom. / Calculated Material: Dual_Phase_980_HY	
Nom. / Calculated Sheet Thickness: 2.000 mm	

Method Info

Method Plan No.:	
Drawing No.:	Rev:

Part

Criterion		OK	n OK	Status
FLD	5.2	☑	☐	
Flanging	5.24	☑	☐	
Gravity	5.3	☑	☐	
Closing	5.4	☑	☐	
Forming	5.5	☑	☐	
Thinning	5.6	☑	☐	
Strain	5.7	☑	☐	
Wrinkles	5.8	☑	☐	
Springback	5.9	☑	☐	

Simulation Info:

Filename:
ARRK_03506010_Frt_Rail_Angled_Outer_NMS_15-8-22_it4 - EXTENSION MODS 2 -

AutoForm AutoForm Forming Solver R10.0.0	Memory: 262.89 MB

Process - Blank Die / Crash & Flange / Form

Input Data	Material & Blank

Calculated Material	Dual_Phase_980_HY	Calc. Sheet Thickness			2.000 mm	
Yield Stress	745.58 MPa	r0	0.93	r90	1.04	
n-Value	0.128	r45	0.95	E-Module	2.10E+05 MPa	

Yield Curve

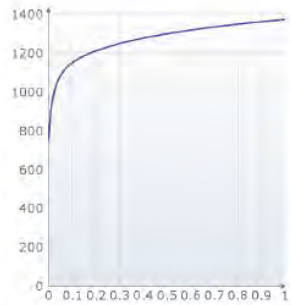

MU - Part to Blank

100%

Yield Surface

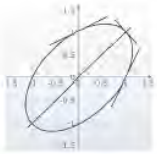

Forming Limit Curve

Blank Info	
☐ Rectangular Blank	
☑ Shaped Blank	
Meshing	
Roll angle	0.00 °
Initial Element Size	20.00 mm
Refinement Level	6
Max Element Angle	22.50 °

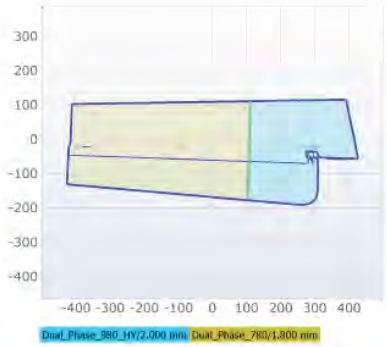

Formability	T-30

Advanced Formability

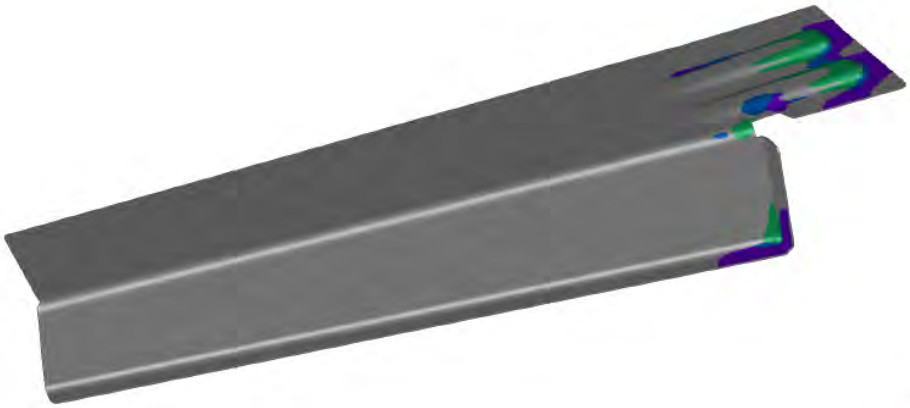

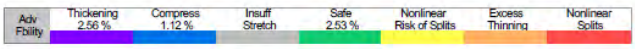

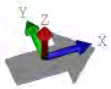

Thinning	T-30	

Thinning

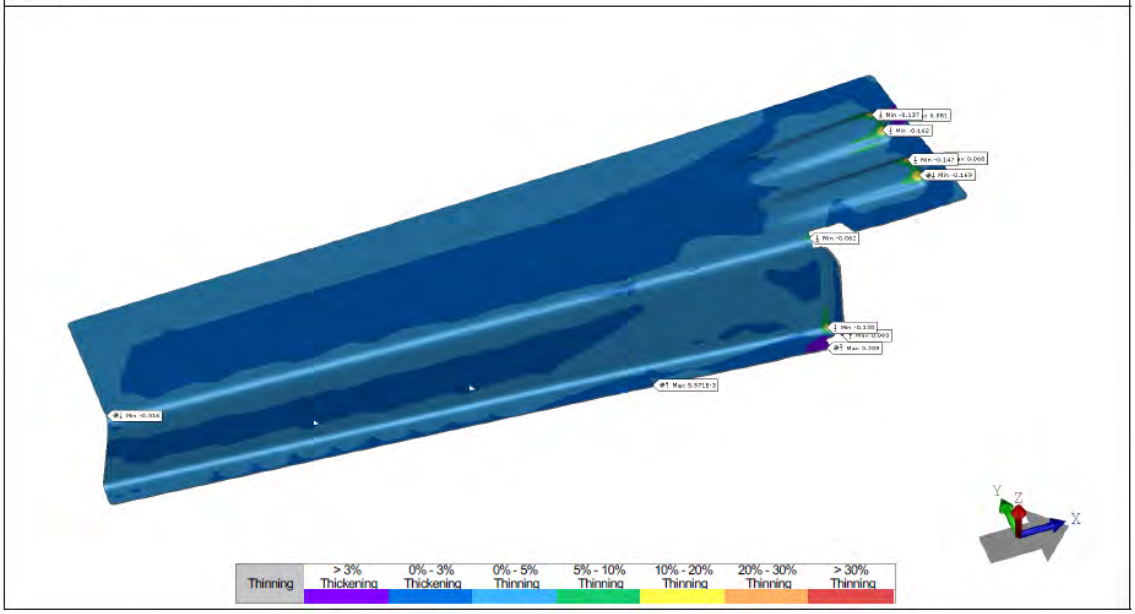

Wrinkles	T-30	

Wrinkles

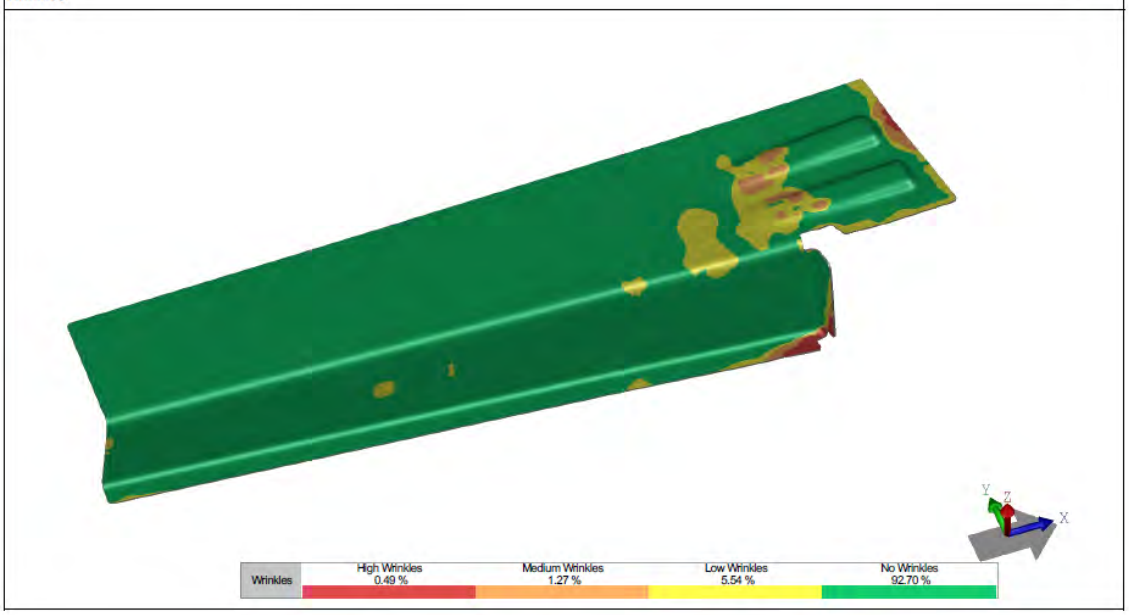

Max Failure	T-30	

Max Failure (Advanced)

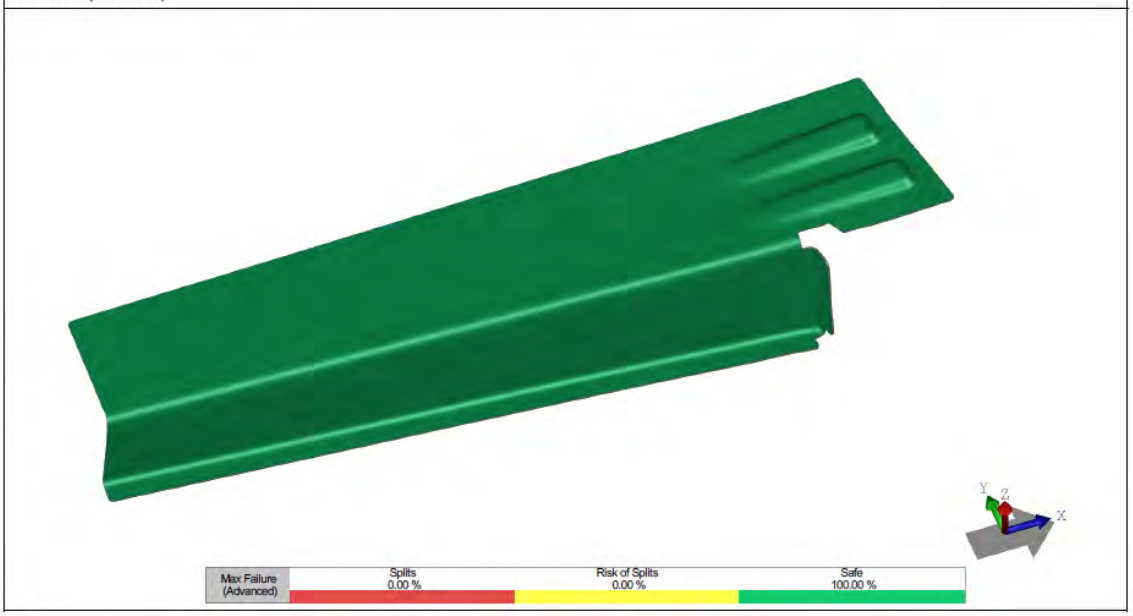

Springback	M-40	

Springback

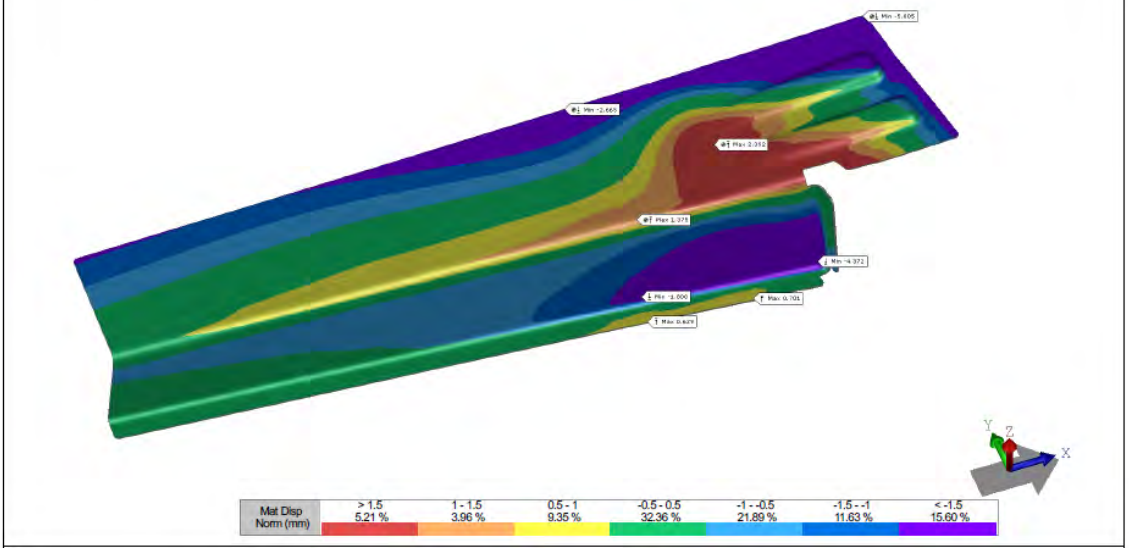

Front longitudinal rail inner

Overview and Summary

Part Info

Designation: 03506011 FRONT RAIL ANGLED INNER LH	Type:
Part No.:	Drawing No.:
Nom. / Calculated Material: Dual_Phase_980_HY	
Nom. / Calculated Sheet Thickness: 2.000 mm	

Method Info

Method Plan No.:	
Drawing No.:	Rev:

Part

Criterion		OK	n OK	Status
FLD	5.2	☑	☐	
Flanging	5.24	☑	☐	
Gravity	5.3	☑	☐	
Closing	5.4	☑	☐	
Forming	5.5	☑	☐	
Thinning	5.6	☑	☐	
Strain	5.7	☑	☐	
Wrinkles	5.8	☑	☐	
Springback	5.9	☑	☐	

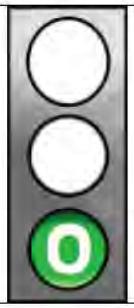

Simulation Info:

Filename: ARRK_03506011_Longit_Mid_Rail_Inr_Frt_NMS_14-8-22_it3 - EXTENSION MODS 1 -

AutoForm AutoForm Forming Solver R10.0.0	Memory: 227.53 MB

Process - Blank Die / Crash & Flange / Form / CAM form & CAM Pierce

Input Data — Material & Blank

Calculated Material	Dual_Phase_980_HY	Calc. Sheet Thickness			2.000 mm
Yield Stress	745.58 MPa	r0	0.93	r90	1.04
n-Value	0.128	r45	0.95	E-Module	2.10E+05 MPa

Yield Curve

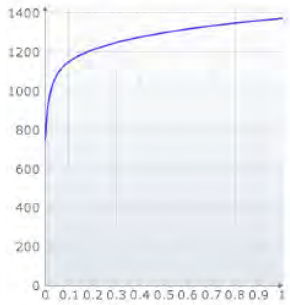

Yield Surface

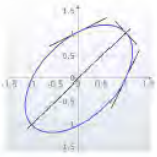

Forming Limit Curve

MU - Part to Blank

100%

Blank Info

☐ Rectangular Blank

☑ Shaped Blank

Meshing

Roll angle	0.00 °
Initial Element Size	20.00 mm
Refinement Level	6
Max Element Angle	22.50 °

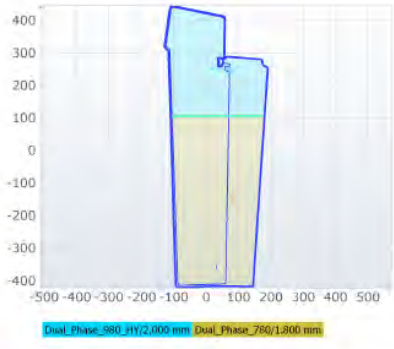

Formability	F-40

Advanced Formability

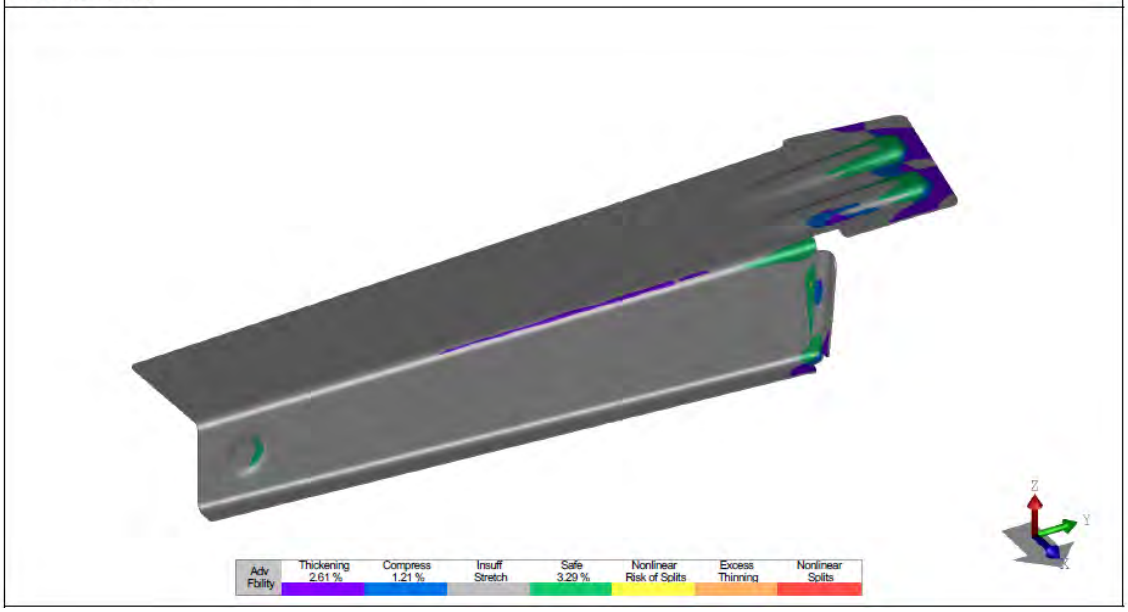

Thinning	F-40

Thinning

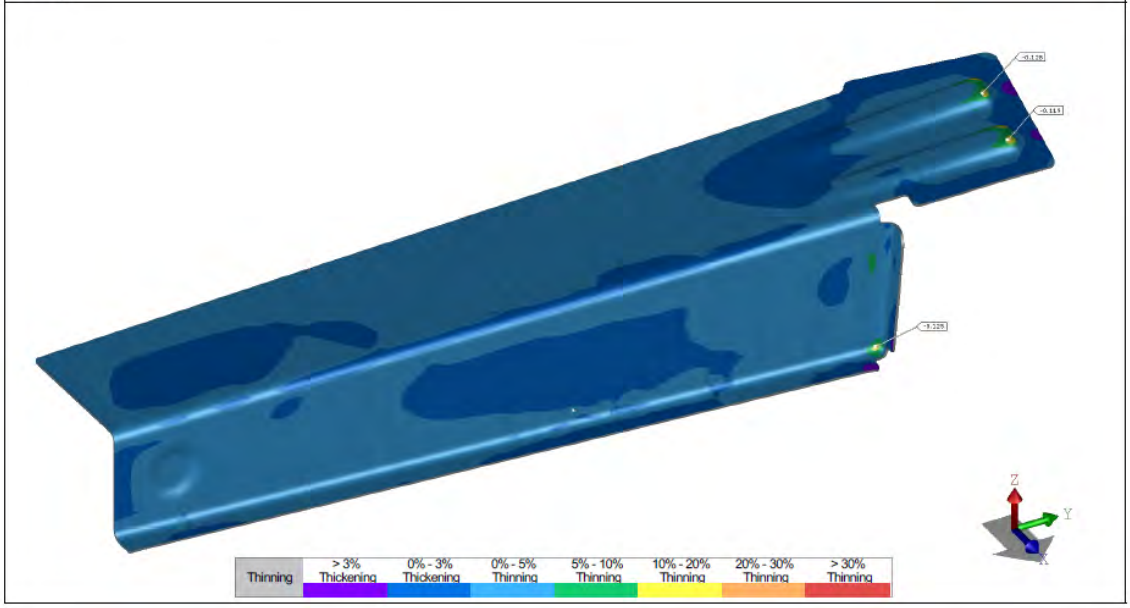

Wrinkles	F-40	

Wrinkles

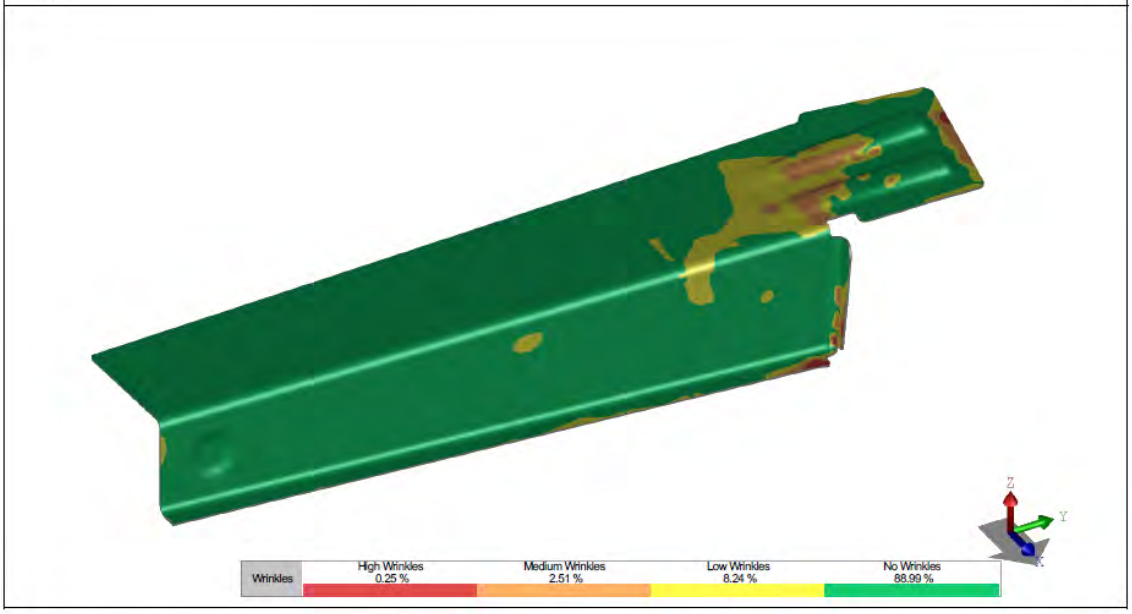

Max Failure	F-40	

Max Failure (Advanced)

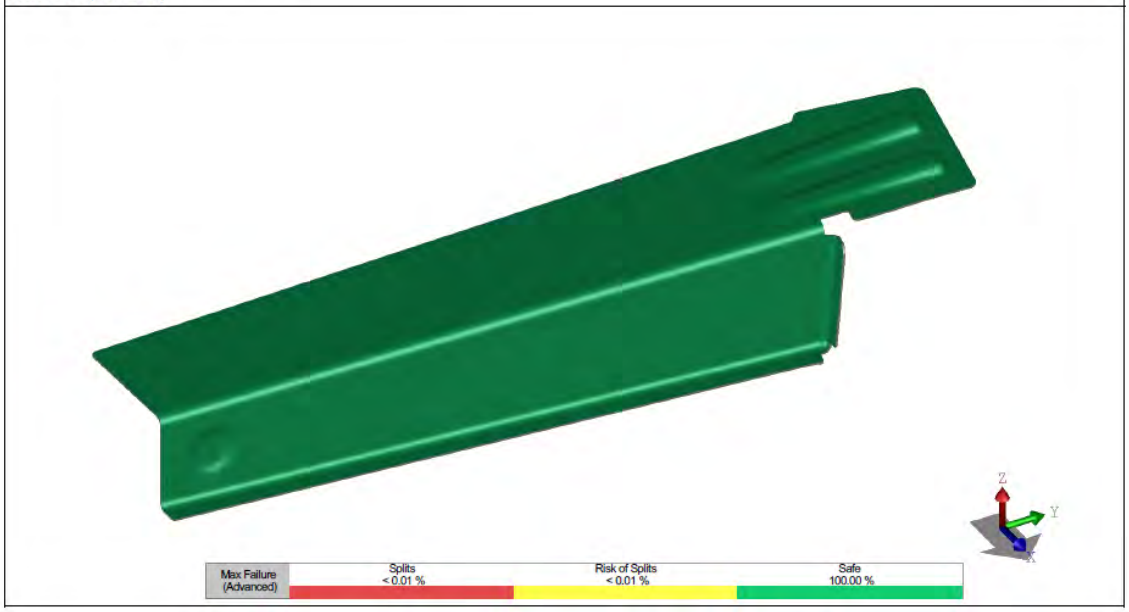

Springback	T-30

Springback

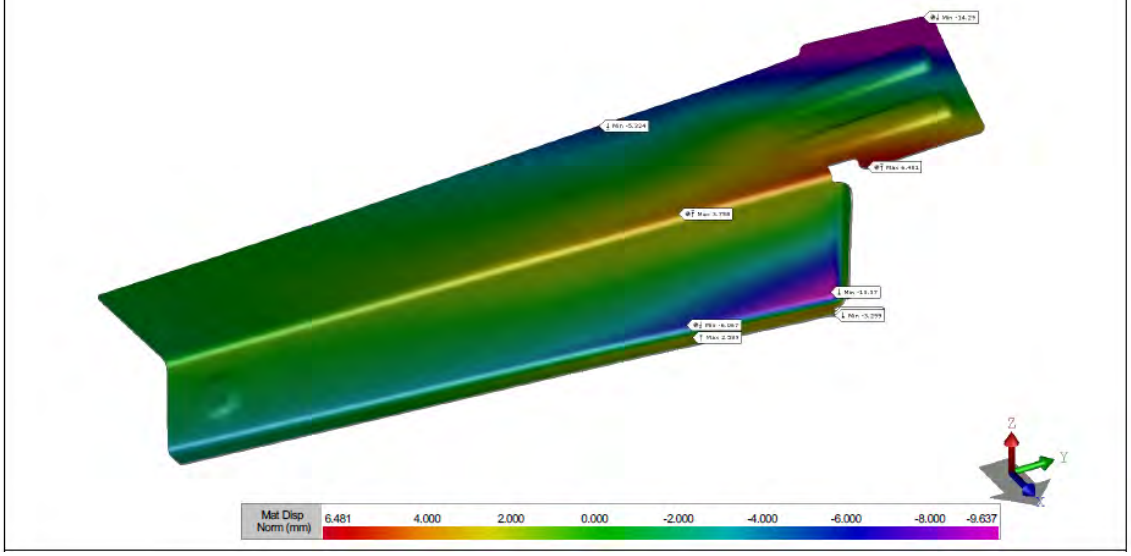

Glance beam inner

Overview and Summary

Part Info

Designation: 03585862-Body.1 | Type: Form Trim Pierce

Part No.: | Drawing No.:

Nom. / Calculated Material: 22MnB5

Nom. / Calculated Sheet Thickness: 1.000 mm

Method Info

Method Plan No.:

Drawing No.: | Rev:

Part

Criterion		OK	n OK	Status
FLD	5.2	☑	☐	
Flanging	5.24	☐	☐	
Gravity	5.3	☑	☐	
Closing	5.4	☑	☐	
Forming	5.5	☑	☐	
Thinning	5.6	☑	☐	
Martensite	5.7	☑	☐	
Temperature	5.8	☑	☐	
Hardness		☑	☐	

Simulation Info:

Filename:
ARRK_03585862_Glance_Beam_Inr_LH_NMS_17-8-22_it9 - EXTENSION MODS 4 -

AutoForm | Memory: 674.20 MB
AutoForm Forming Solver Thermo R10.0.0

Remarks: Wrinkles are now all under control by modifying the process but there is still slightly high thinning on the two end tabs (23%). I believe this is OK for Green status for prototype stage.

Process - Blank Die / Heating / Draw / Quenching / Laser Trim

Input Data	Material & Blank

Calculated Material	22MnB5	Calc. Sheet Thickness			1.000 mm	
Yield Stress		r0	1.00	r90	1.00	
n-Value		r45	1.00	E-Module		

Yield Curve

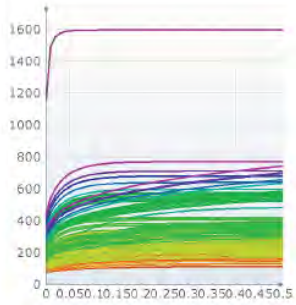

Yield Surface

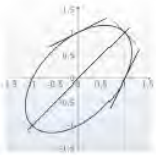

MU - Part to Blank

73.85 %

RAM Tonnage - 153.0 tf

Blank Info

- ☐ Rectangular Blank
- ☑ Shaped Blank

Meshing

Roll angle	0.00 °
Initial Element Size	40.00 mm
Refinement Level	7
Max Element Angle	30.00 °

Blank Size - 1158.31 mm X 1497.64 mm

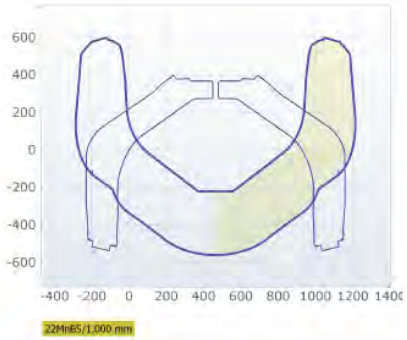

Formability	T-40

Advanced Formability

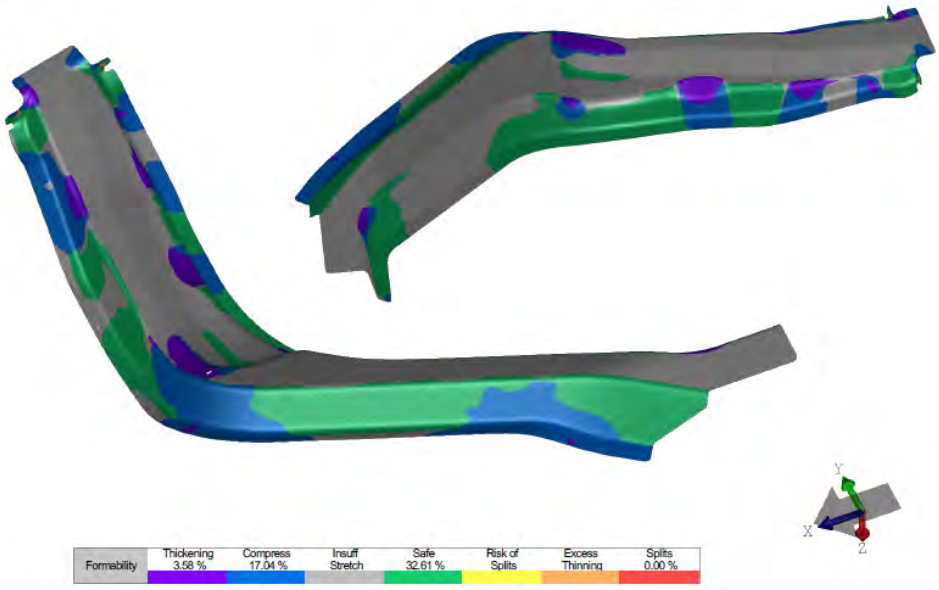

Thinning	T-40	

Thinning

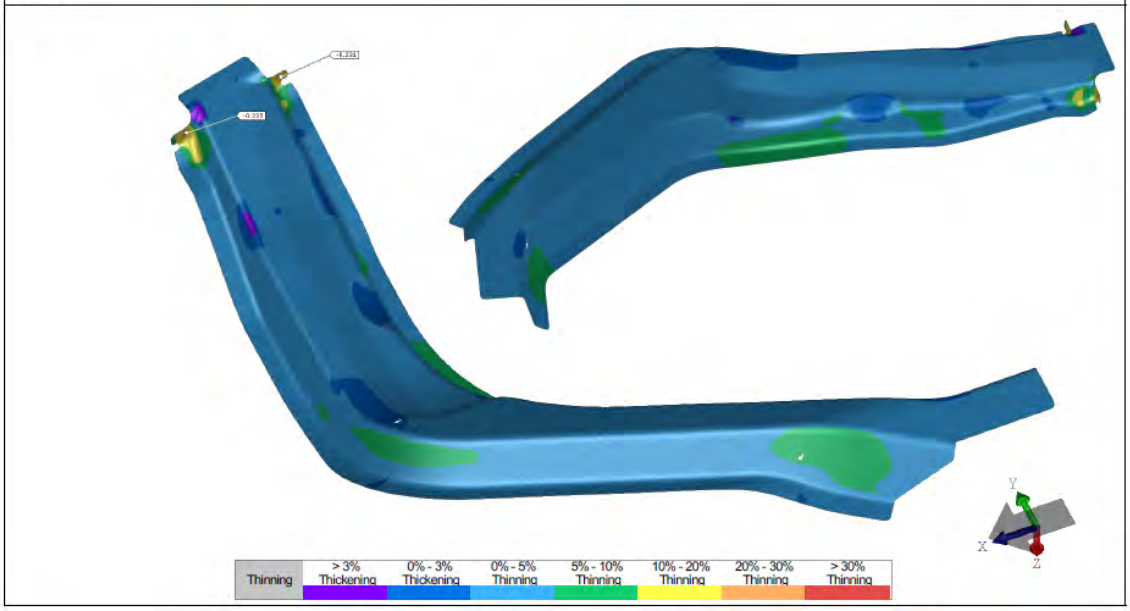

Wrinkling	T-40	

Thickness

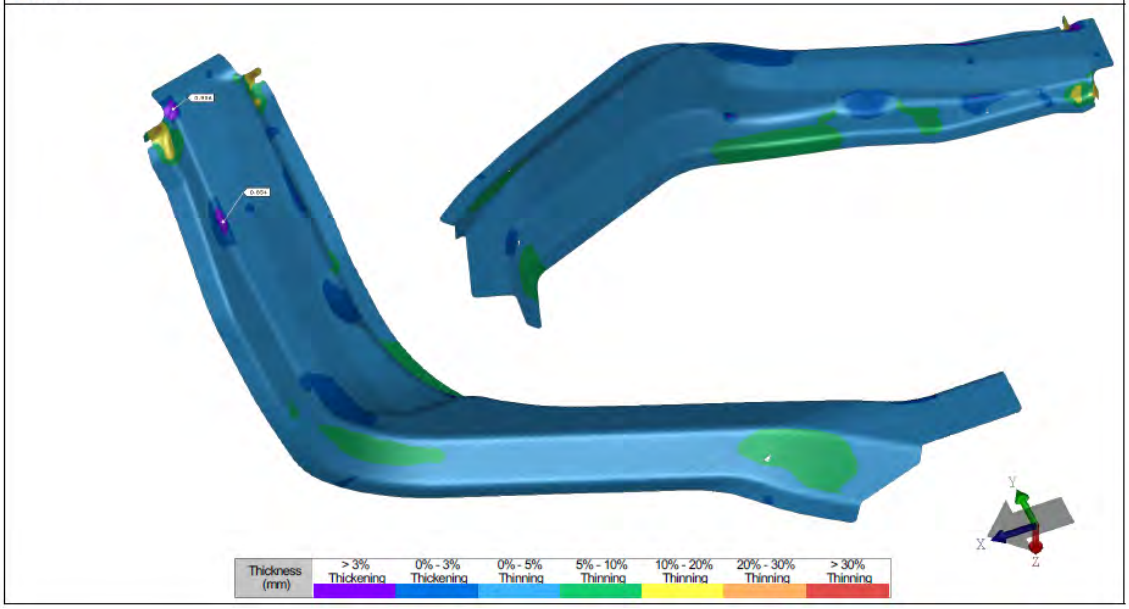

/

Wrinkling Behavior	H-10
Wrinkling at	Wrinkling at
	
Wrinkling at	Wrinkling at
	

Glance beam outer

Overview and Summary

Part Info

Designation: 03585867-Body.2	Type: Single Action Draw
Part No.:	Drawing No.:
Nom. / Calculated Material: Usibor1500_200mm_700C	
Nom. / Calculated Sheet Thickness: 1.500 mm	

Method Info

Method Plan No.:	
Drawing No.:	Rev:

Part

Criterion		OK	n OK	Status
FLD	5.2	☑	☐	
Flanging	5.24	☐	☐	
Gravity	5.3	☑	☐	
Closing	5.4	☑	☐	
Forming	5.5	☑	☐	
Thinning	5.6	☑	☐	
Martensite	5.7	☑	☐	
Temperature	5.8	☑	☐	
Hardness		☑	☐	

Simulation Info:

Filename:
ARRK_03585867_Glance_Beam_Otr_LH_NMS_8-9-22_it12 - EXTENSION MODS 8 -

AutoForm AutoForm Forming Solver Thermo R10.0.0	Memory: 492.67 MB

Process - Blank Die / Heating / Draw / Quenching / Laser Trim

Input Data	Material & Blank

Calculated Material	Usibor1500_200mm	Calc. Sheet Thickness			1.500 mm
Yield Stress		r0	1.00	r90	1.00
n-Value		r45	1.00	E-Module	

Blank Info

- ☐ Rectangular Blank
- ☑ Shaped Blank

Meshing

Roll angle	0.00 °
Initial Element Size	20.00 mm
Refinement Level	6
Max Element Angle	30.00 °

Yield Curve

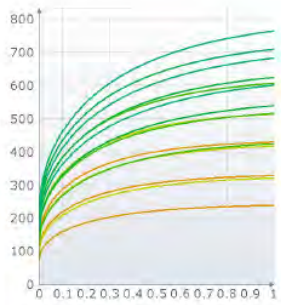

Yield Surface

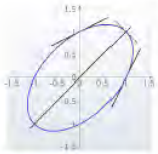

Blank Size - 1310.15 mm X 719.70 mm

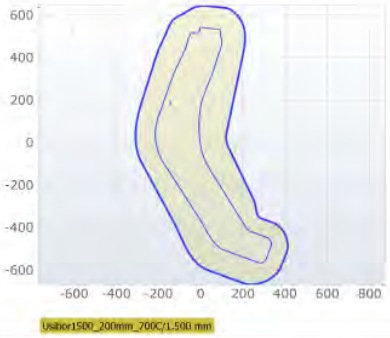

MU - Part to Blank

52.12 %

RAM Tonnage - 300.0 tf

Input Data	D-20	D-20

Tool Info

Meshing Tolerance	0.05 mm		
Process Type	Single Action Draw		
Tool Geometry Refers to	Lower Side of Initial Blank		
Tools	Contact Side	Type	Gap
Die	Upper Side of Blank	Rigid	
Pad	Upper Side of Blank	Force Controlled	
Punch	Lower Side of Blank	Rigid	

Process Data

Friction Coefficient		
Constant	0.400	
Die - Blank	-	
Punch - Blank	-	
Binder - Blank	-	
Binderforce		
RAM	300.0 tf	
Binderforce/-pressure	3.8 tf	

Tool Geometry 1st opp

Formability	T-30	

Advanced Formability

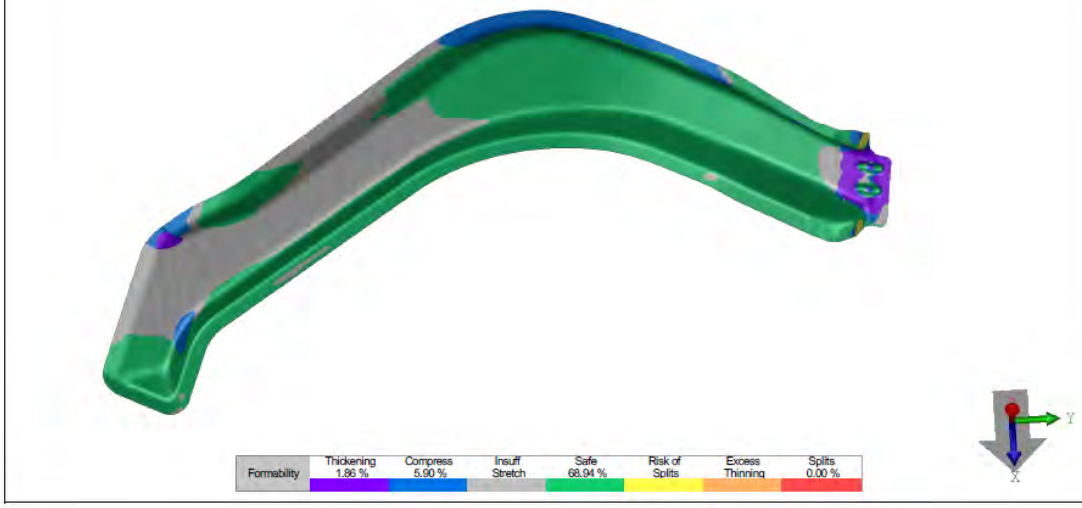

Wrinkling Behavior	K-40	

Wrinkling at -79.60 mm

Wrinkling at -37.56 mm

Wrinkling at -9.98 mm

Wrinkling at -0.50 mm

Front Vertical Dash Brace

Overview and Summary

Part Info

Designation: 03593060-Body.1 | Type:

Part No.: | Drawing No.:

Nom. / Calculated Material: CR820Y1180T_RA_CE+

Nom. / Calculated Sheet Thickness: 1.600 mm

Method Info

Method Plan No.:

Drawing No.: | Rev:

Part

Criterion		OK	n OK	Status
FLD	5.2	☑	☐	
Flanging	5.24	☐	☐	
Gravity	5.3	☑	☐	
Closing	5.4	☑	☐	
Forming	5.5	☑	☐	
Thinning	5.6	☑	☐	
Strain	5.7	☑	☐	
Wrinkles	5.8	☑	☐	
Springback	5.9	☑	☐	

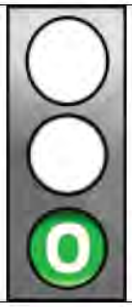

Simulation Info:

Filename:
ARRK_03593060_Vertical_Dash_Brace_Upr_LH_NMS_8-9-22_it8 - EXTENSION MODS

AutoForm | Memory: 213.46 MB
AutoForm Forming Solver R10.0.0

Process - Blank / Form / Trim

Input Data — Material & Blank

Calculated Material	CR820Y1180T_RA_(	Calc. Sheet Thickness			1.600 mm
Yield Stress	869.85 MPa	r0	0.56	r90	0.61
n-Value	0.119	r45	0.77	E-Module	2.10E+05 MPa

Yield Curve

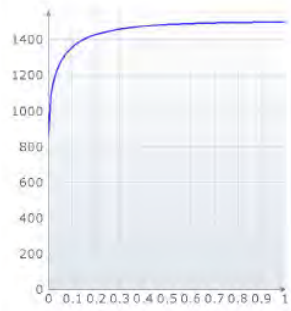

Yield Surface

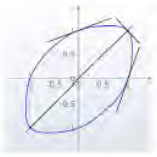

Forming Limit Curve

MU - Part to Blank

72.90 %

Blank Info

☐ Rectangular Blank

☑ Shaped Blank

Meshing

Roll angle	0.00 °
Initial Element Size	20.00 mm
Refinement Level	6
Max Element Angle	22.50 °

Blank size 521.93 X 581.17

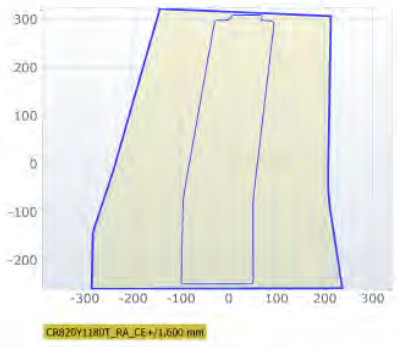

Input Data	F-10

Tool Info			
Meshing Tolerance	0.05 mm		
Process Type	Form Trim Pierce		
Tool Geometry Refers to	Upper Side of Initial Blank		
Tools	Contact Side	Type	Gap
Pad	Upper Side of Blank	Rigid	
Post	Lower Side of Blank	Force Controlled	
Steel	Lower Side of Blank	Rigid	

Process Data		
Friction Coefficient		
Constant	0.150	
Die - Blank	-	
Punch - Blank	-	
Binder - Blank	-	
Binderforce		
RAM	98.1 tf	
Binderforce/-pressure	31.3 tf	

Tool Geometry 1st opp

Formability	T-20

Advanced Formability

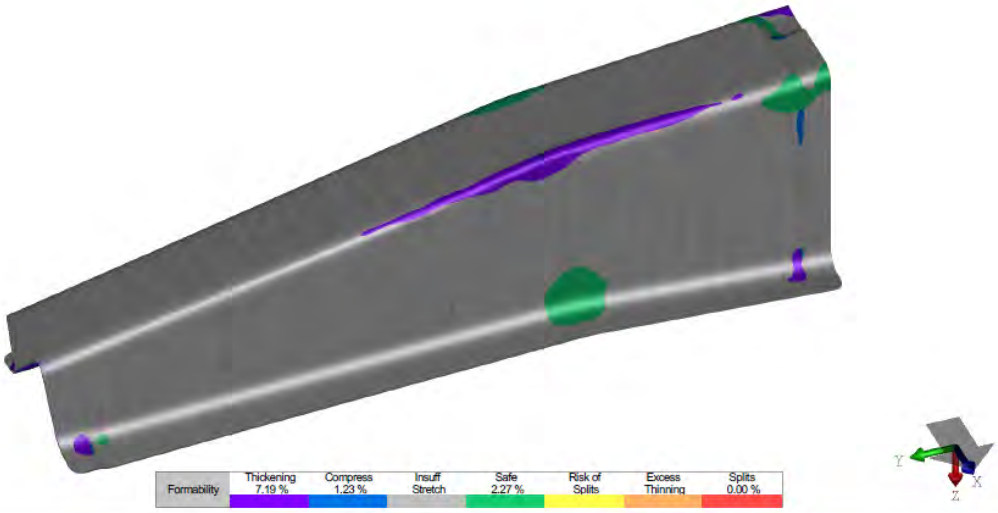

Formability	F-10

FLD

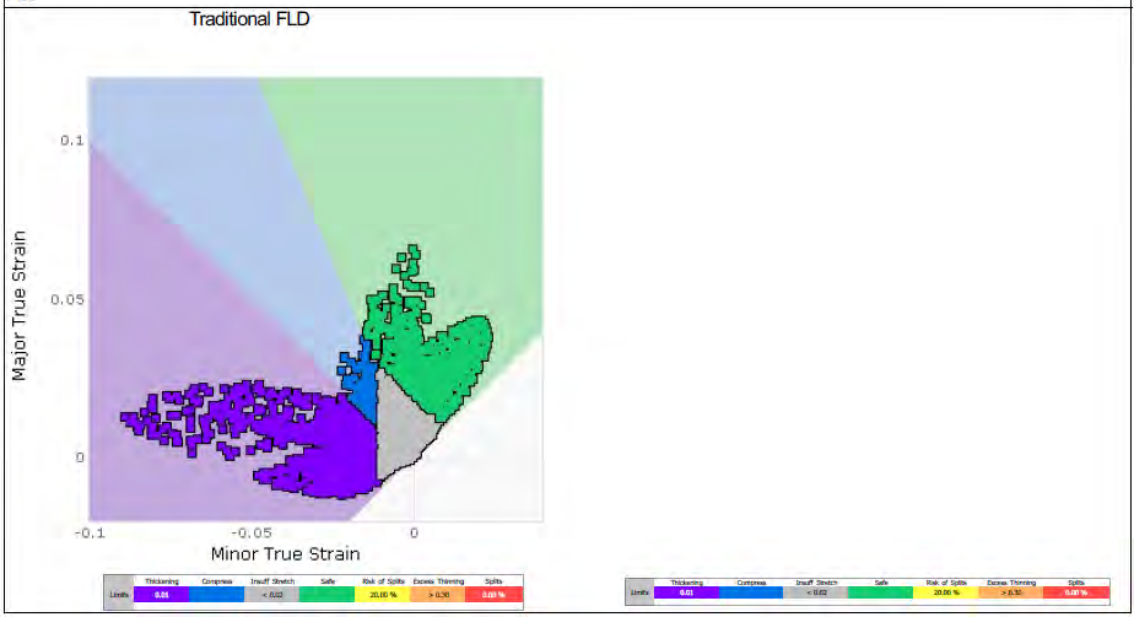

Thinning	T-20

Thinning

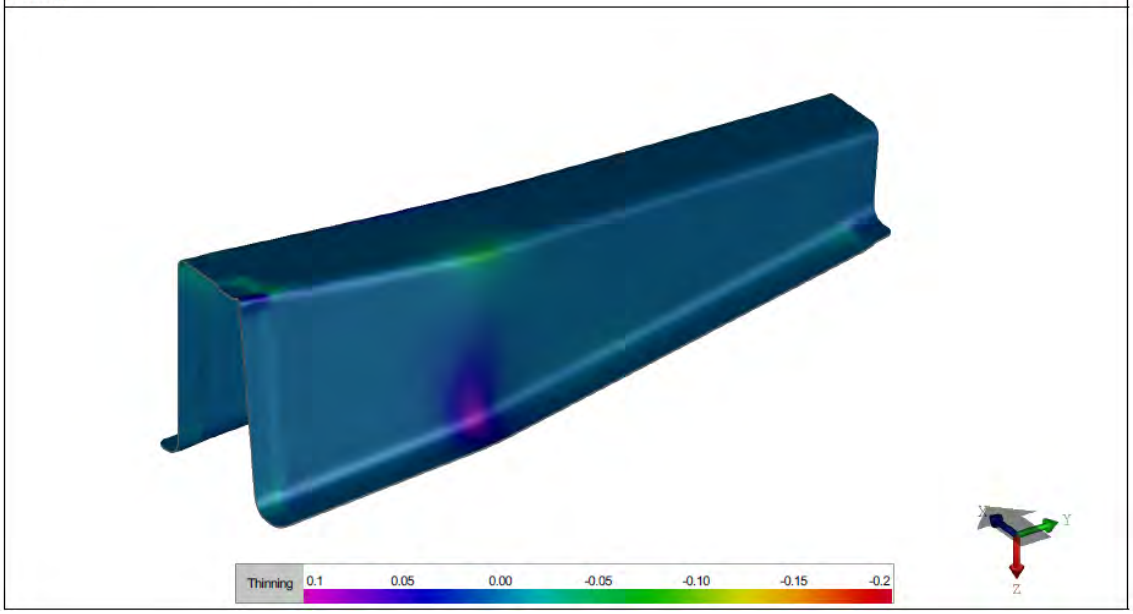

Wrinkles	T-20	

Wrinkles

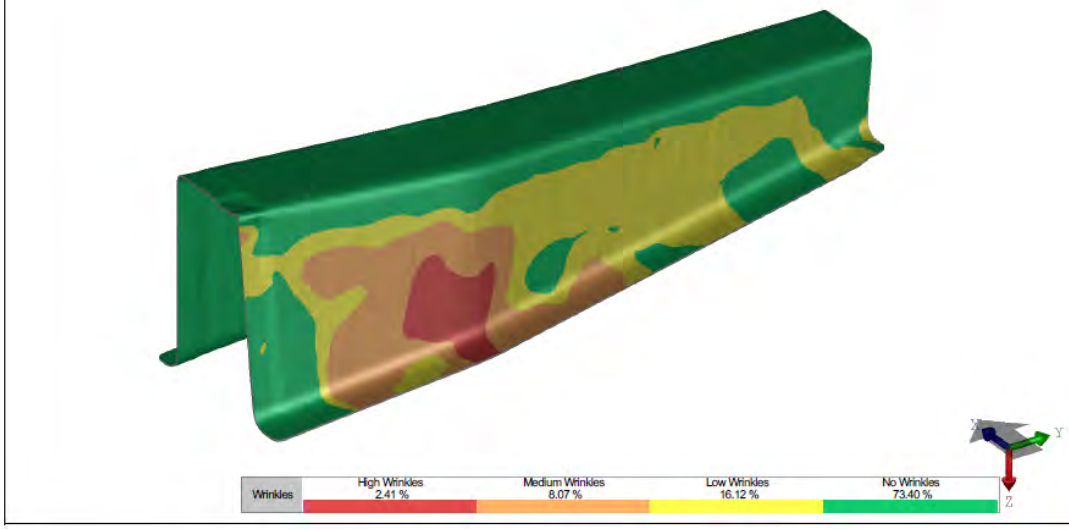

Springback		

Springback

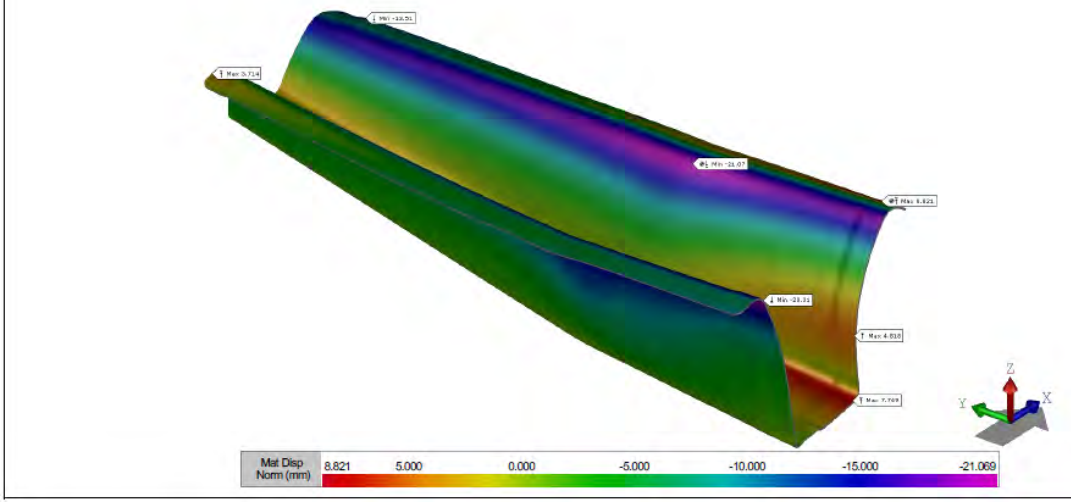

Rear inner roof header gusset

Overview and Summary

Part Info

Designation: 03599233 Rear Inr Roof Hdr Gst | Type:Form Trim Pierce

Part No.: | Drawing No.:

Nom. / Calculated Material: DC04

Nom. / Calculated Sheet Thickness: 0.800 mm

Method Info

Method Plan No.:

Drawing No.: | Rev:

Part

Criterion		OK	n OK	Status
FLD	5.2	☑	☐	
Flanging	5.24	☑	☐	
Gravity	5.3	☑	☐	
Closing	5.4	☑	☐	
Forming	5.5	☑	☐	
Thinning	5.6	☑	☑	
Strain	5.7	☑	☑	
Wrinkles	5.8	☑	☐	
Springback	5.9	☑	☐	

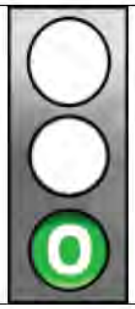

Simulation Info:

Filename:
ARRK_03599233_Rear_Inr_Roof_Header_Gusset_Mount_NMS_21-9-22_it4 -

AutoForm
AutoForm Forming Solver R10.0.0 | Memory: 123.37 MB

Process - Blank / Form / Laser Trim / Flange / Laser Trim

Input Data — Material & Blank

Calculated Material	DC04	Calc. Sheet Thickness			0.800 mm
Yield Stress	167.85 MPa	r0	1.87	r90	2.14
n-Value	0.211	r45	1.30	E-Module	2.10E+05 MPa

Yield Curve

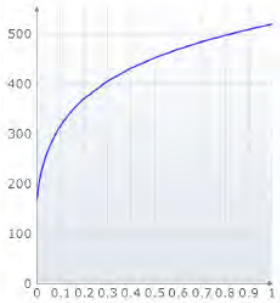

Yield Surface

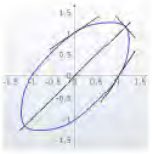

Forming Limit Curve

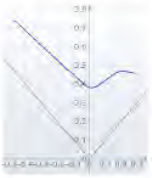

MU - Part to Blank

0.00 %

Blank Info

☐ Rectangular Blank

☑ Shaped Blank

Meshing

Roll angle	0.00 °
Initial Element Size	40.00 mm
Refinement Level	7
Max Element Angle	30.00 °

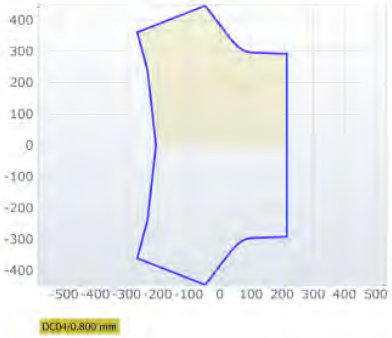

Input Data	F-10	F-10

Tool Info				Process Data		
Meshing Tolerance	0.05 mm			Friction Coefficient		
Process Type	Form Trim Pierce			Constant	0.080	
Tool Geometry Refers to	Upper Side of Initial Blank			Die - Blank	-	
Tools	Contact Side	Type	Gap	Punch - Blank	-	
Pad	Upper Side of Blank	Force Controlled		Binder - Blank	-	
Steel	Upper Side of Blank	Rigid		Binderforce		
Post	Lower Side of Blank	Rigid		RAM	45.7 tf	
				Binderforce/-pressure	8.8 tf	

Tool Geometry 1st opp

Tool Geometry 2nd opp

Formability	T-40

Advanced Formability

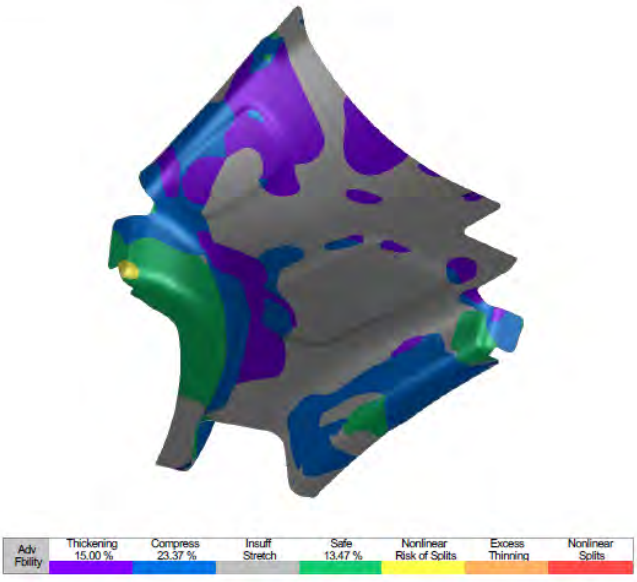

Wrinkling Behavior	
Wrinkling at -25.68 mm	**Wrinkling at 0.00 mm**
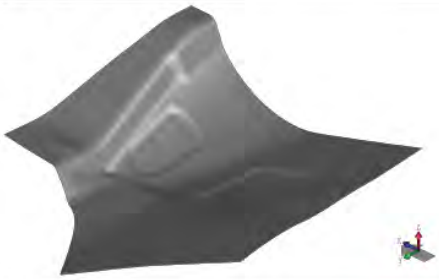	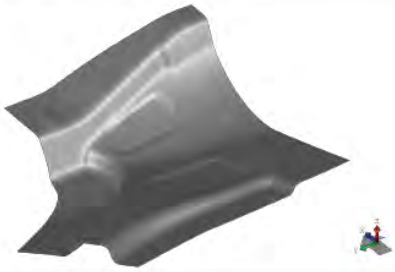
Wrinkling at -18.68 mm	**Wrinkling at -1.00 mm**
	

Glance Beam Upper Triangulation Outer

Overview and Summary

Part Info

Designation: 03601006-Body.1 | Type: Form Trim Pierce

Part No.: | Drawing No.:

Nom. / Calculated Material: 22MnB5

Nom. / Calculated Sheet Thickness: 1.000 mm

Method Info

Method Plan No.:

Drawing No.: | Rev:

Part

Criterion		OK	n OK	Status
FLD	5.2	☐	☐	
Thickness	5.24	☑	☐	
Gravity	5.3	☑	☐	
Closing	5.4	☑	☐	
Forming	5.5	☑	☐	
Thinning	5.6	☑	☐	
Martensite	5.7	☑	☐	
Temperature	5.8	☑	☐	
Hardness		☑	☐	

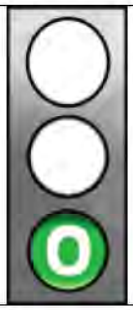

Simulation Info:

Filename:
ARRK_03601006_Glance_Beam_Upr_Triangulation_Otr_LH_NMS_1-9-22_it5 -

AutoForm | Memory: 343.38 MB
AutoForm Forming Solver Thermo R10.0.0

Process - Blank Die / Heating / Form / Quenching / Laser Trim

Input Data	Material & Blank

Calculated Material	22MnB5	Calc. Sheet Thickness				1.000 mm
Yield Stress		r0	1.00	r90	1.00	
n-Value		r45	1.00	E-Module		

Yield Curve

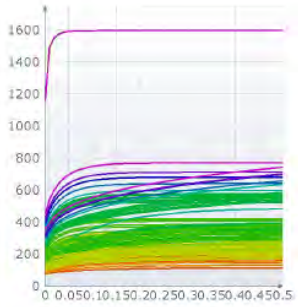

Yield Surface

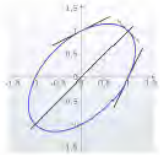

MU - Part to Blank

87.46 %

RAM Tonnage - 153.0 tf

Blank Info

- ☐ Rectangular Blank
- ☑ Shaped Blank

Meshing

Roll angle	0.00 °
Initial Element Size	20.00 mm
Refinement Level	5
Max Element Angle	22.50 °

Blank Size - 663.12 mm X 352.75 mm

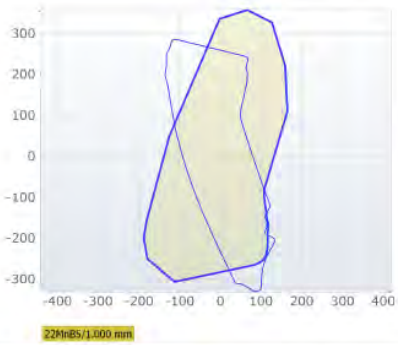

Formability	T-40

Advanced Formability

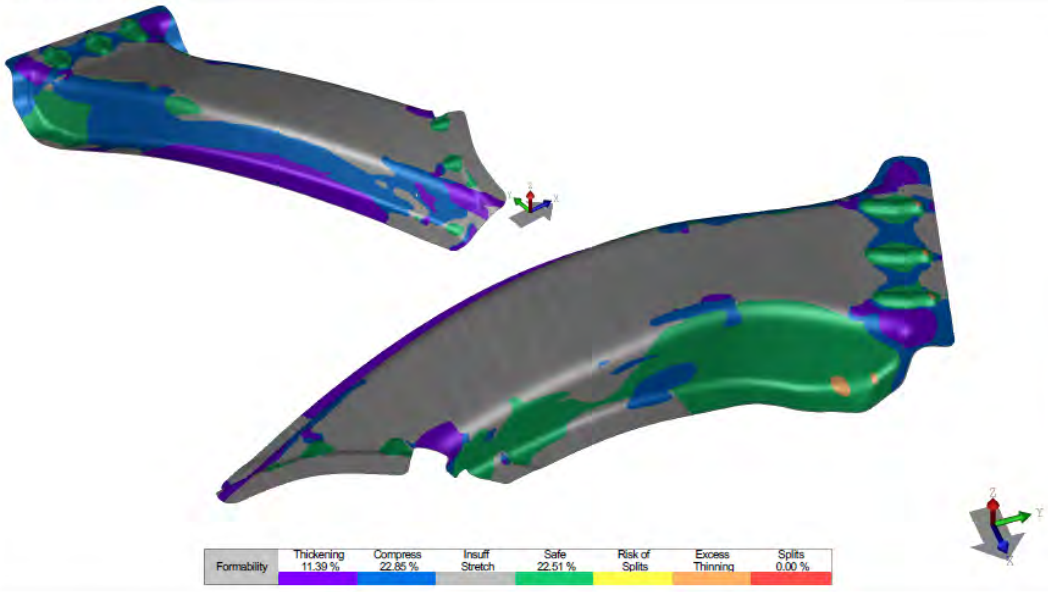

Thinning	T-40	

Thinning

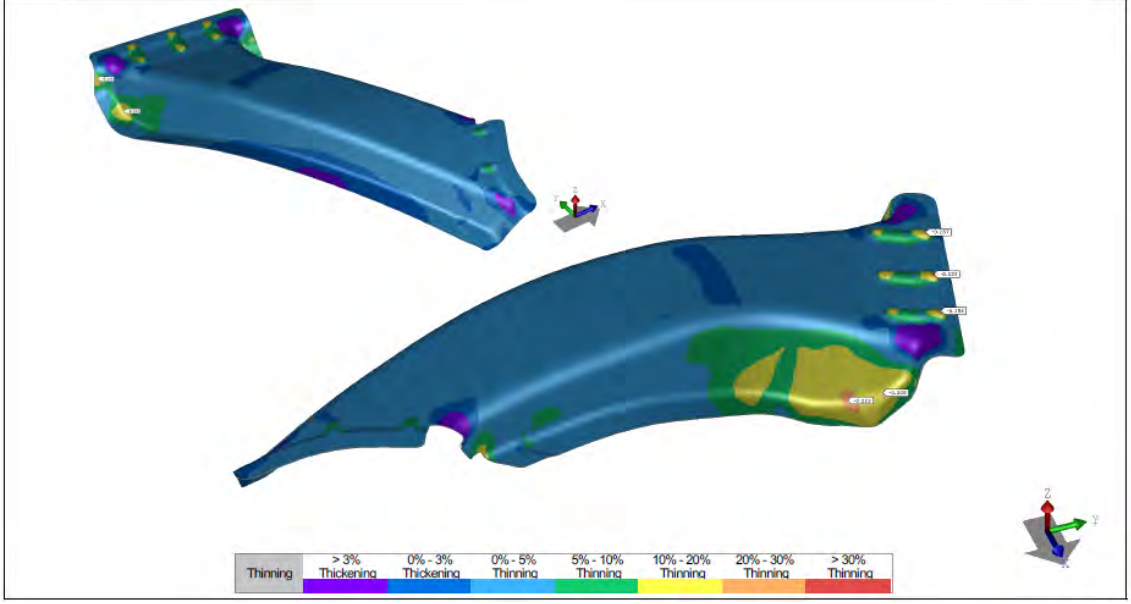

Wrinkling Behavior	K-30	

Wrinkling at 63mm To Bottom

Wrinkling at 36mm To Bottom

Wrinkling at 13mm To Bottom

Wrinkling at 2mm To Bottom

Front Vertical Dash Brace Lower

Overview and Summary

Part Info

Designation: 03630344 VERTICAL DASH BRACE LOWER	Type: Single Action Draw
Part No.:	Drawing No.:
Nom. / Calculated Material: Usibor1500_100mm_600C	
Nom. / Calculated Sheet Thickness: 2.000 mm	

Method Info

Method Plan No.:	
Drawing No.:	Rev:

Part

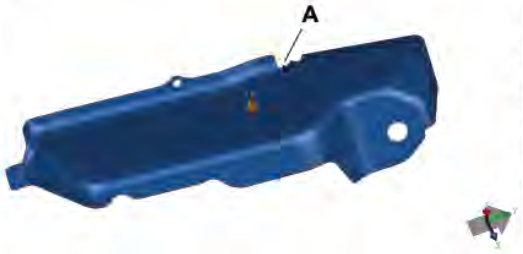

Criterion		OK	n OK
FLD	5.2	☐	☐
Flanging	5.24	☐	☐
Gravity	5.3	☑	☐
Closing	5.4	☑	☐
Forming	5.5	☑	☐
Thinning	5.6	☑	☐
Martensite	5.7	☑	☐
Temperature	5.8	☑	☐
Hardness		☑	☐

Status

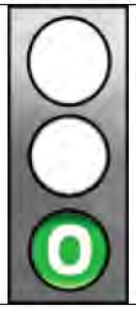

Simulation Info:

Filename:
ARRK_03630344_Vertical_Dash_Brace_Lower_Inr_LH_NMS_3-9-22_it4 - EXTENSION

AutoForm — Memory: 771.96 MB
AutoForm Forming Solver Thermo R10.0.0

Process - Blank Die / Heating / Draw / Quenching / Laser Trim

Input Data — Material & Blank

Calculated Material	Usibor1500_100mm	Calc. Sheet Thickness			2.000 mm
Yield Stress		r0	1.00	r90	1.00
n-Value		r45	1.00	E-Module	

Yield Curve

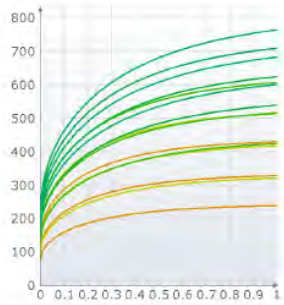

Yield Surface

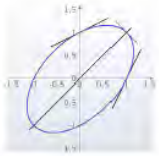

MU - Part to Blank
45.96 %

RAM Tonnage - 130.7 tf

Blank Info

☐ Rectangular Blank
☑ Shaped Blank

Meshing

Roll angle	0.00 °
Initial Element Size	20.00 mm
Refinement Level	5
Max Element Angle	20.00 °

Blank Size - 724.59 mm X 443.70 mm

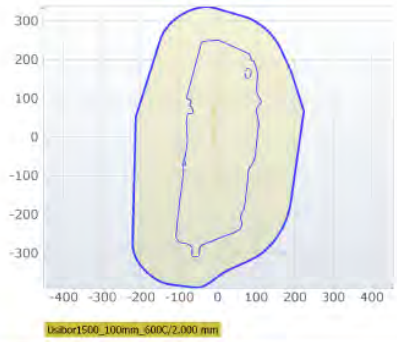

Thinning	T-40	

Thinning

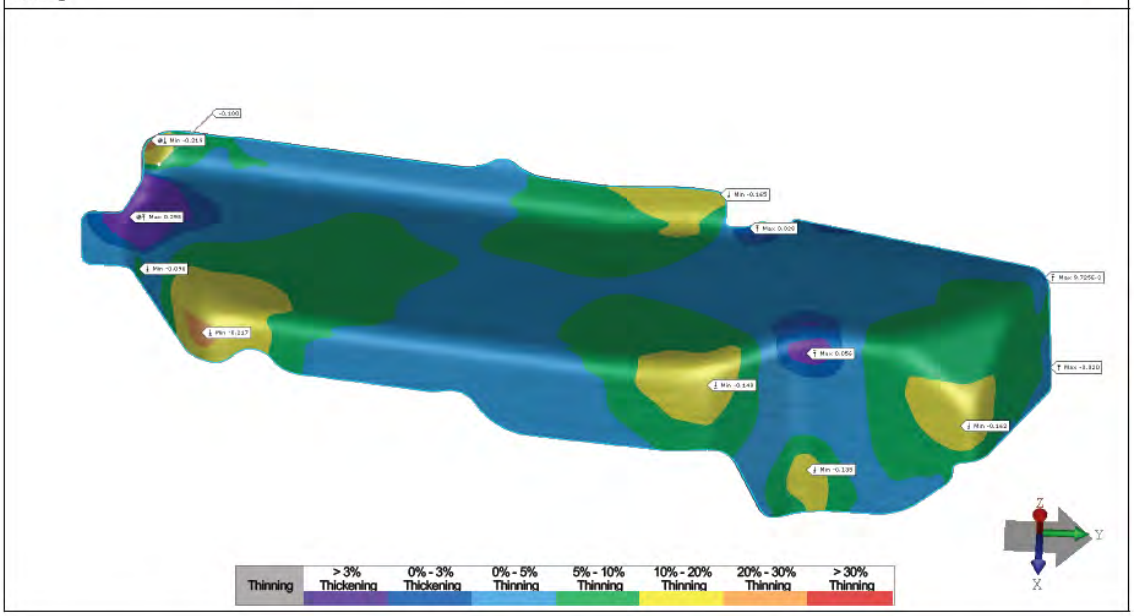

Wrinkling Behavior	T-40	

Wrinkling at -54mm

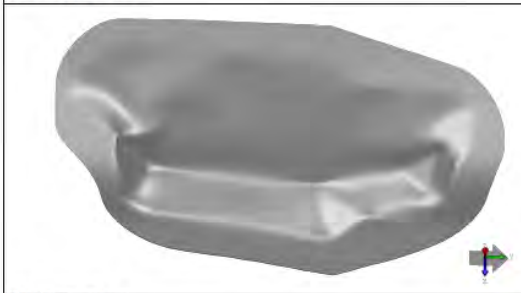

Wrinkling at -21mm

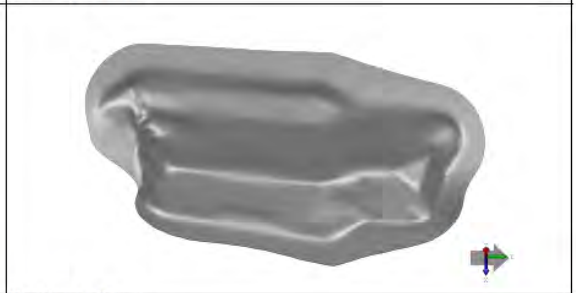

Wrinkling at -8mm

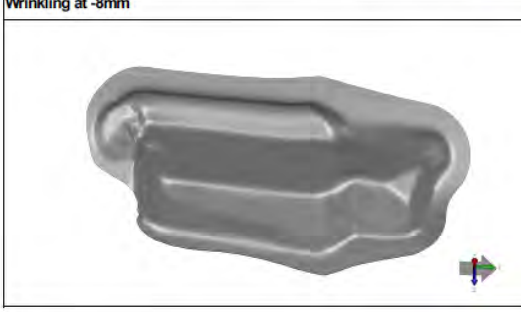

Wrinkling at -0.5mm

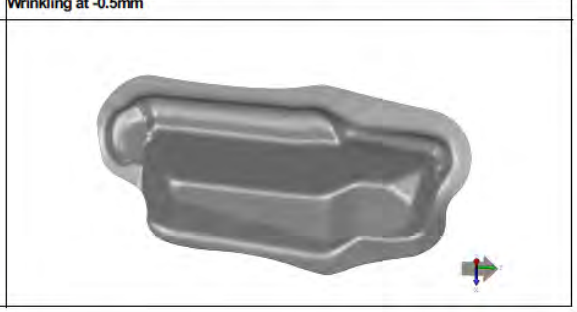

Rear Dash Brace Lower

Overview and Summary

Part Info

Designation: 03630350 - Rear Dash Brace	Type:
Part No.:	Drawing No.:
Nom. / Calculated Material: CR820Y1180T_RA_CE+	
Nom. / Calculated Sheet Thickness: 1.000 mm	

Method Info

Method Plan No.:	
Drawing No.:	Rev:

Part

Criterion		OK	n OK
FLD	5.2	☑	☐
Flanging	5.24	☑	☐
Gravity	5.3	☑	☐
Closing	5.4	☑	☐
Forming	5.5	☑	☐
Thinning	5.6	☑	☐
Strain	5.7	☑	☐
Wrinkles	5.8	☐	☑
Springback	5.9	☑	☐

Status

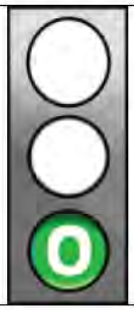

Simulation Info:

Filename:
ARRK_03630350_Rear_Dash_Brace_A_LH_NMS_20-9-22_it9 - EXTENSION MODS 7 -

AutoForm AutoForm Forming Solver R10.0.0	Memory: 227.44 MB

Remarks: After many modifications and many simulations we have a result which is good enough for prototype stage.

Input Data — Material & Blank

Calculated Material	CR820Y1180T_RA_(	Calc. Sheet Thickness			1.000 mm
Yield Stress	869.85 MPa	r0	0.56	r90	0.61
n-Value	0.119	r45	0.77	E-Module	2.10E+05 MPa

Yield Curve

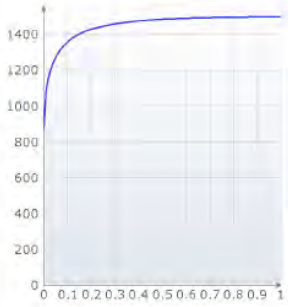

Yield Surface

Forming Limit Curve

Blank Info

☑ Rectangular Blank
☐ Shaped Blank

Meshing

Roll angle	0.00 °
Initial Element Size	40.00 mm
Refinement Level	7
Max Element Angle	30.00 °

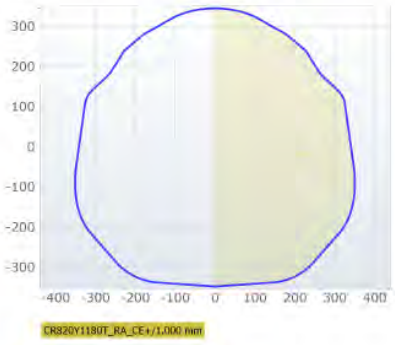

Input Data	D-20

Tool Info				Process Data		
Meshing Tolerance	0.05 mm			Friction Coefficient		
Process Type	Single Action Draw			Constant	0.100	
Tool Geometry Refers to	Lower Side of Initial Blank			Die - Blank	-	
Tools	Contact Side	Type	Gap	Punch - Blank	-	
Die	Upper Side of Blank	Rigid		Binder - Blank	-	
Punch	Lower Side of Blank	Rigid		Binderforce		
Binder	Lower Side of Blank	Force Controlled		RAM	117.0 tf	
				Binderforce/-pressure	21.2 tf	

Tool Geometry 1st opp

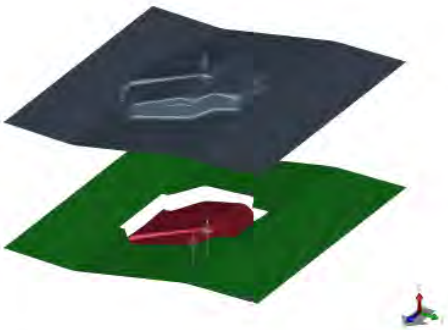

Tool Geometry 2nd opp

Formability	D-20

Advanced Formability

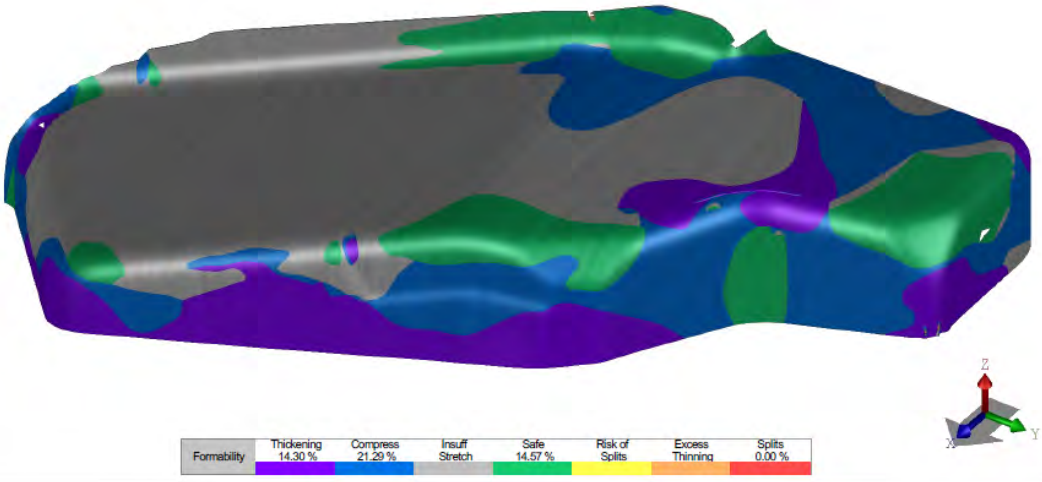

Wrinkling Behavior	D-20	

Wrinkling at -45mm	Wrinkling at -20mm
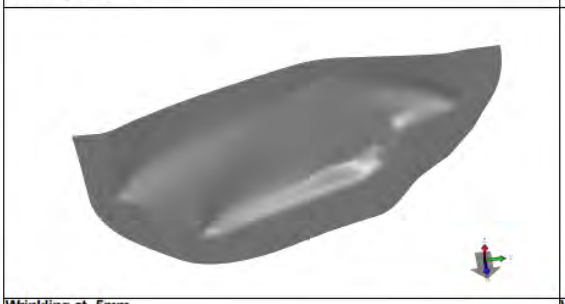	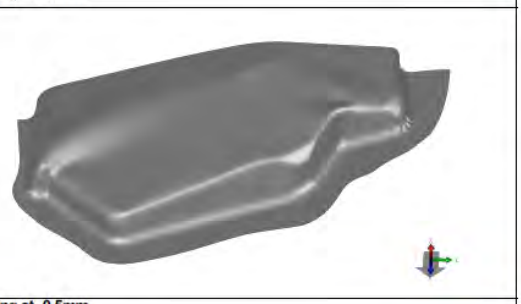
Wrinkling at -5mm	**Wrinkling at -0.5mm**
	

Front Strut Top

Overview and Summary

Part Info

Designation: 03603910-Body.1 | Type:

Part No.: | Drawing No.:

Nom. / Calculated Material: CR_1180DP_AF_RevA

Nom. / Calculated Sheet Thickness: 2.400 mm

Method Info

Method Plan No.:

Drawing No.: | Rev:

Part

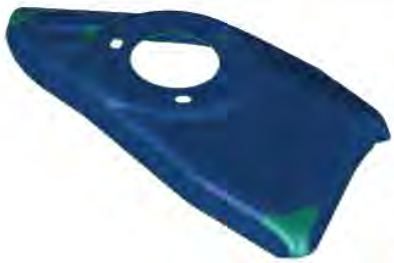

Criterion		OK	n OK	Status
FLD	5.2	☑	☐	
Flanging	5.24	☐	☐	
Gravity	5.3	☑	☐	
Closing	5.4	☑	☐	
Forming	5.5	☑	☐	
Thinning	5.6	☑	☐	
Strain	5.7	☑	☐	
Wrinkles	5.8	☑	☐	
Springback	5.9	☑	☐	

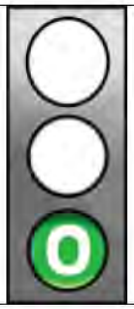

Simulation Info:

Filename:ARRK_03633910_Strut_Top_Front_LH_NMS_10-6-22_it2 - MOD TIP.afd

AutoForm
AutoForm Forming Solver R10.0.0 | Memory: 164.93 MB

Proces - Blank Die / Draw / CAM Trim & Pierce / CAM Trim /

Input Data — Material & Blank

Calculated Material	CR_1180DP_AF_Re	Calc. Sheet Thickness				2.400 mm	
Yield Stress	927.64 MPa	r0	0.80	r90	0.82		
n-Value	0.095	r45	0.74	E-Module	2.10E+05 MPa		

Yield Curve

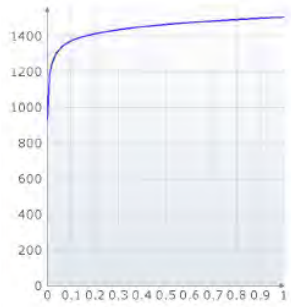

Yield Surface

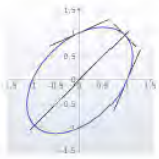

Forming Limit Curve

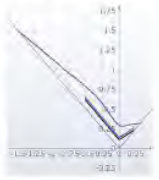

MU - Part to Blank

48.71 %

Blank Info

- ☐ Rectangular Blank
- ☑ Shaped Blank

Meshing

Roll angle	0.00 °
Initial Element Size	40.00 mm
Refinement Level	7
Max Element Angle	30.00 °

Blank Size - 630.81 mm X 443.46 mm

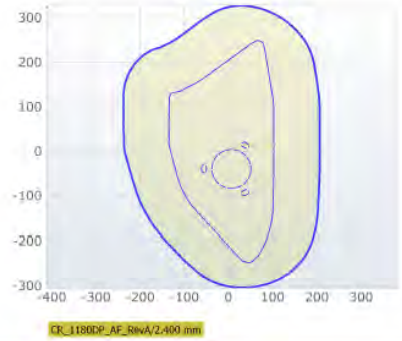

Wrinkling Behavior — D-20

Wrinkling at -54.95 mm

Wrinkling at -34.74 mm

Wrinkling at -8.56 mm

Wrinkling at -1.00 mm

Front Strut Cross Member

Overview and Summary

Part Info

Designation: 03640758-Body.1 | Type:Form Trim Pierce

Part No.: | Drawing No.:

Nom. / Calculated Material: Usibor2000UFG_200mm_700C

Nom. / Calculated Sheet Thickness: 1.000 mm

Method Info

Method Plan No.:

Drawing No.: | Rev:

Part

Criterion		OK	n OK
FLD	5.2	☑	☐
Flanging	5.24	☐	☐
Gravity	5.3	☑	☐
Closing	5.4	☑	☐
Forming	5.5	☑	☐
Thinning	5.6	☑	☐
Martensite	5.7	☑	☐
Temperature	5.8	☑	☐
Hardness		☑	☐

Status

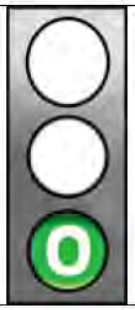

Simulation Info:

Filename:
ARRK_03640758_Strut_X_Mbr_Frt_NMS_6-9-22_it1 - EXTENSION MODS 2 - NEW

AutoForm | Memory: 673.94 MB
AutoForm Forming Solver Thermo R10.0.0

R
S
H
fi

Process - Blank Die / Heating / Form / Quenching / Laser Trim

Input Data — Material & Blank

Calculated Material	Usibor2000UFG_200	Calc. Sheet Thickness			1.000 mm
Yield Stress		r0	1.00	r90	1.00
n-Value		r45	1.00	E-Module	

Yield Curve

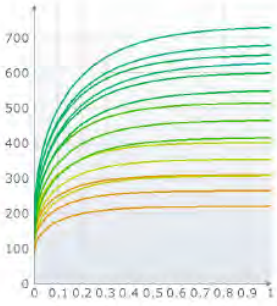

Yield Surface

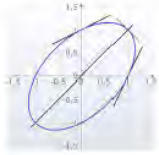

MU - Part to Blank
92.90 %

RAM Tonnage - 300.0 tf

Blank Info

☐ Rectangular Blank
☑ Shaped Blank

Meshing

Roll angle	0.00 °
Initial Element Size	40.00 mm
Refinement Level	5
Max Element Angle	22.50 °

Blank Size - 1416.97 mm X 432.08 mm

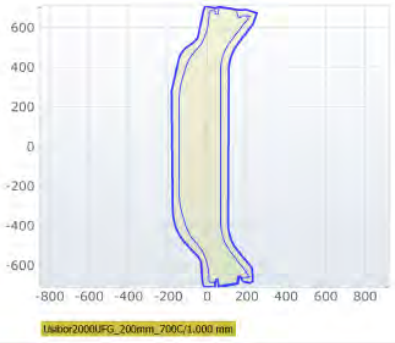

Formability	T-40	

Advanced Formability

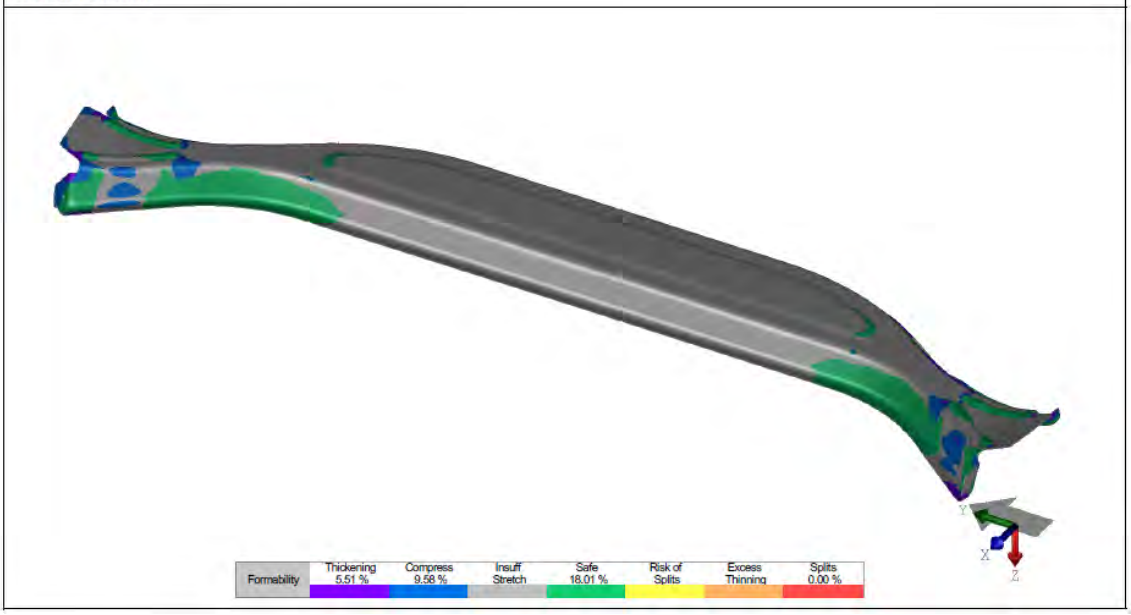

Wrinkling Behavior	T-40	

Wrinkling at -78.0mm

Wrinkling at -38.0mm

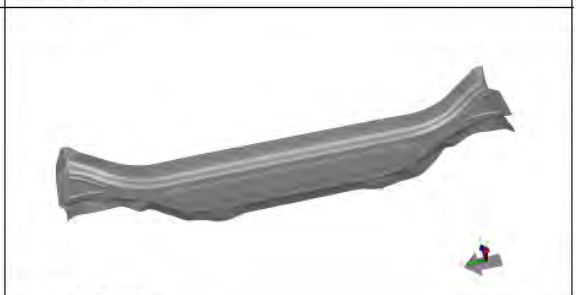

Wrinkling at -9mm

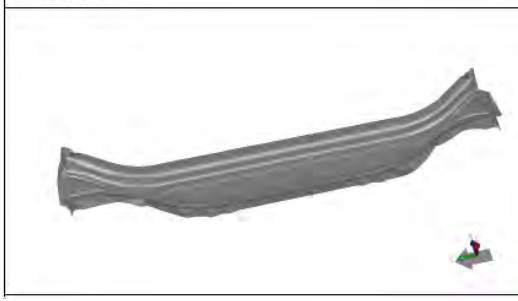

Wrinkling at -1.5mm

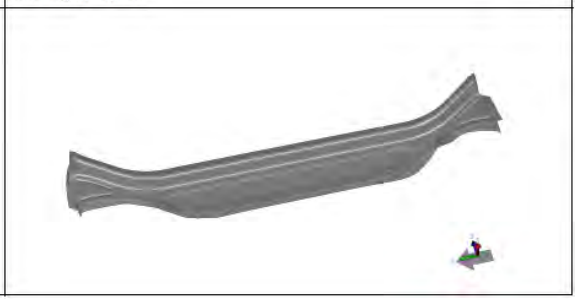

Glance Beam Upper Reaction

Overview and Summary

Part Info

Designation: 03640760-Body.1 | Type:

Part : | Drawing No.:

Nom. / Calculated Material: Usibor1500_200mm_700C

Nom. / Calculated Sheet Thickness: 0.800 mm

Method Info

Method Plan No.:

Drawing No.: | Rev:

Part

Criterion		OK	n OK	Status
FLD	5.2	☑	☐	
Flanging	5.24	☑	☐	
Gravity	5.3	☑	☐	
Closing	5.4	☑	☐	
Forming	5.5	☑	☐	
Thinning	5.6	☑	☐	
Strain	5.7	☑	☐	
Wrinkles	5.8	☑	☐	
Springback	5.9	☑	☐	

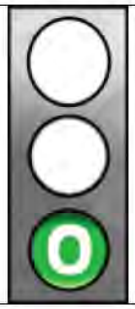

Simulation Info:

Filename:
ARRK_03640760_Glance_Beam_Upr_Reaction_LH_NMS_7-9-22_it9 - EXTENSION

AutoForm | Memory: 389.41 MB
AutoForm Forming Solver Thermo R10.0.0

Process - Blank / Heating / Draw / Cooling / Trim

Input Data — Material & Blank

Calculated Material	Usibor1500_200mm	Calc. Sheet Thickness			0.800 mm
Yield Stress		r0	1.00	r90	1.00
n-Value		r45	1.00	E-Module	

Yield Curve

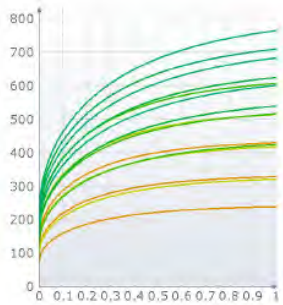

Yield Surface

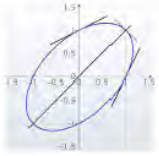

Forming Limit Curve

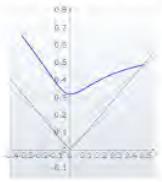

MU - Part to Blank

41.31 %

Blank Info

☐ Rectangular Blank

☑ Shaped Blank

Meshing

Roll angle	0.00 °
Initial Element Size	40.00 mm
Refinement Level	6
Max Element Angle	22.50 °

Blank Size - 565.99 mm x 326.44 mm

Input Data	D-20

Tool Info				Process Data		
Meshing Tolerance	0.05 mm			Friction Coefficient		
Process Type	Single Action Draw			Constant	0.450	
Tool Geometry Refers to	Lower Side of Initial Blank			Die - Blank	-	
Tools	Contact Side	Type	Gap	Punch - Blank	-	
Die	Upper Side of Blank	Rigid		Binder - Blank	-	
Punch	Lower Side of Blank	Rigid		Binderforce		
Binder	Lower Side of Blank	Gap Controlled		RAM	200.0 tf	
				Binderforce/-pressure	0.8 tf	

Tool Geometry 1st opp

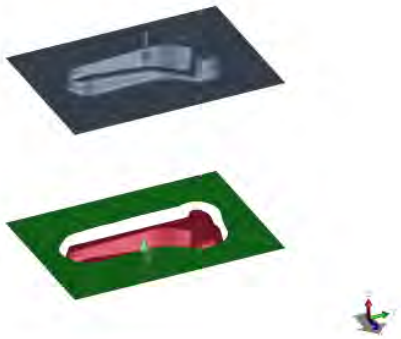

Wrinkling Behavior	D-20

Wrinkling at 10mm To Bottom 1st stage

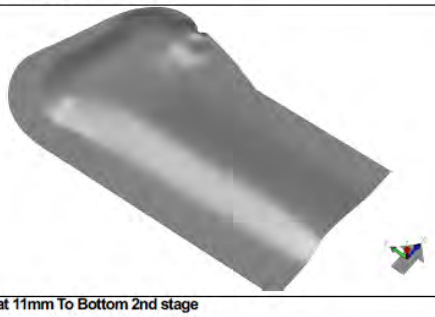

Wrinkling at Bottom 1st stage

Wrinkling at 11mm To Bottom 2nd stage

Wrinkling at 1.5mm To Bottom 2nd stage

Glance Beam Lower Reaction

Overview and Summary

Part Info

Designation: 03642244-Body.1 | Type:

Part : | Drawing No.:

Nom. / Calculated Material: SSAB_CR1220Y1500T_MS

Nom. / Calculated Sheet Thickness: 0.800 mm

Method Info

Method Plan No.:

Drawing No.: | Rev:

Part

Criterion		OK	n OK	Status
FLD	5.2	☑	☐	
Flanging	5.24	☑	☐	
Gravity	5.3	☑	☐	
Closing	5.4	☑	☐	
Forming	5.5	☑	☐	
Thinning	5.6	☑	☐	
Strain	5.7	☑	☐	
Wrinkles	5.8	☑	☐	
Springback	5.9	☑	☐	

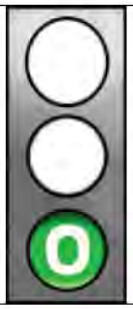

Simulation Info:

Filename:
ARRK_03642244_Glance_Beam_Lwr_Reaction_LH_NMS_31-8-22_it3 - EXTENSION

AutoForm | Memory: 123.45 MB
AutoForm Forming Solver R10.0.0

Process - Blank / Crash / Flange Up / Form / Laser Trim

Input Data — Material & Blank

Calculated Material	SSAB_CR1220Y150	Calc. Sheet Thickness				0.800 mm	
Yield Stress	1296.54 MPa	r0	0.93	r90	0.96		
n-Value	0.084	r45	0.94	E-Module	2.00E+05 MPa		

Yield Curve

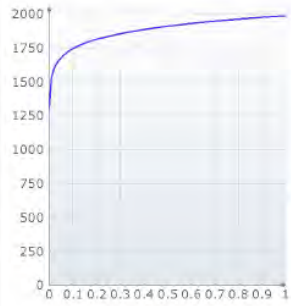

Yield Surface

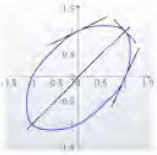

Forming Limit Curve

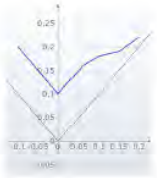

MU - Part to Blank

98.70 %

Blank Info

☐ Rectangular Blank

☑ Shaped Blank

Meshing

Roll angle	0.00 °
Initial Element Size	40.00 mm
Refinement Level	6
Max Element Angle	22.50 °

Blank Size - 451.50 mm x 228.35 mm

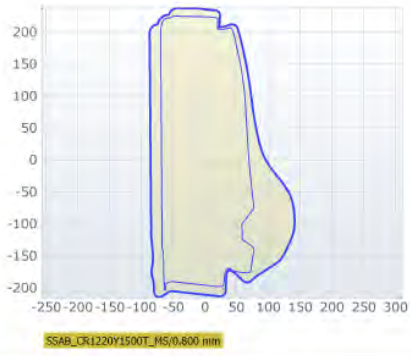

Input Data	C-20

Tool Info				Process Data		
Meshing Tolerance	0.05 mm			Friction Coefficient		
Process Type	Crashform Up			Constant	0.100	
Tool Geometry Refers to	Lower Side of Initial Blank			Die - Blank	-	
Tools	Contact Side	Type	Gap	Punch - Blank	-	
Die	Upper Side of Blank	Rigid		Binder - Blank	-	
Punch	Lower Side of Blank	Rigid		Binderforce		
				RAM	39.6 tf	
				Binderforce/-pressure	4.70 N	

Tool Geometry 1st opp

Tool Geometry 2nd opp

Tool Geometry 3rd opp

Wrinkles	T-50

Wrinkles

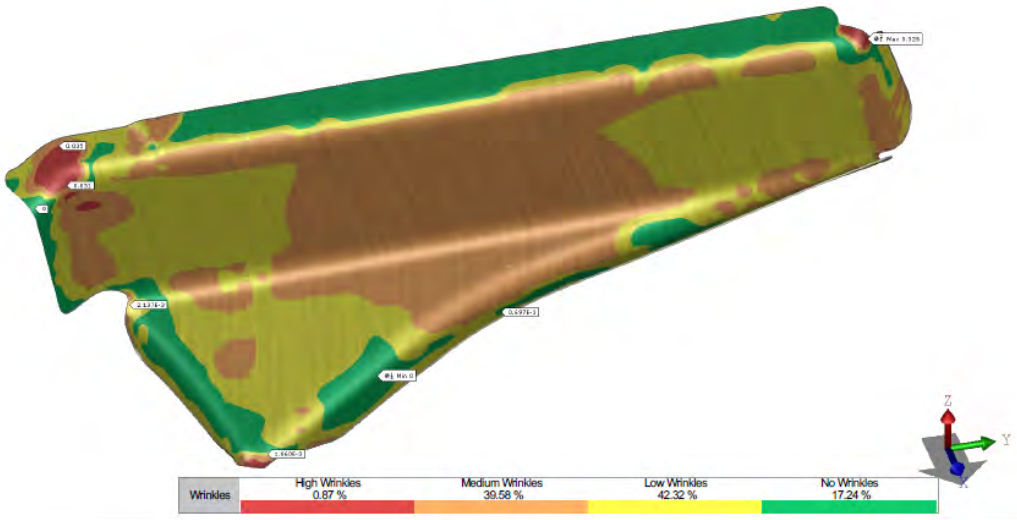

Springback	M-60	

Springback

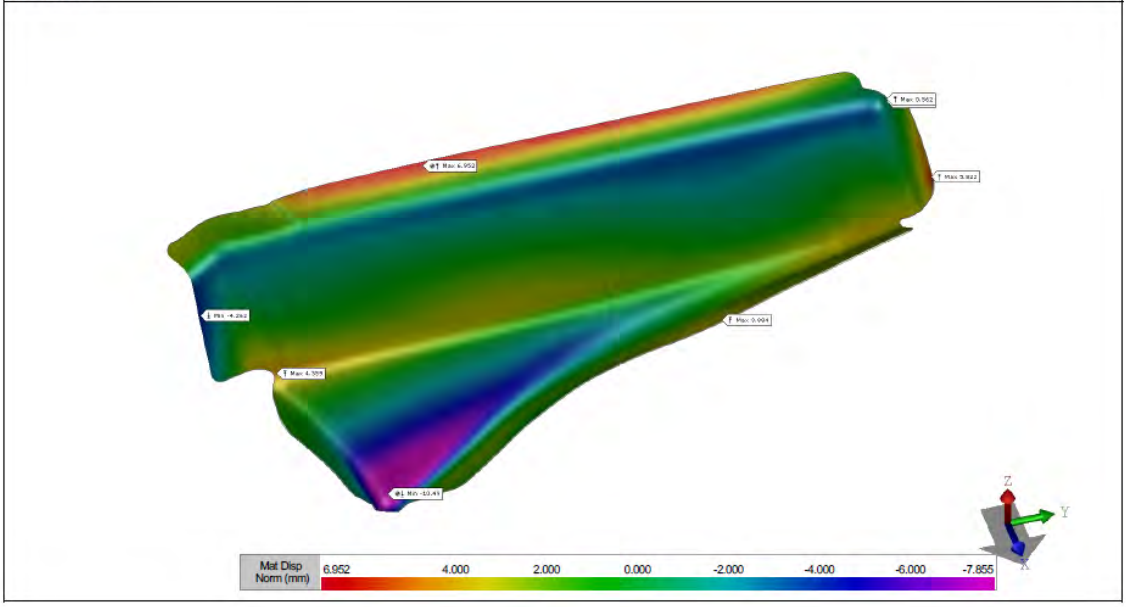

One bar outer upper

Overview and Summary

Part Info

Designation: 03670457 One_Bar_Outer_Upper	Type:
Part No.:	Drawing No.:
Nom. / Calculated Material: SSAB_CR1220Y1500T_MS	
Nom. / Calculated Sheet Thickness: 2.000 mm	

Method Info

Method Plan No.:	
Drawing No.:	Rev:

Part

Criterion		OK	n OK
FLD	5.2	☑	☐
Flanging	5.24	☑	☐
Gravity	5.3	☑	☐
Closing	5.4	☑	☐
Forming	5.5	☑	☐
Thinning	5.6	☑	☐
Strain	5.7	☑	☐
Wrinkles	5.8	☑	☐
Springback	5.9	☑	☐

Status

Simulation Info:

Filename:
ARRK_03670457_One_Bar_Outer_Upr_NMS_5-9-22_it2 - EXTENSION MODS 2 -

AutoForm AutoForm Forming Solver R10.0.0	Memory: 207.26 MB

Process - Blank Die / Crash /Flange / Form / Re-strike

Input Data	Material & Blank

Calculated Material	SSAB_CR1220Y150	Calc. Sheet Thickness			2.000 mm
Yield Stress	1296.54 MPa	r0	0.93	r90	0.96
n-Value	0.084	r45	0.94	E-Module	2.00E+05 MPa

Yield Curve

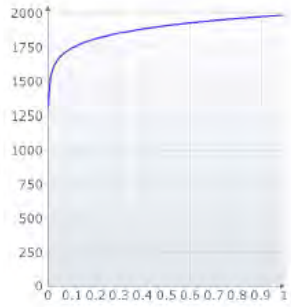

Yield Surface

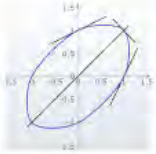

Forming Limit Curve

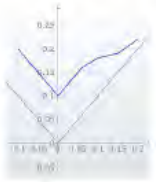

MU - Part to Blank

102.26 %

Blank Info

- ☐ Rectangular Blank
- ☑ Shaped Blank

Meshing

Roll angle	0.00 °
Initial Element Size	40.00 mm
Refinement Level	6
Max Element Angle	22.50 °

Blank size - 710.55 mm X 231.68 mm

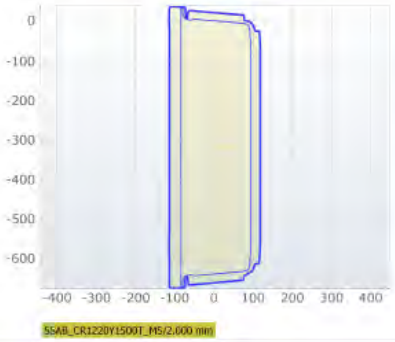

Formability	F-50

Advanced Formability

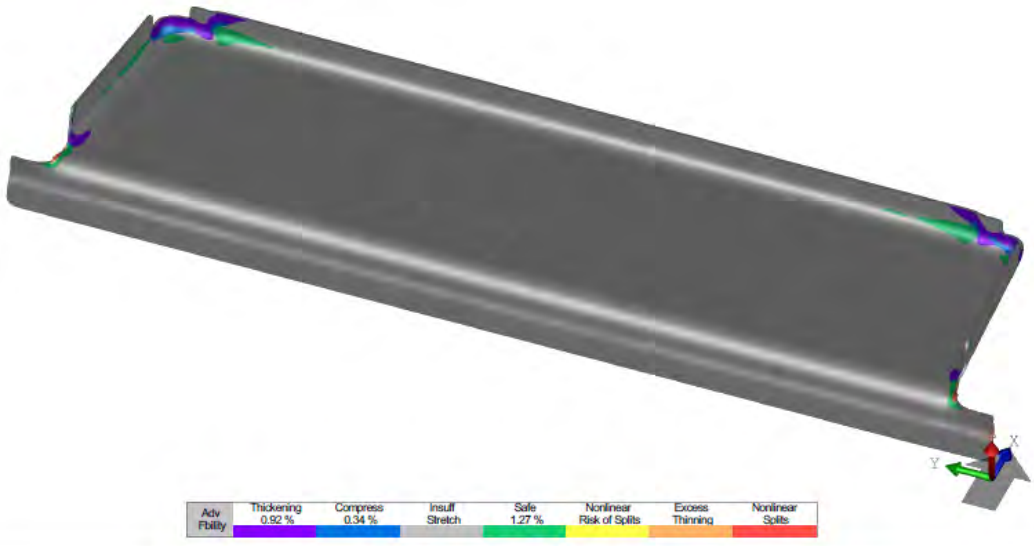

Wrinkles	F-50

Wrinkles

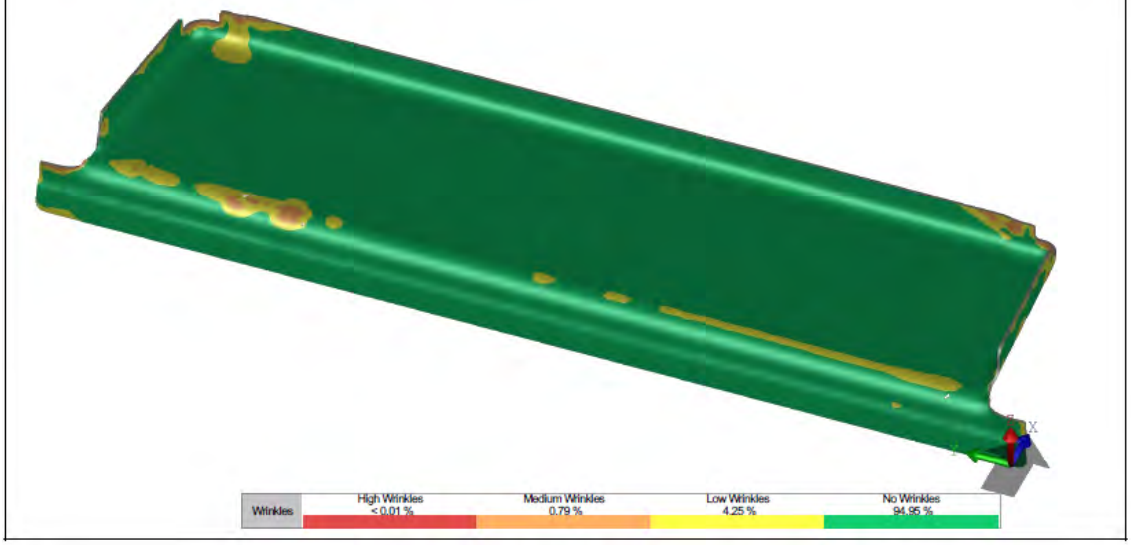

Front Vertical Dash Brace Upper

Overview and Summary

Part Info

Designation:	Type: Single Action Draw
Part No.:	Drawing No.:
Nom. / Calculated Material: USS_CAL_MS1500_AF_RevB	
Nom. / Calculated Sheet Thickness: 1.600 mm	

Method Info

Method Plan No.:	
Drawing No.:	Rev:

Part

Criterion		OK	n OK	Status
FLD	5.2	☑	☐	
Flanging	5.24	☑	☐	
Gravity	5.3	☑	☐	
Closing	5.4	☑	☐	
Forming	5.5	☑	☐	
Thinning	5.6	☑	☐	
Strain	5.7	☑	☐	
Wrinkles	5.8	☑	☐	
Springback	5.9	☑	☐	

Simulation Info:

Filename:
ARRK_03671385_Vertical_Dash_Brace_Upr_Frt_NMS_21-9-22_it1 - EXTENSION

AutoForm AutoForm Forming Solver R10.0.0	Memory: 73.36 MB

Process - Blank / Form / Laser trim / Form / Laser Trim

Input Data	Material & Blank

Calculated Material	USS_CAL_MS1500_	Calc. Sheet Thickness			1.600 mm
Yield Stress	1359.15 MPa	r0	1.24	r90	0.83
n-Value	0.061	r45	0.50	E-Module	2.10E+05 MPa

Yield Curve

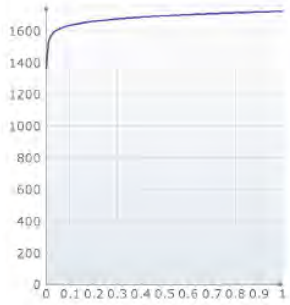

Yield Surface

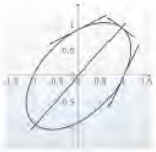

Forming Limit Curve

Blank Info

- ☐ Rectangular Blank
- ☑ Shaped Blank

Meshing

Roll angle	0.00 °
Initial Element Size	40.00 mm
Refinement Level	7
Max Element Angle	30.00 °

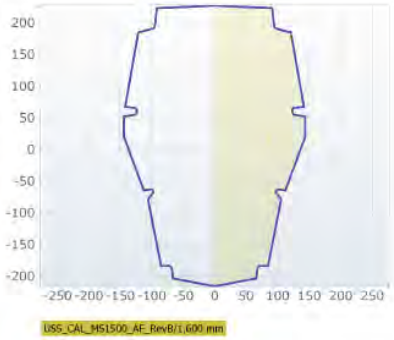

Formability	T-30

Advanced Formability

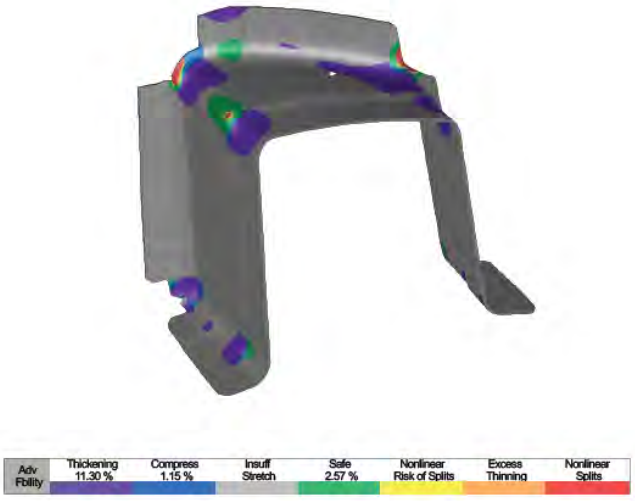

Wrinkles	T-30	

Wrinkles

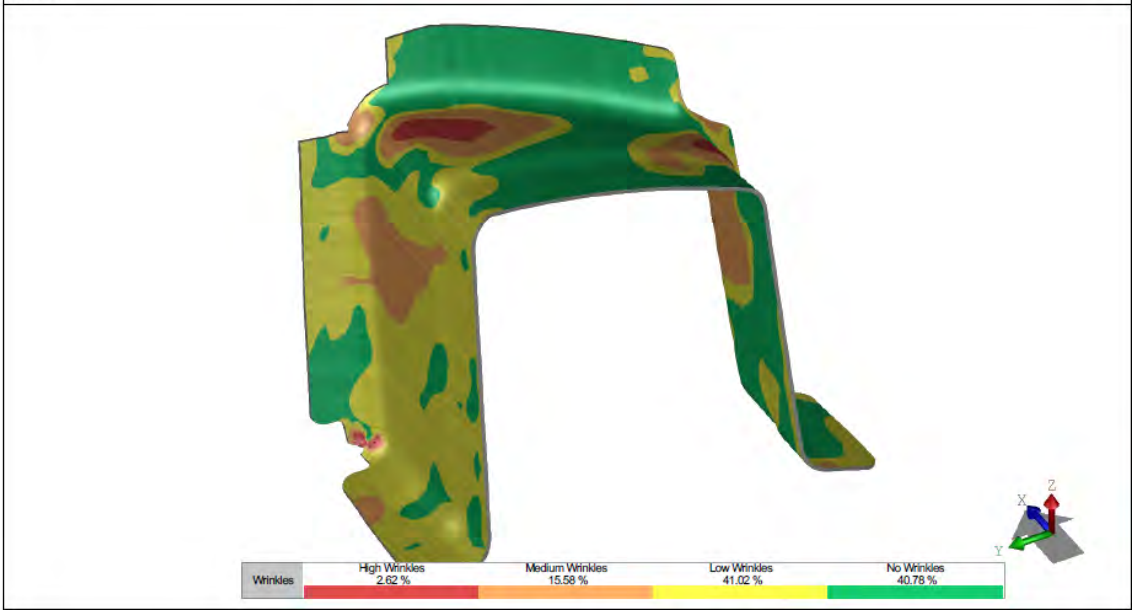

Front torque box outer

Overview and Summary

Part Info

Designation: 03691527-Body.1	Type:
Part No.:	Drawing No.:
Nom. / Calculated Material:	
Nom. / Calculated Sheet Thickness: 1.000 mm	

Method Info

Method Plan No.:	
Drawing No.:	Rev:

Part

Criterion		OK	n OK	Status
FLD	5.2	☑	☐	
Flanging	5.24	☑	☐	
Gravity	5.3	☑	☐	
Closing	5.4	☑	☐	
Forming	5.5	☑	☐	
Thinning	5.6	☑	☐	
Strain	5.7	☑	☐	
Wrinkles	5.8	☑	☐	
Springback	5.9	☑	☐	

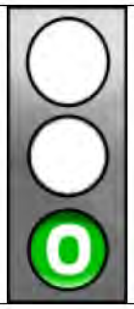

Simulation Info:

Filename:
ARRK_03691527_Torque_Box_NMS_14-8-22_it3 - EXTENSION MODS 1 - NEW CAD

AutoForm AutoForm Forming Solver R10.0.0	Memory: 242.03 MB

Process - Blank Die / Crash & Flange / Form /

Input Data	Material & Blank

Calculated Material	CR850Y1180T-DH-UC-EG_DP1200-	Calc. Sheet Thickness			1.000 mm
Yield Stress	957.78 MPa	r0	0.85	r90	0.94
n-Value	0.132	r45	1.04	E-Module	2.10E+05 MPa

Yield Curve

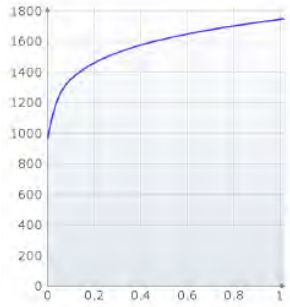

Yield Surface

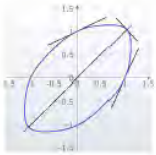

Forming Limit Curve

MU - Part to Blank

94.60 %

Blank Info

- ☐ Rectangular Blank
- ☑ Shaped Blank

Meshing

Roll angle	0.00 °
Initial Element Size	20.00 mm
Refinement Level	6
Max Element Angle	22.50 °

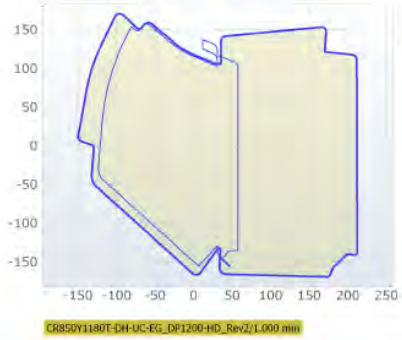

Formability	T-30

Advanced Formability

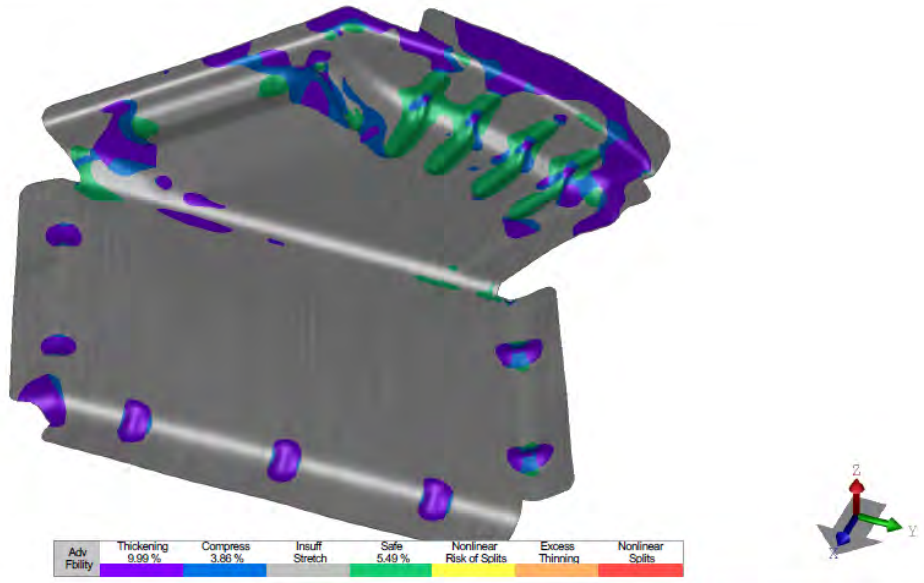

Wrinkles	T-30

Wrinkles

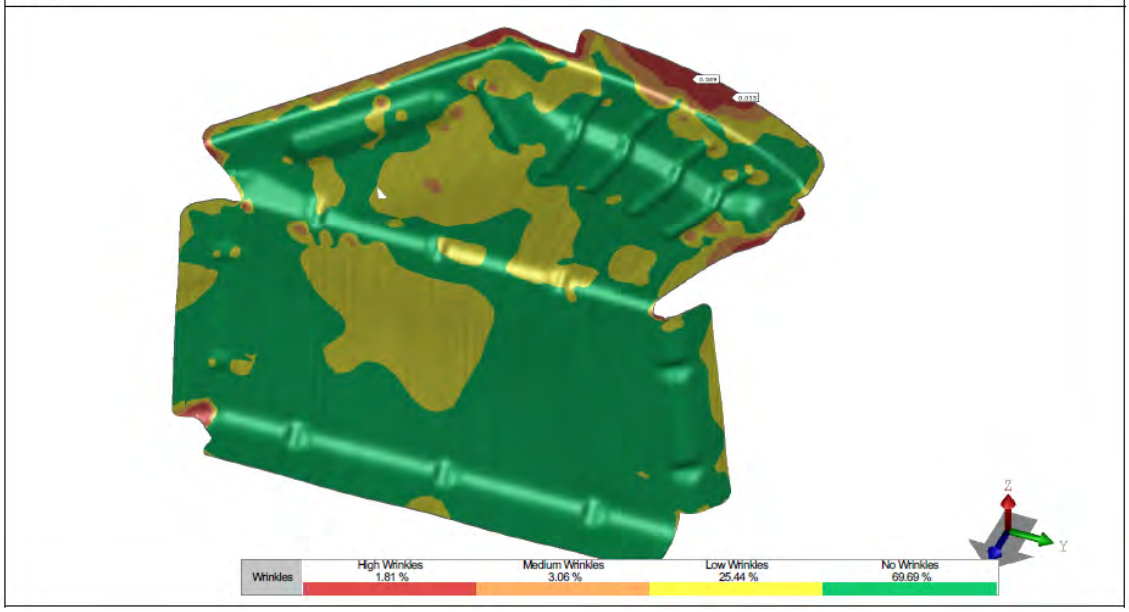

Door Ring Outer (TWB)

Overview and Summary

Part Info

Designation: 03694699-Body.1	Type:Heating
Part No.:	Drawing No.:
Nom. / Calculated Material: Usibor 2000 / Usibor 1500 / Ductibor 1000	
Nom. / Calculated Sheet Thickness: 1.2mm / 1.5mm / 0.8mm	

Method Info

Method Plan No.:	
Drawing No.:	Rev:

Part

Criterion		OK	n OK	Status
FLD	5.2	☐	☐	
Thickness	5.24	☑	☐	
Gravity	5.3	☑	☐	
Closing	5.4	☑	☐	
Forming	5.5	☑	☐	
Thinning	5.6	☑	☐	
Martensite	5.7	☐	☐	
Temperature	5.8	☑	☐	
Hardness		☐	☐	

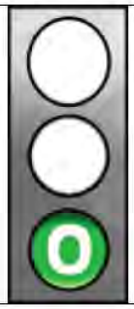

Simulation Info:

Filename:
ARRK_03694699_Outer_Ring_TWB_NMS_7-9-22_it3 - EXTENSION MODS 8 - MOD

AutoForm
AutoForm Forming Solver Thermo R10.0.0

Memory: 2068.16 MB

Process - TWB blank manufacture / Heating / Draw / Quenching / Laser Trim

Input Data	Material & Blank

Calculated Material	Usibor2000UFG_100	Calc. Sheet Thickness				1.200 mm
Yield Stress		r0	1.00	r90	1.00	
n-Value		r45	1.00	E-Module		

Blank Info	
☐ Rectangular Blank	
☑ Shaped Blank	
Meshing	
Roll angle	0.00 °
Initial Element Size	20.00 mm
Refinement Level	6
Max Element Angle	30.00 °

Yield Curve

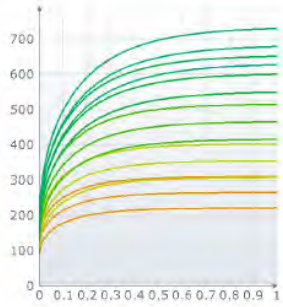

Yield Surface

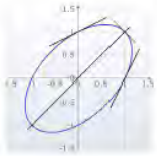

MU - Part to Blank

0.00 %

RAM Tonnage - 691.0 tf

Blank Size - 2980.00 mm X 1942.98 mm

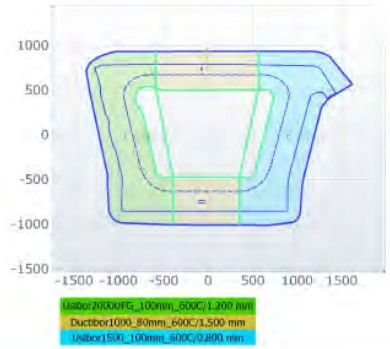

Formability	T-30

Advanced Formability

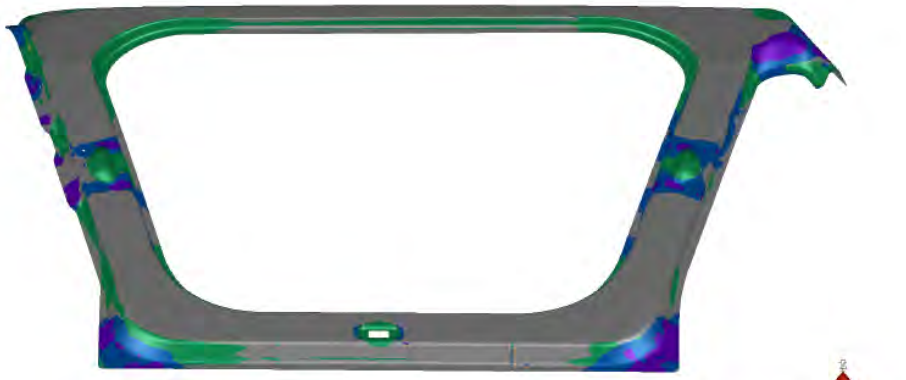

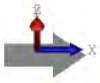

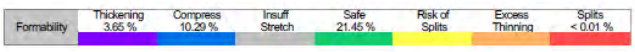

Formability	T-30	

Advanced Formability

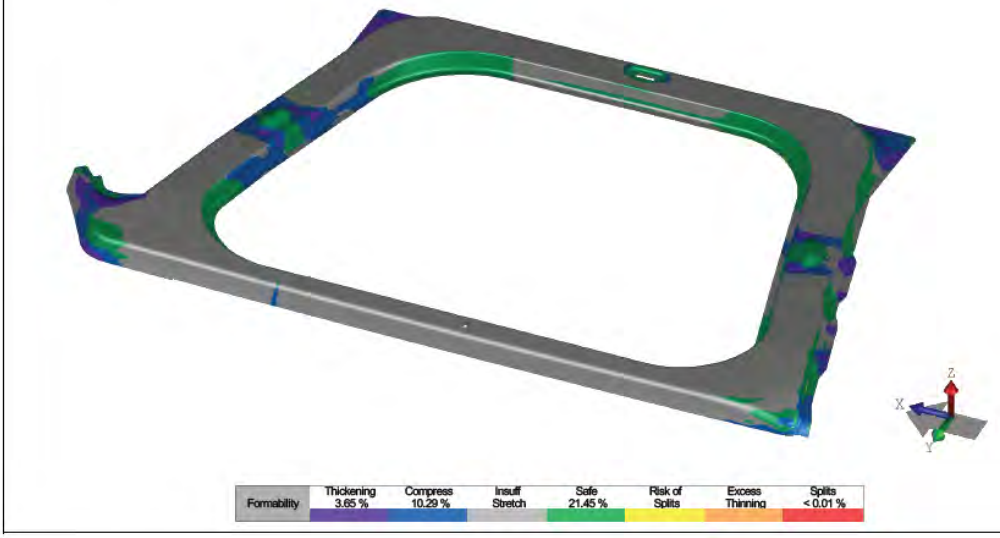

Thinning	T-30	

Thinning

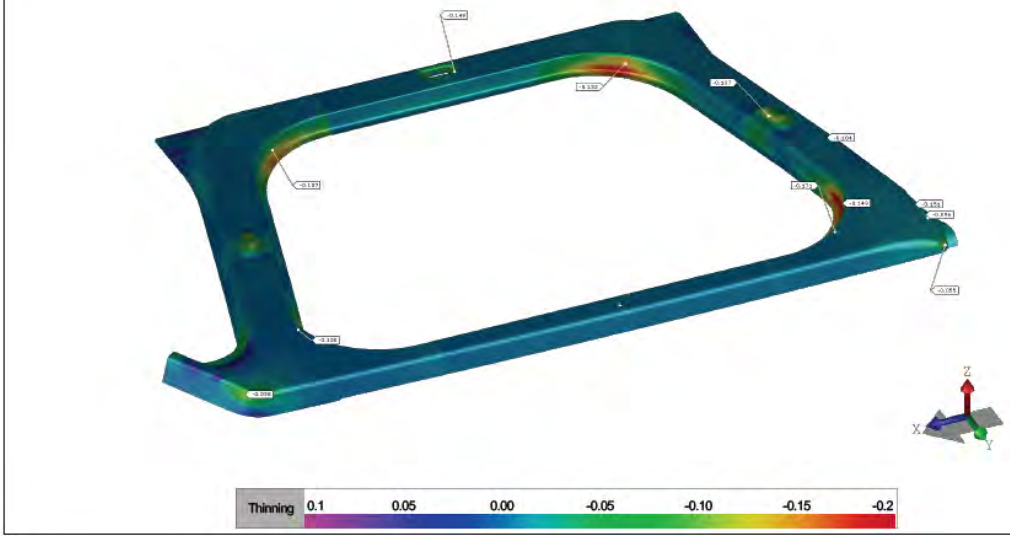

Wrinkling Behavior	H-10
Wrinkling at -34mm	Wrinkling at -22mm
	
Wrinkling at	Wrinkling at
	

Rear Torque Box

Overview and Summary

Part Info

Designation: 03750809 Rear Torque Box | Type: Single Action Draw

Part No.: | Drawing No.:

Nom. / Calculated Material: RA780 - CE

Nom. / Calculated Sheet Thickness: 1.600 mm

Method Info

Method Plan No.:

Drawing No.: | Rev:

Part

Criterion		OK	n OK	Status
FLD	5.2	☑	☐	
Flanging	5.24	☑	☐	
Gravity	5.3	☑	☐	
Closing	5.4	☑	☐	
Forming	5.5	☑	☐	
Thinning	5.6	☑	☐	
Strain	5.7	☑	☐	
Wrinkles	5.8	☑	☐	
Springback	5.9	☑	☐	

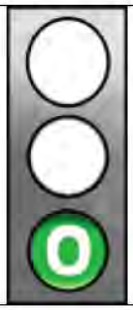

Simulation Info:

Filename:
ARRK_03750809_Rear_Torque_Box_NMS_20-9-22_it9 - EXTENSION MODS 6 - CAD

AutoForm
AutoForm Forming Solver R10.0.0

Memory: 142.44 MB

Process - Blank / Form / Laser Trim / Form / Laser Trim

Input Data — Material & Blank

Calculated Material	RA780 - CE	Calc. Sheet Thickness				1.600 mm
Yield Stress	509.85 MPa	r0	1.00	r90	1.00	
n-Value	0.186	r45	1.00	E-Module	2.10E+05 MPa	

Yield Curve

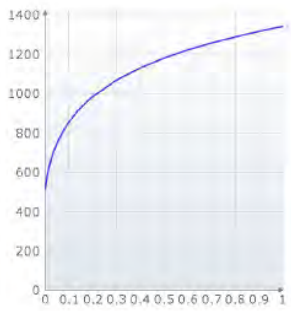

Yield Surface

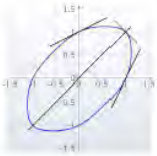

Forming Limit Curve

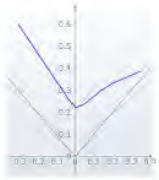

Blank Info

- ☐ Rectangular Blank
- ☑ Shaped Blank

Meshing

Roll angle	0.00 °
Initial Element Size	40.00 mm
Refinement Level	7
Max Element Angle	30.00 °

Formability — F-40

Advanced Formability

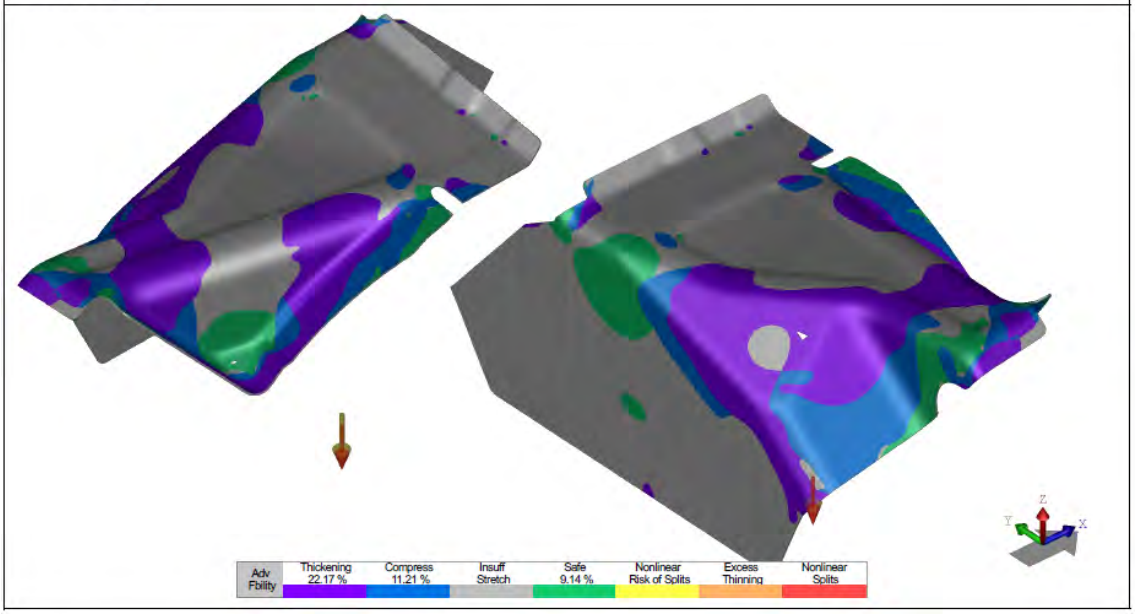

Wrinkling Behavior	D-20

Wrinkling at -234.98 mm	Wrinkling at -94.21 mm
	
Wrinkling at -13.10 mm	**Wrinkling at -1.00 mm**
	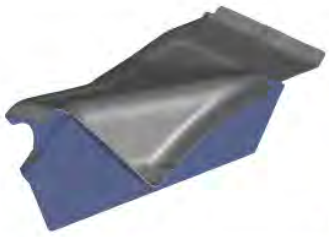

Battery Tray Lower

Overview and Summary

Part Info

Designation: 03647933 - Battery Tray Side	Type:
Part No.:	Drawing No.:
Nom. / Calculated Material: SDSTEEL_CR420-780DP_1.2mm(1)	
Nom. / Calculated Sheet Thickness: 0.700 mm	

Method Info

Method Plan No.:	
Drawing No.:	Rev:

Part

Criterion		OK	n OK	Status
FLD	5.2	☑	☐	
Flanging	5.24	☐	☐	
Gravity	5.3	☑	☐	
Closing	5.4	☑	☐	
Forming	5.5	☑	☐	
Thinning	5.6	☑	☐	
Strain	5.7	☑	☐	
Wrinkles	5.8	☑	☐	
Springback	5.9	☑	☐	

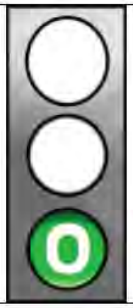

Simulation Info:

Filename: ARRK_03647933_Battery_Tray_Lower_NMS_19-9-22_it5 - EXTENSION MODS 4 -	
AutoForm AutoForm Forming Solver R10.0.0	Memory: 810.42 MB

n

Process - Blank / Draw / Laser Trim

Input Data	Material & Blank

Calculated Material	SDSTEEL_CR420-78	Calc. Sheet Thickness				0.700 mm
Yield Stress	452.85 MPa	r0	0.91	r90	0.82	
n-Value	0.186	r45	0.81	E-Module	2.10E+05 MPa	

Yield Curve

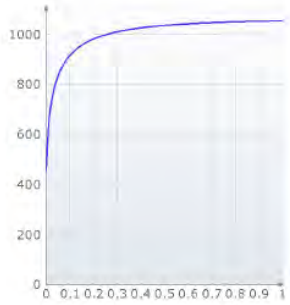

Yield Surface

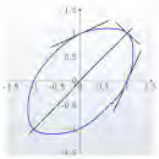

Forming Limit Curve

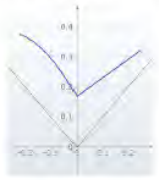

Blank Info	
☑ Rectangular Blank	
☑ Shaped Blank	
Meshing	
Roll angle	0.00 °
Initial Element Size	40.00 mm
Refinement Level	6
Max Element Angle	22.50 °

Blank Size 1680.00 X 1480.00

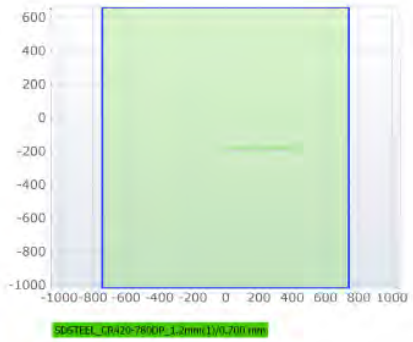

Input Data	D-20

Tool Info			
Meshing Tolerance	0.05 mm		
Process Type	Single Action Draw		
Tool Geometry Refers to	Lower Side of Initial Blank		
Tools	Contact Side	Type	Gap
Die	Upper Side of Blank	Rigid	
Punch	Lower Side of Blank	Rigid	
Binder	Lower Side of Blank	Force Controlled	

Process Data		
Friction Coefficient		
Constant	0.100	
Die - Blank	-	
Punch - Blank	-	
Binder - Blank	-	
Binderforce		
TOTAL TONNAGE	378.5 tf	Half blank so total is x 2
Binderforce/-pressure	250.0 tf	

Tool Geometry 1st opp

Wrinkling Behavior	D-20

Wrinkling at -17.28 mm	Wrinkling at -4.91 mm
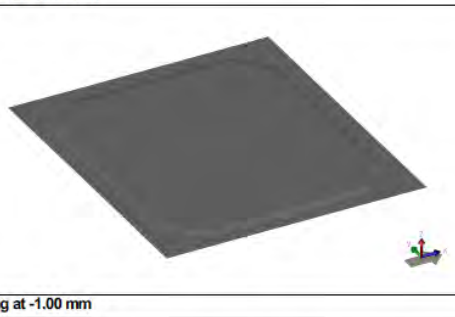	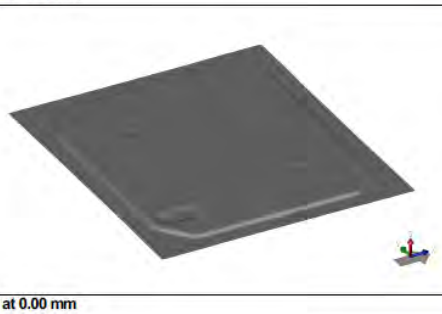
Wrinkling at -1.00 mm	**Wrinkling at 0.00 mm**
	

Battery Frame Longitudinal

Overview and Summary

Part Info

Designation: 03702273_Battery_Longit-LONGITUDIONAL	Type:Crashform Up
Part No.:	Drawing No.:
Nom. / Calculated Material: Dual_Phase_450	
Nom. / Calculated Sheet Thickness: 1.800 mm	

Method Info

Method Plan No.:	
Drawing No.:	Rev:

Part

Criterion		OK	n OK	Status
FLD	5.2	☑	☐	
Flanging	5.24	☑	☐	
Gravity	5.3	☑	☐	
Closing	5.4	☑	☐	
Forming	5.5	☑	☐	
Thinning	5.6	☑	☐	
Strain	5.7	☑	☐	
Wrinkles	5.8	☑	☐	
Springback	5.9	☑	☐	

Simulation Info:

Filename:
ARRK_03702273_Longit_Munich_Left_NMS_14-9-22_it12 - EXTENSION MODS 3 -

AutoForm AutoForm Forming Solver R10.0.0	Memory: 1326.47 MB

Process - Blank Die / Crash / Flange / CAM flange / CAM Flange / Flange Up / CAM Form / CAM Trim

Input Data	Material & Blank

Calculated Material	Dual_Phase_450	Calc. Sheet Thickness				1.800 mm
Yield Stress	271.84 MPa	r0	1.04	r90	1.32	
n-Value	0.220	r45	0.88	E-Module	2.10E+05 MPa	

Yield Curve

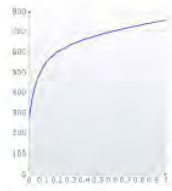

Yield Surface

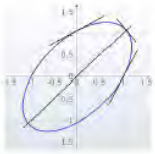

MU - Part to Blank 88.46 %

Forming Limit Curve

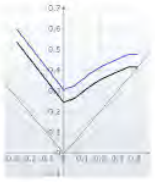

Blank Info

- ☐ Rectangular Blank
- ☑ Shaped Blank

Meshing

Roll angle	0.00 °
Initial Element Size	40.00 mm
Refinement Level	7
Max Element Angle	30.00 °

Blank Size - 1782.59 mm X 367.29 mm

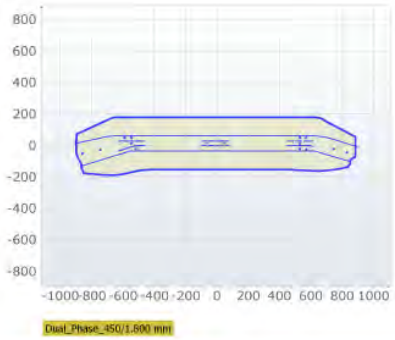

Formability	F-60

Advanced Formability

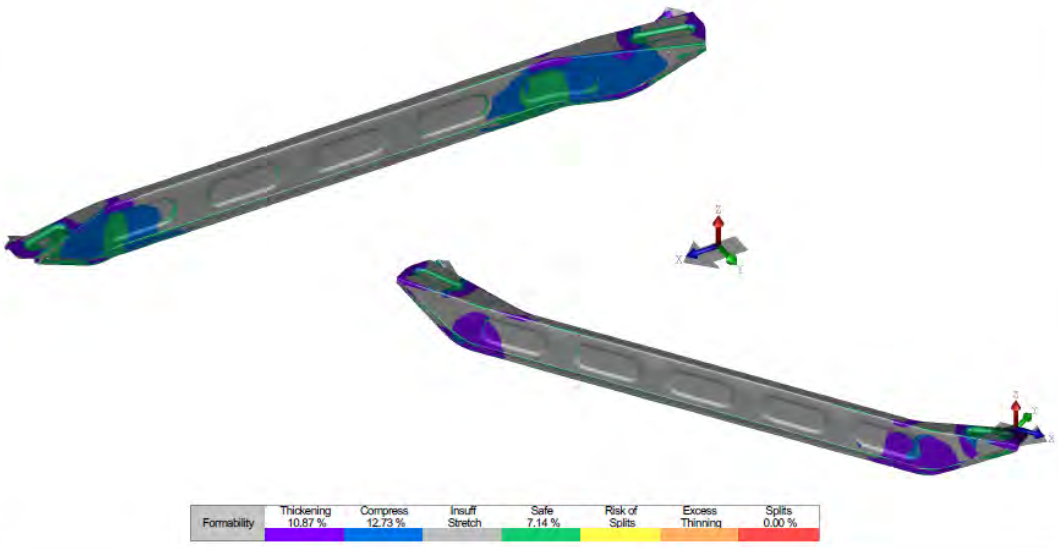

Wrinkling Behavior	F-30
Wrinkling at -1.81 mm	Wrinkling at -2.11 mm
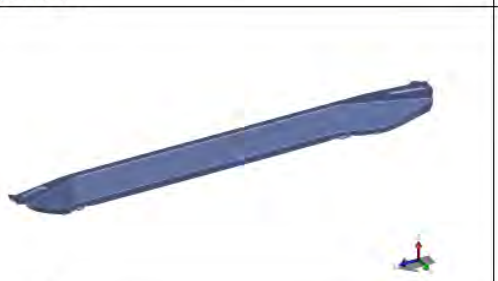	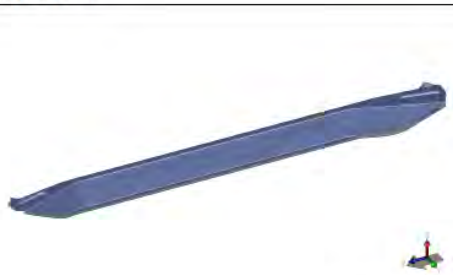
Wrinkling at -1.00 mm	
	

Side (scissor) door rear outer

Overview and Summary

Part Info

Designation	Type: Single Action Draw
Part No.:03750084 Rear Side Door Otr	Drawing No.:
Nom. / Calculated Material: BH280_HD_AF	
Nom. / Calculated Sheet Thickness: 0.700 mm	

Method Info

Method Plan No.:	
Drawing No.:	Rev:

Part

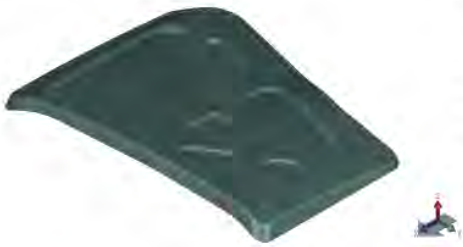

Criterion		OK	n OK	Status
FLD	5.2	☑	☐	
Flanging	5.24	☑	☐	
Gravity	5.3	☑	☐	
Closing	5.4	☑	☐	
Forming	5.5	☑	☐	
Thinning	5.6	☑	☐	
Strain	5.7	☑	☐	
Wrinkles	5.8	☑	☐	
Springback	5.9	☑	☐	

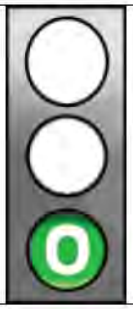

Simulation Info:

Filename:
ARRK_03750084_Side_Rear_Door_Otr_NMS_20-9-22_it1 - EXTENSION MODS 1 -

AutoForm AutoForm Forming Solver R10.0.0	Memory: 4017.68 MB

Process - Blank / Draw / Laser Trim / Flange / Flange

Input Data	Material & Blank

Calculated Material	BH280_HD_AF	Calc. Sheet Thickness				0.700 mm
Yield Stress	294.74 MPa	r0	1.12	r90	1.35	
n-Value	0.159	r45	1.34	E-Module	2.10E+05 MPa	

Yield Curve

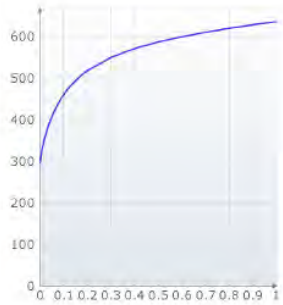

Yield Surface

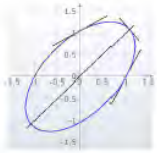

Forming Limit Curve

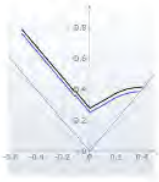

Blank Info

- ☐ Rectangular Blank
- ☑ Shaped Blank

Meshing

Roll angle	0.00 °
Initial Element Size	40.00 mm
Refinement Level	6
Max Element Angle	22.50 °

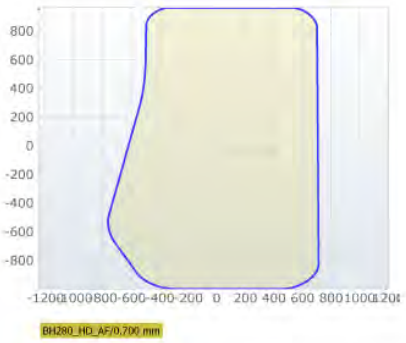

Input Data	D-20	D-20

Tool Info

Meshing Tolerance	0.05 mm		
Process Type	Single Action Draw		
Tool Geometry Refers to	Upper Side of Initial Blank		
Tools	Contact Side	Type	Gap
Die	Upper Side of Blank	Rigid	
Punch	Lower Side of Blank	Rigid	
Binder	Lower Side of Blank	Force Controlled	

Process Data

Friction Coefficient		
Constant	0.110	
Die - Blank	-	
Punch - Blank	-	
Binder - Blank	-	
Binderforce		
RAM	606.5 tf	
Binderforce/-pressure	280.0 tf	

Tool Geometry 1st opp

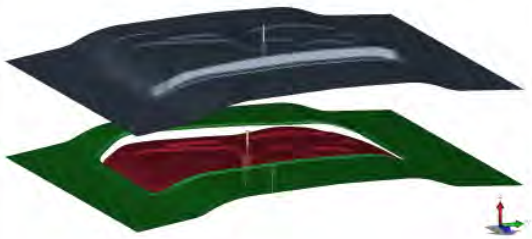

Formability	D-20	

Advanced Formability

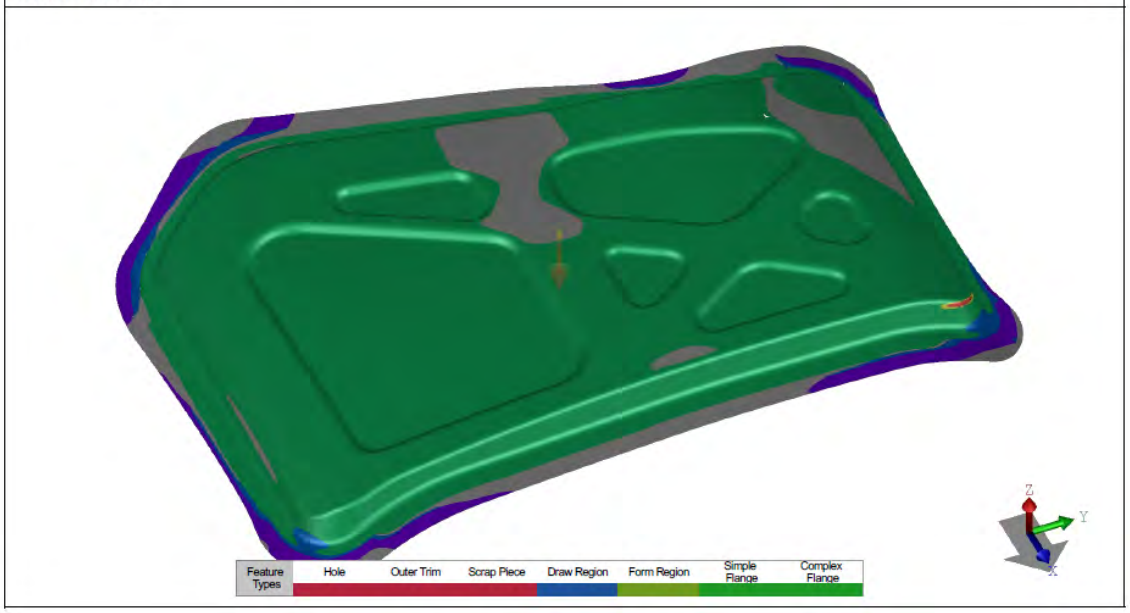

Thinning	D-20	

Thinning

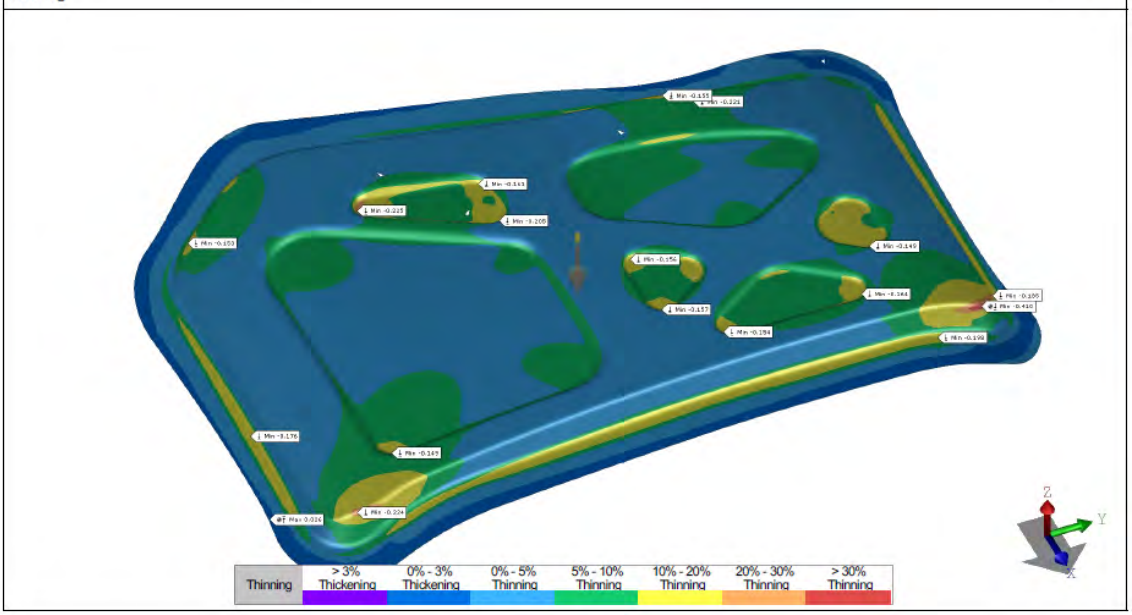

Wrinkles	D-20	

Wrinkles

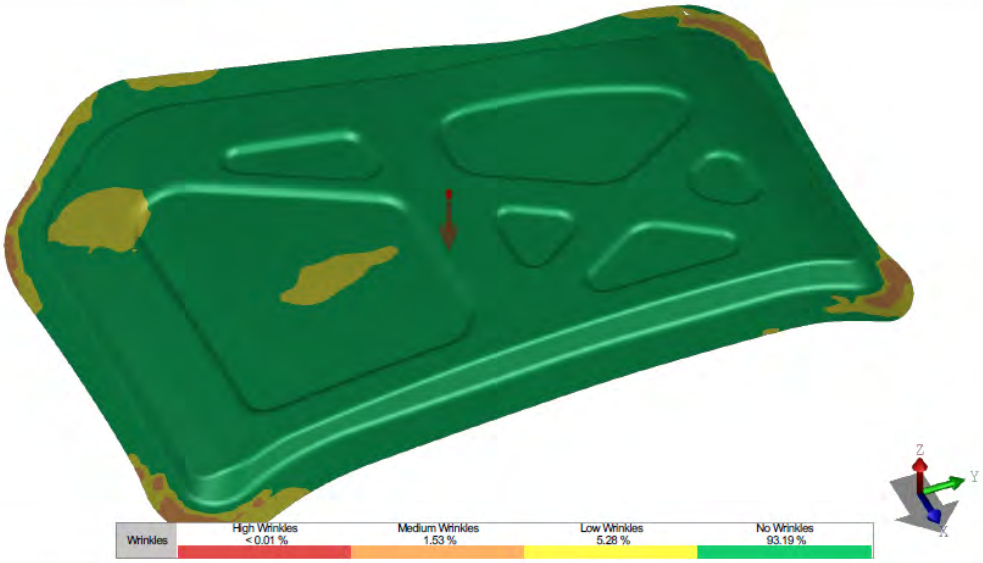

Wrinkling Behavior	D-20	

Wrinkling at -50.61 mm

Wrinkling at -27.61 mm

Wrinkling at -13.98 mm

Wrinkling at -4.64 mm

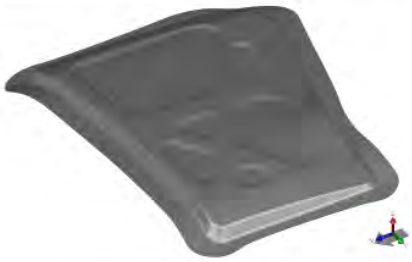

Side (scissor) door rear inner

Overview and Summary

Part Info

Designation: 30082022_DS-WAS-1430_SCISSOR DOOR	Type: Single Action Draw
Part No.:	Drawing No.:
Nom. / Calculated Material: DX56D	
Nom. / Calculated Sheet Thickness: 1.200 mm	

Method Info

Method Plan No.:	
Drawing No.:	Rev:

Part

Criterion		OK	n OK	Status
FLD	5.2	☑	☐	
Flanging	5.24	☐	☑	
Gravity	5.3	☑	☐	
Closing	5.4	☑	☐	
Forming	5.5	☑	☐	
Thinning	5.6	☑	☑	
Strain	5.7	☑	☐	
Wrinkles	5.8	☑	☐	
Springback	5.9	☑	☐	

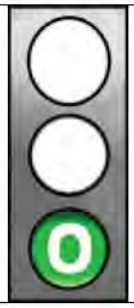

Simulation Info:

Filename:
ARRK_03750471_Side_Frt_Door_Inr_NMS_2-9-22_it2 - EXTENSION MODS 2 -

AutoForm AutoForm Forming Solver R10.0.0	Memory: 1322.95 MB

Process - Draw / Laser Trim / Flange / CAM Form

Input Data — Material & Blank

Calculated Material	DX56D	Calc. Sheet Thickness			1.200 mm
Yield Stress	157.05 MPa	r0	2.05	r90	2.50
n-Value	0.226	r45	1.73	E-Module	2.10E+05 MPa

Yield Curve

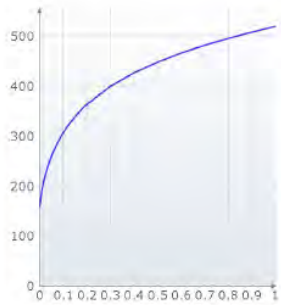

Yield Surface

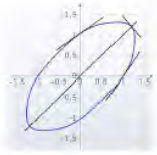

Forming Limit Curve

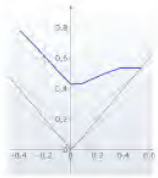

MU - Part to Blank

58.26 %

Blank Info

☐ Rectangular Blank

☑ Shaped Blank

Meshing

Roll angle	0.00 °
Initial Element Size	40.00 mm
Refinement Level	6
Max Element Angle	22.50 °

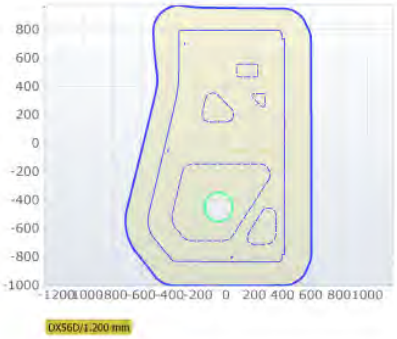

Input Data	D-20	D-20

Tool Info			
Meshing Tolerance	0.05 mm		
Process Type	Single Action Draw		
Tool Geometry Refers to	Lower Side of Initial Blank		
Tools	Contact Side	Type	Gap
Die	Upper Side of Blank	Rigid	
Punch	Lower Side of Blank	Rigid	
Binder	Lower Side of Blank	Force Controlled	

Process Data		
Friction Coefficient		
Constant	0.100	
Die - Blank	-	
Punch - Blank	-	
Binder - Blank	-	
Binderforce		
RAM	661.2 tf	
Binderforce/-pressure	201.3 tf	

Tool Geometry 1st opp

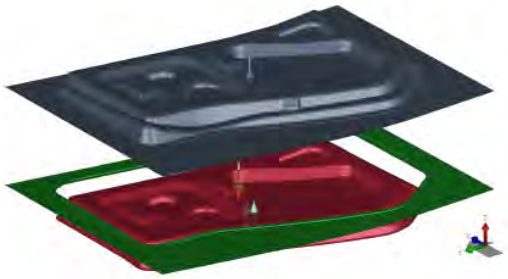

Tool Geometry 2nd opp

Tool Geometry 3rd opp

Formability	F-50

Advanced Formability

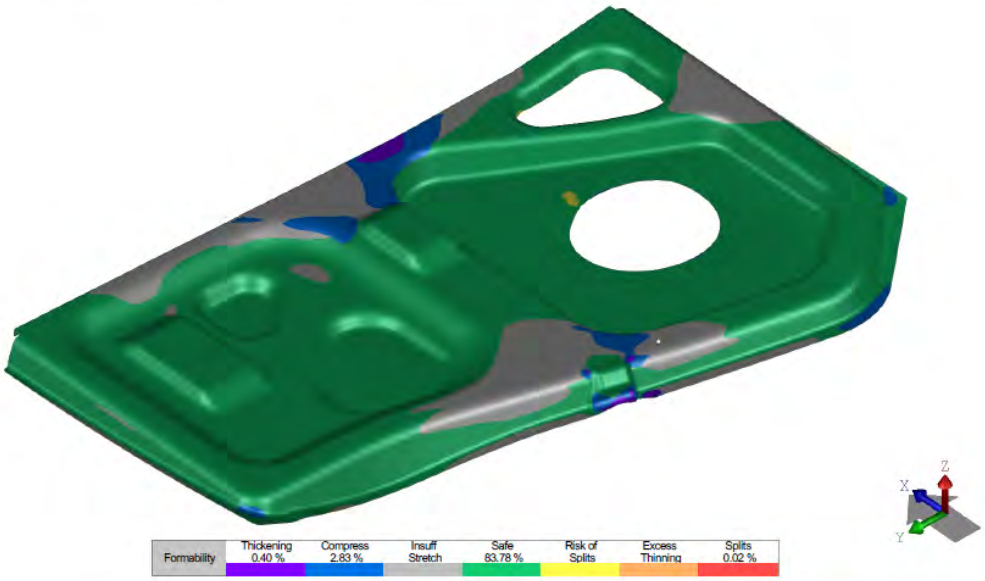

Thinning	F-50	

Thinning

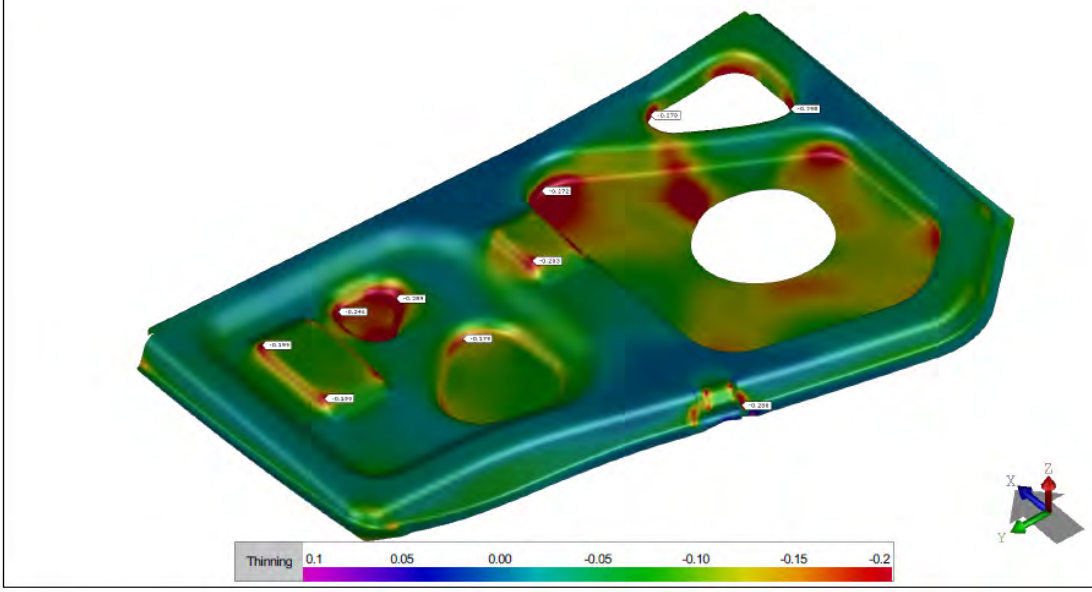

Wrinkles	F-50	

Wrinkles

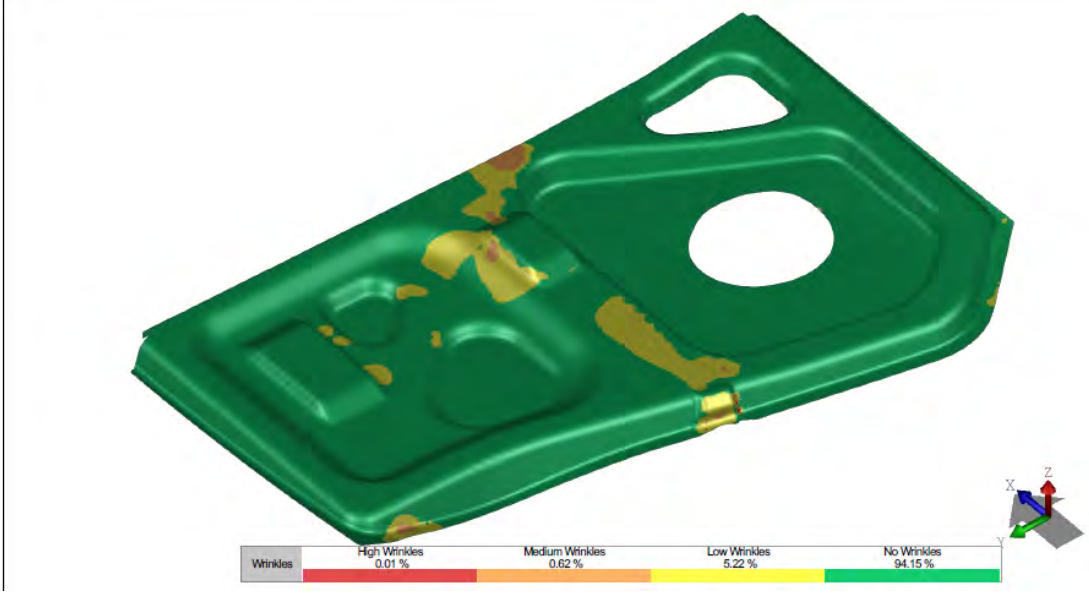

Wrinkling Behavior	D-20

Wrinkling at -58.73 mm

Wrinkling at -28.03 mm

Wrinkling at -11.07 mm

Wrinkling at -1.00 mm

Side (scissor) door outer front

Overview and Summary

Part Info

Designation:	Type:
30082022_DS-WAS-1430_SCISSOR DOOR	Single Action Draw
Part No.:	Drawing No.:
Nom. / Calculated Material: BH280_HD_AF	
Nom. / Calculated Sheet Thickness: 0.700 mm	

Method Info

Method Plan No.:	
Drawing No.:	Rev:

Part

Criterion		OK	n OK	Status
FLD	5.2	☑	☐	
Flanging	5.24	☑	☐	
Gravity	5.3	☑	☐	
Closing	5.4	☑	☐	
Forming	5.5	☑	☐	
Thinning	5.6	☑	☐	
Strain	5.7	☑	☐	
Wrinkles	5.8	☑	☐	
Springback	5.9	☑	☐	

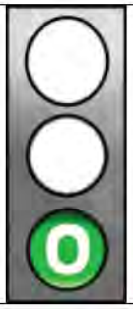

Simulation Info:

Filename:
ARRK_03750465_Side_Frt_Door_Otr_NMS_6-9-22_it2 - EXTENSION MODS 3 -

AutoForm AutoForm Forming Solver R10.0.0	Memory: 3901.13 MB

Process - Blank / Draw / Laser Trim / Flange / Flange

Input Data	Material & Blank

Calculated Material	BH280_HD_AF	Calc. Sheet Thickness				0.700 mm
Yield Stress	294.74 MPa	r0	1.12	r90	1.35	
n-Value	0.159	r45	1.34	E-Module	2.10E+05 MPa	

Yield Curve

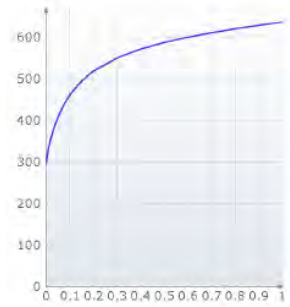

Yield Surface

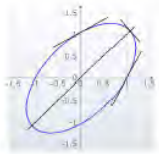

Forming Limit Curve

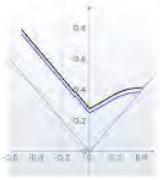

MU - Part to Blank

50.50 %

Blank Info

- ☐ Rectangular Blank
- ☑ Shaped Blank

Meshing

Roll angle	0.00 °
Initial Element Size	40.00 mm
Refinement Level	6
Max Element Angle	22.50 °

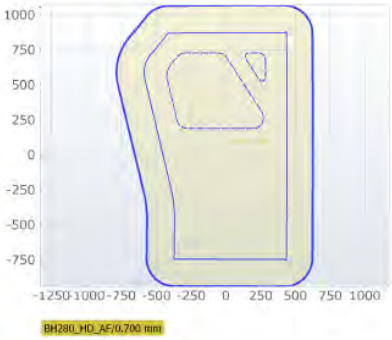

Input Data	D-20	D-20

Tool Info

Meshing Tolerance	0.05 mm		
Process Type	Single Action Draw		
Tool Geometry Refers to	Upper Side of Initial Blank		
Tools	Contact Side	Type	Gap
Die	Upper Side of Blank	Rigid	
Punch	Lower Side of Blank	Rigid	
Binder	Lower Side of Blank	Force Controlled	

Process Data

Friction Coefficient		
Constant	0.110	
Die - Blank	-	
Punch - Blank	-	
Binder - Blank	-	
Binderforce		
RAM	619.6 tf	
Binderforce/-pressure	280.0 tf	

Tool Geometry 1st opp

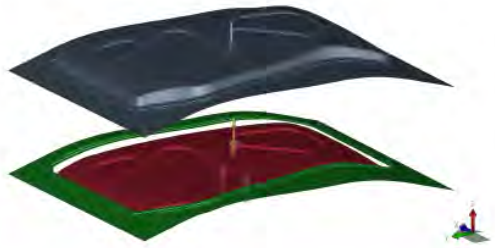

Formability	F-50	

Advanced Formability

Thinning	F-50	

Thinning

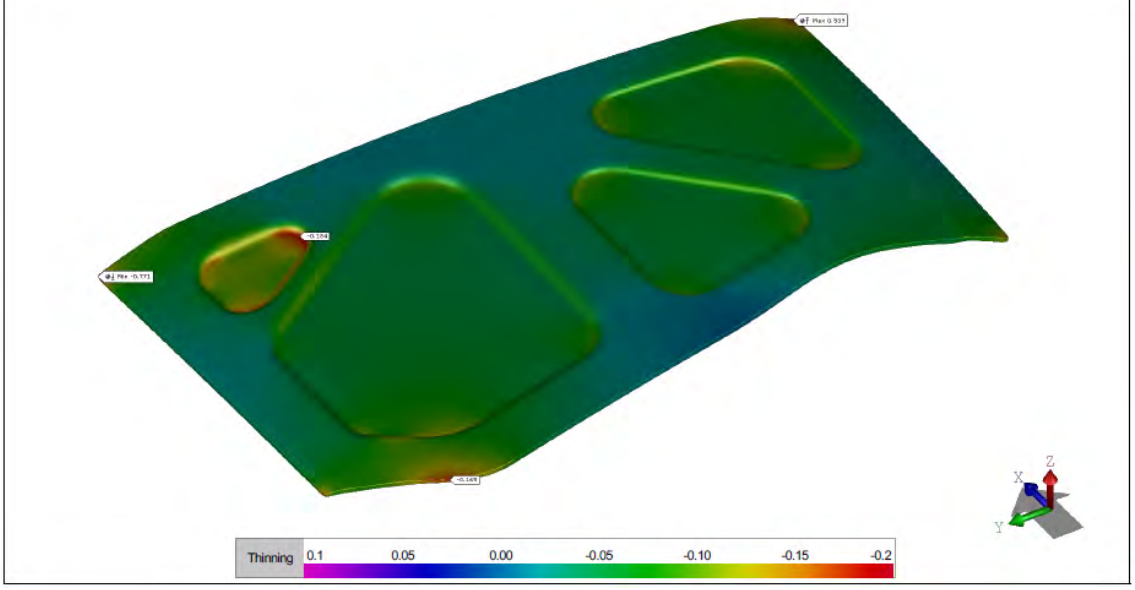

Wrinkling Behavior	D-20

Wrinkling at -50.24 mm	Wrinkling at -18.13 mm
	
Wrinkling at -5.32 mm	**Wrinkling at -0.50 mm**
	

Side (scissor) door front inner

Overview and Summary

Part Info

Designation:	Type:
30082022_DS-WAS-1430_SCISSOR DOOR	Single Action Draw
Part No.:	Drawing No.:

Nom. / Calculated Material: DX56D

Nom. / Calculated Sheet Thickness: 1.200 mm

Method Info

Method Plan No.:

Drawing No.:	Rev:

Part

Criterion		OK	n OK	Status
FLD	5.2	☑	☐	
Flanging	5.24	☐	☑	
Gravity	5.3	☑	☐	
Closing	5.4	☑	☐	
Forming	5.5	☑	☐	
Thinning	5.6	☑	☑	
Strain	5.7	☑	☐	
Wrinkles	5.8	☑	☐	
Springback	5.9	☑	☐	

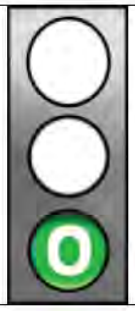

Simulation Info:

Filename:
ARRK_03750471_Side_Frt_Door_Inr_NMS_2-9-22_it2 - EXTENSION MODS 2 -

AutoForm	Memory: 1322.95 MB
AutoForm Forming Solver R10.0.0	

Process - Draw / Laser Trim / Flange / CAM Form

Input Data	Material & Blank

Calculated Material	DX56D	Calc. Sheet Thickness				1.200 mm
Yield Stress	157.05 MPa	r0	2.05	r90	2.50	
n-Value	0.226	r45	1.73	E-Module	2.10E+05 MPa	

Yield Curve

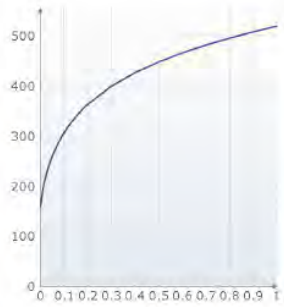

Yield Surface

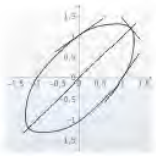

Forming Limit Curve

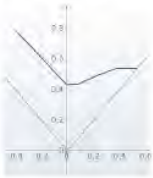

MU - Part to Blank

58.26 %

Blank Info

- ☐ Rectangular Blank
- ☑ Shaped Blank

Meshing

Roll angle	0.00 °
Initial Element Size	40.00 mm
Refinement Level	6
Max Element Angle	22.50 °

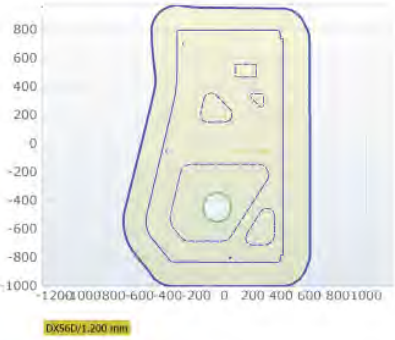

Input Data	D-20	D-20

Tool Info

Meshing Tolerance	0.05 mm		
Process Type	Single Action Draw		
Tool Geometry Refers to	Lower Side of Initial Blank		
Tools	Contact Side	Type	Gap
Die	Upper Side of Blank	Rigid	
Punch	Lower Side of Blank	Rigid	
Binder	Lower Side of Blank	Force Controlled	

Process Data

Friction Coefficient		
Constant	0.100	
Die - Blank	-	
Punch - Blank	-	
Binder - Blank	-	
Binderforce		
RAM	661.2 tf	
Binderforce/-pressure	201.3 tf	

Tool Geometry 1st opp

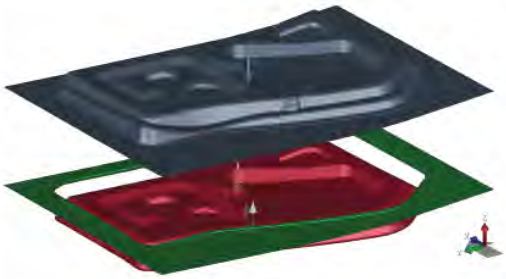

Tool Geometry 2nd opp

Tool Geometry 3rd opp

Formability	F-50	

Advanced Formability

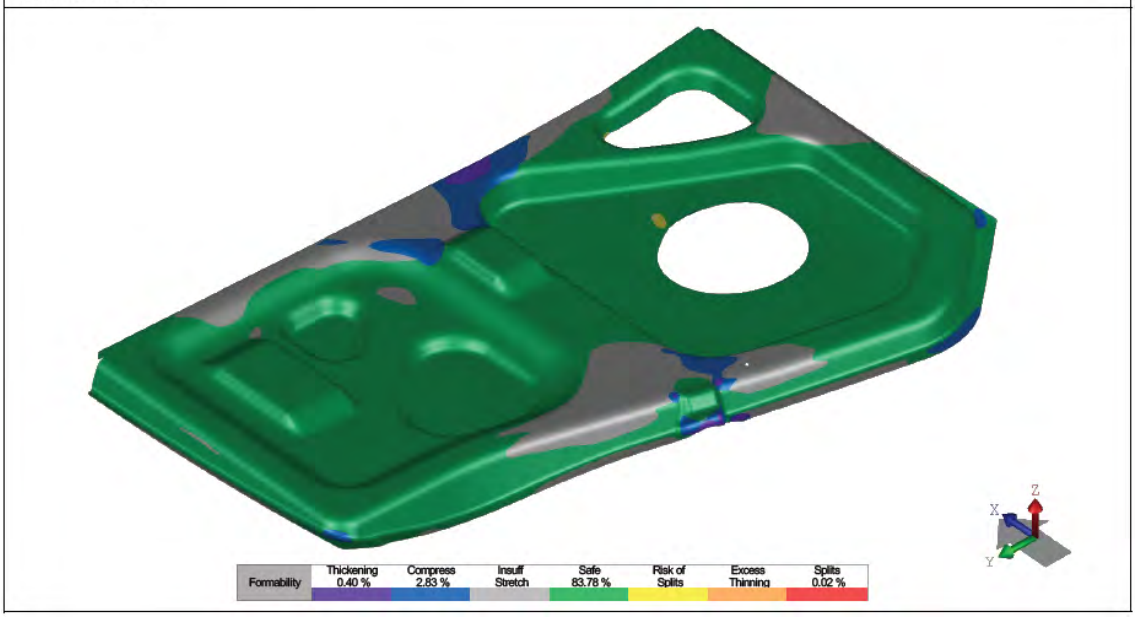

Thinning	F-50	

Thinning

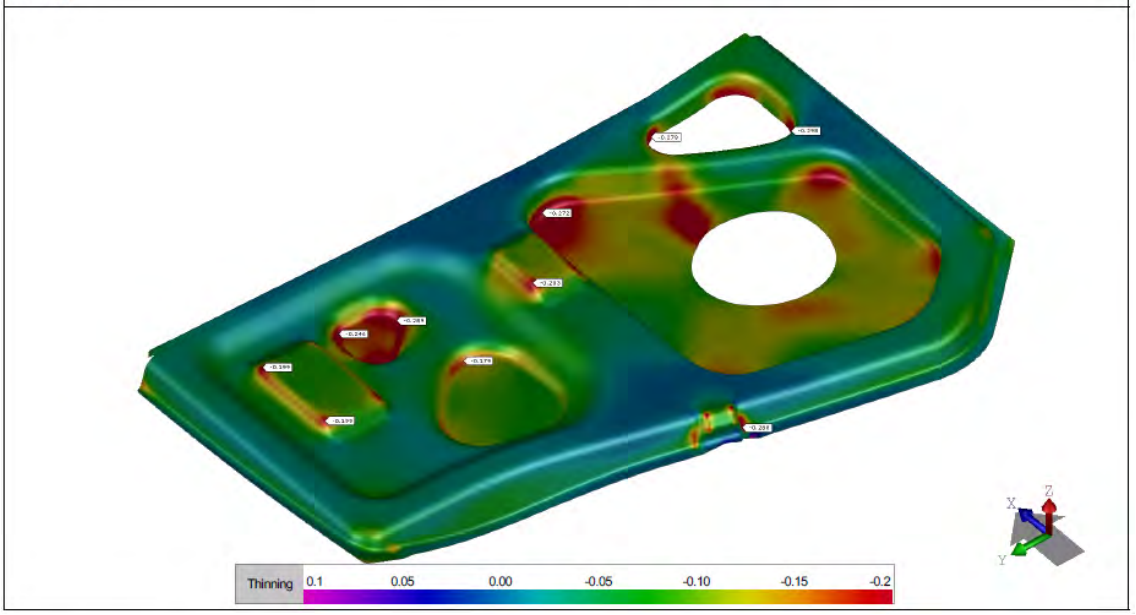

Wrinkling Behavior	D-20	

Wrinkling at -58.73 mm	Wrinkling at -28.03 mm
	
Wrinkling at -11.07 mm	**Wrinkling at -1.00 mm**
	

Coach Door Outer

Overview and Summary

Part Info

Designation: 03777906-A-Surface Coach Door Sheet
Type:
Part No.:
Drawing No.:
Nom. / Calculated Material: BH280_HD_AF
Nom. / Calculated Sheet Thickness: 0.700 mm

Method Info

Method Plan No.:
Drawing No.:
Rev:

Part

Criterion		OK	n OK	Status
FLD	5.2	☑	☐	
Flanging	5.24	☑	☐	
Gravity	5.3	☑	☐	
Closing	5.4	☑	☐	
Forming	5.5	☑	☐	
Thinning	5.6	☑	☐	
Strain	5.7	☐	☑	
Wrinkles	5.8	☑	☐	
Springback	5.9	☑	☐	

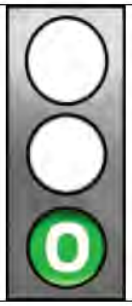

Simulation Info:

Filename:
ARRK_03777906_Coach_Door_Outer_NMS_19-8-22_it2 - EXTENSION MODS 2 - INC

AutoForm
AutoForm Forming Solver R10.0.0
Memory: 4434.52 MB

Process - Blank Die / Draw / Laser Trim / Flange

Input Data	Material & Blank

Calculated Material	BH280_HD_AF	Calc. Sheet Thickness				0.700 mm
Yield Stress	294.74 MPa	r0	1.12	r90	1.35	
n-Value	0.159	r45	1.34	E-Module	2.10E+05 MPa	

Blank Info

- ☐ Rectangular Blank
- ☑ Shaped Blank

Meshing

Roll angle	0.04 °
Initial Element Size	20.00 mm
Refinement Level	6
Max Element Angle	22.50 °

Yield Curve

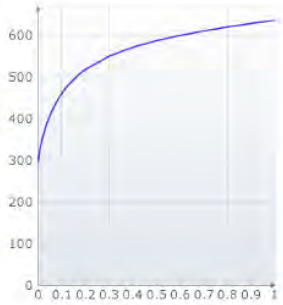

Yield Surface

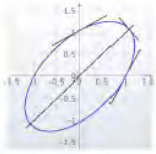

Forming Limit Curve

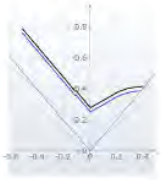

MU - Part to Blank

59.20 %

Blank size 1312.80 X 1939.59

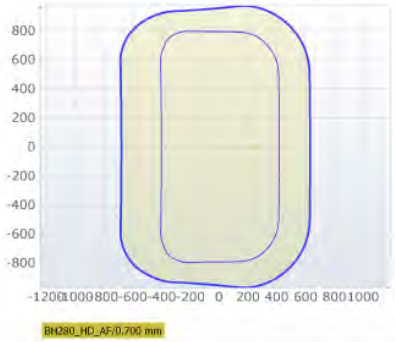

Input Data	D-20

Tool Info

Meshing Tolerance	0.05 mm		
Process Type	Single Action Draw		
Tool Geometry Refers to	Upper Side of Initial Blank		
Tools	Contact Side	Type	Gap
Die	Upper Side of Blank	Rigid	
Punch	Lower Side of Blank	Rigid	
Binder	Lower Side of Blank	Force Controlled	

Process Data

Friction Coefficient		
Constant	0.100	
Die - Blank	-	
Punch - Blank	-	
Binder - Blank	-	
Binderforce		
RAM	599.3 tf	
Binderforce/-pressure	300.0 tf	

Tool Geometry 1st opp

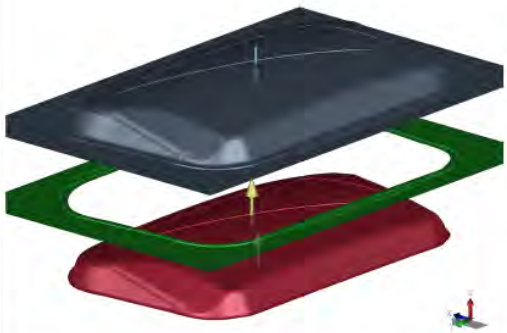

Tool Geometry 2nd opp

Formability	F-40	

Advanced Formability

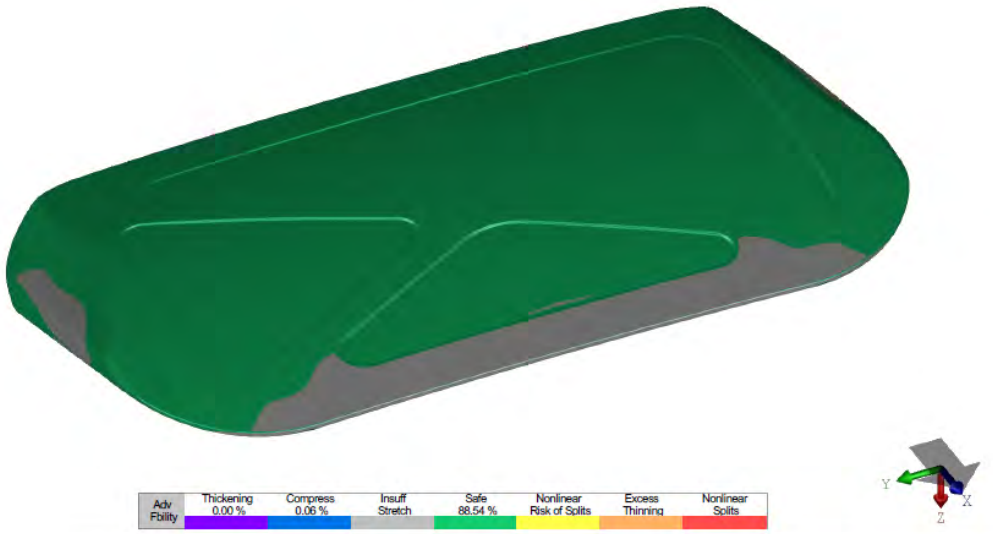

Wrinkling Behavior	D-20	

Wrinkling at

Wrinkling at

Wrinkling at

Wrinkling at

Springback	M-50	
Springback		

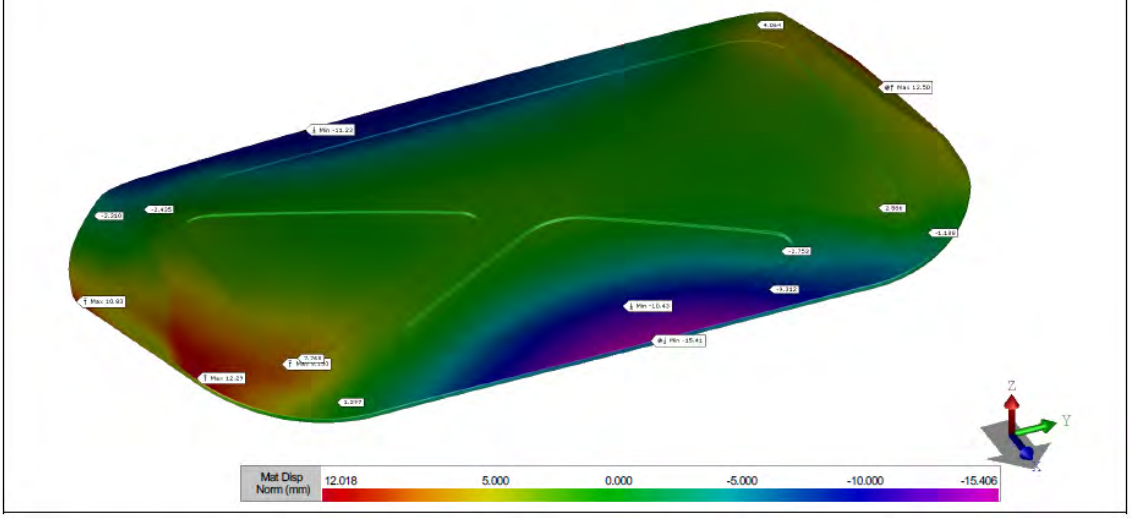

Coach door inner

Overview and Summary

Part Info

Designation:	Type:
Part No.:	Drawing No.:
Nom. / Calculated Material: DX56D	
Nom. / Calculated Sheet Thickness: 1.200 mm	

Method Info

Method Plan No.:	
Drawing No.:	Rev:

Part

Criterion		OK	n OK
FLD	5.2	☑	☐
Flanging	5.24	☑	☐
Gravity	5.3	☑	☐
Closing	5.4	☑	☐
Forming	5.5	☑	☐
Thinning	5.6	☑	☐
Strain	5.7	☑	☐
Wrinkles	5.8	☑	☐
Springback	5.9	☑	☐

Status

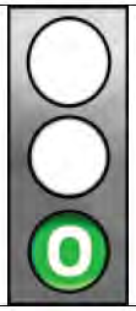

Simulation Info:

Filename:
ARRK_03777910_Coach_Door_Inner_NMS_19-9-22_it5 - EXTENSION MODS 5 - CAD

AutoForm AutoForm Forming Solver R10.0.0	Memory: 1160.17 MB

Remarks: Changes implemented worked well.

Process - Blank / Draw / Laser Trim / Form Up

Input Data	Material & Blank

Calculated Material	DX56D	Calc. Sheet Thickness				1.200 mm
Yield Stress	157.05 MPa	r0	2.05	r90	2.50	
n-Value	0.226	r45	1.73	E-Module	2.10E+05 MPa	

Blank Info

- ☐ Rectangular Blank
- ☑ Shaped Blank

Meshing

Roll angle	0.00 °
Initial Element Size	40.00 mm
Refinement Level	6
Max Element Angle	22.50 °

Yield Curve

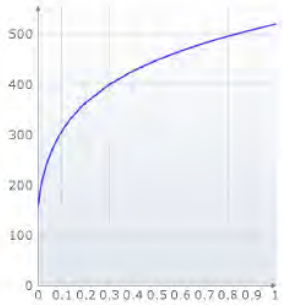

Yield Surface

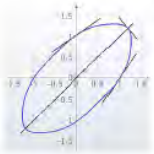

Forming Limit Curve

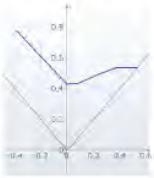

Blank size 1131.64 X 2031.05

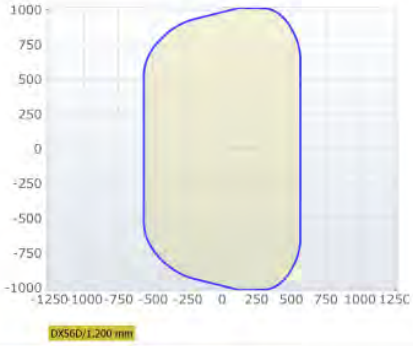

Input Data	D-20

Tool Info

Meshing Tolerance	0.05 mm		
Process Type	Single Action Draw		
Tool Geometry Refers to	Lower Side of Initial Blank		
Tools	Contact Side	Type	Gap
Die	Upper Side of Blank	Rigid	
Punch	Lower Side of Blank	Rigid	
Binder	Lower Side of Blank	Force Controlled	

Process Data

Friction Coefficient		
Constant	0.100	
Die - Blank	-	
Punch - Blank	-	
Binder - Blank	-	
Binderforce		
RAM	581.0 tf	
Binderforce/-pressure	218.9 tf	

Tool Geometry 1st opp

Formability	D-20	

Advanced Formability

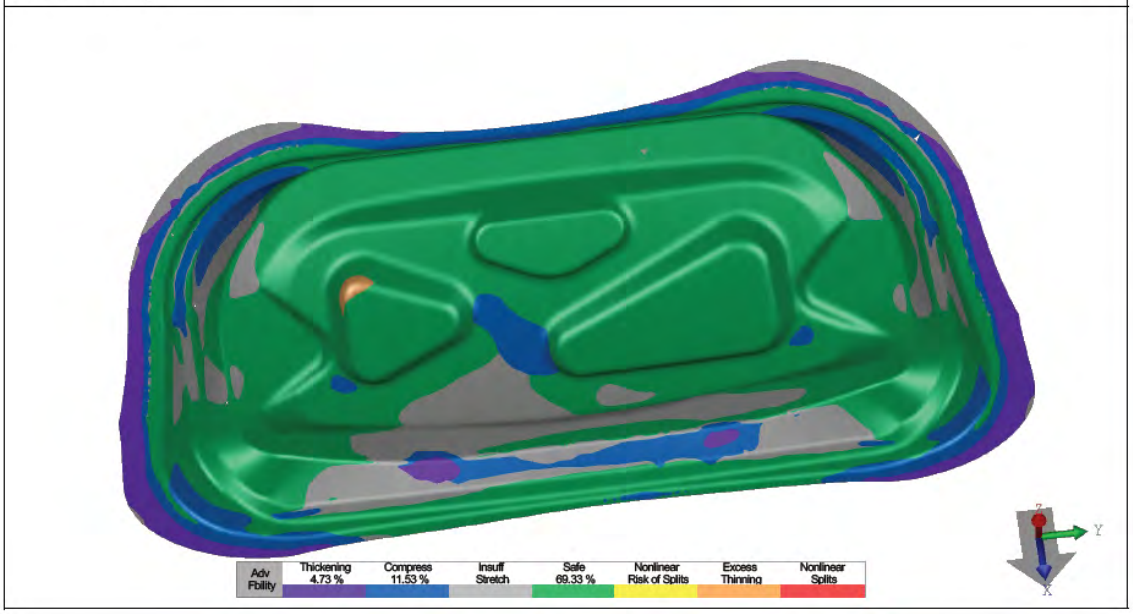

Wrinkling Behavior	D-20	

Wrinkling at 90mm To Bottom

Wrinkling at 61mm To Bottom

Wrinkling at 23mm To Bottom

Wrinkling at 5mm To Bottom

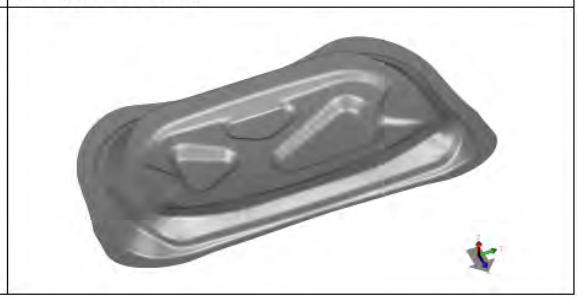

Appendix 2.2 SEM1 BIW section profiles

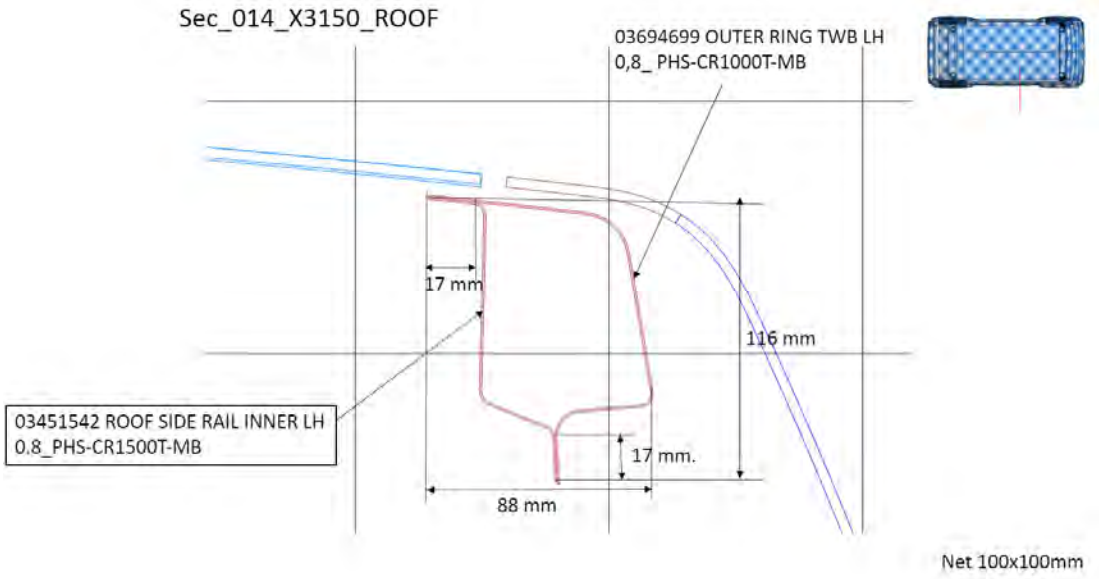

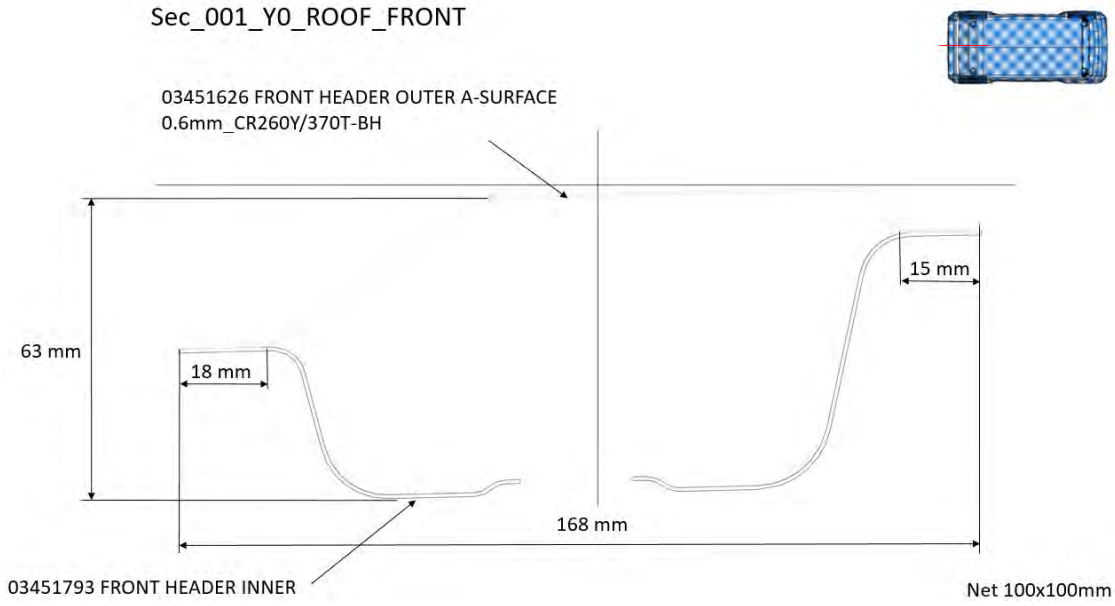

Sec_001_Y0_ROOF_REAR

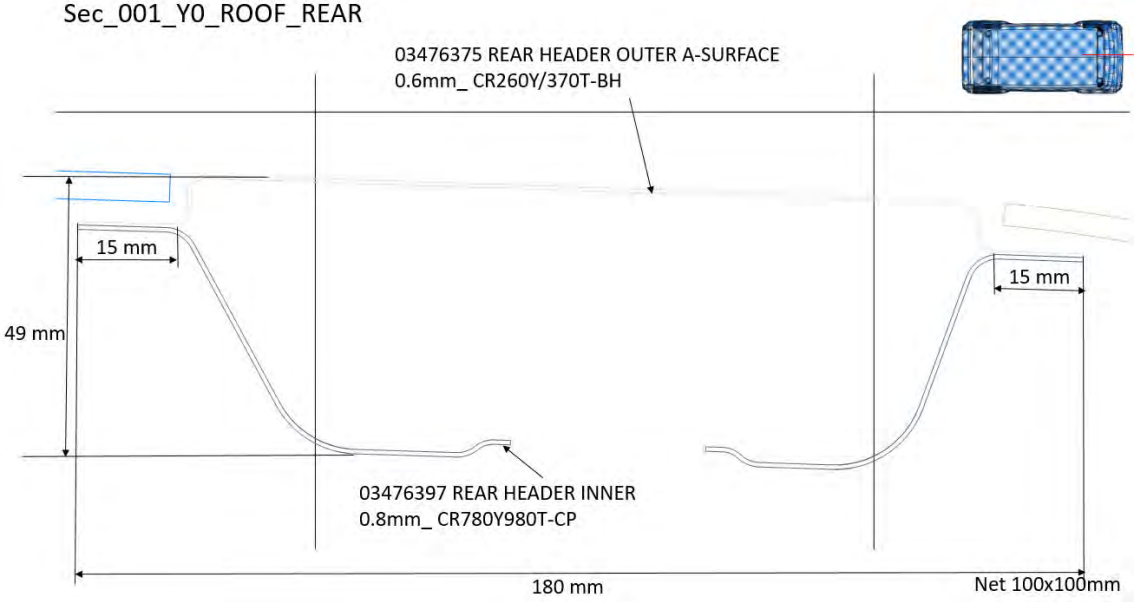

Sec_003_Y_-505_SECTION FRONT CRASH

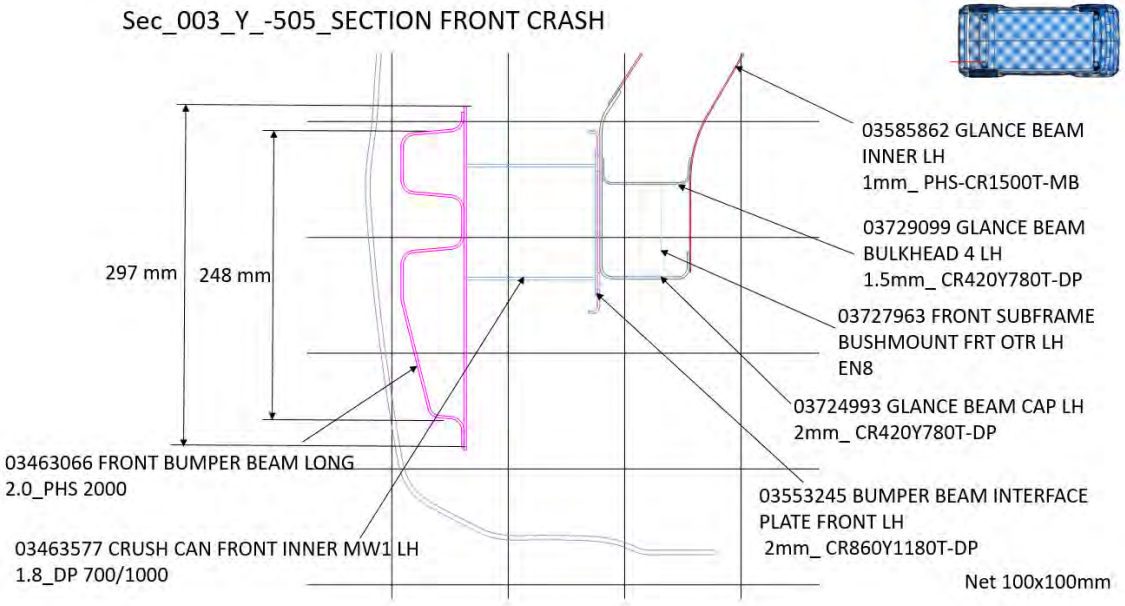

Sec_004_Y_-405_SECTION REAR CRASH

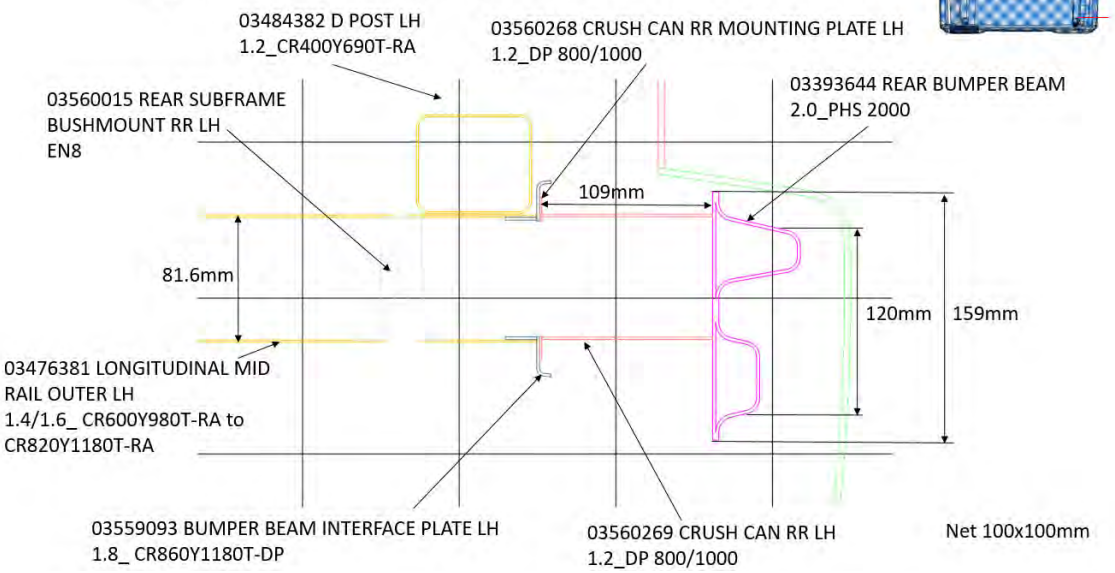

Sec_005_Y_-505_SECTION BATTERY FRONT

Sec_028_Z1341.7_LOWER_HINGE

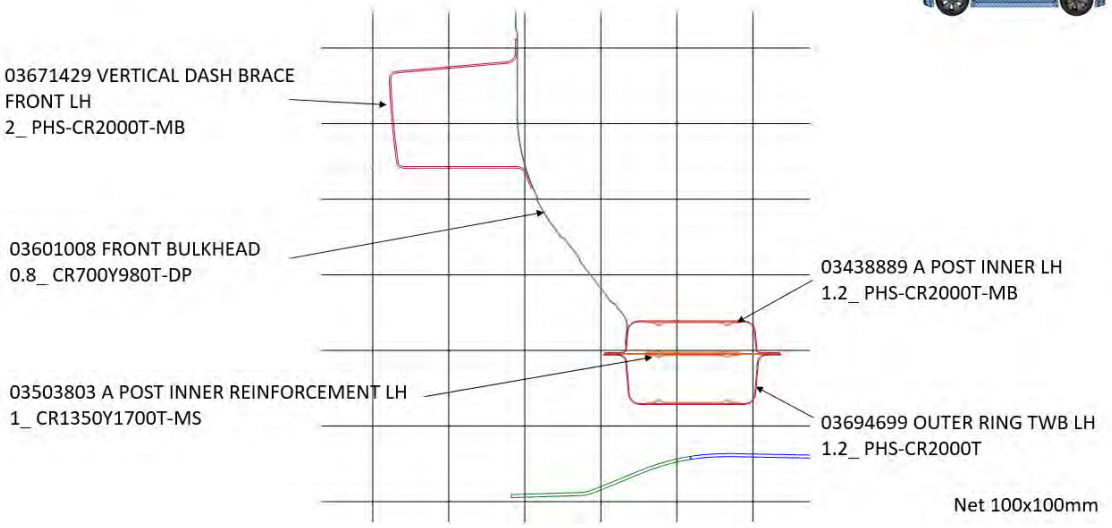

Sec_028_Z1341.7_LOWER_HINGE_REAR

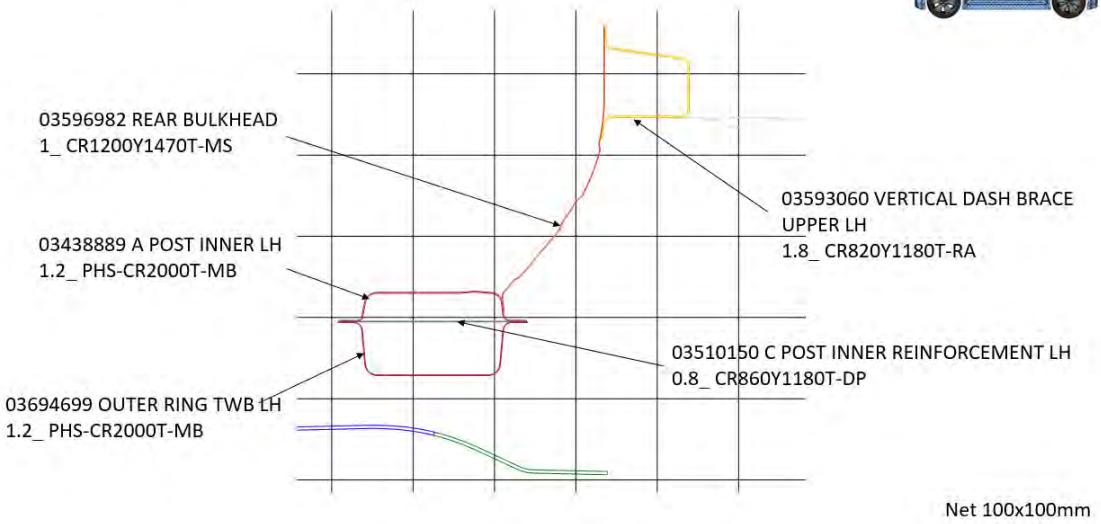

Sec_026_Z1641.7_UPPER_HINGE_FRONT

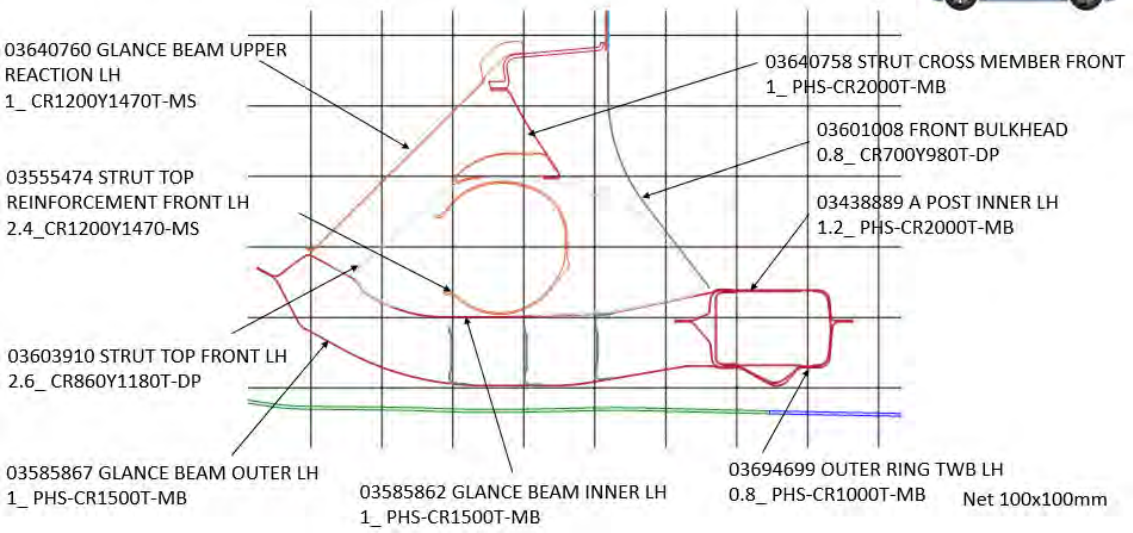

Radial_ Section_D-Pillar

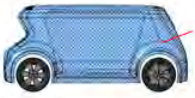

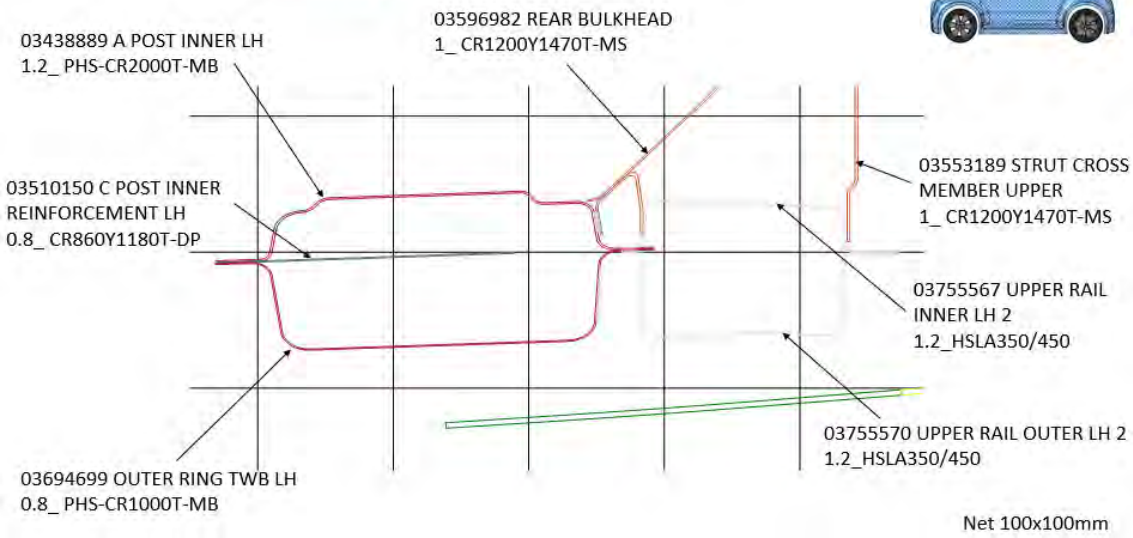

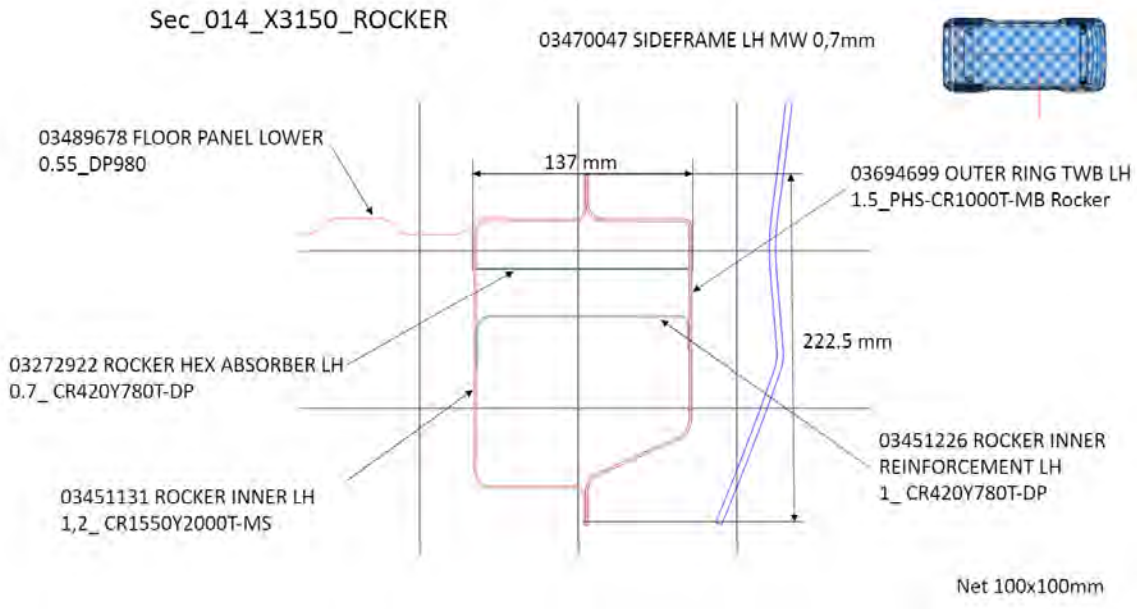
Sec_014_X3150_ROCKER
03470047 SIDEFRAME LH MW 0,7mm
03489678 FLOOR PANEL LOWER
0.55_DP980
137 mm
03694699 OUTER RING TWB LH
1.5_PHS-CR1000T-MB Rocker
222.5 mm
03272922 ROCKER HEX ABSORBER LH
0.7_ CR420Y780T-DP
03451226 ROCKER INNER
REINFORCEMENT LH
1_ CR420Y780T-DP
03451131 ROCKER INNER LH
1,2_ CR1550Y2000T-MS
Net 100x100mm

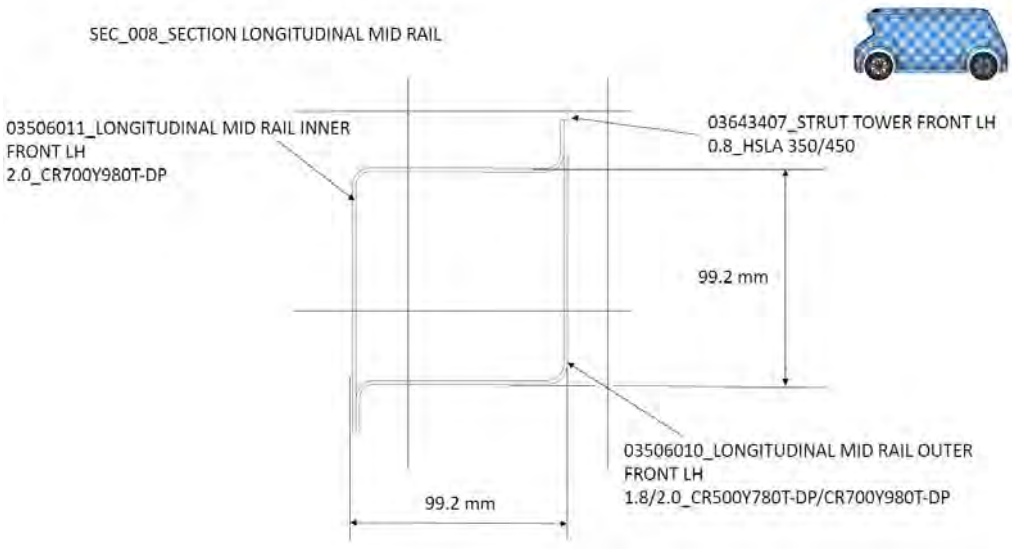
SEC_008_SECTION LONGITUDINAL MID RAIL
03506011_LONGITUDINAL MID RAIL INNER
FRONT LH
2.0_CR700Y980T-DP
03643407_STRUT TOWER FRONT LH
0.8_HSLA 350/450
99.2 mm
03506010_LONGITUDINAL MID RAIL OUTER
FRONT LH
1.8/2.0_CR500Y780T-DP/CR700Y980T-DP
99.2 mm

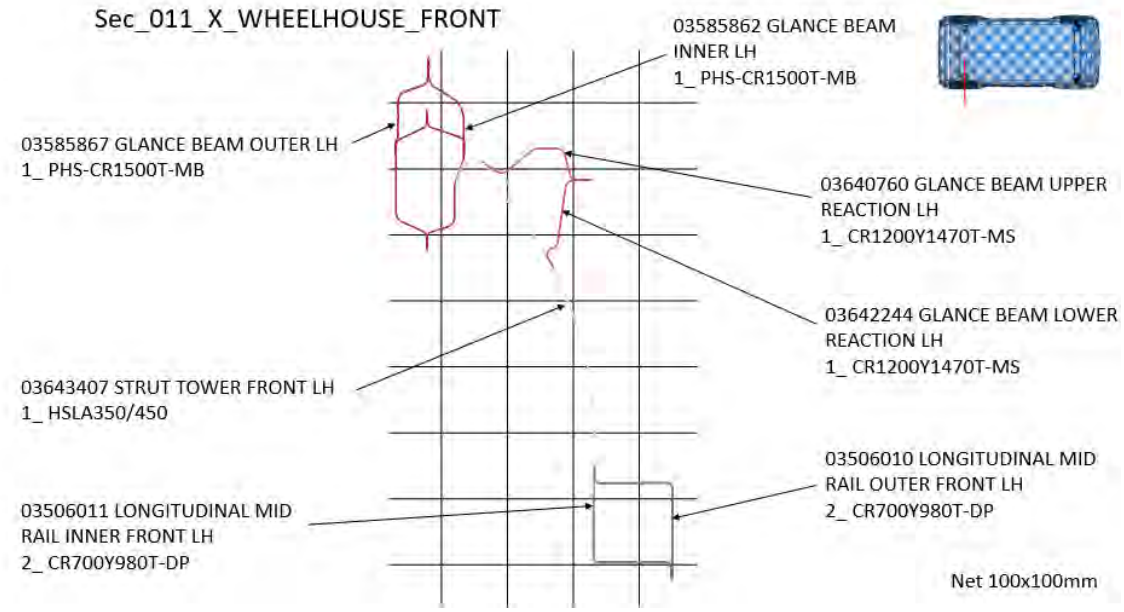
Sec_011_X_WHEELHOUSE_FRONT
03585862 GLANCE BEAM INNER LH
1_ PHS-CR1500T-MB
03585867 GLANCE BEAM OUTER LH
1_ PHS-CR1500T-MB
03640760 GLANCE BEAM UPPER REACTION LH
1_ CR1200Y1470T-MS
03642244 GLANCE BEAM LOWER REACTION LH
1_ CR1200Y1470T-MS
03643407 STRUT TOWER FRONT LH
1_ HSLA350/450
03506010 LONGITUDINAL MID RAIL OUTER FRONT LH
2_ CR700Y980T-DP
03506011 LONGITUDINAL MID RAIL INNER FRONT LH
2_ CR700Y980T-DP
Net 100x100mm

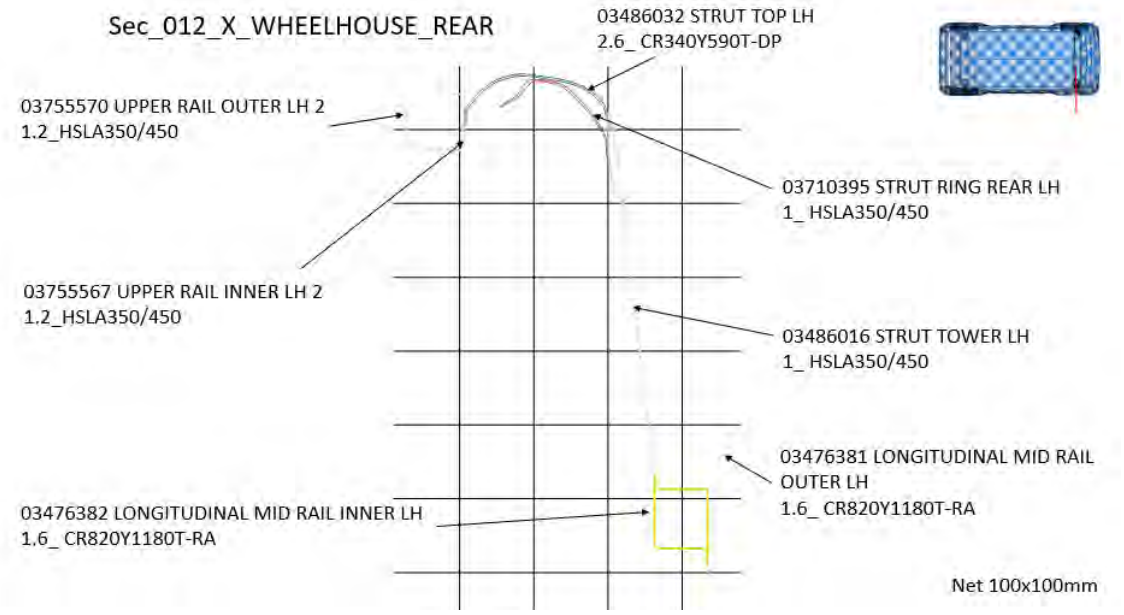
Sec_012_X_WHEELHOUSE_REAR
03486032 STRUT TOP LH
2.6_ CR340Y590T-DP
03755570 UPPER RAIL OUTER LH 2
1.2_HSLA350/450
03710395 STRUT RING REAR LH
1_ HSLA350/450
03755567 UPPER RAIL INNER LH 2
1.2_HSLA350/450
03486016 STRUT TOWER LH
1_ HSLA350/450
03476381 LONGITUDINAL MID RAIL OUTER LH
1.6_ CR820Y1180T-RA
03476382 LONGITUDINAL MID RAIL INNER LH
1.6_ CR820Y1180T-RA
Net 100x100mm

Appendix 3 Body in White Assemblies

„Engineering support for Future Steel Mobility"

Underbody Front Zone

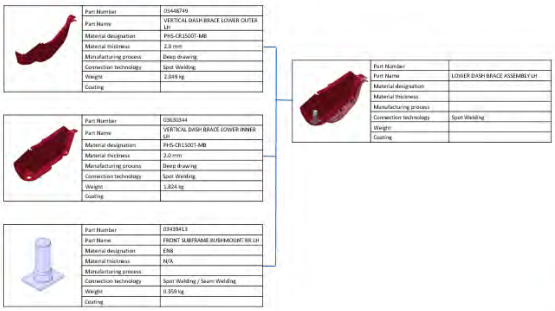

„Engineering support for Future Steel Mobility"

Underbody Front Zone

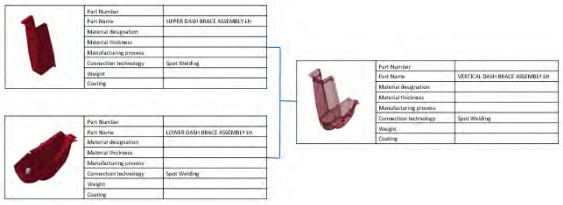

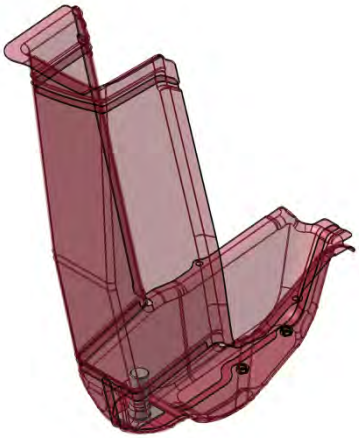

„Engineering support for Future Steel Mobility"

Underbody Front Zone

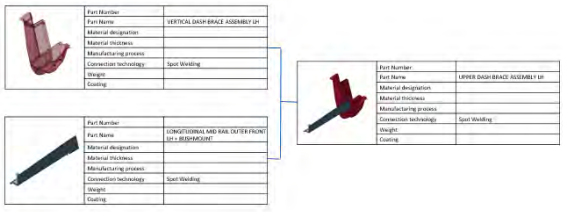

Part Number	
Part Name	VERTICAL DASH BRACE ASSEMBLY LH
Material designation	
Material thickness	
Manufacturing process	
Connection technology	Spot Welding
Weight	
Coating	

Part Number	
Part Name	UPPER DASH BRACE ASSEMBLY LH
Material designation	
Material thickness	
Manufacturing process	
Connection technology	Spot Welding
Weight	
Coating	

Part Number	
Part Name	LONGITUDINAL MID RAIL OUTER FRONT LH + REINFMOUNT
Material designation	
Material thickness	
Manufacturing process	
Connection technology	Spot Welding
Weight	
Coating	

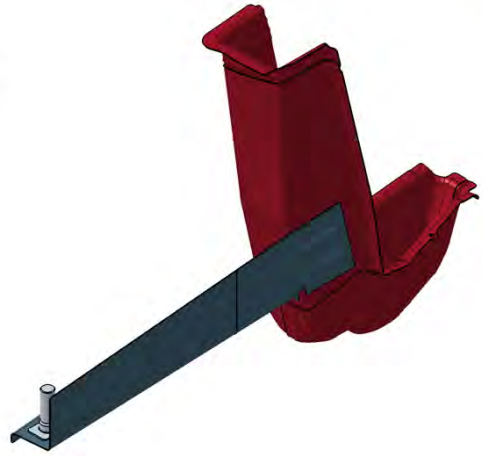

„Engineering support for Future Steel Mobility"

Underbody Front Zone

Part Number	
Part Name	FRONT RAIL DASH BRACE ASSEMBLY LH
Material designation	
Material thickness	
Manufacturing process	
Connection technology	Spot Welding
Weight	
Coating	

Part Number	
Part Name	FRONT RAIL DASH BRACE ASSEMBLY LH
Material designation	
Material thickness	
Manufacturing process	
Connection technology	Spot Welding
Weight	
Coating	

Part Number	01500211
Part Name	LONGITUDINAL MID RAIL INNER FRONT LH
Material designation	CR500Y780T-DP to CR700Y980T-DP
Material thickness	1.8 to 2.0 mm
Manufacturing process	
Connection technology	Spot Welding
Weight	3.162 kg
Coating	

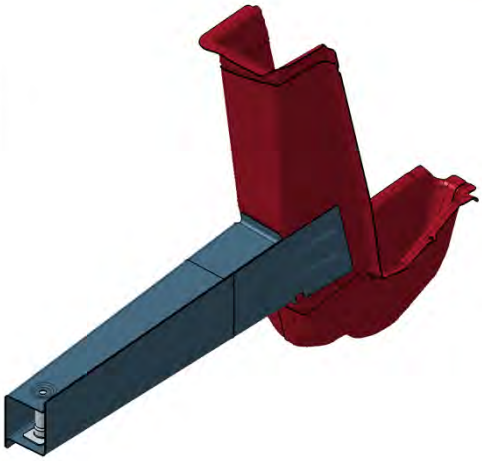

„Engineering support for Future Steel Mobility"

Underbody Front Zone

Part Number	03469873
Part Name	TORQUE BOX FRONT LH
Material designation	CR400Y780T-RA
Material thickness	2 mm
Manufacturing process	Deep Drawing
Connection technology	Spot Welding
Weight	2.149 kg
Coating	

Part Number	
Part Name	TORQUE BOX ASSEMBLY LH
Material designation	
Material thickness	
Manufacturing process	
Connection technology	Spot Welding
Weight	
Coating	

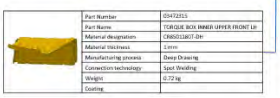

Part Number	03472315
Part Name	TORQUE BOX INNER UPPER FRONT LH
Material designation	CR650Y1180T-DH
Material thickness	1 mm
Manufacturing process	Deep Drawing
Connection technology	Spot Welding
Weight	0.72 kg
Coating	

„Engineering support for Future Steel Mobility"

Underbody Front Zone

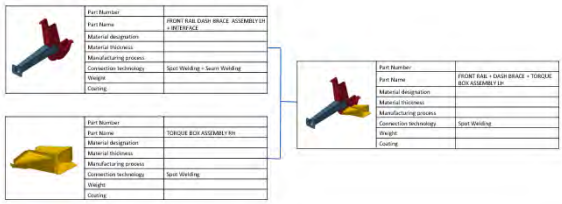

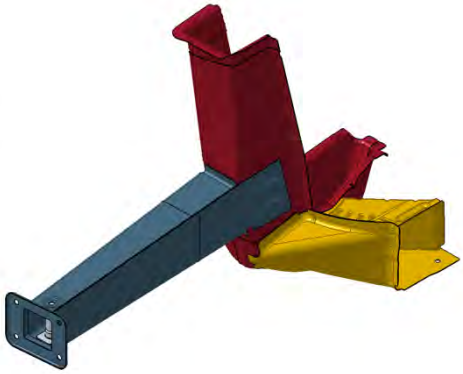

„Engineering support for Future Steel Mobility"

Underbody Front Zone

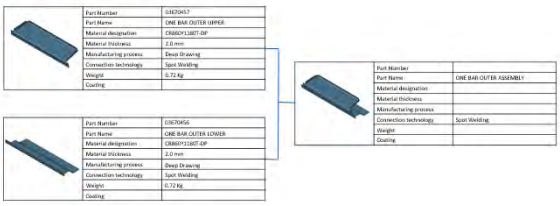

„Engineering support for Future Steel Mobility"

Underbody Front Zone

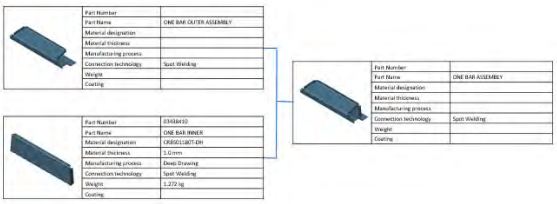

„Engineering support for Future Steel Mobility"

Underbody Front Zone

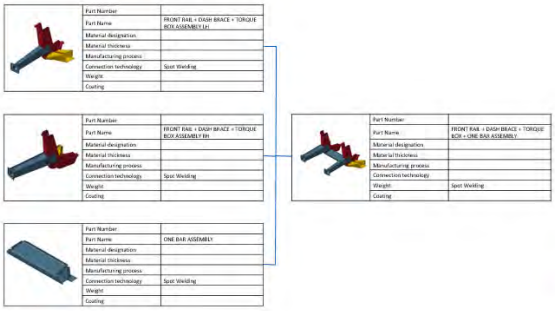

Part Number	
Part Name	FRONT RAIL + DASH BRACE + TORQUE BOX ASSEMBLY LH
Material designation	
Material thickness	
Manufacturing process	
Connection technology	Spot Welding
Weight	
Coating	

Part Number	
Part Name	FRONT RAIL + DASH BRACE + TORQUE BOX ASSEMBLY RH
Material designation	
Material thickness	
Manufacturing process	
Connection technology	Spot Welding
Weight	
Coating	

Part Number	
Part Name	FRONT RAIL + DASH BRACE + TORQUE BOX + ONE BAR ASSEMBLY
Material designation	
Material thickness	
Manufacturing process	
Connection technology	Spot Welding
Weight	
Coating	

Part Number	
Part Name	ONE BAR ASSEMBLY
Material designation	
Material thickness	
Manufacturing process	
Connection technology	Spot Welding
Weight	
Coating	

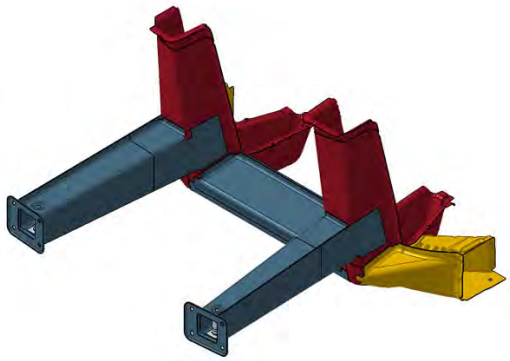

„Engineering support for Future Steel Mobility"

Underbody Front Zone

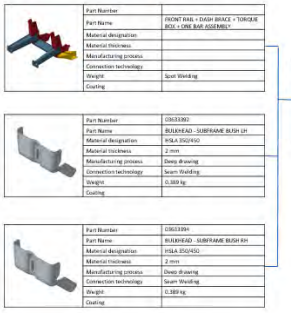

Part Number	
Part Name	FRONT RAIL + DASH BRACE + TORQUE BOX + ONE BAR ASSEMBLY
Material designation	
Material thickness	
Manufacturing process	
Connection technology	
Weight	Spot Welding
Coating	

Part Number	
Part Name	LOWER DASH BRACE ASSEMBLY LH
Material designation	
Material thickness	
Manufacturing process	
Connection technology	Seam Welding
Weight	
Coating	

Part Number	03633002
Part Name	BULKHEAD - SUBFRAME BUSH LH
Material designation	HSLA 350/450
Material thickness	2 mm
Manufacturing process	Deep drawing
Connection technology	Seam Welding
Weight	0.369 kg
Coating	

Part Number	03633004
Part Name	BULKHEAD - SUBFRAME BUSH RH
Material designation	HSLA 350/450
Material thickness	2 mm
Manufacturing process	Deep drawing
Connection technology	Seam Welding
Weight	0.369 kg
Coating	

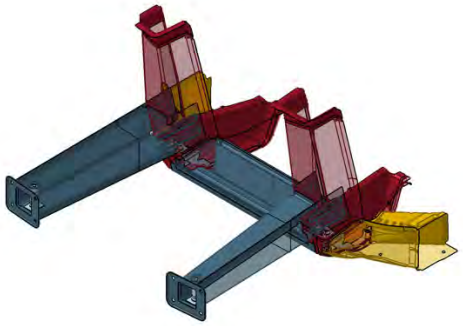

„Engineering support for Future Steel Mobility"

Underbody Front Zone

Part Number	03603002
Part Name	STRUT TOP FRONT LH
Material designation	CR600Y1180T-DP
Material thickness	2.6 mm
Manufacturing process	Deep Drawing
Connection technology	Spot Welding
Weight	2.286 kg
Coating	

Part Number	03603407
Part Name	STRUT TOWER FRONT LH
Material designation	HSLA 350/450
Material thickness	1 mm
Manufacturing process	Deep Drawing
Connection technology	Spot Welding
Weight	1.826 Kg
Coating	

Part Number	
Part Name	STRUT TOWER ASSEMBLY LH
Material designation	
Material thickness	
Manufacturing process	
Connection technology	Spot welding
Weight	
Coating	

„Engineering support for Future Steel Mobility"

Underbody Front Zone

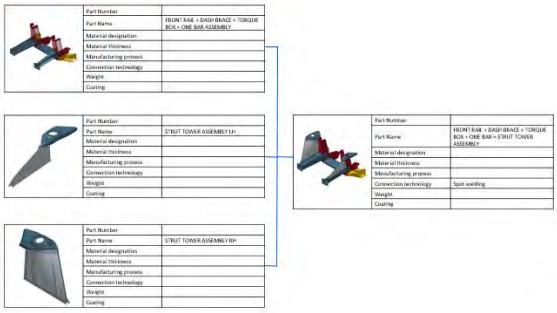

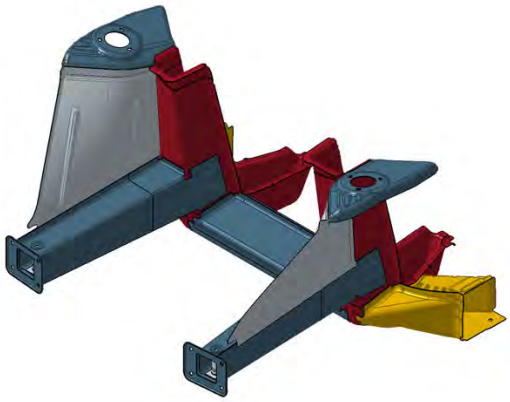

„Engineering support for Future Steel Mobility"

Underbody Front Zone

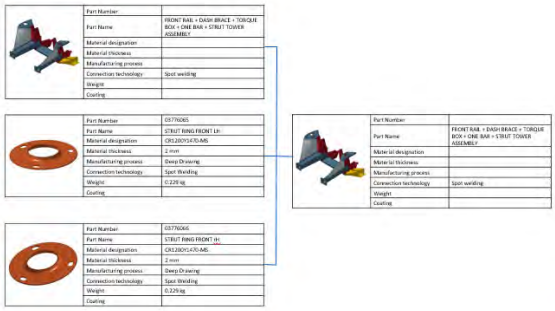

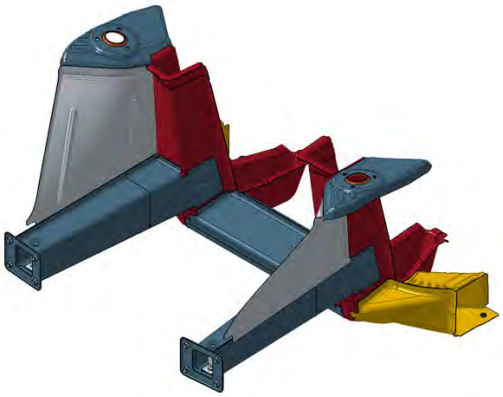

„Engineering support for Future Steel Mobility"

Underbody Front Zone

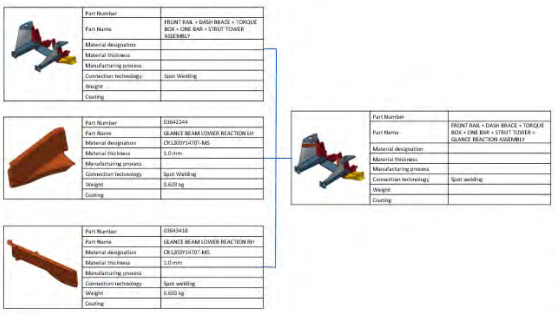

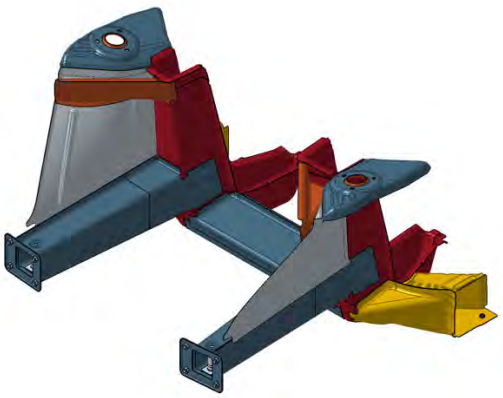

„Engineering support for Future Steel Mobility"

Underbody Front Zone

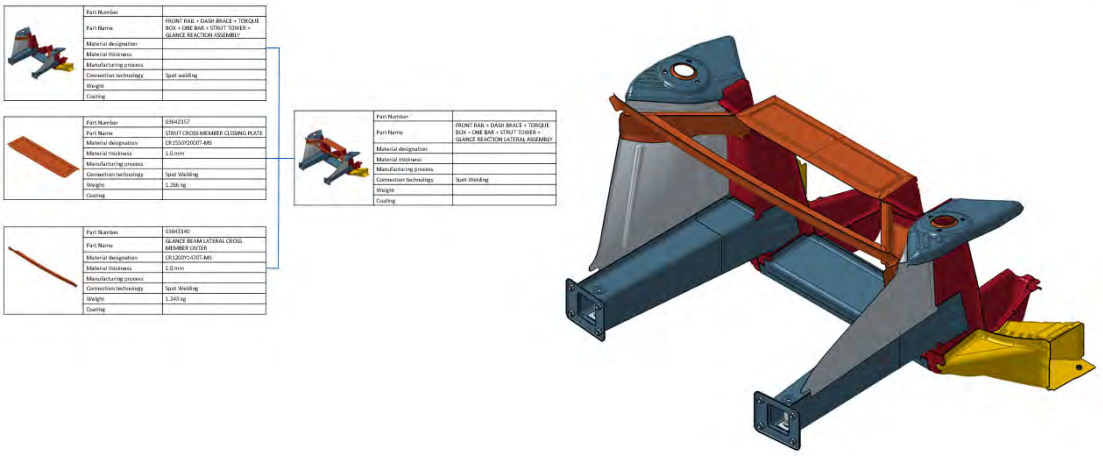

„Engineering support for Future Steel Mobility"

Underbody Front Zone

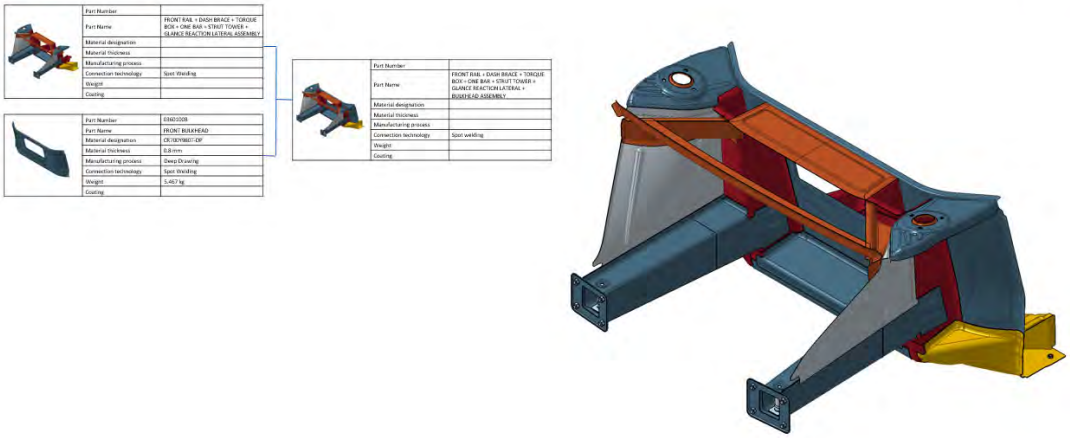

„Engineering support for Future Steel Mobility"

Underbody Front Zone

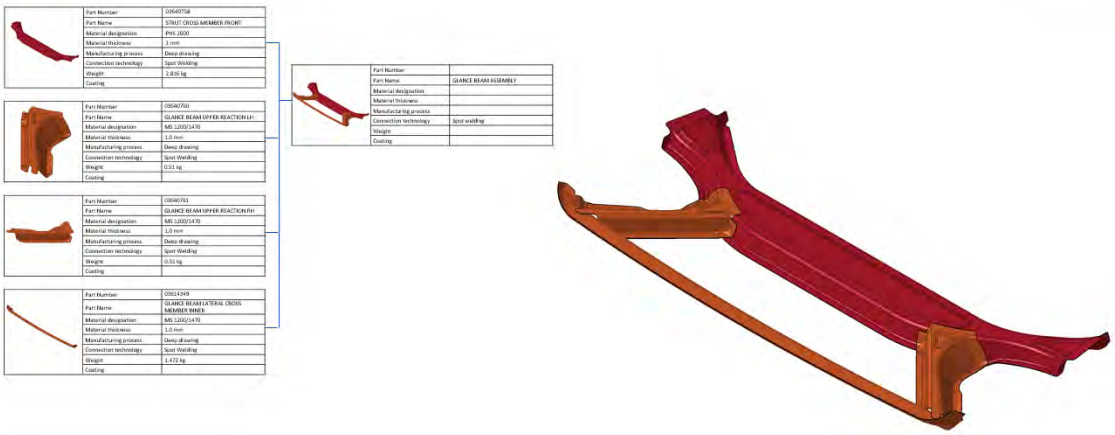

„Engineering support for Future Steel Mobility"

Underbody Front Zone

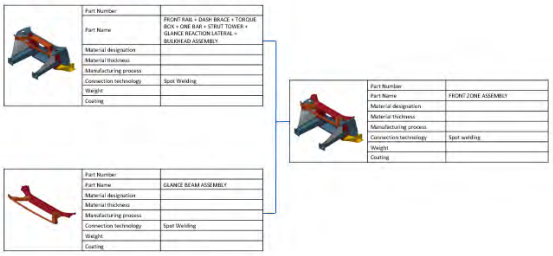

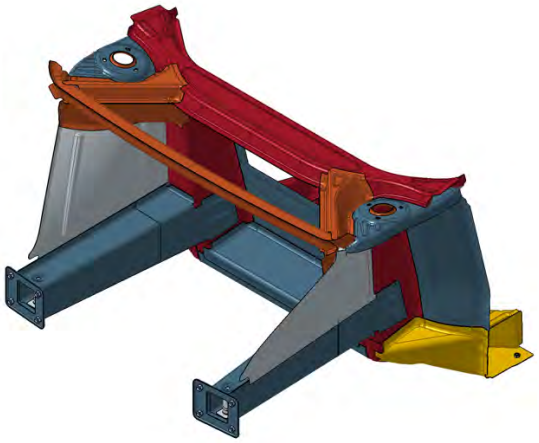

„Engineering support for Future Steel Mobility"

Underbody Front Zone

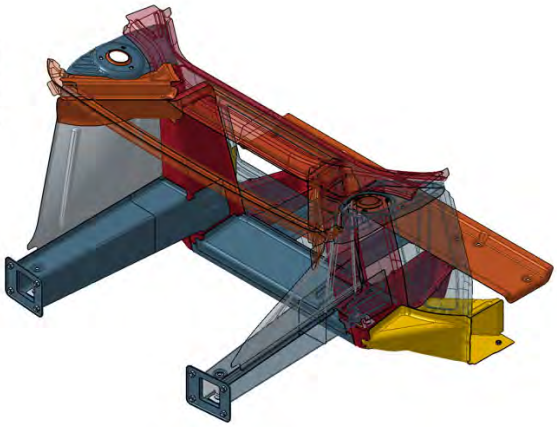

Mid Zone Floor Assembly

„Engineering support for Future Steel Mobility"

Underbody Middle area

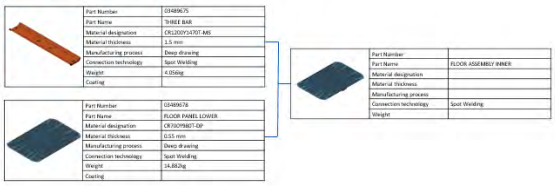

Rear Zone Assembly

„Engineering support for Future Steel Mobility"

Underbody Rear Zone

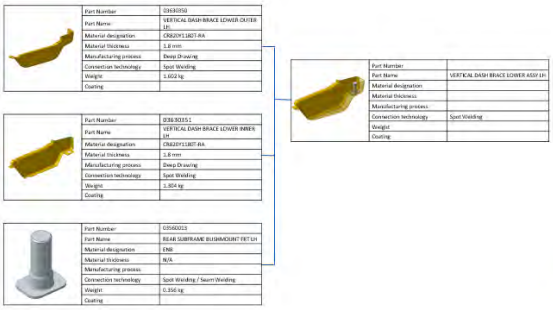

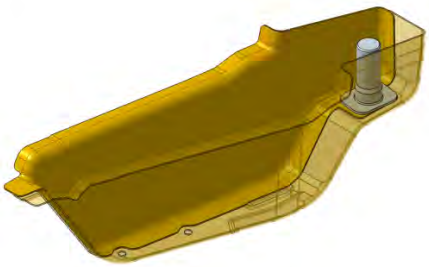

„Engineering support for Future Steel Mobility"

Underbody Front Zone

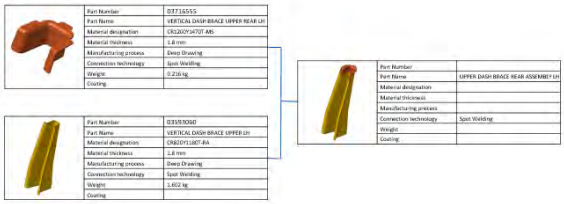

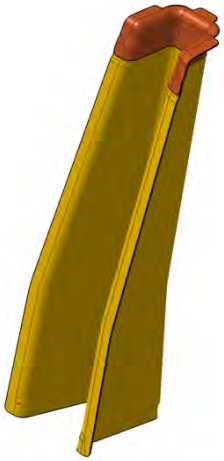

„Engineering support for Future Steel Mobility"

Underbody Rear Zone

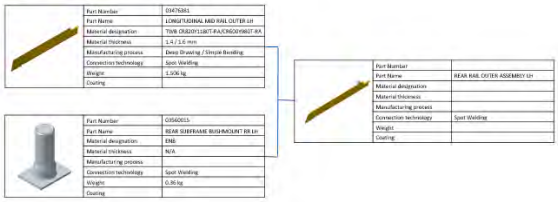

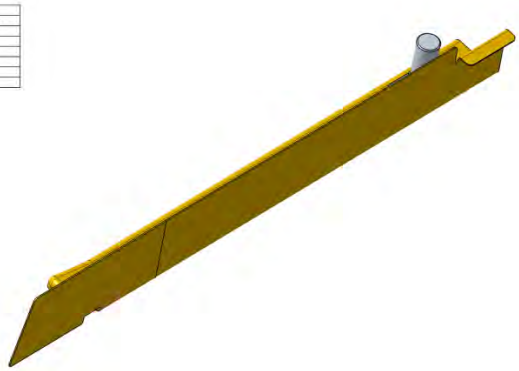

„Engineering support for Future Steel Mobility"

Underbody Rear Zone

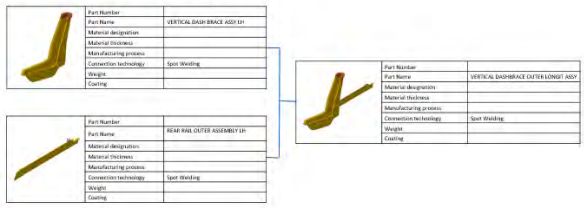

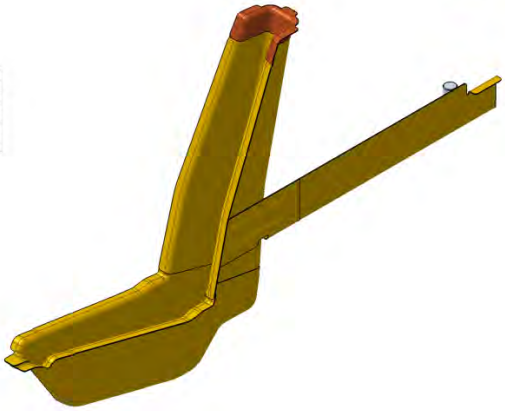

„Engineering support for Future Steel Mobility"

Underbody Rear Zone

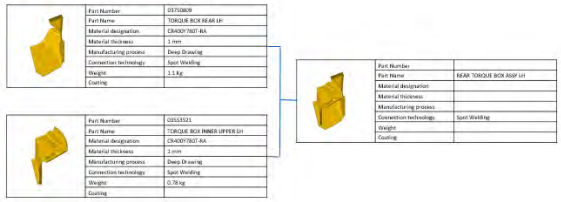

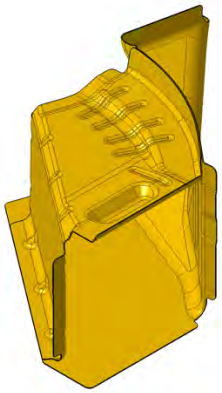

„Engineering support for Future Steel Mobility"

Underbody Rear Zone

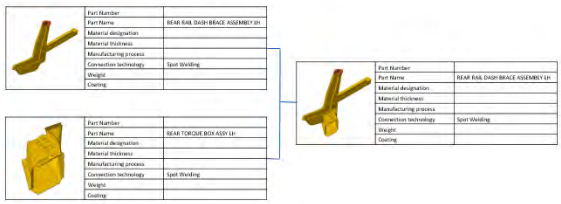

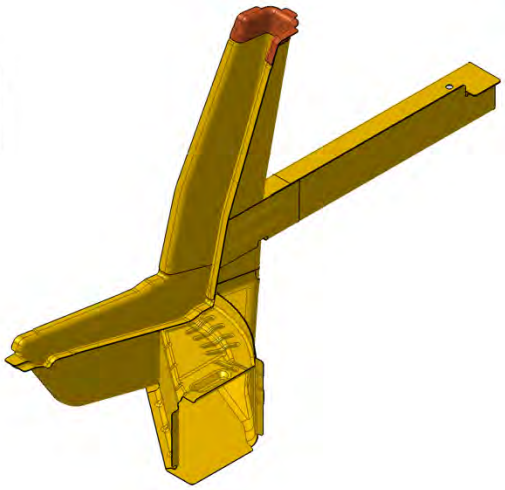

„Engineering support for Future Steel Mobility"

Underbody Rear Zone

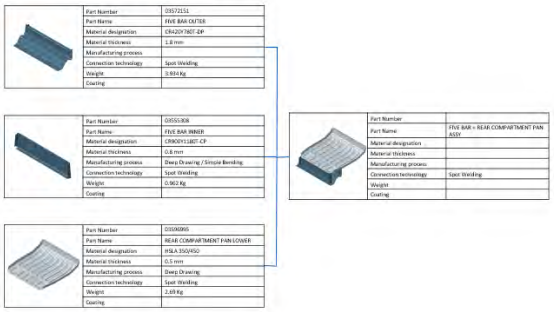

„Engineering support for Future Steel Mobility"

Underbody Rear Zone

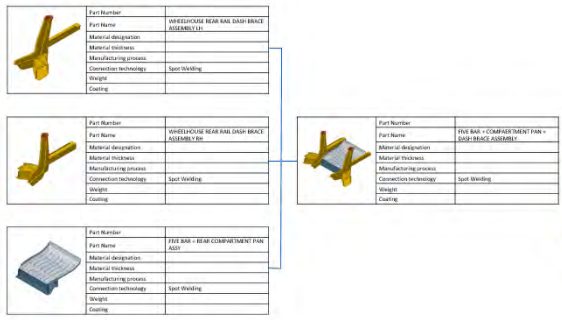

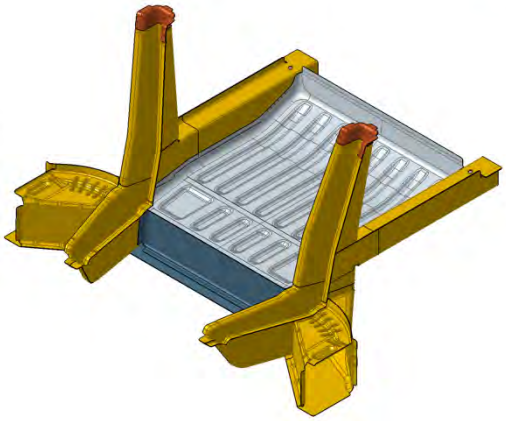

„Engineering support for Future Steel Mobility"

Underbody Rear Zone

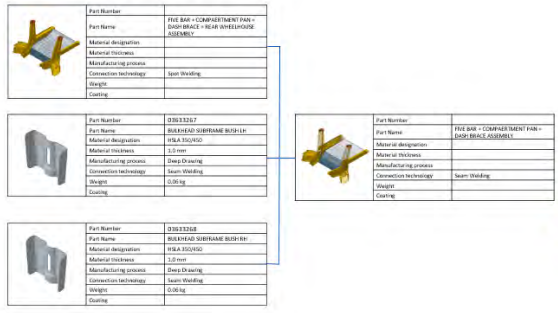

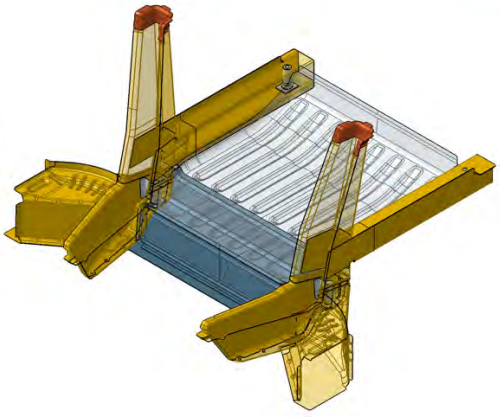

„Engineering support for Future Steel Mobility"

Underbody Front Zone

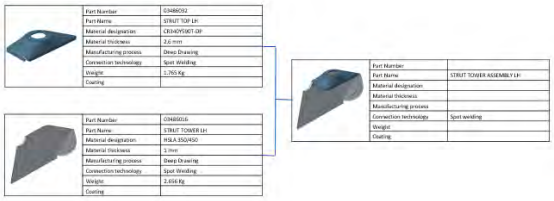

„Engineering support for Future Steel Mobility"

Underbody Rear Zone

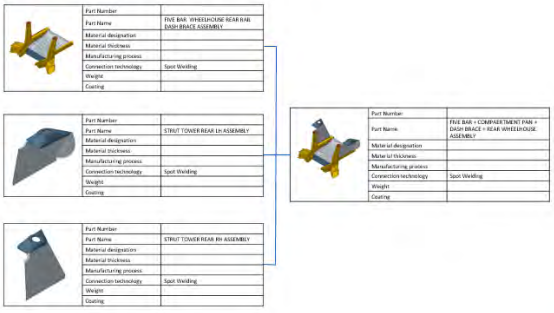

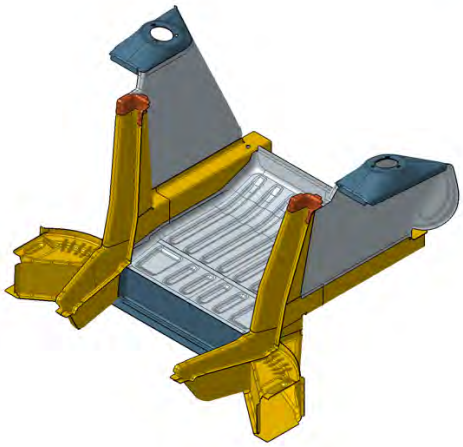

„Engineering support for Future Steel Mobility"

Underbody Rear Zone

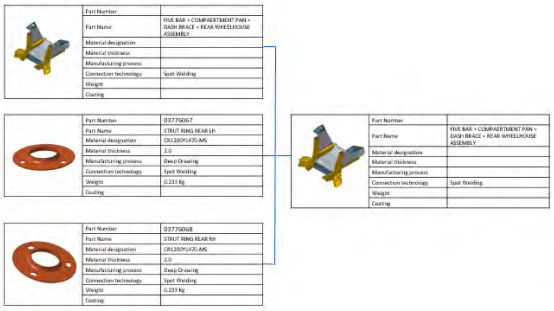

„Engineering support for Future Steel Mobility"

Underbody Rear Zone

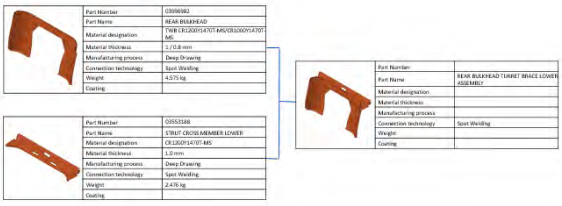

„Engineering support for Future Steel Mobility"

Underbody Rear Zone

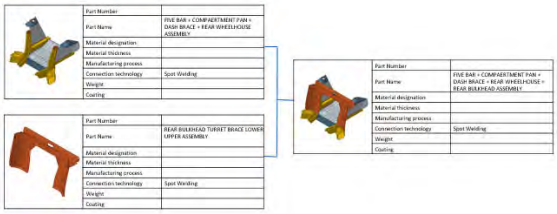

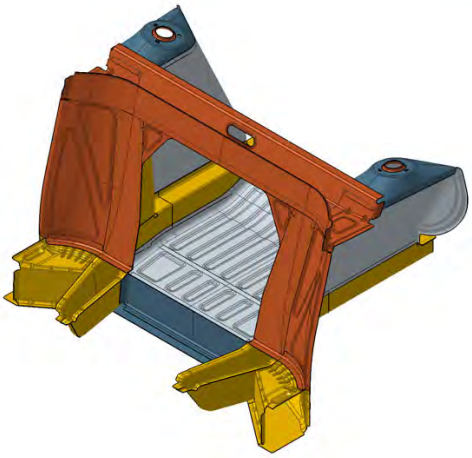

„Engineering support for Future Steel Mobility"

Underbody Rear Zone

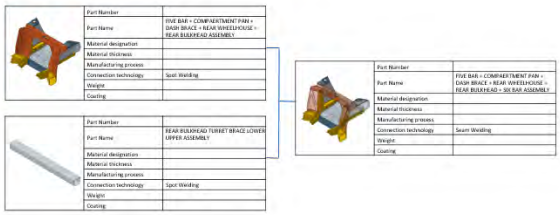

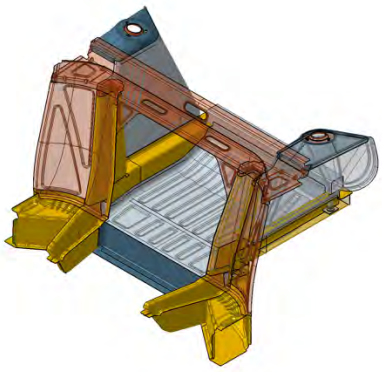

„Engineering support for Future Steel Mobility"

Underbody Rear Zone

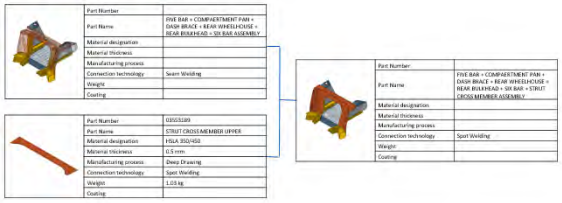

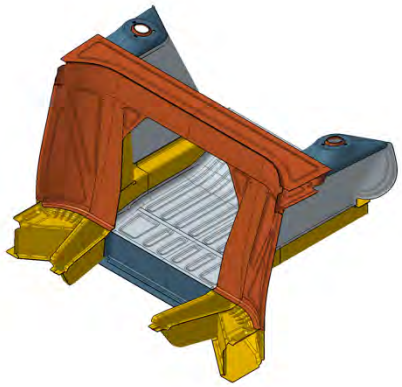

„Engineering support for Future Steel Mobility"

Underbody Rear Zone

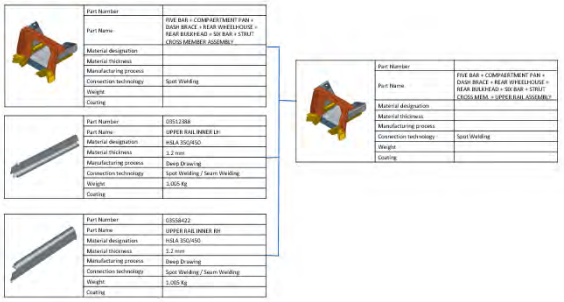

„Engineering support for Future Steel Mobility"

Underbody Rear Zone

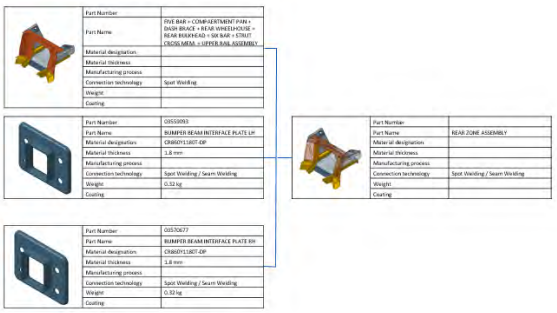

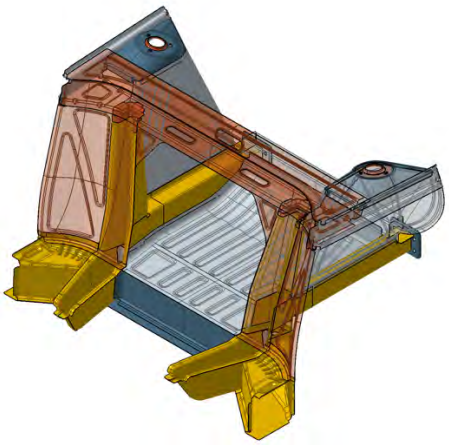

„Engineering support for Future Steel Mobility"

Underbody Rear Zone

Part Number	
Part Name	REAR ZONE ASSEMBLY
Material designation	
Material thickness	
Manufacturing process	
Connection technology	Spot Welding / Seam Welding
Weight	
Coating	

Part Number	
Part Name	REAR ZONE + FOUR BAR ASSEMBLY
Material designation	
Material thickness	
Manufacturing process	
Connection technology	Spot Welding
Weight	
Coating	

Part Number	09489676
Part Name	FOUR BAR
Material designation	CR1200Y1470T-MS
Material thickness	1.5 mm
Manufacturing process	Deep Drawing
Connection technology	Spot Welding
Weight	4.052 kg
Coating	

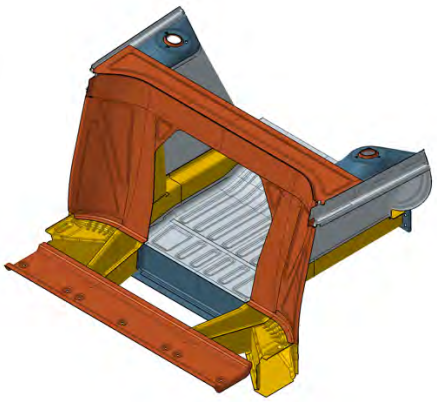

„Engineering support for Future Steel Mobility"

Underbody Rear Zone

Part Number	09484362
Part Name	D POST LH
Material designation	CR420Y690T-RA
Material thickness	1.2 mm
Manufacturing process	Hydroforming
Connection technology	Seam Welding
Weight	3.038 Kg
Coating	

Part Number	
Part Name	D POST ASSEMBLY LH
Material designation	
Material thickness	
Manufacturing process	
Connection technology	Seam Welding / Spot Welding
Weight	
Coating	

Part Number	69763727
Part Name	COACH DOOR LATERAL BAR REINFORCEMENT INNER LH
Material designation	HSLA350/450
Material thickness	0.7 mm
Manufacturing process	Deep Drawing
Connection technology	Seam Welding / Spot Welding
Weight	0.196 kg
Coating	

„Engineering support for Future Steel Mobility"

Underbody Rear Zone

Part Number	69763730
Part Name	COACH DOOR LATERAL BAR REINFORCEMENT OUTER LH
Material designation	HSLA350/450
Material thickness	0.8 mm
Manufacturing process	Deep Drawing
Connection technology	Seam Welding / Spot Welding
Weight	0.311 Kg
Coating	

Part Number	
Part Name	COACH DOOR OUTER REINFORCEMENT ASSEMBLY LH
Material designation	
Material thickness	
Manufacturing process	
Connection technology	Seam Welding / Spot Welding
Weight	
Coating	

Part Number	69738010
Part Name	BRACKET COACH DOOR UPPER LH
Material designation	HSLA350/450
Material thickness	1.5 mm
Manufacturing process	Deep Drawing
Connection technology	Spot Welding
Weight	0.048 kg
Coating	

„Engineering support for Future Steel Mobility"

Underbody Rear Zone

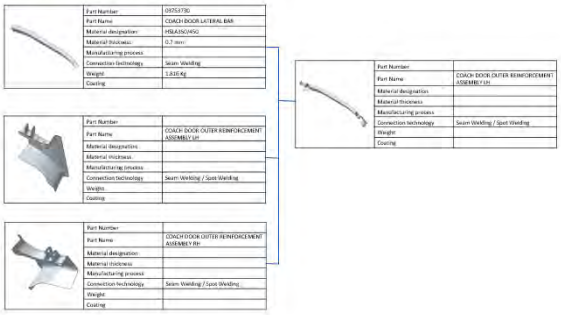

Side Assembly

„Engineering support for Future Steel Mobility"

Side ASSEMBLY

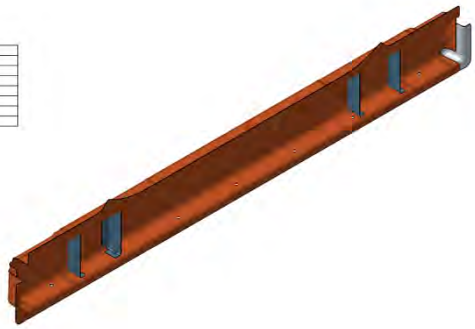

„Engineering support for Future Steel Mobility"

Side ASSEMBLY

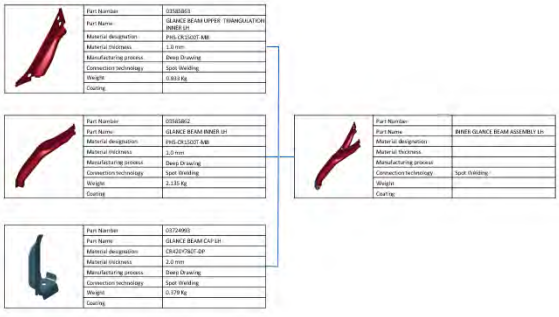

„Engineering support for Future Steel Mobility"

Side ASSEMBLY

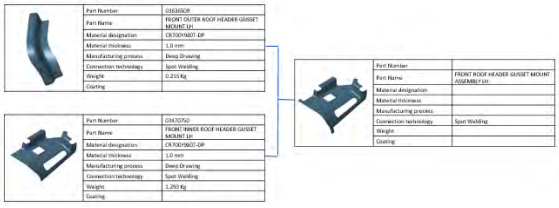

„Engineering support for Future Steel Mobility"

Side ASSEMBLY

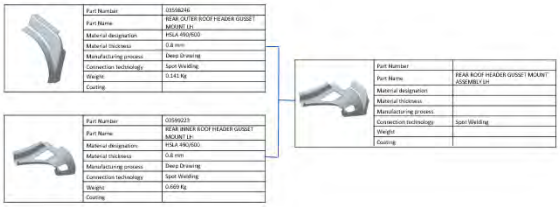

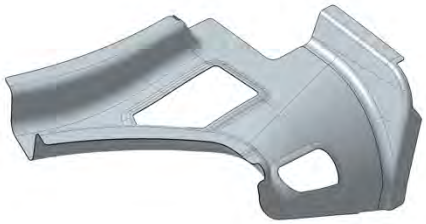

„Engineering support for Future Steel Mobility"

Side ASSEMBLY

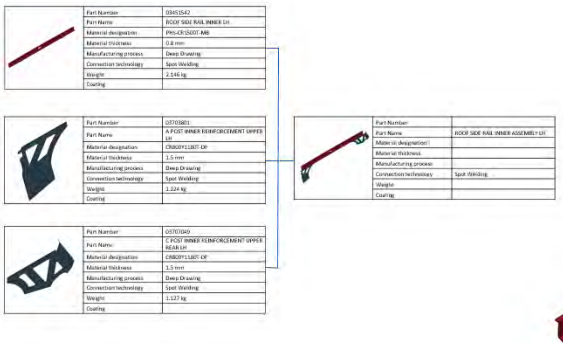

„Engineering support for Future Steel Mobility"

Side ASSEMBLY

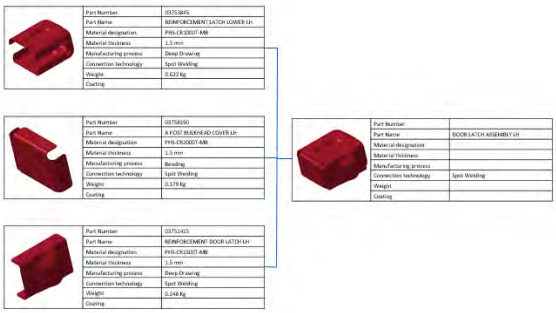

„Engineering support for Future Steel Mobility"

Side ASSEMBLY

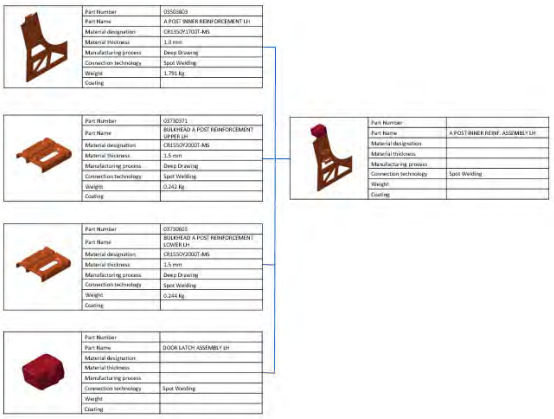

„Engineering support for Future Steel Mobility"

Side ASSEMBLY

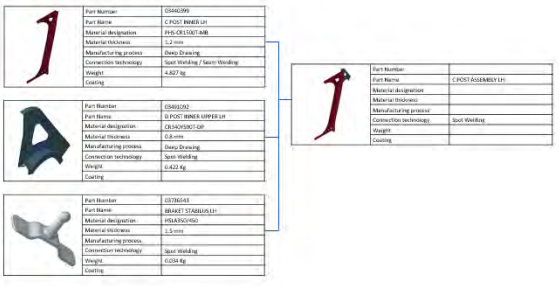

„Engineering support for Future Steel Mobility"

Side ASSEMBLY

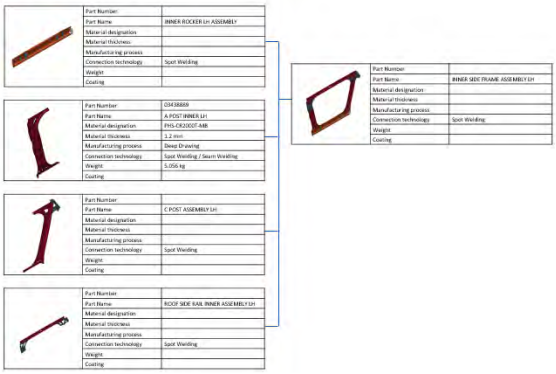

„Engineering support for Future Steel Mobility"

Side ASSEMBLY

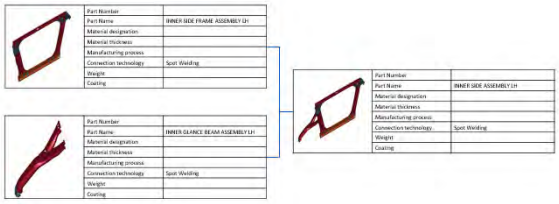

„Engineering support for Future Steel Mobility"

Side ASSEMBLY

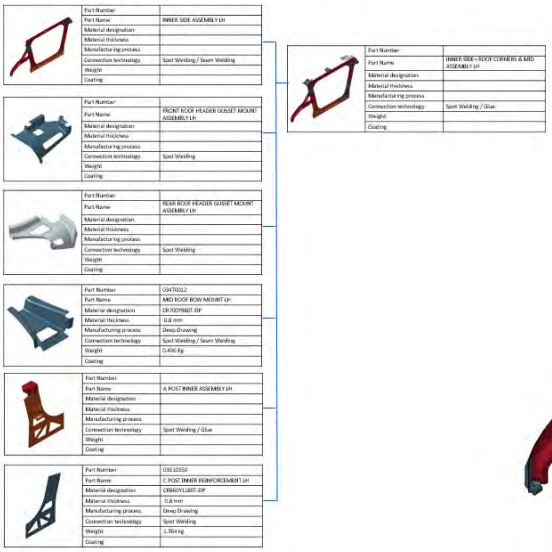

„Engineering support for Future Steel Mobility"

Side ASSEMBLY

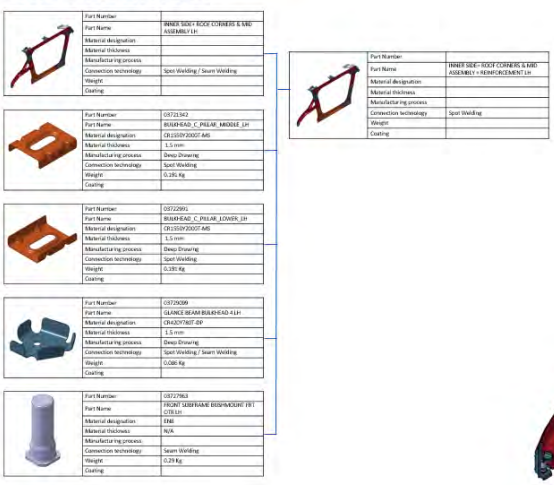

„Engineering support for Future Steel Mobility"

Side ASSEMBLY

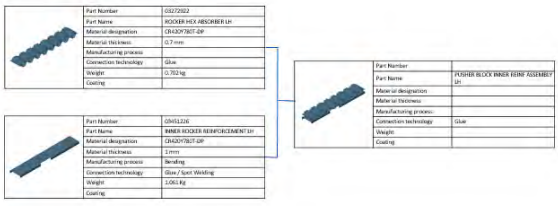

„Engineering support for Future Steel Mobility"

Side ASSEMBLY

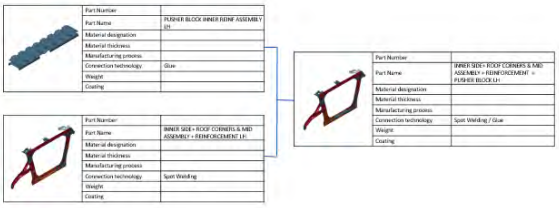

„Engineering support for Future Steel Mobility"

Side ASSEMBLY

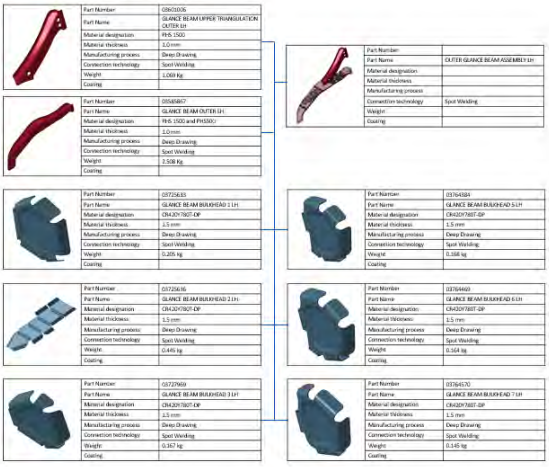

„Engineering support for Future Steel Mobility"

Side ASSEMBLY

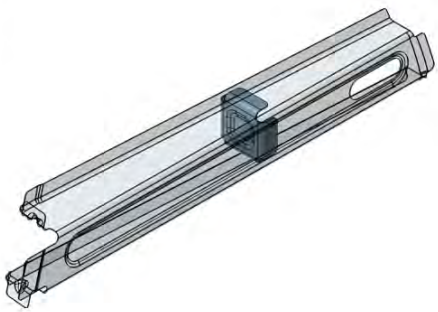

„Engineering support for Future Steel Mobility"

Side ASSEMBLY

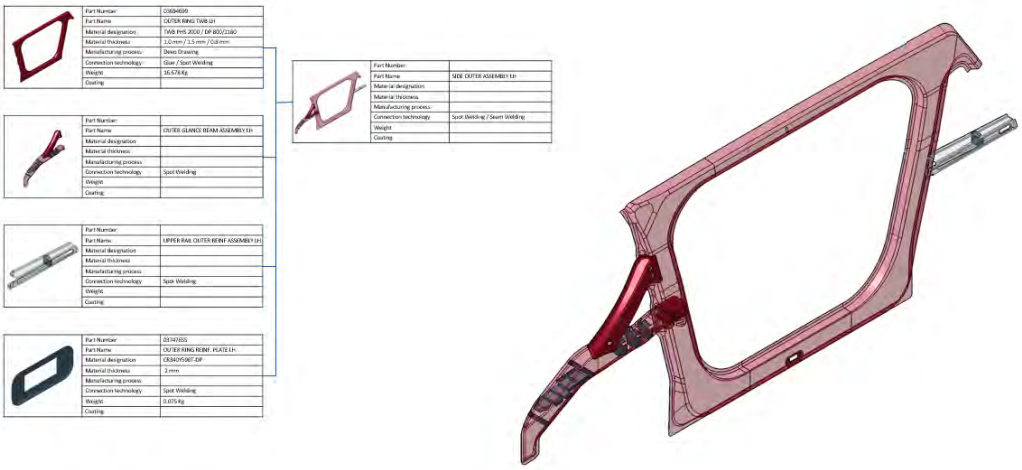

Roof Assembly

„Engineering support for Future Steel Mobility"

Roof ASSEMBLY

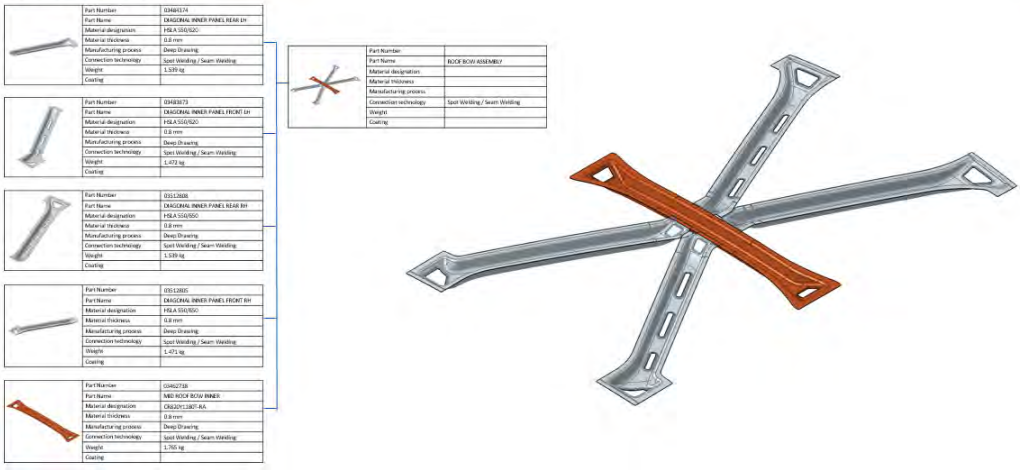

„Engineering support for Future Steel Mobility"

Roof ASSEMBLY

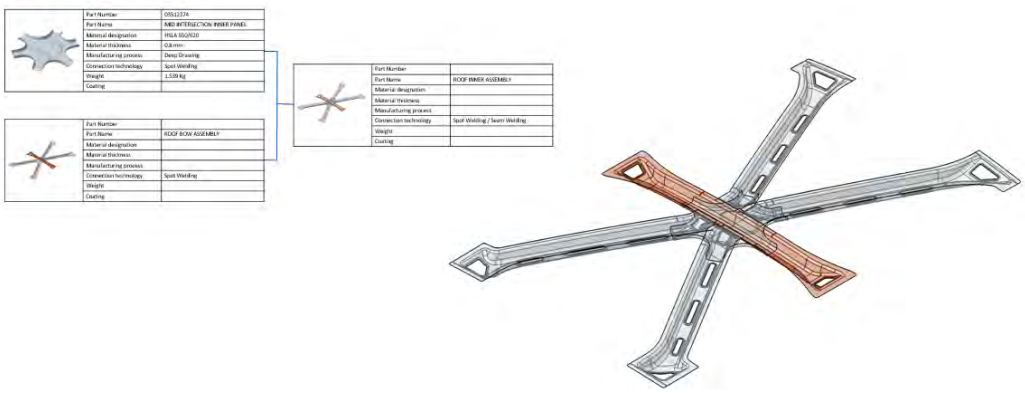

„Engineering support for Future Steel Mobility"

Roof ASSEMBLY

Part Number	
Part Name	ROOF INNER ASSEMBLY
Material designation	
Material thickness	
Manufacturing process	
Connection technology	Spot Welding / Seam Welding
Weight	
Coating	

Part Number	03476397
Part Name	REAR HEADER INNER MW
Material designation	CR780Y980T-CP
Material thickness	0.8 mm
Manufacturing process	Deep Drawing
Connection technology	Spot Welding / Seam Welding
Weight	1.685 kg
Coating	

Part Number	
Part Name	ROOF INNER MIDDLE ASSEMBLY
Material designation	
Material thickness	
Manufacturing process	
Connection technology	Spot Welding / Seam Welding
Weight	
Coating	

Part Number	03455790
Part Name	FRONT HEADER INNER MW
Material designation	CR780Y980T-CP
Material thickness	0.8 mm
Manufacturing process	Deep Drawing
Connection technology	Spot Welding / Seam Welding
Weight	1.076 kg
Coating	

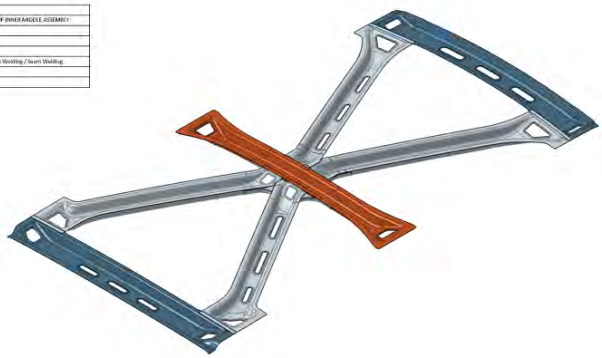

„Engineering support for Future Steel Mobility"

Roof ASSEMBLY

Part Number	03475997
Part Name	DIAGONAL OUTER A-SURFACE PANEL FRONT LH
Material designation	CR260Y370T-BH
Material thickness	0.6 mm
Manufacturing process	
Connection technology	Spot Welding / Seam Welding
Weight	0.781 kg
Coating	

Part Number	03476383
Part Name	DIAGONAL OUTER A-SURFACE PANEL REAR LH
Material designation	CR260Y370T-BH
Material thickness	0.6 mm
Manufacturing process	
Connection technology	Spot Welding / Seam Welding
Weight	0.809 kg
Coating	

Part Number	03496795
Part Name	MID INTERSECTION OUTER A-SURFACE PANEL
Material designation	CR260Y370T-BH
Material thickness	0.6 mm
Manufacturing process	
Connection technology	Spot Welding / Seam Welding
Weight	0.634 kg
Coating	

Part Number	03512806
Part Name	DIAGONAL OUTER A-SURFACE PANEL REAR RH
Material designation	CR260Y370T-BH
Material thickness	0.6 mm
Manufacturing process	
Connection technology	Spot Welding / Seam Welding
Weight	0.809 kg
Coating	

Part Number	03512803
Part Name	DIAGONAL OUTER A-SURFACE PANEL FRONT RH
Material designation	CR260Y370T-BH
Material thickness	0.6 mm
Manufacturing process	
Connection technology	Spot Welding / Seam Welding
Weight	0.781 kg
Coating	

Part Number	03465692
Part Name	FRONT HEADER OUTER A-SURFACE
Material designation	CR260Y370T-BH
Material thickness	0.6 mm
Manufacturing process	
Connection technology	Spot Welding / Seam Welding
Weight	1.045 kg
Coating	

Part Number	
Part Name	ROOF OUTER ASSEMBLY
Material designation	
Material thickness	
Manufacturing process	
Connection technology	Spot Welding / Seam Welding
Weight	
Coating	

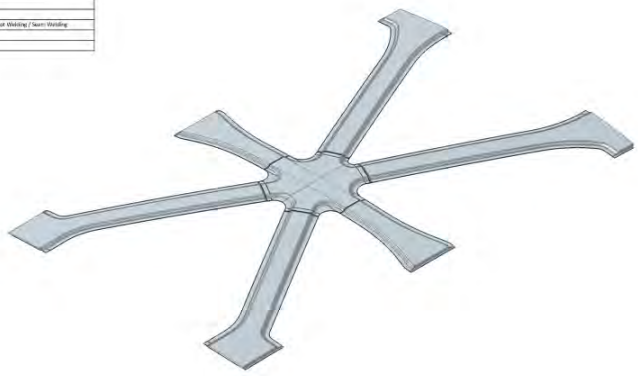

„Engineering support for Future Steel Mobility"

Roof ASSEMBLY

Part Number	10451626
Part Name	FRONT HEADER OUTER A-SURFACE
Material designation	CR260Y/370T-BH
Material thickness	0.6 mm
Manufacturing process	Deep Drawing
Connection technology	Spot Welding / Seam Welding
Weight	1.151 kg
Coating	

Part Number	10476375
Part Name	REAR HEADER OUTER A-SURFACE
Material designation	CR260Y/370T-BH
Material thickness	0.6 mm
Manufacturing process	Deep Drawing
Connection technology	Spot Welding / Seam Welding
Weight	1.207 kg
Coating	

General Assembly

„Engineering support for Future Steel Mobility"

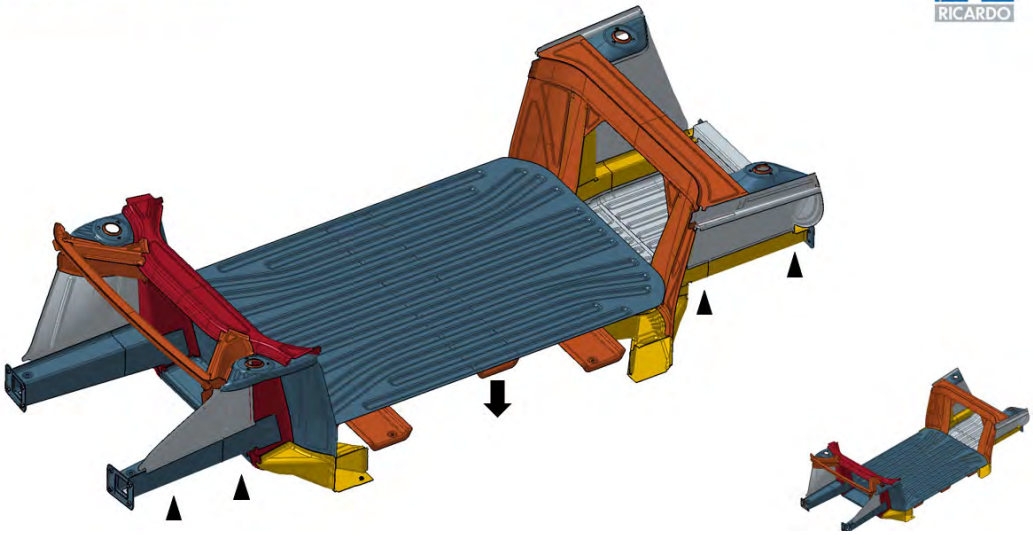

„Engineering support for Future Steel Mobility"

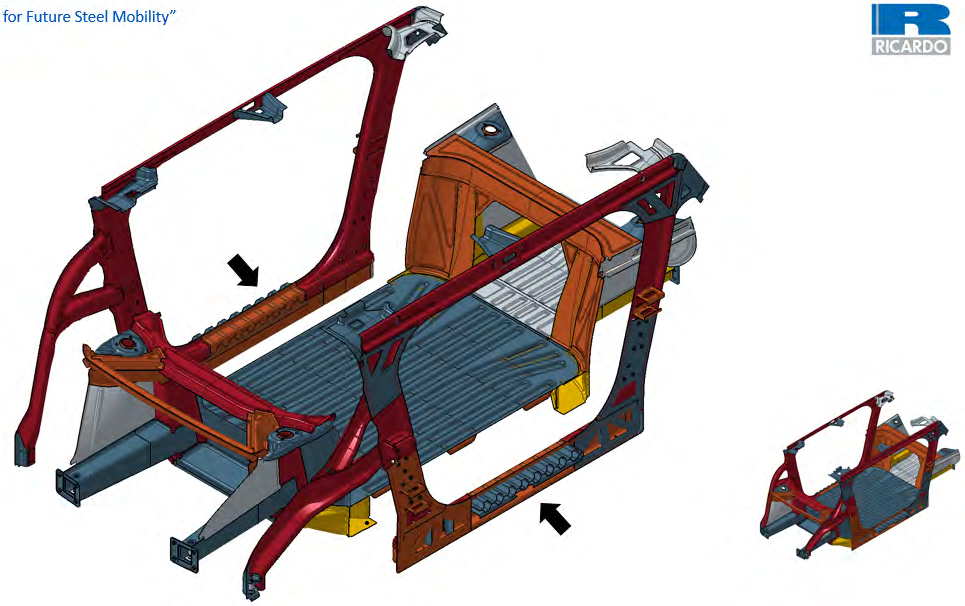

„Engineering support for Future Steel Mobility"

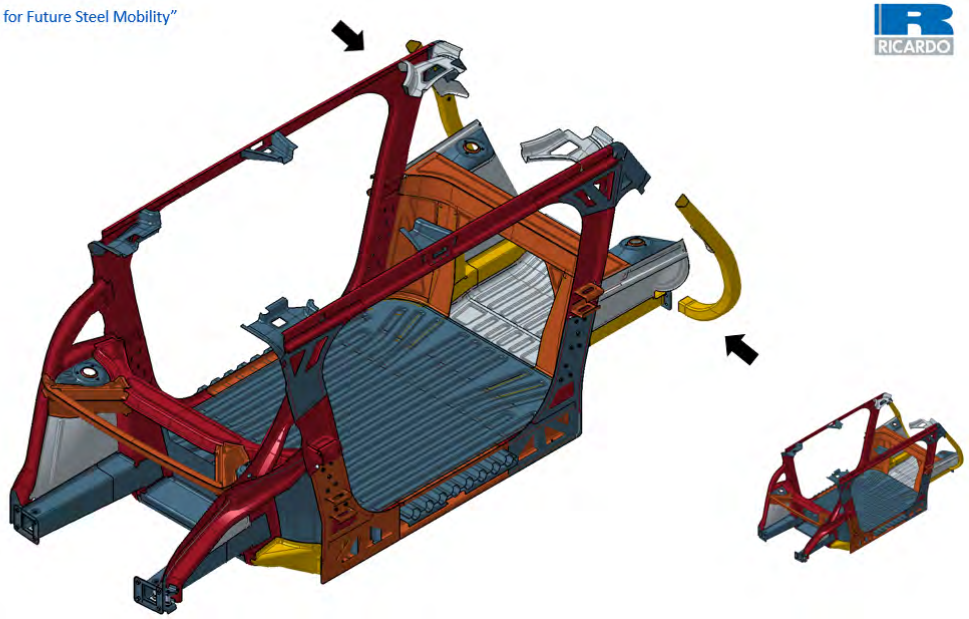

„Engineering support for Future Steel Mobility"

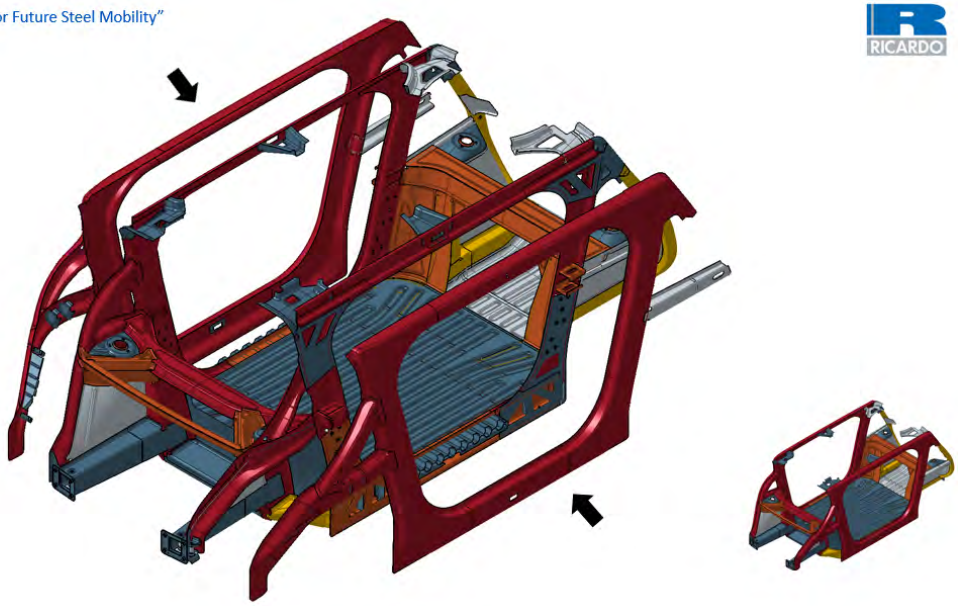

„Engineering support for Future Steel Mobility"

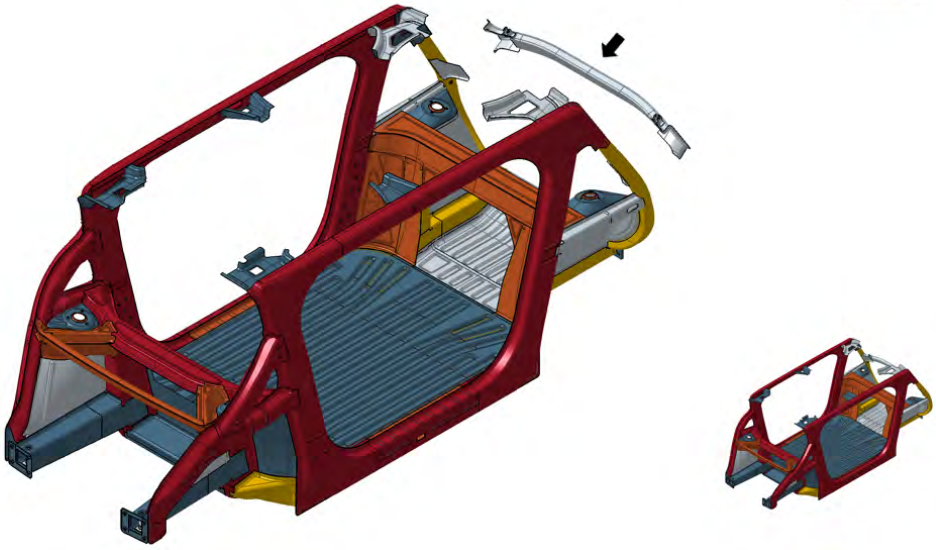

„Engineering support for Future Steel Mobility"

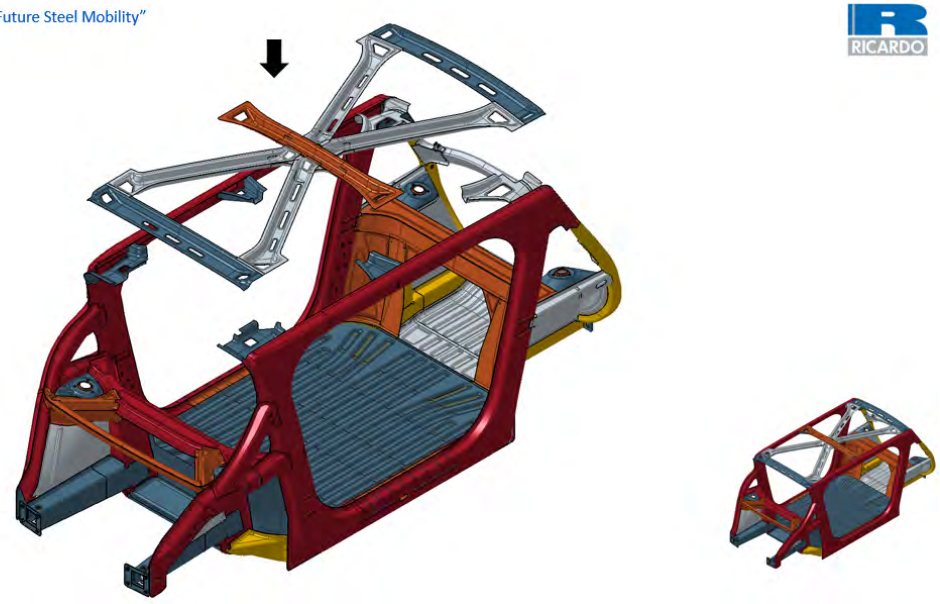

„Engineering support for Future Steel Mobility"

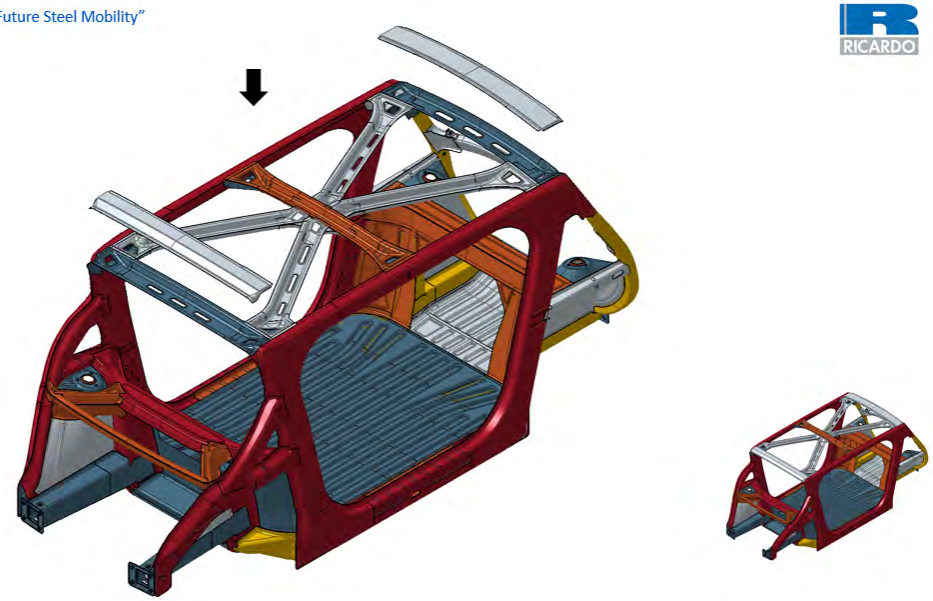

„Engineering support for Future Steel Mobility"

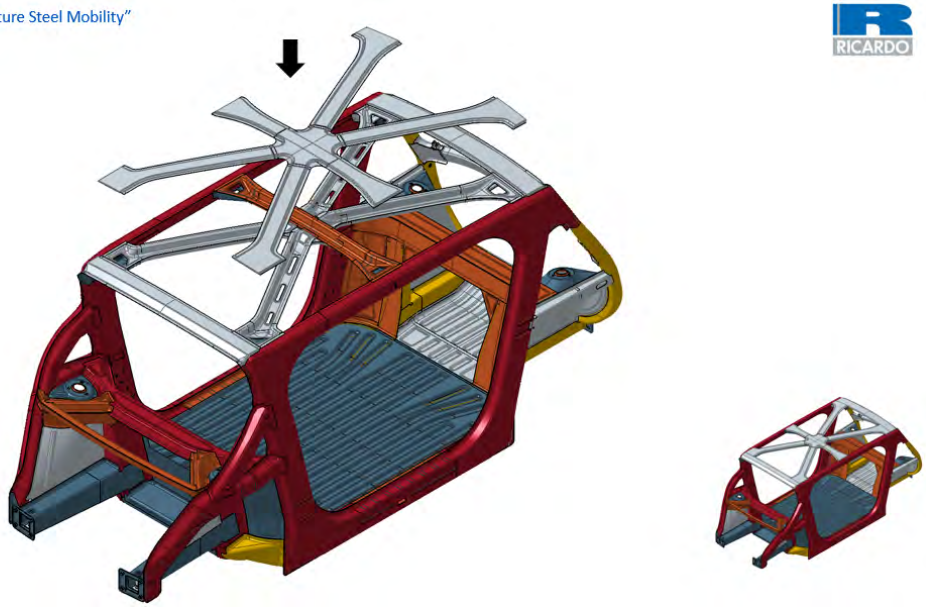

„Engineering support for Future Steel Mobility"

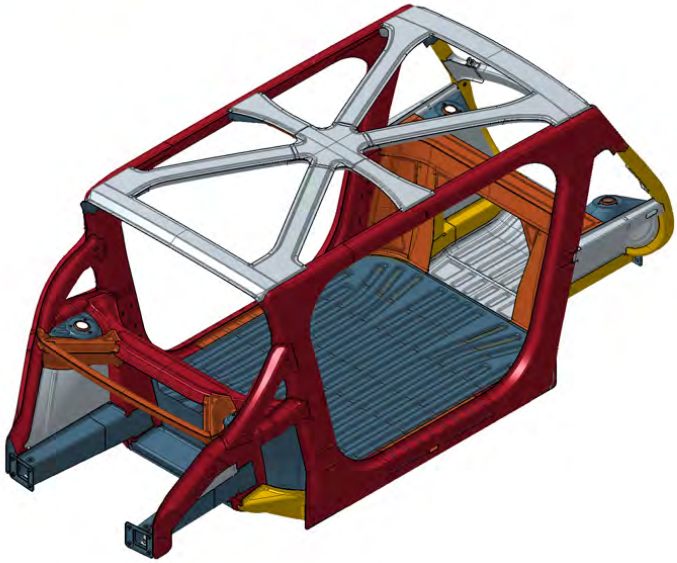

Appendix 4 Full size images and figures

Figure 3.4.1 Autonomous vehicle and Mobility as a Service roadmap

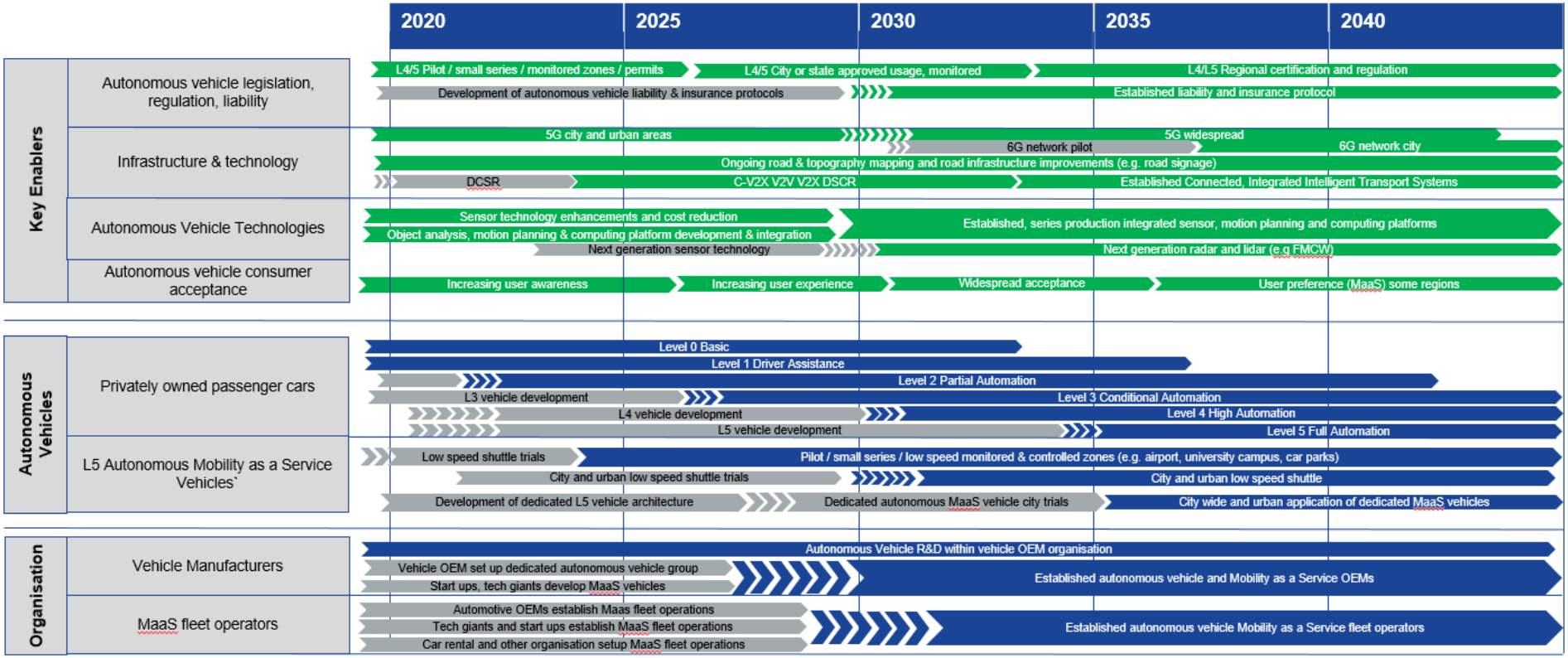

Figure 6.2.5.1.1 Extracts from creative design poll questions and response

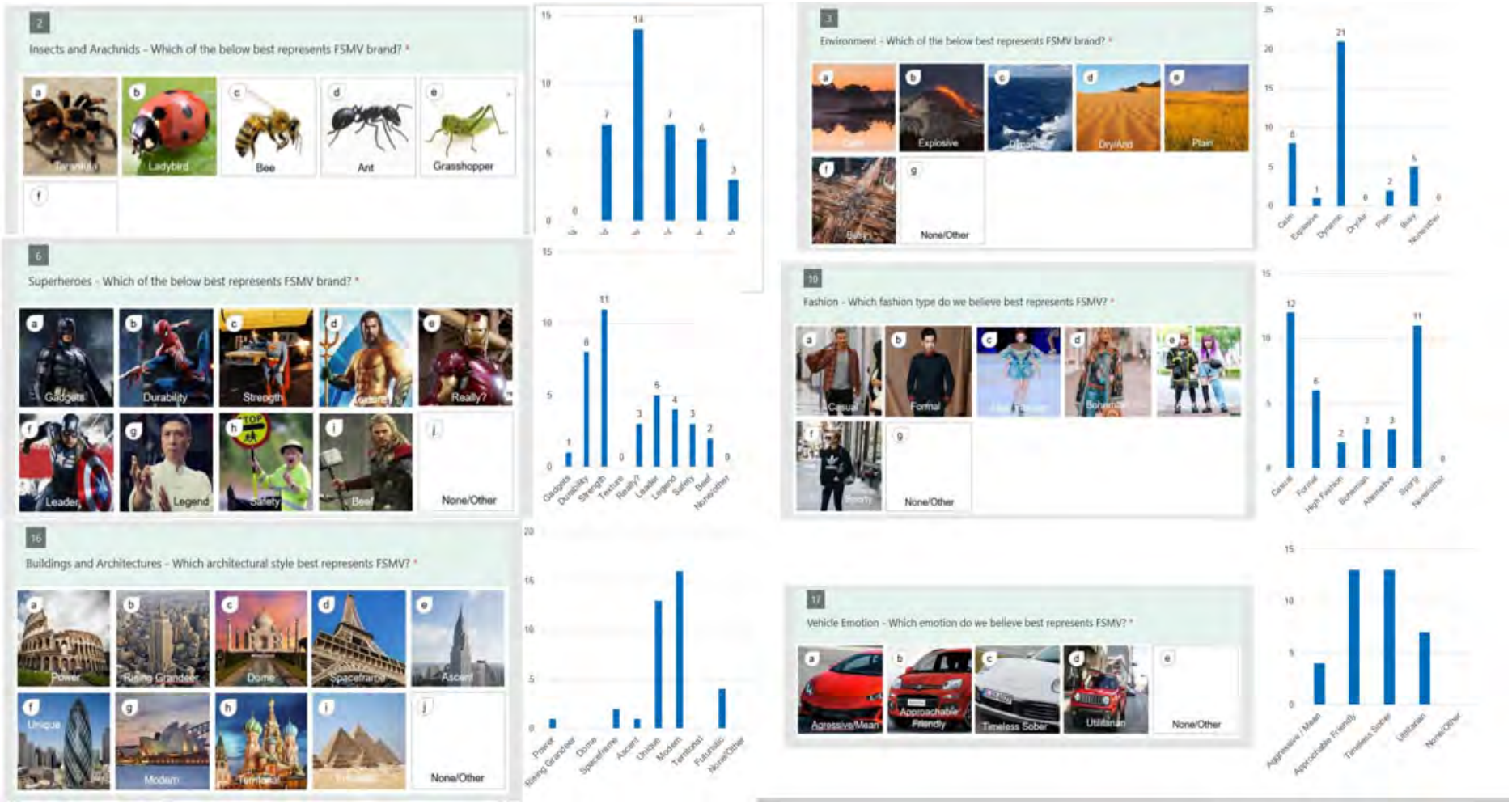

Figure 6.2.5.1.6 Engineering appraisal of 3 selected concepts

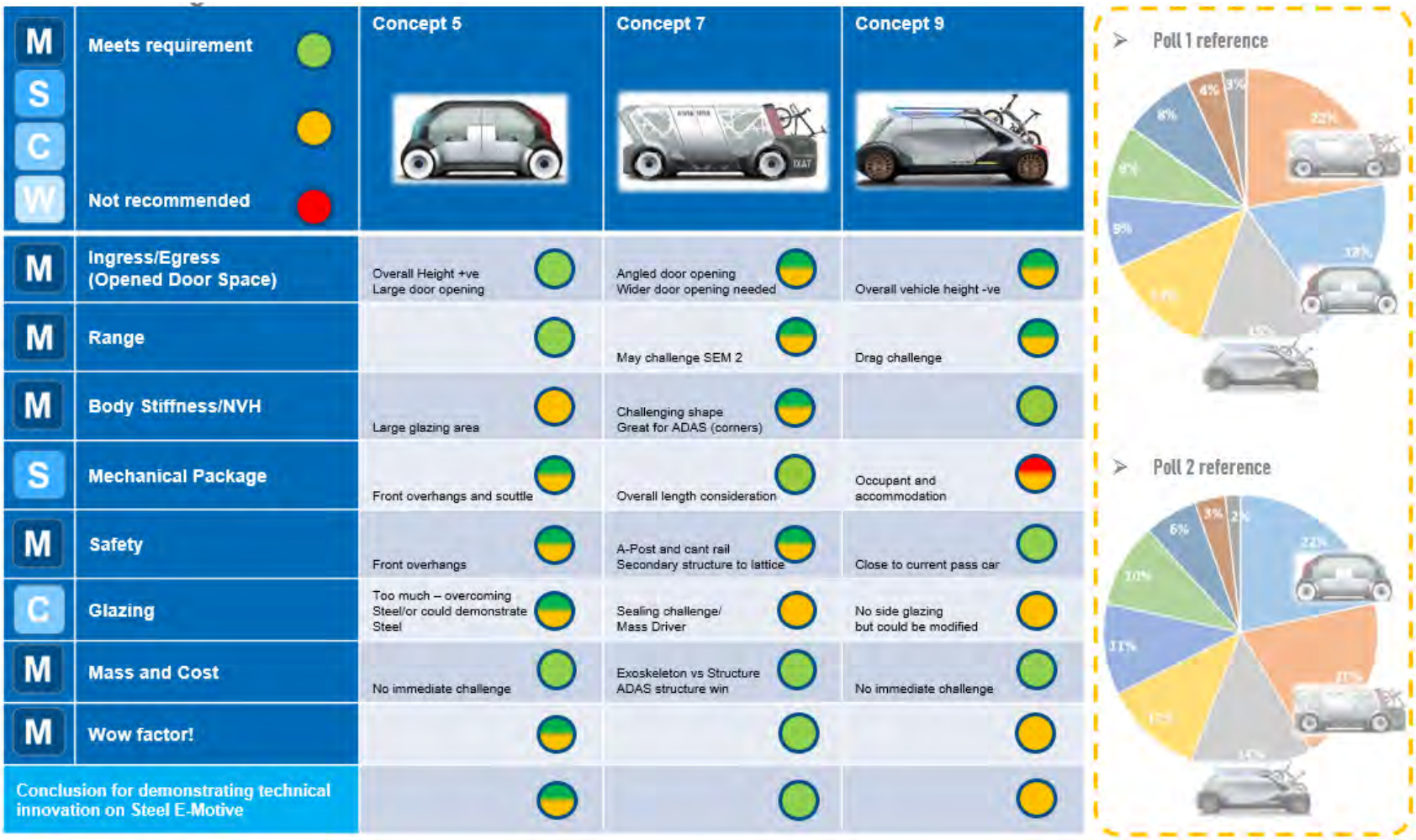

Figure 6.3.3.3 Front crash structure FEA concept design studies evaluating longitudinal crush rail and front subframe configurations

			Concept 1	Concept 3a	Concept 3b	Concept 3c
Front Longitudinal Crush Rail Design			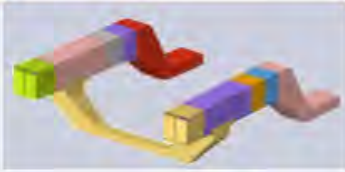	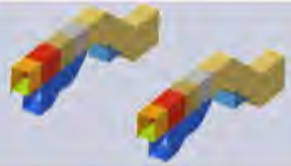	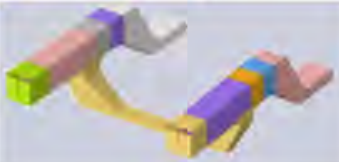	
Chassis/subframe design						(no subframe)
Metric		CAE Target (interim)				
FFB	Acceleration	<48G	43	51	56	54
FFB	Intrusion	- [mm]	363	398	375	400
FFB	Max longitudinal force	<350kN	265	261	334	256
ODB	Acceleration	<40G	39	36	X	37
ODB	Intrusion	- [mm]	893	820	X	777
ODB	Max longitudinal force	<350kN	293	253	X	268
Mass - longitudinal		- [kg]	13.6	10.2	13.6	12
Mass - subframe		- [kg]	15.6	14	7.2	X
Overall performance status						

Figure 6.3.3.5 Rear crash structure FEA concept design studies

		Concept 1a	Concept 1b	Concept 2	Concept 3a	Concept 3b
Body structure design			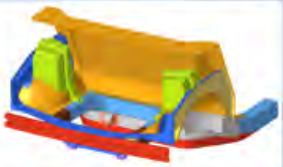	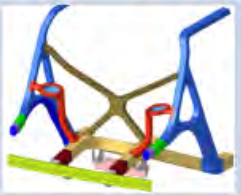		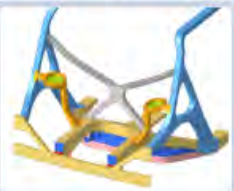
Rear subframe design		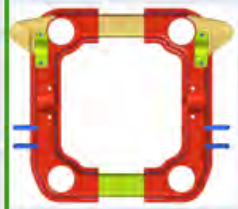	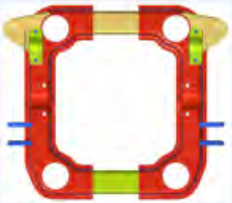	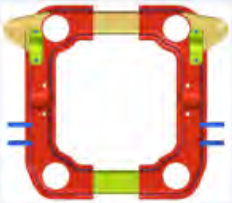	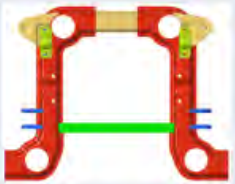	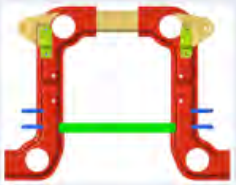
Metric	**CAE Target (subsystem/ interim)**					
Accelerations	<20G	30G	42G	30G	41G	49G
Battery Forces	<70kN	88kN	103kN	79kN	85kN	147kN
Door Intrusion	<40mm	127mm	69mm	48mm	79mm	15mm
Longitudinal Efficiency	-	37%	36%	51%	36%	44%
Body Mass	-	148kg	161kg	132kg	148kg	129kg
Subframe Mass		18.4kg	18.4kg	18.4kg	21.1kg	21.1kg
Overall performance status						

Figure 6.3.3.8 Preliminary rocker concept FEA studies, including aluminium extrusion benchmark

		(Benchmark study)	Concept 2	Concept 5	Concept 7.3.2
Mid-Zone Design (cross section profile)		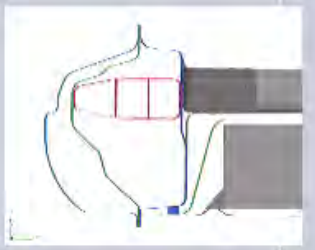	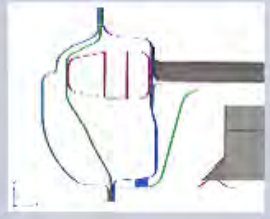		
Design concept		Extruded aluminium crush element, AHSS protection	Fabricated Advanced High Strength Steel crush element	**Coverless battery pack.** Body floor & crossmembers provide top cover.	**Sliding door concept** Re-profiled reinforcement sections, with stabilisers. Swages added to crossmembers. Sill inner increased thickness.
Metric	**CAE Target (subsystem model)**				
Rebound	-	35ms	43ms	33ms	29ms
Pole Force	-	625kN	560kN	552kN	544kN
Floor crush	<25mm	15mm	80mm	11mm	40mm
Rocker energy	>80%	82%	53%	95%	77%
Rocker Mass	<18kg/m	19.8kg/m	14.9kg/m	-	21.9kg/m

Figure 6.3.3.9 Development and assessment of rocker crush element designs

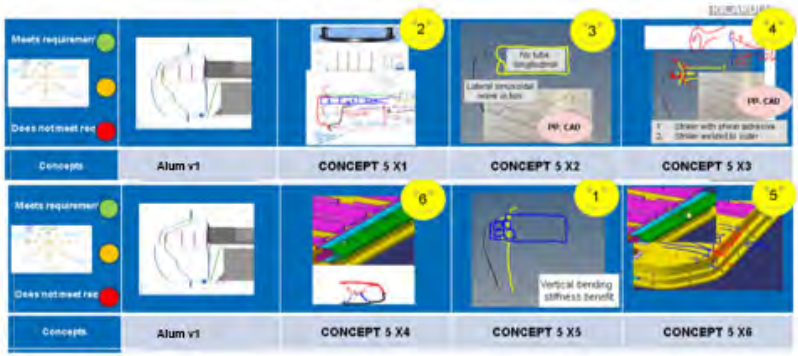

Base 4	Concept-5 X1	Concept-5 X2	Concept-5 X3	Concept-5 X4	Concept-5 X5	Concept-5 X7
Base model 3-part pusher Model 5444	D50mm Crashcans & stiff armature	Sine beam crush	Plunge & crush mechanism	Clamshell 2-Part pusher	D25mm crush tubes	Crush planes
Developed for Concept-5 mid-zone	Difficult to make work between crossmembers Armature heavy	Works well & very mass efficient	(Not evaluated)	Works well, comparable with base 3-part M5444	Tubes need to be joined to container & upper/lower surfaces along length	Stable crush of planes difficult to achieve
9.2kg/m	11kg to 14kg estimate	5.7kg/m		7.9kg/m	8.0kg/m	9.0kg/m
MS1700	Cans DP1180 Armature MS1700	DP1180		MS1700	MS1700	DP1180

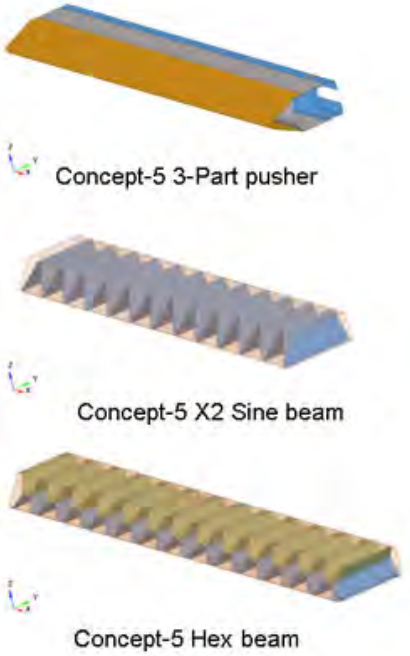

Figure 6.3.4.4 Battery concept #8 assembly process (battery into vehicle only)

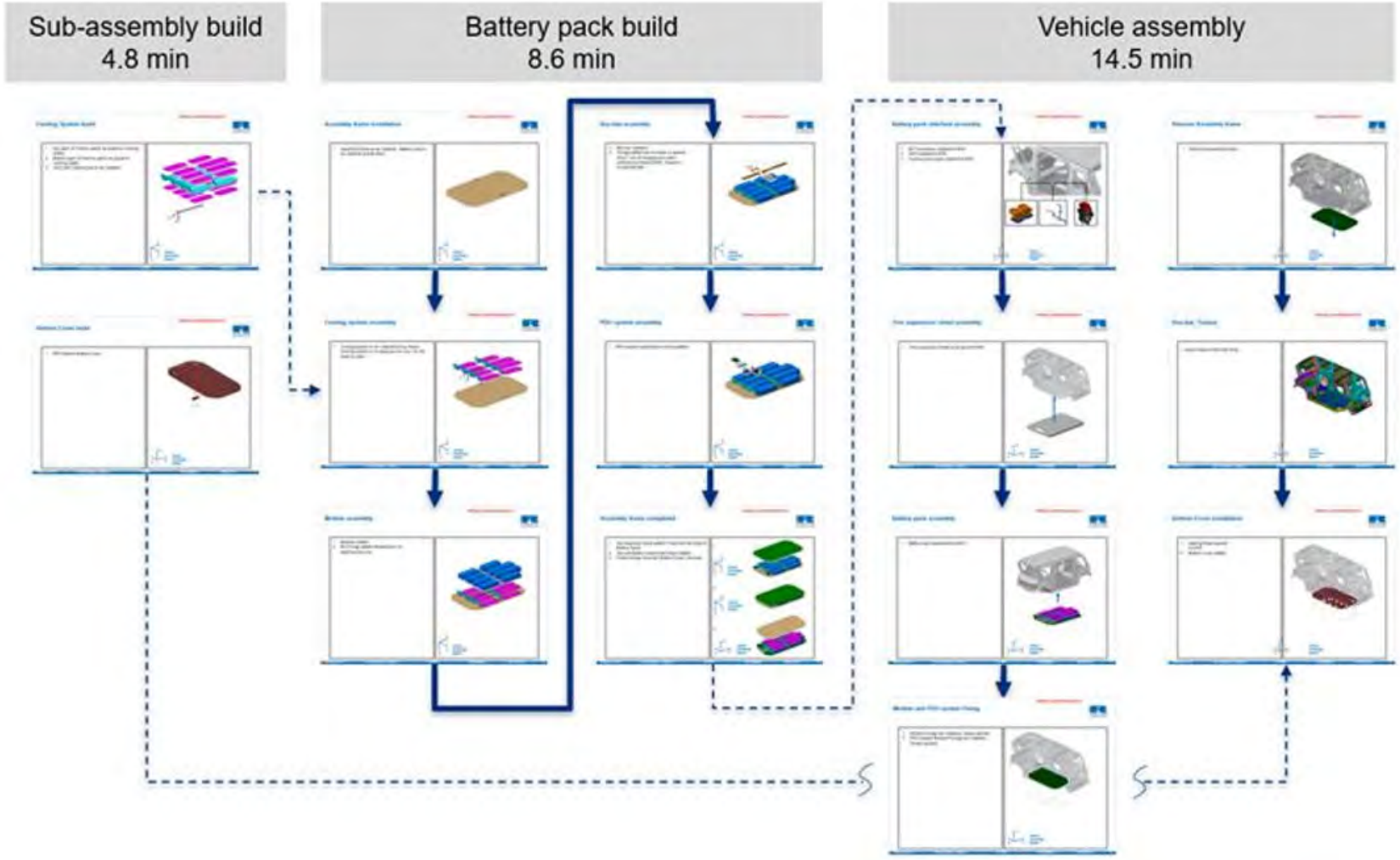

Figure 6.3.4.7 Battery concept #11

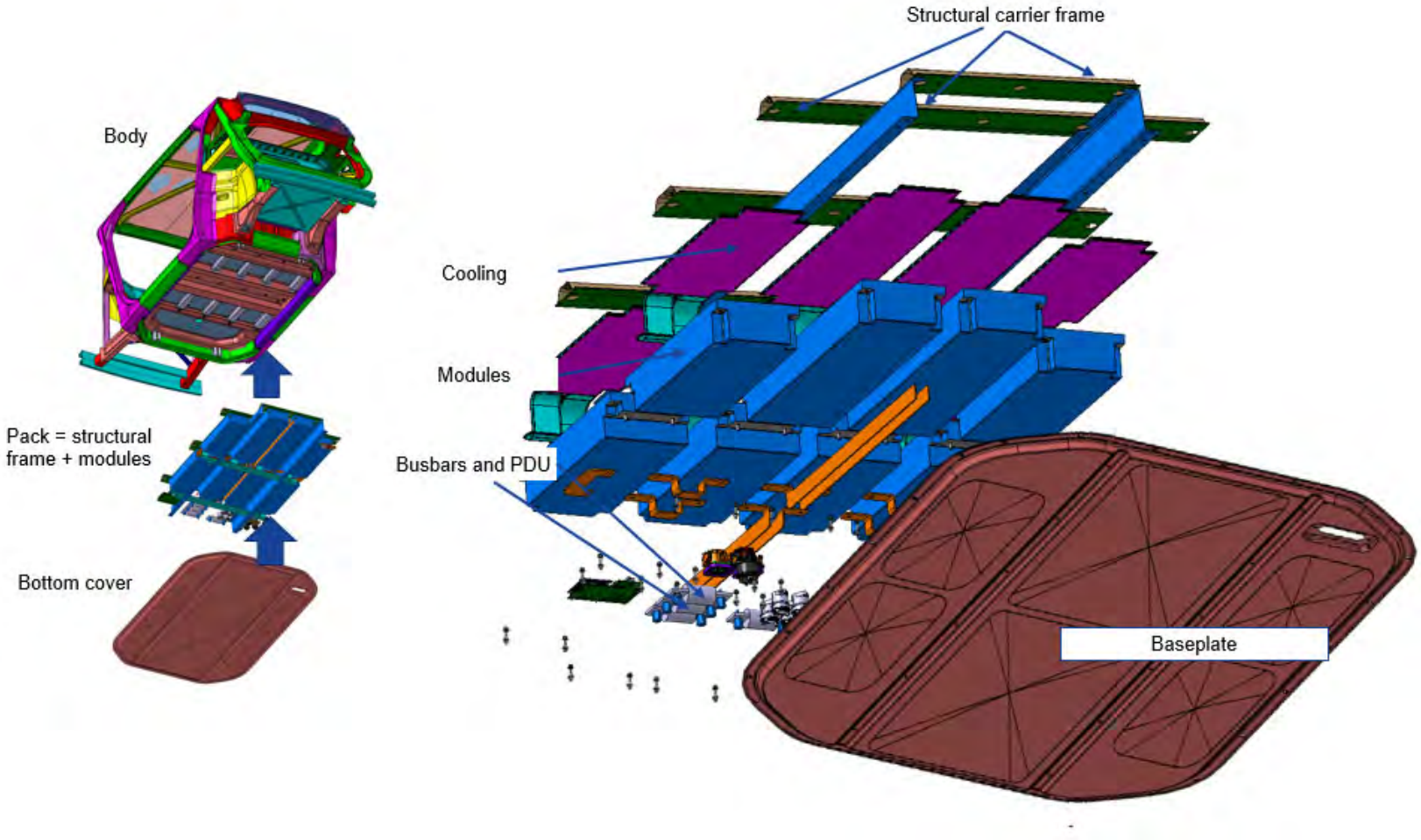

Figure 6.3.5.3.2 Rear closures concept selection matrix

	BASELINE					SELECTED		
Attribute	**Concept 1 – Conventional Liftgate**	**Concept 2 – Club Door**	**Concept 3.1 – Half Liftgate with Exposed Hinge**	**Concept 3.3 – Half Liftgate with Fiat 500 Hinge**	**Concept 4.1 – Coach Door**	**Concept 4.5 – Coach Door Revision**	**Concept 5 – Double Link Hinge**	**Concept 6 – Split Liftgate**
Tailgate Opening (mm)	1431	449	449	610	688	690	462	1431
Interior Intrusion	N/A	N/A	N/A	N/A	235mm (x) from back of closest passenger	Crank of looped arms currently sits 352mm (x) from back of closest passenger	N/A	N/A
Mechanical Package	Simple hinge design with powered strut mounted to BIW	Connecting arm must be exposed to allow for secondary hinge axis to be outside the vehicle Requires A-Surface to move	Hinges must be exposed to allow for correct sweep that doesn't clash with glazing	Full hinge assembly with base/door plates packages well into BIW	Large connecting arms difficult to package Hinge axis can be changed to allow for more efficient package and eliminate some current clashes	Needs consideration for driving mechanism (Stabilus Powerise or motor) Connecting arms package more efficiently than previous concept 4.1 due to reduced crank throw	Concept needs to be further developed to efficiently package hinge design without BIW clashes	Concept needs to be further developed to efficiently package hinge design without BIW clashes
Kerbside Ingress (mm)	N/A	635	N/A	N/A	N/A	N/A	N/A	N/A
Vehicle Height Impact (m)	1.99 (+0.11)	N/A	N/A	N/A	2.03 (+0.15)	2.03 (+0.15)	1.98 (+0.10)	2.02 (+0.14)
Rear Overhang (mm)	646	695	363	447	185	197	113	296
Overhang at Open Position (mm) (measured from bumper A-Surface)	653	-114	/	258*	/	-66	-40	296
Fixed Glazing	N	Y	Y	Y	Y	Y	Y	N
Rear Box Section Potential (global stiffness contribution)	N	Y	Y	Y	Y	Y	Y	N
Door Panel Mass Estimate (kg)	19.62	7.47	/	10.6	/	11.8	10.6	19.2
Cost Estimate	WIP							

Figure 6.3.6.2.4 SEM1 IIHS 64kph SORB front crash strategy

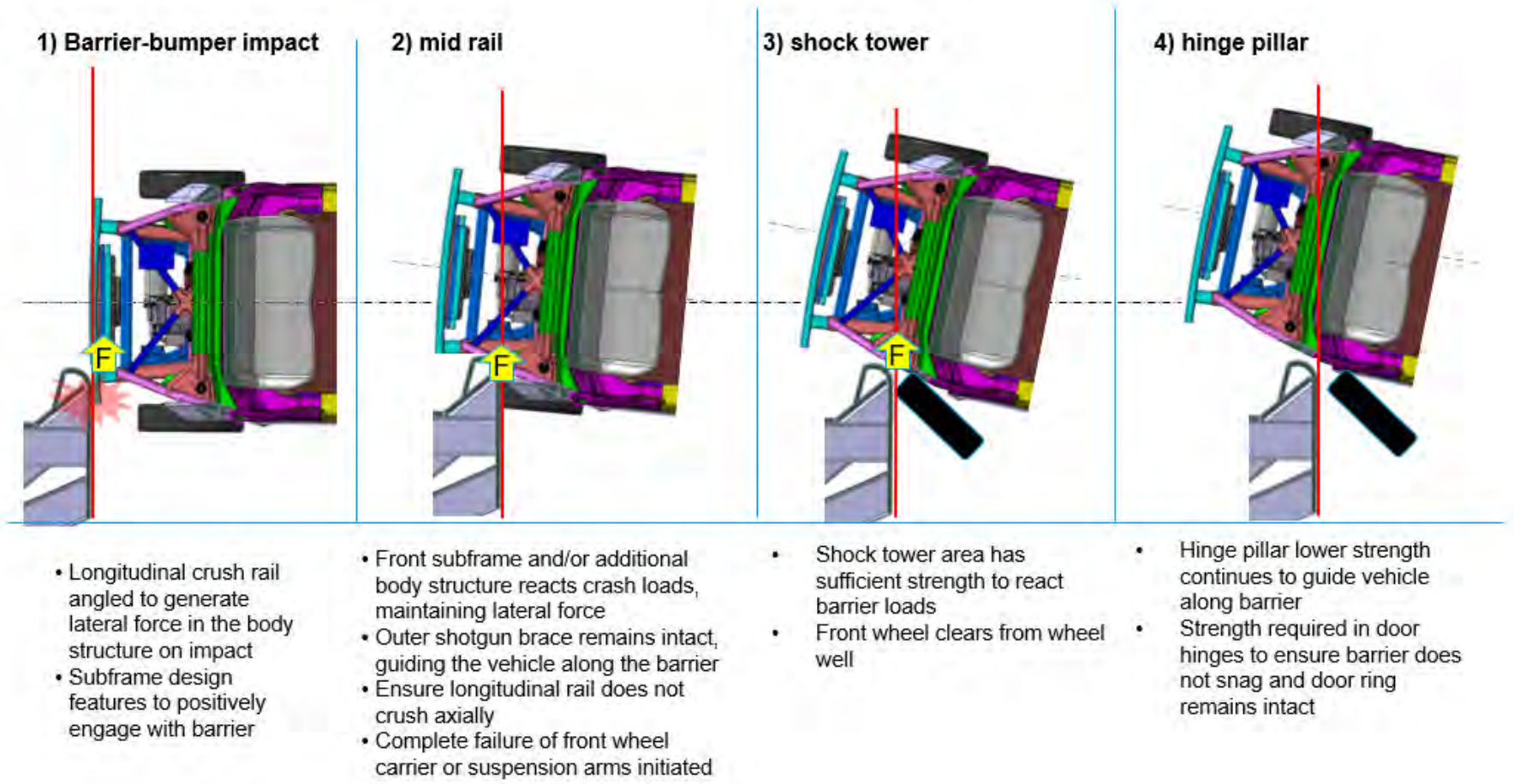

Figure 6.3.6.5.1 Considerations and approach for protection of the rear facing front occupants in a frontal collision

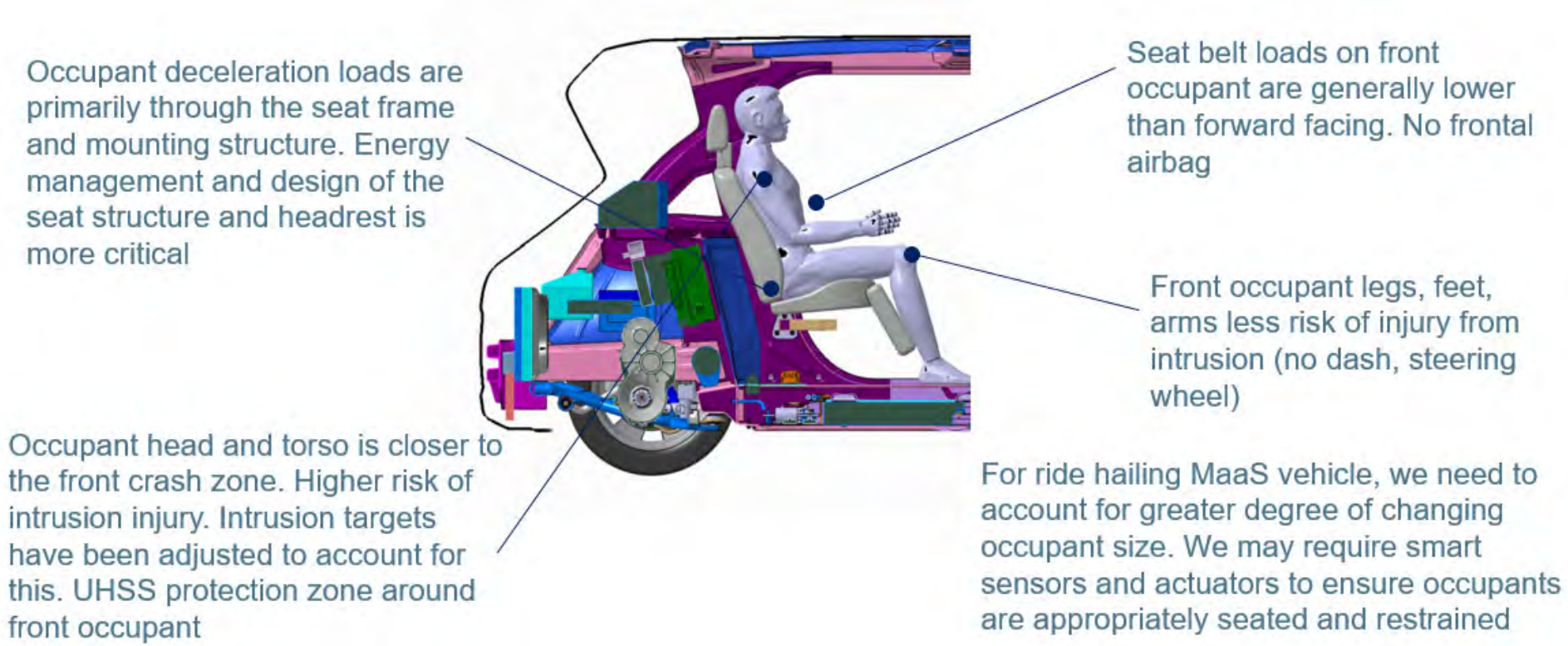

Figure 7.1.1 Engineering 3D CAD image of SEM1 vehicle. Key design features and achievements

SAE Level 5 autonomous driving:
- Fully autonomous, SAE level 5
- Deletion of direct driver controls (steering wheel, pedals, dashboard)
- Package accommodation of autonomous vehicle sensors
- Suitable for deployment on existing highway networks, operating alongside Level 1 to 4 vehicles

Spacious, comfortable cabin interior
- Inward facing seating configuration
- Scissor doors with wide door aperture providing improved entry and egress for passengers
- Glazing surfaces maximised, enabling light and airy cabin space environment
- Steel E-Motive frame mounted integrated battery solution results in a flat floor interior and low step in height
- Vehicle systems packaged and positioned to provide maximum interior space

Advanced High Strength Steel Body Structure:
- Achieves high speed vehicle crashworthiness standards. Predicted to achieve IIHS “good” rating
- High stiffness and strength body structure. Good levels of comfort and NVH
- Lightweight steel design
- Significant reduction in lifecycle greenhouse gas emissions comparing 2035 operation to 2020 conventional battery electric vehicle

Optimised propulsion system
- 75kWh battery electric powerunit. Front electric drive unit. Potential for 12 hour operation on a single charge
- Potential for conversion to hydrogen fuel cell powertrain
- All wheel steer, enabling 7.4m turning circle

Figure 7.1.5.2 Vehicle curb weight versus box volume comparison. Reference vehicle data source www.a2mac1.com

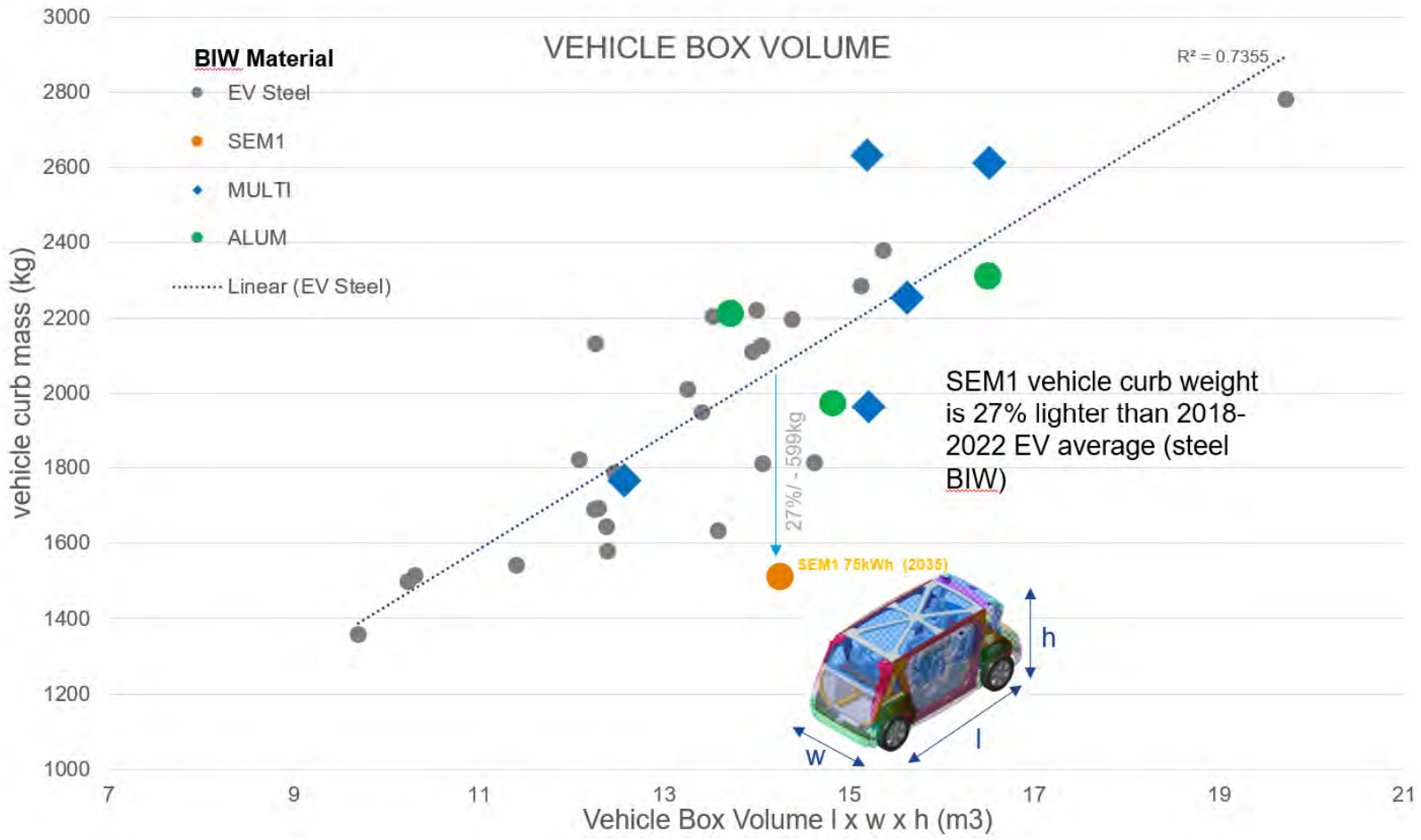

Figure 7.2.1.1 Steel E-Motive SEM1 BIW design and distribution of AHSS

Figure 7.2.1.2 Steel E-Motive BIW AHSS grade allocation

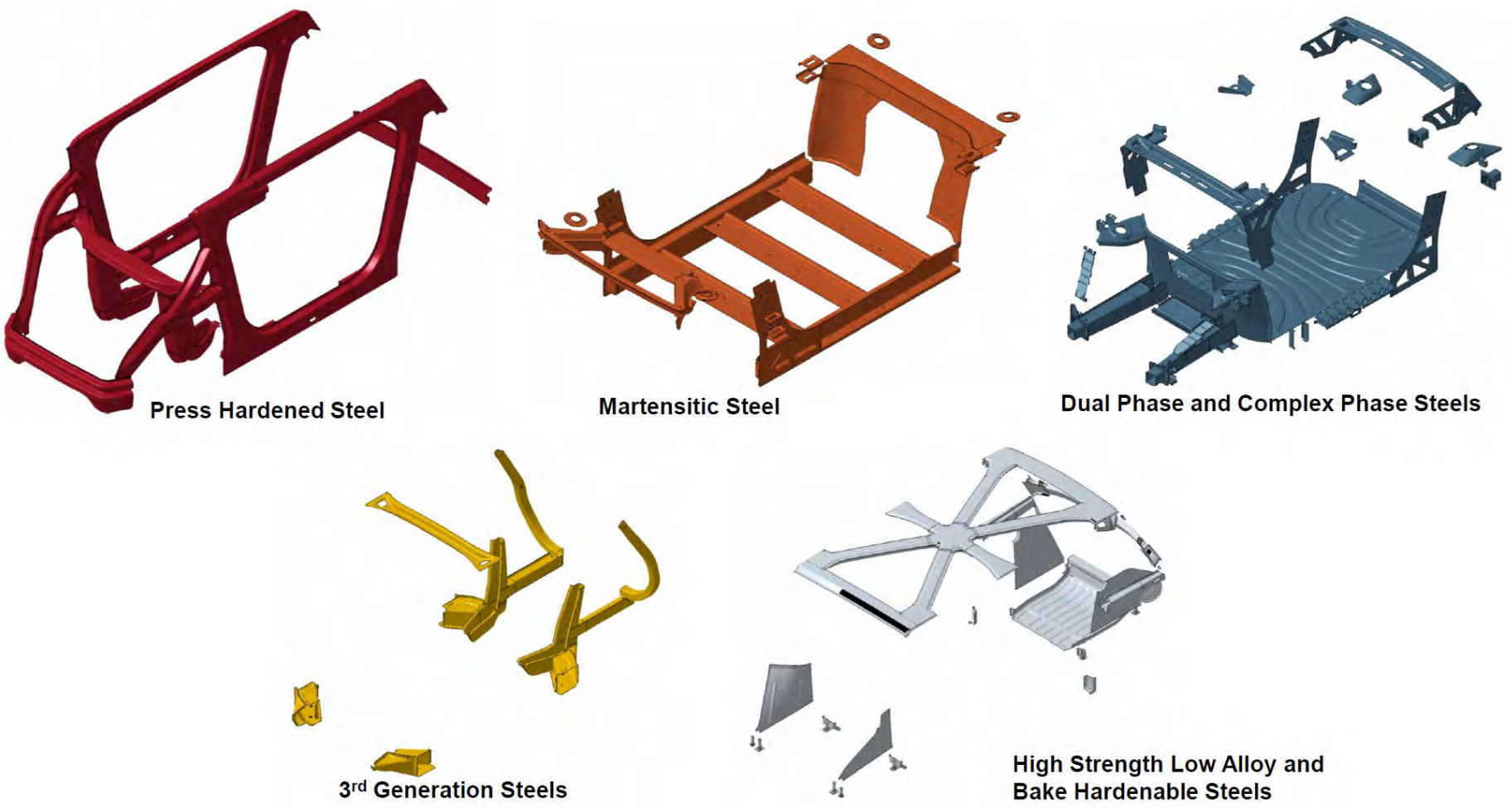

Figure 7.2.1.3 Steel E-Motive BIW AHSS grade distribution

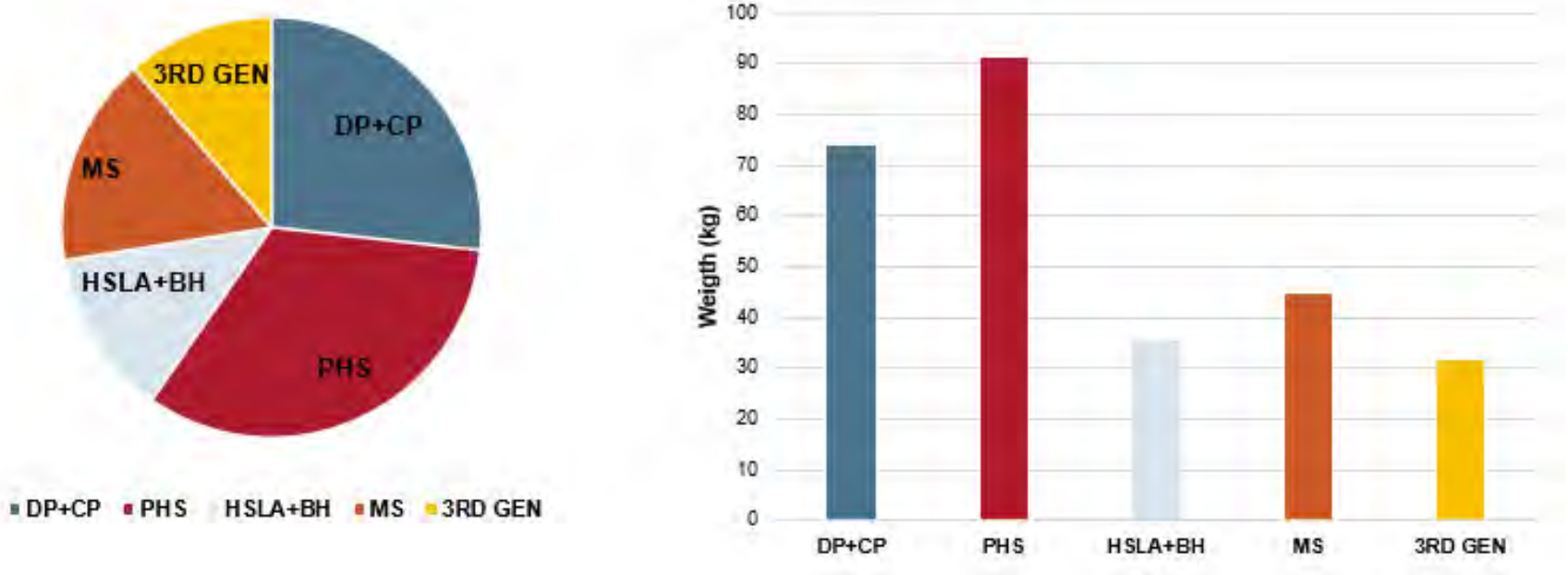

Figure 7.2.1.4 Steel E-Motive SEM1 BIW AHSS grades (exploded view)

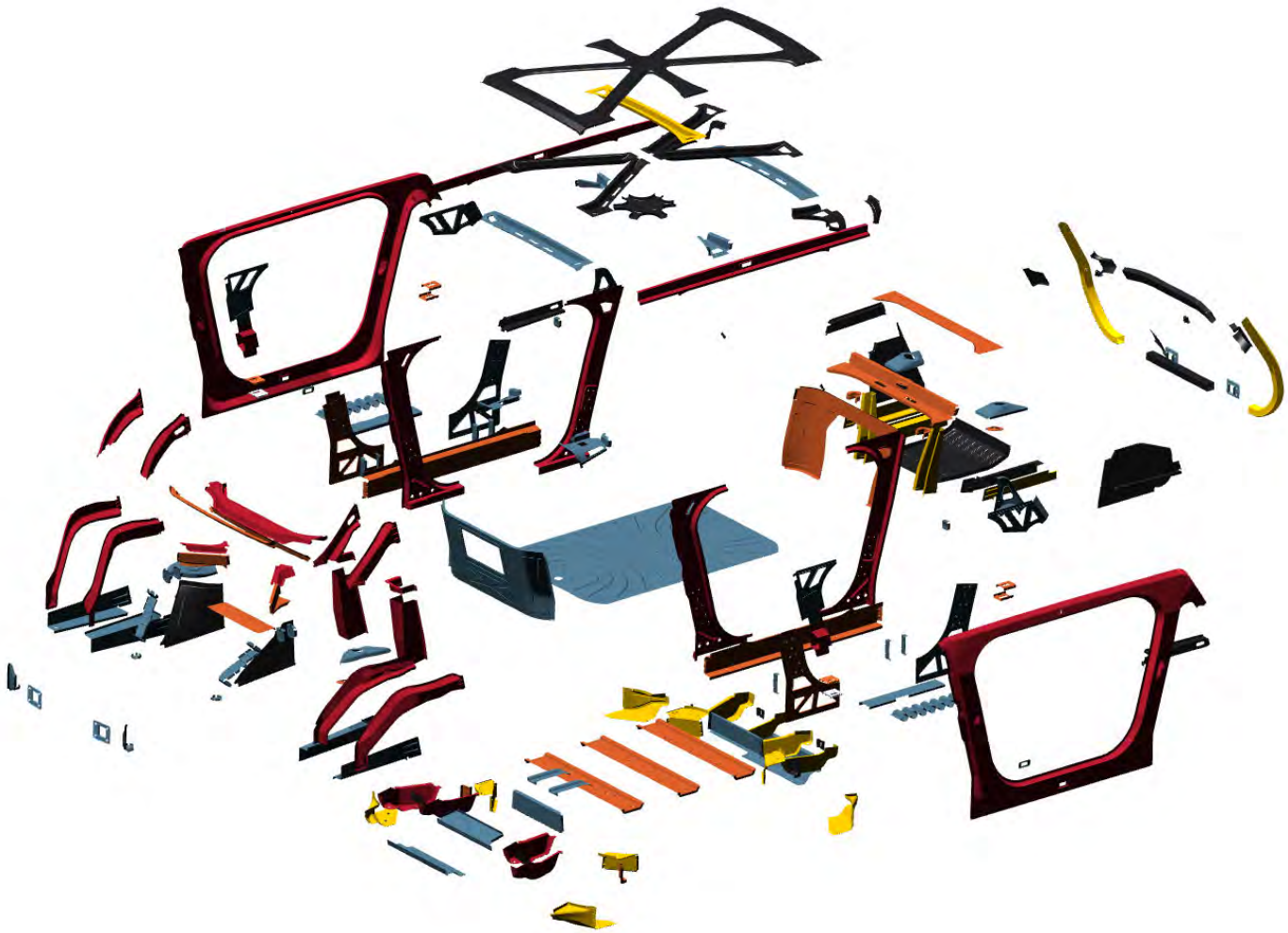

Figure 7.2.2.2 Body In White weight regression analysis

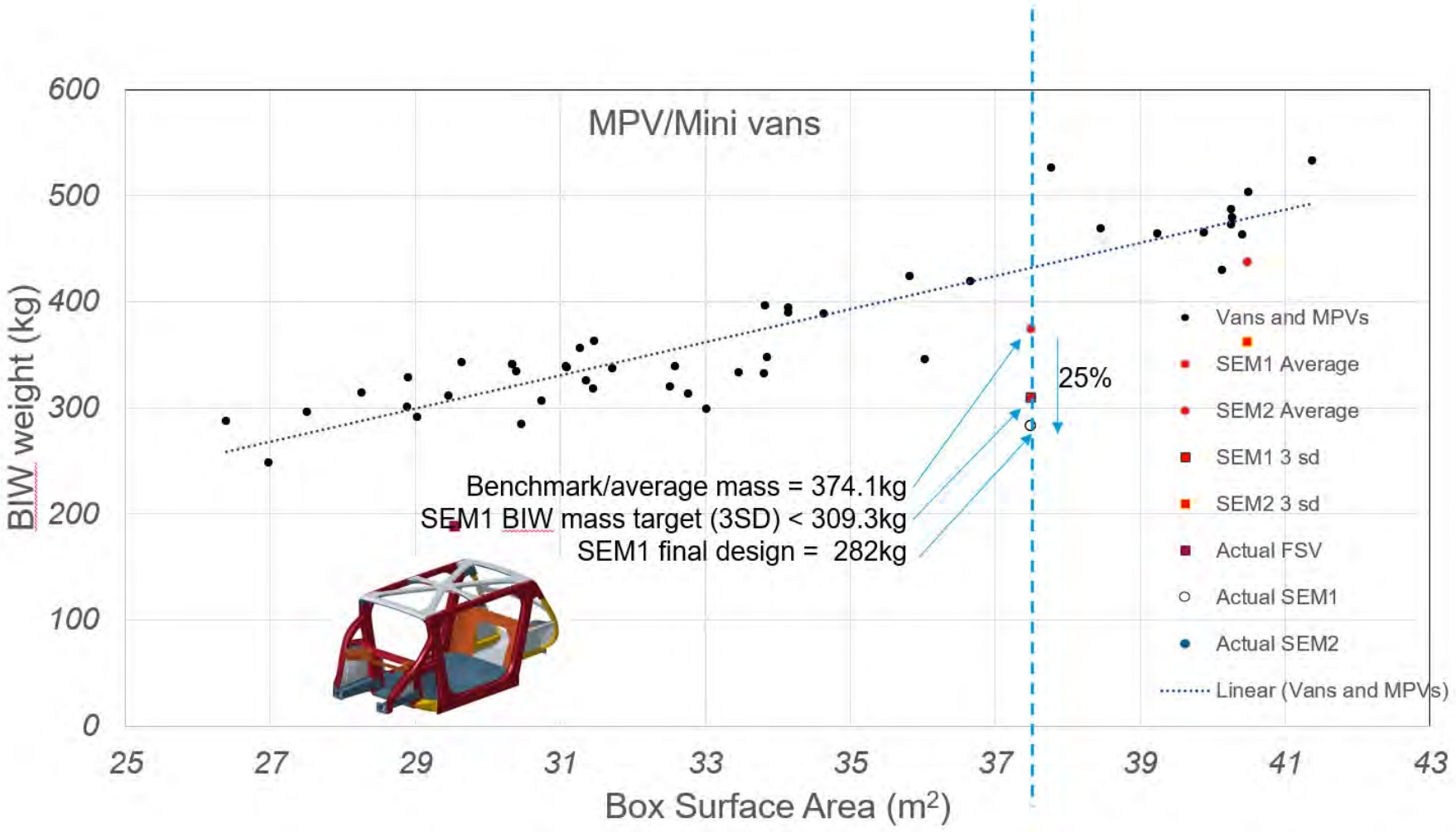

Figure 7.2.2.4 SEM1 body structure key loadpaths

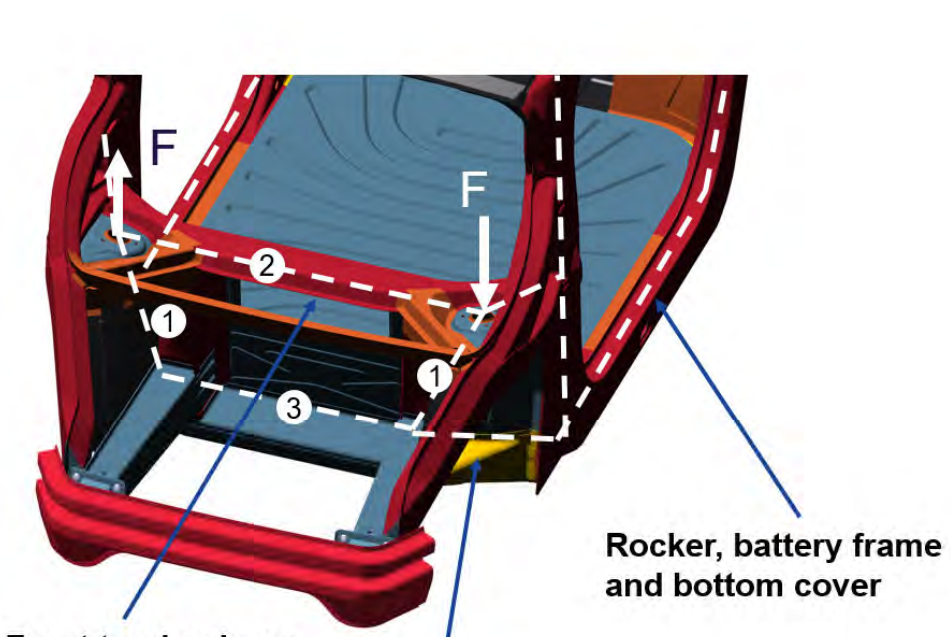

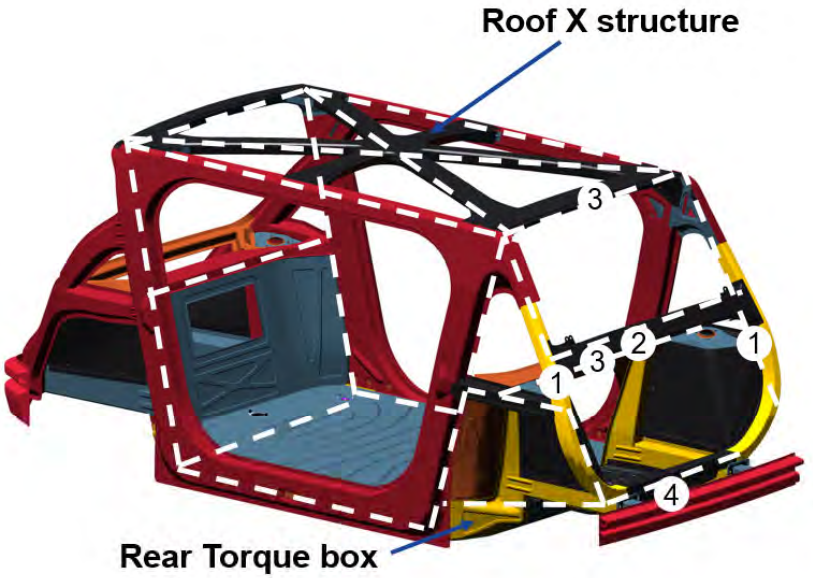

Rear torsion loop:

1) Hydrofrom D pillar
2) Coach door lateral brace
3) Rear roof header
4) #6 bar
5) Lateral strut brace

Figure 7.2.2.5 BIW section in X-X through front strut top mounts

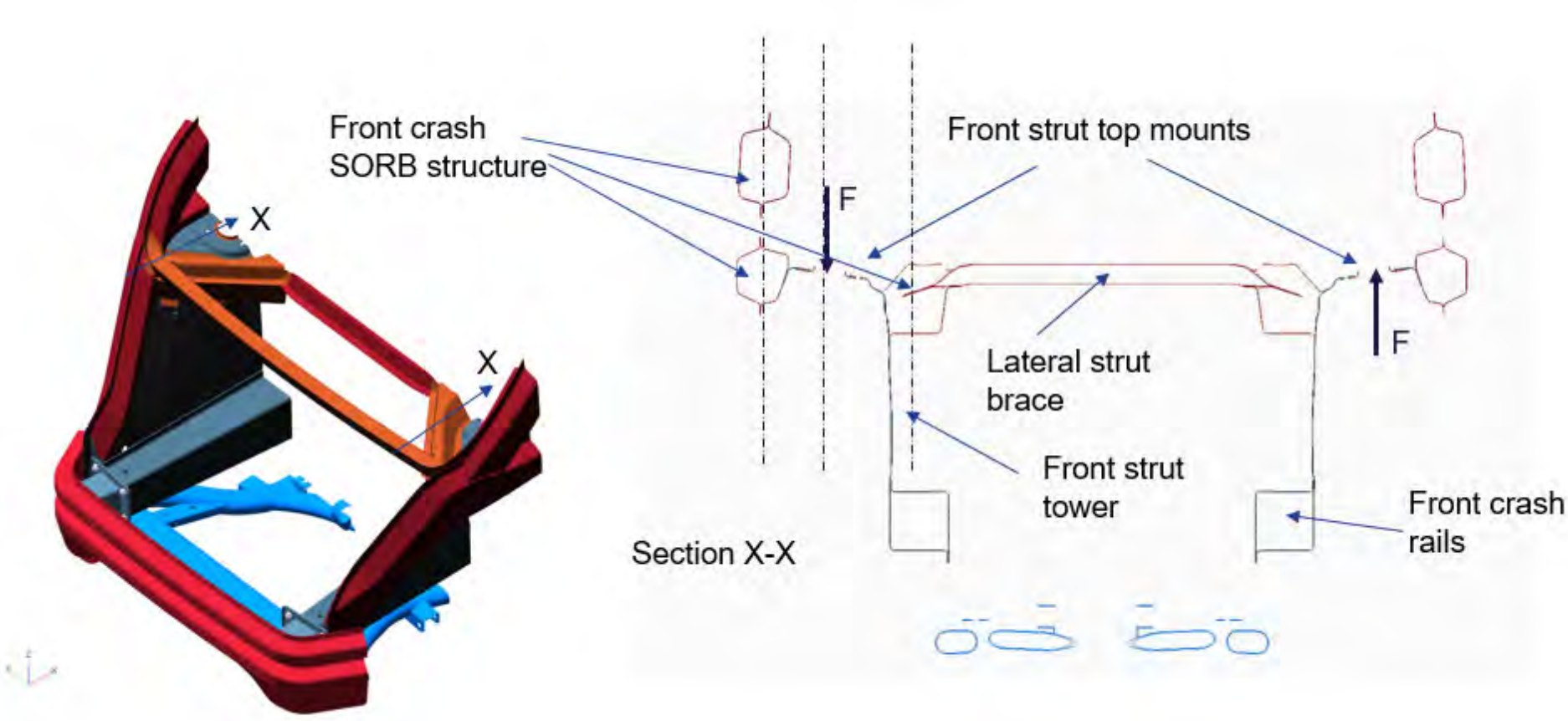

Figure 7.2.2.8 Battery carrier frame fixings to body in white

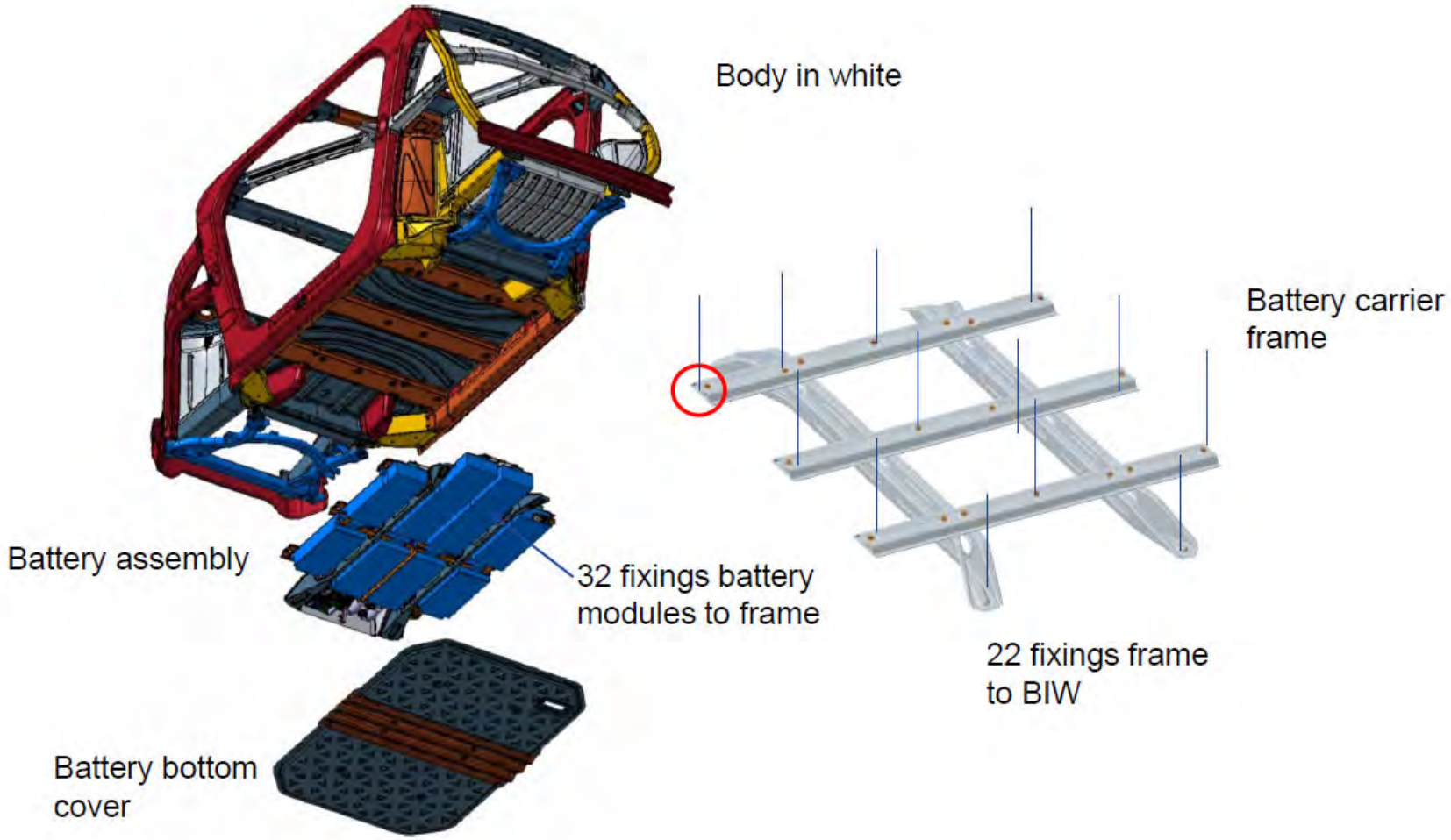

Figure 7.2.2.10 Localised gusset reinforcements adding efficient stiffness and strength improvements

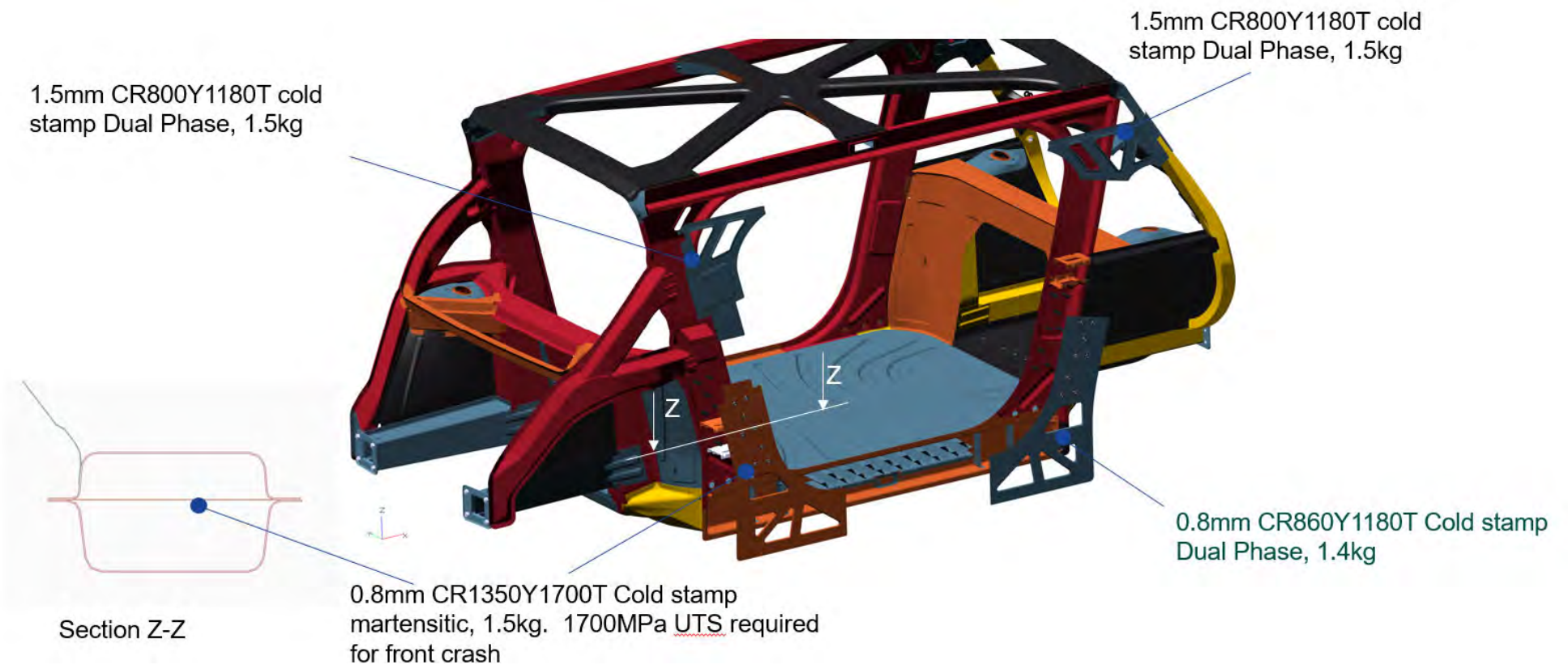

Figure 7.2.2.14 Gauge thickness assignment in SEM1 BIW (exploded view)

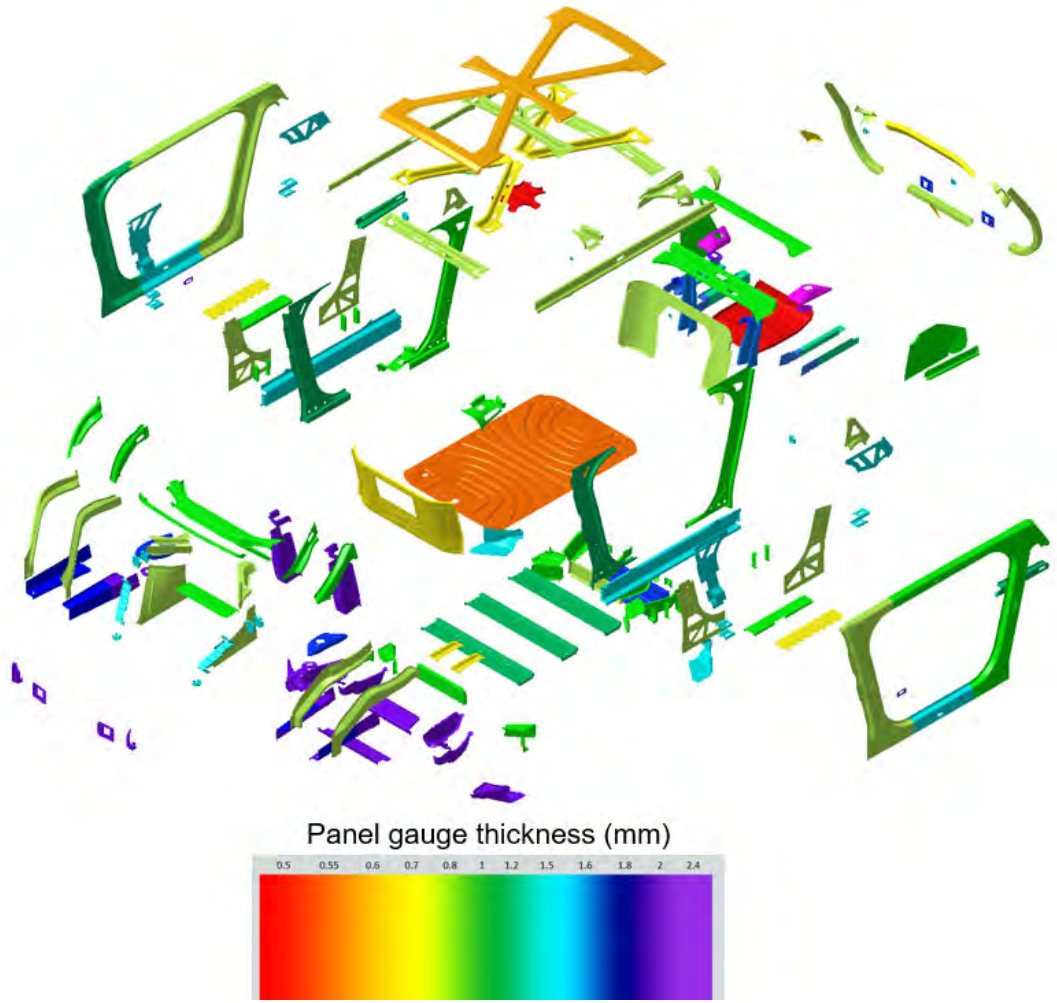

Figure 7.2.2.14 Body in White joining methods

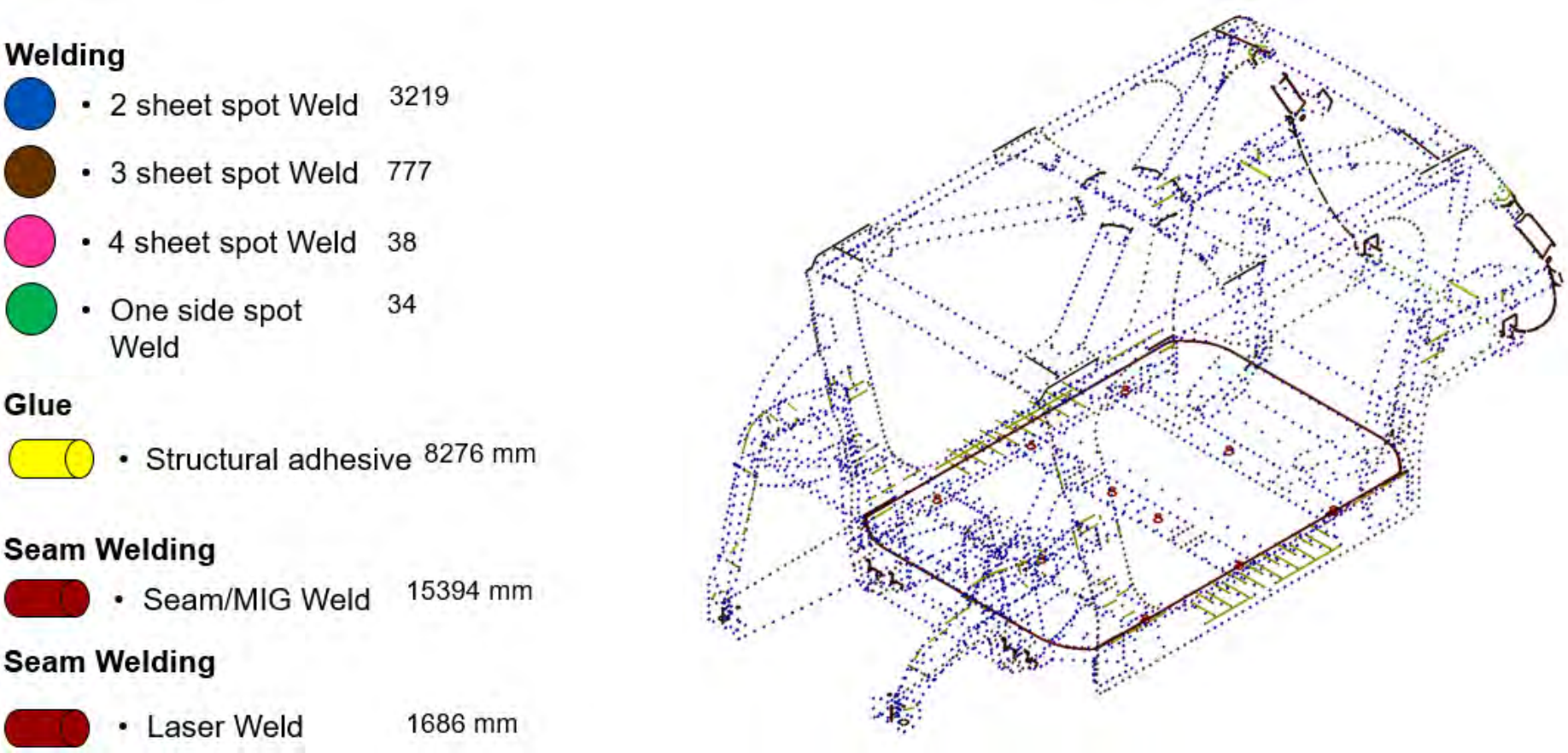

Figure 7.2.2.24 SEM1 Vehicle NVH modal map

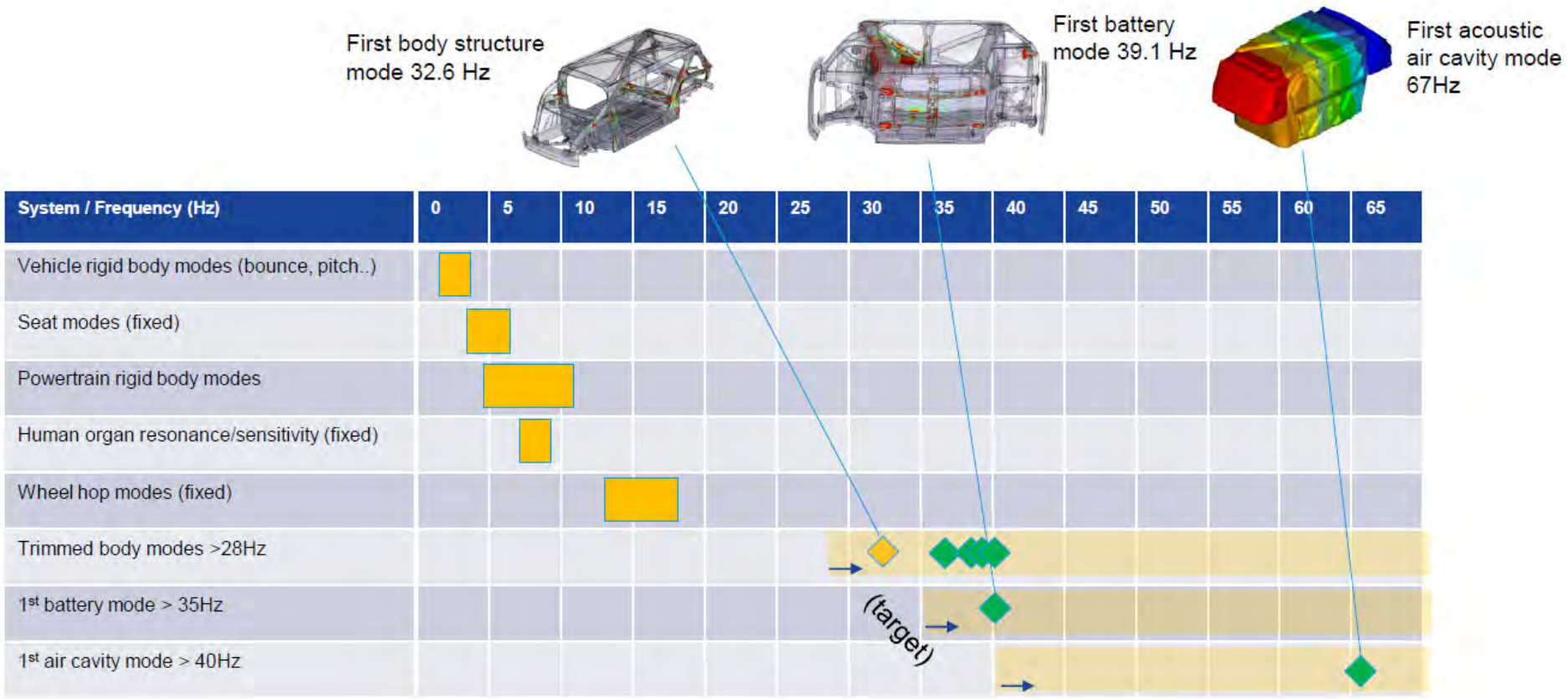

Figure 7.2.3.1 Primary subassemblies in SEM1 front crash structure

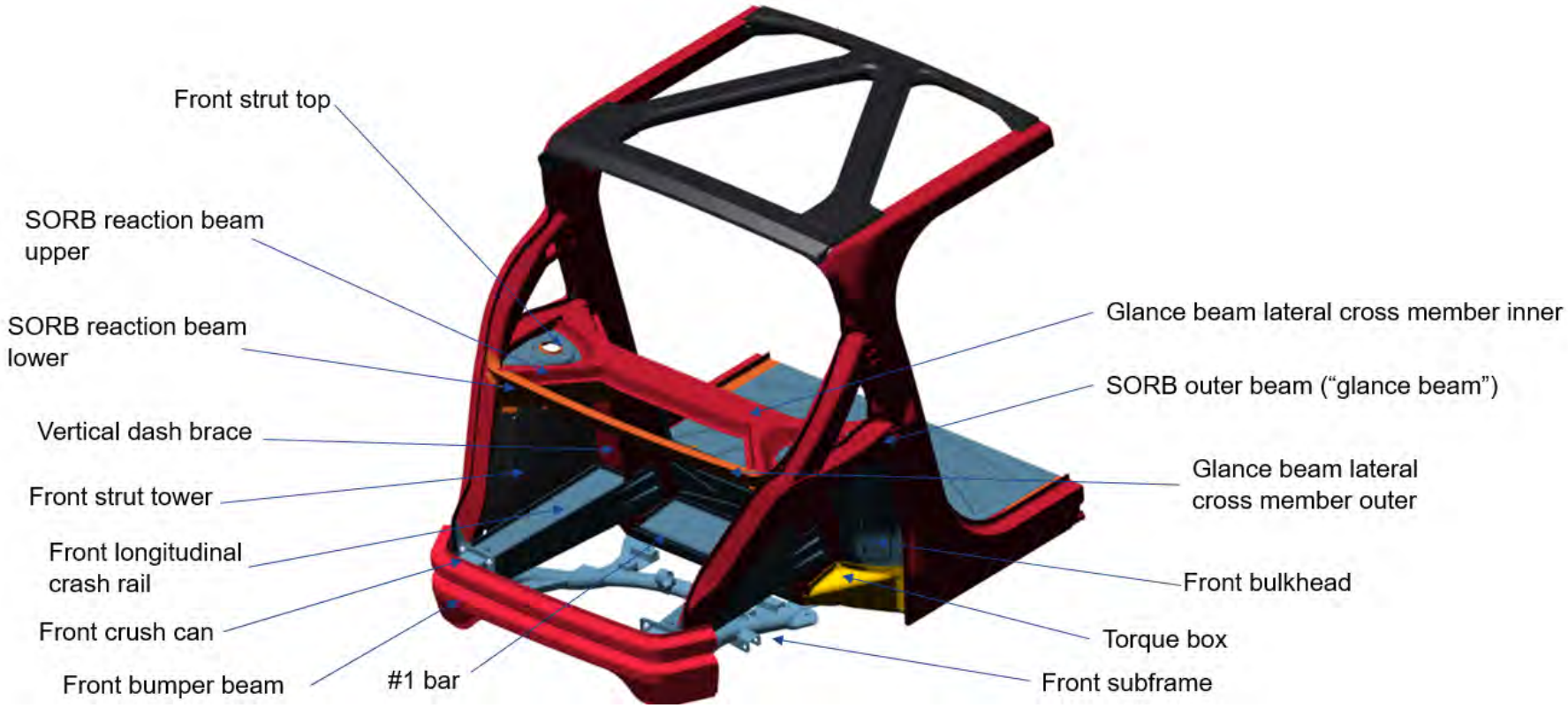

Figure 7.2.3.2 USNCAP 56kph FFB crash test. Vehicle CAE simulation showing the front crush zone deformation behaviour (some parts removed for clarity)

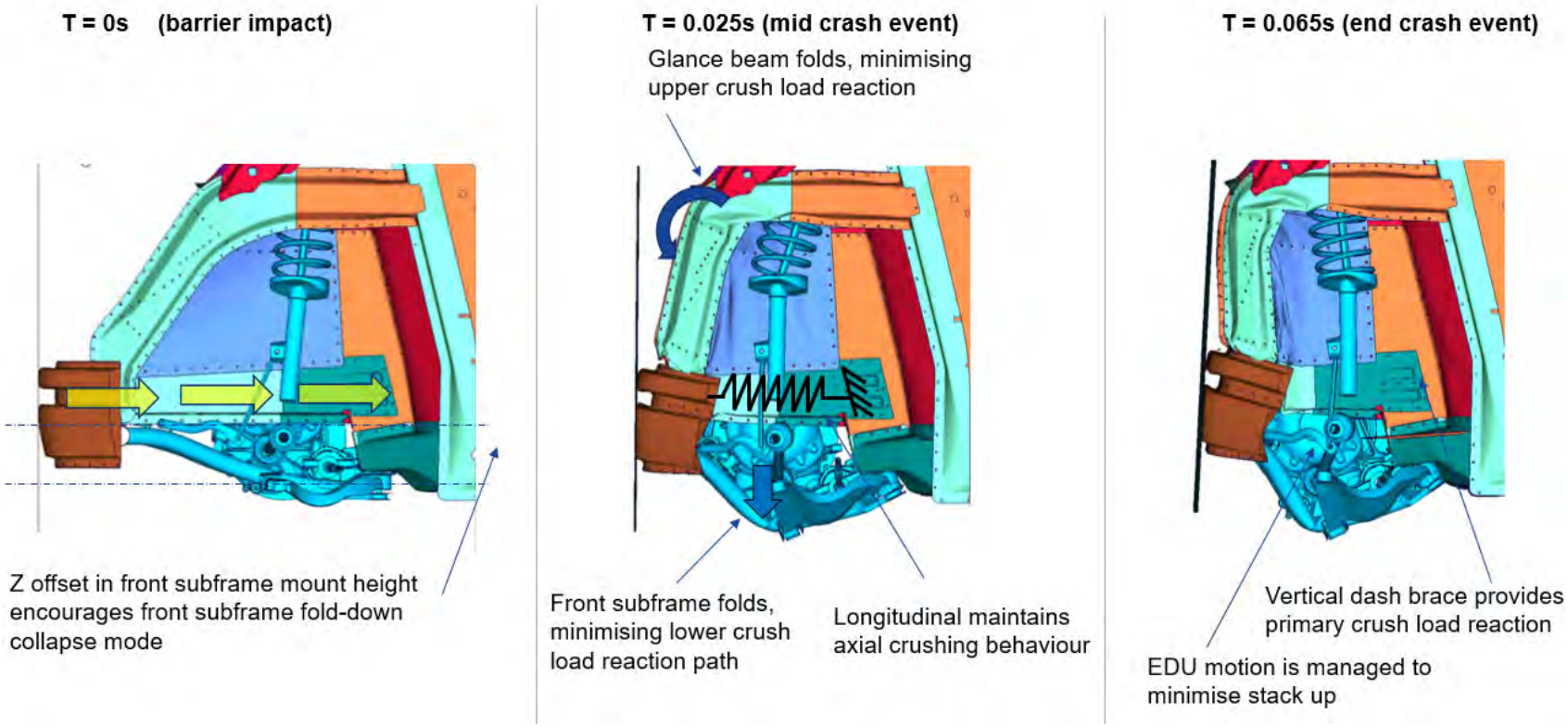

Figure 7.2.3.2b USNCAP 56kph FFB crash test. Vehicle CAE simulation showing the front crush zone deformation behaviour (some parts removed for clarity)

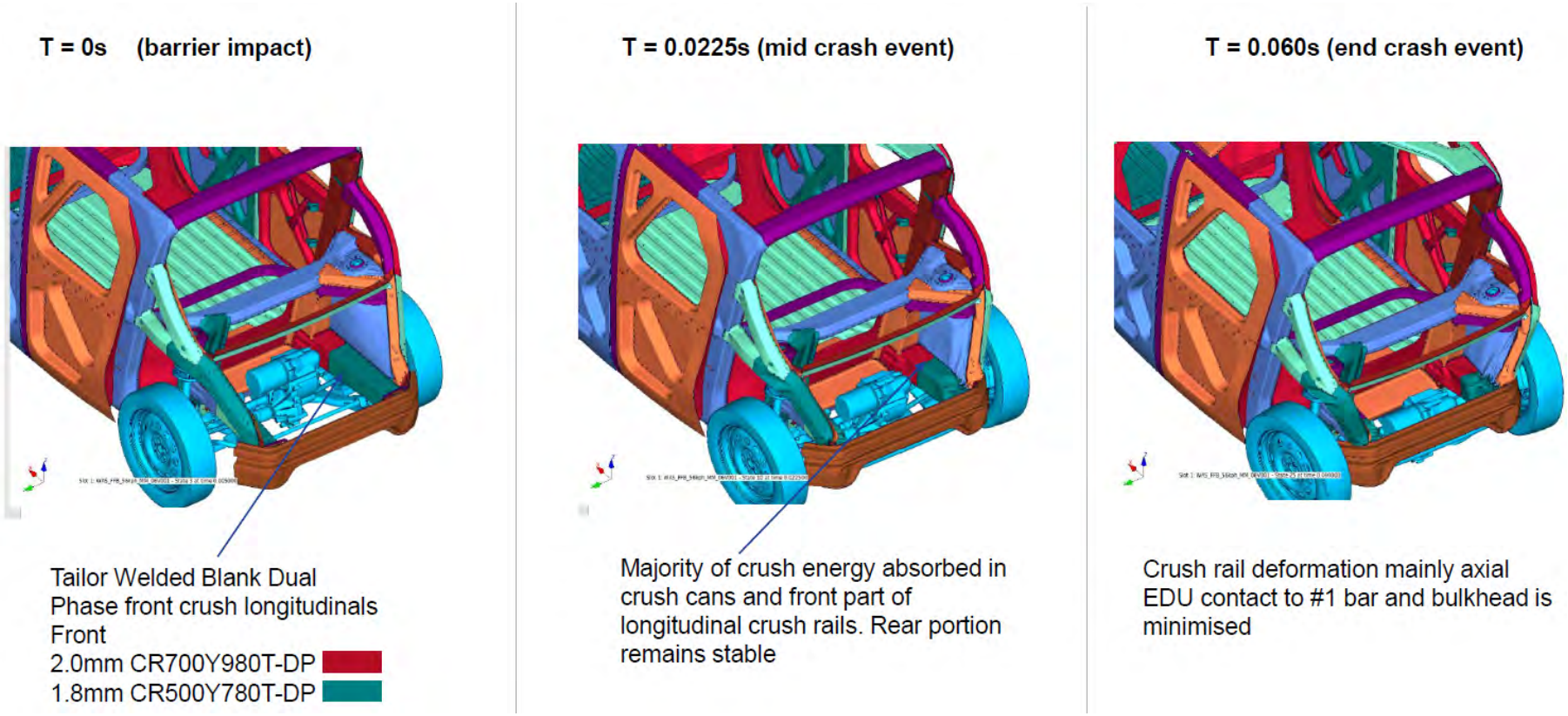

Figure 7.2.3.5 Front crash FFB and ODB key components and AHSS grades & gauges

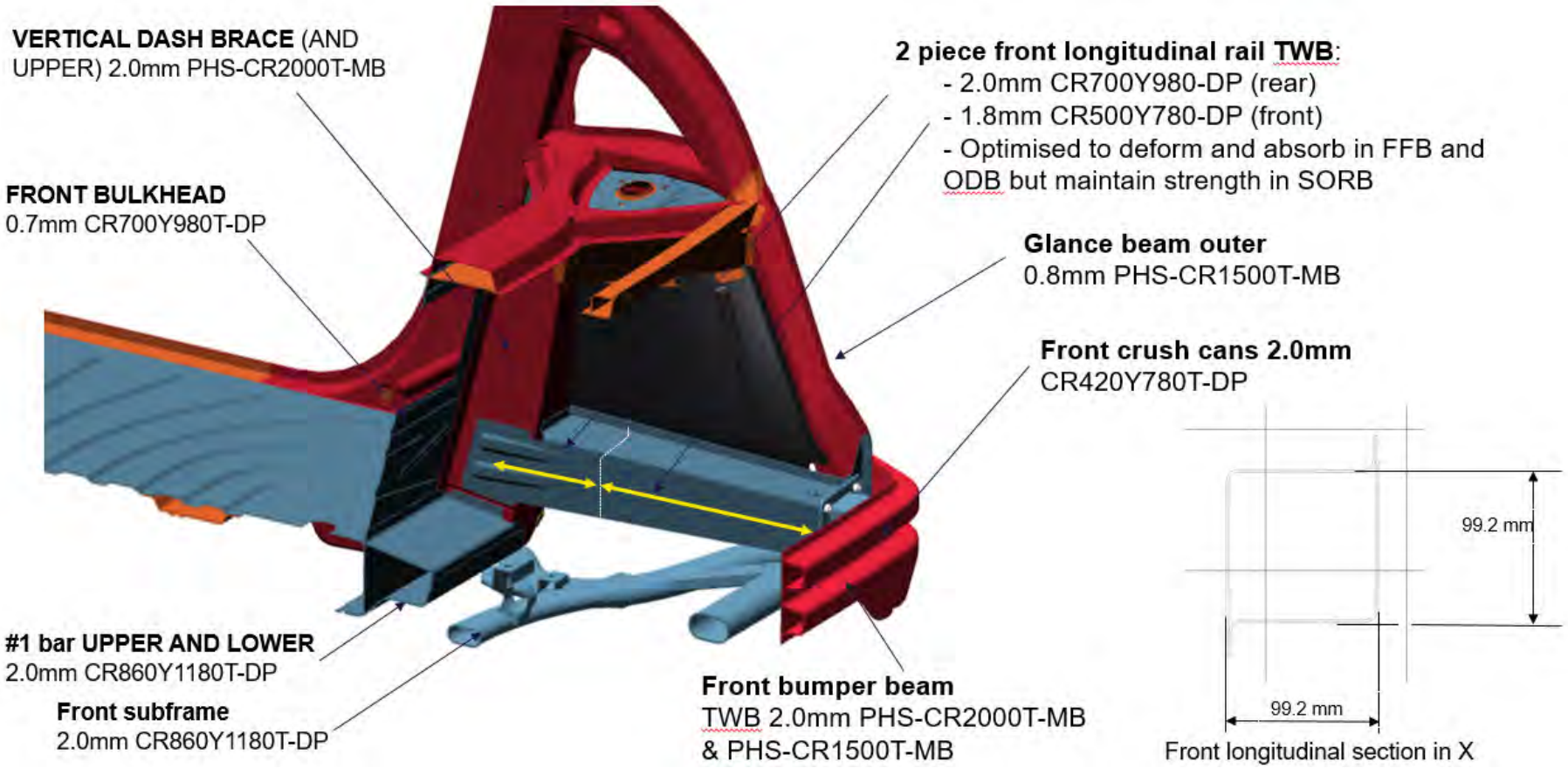

Figure 7.2.3.14 Front bumper beam AHSS grades

Front Bumper Beam	
Geometry/design	Bumper beam outer faces angled and oriented to align with IIHS SORB barrier impact location. In early stage of SORB crash event the bumper beam deforms to contact with front subframe providing lateral force loadpath to initiate glance off motion
Part 1: front bumper panel	2.0mm PHS-CR2000T-MB / Hot form
Part 2: rear bumper panel	2.0mm PHS-CR1500T-MB/ Hot form
Part 3: front crush cans	2.0 mm CR420Y780T-DP / Cold Stamp
Part 4: interface panel	1.2mm CR780Y980T-CP / Cold Stamp

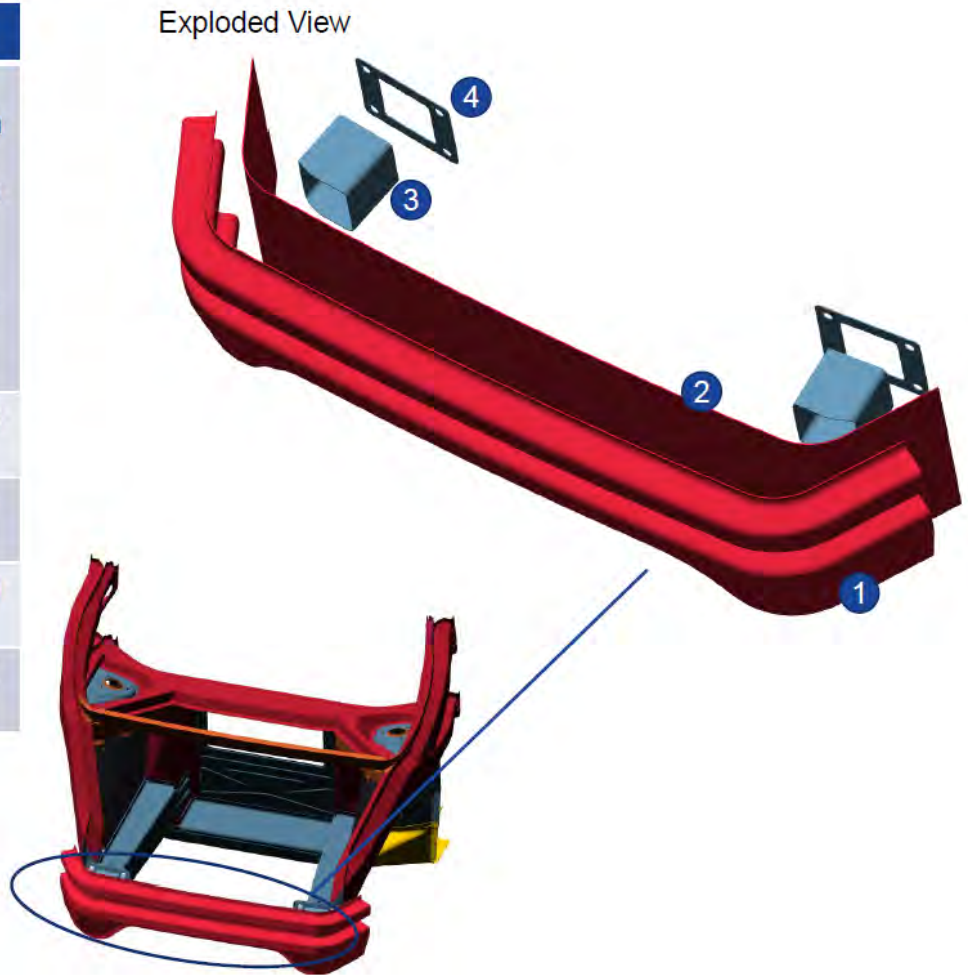

Figure 7.2.3.15 Front crush zone AHSS grades

Front crush zone	
Geometry/design	Longitudinal crush rails 1 and 2 provide primary crush absorption for FFB, ODB and MPDB tests. Tailor Welded blank parts enable uniform axial crush performance and vehicle deceleration. Vertical dash brace parts 4,5, 6 and 7 provide crush load reaction and limits intrusion. One bar parts 8,9 & 10 limit lower intrusion and protect battery
Part 1: LONGITUDINAL MID RAIL INNER FRONT RH	TWB 1.8/2.0_CR500Y780T-DP/CR700Y980T-DP / Cold stamp
Part 2: LONGITUDINAL MID RAIL OUTER FRONT RH	TWB 1.8/2.0_CR500Y780T-DP/CR700Y980T-DP / Cold stamp
Part 3: BUMPER BEAM INTERFACE PLATE FRONT RH	2.0mm CR860Y1180T-DP / Cold stamp
Part 4:VERTICAL DASH BRACE FRONT LH	2.0mm PHS-CR2000T-MB / Hot form
Part 5: VERTICAL DASH BRACE UPPER FRONT	2.0mm PHS-CR2000T-MB / Hot form
Part 6 & 7: VERTICAL DASH BRACE LOWER INNER & OUTER	2.0mm PHS-CR2000T-MB / Hot form
Part 8 & 9: ONE BAR UPPER AND LOWER	1.0mm CR860Y1180T-DP / Cold stamp
Part 10: ONE BAR INNER	2.0mm CR8501180T-DH / Cold stamp
Part 11: STRUT TOWER FRONT RH	0.8mm CR350Y/450T-LA / Cold stamp
Part 12: STRUT TOP FRONT RH	1.8mm CR860Y1180T-DP / Cold stamp
Part 13: STRUT RING FRONT	2.0mm CR1200Y1470-MS / Cold stamp

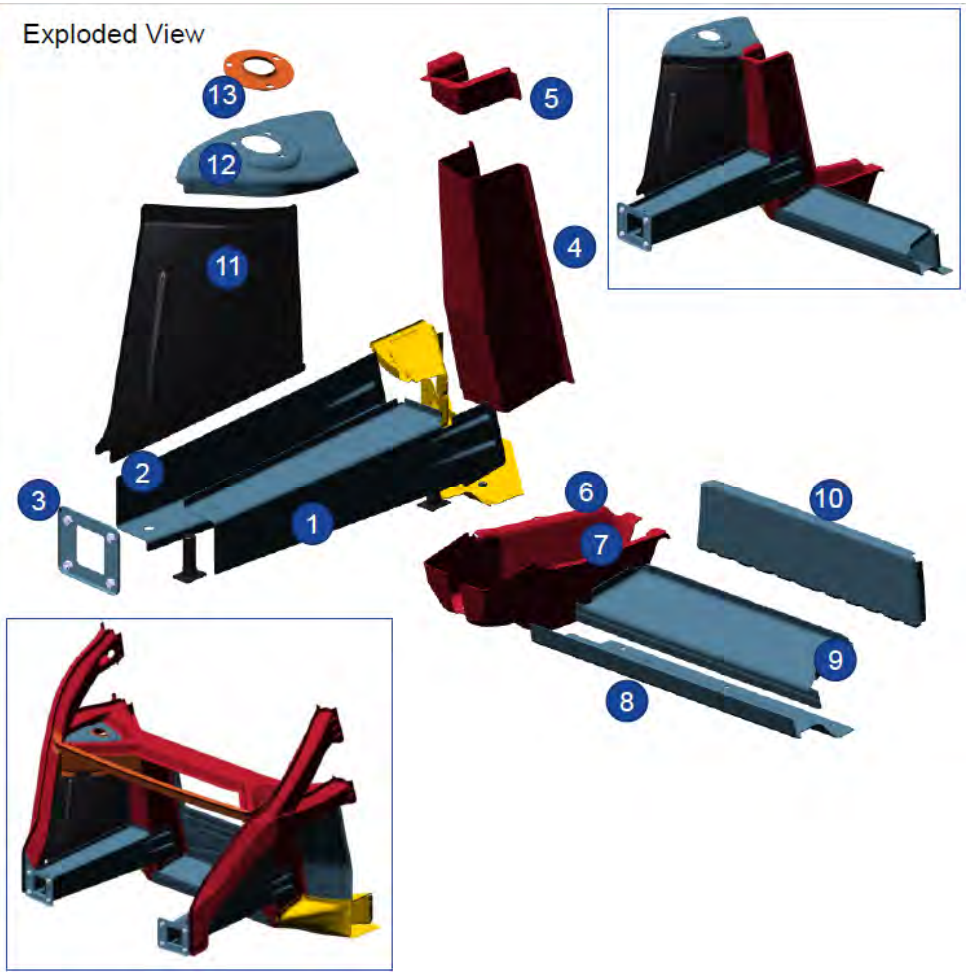

Figure 7.2.3.16 Glance beam AHSS grades

Glance Beam	
Geometry/design	Plan view profile optimised to guide vehicle along desired SORB barrier trajectory. Design and grades optimised to enable fold in FFB and no rupture in SORB
Part 1: GLANCE BEAM OUTER LH	0.8mm PHS-CR1500T-MB / Hot form
Part 2: GLANCE BEAM INNER LH	0.8mm PHS-CR1500T-MB / Hot form
Part 3: GLANCE BEAM UPPER TRIANGULATION OUTER LH	2.0 mm CR420Y780T-DP / Cold Stamp
Part 4:GLANCE BEAM UPPER TRIANGULATION INNER LH	1.2mm CR780Y980T-CP / Cold Stamp
Part 5: GLANCE BEAM BULKHEADS	1.5mm CR420Y780T-DP CR780Y980T-CP / Cold Stamp
Part 6:GLANCE BEAM BULKHEADS	1.5mm CR420Y780T-DP CR780Y980T-CP / Cold Stamp
Part 7: GLANCE BEAM CAP (and subframe bolt)	2.0mm CR420Y780T-DP / Cold stamp

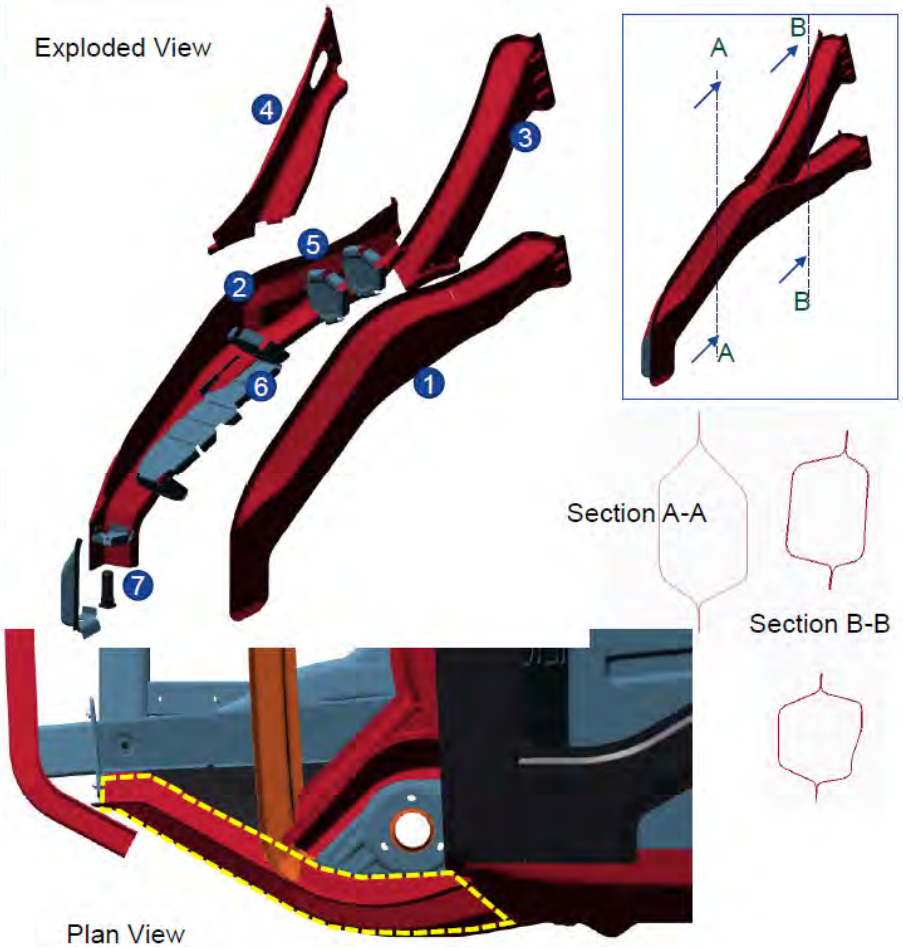

Figure 7.2.3.17 SORB glance reaction beam and damper strut top AHSS grades

SORB Glance Reaction Beams and Damper Strut Top	
Geometry/design	Grades and geometry enable SORB lateral loadpath for glance behaviour
Part 1:GLANCE BEAM UPPER REACTION LH	0.8mm PHS-CR1500T-MB / Hot form
Part 2:GLANCE BEAM LOWER REACTION LH	0.8mm CR1200Y1470T-MS / Cold stamp
Part 3: GLANCE BEAM LATERAL CROSS MEMBER OUTER	1.0mm CR1200Y1470T-MS / Cold stamp
Part 4: GLANCE BEAM LATERAL CROSS MEMBER INNER	1.0mm CR1200Y1470T-MS / Cold stamp
Part 5: STRUT CROSS MEMBER FRONT	1.0mm PHS-CR2000T-MB / Hot form
Part 6: STRUT CROSS MEMBER CLOSING PLATE	1.0mm CR1550Y2000T-MS / Cold stamp
Part 7: STRUT TOP FRONT	1.8mm CR860Y1180T-DP / Cold stamp
Part 8: STRUT RING FRONT	2.0 mm CR1200Y1470-MS / Cold stamp
Part 9: VERTICAL DASH BRACE UPPER FRONT	2.0mm PHS-CR2000T-MB / Hot form
Part 10: VERTICAL DASH BRACE FRONT LH	2.0mm PHS-CR2000T-MB / Hot form
Part 11: STRUT TOWER FRONT LH	0.8mm CR350Y/450T-LA / Cold stamp

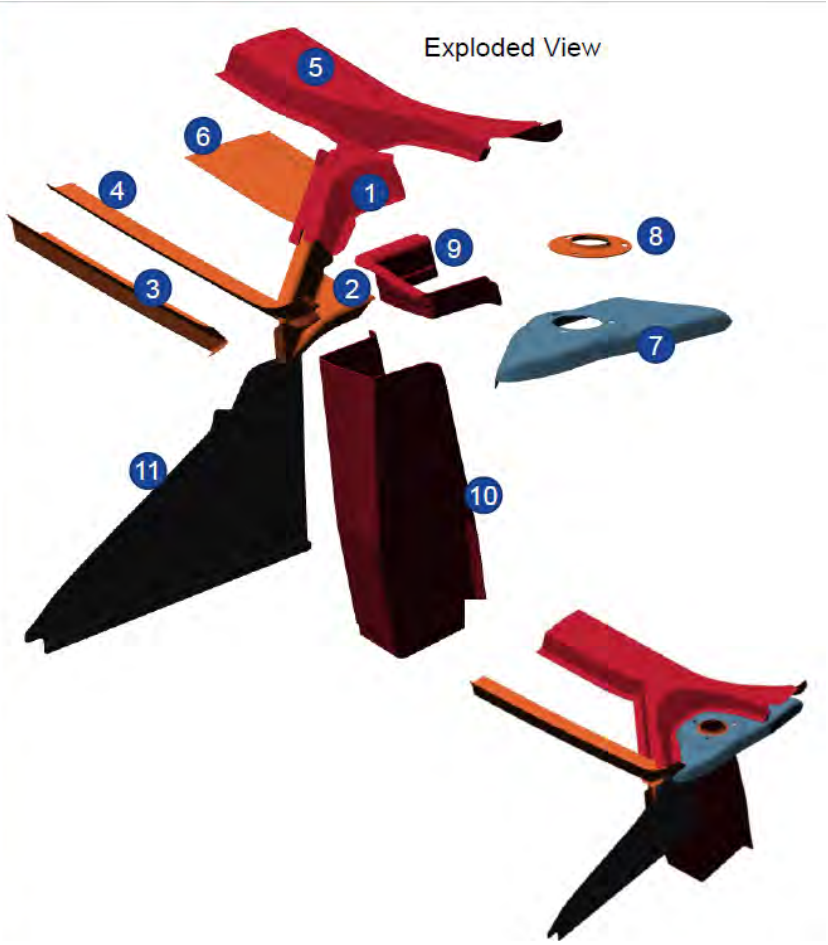

Figure 7.2.3.18 Front subframe AHSS grades

Front Subframe	
Geometry/design	Rigidly connected to BIW at points A (front longitudinal crush rails) B (glance beam), C (Vertical dash brace lower). Provides global body stiffness contribution and crash loadpaths. Front lateral beam (1) provides SORB lateral loadpath Z offset (D) promotes subframe folding collapse mechanism in front FFB, ODB and MPDB loadcases 2.0mm gauge selected as standard for corrosion resistance for chassis parts
Part 1:FRONT SUBFRAME LATERAL BEAM (FRONT)	2.0mm CR860Y1180T-DP / Cold rolled tube
Part 2:FRONT SUBFRAME LONGITUDINAL LH	2.0mm CR860Y1180T-DP / Cold rolled tube
Part 3: FRONT SUBFRAME LATERAL BEAM (REAR)	2.0mm CR860Y1180T-DP / Cold rolled tube
Part 4: MISC. BRACKETS	2.0mm CR860Y1180T-DP / Cold stamp

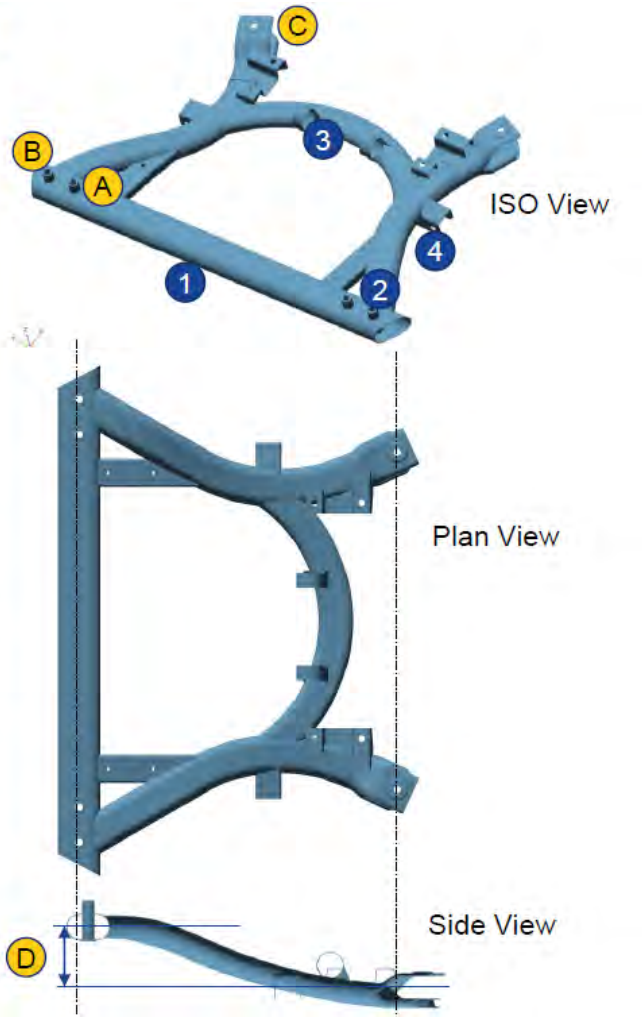

Figure 7.2.3.19 Front crash protection / intrusion prevention zone AHSS grades

Front Crash Protection / Intrusion Zone	
Geometry/design	
Part 1:VERTICAL DASH BRACE FRONT LH	2.0mm PHS-CR2000T-MB / Hot form
Part 2:VERTICAL DASH BRACE UPPER FRONT LH	2.0mm PHS-CR2000T-MB / Hot form
Part 3: VERTICAL DASH BRACE LOWER INNER & OUTER	2.0mm PHS-CR2000T-MB / Hot form
Part 4: ONE BAR UPPER AND LOWER	1.0mm CR860Y1180T-DP / Cold stamp
Part 5: ONE BAR INNER	2.0mm CR8501180T-DH / Cold stamp
Part 6: FRONT BULKHEAD	2.0mm CR860Y1180T-DP / Cold stamp
Part 7: TORQUE BOX OUTER AND INNER	2.0mm CR400Y780T-RA (outer), 1.0mm INNER / Cold stamp
Part 8: STRUT CROSS MEMBER FRONT	1.0mm PHS-CR2000T-MB / Hot form
Part 9: STRUT CROSS MEMBER CLOSING PLATE	1.0mm CR1550Y2000T-MS / Cold stamp
Part 10: A PILLAR OUTER	1.2mm PHS-CR2000T-MB / Hot form (part of TWB OUTER RING)
Part 11: A PILLAR INNER	1.2mm PHS-CR2000T-MB / Hot form

Figure 7.2.5.2 SEM1 side crash barrier alignment and strategy for loadpath and intrusion management

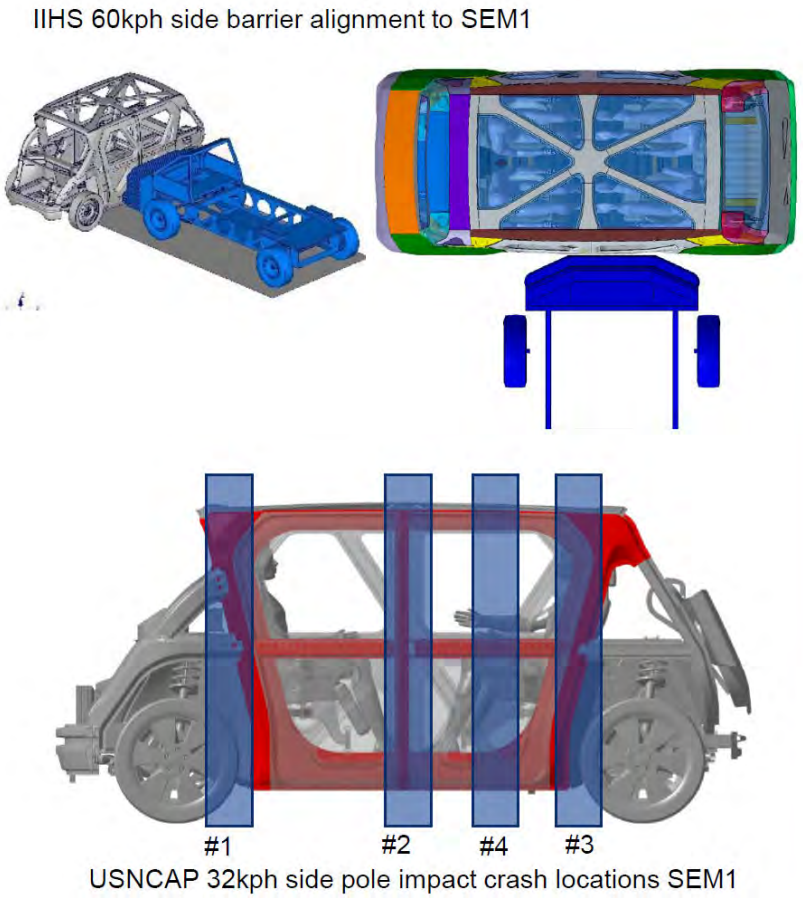

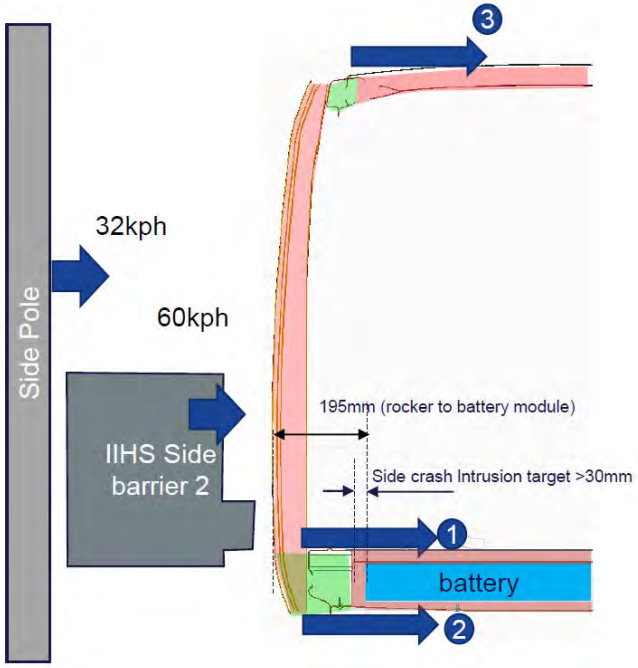

- Crush zones in rocker and cantrail to absorb side pole energy. High strength door, floor and roof structure intrusion zones
- Side pole crash loadpaths 1) Upper lateral cross members 2) Structural battery cover 3) roof structure
- Ensure >30mm crush intrusion target to protect battery modules

Figure 7.2.5.4 Crash CAE simulation of IIHS 60kph side barrier. Predicted intrusion values are in the IIHS “good” zone

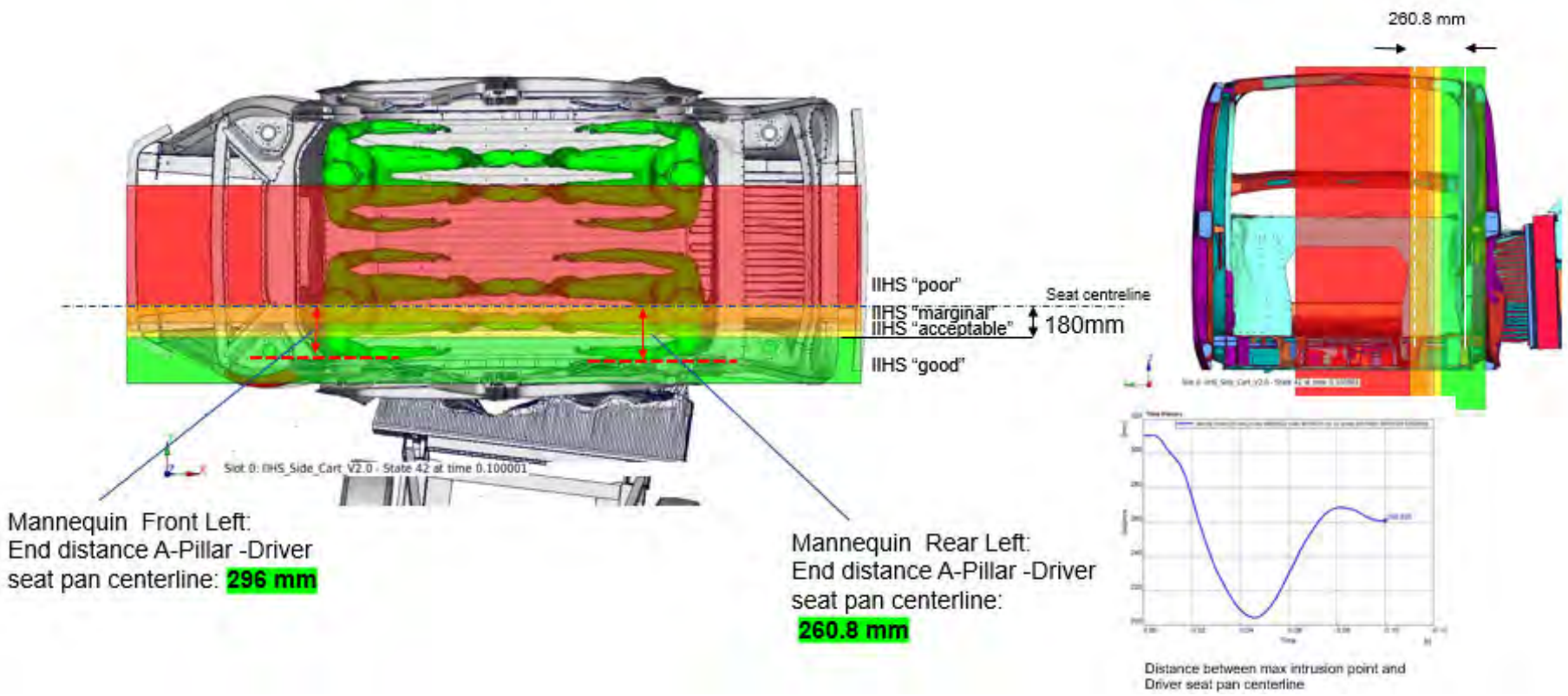

Figure 7.2.5.6 USNCAP 32kph side pole, predicted intrusion values for 4 test locations

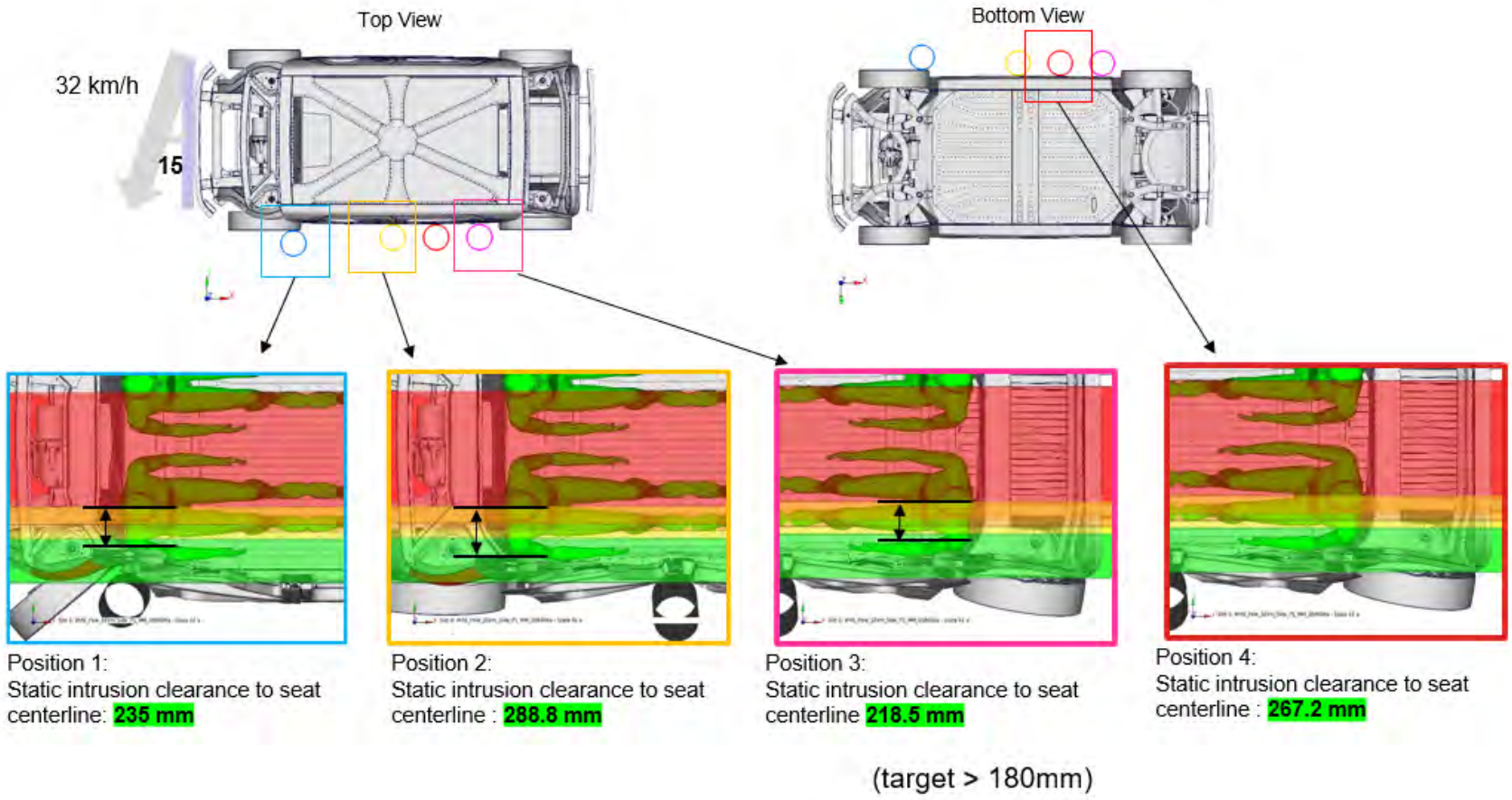

Figure 7.2.5.7 predicted intrusion values for the USNCAP 32kph side pole test (4 locations)

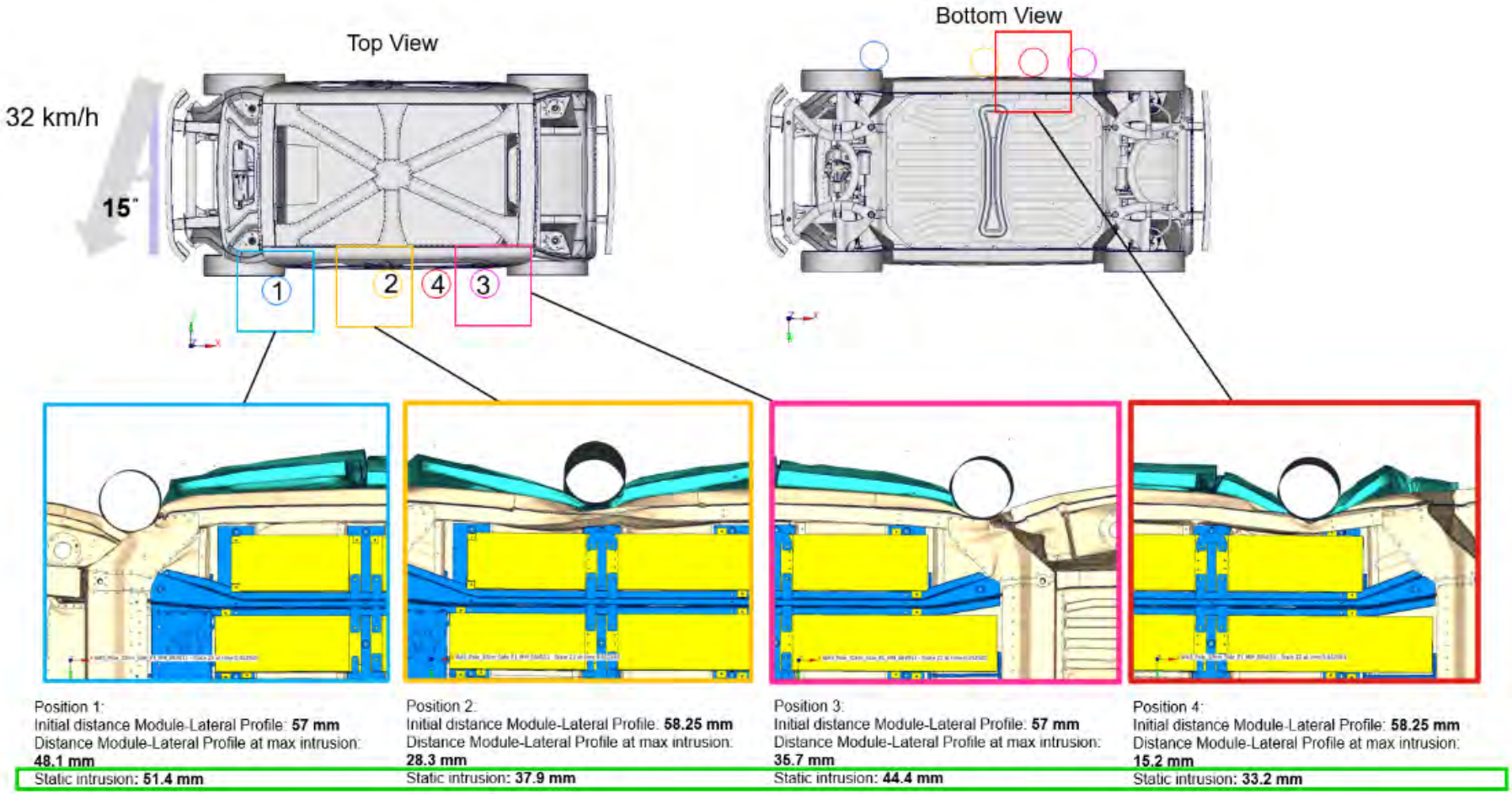

Figure 7.2.5.8a Door structural members and loadpaths into body structure for the IIHS side barrier loadcase (body structure shown for clarity)

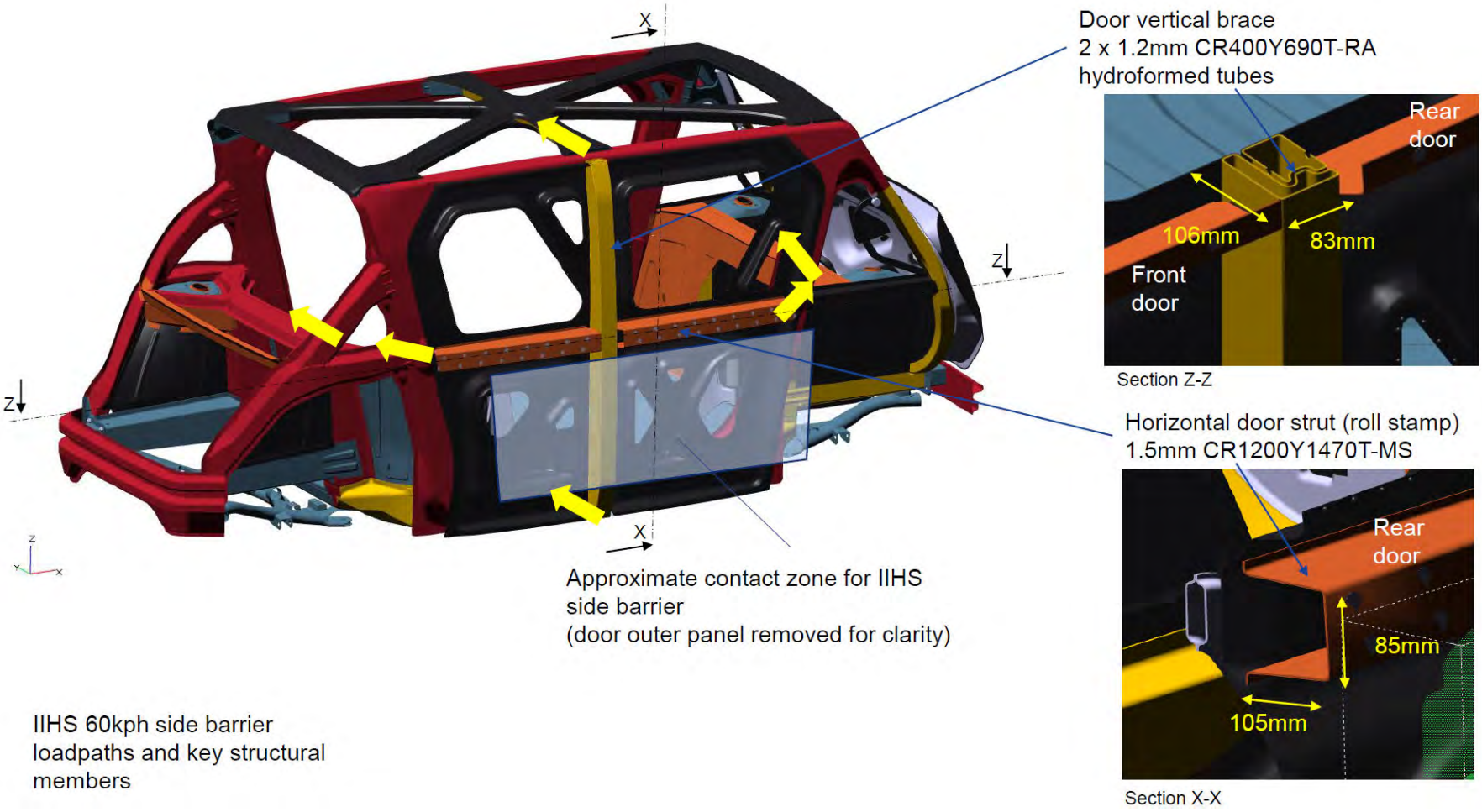

Figure 7.2.5.8b Door structural members and loadpaths into body structure for the IIHS side barrier loadcase (body structure shown for clarity)

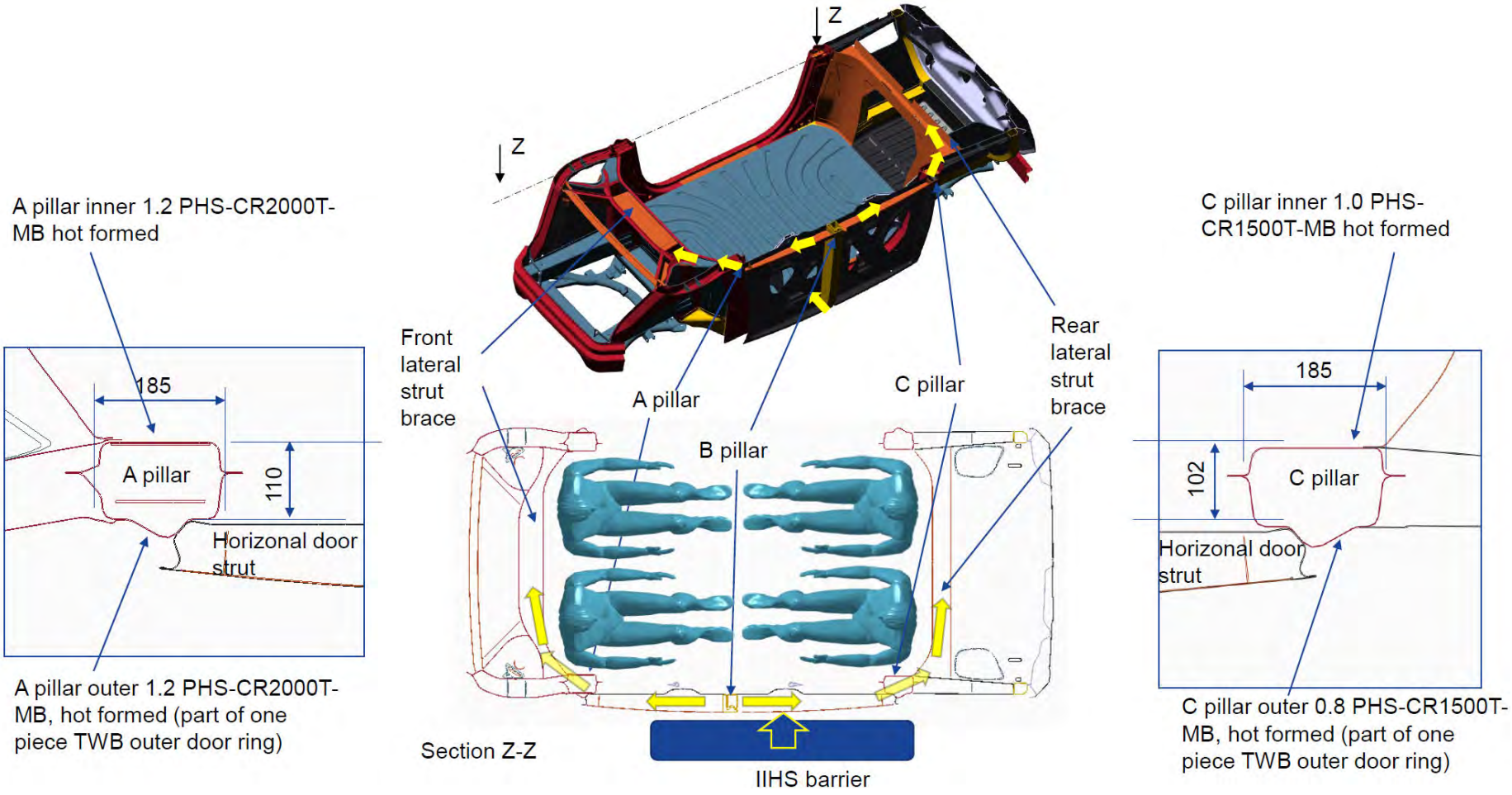

Figure 7.2.5.11 USCAP 32kph side pole crash loadcase, position 1. Loadpaths and crash simulation result

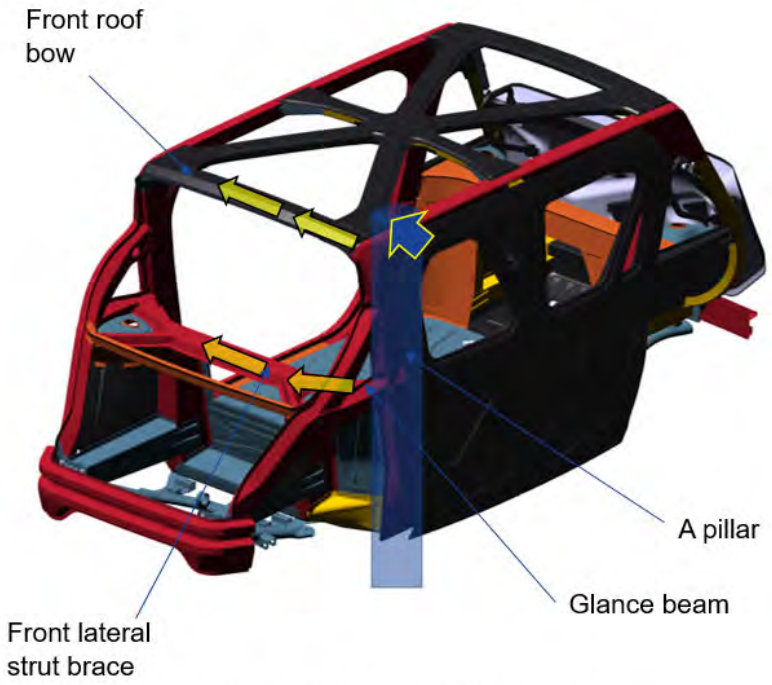

Side pole impact position 1, front occupant

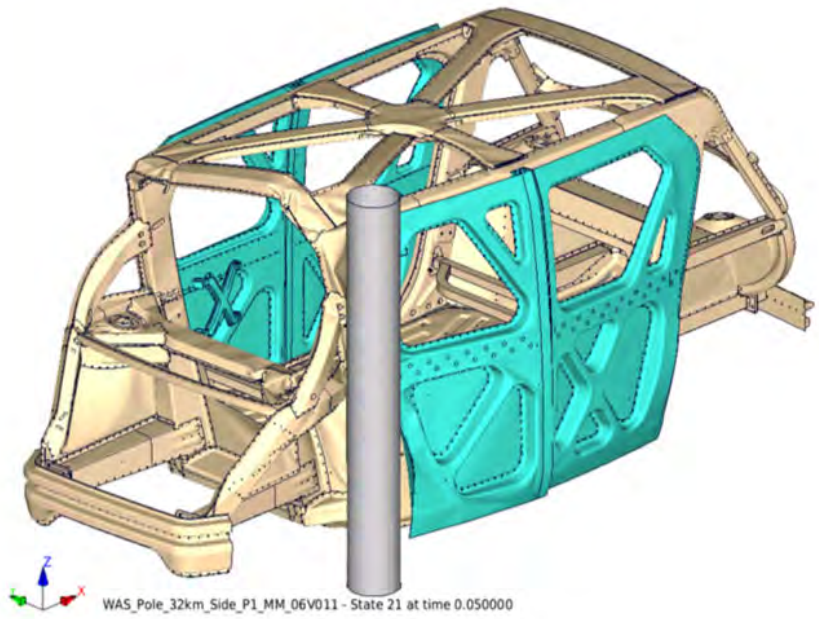

Side pole crash simulation, 50ms

Figure 7.2.5.12 USCAP 32kph side pole crash loadcase, position 3. Loadpaths and crash simulation result

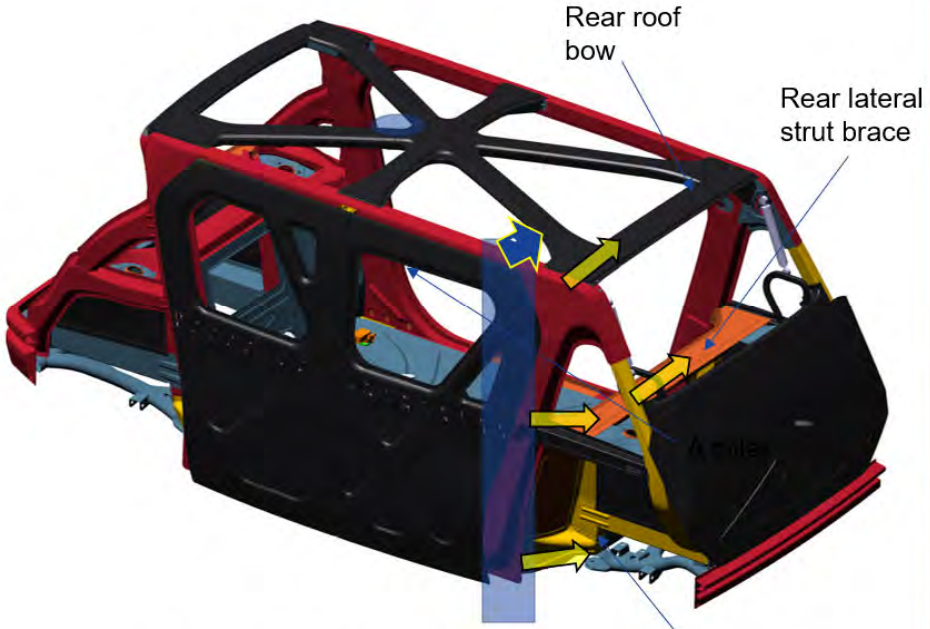

Side pole impact position 3, rear occupant

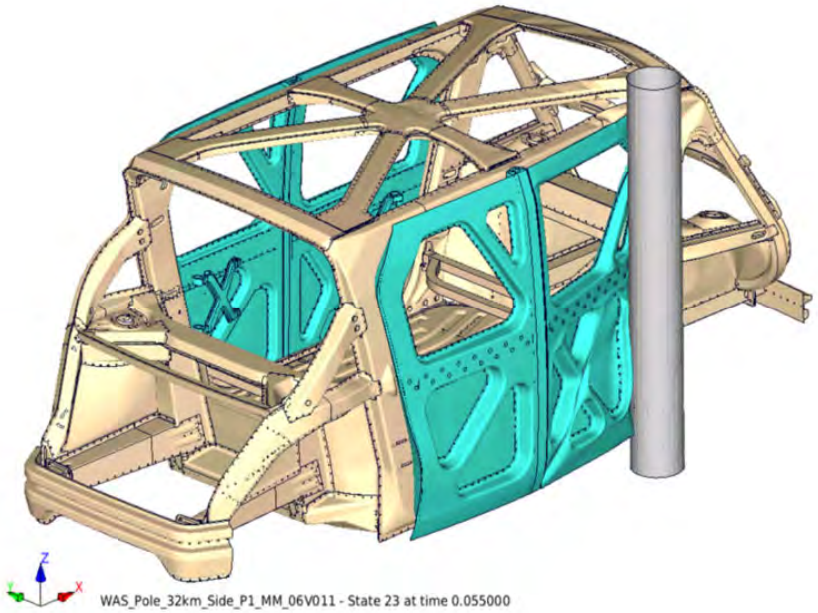

Side pole crash simulation, location 3, @55ms

Figure 7.2.5.14 body structure cross section in X at door split point, side pole position 2. (battery modules, cooling plates, interconnects removed for clarity)

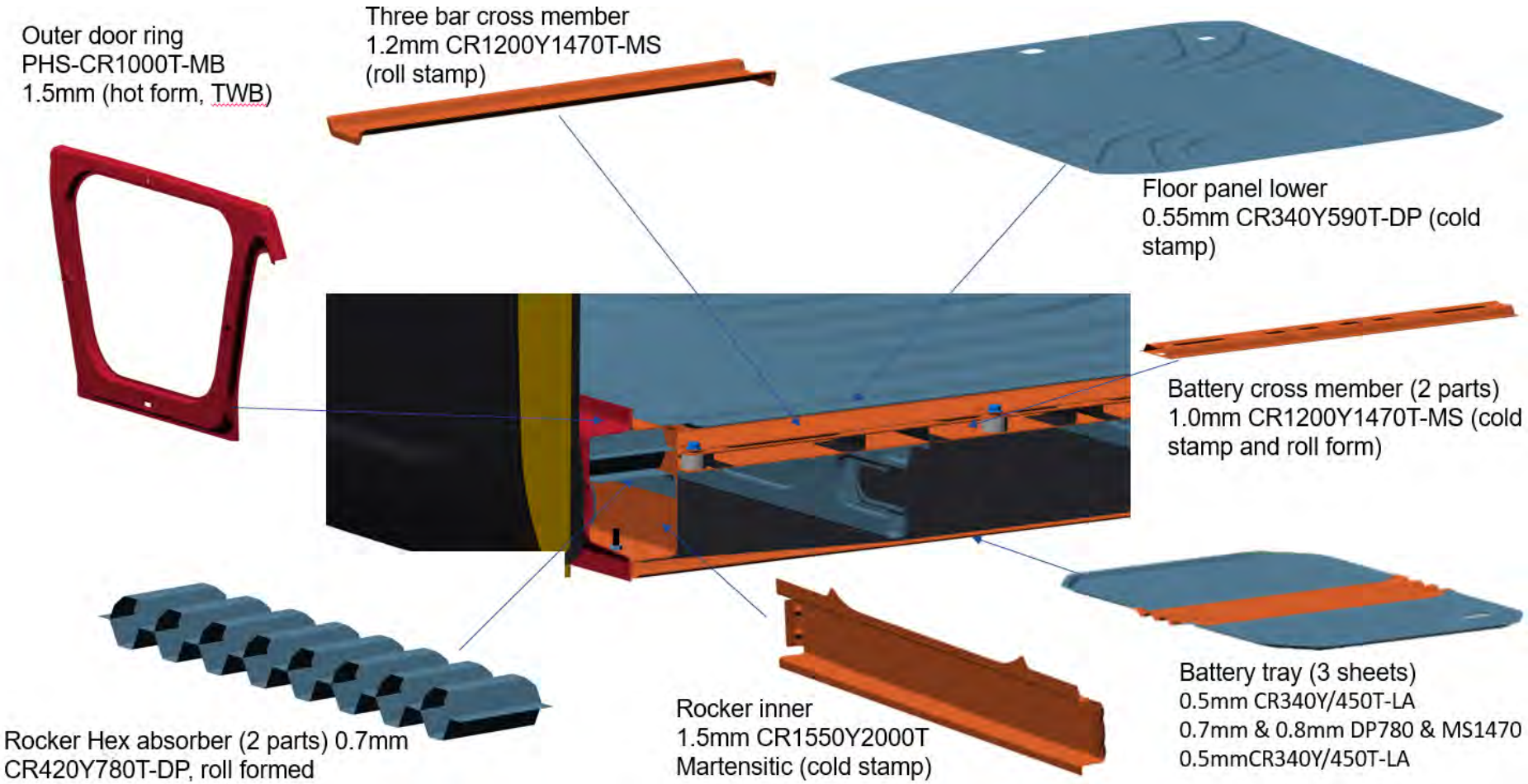

Figure 7.2.5.15 body structure cross section in X showing side pole crash intrusion prevention measures and upper & lower loadpaths

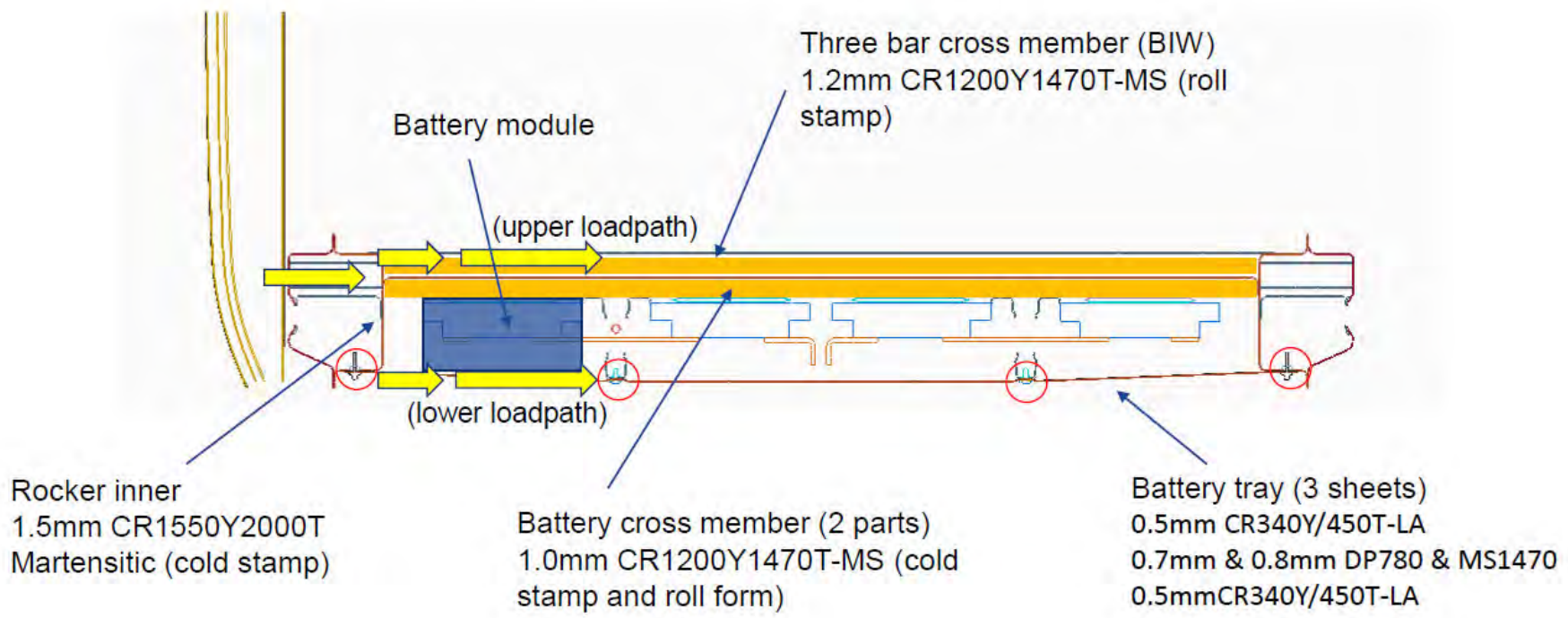

Figure 7.2.5.16 Body structure (floor panel removed) showing body cross members (two, three and four bar) and battery cross members (upper loadpaths)

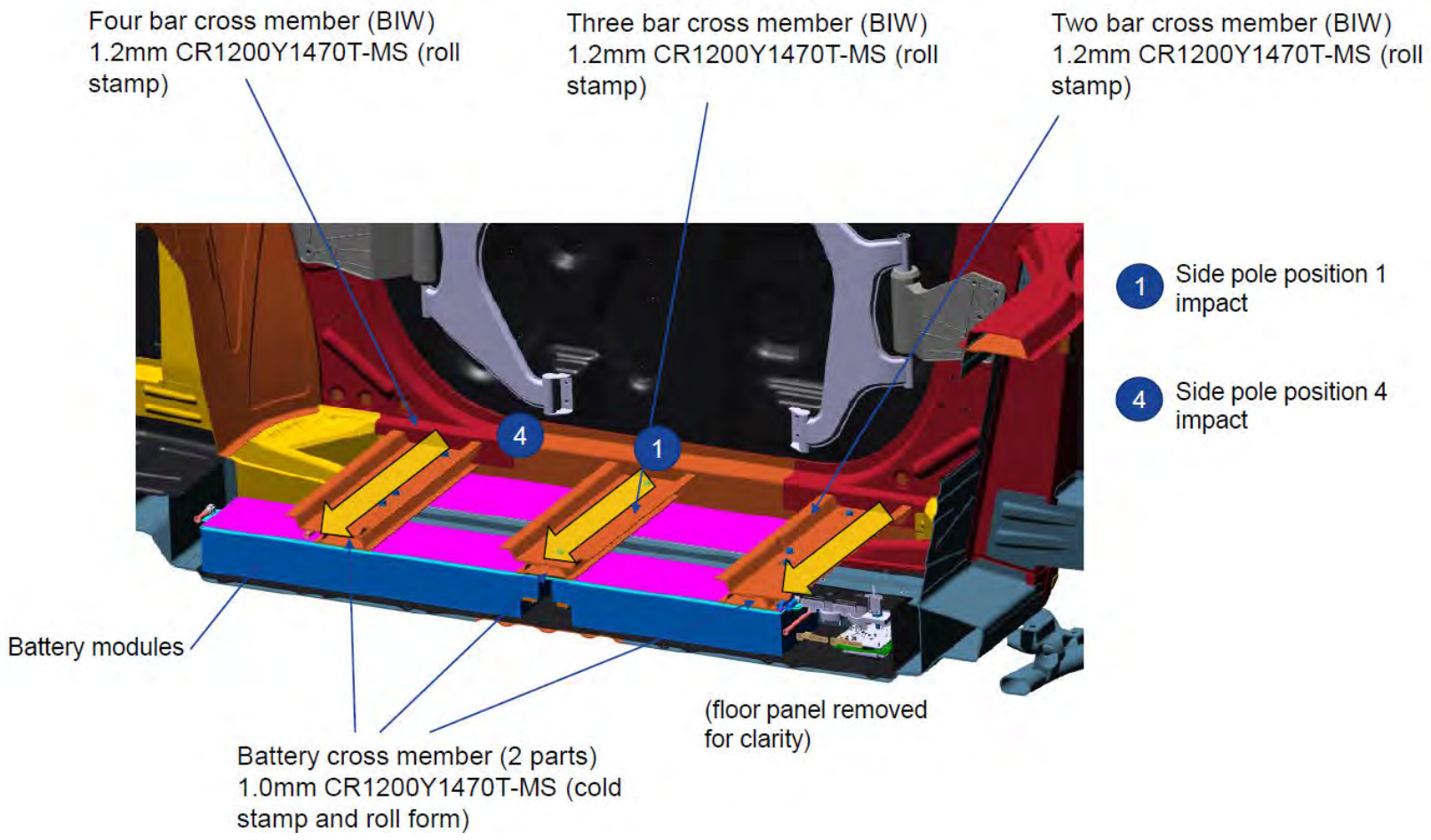

Figure 7.2.5.18 SEM1 mid zone upper structure AHSS grades

Roof structure (front)	
Part 1:OUTER RING TWB LH	TWB (A PILLAR PHS-CR2000T-MB 1.2mm, C PILLAR PHS-CR1500T-MB 0.8mm, Cantrail/roof outer PHS-CR1000T-MB 1.5mm, Rocker PHS-CR1000T-MB 1.5mm
Part 2:A POST INNER REINFORCEMENT UPPER	1.5mm CR800Y1180T-DP / Cold stamp
Part 3: ROOF SIDE RAIL INNER LH	0.8mm PHS-CR1500T-MB / Hot form
Part 4: FRONT HEADER INNER	0.8mm CR780Y980T-CP / Cold stamp
Part 5: FRONT HEADER OUTER A-SURFACE	0.6mm CR260Y/370T-BH / Cold stamp
Part 6:DIAGONAL INNER PANEL FRONT	0.7mm CR550Y/620T-LA/ Cold stamp
Part 7: FRONT INNER ROOF HEADER GUSSET MOUNT	1.0mm CR700Y980T-DP / Cold stamp
Part 8: FRONT OUTER ROOF HEADER GUSSET MOUNT	1.0mm CR700Y980T-DP / Cold stamp

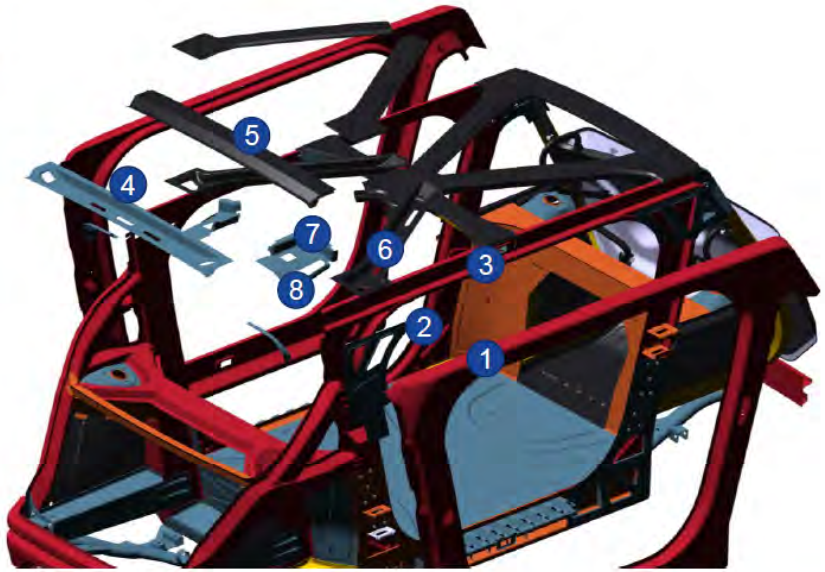

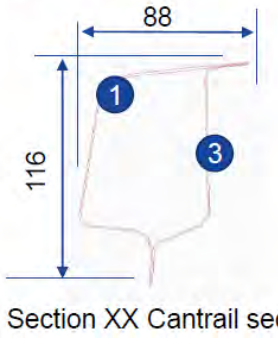

Section XX Cantrail section

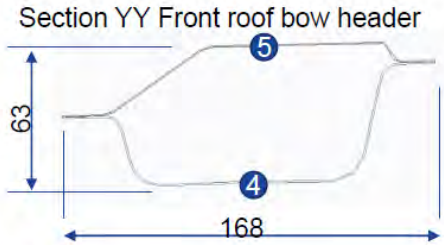

Figure 7.2.5.19 SEM1 mid zone roof structure and AHHS grades

Roof structure (middle)	
Geometry/design	
Part 1:MID ROOF BOW OUTER A-SURFACE	0.6mm CR260Y/370T-BH / Cold stamp
Part 2:MID ROOF BOW INNER	0.8mm CR820Y1180T-RA / Cold stamp
Part 3:MID INTERSECTION OUTER A-SURFACE PANEL	0.6mm CR260Y/370T-BH / Cold stamp
Part 4: MID INTERSECTION INNER PANEL	0.5_CR260Y/370T-BH / Cold stamp
Parts 5, 7 8 & 9 : DIAGONAL OUTER A SURFACE	0.6mm CR260Y/370T-BH / Cold stamp
Parts 10, 11, 12, 13 :DIAGONAL INNER PANEL	0.7mm CR550Y/620T-LA/ Cold stamp

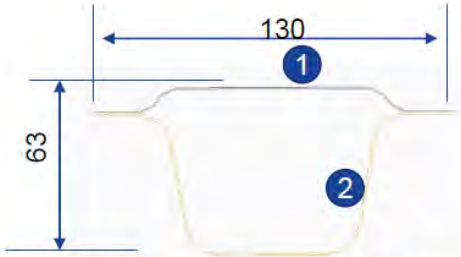

Section YY Middle roof bow

Figure 7.2.5.20 SEM1 outer ring and approach for A surfaces

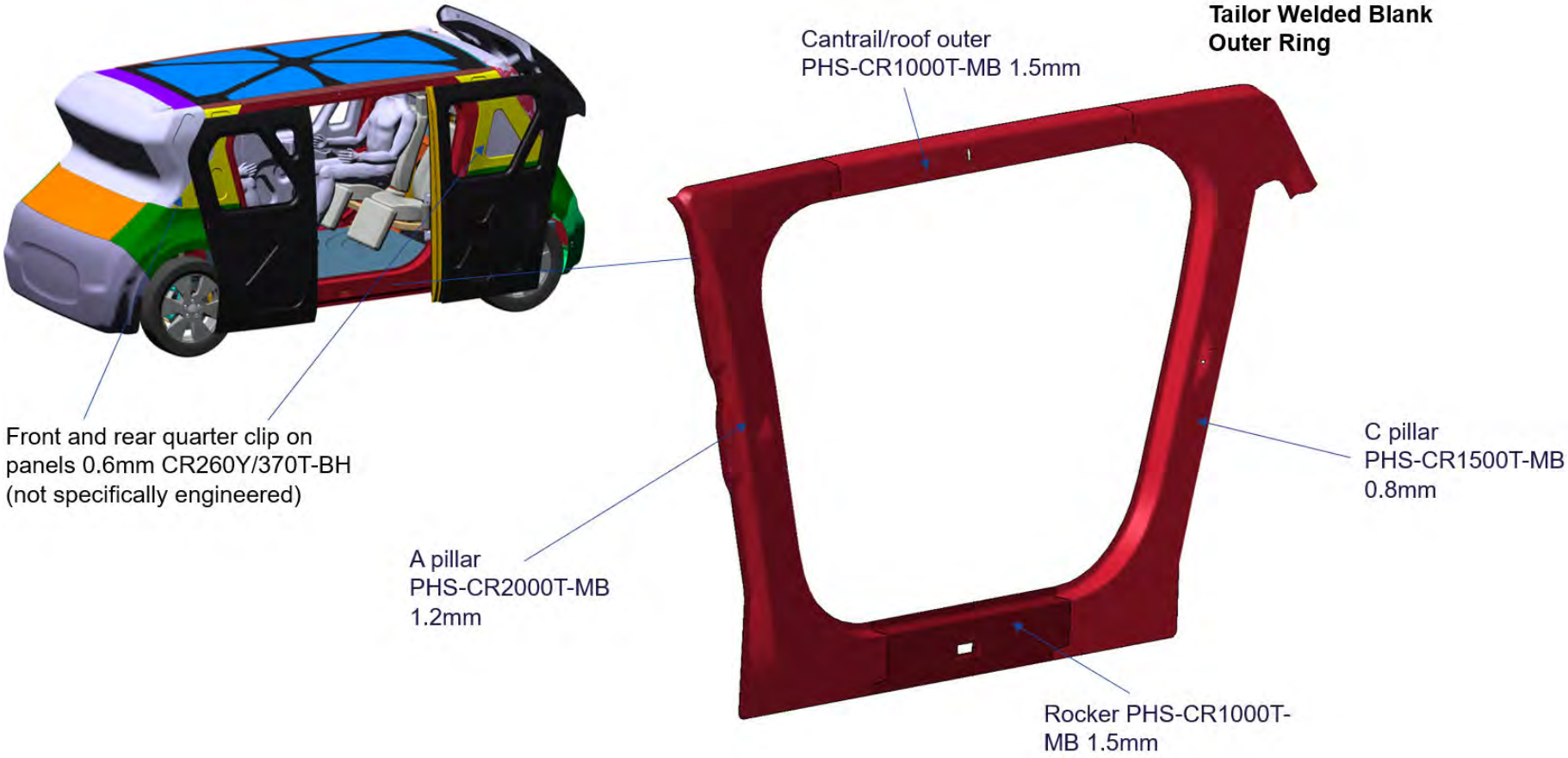

Figure 7.2.5.1 IIHS Roof Crush Strength Evaluation 1 and SEM1 CAE calculation

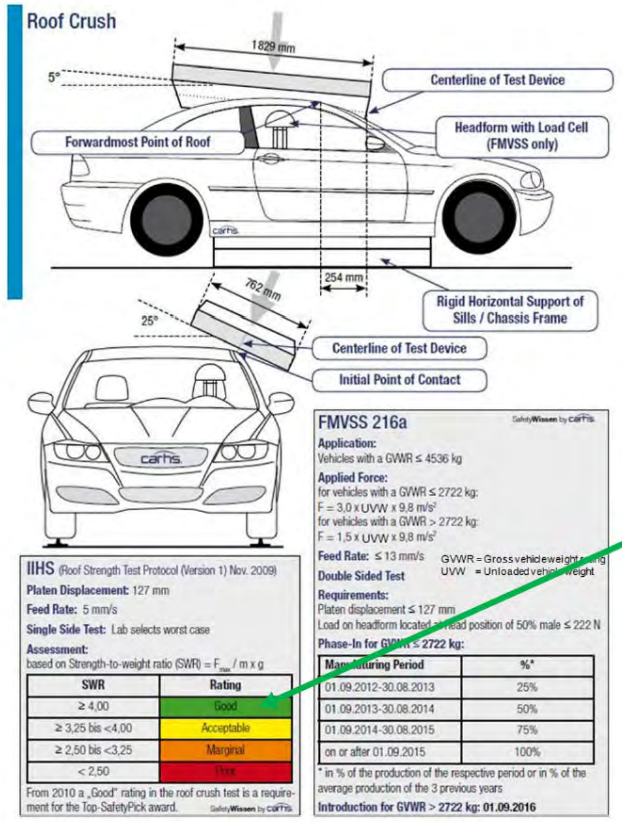

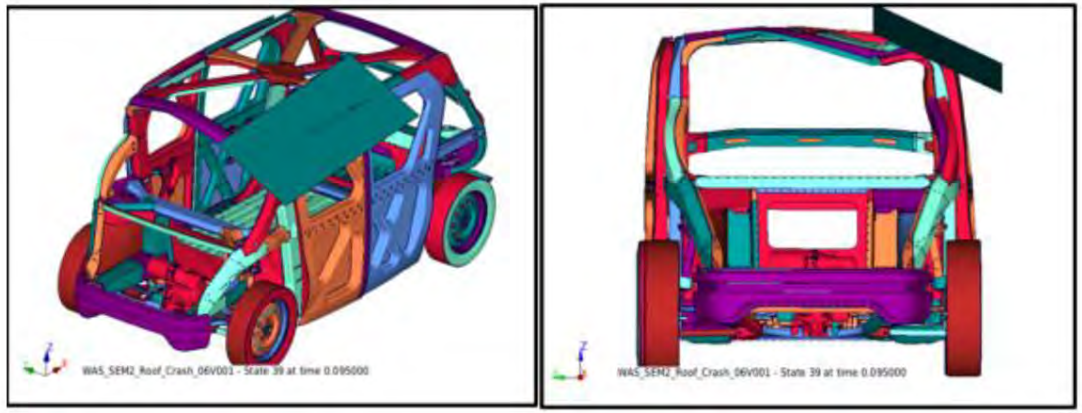

SWR = Fmax / m x g

SWR = 148.2 / 1512 x 9,81

SWR = 9,58 > 4,00

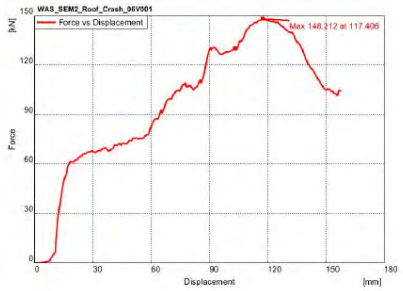

Figure 7.2.6.1 Rear zone subassemblies

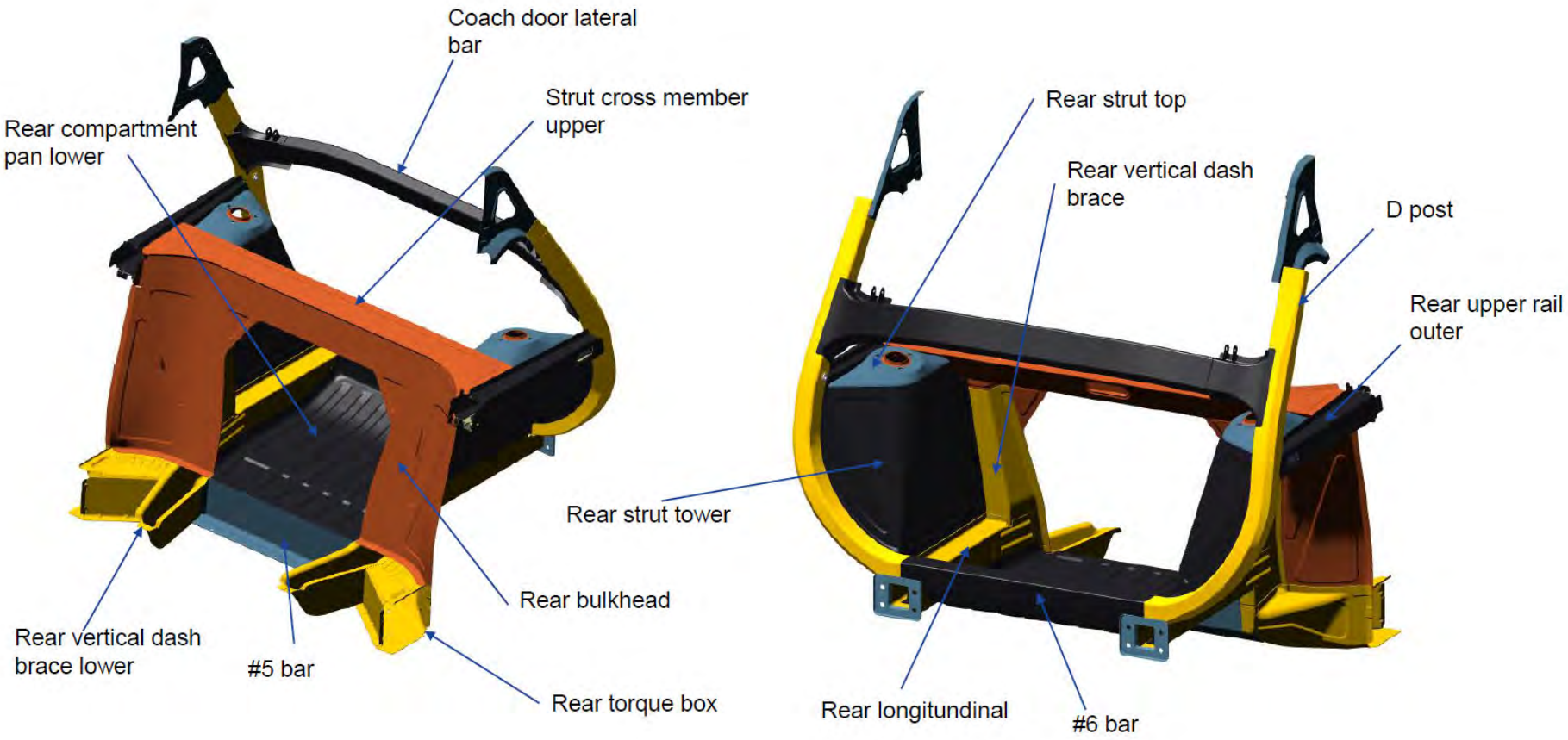

Figure 7.2.6.4 SEM1 Body structure rear zone

Rear body structure (crush zone)	
Geometry/design	Crush cans (2) and longitudinal rails (3) tuned to crush axially under FMVSS305 EV loadcase. Longitundinals are 2 grade TWB. Rear subframe is rigidly bolted to BIW and engineered to fold in rear crash
Part 1: REAR BUMPER BEAM	2.0mm PHS-CR2000T-MB / hot formed
Part 2: REAR CRUSH CAN	1.5mm CR350Y600T DP / cold formed
Parts 3: REAR LONGITUDINAL RAILS (2 PARTS)	TWB: (A) 1.6mm CR820Y1180T-RA (B) 1.4mm CR600Y980T-RA / cold formed
Part 4: REAR SUBFRAME	2.0mm CR860Y1180T-DP / hydroformed tubes
Part 5: REAR COMPARTMENT PAN LOWER	0.5mm CR350Y/450T-LA / cold formed

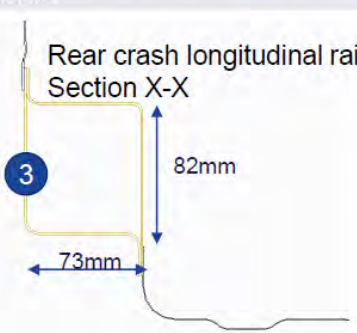

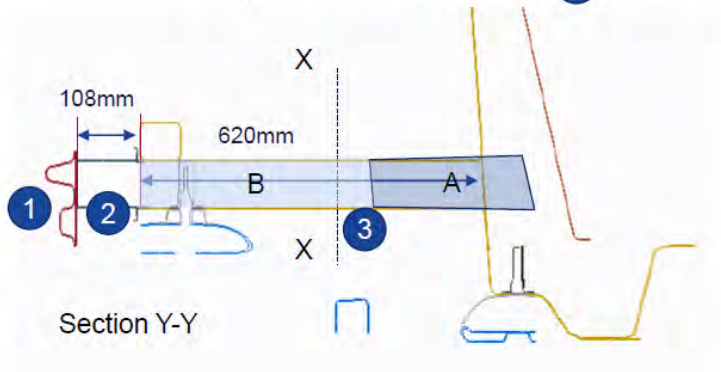

Figure 7.2.6.5 SEM1 Body structure rear zone

Rear body structure (intrusion zone)	
Geometry/design	Vertical dash braces provides primary crash load reaction in rear crash. Five bar provides intrusion protection for battery. Rear strut cross member and rear bulkhead provide crush load reaction and intrusion strength
Part 1: REAR VERTICAL DASH BRACE	1.6mm CR820Y1180T-RA / cold formed
Parts 2 & 3: FIVE BAR (INNER & OUTER)	0.8mm CR900Y1180T-CP & 1.8mm CR420Y780T-DP / cold formed
Parts 4 & 5: REAR STRUT CROSS MEMBER (UPPER AND LOWER)	1.0mm CR1200Y1470T-MS
Part 6: REAR BULKHEAD	TWB (A) 1.0mm CR1200Y1470T-MS & (B) 0.8mm CR1000Y1470T-MS

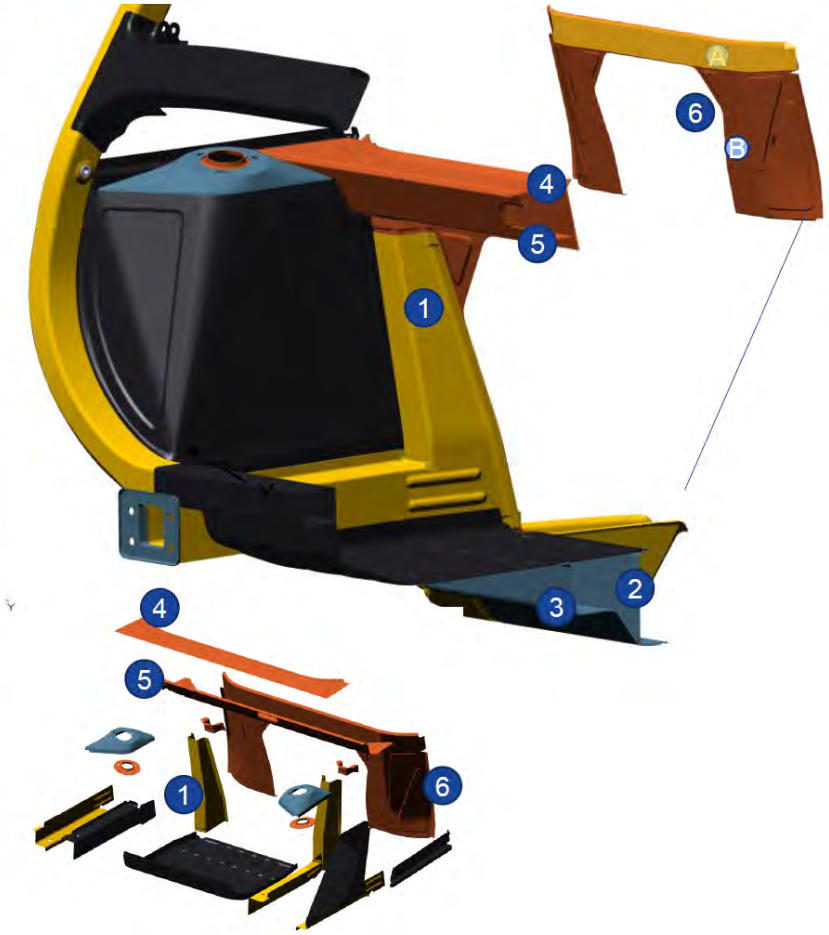

Figure 7.2.6.6 Rear torque box and five bar assembly

Rear body structure (torque box, five bar, lower vertical dash brace)	
Geometry/design	Rear torque box and five bar assembly forms the lower part of the rear crash intrusion zone. The assembly also provides contribution to global body stiffness
Parts 1 & 2: REAR VERTICAL DASH BRACE LOWER (INNER & OUTER)	1.0mm CR820Y1180T-RA / cold formed
Parts 3 & 4: TORQUE BOX REAR (INNER & OUTER)	1.5mm CR400Y780T-RA / cold formed
Part 5: FIVE BAR OUTER	0.8mm CR900Y1180T-CP / cold formed
Part 6: FIVE BAR INNER	0.8mm CR900Y1180T-CP / cold formed

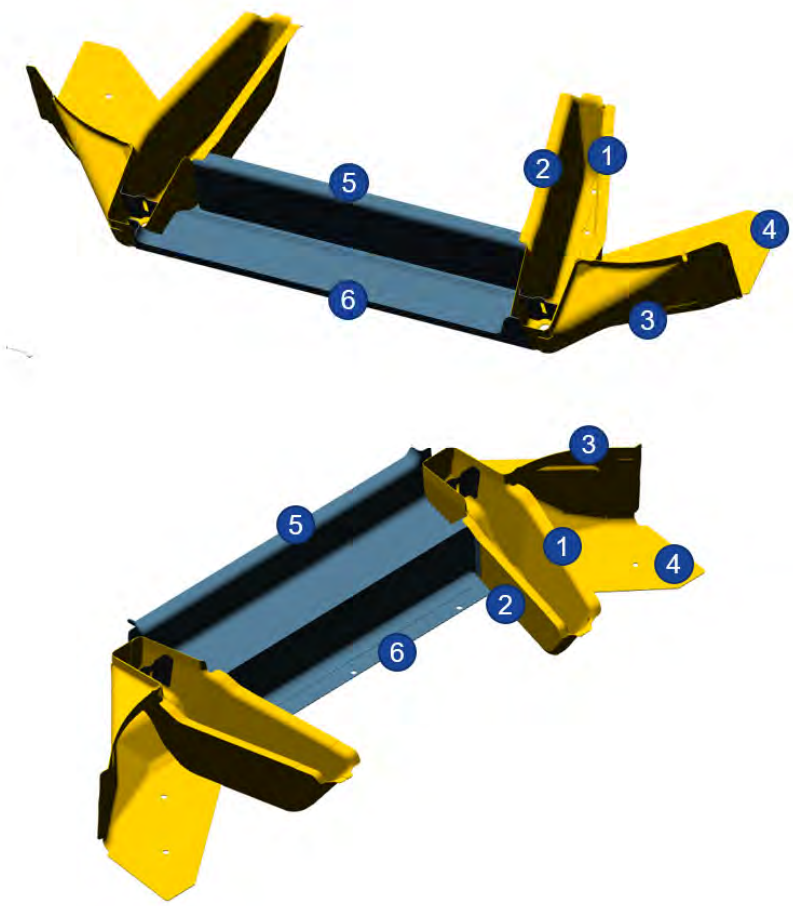

Figure 7.3.2.1 SEM1 battery carrier frame design and AHSS grades

Battery carrier frame	
Part 1 : CARRIER FRAME LONGITUDINAL (LEFT & RIGHT)	1.8mm CR260Y450T-DP / cold formed
Part 2: UPPER CROSS MEMBER #3	1.0mm CR1200Y1470T-MS / roll stamp
Parts 3 & 4: UPPER CROSS MEMBER #2 & 3	1.0mm CR1200Y1470T-MS / roll form
Parts 5,6 & 7: LOWER CROSS MEMBERS #3, #2, #1	1.0mm CR1200Y1470T-MS / roll form

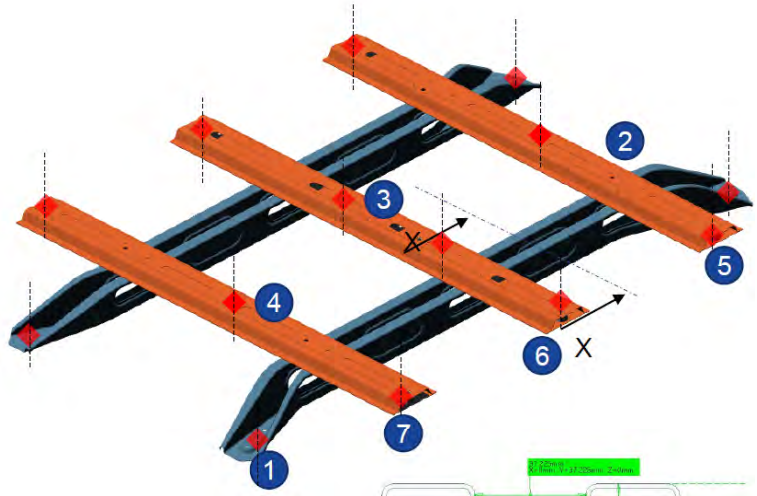

◆ Fixing position to body structure

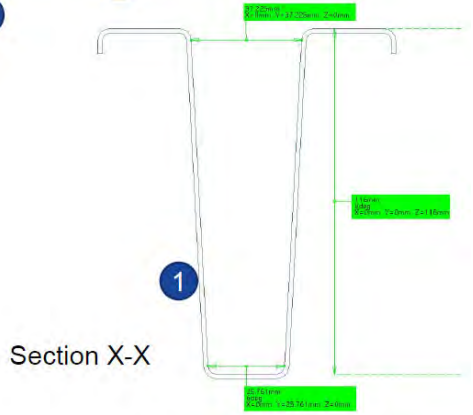

Section X-X

Figure 7.3.3.1 Battery tray design and AHSS grades

Battery tray (bottom cover)	
Geometry/design	3 sheet steel sandwich cover combines to provide high stiffness and strength. Triangular stamping in 2 provides section depth for stiffness and strength Use of 0.5mm and 0.7mm gauge helps achieve total weight 33.2kg Joining methods: spotweld, laser weld, adhesive
Part 1: BATTERY TRAY UPPER	0.5mm CR340Y/450T-LA / cold formed
Part 2 : BATTERY TRAY TRIANGLECOMB FRONT & REAR	0.5mm CR340Y/450T-LA / cold formed
Part 3: BATTERY TRAY LOWER	TWB (A) 0.7mm CR420Y780T-DP (B) 1.0mm CR1200Y1470T-MS / cold formed

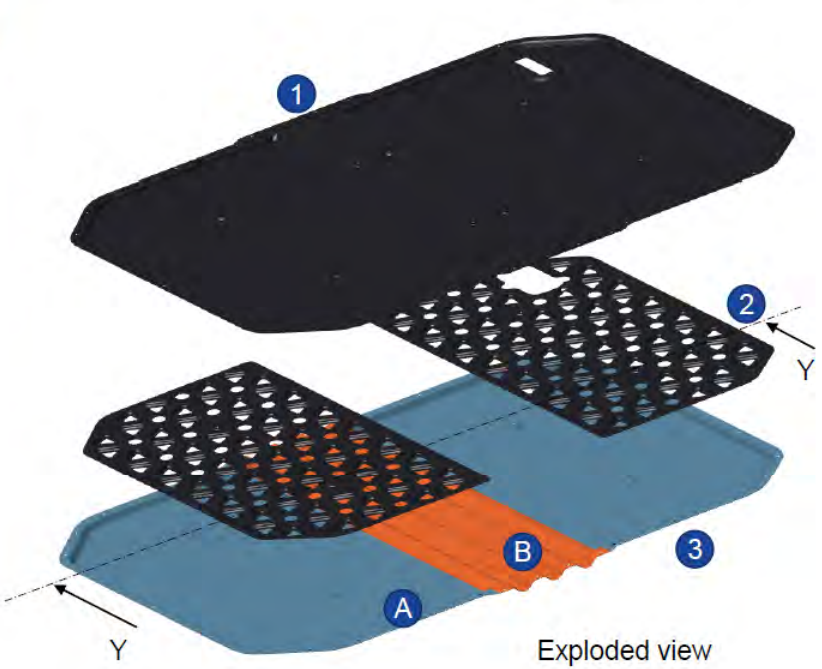

Figure 7.3.3.2 CAE results of battery tray debris and jacking loadcases

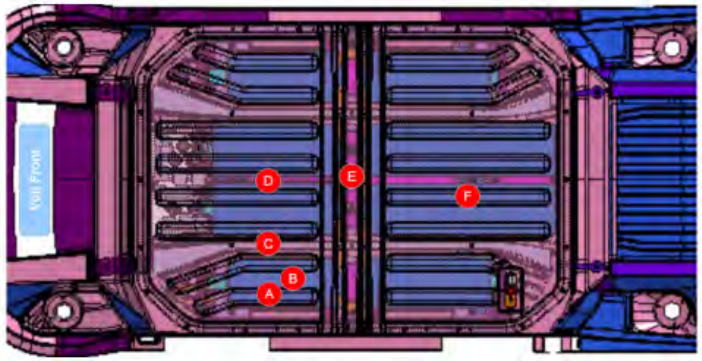

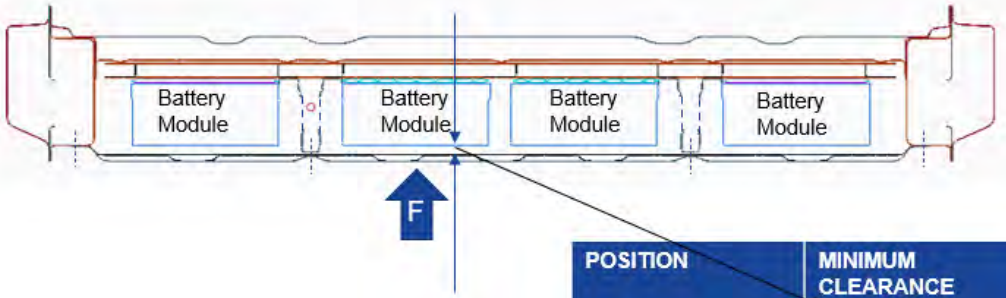

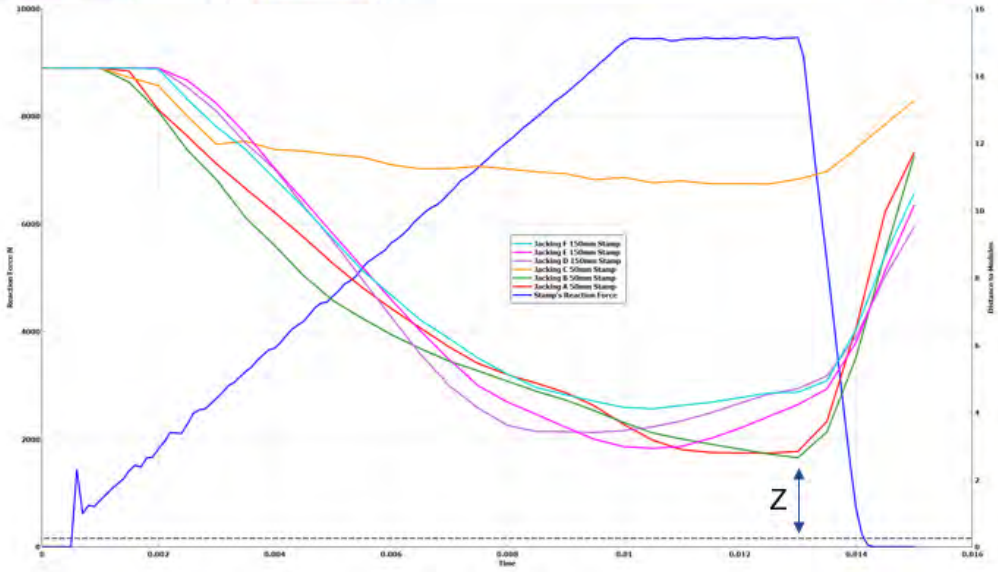

POSITION	MINIMUM CLEARANCE (Z) [mm]
A 50mm Stamp	2.78
B 50mm Stamp	2.64
C 50mm Stamp	10.79
D 150mm Stamp	3.40
E 150mm Stamp	2.92
F 150mm Stamp	4.10

Figure 7.3.3.4 Battery durability FEA. Predicted Von-Mises stresses (Root Mean Square)

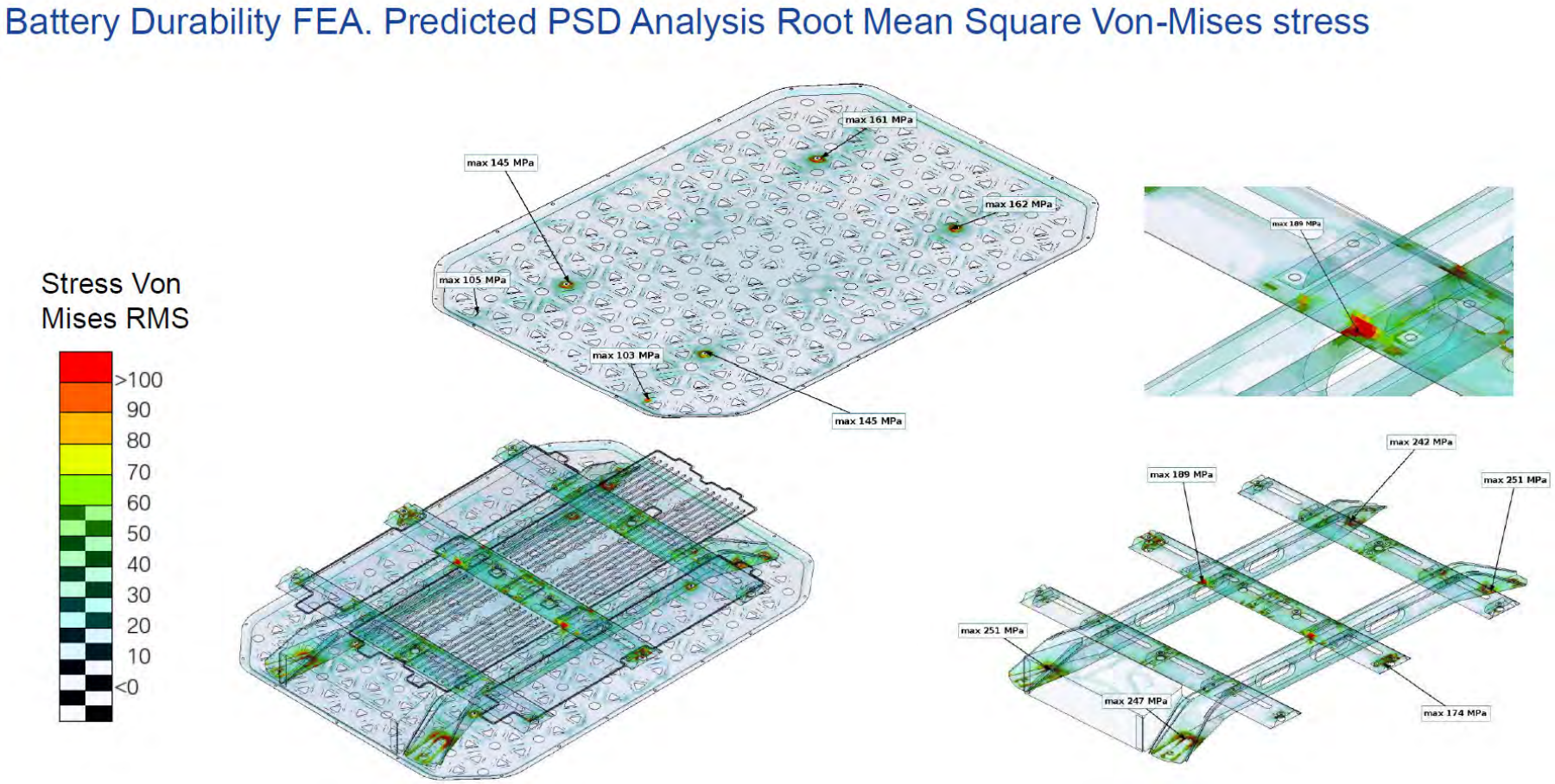

Figure 7.3.3.6 Steel E-Motive battery tray sealing configuration

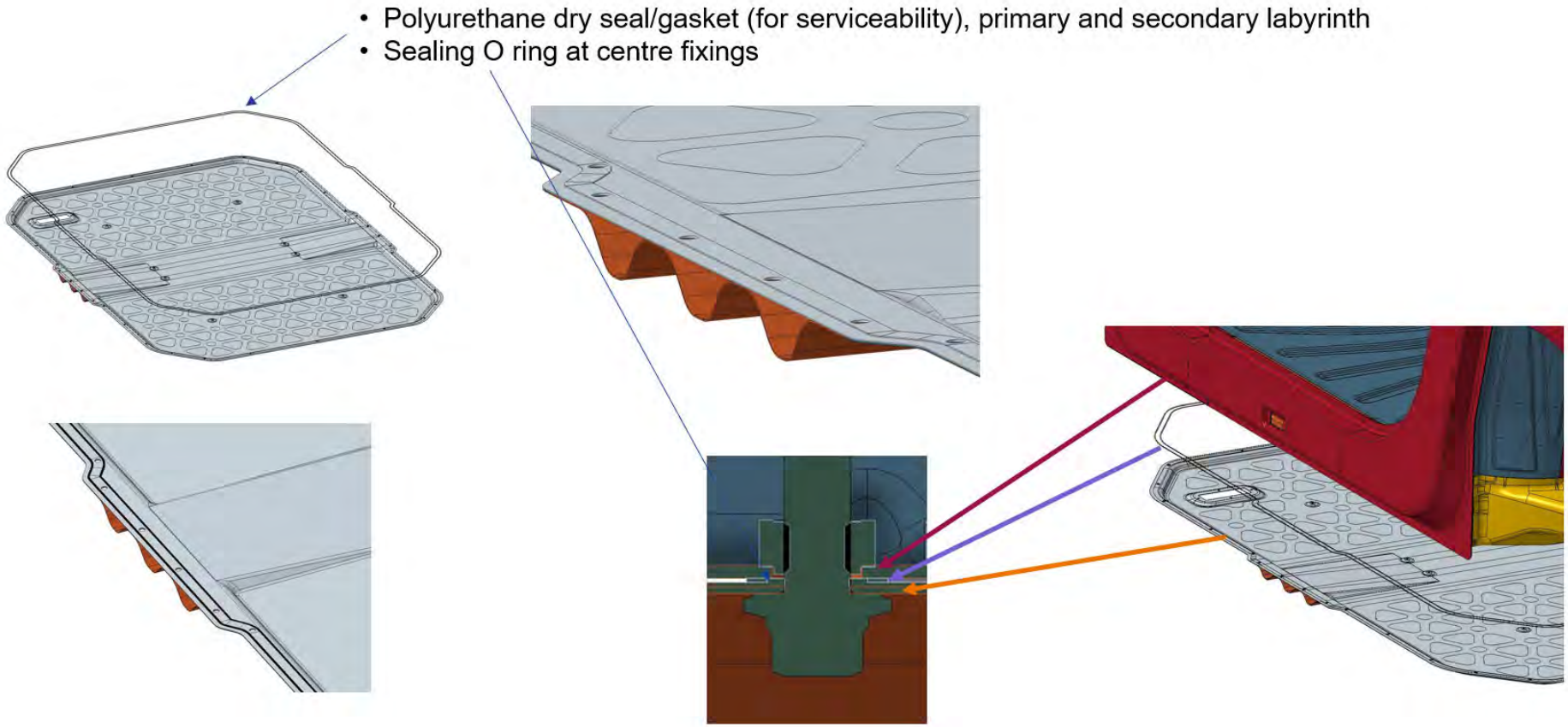

Figure 7.4.1.2.4 AHSS grades in SEM1 scissor doors

Scissor Door Structure	
Geometry/design	B pillars (1 & 2) and horizontal door struts (3 & 4) provide main crash loadpaths for IIHS side barrier. B pillars overlap the cantrail (top) and rocker sections (bottom) to provide crash loadpath into BIW structure. Mild steel door inner panels and bake hardenable outer panels. Lattice features provide some
Parts 1 & 2: B PILLAR (FRONT AND REAR)	1.2mm CR400Y690T-RA / Hydroformed
Parts 3 & 4: HORIZONTAL DOOR STRUTS (FRONT AND REAR)	1.5mm CR1200Y1470T-MS / roll stamp
Parts 5 & 6: DOOR INNER PANEL (FRONT AND REAR)	1.2mm Mild140/270 / cold stamp
Parts 7 & 8: DOOR OUTER PANEL(not shown) (FRONT AND REAR)	0.7mm CR280Y/400T-BH / cold stamp

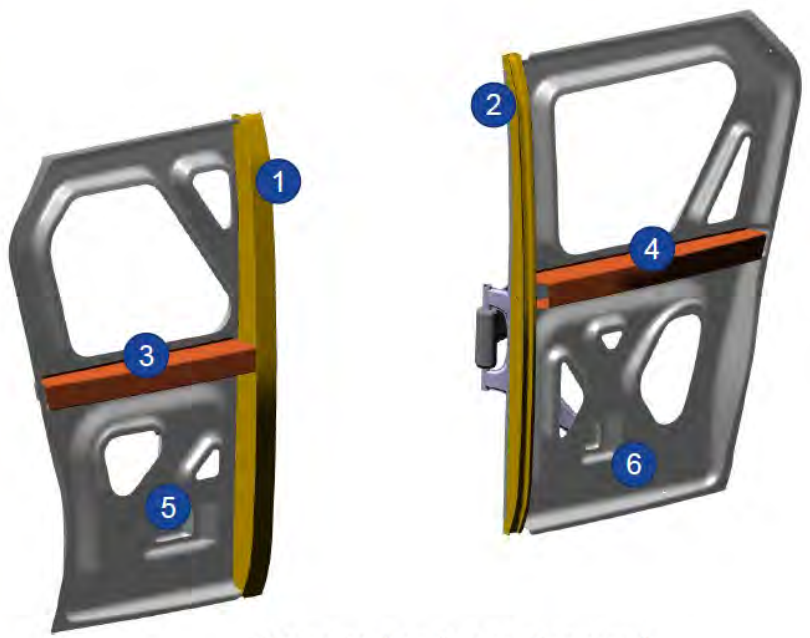

(door outer A surface panel removed)

Figure 7.6.2.3 Pareto of the highest 45 part costs in the SEM1 BIW

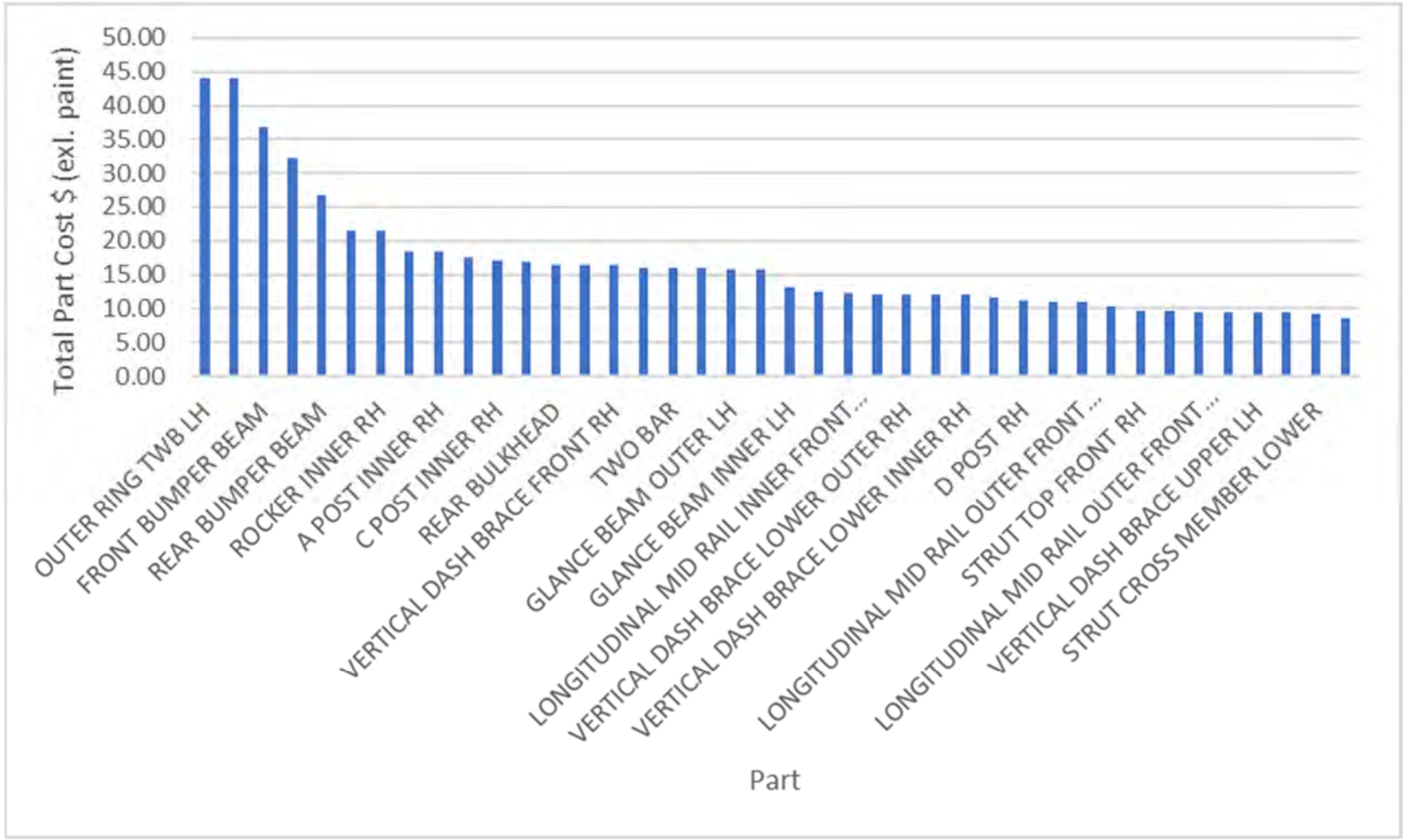

Figure 8.2.1 SEM1 front crashworthiness results (from full vehicle simulation)

	Vehicle Crashworthiness			
	Loadcase	**Target Value**	**Result Value**	**Comments**
Front (core loadcases)	US - NCAP 56 km/h FFB	<35 G Deceleration	33.1	- progressive, controlled collapse of crush rail - front subframe collapse encourages EDU ride down, reducing impact to front bulkhead
		< 40 mm bulkhead intrusion	2.5	- see Figure 8.2.2
	IIHS 64 km/h 40% ODB	<35 G Deceleration	20.5	Targets described in Figure 4.2.3.
		Footwell intrusion (1,2,3) < 150mm	1) 2.4 2) 4.1 3) 1.4	Intrusion values are within IIHS "good" rating
		Bulkhead Intrusion (4,5) < 50mm	4) 3.4 5) 5.2	- see Figure 8.2.3
		A pillar Y intrusion (6,7) >180mm clearance to seat centreline	6) >180mm 7) >180mm	
		No contact body structure to battery	(no contact observed)	
	IIHS 64 km/h 25% SORB	<35 G Deceleration	19.9	- IIHS "good" rating achieved. Vehicle exhibits "glance off" motion with 420mm lateral deflection - intrusion levels close to target but within 75mm IIHS "good" target
		Footwell intrusion (1,2,3) < 150mm	1) 2.0 2) 2.4 3) 4.2	- very stable A pillar and door ring - see Figure 8.2.4
		Bulkhead Intrusion (4,5) < 75mm	4) 53.8 5) 48.9	
		A pillar Y intrusion (6,7) >180mm clearance to seat centreline	6) >180 7) >180	
		No contact body structure to battery	(no contact observed)	
Front (reference loadcase)	OEM Centre Rigid Pole 64km/h, 253mm Pole	<40 G Deceleration	39	<40g pulse for all loadcases < 70mm dash intrusions
		< 80 mm bulkhead intrusion	1.6	Passenger cell integrity remains good
	NHTSA 90kph 35% 15 degree oblique	<40g	31.9	- see Figure 8.2.5 to 8.2.7
		<80mm intrusion	70	
	NCAP - MPDB	<40 G Deceleration	33.3	
		< 80 mm bulkhead intrusion	1.3	

Figure 8.3.2 IIHS 60KPH side barrier (II) crash simulation results

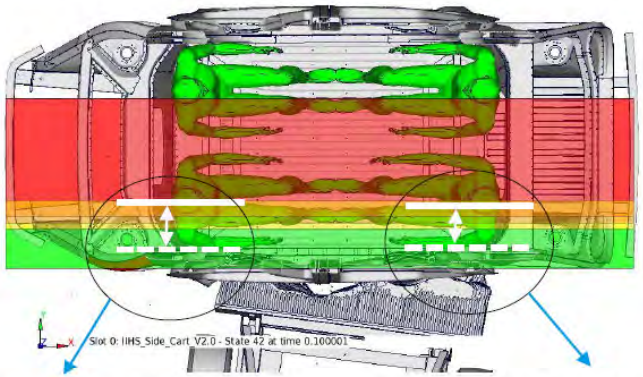

Mannequin Front Left:
End distance A-Pillar -Driver seat pan centerline: **297.8 mm**

Mannequin Rear Left:
End distance A-Pillar -Driver seat pan centerline: **292.8 mm**

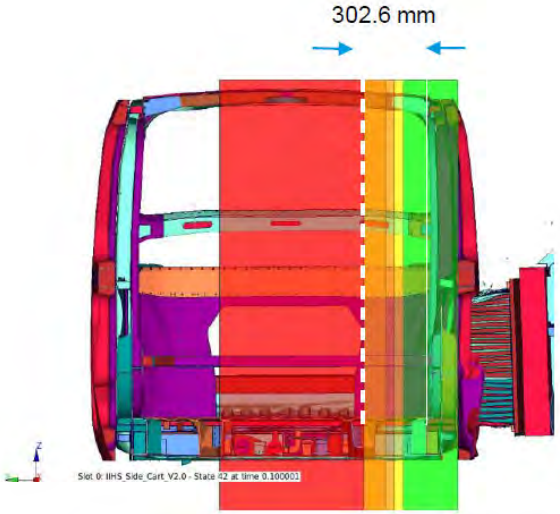

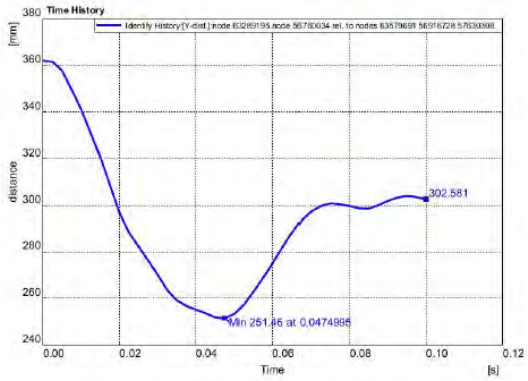

Distance between max intrusion point and Driver seat pan centerline

Figure 8.3.3 USNCAP 32kph side pole crash simulation results, battery protection

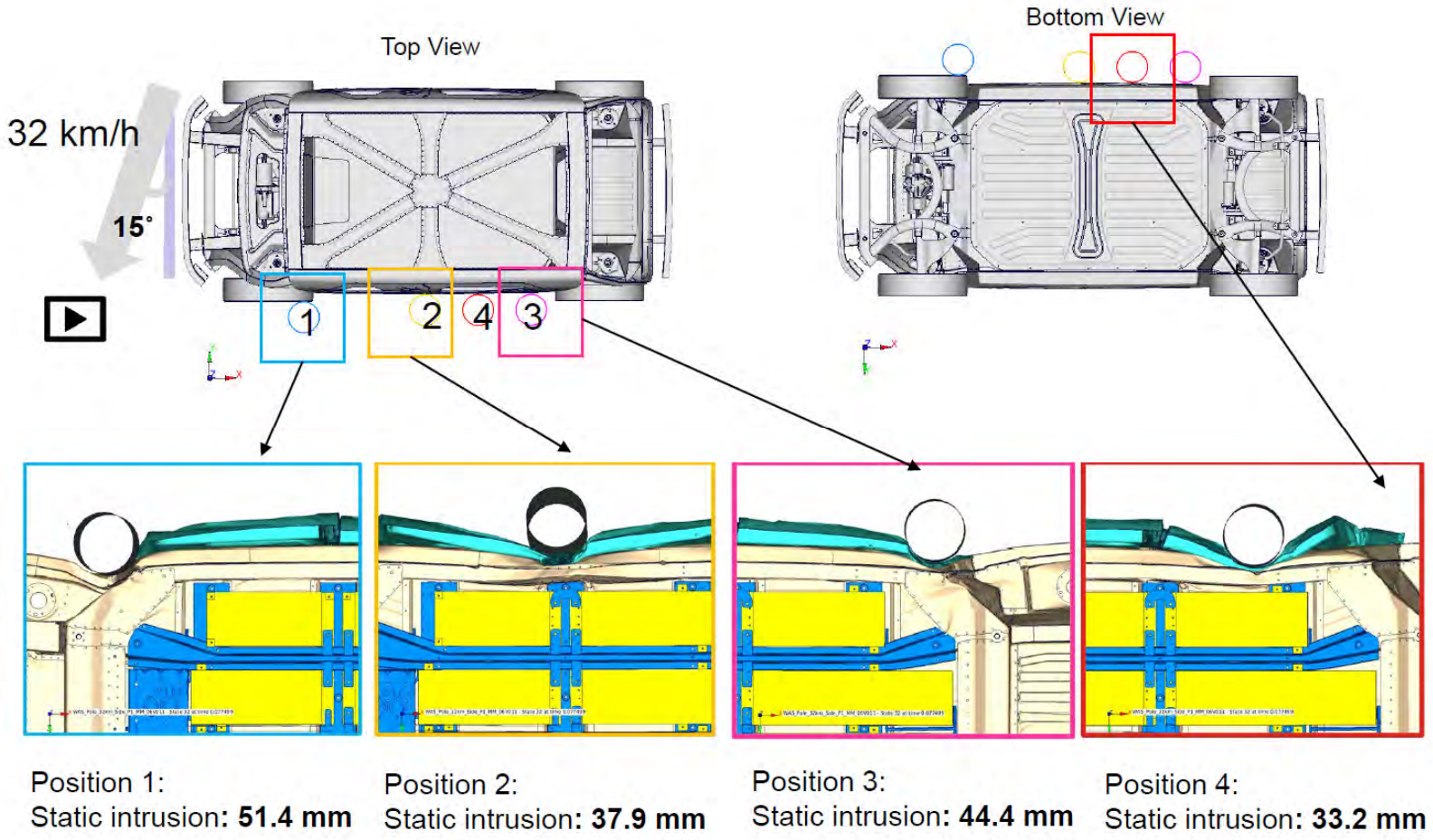

Figure 8.3.4 USNCAP 32kph side pole crash simulation results, occupant protection

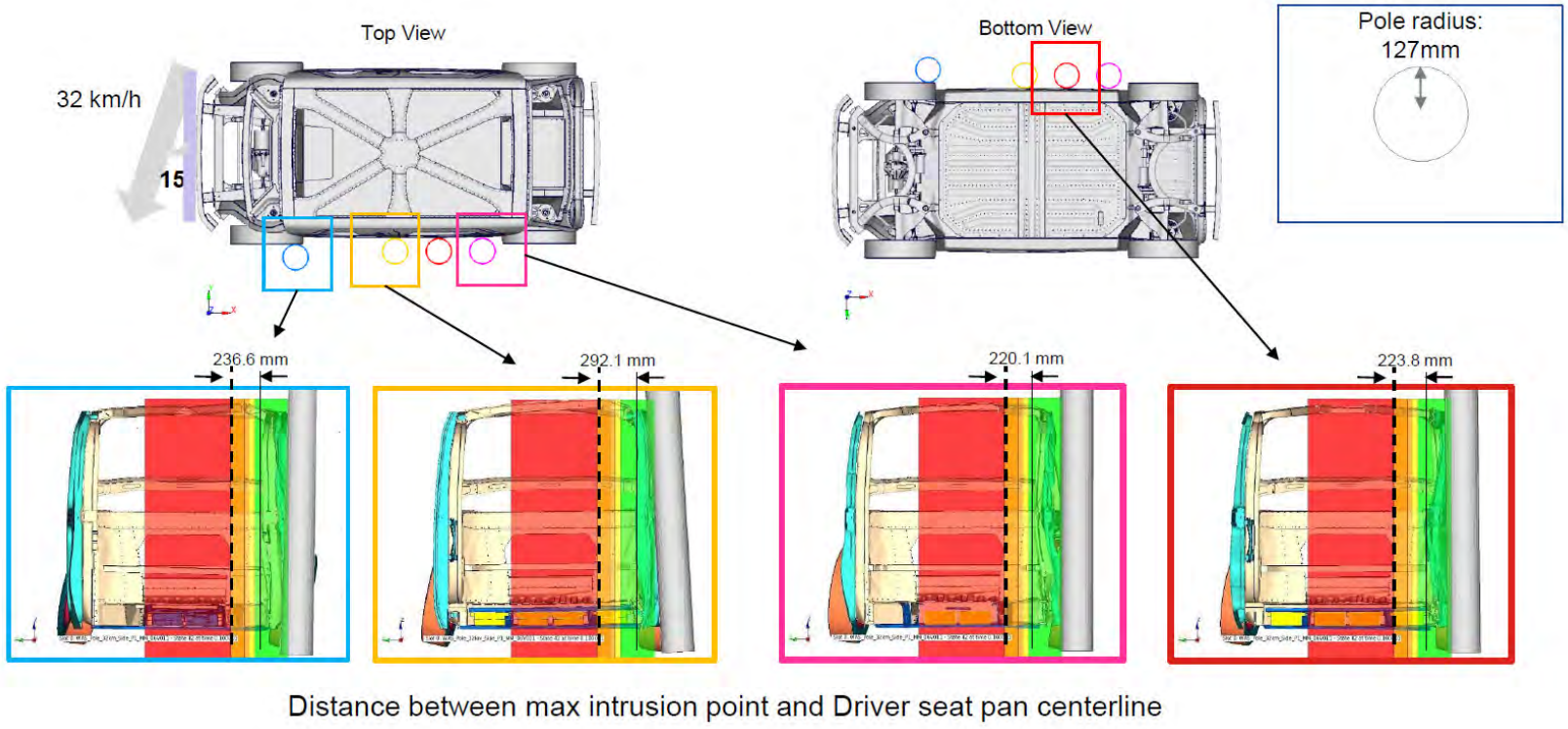

Figure 8.3.5 USNCAP 32kph side pole crash simulation results, occupant protection

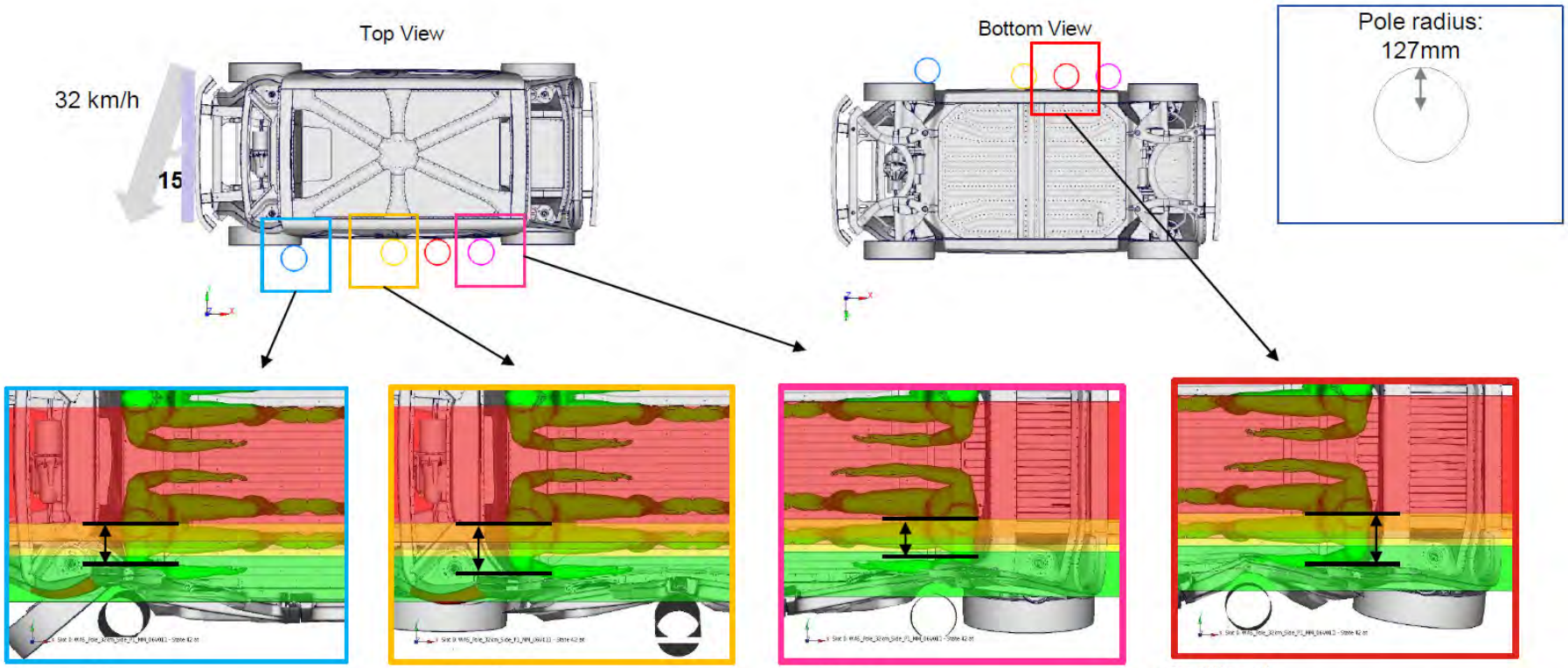

Figure 9.2.1 UCSB Life Cycle Analysis tool data flow

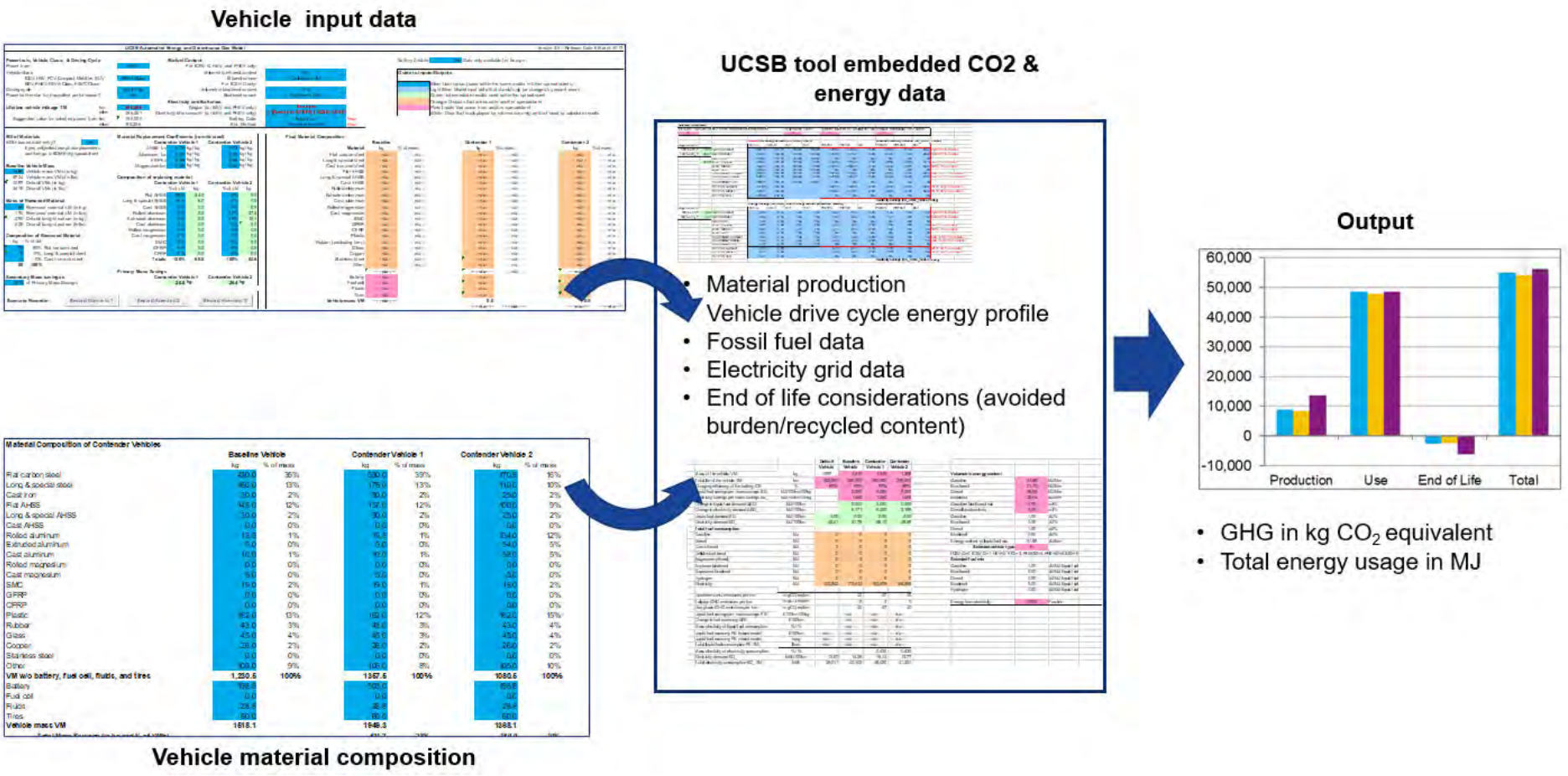

Figure 9.2.2 LCA model input parameters

LCA parameter	Value
description	Text description of the LCA model (e.g. “reference”, “Steel E-Motive baseline”
Su-title Level 1	Further model description (e.g. “drivecycle smoothing” study
power train	(is Battery Electric for all vehicles in the LCA study)
% ethanol	(=0% for all (BEV) vehicles in the LCA study)
Vehicle class	(= “FSV A class” for all vehicles in the LCA study. This is standard option in UCSB tool
Driving cycle	Standard test drive cycle used for use phase calculation (e.g. WLTP)
Driving cycle smoothing reduction	% reduction in drive cycle energy, based on autonomous vehicle speed and throttle control potential
Lifetime km	Total expected life of vehicle (kilometers)
Battery lifetime (km)	Total expected life of propulsion battery (kilometers)
pyrometall. LIB recycling share	Propulsion battery recycling approach
Grid mix (both SDS and STEPS for future scenarios)	Electricity grid supply timeline (data from IEA)
Region	Vehicle operation (grid supply) location (Europe, US, Japan, China, India)
EoL method	LCA End of life methodology (avoided burden, recycled content)
"green" steel share	% steel of reduced carbon production steel used (100% = all steel used in vehicle is manufactured using decarbonised process)
"green" Al share	% of reduced carbon production aluminium used (100% = all aluminium used in vehicle is manufactured using decarbonised process)
Vehicle occupancy (ride sharing)	Number of vehicle occupants in LCA calculations

Figure 9.3.2.1.2 Life Cycle Analysis modelling considerations for BF-BOF and DRI-EAF steel production methods

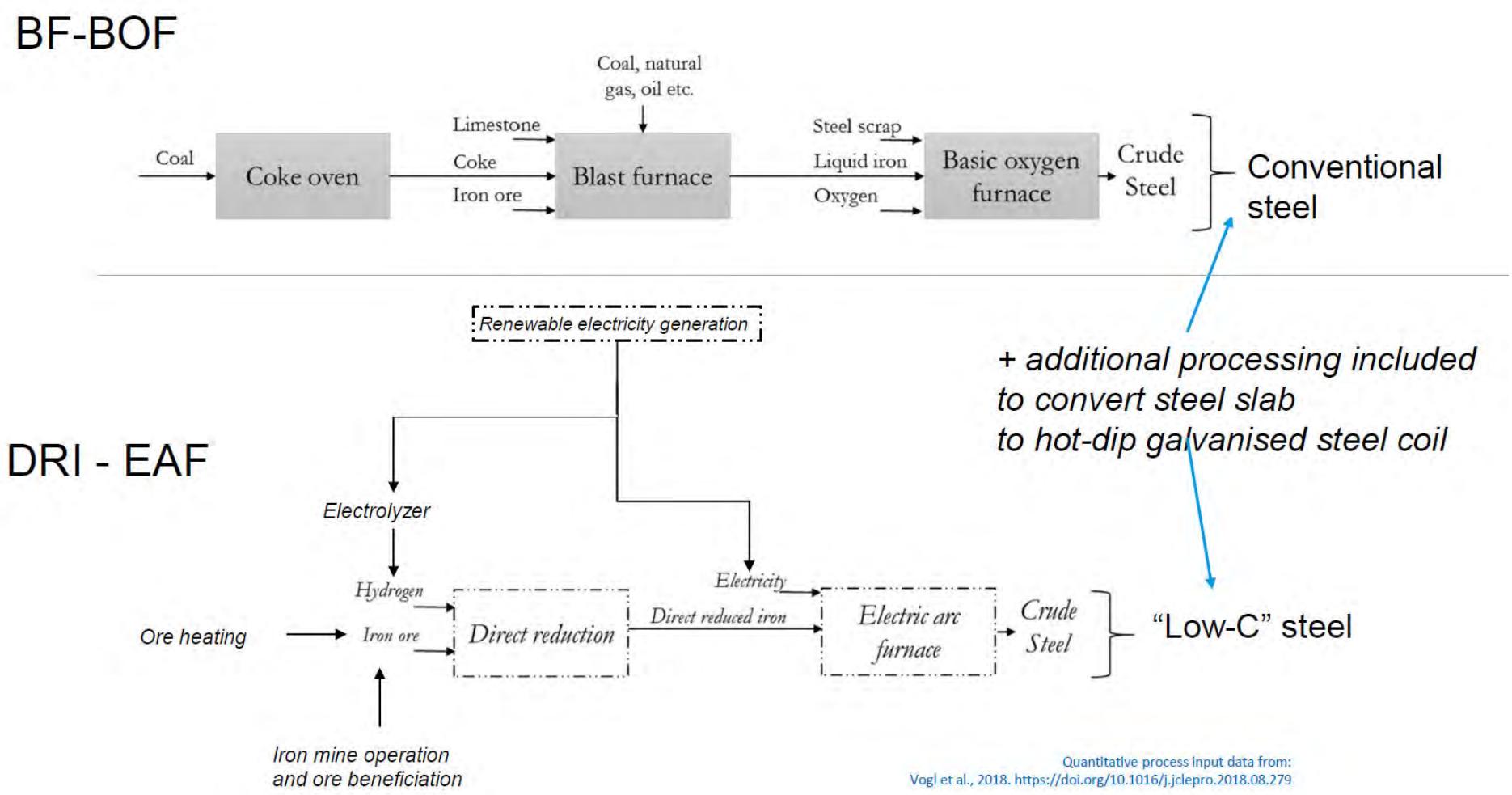

Figure 9.3.2.1.3 GaBi modelling of DRI-EAF steel production

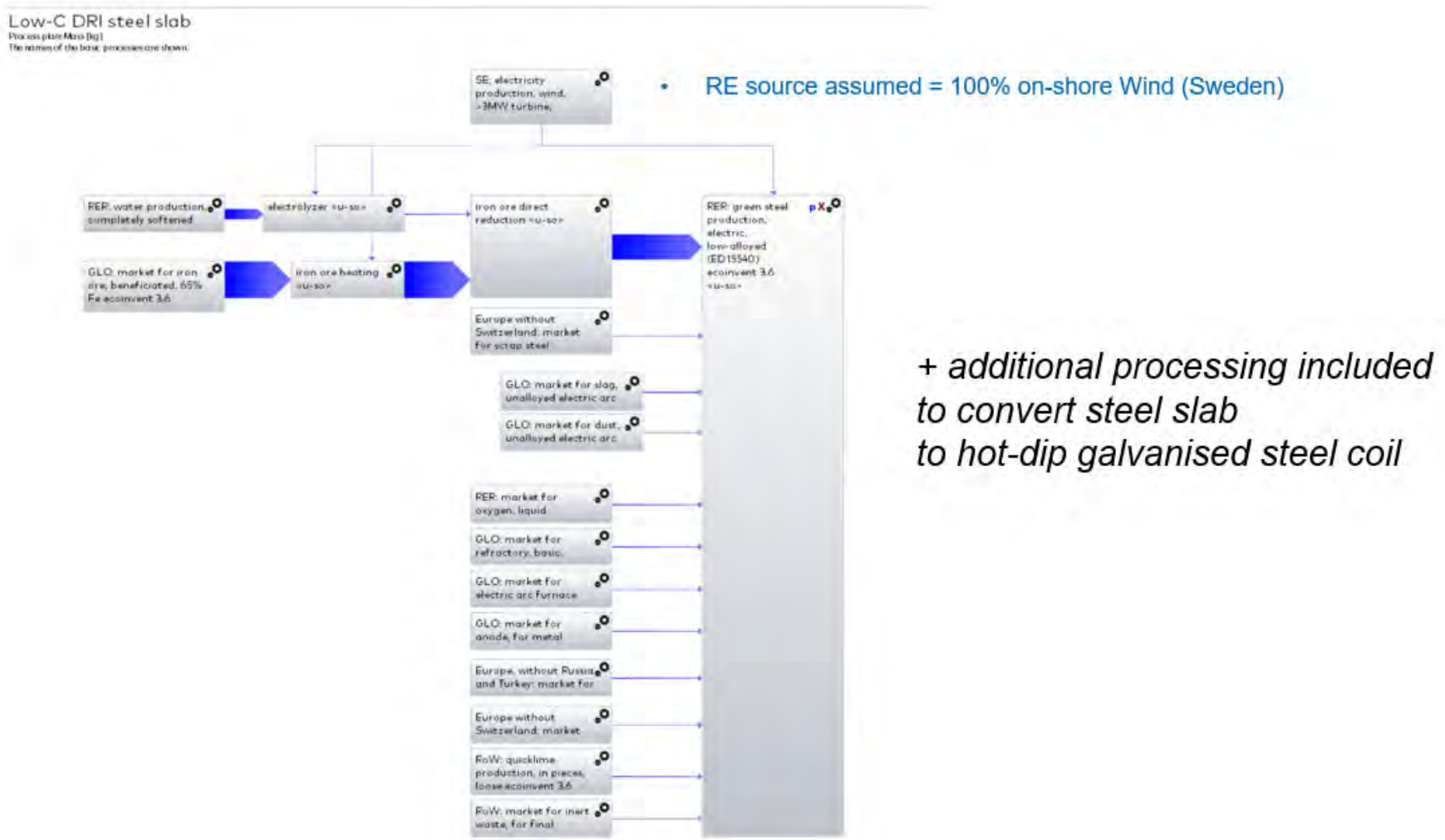

Figure 9.3.2.1.4 Predicted GHG emissions and fossil fuel primary energy demand effects of “green” steel production. (BF-BOF data provided by WorldSteel association).

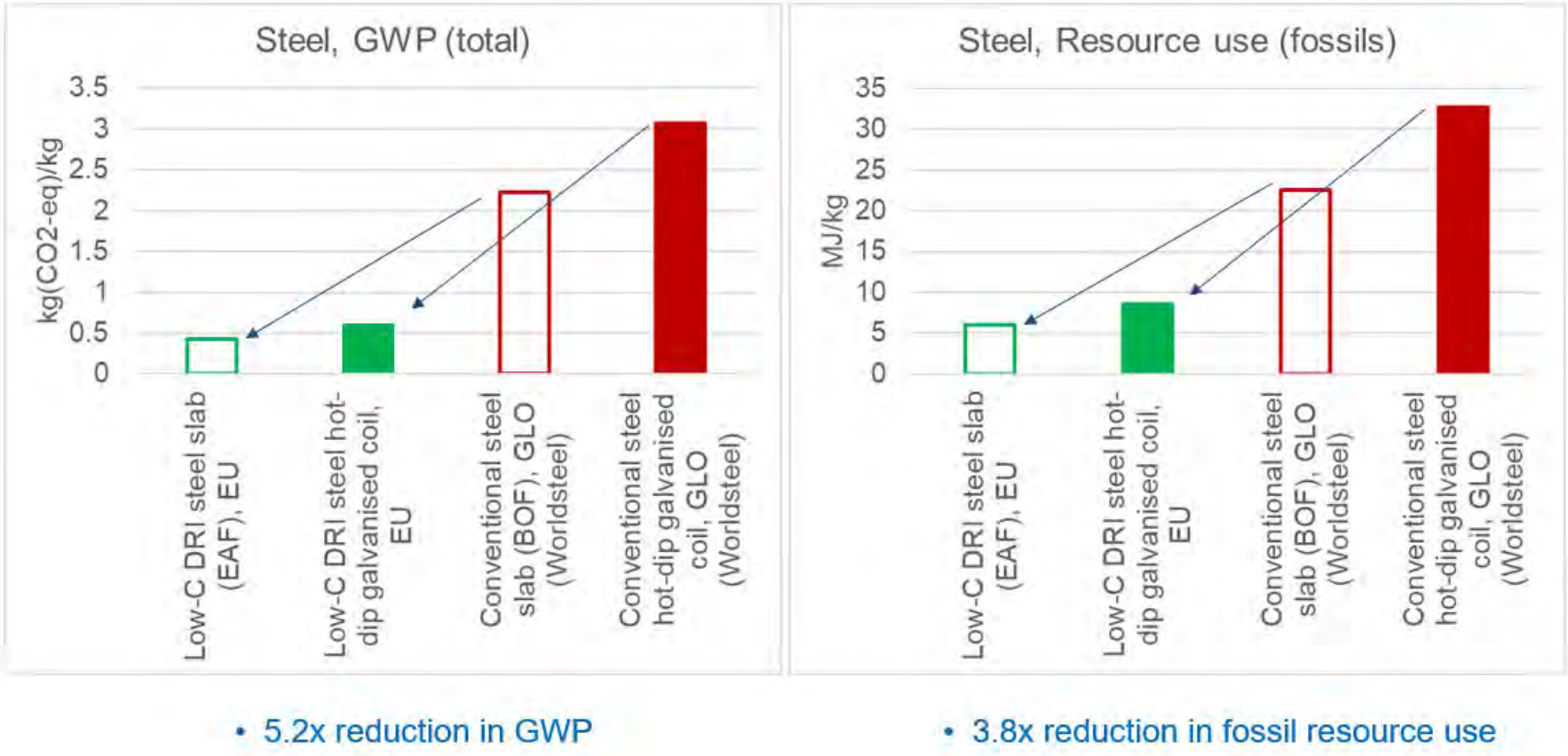

Figure 9.3.2.5.2 1D IGNITE vehicle energy simulation model schematic

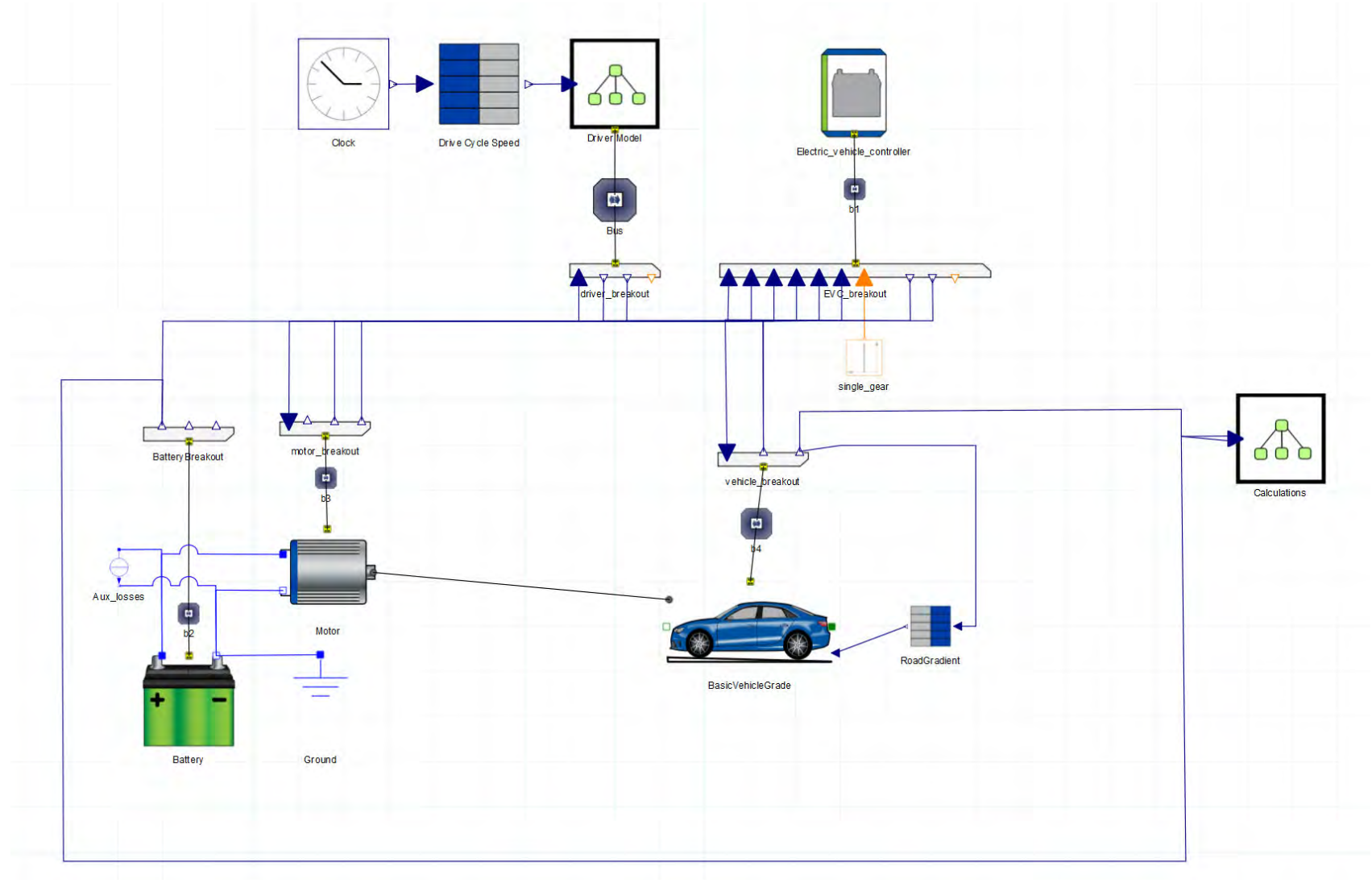

Figure 9.3.2.5.3 Traffic & drive cycle generation, vehicle energy simulation, Life Cycle Analysis process flow applied in Steel E-Motive

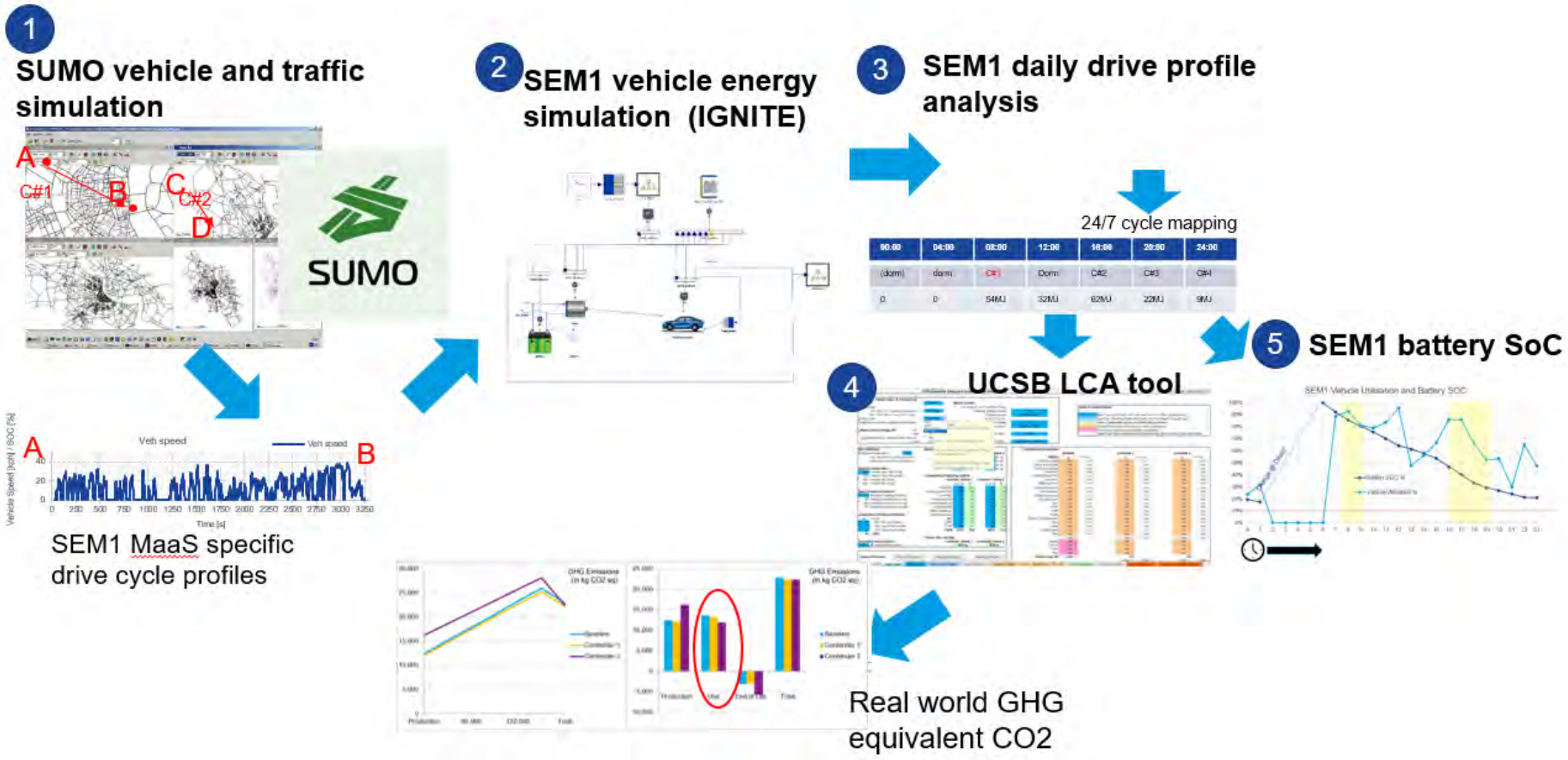

Figure 9.3.2.5.4 Map of SEM1 SUMO model mission routes

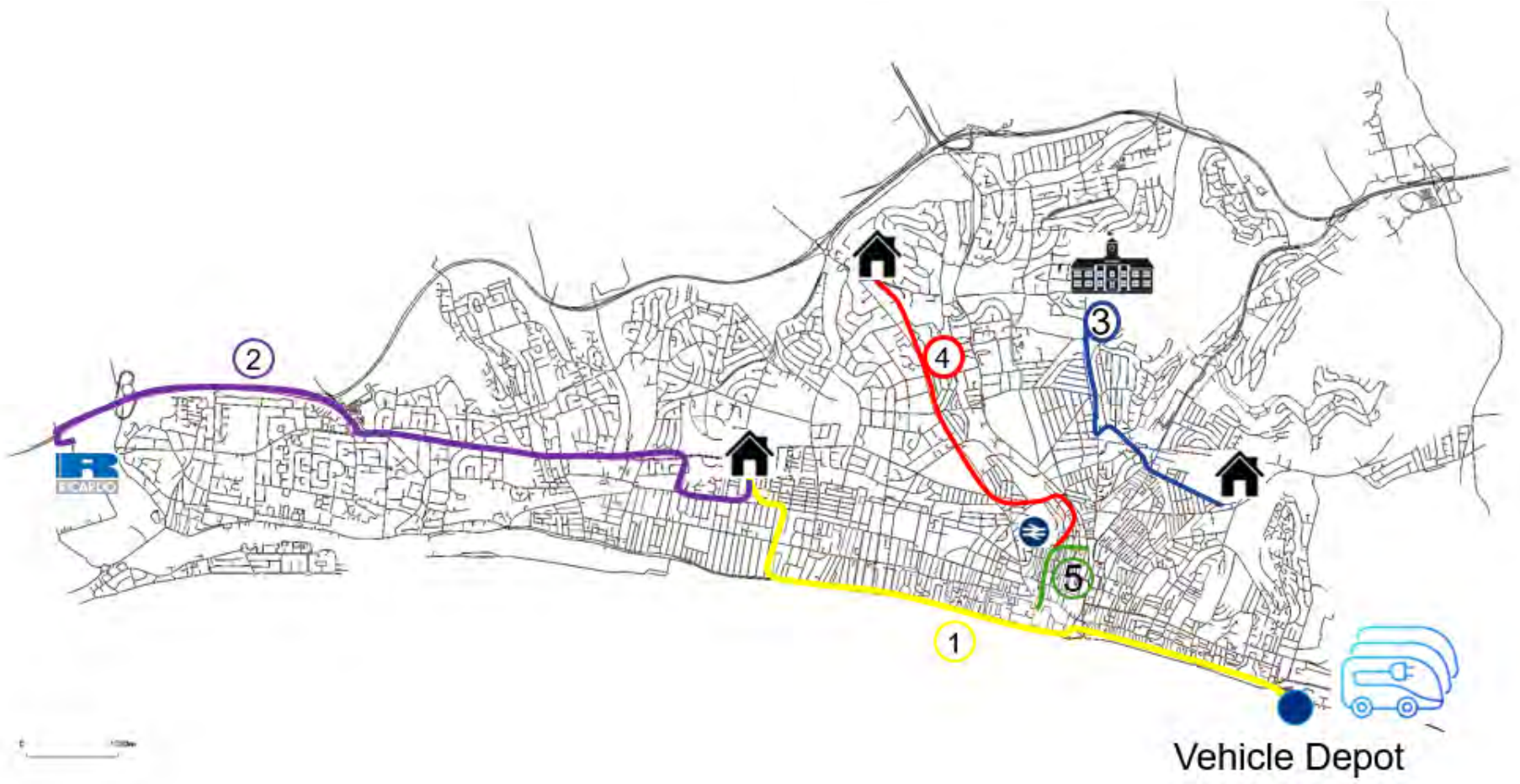

Table 9.3.2.5.5 SUMO traffic modelling output for SEM1 missions

Mission number	Description	Journey distance (km)	Journey type	Journey time (minutes) (low traffic/off peak)	Average vehicle speed (km/h) (low traffic/off peak)	Journey time (minutes) (high traffic/peak)	Average vehicle speed (km/h) (high traffic/peak)
1	Depot to home collection	8.37	Suburban to suburban	11.9	41.7	13	37.6
2	Home to office	9.11	Suburban to rural	10.0	53.8	10.0	53.8
3	Home to school	3.22	Suburban to suburban	6.2	30.4	6.2	30.4
4	Home to city centre train station	4.08	Suburban to city	7.1	33.9	7.1	33.9
5	City centre journey	1.67	City centre	3.6	27.1	9.2	11.5

Figure 9.3.2.5.7 SUMO traffic modelling drive cycle profiles for low and high traffic scenarios

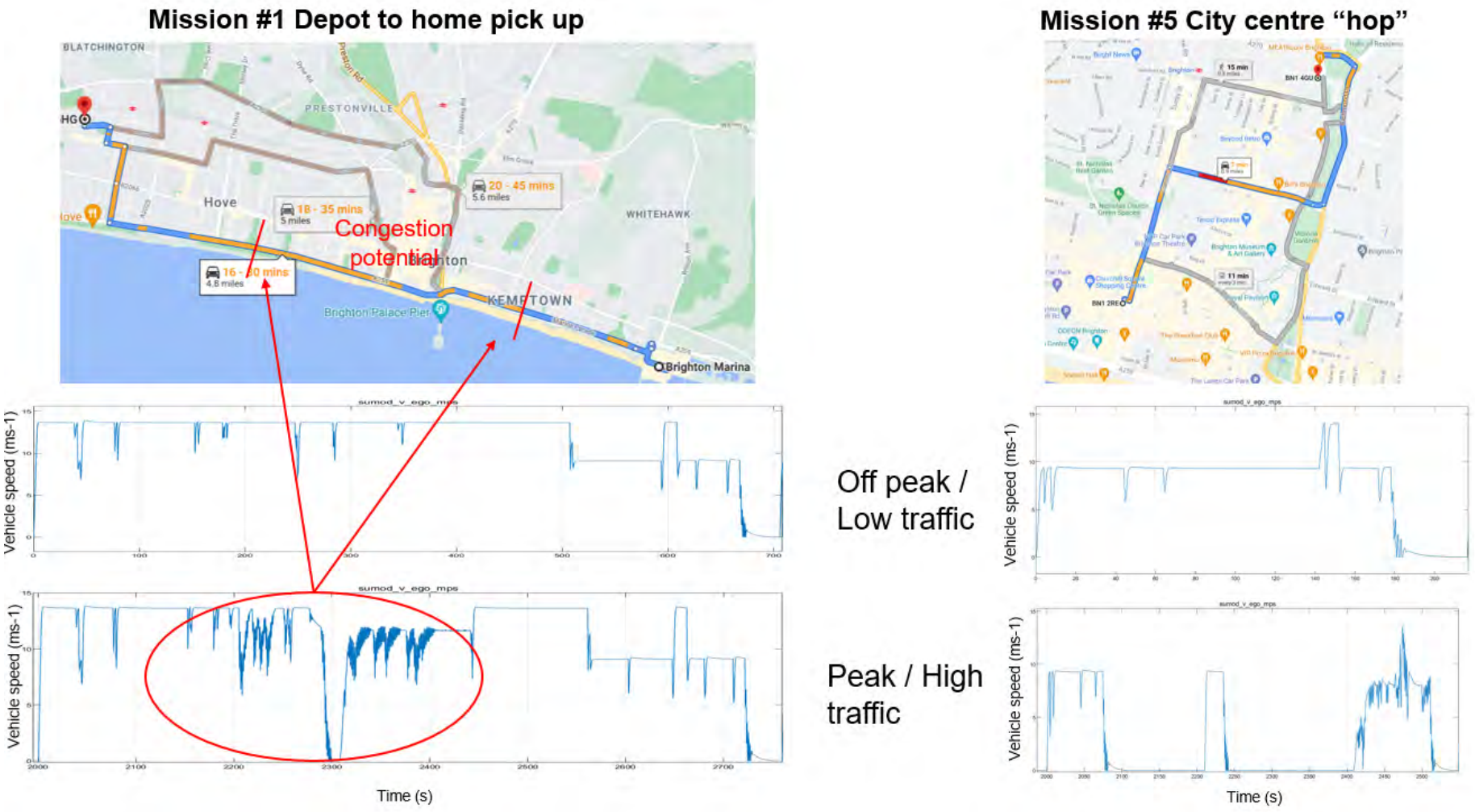

Figure 9.3.2.5.8 24-hour SEM1 vehicle mission profile, combining mission segments #1 to #5, at low/high traffic and low/high weight

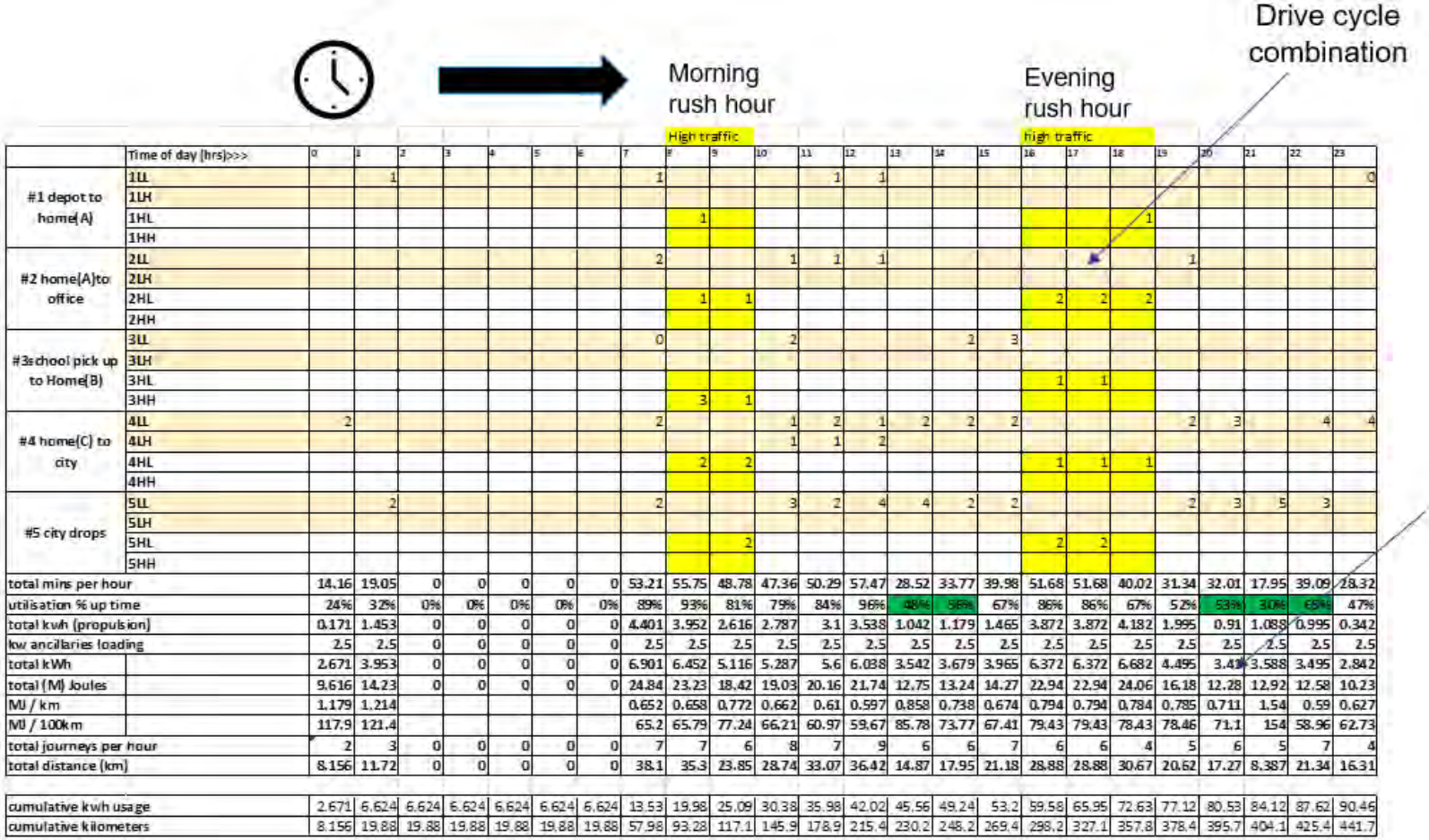

	Time of day (hrs)>>>	0	1	2	3	4	5	6	7	8	9	10	11	12	13	14	15	16	17	18	19	20	21	22	23
#1 depot to home(A)	1LL		1						1				1	1											0
	1LH																								
	1HL									1											1				
	1HH																								
#2 home(A)to office	2LL								2			1	1	1							1				
	2LH																								
	2HL									1	1							2	2	2					
	2HH																								
#3school pick up to Home(B)	3LL								0			2				2	3								
	3LH																								
	3HL																	1	1						
	3HH									3	1														
#4 home(C) to city	4LL	2							2			1	2	1	2	2	2				2	3		4	4
	4LH											1	1	2											
	4HL									2	2							1	1	1					
	4HH																								
#5 city drops	5LL		2						2			3	2	4	4	2	2				2	3	5	3	
	5LH																								
	5HL										2							2	2						
	5HH																								
total mins per hour		14.16	19.05	0	0	0	0	0	53.21	55.75	48.78	47.36	50.29	57.47	28.52	33.77	39.98	51.68	51.68	40.02	31.34	32.01	17.95	39.09	28.32
utilisation % up time		24%	32%	0%	0%	0%	0%	0%	89%	93%	81%	79%	84%	96%	48%	56%	67%	86%	86%	67%	52%	53%	30%	65%	47%
total kwh (propulsion)		0.171	1.453	0	0	0	0	0	4.401	3.952	2.616	2.787	3.1	3.538	1.042	1.179	1.465	3.872	3.872	4.182	1.995	0.91	1.088	0.995	0.342
kw ancillaries loading		2.5	2.5	0	0	0	0	0	2.5	2.5	2.5	2.5	2.5	2.5	2.5	2.5	2.5	2.5	2.5	2.5	2.5	2.5	2.5	2.5	2.5
total kWh		2.671	3.953	0	0	0	0	0	6.901	6.452	5.116	5.287	5.6	6.038	3.542	3.679	3.965	6.372	6.372	6.682	4.495	3.41	3.588	3.495	2.842
total (M) Joules		9.616	14.23	0	0	0	0	0	24.84	23.23	18.42	19.03	20.16	21.74	12.75	13.24	14.27	22.94	22.94	24.06	16.18	12.28	12.92	12.58	10.23
MJ / km		1.179	1.214						0.652	0.658	0.772	0.662	0.61	0.597	0.858	0.738	0.674	0.794	0.794	0.784	0.785	0.711	1.54	0.59	0.627
MJ / 100km		117.9	121.4						65.2	65.79	77.24	66.21	60.97	59.67	85.78	73.77	67.41	79.43	79.43	78.43	78.46	71.1	154	58.96	62.73
total journeys per hour		2	3	0	0	0	0	0	7	7	6	8	7	9	6	6	7	6	6	4	5	6	5	7	4
total distance (km)		8.156	11.72	0	0	0	0	0	38.1	35.3	23.85	28.74	33.07	36.42	14.87	17.95	21.18	28.88	28.88	30.67	20.62	17.27	8.387	21.34	16.31

cumulative kwh usage	2.671	6.624	6.624	6.624	6.624	6.624	6.624	13.53	19.98	25.09	30.38	35.98	42.02	45.56	49.24	53.2	59.58	65.95	72.63	77.12	80.53	84.12	87.62	90.46
cumulative kilometers	8.156	19.88	19.88	19.88	19.88	19.88	19.88	57.98	93.28	117.1	145.9	178.9	215.4	230.2	248.2	269.4	298.2	327.1	357.8	378.4	395.7	404.1	425.4	441.7

Figure 9.4.1 Lifecyle analysis studies and model boundary conditions

Scenario n.	1	2	3	4	5	6	7	8	9	10	11
description	*BASELINE: 2018-2030 grid mix, private/taxi, EU*	*Future grid mix, private/taxi, EU*	*Future grid mix, private/taxi, EU, recycled content EoL*	*Future grid mix, 100% low-C steel, private/taxi, EU*	*Future grid mix, extended life, 2 batt, private/taxi, EU*	*Future grid mix, extended life, 1 batt, private/taxi, EU*	*Future grid mix, private/taxi, "real world" cycle, EU*	*Future grid mix, autonomous, private/taxi, "real world" cycle, EU*	*Future grid mix, ride sharing low, EU*	*Future grid mix, ride sharing high, EU*	*Future grid mix, extended life, 100% low-C steel, autonomous, ride sharing high, EU*
Title Level 1	*Baseline vehicle 2018*	*Steel e-Motive; Default*	*Recycled*	*Low-C steel*	*Extended life, 2*	*Extended life, 1*	*"Real-World"*	*"Real-World"*	*Increased Ride sharing low*	*Ride sharing*	*Extended life,*
Title Level 2											
Title Level 3	*Baseline*										
power train	**BEV**	**BEV**	**BEV**	**BEV**	**BEV**	**BEV**	**BEV**	**BEV**	**BEV**	**BEV**	**BEV**
% ethanol	0%	0%	0%	0%	0%	0%	0%	0%	0%	0%	0%
Vehicle class	FSV A-class	FSV A-class	FSV A-class	FSV A-class	FSV A-class	FSV A-class	FSV A-class	FSV A-class	FSV A-class	FSV A-class	FSV A-class
Driving cycle	WLTP	WLTP	WLTP	WLTP	WLTP	WLTP	real-world cycle	real-world cycle	WLTP	WLTP	WLTP
Driving cycle smoothing reduction	0%	0%	0%	0%	0%	0%	0%	-15%	0%	0%	0%
Lifetime km	300,000	300,000	300,000	300,000	600,000	600,000	300,000	300,000	300,000	300,000	600,000
Battery lifetime (km)	300,000	300,000	300,000	300,000	300,000	600,000	300,000	300,000	300,000	300,000	600,000
pyrometall. LIB recycling share	50%	0%	0%	0%	0%	0%	0%	0%	0%	0%	0%
Grid mix (both SDS and STEPS for future scenarios)	2018	2030-2040	2030-2040	2030-2040	2030-2040	2030-2040	2030-2040	2030-2040	2030-2040	2030-2040	2030-2040
Region	**Europe**	**Europe**	**Europe**	**Europe**	**Europe**	**Europe**	**Europe**	**Europe**	**Europe**	**Europe**	**Europe**
EoL method	Av.Burden	Av.Burden	Recycled content	Av.Burden	Av.Burden	Av.Burden	Av.Burden	Av.Burden	Av.Burden	Av.Burden	Av.Burden
"green" steel share	0%	0%	0%	100%	0%	0%	0%	0%	0%	0%	100%
"green" Al share	0%	0%	0%	0%	0%	0%	0%	0%	0%	0%	0%
Vehicle occupancy (ride sharing)	1.4	1.4	1.4	1.4	1.4	1.4	1.4	1.4	2	3	3

Figure 9.4.2 lifecycle analysis GHG CO_2 calculations (CO_2 equivalent per passenger-kilometers)

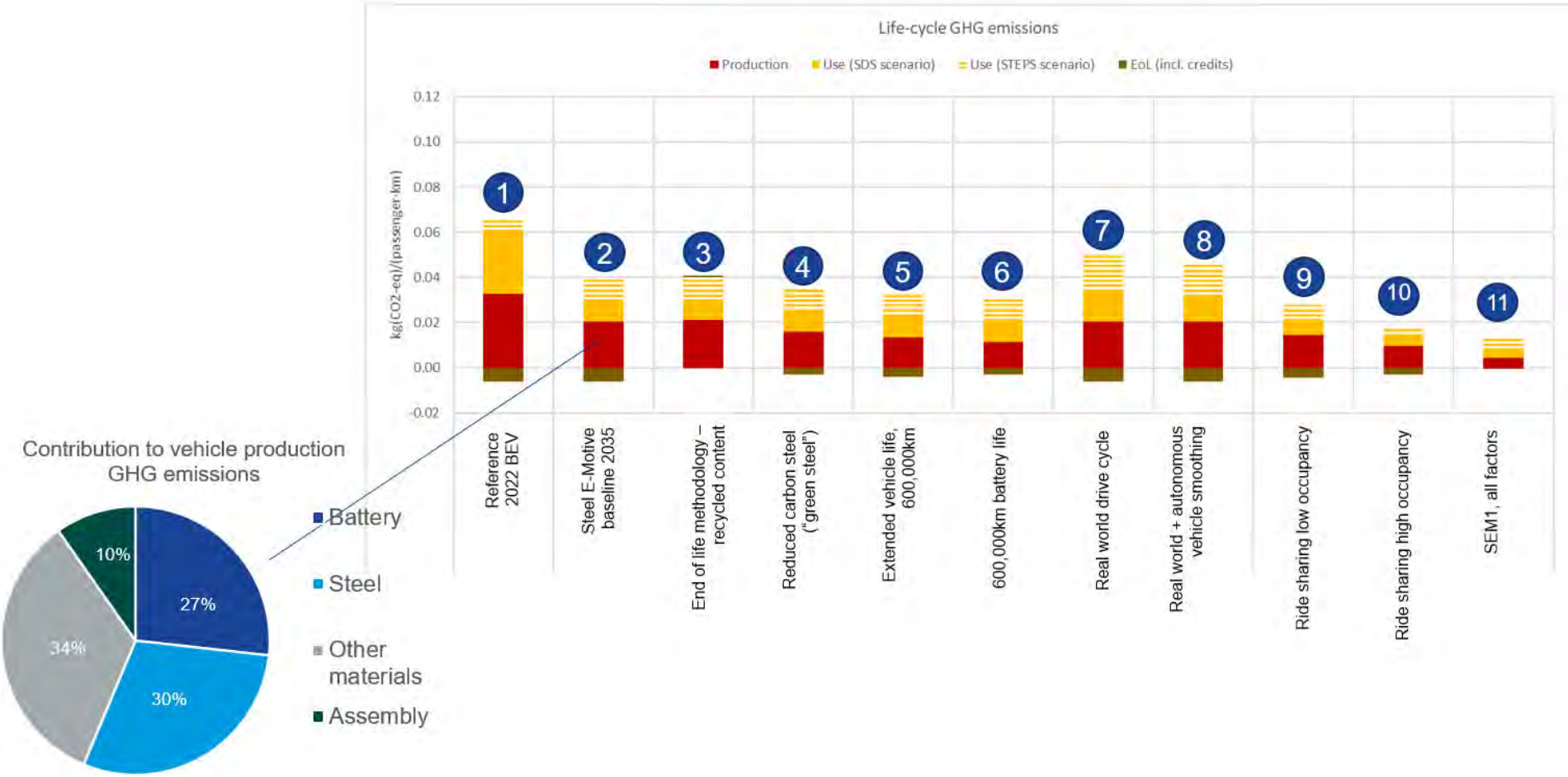

Figure 9.4.3 lifecycle analysis GHG CO_2 calculations, expressed as % of reference 2022 BEV

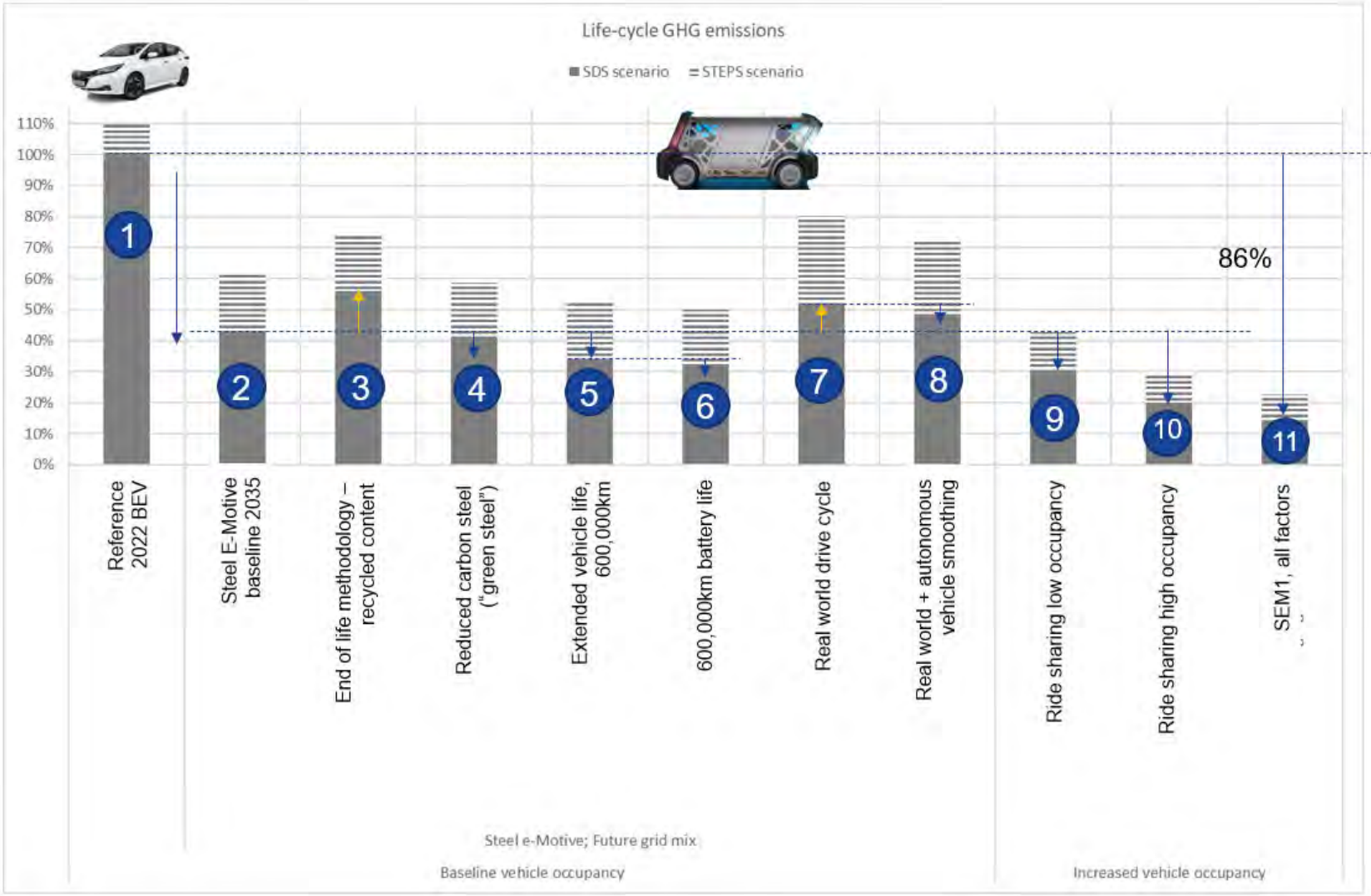

Figure 9.4.4 LCA results narrative

Model/result number	Description	Key Result
1	Reference BEV, 2022	Used as datum/reference for SEM
2	Baseline Steel E-Motive. 25% vehicle weight reduction versus (1), 2030-2040 electricity grid mix	57% life cycle GHG reduction compared to (1)
3	Steel E-Motive. As (2) with End of Life methodology changed from *avoided burden* method to *recycled content*	Recycled content EOL methodology results in a 13% increase in lifecycle GHG
4	Steel E-Motive. As (2) with all AHSS in the vehicle substituted with decarbonised steel production	22% reduction in vehicle production GHG emissions. 3% decrease in GHG over vehicle lifecycle. Note, the effect is diluted due to the GHG contribution in the use phase
5	Steel E-Motive. As (2), with vehicle lifetime kilometers increased from 300,000km (2) to 600,000km (5)	20% reduction in vehicle lifecycle GHG
6	Steel E-Motive. As (5), with battery lifetime increased from 300,000km to 600,000km	A further 7% reduction in lifecycle GHG emissions compared to (5)
7	Steel E-Motive. As (2) with real-world driving cycle. (all other models assume a standard WLTP drive cycle)	Real world drive cycle results in overall 21% increase in lifecycle GHG emissions
8	Steel E-Motive. As (7) with effect of autonomous vehicle drive cycle smoothing	7% reduction in lifecycle GHG emissions compared to (7)
9	Stee E-Motive. As (2) with vehicle occupancy passenger increased from 1.4 to 2.0	30% reduction in lifecycle GHG emissions compared to (2)
10	Stee E-Motive. As (2) with vehicle occupancy passenger increased from 1.4 to 3.0	53% reduction in lifecycle GHG emissions compared to (2)
11	Steel E-Motive. As (2), with combined effects of (4), (5), (6), (10)	86% reduction in lifecycle GHG emissions compared to reference 2022 BEV vehicle (1))

Figure 9.4.5 Lifecycle calculations for Eu, US, China and Japan regions

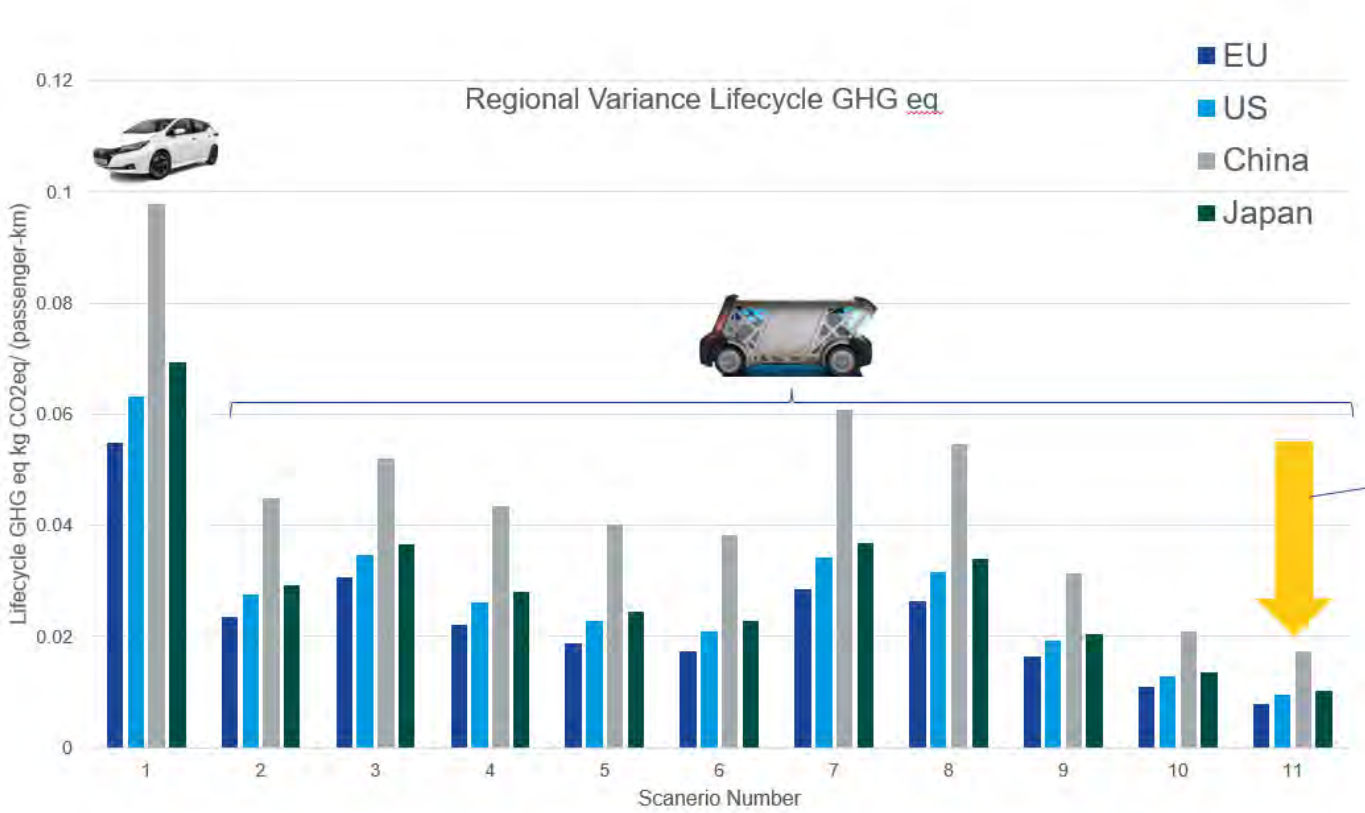

Country	Max GHG Potential from 2022 Reference
EU	86%
US	85%
China	82%
Japan	85%

Figure 11.4.2.2 Unique SEM2 BIW parts: front zone

Part Number	Part Name	AHSS Grade	Gauge (mm)	C = Carry over SEM1 G = grade/gauge change N = New geom	Part Mass (kg)	SEM2 change
03643418_2	GLANCE BEAM LOWER REACTION RH	CR1200Y1470T-MS	1.2	G	0.72	change from 0.8mm to 1.2mm
03640761_2	GLANCE BEAM UPPER REACTION RH	PHS-CR1500T-MB	1.0	G	0.52	change from 0.8mm to 1.2mm
03553269_2	LONGITUDINAL MID RAIL OUTER FRONT RH	CR500Y780T-DP/CR700Y980T-DP	2.0	G	3.51	change from 1.8mm/2.0mm TWB to to 2.0mm throughout
03506010_2	LONGITUDINAL MID RAIL OUTER FRONT LH	CR500Y780T-DP/CR700Y980T-DP	2.0	G	3.51	change from 1.8mm/2.0mm TWB to to 2.0mm throughout
03585863_2	GLANCE BEAM UPPER TRIANGULATION INNER LH	PHS-CR1500T-MB	1.2	G	1.12	change from 0.8mm to 1.2mm
03642244_2	GLANCE BEAM LOWER REACTION LH	CR1200Y1470T-MS	1.2	G	0.72	change from 0.8mm to 1.2mm
03553270_2	LONGITUDINAL MID RAIL INNER FRONT RH	CR500Y780T-DP/CR700Y980T-DP	2.0	G	3.79	change from 1.8mm/2.0mm TWB to to 2.0mm throughout
03618387_2	GLANCE BEAM OUTER RH	PHS-CR1500T-MB	1.2	G	2.63	change from 0.8mm to 1.2mm
03618391_2	GLANCE BEAM UPPER TRIANGULATION OUTER RH	PHS-CR1500T-MB	1.2	G	1.27	change from 0.8mm to 1.2mm
03640760_2	GLANCE BEAM UPPER REACTION LH	CR1200Y1470T-MS	1.2	C	0.42	change from 0.8mm to 1.2mm
03618390_2	GLANCE BEAM UPPER TRIANGULATION INNER RH	PHS-CR1500T-MB	1.2	G	1.12	change from 0.8mm to 1.2mm
03643340_2	GLANCE BEAM LATERAL CROSS MEMBER OUTER	CR1200Y1470T-MS	1.2	G	1.52	change from 0.8mm to 1.2mm
03601006_2	GLANCE BEAM UPPER TRIANGULATION OUTER LH	PHS-CR1500T-MB	1.2	G	1.27	change from 0.8mm to 1.2mm
03506011_2	LONGITUDINAL MID RAIL INNER FRONT LH	CR500Y780T-DP/CR700Y980T-DP	2.0	G	3.51	change from 1.8mm/2.0mm TWB to to 2.0mm throughout
03640758_2	STRUT CROSS MEMBER FRONT	PHS-CR2000T-MB	1.2	G	3.31	change from 1.0mm to 1.2mm
03618389_2	GLANCE BEAM INNER RH	PHS-CR1500T-MB	1.2	G	2.56	change from 0.8mm to 1.2mm
03585867_2	GLANCE BEAM OUTER LH	PHS-CR1500T-MB	1.2	G	2.63	change from 0.8mm to 1.2mm

Figure 11.4.2.2 Unique SEM2 BIW parts: rear zone

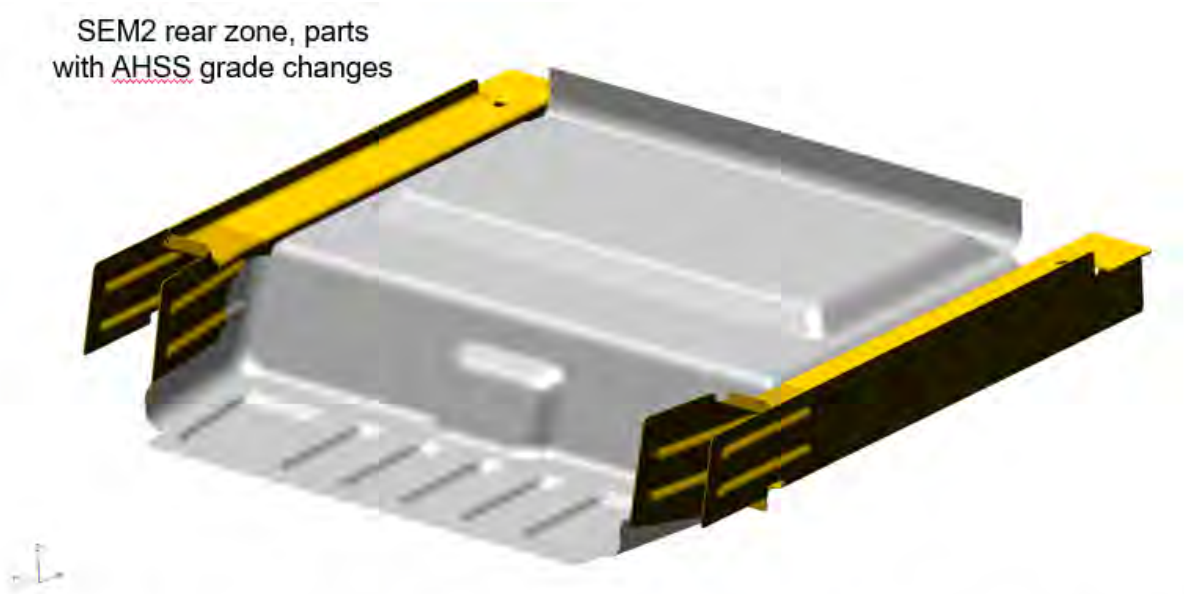

Part Number	Part Name	AHSS Grade	Gauge (mm)	C = Carry over SEM1 G = grade/gauge change N = New geom	Part Mass (kg)	SEM2 change
03596995_2	REAR COMPARTMENT PAN LOWER	CR_HSLA350/450	0.5	N	2.89	New geometry for rear EDU package
03477701_2	LONGITUDINAL REAR RAIL INNER RH	CR820Y1180T-RA_1.4_CR600Y980	1.8	G	1.90	change from 1.4mm/1.6mm TWB to 1.6mm
03476382_2	LONGITUDINAL REAR RAIL INNER LH	CR820Y1180T-RA_1.4_CR600Y980	1.6	G	1.90	change from 1.4mm/1.6mm TWB to 1.6mm
03477703_2	LONGITUDINAL REAR RAIL OUTER RH	CR820Y1180T-RA_1.4_CR600Y980	1.6	G	1.81	change from 1.4mm/1.6mm TWB to 1.6mm
03476381_2	LONGITUDINAL REAR RAIL OUTER LH	CR820Y1180T-RA_1.4_CR600Y980	1.6	G	1.81	change from 1.4mm/1.6mm TWB to 1.6mm

Figure 11.5.1 Subjective performance evaluation for SEM2

Attribute/Requirement	Impact of SEM1 to SEM2	Design mitigation and countermeasures
Front crash	SEM2 higher 24% curb mass, therefore front crash will have higher energy levels to manage	Increase strength of front longitudinals to enable greater energy absorption. Increase gauge thickness of PHS2000 SORB parts
Side crash	IIHS side barrier. Larger side aperture. Heavier vehicle. SEM1 has very good side barrier crash performance Pole: Alignment to occupant won't change so no issue expected. Pole to HV battery potentially an issue with stretched door aperture	Additional C pillar to protect 3rd row occupants
Rear crash & roof crush	Higher GVW. SEM1 performance is comfortable so no significant issue expected	None
Body stiffness and NVH	Stretched, longer body structure therefore modal frequencies expected to reduce, potentially below target. Higher battery mass will further reduce the batter first mode	Additional structural adhesive applied to recover NVH modal frequencies
Durability	Higher curb mass = higher durability loads. SEM1 has some margin on durability performance so no change is expected	None
BIW Mass	SEM2 BIW mass increase will be: additional/stretch mid-zone section. Impact of secondary countermeasures. There could be a –ve mass spiral effect with more mass being required due to higher curb mass. E.g. body needs to be heavier due to heavier battery	None
Cost	New mid-zone panels (tooling) and increased grade and gauges in front zone	Cost increases expected to be in line with other vehicle platform approach
Life Cycle Assessment	Higher vehicle mass, more steel. Less aggressive real world duty cycle (less city stop-start) Need to ensure high occupancy rate >2	None
Manufacture & assembly	Don't expect significant manufacture issues beyond usual vehicle variant lines	
HV battery, jacking, China crush, PSD	Higher mass, higher jacking load. Larger battery cover area. More challenging to meet targets	None

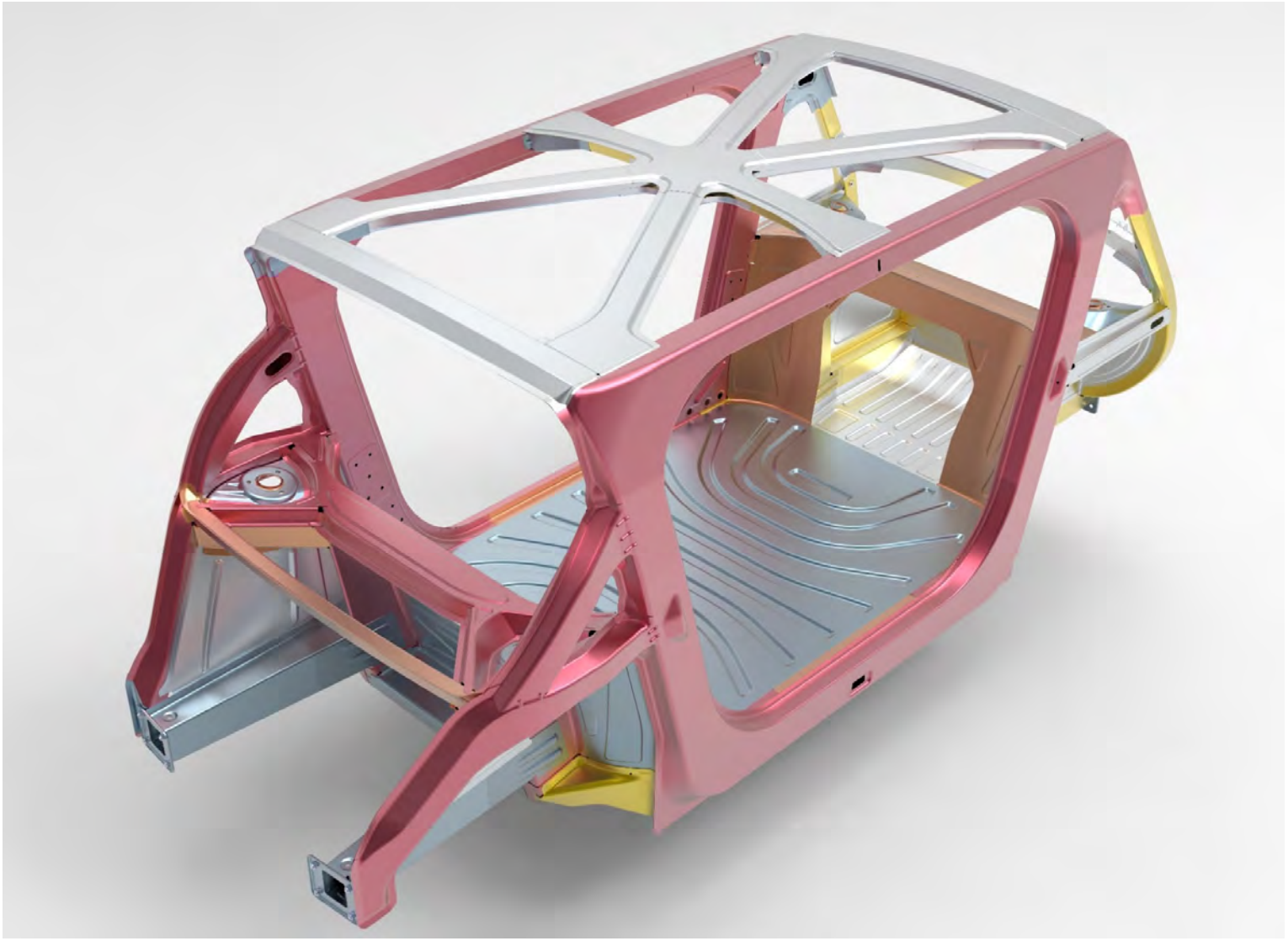

END OF REPORT